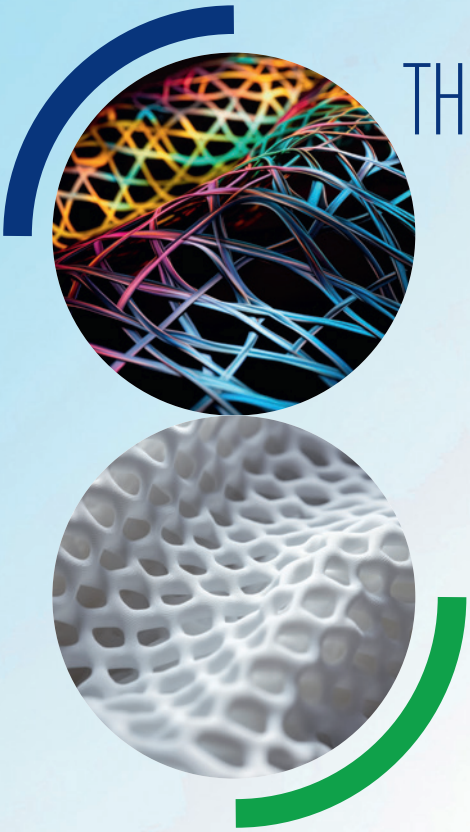
EUROGEO 8
LILLE 2025 15-18 September



8TH

EUROPEAN GEOSYNTHETICS CONFERENCE

CONFERENCE PROCEEDINGS



15-18 SEPTEMBER 2025
LILLE GRAND PALAIS - FRANCE

ORGANIZED BY CFG

COMITÉ FRANÇAIS DES GÉOSYNTHÉTIQUES

UNDER THE AUSPICES OF IGS

INTERNATIONAL GEOSYNTHETICS SOCIETY

Dear Participants in Eurogeo8, Dear Sponsors and Exhibitors,

Dear Friends,

Warm welcome to France,

Almost 50 years after the first International Conference on Geosynthetics in 1977 on the Use of Fabrics in Geotechnics in Paris, and 23 years after the 7th International Conference on Geosynthetics in Nice in 2002, the CFG French Chapter of IGS is happy to welcome you for this 8th European Conference in the nice and warm city of Lille.

The main theme of the Conference is: Technical Challenges and Environmental Imperatives for the 21st Century. The new challenges faced by construction professionals, environmental concerns, innovation and risk management will be at the heart of the discussions and presentations.

The Conference Program includes opportunities to attend two full one-day workshops, 4 Keynote Lectures, a Lecture about Diversity, 21 scientific sessions run in 4 parallel rooms, including 3 sessions in French and 135 oral presentations, and additional activities.

An Exhibition area welcomes you to visit and stop by any of the 77 booths from 27 countries; we hope you find time to stop and chat with representatives of the 25 main sponsors and companies, some of whom have travelled long distances to be here.

The Conference is not only oriented on science and geosynthetic product but includes a number of social activities within the program. 600 delegates from 51 countries are expected to attend the Conference and we are sure many new international relationships will be created.

We hope that you will enjoy time in Lille, discover a little bit of France, and hopefully come back in the near future.

This conference couldn't happen without the support of the Exhibitors and Sponsors to whom I address very special thanks. We all appreciate your dedication and desire to see regional geosynthetic events such as EuroGeo conference happen again.

Together with my colleagues of the Organisation and Scientific Committees, we wish you all very best time in Lille.

Yours sincerely

Dr Jean-Pierre Magnan
Conference Chair, President of French Chapter of the IGS

Edited by vertcom

CONFERENCE COMMITTEES

The Organizing Committee is led by IGS France expert members who represent industry, academia, and professional practice. Additionally, the committee is supported by leaders from throughout the IGS Chapters in Europe.

Organizing Committee

Jean-Pierre	MAGNAN	*Chairman of EuroGeo 8, President of the French Chapter*
Guillaume	STOLTZ	*General Secretary of EuroGeo 8, INRAe, Aix-Marseille University*
Abdelkader	ABDELOUHAB	*Solmax*
Anne-Laure	BACKES	*DuPont de Nemours*
Xavier	DE MAUNY	*BMIgroup France*
Paul	GUINARD	*Soprema*
Véronique	HEILI	*Vice-Chair of EuroGeo 8, Treasurer of the French Chapter, CEREMA Est*
Pierre	LEBON	*ASQUAL*
Alain	NANCEY	*Solmax*
Jean-Frédéric	OUVRY	*French Chapter of IGS*
Jean-Christophe	PELLEZ	*Sol Solution*
Mathilde	RIOT	*Afitexinov*
Jacques	SAINTOT	*AFAG*
Antoine	SEGUIN	*BMIgroup France*
Olivier	SNIEHOTTA	*Fibertex*
Hélène	SZULC	*AQUAGEO Etanchéité*
Sébastien	VERBRUGGHE	*TERAGEOS*
Thomas	WOHLHUTER	*AnteaGroup*
Séverine	BEAUNIER	*École des Ponts Formation Continue*

CONFERENCE COMMITTEES

Scientific Committee

Chair:

Laetitia	VAN SCHOORS	*Gustave Eiffel University*

Co-chairs:

Laurent	BRIANÇON	*INSA de Lyon*
Philippe	DELMAS	*French Chapter of IGS*
Jean-Pierre	GOURC	*Grenoble University*
Véronique	HEILI	*CEREMA Est*
Orianne	JENCK	*Grenoble INP*
Guillaume	STOLTZ	*INRAe Aix Marseille University*

Extended Scientific Committee:

Abdelkader ABDELOUHAB, **France**
Julien AUBRIET, **France**
Anne-Laure BACKES, **Luxembourg**
Adam BEZUIJEN, **Belgium**
Stefania BILARDI, **Italy**
Giovani BIONDI, **Italy**
Eric BLOND, **Canada**
Olivier BORY, **France**
Gerhard BRAU, **Germany**
Francesco CAFARO, **Italy**
Laura CARBONE, **Germany**
Giuseppe CARDILE, **Italy**
Davis CARLOS, **Portugal**
José Ricardo CARNEIRO, **Portugal**
Paolo CARRUBBA, **Italy**
Victor CAVALEIRO, **Portugal**
Daniele CAZZUFFI, **Italy**
Sabatino CUOMO, **Italy**
Tonguc DEGER, **Turkey**
Mattos DELMA VIDAL, **Brazil**
Oliver DETERT, **Germany**
Gemmina DI EMIDIO, **Belgium**
Yuli DOULALA-RIGBY, **UK**
Isabel FALORCA, **Portugal**
Fabienne FARCAS, **France**
Fernanda FERREIRA, **Portugal**
Francesco FONTANA, **Italy**
Juha FORSMAN, **Finland**
Ian FRASER, **UK**
Patrick GARCIN, **France**
Domenico GAUDIO, **Italy**
Yves GERARD, **France**
Domenico GIOFFRÉ, **Italy**
Thierry GISBERT, **France**
Guido GOTTARDI, **Italy**
Fredrik GRIWELL, **Sweden**

CONFERENCE COMMITTEES

Nicolo GUARENA, **Italy**
Patricia GUERRA-ESCOBAR, **UK**
Erol GULER, **Turkey**
Oddur HAGALIN, **Iceland**
Leos HORNICEK, **Czech Republic**
Mehrez JAMEI, **Tunisia**
Jacek KAWALEC, **Poland**
Elzbieta KOKOCINSKA-PAKIET, **Poland**
Jean LAFLEUR, **Canada**
Stephane LAMBERT, **France**
Minna LEPPÄNEN, **Finland**
Monica LÖFMAN, **Finland**
Andrzej LOPATKA, **Poland**
Giulia LUGLI, **Italy**
Philippe MAILLER, **France**
Maria Clorinda MANDAGLIO, **Italy**
Viviana MANGRAVITI, **Italy**
João MANSO, **Portugal**
Anna MARKIEWICZ, **Poland**
Ioannis MARKOU, **Greece**
Veronique MEYDIOT, **France**
Aníbal MONCADA, **Spain**
Omar NACIRI, **France**
Alain NANCEY, **France**
Jose NEVES, **Portugal**
Ali Hakan ÖREN, **Turkey**
Hakan OZCELIK, **Turkey**
Jean-Christophe PELLEZ, **France**
Margarida PINHO-LOPES, **Portugal**
Marilene PISANO, **Italy**
Heraldo PITANGA, **Brazil**
William POWRIE, **UK**
Damians PUIG, **Spain**
Piergiorgio RECALCATI, **Italy**
Jan RETZLAFF, **Germany**
Pietro RIMOLDI, **Italy**
Laurent SAUGER, **France**
Richard THIEL, **USA**
Nathalie TOUZE, **France**
Fabrizia TROVATO, **Italy**
Karen VARAIN, **France**
António Miguel VERDELHO PAULA, **Portugal**
Castorina VIEIRA, **Portugal**
Pascal VILLARD, **France**
Hauke ZACHERT, **Germany**
Kasia ZAMARA, **UK**
Helmut ZANZINGER, **Germany**
Martin ZIEGLER, **Germany**

International Advisory Committee:

Sam	ALLEN	*President of IGS*
Domenico	GAUDIO	*Chair of Europe Region IGS Young Members Committee*
Patricia	GUERRA-ESCOBAR	*Chair of ERAC (European Regional Activities Committee) of IGS*
John	KRAUS	*Executive Director of IGS*
Viviana	MANGRAVITI	*Chair of IGS Young Members Committee*
Elise	OATMAN	*Secretariat Manager of IGS*

LIST OF EXHIBITORS

Platinium Sponsors

CETCO
A MINERALS TECHNOLOGIES COMPANY

MACCAFERRI

VIGANO PAVITEX S.P.A.

RENOLIT
Rely on it.

THRACE GROUP
A WORLD OF MATERIALS & SOLUTIONS

Gold Sponsors

BONTEXGEO GROUP

COLETANCHE

CONCRETE CANVAS

ECOFIBRE
GÉOTEXTILES NON TISSÉS

Edilfloor

GEOMAS
GEOKOMPOZIT

HUESKER
Ideen. Ingenieure. Innovationen.

SOLMAX

TENAX

LIST OF EXHIBITORS

Silver Sponsors























LIST OF EXHIBITORS

Exhibitors









































LIST OF EXHIBITORS

Exhibitors









































KEYNOTE LECTURES



Life cycle assessment of geosynthetics: a pathway to sustainability

Dr. Enrico Benetto

Head of Unit, Environmental Sustainability and Circularity Assessment Research Unit, Luxembourg institute of Science and Technology

Biography

Enrico focuses on developing science-based methods and indicators to guide industry and society toward climate targets and sustainability transitions. With 25 years of leadership in R&D institutions, his work in Sustainability Science spans the design of products, technologies, and policies. He has co-authored over 120 peer-reviewed papers, 150 conference proceedings, 18 book chapters, and edited the open-access book Designing Sustainable Technologies, Products and Policies (Springer, 1.4M accesses). Enrico has contributed to over 50 European research projects and 30 collaborative partnerships with SMEs, policymakers, and large industries, advancing sustainability knowledge and practice.

Enrico has built strategic partnerships with national ministries and organizations like the World Alliance for Efficient Solutions. He serves in prominent advisory roles, including the EU Platform on Sustainable Finance, the Climate Policy Observatory of Luxembourg, and the Scientific Advisory Board of the Luxembourg Sustainable Finance Initiative (LSFI), driving innovative approaches for a sustainable future.

Abstract

In this lecture we will explore the life cycle assessment (LCA) of geosynthetics, a crucial tool for understanding the environmental impacts of these materials from cradle to grave. Geosynthetics have revolutionized infrastructure, water management, and soil stabilization, often outperforming traditional materials by reducing excavation needs, transportation costs, and carbon footprint. Yet, as sustainability becomes a global imperative, we must evaluate their life cycle to align innovation with environmental stewardship.

The LCA framework reveals both opportunities and challenges. Geosynthetics enhance resource efficiency and extend infrastructure lifespan, minimizing emissions over time. However, challenges persist, particularly in the production phase, which relies heavily on fossil fuels, contributing to greenhouse gas emissions. End-of-life management is another critical issue, as recycling remains technically complex and economically unviable in many contexts, leaving landfilling and incineration as predominant options.

Methodological challenges further complicate LCA implementation. Data gaps, variability, and region-specific limitations hinder accuracy. Defining functional units for long-term applications and deciding on system boundaries—whether to include secondary effects such as reduced maintenance—add layers of complexity. Additionally, the lack of harmonized standards across industries limits comparability and policy development.

To address these challenges, the field should prioritize innovation in material science, such as developing bio-based and recyclable geosynthetics, while improving recycling systems. Collaboration between researchers, industry stakeholders, and policymakers is essential to establish standardized methodologies and incentivize sustainable practices.By integrating robust LCA into decision-making, we can advance technologies that meet engineering demands while respecting planetary boundaries.

KEYNOTE LECTURES



Committee DEI – Approach to Diversity, Equity, and Inclusion
Awakening Perceptions: Challenging Minds to Lead with Empathy

Daniela Felletti

Global Diversity, Equity and Inclusion Practitioner, Educator & Speaker

Biography

Daniela is a multilingual professional, with +19 years of experience in Europe and a background in behavioral science.

Applying culturally aware approaches to human behavior for more ethical engagement, she helps organizations transform their perceptions and actions towards a more inclusive world. Daniela' specialism is in Diversity, Equity & Inclusion Advisory at the executive Level and she is also an experienced Lecturer in Higher Education and an international corporate Speaker.

Through her training, she evokes the importance of exploring the different perceptions of the brain (thus of the unconscious) towards the other through sensory, introspective and active listening activities. A profound and effective way to create meaningful connections, to release curiosity and to awaken perceptions with empathy and authenticity.

Daniela has presented at many international events and organisations and her clients include FIA (Féderation International Automobile), AECOM, Trane Technology, Bristol Meyers Squib, West Pharm, Nelson's, Heineken and Michigan State University.

Daniela is an expert that inspires her work on behavioural science aiming to help individuals and organisations transform and evolve the way they perceive and act on Diversity, Equity and Inclusion.

Daniela has advised +300 executives and trained +5000 individuals on these topics on 3 continents.

Fluent in Brazilian Portuguese, Italian, English, French and Spanish. Currently exploring the Arabic language.

Abstract

Daniela will deliver a groundbreaking talk designed to challenge perspectives and awaken a deeper understanding of Diversity, Equity, and Inclusion (DEI). This subject fundamentally impacts everyone – which is why every congress member's participation matters, not just as attendees but as active contributors to change. Moving beyond awareness, this session will provide all participants with concrete tools and actionable strategies. By cultivating both empathy and accountability, attendees will start to develop a more conscious approach to DEI – empowering them to consistently apply these principles in their leadership during the forum and in all future decisions and interactions.

KEYNOTE LECTURES



Geosynthetics in the northern countries: geotechnical and environmental challenges

Arnstein Watn

Managing director/Daglig leder WatnConsult ASManaging Director WatnConsult AS/Senior Advisor Norwegian University of Science and Technology (NTNU)

Biography

M.Sc geotechnical Engineering from NTNU 1981. More than 40 years experience with varied geotechnical consulting, public authority, research and education. Project Manager for national and international design, construction and research project in geotechnics. Participation and project director for a number of large construction projects and research and development projects nationally and internationally including climate adaption, roads, railroads, quays, airfields, dam structures and more.

30 years of experience as sensor and research fellow at University level. More than 150 scientific publications. Long experience in giving courses, leading work-shops and giving presentations at seminars and conferences nationally and internationally. 30 years of experience from national and international standardisation work on geosynthetics, lightweight materials and geotechnical work. Previous board member of the Norwegian Geotecnical society (NGS), leader of the NGS geosynthetic committee and past President of IGS Norwegian Chapter.

Abstract

Nordic countries commonly have challenging conditions with soft subsoil and changing climate and soil improvement based on natural vegetation (trees, bushes, weeds) has been used in the Nordic countries since more than 1000 years. The introduction of geosynthetics around 1970 provided a good possibility for providing environmental friendly structural solutions that were beneficial technically and economically. A system for classification of geosynthetics for separation and filtration was proposed by the Norwegian Directorate of roads in 1978. This has been the basis for NorGeoSpec, a common system for certification of geosynthetics operating for more than 20 years covering Estonia, Finland, Sweden and Norway.

A guideline for design and construction of reinforced soil structures were developed as a co-operation between the Nordic geotechnical societies in 2000. Geosynthetics have been used for large number of construction projects. Special structural solutions include vegetated steep slopes with peat block front for frost insulation and a combination of geosynthetic reinforcement and light weight clay aggregate to provide light wight structural solutions with frost insulation.

A number of research projects have been carried out to develop structural solutions and construction methods for Nordic conditions. The projects include testing of geosynthetic for erosion control in Arctic conditions as far north as Svalbard. The possibility for installing geosynthetics under temperatures down to -25 were carried out in Kemi in Finland close to the Swedish border as a co-operation between the Nordic Traffic authorities, Universities , research institutes and a group of producers.

There has been a long tradition of co-operation in the field of geosynthetics between the Nordic countries related to research, education, certification and on marketing and sales. A common Nordic chapter of IGS which was formerly established from 2023 and hopefully will be the basis for further development of geosynthetics "under Aurora Borealis".

KEYNOTE LECTURES



LMNS lecture
Suitable design approaches for the different interfaces including geosynthetics in different loading and flow conditions

Prof. Eng. Nicola Moraci, Ph.D
Mediterranean University of Reggio Calabria

Biography

Full Professor of Geotechnical Engineering at the Mediterranean University of Reggio Calabria where he was Pro-Rector for Research, Head of the Department of Civil, Energy, Environmental and Materials Engineering; Member of the Academic Senate; Member of the Board of Administrators; Coordinator of the Doctorate in Geotechnical Engineering. He has been Tutor of 22 PhD theses in Geotechnical Engineering. He was President of the Italian Geotechnical Society (AGI) (2015-2022). The research activity has developed along multiple themes including landslides and landslide risk mitigation, use of geosynthetics in civil and environmental works, controlled landfills and remediation of contaminated sites, soil reinforcement, protective filters, innovative technologies and materials, sustainable geotechnical works. The research activity has led to the editing of more than 250 papers mostly published in important international journals and international and national conferences. He has received awards for research activities, including the IGS (International Geosynthetics Society) Award 2008, the Best Paper Awards from the Geotextiles and Geomembranes Journal (2017) and from the Geosynthetics International Journals (2022). He is currently Associate Editor of the Geotextiles and Geomembranes Journal, and Member of the Editorial Board of others important international Journals. He has been scientific director of numerous research projects funded on the basis of competitive calls for bids that provide for peer review. He has been invited lecturer at several International and National Conferences, as well as a member of Scientific and Organization Committees of several International and National Conferences. He has been a member of numerous Technical and Scientific Committees for the ISSMGE, the CEN, the IGS, the Ministry for Environment, Land and Sea Protection of Italy, and the AGI.

Abstract

The topic I would like to develop in the LMNS Lecture aims to systematically integrate the findings from my years of research, with a particular emphasis on studies regarding the interaction between various interfaces where geosynthetics are employed to serve different functions. This pertains to the ultimate or serviceability limit states of the structures in which they are used, under different loading or flow conditions.

Given the limited time available, I plan to focus on the importance of proper interface characterization concerning the design of reinforced earthworks, landfill cover systems and drainage systems in earthworks or slopes. Specifically, the research I carried out, which I will summarize in the Lecture and has been the subject of several scientific publications and international awards, has helped to clarify the approaches to be considered for:

1. the correct characterization of the soil-geosynthetic interface in geosynthetic-reinforced soil structures under static and cyclic conditions, both in the short and long term. Clear guidance is provided for the correct selection of materials and interface parameters necessary for designing structures under ultimate and serviceability limit state conditions.
2. the correct characterization of the interface between different geosynthetics in landfill cover systems under static and seismic loading conditions. In this context, the roles played by low contact stresses, mechanical damage due to high relative displacements and the presence of interstitial fluid at the interface are highlighted.
3. the proper evaluation of the limit states of soil/geotextile filter interface in contact with internally stable and unstable granular soils under different flow conditions (unidirectional or alternating flow), while highlighting the limitations of the approaches generally used for both the characterization of interacting materials and the design of filters. These findings enabled the development of a new approach for the design of geotextile filters in contact with internally stable and unstable cohesionless soils and the development of a procedure useful in geotextile filter design under critical/severe conditions.

KEYNOTE LECTURES



Geosynthetic reinforced soil : from the experimentation to design methods

Prof. Laurent Briançon
INSA, Lyon

Biography

Laurent Briançon is a professor and researcher at the National Institute of Applied Sciences (INSA) of the University of Lyon in France. He received a PhD degree in Civil Engineering from the University of Bordeaux in 2001 and, later in 2024 the title of "Habilitation" in Civil Engineering. He worked for 9 years as an Assistant Professor at the Conservatoire National des Arts et Métiers, for 2 years at the engineering consultancy Antea Group, and since 2014 as an Assistant Professor at the National Institute of Applied Sciences. His activities involve research, teaching, and consulting in the field of soil reinforcement and geosynthetics. Laurent's research combines laboratory tests and field monitoring approaches to propose practical design methods. He specifically worked on the reinforced platforms by GSY on cavities and participated in the redaction of the French Standard XP G38-065 on this topic. He also participated in the French research project ASIRI on the pile-supported embankment and manages the new project ASIRI+ in this field since 2019. So far, he has supervised over 17 PhD. He has published 30 journal papers and 3 books. He is the Vice president of the French Chapter of IGS and has been a member of the technical committee of the French chapter of ISSMGE.

Abstract

Construction on poor-quality soils or with a risk of loss of bearing capacity over time is a major challenge for the planning of land and economic development of a country. Environmental considerations imposed since the 2000s have strengthened economic choices on soil improvement and reinforcement solutions. Geosynthetic reinforcement has found a place of choice in structures to reduce the risk, improve load transfer and more generally control the settlements. Geosynthetic reinforcement of the granular layers also reduces their thickness and thus limits the extraction of natural material and its transport.

These innovative techniques are often the subject of research projects that propose rules for their design and setup. These studies require laboratory experiments to identify mechanisms and characterize the interactions between soils and geosynthetic sheets. They are often paired with numerical models calibrated on the experimental results to put into equations mechanisms and eventually propose design rules. Full-scale validations are also essential for a complete engineering transfer. The diversity of geosynthetic sheets and the complexity of interaction mechanisms require R&D actions to bring together researchers, producers, and designers.

This scientific and technical path will be detailed on three geosynthetic reinforcement applications:

1. For granular platforms with cavity risk

   In this field, French research began in 1997 with the project RAFAEL and went on for more 20 years with full-scale experimentations, laboratory tests, DEM simulations in the projects GEOINOV or PITAGOR to result in the French Standard XP G38-065 (2020).

2. For load transfer platforms of pile-supported embankment

   Several research projects have addressed this topic to study the role of the geosynthetic on the efficiency of this technique. In France, two research projects investigated pile-supported embankments (ASIRI, 2012; ASIRI+, 2025) and more particularly the role of the geosynthetic in the granular platform.

For granular platform laid over weak soil subjected to traffic loading

Two French Thesis have recently investigated this problem by developing a traffic loading simulator, performing laboratory tests at a real scale, and DEM simulations (Khoueiry, 2019; Abou Chaz, 2024). The results of these studies will be compared to others to highlight the complexity and the variability of mechanisms depending on the type of geosynthetics, their location, and the compressibility of the subgrade soil.

TECHNICAL SESSIONS

TECHNICAL SESSION	TITLE	PAPER AUTHORS
SESSION 1 A- SUSTAINABILITY AND DURABILITY (1)	Geosynthetics, a key brick of the energy transition	Wetzel H., Van Helden W., Sørensen P.A., Micollier V.
	Greener unpaved forest roads: costs and emissions analysis of solutions with an industrial byproduct and a geosynthetic	Rodrigues D., Martins C., Carlos D., Preiswerk S., Montez P., Macedo J., Pinho-lopes M.
	Comparative Life Cycle Assessment of a slope protection on a railway embankment	Wittl T., Klügel S., Vollmert, Ehrenberg H.
	Technical solutions for reducing CO2 footprint in MSE wall constructions	Grandclerc A., Joussellin T.
	Comparative environmental life cycle assessment of a temporary road, a study on behalf of the EAGM	Ehrenberg H., Gruber J.
	Sustainability assessment of liquefaction instability mitigation solutions for the World's highest observation wheel project in Dubai	Puthiya Veettil J., Trovato F., Lugli G.
	Effects of ageing in a saturated environment on the functional properties of hemp geotextiles	Dabiret S. A., Roure, F., Farcas F., Makki L., Mailler P., Reiffsteck P., Schoors L.
SESSION 2 A- SUSTAINABILITY AND DURABILITY (2)	Geosynthetic multilayered composite: innovative development, applications and life cycle assessment	Ferrara M., Lugli G.
	Potential release of microplastics from geosynthetic applications: a case study in Europe	Cazzuffi D., De Meyer S., Fontana F.
	Potential microplastic release from gabion mattresses: a quantitative assessment	Brocca G., Masola F., Born M.P., Schiller S.
	High performance and recyclable geosynthetic for stabilisation and platform reinforcement	Nancey A., Abdelouhab A.
	Geotextile durability by outdoor weathering and tensile creep: case study	Alves Guimarães M. G., Urashima D.,Urashima B. M.
	Evaluation of the degradation of polypropylene geotextiles under real coastal conditions and UV radiation exposure	Weynemi Cavalcante Dos Santo E., Lizandra Maria Ferreira Gurgel L., Felinto de Lima Neto F., Alexandre Nunes de França F.
	Water storages with PVC liners and floating covers	Sadlier M.

TECHNICAL SESSIONS

TECHNICAL SESSION	TITLE	PAPER AUTHORS
SESSION 1 B- TESTING, QUALITY (1)	Assessing the shear-strength properties of geomembranes textured using the spray-on technique	Blond E., Tarnowski C.
	Experience of a certification body with the quality of external testing in the certification process	Hessing C., Recker C.
	The influence of seating time on water flow of nonwoven geotextiles in permeability tests	Markiewicz A., Koda E., Skrońc A., Soszyński P.
	Laboratory tests on stabilization of railway ballast with geogrid	Somov D., Petriaev A.
	Dry abrasion evaluation of geotextiles with different test standards	Fierro G.
	Considering the deformation of nonwovens to follow the behavior on site	Ehrenberg H., Retzlaff J.
	Studies on the sound generated during the tensile test on nonwoven geotextiles	Niccolai F.
SESSION 2 B- TESTING, QUALITY (2)	Design of unpaved forest roads - stress-strain response of a reinforced soil under triaxial conditions	Carlos D., Cafôfo O., Macedo J., Pinho-lopes M.
	Enhancing reinforced soil performance: polymeric coated steel woven wire mesh and geogrid interaction in composites systems	Brocca G., Vicari M., Lugli G.
	Development of shear resistance at cohesive soil – geotextile interfaces	Markou I., Evangelou E.
	Evaluating the interaction between geogrid and recycled aggregate using pullout tests	Khan A. R., Di Emidio G., Denies N.
	Influence of construction method on pullout resistance of polymeric strap reinforcement	Moncada A., Girbau N., Damians I.P., Olivella S., Bathurst R. J.
	Fibre reinforcement of a uniform sand: stress-penetration and stress-strain responses	Martins C., Rodrigues D., Carlos D., Morais S., Macedo J., Pinho-lopes M.

TECHNICAL SESSIONS

TECHNICAL SESSION	TITLE	PAPER AUTHORS
SESSION 1 C- REINFORCEMENT APPLICATIONS (1)	Experimental studies on groups of stone columns with various shapes of geotextile	Bazzazian Bonab S., Lajevardi S. H.
	Soil arching in geosynthetic and steel grid-reinforced pile-supported embankments	Van Eekelen S., Schneider M., Hell M., Pandrea P., Schauber P., Topolnicky M., Makowska K., Zachert H., Bezuijen A.
	Experimental and numerical model in geosynthetic pile embankment	Lajevardi S. H., Tardast A., Briançon L., Mirhoseini S. M.
	Piled embankments - Behaviour of geosynthetic basal reinforcement in condition of change of soft soil reaction	Łopatka A.
	On the construction rate of geosynthetic-reinforced and pile-supported embankments	Mangraviti V.
	Design of geosynthetics for rigid inclusion ground improvement: a simplified analytical method	Alzate A.M., Simon B., Briançon L.
	Lessons learned from the ASIRI+ project on the use of geosynthetics in load transfer platform	Nancey A., Briançon L.
SESSION 2 C- REINFORCEMENT APPLICATIONS (2)	Microgrid reinforcement of scaled railway ballast	Anjos R., Neto V., Pinho-lopes M., Powrie W.
	Geogrid-stabilized eco-friendly aggregates for pavement base – quantitative assessment using bender element sensor technology	Wang H., Ko H., Kang M., Tutumluer E., Shoup H.
	Experimental studies on the cyclic behaviour of reinforced unbound railway base courses	Bräunig C., Herle I., Weisemann U.
	Compaction of a geotextile-reinforced sand contaminated with tyre microplastics	Ozhan H., Yavuz M.
	Ensuring the stability of high embankments on Ukrainian highways during reconstruction and repair using geosynthetic materials	Gameliak I., Zhurba G., Diakovska T.

TECHNICAL SESSIONS

TECHNICAL SESSION	TITLE	PAPER AUTHORS
SESSION 1 D- DESIGN AND MODELISATION (1)	Effects of grains characteristics and geogrid shape and rigidity on the behavior of reinforced granular soil – 3D DEM study	El Ayoubi A., Emeriault F., Villard P., Sibille L.
	Laboratory tests and numerical studies of a geosynthetic reinforced pile-supported embankment	Hu Y., Briançon L., Dias D.
	Strength prediction models for fiber-reinforced soils under effective stress triaxial compression testing	Bantralexis K.E., Vassou A.G., Markou I.N.
	Geosynthetic overlap for reinforced piled embankment : centrifuge modelling	Thorel L., Guerois M., Dubreucq Th., Blanc M.
	Finite element modelling of geogrids in stabilisation function - comparison study	Ria Zamara K., Lees A., Gorrill B., Kawalec J.
	Numerical modelling of soil-reinforcement direct shear test with Mohr-Coulomb plasticity	Xiao S., Damians I. P., Hu W.
	Prediction of rainfall induced geosynthetic-reinforced slope instability: machine learning algorithms perspective	Jamei M., Selmi M., Hamroumi F.
SESSION 2 D- DESIGN AND MODELISATION (2)	Reinforced platforms with geocells over tree root protection zones for the construction of an elevated woodland walkway	Tahir M., Bernardini P., Saeed R.
	Comprehensive overview of soil erosion control: design of anti-erosive geomats for effective slope stabilization	Santoli F.M., Lugli G., Trovato F.
	Impact of structural intersections on reinforced soil structures: design and construction considerations	Masola F., Trovato F., Brocca G., Vicari M.
	Numerical modelling of MSE walls subjected to strong earthquake motions	Korini O.
	Attenuation of environmental vibrations using geosynthetics	Herault A., Jean P., Jolibois A.
	A numerical assessment of the influence of compaction on the seismic performance of Geosynthetic-Reinforced Earth retaining walls	Gaudio D., Cioffi L., Masini L.

TECHNICAL SESSIONS

TECHNICAL SESSION	TITLE	PAPER AUTHORS
SESSION 3 A- SUSTAINABILITY AND DURABILITY (3)	Reuse and recycling of geosynthetics – Insights into an interdisciplinary research project for a circular economy	Depenbrock N., Heimbecher F., Flamme S., Ebbert S., Tazl M.
	Towards a collaborative circular European geosynthetic economy	Denoo F., de Meyer S., Zamora S.
	Recycling of geotextiles: a collaborative approach to enhance circularity in construction.	Groen G., Gruber J.
	Simple constitutive methods to represent the tensile response of a laboratory-aged nonwoven geotextile	Paula A. M., Carneiro J.R., Pinho-lopes M.
	Investigation of durability of geotextiles tubes in marine conditions	Chew S. H.,Soh J. M., Lim Y. M., Deng J., Tan Y.G., Yim A., Quek A., Lim D. J., Low S., Chang D.
SESSION 4 A- MANDATORY EUROPEAN FRAMEWORK FOR GEOSYNTHETICS - BEYOND SUSTAINABILITY	Construction Products Regulation: environmental approach for geosynthetics	Delmas Ph.
	On going Work on the Mandatory requirements for geosynthetics	VON Maubeuge K.
	Geosynthetics - Assessment of Release of dangerous substances	Heili V.
	Geosynthetics - Environmental performance – product category rules	Henning H.
	Geosynthetics - Circular Economy – requirements: materials and products	Fontana F.
	Geosynthetics - Potential release of microplastics	Fraser I.
	Discussions	VON Maubeuge K.
	Summary and conclusions	Delmas Ph.

TECHNICAL SESSIONS

TECHNICAL SESSION	TITLE	PAPER AUTHORS
SESSION 5 A- SUSTAINABILITY AND DURABILITY (4)	Long-term durability of HDPE geomembranes in mining: A non-parametric statistical approach	Urashima B. M., Inui T., Deleon L., Ribeiro Duarte A., Urashima D., Santos R.
	Durability assessment of HDPE geomembrane in a concrete water supply canal: A 10-year case study.	Urashima B. M., Inui T., Deleon L., Carvalho Urashima D., Meucci D.
	Comparative performance evaluation of smooth and textured white geomembranes under UV exposure	Aparicio-ardila M. A., Lins Da Silva J.
	Service life of bituminous geosynthetic barrier: accelerated ageing tests	Hahn W., Kroh R, Zanzinger H., Armani A., Breul B., Doledec E.
	Durability of three PVC-P geomembranes during two years of accelerated ageing laboratory tests	Stoltz G., Aubriet J., Bambara G., Sauger L., Chamoley D., Bouteille S.
	Aging of PVC geomembranes for dams: monitoring of aging and end of service life	Bory O., Cintract J., Martin L.
SESSION 6 A- SUSTAINABILITY AND DURABILITY (5)	Determination of the reduction factors applied to polymeric coated woven steel wire mesh reinforcement according to German recommendation	Masola F., Gualandi P., Rimoldi P., Schiller P., Vicari M.
	Durability analysis of High-Density Polyethylene geomembrane immersed in brine and tailings solutions	Paulson S.
	25 years of experience with a lysimeter system with geosynthetic clay liners	Muller -Kirchenbauer A.,Ehrenberg H.
	Evolution of recycled construction aggregates (RCA) pH and its compatibility with geosynthetics	Abdelouhab A., Nancey A., Janse D.
	Long-term performance of pet geogrids with LLDPE coating in alkaline conditions	Lugli G., Napoelonie Q; Scotto M.
SESSION 3 B- TESTING, QUALITY (3)	Laboratory investigation of geopolymer stabilized subgrade soil reinforced with Alkaline binder-coated Natural Jute Sheet	Aaqib A., Syed M., Mubashir A., Umair A.
	Laboratory tests of the impact of stones on geotextile and calculation model	Bezuijen A.
	Study of installation of prefabricated vertical drain through a geotextile tube bund	Soh J. M., Chew S. H., Lim Y. M., Deng J., Tan Y. C., Yim A., Quek A., Lim D. J., Low S., Chang D.
	Interaction properties between cohesive soils and woven geotextiles – experimental and numerical analysis	Serbulea M.-S.
	Simulation and applicability evaluation of nonwoven geotextile composite for adsorption of cesium Ions in radiation-contaminated soil JEON H.Y., NAM G., CHA J.H.	Jeon H.Y., Nam G., Cha J.H.

TECHNICAL SESSIONS

TECHNICAL SESSION	TITLE	PAPER AUTHORS
SESSION 4 B- TESTING, QUALITY (4)	Geosynthetic Clay Liners, why hydraulic conductivity (k-value) is the wrong value for a tender	Ehrenberg H., Niehues C.
	Parameters affecting the vertical deformations of GCLs during hydraulic conductivity tests	Demirci N., Özdamar Kul T., Ören A. H.
	Hydraulic conductivity of geosynthetic clay liner containing polymerized bentonite with low mass per unit area	Ören A. H., Aytekin T. C.
	Semi-permeable membrane behaviour of conventional and enhanced Geosynthetic Clay Liners	Bernardo D., Domizi J., Fratalocchi E., Mazzieri F.
	Laboratory procedures for the modification of soluble and exchangeable cations of geosynthetic clay liners	Guarena N., Mazzieri F., Dominijanni A., Fratalocchi E., Manassero M.
SESSION 5 B- HYDRAULIC APPLICATIONS (1)	Issues of steep sideslope liners that remain exposed and are later covered	Thiel R.
	Performance of geosynthetics in methane oxidation systems	Di Battista V., Filion S., Cabral A.
	Gas capture and extraction using multi-linear drainage composite	Bannour H., Beaumier D., Fourmont S.
	Feedback on the long-term integrity of multi-linear drainage geocomposites installed on landfill final covers after 10 and 12 years of operation	Riot M., Ciuperca C., Saunier P., Fourmont S.
	Installation of geosynthetics at the Cerro do Lobo Tailings Storage Facility.	Barroso M., Manso J., Brito A., Marcelino J., Galrao R., Oliveira M.
	Raising waste storage facilities-design in line with the latest French recommendations	Faye C., Abdelouhab A.
SESSION 6 B- HYDRAULIC APPLICATIONS (2)	First innovative and sustainable GCL-application in Dutch flood defence at Beesel	Gerritsen R., Bardoel J.W., Dorst K., Meerkerk J.
	Benefits in cost and environment for channel revetment with geocells	Caressato Junior W., Fierro G.
	Central quay, Cardiff - regenerated concrete river bank	Bernardini P., Guerra-escobar P., Saeed R., Tahir M.
	Innovation in reservoir design with bituminous geomembranes (BGM)	Daly N., Doledec E., Aguirre T., Escobar E.
	Climate resistance of GCL-reinforced sealing systems based on lysimeter testing	Niehues C., Vollmert L.

TECHNICAL SESSIONS

TECHNICAL SESSION	TITLE	PAPER AUTHORS
SESSION 3 C- REINFORCEMENT APPLICATIONS (3)	Enhanced evaluation methodology for asphalt reinforcement: methodological updates and laboratory testing protocols	Sadeghian M., Vromans E., Auray G.
	Geogrids in road applications for mitigating reflective cracking: A case study from Portugal	Neves J., Caetano F., Beja C.
	Comparative analysis of thermal and mechanical degradation in glass fiber and PVA geocomposites in asphalt pavement	Castro Dos Santos P.J., Dos Anjos E Mello M., Alexandre Nunes de França F., Claudio Marques Silva Júnior F., Fernandes Amorim Ê.
	Evaluation of geotextiles' stiffening function using accelerated pavement testing	Sicha G.
	Instrumentation of geogrids using novel non-invasive electrical sensing	Sharp T., Mias C., Zamara K., Fowmes G.
SESSION 4 C- REINFORCEMENT APPLICATIONS (4)	Use of asphalt interlayer multiaxial geocomposite to enhance an asphalt overlay fatigue performance and bottom-up cracking prevention in motorway rehabilitation project	Golos M., Kornacka K., Kawalec J.
	Influence of different paving geosynthetics on crack growth phases and strain behaviour in asphalt overlays	Correia N.S., Bernardinelli A.L.C.S., Santos K.M., Shahkolahi A.
	Steel geogrids performance and environmental impact in asphalt reinforcement	Auray G., Mekkaoui A.
	Application of geosynthetics in linear concrete pavements improved by adding carbon nanotubes CNTs	Abdessemed M., Ouadah N.
SESSION 5 C- REINFORCEMENT APPLICATIONS (5)	Stabilisation and bearing capacity improvement of granular platform NANCEY A., ABOU CHAZ N., BRIANÇON L., VILLARD P., SILVANI C.	Nancey A., Abou Chaz N., Briançon L., Villard P., Silvani C.
	The role of mechanically stabilized base on the performance of top asphalt layer	Hornícek L., Rakowski Z., Kawalec J., Pospisil J.
	Research on geogrid stabilisation of paved and unpaved roads	Lugli G., Rimoldi P., Spadaro G., Trovato F.
	Case studies of use of multiaxial stabilisation geogrids in heavy duty pavements	Mazurowski P., Zamara K.
	Advanced multi-composite products for road stabilization: a comparative design and LCA analysis	Trovato F., Puthiya V. J., Lugli G., Rimoldi P.
	Refinement of the design method for geogrid stabilisation of railway ballast and subballast	Rimoldi P., Trovato F.

TECHNICAL SESSIONS

TECHNICAL SESSION	TITLE	PAPER AUTHORS
SESSION 6 C- REINFORCEMENT APPLICATIONS (6)	Design of geosynthetic-reinforced soil bridge abutment using river debris as backfill material	Lenart S., Karumanchi S. R.
	Design and construction of non-load bearing reinforced soil bridge abutments for high speed two to span over large diameter sleeve columns	Dalwadi M., Perdikou S., Doulala-rigby C., Kawalec J.
	History and performance of the first MSE walls reinforced with polymeric strips in Türkiye	Ozcelik H.
	Influence of different construction methods on full-height precast facing reinforced soil walls	Malekmohammadi K., Damians I.P.
	The stabilisation of a cut slope utilising percusion driven earth anchors	Harris E.
SESSION 7 B- TESTING AND QUALITY(5)	Comparing continuous filament and staple fibre geotextiles for geomembrane puncture protection	Albertyn M.
	Experimental investigation of a PVC geomembrane response to different tensile loading modes	Akel N., Josseaume L., Stoltz G., Wautier A., Touze N., Nicot F.
	Internal temperature change of various types of geomembranes subjected to tensile test	Tahir H., Stoltz G., Akel N., Veylon G., Peyras L.
	Effect of tensile load and temperature on bituminous geomembrane seams	Blond E., Giroud J.-P., Scheirs J.
	Performance testing of strained BGM welds	Kendall P., Llinas P., Hettihewahe M.
SESSION 7 C- REINFORCEMENT APPLICATIONS (7)	Oosterweel connection - optical fiber monitoring of a 17 meter high reinforced fill structure	Denies N., Van Breusegem M., Couck J., van der Ploeg J., Lauwers N., De Maesschalk S., Masola F., Ruigrok J.
	Geometric changes of reinforced soil walls: monitoring and impact on facing conditions during construction and using stage	Machowski M.
	Numerical study on the performance of reinforced fill structure using marginal fill	Khan A.R., Di Emidio G.
	Green vegetated reinforced soil wall with geogrid and site won materials for Raleigh park, Barnstaple, U.K.	Saeed R., Guerra-escobar P., Bernardini P., Tahir M.
	Slope protection using geosynthetic materials-a case study on the graveyard complex of mataram royal king	Nurjannah D.A., Anindita N.A., Harninto D.S., Badriza A.Subagja J.

TECHNICAL SESSIONS

TECHNICAL SESSION	TITLE	PAPER AUTHORS
SESSION 7 D- DESIGN AND MODELISATION (3)	Seismic performance of reinforced soil walls on the Big Almaty Ring Road in Kazakhstan	Kuznetsova A., Orlov E., Park S.
	Selection of intensity measures for displacement prediction of geosynthetic reinforced soil walls under seismic loading	Cengiz C., Kilic I.E., Guler E.
	Design method for combined geocell and geogrid stabilization of paved roads	Rimoldi P.
	Effects of density of geofoam cushion on seismic performance of the retaining wall: experimental study	Edinçliler A., Demirtas B.S.
SESSION FRANCOPHONE	Réhausse des installations de stockage des déchets (ISD) – conception selon les dernières recommandations françaises	Faye M.C., Abdelouhab A.
	Utilisation des géosynthétiques dans le cadre des travaux de « digues » du site pilote écrêteur de crue Seine-Bassée	Valenziano A., Laugier P.
	Amélioration des sols par inclusions rigides et apport des géosynthétiques	Hamidechi Boulmaali T., Tabti S.
	Techniques de renforcement par géosynthétiques d'un glissement de terrain	Khelifi M., Zermani M.
	Amélioration de la portance d'une plateforme par inclusion de nappes géosynthétiques	Cherifi F., Tabti S.

KEYNOTE LECTURES

A Safe and Sustainable by Design approach to geosynthetics development

Enrico Benetto*

[1] Environmental Sustainability Assessment and Circularity Unit, Luxembourg Institute of Science and Technology, 4662 Esch sur Alzette, Luxembourg

Abstract. The integration of safety and sustainability principles into geosynthetics design has become increasingly critical as global consumption patterns strain planetary boundaries. This paper examines the application of the European Commission's Safe and Sustainable by Design (SSbD) framework to geosynthetics development and procurement. The SSbD framework provides a five-step tiered approach encompassing scoping, safety assessment, sustainability assessment, trade-off analysis, and implementation with iterative improvement. Current geosynthetics face significant sustainability challenges including dependence on petroleum-based polymers, potential microplastic release, complex end-of-life management, chemical additive toxicity concerns, and substantial production-related environmental footprints. While Life Cycle Assessment applications in geotechnical engineering remain limited, emerging research demonstrates potential benefits from bio-based alternatives and improved assessment methodologies. The paper identifies key opportunities for SSbD integration including formal incorporation into ISO/TC 221 standards, alignment with Product Environmental Footprint Category Rules development, integration into engineering specifications and procurement policies, continued research investment in next-generation materials, and comprehensive training programs for designers and engineers. By systematically applying SSbD principles, the geosynthetics industry can continue providing essential infrastructure solutions while minimizing negative impacts on human health and environment, contributing to broader sustainability goals in construction and engineering sectors.

1 introduction

The integration of safety and sustainability principles into materials and product design has become increasingly critical in our resource-constrained world. As global consumption patterns continue to strain planetary boundaries, designers and engineers face the dual challenge of creating products that not only perform effectively but also minimize negative environmental impacts while ensuring human safety.

Contemporary materials science has evolved to embrace life cycle thinking, which examines environmental impacts throughout a product's entire existence—from raw material extraction through manufacturing, distribution, use, and end-of-life management (including

* Corresponding author: enrico.benetto@list.lu

reuse, recycling and cradle to cradle pathways). This approach recognizes that safety and sustainability considerations must be addressed at the earliest design stages rather than as afterthoughts.

Several significant regulations guide safety and sustainability in materials development. The European Union's Registration, Evaluation, Authorization and Restriction of Chemicals (REACH) regulation represents one of the most comprehensive frameworks governing chemical safety. This has fundamentally altered how materials are developed, forcing consideration of potential hazards from the earliest design stages. The EU's Ecodesign for Sustainable Products Regulation (ESPR), which entered into force in July 2024, aims to significantly improve the sustainability of products placed on the EU market by improving their circularity, energy performance, recyclability and durability [1].

Life Cycle Assessment (LCA) has emerged since late 1990s as the gold standard for quantifying environmental impacts. The Life Cycle Initiative partnership of the United Nations Environment Programme (UNEP) and the Society for Environmental Toxicology and Chemistry (SETAC) has enhanced the role of life cycle-based approaches and thinking in several ways and eventually the ISO standardized the methodology (ISO 14040/14044). LCA allows designers to identify "hotspots" where environmental impacts are concentrated, enabling targeted improvements [2]. Life Cycle Sustainability assessment (LCSA) adds to the environment assessment pillar an economic one, through Life Cycle Costing (LCC) assessing cost implications and a social one, through Social Life Cycle Assessment (S-LCA) to examine social consequences [3].

Similarly, to address safety concerns, several approaches have been developed. Chemical Alternatives Assessment provides structured approaches to identifying safer substitute materials; digital tools including materials databases, predictive toxicology software, and computational modelling have revolutionized how designers evaluate material options, allowing for virtual testing before physical prototyping.

Despite progress, significant challenges remain. Material complexity continues to increase, with modern products often containing dozens of specialized materials, making comprehensive assessment difficult. Data gaps persist regarding long-term environmental fate and toxicity of many substances. The scientific imperative for incorporating safety and sustainability into materials design has never been clearer. As our understanding of planetary boundaries and human health impacts deepens, regulatory frameworks continue to evolve, providing both compliance requirements and innovation opportunities. By embracing scientific methodologies for impact assessment and alternative evaluation, designers can create materials and products that contribute to a more sustainable future while ensuring human safety.

2 Safe and Sustainable by Design framework

The Joint Research Centre (JRC) of the European Commission developed the Safe and Sustainable by Design (SSbD) framework to guide the development of chemicals, materials, products, and processes that prioritize both safety and sustainability throughout their lifecycle. This framework emerged as a response to increasing concerns about environmental impacts, resource depletion, and human health effects associated with conventional design approaches [4]. The SSbD approach aligns with the European Green Deal objectives and the Chemicals Strategy for Sustainability, aiming to minimize harmful impacts on human health and the environment while maintaining competitiveness and innovation [5].

The SSbD framework integrates principles from green chemistry, circular economy [6], and lifecycle thinking [7] to create a comprehensive approach that considers safety hazards alongside broader sustainability aspects. By embedding these considerations from the earliest stages of design, the framework aims to prevent harmful impacts rather than mitigating them after products are already in use.

SSbD is a tiered approach involving five sequential steps: Scoping and Problem Definition, Safety Assessment, Sustainability Assessment, Trade-off Analysis and Decision-making and Implementation and Iteration.

Step 1: Scoping and Problem Definition. The process begins with clearly defining the product or material's intended function and performance requirements. This phase establishes system boundaries, identifies stakeholders, and determines which lifecycle stages will be assessed. [8]

Step 2: Safety Assessment. This step involves identifying and characterizing potential hazards, conducting exposure assessments, and characterizing risks. The assessment considers both intrinsic properties of materials and their behaviour across the lifecycle [9]. The JRC recommends a tiered approach to hazard assessment, prioritizing endpoints based on their severity and relevance to the application context. The safety component of SSbD extends beyond conventional risk assessment to consider potential hazards throughout a product's lifecycle. This includes hazard identification for human health (including workers, consumers, and the public); environmental hazards assessment (impacts on ecosystems and biodiversity); exposure assessment across the value chain; consideration of vulnerable populations and sensitive environments; evaluation of both short-term and long-term effects. The methodology builds on established regulatory frameworks (such as REACH) in the EU while expanding their scope to integrate with sustainability concerns.

Step 3: Sustainability Assessment. Multiple sustainability dimensions are assessed using standardized indicators and methodologies: resource efficiency and circular design; climate impacts and energy requirements; water and land use considerations; social aspects including fair labour practices and community impacts; economic viability and value creation and biodiversity protection. The framework emphasizes the importance of using consistent, science-based metrics to enable comparability across different design options. In the common practice, this step typically includes LCA, S-LCA [10], and economic considerations, relying on standardized methodologies such as the Product Environmental Footprint (PEF[†]) and building upon UN Sustainable Development Goals[‡]. In its more advanced implementations, it suggests using absolute sustainability metrics which, in contrast to relative ones (like LCA), compare environmental impacts to "carrying capacity as a reference" to determine if products operate within sustainable levels [11].

Step 4: Trade-off Analysis and Decision-Making. The JRC framework emphasizes that safety and sustainability must be considered holistically rather than as separate aspects [3]. The integration helps identify potential trade-offs and synergies between different objectives, enabling more informed design decisions and leading to more comprehensive solutions compared to siloed assessments. This critical phase examines potential conflicts between safety and sustainability objectives and identifies optimal solutions that balance multiple criteria. Multi-criteria decision analysis (MCDA) tools are often employed to facilitate transparent decision-making that incorporates stakeholder priorities [12] [13].

Step 5: Implementation and Iteration. The framework promotes continuous improvement through feedback loops and refinement of designs based on new data or evolving priorities [3]. This adaptive approach recognizes that sustainability is a moving target requiring ongoing reassessment.

[†] https://eplca.jrc.ec.europa.eu/EnvironmentalFootprint.html
[‡] https://sdgs.un.org/goals

3 How to apply Safe and Sustainable by Design to Geosynthetics Design?

In this chapter we will examine the specificities of geosynthetics over their lifecycle and how the SSbD framework could be applied to enhance their design, development and implementation. Focus will be on the environmental sustainability dimension. Safety and economic considerations will be treated in a more preliminary manner.

3.1 Geosynthetics: Function and Current Challenges

Geosynthetics are engineered materials used in civil engineering, environmental protection, and construction applications to enhance soil properties, control erosion, provide filtration, and manage drainage. While their use has revolutionized many construction practices and provided technological solutions for numerous environmental challenges, there are significant sustainability concerns associated with their lifecycle, which could be summarized as follows:

- They are predominantly manufactured from petroleum-based polymers. [14]
- They involve a significant potential for microplastic release into environments. [15]
- End-of-life management presents several issues. [16]
- Chemical additives to geosynthetics may pose toxicity concerns. [17]
- Environmental Footprint associated with their production is significant and may vary substantially depending on several factors. [18]

3.1.1 Use of Petroleum-Based Polymers

Most conventional geosynthetics are designed to contribute to the long-term stability of the soil structure, requiring materials with little change in long-term performance. While this durability provides functional benefits, it relies heavily on non-renewable resources. Indeed, a fundamental sustainability challenge for geosynthetics stems from their primary composition of petroleum-derived polymers. This dependence on fossil resources creates multiple environmental concerns throughout their lifecycle.

Life Cycle Assessments reveal that environmental impacts of the geosynthetic production are dominated by the raw material provision and electricity consumption during manufacturing [14]. A very large portion of plastics used in geosynthetics are still synthesized from non-renewable sources, increasing dependence on fossil resources. Studies show that energy consumption in polymer production is a major environmental issue. This leads to significant carbon emissions, with plastic raw materials responsible for between 4% and 80% of the overall impacts in different environmental impact categories [18]. The "take-make-dispose" linear production model applied to these materials yields a plastic economy that is unsustainable from both resource economy and global health perspectives [19].

3.1.2 Potential for Microplastic Release into Environment

The durability that makes synthetic geotextiles valuable in engineering applications has another significant downside: their potential to contribute to microplastic pollution. As these materials degrade over their long service life, they can shed synthetic particles into soil and water systems, particularly when exposed to UV radiation, mechanical stress, or weathering processes. Microplastic pollution is identified as a key concern in the LCA of geosynthetics, leading to harmful effects on aquatic ecosystems, marine life and eventually human health through ingestion of microplastics and chemical exposure [15].

The challenge is naturally particularly acute in aquatic applications, where geotextiles may be directly exposed to water bodies, increasing the risk of microplastic migration into sensitive ecosystems. Coastal protection measures, riverbank stabilization, and drainage systems are all applications where microplastic shedding poses heightened environmental risks. However, [20] identifies critical gaps that remain in current knowledge and practice regarding the full environmental impacts of geotechnical materials, including aspects related to microplastic pollution. This highlights the need for further research and monitoring to fully understand and address this challenge.

3.1.3 End-of-Life Management Issues

The disposal or recycling of geotextiles at the end of their useful life represents another critical sustainability hotspot. As said, many synthetic geotextiles are not biodegradable and can contribute significantly to landfill waste, while even natural geotextiles may have different degradation rates and environmental impacts depending on treatment chemicals and processing methods.

End-of-life management is complicated by several factors. First, the long service life of many geosynthetics—often measured in decades—means that disposal concerns may be deferred but not eliminated. Second, when removal is eventually necessary, geotextiles are typically contaminated with soil, biological material, and potentially pollutants, making recycling technically challenging, economically costly, limiting the potential for closed-loop recycling systems and eventually creating a substantial barrier to circular economy.

Studies indicate that only less than 9% of the over 6.3 billion metric tons of plastic waste generated since the 1950s has been recycled [21]. This low recycling rate highlights the significant challenge of waste management for petroleum-based polymers used in geosynthetics. The disposal of petroleum-based geosynthetics creates long-term environmental liabilities, as these materials are not biodegradable and can persist in the environment for hundreds of years, raising concerns about landfill space and environmental contamination. A contributing factor to these challenges is the material composition of many geotextiles. They often contain additives, coatings, and mixed polymer types that complicate separation and recycling processes. The durability that makes geotextiles valuable during their service life becomes problematic at end-of-life.

3.1.4 Chemical Additives Posing Toxicity Concerns

Chemical additives enhancing performance characteristics such as UV resistance, durability, and flexibility can pose additional concerns with regard to their toxicity when they leach into the surrounding environment during the product's lifecycle. The potential for chemical leaching is particularly concerning in water management applications, where geotextiles come into direct contact with groundwater or surface water. The toxicity concern extends beyond the use phase to disposal, where chemicals may be released as materials degrade in landfills or other disposal environments. This creates another long-term environmental liability that extends well beyond the service life of the product. [20] identifies gaps in current assessment methods, noting that currently reported environmental indicators may not effectively or fully capture important environmental impacts and trade-offs associated with geotechnical systems. This suggests that chemical toxicity concerns may be underrepresented in current sustainability assessments of geotextiles.

3.1.5 Environmental Footprint Associated with Production

Overall, the production of synthetic geotextiles is resource-intensive, requiring significant amounts of energy and water, which can lead to depletion of resources and

increased environmental stress. Indeed, the environmental impacts of manufacturing processes for geotextiles span multiple environmental categories and occur across various production stages.

Life Cycle Assessment (LCA) studies identify several impact categories for evaluating the environmental performance of geosynthetics, including cumulative energy demand (CED), global warming potential (GWP), eutrophication, photochemical ozone formation, particulate formation, acidification, land competition, and water consumption impacts [22]. The assessment of these categories reveals the comprehensive environmental footprint of geosynthetic production. For example, the global warming potential associated to the lifecycle of geosynthetics as filter layer for four different uses (road, landfill, slope retention), equals to 0.81 kg CO_2-eq/m^2 [18].

Transportation impacts are repeatedly highlighted as important contributors. [23] found that the transportation phase is the main contributor to almost every environmental impact category in their life cycle assessment of palm-fibre geotextiles.

Energy consumption during manufacturing represents another major impact area as noted by [18]: environmental impacts of the geosynthetic production are dominated by the raw material provision (plastic granulate) and electricity consumption during manufacturing.

Eutrophication is another significant environmental impact category associated with geosynthetic materials. Studies indicate that petroleum-based polymers contribute to eutrophication, which leads to excessive algae growth in water bodies [20]. This can have substantial negative effects on aquatic ecosystems.

Water consumption is a significant environmental concern as well. Even natural alternatives may present challenges in this regard, with [23] noting that palm-fibre geotextile's water consumption exceeds that recorded for synthetic geotextiles.

3.2 Safety Assessment of Geosynthetics

Safety assessment focuses on human health and environment.

Regarding human health safety, main assessment concerns are worker exposure during manufacturing and installation, potential leaching of additives (plasticizers, UV stabilizers, flame retardants) [24], dust generation during installation and maintenance and end-of-life exposure scenarios.

Regarding environmental safety, main assessment concerns are ecotoxicity of polymer degradation products [15], persistence in the environment and bioaccumulation potential, physical entrapment risks for wildlife and soil ecosystem impacts [25]. Research demonstrated that weathered geosynthetics can release microplastics and leachates that affect soils, potentially disrupting key ecosystem services.

3.3 Sustainability Assessment of Geosynthetics

3.3.1 Environmental Sustainability

As [20] notes, Life Cycle assessment (LCA) has only had limited application in the geotechnical engineering discipline, though it has been widely applied to civil engineering systems such as pavements and roadways. This limited adoption creates fundamental challenges in developing consistent methodologies. Furthermore, the few comprehensive applications of Life Cycle Assessment (LCA) to geotextiles faced numerous challenges in both data collection and impact assessment methodologies. Remarkable assessment challenges were related to high variability in material selection and manufacturing processes [18] and to the quantification of water usage during production and of land use impacts during resource extraction. Comparative LCA studies found that while geosynthetics often reduce

overall environmental impacts compared to traditional construction materials, their production phase remains significant and requires a careful assessment. However, comparative assessments mostly showed that geosynthetics can offer environmental advantages over traditional construction materials [26], e.g. using geosynthetics results in less masses that must be excavated, transported and installed compared to traditional methods. [18] quantified this benefit, finding that the cumulative greenhouse gas emissions amount to 7.8 kg CO_2-eq (mineral filter) and to 0.81 kg CO_2-eq (geosynthetic filter), showing a significant reduction in climate impact when using geosynthetic alternatives.

Main innovations in geotextile designs to address the several challenges highlighted in §3.1, that were assessed using a LCA approach, involve the use of more sustainable material sources, transitioning away from petroleum dependence while maintaining necessary performance characteristics. As an example, [23] demonstrates that palm-fibre-based geotextile presented the lower impacts in all the categories, except for eutrophication and ozone layer depletion potentials, its carbon footprint is relatively low and can save an average of 0.84 Kg CO_2 eq. per surface unit (1 m^2). Researchers note that palm-fibre geotextile can compete with the synthetic ones used in soil erosion, it is designed from renewable resource, naturally biodegradable, requires little energy for its production, and contribute to the reduction of greenhouse gas emissions. Such natural alternatives eliminate the microplastic concern while potentially offering comparable performance for certain applications.

Water consumption presents a complex trade-off in geotextile material selection. While palm-fibre geotextiles show advantages in most impact categories, [23] found that their water consumption exceeds that recorded for synthetic geotextiles. This indicates that natural alternatives may have environmental advantages in some categories but disadvantages in others.

Overall, main challenges in the implementation of sustainability assessment arise from material variability which complicates inventory development, i.e. significant diversity in geotextile characteristics, including variations in size and shape of textile fibre and variations in type of polymer. Standardization concerns persist, the absence of uniform standards remains a critical issue. [20] recommends that further research is needed to develop guidelines for life-cycle assessments tailored to geotechnical systems to establish common criteria and methods for future studies.

In conclusion, LCA of geotextiles reveals complex trade-offs between different environmental impact categories and materials. While methodological challenges persist in data collection and impact assessment, emerging research points to potential sustainability benefits from alternative materials and improved assessment approaches.

3.3.2 Social Sustainability

Main issues of concern related to social sustainability are worker conditions throughout the supply chain, community impacts near manufacturing facilities, benefits to local communities through improved infrastructure and accessibility and equity considerations, particularly in developing regions.

The production and application of geotextiles, particularly natural alternatives, can offers socio-economic benefits. Bio-based geotextiles could improve socio-economic foundations for sustainable development, with potential benefits for developing countries potentially including poverty alleviation, engagement of disadvantaged groups as stakeholders, employment opportunities, small and medium enterprise (SME) development, environmental education, and local community involvement in reclamation and environmental improvement programs. These benefits are achieved through promotion of sustainable and environmentally-friendly agriculture to discourage deforestation and promote reforestation and agroforestry. Field and laboratory studies suggest geotextile mats constructed from palm leaves are an effective, sustainable, and economically viable soil conservation technique. The

development of palm geotextiles also contributes to the stabilization of rural populations, thus decreasing migration to urban areas [27].

Community engagement is essential for sustainable outcomes in geotextile production and civil engineering applications. Rather than taking the lead on projects, companies can adopt multi-stakeholder processes to involve local communities, enabling targeted local economic development plans for operational areas.

3.3.3 Economic Sustainability

Main economic aspects related to geotextiles are lifecycle cost assessment including installation, maintenance, and replacement, value creation and distribution across the supply chain, market potential for innovative designs and long-term economic viability. While sustainable geosynthetics may have higher upfront costs, they often deliver better lifecycle value through extended service life and reduced maintenance requirements.

Life Cycle Costing represents a comprehensive evaluation method that analyzes the total costs associated with geotextile products throughout their entire lifecycle, including installation, maintenance, and replacement. These assessments are realized by the reduction of several thousand cubic meters of granular base course and decreased excavation costs. In pavement structures, geogrids are generally cost competitive against the granular material they replace, either through lower initial cost or through extended service life of the pavement structure.

The ability to perform whole-life economic analysis associated with long-term infrastructure assets is important to long-term sustainability. By comparing the present value of initial construction and future preservation costs across different structures and technologies, an accurate assessment of construction and design options is achievable.

3.4 Examples of geosynthetics designs benefitting from Safe and Sustainable by Design approaches

As the SSbD framework and approach is relatively recent, comprehensive applications to new geosynthetic designs are lacking. However, several examples of previous developments could be revisited through the lens of SSbD.

The development of partially or fully bio-based alternatives to fossil-based polymers, using natural fibres (jute, coir, hemp) and hybrid materials combining conventional and bio-based components is a seminal example. These materials could address sustainability concerns while maintaining necessary performance characteristics for specific applications. [28] demonstrated that jute-PLA composite geotextiles provided comparable short-term reinforcement to conventional polyester materials while offering improved end-of-life scenarios.

Geotextile designs have evolved to address toxicity and safety concerns throughout their lifecycle. Various approaches have been developed to create more environmentally friendly and less hazardous materials while maintaining or improving performance characteristics. SSbD could led to elimination of hazardous additives, development of alternative UV stabilizers with improved safety profiles. Utilizing water-based rather than solvent-based coatings for geotextiles can significantly reduce the release of volatile organic compounds (VOCs) and other hazardous substances during production and use. This approach improves both worker safety and environmental impact.

Advanced designs could incorporate recyclability considerations in polymer selection and mono-material designs that facilitate recycling, Material and polymer chemistry innovation involves research and development of new materials that are both high-performance and recyclable. Sustainable geotextile innovations could include design approaches that incorporate biodegradable materials, modular systems, and recycled inputs

to enhance environmental sustainability. Manufacture of recycled geotextiles may be a good opportunity to boost the use of textile and plastic waste as raw materials.

Sustainable sourcing would focus on obtaining raw materials from suppliers who prioritize environmental responsibility and recyclability in their production processes, enhancing the overall sustainability of geotextile products. Standardization of materials advocates for consistency in materials used across geotextile products to simplify recycling processes, making it easier to develop recycling protocols and facilities. Recycled geotextiles may be suitable to carry out the functions usually assigned to agro-textiles, which can be applied in agriculture, horticulture or gardening.

SSbD-optimized geosynthetics would also include biodegradable options for temporary applications, retrievable designs for permanent installations and consideration of degradation pathways and breakdown products. A framework should provide guidance on incorporating end-of-life considerations into geosynthetic selection, focusing on both technical and environmental factors. Biodegradable geotextiles represent indeed an environmentally conscious alternative to conventional synthetic geosynthetics, particularly for temporary applications where long-term durability is not required. These materials are designed to decompose over time, providing necessary functionality during their service period before breaking down naturally in the soil. For example, biodegradable turf reinforcement mats are used to stabilize grassed areas, prevent erosion and provide temporary support for vegetation, decomposing after the grass is established. Similarly, biodegradable silt fences are temporary barriers made from biodegradable materials used to control sediment runoff during construction, providing necessary protection while being designed to decompose after project completion.

4 Possible future directions for SSbD of geosynthetics

The integration of Safe and Sustainable by Design (SSbD) principles into geosynthetics design, engineering specifications and procurement policies is in its early developmental stages. While the EU SSbD framework provides a solid foundation for chemicals and materials assessment, specific application to geosynthetics procurement remains limited. Its application to geosynthetics represents an important shift toward more responsible material development in geotechnical engineering. Moving forward, several priorities emerge.

First, more formal integration of SSbD assessment methodologies in the development of standards on geosynthetics, for example within the ISO/TC 221 and the ongoing development of the ISO/TR 18228 series. This could build on i) current advances, which acknowledge that geosynthetics contribute to sustainable construction practices by minimizing environmental impact and reducing the need for traditional construction materials; ii) further alignment to Sustainable Development Goals, recognizing that SSbD driven geosynthetic development may provide alternatives to unsustainable traditional construction methods.

Second, explore the opportunity to align the integration of SSbD consideration in standardisation with the development of Product Environmental Footprint Category Rules (PEFCR). The Product Environmental Footprint (PEF) is a LCA-based measure of the environmental performance of a good or service throughout its life cycle, developed by the European Commission to measure and communicate potential life cycle environmental impacts of products [29]. PEFCRs provide specific guidelines for individual product categories and are developed to improve reproducibility, comparability, and verifiability of results for specific product groups. Since EN 15804+A2 has been aligned with PEF methodology and covers construction products generally, geosynthetics could potentially be assessed within this broader framework. The geosynthetics industry, through organizations like ISO/TC 221 or industry associations, could proactively develop a PEFCR for geosynthetics products. This would provide standardized environmental assessment

methods, enable comparisons between different geosynthetic products, support substantiated environmental claims and contribute to preparing the industry for potential future regulatory requirements.

Third, integrate SSbD principles into engineering specifications and procurement policies. Engineering specifications should require hazard profiles of polymer components, worker safety documentation during manufacturing and installation, environmental exposure evaluations throughout service life, and comprehensive end-of-life management protocols. Performance specifications should also consider Environmental Product Declarations aligned with SSbD principles. Procurement frameworks should establish pre-qualification criteria evaluating supplier SSbD implementation capabilities and environmental management certifications. Contract requirements should mandate continuous SSbD assessment reporting, establish sustainability improvement commitments, and require supply chain transparency for materials traceability.

Fourth, EU should continue investing in research for next-generation materials that optimize both safety and sustainability of geosynthetics. Research investment should focus on multi-functional geosynthetic materials integrating performance criteria with SSbD compliance, novel manufacturing processes using green chemistry approaches, greater integration of artificial intelligence for predicting material performance and impacts, expanded use of bio-based and circular materials, and more sophisticated methods for evaluating complex material mixtures. Successful funding applications require multidisciplinary consortiums encompassing materials science institutes, industry partners, SSbD specialists, and regulatory expertise, emphasizing contribution to EU Green Deal objectives and circular economy principles.

Finally, training and education for designers and engineers on Safe and Sustainable by Design implementation in geosynthetics requires a comprehensive approach that integrates technical competencies with lifecycle thinking and regulatory awareness. Professional development programs should encompass the four-step SSbD assessment framework including hazard evaluation of polymer components, occupational safety during manufacturing and installation, environmental exposure assessment during service life, and comprehensive lifecycle impact analysis aligned with PEF methodologies. Training modules must address practical implementation challenges including data availability and quality requirements, scaling laboratory findings to industrial applications, and integrating functionality requirements with sustainability metrics throughout the design process.

By systematically applying SSbD principles, the geosynthetics industry can continue to provide essential infrastructure solutions while minimizing negative impacts on human health and the environment, contributing to broader sustainability goals in the construction and engineering sectors [30].

References

1. European Commission. (2024). *Ecodesign for Sustainable Products Regulation*. Retrieved from https://commission.europa.eu/energy-climate-change-environment/standards-tools-and-labels/products-labelling-rules-and-requirements/ecodesign-sustainable-products-regulation_en
2. Hellweg, S., Benetto, E., Huijbregts, M.A.J., Veriones F., Wood R. (2023). Life-cycle assessment to guide solutions for the triple planetary crisis. *Nat Rev Earth Environ* 4, 471–486. https://doi.org/10.1038/s43017-023-00449-2
3. Ciroth, A., Finkbeiner, M., Traverso, M., Hildenbrand, J., Kloepffer, W., Mazijn, B., ... & Vickery-Niederman, G. (2011). *Towards a life cycle sustainability assessment: making informed choices on products*. UNEP Life Cycle Initiative. https://www.lifecycleinitiative.org/wp-content/uploads/2012/12/2011%20-%20Towards%20LCSA.pdf

4. Caldeira, C., Farcal, R., Garmendia Aguirre, I., Mathieux, F., & Tecchio, P. (2022). *Safe and Sustainable by Design chemicals and materials - Review of safety and sustainability dimensions, aspects, methods, indicators, and tools*. EUR 30991 EN, Publications Office of the European Union, Luxembourg, JRC127109.
5. European Commission. (2020). *Chemicals Strategy for Sustainability: Towards a Toxic-Free Environment*. COM(2020) 667 final.
6. Ellen MacArthur Foundation. (2019). *Completing the Picture: How the Circular Economy Tackles Climate Change*. https://circulareconomy.europa.eu/platform/sites/default/files/emf_completing_the_picture.pdf
7. JRC. (2010). Making sustainable consumption and production a reality. A Guide for business and policy makers to Life Cacle Thinking and Assessment. https://eplca.jrc.ec.europa.eu/uploads/LCT-Making-sustainable-consumption-and-production-a-reality-A-guide-for-business-and-policy-makers-to-Life-Cycle-Thinking-and-Assessment.pdf
8. European Commission, Joint Research Centre, Abbate, E., Garmendia Aguirre, I., Bracalente, G.,cMancini, L., Tosches, D., Rasmussen, K., Bennett, M.J., Rauscher, H. and Sala, S., Safe and Sustainable by Design chemicalscand materials - Methodological Guidance, Publications Office of the European Union, Luxembourg, 2024, https://data.europa.eu/doi/10.2760/28450, JRC138035.
9. Apel, C., Kümmerer, K., Sudheshwar, A., Nowack, B., Som, C., Colin, C., Walter, L., Breukelaar, J., Meeus, M., Ildefonso, B., Petrovykh, D., Elyahmadi, C., Huttunen-Saarivirta, E., Dierckx, A., Devic, A. C., Valsami-Jones, E., Brennan, M., Rocca, C., Scheper, J., Strömberg, E., & Soeteman-Hernández, L. G. (2024). Safe-and-sustainable-by-design: State of the art approaches and lessons learned from value chain perspectives. *Current Opinion in Green and Sustainable Chemistry*, *45*, 100876. https://doi.org/10.1016/j.cogsc.2023.100876
10. Benoît, C., & Mazijn, B. (Eds.). (2009). *Guidelines for Social Life Cycle Assessment of Products: Social and socio-economic LCA guidelines complementing environmental LCA and Life Cycle Costing, contributing to the full assessment of goods and services within the context of sustainable development*. United Nations Environment Programme. https://wedocs.unep.org/bitstream/handle/20.500.11822/7912/-Guidelines%20for%20Social%20Life%20Cycle%20Assessment%20of%20Products-20094102.pdf?sequence=3&amp%3BisAllowed=
11. Rockström, J., Steffen, W., Noone, K., Persson, Å., Chapin, F. S., III, Lambin, E., Lenton, T. M., Scheffer, M., Folke, C., Schellnhuber, H. J., Nykvist, B., de Wit, C. A., Hughes, T., van der Leeuw, S., Rodhe, H., Sörlin, S., Snyder, P. K., Costanza, R., Svedin, U., Falkenmark, M., Karlberg, L., Corell, R. W., Fabry, V. J., Hansen, J., Walker, B., Liverman, D., Richardson, K., Crutzen, P., & Foley, J. (2009). Planetary boundaries: Exploring the safe operating space for humanity. *Ecology and Society*, 14(2), 32. http://www.ecologyandsociety.org/vol14/iss2/art32/
12. Benetto E., Dujet C., Rousseaux P. (2008). Integrating fuzzy multicriteria approach with uncertainty analysis for Life Cycle Assessment. *Environmental Software and Modelling*, 23 (12), 1461-1467.
13. Dias, L. C., Caldeira, C., & Sala, S. (2024). Multiple criteria decision analysis to support the design of safe and sustainable chemicals and materials. *Science of the Total Environment*, 916, 169599.
14. Cislaghi, A., Sala, P., Borgonovo, G., Gandolfi, C., & Bischetti, G. B. (2021). Towards more sustainable materials for geo-environmental engineering: The case of geogrids. *Sustainability*, 13, 2585.

15. Monkul, M. M., & Özhan, H. O. (2021). Microplastic contamination in soils: A review from geotechnical engineering view. *Polymers*, 13(23), 4129.
16. Damians, I. P., Bathurst, R. J., Adroguer E.g., Josa, A., & Lloret, A. (2017). Environmental assessment of earth retaining wall structures. *Environmental Geosynthetics*, 4(6), 415-431.
17. Teuten, E. L., Saquing, J. M., Knappe, D. R., Barlaz, M. A., Jonsson, S., Björn, A., Rowland, S. J., Thompson, R. C., Galloway, T. S., & Yamashita, R. (2009). Transport and release of chemicals from plastics to the environment and to wildlife. *Philosophical Transactions of the Royal Society B: Biological Sciences*, 364(1526), 2027-2045.
18. Stucki, M., Büsser, S., Itten, R., Frischknecht, R., & Wallbaum, H. (2011). Comparative life cycle assessment of geosynthetics versus conventional construction materials. *ESU-services Ltd. commissioned by European Association for Geosynthetic Manufacturers (EAGM), Uster and Zürich, CH*.
19. Fagnani, D. E., Jehanno, C., Sardon, H., & McNeil, A. J. (2022). Sustainable green polymerizations and end-of-life treatment of polymers. *Macromolecular Rapid Communications*, 43(13), 2200446.
20. Raymond, A. J., Tipton J.R., Kendall A., Dejong J. (2019). Review of impact categories and environmental indicators for life cycle assessment of geotechnical systems. *Journal of Industrial Ecology*, 24(3), 485-499.
21. Geyer R, Jambeck J. R., Law K. L. (2017). Production, use, and fate of all plastics ever made. *Sci. Adv*. 3, e1700782.
22. Frischknecht, R., Stucki, M., Büsser, S., Itten, R., & Wallbaum, H. (2012). Comparative life cycle assessment of geosynthetics versus conventional construction materials. *Ground Engineering*, *45*(10), 24-28.
23. Laasri, L., & Naim, H. (2022). Evaluation of Environmental Impact of Palm-Fiber Based Geotextile Using a Life Cycle Method. *Key Engineering Materials*, 925, 9–16.
24. Lithner, D., Larsson, Å., & Dave, G. (2011). Environmental and health hazard ranking and assessment of plastic polymers based on chemical composition. *Science of the Total Environment*, 409(18), 3309-3324.
25. Gewert, B., Plassmann, M. M., & MacLeod, M. (2015). Pathways for degradation of plastic polymers floating in the marine environment. *Environmental Science: Processes & Impacts*, 17(9), 1513-1521.
26. Heerten, G. (2012). Reduction of climate-damaging gases in geotechnical engineering practice using geosynthetics. *Geotextiles and Geomembranes.* 30, 43-49.
27. Fullen, M. A., Booth, C. A., et al. (2007). Contributions of biogeotextiles to sustainable development and soil conservation in developing countries: the BORASSUS Project. *WIT Transactions on Ecology and the Environment*, 106, 123-141.
28. Prambauer, M., Wendeler, C., Weitzenböck, J., & Burgstaller, C. (2019). Biodegradable geotextiles – An overview of existing and potential materials. *Geotextiles and Geomembranes*, 47, 48-59.
29. Zampori, L., & Pant, R. (2019). *Suggestions for updating the Product Environmental Footprint (PEF) method*. EUR 29682 EN, Publications Office of the European Union, Luxembourg, JRC115959.
30. European Commission. (2023). *Safe and Sustainable by Design Framework for the Assessment of Safety and Sustainability of Chemicals and Materials*. Publications Office of the European Union.

Geosynthetics in the Northern countries: geotechnical and environmental challenges

Arnstein Watn [1,2*] and *Inge Hoff*[2]

[1]WatnConsult AS, Trondheim, Norway
[2] Norwegian University of Science and Technology, Trondheim, Norway

Abstract. Nordic countries have challenging conditions both related to Nordic countries commonly have challenging conditions with soft subsoil and changing climate. The introduction of geosynthetics around 1970 provided a good possibility for providing environmentally friendly structural solutions that were beneficial technically and economically. A system for classification of geosynthetics for separation and filtration was proposed by the Norwegian Directorate of Roads in 1978. This has been the basis for NorGeoSpec, a common system for certification of geosynthetics operating for more than 20 years covering Estonia, Finland, Sweden, and Norway. A guideline for design and construction of reinforced soil structures was developed as a co-operation between the Nordic geotechnical societies in 2000. Geosynthetics have been used for large number of construction projects. Special structural solutions include vegetated steep slopes with peat block front for frost insulation and a combination of geosynthetic reinforcement and lightweight clay aggregate to provide light wight structural solutions with frost insulation. A number of research projects have been carried out to develop structural solutions and construction methods for Nordic conditions. The projects include testing of geosynthetic for erosion control in Arctic conditions as far north as Svalbard. A project to investigate the possibility for installing geosynthetics under temperatures down to -25 was carried out in Kemi in Finland close to the Swedish border as a co-operation between the Nordic Traffic authorities, Universities, research institutes, and a group of producers.

1 Introduction

Nordic countries extending beyond the Arctic Circle have several common features relevant to the construction and maintenance of infrastructure and buildings. Population density is low, and the total length of the road network in relation to the population is considerably large.

Heavy transport, which extends to the lower-class road network, is of great importance to the economies of the Nordic countries. Transport needs are primarily related to the forestry industry, the fishing industry (Norway), industry, agriculture and livestock cover almost the entire road network in all three countries.

Buildings, structures, and other types of infrastructures have to be designed and built considering the need for resistance to freeze and thaw during seasonal variations. Climate change is adding additional challenges, with more intense precipitation increasing the frequency of landslides and flooding. Hence, design and construction must be more robust to cope with a changing climate. At the same time, there is a need for innovative solutions to reduce CO_2 emissions and environmental impact from construction and maintenance works.

* Corresponding author: arnstein.watn@watnconsult.no

Climatic conditions

Frost heaves caused by seasonal frost, the melting of snow and the thawing phase of frost in the spring is critical regarding the condition and durability of road structures. Figure 1 shows a road in Norway becoming unpassable during the spring thaw.



Fig. 1. Gravel road during spring thaw

Temperature fluctuations combined with precipitation and snow melting commonly lead to flooding, erosion, and water-triggered landslides which may pose threats to life and health and cause considerable damage.

Seasonal frost affects most of Finland, Sweden and Norway, but there is no permafrost in the Nordic countries, except for the Svalbard islands in Norway. During the coldest winters, the freezing index in inland Norway, northern Sweden, and northern Finland can exceed 60,000 Kh (2,500 Kdays), which corresponds to a frost penetration depth of more than two metres in typical subgrade conditions, and in open-graded blasted or crushed rock significantly deeper. In the coastal regions and in the very southern parts of the countries, however, the penetration depth of frost remains at a few tens of centimetres.

The variation in air temperature during the year in the inland area east of the Scandinavian mountains is considerable. The coldest temperatures in the northern regions of Finland and Sweden can be as low as - 40 degrees, while the highest summer temperatures in the same regions can reach +30 degrees. However, especially in coastal areas, the differences in temperature extremes are smaller.

The annual rainfall is highest in the mountainous area of the west coast of Norway, about 3,000 mm/year, while in the inland areas of Sweden and Finland, east of the Scandinavian mountain range, it is about 600 mm/year. Correspondingly, the thickness of snow cover varies both geographically and annually, but in Swedish and Finnish Lapland snow thicknesses of more than one meter are common. In the mountainous areas of Norway and Sweden, there can be snow in places more than two meters thick.

1.1 Traffic situation

To reduce the climate impact of transport the maximum permissible weights of heavy vehicles have increased significantly. In Finland, trucks with a total weight of 76 tons are allowed to operate on the entire public road network, unless temporary weight restrictions impose other limits. With special permits on certain routes important for heavy transport,

super-heavy trucks weighing up to one hundred tons (eventually up to 400-500 tons with special permits) are currently possible in Finland. The same tendency is seen also in the other Nordic countries.

In Norway an R&D-project "Bedre utnyttelse av bæreevnen" (Better utilization of the bearing capacity) led to the axle-load restrictions in the thaw period being partly cancelled, as these restrictions imposed increased costs for truck transport.

1.2 Topography and soil conditions

The highest points in the Nordic countries, almost 2,500 meters above sea level, are located in Norway in the region of Jotunheimen. On the Finnish and Swedish sides, however, the mountains have been lowered and become more gentle fells due to the wear and tear caused by the ice ages. The geological formations formed during the melting phase of the latest glaciation period, which ended about 10,000 years ago, are otherwise characteristic for the Nordic topography and soil conditions.

Typical features include:

The soil cover above the bedrock surface is typically fairly thin (usually only a few metres and at most only a few tens of metres). In many places, the bedrock surface is visibly bare and completely without soil cover.

Especially in areas further away from the coastal areas, the very mixed-grained moraine is the most common soil type. The moraine is typically tightly packed and practically always consists of frost-susceptible material.

Fine-grained clay and silt are the most common soil types in coastal areas, that especially in Sweden and Finland are generally fairly flat.

The highest population and road network densities are also concentrated on these fine-grained marine deposits that are characterized by both low shear strength and very high compressibility.

The marine clays may, if the salty porewater is washed out and replaced by fresh water, become quick-clay, which will collapse and behave like a fluid if disturbed. This may lead to catastrophic landslides involving large areas and represents a considerable risk to life and damage, Figure 2.



Fig. 2. Quick-clay landslide in Småröd, Munkedal, Sweden, 2006 (Photo SGI)

In many areas, the top layer of soil is peat, which consists entirely of organic material and is even more problematic than fine-grained clays and silts, because the settlements in peat are

not only large but could continue to develop for a long time. Construction works in peat areas may impose significant challenges related to stability and deformations. Figure 3.



Fig. 3. Road construction on peat in Lofoten, Norway and in swampy area Kemi, Finland

Until recently, peatlands were considered only a technical challenge, but the focus has now shifted towards preserving peat to avoid releasing the vast amounts of carbon stored in the organic material.

2 Geosynthetics – applications, design and specification

Soil improvement based on vegetation (trees, bushes, weeds) has been used in the Nordic countries for more than 1000 years. The introduction of geosynthetics around 1970 provided an opportunity for providing environmentally friendly structural solutions that were beneficial technically and economically. Initially, the main focus on the use of geosynthetics was focused on road construction. Given the combination of frost penetration and soft and frost susceptible soil all the Nordic countries are focusing on road structures which have sufficient bearing capacity and frost protection. This was traditionally solved by relatively thick road structures based on natural sand/gravel in combination with crushed rock. The introduction of geosynthetics introduced a possibility to be able to build on soft subsoil and to reduce time and costs for the construction.

2.1 The specification of geotextiles for separation in roads and other traffic areas

In the mid 70-ties the Norwegian Road Authorities (NPRA) in co-operation with the Norwegian University of Science and Technology (NTNU) were looking into how to establish a system for specification of geosynthetics for separation (between fine and coarse materials) in roads and other traffic structures. The proposal for a classification system for geosynthetics for separation and filtration in roads was published in the International Conference on Fabrics in Geotechnics in Paris in 1977 [1]. The classification system was based on a combination of required properties from two different test methods: the CBR-test and the Cone-drop test. Based on the results from the testing, the products would be classified into five different application classes. The selection of relevant application class was based on guidelines with input on subsoil (soft - firm), fill material (fine - coarse) and construction and installation conditions. The classification system was implemented in the national requirements in Norway, Sweden, and Finland [2].

Over time, the specifications were modified in the different Nordic countries related both to the requirements, the testing methods and the procedures. The requirements to be “fit for purpose” would differ between the countries. In addition, there was no system for quality control of the test results and no system for keeping track of the relevant status for a product. In principle, a product could have test results from different laboratories with different results

and resulting in different application classes [3]. The situation caused a lot of confusion for the end users related to requirements on specification requirements and product documentation.

The development of common European standards through CEN provided common rules both on the required properties for a specific function and application and for the testing equipment and procedures. In 1999 an internordic project was started to harmonise the requirements and prepare a new common system for specification and control. The requirements were based on the experiences with the old classification systems and results from performed research and development projects [4].

Experiences from the field and research projects have verified that the requirements for the mechanical properties are strongly related to the installation and construction phase. Full-scale experiments were carried out as a basis for evaluation of relevant properties and requirements for the survivability of geotextiles during installation and construction to ensure the function during the service lifetime, Figure 4.



Fig. 4. Installation of geosynthetics for testing of survivability

The results showed considerable differences in the susceptibility to damage during the installation and construction between different types of geotextiles. The requirements are based on the need for the geotextile after the installation to fulfil its function in the structure for a sufficient service lifetime. Both these aspects have to be taken into consideration for the preparation of the revised specification requirements.

2.2 NorGeoSpec 2002

The revised requirements, named NorGeoSpec 2002, were implemented into the national guidelines combined with a common system for product certification, NorGeoSpec. The system is run with an independent Notified Body, SINTEF, responsible for product sampling and administration of the certification procedure. The testing is carried out by a group of certified laboratories in France, Germany, and England. A Technical committee including the Traffic authorities in Estonia, Finland, Sweden and Norway is responsible for the revision of the guidelines and there is also an advisory board including representatives from European Association for Geosynthetic Manufacturers (EAGM) for technical discussions and recommendations for possible revisions of the system.

The system has later been extended and is now also covering geosynthetics for reinforcement. The NorGeoSpec system have now been in use for more than 20 years and is basis for the specification of geosynthetics in Estonia, Finland, Sweden and Norway.

2.3 Geosynthetics for soil reinforcement

The possibilities for using geosynthetics for soil reinforcement were early recognised as a way to deal with challenging soil conditions and harsh environments.

2.3.1 Reinforced soil wall full-scale test near Oslo, Norway

A research project was established in 1987 to study geosynthetics for reinforced steep slopes and walls. The project included the construction of a full-scale test wall in a gravel pit located 25 km north of Oslo /5/. The test wall was 20m long, 4,8m high and front inclination 2(v):1(h). 8 layers of geogrid with length 2,2m were placed with an equal vertical spacing of 0,6m and sand backfill. The test wall was loaded with a static surcharge loading for two months by using water filled tanks on top of the slope. Upon completion, instrumentation established a maximum tensile load per unit width T_{max}=1,4kN/m at the bottom of the slope and values 2,1< T_{max} <3,0 kN/m for the subsequent layers. Corresponding strain was measured in the range of 0,2<ε_{max}<0,8%. The mobilized tensile force and corresponding strain were relatively low but corresponded well with the geotechnical analyses. The results from the test were used as a basis for recommendations for design and construction of reinforced soil walls in the National regulations from the Norwegian Public Road Authorities /6/.

The structure is still existing and a program of field sampling of the geogrid reinforcement was conducted about 25 years after the initial construction in 2013 [7]. The durability assessment was based on visual inspection and a series of index and strength tests focusing on the identification of possible physical damage and/or degradation. Visual inspection and microscopic imaging revealed no installation damage of any significance. Rapid loading creep test data to 10.000h showed excellent agreement between incremental strain is specimens of the exhumed geogrid and typical values for the original product type. The assessment lends confidence in the use of isochronous load-strain-time data for predicting the long-term strain of geogrid reinforced structures for design practice.

2.4 Regulations and guidelines for reinforced soil structures

Regulations and guidelines for design and construction of reinforced soil structures in the Nordic countries were generally based on rules from other countries, mainly UK, Germany, and USA. In general, the theoretical background for the design regardless the background was based on limit equilibrium analyses, but functional requirements, design input and safety approach could vary from project to project dependent on the basis used. This commonly resulted in misunderstandings and discussions especially related to required properties and corresponding documentation for the reinforcement products. There were also examples where the lack of a common basis would lead to failures and inadequate design. A project in Åre in Sweden with reinforced backfill for a basement wall had major deformation and cracking due to improper design with too short reinforcement and ice and snow in the backfill [8].

The rehabilitation of the reinforced wall resulted in a considerable overdesign. First material factors were applied to the soil backfill properties according to national Swedish regulations and then the design was including an overall material factor according to UK regulations, Figure 5.



Fig. 5. Åre School, Sweden: Original design, failure mode, after excavation

In the common European work on developing common European Standards the Nordic countries established a co-operation, The Nordic Geosynthetic Group (NGG), to ensure that specific challenges for the regions were addressed in the Standardisation work. This was typically focusing on challenges related to climate (low temperature, freeze/thaw), soil conditions (soft and compressible subsoils) and backfill material (typically crushed angular rock).

Based on the experiences from this co-operation in the European Standardisation work it was agreed to prepare common Nordic guidelines for design and construction of reinforced soil structures. NGG initiated these guidelines and the project group was organised by the geotechnical societies in Denmark, Finland, Norway and Sweden with financial contribution from the traffic authorities in the Nordic countries and from the Nordic Industrial funding [9], Figure 6.

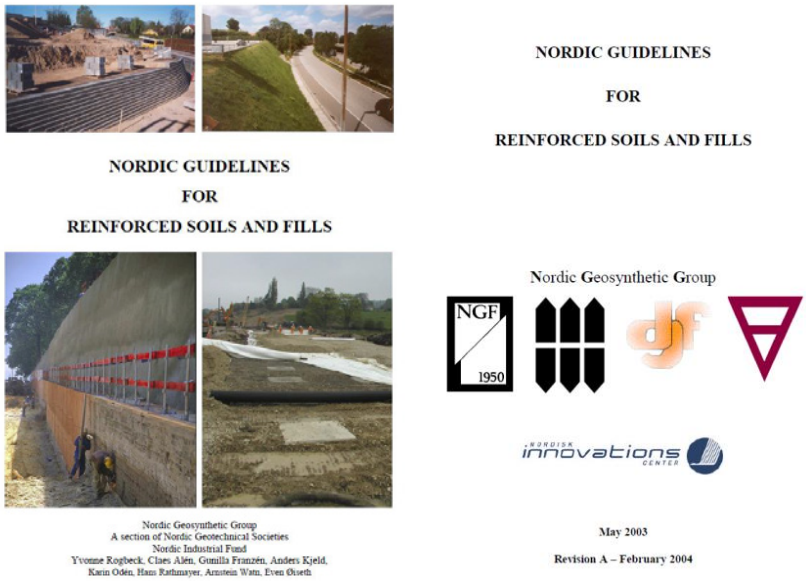


Fig. 6. Nordic guidelines for reinforced soil and fill [9]

The Nordic Guidelines for strengthened/reinforced soils and other fills are guidelines with recommendations for different applications. The guidelines are based on a limit state approach using partial factors of safety in the design. The base of the design is existing Eurocodes, ENV 1991-1 “Basis of Design and Actions of Structures” and ENV 1997-1“Geotechnical Design”. The guidelines covered four applications: Vertical walls and slopes, Embankment on soft soil, Embankment on improved soil and Soil-nailing (excavated vertical

wall and natural slope). The guidelines include general information on reinforcement properties and test method, functional requirements, guidelines for design, construction, monitoring and measurements and recommendations for procurement. The guidelines is a common reference used in the national regulations for reinforced soil in the Nordic countries.

2.5 Stabilisation and improved bearing capacity in roads and other traffic areas

2.5.1 Challenges and deterioration mechanism

As previously stated, all the Nordic countries are relatively sparsely populated and accordingly, there are relatively many km of roads and other traffic areas per capita. Large part of the road network has a relatively small traffic volume, but still the traffic may impose significant loading from heavy trucks from timber transport, fish farming etc. In addition, soft subsoil and freeze/thaw actions typically results in extensive road deterioration with rutting and cracking of the asphalt pavement, Figure 7.



Fig. 7. Cracking of asphalt pavement due to edge deformation and frost heave

Typically, the deterioration and need for upgrading and rehabilitation of small volume roads in the nordic countries are related to plastic deformations and not so much due to elastic deformations, Figure 8 and 9.

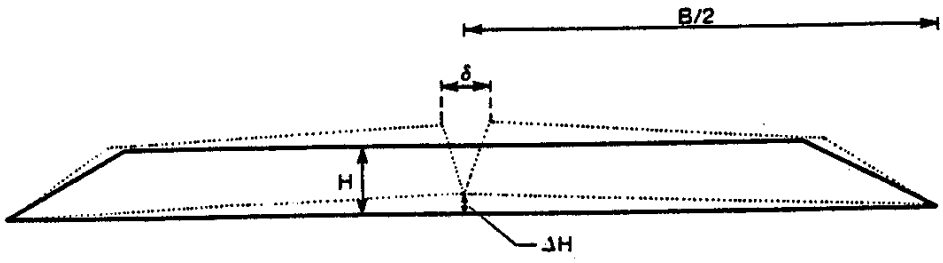


Fig. 8. Deformations and cracking of road structures due to frost heave

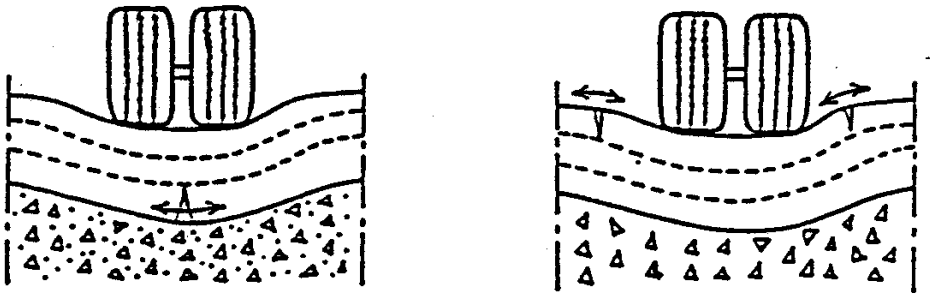


Fig. 9. Cracking of asphalt pavement due to plastic déformations from rutting

Geosynthetic reinforcement for stabilisation of roads in general has very little impact on the elastic stiffness of the road but may significantly improve the resistance against plastic déformations (rutting, edge déformations, frost heave). Basically the use of geosynthetics for improving bearing capacity and reduced déformations accordingly seem to be a very useful possibility.

2.5.2 Test road in Myre in Vesterålen, Norway

The Norwegian University of Science and Technology (NTNU) and SINTEF were initiating a research project in 1982 to look into the potential use of geosynthetic reinforcement for road construction on soft subsoil. The project included the construction of a full-scale test road on peat in Myre in Vesterålen, Norway, Figure 10.



Fig. 10. Installation of geogrid for road construction on peat in Myre, Vestrålen in Norway (1984). Foto SINTEF. [10]

A common problem in these areas is strengthening and paving of gravel roads on soft subsoil. In this case the old road was located in an area of peat subsoil with thicknesses up to

3m. The road had insufficient bearing capacity during the thawing period and was also subjected to extensive differential settlements. The strengthening of the road was done by using geogrid reinforcement directly on the old road and then placing a bearing layer with a thickness up to 1 m on top of the grid before the asphalt overlay was installed.

Measurements after the rehabilitation indicated that the reinforcement increased the bearing capacity of the subsoil and reduced differential settlements. The road has now been in use for more than 30 years since the rehabilitation was completed. Generally, the experience has been good but repaving due to cracking of the asphalt overlay has been carried out including geosynthetic reinforcement in the asphalt overlay [11].

2.5.3 Collecion of experience - the Cost Reipas project

In the COST Reipas project the existing knowledge on reinforcement in roads was mapped through a set of questionnaires amongst the experts in the participating countries [12], [13], [14]. These resulted in descriptions of the damage cases for which reinforcement products are relevant and in an overview of assessment methods and in addition in a review of previous and ongoing research on the subject of reinforcement of pavements.

The purposes of using reinforcement reported in the survey were:
-increase pavement fatigue life,
-minimize differential and total settlement,
-reduce rutting – surface and subgrade,
-prohibit or limit reflective cracking,
-increase resistance to cracking due to frost heave,
-reduce natural mineral usage,
-reduce maintenance costs,
-increase bearing capacity,
-enable bridging over voids,
-enable economic construction platforms.

Reinforcement in roads is to a large extent used is to reduce deterioration dependent on local conditions. Foundation, moisture, temperature and traffic conditions, types of granular materials, types of overlay, precipitation etc., all are influencing the structural solutions, the types of reinforcement to be used and what effects can be achieved. In the Nordic countries a major basis for the design of roads and other traffic areas is to prevent frost from penetrating into frost susceptible subsoil underneath the structure. Frost penetration may cause considerable frost heave during the winter and loss of bearing capacity when the frost is melting in the spring. Accordingly in general it is generally not recommended to reduce the aggregate thickness of the structure by using geosynthetics. The general recommendation is that geosynthtics for stabilisation of traffic areas can be used to increase bearing capacity for access roads and temporary roads and to reduce rutting during the service lifetime.

2.5.4 Guidelines for design and construction

The national guidelines for design and construction of roads in Norway include the possibility for the use of geosynthetics for stabilisation of roads and traffic areas but there is no general recommendation for the design and construction [15]. Accordingly guidelines in general are left to the specific designers and contractors which again mostly rely on product specific recommendations provided by producers and distributors. The lack of general national guidelines is a challenge for the designers and users as this implies they will be responsible for any possible damage and or lack of function which can be linked to the specific design and construction. Despite the lack of common regulations and guidelines geosynthetics are commonly used especially for rehabilitation and upgrading of roads.

SINTEF initiated a research project in 1990 focusing on the possibility for using geosynthetics for improving bearing capacity of roads and airfields. The research project was carried out in co-operation with NPRA, the Norwegian Army and the Norwegian Aviation Authorities. The theoretical basis for the use of reinforcement was presented in a report in 1991 [16]. It was concluded that geosynthetic reinforcement to a limited extent would improve the elastic stiffness but could significantly improve the resistance against plastic deformations. The project concluded that geosynthetic reinforcement could beneficially be used to improve bearing capacity and reduce rutting. It especially pinpointed the possibility related to reducing deterioration caused by plastic deformations, e.g rutting caused by reduced bearing capacity during the thawing period. It also pinpointed that the lack of common regulations and product independent guidelines for design and construction were a major obstacle for utilising reinforcement in roads and traffic areas. Based on the results from the project it was prepared a proposal for guidelines for the use of geosynthetics for stabilisation of roads and airfields [17]. The proposal for guidelines included a basis for evaluation of potential benefits from using reinforcement, recommendations for design and construction and covers reinforcement both in granular layers and in the asphalt overlay.

Despite the positive effects of using geosynthetics for stabilisation are verified through experiences, no technically sound design model is existing. This is a major obstacle to have a sound design method and possibility of evaluation of effects related to other solutions.

A comprehensive research project GeoRePave was executed by MSU (Montana State University, USA) and SINTEF (Trondheim, Norway) [18-24]. The objective of this project was to develop design methods for reinforced unbound base course layers in roads and included the development of numerical material models and numerical modelling methods for road foundations. This research project has resulted in a proposed design procedure.

The motivation for including reinforcement in unbound base course materials is to reduce the construction and maintenances cost of the road. The latter should be evaluated in terms of life cycle cost. The life cycle cost can be split into:

- construction costs including materials
- maintenance costs over the road lifetime
- environmental impact from the use of construction materials

The cost reduction due to the use of reinforcement may be evaluated in terms of reduced required thickness of the unbound layer or increased number of traffic passes before maximum allowable deformation of the road is exceeded. This may be expressed with so-called benefit ratio's:

- Traffic Benefit Ratio (TBR): ratio of allowable traffic passes for a reinforced base course.
- Base Course reduction Ratio (BCR): ratio for the reinforced base thickness

If the TBR ratio is applied, the reduction in maintenance costs in the future must be larger than the cost for purchasing and installing the reinforcement. The life cycle cost may however be the easiest to determine on basis of the BCR, since this compares designs for the same traffic load (same number of passes before the design criteria on allowable traffic is reached).

To be comparable with the unreinforced design, the design method for reinforced base courses must include parts of the experience and empirical relations derived from field tests. It is therefore a difficult task to compare the design of reinforced and unreinforced pavements in engineering terms.

Design of reinforced pavements has thus to be performed in relation to conventional road design. Starting from a 2D-axial symmetric Finite Element Model the unreinforced structure is dimensioned. The effect of compaction, traffic load and reinforcement on the horizontal and shear stresses is calculated stepwise. Due to its complexity, this procedure needs to be incorporated into a software/design package in order to be used on a routine basis in practice.

The research in the GeoRePave project has provided the outline of the methods and is published on the web address http://www.coe.montana.edu/wti/wti/display.php?id=89.

The proposed design method is based on the following in-put related to geosynthetic properties:

a) material properties for the reinforcement. Stiffness in MD and CMD direction, Poisson's ratio and in plane shear-modulus.

b) interface properties between reinforcement and the base aggregate.

c) identification of shear stress growth functions for the reinforcement-aggregate interface.

The following test methods will be required to measure the reinforcement and interaction properties:

a) stiffness - wide with tensile test

b) Poisson's ratio – biaxial tensile tests

c) in plane shear modulus – a fully appropriate test method does not exist

d) cyclic pullout tests to define interaction properties

e) cyclic loading model tests on a reinforced pavement structure

f) cyclic triaxial tests on base course material to define permanent deformation properties

Pavement reinforcement with geosynthetics has been used for more than 40 years, steel reinforcement for more than 3 decades in Europe. Reinforcement in road pavements has a promising potential and the beneficial effects of the reinforcement may both reduce construction costs and enhance the road performance. However, despite the large amount of research projects and a large number of successful projects in the field with good experience, pavement reinforcement is still not recognised as a solution at the same level with conventional methods. This is to a large extent due to the lack of technically sound models for the function mechanisms of the reinforcement and proper non product related design models.

3 Installation and Construction

The Nordic conditions are challenging when it comes to installation and construction. Short working hours with daylight during the winter, soft and frost-susceptible soils, low temperatures, ice, snow, and frozen subsoil imply that installation and construction may cause damage to the products and improper installation. The general regulations and guidelines accordingly give limitations on when installation and construction with geosynthetics can be carried out.

The restrictions on installation and construction have a major impact on the possible use and economic benefits of using geosynthetics. Especially the limitations related to installation in cold temperatures have major consequences, as this implies that construction using geosynthetic in general can't be done during the winter. The basis for the limitation in cold temperatures was experiences where geosynthetics had exhibited damage by cracking when installed and covered with fill material at low temperature, Figure 11.



Fig. 11. Damage on geogrid from installation at low temperature (Photo Trafikverket, Sweden).

3.1 The Rough project-installation and construction under Nordic conditions

Users, contractors and producers/distributors had a common interest in extending the time period for installation and construction with geosynthetics. Experiences revealed a lack of relevant requirements related to the installation and function of geosynthetics in a cold climate especially when temperature are largely below 0 °C. A development project ROUGH (RecOmmendations for the Use of GeosyntHetics in Nordic conditions) was established to identify special requirements for geosynthetics to ensure technically and economically optimal solutions in country-specific climates and soils. Traffic Authorities in Finland, Sweden and Norway, research institutes, universities and a group of producers participated in the project.

The objective of the ROUGH project was specially to focus on cold temperature by using local soil conditions in the Nordic countries and local construction methods and typical aggregate materials. The project included a survey of experiences, literature studies, laboratory investigations and a full-scale field test. Depending on the type of geosynthetics the main means implemented were:

1- a full scale on-site experiment in Kemi (Northern Finland) on installation under Nordic conditions for the applications with the functions reinforcement / stabilisation, filtration, drainage;

2- considering the difficulty of the realisation of a similar on-site experiment for sealing applications, it was decided to realise a literature study associated with a synthesis of the state of the art for this function.

Long term behaviour like freeze/thaw action and traffic loading is obviously important for the function but the ROUGH-project was limited to the installation and construction.

The test site was established along an ongoing construction project to upgrade the Highway 4 (E8/E75) (Northern Finland), close to the border to Sweden, Figure 12 [26].

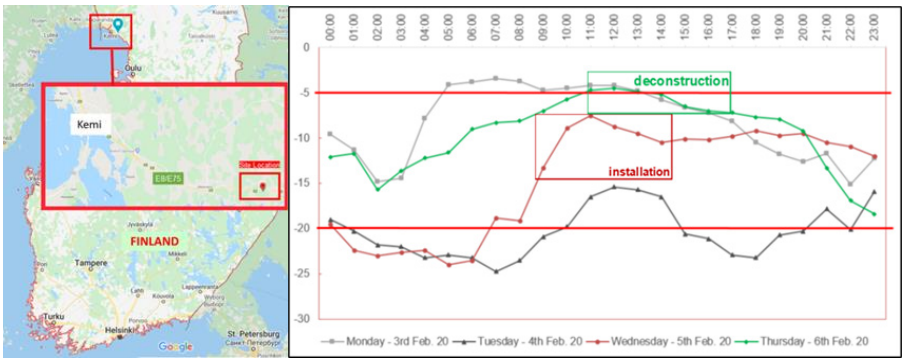


Fig. 12. Location of the field tests (Screenshot Google Maps) and temperatures during installation and recovery [°C]

Altogether 13 products were installed covering the functions reinforcement/ stabilization, filtration, and drainage. The products were installed as a part of a road structure and of a drainage ditch at an average temperature - 10 °C (down to - 15 °C). The installation and compaction were carried out according to pre-determined procedures, Figure 13.



Fig. 13. Installation of geosynthetic samples for reinforcement/stabilisation function.

The procedures for the extraction of the products had to be specially adapted to be able to remove the fill material on top of the geosynthetics, without creating added potential damages due to excavation. To avoid additional damage to the samples during the recovery of the geosynthetics, a vacuum/sucking lorry was used. The first 20 cm of the base crushed rock layer were removed by careful use of an excavator. The remaining 10 cm of the base crushed rock layer was successfully removed by the vacuum lorry, Figure 14.

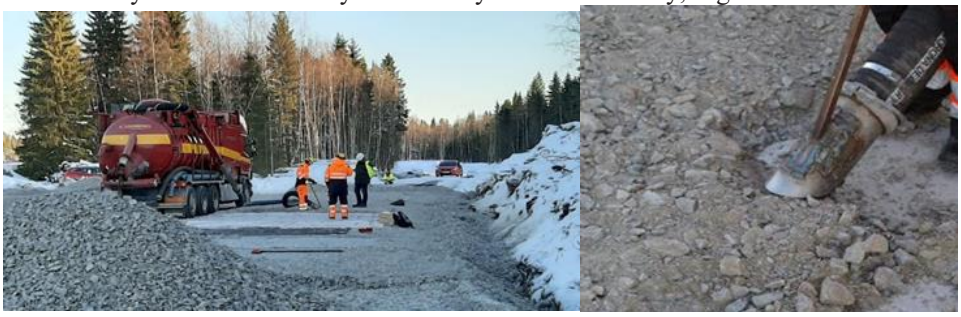


Fig. 14. Vacuum lorry and system for sucking of material from the geosynthetics.

The ROUGH project allowed to bring the important conclusions for the geotextiles and related products tested during the full-scale experiment. If geosynthetics are correctly designed for a positive temperature (e.g., + 20 °C) for the defined geotechnical conditions of installation (type of soils, drop height, compaction, etc.), no additional installation damage is observed on the essential characteristics when the products are installed under the same conditions at - 10°C:

- tensile strength and tensile stiffness for reinforcement/stabilisation,
- robustness factor and characteristic opening size for filtration,
- water flow capacity for geosynthetic drainage composites.

The field test in Kemi did not reveal similar types of junction-damage on the grids installed as previously experienced. The susceptibility for this type of damage is likely to be heavily influenced by the polymer type and additives and the production procedure. The result from the ROUGH-project is valid for the geosynthetics tested during the full-scale experiment in Kemi and for the products of the same family (same production process, same polymer, same function).

The results from the ROUGH-project is basis for recommendation and guidelines for installation and construction with geosynthetics under Nordic conditions [26].

4 Project examples

Geosynthetics have been used for more than five decades in the Nordic countries including a large number of applications, functions and products. Below a limited number of examples are shown to present some of the innovative structural solutions and construction methods that is completed.

4.1 Green vegetated slopes

Geosynthetics can be used as soil reinforcement to establish green vegetated slopes that are environmentally friendly and economically beneficial. To establish and keep the vegetation green would however generally require the use of backfill which contains moisture. For the Nordic countries this generally implies the use of backfill material containing some fine particles to keep a minimum moisture content during dry periods. The content of fines however will also imply the soil will be more frost-susceptible and possibly create deformations and damage during the frost period.

SINTEF in co-operation with the company Halling Torv developed a solution where “peat-blocks” were used in the front of the structure as frost-insulation and “moisture magazine”. The peat-blocks are produced from peat with a natural-based binder and has a size of 30cmx40cmx12cm. The blocks can be stapled on top of each other without any scaffolding system using a geogrid wrap-around solution to keep the front stable, Figure 15.

A number of these structures have been established in the Nordic countries and has proven to be environmentally friendly and economically beneficial with short construction time and low costs [27].

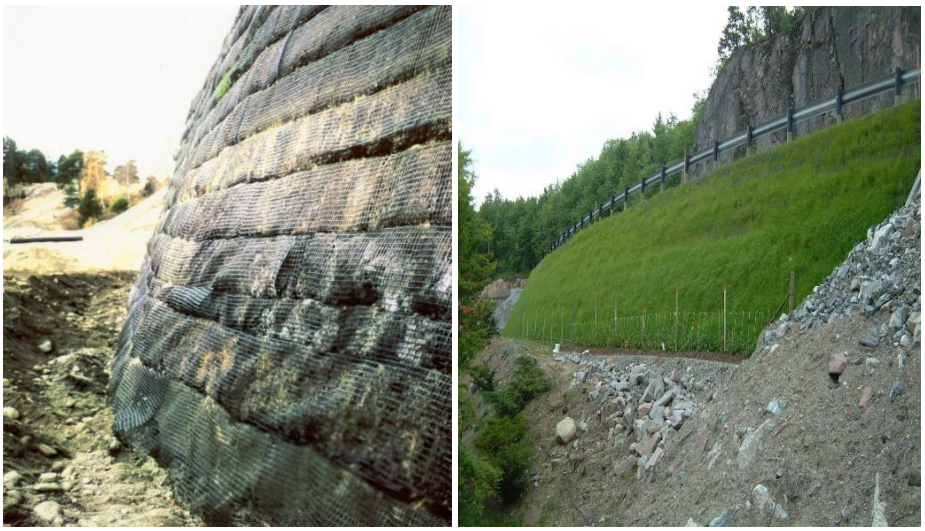


Fig. 15. Green vegetated steep slope with peat block front and geogrid reinforcement

4.2 Upgrading and rehabilitation of roads

Geosynthetics have, despite the lack of independent design methods, been successfully used for stabilisation of roads. Especially in rehabilitation and upgrading of existing roads geosynthetics from experience have proven to be a technically sound and economically beneficial solution to traditional methods. In the island of Hitra outside the northwestcoast of Norway geosynthetic reinforcement was used for rehabilitation of an old gravel road on very soft subsoil subjected to settlements and low bearing capacity in the thawing period. The aim of the rehabilitation was to improve the bearing capacity of the road to avoid restrictions on the axle load during the thawing period and to restrict the deformations of the surface to avoid cracking of the asphalt pavement. The structural layout was designed by the municipality of Hitra with assistance from the local road authorities, **Erreur ! Source du renvoi introuvable.**.

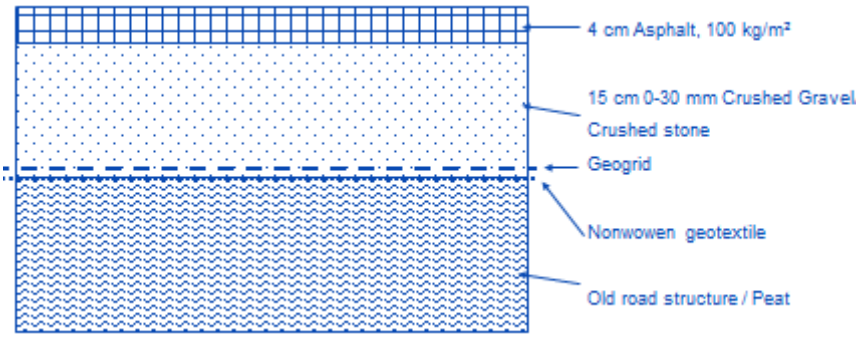


Fig. 16. Structural lay-out, test road at Hitra, Norway

The rehabilitation was performed in section over a period of several years and different types of geogrid reinforcement were used. Pictures from the installation of the reinforcement is shown in **Erreur ! Source du renvoi introuvable.**.



Fig. 17. Road rehabilitation, Hitra Norway [28]

SINTEF was responsible for evaluating the results from the rehabilitation and performed rutting measurements and Falling Weight Deflectometer (FWD) as basis for the evaluation [28]. The evaluation of the results indicated that the rehabilitation works had been successful as no substantial rutting or cracking of the asphalt overlay has been observed on any of the test sections.

Falling Weight Deflectometer (FWD) show the effect on elastic properties while the beneficial effect of the reinforcement generally was related to the plastic deformations. The FWD test confirms that very little effect could be found on the elastic stiffness.

4.3 Erosion control at sea-shore in the Arctic

Climate change has caused thawing of permafrost and increased erosion at sea-shore in several areas in the Arctic. Increasing erosion is causing loss of land and properties and several attempts have been made to try to reduce the erosion from current and waves.

Geosynthtics have successful been used in several project for sea-shore protection but arctic conditions with permafrost, extreme low temperatures and ice-covered sea represents challenges beyond previous experiences, Figure 18.



Fig. 18. Ice covered sea and sea-shore erosion in Longyearbyen, Svalbard, Spitsbergen

The University Centre in Svalbard, SINTEF and Bidim established a research project, GISSAC, aiming at developing a geosynthetic based erosion control system for seashore protection in Svalbard [29]. The system included a sand-filled geosynthetic bag tailor-made to be able to resist very low temperatures, wave action and abrasion from ice. As a part of the project a test-site was established at the break-water structure in Svea, a mining city at

Svalbard. Six years after construction, the overall performance was good. The observations indicate that the abrasion from sea ice is the dominating action wearing down the geosynthetics. Several bags were damaged and worn, but the flexibility of the geotextile bag structures still secured the stability. The structures are stable, and erosion at the sites have seized. Successful replacements of missing and damaged bags have been performed annually in the summer based on visual observation.

Based on the results from the research project the system has later been used in coastal protection in the harbour area in Longyearbyen, Figure 19.



Fig. 19. Geosynthetic bags for erosion protection at the harbour in Longyearbyen

One of the major challenges in working in the Arctic areas are the challenges related to installation and construction under extreme conditions. Ice, snow, wind and waves all contribute to very difficult conditions which requires very skilled persons for obtaining a good result. In Svalbard also nature has other challenges which has to be handled. During the research project the test site in Svea had visit from a polar bear with to babies, Figure 20.



Fig. 20. Polar bears visiting the test site at Svea in Svalbard, Spitsbergen

5 References

1. Alfheim, Sørlie, Testing and classification of fabrics for applications in road constructions. (International Conference on the use of fabric in geotechnics Paris 1977, Vol 2, pp 33-338).
2. Rathmayer. Nonwoven Geotextiles in Road constructipons. Quality Requirements- The VTT-GEO Geotextiles Specification. (Finnish National Road Administration, FinnRa Reports 71/1993).
3. Schalin, A comparison among the Swedish, the Finnish and the Norwegian requirements for separation layers of geotextiles. (Norwegian Road Research Laboratory, internal report no. 1786).
4. Watn and Eiksund, Mechanische Anforderungen an Geotextilien zur Anwendung als Trenn- und Filterschicht im Strassenbau. (K-Geo, TU München, 2001).
5. Fannin and Hermann, Performance data for a Sloped Geogrid Reinforced Soil wall, (Canadian Geotechnical Journal 27/5-1990).
6. Norwegian Public Road Authorities, N-V220 Geotechnical Engineering in Road construction (in Norwegian). (https://store.vegnorm.vegvesen.no/svv-proj-1464979).
7. Fannin and Quinteros, Durability of geogrid reinforcement from a sloped retaining wall after 25 years in-service. (Geosynthetics : Leading the Way to a Resilient Planet. Proceedings of 6th European Conference on geosynthetics)
8. Watn, Lessons learned from failures of reinforced soil structures. (17 Prazke Geotecnicke, DNY/, 2009).
9. Nordic Geosynthetic Group, Nordic Guidelines for Reinforced Soils and Fills. (The Nordic Geotechnical Societies and Nordic Industrial Funding, 2004).
10. Myhre, J. (1985): Strengthening of a road on peat using Tensar geogrid and Terram Geotextile. (SINTEF report STF61 F85011, 1985).
11. Watn, Hoff and Recker, Geosynthetic reinforcement for road pavements in cold climate. (Proceeding Conference EuroGeo 6, Ljubljana Slovenia, 2016). EuroGeo6 2016.
12. Cost Action 348 (2004), Reinforcement of pavements with steel meshes and geosynthetics (REIPAS). Draft Report of WG 1 chaired by Chris Jenner.
13. Cost Action 348 (2004), Reinforcement of pavements with steel meshes and geosynthetics (REIPAS). Design Models and Procedures for Geosynthetics in Pavements, draft report of WG 4 chaired by Arian de Bondt.
14. Cost Action 348 (2004), Reinforcement of pavements with steel meshes and geosynthetics (REIPAS). Development and testing work, draft report of WG 3 chaired by Gudmund Eiksund.
15. Norwegian Public Road Authorities, N200 Road Construction (in Norwegian), N200 Vegbygging | Statens vegvesen.
16. Watn and Solheim (1991), Reinforcement for Roads and Traffic Areas. Upgrading and new Construction-Design Basis. SINTEF report STF69 A91020 (in Norwegian).
17. Watn and Solheim (1993), Reinforcement for Strengthening and Rehabilitation of Roads and Airfields. SINTEF report STF69 A93021 (in Norwegian).
18. Perkins, S.W. & Eiksund, G.R., 2005. Geosynthetic Material Properties for Use in 2-D Finite Element Pavement Response Models. Proceedings of the Seventh International Conference on the Bearing Capacity of Roads, Railways and Airfields, Trondheim, Norway.
19. Perkins, S.W. & Svanø, G. 2006. Assessment of Interface Shear Growth from Measured Geosynthetic Strains in a Reinforced Pavement Subject to Repeated Loads. Eighth International Conference on Geosynthetics, Yokohama, Japan , J. Kuwano & J. Koseki eds., Vol. 3, pp. 813-816.
20. Perkins, S.W., Christopher, B.R., Cuelho, E.V., Eiksund, G.R., Schwartz, C.S. & Svanø, G. 2009. A Mechanistic-Empirical Model for Base-Reinforced Flexible Pavements. International Journal of Pavement Engineering, Vol. 10(2), pp. 101-114.

21. Perkins, S.W., Christopher, B.R. & Lacina, B.A. 2008. Mechanistic-Empirical Design Method for Unpaved Roads Using Geosynthetics. Proceedings of the 4th European Geosynthetics Conference EuroGeo4, Edinburgh Scotland, Paper No. 228.
22. Perkins, S.W., Christopher, B.R., Eiksund, G.R., Schwartz, C.S. & Svanø, G. 2005. Modelling Effects of Reinforcement on Lateral Confinement of Roadway Aggregate. Proceedings of the Conference GeoFrontiers, Geotechnical Special Publication 130, Advances in Pavement Engineering, ASCE, Austin, Texas.
23. Perkins, S.W., Christopher, B.R., Cuelho, E.L., Eiksund, G.R., Hoff, I., Schwartz, C.W., Svanø, G., & Watn, A. 2004. Development of Design Methods for Geosynthetic Reinforced Flexible Pavements. U.S. Department of Transportation, Federal Highway Administration, Washington, DC, FHWA Report Reference Number DTFH61-01-X-00068, 263p.
24. Eiksund, G.R., Hoff, I. & Perkins, S.W. 2004. Cyclic Triaxial Tests on Reinforced Base Course Material. Proceedings of the Conference EuroGeo 2004, Munich, Germany, pp. 619-624.
25. Delmas, Watn and Recker. 2022. ROUGH – Tests on damage during installation at low temperature (SINTEF report 2022-00635)
26. Delmas, Watn, Uotinen, Vaslestad, Griwell and Recker, ROUGH - RecOmmendations for the Use of GeosyntHetics in Nordic conditions. (Geosynthetics: Leading the Way to a Resilient Planet, proceedings 12 ICG, Rome, Italy).
27. Halling Torv, Green wall, hallingtorv.no/file/b514d5598845/ (in Norwegian).
28. Watn and Øiseth. 2000. Geosynthetic Reinforcement in Roads – test Road at Hitra, Sør-Trøndelag, Norway. SINTEF report STF22 F00604.
29. Finseth, Bæverfjord, Lothe, Watn and Delmas, Use of geosynthetics for coastal protection in Arctic areas. (Proceedings of the 5th European Geosynthetics Congress, 2012).

Suitable design approaches for interfaces involving geosynthetics under various loading and flow conditions

Nicola Moraci[1*], *Giuseppe* Cardile[1], *Marilene* Pisano[1], *Paolo* Carrubba[2], *Maria Clorinda* Mandaglio[3] and *Stefania* Bilardi[1]

[1]Mediterranean University of Reggio Calabria, DICEAM Department, 89122 Reggio Calabria, Italy
[2]University of Padova, Department ICEA, School of Engineering, 35129 Padova, Italy
[2]University of Salerno, Department DICIV, 84084 Fisciano, Italy

Abstract. This work integrates the research results conducted over several years, focusing on the behaviour of interfaces in applications involving geosynthetics. It addresses the importance of accurately characterizing the interfaces of geosynthetic-reinforced soil walls and steep slopes, landfill cover systems, and drainage systems to ensure their performance under both ultimate and serviceability limit states. For geosynthetic-reinforced soil walls and steep slopes, the research emphasizes the proper characterization of soil-geosynthetic interfaces under static and cyclic loading conditions, both in the short- and long-term. It provides essential guidelines for selecting design parameters for these structures, ensuring their stability under various loading scenarios. In landfill cover systems, the study investigates the behaviour of interfaces between different geosynthetics under static and seismic loading conditions, with special attention to potential damage arising from improper installation. The lecture offers a comprehensive approach to understanding these interactions and their impact on the long-term performance of landfill systems. Lastly, the research examines the soil/geotextile filter interfaces in drainage systems, particularly in contact with unstable cohesionless soils under different boundary conditions. It challenges conventional design methods and introduces a new methodology to design filter transitions in contact with internally unstable soils. These findings significantly contribute to designing and optimising geosynthetic applications in civil engineering, advancing theoretical understanding and practical implementation.

1 Introduction

Geosynthetics in engineering applications are now recognized as a sustainable and well-established technological solution. On a global scale, there is an increasing focus on the negative impacts of plastics, particularly "single-use plastics," and the subsequent generation of microplastics, which contribute to a pollution process with severe environmental risks. Geosynthetics, which are durable building materials designed for long-term use in engineering projects, offer a sustainable alternative as they align with the concept of sustainable development.

Concerning the United Nations' "2030 Agenda," which aims to transform the world sustainably and eradicate poverty in all its forms, geosynthetics can play a significant role in achieving key objectives such as clean water and sanitation, industry innovation and infrastructure, responsible consumption and production, climate action, and global partnerships.

Climate change is a primary driver of increasing natural disasters, including typhoons, landslides, and floods, which are becoming more frequent and severe. This phenomenon substantially threatens human health, food security, migration patterns, and the global economic and political balance. Reducing greenhouse gas (GHG) emissions, especially carbon dioxide (CO_2), will be a vital and urgent priority in the coming years. To accurately assess the environmental impact of a product or system, it is essential to evaluate its entire life cycle (Life Cycle Assessment, LCA), with a particular focus on CO_2 emissions. This evaluation should consider the entire process, from raw material extraction to industrial production, end-use applications, and potential recycling and final waste disposal. In conducting these assessments, various indicators must be considered, including energy supply and demand, climate change, ozone depletion, particulate formation, acidification, eutrophication, land use, water resources, human health, biodiversity preservation, and resource availability. LCA studies of geosynthetic applications have demonstrated that these materials significantly reduce GHG emissions compared to traditional geotechnical solutions.

Geosynthetics can also play a significant role in adapting to ongoing climate change. Adaptation involves proactively addressing the negative impacts of climate change by implementing measures to prevent or mitigate the potential damage. Research has shown that early and well-planned adaptation efforts can lead to substantial savings in both financial and human terms. The use of geosynthetics in protection barriers for landslide risk mitigation, dams and levees, erosion control solutions, and in earth structures for slope re-profiling contributes significantly to enhancing the resilience of communities and infrastructure against natural hazards like earthquakes, floods, landslides, and droughts.

The construction methods involving geosynthetics offer a notable reduction in construction time due to their simplicity compared to traditional techniques, resulting in cost savings arising from the use of more affordable materials, whose mechanical characteristics and properties are rigorously tested and certified according to strict quality standards before entering the market, reduced reliance on highly skilled labour, and decreased equipment rentals. Additionally, substantial cost reductions can be achieved by utilizing on-site granular soil or a portion of it, which eliminates or decreases the need for transport from quarries. Furthermore, the use of geosynthetics in road and railway embankments allows for steeper slopes, leading to potential savings in land acquisition costs. Geosynthetic solutions also offer considerable long-term cost savings, particularly in reduced maintenance and improved performance, especially during seismic events.

Among the various functions that geosynthetics can perform, this paper specifically focuses on reinforcement and filtration.

The reinforcement function aims to improve the shear strength and deformability of the soil by incorporating a geosynthetic material with high tensile strength and stiffness. Geosynthetics, such as woven geotextiles, geogrids, and geocells, are widely used in soil

reinforcement applications, including the construction of retaining walls, bridge abutments, embankments, steep slopes, and cover barrier systems for landfills. In these applications, it is necessary to account for the soil-geosynthetic interface resistance considering different short- and long-term loading conditions.

In the context of the filtration function, geosynthetics play a fundamental role in preventing the migration of soil particles, thus avoiding erosion while allowing the free movement of water through the soil. This helps to prevent increases in pore water pressures within the system (soil–geotextile filter), which could otherwise compromise the drainage capacity and potentially destabilize the structure. Geosynthetics used for filtration, such as geotextiles and geocomposite filters, are essential in applications like dams, embankments, drainage trenches, coastal structures, revetments, scour protections, permeable reactive barriers, and both vertical and horizontal drains. In these cases, carefully considering the soil-geotextile interaction during the design phase is important to ensure optimal performance.

2 Soil-geosynthetic interface strength in the design of reinforced walls and steep slopes

The evolution of the design of geosynthetics-reinforced soil (GRS) structures over the years can primarily be traced to advances in understanding the mechanical behaviour of both soil and geosynthetics, the durability of geosynthetics, soil-reinforcement interaction, and design methods. The design of GRS walls and steep slopes, constructed by alternating layers of reinforcing geosynthetics with compacted soil, involves several critical decisions. These include the selection of the backfill soil and the compaction techniques; the choice of the reinforcing geosynthetic and the polymer characteristics that ensure durability under specific environmental conditions; the selection of construction methods (and the type of facing); the determination of interface parameters, and consequently, the length and spacing of the reinforcements; the design of the drainage system both upstream and behind the structure; as well as the preparation of technical specifications for construction and long-term monitoring of the structure.

The design of reinforced earth structures using geosynthetics must ensure adequate safety margins concerning both ultimate and serviceability limit states in accordance with the applicable technical standards in the country where the construction takes place. In particular, regarding the internal stability of these structures, it is necessary to consider the possible failure mechanisms during designing, which may result from insufficient tensile strength of the polymeric reinforcement, inadequate pullout resistance of the reinforcement from the anchorage zone, or insufficient sliding resistance of a portion of the reinforced block along a soil-geosynthetic interface. These resistances arise from the interaction between the reinforcement and the compacted soil in which it is embedded. Therefore, in this context, it is essential to understand the soil-reinforcement interaction parameters and their evolution over time with regard to the type of applied load. The length of the reinforcement, and consequently the size of the reinforced block, depends on the apparent coefficient of friction at the interface, which is adopted in the design.

The complex behaviour at the soil-geosynthetic interface is generally simplified by introducing equivalent shear stress, which allows for the determination of the overall resistance associated with the entire surface of the reinforcement. The soil-geosynthetic interaction can be very complex as it is influenced by the structural, geometric, and mechanical characteristics of the geosynthetic, the mechanical and grain size characteristics of the soil, and the loading and boundary conditions.

The reinforcement action is exerted through various soil-geosynthetic interaction mechanisms. To provide further detail, skin friction due to sliding is the only mechanism that develops when the interface consists of soil in contact with a continuous geosynthetic (e.g., geotextiles). However, the interaction becomes more complex for a geogrid due to its open mesh structure. Specifically, in this case, three different elementary mechanisms can be

mobilized at the interface: skin friction between the soil and the solid portion of the reinforcement; bearing resistance developed along the transverse elements of the geogrid, positioned orthogonally to the pullout direction; and friction due to sliding between the soil portions enclosed within the openings of the reinforcement and the soil above and below it.

One or more of the aforementioned elementary interaction mechanisms may be mobilised depending on the considered ultimate limit state, the reinforcement's geometric structure, and the soil's grain size characteristics. Figure 1 shows one of the possible ultimate limit states of a GRS structure, specifically the pullout mechanism. Pullout tests are performed using a large-scale apparatus to simulate it in the laboratory.

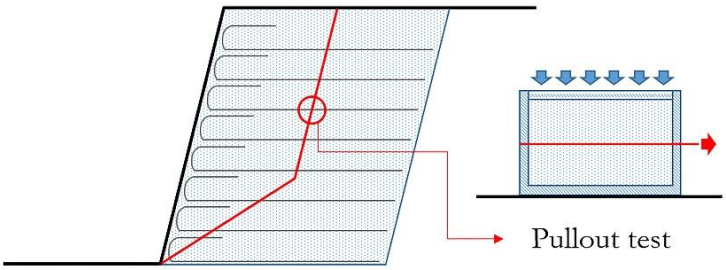


Fig. 1. Ultimate limit state (pullout) and corresponding laboratory test used to simulate the behaviour at the soil-geosynthetic interface.

The peak pullout resistance that the soil-geogrid interfaces oppose to the tensile loads acting on the reinforcements during the service life of a GRS structure can be expressed as follows:

$$P_R = 2 \cdot L_R \cdot \sigma_n' \cdot f_b \cdot \tan\phi' \quad (1)$$

In equation (1): P_R is the maximum pullout resistance per unit width; L_R is the length of the reinforcement in the anchorage zone; σ'_n is the effective normal stress acting orthogonally to the reinforcement plane; ϕ' is the shear strength angle of the soil; f_b is the soil-geosynthetic interaction coefficient under pullout conditions.

Jewell et al. [1] provided a theoretical equation for determining the f_b coefficient of the equation (1), but several studies have demonstrated the limitations of this formulation [2-4]. The f_b values can also be obtained using results from pullout tests. The choice of the shear strength angle mobilized for use in the expressions of f_b is very important. Still, it is quite challenging due to the three-dimensional effects, dilation phenomena, and the effects related to the extensibility of the reinforcement.

The problem of determining the pullout resistance can be solved by using the peak apparent coefficient of friction at the soil-geosynthetic interface, $\mu^P_{S/GSY}$, which can be derived from the equation:

$$\mu^P_{S/GSY} = f_b \cdot \tan\phi' = \frac{P_R}{2 \cdot L_R \cdot \sigma_n'} \quad (2)$$

It is important to note that the use of this expression does not require any assumption regarding the values of the shear strength angle mobilized along the interface, as all the parameters in this equation can be easily determined through pullout tests conducted in the laboratory with large-scale apparatus.

To predict the pullout resistance of geogrids embedded in compacted granular soils, Moraci and Gioffrè [5] proposed a simple method suitable for geogrids where scale and

interference effects are negligible. Moreover, the method accounts for both reinforcement extensibility and soil dilatancy effects. According to this method, the pullout resistance of extruded geogrids embedded in a compacted granular soil is given by the sum of the skin friction between the soil and the solid surface areas of the reinforcement and the bearing resistance developed against the transverse elements, as expressed in the following equation:

$$P_R = 2 \cdot C_{\alpha S} \cdot \alpha_S \cdot L_R \cdot \sigma'_n \cdot tan\delta + n_t \cdot n_{tb} \cdot A_b \cdot \sigma'_b \quad (3)$$

where $C_{\alpha S}$ is a reduction coefficient for geogrid area where skin friction develops; δ is the mobilized skin friction angle between soil and geogrid, influenced by soil dilatancy and reinforcement extensibility; $n_t = L_R/S$ is the number of geogrid bearing members; n_{tb} is the number of nodes in a transverse bar; $A_b = A_t + A_r$ is the area of each rib element (including the single node and the bar portion between two nodes) where bearing resistance can be mobilized; and σ'_b is the bearing stress, evaluated according to Matsui et al. [6]. Furthermore, the complex geometry of transverse bars was simplified by assuming an equivalent strip geometry with uniform thickness (Fig. 2).

The evaluation of interaction factors is complex: $C_{\alpha S}$ depends on the extent of passive and active failure surfaces (assumed to be 1 in the absence of interference effects); δ depends on soil dilatancy and reinforcement extensibility; σ'_b depends on soil dilatancy, reinforcement extensibility, and the failure mechanism.

The peak shear strength angle was considered variable with the applied effective vertical stress to account for the curvature of the soil failure envelope, and δ was assumed to be a fraction of the mobilized soil shear strength angle, depending on the geogrid type. To incorporate reinforcement extensibility, the following assumptions were made:

- For short reinforcements and long reinforcements under low effective vertical stresses, the interaction mechanisms are activated simultaneously along the whole reinforcement [7]. The peak shear strength angle was used for both components of pullout resistance;
- For long reinforcements under high effective vertical stresses, the two interaction mechanisms are mobilized progressively [7]. The skin friction component was evaluated using the mean value between the peak shear strength angle and the constant-volume shear strength angle, while the bearing resistance component was evaluated using the peak shear strength values corresponding to different vertical effective stresses.
- In residual conditions, the shear strength angle at constant volume was used.

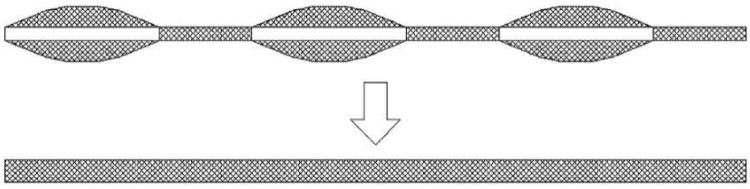


Fig. 2. Assumed equivalent geometry [5].

The mobilization of bearing resistance is significantly influenced by the interference phenomenon in closely spaced bearing members (i.e., for a small ratio between S and the thickness of transverse ribs, B_{eq}). Actually, this phenomenon also involves a substantial part of the surface of the longitudinal members, resulting in a decrease in skin friction.

Bearing resistance depends on both the ratio of the transverse rib thickness B_{eq} to the average particle size of the soil, D_{50} (i.e., the scale effect) and the shape of the transverse ribs [3, 8-12].

Cardile et al. [13, 14], based on the results of several large-scale pullout tests [14-18], improved the Moraci and Gioffrè [5] model by accounting for the interference mechanism in closely spaced bearing members (i.e. for $S/B_{eq} < 50$) by adding a $C_{\alpha b}$ coefficient in the second term of the equation (2). Figure 3 shows the interference reduction factors $C_{\alpha b}$, fitted by linear regression, for varying S/B_{eq} ratios. When $S/B_{eq} > 50$, the interference phenomenon can be considered negligible, meaning the interference reduction factor $C_{\alpha b}$ is equal to one.

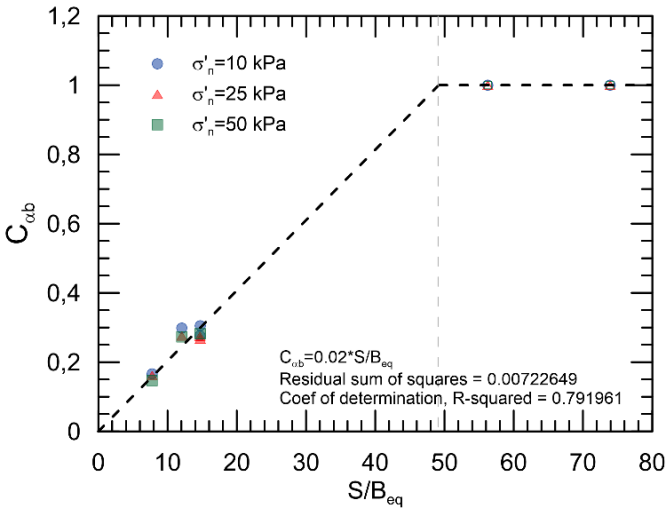


Fig. 3. Variation of the reduction factor for the bearing resistance with varying the normalised spacing between transversal members [13].

2.1 Test apparatus for the interface characterization

The pullout tests allow for studying the behaviour of the reinforcement in the anchorage zone in the laboratory; consequently, they allow for analysing the elementary interaction mechanisms that develop at the soil-geosynthetic interface. Through these tests, it is possible to obtain the load-displacement curves representing the pullout load measured at the reinforcement head as a function of the displacement of the first confined section (pullout curves), as well as the curves representing the deformative behaviour of the specimen.

The pullout apparatus consists of a rigid steel box, a system for applying vertical confining pressure, a system for applying and controlling the pullout force, a geosynthetic clamping device, transducers to measure the displacement of the reinforcement specimen, and the required control and data acquisition system.

The test method is intended to be a performance test conducted as closely as possible to replicate in situ conditions. In the case of reinforcements embedded in compacted granular soils (the most common case), the test results depend on the particle size distribution, the compaction state, and the mechanical characteristics of the granular soil, as well as the geometric, structural, and mechanical characteristics of the geosynthetic, the confining pressure, and the loading conditions (e.g., monotonic, cyclic, multi-stage). Moreover, the experimental results may also depend on the apparatus characteristics and the testing procedure employed.

The different pullout apparatuses currently used around the world vary in the box dimensions and the methods adopted to minimize the boundary effects on the test results. Moreover, different testing procedures are also used. In the last three decades, different researchers carried out pullout tests using these various prototype apparatuses to study the influence of boundary conditions and the scale effects of devices [3, 7, 12, 19-25]. The

outcome of these studies allowed the identification of the following factors affecting pullout test results: the influence of the vertical load application system; the influence of the boundary conditions at the front wall; the efficiency of methods used to minimize friction between side walls and soil; the influence of the box sizes (specifically the thickness of soil below and above the geosynthetic specimen) to avoid boundary effects; the influence of geosynthetic specimen width compared to the pullout box width; the influence of the clamping device; the influence of the displacement rate used in the test. Based on the findings obtained by the research on this topic, the following recommendations can be summarized to define the characteristics that a pullout apparatus must have to ensure test results are not affected by the factors mentioned above:

– Vertical confining pressure should be applied using a flexible membrane;
– The side walls of the pullout box should be lined with low-friction materials;
– Sleeves of at least 200–300 mm in length should be utilized;
– An internal clamping system should be employed to maintain specimen confinement throughout the test duration;
– The soil height within the pullout box should be no less than 600 mm;
– The geosynthetic specimen width should be nearly equal to the width of the pullout box;
– The dimensions of the pullout box should be sufficiently large to accommodate a representative geosynthetic specimen.

Given these considerations, Moraci and Recalcati [7] designed a large-scale prototype apparatus for conducting pullout tests under monotonic and multi-stage loading conditions. This apparatus consists of a large rigid steel box, a pair of 200 mm-long metal sleeves, an internal clamping system, a pneumatic system for applying vertical loads, a hydraulic actuator for applying horizontal loads, six RVDTs, and a data acquisition system (Fig. 4).

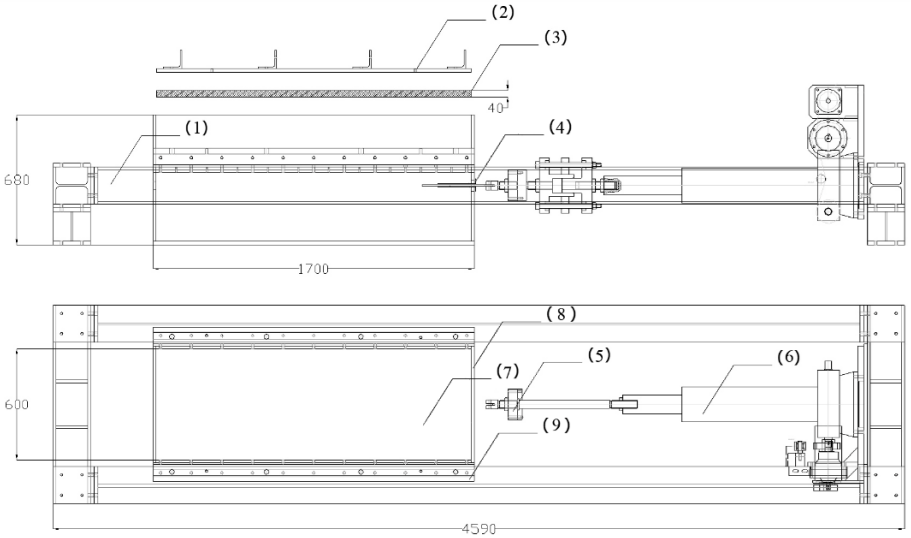
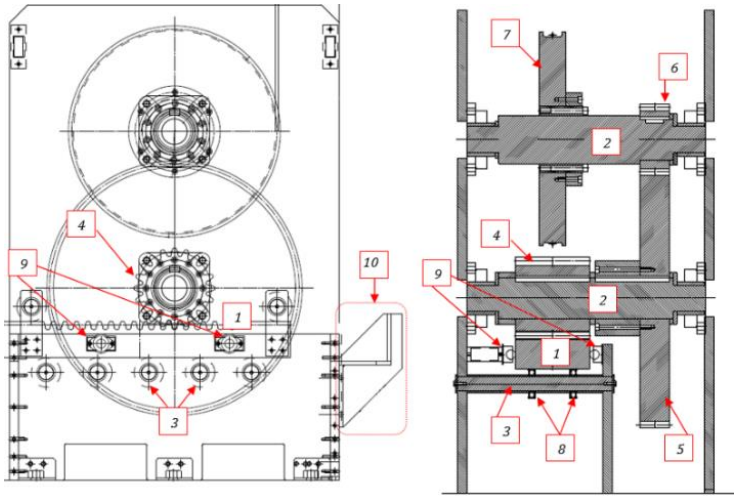


Fig. 4. Scheme of pullout test apparatus: 1) frame; 2) steel plate; 3) air bag; 4) sleeves; 5) load cell; 6) hydraulic actuator; 7) 1700x600x680 mm pullout box; 8) front wall; 9) side wall (modified from [7]).

Subsequently, to investigate the long-term behaviour of geosynthetics used for reinforcement purposes, Cardile et al. [26] designed a new large-scale prototype apparatus to analyze the time-dependent variation of geosynthetic strains resulting from interaction with soil under sustained pullout loading conditions. The long-term pullout apparatus is similar to that used for conventional pullout tests; however, it differs in the system for applying the horizontal load. In this new apparatus, the horizontal load application is entirely mechanical. It consists of a set of weights that descend vertically under gravity, connected to a pulley via a steel cable (Fig. 5). A gear system amplifies the applied load while reducing displacement.

The overall load is transferred to a gear rack that is rigidly connected to the clamp holding the geosynthetic specimen.



(a) (b)

1) Gear rack; 2) Main axles; 3) Axles in support of gear rack; 4) Gearwheel 1; 5) Gearwheel 2; 6) Gearwheel 3; 7) Pulley; 8) Bearing in support of gear rack; 9) Gear rack lateral supports; 10) Shock absorber for gear rack.

Fig. 5. Longitudinal (a) and transverse (b) cross-sections of the system for the application of pullout load [27].

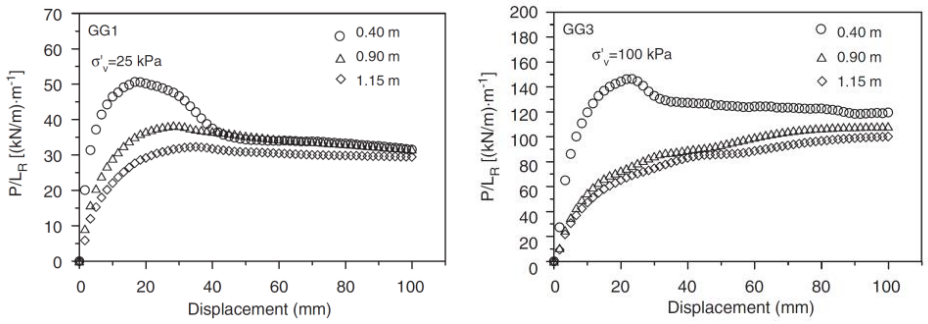
2.2 The static interface strength

The results obtained from various studies [7, 18, 28-30] carried out on geogrids embedded in compacted granular soils and subjected to a monotonic load indicate that the pullout behaviour of a given geosynthetic depends on both the reinforcement length and the applied confining stress.

Pullout tests conducted on "long" specimens generally exhibit strain-hardening behaviour. In this case, the pullout resistance progressively increases as the displacement of the first confined section of the geogrid increases, reaching a peak value beyond which only minimal variations in resistance occur as the pullout process continues. Conversely, tests performed on "short" specimens typically display strain-softening behaviour, characterized by a progressive reduction in pullout resistance after reaching a peak value.

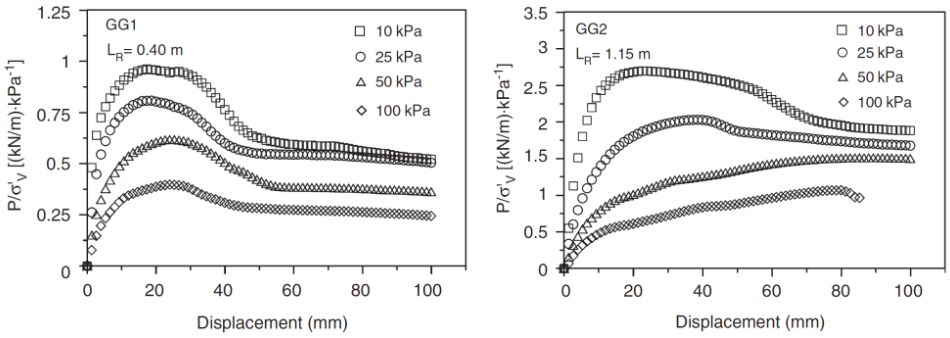
Therefore, the trend of the pullout curves is due to the different deformation behaviour of the reinforcement specimens. Specifically, longer reinforcements exhibit pronounced extensibility effects, especially under high effective confining stresses. This phenomenon induces a progressive mobilization of the interaction mechanisms at the interface, which govern the pullout resistance. On the other hand, shorter specimens (and, in general, longer specimens tested under low effective confining stresses) display a pullout behaviour characterized by limited longitudinal deformations (and thus reduced extensibility effects). As a result, interaction mechanisms are mobilized almost simultaneously along the entire reinforcement length, leading to response patterns similar to stress-strain curves for compacted soils.

The influence of reinforcement extensibility on interface behaviour can be observed in Figure 6, which shows that, in general, extensibility effects are more pronounced for longer reinforcements and at higher effective confining stresses. Due to these effects, the normalized resistance values mobilized in shorter specimens are higher than those mobilized in longer specimens.



(a) (b)

Fig. 6. Normalization of the pullout test results: the effect of reinforcement extensibility (σ'_v=const.) [7].



(c) (d)

Fig. 7. Normalization of the pullout test results: the effect of soil dilatancy (L_R=const.) [7].

The primary factor influencing pullout resistance is soil dilatancy. This can be highlighted by plotting the results in terms of pullout resistance normalized by the applied effective normal stress (Fig. 7). Due to dilatancy effects, the normalized resistance values mobilized under low confining stresses are higher than those mobilized under high confining stresses. The magnitude of the dilatancy effect decreases as the effective normal confining stress increases. This phenomenon is associated with forming three-dimensional passive failure surfaces, which develop against protrusions at the geogrid nodes and against the transverse bars oriented perpendicular to the pullout direction [7].

To understand the actual behaviour of soil-geosynthetic interfaces during load transfer and pullout phases—both characteristic of the pullout process—it is essential to evaluate the active length, L_A, which represents the geogrid's portion where the mobilization of interaction mechanisms withstands the applied pullout load [18]. As long as the geogrid's last transverse bar does not begin to move (i.e., the onset of the pullout phase), the specimen length does not influence the pullout behaviour of the interface. Under the same geogrid and soil conditions, this behaviour depends solely on the applied confining stress.

The tensile load applied at the geogrid's head induces elongation, which occurs only in the active reinforcement portion. This active length varies throughout the test. Cardile et al.. [18] defined the average longitudinal strain, ε_A, as the ratio between the mobilized elongation of the specimen, ΔL, and the corresponding active length L_A, reduced by ΔL. At any given moment during the test, the active length corresponds to the portion affected by interaction mechanisms plus the elongation it undergoes due to the applied load.

Figure 8 illustrates the results of pullout tests conducted at the same confining stress on specimens of different lengths. The graph in the upper part plots the active length as a function of the displacement of the clamp (i.e., the displacement of the first confined section of the geogrid). The lower part presents the values of ε_A, calculated for different clamp displacement values. The X symbols in the graphs indicate the onset of the pullout phase: from this point onward, the increase in active length is solely due to the elongation of the geogrid (i.e., the entire reinforcement length has been mobilized). The slope of the average longitudinal strain curves during the tensile load transfer phase is lower than that observed during the pullout phase. The onset of pullout failure occurs when the average longitudinal strain ceases to increase (in other words, when the curves in the lower graph of Figure 8 become parallel).

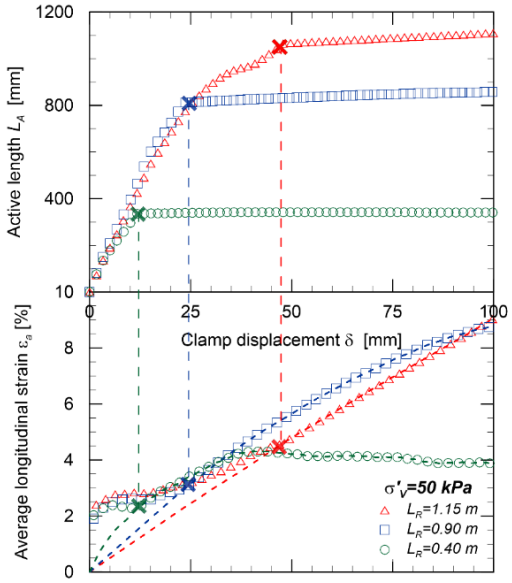


Fig. 8. Active length (upper graph) and average longitudinal strain (lower graph) versus clamp displacement for a normal effective stress of 50 kPa and varying the specimen length [18].

To investigate the deformation behaviour of interfaces subjected to sustained pullout loads over time (confined creep), Cardile et al. [26] conducted long-term pullout tests using two long-term twin apparatuses on the same geogrid and compacted soil specimens under identical vertical effective stress conditions. The difference between the two tests lies in the level of applied tensile load, which was set at 50% and 70% of the peak pullout resistance obtained from conventional pullout tests, respectively.

Displacement data recorded at various points along the geogrid were used to calculate the total tensile strains. By normalizing these values with respect to the cumulative strain measured at the first hour, the graph in Figure 9 was obtained, where $\varepsilon_{H\text{-}B1,conf}$ are the strains calculated along the geogrid portion closest to the clamp, and $\varepsilon_{in\text{-}air}$ are strains obtained from in-air tensile creep tests conducted at the same load level. The results indicate that the strains accumulating due to the application of a sustained load are lower in the case of the confined test due to the soil confinement effect. Furthermore, data analysis reveals that initially (during the first 20 hours), the two curves exhibit a similar gradient. However, after reaching the 20-hour mark, the $\varepsilon_{H\text{-}B1,conf}$ strains show a lower gradient for the whole test duration. If this trend persists, the time required to reach potential creep rupture under pullout conditions would be significantly longer than the time recorded in conventional creep tests. This suggests that the creep reduction factor extrapolated at the design working life through accelerated laboratory

tests [31]—commonly used to reduce the geosynthetic tensile strength in current design practice—could be overly conservative.

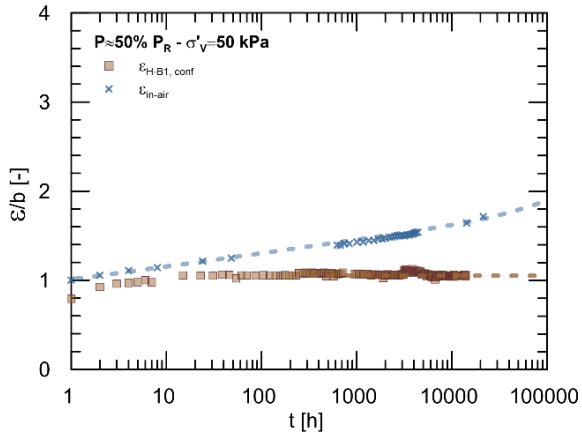


Fig. 9. Comparison between normalized values of $\varepsilon_{H\text{-}B1,conf}$ strains and those obtained by in-air tensile creep tests carried out at same load level (50% P_R) [26].

2.3 The cyclic interface strength

Regarding soil-geosynthetic interaction under cyclic and post-cyclic pullout conditions, several studies have been conducted [32-39].
Moraci and Cardile [40, 41], and Cardile et al. [42] proposed a multi-stage testing procedure to evaluate geosynthetic pullout behaviour under cyclic and post-cyclic loading conditions. This procedure consists of three distinct stages:

- a displacement-controlled stage at a constant rate of displacement (CRD) equal to 1 mm/min, reaching a fixed pullout load P_i;
- a load-controlled cyclic stage using a sinusoidal function, with a fixed tensile loading amplitude A and frequency f = 1 Hz, for N = 1000 cycles in total;
- a post-cyclic stage, which is another displacement-controlled stage at CRD = 1 mm/min, continued until a maximum horizontal displacement equal to 100 mm, full pullout of the specimen, or its rupture occurs.

These studies [40-44] enabled the assessment of the effects of cyclic pullout loads on the interface behaviour. The comparison between the pullout curves from monotonic and multi-stage tests showed that, for geogrids embedded in well-compacted granular soils, the applied cyclic loading history can lead to a reduction in post-cyclic pullout resistance (Figure 10). Specifically, depending mainly on the applied cyclic load amplitude and the acting confinement stress, a decrease in post-cyclic peak pullout resistance was observed, ranging from 10% to 33%. The most significant reductions were recorded at lower confinement stresses and higher investigated cyclic tensile load amplitudes.

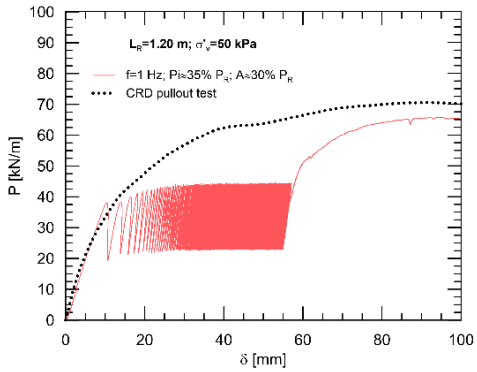


Fig. 10. Comparison between load-displacement trends obtained in CRD and multistage conditions for tests with $\sigma'_v = 50$ kPa, at $A \approx 30\% P_R$ [42].

The deformation behaviour of the reinforcement specimen during the cyclic phase was analyzed [41-43] using the double graphs shown in Figure 11. These graphs illustrate the results of multi-stage (MS) pullout tests conducted at the same vertical effective stress ($\sigma'_v = 50$ kPa) and $P_i \approx 35\%$ P_R, but with two different loading amplitudes ($A \approx 30\%$ P_R; $A \approx 45\%$ P_R). These graphs examine the influence of cyclic load amplitude and confining stress for a fixed frequency.

In the upper section of each graph, the number of cycles (N) is plotted against the cumulative displacement ($\Delta\delta^h$) measured at the geogrid's head during the cyclic phase. A stable behaviour is characterized by a curve that is markedly concave upward, where the cyclic displacement increments decrease as the number of cycles increases. Conversely, the soil–geogrid interface exhibits cyclic instability when the cyclic displacement increments become constant or start increasing with the number of cycles. In the latter case, the N-$\Delta\delta^h$ curve develops an inflection point, becoming concave downward; that is, the accumulation rate of displacement increases with N, potentially leading to reinforcement failure due to insufficient interaction resistance between the soil and the reinforcement under pullout conditions. In the lower section of each graph, the cumulative cyclic displacement of the specimen's rear end, $\Delta\delta^e$, is plotted against $\Delta\delta^h$. These data provide further insights into the onset of critical pullout failure in the soil–geogrid interface during the cyclic phase.

With regard to the influence of loading amplitude A, when $A \approx 30\%$ P_R, the soil-reinforcement interface exhibits stable behaviour throughout the cyclic stage, as $\Delta\delta^h$ tends to stabilize towards a constant value with an increasing number of cycles (Figure 11a). The same conclusion can be drawn from Figure 11b, where the cyclic displacement increment measured at the rear end is consistently lower than the cyclic displacement increment of the geogrid's head. Conversely, for $A \approx 45\%$ P_R, an unstable behaviour is observed. In this case, an inflection point appears, and $\Delta\delta^h$ continues to increase as the number of cycles increases. The instability is also evident in the bottom graph, as the $\Delta\delta^e$–$\Delta\delta^h$ curve becomes parallel to the boundary line between the admissible and inadmissible areas, which defines the pullout failure condition ($\Delta\delta^e_{part} = \Delta\delta^h_{part}$). This confirms that the stability of the soil–geogrid interface progressively worsens as the cyclic loading amplitude increases.

To evaluate the influence of the vertical effective stress (σ'_v) applied to the soil-geogrid interface, Figures 11c and 11d show that a stable response is obtained only for σ'_v=100 kPa. For all other applied vertical effective stress levels, the cumulative cyclic displacement of the specimen's head keeps on increasing with N and the $\Delta\delta^e$-$\Delta\delta^h$ curves become parallel to the boundary line that separates the admissible and inadmissible regions. This indicates that an increase in vertical effective stress exerts a stabilizing effect on the interface behaviour.

The reduction in interface parameters under cyclic loading can be analyzed using the P–ε/δ–ε double graph, which relates the displacement of the first confined section (δ) to the pullout average strain (ε) for a given pullout load P and vertical effective stress (Fig. 12).
A key observation from point 5 vs. point 1 in Figure 12b is that cyclic loading leads to both higher geogrid deformation (due to its viscous effects under a quasi-constant average load) and greater head displacement, with the MS δ–ε slope increasing as the cyclic loading amplitude rises. This implies that at the start of the third MS phase (point 5), internal geogrid displacements are greater than those mobilized at the same pullout load level P_i in the monotonic test. Figure 12c (square c-1) qualitatively illustrates that lower vertical effective stress results in greater displacements, pushing the interface closer to pullout failure compared to static loading.

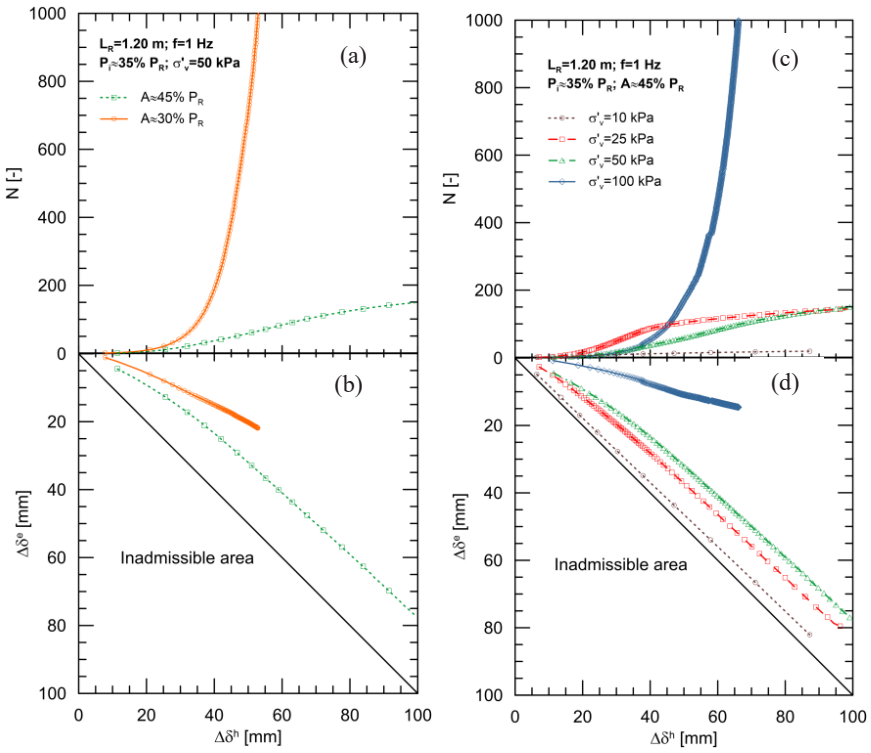


Fig. 11. Number of loading cycles versus cumulative cyclic displacement measured at the first confined section of specimen (a),(c) and $\Delta\delta^h$ versus cumulative cyclic displacement measured at the rear end of the specimen (b),(d) [42].

During the third stage, the MS δ–ε curve initially follows a trend similar to the CRD δ–ε curve at the same strain level (point 5 vs. point 2, Figure 12b), as both are now displacement-controlled tests. The CRD δ–ε curve appears shifted downward (path 5-7) by an amount $\delta_{2\text{-}5}$, corresponding to the difference between cyclic ($\delta_{1\text{-}5}$) and static ($\delta_{1\text{-}2}$) displacements at the same strain level. Despite this, the interface still attempts to mobilize the same pullout strength as in the static case (no intrinsic reinforcement degradation), showing hardening behaviour (path 5-6b with greater incremental pullout stiffness than path 2-4, Figure 12a).

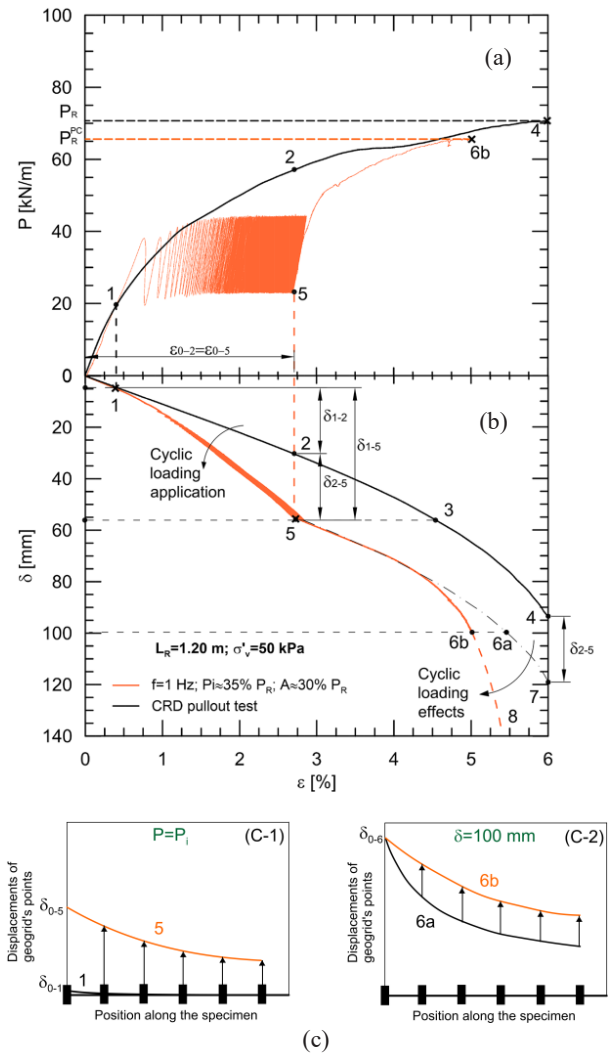


Fig. 12. Comparison between P–ε (a) and δ–ε (b) trends obtained in CRD and multistage conditions for tests with $\sigma'_v = 50$ kPa, at $A \approx 30\%$ P_R, and qualitative distribution of the geogrid's points displacements at the same pullout load level P_i for CRD test and MS test at N=1000 (c-1) and at $\delta = 100$ mm for MS test following the "ideal" or the real path (c-2) [44].

However, cyclic loading accelerates the use of the geogrid portion that resists the applied load, bringing the interface closer to pullout failure compared to monotonic loading. If interaction mechanisms had not progressed further, the MS δ–ε curve would have ideally followed the dashed path 5-7 in Figure 12b, meaning the difference $\delta_{2\text{-}5}$ would remain constant. However, the actual curve deviates from this ideal path due to cyclic loading effects, which degrade the interface, reducing geogrid deformation at a given head displacement and mobilizing lower pullout strength. These effects are further evident when considering the displacement distribution of internal geogrid points at $\delta = 100$ mm (Figure 12c, square c-2). The displacements at point 6b exceed those at point 6a, confirming that cyclic loading accelerates the pullout process, leading the geogrid to reach its limit state earlier. Smaller internal displacements indicate a more ideal δ–ε trend.

In summary, reaching the pullout average strain corresponding to peak pullout resistance (P_R) obtained under static conditions is theoretically possible—unless pullout failure occurs first. This can be visualized by extending the MS δ–ε curve (dashed line, Figure 12b), where achieving P_R requires a greater head displacement than in static conditions.

2.4 The use of interface strength in practice

The interface parameter used for designing reinforced soil walls and steep slopes is the apparent coefficient of friction mobilized at peak, $\mu^P_{S/GSY}$, defined in Eq. (2) of §2.2. This parameter allows for determining the reinforcement length in the anchorage zone and, consequently, the size of the reinforced soil block. As shown in Figure 13, a significant reduction in $\mu^P_{S/GSY}$ can be observed for both long and short reinforcement specimens when transitioning from low to high confinement stresses. These results confirm previous observations on the influence of soil dilatancy and, to a lesser extent, reinforcement extensibility on soil-geosynthetic interaction. From a practical perspective, this finding highlights the importance of considering $\mu^P_{S/GSY}$ values that vary with the effective normal stress acting at a given depth when designing reinforced soil retaining structures. In practical terms, this implies adopting different $\mu^P_{S/GSY}$ values for each reinforcement level within the structure.

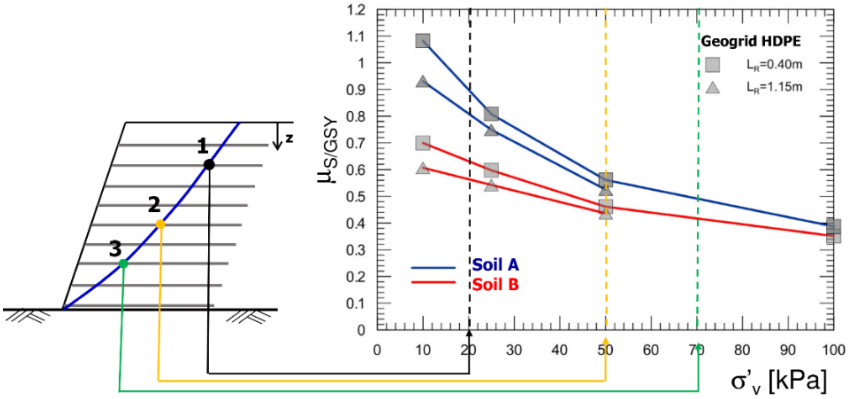


Fig. 13. Peak apparent coefficient of friction at interface versus applied effective vertical stress for different reinforcement lengths and soil types: Soil A=uniform medium sand; Soil B=gravel with silty sand [45].

In current design practice, even under cyclic/seismic conditions, the interface parameters are typically derived from monotonic pullout tests. However, as discussed in §2.3, under cyclic tensile loads, the pullout behaviour is influenced by the frequency, amplitude, and number of cycles of the cyclic loading history, as well as the pre-existing static tensile load acting on the geosynthetic at the onset of cyclic loading.
In the MS pullout tests conducted by Cardile et al. [42], a reduction of up to 30% in the post-cyclic apparent friction coefficient was observed compared to values obtained in monotonic pullout tests (Figure 14). For a given A, this reduction is more pronounced at lower vertical effective stresses (becoming negligible at higher σ'_v values) and increases with the amplitude of cyclic loading. The decrease in interface parameters appears to be related to the progressive transfer of interaction mechanisms along the specimen during the cyclic phase, which may lead to premature pullout occurring within this stage. As a result, during the post-cyclic phase, the available resistance at the interface is depleted.

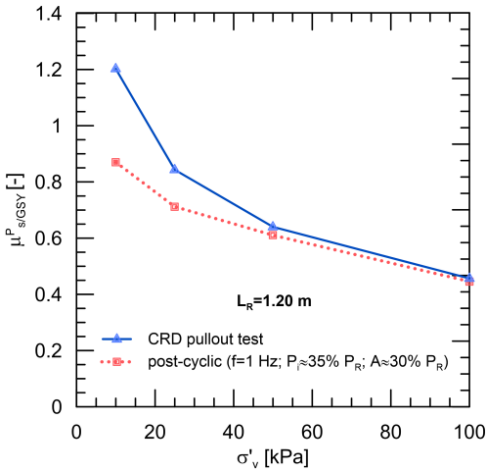


Fig. 14. Normalised post-cyclic peak pullout resistance (a) and peak apparent coefficient of friction (b) for varying vertical effective stress, considering CRD and multi-stage tests at A ≈ 30% P_R [44].

These effects should be carefully considered when designing geosynthetic-reinforced soil (GRS) structures in seismic areas, appropriately reducing the interface parameters typically obtained from CRD pullout tests. This is particularly important because the reduction in interface strength mainly affects the shallow reinforcement layers, which are the most susceptible to the pullout limit state.

Given that creep and relaxation phenomena influence the geosynthetic deformation over time, it is essential to assess the extent to which the apparent coefficient of friction mobilized at the interface should be reduced to account for these effects. To achieve this, the equation (2) should not use the maximum pullout resistance per unit width obtained from conventional pullout tests, but rather the sustained pullout load obtained from long-term pullout tests, such as those conducted in [26].

To examine the impact of viscous behaviour at the interface under serviceability conditions, Cardile et al. [26] developed isochronous curves in the $\mu_{s/GSY}$-ε_{conf} plane, where ε_{conf} represents the strains measured along the section of the geogrid closest to the clamp (i.e., the most stressed portion, extending from the first confined section to the first transverse bar). The isochronous curves were generated based on values of $\mu_{s/GSY}$ derived from two levels of sustained loading obtained experimentally (P = 50% P_R and 70% P_R). For each case, the corresponding strains ε_{conf} were determined at specific time intervals (t = 1 h, 10 h, 100 h, 1000 h, 10000 h). The data pairs ($\mu_{s/GSY}$-ε_{conf}) were then processed using curve-fitting techniques, resulting in the isochronous trends illustrated in Figure 15. As observed in the figure, the relationship between $\mu_{s/GSY}$ and ε_{conf} is generally linear, provided that no local rupture phenomena or tertiary creep occurs.

As expected, the results indicate that reinforcement strains in the anchorage zone progressively increase over time as $\mu_{s/GSY}$ is mobilized to maintain structural stability. This trend is observed at all reinforcement levels, corresponding to different vertical effective stresses. Since tensile strains continue to develop, it is important to evaluate whether the final strain value, reached at the end of the design working life, remains within acceptable serviceability limits. Additionally, when moving between successive time intervals in a logarithmic scale, a progressive reduction in cumulative strain increments is observed for a given coefficient of friction, except for the t = 10000 h isochrone. At this point, a deviation from the expected trend is noticeable, which may be attributed to the onset of tertiary creep.

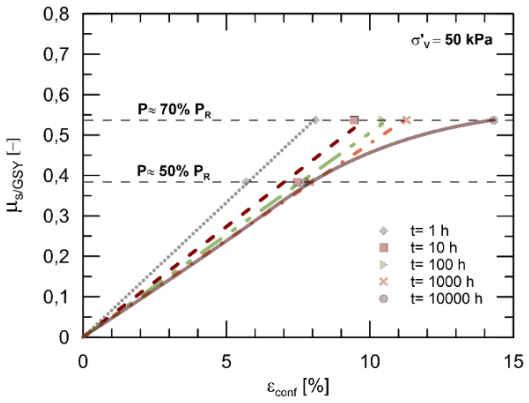


Fig. 15. Isochronous interaction curves under long-term pullout conditions [27].

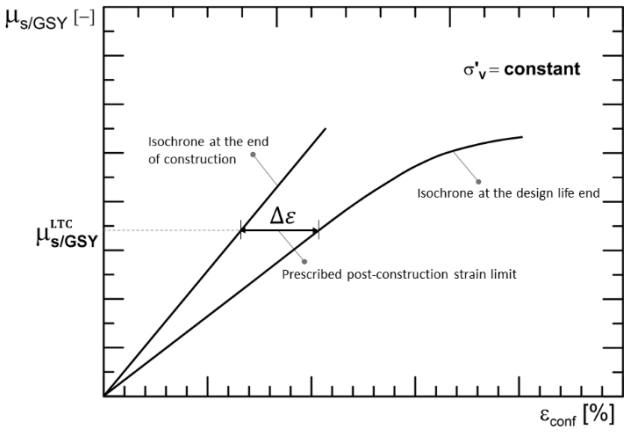


Fig. 16. Long-term apparent coefficient of friction assessed at a prescribed limiting value of post-construction strain in reinforcement by using isochronous curves [27].

Developing isochronous curves corresponding to different vertical effective stresses could provide a valuable tool for structural design, allowing engineers to select an appropriate apparent coefficient of friction that accounts for the long-term behaviour of geosynthetics. When using design approaches based on the ultimate limit state [46], the $\mu_{s/GSY}$ value can be determined using the $\mu_{s/GSY}$-ε_{conf} isochronous curves, thereby integrating serviceability limit state considerations into the design process. Specifically, as illustrated in Figure 16, the proposed design procedure involves:

- Selecting the isochronous $\mu_{s/GSY}$-ε_{conf} graph corresponding to the given vertical effective stress;
- Identifying a horizontal segment on the graph that represents the allowable strain for the specific structure to be designed;
- Determining the long-term creep apparent coefficient of friction ($\mu^{LTC}{}_{s/GSY}$) as the vertical coordinate of the intersection point between the horizontal segment and the isochronous curves for the strain at the end of the design working life and the strain at the end of construction.

The allowable strain can be estimated through numerical analysis and/or full-scale measurements, correlating the strain in the most stressed reinforcement segment with the actual deformation of the structure (e.g., horizontal displacement of a GRS wall facing). This

process enables the determination of threshold strain values, ensuring that commonly used ultimate limit state design methods (e.g., Limit Equilibrium Design) also account for serviceability requirements.

3 Geosynthetic/geosynthetic or soil/geosynthetic interface strength in landfill cover system

In landfill cover barriers, geosynthetics can carry out different and simultaneous geotechnical functions, such as: drainage of the ascending biogas, drainage of the descending rainwater, waste waterproofing, cover reinforcing and soil erosion preventing.

Drainage of the rainwater may be guaranteed by a drainage geocomposite which is made of a geotextile in contact with the soil to be drained and a geospacer for collecting and channel rainwater. The geotextile should be provided of appropriate filter opening to prevent blinding and clogging, both unwanted phenomena capable of invalidating the long-term drainage of the cover soil. The geospacer should have an appropriate discharge capacity to avoid the growth of water table inside the above soil and the subsequent collapse of the cover itself.

Waterproofing for both rainwater and biogas emissions is achieved with the help of a geomembrane, possibly coupled with an underlying geocomposite clay liner if it is not possible to install a clay barrier of adequate thickness. A geonet may be placed over the geomembrane with the aim of avoiding lacerations and perforations during the subsequent phase of laying the drainage geocomposite.

In order to allow drainage of the ascending biogas, another geocomposite drainage may be provided beneath the waterproofing barrier.

If the cover lies on a slope and/or in areas where differential settlements are expected, some geogrids inserted into the cover package allow to increase the cover strength to slippage and to relieve any tensile forces in the less resistant geosynthetics.

Geocell or geomat can be placed to prevent the soil erosion exposed to atmospheric agents and also to allow for natural greening or hydro-seeding.

A typical succession of geosynthetics in landfill covers is shown in Figure 17, from a qualitative point of view. These geosynthetics offer continuous and/or discontinuous contact surfaces which work at low contact stress and low friction. The most critical interfaces, characterized by low friction, are: geotextile-soil (GTX-Soil), geotextile-geonet (GTX-GNT), geotextile-geomembrane (GTX-GMB), geonet-geomembrane (GNT-GMB), geomembrane-geocomposite clay liner (GMB-GCL) and geocomposite clay liner-geotextile (GCL-GTX). It is, therefore, necessary to characterize the interface strength of these contacts for the right design of the reinforcement geogrids and of the anchoring trenches.

The main purpose of this chapter is to summarize the results of laboratory tests carried out on geosynthetic interfaces using two experimental equipment recently developed [47-49]. These instrumentations consist of an inclined plane device and a direct shear device at a constant loading rate. Both devices allow for the characterization of the geosynthetic interface friction under low contact stresses. Since these devices provide perfectly comparable results, they can be considered complementary and interchangeable, benefitting the test modalities that may be considered appropriate for the proper characterization of the geosynthetic interface strength. The results of these experiments confirm how the interface friction of a landfill cover is a crucial parameter for the stability of the cover itself. The main aspect is the kinematic mode of failure, a function of the types of geosynthetics placed in contact; also worthy of consideration is the state of wear of the contact surfaces, the presence or absence of interstitial fluid and, finally, the relative density of the granular soil in contact with the geosynthetic.

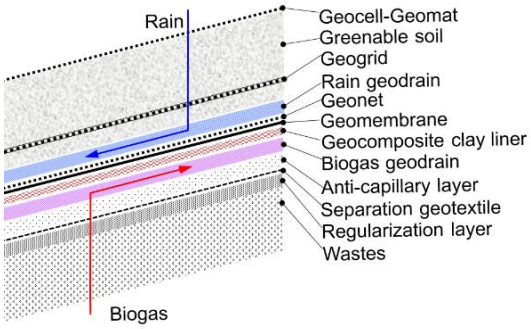


Fig. 17. Schematic representation of a geosynthetics succession in a sloping landfill cover.

3.1 Laboratory evaluation of geosynthetic interface strength

The interface geosynthetics strength can be evaluated in the laboratory with different types of test for different loading conditions: static, cyclic and seismic, as well as for low and high normal stresses.
Referring only to the low-contact stress case, the most widespread procedures in the technical literature are: the direct shear test at constant displacement speed, the direct shear test at constant load speed and the inclined plane test. Further study made use of large displacement devices such as the annular shear device, similar to the Bromhead apparatus for clay soils [50, 51], and the cylindrical shear apparatus [52] in which one interface element is wrapped around a cylinder subjected to rotation while the other element remains fixed.
Finally, as shown in §2, the pull-out test apparatus has also been used to study the ultimate interface strength developed along the upper and the lower sides of a geosynthetic in contact with soil.

3.2 The static interface strength

The standard direct shear test at constant displacement speed is perhaps the most widespread in the technical literature and has been the subject of standardization [53]. It is performed on the interface specimen with a minimum size of 0.30 × 0.30 m; one interface element remains fixed while the other can slide relative to the first. The mobile box slides during the test at constant normal pressure, σ_0, and constant displacement speed, while the shear stress, τ_0, is monitored with respect to the relative displacement. To identify the failure envelope, the tests are repeated for at least three values of the normal stress σ_0 (50 kPa, 100 kPa, and 150 kPa, following the European standard) and the shear strength parameters (adhesion, α, and slope envelope, φ_{tan}) are evaluated via linear interpolation of the results. In this regard, it should be noted [54-56] that the failure envelope of geosynthetic interfaces can be strongly curvilinear in the transition from low to high contact stresses (Fig. 18), so that the evaluation of the secant friction angles, φ_{sec}, instead of α and φ_{tan}, proves to be more in line with the actual performance of the cover package in which the maximum normal stress can be less than 50 kPa.
A prototype of a direct shear device working at constant speed of loading has been recently developed [48, 49]. Figure 19 shows the device's operational scheme. It consists of a mobile box, 0.30×0.30 m in sides, placed on a horizontal plane. One geosynthetic specimen is fixed on the base of the mobile box, while the other is fixed on the base of the device.
The box is connected, via a steel cable, to a counterweight and a load cell, placed between the box and the cable, allowing the horizontal force acting on the box to be measured during the test. The counterweight increases its load over time in such a way as to give a constant

loading speed at the interface until a maximum relative displacement of 50 mm is reached. Assuming that the horizontal load can be considered to be applied statically, i.e. for low values of the relative sliding speed of the interface, the mobilized friction angle can be evaluated as follows:

$$tan\varphi_{sec}(t) = \frac{H(t)}{W} \tag{4}$$

where the horizontal force at the box, *H(t)*, increases at a constant loading speed, while the weight of the box, *W*, remains constant during the test.

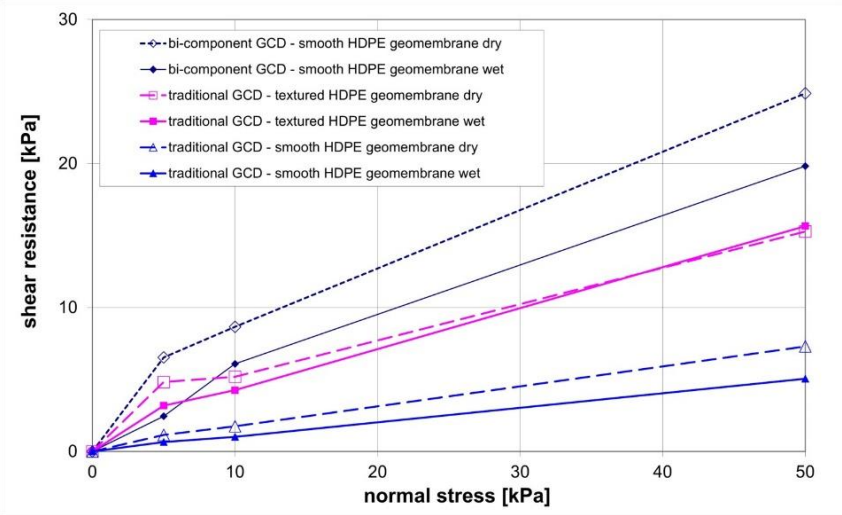


Fig. 18. Non linearity of geosynthetic interface envelops tested at low normal stress [56].

Referring to the differences with the standard direct shear test it should be noted that in the standard device the displacement occurs at a constant rate of about 1 mm/min, so that the mobilised interface strength could be erased at very low displacements. Conversely, at constant loading rate the mobilised shear stress increases gradually, allowing more accuracy in friction measurement as soon as the interface start to slide. This loading mode is analogous to what occurs in the inclined plane test and discussed below.

Another important difference between the standard direct shear test at constant displacement speed and the direct shear test at constant loading speed concerns the value of the minimum normal stress; due to how the stress is applied in the standard direct shear test, by using a hydraulic press, the minimum contact stresses that can be reached are roughly 20 kPa. Instead, the prototype direct shear device at a constant loading rate can perform tests at normal stresses as low as 5 kPa.

Figure 20 shows the result of a direct shear test at constant loading speed for an interface GMB_{smooth}-GCD made of a smooth geomembrane coupled with a drainage geocomposite [48], while the results of a similar test carried out for an interface $GMB_{textured}$-GCD made of a structured geomembrane coupled with a drainage geocomposite is shown in Figure 21 [49]. The first interface shows a slow mode of failure with a maximum speed of a few mm/s, whereas the second shows a fast one, where the maximum displacement speed may reach a value of about 60 mm/s. Although Equation (4) would no longer be valid in this second interface, it was noted that the static interpretation criterion may still be used since the interface strength is attained at a low level of displacement in both cases with a negligible kinematic effect.

A further possibility offered by direct shear tests, both standard and with a controlled loading rate, is the option to carry out the shear tests in the presence of fluid. This circumstance is not possible in the subsequent inclined plane test, where, at best, only wet conditions can be examined.

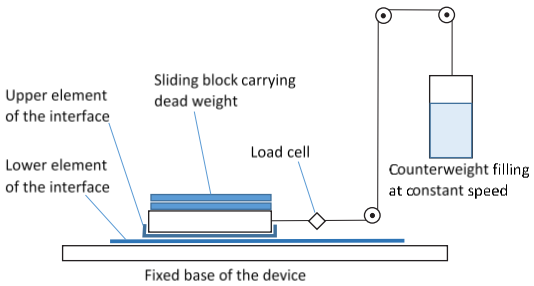


Fig. 19. Operational scheme of the direct shear device working at constant loading rate, made at the geotechnical laboratory of the University of Padua.

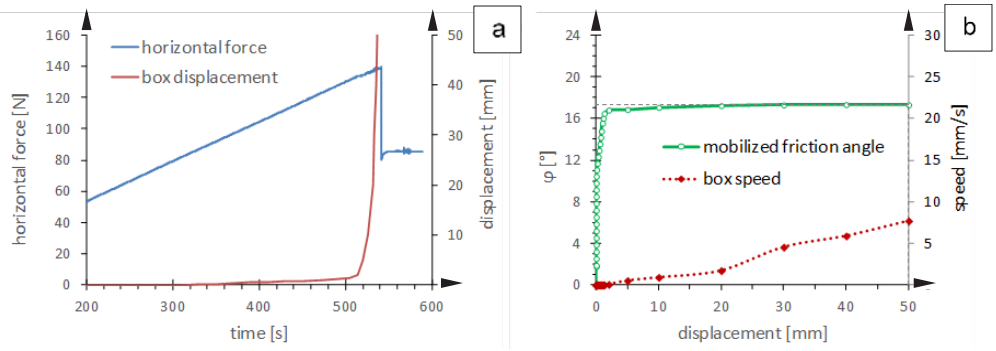


Fig. 20. Results of a direct shear test at constant loading speed for an interface made of a smooth geomembrane coupled with a drainage geocomposite GMB_{smooth}-GCD: a) evolution of the horizontal force and box displacements over time; (b) mobilized friction angle and block speed versus displacement.

The inclined plane test [57-60] has been standardized according to the European standard [61]. Strictly speaking, this standard refers only to interfaces between soil and geosynthetics, but its indications can also be easily extended to cases featuring contact between geosynthetics.

The equipment developed at the geotechnical laboratory of the University of Padua consists of a tilting plane, above which is a steel box that is free to slide along the plane. The box's motion can be controlled via lateral guides and trolleys positioned outside the contact zone of the geosynthetics. One geosynthetic of the interface is fixed on the inclined plane, while the other one is fixed to the bottom of the box. According to the European standard, the specimen to be tested should have a minimum dimension of 0.30 × 0.30 m, analogous to the standard for the direct shear test. The test starts from the horizontal position of the plane; then, the table inclination is gradually increased with a constant speed of 3 ± 0.5°/min.

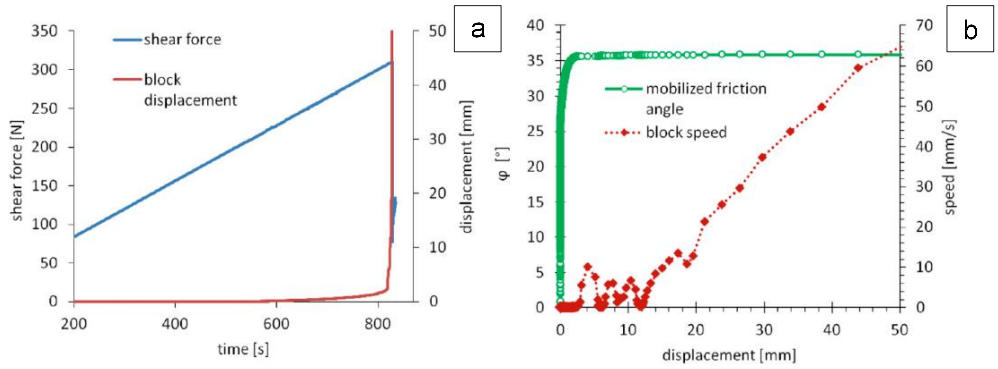


Fig. 21. Results of a direct shear test at constant speed of loading for a structured geomembrane coupled with a drainage geocomposite $GMB_{textured}$-GCD: a) evolution of the horizontal force and box displacements over time; b) mobilized friction angle and block speed versus displacements.

The plane inclination, β_{50}, for which the box reaches 50 mm in displacement, must be identified; under this condition, the interface strength angle, φ_{stand}, is evaluated with the following expression:

$$tan\varphi_{stand} = tan\beta_{50} \tag{5}$$

Although not expressly specified in the European standard, it is possible to define a first interface strength angle for a minimum reference displacement of the box, for example of 1 mm. Under this hypothesis, a first detachment friction angle, φ_0, may be defined when the plane inclination, β_0, allows the box to reach a displacement of 1 mm. Therefore, the first detachment friction angle is given by:

$$tan\varphi_0 = tan\beta_0 \tag{6}$$

It should be noted that the displacement of 50 mm actually constitutes an arbitrary reference since Equation (5) is based on the hypothesis that the box is in static equilibrium while it is moving with speed and acceleration that are not always negligible [62].
In this regard, various types of motion are possible, such as sudden sliding or gradual sliding. The sudden sliding mode is defined as that for which, once φ_0 is reached, the box goes forward with uniformly accelerated motion, and the friction strength becomes dynamic. It can be evaluated by means of the dynamic equilibrium equation, in which both the box accelerations, a, and the gravity, g, are included:

$$tan\varphi_{dyn} = tan\beta - \frac{1}{cos\beta} \times \frac{a}{g} \tag{7}$$

also, $\beta \geq \beta_0$
Therefore, within the European standard framework, the evaluation of the friction parameter through Equation (5) represents, in this circumstance, an index parameter, not a static nor a dynamic one; the latter can be obtained from Equation (7) if box acceleration is detected during the sliding phase.
The gradual sliding mode is defined as one in which, once φ_0 is reached, the box goes forward with uniform motion ($a_{box} = 0$), whose speed, v, becomes a function of the plane inclination, $\beta(t)$, when the latter exceeds the value β_0; in this case, a part of the friction associated to the box motion comes from the viscous strength component ($\tau = c \times v$). Under the hypothesis that the speed remains constant in correspondence with the table inclination $\beta(t)$, a kinematic strength angle, φ_{kin}, is provided by the following expression:

$$tan\varphi_{kin}(\beta) = tan\beta \tag{8}$$

being $\beta \geq \beta_0$.
This kinematic strength angle may be greater than φ_0 because part of the mobilised strength is given by a viscous mechanism.
In addition to the European standard test, the inclined plane device allows for the evaluation of the interface friction by means of a further procedure, namely the force method [63].

This test method is not standardized and can be performed at the end of the standard test [60]: at the end of the slide phase along the plane, the block is held by a cable, parallel to the plane, and the constraint force (F), exerted by the cable, is measured using a load cell. From the static balance of forces, it is possible to evaluate a new parameter, defined as the limiting friction angle, φ_{lim}, given by the following expression:

$$tan\varphi_{lim} = tan\beta - \frac{F(\beta)}{Wcos\beta} \tag{9}$$

where W is the weight of the box.
Even if the inclination of the plane continues to vary, the constraint reaction exerted by the cable changes in such a way that φ_{lim} remains constant, thus allowing another measure of the interface friction in the absence of block motion, whether accelerated or uniform. The parameter φ_{lim} is less than φ_0 both in the gradual and sudden sliding modes of failure. The complete procedure for measuring all the geosynthetic interface strengths with the inclined plane test is summarised in Figure 22.

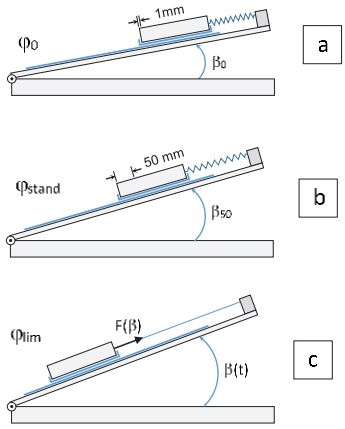


Fig. 22. Complete procedure for measuring geosynthetic interface strength with the inclined plane test: a) friction angle at detachment, φ_0; b) standard friction angle, φ_{stand}; c) force method for measuring the limit angle, $\varphi_{lim.}$

Figure 23 [64] proposes two typical interface behaviours to illustrate the diversity with which friction is mobilized between geosynthetics during inclined plane tests.
The first case (Fig. 23a) reflects the behaviour of an interface between a rough geomembrane coupled with a drainage geocomposite ($GMB_{textured}$-GCD) which shows a *sudden sliding mode of failure*: φ_0 is reached for minimal displacements, less than one millimetre, after which the almost instantaneous slippage of the box occurs under constant acceleration: in this case, $\beta_0 \cong \beta_{50}$. Still following the static approach outlined by equations (5) and (6), it is deduced that $\varphi_0 \cong \varphi_{stand}$.
Conversely, Figure 23b shows the behaviour of a geosynthetic interface between a smooth geomembrane coupled with the same drainage geocomposite of the previous case (GMB_{smooth}-GCD): a succession of kinematic equilibria is established until the conventional

failure inclination, β_{50}, with movements progressively increasing in speed as long as β increases beyond β_0: in this case, $\beta_0 < \beta_{50}$. Still following the static approach outlined by equations (5) and (6), it is deduced that $\varphi_0 < \varphi_{stand}$. For this second interface, which can be classified in the *gradual sliding mode of failure*, the conventional angle of interface strength, φ_{stand}, may include a viscous strength component proportional to the sliding speed, whereas φ_0 is not affected by viscous resistance to motion.
For example, a rough geomembrane in contact with the nonwoven geotextile of a drainage geocomposite can give rise to considerable displacements, even well beyond β_{50}, due to the effect of the interpenetration of the geotextile fibres within the roughness of the geomembrane. Interfaces of particular polymers and geometries can manifest *non-uniform motion* during sliding, as in the case of the stick-slip mode of failure. It is a kinematic phenomenon characterized by sudden accelerations and stops when the abrupt transition from static to dynamic friction occurs. The resulting motion alternates stick and slip phases, which do not allow for a clear failure point to be identified.
In both the *gradual sliding mode of failure* and the *non-uniform motion sliding*, φ_{stand} has to be considered a convenient parameter rather than an effective design parameter, useful for difficult geosynthetic interfaces.

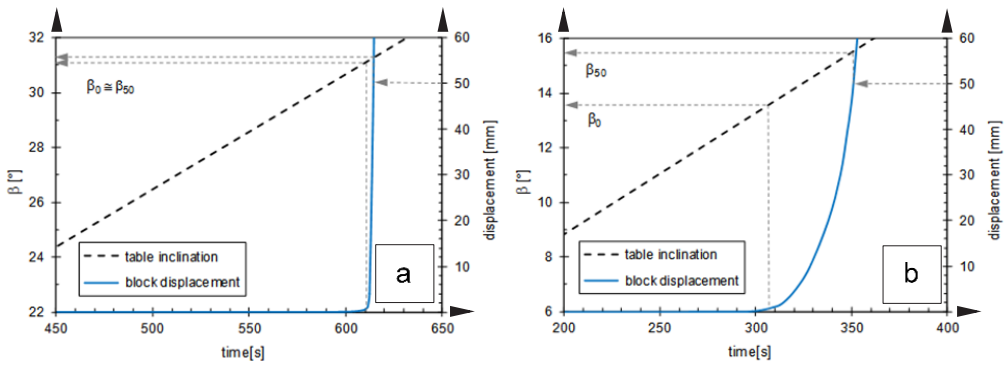


Fig. 23. Two different HDPE geomembranes in contact with a nonwoven geotextile under dry conditions: a) the interface $GMB_{textured}$-GCD shows a sudden sliding behaviour; b) the GMB_{smooth}-GCD interface shows a gradual sliding behaviour.

For both interface failure modes—gradual sliding and sudden sliding—the limit friction angle, φlim, provides the most conservative parameter of those obtainable with the inclined plane test since the viscous strength component becomes zero and the detachment friction, φo, has already been reached. The inclined plane tests also allow experiments on the degradation of the interface friction between geosynthetics as the relative sliding varies [60, 65].
Figure 24 [65] reports the results of large displacement inclined plane tests relating to an interface between a draining geocomposite and a woven bentonite geocomposite (GCD-GCL), with gradual sliding behaviour in both the wet and the dry conditions. It is possible to note how the presence of fluid at the interface determines a lower frictional resistance and how the parameter φ_{lim} is always lower than φ_o, and φ_{stand}, in both dry and wet conditions.

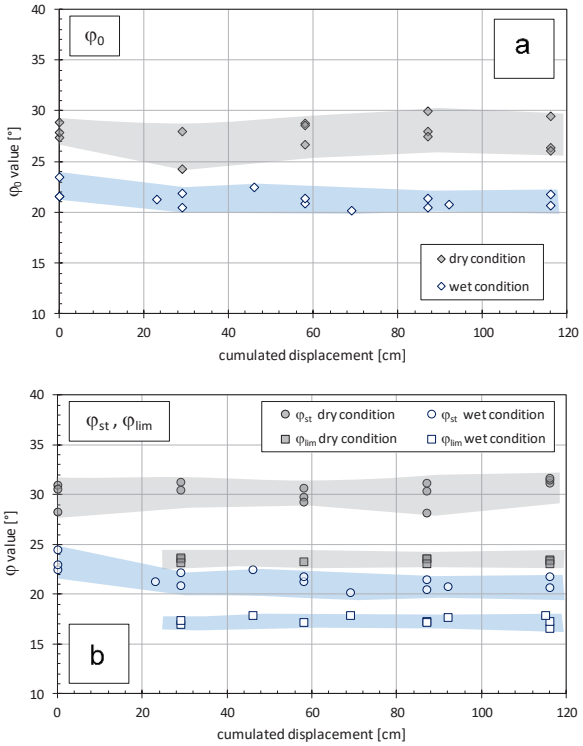


Fig. 24. Friction variation versus cumulative displacements for a GCD-GCL interface: a) ranges of φ_0 values for both dry and wet conditions; b) ranges of φ_{stand} and φ_{lim} for both dry and wet conditions.

3.3 The seismic interface strength

In addition to evaluating static interface strength, there is a whole area related to dynamic conditions, such as those that can occur in seismic situations, which can be studied by means of the shaking table device, the dynamic direct shear test and the inclined plane test.
The most common tests are carried out by means of the shaking table device; the table carries one of the geosynthetics of the interface, while the other is bound to a free-sliding block resting over the table. The case of an interface placed on a horizontal plane and subjected to regular cyclical loadings and/or replicas of real seismic events has been studied by many authors [60, 66-71], as well as experiments with dynamic direct shear devices [68, 72-75].
Other studies have analysed a sliding block resting over an inclined plane, connected to the shaking table and subjected to a horizontal dynamic loading [47, 76-78]. The basic approach for interpreting this test is based on Newmark's sliding block [79]; during table motion, with horizontal acceleration a_g, the block moves in tandem with the table until its acceleration does not exceed the critical acceleration a_{crit}:

$$\frac{a_{crit}}{g} = \tan(\varphi_0 - \beta) \tag{10}$$

When a_g exceeds the critical acceleration, the block slides downwards, and the dynamic interface friction may be evaluated as follows:

$$tan\varphi_{dyn} = \frac{sen\beta + \left(\frac{a_g - a_{crit}}{g}\right)cos\beta}{cos\beta - \left(\frac{a_g - a_{crit}}{g}\right)sen\beta} \tag{11}$$

Lastly, dynamic friction was also measured by means of free sliding tests on the inclined plane for inclinations equal to or greater than β_0 [47, 60], by monitoring the kinematics of the block while it slides with both uniformly accelerated or uniform motions, according to equations (7) and (8).

Figure 25 [47] reports the relationship between interface friction and slip speed for two interfaces (one of the sudden sliding type and the other of the gradual sliding type) in dry conditions. The interface of Figure 25a, refers to a nonwoven geotextile in contact with a textured geomembrane (GTX2-$GMB_{textured}$), while the interface of Figure 25b, refers to another nonwoven geotextile in contact with a smooth geomembrane (GTX1-GMB_{smooth}). To establish such a relationship, free sliding and vibrating table tests have been carried out using the inclined plane.

Looking at Figure 25 we note how in the sudden sliding type of interface, the dynamic friction is lower or close to the static friction of the first detachment, the latter available at zero sliding speed, while in the gradual sliding type interface, the dynamic friction is generally higher than the first detachment friction due to a non-negligible contribution of the viscous resistance, which is more influential as the relative sliding speed increases.

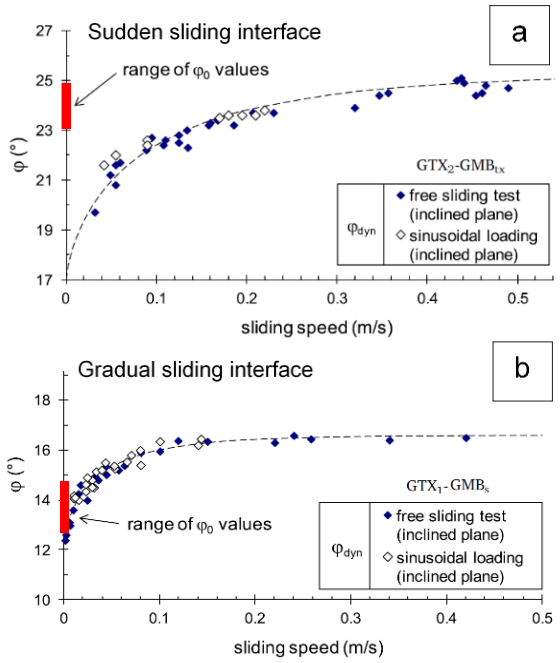


Fig. 25. Dynamic friction expressed as a function of the relative sliding velocity for two geomembranes in contact with two nonwoven geotextiles: a) interface showing sudden sliding behaviour; (b) interface showing gradual sliding behaviour.

3.4 The use of interface strength in practice

Based on the discussed data, it can be inferred that the correct characterization of the interface strength between the geosynthetics employed in a landfill cover can be achieved using laboratory equipment at low contact stresses, such as the inclined plane and the direct shear at a constant loading rate. With such equipment, it is possible to observe the interface failure modes (i.e. sudden sliding, gradual sliding and non-uniform sliding) to establish which is the

most suitable shear strength angle between φ_0, φ_{stand}, φ_{lim}, φ_{kin} and φ_{dyn}, in order to guarantee the level of safety with respect to the slipping risk on the slope and to the tear due to the differential settlements that may occur in different areas of the plant (Table 1).
Similar recommendations can also be extended to the case of seismic loading for predicting post-seismic displacements of the cover and/or tensile force induced in the geosynthetics by the displacements themselves.
Given the low level of contact stresses, it is emphasized that the design parameter of interface resistance should be more accurately represented by the secant value rather than the tangent ones, which are usually supplied by the standard direct shear test.
Finally, the standard methodology for establishing interface failure, φ_{stand}, may be acceptable when the kinematic behaviour is *non-uniform*; conversely, interface failure showing both uniform and uniformly accelerated motions should be characterized by the angles φ_0 or φ_{lim}, depending on the level of safety to be achieved.

Table 1. The use of interface strength in practice

TYPE OF FAILURE		
Sudden sliding Failure mode showing uniformly accelerated motion	**Gradual sliding** Failure mode showing uniform motion	**Non-uniform sliding** Failure mode showing non-uniform motion, such as in the case of stick slip mode
$\varphi_0 \cong \varphi_{stand}$ $\varphi_{lim} < \varphi_0$ $\varphi_{dyn} \leq \varphi_0$	$\varphi_0 < \varphi_{stand}$ $\varphi_{lim} < \varphi_0$ $\varphi_{kin} \geq \varphi_0$ $\varphi_{dyn} \geq \varphi_0$	$\varphi = \varphi_{stand}$
Behavior unfavorable to stability in seismic conditions	Stable behavior under seismic conditions	Stable behavior under seismic conditions

4 Soil–geotextile interaction in filtering systems

Internal erosion or piping in soils represents a serious problem in geotechnical and environmental structures. To control seepage and to avoid internal erosion of base soil, granular or geotextile filters are used. In filtering systems, the boundary conditions (flow conditions, effective stresses, continuity of contact between filter and base soil etc.) can be very different.

Geotextile filters are usually designed according to two criteria that appear to be in disagreement: the retention and permeability criteria.

According to the retention criterion, the main function of a geotextile filter is to prevent the movement of fine particles from the base soil, avoiding soil erosion, whereas, to meet the permeability criterion, the geotextile must have a long-term high permeability to guarantee the required flow-rate and avoid the development of excessive pore water pressure at the base soil and geotextile filter interface.

Therefore, to meet the retention and permeability criteria, the porometry and geotextile filter openings must be less or greater than certain limits.

If the geotextile filter is not correctly designed, different limit states can occur. In particular, the main limit states of the filtering systems, which can lead to the inefficiency of the drainage system or to the failure of the structure, are base soil erosion (piping), geotextile filter blinding and/or clogging, and geotextile filter flapping.

The design of a suitable filter requires the knowledge of the interaction between base soil and geotextile filter, which is a very complex phenomenon due to the large number of factors involved (Fig. 26). In particular, the selection of an appropriate geotextile filter depends on

the design and boundary conditions, on the geotechnical characteristics of the base soil and on the criticality/severity of application.

The factors related to cohesionless soil that can affect soil-geotextile filter interaction are relative density (DR), grain size distribution (GSD), internal stability and permeability. In some applications, such as bank revetments and landfill cover systems, the shear strength and deformability of the base soil must also be considered.

Regarding geotextile properties, the filter design criteria are generally based on geotextile filtration opening size (O_F), pore size distribution (PSD) and geotextile permeability (k_{ng}) or permittivity (Ψ_g). Depending on field application, the geotextile can be subjected to compression, tension, shear and impregnation (λ) due to placement and base soil compaction, which can modify the geotextile thickness and porosity, producing a variation in filtration opening size (O_F^*) and permeability (k_{ng}'). For this reason, other properties such as geotextile thickness, porosity, compressibility, tensile strength, deformability and durability are also involved in the design.

The factors related to boundary conditions are spreading and base soil compaction, flow conditions, hydraulic gradient, continuity of the contact at the base soil-filter interface, effective and shear stress at the soil-filter interface and type of permeant.

Typical applications of one-way flow conditions are earth dams, embankments, retaining walls, landfills, shallow foundations, drainage trenches and vertical and horizontal drainages. Whereas, typical applications under reversing flow conditions are bank revetments, separation and reinforcing layers in submerged or submersible foundations, offshore foundations, scour protections and pipeline protections.

Another boundary condition is the continuity of soil-filter contact at the interface. It depends on construction procedures, density of base soil and stiffness of geotextile filter.

Finally, the filter design should consider the application's criticality and severity. As shown in Figure 26, the criticality of a filter application depends on the risk of failure and/or the consequences in case of filter failure, the possibility of accessing it for maintenance or replacement and the signs of rupture before potential failure. The application can be considered critical when the risk of failure or the consequences in case of filter failure are high and/or when the repair costs are much higher than the installation costs and/or when there is no evidence of the inception of limit states before potential failure. The application can be considered less critical when there is no risk of failure, when the repair costs are equal to or less than the installation costs and when the inception of limit states before potential failure is evident. The severity of a filter application depends on the internal stability of the base soil, the hydraulic gradient and flow conditions. The application can be considered severe for internally unstable base soils (or internally stable soils with a high fine fraction) and/or in the presence of high hydraulic gradients and/or in reversing flow conditions (dynamic, cyclic, or pulsating).

Several researchers studied the factors affecting the design of geotextile filters and indicated the precautions to be taken in each case [80-87].

However, many studies indicate that the internal stability of cohesionless base soils needs further investigation.

The authors were engaged in this aspect for years, developing reliable methods for evaluating the internal stability of cohesionless base soils, equipment capable of analysing the geotextile filter-base soil compatibility by means of long-term performance tests under severe conditions to quantify the occurrence of different limit states, and an innovative design methodology based on a geometrical, experimental and micro-structural approach. The following sections are related to the description of these aspects.

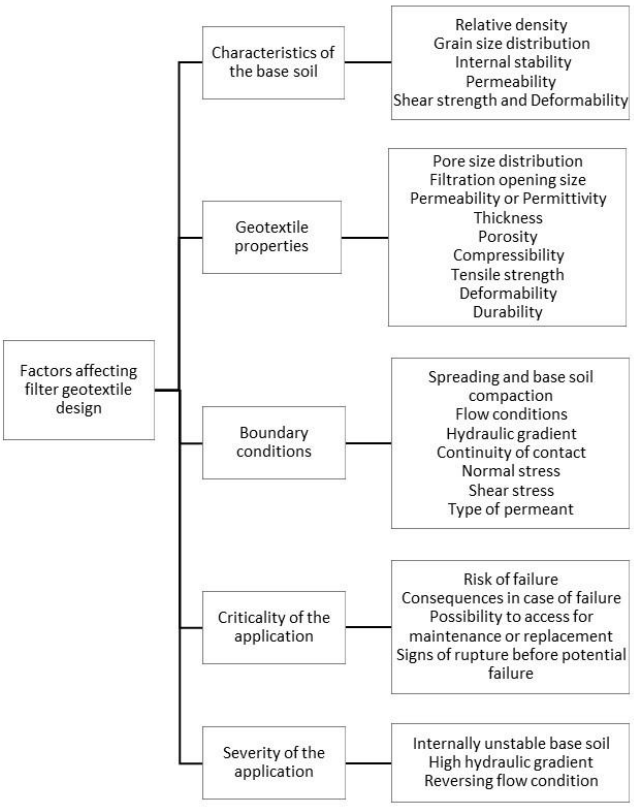


Fig. 26. Schematic representation of the factors affecting the design of geotextile filter for cohesionless soils.

4.1 Internal stability of cohesionless soils

Among the factors affecting the soil geotextile filter interaction, the internal stability of base soil is a key factor for the filter design in contact with cohesionless soils.

A cohesionless soil is internally stable when all the soil particles belong to the soil skeleton that supports the loads and transfers the stresses. On the other hand, the soil is internally unstable when a portion of particles exists inside pores generated by soil skeleton particles that are free to move in the bordering pores. The movement of this fraction occurs when the network of pores is characterized by constrictions (the narrow throat that connects two pores) whose minimum dimensions are large enough to allow the movement of some particles of the same soil, which can be dragged by the flow. This process of internal erosion is called suffusion.

Internal stability mainly depends on soil GSD, relative density, and applied hydraulic gradient. On the basis of the GSD curve, internally unstable cohesionless soils are concave upward, gap-graded, and broadly graded soils. Potential instability generally increases with increasing soil uniformity coefficient, decreasing relative density, and increasing applied hydraulic gradient [88].

Skempton and Brogan [89] showed that a critical content of fines, below which the fine particles in a gap-graded soil do not fill the voids in the coarse component, exists. It depends on the porosities of the coarse and fine fractions. In particular, it is 29% by weight in loose packing and 24% in dense packing.

Moreover, if the fines content exceeds about 35%, the coarse particles are no longer in contact with each other and are dispersed in a matrix of fines.

In internally unstable soils, the Moraci [90] retention design criterion is strictly related to the critical diameter of suffusion (D_c) representing the diameter of the largest particle free to move inside the soil solid constrictions.

The internal stability of cohesionless soils and the critical diameter of suffusion can be evaluated through semi-empirical, theoretical and graphical methods.

The semi-empirical criteria are Kezdi [91], Sherard [92] and Kenney and Lau [93] methods. Kezdi [91] and Sherard [92] methods consist of dividing the soil grain size distribution (for different values of soil diameter) into a coarse and a fine component. The selected soil is internally unstable if $D_{15coarse}/D_{85fine} \geq 4$, according to Kezdi [91], or $I_r = D_{15coarse}/D_{85fine} \geq 5$, according to Sherard [92]. The larger diameter of the base soil for which the above-mentioned equations are verified represents the critical diameter of suffusion, D_c.

Kenney and Lau [93-94] proposed a method consisting in the construction of the 'shape of the grading curve,' that is built as follows. At any point on the grain size distribution of the base soil, corresponding to a value of 'mass fraction smaller than', denoted as *F*, and a particle diameter *D*, the mass of fraction *H* is measured between particles *D* and *4D* and plotted with the corresponding value of F. They found that the limiting gradation curve of a stable soil, in medium dense conditions, is the curve where the weight percentage of particles having a size between *D* and *4D* (*H*) represents at least 1.0 time the weight percentage of particles smaller than *D(F).* Therefore, according to this method, a granular material can be considered internally unstable if $H<F$.

Chapuis [95] showed that the previous criteria can have a similar mathematical expression in terms of the limit slope of GSD. Therefore, the secant slope of the grain size distribution curve indicates the potential of internal instability (Fig. 27). In Kezdi's method, the soil that has in the grain size distribution curve a slope lower than S=24.9% is considered internally unstable. In Sherard's method, the value of the slope is equal to S=21.5%. Finally, in the Kenney and Lau [93] method, the soil is considered internally unstable if the slope of the grain-size distribution curve is lower than S=1.66F. Therefore, Kenney and Lau's slope limit increases in magnitude with progression along the gradation curve (Fig. 27).

The theoretical method "Simulfiltr" proposed by Moraci et al. [96-97] develops in three steps. In the first one, the soil grain-size distribution is divided into two parts for each diameter, called division diameter, beginning from the lowest and ending with the largest diameter. The soil grain-size distribution is divided as many times as the diameters. For each division diameter, two grain-size distribution curves are created: the first one of the coarser soil (Fig. 28) that represents the solid skeleton (soil 1, dash dot line), and the second one of the finer soil (soil 2, dotted line) that represents the fine particles potentially free to move through the soil 1 constrictions. For each of the division diameters considered, the soil numerical percentage constriction-size distribution is obtained from the soil 1 grain-size distribution by means of Silveira [98] probabilistic geometric method, considering the relative density.

In the second step, the schematisation of the soil in layers is carried out. The soil is represented by means of a set of layers ($m \times n$), parallel to each other, where each layer, *s*, is formed by the soil 1 constrictions and by the soil 2 fine particles in alternate positions (Fig. 29). Since the solid skeleton is formed by particles in a fixed position, the relative constrictions can also be considered in fixed position. Assuming a three-dimensional distribution, the theoretical distance between the constrictions in the hydraulic flow direction (assumed normal to the soil layers) depends on the soil relative density. It is equal to the sphere diameter, *D*, in a loose state (cubic distribution), and 0.82 times the sphere diameter, *D*, in a dense state (tetrahedral distribution). Therefore, the distance between the layers is obtained by means of linear interpolation between the *D* values, equal to the mean diameter of the particles if the relative density is typical of loose state and 0.82*D* if the relative density is typical of dense one. However, the soil fine particles and the soil constriction sizes in each

different layer, in which one of the soils has been divided, are obtained by applying a sampling stochastic method at the constrictions and fine particles numerical percentage cumulative grain-size distributions. The sample size that simulates the soil depends on the shape and extension of the initial soil grain-size distribution. If the soil grain-size distribution is wide, the sample size will be larger.

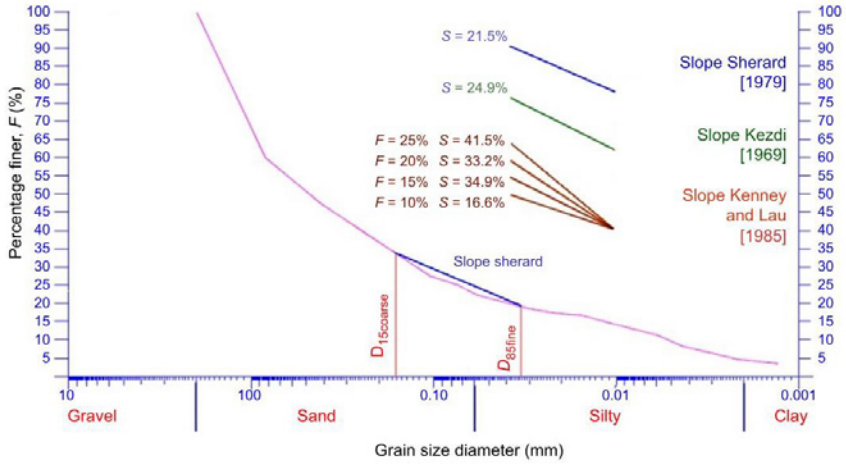


Fig. 27. Internal stability criteria in terms of grain size distribution limit slope.

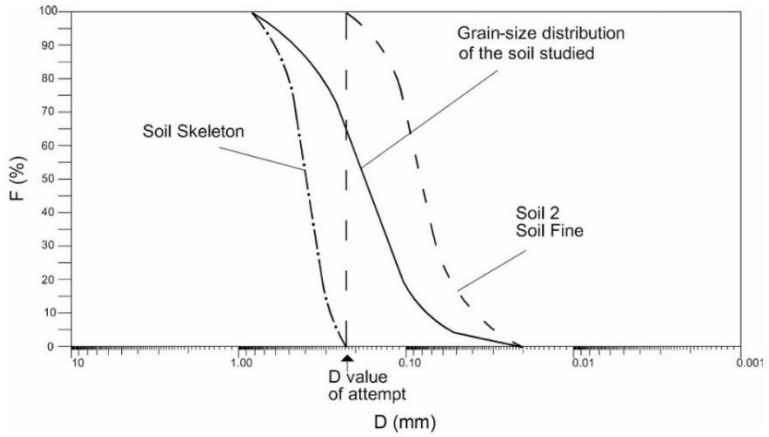


Fig. 28. 1st step of Simulfiltr method: division of soil grain-size distribution.

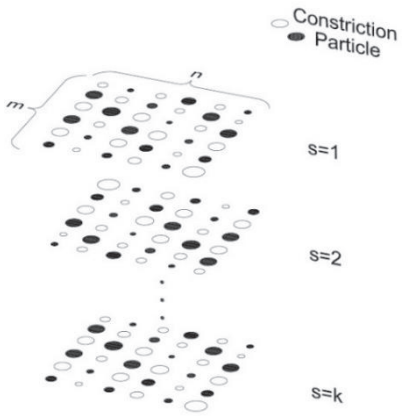


Fig. 29. 2nd step of Simulfiltr method: schematisation of the soil in s layers.

The third step simulates the filtration process of the fine particles, which constitute soil 2, through the soil 1 constrictions inside the number of layers, n, representing the soil. A generic particle inside the first layer is chosen and compared with the relative constrictions inside the next layer (Fig. 30). If the considered particle size is lower than that of the compared constriction size, the particle can move to the next layer. The procedure is repeated for all the layers representing the soil, and the cumulative grain-size distribution of the passing soil is obtained. Finally, the largest diameter of the passing soil (D_{95}) and the mass ratio between the moved mass and the average mass of the layers ($M_{f/s}$) are determined. For the diameter considered, a set of possible simulations (Monte Carlo method) is carried out, changing randomly the constrictions and the fine particle sizes in each layer. A set of large diameters of passing soil is so obtained. As a result of the weak law of large numbers, these values converge with the increase of the simulation number to a single value taken as the final value. The procedure is repeated for each division diameter of the analysed soil grain-size distribution, and couples (D_{95}, $M_{f/s}$) for each division diameter of the soil grain-size distribution are obtained. The critical diameter of suffusion, D_c, corresponds to the largest diameter D_{95} among the couples that show a ratio between moved mass and average mass of the layers, $M_{f/s}$, equal to or greater than 0.60. This value, 0.60, was obtained by calibrating the model based on the experimental results of long-term filtration tests on stable and unstable cohesionless soils carried out by the authors and other researchers.

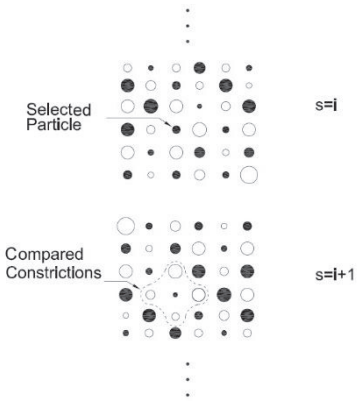


Fig. 30. 3rd step of Simulfiltr method: scheme of comparison between particle and constrictions.

The results derived by long-term filtration tests performed using a rigid-wall permeameter on different internally stable and unstable granular soils [96-99] were also used to evaluate the reliability of this theoretical method.

As previously described, Chapuis' method transforms the semi-empirical methods into graphic form, identifying the limit values of the secant slopes to the grain size distribution curve of the soil under examination.

Butterfly Wings is a graphical method proposed by Moraci et al. [100-101] that allows us to evaluate the internal stability considering in which zone of the chart (Fig. 31) the representative point of soil, expressed in terms of average value of finer percentage (F) and of minimum slope of the grain-size distribution (S_{min}), falls. The Butterfly Wings chart is divided into four zones. The first one is the zone where the soils are unstable, the second one is the zone where the soils are stable, the zones A and B are the zones where the soils are stable according to some empirical criteria and unstable for others.

The evaluation of F and S_{min} is complex and was explained in detail in Moraci et al. [101].

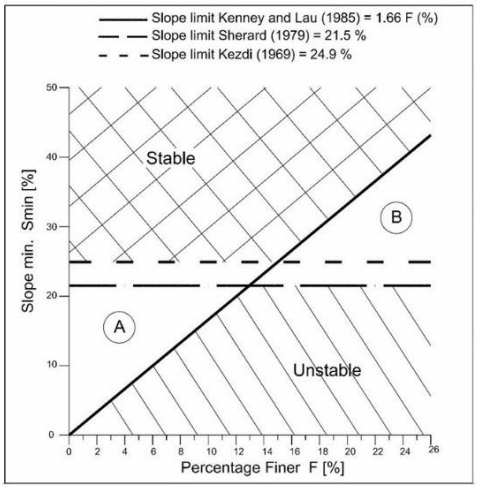


Fig. 31. Butterfly Wings chart.

4.2 Experimental methods to evaluate the long-term behaviour of filtering systems

The behaviour of soil-geotextile filtering systems can be analysed by means of long-term filtration tests. If the geotextile filter is not compatible with the base soil under specific experimental conditions, base soil erosion, geotextile filter blinding and/or clogging can occur [102, 83, 88].

The Figure 32 shows typical one-way filtration performance test results in terms of soil-geotextile system permeability and mass of passing soil through the filter over time. Figure 32a shows a typical result in which the system reaches a base soil erosion limit state. In this condition, there is a continuous loss of soil particles and an increase of the permeability over time. Base soil erosion occurs if the geotextile filter's pore sizes are too large and do not retain the movement of base soil particles. This limit state occurs when the base soil particles, forming the solid skeleton, are dragged away by the hydraulic flow. Figure 32b shows a typical trend of a stable soil-geotextile filtering system where the system permeability stabilizes after an initial transitory phase and no particles pass through the geotextile filter over time. The time required for the stabilization of the filtering system can vary from a few hours to weeks or even months depending on the base soil characteristics, on the geotextile filter characteristics and on the applied boundary conditions in terms of hydraulic gradients

and normal stresses acting at the soil-filter interface. Finally, Figure 32c shows typical results of clogging or blinding limit states, in which the permeability of the system continuously decreases over time.

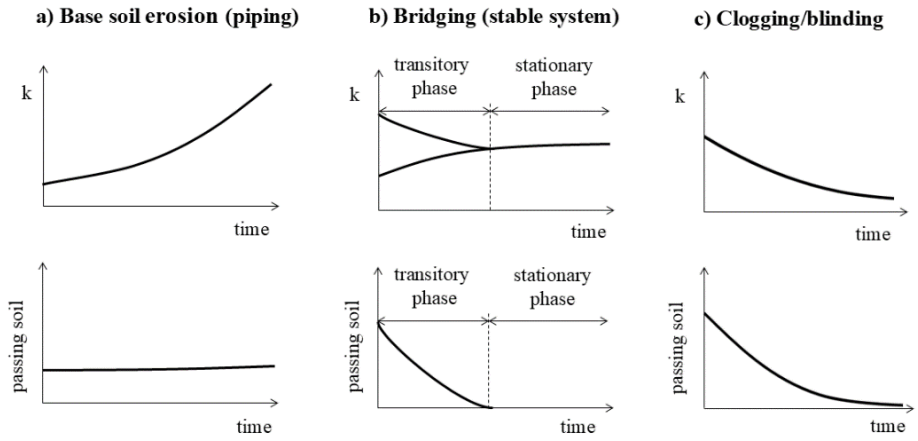


Fig. 32. Typical profiles of the soil-geotextile system permeability and mass of passing soil through the filter over time when the system reaches a) the base soil erosion limit state, b) the stability and c) the clogging or blinding limit states.

The blinding limit state generally occurs when the geotextile filter is in contact with internally unstable soils. In these conditions, if the hydraulic flow moves the base soil particles not forming the soil skeleton with dimensions larger than the geotextile pores, these particles accumulate at the base soil–geotextile filter interface and a low permeability zone is created (filter cake). The development of excessive pore water pressures related to the decrease of permeability at the soil–filter interface and the consequent reduction of flow rate could generate a limit state. Blinding could also occur when the filter is permeated by other types of fluid.

The clogging limit state yields a decrease in nonwoven geotextile filter permeability and pore sizes due to the accumulation of soil particles, and chemicals and biological materials in geotextile pores and fibres. The phenomenon results in a decrease of the permeability of the filtering system, in a reduction of the system flow rate, and in an increase of pore water pressure.

Long-term filtration tests can be performed in the laboratory placing the base soil in contact with the geotextile filter under the flow conditions expected in the application. Different test devices and procedures were developed according to the flow conditions (one way or reversing flow).

In USA the test method commonly used under one-way flow conditions for determining the soil-geotextile clogging potential is the Gradient Ratio (GR) test in which a specific soil is placed above the geotextile filter in a rigid wall permeameter, and a flow of water passes vertically through the soil-geotextile filter system under a range of hydraulic heads and without the application of vertical stress [103]. To simulate the soil-geotextile filtering system subject to different vertical stresses, a more advanced equipment able to perform gradient ratio tests with vertical stresses up to 2000 kPa was developed by Palmeira et al. [104]. According to these procedures, the ratio of the hydraulic gradient across a soil-geotextile interface i_{LG}, to that through the soil i_s represents the gradient ratio, GR (equation 12):

$$GR = \frac{i_{LG}}{i_s} \tag{12}$$

Equation 12 allows the calculation of GR by different definitions, depending on the considered piezometer. An increase in the GR value during the filtration test indicates that soil particles accumulate inside (clog) the geotextile or blind its surface. If GR value continues to decrease below one, it means that fine soil particles are passed through the filter and piping can occur. The GR value calculated by equation 12 does not allow for distinguishing between clogging and blinding phenomena.

To overcome these limitations, Moraci [90] proposed a test methodology, capable of distinguishing between clogging and blinding phenomena and also able to analyse the base soil erosion (piping) and the evolution of the permeability of the soil-geotextile system k_{sys} over time.

The test device (Figure 33) consists of three units. The upper unit permits the application of a constant head boundary condition to the top of the specimen. The middle unit is the permeameter where the base soil specimen is placed. The permeameter is equipped with piezometers located at different heights, which allow measurement of the hydraulic head and determination of the average hydraulic gradient along the specimen and the cumulative percentage of hydraulic head lost at each piezometer. The lower unit of the permeameter contains a soil-geotextile support screen and permits collection of the particles passing through the geotextile.

Various parameters are measured during the test to evaluate the long-term compatibility between the base soil and geotextile filter: water flow, water temperature, hydraulic heads along soil–geotextile filtering system and mass of base soil passing through the filter. These parameters allow us to determine the evolution over time of the piping and the permeability of the soil–geotextile filtering system.

After the test, it is possible to determine the permeability of the geotextile normal to the plane and the geotextile impregnation level λ. Knowledge of these parameters and the hydraulic heads measured during the test allows us to determine the clogging level at the end of the test and the evolution of the blinding factor over time.

The blinding factor, $BF = i_{cz}/i_s$, is defined as the ratio between the gradient in the filter-soil contact zone (equation 13) and the gradient in the adjacent soil (equation 14). To evaluate these gradients, the following expressions are introduced (referring to the hydraulic scheme illustrated in Figure 33):

$$i_{cz} = \frac{(h_5 - h_6)}{L_s''' \left[\left(\frac{t_g}{L_s'''} \frac{k_s}{k'_{ng}} \right) + \left(\frac{L_{gr}}{L_s'''} \frac{k_s}{k'_{gr}} \right) + 1 \right]} \tag{13}$$

$$i_S = \frac{(h_2 - h_5)}{L_{2,5}} \tag{14}$$

where: h_2, h_5 and h_6 are the hydraulic heads measured, respectively, in the piezometric stand pipes 2, 5 and 6; $L_{2,5}$ is the distance between piezometric stand pipes 2 and 5; t_g is the geotextile thickness; L_{gr} is the thickness of the gravel drainage layer, L_s''' is the thickness of the soil in contact with the filter; k_s is the permeability of the base soil; k'_{ng} is the permeability of the geotextile after clogging and k'_{gr} is the permeability of the gravel drainage layer after the test.

The i_{cz} definition makes it possible to eliminate the influence of clogging on the measured hydraulic heads and to evaluate the blinding and the clogging levels separately.

In internally unstable soils or in non-homogenous soil specimens, the interpretation of the obtained values of BF or GR can be complex due to the influence of soil particles migration or soil heterogeneities on the values of i_{cz} (or i_{LG}) or i_s, or on both. In this case, the hydraulic gradient away from the geotextile may be affected by suffusion that takes place during test, influencing the value of the BF or GR and the permeability along the soil thickness.

Therefore, due care is recommended when deciding on the acceptance of a geotextile filter based only on the value of BF or GR from laboratory tests on internally unstable soils. In such cases, the flow rate variation with time (i.e. k_{sys} values) and the requirements from the project itself (minimum required flow rate or maximum acceptable pore pressure at the contact zone, for instance) must also be considered for a final decision. Therefore, the value of BF or GR is not sufficient to establish the effectiveness of the filter because it is also necessary to evaluate if the permeability of the system k_{sys} is maintained and there is the establishment of some recognizable equilibrium or stabilization of the system. Therefore, the allowable BF or GR values and related flow rates for various soil-geotextile systems will depend on the specific site application.

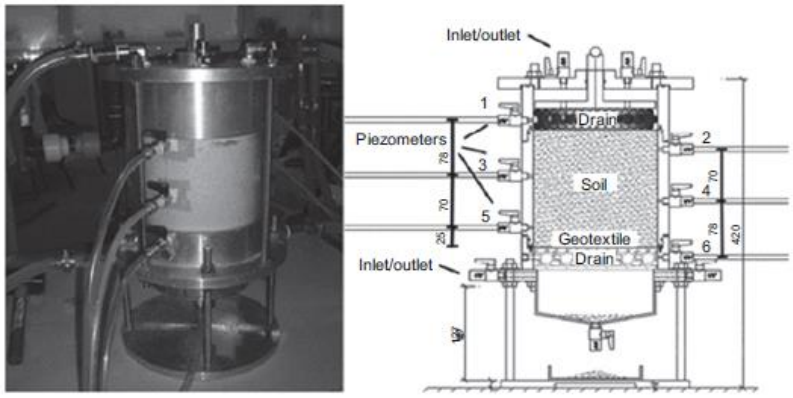


Fig. 33. Test apparatus to evaluate the long-term behaviour of filtering systems.

For instance, referring to the test apparatus developed by Moraci [90] a BF equal to 3 means a head loss in the contact zone equal to 35% of the applied hydraulic head and a permeability of the contact zone equal to $0.33k_s$. These values could be acceptable or not depending on the flow direction, base soil thickness, pore pressure, and flow rate requirements characteristics of the real application.

The effect of soil particle accumulation inside the geotextile (clogging) can be evaluated by introducing a clogging ratio (CR) defined (considering the permeability criterion) as the ratio between the geotextile permeability normal to the plane after clogging (k'_{ng}) and the permeability of base soil (k_s):

$$CR = \frac{k'_{ng}}{k_s} \tag{15}$$

The acceptable values of the clogging ratio depend on the flow direction, soil and geotextile filter thickness, as well as the pore pressure and flow rate requirements characteristic of the real application. A value of CR greater or equal to 1 is always acceptable.

The clogging level of a geotextile can also be quantified by means of the geotextile impregnation level λ calculated as the ratio between the total mass of particles in the geotextile (M_s) and the total mass of geotextile fibres (M_f) [105]:

$$\lambda = \frac{M_s}{M_f} \tag{16}$$

The porosity of the geotextile after long-term filtration tests n', can be determined according to Palmeira and Gardoni [105] as follows:

$$n' = 1 - (1 - n) \cdot \left(1 + \frac{\rho_f}{\rho_s}\right) \lambda \tag{17}$$

where n is the porosity of the virgin geotextile given by equation 18

$$n = 1 - \frac{\mu_g}{\rho_f t_g} \tag{18}$$

where μ_g is the mass per unit area of geotextile, ρ_f is the geotextile fibre density, ρ_s is the density of the solid particles and t_g is the geotextile thickness.

A maximum value of λ (i.e. λ_{max}) considering a mass of soil particles (smaller than the geotextile voids) uniformly distributed inside the geotextile can be estimated by equation (19) [87]:

$$\lambda_{max} = \frac{\rho_s}{\rho_f}(1 - n_s) \cdot \frac{n}{1-n} \tag{19}$$

where n_s is the porosity of the mass of particles in the geotextile voids.

If all the geotextile voids are entirely occupied by a solid mass, which would be an extreme case of geotextile impregnation yielding to k_{ng} = 0, where k_{ng} is the geotextile permeability coefficient, equation 19 can still be used, making n_s = 0. According to this approach it is possible to define a clogging level CL as the ratio expressed in percentage by the value of λ, determined at the end of the test, and the maximum value of λ_{max}

$$CL = \frac{\lambda}{\lambda max} * 100 \tag{20}$$

Moreover, the permeability normal to the plane after impregnation (clogging) can be determined using the equation proposed by Palmeira and Gardoni [105]:

$$k'_{ng} = \frac{\beta \rho_w g}{\eta_w} \frac{\left[n - \lambda\left(\frac{\rho_f}{\rho_s}\right)(1-n)\right]^3}{\left(\frac{4}{d_f} + \lambda\left(\frac{\rho_f}{\rho_s}\right)\left(\frac{6}{d_s}\right)\right)^2 (1-n)^2} \tag{21}$$

where β is a dimensionless shape factor which is related to the tortuosity of the path followed by the fluid (that could be assumed equal 0.37 for nonwoven), ρ_w is the density of the fluid, g is the acceleration of gravity, η_w is the dynamic viscosity of the fluid, n is the porosity of the geotextile without considering the presence of the soil particles in the voids, λ is the geotextile impregnation level, ρ_f is the density of the geotextile fibres, ρ_s is the density of the soil particles, d_f is the fibre diameter and d_s is the average diameter of the soil particles inside the geotextile (see Palmeira and Gardoni [105] for predictions of d_s).

Once the geotextile permeability normal to the plane after clogging is known, the previously defined clogging ratio can also be calculated in this case.

At the end of the test, in addition to the measure of the residual permeability of the geotextile and its impregnation, the determination of its O_F and pore size distribution can provide useful information about the retention capability of the geotextile after impregnation [106].

Moreover, some portions of the base soil after filtration test, may be subject to grain size analysis. In particular, the comparison among the GSD of the soil in contact with the geotextile, with those of the central and upper part of the specimen can provide information on the movement of the base soil and therefore further information on the internal stability of the soil, but also to support experimental data on the occurrence of blinding or clogging phenomena.

Another parameter, determined after filtration test and used in literature is the piping failure limit obtained dividing the soil mass passing through geotextile by the specimen area.

For internally unstable soils, it is rather difficult to establish a limit for piping, as discussed above in relation to the acceptable values of GR or BF. Some researchers suggest that the piping limit should be defined based on gradation of the particles that constitute less than 30% (for uniformly graded soils) or 20% (for broadly graded soil) of the original soil gradation [107,87].

Cazzuffi et al. [102] studied the behaviour of geotextile filtering systems under reversing flow conditions. The test apparatus (Fig. 34) was designed to study interaction phenomena in filtering systems subjected to cyclic hydraulic loads with different boundary conditions.

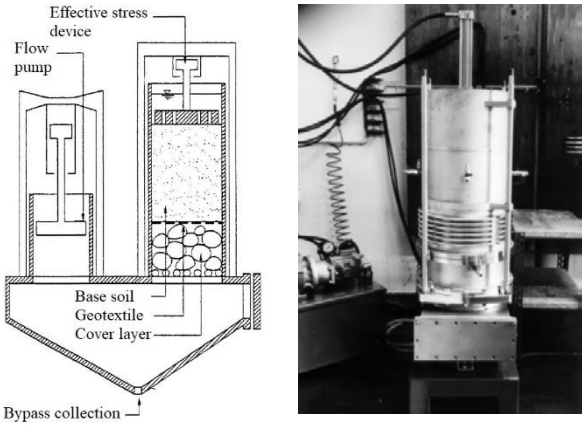


Fig. 34 Laboratory equipment for cyclic filtration performance test: set up for reversing flow perpendicular to the interface [102].

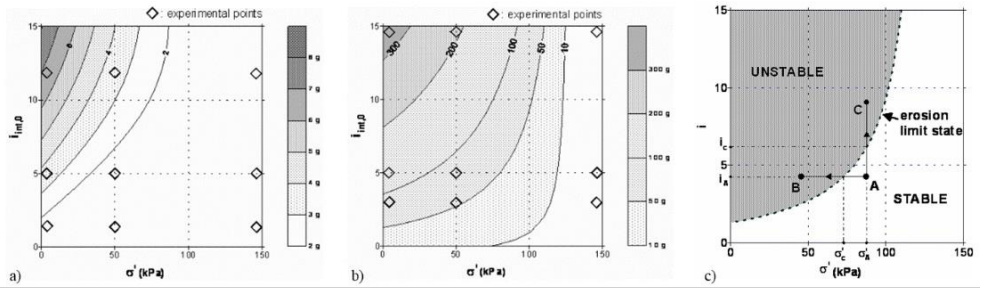


Fig. 35 Experimental results of cyclic filtration tests: a) nonwoven; b) woven; c) influence of vertical effective stress and of hydraulic cyclic gradient [102].

In particular, using this device, it is possible to reproduce a cyclic reversing flow perpendicular or parallel to the interface and also to change the boundary conditions in terms of normal effective stress and contact geometry between the geotextile and the protection layer or external cover layer. The test apparatus may be assembled in two different ways to perform experiments with the flow either perpendicular or parallel to the interface, respectively. The water flow is induced by two different flow devices. A small cylinder is used to push the water through the perpendicular flow specimen, where a limited discharge has to be generated, vice versa in the parallel flow tests a larger cylinder is used, since a larger discharge is necessary. Typical wave periods are simulated in the experiments range from 2 s to 20s. Of course, higher periods are limited by the finite volume that may be achieved by the flow pump in the case of highly permeable test specimens, with a large discharge necessary to reach the required gradient. The maximum volume that the large cylinder may achieve is about 12l, while it can be up to 0.5l for the smaller one. The pushing apparatus can

be set by acting on the velocity and on the stroke regulation device in the pushing unit. A detailed description of the experimental set-ups can be found in Cazzuffi et al. [102,108].

The researchers showed that in the case of the cyclic flow, the retention criterion of the filter depends on the applied hydraulic gradients, the vertical effective stresses, the filter stiffness and the type of contact. It has also been shown that a stable soil-geotextile interface can reach instability because of an increase in the hydraulic gradient (path from A to C) or a decrease in vertical effective stress (path from A to B), as shown in Figure 35.

4.3 A geometrical, experimental and microstructural approach for assess long-term filter compatibility

Cazzuffi and Moraci [109] showed that the filter design criteria in one-way flow conditions are conservative for stable uniform cohesionless soils. For these materials, the existing theoretical and experimental retention criteria are reliable. Therefore, many researchers have turned to the design of geotextile filters in contact with internally unstable cohesionless soils.

Few design criteria exist for these soils [90, 110-112]. Some researchers [110, 112] defined only the upper limit of the critical retention ratio O_F/D_{85}, whereas others [90, 111] defined both the upper and lower limits.

Bhatia and Huang [110] found that O_F value combined with the porosity of the geotextile (k_{ng}) controls the geotextile filter performance. According to geotextile porosity, they proposed two different criteria. In particular, for $n_{gt} > 60\%$ the retention ratio depends on D_{85} and the coefficient of curvature Cc. The experimental results, obtained by different authors, were compared [109] to the different design criteria in terms of maximum retention critical ratio (RR=O_F/D_{85}) proposed by Bhatia and Huang [110]. The experimental results showed that a lot of filter failures occurred for $O_F/D_{85} << 1$. These results highlighted the need to introduce a lower limit to the filter opening size.

Moraci [90] and Lafleur [111] introduced both the upper and lower limits of the critical retention ratio. The upper limit of the retention criterion controls the retention of the base soil, whereas the lower limit allows soil particles to cross or clog the filter. Therefore, in the case of internally unstable soils, the designer must decide whether to specify a geotextile open enough to allow the passage of fine-grained soil particles or a less porous geotextile that will retain these particles. A too-open geotextile may allow excessive piping of soil particles that may cause problems in the drainage layer. On the other hand, retaining too many soil particles may cause soil blinding and a severe reduction of flow rate with an increase of pore pressures in the vicinity of the filter layer. These effects could be unacceptable for the specific application's pore pressure and flow rate requirements. For these reasons, long-term filtration tests are recommended for geotextile filter design in contact with unstable cohesionless soils.

The different long-term filtration test results existing in literature were compared [109] to the lower limit of the retention ratio proposed by Lafleur [111]. It was possible to observe that for values of retention ratio lower than the minimum critical one O_F/D_{30} the behaviour of filters may be stable in some cases and unstable in other ones. Therefore, the authors concluded that the critical diameter D_{30} used by Lafleur [111] is not always representative for unstable soils.

The comparison of filtration test results with the upper and lower limits of critical ratio proposed by Moraci [90] showed that this filter design criterion is generally reliable but needs further developments.

In order to assess the soil/geotextile filter compatibility in the complex case of internally unstable soils, Moraci et al. [106] proposed a new methodology based on a geometrical, experimental and microstructural approach.

The geometrical approach consists of considering the pore size distribution (PSD) of the geotextile filter and the GSD of the base soil, comparing the values of O_F with the values of the critical diameter of suffusion, D_c. This comparison allows us to understand better whether

the mass of soil particles with a diameter lower than D_c could pass through the filter, clog the filter, or accumulate at the soil-filter interface, causing blinding.

The experimental approach is based on the results of long-term filtration tests, which allow the evaluation of blinding, clogging, and piping limit states (see §4.2).

The micro-structural approach is based on the analyses of SEM images taken on the tested geotextiles to observe the clogging and blinding phenomena and compare them with results obtained with geometrical and experimental approaches.

This methodology has been applied to different cohesionless soils in contact with different nonwoven geotextiles [106, 113]. For example, the application of the proposed methodology to two cohesionless soils in contact with a thick needle-punched (NP) geotextile and a thin heat-bonded (HB) needle-punched geotextile is illustrated below. The soils were reconstituted using gravel and marbles of various colours, and the critical diameter of suffusion was obtained according to SimulFiltr method. The properties of the tested geotextiles are shown in Table 2.

Figure 36 shows the application of the geometrical approach to the 9/WF soil in contact with the HB (Fig. 36a) and NP geotextile (Fig.36b) and to the 4R/WF soil in contact with the HB (Fig. 36c) and NP geotextile (Fig.36d).

According to the geometrical approach (Figure 36), the soil particles free to move inside the solid skeleton (with a diameter lower than D_c) can clog (yellow zone), cross the geotextile filter (green zone) or accumulate at the soil-geotextile filter interface (red zone). The division between the weight percentages of soil that can clog (yellow zone) or cross (green zone) the geotextile filter is simplified because a part of the yellow fraction could cross the filter due to the pore size distribution of the geotextile filter. Therefore, it could happen to measure piping experimentally also in the absence of a green fraction. Moreover, not all the soil particles in the green zone or the yellow zone can cross or clog the geotextile filter when there is a fraction of soil particles (red zone) that can accumulate at the interface (i.e. if D_c is greater than O_F) because this fraction stops at the soil/geotextile interface generating a blinding phenomenon that produces a porosity decrease at the soil-filter interface and a new soil grain and pore size distribution at the interface.

Table 2. Geotextile properties.

Geotextile	Typology	μ_g [g/m^2]	t_g [mm]	O_F [mm]
HB	PP, HB NP	80	0.7	0.187
NP	PET, NP	600	2.8	0.055

Note: PET, polyester; PP, polypropylene.

Comparing the GSD of 9/WF soil with PSD of HB geotextile (Fig. 36a), it can be observed that the piping, clogging and blinding phenomena could occur. Piping becomes negligible when the same soil is in contact with NP GT (Fig. 36b), while the blinding susceptibility increases for the 9/WF-NP GT contact with the increase of percentage by weight of soil particles falling in the red zone. Therefore, passing from HB to NP geotextile, it can be noted that susceptibility to blinding increases according to a reduction of O_F.

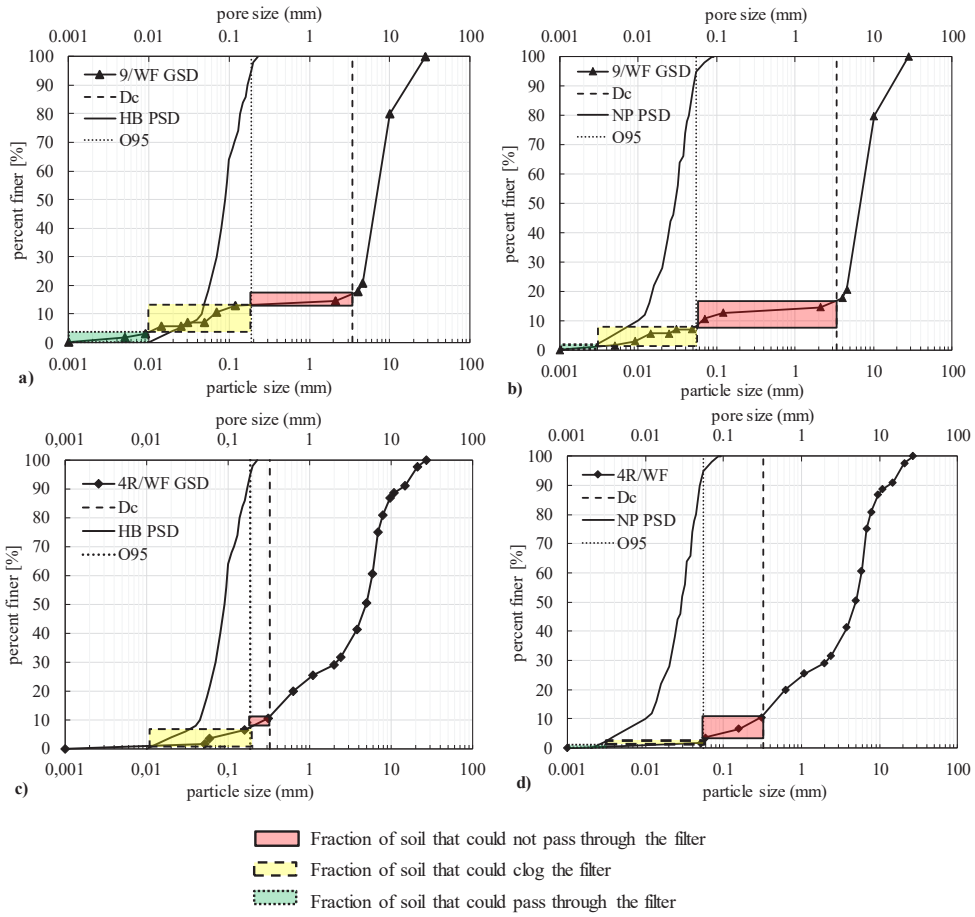


Fig. 36. GSD of the base soil, PSD of the geotextile and schematization of the fraction of soil that could not pass through the filter, clog the filter or pass through the filter for 9/WF soil in contact with a) HB and b) NP geotextile, and for 4R/WF soil in contact with c) HB and d) NP geotextile.

Considering 4/WR soil in contact with HB geotextile (Fig. 36c), negligible blinding and moderate clogging and blinding could occur. Passing to NP geotextile, the geotextile's susceptibility to blinding phenomena increases, while the levels of clogging and piping become negligible (Fig. 36d).

In all the tests, a level of clogging is always expected due to the impregnation of the geotextile during the soil specimen preparation.

The results derived from the geometrical approach were compared with the long-term filtration test results performed under low normal stress and high hydraulic gradients on the same interfaces.

Table 3 summarizes the results of the long-term filtration tests performed on the same soils in contact with the same geotextiles and the results obtained from applying the geometrical approach. In Table 3 the percentage by weight of soil particles that could blind (B, red zone), clog (C, yellow zone) the filter or pass through the filter (P, green zone), the blinding factor BF, the mass of soil passing through geotextile M_P, the ratio between M_P and the total mass of the specimen M_{tot} and the impregnation level of geotextile λ are shown. Moreover, in all the performed filtration tests, the long-term permeability of the system remained in the same order of magnitude as the initial one. The flow rate reduction ranged

from 0% (for both geotextiles in contact with soil 4R/WF) to 50% (for NP in contact with soil 9/WF).

Table 3. Results derived from the geometrical and the experimental approaches.

	B	*C*	*P*	*BF*	M_P	M_P/M_{tot}	λ
	[%]	[%]	[%]	[-]	[g]	[%]	[-]
HB - 9/WF	5	10	3	> 3	114.43	2.36	2.90
NP - 9/WF	10	6	2	> 3	1.69	0.035	1.58
HB - 4R/WF	4	7	0	≅ 3	25.8	0.53	1.13
NP - 4R/WF	8	3	0	> 3	0	0	1.66

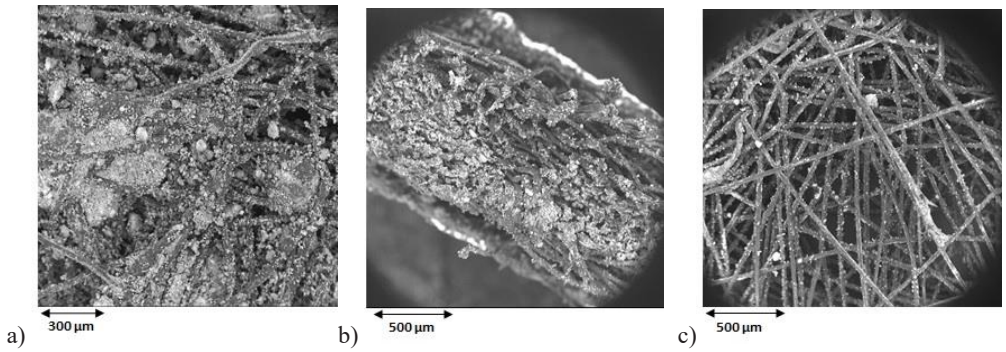
For the 9/WF soil in contact with the two geotextiles, according to the geometrical approach, the percentage by weight of soil particles that could blind the filter (B) is equal to 5 % and 10 % for the HB and NP geotextile, respectively. These percentages agree with the BF values obtained by long-term filtration tests that are greater than 3. The percentage by weight of soil particles potentially able to clog the filter (C) is equal to about 10 % and 6 % for the HB and NP geotextile, respectively. The percentage by weight of soil particles potentially able to pass through the filter (P) is equal to about 3 % and 2 % for the HB and NP geotextile, respectively. Due to the greater amount of soil particles that accumulate on the surface of the NP geotextile, clogging and piping decrease as confirmed by the Piping and impregnation levels evaluated at the end of the long-term filtration test.

Regarding 4R/WF soil in contact with the two geotextiles, the base soil fraction capable of blinding the filter (red zone) is equal to 4 % and 8 % for the HB and NP geotextile, respectively. An increase of blinding is expected for the NP geotextile. This result was confirmed by long-term filtration test results where a value of BF greater than 3 was determined. For HB geotextile, the soil fractions able to clog or pass through the filter are low (7 % by weight) and, therefore, the piping and clogging levels expected are also limited, as confirmed by test results.

Microscopic observations are another useful tool to support experimental data and evaluate the extent of blinding or clogging phenomena and the variation in the geotextile internal structure (fibres and voids) [106, 114-115]. In particular, scanning electron microscope (SEM) images referred to the upstream face of the geotextile (i.e. the surface directly in contact with the base soil) give information about blinding phenomenon, whereas the cross-section of the geotextile is helpful to evaluate the clogging level along the geotextile thickness.

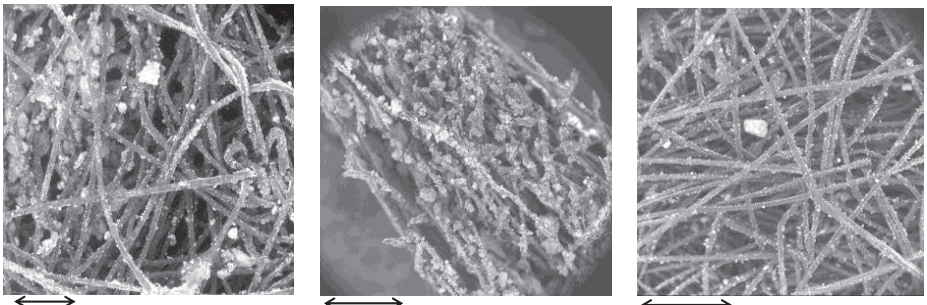
Therefore, the microstructural approach provided further useful information about blinding and clogging phenomena and confirmed the experimental and geometrical analysis results. Figure 37 shows SEM images of the upstream face (i.e., the surface directly in contact with the base soil), cross-section, and downstream face of the HB geotextile in contact with 9/WF soil.

A large number of fine particles on the upstream face of the geotextile and the presence of precipitates (Figure 37a) are observed according to the level of blinding (BF > 3) experimentally determined. The SEM analyses of the geotextile cross-section (Figure 37b) show the presence of soil particles entrapped in the geotextile voids and of precipitates for the whole thickness. As a result, geotextile porosity decreases almost uniformly along the thickness.



a) b) c)

Fig. 37. SEM images of HB geotextile in contact with 9/WF soil: a) upstream face (magnification 220x); b) cross-section (magnification 145x) and c) downstream face (magnification 220x).



a) b) c)

Fig. 38. SEM images of HB geotextile in contact with 4R/WF soil: a) upstream face (magnification 195x), b) cross-section (magnification 145x) and c) downstream face (magnification 175x).

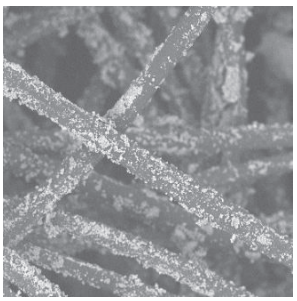


Fig. 39. Example of SEM images of the fibres of a heat-bonded needle-punched geotextile after long-term filtration test.

The SEM analyses also confirm the value of λ (i.e. 2.90) obtained in the test. In the downstream face (Figure 37c), a negligible amount of fine particles and the presence of precipitates are observed. SEM images of the HB geotextile in contact with 4R/WF soil (Fig. 38) confirm the stable behaviour of the filter system with acceptable levels of blinding, clogging and piping observed in the long-term filtration test. Indeed, the upstream face of the geotextile after a long-term filtration test (Fig. 38a) shows an acceptable level of blinding, the cross-section shows a limited level of clogging (Fig. 38b), and the downstream face (Fig. 38c) shows a negligible presence of soil particles.SEM images can also determine fibre diameter of geotextile, before (d_f) and after filtration tests (d_f'), through Fibermetric software [106]. Figure 39 shows an example of geotextile fibres after a filtration test; in this case, an

increase in fibre diameter due to the formation of precipitates that coat the fibres was observed [106].

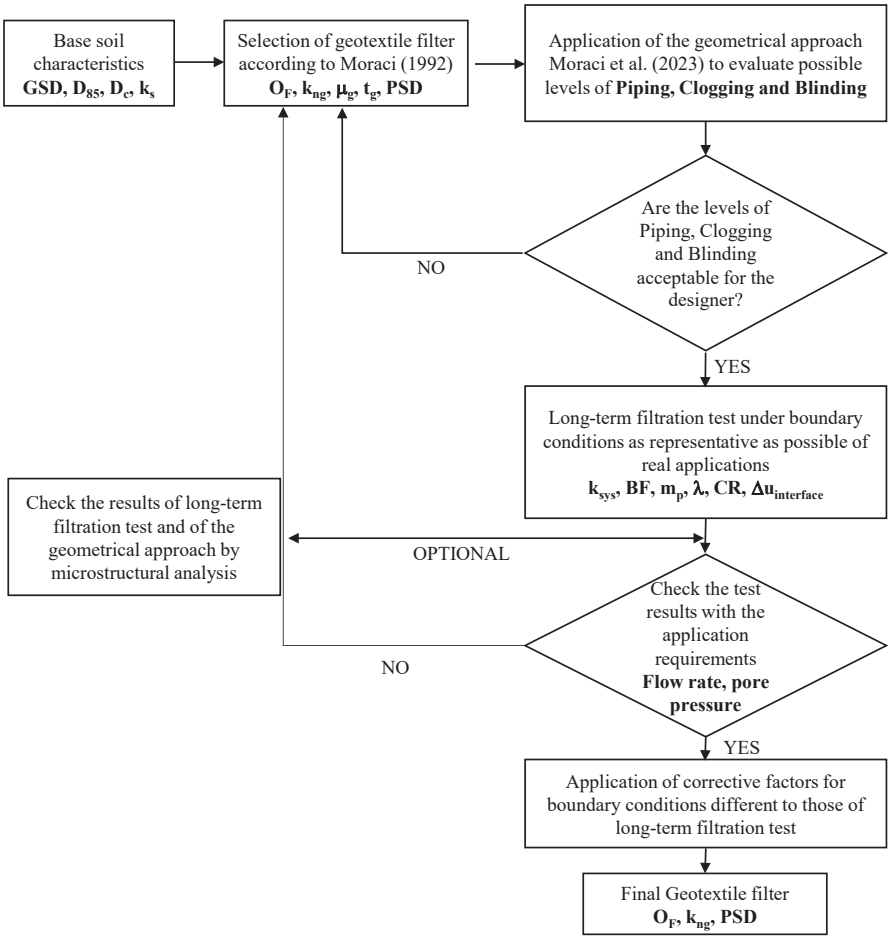


Fig. 40. Design approach for geotextile filter in contact with internally unstable cohesionless soils.

The authors' methodology for the design of geotextile filters in contact with internally unstable cohesionless soils is summarized in the flow chart shown in Figure 40. The proposed methodology, based on the characteristics of the base soil (GSD, D_{85}, D_c and k_s), provides a first pre-sizing of the geotextile filter (O_F, PSD, t_g, μ_g, k_{ng}) using the retention and permeability criteria proposed by Moraci [90]. Once the filter has been pre-sized, the levels of piping, clogging and blinding are evaluated using the geometrical approach (first phase of the methodology described above). If these levels, although indicative, are not considered admissible by the designer, another filter whose characteristics (O_F, PSD, t_g, v_g, k_{ng}) satisfy the aforementioned design criteria is chosen

When the selected filter satisfies the requirements deemed admissible by the designer, the experimental verification (second phase of the proposed methodology), in boundary conditions as representative as possible of the real application, is carried out on the soil-geotextile system, evaluating the results in terms of BF, CR, k_{sys}, M_p, λ, and Δu with reference to the design requirements. The geotextile specimens can also be subjected to microscopic observations at the end of the long-term filtration tests (third phase of the proposed methodology) to further validate the experimental results in terms of the extent of blinding

or clogging phenomena and the variation in the geotextile internal structure (fibres and voids).

Once the compatibility between base soil and geotextile filter has been verified by means of the geometrical, experimental and microstructural methodology, the final characteristics of the filter (O_F, k_{ng}) can be obtained by applying any other corrective factors deriving from boundary conditions not considered in the experimentation by referring to the studies available in the scientific literature and summarised in Table 4.

Table 4. Literature studies that have quantified the effects of factors affecting geotextile filter design.

Factor	Quantification of the effect on geotextile filter behaviour
Partial clogging (impregnation)	Palmeira and Gardoni [105,116], Palmeira and Trejos-Galvis [117], Palmeira [87]
Compressive stresses	Palmeira and Gardoni [116], Palmeira et al. [104]; Palmeira and Trejos-Galvis [117]
Tensile strains	Palmeira et al. [118]
Continuity of soil-filter contact	Cazzuffi et al. [102], Koerner and Koerner [84]
Type of permeant	Palmeira [87]

5. Conclusions

The present lecture provides a comprehensive assessment of soil-geosynthetic interaction mechanisms under different loading conditions, focusing on monotonic, cyclic, and long-term pullout behaviour. The analysis highlights that the interface strength is significantly influenced by confinement stress, cyclic loading history, and sustained loading effects over time, emphasizing the need for refined design approaches that account for these parameters in geosynthetic-reinforced soil structures.

Under monotonic conditions, the interaction mechanisms governing the mobilization of pullout resistance are primarily controlled by soil dilatancy effects and reinforcement extensibility. The results confirm that the apparent coefficient of friction decreases with increasing confinement stress, an effect that must be carefully considered in the design of reinforced soil retaining structures. Current design methodologies, which often assume a constant interface strength, may lead to underestimations of the available pullout resistance since soil dilatancy effects are not considered.

When subjected to cyclic loading, the soil-geosynthetic interface exhibits progressive degradation, with post-cyclic pullout resistance reductions ranging from 10% to 33%, depending on the amplitude of cyclic loading and the applied confinement stress. The experimental results demonstrate that lower confinement stresses and higher cyclic load amplitudes exacerbate interface degradation, leading to an increased accumulation of displacements and, in some cases, unstable cyclic behaviour. The stability of the interface is strongly dependent on the applied vertical effective stress, with higher confinement pressures mitigating cyclic-induced degradation effects. These findings underscore the necessity of incorporating cyclic loading effects into the design of geosynthetic-reinforced soil structures, particularly in seismic regions where cyclic tensile loads can significantly alter interface response and reinforcement mobilization.

Investigating long-term pullout behaviour further reveals that creep and relaxation phenomena play a key role in the evolution of interface strength over time. The development of isochronous curves provides a valuable tool for quantifying the reduction in the apparent coefficient of friction due to sustained loading, allowing for a more rigorous evaluation of long-term geosynthetic performance. The experimental results confirm that reinforcement strains progressively accumulate as the interface mobilizes resistance to maintain structural

stability. The integration of isochronous response into the design process enables the selection of an appropriate long-term apparent coefficient of friction, ensuring that serviceability requirements are met throughout the design life of the structure.

Overall, the results demonstrate that the conventional approach of deriving interface parameters solely from monotonic pullout tests may be inadequate for accurately predicting geosynthetic performance under realistic loading conditions. The observed reductions in pullout resistance due to cyclic and long-term effects highlight the need for a more nuanced approach that explicitly considers the loading history and time-dependent behaviour of the interface.

The correct characterization of the interface strength between the geosynthetics employed in a landfill cover system can be achieved using laboratory equipment at low contact stresses, such as the inclined plane and the direct shear at a constant loading rate. With such equipment, it is possible to observe the interface failure modes, sudden sliding, gradual sliding and non-uniform sliding, to establish which is the most suitable shear strength angle, between φ_0, φ_{stand}, φ_{lim}, φ_{kin} and φ_{dyn}, to guarantee the level of safety with respect to the slipping risk on the slope and to the tear due to the differential settlements that may occur in different areas of the plant.

Similar recommendations can also be extended to the case of seismic loading for predicting post-seismic displacements of the cover and/or tensile force induced in the geosynthetics by the displacements themselves.

Given the low level of contact stresses, it is emphasized that the design parameter of interface resistance should be more accurately represented by the secant value rather than the tangent ones, which are usually supplied by the standard direct shear test.

Finally, the standard methodology for establishing interface failure, φ_{stand}, may be acceptable only when the kinematic behaviour is non-uniform; conversely, interface failure showing both uniform and uniformly accelerated motions should be characterized by the angles φ_0 or φ_{lim}, depending on the level of safety to be achieved.

Several researchers studied the different factors affecting the design of geotextile filters, indicating the precautions to be used for each. Nevertheless, many studies point out that the design of geotextile filters for internal unstable cohesionless soils is a critical aspect that needs further investigation, as no design criteria recognized as reliable by the scientific community are currently available.

The authors were engaged in these aspects, developing two reliable methods for evaluating the internal stability of cohesionless base soils (SimulFiltr and Butterfly-Wings), two equipment capable of analysing the long-term geotextile filter-base soil compatibility under different boundary conditions, and a new methodology to assess the compatibility of geotextile filter in contact with an internally unstable cohesionless soil. The proposed methodology is based on a geometrical, experimental and microstructural approach.

The geometrical approach consists of considering the pore size distribution (PSD) of the geotextile filter with the grain size distribution (GSD) of the base soil, comparing the values of O_F and the values of the critical diameter of suffusion, D_c. This comparison enables a more accurate determination of whether the mass of soil particles with a diameter lower than Dc could pass through the filter, clog the filter, or accumulate at the soil-filter interface, causing blinding.

The experimental approach is based on the results of long-term filtration tests that allow for the evaluation of long-term system permeability (or flow rate), blinding, clogging and piping. The micro-structural approach is based on the analyses of SEM images taken on the tested geotextiles to observe the clogging and blinding phenomena and compare them with the geometrical approach and long-term filtration test results. A new design procedure was finally proposed according to this new methodology.

Acknowledgments

I want to express my sincere gratitude to all those who, over the years, have contributed to the advancement of research on soil–geosynthetic interfaces, the outcomes of which are partially summarized in this lecture. First and foremost, I wish to thank the co-authors who equally contributed to the preparation of this paper: Giuseppe Cardile and Marilene Pisano, for their continuous support in the development of research on soil–reinforcement interaction under pullout conditions (Chapter 2); Paolo Carrubba, with whom the challenging topic of interface characterization via inclined plane tests was explored (Chapter 3); and Maria Clorinda Mandaglio and Stefania Bilardi, who helped further the studies on geotextile filters (Chapter 4). My gratitude also extends to the many Ph.D students, manufacturers, and colleagues who contributed to the research efforts. Though too numerous to list in full, I would like to give special recognition to Piergiorgio Recalcati, Domenico Gioffrè, Lidia Sarah Calvarano, Laura Carbone, and Paolo Pavanello, whose contributions to interface strength studies have been particularly significant. Finally, a heartfelt thank you goes to my friends Alberto Mazzucato and Daniele Cazzuffi, who instilled in me a passion for geotechnical and geosynthetic engineering from a very young age.

References

1. R.A. Jewell, G.W.E. Milligan, R.W. Sarsby, D. Dubois, Interaction between soil and geogrids. T. Telford (Ed.), Symposium on Polymer Grid Reinforcement in Civil Engineering, pp. 18-30 (1985).
2. N. Moraci, F. Montanelli, Analisi di prove di sfilamento di geogriglie estruse installate in terreno granulare compattato. Ital Geotech J. **4**, 5-21 (2000).
3. E.M. Palmeira, G.W.E. Milligan, Scale and other factors affecting the results of pull-out tests of grid buried in sand. Géotechnique **39**, 511-524 (1989). https://doi.org/10.1680/geot.1989.39.3.511
4. R.F. Wilson-Fahmy, R.M. Koerner, Finite element modelling of soil-geogrid interaction with application to the behavior of geogrids in a pullout loading condition. Geotext Geomembranes **12**, 479-501 (1993). https://doi.org/10.1016/0266-1144(93)90023-H
5. N. Moraci, D. Gioffrè, A simple method to evaluate the pullout resistance of extruded geogrids embedded in a compacted granular soil. Geotext Geomembranes **24**, 198-199 (2006). https://doi.org/10.1016/j.geotexmem.2005.11.001
6. T. Matsui, K.C. San, Y. Nabeshima, U.N. Amin, Bearing mechanism of steel grid reinforcement in pullout test. In Proceedings of International Symposium on Earth Reinforcement, Fukuoka, Kyushu, Japan, pp. 101-105 (1996).
7. N. Moraci, P. Recalcati, Factors affecting the pullout behaviour of extruded geogrids embedded in compacted granular soil. Geotext Geomembranes **24**, 220-242 (2006). https://doi.org/10.1016/j.geotexmem.2006.03.001
8. G.W.E. Milligan, R.F. Earl, D.I. Bush, Observations of photo-elastic pullout tests on geotextiles and geogrids. In Proceedings of 4th International Conference on Geotextiles, Geomembranes and Related Products, pp. 747-751 (1990).
9. D.T. Bergado, R. Shivashankar, M.C. Alfaro, J.-C. Chai, A.S. Balasubramaniam, Interaction behaviour of steel grid reinforcements in a clayey sand. Géotechnique **43**, 589-603 (1993).
10. R.A. Jewell, Soil Reinforcement with geotextile. CIRIA Thomas Telford, London (1996).
11. E.M. Palmeira, Bearing force mobilisation in pullout tests on geogrids. Geotext Geomembranes **22**, 481-509 (2004). https://doi.org/10.1016/j.geotexmem.2004.03.007

12. E.M. Palmeira, Soil–geosynthetic interaction: modelling and analysis. Geotext Geomembranes **27**, 368-390 (2009). https://doi.org/10.1016/j.geotexmem.2009.03.003
13. G. Cardile, D. Gioffrè, N. Moraci, L.S. Calvarano, Modelling interference between the geogrid bearing members under pullout loading conditions. Geotext Geomembranes **45**, 169-177 (2017). https://doi.org/10.1016/j.geotexmem.2017.01.008
14. G. Cardile, M. Pisano, N. Moraci, A predictive model for pullout bearing resistance of geogrids embedded in a granular soil. F. Calvetti, F. Cotecchia, A. Galli, C. Jommi (Eds.), Geotechnical Research for Land Protection and Development, Springer International Publishing, Cham, Lecture Notes in Civil Engineering, 40, pp. 438-445 (2020). https://doi.org/10.1007/978-3-030-21359-6_46
15. G. Cardile, L.S. Calvarano, D. Gioffrè, N. Moraci, Experimental evaluation of the pullout active length of different geogrids. In Proceedings of 10th International Conference on Geosynthetics, ICG 2014, Berlin, Germany, pp. 1184-1190 (2014).
16. D. Cazzuffi, N. Moraci, L.S. Calvarano, G. Cardile, D. Gioffrè, P. Recalcati, The influence of vertical effective stress and of geogrid length on interface behaviour under pullout conditions. Geosynthetics **32**, 40-50 (2014).
17. N. Moraci, D. Cazzuffi, L.S. Calvarano, G. Cardile, D. Gioffrè, P. Recalcati, The influence of soil type on interface behavior under pullout conditions. Geosynthetics **32**, 42-50 (2014).
18. G. Cardile, N. Moraci, L.S. Calvarano, Geogrid pullout behaviour according to the experimental evaluation of the active length. Geosynth. Int. **23**, 194-205 (2016). https://doi.org/10.1680/jgein.15.00042
19. R.S. Johnston, K.M. Romstad, Dilation and boundary effects in large scale pullout test. In Proceedings of 12th International Conference on Soil Mechanics and Foundation Engineering, Rio De Janeiro, 2, pp. 1263-1266 (1989).
20. S. Hayashi, M.C. Alfaro, K. Watanabe, Dilatancy effects of granular soil on the pullout resistance of strip reinforcement. In Proceedings of International Symposium on Earth Reinforcement, Fukuoka, Kyushu, Japan, pp. 39-44 (1996).
21. M.L. Lopes, M. Ladeira, Influence of confinement, soil density and displacement rate on soil-geogrid interaction. Geotext Geomembranes **14**, 543-554 (1996). https://doi.org/10.1016/S0266-1144(97)83184-6
22. D.T.-T. Chang, F.C. Chang, G.S. Yang, C.Y. Yan, The influence factors study for geogrid pullout test. ASTM STP1379-EB Grips, Clamps, Clamping Techniques, and Strain Measurement for Testing of Geosynthetics, Ed. Stevenson, 14 p. (2000). https://doi.org/10.1520/STP13477S
23. K. Farrag, M. Morvant, Effect of clamping mechanism on pullout and confined extension tests. ASTM STP1379-EB Grips, Clamps, Clamping Techniques, and Strain Measurement for Testing of Geosynthetics, Ed. Stevenson, pp. 89-96 (2000). https://doi.org/10.1520/STP13474S
24. I. Schmid, M. Kazda, Vertical distribution and radial growth of coarse roots in pure and mixed stands of Fagus sylvatica and Picea abies. Can. J. For. Res. **31**, 539-548 (2001). https://doi.org/10.1139/x00-195
25. M. Sugimoto, A.M.N. Alagiyawanna, K. Kadoguchi, Influence of rigid and flexible face on geogrid pullout tests. Geotext Geomembranes **19**, 257-277 (2001).
26. G. Cardile, M. Pisano, P. Recalcati, N. Moraci, A new apparatus for the study of pullout behaviour of soil-geosynthetic interfaces under sustained load over time. Geotext Geomembranes **49**, 1519-1528 (2021). https://doi.org/10.1016/j.geotexmem.2021.07.001

27. M. Pisano, G. Cardile, N. Moraci, P. Recalcati, Long-term pullout tests to analyse the soil-geogrid interaction. In Proceedings of 12th International Conference on Geosynthetics, September 17-21, 2023, Rome, Italy, pp. 617–622 (2023).
28. D. Cazzuffi, L.S. Calvarano, G. Cardile, N. Moraci, P. Recalcati, European experience in pullout tests: The influence of geogrid's geometry and structure on interface behaviour. Geosynthetics **29**, 42-51 (2011).
29. N. Moraci, G. Cardile, Pullout behaviour of different geosynthetics embedded in granular soils. In Proceedings of 4th Asian Regional Conference on Geosynthetics, Shanghai, China, 17-20 June 2008, pp. 146-150 (2008).
30. N. Moraci, G. Cardile, The use of pullout test results in the serviceability limit states design of earth reinforcement structures. In Proceedings of GeoAfrica 2009, Cape Town, 2-5 September 2009, 6 p. (2009).
31. ISO/TR 20432, Guidelines to the determination of long-term strength of geosynthetics for soil reinforcement. International Organization for Standardization, ISO, Ginevra (2007).
32. T.H. Hanna, M. Touahmia, Comparative behavior of metal and tensar geogrid strip under static and repeated loading. In Proceedings of Geosynthetics '91, Atlanta, GA, USA, February 1991, pp. 575-585 (1991).
33. N. Meyer, A. Nernheim, U. Kohler, Geosynthetic-soil interaction under cyclic loading. In Proceedings of 3rd European Geosynthetics Conference, Munich, Germany, pp. 635-639 (2004).
34. Y. Min, D. Leshchinsky, H.I. Ling, V.N. Kaliakin, Effects of sustained and repeated tensile loads on geogrids embedded in sand. Geotech. Test. J. **18**, 204-225 (1995).
35. A. Nernheim, Interaktionsverhalten von geokunststoff und erdstoff bei statischen und zyklishen beansprungen. Dissertation an der Technischen Universität Clausthal (2005).
36. D.J. Raju, J. Fannin, Monotonic and cyclic pull-out resistance of geogrids. Géotechnique **47**, 331-337 (1997).
37. D.J. Raju, J. Fannin, Load-strain-displacement response of geosynthetic in monotonic and cyclic pullout. Can. Geotech. J. **35**, 183-193 (1998).
38. D.J. Raju, Monotonic and cyclic pullout resistance of geosynthetic. Ph.D. Thesis, University of British Columbia, Vancouver, Canada (1995).
39. S. Yasuda, H. Nagase, H. Marui, Cyclic pull-out test of geogrids in soils. In Proceedings of International Symposium on Earth Reinforcement Practice, Fukuoka, Japan, pp. 185-190 (1992).
40. N. Moraci, G. Cardile, Influence of cyclic tensile loading on pullout resistance of geogrids embedded in a compacted granular soil. Geotext Geomembranes **27**, 475-487 (2009). https://doi.org/10.1016/j.geotexmem.2009.09.019
41. N. Moraci, G. Cardile, Deformative behaviour of different geogrids embedded in a granular soil under monotonic and cyclic pullout loads. Geotext Geomembranes **32**, 104-110 (2012). https://doi.org/10.1016/j.geotexmem.2011.11.001
42. G. Cardile, M. Pisano, N. Moraci, The influence of a cyclic loading history on soil-geogrid interaction under pullout condition. Geotext Geomembranes **47**(4), 552-565 (2019). https://doi.org/10.1016/j.geotexmem.2019.01.012
43. M. Pisano, G. Cardile, N. Moraci, The influence of cyclic loading histories on soil-geogrid interface behaviour under pullout conditions. In Proceedings of 11th International Conference on Geosynthetics, September 16-21, 2018, Seoul, Korea, pp. 2543–2548 (2018).

44. M. Pisano, G. Cardile, N. Moraci, Soil-geogrid interface behaviour under cyclic pullout conditions. In Proceedings of the 7th International Conference on Earthquake Geotechnical Engineering, June 17-20, 2019, Rome, Italy, pp. 4507–4514 (2019).
45. N. Moraci, G. Cardile, M. Pisano, Soil-geosynthetic interface behaviour in the anchorage zone [Comportamento all'interfaccia terreno-geosintetico nella zona di ancoraggio]. Ital Geotech J. **51**(1), 5-25 (2017). https://dx.doi.org/10.19199/2017.1.0557-1405.005
46. G. Cardile, M. Pisano, Advances in soil reinforcement with geosynthetics: from laboratory tests to design practice. Ital Geotech J. **54**(3), 52–82 (2020). https://dx.doi.org/10.19199/2020.3.0557-1405.052
47. P. Pavanello, P. Carrubba, N. Moraci, Dynamic friction and the seismic performance of geosynthetic interfaces. Geotext Geomembranes **46**, 715-725 (2018a). https://doi.org/10.1016/j.geotexmem.2018.06.005
48. P. Pavanello, P. Carrubba, N. Moraci, Evaluation of geosynthetic interface friction at low normal stress: Comparison between two different test procedures. Acta Sci. Pol. Archit. **21**, 3–10 (2022a). https://doi.org/10.22630/ASPA.2022.21.4.25
49. P. Pavanello, P. Carrubba, N. Moraci, Geosynthetic interface friction at low normal stress: Two approaches with increasing shear loading. Appl. Sci. **12**(3), 1065 (2022b). https://doi.org/10.3390/app12031065
50. T.D. Stark, A.R. Poeppel, Landfill liner interface strengths from torsional ring shear tests. J. Geot. Eng. **120**(3), 597-615 (1994). https://doi.org/10.1061/(ASCE)0733-9410(1994)120:3(597)
51. T.D. Stark, T.A. Williamson, H.T. Eid, HDPE geomembrane/geotextile interface shear strength. J. Geot. Eng. **122**(3), 197-203 (1996). https://doi.org/10.1061/(ASCE)0733-9410(1996)122:3(197)
52. A. Moss, L. Anderson, Cylinder direct shear: a new test method. Advances in transportation and geoenvironmental systems using geosynthetics, In Proceedings of the Geo-Denver 2000, Denver, CO, USA, 5–8 August 2000; pp. 106–116 (2000). https://doi.org/10.1061/40515(291)7
53. EN ISO 12957-1, Geosynthetics - determination of friction characteristics - part 1: direct shear test. European Committee for Standardization, CEN, Brussels, Belgium (2018).
54. B.M. Bacas, H. Konietzky, J.C. Berini, C. Sagaseta, A new constitutive model for textured geomembrane/geotextile interfaces. Geotext Geomembranes **29**(2), 137–148 (2011). https://doi.org/10.1016/j.geotexmem.2010.10.014
55. B.M. Bacas, J. Cañizal, H. Konietzky, Shear strength behavior of geotextile/geomembrane interfaces. J. Rock Mech. Geotech. Eng **7**(6), 638-645 (2015). https://doi.org/10.1016/j.jrmge.2015.08.001
56. D. Cazzuffi, P. Recalcati, L.S. Calvarano, Direct shear and inclined plane experimental activities for different interfaces among geosynthetics and soils. In Proceedings of Geo-Congress, Los Angeles, CA, USA, March 26–29, 2023 (2023). https://doi.org/10.1061/9780784484685.05
57. S. Lalarakotoson, P. Villard, J.P. Gourc, Shear strength characterization of geosynthetic interfaces on inclined planes. Geotech. Test. J. **22**(4), 284-291 (1999). https://doi.org/10.1520/GTJ11240J
58. R. Reyes-Ramirez, J.P. Gourc, Use of the inclined plane test in measuring geosynthetic interface friction relationship. Geosynth. Int. **10**(5), 165-175 (2003). https://doi.org/10.1680/gein.2003.10.5.165

59. H.N. Pitanga, J.P. Gourc, O.M. Vilar, Interface shear strength of geosynthetics: Evaluation and analysis of inclined plane tests. Geotext Geomembranes **27**(6): 435–446 (2009). https://doi.org/10.1016/j.geotexmem.2009.05.003
60. L. Carbone, J.P. Gourc, P. Carrubba, P. Pavanello, N. Moraci, Dry friction behaviour of a geosynthetic interface using inclined plane and shaking table tests. Geotext Geomembranes **43**(4), 293-306 (2015). https://doi.org/10.1016/j.geotexmem.2015.05.002
61. EN ISO 12957-2, Geosynthetics - determination of friction characteristics - part 2: inclined plane test. European Committee for Standardization, CEN, Brussels, Belgium (2005).
62. J.P. Gourc, R. Reyes-Ramirez, Dynamics-based interpretation of the interface friction test at the inclined plane. Geosynth. Int. **1**(6), 439–454 (2004). https://doi.org/10.1680/gein.2004.11.6.439
63. L. Briançon, H. Girard, J.P. Gourc, A new procedure for measuring geosynthetic friction with an inclined plane. Geotext Geomembranes **29**(5), 472-482 (2011). https://doi.org/10.1016/j.geotexmem.2011.04.002
64. P. Pavanello, P. Carrubba, N. Moraci, The characterisation of geosynthetic interface friction by means of the inclined plane test. Geotext Geomembranes **49**(1), 257-275 (2021). https://doi.org/10.1016/j.geotexmem.2020.10.027
65. P. Pavanello, P. Carrubba, N. Moraci, P. Pezzano, M. Miuzzi, Parameters and conditions affecting friction angles in geosynthetic interfaces. In Proceedings of the Eurogeo 6, Ljubljana, Slovenia, 25–28 September (2016).
66. M.K. Yegian, A.M. Lahlaf, Dynamic interface shear strength properties of geomembranes and geotextiles. J. Geotech. Eng. **118**(5), 760-779 (1992).
67. M.K. Yegian, Z.Y. Yee, J.N. Harb, Seismic response of geosynthetic/soil systems. Geoenvironment 2000. In Proceedings of a Specialty Conference of Geotechnical Engrg. And Envir. Engrg., ASCE, February 24-26, New Orleans, Louisiana (1995).
68. A. De, T.F. Zimmie, Estimation of dynamic interfacial properties of geosynthetics. Geosynth. Int. **5**(1–2), 17–39 (1998).
69. I.J. Park, M.W. Seo, J.B. Park, S.Y. Kwon, J.S. Lee, Estimation of the dynamic properties for geosynthetic interfaces. In Proceedings of 13th World Conference on Earthquake Engineering, Vancouver, Canada, 1–6 August (2004).
70. M.K. Yegian, U. Kadakal, Foundation isolation for seismic protection using a smooth synthetic liner. J. Geotech. Geoenviron. Eng. **130**(11), 1121 (2004). https://doi.org/10.1061/(ASCE)1090-0241(2004)130:11(1121)
71. E. Kavazanjian, X. Wu, M. Arab, N. Matasovic, Development of a numerical model for performance-based design of geosynthetic liner systems. Geotext Geomembranes **46**, 166-182 (2018). https://doi.org/10.1016/j.geotexmem.2017.11.005
72. M.K. Yegian, U. Kadakal, Geosynthetic interface behavior under dynamic loading. Geosynth. Int. **5**(1–2), 1-16 (1998).
73. J. Kim, M. Riemer, J.D. Bray, Dynamic properties of geosynthetic interfaces. Geotech. Test. Journ. **28**(3), 288-296 (2005). https://doi.org/10.1520/GTJ11856
74. P.J. Fox, C.J. Nye, T.C. Morrison, J.G. Hunter, J.T. Olsta, Large dynamic direct shear machine for geosynthetic clay liners. Geotech. Test J. **29**(5), 392-400 (2006). https://doi.org/10.1520/GTJ100183
75. J.D. Ross, P.J. Fox, Dynamic shear strength of GMX/GCL composite liner for monotonic loading. J. Geotech. Geoenviron. Eng. **141**(7), 11 (2015). https://doi.org/10.1061/(ASCE)GT.1943-5606.0001198

76. M.K. Yegian, J.N. Harb, Slip displacements of geosynthetic systems under dynamic excitation. In: Earthquake Design and Performance of Solid Waste Landfills, ASCE (1995).
77. J. Wartman, J.D. Bray, R.B. Seed, Inclined plane studies of the Newmark sliding block procedure. J. Geotech. Geoenviron. Eng. **129**(8), 673-684 (2003). https://doi.org/10.1061/(ASCE)1090-0241(2003)129:8(673)
78. P. Pavanello, P. Carrubba, N. Moraci, The determination of interface friction by means of vibrating table tests. Geotext Geomembranes **46,** 830-835 (2018b). https://doi.org/10.1016/j.geotexmem.2018.06.006
79. N. Newmark, Effects of earthquakes on dams and embankments. Géotechnique **15**(2), 139-160 (1965).
80. J.P. Giroud, Granular filters and geotextile filters, in Proceeding of Geofilters '96, Montréal, Canada, May (1996), pp. 565-680.
81. J.P. Giroud, Quantification of geosynthetic behavior. Geosynth. Int. **12**, 2-27 (2005).
82. R.D. Holtz, B.R. Christopher, R.R. Berg, Geosynthetic Design and Construction Guidelines, (U.S. Federal Highway Administration, National Highway Institute, Washington, D.C., Publication No. FHWA-NHI-07-092, 592 p. 1998).
83. N. Moraci, Geotextile filters: Design, characterization and factors affecting clogging and blinding limit states, Proceeding of 9th International Conference on Geosynthetics - Geosynthetics: Advanced Solutions for a Challenging World, Guaruja, Brazil, USA, May 23-27 (2010), pp. 413-438.
84. G.R. Koerner, R.M. Koerner, Lessons learned from geotextile filter failures under challenging field conditions. Geotext. Geomembr. **43**, 272-281 (2015).
85. E.M. Palmeira, A review on some factors influencing the behaviour of nonwoven geotextile filters. Soils and Rocks, **43**, 351–368 (2020).
86. N. Moraci, S. Bilardi, M. C. Mandaglio, Factors affecting geotextile filter long term behaviour and their relevance in the design. Geosynth. Int. **29**, 19-42 (2022).
87. E.M. Palmeira, Geotextile filters: from idealization to real behaviour (Giroud Lecture 2023). Geosynth. Int. **32**, 2-39 (2025).
88. N. Moraci, D. Ielo, M.C. Mandaglio, Assessment of internal stability of granular soils. Rivista Italiana di Geotecnica, **50**, 27-43 (2016).
89. A.W. Skempton, J.M. Brogan, Experiments on piping in sandy gravels. Gèotechnique **44**, 449-460 (1994).
90. N. Moraci, The filter action of geotextiles on contact with granular soils: characterization, interaction and modeling. Ph.D Thesis in Geotechnical Engineering, University of Padova, Italy, (1992).
91. A. Kezdi, Increase of protective capacity of flood control dikes. Department of Geotechnique, Technical University, Budapest, Report No.1. (In Hungarian), 1969.
92. J.L. Sherard, Sinkholes in dams of coarse, broadly graded soils, in Proceeding of 13th International Congress on Large Dams, Vol. 2, New Delhi, India, October - November (1979).
93. T.C. Kenney, D. Lau, Internal stability of granular filters. Can. Geotech. J. **22**, 215-225 (1985).
94. T.C. Kenney, D. Lau, Reply: Internal stability of granular filters. Can. Geotech. J. **23**, 420-1040 (1986).
95. R.P. Chapuis, Similarity of internal stability criteria for granular soils. Can. Geotech. J. **29**, 711-713 (1992).

96. N. Moraci, M.C. Mandaglio, D. Ielo, A new theoretical method to evaluate the internal stability of granular soils. Can. Geotech. J. **49**, 45-58 (2012).
97. N. Moraci, M.C. Mandaglio, D. Ielo, Reply to the discussion by Dallo and Wang on "A new theoretical method to evaluate the internal stability of granular soils". Can. Geotech. J. **49**, 869-874 (2012).
98. A. Silveira, An analysis of the problem of washing through in protective filters, in Proceeding of 6th international conference on soil mechanics and foundation engineering, Montreal, Canada, September (1965).
99. M.C. Mandaglio, N. Moraci, E. Polimeni, Assessment of internal stability of granular soils by means of theoretical and laboratory methods, in book: Internal Erosion in Earthdams, Dikes and Levees, S. Bonelli et al. (Eds.) Springer International Publishing, 60-68. (2019).
100. N. Moraci, M.C. Mandaglio, D. Ielo, Analysis of the internal stability of granular soils using different methods. Can. Geotech. J. **51**, 1063-1072 (2014).
101. N. Moraci, M.C. Mandaglio, D. Ielo, Reply to the discussion by Ni et al. on "Analysis of the internal stability of granular soils using different methods". Can. Geotech. J. **52**, 385-391 (2015).
102. D. Cazzuffi, A. Mazzucato, N. Moraci, M. Tondello, A new test apparatus for the study of geotextiles behaviour as filters in unsteady flow conditions. Geotext. Geomembr. **17**, 313-329 (1999).
103. ASTM D5101. Standard Test Method for Measuring the Filtration Compatibility of Soil-Geotextile Systems, American Society for Testing and Materials, West Conshohocken, PA, USA.
104. E.M. Palmeira, M.G. Gardoni, D.W. Bessa da Luz, Soil–geotextile filter interaction under high stress levels in the gradient ratio test. Geosynth. Int. **12**, 162–175 (2005).
105. E.M. Palmeira, M.G. Gardoni, The influence of partial clogging and pressure on the behaviour of geotextiles in drainage systems. Geosynth. Int. **7**, 403–431 (2000).
106. N. Moraci, M.C. Mandaglio, S. Bilardi, Soil/geotextile filter compatibility: a geometrical, experimental and micro-structural approach. Geosynth. Int. **30**, 29 - 46 (2023).
107. M.W. Khan, A.R. Dawson, A.M. Marshall, Filtration performance of nonwoven geotextiles with internally-stable and –unstable soils under dynamic loading. Geotext. Geomembr. **50**, 293 – 311 (2022).
108. D. Cazzuffi, A. Mazzucato, N. Moraci, M. Tondello, A new test apparatus for the study of geotextiles behaviour as filters in unsteady flow conditions, Proceeding of Geofilters '96, Montreal, Canada, May (1996).
109. D. Cazzuffi, N. Moraci, Design of geotextile filters in contact with granular soils, Proceeding of the 4th Asian Regional Conference on Geosynthetics, Shanghai, China, September (2008).
110. S.K. Bhatia, Q. Huang, Geotextile filters for internally stable/unstable soils. Geosynth. Int. **2**, 537-565 (1995).
111. J. Lafleur, Selection of geotextiles to filter broadly graded cohesionless soils. Geotext. Geomembr. **17**, 299-312 (1999).
112. C.F.E.M. (Canadian Foundation Engineering Manual), 4th edition, Canadian Geotechnical Society, (2006).
113. N. Moraci, M.C. Mandaglio, S. Bilardi, Behaviour of geotextile filters in contact with internally unstable cohesionless soils, in Proceedings of the 12ICG, Geosynthetics: Leading the Way to a Resilient Planet, Roma, Italy, September 17-21, (2023).

114. S. Qureshi, R.M. Kogler, S.K. Bhatia. Long term filtration behavior of nonwoven geotextiles. Geotextiles, Geomembrane and Related Products, Den Hoedt (ed.), Balkema, Rotterdam, (1990).
115. E.M. Palmeira, R.J. Fannin, Y.P. Vaid, A study on the behaviour of geotextile systems in filtration tests. Can. Geotech. J. **33**, 899–912 (1996).
116. E.M. Palmeira, M.G. Gardoni, Drainage and filtration properties of non-woven geotextiles under confinement using different experimental techniques. Geotext. Geomembr. **20**, 97–115 (2002).
117. E.M. Palmeira, H.L. Trejos-Galvis, Opening sizes and filtration behaviour of nonwoven geotextiles under confined and partial clogging conditions. Geosynth. Int. **24**, 125-138 (2017).
118. E.M. Palmeira, D.L.A. Melo, I.P. Moraes-Filho, Geotextile filtration opening size under tension and confinement. Geotext. Geomembr. **47**, 566–576 (2019).

Geosynthetic-reinforced granular platforms: from experimentation to design

Laurent Briançon
GEOMAS, Université de Lyon, INSA-Lyon, Villeurbanne, France

Abstract. Geosynthetic soil reinforcement techniques are simple and cost-effective solutions, improving the mechanical properties of the granular platform, reducing its thickness and thus decreasing its environmental footprint. These innovative techniques are often the subject of research projects that propose rules for their design and setup. These studies require experimental and numerical approaches to define the interaction laws between the geosynthetic and the surrounding soil, and to achieve the objectives of proposing standards for each application.

1 Introduction

Construction on poor-quality soils or with a risk of loss of bearing capacity over time is a major challenge for the planning of land and economic development of a country. Environmental considerations imposed since the 2000s have strengthened economic choices on soil improvement and reinforcement solutions. Geosynthetic reinforcement has found a place of choice in structures to reduce the risk, improve load transfer and thus control the settlements. Geosynthetic reinforcement of the granular layers also reduces their thickness and therefore limits the extraction of natural material and its transport.

These innovative techniques are often the subject of research projects that propose rules for their design and setup. These studies require laboratory experiments to identify mechanisms and characterize the interactions between soils and geosynthetic sheets. They are often paired with numerical models calibrated on the experimental results to put into equations, mechanisms and eventually propose design rules. Full-scale validations are also essential for a complete engineering transfer. To achieve all these objectives, the first step is to make a full state of the art to determine the scientific and technical obstacles and situate your study in this context.

The diversity of geosynthetic sheets and the complexity of interaction mechanisms require R&D actions to bring together researchers, producers, and designers.

In the present paper, this scientific and technical path will be detailed on two geosynthetic reinforcement applications:

1. For granular platforms with cavity risk

In this field, French research began in 1997 with the project RAFAEL and continued for more than twenty years with full-scale experimentations, laboratory tests, and DEM simulations in the projects GEOINOV or PITAGOR, resulting in the French Standard XP G38-065 (2020).

2. For load transfer platforms of pile-supported embankment

Several research projects have addressed this topic to study the geosynthetic's role on this technique's efficiency. In France, two research projects investigated pile-supported embankments (ASIRI, 2012; ASIRI+, 2025) and, more particularly, the role of the geosynthetic in the granular platform.

2 Geosynthetic-reinforced platform overlying voids

In a first approach, the geosynthetic reinforcement of a granular platform overlying voids is simple. The geosynthetic is usually set at the base of the platform, and when a cavity appears below it, it avoids a collapse by the membrane effect. The efforts applied to the geosynthetic, on the void, are equilibrated by friction with the soil in the anchorage areas around the void (Fig. 1).

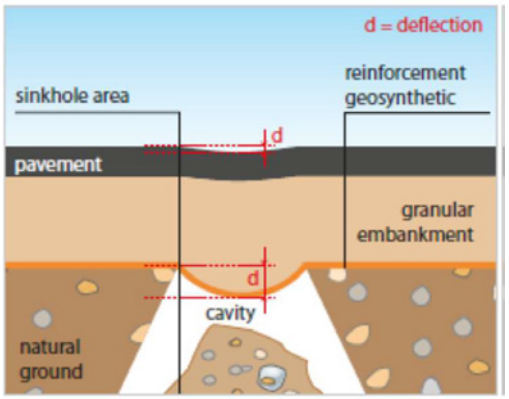


Fig. 1. Principle of Geosynthetic-reinforced platform overlying voids

2.1 Initial studies

Experimental and theoretical studies on this topic [1], [2], [3], [4], [5] have given rise to analytical design methods in British standard [6], German standard [7] and French recommendations [8]. Using simple assumptions, it is possible to determine the load applied on the geosynthetic, to predict its vertical displacements and the surface settlement, knowing the stiffness of the geosynthetic and the size of the cavity. It was generally assumed that the geosynthetic was fixed at the edge of the cavity.

2.1.1 Determination of the load applied to the geosynthetic

In the first studies (before 2000), two collapse mechanisms were proposed, giving different loading cases on the geosynthetic. The first one, used in the British standard [6] supposed a soil collapse with an angle of draw approximately equal to the peak friction angle of the fill soil (Fig. 2a). The load applied on the geosynthetic is supposed equal to the sum of the weight of the layer above the geosynthetic and the overload applied at the surface (eq 1).

$$q = \gamma.H + p \qquad (1)$$

The second one, proposed by Gourc [1] and Giroud [3] and observed in a full-scale experiment performed in the framework of the French project RAFAEL [6], [8] supposed a cylindrical collapse of the soil layer located on the geosynthetic above the cavity and a parabolic shape of the geosynthetic deflexion (Fig. 2b). In this case, the arching theory

developed by Terzaghi for the case of a trapdoor [9] is adapted considering that the soil immediately above the cavity tries to move in a vertical column between the adjacent masses of soil which have remained stable. The shear strength along the slip lines resists the displacement of the active soil mass, reducing stresses on the geosynthetic sheet above the cavity and increasing vertical stresses at the edge of the cavity (eq 2).

$$q = \frac{\gamma.D}{4.K.tan\emptyset}\left(1 - e^{-\left(\frac{4.K.H.tan\emptyset}{D}\right)}\right) + pe^{-\left(\frac{4.K.H.tan\emptyset}{D}\right)} \quad (2)$$

The assumption of truncated geometry for the collapse leads to solutions, which, in certain cases, may be very different from those obtained by the design method based on cylindrical soil collapse over the cavity.

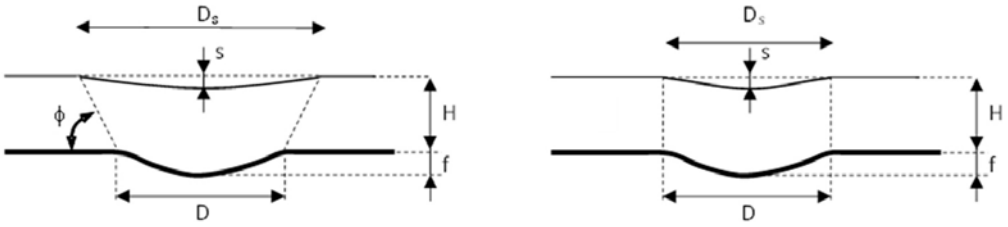


Fig. 2. Mechanisms of collapse during the opening of a sinkhole

2.1.2 Determination of the geosynthetic behaviour

Due to their structure, geosynthetics have low bending rigidity and can therefore be strained only by tensile forces. When they are submitted to stresses that are perpendicular to their horizontal plane, they take the shape of a membrane so that the tensile forces guarantee the static equilibrium of the sheet. For 2D applications, analytical formulations of the membrane effect, which can be used to evaluate tensile forces and sheet strains, have been developed for homogeneous and isotropic sheets and simple load geometries [3], [10]. It was generally assumed that the geosynthetic was fixed at the edge of the cavity and that there was a decrease of tension at the edge of the cavity due to the change of orientation of the geosynthetic. The equilibrium of the part of the geosynthetic sheet allows writing the relation between the maximal tension T_{max}, the applied load q, the stiffness of the geosynthetic J, and the diameter of the cavity D (eq 3):

$$T_{max} = \frac{q.D}{2}\sqrt{1 + \frac{1}{6.\varepsilon_{max}}} = J.\varepsilon_{max} \quad (3)$$

A simplified equation links the maximal strain ε_{max} the geosynthetic with its maximal vertical displacement f and the diameter of the cavity (eq 4):

$$\varepsilon_{max} = \frac{8}{3}\left(\frac{f}{D}\right)^2 \quad (4)$$

2.1.3 Determination of the soil behaviour

When a granular material is subjected to a collapse, particles move together, increasing its apparent volume. The increase in soil volume is linked to the nature, granular distribution, initial compactness and state of stresses applied to the material. The ratio between the new soil volume and the initial soil volume is called the expansion coefficient Ce. This mechanism

has been used to explain the difference of vertical displacement between the geosynthetic and the surface in the full-scale experimentation of RAFAEL and it has been proposed that when a cylindrical soil collapse is assumed, the significant reduction in settlement at the surface is due to the expansion of the soil above the cavity.
Assuming that the deformed shapes of both the geosynthetic and the free surface of the fill are parabolic, it is thus possible to find a relation between the maximum surface displacement s, the maximum geosynthetic vertical displacement f, the expansion coefficient Ce and height of soil cover H (eq 5):

$$s = f - 2H(Ce-1) \quad (5)$$

2.2 Soil/Geosynthetic interactions highlighting

Following an experimental work made to validate a process of monitoring [11], new developments validated by numerical simulations [12] were proposed [13], [14] to significantly improve the RAFAEL method. The originality of this experimental work was to perform a full-scale experimentation of cavity opening below a geosynthetic-reinforced platform and to monitor the geosynthetic with optical fibers above the cavity and in the anchorage areas. The main result of this experimentation was to highlight the displacement of the geosynthetic in the anchorage areas. From this observation, new assumptions were made to simulate the behavior of the geosynthetic taking into account the frictional behavior of the geosynthetic sheet in the anchorage areas through a Coulomb friction law (Fig. 3). The stretching of the geosynthetic sheet in the anchorage areas leads to an increase of the vertical displacement of the sheet and the friction and a change in the orientation of the sheet at the edge of the cavity. For classical values of the friction between soil and geosynthetic, these developments lead (comparatively to the classic RAFAEL method) to a doubling of the value of the tensile stiffness of the product to ensure the surface deflexion criterion.

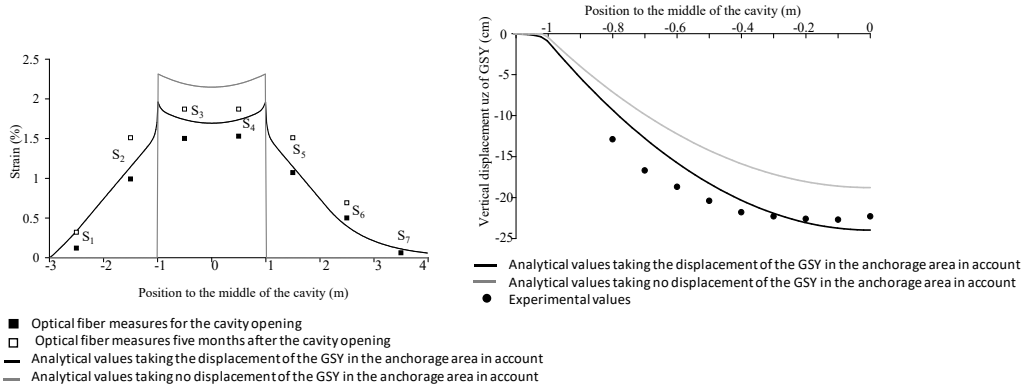


Fig. 3. Comparison between experimental and analytical values [14]

2.3 Cavity opening process highlighting

A new study was launched in the framework of the French project GEOINOV, particularly in the thesis of [15], to verify the new analytical development proposed by [14] and calibrate a numerical model with DEM. This study consists of a full-scale experimentation of geosynthetic-reinforced platforms under cavities, DEM simulations, and a comparison of experimental and numerical values with analytical ones.

2.3.1 Full-scale experimentations

These experiments aim to simulate the opening of a circular sinkhole under a reinforced granular embankment and to analyze the behavior of the fill material over the cavity for two experimental sections reinforced by two different geosynthetics.

These sections are located around a manhole that enables for triggering the opening of the sinkholes to proceed to monitoring. After the progressive opening of the sinkhole, the cavity was cleaned, and loading tests were conducted. Specific instrumentation was set up to measure the strain and the deflection of the geosynthetic, the displacements within the embankment, the load transfer towards the edges of the cavity, and the surface settlement during the entire experiment.

The embankment used was 1 m high and was made of cleaned, rounded gravel with particle sizes from 20 to 40 mm. The geosynthetics used in the two reinforced sections were chosen to have weakened capacities, thus allowing for easy monitoring of their deformation during the tests. Their tensile properties were relatively similar to enable easy comparison between tests. GSY 1 is a high tenacity yarn of polyester cables combined with a woven fabric (Tensile strength at 2% strain = 65.2 kN/m). GSY 2 is a warp-knitted grid combined with high tenacity polyester cables (Tensile strength at 2% strain = 8.9 kN/m). More details of materials and instrumentation are given in [16].

A specific device was designed and built to enable the progressive opening of a circular sinkhole in three stages, corresponding to diameters of approximately 0.75, 1.25, and 2.2 m. The device consists of a vertical pipe, one meter high and 2.2 m in diameter, separated in two parts of equal height by a metallic plate on which a trapdoor is centered (Fig. 4). The lower part, under the trapdoor, is initially empty, whereas the upper part is initially filled and then emptied during the experiment to simulate the formation of a sinkhole. The upper part of the opening device is filled with two levels of concentric inflated tubes: one external large tube, with an external diameter of nearly 2.2 m, an internal diameter of 1 m and a height of approximately 0.5 m, and two smaller tubes in the middle of the large tube, one on top of the other (Fig. 3). These two smaller tubes have an external diameter of 1 m, for an internal diameter of 0.5 m and a total height reaching 0.5 m. The remaining volume above the trapdoor and the tubes is filled with clay pebbles.

The progressive cavity opening under the embankment can be physically simulated by opening the trapdoor to create a cavity 0.75 m in diameter, by deflating the two inner tubes to create a cavity 1.25 m in diameter, and by deflating the two outer tubes to create a cavity 2.2 m in diameter.

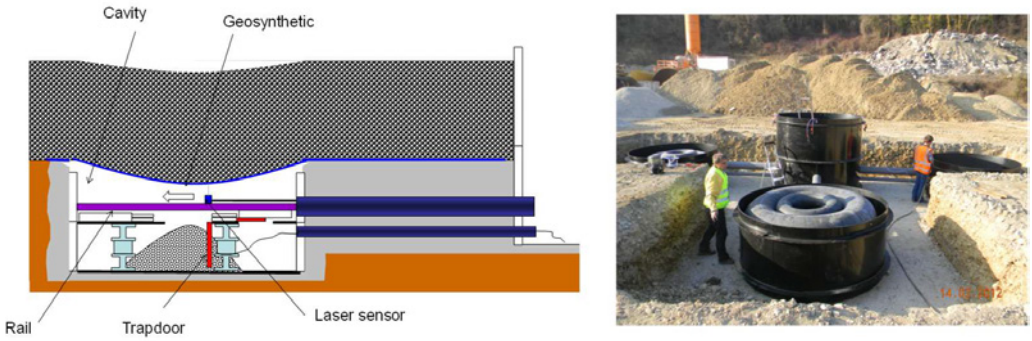


Fig. 4. Full-scale experimentation facilities [15]

The monitoring of the experimental sections was designed to measure the following during the emptying of the cavity and the traffic tests:

- the strain of the GSY by Bragg gratings optical fibers,

- the deflection of the geosynthetic sheet with a laser distance sensor moving on a rail inside the cavity,
- the displacements within the embankment with a Ground Penetrating Radar analysis,
- the load transfer mechanisms with Earth Pressure Cells,
- the surface displacements with topographic and manual measures.

During the opening of the cavity, movements within the embankment could be observed by the two layers of metallic landmarks and the GPR analysis. Fig. 5a highlights the kinematic behavior of section 2 during the opening of the sinkhole. Section 2 is presented because it enabled monitoring of the most important displacements. Fig. 5a illustrates the consistency of the displacements during the opening of the sinkhole on all sections and at every considered level (geosynthetic sheet, first and second level of metallic landmarks). These results should be considered cautiously because they were obtained consecutively with an arduous calibration and the combination of GPR measurements, topography, and landmark positions. Hence, the precision is the size of the granular particles of the embankment (± 0.02 or 0.03 m).

An interesting point to note is the relatively "cylindrical" geometry of the collapsed portion of the embankment over the opened sinkhole.

From the vertical displacement of the reinforcement and the surface settlement, it is possible to estimate the expansion coefficient of the embankment, taking into account the cylindrical shape of the collapse area. To do so, surface and geosynthetic deflections are assumed to be a paraboloid of revolution. The expansion factor Ce is obtained by the volume variation of the granular material inside the collapsed soil cylinder (eq 5): $Ce_1 = 1.04$; $Ce_2 = 1.035$.

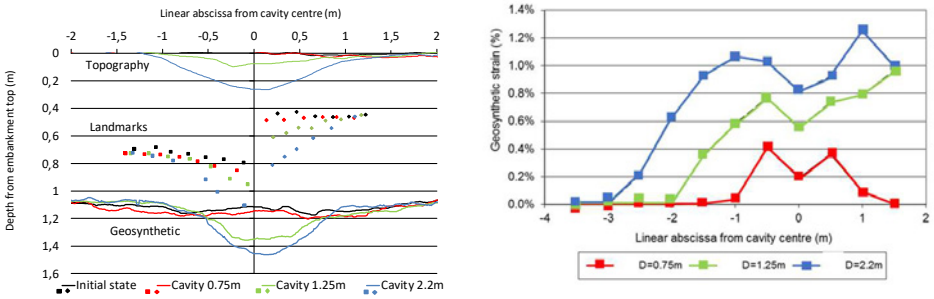


Fig. 5. Main results of the full-scale experimentation [16]

Fig. 5b. presents the evolution of the geosynthetic strains measured in section 1 with optic fibers during the sinkhole opening. It can be noted that: the strains increase with the opening of the cavity, the maximum strain value is located above the sinkhole and its edges, and for a given diameter cavity, the strain values decrease in the anchorage areas due to friction mobilization. These observations confirm those made by [11].

2.3.2 DEM simulations

The 3D numerical model used in this study [17] is a coupling method that combines the finite and discrete element methods [12] and allows consideration of the discrete nature of the granular material, the fibrous and continuous nature of the geotextile sheet and the complex frictional interaction at the interface between the soil particles and the finite elements used to describe the geotextile behaviour (rolling sliding and friction).

The finite elements used to describe the 3D geotextile behaviour are thin, triangular elements. An anisotropic tensile behaviour of the geosynthetic (no compression or bending

strength) can be considered according to the definition of specific stiffness values of the fibres in particular directions - for example, in reinforcement directions [8].
The discrete nature of the granular embankment is described using elementary rigid particles of various sizes interacting through contact points [18]. A classical linear elastic contact law [19] characterized by a friction coefficient μ and two stiffness coefficients kn and ks in the normal and tangential directions, respectively, is used.

The macroscopic behaviour of the numerical sample is a function of shape and grading of the particles, the numerical bulk density of the granular assembly and the intrinsic microscopic contact parameters [20], [21]. Since there is no direct relation between the microscopic parameters (normal and tangential stiffness, contact friction coefficient, grading, particle shape and density of the numerical sample) and macroscopic parameters (Young's modulus, Poisson's ratio and internal friction angle), a specific calibration process is required. A classical way to obtain the micromechanical parameters is to simulate laboratory tests performed in well-controlled conditions and compare the numerical results to the experimental ones. In this study, a numerical process based on comparisons between numerical and experimental triaxial test results [20] is used to calibrate the numerical parameters. The main advantage of the DEM method compared to the others lies to the possibility to simulate large displacements, collapse, compaction or expansion and to easily consider the change of the granular behaviour consecutively with the variation of its density (due to collapse, for example) or of the loading process (loading, unloading, cycles). The numerical procedure needed to solve the problem is described in [17].

The numerical models (Fig. 6) used for this study include, from top to bottom:

- an assembly of clumps of two spheres describing the behaviour of the granular embankment,
- thin, finite, triangular elements to consider the geotextile behaviour,
- a layer of spheres regularly distributed in a square mesh at the base of the model to mimic the action of an elastic supporting soil and well-simulate the sinkhole opening process.

Frictionless lateral walls are used to consider the symmetry so that the cavity is located on a corner of the numerical model.
Two numerical opening processes are defined:

- Process A - a progressive opening of the cavity by an increase of the cavity diameter D,
- Process B - a gradual downward movement of all spheres under the geosynthetic included in a circular area of diameter D.

The velocity of the opening processes is low enough to avoid dynamic effects.

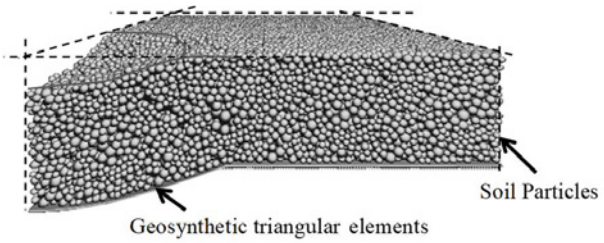


Fig. 6. Geometry of the numerical samples [17]

2.3.3 Comparison between experimental and numerical results

The experimental results of the geosynthetic deflexion and the surface settlements are compared in Fig. 7a to the numerical results obtained with the two cavity opening processes. The numerical results corresponding to Process A match well with the experimental results established with a similar opening process, whereas the results of Process B significantly underestimate the geosynthetic deflexion and the surface settlement. This shows that the opening process is of primary importance to the design of such reinforced structures and should be considered in a proper estimation of the surface settlement. Note that the good concordance between the experimental and numerical results of the surface settlements in the case of the progressive cavity opening process shows that when roughly similar shape and grading for the numerical and experimental soils are used, it is possible to well describe the expansion mechanism involved within the granular embankment. Fig. 7b compares the geosynthetic strain measured in the axis of the cavity by optical fibres and the numerical strain obtained using the progressive cavity opening process: experimental and numerical geosynthetic strains are close, providing new evidence of the relevance of the numerical tool. Concerning the expansion mechanism, it can be noted that the numerical average value of the expansion coefficient of 1.048, computed for the progressive cavity opening process, is consistent with the average experimental value of 1.037 obtained by considering the experimental results of full-scale experiments [16].

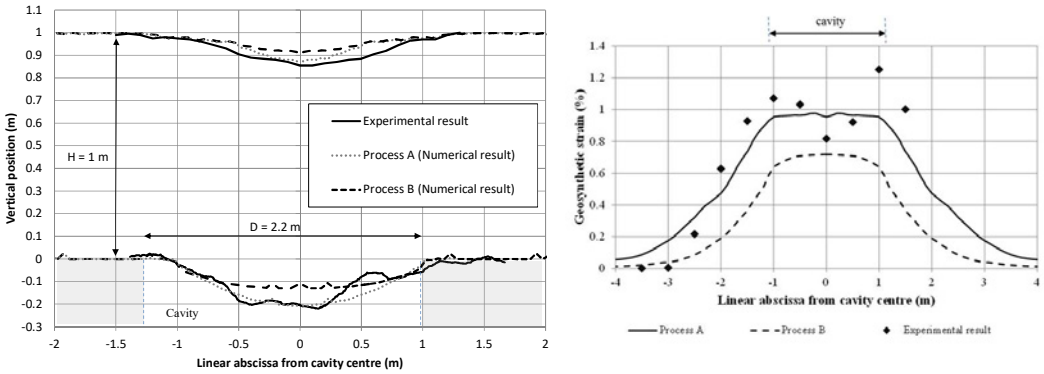


Fig. 7. Comparison between experimental and numerical results a) Surface settlement and geosynthetic deflexion b) Geosynthetic strain [17]

2.3.4 Design rule improvement

The comparison between the experimental and the numerical values highlighted that the numerical model was able to well simulate the mechanisms. Then, it was used to analyse the load transfer mechanisms inside the platform.

A comparison between the two opening processes can be made for a given value of the cavity diameter (D/H = 2.2) by the vertical displacements of the geosynthetic f, the surface settlements s and the expansion coefficients Ce. The numerical average values of the expansion coefficient are computed by considering the volume resulting from the surface settlement Vs, the volume due to the deflexion of the geosynthetic sheet Vg, and the initial volume V0 of the column of soil located above the cavity (Ce = (V0+Vg-Vs)/V0). As seen in Table 1, a comparison between the numerical average expansion coefficients for the two opening processes indicates a significant difference in the expansion mechanisms within the granular embankments as a function of the kinematic of the opening process. The maximal vertical displacements of the geotextile and the maximal surface settlements presented in Fig. 8a are also very different from one opening process to another. Considering that the total

vertical loads acting on the geotextile are quite similar from the two opening processes (equivalent efficiency), the differences obtained for the vertical displacement of the geotextile and the surface settlement can appear to be strange unless the load distributions acting on the geosynthetic are different from one case to another.

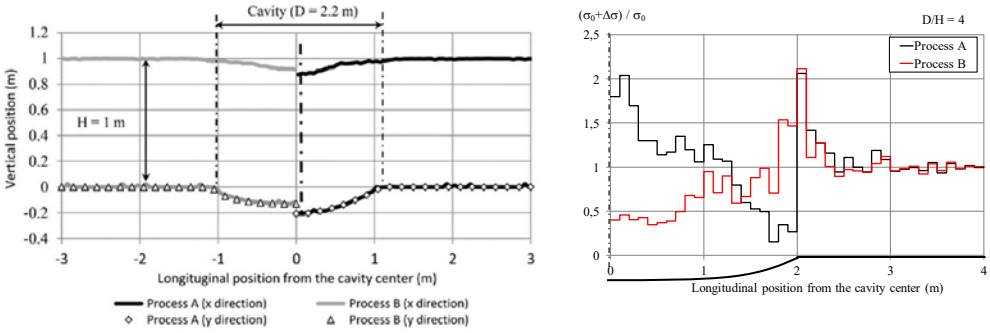


Fig. 8. Analysis of the mechanisms a) Vertical geosynthetic displacements and surface settlements (m) for both processes and for H/D = 2.2 b) Increase in the vertical stresses acting on the upper face of the geosynthetic for H/D = 4

Table 1. Comparison between the two processes.

	Process A	Process B
Maximal vertical displacements of the geotextile (m)	0.207	0.13
Maximal surface settlements (m)	0.126	0.086
Coefficient of expansion Ce	1.048	1.036

To explain this difference of values, the increase of stresses $(\sigma_0+\Delta\sigma)/\sigma_0$, where σ_0 represents the initial vertical stresses acting on the upper face of the geosynthetic, are computed in both opening processes through the vertical contact forces at the upper soil/geotextile interface. Stresses are computed on annular areas centred on the cavity. Results are presented Fig. 8b for D/H = 4. Note that similar results are obtained for each cavity diameter considered.

The load distribution (Fig. 8b) obtained in the case of the increasing diameter process (Process A) takes an approximate conical shape whereas the load distribution is rather constant or slightly inverted in the case of the gradual settlement process (Process B). The load transfer mechanisms occurring within the granular embankment at the beginning of the gradual settlement process are not disturbed during the opening process, and the load transfer mechanisms are continually modified during the increase of the cavity diameter. In both cases, at the end of the opening process, the shearing forces at the periphery of the soil cylinder sited over the cavity are rather similar such that the efficiencies and the total loads acting on the part of the geosynthetic located above the cavity are equivalent.

These experimental and numerical studies highlighted that:

- the mechanisms developed inside the granular platform depended on the cavity opening process,
- the assumption of a uniform load applied on the geosynthetic above the cavity was wrong,
- the assumption of the geosynthetic displacement in the anchorage area was true

From these important new results, the design method proposed by [13] has been improved by the implementation of new load distribution shapes above the cavity. This involves an iterative process to resolve the equations of equilibrium of both horizontal and vertical efforts on any part of the geosynthetic sheet (above the cavity and in the anchorage areas). In the present case, the original analytical formulation proposed by [13] is adapted for approximate conical and inverted parabolic distributions (Fig. 9).

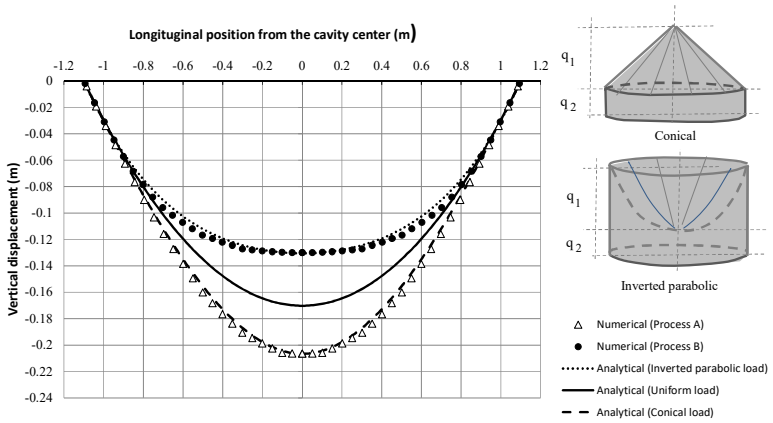


Fig. 9. Comparison between analytical and numerical geosynthetic deflection [17]

A second improvement consists of keeping the assumption proposed by Terzaghi of a moving cylinder of soil between fixed areas, that seems from a kinematic point of view, relevant for the two opening processes as long as the ratio D/H is sufficiently large. However, the comparison between the analytical and numerical models shows that the coefficient Ka of the (eq 2) must be equalled to 1.3 for this experimentation. A similar analysis of the literature performed by [22], dealing with the numerical and experimental studies of the trapdoor problem, shows that values of K of 1.17 and 1.46 for sands and coarse granular materials, respectively, are needed to fit Terzaghi's formulation. All these results show that the usual value of Ka is not well adapted to evaluate the load transfer mechanisms.

2.4 Validation

Comparison between numerical and analytical values of geosynthetic strain shows a good agreement (Fig. 10). Process B has been validated with experimental results of [15], but Process A remains to be validated experimentally. This validation was made from laboratory tests [23] where a specific device was designed to simulate the two processes (Fig. 11):

- For the progressive procedure (Process A), a cone filled with sand was emptied making it possible to simulate a concentric opening of the cavity under the geosynthetic sheet. The cone was connected under the table using screws, and the filled sand was kept in the cone by a lock. When the lock is opened, the sand will fall out of the cone vertically with the same duration for each test (500 seconds), hence leading to the opening of the cavity.
- For the trapdoor procedure (Process B), a rigid circular plate combined with a jack was used to simulate the cavity opening.

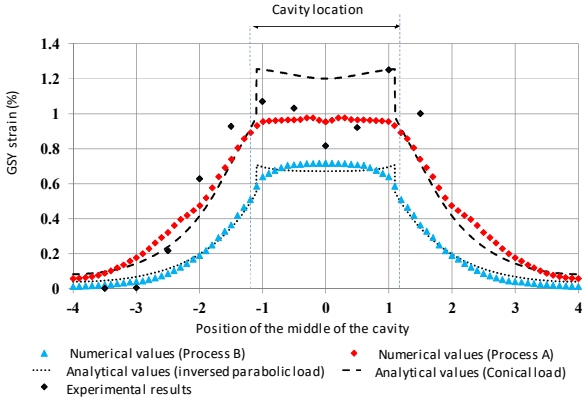


Fig. 10. Comparison between analytical and numerical geosynthetic strain [17]

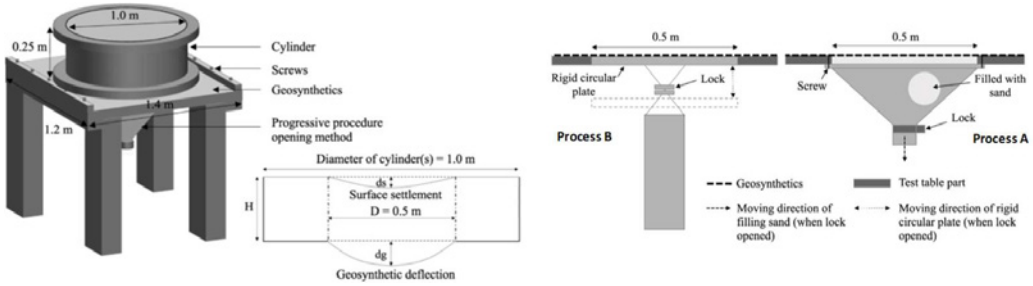


Fig. 11. a) Experimental device [23] b) Opening processes

From 50 tests for two cavity openings, two geosynthetic, three heights of embankment, and three types of granular soil, the following conclusions were exposed:

- Thanks to a network of tactile pressure sensors, placed on and at the edges of the cavity, enabled the measurement of the load distribution during the cavity opening, this experimentation showed the differences in behavior for two opening processes and confirmed findings from previously published numerical studies (Fig. 8b)
- In the case where the trapdoor was used as an opening mode, the surface settlement and deflections of geosynthetics were lower than those of the progressive mode for both woven and nonwoven geosynthetics as proposed in [17]

Finally, a numerical model based on DEM and FEM [24] coupling was used to reproduce the laboratory experiments performed by [23]. These numerical and experimental coupled studies highlighted the complex mechanisms developed within the reinforced mattress over the cavity. The numerical and experimental results of the surface settlement of the embankment, the geosynthetic deflection, and the global expansion coefficient over the cavity area (which was generally not estimated in practice) were compared for three different heights of granular embankment (H/D=0.5, 1, 1.5), two cavity-opening modes (trapdoor and progressive) and different geotextile stiffnesses (woven and nonwoven). For the cases presented in this study, the numerical model was a relevant tool to analyze the load transfer mechanisms within the granular embankment and predict the reinforced embankment behavior. Its main advantage was its ability to provide extra microscopic information at the grain level that was difficult to measure experimentally, such as: local deformations, grain displacements, the network of contact forces, and stress distribution within the granular mattress.

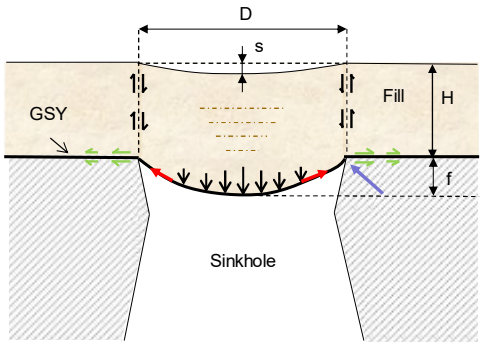
This numerical study confirmed that, for a given embankment height, soil geometrical characteristics mainly affected the surface settlement values owing to different expansion phenomena, while the geosynthetic deflection remained slightly affected. The numerical results also confirmed that the vertical displacements of the geosynthetic were similar for the studied thicknesses of the granular soil layers because a higher embankment is more prone to the load transfer mechanisms. As expected, the surface settlement and geosynthetic deflection were functions of the geosynthetic tensile stiffness [24]. The sensitivity analysis also showed that the local expansion coefficient over the cavity was not uniform over the depth of the embankment and depended on the cavity-opening mode, grain shape, soil density, shear strain rate, and height of the embankment. The obtained stress profiles confirmed previous numerical studies showing that the stress was not uniform over the cavity, as was commonly considered in most existing design methods. The shear stress within the granular embankment was also computed, and the results showed that the direction of shearing for both opening modes was not the same. While shearing progresses from the cavity center to its borders for progressive openings, it progresses from the borders toward the center in the trapdoor-opening mode, which explains the load distribution acting on the geotextile sheet for different opening modes.

2.5 French Standard

Despite such uncertainty on parameters such as the expansion coefficient, a French standard [24] has been proposed based on all previous studies. This standard considers for a ratio between the heigh of the embankment and the cavity diameter $1.5/4 < H/D < 3$:

- The cylindrical collapse above the cavity
- The geosynthetic membrane effect
- The geosynthetic displacement in the anchorage areas
- The load transfer from Terzaghi's formula with a correct coefficient K = 1.

Due to the difficulty in defining the cavity opening process, its role in the applied load on the geosynthetic has not been considered, and a uniform load distribution is proposed (Fig. 12). This standard could be revised when future studies bring new developments, particularly considering the expansion coefficient.



	Observed mechanisms	Considered mechanisms in the standard
↕	Shearing (Terzaghi formula) and cylindrical collapse	
↓	Non uniform load on geosynthetic	Uniform load on geosynthetic
→	Membrane effect	
⇌	Friction in anchorage area	Friction in anchorage area
↖	Increase in tension at the edge of the cavity	
	Non uniform expansion of soil	Uniform expansion of soil

Fig. 12. Considered mechanisms in the French Standard

This example shows that, thanks to a combination of complementary experimental and numerical studies, it has been possible to completely describe the complex mechanisms inside the granular platform and between the geosynthetic and the surrounding soil to propose a design method usable by engineers.

3 Geosynthetic-reinforced pile-supported embankment

Pile-supported embankments have been widely used as a soil-reinforcement technique over the last 50 years [25]. Piles known as rigid inclusions are installed in soft soil and a load transfer platform (LTP) is placed on the pile head. Granular LTPs created using sand or gravel are often reinforced using geosynthetics, e.g., in Geosynthetic-Reinforced Pile-Supported Embankments (GRPSE).

This technique aims to transfer the load of a new construction by the vertical rigid inclusions to the substratum to avoid loading the soft soil layer. Generally, a granular layer (called LTP) is set up between the construction and the rigid inclusions to improve the load transfer to the pile head. A part of the load is also transferred to the soft soil which can settle and transfer this load by friction to the pile (Fig. 13). Several standards on recommended design methods for GRPSEs are available [26], [27], [28], and [29]. All existing standards recommend reinforcing the granular LTP using geosynthetics. However, no rule is available to choose between geotextile or geogrid, identify the optimum installation location or the number of geosynthetics. Moreover, although geosynthetic reinforcement seems to improve load transfer to the piles, some issues regarding its role in settlement reduction or load transfer remain unresolved.

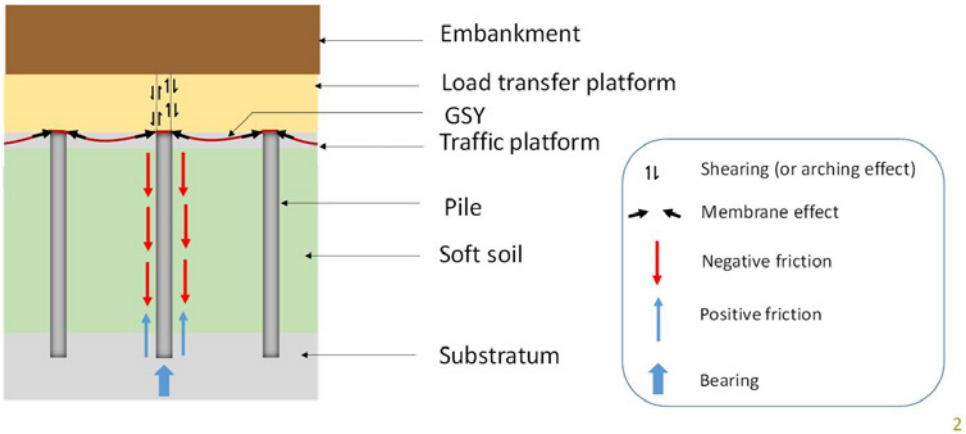


Fig. 13. Mechanisms developed inside a GRPSE

In France, this technique was studied under the ASIRI project between 2005 and 2012. This project specifically studied the behavior of reinforced soil under embankment and slab. Recommendations were published in 2012. In 2016, following a survey in this area, it appeared that some topics could be further studied, such as the mechanisms developed inside the LTP or the behavior of reinforced soils under complex solicitations, and a new project called ASIRI+ was launched. The new recommendations will be published in 2025.

As part of the French national project ASIRI+ (2019–2025), specific studies on the role of geosynthetics in the mechanisms developed inside the LTP were launched. They are based on:

- a strongly state-of-the art review
- an experimental study
- a numerical simulation

3.1 State-of-the-art review

The objective of this state-of-the-art review based on full-scale experiments and laboratory tests was to highlight how the role of geosynthetics has been investigated in an attempt to design the most effective and representative experiment.

3.1.1 Full-scale tests review

The advantages of the full-scale experiments are the presence of soft soil and that all the construction stages are realistic. The difficulties encountered with full-scale tests are the homogeneity of the soft soil over the test area and the low number of trials tested in the same study.

3.1.1.1 Experimentation without comparison with unreinforced section

Many studies are performed to validate the design of the GRPSE or to analyze the mechanisms inside the LTP but the geosynthetic reinforced section is not compared to an unreinforced section [30] to [38]. These experiments still allow bringing components of understanding on the contribution of the geosynthetic to the load transfer.

Almeida et al. [30] presented a full-scale GRPSE experiment over very soft soil to highlight the behavior of a biaxial geogrid placed directly on the pile head. A 1 m excavation under the geogrid was conducted to induce rapid mobilization of the geogrid and compare it with its behavior in a non-excavated area. This study showed that settlement occurred during embankment construction and was slightly delayed in non-excavated areas.

Wachman et al. [31] monitored a GRPSE using a granular platform reinforced with three monoaxial geogrids. The strain gauges installed on the metallic piles and the earth pressure cells located on the soil below the granular platform highlighted the load transfer. The construction of the first meter of the embankment increased the stress on the piles and soil; the stress on the pile increased significantly during the construction of the second part of the embankment, whereas it decreased in the soil. Load transfer also occurred at the base of the embankment because of the hard spot at the vertical end of the pile in the granular platform. The strain gauges installed in the upper geogrid showed that the geogrid was mobilized during the first stage of the embankment construction, and was not mobilized further when the stress applied to the soil decreased. Unfortunately, the strain in the two lower geogrids and settlement could not be measured owing to the failure of some sensors during setup.

Cheng et al. [32] monitored a GRPSE using a granular platform reinforced with three biaxial geogrids. The earth pressure highlighted that load transfer occurred during embankment construction. The settlement measured below the load-transfer platform increased during the first 60 days and reached a plateau before the end of embankment construction. This change in trend corresponds to a decrease in the stress measured on the soil between the piles.

Nguyen et al. [33] monitored a GRPSE using a granular platform reinforced with two biaxial geogrids. Using stress measurements, they calculated the efficiency, compared it with that of several design methods, and observed that most of them slightly overestimated the efficiency. The differential settlement was stabilized after setting up 0.5 m of embankment. The non-mobilization of the geogrid could be attributed to the absence of differential settlement. Interestingly, the same experimental efficiency was observed in all the design methods, considering the high mobilization of the geogrid. In this study, the load transfer was only due to the arching effect inside the granular platform. This difference between the design methods and the measurements is probably due to poor simulation of the behavior of the piles; they were not anchored, and their settlement was not considered, which led to overestimation of the differential settlement, and thus the tension in the geogrids.

Pan et al. [34] monitored two GRPSEs using a granular platform reinforced with two biaxial geogrids. Floating piles were present in both embankments but with different lengths (L = 8 m and L = 15 m). The embankments were constructed in two stages with an equilibrium stage after each construction stage. The evolution of soil arching and the deformation of the soil, piles, and geogrids during the construction and equilibrium stages of the embankments were monitored. Based on this experiment, the authors proposed a schematic diagram of the grid strain, pile-soil stress ratio, and pile-soil differential settlement evolution under different soil arching states. They identified three stages in the evolution of soil arching: no soil arching, formation of soil arching, and stabilization of soil arching (Fig. 14):

- At the beginning of the construction, a large differential settlement was observed because the arching was incomplete, and geogrids were solicited (stage b)
- When the arching was full, the floated piles were loaded, and their settlement decreased the differential settlement and the mobilization of the geogrids (stage c)
- After stage c, even when the construction of the embankment was followed, there was no new differential settlement between the soil and piles; thus, no new strain developed in the geogrids (stage d).

This study shows that, for this specific experiment with floating piles, the strain of the geogrid mainly occurs in the initial stage of filling, which is caused by the differential settlement of the pile and soil during the filling process. However, the strain in the second filling process is small, mainly owing to the overall settlement of the composite foundation.

Riccio et al. [35] monitored deep-soil-mixing column-supported embankments without a load-transfer platform. The biaxial geogrid was placed in the middle of the 0.20 m sand layer to prevent mechanical damage. Unlike the previous studies, differential settlement occurred during the last part of the embankment construction. This situation might be attributed to the absence of a load-transfer platform and the presence of a thick traffic platform that can support the load brought by the first meter of the embankment. A comparison of the stress of sensors located over the column and over the geogrid and the sensors located between the columns and the geogrid indicated that the stress measured on the GGR above the pile is 2.5 times higher than the stress measured below the GGR above the pile. In this specific case, the role of the geogrid is predominant.

King et al. [36] monitored a GRPSE using a granular platform reinforced with two monoaxial geogrids. Earth pressure cell data showed the development of the arching stress. During the load-transfer platform construction, the measured stresses closely matched the overburden stress. Partial arching was observed as an increase of the stress on the pile and a reduction of the stress measured between two piles below the geogrids after an increase in the embankment height from 0.65 m to 1.90 m. After the embankment construction, the arching behavior was well established, except when several columns were installed near the monitored area. The strain gauges installed on the geogrids did not exhibit mobilization of the geogrid during the construction of the embankment, with the strain measured to be below 0.15%.

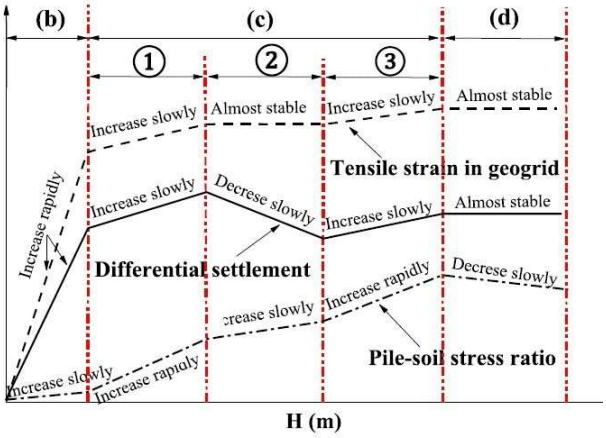


Fig. 14. Schematic diagram of grid strain, pile-soil stress ratio, and pile-soil differential settlement evolution under different soil arching states [34]

Gunnvard et al. [37] monitored a GRPSE using a granular platform reinforced with two monoaxial geogrids. The embankment was constructed on 8 m long untreated timber piles with 1.1 m spacing in a triangular pattern without pile caps. The earth pressure cell data showed that after the construction of the embankment and road, pile efficiency remained relatively constant (0.29–0.48) for most of the monitoring period. The extensometers installed on both geogrids measured very low strain (< 0.2%), highlighting the partially mobilized geogrids. This non-mobilization could be attributed to the lack of differential settlement between the piles and soil owing to the floating piles.

Khansari and Vollmert [38] monitored geosynthetic-reinforced pile-supported structures. The prediction models in three design codes ([26], [27], [28]) are applied to estimate the loads and strains in different structural components of the embankment. The results show that the models fail to accurately estimate the geogrid reinforcement deflection and overestimate the loads on the pile foundation in this project:

- 189%, 15% and 32% by EBGEO [27], BS8006-1 [26] and CUR 226 [28], respectively for the stress on the mid-span GR,
- 43%, 75% and 89% by the models in EBGEO [27], BS8006-1 [26] and CUR 226 [28], respectively for the forces on the pile foundation

Even if these studies do not compare reinforced sections with an unreinforced section, the instrumentation allows noticing that the geosynthetic requires large differential settlement to be mobilized and in many experimentations, the strain of geosynthetic is very low, highlighting that the major part of the load transfer is due to the shearing inside the granular platform.

3.1.1.2 Experimentation with comparison with unreinforced section

Some authors were able to compare reinforced and non-reinforced granular platforms ([39] to [42]).

Oh and Shin [39] performed full-scale experimentation of pile-supported embankment with four sections: three with a load transfer platform reinforced by three geogrids of various grid sizes and one without geogrid. According to the results of vertical stress and settlement analysis:

- The mechanisms occurred during the embankment construction,
- Geogrids brought a reduction of settlement compared to the section without geogrid but required a differential settlement to be mobilized and finally, the reduction of settlement reached 30% for this specific experimentation,

- Geogrids brought an increase of stress on the pile head but a great part of the efficiency was due to the arching effect inside the granular platform.

Briançon and Simon [40] performed full-scale experimentation of pile-supported embankment on soft soil with four sections: section 1 without pile, section 2 with piles but without a load transfer platform, sections 3 and 4 with piles and a granular platform reinforced respectively by a biaxial geotextile and by two monoaxial geogrids. For the three pile-supported embankment sections, a large part of the mechanisms occurred during the construction. The sections with a reinforced granular platform brought a better load transfer. For the three reinforced sections, the settlement of soil was reduced by a factor between 2.5 and 4. Settlement slightly increased after the end of the embankment construction for all three reinforced sections. This full-scale experimentation highlights the great efficiency of the reinforced granular platform and a significant reduction of settlement. Unfortunately, the lack of a non-reinforced granular platform in section 2 does not allow identifying the exact role of the geosynthetic in this efficiency. Even if this experimentation was not able to identify the exact role of geosynthetics, an instrumentation of the geosynthetics with optical fiber allowed to show that the maximum strain took place at the edge of the pile heads after embankment construction in the geotextile for section 3, and in the geogrid in section 4R (Fig.15).

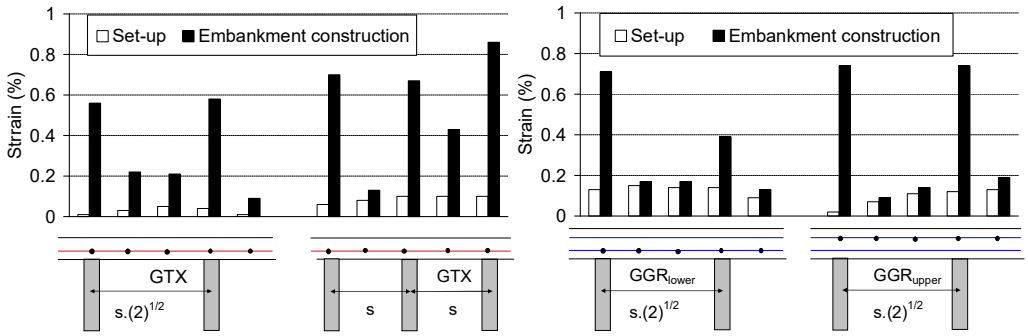


Fig. 15. a) Geosynthetic strain in section 3, (b) Geosynthetic strain in section 4 [40]

A recent study [43] compared the results of [40] with Design Guidelines. They show that all Design Guidelines overestimated the geosynthetic tension.

In the frame of the construction of the new South Europe Atlantic high-speed line, full-scale experimentation has been performed to validate a GRPSE solution [41]. Two configurations have been evaluated: “Pile-supported Embankment” (PSE) with pile cap, and GRPSE with two geogrids inside the granular platform. Comparing both sections, it is noticed that the GRPSE solution leads to the same load transfer to the pile head as the PSE solution. A great part of the settlement occurred during the embankment construction for both sections. The differential settlement at the pile head level between the pile and the soil was higher in the GRPSE section but since it happened during the construction phase, there was no negative impact at the surface of the embankment.

Geogrid strain was measured during the embankment construction and during the period of six months following the embankment construction. Fig.16 presents the strain in both geogrids at the end of this monitoring period. For the three GRPE sections, the maximum strain is found at the on and around the pile for both geogrids. The strain decreases at increased distances from the piles. Note that strains are higher in the lowest geogrid, which is more mobilised. All these results are in concordance with results of [40], especially for the distribution of strain inside the geogrids.

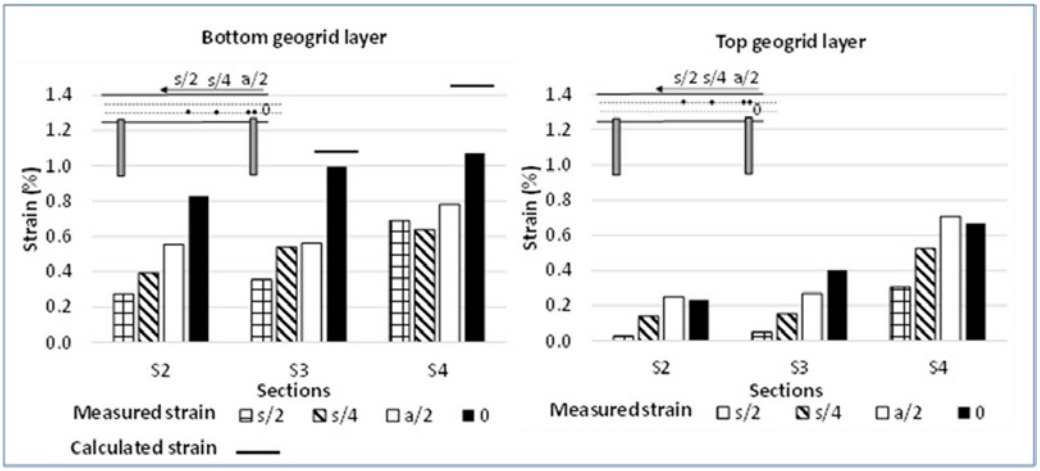


Fig. 16. a) Lower geogrids strain, (b) Upper geogrid strain [41]

Wang et al. [42] performed two large-scale field tests of the pile-supported embankments for an international motor-racing circuit in China. In the first section, there was no geosynthetic in the load transfer platform. In the second section, the load transfer platform was reinforced by three triaxial geogrids. In the non-reinforced section, during the embankment construction, the stress applied on soil is higher than the one in the reinforced section and decreases after the embankment construction to reach the same value. In the non-reinforced section, the stress on the pile head is 15% lower than in the reinforced section.

3.1.2 Laboratory tests review

The advantages of the laboratory tests are the control of initial conditions (same soft soil for all the tests), the possibility to test many configurations on the same reinforced soil, and the lack of constraint of time to perform the tests. The difficulties of laboratory tests are the respect to the scale without boundary effect, the geometry and the way to reproduce the compressibility of the soft soil, and the various stages of the construction. In the laboratory tests of Zaeske [44] or Eekelen [45], all these considerations were not respected: only four piles were tested, the geosynthetic was anchored on the frame of the box, the similitude laws were not respected. Even if Zaeske and Eekelen's works brought important progress in the understanding of the mechanisms developed inside the LTP, their experimental conditions seem to increase the role of the geosynthetic on the mechanisms.

The full-scale experimentation of Sloan [46] performed on nine piles can be classified as a laboratory test because all tests were performed in the same location and the settlement of the soft soil is simulated by the dissolution of geofoam after the construction of the embankment. The geometry of these tests was at a good scale but the settlement was triggered after the construction and, after the dissolution of the geofam, there was no reaction of the soft soil below the geogrids. Even if the settlement was blocked during the construction of the embankment, it is interesting to note that the load transfer began during the construction of the embankment before the mobilization of the geogrid (probably due to the compressibility of the geofoam). This observation shows that the differential settlement required to transfer the load by shearing in the granular platform is very small. As the mobilization of the geogrids requires a larger differential settlement, the load transfer is firstly due to the shearing in the granular layer. This experimentation highlights that the blockage of the settlement during the construction of the embankment does not allow well to simulate the mechanism inside the load transfer platform.

Lee et al. [47] performed a real-scale laboratory experiment where they compared many configurations of GRPSE. The use of 16 piles allowed isolating the central grid from the boundary effects. The soft soil was simulated by a compressible foam (Elastic modulus = 50 kPa). The earth pressure cells data showed that the section with the geotextile brought the best efficiency at the end of the embankment construction. The efficiency of the reinforced section by geogrids was the same as this one in the section without geosynthetic. The section with the geotextile was also the only one able to reduce the settlement compared to the case without reinforcement. The bad results obtained with the two sections reinforced with geogrids can be attributed to using sand at the base of the embankment in contact with the geogrids, not being able to mobilize correctly the membrane effect due to the size of the grains.

To overcome the scaling effect, centrifuge tests on GRPSE, which can be representative of the behavior of a full-scale structure, were performed by many researchers ([48], [49], [50]). For all of them, the settlement of the soft soil was simulated by the displacement of a horizontal plateau and they are not able to represent all the materials explicitly (it is not possible to test a real geosynthetic for example). The results of these experimentations must be considered with prudence because the real conditions of the soft soil settlement were not respected.

From all these experimentations, we can conclude that it is not easy to highlight the exact role of geosynthetic in the efficiency of GRPSE. To try to identify this role, it is necessary to compare a section with geosynthetic with a section without geosynthetic in the same geometrical and geotechnical conditions. In particular, the behavior of the soft soil is a key parameter that has to be simulated with care.

3.1.3 Highlights gaps in the existing literature

Field and laboratory experiments have identified many load transfer mechanisms and provide key insights on how to conduct new studies best. Field experiments to validate a GPRS were often conducted without a reference section (without a geosynthetic). Although they have provided many elements on the mechanisms, such as a large part of the settlement is done during the embankment's construction, they cannot highlight the geosynthetic's real role. These field experiments are essential to validate existing design methods or to calibrate numerical simulations. They are also a source for designing effective instruments for new experiments. Small-scale laboratory tests were conducted to understand the mechanisms within the load transfer platform. However, experimental conditions and the failure to respect the similitude laws do not allow a comparison of their results with those of design methods. From this bibliographical analysis, it seems that the best way to highlight the role of geosynthetics on the mechanisms is to propose laboratory tests at a real scale with enough piles to isolate a central grid and try to simulate well the soft soil behavior with an analogic material to obtain the same initial state of each test.

The main parameters of the experimentations used in the background section have been presented in Table 2 for a better understanding of the effects found in the research.

Table 2. Main parameters of the existing experimentations.

Authors	H/(s-D)	J (kN/m)	Ks (kN/m^3)
Almeida et al. [30]	0.7	1615	0
Wachman et al. [31]	1.6	-	-
Cheng et al. [32]	2.8	-	-
Nguyen et al. [33]	11.1	2360	428
Pan et al. [34]	6.8	-	466
Riccio et al. [35]	3.7	2770-3050	625
King et al. [36]	5	2000	-
Gunnvard et al. [37]	1.7	1050	89 - 214
Khansari and Vollmert [38]	1.0	2720 - 5440	375
Oh & Shin [39]	2.2-3.9	235	236
Briançon & Simon [40]	2.0	600 - 700	355
Briançon & Simon [41]	2.25-2.99	12600	312
Wang et al. [42]	2.0	480	240
Sloan [46]	0.94-1.16	493 - 569	0
Lee at al. [47]	2.28	-	125

3.2 Experimental study

Laboratory tests were designed to simulate a GRPSE most accurately concerning the 3D geometry, scale, materials, settlement of soft soil, and different stages of construction. Previous studies have highlighted the importance of ensuring that most settlement occurs during embankment construction.

3.2.1 Test facilities

Tests were performed in an experimental pit to analyze the mechanisms inside the LTP of the pile-supported embankment. The 64-m² pit featured 16 concrete piles with 30-cm diameter and 1-m height, set up in a 2 m-interval square mesh (Fig. 17a). Soft soil was simulated using four layers of materials (Fig. 17b):

- a 2.5 cm-thick wooden grating,
- a 10 cm-thick layer of honeycomb cardboard planks (called Biocofra),
- a 50 cm-thick layer of tire aggregates (called Deltagom), and
- a 37.5 cm-thick layer of sand.

Honeycomb cardboard planks are very rigid when dry, but biodegrade uniformly throughout their thickness in the presence of water; hence, we added a grating layer to facilitate water supply. The honeycomb cardboard planks were dissolved at the end of the test to remove the soft soil reactions and reach an extreme case. The compressibility of soft soil was simulated using a layer of tire aggregates. The LTP was compacted using the sand layer. The combination of sand and tire aggregate layers represented the compressibility of soft soil found in real-world sites reinforced with rigid inclusions.

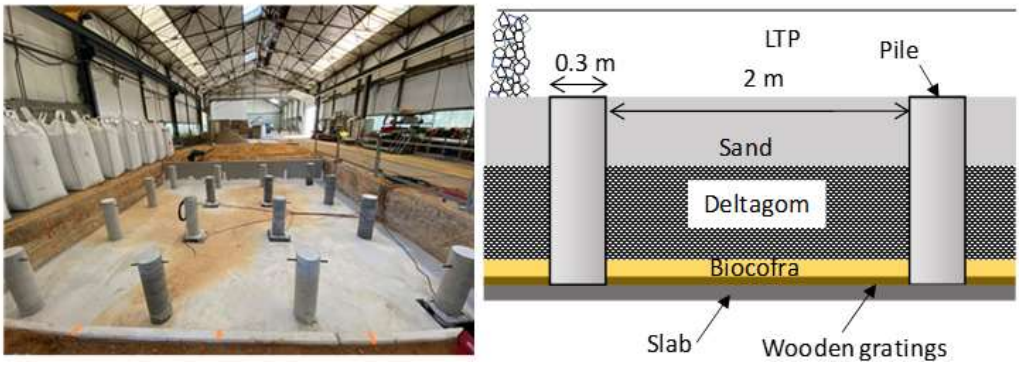


Fig. 17. a) Experimental pit, (b) Various layers constituting the experimental cross-section

3.2.2 Tested material

Deltagom particles were constituted by rubber granulates collected from end-of-life tires of French automotive professionals. The size of the particles ranged between 3–8 mm. It exhibited a specific gravity of 1, a void ratio of 0.95, and a bulk density of 0.51. Its compressibility was determined using large odometer tests. The strain on this layer was high even when the stress was low, owing to the large void ratio. After the first settlement, a second settlement occurred due to the compressibility of the particles themselves. The second layer, constituting soft soil, was a sand layer with a friction angle of 32° and a cohesion of 0 kPa. A gravel with a D_{max} of 31.5 mm (crushed material), a friction angle of 40°, and a cohesion of 2 kPa was used in the LPT. When compacted, its bulk density was 1.9. Two monoaxial geosynthetics were used: a geotextile and a geogrid. For confidentiality considerations, we cannot provide additional descriptions of these geosynthetics than those given in Table 3.

Table 3. Geosynthetics properties

Property	Unit	GGR	GTX
Type of GSY	-	PET - Mono-axial	PET - Mono-axial
Max. tensile strength md/cmd	kN/m	> 600 / 50	600 / 50
Elongation at nominal strength md/cmd	%	< 10 / 10	10 / 12
Tensile strength at 2% elongation md/cmd	kN/m	> 130	135
Tensile strength at 5% elongation md/cmd	kN/m	> 250	300
Aperture size md x cmd	mm x mm	30 x 30	-

The soil used in the embankment was gravel with a D_{max} of 63 mm, a friction angle of 33°, and a cohesion of 8 kPa. When compacted, its bulk density was 1.8.

3.2.3 Instrumentation

During each test, multiple sensors were installed in the LTP, soft soil, and embankment to measure load transfer and settlement (Fig. 18):

- Earth pressure cells (EPCs) were placed on the four central piles, in the soil underneath the Deltagom layer, and both above and beneath the LTP.
- Load cells (LCs) were placed at the feet of the four central piles.

- A liquid-levelling system consisting of a series of pressure transmitters hydraulically connected to a reference tank positioned in a stable location.

All sensors were connected to a data logger. To limit potential errors, the four piles in the central grid were monitored on their heads with earth pressure cells and at their toes with load sensors. The measures of the four sensors at the top and the four at the toe were compared before taking the mean value into account. Concerning the settlement sensors, the risk of a potential error could be due to a leak in the pressure line; the reference sensor installed below each reservoir was fixed and a leak was detected if the reference sensor measured a pressure difference.

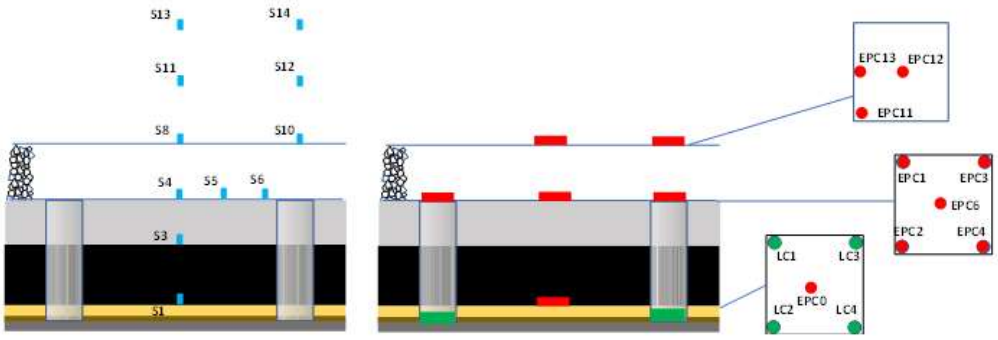


Fig. 18. Instrumentation

3.2.4 Program and experimental set-up

Full-scale experiments were conducted using five different geosynthetics and installation methods. Test 1 involved an unreinforced condition with no installed geosynthetics. Tests 2 and 5 involved reinforced conditions, in which two monoaxial geotextiles were installed 10 cm above the pile head (test 2) and directly on the pile head (test 5). Tests 3 and 4 involved reinforced conditions, in which two monoaxial geogrids were installed 10 cm and 30 cm above the pile head, respectively. To compare the test results, the thicknesses of the LTP and embankment, the grid size, and the soft soil composition were held constant. These configurations correspond to a relation H/(s-d) = 0.79. The height of the embankment is higher than the critical height defined in the standard recommendations [26], [29]. The diameter of the pile has been chosen to match the use in France.

For each test, 16 piles were installed in the pit and monitored. Wooden gratings were installed on the floor around the piles. Honeycomb cardboard planks were placed on the wooden gratings. Both layers of tire aggregates and sand were set up without compaction. Granular platforms were installed with and without reinforced geosynthetics. The embankment was set up in three stages of 0.5 m. One month after the completion of embankment construction, an overload was placed on the surface of the embankment (only in tests 4 and 5). Finally, the honeycomb cardboard planks dissolved owing to the saturation of the wooden gratings.

3.2.5 Experimental results

3.2.5.1 Load transfer measured at the end of each stage

Fig. 19(a) and (b) depict the stresses measured on the piles and at their feet, respectively, at the end of each construction step during the five tests. These values were the averages of the stresses measured for the four piles in the central grid. Overloading, by concrete blocks installed on the embankment, was performed only in the final two tests. The stress at the feet

of the piles was higher than that on the pile head, highlighting load transfer by negative friction along the piles. Load transfer occurred during embankment construction and exhibited an increasing trend over the subsequent month. All reinforced LTPs exhibited better load transfer than those with non-reinforced granular platforms. Among the reinforced platforms, after one month from the completion of embankment construction, geogrid-reinforced LTP (Tests 3 and 4) exhibited the highest load transfer on the pile head. In contrast, geotextile-reinforced LTP placed directly on the pile head (Test 5) exhibited the best load transfer at the feet of the piles. The same trend was observed when an overload was applied on the embankment.



Fig. 19. (a) Stress on the pile head (b) Stress at the toe of the piles

3.2.5.2 Settlement

Fig. 20a presents the settlements measured in the middle of the central grid below the LTP during each stage. Because there was no settlement of the piles, soil settlement was also the differential settlement between the pile and the soil. As observed in all tests, a significant portion of the settlement was achieved during the construction of both the LTP and the embankment. Settlement of reinforced LTP was not lower than that of non-reinforced LTP, except when the geotextiles were directly placed on the pile head (Test 5). Overloading was only applied in the final two tests. Test 5, where the geotextiles were placed directly on the pile head, yielded better stability than Test 4, where geogrids were placed inside the LTP.

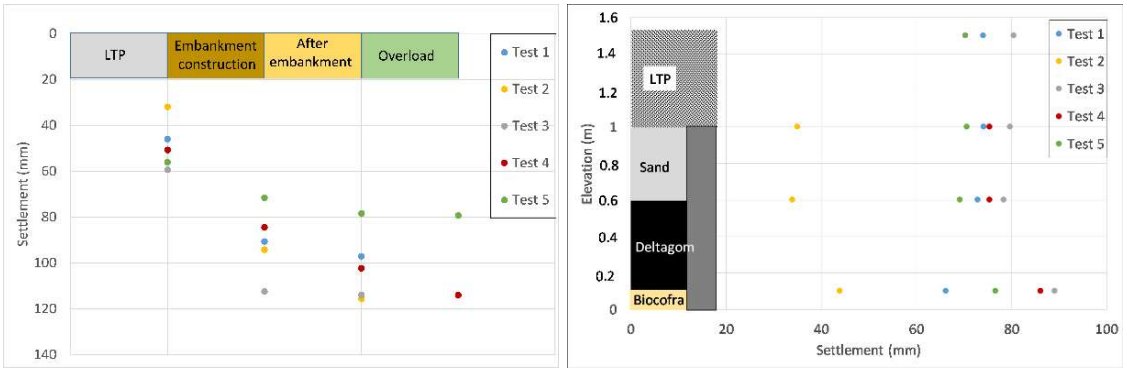


Fig. 20. (a) Soil settlement in the middle of the central grid (b)

Fig. 20b presents settlements induced by the dissolution of the Biocofra planks measured at the top of the Biocofra, Deltagom, and sand layers, as well as the LTP. In all tests with geosynthetics, the settlement on Biocofra was higher than those on the other layers. Even if geosynthetics did not reduce settlement during the construction stages, they played a role in large displacements. In Test 1 (without Geosynthetic), the vertical displacement was not

reduced, and the settlements of the upper layers were higher than the displacement induced by Biocofra dissolution owing to strain within the Deltagom layer.

3.2.5.3 Observations after the test

In Test 4, the location of the LTP on and near the pile head following Biocofra dissolution after removing the embankment and LTP were observed using gravel colouring on the pile head and the final location of the geogrids (Fig. 21).

These observations explain why the test scenarios involving geosynthetics inside LTP (Tests 2–4) did not yield any increase in efficiency or reduction in settlement during the construction stages. The 10 cm-thick layer between the pile head and the first geosynthetic did not maintain its thickness, and the geosynthetic only functioned for large displacements (during the dissolution stage). The upper geosynthetic was not mobilized and remained straight, even after the dissolution stage.

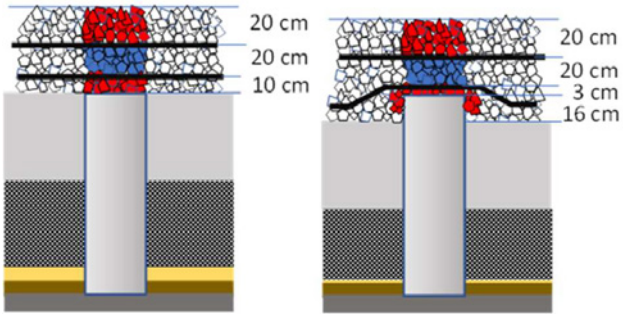


Fig. 21. Observation of LTP behavior in Test 4 after embankment removal

In Test 5, the geotextile transferred the load more quickly because it was blocked on the pile head, and the differential settlement could mobilize the tension in the geotextile during the initial construction stages.

3.2.6 Conclusion

The following conclusions were drawn under the tested geometrical and compressibility conditions:

- Platforms reinforced with geosynthetic placed directly on the pile head yielded the best load transfer efficiency and settlement reduction.
- A large part of the efficiency was attributed to the shearing mechanisms inside the granular platform.
- A large proportion of settlement occurred during the construction stage.
- Non-reinforced granular platforms were observed to be incapable of supporting large displacements.
- The type of geosynthetic used did not influence load transfer efficiency.
- Geosynthetics did not reduce settlement at the pile head significantly because they required large displacements to be mobilized. However, they ensured stability at the base of the embankment after its construction.

These conclusions are consistent with the results of other studies. In particular, the major part of the final settlement occurring during the construction stages and the low mobilization of geosynthetics were corroborated. Based on a comparison between non-reinforced and reinforced platforms with identical configurations and initial conditions using accurate

simulations of the real behavior of soft soil, our experiments definitively elucidated the influence of geosynthetics on load transfer efficiency and settlement reduction: even if the presence of the geosynthetic increases the efficiency of the platform, it is not able to reduce significantly the settlement for slight displacements but it plays its role for large displacement by membrane effect to increase the efficiency and reduce the settlement. Geosynthetic brings stability and safety.

They should be mobilized from the beginning of construction to increase the influence of geosynthetics. The optimal location for geosynthetic installation to maximize the differential settlement, is the pile head level. The disadvantage of this configuration is the risk of puncture by the pile head; thus, we recommend installing a protective geotextile between the pile and the geosynthetic that is comparable in size to the pile head.

3.3 Numerical studies

3.3.1 DEM simulation

In the framework of the project ASIRI+, a numerical simulation, based on the discrete element method, was made to evaluate the mechanisms inside the LPT and determine the role of the GSY [51]. This simulation makes it possible to take the discrete nature of the soils into account, the texture of the reinforcement and the interaction on a local scale between the granular particles and the reinforcement. They were carried out to describe the in-service behavior of a structure subjected to settlements of reasonable amplitude. Fig. 22a presents the basic geometry used for the modelling. To limit calculation times, a quarter of the mesh of the pile network was subsequently modelled.

The numerical model [52] consists of a granular mattress (apparent density of 1550 kg/m^3) made up of clumps arranged in such a way that the macroscopic behavior of the numerical sample corresponds to a granular material with an internal friction angle at the peak of 40° and a Young modulus of 20 MPa (Fig. 22b). Each clump is made up of two spheres of diameter D, overlapped and inseparable, whose centers are spaced a distance of 0.8 D. Many heights of the granular embankment were tested: H_1 = 0.75 m (16000 clumps), H_2 = 1.5 m (32000 clumps), H_3 = 2.25 m (48000 clumps) and H_4 = 3 m (64000 clumps).

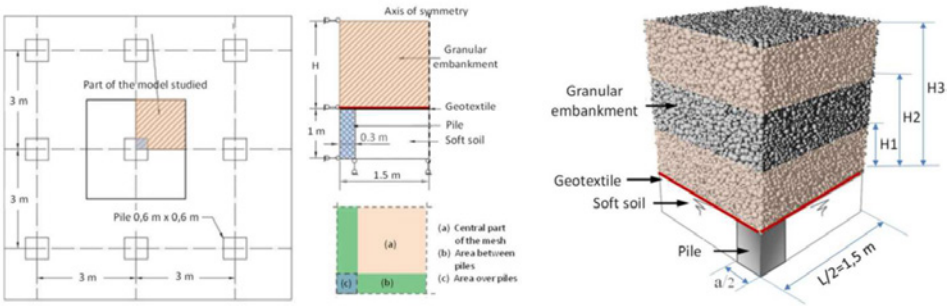


Fig. 22. Geometry of the simulated problem

The geosynthetic layer (2738 thin three-node triangular elements), positioned at the base of the granular embankment, is reinforced in two directions (longitudinal and transverse directions). The tensile stiffnesses of the geosynthetic in the longitudinal and transverse directions are respectively: Jx=3000 kN/m and Jy=3000 kN/m. A set of spheres regularly distributed under the geosynthetic reinforcement is used to materialize the soft soil and the action of the piles on the reinforcement sheet. The behaviors of the compressible soil and the piles are governed by springs that act vertically on the particles located under the

geosynthetic. The compressibility modulus of the soil Ks is defined as the ratio between the oedometric modulus of the soil and the thickness of the soft soil (by default a value of 0.2 MN/m^3 is used for the soft soil and a value of 2000 MN/m^3 for piles).

The numerical results showed that the vertical loads due to the granular embankment are transferred, on the one hand to the piles by load transfer within the granular mattress, by membrane effect following the curvature of the geosynthetic sheet, and to the soft soil which undergoes a vertical settlement. It proves that the best location for the geosynthetic is when it is directly laid out over the pile head. The geosynthetic strips located between the piles are the most stressed and contribute mainly to the reinforcement (Fig. 23a). The distribution of stresses on these geosynthetic strips takes a third-degree polynomial form corresponding to 85% of the total loads mobilized by the geosynthetic sheet (Fig. 23b). It has also been shown that the load transfer mechanisms within the granular fill are little affected by the presence of the geosynthetic sheet. All these conclusions will lead, by studying the vertical equilibrium of a portion of the geosynthetic sheet, to developing a design method for the geosynthetic.

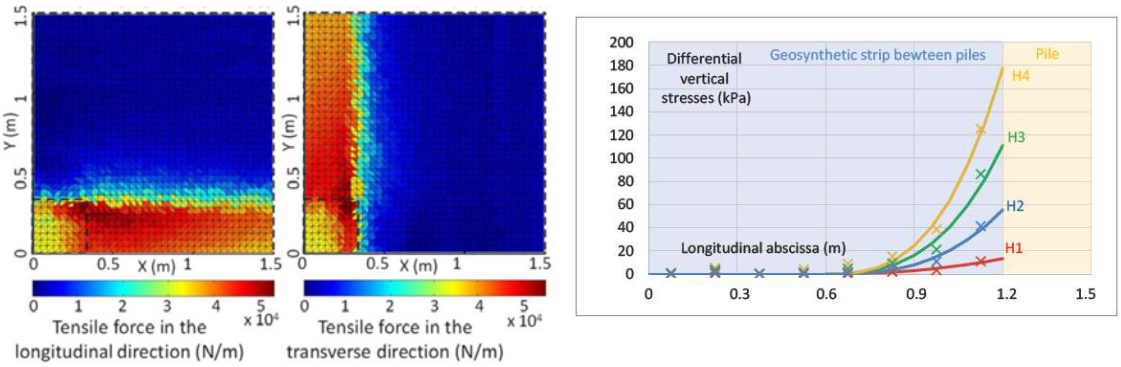


Fig. 23. (a) Tensile forces in the longitudinal and transverse directions (b) Differential vertical stresses acting on the geosynthetic strip located between piles (Ks=0.2 MN/m^3).

3.3.2 Analytical model

Following the ASIRI project [29], a biphasic model applied inside an elementary unit cell (Fig. 20) has been developed in France and implemented in the Software Taspie+. The results brought by the experiments of the ASIRI+ project were added by integrating the geosynthetic inside the biphasic model [53].

Taspie+ model aims to study the behavior of an elementary cell centered on an inclusion subjected to vertical loading. This volume is decomposed into two domains: the « pile » domain, consisting of the inclusion and the surrounding soil volumes that extend it to the lower or upper limits of the model, and the « soil » domain, consisting of the complementary soil volume (Fig. 24). The interaction between these two domains is assumed to be fully described by the shear τ that develops on their vertical boundary. A « t-z » load transfer curve, characterized by a slope parameter kt and a limiting shear value qs, is used to describe the shear at the interface. For large structures such as slabs, rafts, or embankments, the model is assumed to be periodic, which implies that the shear is equal to zero on the outer vertical faces.

The presence of a load transfer platform (LTP) and/or a fill layer is treated by fictively extending the « pile » domain to the top of the model. The load transfer induced by the arching effect is modeled through a negative vertical friction between the « pile » and « soil » domains. The limiting value of this friction is taken as q_{sn} = ktanδ.σ'v. The factor ktanδ is an empirical parameter that represents the product of a soil-pile friction coefficient tanδ and a

passive earth pressure coefficient k (such that $\sigma'_N = k\sigma'_N$). In practice, the factor ktanδ is capped at a value of 1 within the mattress.

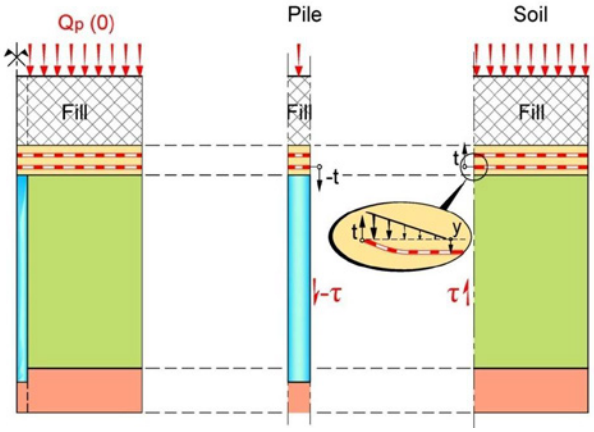


Fig. 24. Biphasic model on an elementary unit cell

Geosynthetics are integrated inside the Taspie+ model by introducing, at the geosynthetic level, the relationship between the geosynthetic displacement Δy and the load R it transfers to the « pile » domain. The Δy value corresponds to the deflection of the geosynthetics, and can be approximated in the elementary unit cell model as the differential settlement between « soil » and « pile » domains at the geosynthetics level.

The relationship R= f (Δy) is derived from an analytical model that considers the geogrids as membranes facilitating the transfer of some extra load to the « pile » domain. This load transfer is mainly operated by orthogonal strips within the geogrid (Fig. 25). The strips are assumed to be loaded by an inverse triangularly distributed load and rest on a width a, determined by a 1H:2V diffusion ratio from the inclusion heads (a = B + h).

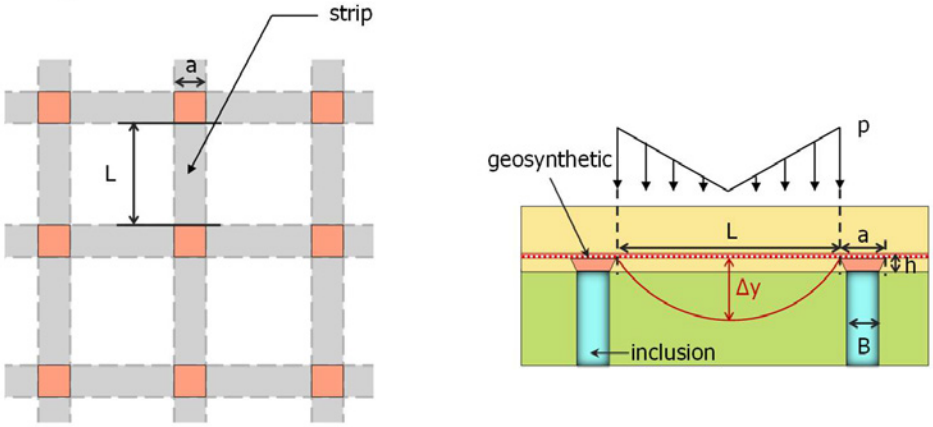


Fig. 25. Geosynthetic loading

The elastic equilibrium of the strip is studied taking into account second-order effects, and its resolution allows for establishing a direct nonlinear relationship between the pressure p and the resulting deflection Δy. This relationship depends on the secant stiffness J (kN/m) of the strip and the distance between the supports.

The total force R transferred by the geogrid to the inclusion tops is calculated by integrating the pressure p over a specific portion of the mesh area. This portion is defined as

twice the strip area: an area with the same length but twice the bearing width (d = 2a, Fig. 26). This approach assumes that each strip captures a fraction of the load applied to the mesh area through a membrane effect. The approach also accommodates the anisotropic behavior of geosynthetics by summing contributions from strips in both longitudinal and transverse directions (Fig. 26).

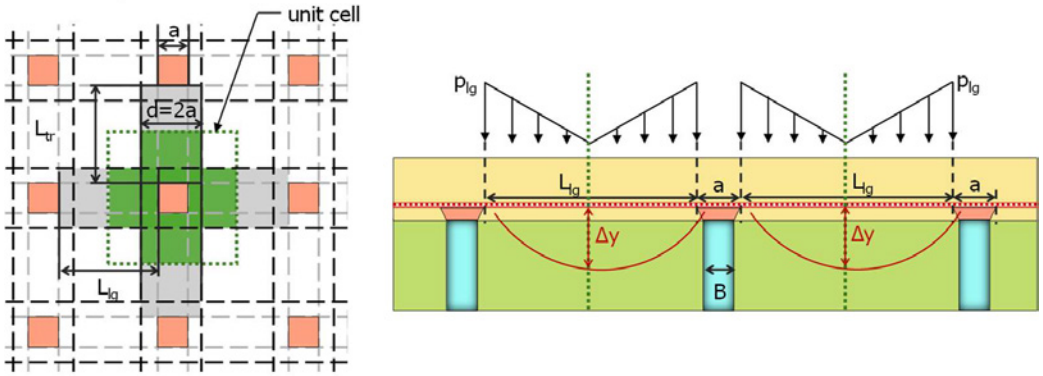


Fig. 26. Portion of the mesh area used for the integration of pressure p

The Test 5 of the experiment (section 3.2) has been calculated with the Taspie+ model. Fig. 27 presents the vertical settlement profile on soil and the vertical stress profile within the inclusions after the construction of the embankment. The experimental results indicate that settlements at the base of the fill and LTP are smaller than those at the base of the sand. These results suggest an extension of these layers and are not considered in the analysis, in line with the approach used during the parameter calibration stage. The experimental data closely align with the Taspie+ results in terms of both settlements and the stress profile within the inclusions. This confirms the validity of the triangular load distribution. The settlement of Biocofra could not be fully modeled because Taspie+ doesn't allow for displacement to be directly imposed (it works with constraints, not displacements). Therefore, the deformation of the Biocofra is controlled by the modulus derived from the calibration phase (0.35 MPa) and the stress at the top of the layer, which is lower in the presence of geosynthetics compared to the stress applied during the calibration.

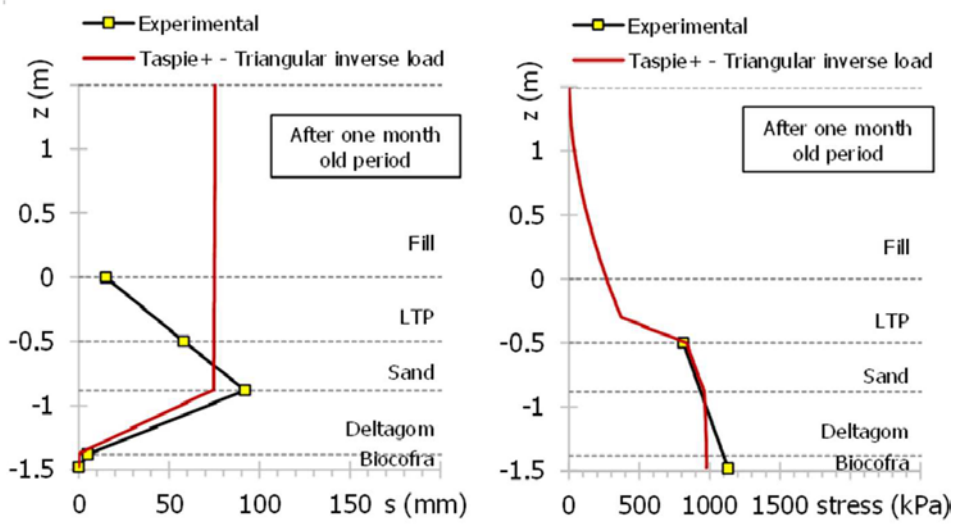


Fig. 27. Comparison between experimental results and calculated values (a) vertical settlement profile on soil (b) vertical stress profile within the inclusions

3.4 Conclusion

From a thorough state-of-the-art review, it was possible to highlight the key parameters for simulating the behavior of LTP in the embankment. The following conclusions were drawn under the tested geometrical and compressibility conditions:

- Platforms reinforced with geosynthetic placed directly on the pile head yielded the best load transfer efficiency and settlement reduction.
- A large part of the efficiency was attributed to the shearing mechanisms inside the granular platform.
- A large proportion of settlement occurred during the construction stage.
- Non-reinforced granular platforms were observed to be incapable of supporting large displacements.
- The type of geosynthetic used did not influence load transfer efficiency.
- Geosynthetics did not reduce settlement at the pile head significantly because they required large displacements to be mobilized. However, they ensured stability at the base of the embankment after its construction.

These conclusions are consistent with the results of other studies. In particular, the major part of the final settlement occurring during the construction stages and the low mobilization of geosynthetics were corroborated. Based on a comparison between non-reinforced and reinforced platforms with identical configurations and initial conditions using accurate simulations of the real behavior of soft soil, this experiment definitively elucidated the influence of geosynthetics on load transfer efficiency and settlement reduction: even if the presence of the geosynthetic increases the efficiency of the platform, it is not able to reduce significantly the settlement for slight displacements but it plays its role for large displacement by membrane effect to increase the efficiency and reduce the settlement. Geosynthetic brings stability and safety.

To increase the influence of geosynthetics, they should be mobilized from the beginning of construction. The pile head is the optimal location for geosynthetic installation to maximize the differential settlement. This important result was confirmed by a numerical study based on a discrete element model. This study also showed that the geosynthetic strips located between the piles were the most stressed and contributed mainly to the reinforcement and that the distribution of stresses on these geosynthetic strips took a third-degree polynomial form corresponding to 85% of the total loads mobilized by the geosynthetic sheet.

All these results were used to improve the biphasic model integrating the geosynthetic effect. This design method will be proposed in the new French recommendations ASIRI+.

4 Conclusion

Through these two applications, we wanted to show the research strategy to reach the objective of proposing design rules. This strategy is based on a thorough state-of-the-art review to define the best way to simulate the mechanisms developed inside the reinforced soil. Interaction mechanisms between geosynthetics and the surrounding soil are complex and depend on many parameters. Modeling these mechanisms under controlled test conditions at a real scale is a means of taking the setup stages into account and controlling the initial conditions. Even if laboratory tests at scale 1 or full-scale experimentation under controlled conditions are expensive tests without an easy comeback, they remain the cornerstone of our studies. Experimentation cannot be separated from numerical simulations. Indeed, many mechanisms cannot be perfectly described from instrumentation, and a

numerical model, well-calibrated on the experimental results, allows multiplying the studied cases and deeply analysing complex mechanisms. The use of high technology sensors like optical fibres to measure the geosynthetic strain and performant numerical models to describe well the interaction between the granular soil and the geosynthetic were significantly helped to improve the understanding of the mechanisms.

To resume, a thorough state-of-the-art review, experimental studies associated with numerical simulations can improve the understanding of developed mechanisms inside the reinforced soil. The following stage is essential: the transfer of the research results to the engineers, knowing that the research numerical programs are not often adapted to the usual designs. For this transfer, it is sometimes necessary to simplify the problem or not take some mechanisms into account if their role is not essential in global behavior. From simplifying assumptions, it is possible to propose some practicable equations in recommendations or standards.

Concerning reinforced platforms on cavities, many mechanisms have not been properly taken into account in the previous standards. It took us 20 years to carry out numerous experimental and numerical studies in order to significantly improve the understanding of mechanisms, describe them, and propose a design method in a French standard.

Concerning the role of geosynthetics inside pile-supported embankments, many studies were performed and from them, it has been possible to design a laboratory experiment allowing simulating faithfully the real conditions. From these experimental results and thanks to DEM simulations, we have confirmed some mechanisms highlighted by other authors and well described the behaviour of the reinforced load transfer platform. These results were integrated into commercial software for the engineers. Our method differs from other design methods proposed in Standards and the next stage will be to compare all these design methods on monitored real cases.

All these studies are possible thanks to a strong partnership between research laboratories, geosynthetic producers, engineering consultancies, and geotechnical firms. The French Ministry of Research often supports these projects.

Acknowledgment

The author would like to thank all his PhD Students working on these two topics, his colleagues P. Villard, B. Simon, D. Dias, A.M. Alzate for their numerical studies and all members (GSY producers, geotechnical firms, geotechnical design offices, Universities) of projects ASIRI, GEOINOV and ASIRI+.

Notations

B	Diameter of the pile (m)
C_e	Expansion coefficient (-)
D	Cavity diameter (m) / Pile diameter (m)
f	Maximum vertical displacement of the geosynthetic sheet (m)
H	Fill soil thickness (m)
J	Geosynthetic stiffness defined per width unit (N/m)
K	Ratio between the horizontal stress and the vertical stress
Ks	Soil stiffness (N/m^3)
K_a	Active soil pressure (-)
L	Pile length (m)
p	Vertical overload applied on the fill soil surface (kPa)
q	Vertical load acting over the cavity (kPa)

s	Vertical displacement at the surface of the soil / Distance between piles (m)
T_{max}	Maximal tensile force acting on the geosynthetic sheet (N/m)
ε_{max}	Maximal sheet strain (-)
ϕ	Interface friction angle of fill soil (°)
γ	Unit weight of fill soil (N/m^3)

References

1. J.P. Gourc. Quelques aspects du comportement des géotextiles en mécanique des sols. PhD Thesis, University of Grenoble, France (1982)
2. T.C. Kinney and B. Connor. Geosynthetics Supporting Embankments Over Voids. Journal of Cold Regions Engineering **1**, 158-170 (1987)
3. J.P. Giroud. Determination of geosynthetic strain due to deflexion. Geosynth. Int. **2**, 635-641 (1995)
4. H. Giraud. Renforcements des zones d'effondrement localisé - Modélisations physique et numérique. PhD thesis, University of Grenoble, France (1997)
5. J.P. Gourc, H. Giraud, P. Villard, J.C. Blivet, M. Khay, B. Imbert, A. Morbois and Ph. Delmas, 1999. Reinforcement of motorway and railway embankments on localised sinkhole area – Large scale experiment. in Proceedings of Rencontres Géosynthetiques 99, Bordeaux, France 12-13 October (1999) 7-44
6. British Standard BS 8006. Code of practice for strengthened/reinforced soils and other fills, British Standard Institution, London, 162p. (1995)
7. EBGEO. Empfehlungen für Bewehrungen aus Geokunststoffen. Deutesche Gesellschaft für Geotechnik (Hrsg). Verlag Ernst Sohn, Berlin (1997)
8. P. Villard, J.P. Gourc and H. Giraud. A geosynthetic reinforcement solution to prevent the formation of localized sinkholes. Canadian Geotechnical Journal **37**(5), 987-999 (2000)
9. K. Terzaghi. Theoretical soil mechanics, John Wiley & Sons, New York (1943)
10. Ph. Delmas 1979. Sols renforcés par géosynthétiques – Premières études. PhD thesis, University of Grenoble, France (1979)
11. L. Briançon, A. Nancey and P. Villard. Development of Geodetect: a new warning system for the survey of reinforced earth constructions. Studia Geotech. Mech. **XXVII** (1-2), 23-32 (2005)
12. P. Villard, B. Chevalier, B. Le Hello and G. Combe. Coupling between finite and discrete element methods for the modelling of earth structures reinforced by geosynthetic. Comput. Geotech. **36** (5), 709-717 (2009)
13. L. Briançon and P. Villard. Design of geosynthetic-reinforced platforms spanning localized sinkholes. Geotext & Geomembr. **26**, 416-428 (2008)
14. P. Villard and L. Briançon. Design of geosynthetic reinforcements for platforms subjected to localized sinkholes. Can. Geotech. J. **45**, 196-209 (2008)
15. A. Huckert. Approches expérimentale et numérique du dimensionnement de renforcements géosynthétiques sur cavités et inclusions rigides. PhD thesis, University of Grenoble, France (2014)

16. A. Huckert, L. Briançon, P. Villard, and P. Garcin, P., 2016. Load transfer mechanisms in geotextile-reinforced embankments overlying voids: experimental and analytical approaches. Geotext & Geomembr. **44** (3), 442-456 (2016)
17. P. Villard, A. Huckert and L. Briançon. Load Transfer Mechanisms In Geotextile-Reinforced Embankments Overlying Voids: Numerical Approach And Design. Geotext & Geomembr. **44** (3), 381-395 (2016)
18. P.A. Cundall and O.D.L. Strack. A discrete numerical modelling method for granular assemblies. Geotechnique **29** (1), 47-65 (1979)
19. F.V. Donzé and S.A. Magnier. Formulation of a three dimensional numerical model of brittle behavior. Geophys. J. Int. **122**, 790-802 (1995)
20. C. Salot, Ph. Gotteland and P.Villard. Influence of relative density on granular materials behavior: DEM simulations of triaxial tests. Granular Matter. **11** (4), 221-236 (2009)
21. K. Szarf, G. Combe and P. Villard. Polygons vs. clumps of discs: A numerical study of the influence of grains shape on the mechanical behaviour of granular materials, Powder Technology **208** (2), 279-288 (2011)
22. B. Chevalier, G. Combe and P. Villard. Experimental and Discrete Element Modelling studies of the trapdoor problem: influence of the macro-mechanical frictional parameters. Acta Geotech. **7** (1), 15-39 (2012)
23. M.T. Pham, L. Briançon, D. Dias and A. Abdelouhab. Investigation of load transfer mechanisms in granular platforms reinforced by geosynthetics above cavities. Geotext & Geomembr. **46**, 611-624 (2018)
24. XP G38-065. Géosynthétiques, géotextiles et produits apparentés - Renforcement de la base des remblais sur zones à risques d'effondrement - Justification du dimensionnement et éléments de conception. Afnor editions (2020)
25. S. Eekelen and J. Han. Geosynthetic-reinforced pile-supported embankments: state of the art. Geosynthetics International **27**(2): 112-141 (2020)
26. BS 8006-1. Code of practice for strengthened/reinforced soils and other fills. British Standards Institution BSI, London, UK. ISBN 978-0-580-53842-1 (2010)
27. EBGEO. Recommendations for design and analysis of earth structures using geosynthetic reinforcements-EBGEO. Digital in English. German geotechnical society, Berlin, Germany (2011)
28. CUR 226. Design guideline basal reinforced piled embankments. In: Design guideline basal reinforced piled embankments. CRC press (2016)
29. ASIRI (2013). Recommendations for the design, construction and control of rigid inclusions ground improvements (2013). Paris : Presses des ponts (2013)
30. M. Almeida, M. Ehrlich, A.P. Spotti and M. Marques. Embankment supported on piles with biaxial geogrids. Geotechnical Engineering **160**(GE4): 185-192 (2007)
31. G.S. Whachman, L. Biolzi and F. Labuz. Structural behavior of a pile-supported embankment. Journal Geot. & Geoenv. Eng. **136**(1): 26-34 (2010)
32. Q. Cheng, J. Wu, D. Zhang and F. Ma. Field testing of geosynthetic-reinforced and column-supported earth platforms constructed on soft soil. Frontiers of Structural and Civil Engineering **8**(2): 124-139 (2014)
33. V.D. Nguyen, Q. Luo, T. Wang, L. Zhang, Y. Zhan and T.P. Nguyen. Monitoring of an instrumented geosynthetic-reinforced piled embankment with a triangular pile configuration. Int. journal of rail transp. **11**(1): 69-91(2023)

34. G. Pan, X. Liu, S. Yuan, Y. Wang, D. Sun, Y. Feng and G. Jiang. A Field Study on the Arching Behavior of a Geogrid-Reinforced Floating Pile-Supported Embankment. Transp. Geot. **37** (2022)
35. M. Riccio, F. Bastos, M. Almeida, D. Fagundes, J. Rigolon and C. Ávila C.Numerical Analysis of a Monitored piled-supported Embankment of an Airport Runway. Transp. Geot. **44**: article id. 101157 (2023)
36. D. King, A. Bouazza, J. Gniel, K. Rowe and H Bui. Load transfer platform behaviour in embankments supported on semi-rigid columns: implications of the ground reaction curve. Can. Geot. Journal. **54**(8) (2017)
37. P. Gunnvard, N. Garcia, H. Mattsson, J. Laue and Q. Jia. Monitoring of a timber pile-supported road embankment. in Proceedings of 11th Inter. Conf. on the Bearing Capacity of Roads, Railways and Airfields, Volume 2 – Hoff, Mork & Saba (eds) (2022)
38. A. Khansari and L. Vollmert. Load transfer and deformation of geogrid-reinforced piled embankments: field measurement. Geos. Int. **27**(3): 332-241 (2020)
39. Y.I. Oh and E.C. Shin. Reinforcement and arching effect of geogrid-reinforced and pile-supported embankment on marine soft ground. Marine Georessources & Geotechnology **25**(2): 97-118 (2007)
40. L. Briançon and B. Simon. Performance of pile-supported embankment over soft soil: full-scale experiment. Journal Geotechnical & Geoenvironmental Engineering **138**: 551–561 (2012)
41. L. Briançon and B. Simon. Pile-Supported Embankment over Soft Soil for South Europe Atlantic High-Speed Line. Geosynth. Int. **24**(3): 293-305 (2017)
42. G. Wang, X. Zhang, X. Liu, H. Wang, L. Xu, H. Liu and L. Peng. Soil arching effect in reinforced piled embankment for motor- racing circuit: Field tests and numerical analysis. Transportation Geotechnics **37**(2022)
43. M. Nobahar, M.Y. Abu-Farsakh and M. Izadifar. Evaluating the mechanisms and performance of Geosynthetic-Reinforced Load Transfer Platform of pile-supported embankments design methods. Geotex & Geomemb. **52**(6): 1112-1133 (2024)
44. D. Zaeske. Zur Wirkungsweise von unbewehrten und bewehrten mineralischen Tragschichten über pfahlartigen Gründungselementen. Schriftenreihe Geotechnik, Uni Kassel, Kassel, Germany, Heft 10 (2001)
45. S. Eekelen. Basal Reinforced Piled Embankments: Experiments, field studies and the development and validation of a new analytical design model. Ph.D. Dissertation. Technische Universiteit Delft (2015)
46. J.A. Sloan. Column-supported Embankments: Full-scale Tests and Design Recommendations Ph.D. Dissertation. Blacksburg, VA: Virginia Polytechnic Institute and State University (2011)
47. T. Lee, S.H. Lee, I.W. Lee and Y.H. Jung. Lessons from full-scale experiments on piled embankments with different geosynthetic reinforcements. Geotech. Eng. **25**: 442-450 (2020)
48. M. Blanc, G. Rault, L. Thorel and M. Almeida. Centrifuge investigation of load transfer mechanisms in a granular mattress above a rigid inclusions network. Geotex. & Geomemb. **36**: 92-105 (2013)
49. D. Fagundes, M. Almeida, L. Thorel and M. Blanc. Load transfer mechanism and deformation of reinforced piled embankments. Geotex. and Geomemb. **45**(2): 1-10 (2017)

50. R. Girout, M. Blanc, L. Thorel and D. Dias. Geosynthetic reinforcement on piled-supported embankment Geos. Int. **25**(1) 37-49 (2018)
51. P. Villard. Mechanical behaviour of geosynthetic sheets used to reinforce load transfer mattresses in the case of embankments on soft soils reinforced by rigid inclusions. In Proceedings of the XVIII ECSMGE 2024, Lisbon, Portugal, August 26th-30th (2024)
52. Q.A. Tran, P. Villard and D. Dias. Discrete and continuum numerical modeling of soil arching between piles. International Journal of Geomechanics. **19**(2) (2019)
53. A.M. Alzate., B. Simon and L. Briançon. Design of geosynthetics for rigid inclusion ground improvement: a simplified analytical method. In Proceedings of EUROGEO 8, Lille, France, September 15-18 (2025)

TECHNICAL SESSIONS

SESSION 1 A
SUSTAINABILITY AND DURABILITY (1)

Geosynthetics, a key brick of the energy transition

Hendrik Wetzel[1*], *Wim* van Helden[2], *Per Alex* Sørensen[1] and *Vincent* Micollier[3]

[1]PlanEnergi, Skørping, Denmark
[2]AEE Intec, Gleisdorf, Austria
[3]Vinci Construction, Lyon, France

Abstract. To establish a fully green energy system in Europe, flexible energy management is vital, especially with intermittent sources like wind and solar. As part of the TREASURE project financed by the European Union the pit thermal energy storage (PTES) technology is developed further, and it is aimed to streamline the implementation of this type of storage facility which is critical to the realization of a zero-carbon energy system. PTES are essential for utilizing renewable energy in heating communities and industries, hence geosynthetic products play a key role. The potential in Europe has a cumulative estimated capacity in the range of 35 to 110 TWh. This corresponds to a total water volume between 1 to 3 billion m^3, at a forward/return temperature of 60/90 °C as used in most European district heating networks. Assuming a water volume from 250,000 to 500,000 m^3 per individual PTES, a potential from 2,000 to 12,000 PTES needs to be constructed, although in many cases the water volume can be smaller, with a simultaneous increase in the number of facilities. To waterproof bottom, sides and floating cover of just one PTES with 250,000 m^3 Volume ca. 50,000 m^2 of sealing system is required, for 500,000 m^3 it is ca. 78,000 m^2, which means a European market potential from 160 to 600 million m^2 for geomembranes exposed to high temperatures.

1 Introduction

The EU Green Deal prioritizes a fully decarbonized European energy system by 2050. To ensure this, energy sectors need to be highly flexible in supply and demand, for the successful uptake of intermittent renewable sources. Flexibility also allows for easier coupling of energy sectors (heating, cooling, electricity) and for increasing the overall energy system efficiency. In the heating sector, energy demand can fluctuate drastically over the course of the year depending on the climate conditions, with the peak demand occurring during the coldest months in winter. On the contrary, the availability of renewable heat sources such as solar thermal heat is highest during the warm sunny months of summer, while most waste heat streams are available all year round. To bridge the temporal mismatch in supply and demand and therefore maximising the share of renewables and waste heat in the heating sector, large-scale seasonal thermal energy storages must play a central role in district heating networks.

* Corresponding author: hw@planenergi.dk

The present knowledge about large thermal energy storage is restricted to a small number of projects, mainly in Denmark and based largely on seasonal storage of excess solar heat.

The EU-funded TREASURE project is aimed at ensuring robust, safe, cost effective and sustainable large-scale thermal energy storage, developing secure and smart system integration concepts and increasing the effectiveness of realizing the pit thermal energy storage (PTES) technology in Europe. In the project seven Pit Thermal Energy Storage (PTES) demonstrators in five different countries are developed. It also has a constant interchange with a group of 16 satellite initiatives, collecting its experiences and feeding them with knowledge and experiences from TREASURE.

Geosynthetic materials, especially geomembranes, play a particularly important role in the PTES technology, as large quantities of hot water have to be stored in a watertight reservoir in order to accumulate thermal energy. Such a reservoir typically takes the form of a large inverted truncated pyramid, see figure 1 below.

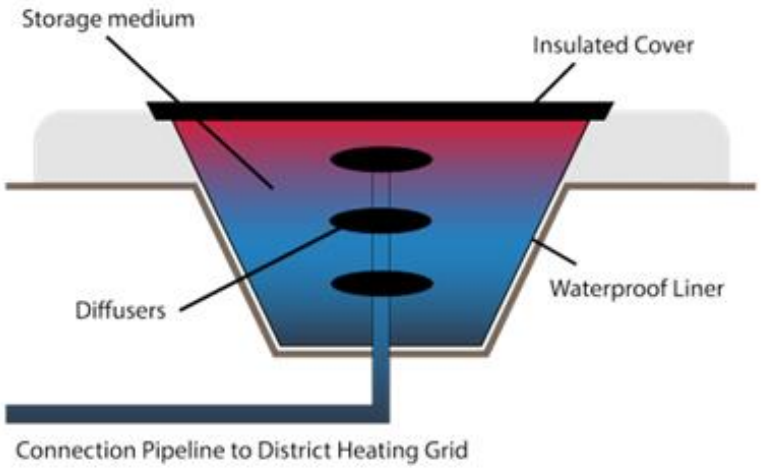


Fig. 1. Basic design of a PTES [1]

The particular advantage of this shape, apart from the benefits of relative ease of construction, lies in its scalability to enormous sizes. This allows very large quantities of water to be stored as a prerequisite for correspondingly large quantities of thermal energy under atmospheric pressure. At the same time, however, the requirements for the polymers used pose a challenge. Especially those materials in direct contact with hot water temperatures at 90 °C or more must be able to achieve a long service life. In addition, the potential size and shape of a PTES can lead to difficulties in finding suitable locations. The attempt of this paper is therefore to provide an outlook on the potential for geosynthetics, particularly for waterproofing systems.

2 Current Situation

Traditionally, district heating systems relied on fossil fuels, that could easily match supply with demand. However, with the EU's ambitious goal to phase out fossil fuels by 2050, a swift integration of renewable and waste heat sources is needed. These sources, while abundant, often pose a challenge due to their intermittent availability and mismatch with peak demand periods.

To bridge this gap, Thermal Energy Storage (TES) emerges as a pivotal solution. TES allows us to store excess heat during periods of abundance and release it when demand peaks. One promising TES system to focus on is Pit Thermal Energy Storage (PTES), which offers flexibility and efficiency in heat storage. Denmark has led the way in PTES technology, demonstrating its effectiveness in various applications. However, expanding PTES systems across Europe requires addressing technical, economic, and environmental considerations unique to different regions.

3 Role of Geosynthetics in PTES

3.1 Waterproofing

In principle, a PTES consists mainly of five components: Earthworks, waterproofing system, the energy storage medium water, an insulating floating cover construction and an inlet/outlet arrangement to pump the water around for energy exchange.

The role of geosynthetics for PTES systems therefore lies primarily in sealing the earthworks to accommodate the storage medium. And the importance of a simple, large-area seal is emphasized by the contour and the associated scalability of the structure. According to [2] a design in different shapes is possible, but "an excavation as a truncated pyramid placed upside down in the ground" is the most straightforward form. This form supports the approach of a mass balance of the necessary earthworks, which improves economic efficiency by minimizing soil transport and handling. The soil from the excavation is then used to construct the surrounding embankments with a typical inclination of 1:2, but in general depending on the geotechnical properties of the excavated material. This contour is then made watertight, which also includes the water surface. An insulating cover construction is applied to a floating geomembrane to prevent heat loss from the heated water. Figure 2 shows the principle of the simple construction method with an inclination of 1:2 to reach mass balance.

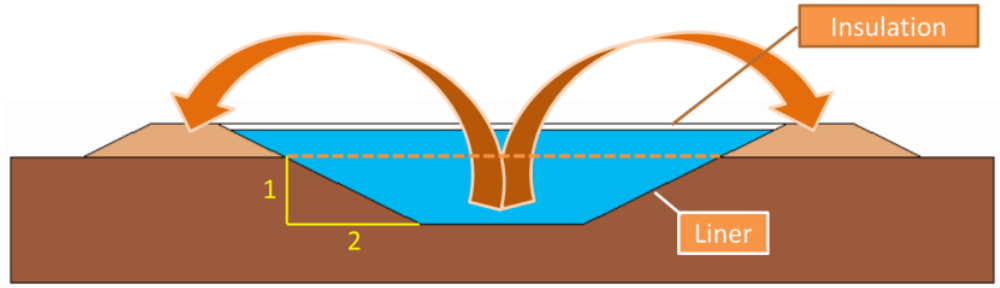


Fig. 2. Principle of a cross section [2]

The main requirement for the waterproofing system is that the geomembrane used must be able to achieve a service life of at least 20 to 25 years in an environment with typically high temperatures. Depending on the system integration of a PTES, a possible exposure condition can be a high water temperature only intermittently or a permanent water temperature of up to 95 °C. High water temperatures have consequences for the approach to material selection. For example, 25,000 m^2 of a new type of Polypropylene liner were used in the 70,000 m^3 PTES in Høje Taastrup, Denmark, commissioned in early 2023, to fulfil the requirements of at least 20 years of service life at 90 °C continuous temperature load [3]. This specific PTES is the first of its kind as it is operated as a weekly buffer storage and thus demands permanent high temperatures in the uppermost water layer. The methods for accelerated ageing testing of plastics described in [4; 5] have been considered in the material selection process.

Compared to e.g. aquifer TES or borehole TES, PTES technology has advantages in scaling both the total amount of energy per unit (the water volume at atmospheric pressure) and the loading and unloading capacity, since in comparison to the other Large Thermal Energy Storage (LTES) technologies mentioned above, no rock interacts with the heat transfer medium water.

3.2 Reduction of the area

One challenge and difficulty with PTES systems is that such facility consumes a relatively large amount of space, especially compared to other LTES variants, which predominantly utilise deeper layers of the subsurface. The outer dimensions of the dam construction can in many respects lead to difficulties in site selection if this is offset by land costs and other particular interests such as urban utilisation scenarios. Increasing the angle of inclination of the inside and outside of the dams offers advantages for the land consumption of a PTES, which would open up a wide range of applications for geosynthetics in the course of reinforced earth solutions. It also improves the surface/volume ratio in terms of the efficiency of the system, which according to the Danish Energy Agency [6] is a "key figure for heat loss per amount of energy stored".

An increase in the slope gradient (α) also means that the excavation depth (d_{exc}) can be significantly reduced if mass balance is applied, and the water column remains unchanged. A less deep excavation pit also offers potential in terms of facilitating the earthworks from a technical and economic point of view (Table 1).

Table 1. Influence of the slope inclination on the area consumption.

	250,000 m³			500,000 m³			
α [°]	a [m]	A [m²]	d_{exc} [m]	a [m]	A [m²]	d_{exc} [m]	A_{red} [%]
26.6°	167	27,959	16.6	205	42,111	21.5	-
33.7°	157	24,536	15.5	192	36,849	19	12
45.0°	146	21,191	13.9	178	31,709	17	25
53.1°	140	19,558	12.8	171	29,207	15	30

As the need for steeper slopes can be highly dependent on the local conditions of each individual plant, a more detailed quantification of potentials is not provided in this paper. In addition, no commercial PTES has yet been equipped with reinforced embankments. However, this approach is being investigated further as part of the German research project "Efficient Pit" [7].

4 Market Potential for PTES

The total District Heating (DH) final energy consumption in 2018 in the EU was 446 TWh, 12% of final energy consumption for space heating and water, with a total installed capacity of 354 GW, with biggest EU markets being Germany (124 TWh consumed, 95 GW installed capacity), Poland (65 TWh/55 GW), Sweden (51 TWh/43 GW), Finland (34 TWh/24 GW), Denmark (31 TWh/25 GW), France (26 TWh/23 GW). [8] It is estimated that in 2021 there were approximately 10,000 heating networks [9] in Europe, representing 12% of EU's heat demand and serving approximately 60 million EU citizens. The current socio-economic and geo-political context (Russia-Ukraine, FitFor55 package) indicates that the District Heating and Cooling (DHC) market will grow exponentially in the EU. This statement is confirmed by the 2050 roadmaps of EU countries, where radical increase is expected in the next three decades confirming the potential of District Heating and Cooling to further integrate renewable heat sources, harvest the potential of renewable electrification but also to offer an effective energy storage solution [10]. The latest IEA report indicates that in 2021 DH

production increased by around 3% compared to 2020. 25% more heat was delivered to end-users through DH in 2021 than in 2020 [11]. If the strong urbanisation trend continues and appropriate investments are put in place, district heating could meet almost half of Europe's heat demand by 2050 [12], meaning an increase with a factor 4 (Table 2).

Table 2. DH market share projections for some of the biggest DH markets [10].

Country	Presently	2030	2040 – 2050
Germany	14%	16%	21 – 25%
Denmark	65%	70%	70%
Sweden	50%	Slight increase	
Finland	38%	45% – 50%	
France	6%	10%	15% – 20%
Czech Republic	38%	40%	43% – 47%

As we can see, most major European markets are planning to extend their District Heating and Cooling market towards 2050, increasing the market potential for other important solutions with which the DH systems are to be coupled, such as PTES. Other studies also indicate a rapid growth in the thermal storage capacity, for instance, for the Nordic and Baltic market the project Flex4RES investigated how sector coupling between different energy systems can support the integration of high shares of wind- and solar power in the Nordic-Baltic energy system [13]. Four scenarios are calculated. The preconditions are that 50% of the district heating market is covered by electricity. In all scenarios, it is economically feasible to implement long term thermal storage. The optimal storage capacity is between 1,169 GWh and 1,360 GWh in the four scenarios in 2050.

In the Heat Roadmap Europe 4 (HRE4) project, the possibilities for extension of district heating have been investigated for the 14 EU member states with the largest heat demands. Halmstad University's database for cities with district heating and cooling systems has been used for the analysis [14]. The project covers 3,207 out of 4,843 district energy systems in the database. One of the findings in the project is that 2,188 district heating systems have either power plants, waste-to-energy plants, or excess heat from industries in the DH area, or in fewer than 20 km, and 64% of the excess heat activities in the countries were found within that 20 km from the DH systems. Altogether there are many existing large DH systems with CHP, and since the utilization of excess heat is only starting to kick off, this amount will be increased significantly in the coming years

5 Derivation of an outlook for waterproofing solutions

With the above information, it is possible to derive the assumed total capacity attributable to PTES as part of annual heat sales in the EU by 2050. This capacity depends on the configuration of the hot water system, the mix of heat sources used; it can vary drastically due to operating temperatures and the size limitations in different networks. Therefore, and to give an order of magnitude of the required operation, 5%, 10% and 15% are considered as the total storage capacity of the annual heat sales to outline scenarios for the geosynthetics industry. For this purpose, as aforementioned the EU-wide annual heat sales in district heating in 2018, the growth factor for the year 2050 and an assumption of a share of PTES as part of large-scale heat storage in district heating networks are considered together as follows.

$$Q_{EU\text{-}wide\ 2018}\ (TWh) = 446 \quad (1)$$

$$Growth\ Factor\ 2050 = 4 \quad (2)$$

$$PTES\ share\ assumption\ 2050 = 40\% \quad (3)$$

The percentage share of PTES capacity of annual heat sales for the three scenarios is then the product of aforementioned PTES share assumption and the scenario consideration:

$$share\ 5\%\ scenario = 0.04 \times 0.05 = 2\% \quad (4)$$
$$share\ 10\%\ scenario = 0.04 \times 0.10 = 4\% \quad (5)$$
$$share\ 15\%\ scenario = 0.04 \times 0.15 = 6\% \quad (6)$$

The assumed total capacity attributable to PTES as part of the annual heat sales in the EU up to 2050 with these 3 scenarios is then calculated as follows.

$$Q_{PTES}\ (GWh) = Scenario \times Q_{EU\text{-}wide\ 2018} \times Growth\ Factor\ 2050$$

The corresponding total water volume can be derived by firstly converting the formula for the heat quantity to the corresponding total mass.:

$$m_{total}\ (kg) = Q_{PTES} / (c_{water}\ \Delta T) \quad (7)$$

The applied temperature difference results from the difference between the forward and return temperatures. In most European district heating networks 60/90 $°C$ is commonly used.

$$\Delta T\ (K) = T_{forward} - T_{return} = 90\ °C - 60\ °C = 30 \quad (8)$$

The specific heat capacity of Water is as follows:

$$c\ (Kj / kg\ K) = 4.20 \quad (9)$$
$$c\ (kWh / kg\ K) = 0.0011667 \quad (10)$$

Due to the scale, the total mass value is converted into gigatons.

$$m_{total}\ (Gt) = m\ (kg) / 1\ 000\ 000\ 000 \quad (11)$$

An average density of water (H_20) of 1,000 kg/m3 is then used to calculate the total water volume for the scenarios in 2050 resulting from the total mass. The assumption in equation 12 is simplified since a change in water temperatures, even though undoubtedly occurring in a PTES, does not have a significant impact on the considerations in this document to derive the outlook for waterproofing solutions.

$$\rho\ (kg / m^3) = 1\ 000 \quad (12)$$
$$V_{total}\ (m^3) = m_{total} / \rho \quad (13)$$

The total volume is then distributed in two different sizes of PTES mentioned under 3.2, 250,000 m^3 and 500,000 m^3, to represent an approximate number of this kind of large thermal energy storage that would be needed to fulfil the three scenarios in 2050. The results are shown below in **table 3**. To enable a better classification of the orders of magnitude, the two example variables are listed individually with the corresponding values.

Table 3. Quantity of PTES with 250,000 or 500,000 m^3 of water; assumed forecast up to 2050.

PTES capacity of annual heat sales		Q [GWh]	m [Gt]	V [10^6 m^3]	250,000 m^3	500,000 m^3
5%	2%	35,680	1,019	1,019	4,078	2,039
10%	4%	71,360	2,039	2,039	8,155	4,078
15%	6%	107,040	3,058	3,058	12,233	6,117

Example for 1 Unit of 250,000 m^3	8.75	0.25	0.25	1	0.5
Example for 1 Unit of 500,000 m^3	17.50	0.50	0.50	0.5	1

The area to be sealed per PTES unit always refers to the basin floor, the embankments and the water surface and from this context a total area (1 layer) can be derived from the number of facilities to be built. With an assumed material thickness d of 2 to 3 mm for the geomembranes used and the area assumptions, a potential total material quantity forecast is possible. To waterproof bottom, sides and floating cover of just one PTES with 250.000 m^3 Volume ca. 50.000 m^2 of sealing system is required, for 500.000 m^3 it is ca. 78.000 m^2. Forecasted total volumes are shown in **table 4**.

Table 4. Order of magnitude for geomembrane quantity in dependence of PTES size; assumed forecast up to 2050.

		Total Quantity [t]		
250 000 m^3	A [m^2]	d = 2,0 mm	d = 2,5 mm	d = 3,0 mm
Example for 1 Unit	50 000	100	125	150
4 078	203 885 714	407 771	509 714	611 657
8 155	407 771 429	815 543	1 019 429	1 223 314
12 233	611 657 143	1 223 314	1 529 143	1 834 971
500 000 m^3				
Example for 1 Unit	78 000	156	195	234
2 039	159 030 857	318 062	397 577	477 093
4 078	318 061 714	636 123	795 154	954 185
6 117	477 092 571	954 185	1 192 731	1 431 278

Thus, depending on the size of the PTES and the thickness of the liner material, a total geomembrane quantity in the range of 0.4 to 1.4 Mton is assumed to be needed.

6 Carbon Footprint Reduction

Quantifying the potential total reduction of carbon emissions as result of PTES implementation is not readily possible, since the potential compilation of different components, assets, requirements and framework conditions in each individual power and heating system varies from one to another.

To, however, give an impression of how a PTES can already contribute to carbon footprint reductions of an energy system and furthermore lead to economical improvements of the same system, the case study PTES Høje Taastrup shall be used as an example instead. This PTES is used for peak load shaving and thus represents a fundamental enhancement of the functional possibilities of this type of large thermal energy storage, away from pure seasonal heat storage. Figure 3 illustrates the setup of the PTES in the district heating network, where it is charged with thermal energy from the transmission network that connects multiple power assets in the capital city and the Greater Copenhagen area with each other. After storing the thermal energy, it is then discharged when needed into the local district distribution network of the Høje Taastrup district.

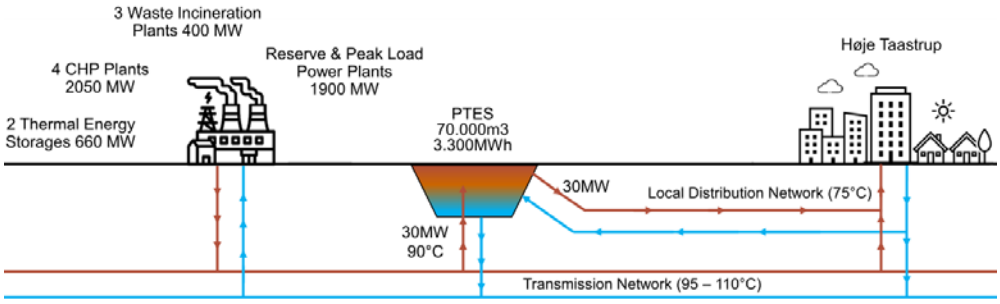


Fig. 3. Setup of the PTES in Høje Taastrup [15]

According to calculations made by Ea Energianalyse the PTES offers a substantial contribution to the district heating network and power system [16; 17]. Peak shaving the combined heat and power plants leads to an annual CO_2 reduction of 3,000 tons, primarily as a result of saved fossil gas. Another 3,200 tons reduction of CO_2 footprint result from the electricity sector due to optimized electricity production possibilities. In relation to the volume of 70,000 m^3 this means an annual greenhouse gas reduction of 43kg of CO_2 per m^3 for savings in peak shaving and 43kg of CO_2 per m^3 from the electricity sector, which is to some extent transferable to other locations as fossil gas is often used to handle peak loads. In addition to this, the entire system profits from a forecasted 1,05 Mio€ annual benefits due to less expenses on fossil, reduced peaks etc., while the construction costs of the PTES itself are around 76 €/m^3 [18].

7 Conclusion

Transformation of energy systems to decrease carbon footprint is an essential approach to reduce the impact on the global climate. Large-scale thermal energy storage is seen as a key to the transformation of the heating sector. In particular, Pit Thermal Energy Storages is a technology with great potential as it offers many opportunities for existing energy systems. The EU-funded TREASURE project aims to establish the technology across Europe, as the use of these systems offers great potential for CO_2 reduction.

Suitable geomembranes represent a core component for the sealing solution, for which, as shown, considerable volumes can be expected. Geosynthetics are therefore of particular importance in this context with the potential to become a key brick of the energy transition.

Acknowledgement. This research has received funding from the European Union under Grant Agreement No. 101136095. Views and opinions expressed are however those of the author(s) only and do not necessarily reflect those of the European Union or CINEA. Neither the European Union nor CINEA can be held responsible for them.

References

1. Source of figure 1. https://www.treasure-project.eu/
2. Task 55 Large Solar Heating & Cooling Systems - Seasonal pit heat storages - Guidelines for materials & construction (2020). https://www.iea-

shc.org/Data/Sites/1/publications/IEA-SHC-T55-C-D.2-FACT-SHEET-Guidelines-seasonal-storages.pdf

3. H. Wetzel, L. Peham, P.A. Sørensen, G.M. Wallner, Polyolefinic geosynthetics as key components in future energy systems: A case study and perspective, Geosynthetics: Leading 28 the Way to a Resilient Planet, Proceeding of the 12th International Conference on Geosynthetics (2023).
   DOI: 10.1201/9781003386889-24
4. G.M. Wallner, K. Grabmayer, S. Beissmann, H. Schobermayr, W. Buchberger, R.W. Lang, Methoden zur beschleunigten Alterungsprüfung von Kunststoffen. erneuerbare energie – Zeitschrift für eine nachhaltige Energiezukunft **2013-01**, 18-20
5. M.K. Grabmann, G.M. Wallner, K. Grabmayer, D. Nitsche, R.W. Lang, Aging behavior and lifetime assessment of polyolefin liner materials for seasonal heat storage using micro-specimen. Solar Energy **170**, 988–990 (2018)
6. Danish Energy Agency, 2018. Technology Data for Energy Storage.
7. G. Bröer, Zwei Erdbecken-Wärmespeicher als Labor, Solarthemen **582**, 12.12.2024
8. Tilia, TU Wien, IREES, Öko-Institut, Fraunhofer ISI - Overview of District Heating and Cooling Markets and Regulatory Frameworks under the Revised Renewable Energy Directive, October 2021
9. Interreg HeatNet NEW - District Heating in North-West Europe A Guide for Energy Consumers
10. DHC Market Outlook 2022, Insights & Trends – Euroheat & Power
11. District Heating – Analysis - IEA
12. Heat Roadmap Europe: https://heatroadmap.eu/
13. https://www.nordicenergy.org/flagship/flex4res
14. https://energyplan.eu/hre4
15. Source of figure 3. Presentation at 12th ICG Rome, 2023. H.Wetzel, L. Peham, Polyolefinic geosynthetics as key components in future energy systems: A case study and perspective
16. P.A. Sørensen, N. From, H. Wetzel, I. Sifnaios, A.R. Jensen, Design, implementation, and monitoring results from the 70,000 m^3 pit thermal energy storage (PTES) in Høje Taastrup, Copenhagen, ENERSTOCK 2024, Proceedings of the 16th IEA ES TCP International Conference on Energy Storage
    DOI: 10.5281/zenodo.13790499
17. P.A. Sørensen, N. From, H. Wetzel, I. Sifnaios, A.R. Jensen, Design, implementation, and monitoring results from the 70,000 m^3 pit thermal energy storage (PTES) in Høje Taastrup, Copenhagen, ENERSTOCK 2024, Proceedings of the 16th IEA ES TCP International Conference on Energy Storage, conference presentation, 05.-07.07.2024
18. H. Wetzel, F. Bruus, Erdbeckenwärmespeicher im Großraum Kopenhagen als Kurzzeitwärmespeicher im Einsatz, EURO HEAT & POWER **9/2023**, 37-41

Greener unpaved forest roads: costs and emissions analysis of solutions with an industrial byproduct and a geosynthetic

Daniela Rodrigues[1], *Catarina* Martins[1], *David* Carlos[1], *Sebastien* Preiswerk[2], *Patricia* Montez[3], *Joaquim* Macedo[1] and *Margarida* Pinho-Lopes[1**]

[1]CERIS_University of Aveiro, Department of Civil Engineering, 3810-193 Aveiro, Portugal
[2]Navigator Forest Portugal, SA, 2901-861 Setúbal, Portugal
[3]Megavia_Construções e Obras Públicas, SA, 2400-119 Leiria, Portugal

Abstract. Unpaved forest roads are vital for forestry activities. They may demand using high-quality aggregates to withstand heavy traffic loads. This poses a significant challenge, related with environmental and economic aspects, due to their production, transport and application requirements. For the pulp and paper industry, forest roads are crucial in the exploitation and management of forest areas, which provide the raw materials essential to their activity. Wastes and byproducts are generated during the associated industrial processes. Some of these materials have the potential to be used in the construction of unpaved forest roads, reducing demand for aggregates and enhancing circular economy and sustainability. Herein, traditional solutions for unpaved road construction are compared with alternative ones considering a byproduct (from the pulp and paper industry) with and without reinforcement (geosynthetics). This analysis considers costs and carbon emissions associated with the construction of roads. Results show that the use of the studied byproduct presents significant benefits by repurposing the material and reducing landfill disposal costs. Transport is relevant in unpaved road construction due to the large amount of material transported. Reinforcement decreased the use of aggregate, resulting in a 42%-75% cost reduction and a 47%-79% decrease in emissions compared to traditional solution.

Full paper published in the September 2025 Special Issue of the French Geotechnical Journal **"Revue Française de Géotechnique"** _https://www.geotechnique-journal.org

* mlopes@ua.pt

Comparative Life Cycle Assessment of a slope protection on a railway embankment

Theresa Wittl[1], *Silvio* Klügel[1*], *Lars* Vollmert[2] and *Henning* Ehrenberg[2]

[1]GEPRO Ingenieurgesellschaft mbH, Dresden, Germany
[2]Naue GmbH & Co. KG, Espelkamp, Germany

Abstract. Where space is limited, abrupt changes in ground level must be secured by supporting structures. Using a railway embankment as an example, two construction methods are compared, taking into account geotechnical, economic and ecological aspects. The evaluation is carried out using the ecological scarcity method in environmental impact points, primarily for greenhouse gas emissions and primary energy requirements. In addition, the results are evaluated in monetary terms according to a proposal by the Federal Environment Agency. The total costs of both methods, including environmental costs, are compared as a basis for discussion.

1 Introduction

Where space is limited, a free-sloping embankment structure is not always possible. A conventional method of securing the resulting ground movement on railway embankments is the angular retaining wall (ARW). Future-oriented planning focuses on ecological construction methods, for which more sustainable alternatives have to be found. For the construction of a new embankment, two solutions for securing the embankment are being analysed. The geotechnical, economic and environmental aspects of both options are compared.

2 Aim and scope of the study

2.1 Overview and aim of the life cycle assessment and Functional Unit

The aim of this LCA is to compare two construction methods for securing a 4.0 m high step on a new railway embankment using the example of the retaining structures presented in the manual 'Erdbauwerke der Bahnen' [1], namely the geogrid-reinforced retaining structure (GRS) and the ARW.
In addition to the life cycle assessment, a monetary assessment will be carried out. The aim of the project is to identify existing knowledge gaps for a holistic view of a retaining structure and the ecological advantages of GRS and to achieve a more intensive application of GRS in railway construction.

* Corresponding author: silvio.kluegel@gepro-dresden.de

The functional unit is defined as a 100 m long retaining structure on a new railway embankment to be built for a service life of at least 50 years. The calculations assume that both retaining structures have the same service life and therefore this is not decisive for the assessment.
In addition, the following general boundary conditions were defined in [1]

- Double track railway line in embankment position,
- v_{max} = 160 km/h,
- Railway traffic loads: LM 71 according to Ril 836.2001, section 3 (3) (2022) [2],
- Own weight of superstructure according to Ril 804.2101, table 2 (2021) [3],
- design situation BS-P,
- Design of GRS according to Ril 836 (2022) [2], EBGEO (2010) [4] and DIN 1054:2021-04 [5]
- Design of ARW according to Ril 836 (2022) [2], DIN 1054:2021-04 [5] and 4085:2017-08 [6].

2.2 Scope of study and system boundaries

Scope of study
In accordance with DIN EN 15804 [7] and DIN EN ISO 14040 [8] and DIN EN ISO 14044 [9], the aim was to analyse the entire life cycle (from cradle to grave) of the supporting structure. The life cycle stages B1 to B7 (Use Stage) have not been considered, as it is assumed that these stages do not differ significantly between the two variants. The life cycle stages A1-3, A4, A5, C1 to C4 and D (see Fig. 3) were therefore analysed.

System boundary
The technical system boundary is defined around the retaining structure, excluding the railway embankment (see Fig. 1 and Fig. 2). The system boundary has been generously defined around the corresponding retaining structure with the associated foundation pad. The geometric parameters excavation depth and excavation width of the excavation pit of the ARW were decisive here, as the foundation pad of the ARW has larger dimensions for structural reasons.

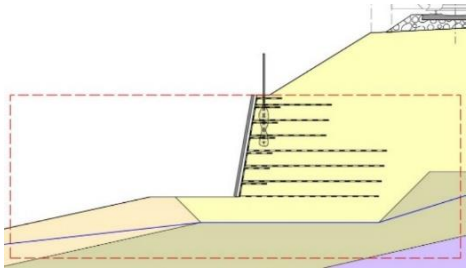


Fig. 1. *Geogrid-reinforced retaining structure (GRS) with illustration of system boundary.*

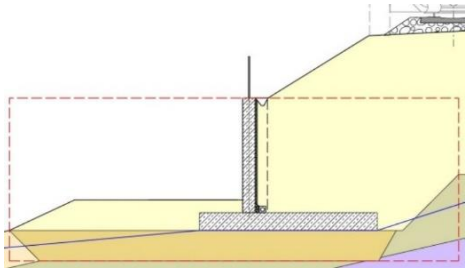


Fig. 2. *Retaining wall (ARW) with illustration of system boundary.*

A further system boundary was required when considering the required infrastructure and machinery. It was assumed that all structures (e.g. concrete plant, etc.) and machinery (e.g. lorries, etc.) required for the considered life cycle stages of the retaining structure were already in place. Therefore, emissions from structures and machinery are not considered separately in the LCA.
The geographical system boundary is the national territory of Germany, as most of the data originate from this geographical area. The LCA was therefore carried out on a fictitious railway embankment in the Deutsche Bahn network.

2.3 Analysed variants

The two support structures considered are GRS and ARW. Both variants were selected on the basis of the available generalised calculation in [1]. They differ in the required dimensions of the retaining structure and the required foundation pad.
In order to be able to create a meaningful and comparable life cycle assessment despite the differences between the two variants, the framework conditions and the design results from [1] were used as a basis.
The required foundation cushion of the ARW is very large compared to the GRS. The dimensioning is based on the calculations in [1]. The following reasons for the large foundation cushion of the ARW are given there:

- The very conservative approaches of the normative regulations for the design of ARWs result in an earth pressure that is about twice as high compared to the GRS.
- The earth pressure to be applied from the strip load of the live load, combined with the lack of vertical component of the earth pressure, results in an unfavourable load on the angular retaining wall.

2.4 Assumptions

Assumptions had to be made to simplify the calculations and due to data gaps. These assumptions relate to the system boundary, the Life Cycle Inventory and Impact Assessment, and the evaluation of the results.

3 Life Cycle Inventory

3.1 Data

The Environmental Product Declarations (EPDs) of the products/construction materials were taken from the ÖKOBAUDAT database [10], with the exception of the geogrid. They all refer to the reference year 2022 and are valid until 2024. Values for the reference region of Germany are given in these data sheets.
The EPD for the geogrid (Secugrid 80/20 R6, PES/PET) [11] was submitted by Naue GmbH & Co. KG. The reference year for this data is 2017 and it is valid until 12/2025 and has a global reference.
The fuel consumption of the machines was determined using the Construction Machinery and Equipment List. An average value was chosen for the calculations. For engine power, the various technical data sheets were used. The power values of the machines are based on experience and estimates. The engine limits for nitrogen oxides and particulate matter were taken from a table published by the German Federal Environmental Agency (UBA) for lorries and from a data sheet from the VDMA e.V. for construction machinery.

3.2 Process modules and calculation methods

The calculations are divided into the different life cycle stages (see Fig. 3). The corresponding process modules have been assigned to the life cycle stages, e.g. the extraction and processing of raw materials for reinforcing steel to life cycle stage A1-3 or the post-compaction of the excavation base to life cycle stage A5.

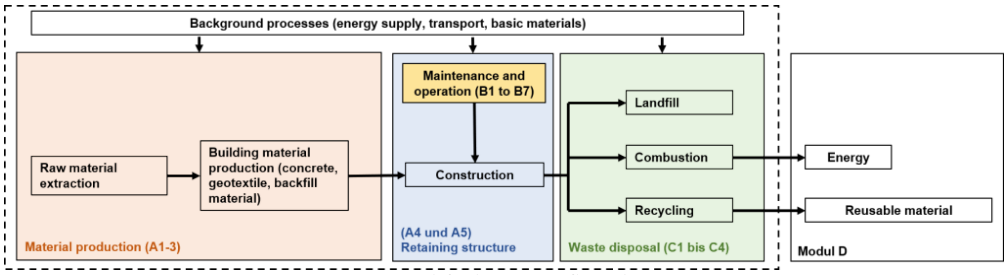


Fig. 3. *Simplified process flow diagram.*

The mass determination is based on the geometric dimensions of the retaining structures and the corresponding foundation. This information was used to determine the cross-sectional areas and volumes of the various construction materials.
For life cycle stages A1-3, A4, C1 - C4 and D, the energy demand and emissions are calculated using the EPD values and the masses determined in the mass balance. The energy demand and emissions for life cycle stage A5 are calculated using the machine running times and the resulting fuel consumption.

3.3 Sensitivity analysis for adjusting the system boundary

In order to define the system boundary, the assumptions made and the boundary conditions defined were critically reviewed prior to the calculations.
For this purpose, a comparative calculation of the influence of the transport routes on the assessment results were carried out. It was found that the variation of the transport route had a linear influence on the CO2 emissions. On this basis, the focus was placed on one transport route.

The large foundation pad of the ARW was critically examined. As the reason for the dimensioning lies in the specifications of DIN 4085:2017-08 [6] and Ril 836.4301 [2], the system limit for both variants was set at the height of the lower edge of the foundation pad of the ARW.

4 Impact Assessment

4.1 Impact Categories, Impact Indicators, Characterisation and Standardisation

The core indicators of DIN EN 15804 [7] were used to define the impact categories, and all impact categories/indicators for which data is available in the environmental product data sheets were included in the impact assessment.

The emission values of the products from the EPDs used already contain characterised values, so no characterisation was performed. The consumption of energy resources in the primary energy impact category and the net use of freshwater resources are material flows.
The emission values for CO_2, oxides of nitrogen and particulate matter for the life cycle stage A5 are direct emissions of air pollutants. The emission values of the Life Cycle Assessment are based on the defined emission limits for nitrogen oxides and particulate matter and do not necessarily correspond to the actual emissions. Therefore, the comparability of these values with the emissions of the other life cycle stages is limited.

5 Evaluation and Discussion

5.1 Ecological scarcity method

The ecological scarcity method allows the results of the Life Cycle Inventory and the Impact Assessment to be weighted. The calculations compare the current total flow of an environmental impact of a country with the critical flow of that environmental impact. The critical flow is derived from the country's environmental policy goals. Both characterised environmental impacts (e.g. climate change) and other environmental impacts (e.g. resource use) can be weighted directly.
The weighting is done using an eco-factor in the unit [UBP] (environmental impact points), which is calculated using the following equation:

$$Eco - factor = K \cdot \frac{1}{Standardisation\ flow} \cdot \left(\frac{current\ flow}{critical\ flow}\right)^2 \cdot 10^{12}\ [UBP]$$

The current flow and the critical flow are compared and squared. This step means that exceeding the target value (critical flow) is weighted disproportionately, so that additional emissions are weighted more heavily the higher the pollution situation already is [12].
It was only possible to calculate the eco-factor for primary energy demand, water consumption, the impact categories climate change and photochemical ozone creation, and air emissions of particulate matter and nitrogen oxides.

The comparison of the eco-factors for 2030 and 2050 makes it possible to identify the material flows that will be important/critical in the future. The eco-factor for greenhouse gas (GHG) emissions in [CO_2-eq] turns out to be the most important factor, with a percentage difference of 851% between 2030 and 2050 (see Fig. 4). For this reason, the analysis and evaluation of the LCA results focused primarily on this impact category.

	Unit	Period 2030	Period 2050	Percentage difference (2030 = 100%)
Consumption of energy resources	UBP/MJ	0,12	0,23	196%
Greenhouse gas emissions	UBP/t CO_2-eq.	3.889	33.103	**851%**
Particulate matter $PM_{2,5}$	UBP/g $PM_{2,5}$	22,6	80	352%
Particulate matter PM_{10}	UBP/g PM_{10}	8,1	19	238%
Nitrogen oxides (NO_x, calculated as NO_2)	UBP/g NO_x	1,5	4,6	317%
Volatile organic compounds without methane (NMVOC)	UBP/kg NMVOC	2.532	12.255	484%
Water use	UBP/m³	80	259	324%

Fig. 4. *Calculated eco-factors*

5.2 Evaluation of the results

When analysing the distribution of GHG emissions over the life cycle (see Fig. 5 and Fig. 6), it is noticeable that the End of Life Stage C1 - C4 cause more than half of the emissions with a share of 60%. For the ARW, however, the majority of GHG emissions (64%) are generated in the Product Stage A1-3.
The Construction Stage A5 has the lowest share in both variants with only 3% and 5% respectively.

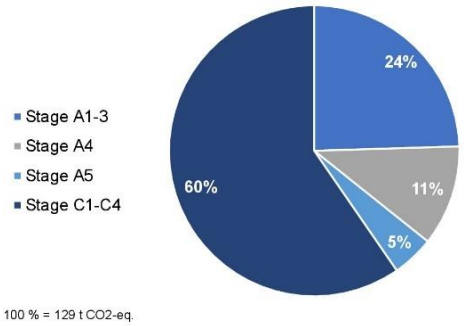


Fig. 5. *Evaluation of GHG emissions GRS.*

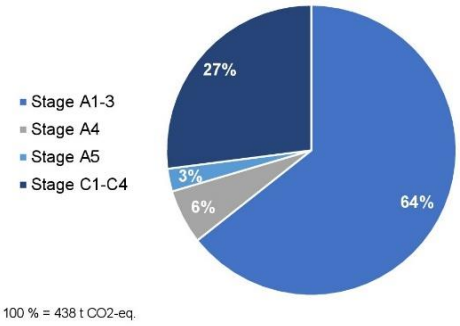


Fig. 6. *Evaluation of GHG emissions ARW.*

The reason for the large difference in the distribution of emissions over the life cycle stages when comparing the two variants can be recognised by taking a closer look at the GHG emissions of life cycle stages A 1-3 and C1 - C4.
The high emissions in life cycle stage C1 - C4 at the GRS originate from the sand/gravel backfill material. This causes the majority of emissions in both the Product Stage and the End of Life Stage. In the End of Life Stage, the proportion of backfill material is 89 % compared to 70 % in the Product Stage. This clearly shows that the sand/gravel causes higher emissions during disposal/waste treatment than during production. The emissions and definitions of the processes behind the different life cycle stages are listed in the ÖKOBAUDAT data sheet 10]. We consider the high values for stages C1 - C3 to be implausible, but the data available at the time of processing means that these emissions are modelled in this way.
In the case of ARW, concrete is clearly the most important building material for GHG emissions, accounting for 66% of emissions in the Product Stage A1-3, while reinforcing steel accounts for 22% and soil replacement/filler material for 12%. This contrasts with a share of just 11% for concrete in the C1 - C4 End of Life Stage, while the share of reinforcing steel is as low as 0.07%. Again, it can be seen that the gravel/sand of the soil replacement and backfill material, with a share of 89%, causes more emissions during disposal than during production. However, the emissions during the production of concrete and reinforcement are greater than those of gravel/sand during disposal, which means that the Product Stage causes the majority of GHG emissions in the ARW.

The evaluation of the assessment shows that the geogrid reinforced retaining structure is the more environmentally friendly option in almost all impact categories analysed.
When comparing the two options in terms of greenhouse gas emissions, the construction of a GRS offers a savings potential of 70% compared to the ARW. In terms of primary energy consumption, the savings potential of the GRS is 60%.

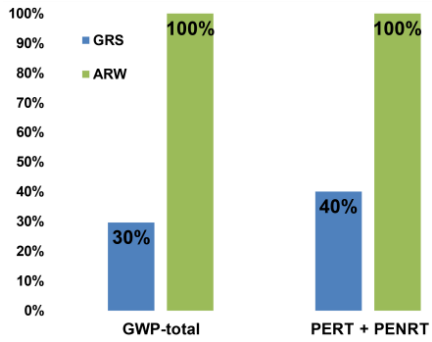


Fig. 7. *Comparison of environmental impacts for the impact categories (GWP) and primary energy demand (PERT+PENRT) in life cycle stages A 1-3, A4, A5 and C1 - C4.*

5.3 Monetary valuation

For the monetary evaluation of the two support structures, a rough estimate of the costs within the limits of the system has been carried out.
The costs of different emissions can be estimated using 13].
A distinction is made between cost factors for '1% pure time preference rate' and '0% pure time preference rate'. A 1% pure time preference rate implies a higher weighting of the welfare of the current generation as opposed to the welfare of future generations. In contrast, the 0% pure time preference rate represents an equal weighting of the welfare of the generations.
The value factors for greenhouse gas emissions [CO_2-eq] and freight transport [tkm] were used to assess the total costs (rough costs for the supporting structure + environmental costs). The value factors for greenhouse gas emissions were taken from 14], as these values are more recent and also less favourable than the value factors given by 13]. The climate costs for 1 [ton CO_2] in 2022 are therefore

- at 1 % pure time preference rate 237 €$_{2022}$ and
- at 0 % pure time preference rate 809 €$_{2022}$.

The environmental costs of transport are taken into account using the value factor from Dr Matthey et al. (2020) for a 14-28 tonne lorry. The values given are for the year 2020. The consumer price index is used to convert these values to 2022. This is 100 for 2020 and 110.2 for 2022, giving a conversion factor of 1.102. The environmental cost per [tkm] in 2022 is therefore

- at 1% pure time preference rate 8.28 €-Cents$_{2022}$ or 0.08 €$_{2022}$ and
- at 0% pure time preference rate 21.57 €-Cents$_{2022}$ or 0.22 €$_{2022}$.

The evaluation of the construction and environmental costs clearly shows that the GRS is the cheaper option. Not only can 59% of the construction costs be saved with the GRS compared to the ARW, but there is also a 67% savings potential in environmental costs.
The share of environmental costs (0% pure time preference rate) is only 39% for the GRS, whereas the share for the ARW is significantly higher at 53%. This means that the GRS is not only cheaper overall, but also has relatively lower environmental costs.

5.4 Research needs and critical points

A number of critical issues arose during the LCA process and research needs were identified. These are analysed in more detail below.

Disposal of concrete and bitumen
The LCA calculations take into account the separate disposal of the concrete and bitumen of the ARW, with the emissions according to the respective EPDs. The prerequisite for this approach is that the two construction materials are separated by type. As this is not yet a standard practice for the dismantling of ARW, a calculation with joint disposal of concrete and bitumen was performed for comparison.
This assumes that the concrete is not treated and processed for reuse as considered in the balance, but that the concrete and bitumen are landfilled/disposed of together. The construction waste landfill data sheet was used for the landfill of the two construction materials.
Comparing the two disposal options for concrete and bitumen, the total life cycle emissions increase by 3% in terms of GHG emissions and 4% in terms of primary energy demand when the two building materials are disposed of or landfilled together. If only the End of Life Stage is compared, the difference of 12% in GHG emissions and 9% in primary energy demand is more apparent. In addition, the benefits in life cycle stage D decrease from - 8 888 kg CO_2-

eq to - 6 033 kg CO_2-eq. This represents a reduction in benefit of approximately 32% and a loss of important raw materials.
This shows that separating building materials by type has a positive impact on sustainability.

Critical analysis of the Product Data Sheet for Gravel 2/32 and Sand 0/2
When evaluating the results in chapter 5.3, it was noticed that the building material sand/gravel allegedly causes higher emissions in the End of Life Stage C1 - C4 than in the Product Stage A 1 - 3. In order to verify this more precisely, the CO_2 eq. emissions from the ÖKOBAUDAT 10] data sheet were broken down into the individual life cycle stages.
The pie chart in Fig. 8 clearly shows that life cycle stage C3 accounts for more than half of the total emissions over the life cycle of the backfill material (53%).
This stage includes the processing of the material for reuse. A processing loss of 25% has been taken into account, which is disposed of in an inert landfill. The resulting emissions are also included in stage C3.

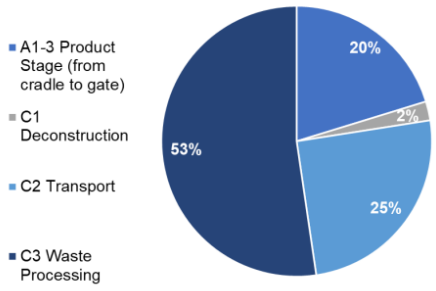


Fig. 8. *Backfill material sand/gravel, share of the various life cycle stages in the GWP-total.*

The high values for life cycle stage C3 are implausible, as even if stage D is included, emissions are much higher than during production. However, the existing data base means that these emissions are modelled in this way.
This is not critical for the comparative LCA as the increased values are applied to both variants. For construction methods with very different amounts of gravel/sand mix, the data base and its selection should be critically reviewed.

5.5 Assessment of data quality

For life cycle stages A1-3, A4, C1 - C4 and D data from Environmental Product Declarations could be used. With the exception of the geogrid, these were taken from the ÖKOBAUDAT online database 10].
The ÖKOBAUDAT EPDs 10] have a reference year of 2022 and are valid until 2024, which is a current time reference. Average values for Germany are given in the EPDs, which means that the values are well suited for the calculations as no exact location is given.
The EPD of the geogrid 11] refers to the year 2017 and is valid until 12/2025. The values given have a global reference and cover Naue as manufacturer.
For the life cycle stage A5 (construction/installation process) there is no data available in the database of the ÖKOBAUDAT 10]. The emissions generated here could only be estimated using our own experience and plausible approaches to machine performance, machine indicators and emission limits.

6 Sensitivity analysis

The sensitivity analysis examines how the length of the retaining structure and the associated change in the choice of machinery and the handling of the excavated material at the construction site affect the balancing of the two retaining structures.

Support structure length for machine selection
In the sensitivity analysis, the length of the support structure is reduced from 100 m to 20 m. Experience has shown that smaller equipment and machines are required for such a site length. Accordingly, there is no need to transport these large machines to the site, but all distribution and compaction work must now be carried out with the smaller machines.
The comparative calculations show that the smaller support structure, both ARW and GRS, generates approximately the same emissions per 1 m of support structure as the larger support structure.

Treatment of excavated material
The sensitivity analysis examines the effects of reusing the excavated slope loam as a foundation for the retaining structure. In order to use the slope loam as a foundation pad, it needs to be improved with a binder. It is assumed that lime with a binder content of 3 M-% is used. The emissions from the disposal/landfilling of the excavated material are estimated using the emission values from the sand/gravel EPD. Comparative calculations have shown that the emissions would be twice as high using the landfill data set. This seems unrealistic as soil is generally not classified as construction waste and the excavated material can even be reused, depending on the soil material class, in accordance with the Substitute Building Materials Ordinance. Only the emissions from the disposal/landfilling of the excavated material and the emissions from the binder, the disposal and landfilling of the remaining excavated material, the savings in the removal of the excavated material and the savings in the production of the gravel and sand backfill material are compared. It can be seen that both the GRS and the ARW result in higher GHG emissions and higher primary energy requirements due to the use of the excavated material as foundation backfill. This is mainly due to the high emissions associated with the production of the lime. The positive effect of saving resources by using less sand/gravel is thus negated in this exemplary LCA. A generalisation of this aspect is not recommended, as resource conservation will become more important in the future and the weighting and evaluation would have to change accordingly.

7 Outlook and summary

Based on the results of this LCA, there are further options to consider. With a view to achieving a high recycling rate, as required by the Substitute Building Materials Ordinance, the use of substitute building materials/recycled materials as backfill material could be further investigated.
Another aspect would be a comparative analysis of the amount of microplastics produced, for example, by tyre abrasion during the transport of all the necessary equipment and building materials to and from the site.
The detailed analysis focused on greenhouse gas emissions and primary energy requirements. An evaluation according to the environmental impact score has not yet been carried out. The weighting of the results makes it possible to compare the majority of the impact categories.
For the retaining structures presented as examples in [1], as a geogrid reinforced retaining structure and an angular retaining wall, a life cycle assessment was carried out over the entire life cycle, including a monetary assessment. A sensitivity analysis was carried out and research needs and critical points were identified.
Within the defined system limits and the assumptions made, it was possible to show that the **geogrid reinforced retaining structure** is both the more **ecological** and the more **economical** option compared to the angled retaining wall. Although simplifications and

assumptions had to be made, the results of this comparative LCA are considered to be meaningful.

References

1. K. Göbel, K. Lieberenz, U. Weisemann (Hrsg.), Handbuch Erdbauwerke der Bahnen, (GRT Global Rail Academy and Meida GmbH, 2022)
2. Deutsche Bahn AG, Handbuch 83601: Erdbauwerke und sonstige geotechnische Bauwerke planen, bauen und instand halten (8. Aktualisierung, 01.05.2022), Ril 836, (2022)
3. Deutsche Bahn AG, Handbuch 80400 - Eisenbahnbrücken (und sonstige Ingenieurbauwerke) planen, bauen und instand halten, Ril 804, (2021)
4. Deutsche Gesellschaft für Geotechnik e.V. (DGGT), Empfehlungen für den Entwurf und die Berechnung von Erdkörpern mit Bewehrungen aus Geokunststoffen - EBGEO, (Ernst & Sohn, 2010)
5. Deutsches Institut für Normen e.V., DIN **1054**: Subsoil - Verification of the safety of earthworks and foundations - Supplementary rules to DIN EN 1997-1, (Beuth Verlag GmbH, 2021)
6. Deutsches Institut für Normen e.V., DIN **4085**: Subsoil - Calculation of earth-pressure, (Beuth Verlag GmbH, 2017)
7. Deutsches Institut für Normen e.V., DIN EN **15804**: Sustainability of construction works - Environmental product declarations - Core rules for the product category of construction products; German version EN 15804:2012+A2:2019 + AC:2021, (Beuth Verlag GmbH, 2022)
8. Deutsches Institut für Normen e.V., DIN EN ISO **14040**: Environmental management - Life cycle Assessment - Principles and framework (ISO 14040:2006 + Amd 1:2020); German version EN ISO 14040:2006 + A1:2020, (Beuth Verlag GmbH, 2021)
9. Deutsches Institut für Normen e.V., DIN EN ISO **14044**: Environmental management - Life cycle assessment - Requirements and guidelines (ISO 14044:2006 + Amd 1:2017 + Amd 2:2020); German version EN ISO 14044:2006 + A1:2018 + A2:2020, (Beuth Verlag GmbH, 2021)
10. Bundesministerium für Wohnen, Stadtentwicklung und Bauwesen, ÖKOBAUDAT Informationsportal Nachhaltiges Bauen, Online Datenbank, https://www.oekobaudat.de/no_cache/datenbank/suche.html (accessed 06/2023)
11. Naue GmbH & Co. KG, Secugrid® Environmental Product Declaration, Declaration number: EPD-Naue-SG-001-ref2 2017, (treeze Ltd., 2017)
12. R. Frischknecht, Lehrbuch der Ökobilanzierung, (Springer-Verlag GmbH Deutschland, 2020)
13. Dr. A. Matthey, Dr. B. Bünger, Methodical Convention 3.1 for the Assessment of Environmental Costs; Value Factors, (German Environment Agency (UBA), 2020)
14. German Environment Agency (UBA) (Hrsg.), Tabelle UBA-Empfehlung zu den Klimakosten, https://www.umweltbundesamt.de/daten/umwelt-wirtschaft/gesellschaftliche-kosten-von-umweltbelastungen#gesamtwirtschaftliche-bedeutung-der-umweltkosten, (2023)

Technical solutions for reducing CO_2 footprint in MSE wall constructions

Anaïs Grandclerc[1*] and *Thomas* Joussellin[1]

[1]Terre Armée, Technical department, 92500 Rueil-Malmaison, France

Abstract. Today, the construction industry is one of the most CO_2-emitting sectors. Actions have been taken for several years to reduce these emissions, but progress is still being made to reach the global greenhouse gas emission reduction targets. Reinforced earth walls are mainly composed of a facing made of concrete or welded mesh panels with a backfill reinforced by metallic or geosynthetic elements. This article deals with the proposal of technical solutions to reduce each component's carbon footprint of a reinforced earth wall (facing, reinforcement, backfill) and to estimate the CO_2 emission reduction at the construction project level (calculations based on a specific and real construction project). Concerning the concrete panels, the replacement of ordinary Portland concrete by low-carbon concrete is a key parameter in the reduction of CO_2 emissions of the construction of a reinforced earth wall (estimation of reduction between 15% and 30% on the total CO_2 emission for this project). Regarding the backfill reinforcement, using geosynthetic reinforcement instead of steel reinforcement is also a way to reduce CO_2 emissions. Indeed, steel reinforcements accounts for around 20% of total CO_2 emissions for this project while geosynthetic reinforcement accounts for around 5%. Finally, regarding backfill, its carbon impact represents about 45% of this project's overall CO_2 emissions, considering the materials and their transportation. Thus, using recycled materials as backfill and reducing transportation distance are essential.

Full paper to be published in:
https://www.e3s-conferences.org/articles/e3sconf/abs/2025/44/contents/contents.html

* Corresponding author: anais.grandclerc@terre-armee.com

Comparative environmental life cycle assessment of a temporary road, a study on behalf of the EAGM

Henning Ehrenberg[1*] and *Jürgen* Gruber[2]

[1]Naue GmbH & Co. KG, 32339 Espelkamp, Germany
[2]Solmax Austria GmbH, 4021 Linz, Austria

Abstract. The European Association of Geosynthetic Product Manufacturers (EAGM) originally commissioned ETH Zurich to quantify the environmental impact of conventionally used building materials (such as concrete, cement, lime or gravel) in comparison to geosynthetics in four cases. In the meantime, the relevance of these cases has been confirmed by treeze AG and a further case (application with filter function (the construction of a filter with geosynthetics in comparison to a mineral filter)) was evaluated in 2020. Another case was evaluated in 2023/2024. The life cycle assessment carried out as part of this study follows a cradle-to-grave approach. The analysed product systems of a temporary road construction include the extraction of raw materials, their processing into construction materials, the construction and dismantling of the temporary road (infrastructure element). The environmental performance of geosynthetics is compared with the performance of competing construction materials. The study shows the advantages of sustainable constructions with geosynthetics.

1 Introduction

Geosynthetic materials are used in many different areas of applications in the construction industry. In most cases, the use of geosynthetics replaces or improves the use of other materials. In 2010, the European Association of Geosynthetic Product Manufacturers (EAGM) commissioned ETH Zurich and ESU-services Ltd. for the first time to quantify the environmental impact of common construction materials (such as concrete, cement, lime or gravel) in comparison to geosynthetics in civil and environmental engineering structures.

To this end, a series of 4 comparative life cycle assessment (LCA) studies was conducted focusing on different use cases, namely filtration systems, foundation-stabilised roads, drainage in landfill constructions, and retaining structures. The environmental performance of geosynthetics and competing construction materials was compared.

It was verified in 2018, if the obtained results were still up to date or whether the study needed to be renewed. EAGM commissioned treeze Ltd (the successor company of ESU-services Ltd) with this review. The assessment confirms the timeliness of the study. The full study, including the results of the critical reviews, is available at: http://www.eagm.eu/. [1, 2]. These results were presented in detail at EUROGEO 7 in Warsaw in 2022.

* Corresponding author: hehrenberg@naue.com

Furthermore, a cost comparison of the 4 cases mentioned above [3, 4] was presented.at EUROGEO 7.

In 2023, at the 12th International Conference on Geosynthetics (12 ICG Roma), a fifth LCA case was presented [5], a life cycle assessment of geosynthetics versus conventional construction materials in a river construction for filtration purposes.

Another study [6] was prepared in 2023 and 2024, and the findings are presented in detail within this paper.

2 Life cycle assessment of a temporary road

This paper presents the results of a case with a geosynthetic as a separation, stabilisation and reinforcement function in comparison to a road construction with mainly soil exchange. The study shows benefits in sustainable constructions using geosynthetics. treeze Ltd. evaluated the study.

The life cycle assessments carried out within this study follow a cradle-to-grave approach. The product systems of the temporary road analysed encompass the extraction of the raw materials, their processing into building materials, the construction and disposal of the materials (infrastructure element, see Fig. 1). Operation and maintenance were excluded. Transport processes and infrastructure are included. All processes describe average European conditions.

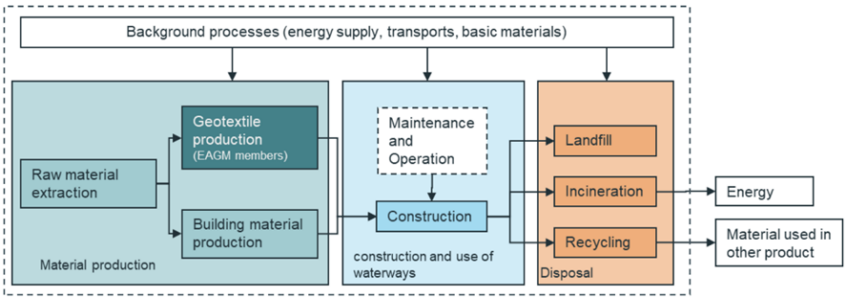


Fig. 1. Simplified process flow chart showing the most important process steps. Maintenance and operation of the infrastructure element are not included in the system boundaries.

The functional unit is 1 meter of a temporary road on low bearing (soft) soil of a width of 5 meters. The geosynthetic layer separates the subbase from the subsoil knowing that without separation the clean subbase will be mixed with subsoil. This additional “extra” function is hard to quantify in the LCA and thus not taken into account. As in this case a temporary road was evaluated, the lifetime is expected to be the same (2 years) for both options assessed in this study.

Data about geosynthetic material production were gathered from 6 individual European producers, all members of the EAGM, using pre-designed questionnaires to be answered. The company-specific life cycle inventories are used to establish an average life cycle inventory of geosynthetic material suited for the technical functionality of temporary roads. Data collection covers manufacturing efforts, raw material and water consumption, production waste and emission of pollutants during manufacturing of geosynthetics. Data on construction and deconstruction efforts were adopted from previous case studies and provided by an industry expert, respectively. They cover diesel consumption of construction equipment as well as transport distances and modes of transportation.

The data collection includes qualitative information of system-relevant products and processes from the producer, information from suppliers of the producer (where possible) as well as data from technical reference documents (e.g. related studies, product declarations,

etc.). An average LCI is established on the basis of a simple average of the environmental performance of products manufactured by the participating member companies suitable for temporary road applications.

The primary source of background inventory data used in this study is UVEK LCI data DQRv2:2022 [7]. The LCA software SimaPro v9.5.0.0 (PRé Consultants 2023) was used to model and calculate the life cycle based environmental impacts.

The study refers to the year 2022. Foreground data about geosynthetic material manufacture gathered by questionnaires refer to the years 2020, 2021 and 2022.

Sensitivity analyses are conducted to verify the reliability of the results. They differ in the specific weight of the geosynthetics used and in the shipping distance of subbase mineral material.

The environmental performance is assessed with the following impact category indicators:

- Climate Change (Global Warming Potential, GWP100),
- Photochemical Ozone Formation,
- Particulate Formation,
- Acidification,
- Eutrophication,
- Land use impacts,
- Abiotic resource depletion (excluding fossil fuels), and
- Cumulative Energy Demand (Primary Energy Consumption), non-renewable.

3 Description and results

3.1 Description of Case 6 of the EAGM LCA Studies

The functional unit is 1 meter of a temporary road on low bearing (soft) soil for a width of 5 meters (see Fig. 2). The geosynthetic layer also separates the base layer from the subsoil. The effect as a separating layer in this case (clean separation of the soil layers by the geosynthetic layer as opposed to mixing of the soil layers without the geosynthetic layer), this additional "extra" function is hard to quantify in the LCA and thus not taken into account.

The subbase has a thickness of 55 cm and 35 cm for the unreinforced and the reinforced alternative, respectively. Three different geosynthetic products are commonly used. Either a woven made of polypropylene (PP), a geosynthetic composite made of nonwoven polypropylene with a geogrid structure on top, or a polypropylene or polyethylene terephthalate (PET) geogrid. The geosynthetic layer is modelled as an average of the three types and has an average specific weight of 360 g/m². As in this case a temporary road was evaluated, the lifetime is expected to be 2 years for both options assessed in this study.

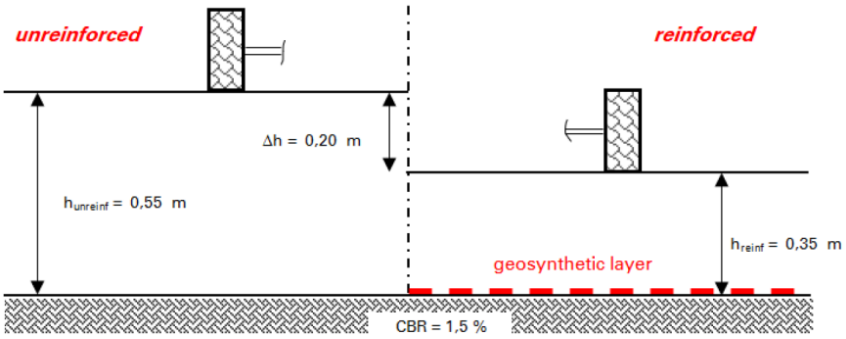


Fig. 2. Cross section of the temporary road on soft soil analysed in this study (left: without geosynthetic and 0.55 m aggregate; right: with geosynthetic and 0.35 m aggregate on top)

The two alternatives are defined such that they can be considered technically equivalent or at least comparable. The geosynthetics used represent a mix of different brands suited for reinforcing the subbase of temporary roads on soft soil (CBR = 1.5 %). The conventional systems represent the most common type of construction.

3.2 Sensitivity analyses

Sensitivity analyses are conducted to verify the reliability of the results. They differ in the specific weight of the geosynthetics used and in the shipping distance of subbase mineral material.

Geosynthetic layers are averaged with a weight per unit of 360 g/m² and vary with + and – 10% for scenario 1 and 2.

Geosynthetic layers are delivered to the construction site (average distance: 650 km by lorry and 1,070 km by cargo ship) in all three calculated scenarios.

The average shipping distance for aggregates is 50 km in the base scenario and varies for scenario 1 and 2.

Table 1. Scenarios applied in case 6

Scenario	**Base**	1	2
Geosynthetics basis weight [g/m²]	**360**	396	324
Distance supply of subbase material [km]	**50**	20	100

3.3 Deconstruction

The deconstruction efforts considered in this comparative LCA are the diesel consumption during deconstruction and first cleaning of the geosynthetic material as well as the transport to the waste management facilities. It is assumed that geosynthetics are sent to a waste incineration facility (conservative assumption). Shipping distances of 20 km to a landfill site and 50 km to a waste incineration plant are assumed.

For their use in cement kilns, further cleaning and treatment would be needed [8].

The deconstruction efforts as well as the efforts for cleaning of recovered geosynthetic materials are expert estimates [6].

First experiments with the recycling of used geosynthetic materials are being made and experiences gained. Extensive work is currently being carried out in the industry on the deconstruction and recycling of geosynthetics. Reports can be found in this conference [9] and [10], to mention just a few current experiences and projects.

3.4 Results of base scenario and scenarios 1 and 2

The base scenario is based on a geosynthetic layer with an average specific weight of **360 g/m²** and a shipping distance of mineral material (gravel/sand) of **50 km**.

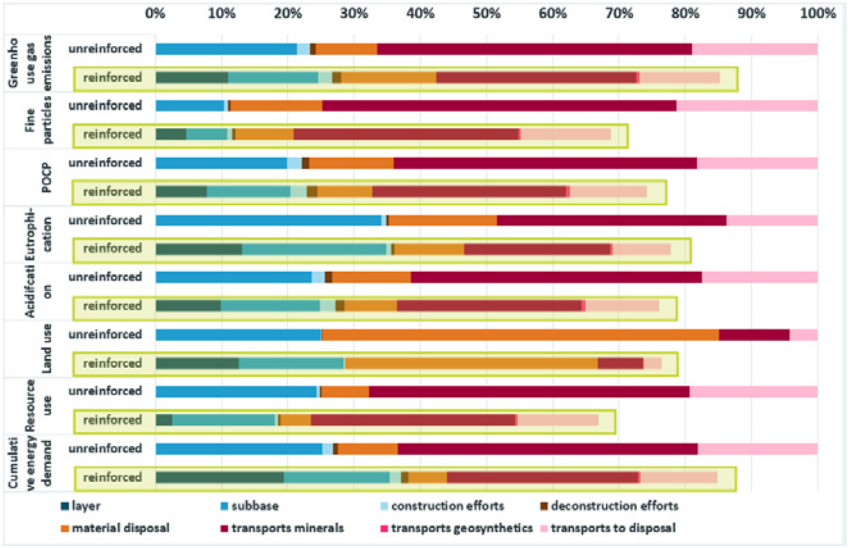


Fig. 3. Environmental impacts and their main contributors caused by 1 m of reinforced temporary road (width of 5 m, highlighted in light green) relative to the environmental impacts of the unreinforced temporary road (which equal to 100 %); base scenario.

Scenario 1 is based on a geosynthetic layer with an average specific weight of **396 g/m²** and a shipping distance of mineral material (gravel/sand) of **20 km**.

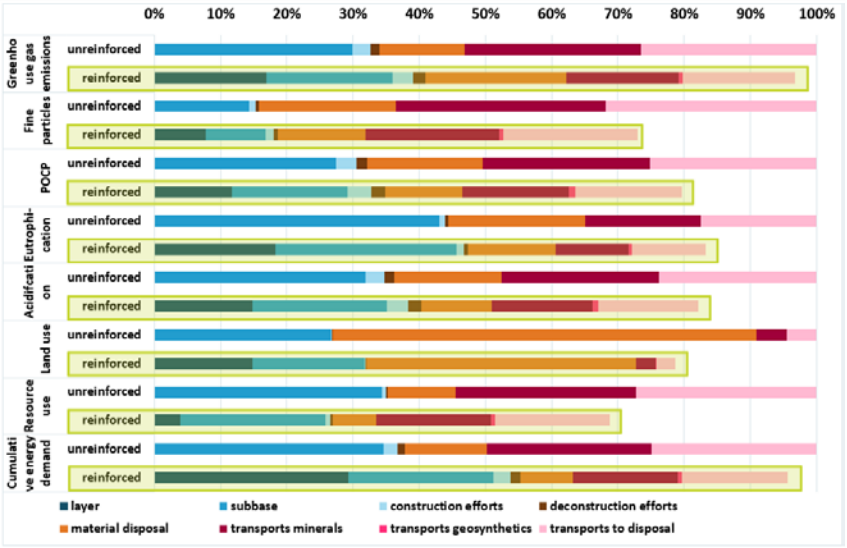


Fig. 4. Environmental impacts and their main contributors caused by 1 m of reinforced temporary road (width of 5 m, highlighted in light green) relative to the environmental impacts of the unreinforced temporary road (which equal to 100 %); scenario 1.

Scenario 2 is based on a geosynthetic layer with an average specific weight of **324 g/m²** and a shipping distance of mineral material (gravel/sand) of **100 km**.

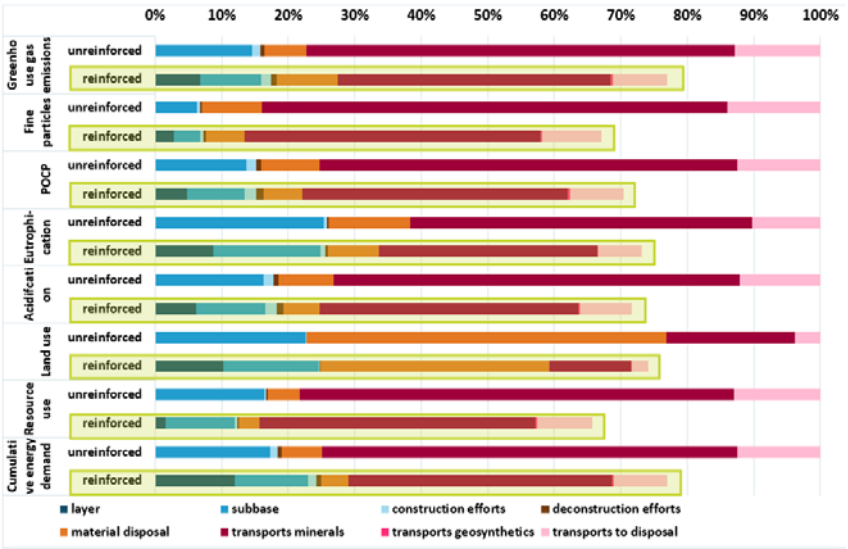


Fig. 5. Environmental impacts and their main contributors caused by 1 m of reinforced temporary road (width of 5 m, highlighted in light green) relative to the environmental impacts of the unreinforced temporary road (which equal to 100 %); scenario 2.

3.5 General summary of results of base scenario and scenarios 1 and 2

The results show that the alternative structure reinforced with geosynthetics has a lower environmental impact than the alternative without geosynthetics in all cases and in all impact categories. Depending on the scenario and impact category, the reduction in environmental impact when using geosynthetics varies between 3 % and 35 %.

The geosynthetic layer separates the base layer from the subsoil, whereas without separation the clean base layer is mixed with the subsoil. This additional function and the advantage it offers, particularly during dismantling and recycling, is currently still difficult to quantify and is therefore not included in this life cycle assessment.

4 Construction costs

At the EUROGEO 7, [3] presents a cost comparison (CASE 2: Foundation stabilisation) to a similar case like the one presented in this paper. Described as: In road construction the subbase needs to meet defined requirements for compaction and bearing capacity. Improvement of some soil characteristics may be necessary when building on weak soils. All products included had an ultimate tensile strength of 30 kN/m in both directions and were manufactured from polypropylene or polyester. The case of a conventional road is compared to a road reinforced with geosynthetics.

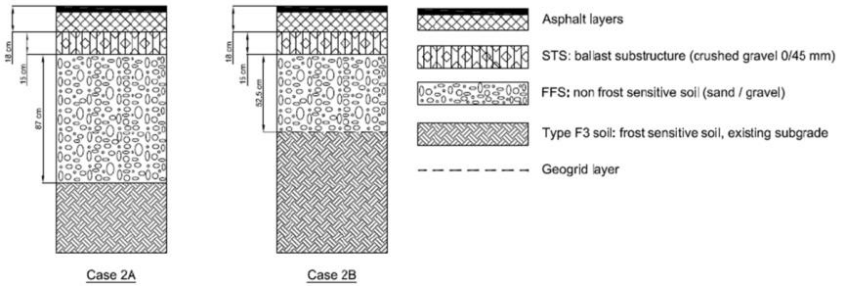


Fig. 6. Cross section of the compared road constructions from case 2

The main difference is that in Case 2B there is 34.5 cm less soil exchange / replacement than in Case 2A, but therefore the use of geogrid/nonwoven in Case 2B which is the basis for the cost calculation.

The Case 2 is not completely comparable to the Case 6 from this paper, but it was shown that the use of geosynthetics can save soil movements on the construction site and reduce required quantities of soil and this clearly leads to significant cost savings. In Case 2, the costs for a “classic construction” are 45 % higher than for the construction with a geosynthetic solution. The cost comparison is based on cost rates for the third quarter of 2021. Since the classic solution always requires more equipment to be used on the construction site and transport to/from the construction site is necessary, the cost advantages of the geosynthetic solution calculated with this cost today are estimated to be even higher due to the significant increase in energy and fuel costs today compared to summer 2021.

5 Summary

Given the goal in the European Climate Law of the European Union to become climate neutral by 2050, a further and substantial reduction in greenhouse gas emissions and other impacts is required. This involves low CO_2 construction equipment and freight transports, and the reduction in greenhouse gas emissions during the manufacture and disposal of geosynthetic materials. Roads constructed in Europe may differ in cross-section and materials used.

Two significant impacts discussed in the last years are climate change (greenhouse gas / CO_2 emissions) and cumulated energy demand. In the last years, the saving of natural resources, e. g. minerals (abiotic resource depletion), is coming more & more into mind.

Fig. 7 shows that the use of a geosynthetic leads to lower impacts compared to the classic construction with a mineral filter layer in all evaluated scenario.

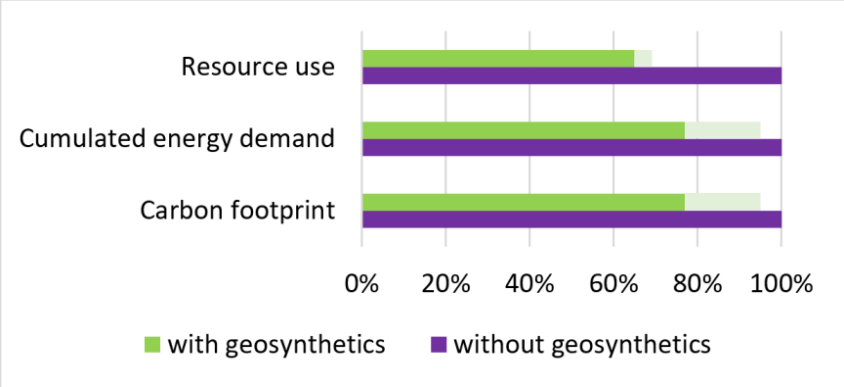


Fig. 7. Relative differences in resource use, cumulated energy demand and carbon footprint; and the fluctuation range of the reduction depending on the scenario under consideration.

The results for the different scenarios are similar and show that the use of a geosynthetic leads to lower impacts compared to the classic construction in all evaluated scenarios in all impact categories. The results can be seen in detail in [6] at www.eagm.eu.

Furthermore, it was shown that the use of geosynthetics means a high saving of natural resources, as minerals such as sand and gravel are saved by using geosynthetics. In addition, an example was shown in which the construction costs of the entire project were significantly reduced through the use of geosynthetics compared to the construction costs using a classic construction method.

References

1. M. Stucki, S. Büsser, R. Itten, R. Frischknecht and H. Wallbaum (2011) Comparative Life Cycle Assessment of Geosynthetics versus Conventional Construction Material. ESU-services Ltd. commissioned by European Association for Geosynthetic Manufacturers (EAGM), Uster and Zürich, CH.
2. P. Stolz & R. Frischknecht 2019. Comparative Life Cycle Assessment of Geosynthetics versus Conventional Construction Materials, treeze Ltd. commissioned by European Association of Geosynthetic product Manufacturers (EAGM), Uster and Zürich, Switzerland.

3. J. Retzlaff, Cost comparison of geosynthetics versus conventional construction materials, a study on behalf of the EAGM, CASE 1: Filter function, CASE 2: Foundation stabilisation, EUROGEO 7, Warshaw (2022)
4. J. Retzlaff, Cost comparison of geosynthetics versus conventional construction materials, a study on behalf of the EAGM, CASE 3: Landfill construction drainage layer, CASE 4: Soil retaining wall, EUROGEO 7, Warshaw (2022)
5. H. Ehrenberg, Comparative life cycle assessment of geosynthetics versus conventional construction materials in infrastructure, filter function in a river construction, a study on behalf of the EAGM, 12th International Conference on Geosynthetics – 12 ICG Roma, (2023)
6. R. Frischknecht, Comparative environmental life cycle assessment of a temporary road, Uster (2024)
7. KBOB, ecobau and IPB (2022) UVEK Ökobilanzdatenbestand DQRv2:2022. Koordinationskonferenz der Bau- und Liegenschaftsorgane der öffentlichen Bauherren c/o BBL-Bundesamt für Bauten und Logistik, retrieved from: www.lc-inventories.ch.
8. Lechtenberg & Partner (2019) Entsorgung von Geotextilien. In proceedings from: Kolloquium – Umweltauswirkungen von Geotextilien im Wasserbau, 23./24. Oktober 2019, Bfg Bundesanstalt für Gewässerkunde, Koblenz.
9. N. Depenbrock, F. Heimbecher, S. Flamme, S. Ebbert, M. Tazl, Reuse and recycling of geosynthetics – Insights into an interdisciplinary research project for a circular economy, EUROGEO 8, Lille (2025)
10. G. Groen, J. Gruber, Recycling of geotextiles: a collaborative approach to enhance circularity in construction, EUROGEO 8, Lille (2025)

Sustainability assessment of liquefaction instability mitigation solutions for the World's highest observation wheel project in Dubai

Jayakrishnan Puthiya Veettil[1*], *Fabrizia* Trovato[2] and *Giulia* Lugli[2]

[1]Maccaferri Middle East, Technical Department, Dubai, UAE.
[2]Officine Maccaferri Group, Geosynthetic Business Unit, Bologna, Italy.

Abstract. 'Ain Dubai,' located on Bluewaters Island in the UAE, is the world's tallest observation wheel, standing at a height of 250 meters. Built between 2015 and 2021, the project includes an artificial island with residential, retail, and leisure spaces. The 12-meter-high shoreline protection structure sits on a 3-meter-thick loose marine sand layer, underlain by competent strata. The initial revetment design accounted for liquefaction risks, and dimensions were set accordingly. However, modifications to the landscaping plan later required raising the platform by 4 meters, reducing the revetment's factor of safety in deep-seated stability. To address this, the designer proposed one primary and three alternative stabilization strategies: (1) jet grouting the existing liquefiable layer, (2) cement stabilization of the top fill, (3) reinforcing the top fill with high-strength geogrids, or (4) extending the quarry run trench for additional toe support. The geosynthetic stabilization option was selected due to its techno-commercial benefits. This paper presents a detailed back analysis of solution options to mitigate liquefaction-induced instability in shoreline protection works through the 'Ain Dubai' case study, providing one of the first comparative evaluations using real project data to encourage sustainable practices for future similar projects in the Arabian Peninsula.

Full paper published in the September 2025 Special Issue of the French Geotechnical Journal **"Revue Française de Géotechnique"** _*https://www.geotechnique-journal.org*

* Corresponding author : p.jayakrishnan@maccaferri.com

Effects of ageing in a saturated environment on the functional properties of hemp geotextiles

Sama Angèle Dabiret[1*], *Frédéric* Roure[2], *Fabienne* Farcas[1], *Lamis* Makki[3], *Philippe* Mailler[4], *Philippe* Reiffsteck[3], and *Laetitia* Van Schoors[1]

[1]Université Gustave Eiffel, Mast/Cpdm, 77454 Marne-la-Vallée Cedex 2, France
[2]Entreprise Géochanvre, Route de Frangey, 89160, Lézinnes, France
[3]Université Gustave Eiffel, Gers/Sro, 77454 Marne-la-Vallée Cedex 2, France
[4]Institut Français du Textile et de l'Habillement, 69130 Ecully, France

Abstract. In road infrastructures, geotextiles perform the essential functions of separation and filtration. For these applications, synthetic geotextiles like those made from polypropylene are widely used for their properties and high durability. However, for temporary road infrastructures, such durability may not be necessary. Replacing these materials with natural geotextiles, such as geotextiles made with hemp fibers appears promising. The aim of this study is to evaluate the relevance of using hemp geotextile for separation and filtration applications in road infrastructures. In this paper we present the evolution of hemp geotextiles properties through a laboratory ageing process. Laboratory ageing was carried out by placing the geotextiles in water-saturated crushed concrete soil for six months. The evaluation focused on functional properties, in particular mechanical and hydraulic performance, supplemented by physicochemical analyses. After six months of ageing, no significant changes in mechanical properties and hydraulic performance were observed. However, morphological and chemical study revealed a slight change in fiber surface. These results highlight promising performance of these geotextiles in this environment.

Full paper to be published in:
https://www.e3s-conferences.org/articles/e3sconf/abs/2025/44/contents/contents.html

* Corresponding author: sama-angele.dabiret@univ-eiffel.fr

SESSION 1 B

TESTING, QUALITY (1)

Assessing the shear-strength properties of geomembranes textured using the spray-on technique

Eric Blond[1*], and *Catrin* Tarnowski[2]

[1]Eric Blond Consultant Inc, Montréal, Québec, Canada
[2]SOLMAX, Hamburg, Germany

Abstract. One of the techniques commonly used to create a surface texture on a polyethylene geomembrane consists in spraying filaments on a smooth geomembrane. When adequately produced, this solution provides a geomembrane exhibiting good friction properties, while preserving the mechanical and durability properties of the base, smooth geomembrane. In the first part of the paper, key aspects related to the manufacturing of spray-on texture are presented, along with key characteristics of the finished product. Despite having been supplied for over 30 years, the quality control and specification of spray-on texture has remained a 'black-box' for end-users. In the second part of the paper, the strategy which has been used over three decades by the BAM (Germany) to assess the reliability of this technology, in a context of product certification. To facilitate acceptance of the spray-on technique on markets relying on conformance testing instead of certification, Blond *et al.* (2022) [1] introduced the inclined-plane compression test, which was successful at measuring an index property reflecting the friction properties of the geomembrane and could be measured on the finished product. Blond *et al.* (2023) [2] also showed that the test offers an opportunity to estimate the peak interface shear strength of geomembrane/geotextile interfaces. In the third part of the paper, an intensive testing program is conducted to assess the repeatability of the test. It is shown that this technique can be successfully used to control, and to specify geomembrane interfaces.

Full paper to be published in:
https://www.e3s-conferences.org/articles/e3sconf/abs/2025/44/contents/contents.html

* Corresponding author: eric@ericblond.com

Experience of a certification body with the quality of external testing in the certification process

Christoph Hessing[1*], *Christian* Recker[1]

[1]SINTEF Certification, Børrestuveien 3, 0373 Oslo, Norway

Abstract. "If a manufacturer loses its certificate, this should be because of poor product quality and not because of a measurement error." (Romain Diederich, Technical Marketing Specialist/Producer of geotextiles) Test results are the basis for the conformity assessment of a certification body. Incorrect testing may result in serious consequences for manufacturers. If the test results are outside a certain specified range, the product loses its certification and can no longer be sold in certain markets. This paper highlights the interaction between product quality and the quality of product testing in the certification process. It underscores the need for robust quality control measures in testing laboratories to prevent unwarranted certificate revocations due to measurement errors. Furthermore the paper describes the evaluation criteria for the submission of obviously incorrect or questionable test results delivered by the testing laboratories, the measures taken, the reactions of the testing laboratories and the interaction between the laboratories and the certification body.

1 Conformity assessment acc. to ISO/IEC 17065

ISO/IEC 17065 [1] is the international standard that outlines the requirements for certification bodies certifying products, processes, and services. It ensures that these bodies operate competently, impartially, and consistently. The goal of application of the standard is to establish confidence and trust in the work of accredited bodies and in the certification of products, processes or services [2].

Given these normative requirements, it is critical for a certification body to ensure that test results from external testing laboratories are reliable and accurate, as these results form the foundation of their conformity assessments. When incorrect results are identified, clear and structured actions must be taken to maintain the integrity of the certification process. ISO/IEC 17065 outlines specific requirements for certification bodies regarding their procedures for conformity evaluation, complaint and appeal handling, and continuous improvement, in addition to general requirements for their organization and resources.

2 Example of a voluntary quality system for geosynthetics

* Corresponding author: christoph.hessing@sintef.no

Each conformity assessment performed by a certification body is based on a certification scheme, outlining an agreed set of rules and procedures for the particular conformity assessment. The certification scheme is defined by a program owner which can be certification bodies, governments and authorities, purchasing agencies, non-governmental organizations, industry and trade associations or consumer organizations. The certification scheme forming the basis for this paper is a voluntary quality system for the certification and quality control testing of geosynthetics for separation, filtration and/or reinforcement. It defines minimum requirements related to the intended purpose (function) of the products. The certification process can be described in five stages:

2.1 Inspection

The producer´s manufacturing facility is inspected by the certification body to assess whether the requirements of the certification scheme are met. The inspection covers the producer's factory production control, its organisation, handling of non-conformities, assessment and approval of suppliers, incoming goods control, finished goods control, product storage and product marking. A successful inspection is required for the initial certification as well as the re-certification every second year.

2.2 Sampling

During the inspection, the certifying body randomly selects rolls from the warehouse which are then sampled, marked and send to an accredited laboratory commissioned by the certification body. Unannounced random product sampling of already certified products may also take place at the manufacturer, in a distributors warehouse or on a construction site.

2.3 Testing

The samples are tested in testing laboratories accredited acc. to ISO/IEC 17025 [3]. The scope of testing is defined by the type of product and its intended function(s) as per Table 1.

Table 1. Certified values with tolerance (in % of values) depending on the function fulfilled by the product

Characteristic	Standard	Unit	Function		
			Filtration	Separation	Reinforcement
Product identification					
Mass per unit area[1)]	EN ISO 9864	g/m²	± 10 %	± 10 %	± 10 %
Tensile elements	Annex F		n.r.	n.r.	Manufacturer's data
Dimensions	Annex F [2)]	mm	n.r.	n.r.	± 15 %
Mechanical tests					
Max tensile strength	EN ISO 10319[3)]	kN/m	-10 %	-10 %	n.r
Tensile strain at max tensile load	EN ISO 10319	%	-20 %	-20 %	n.r
Nominal tensile strength	EN ISO 10319	kN/m	n.r	n.r	-5 %
Tensile strain at nominal strength	EN ISO 10319[3)]	%	n.r.	n.r.	± 20 %
Tensile stiffness at 2, 5, 10% tensile strain	EN ISO 10319	kN/m	n.r.	n.r.	-20 %
Static puncture test	EN ISO 12236	kN	-10 %	-10 %	-10%[4)]
Dynamic perforation resistance	EN ISO 13433	mm	+25 %	+25 %	+25%[4)]
Hydraulic tests					
Permeability normal to the plane without load	EN ISO 11058	mm/s	-30 %	-30 %	-30 %[4)]
Characteristic opening size	EN ISO 12956	µm	±30 %	±30 %	±30 %[4)]

[1)] We regard the plus/minus NGS-tolerance on the mass per unit area as an indication of the process stability. Process stability means that the process delivers constant, predictable results.

[2)] Applicable only for geogrids (definition acc. EN ISO 10318).

[3)] MD and CMD direction. For uniaxial products, test only the direction of load uptake

[4)] Voluntary

n.r. = not required

NorGeoSpec 2012 guideline, part 1, Product Certification [4]

In the given certification scheme, testing laboratories are required to participate in the continuous improvement programme for testing quality, organized by the certification body. This programme is based on regular round robin tests and annual meeting to discuss the results and findings. The accredited testing laboratories can also use the findings from these round robin tests to ensure the validity of their test results, as mandated by ISO/IEC 17025, section 7.7. Additionally, these findings help to identify potential inaccuracies in the testing standards and ensure consistent future testing procedures among all laboratories participating in the certification scheme.

2.4 Assessment

In the given certification scheme product specification profiles are defined for geotextile products used for separation and filtration. The test results obtained are compared against these profiles which form the basis of the conformity assessment.

Table 2. Required values - Product specification

	Function: separation and filtration							
Characteristic	**Testing standard**	**Unit**	**Maximum tolerance [1]**	**Required[2] values corresponding to 95% confidence limit**				
				Product Specification profiles				
				1	**2**	**3**	**4**	**5**
Min tensile strength	EN ISO 10319	kN/m	-10%	6	10	15	20	26
max. load	EN ISO 10319	%	-20%	15	20	25	30	35
Max cone drop diameter	EN ISO 13433	mm	+25%	44	38	28	22	13
Min energy index		kN/m		1.2	2.1	3.2	4.5	6.5
Min velocity index	EN ISO 11058	10^{-3} m/s	-30%	3	3	3	3	3
Max characteristic opening size, O_{90}	EN ISO 12956	mm	±30%	0.2	0.2	0.2	0.15	0.15
Max tolerance for mass per unit area	EN ISO 9864	g/m²	±10%					
Max tolerance for static puncture strength	EN ISO 12236	kN	-10%					

1) The tolerance shall be stated by the manufacturer; this table gives the maximum allowable tolerance.

2) The tolerances are not to be added to the required values. The nominal values ± the tolerance shall fulfil the requirement.

NorGeoSpec 2012 guideline, part 2, Product Specification [4]

The decision rules are described in the certification scheme based on the declared tolerances by the manufacturer and the test results obtained in the testing laboratories. These are defined as:

- If the test result (average of the sample tested) for the particular characteristics is within the 95% NGS-confidence limits, the product is accepted.
- If the test result for one or more of the particular characteristics is outside 1.5 times the tolerance values provided by the manufacturer, the product does not comply with the requirements.
- If the test result for one or more of the particular characteristics is between 1.0 and 1.5 times the tolerance values given by the manufacturer, B-sample shall be tested.
- If the test result of the B-sample for one or more of the same particular characteristics is within the tolerance values provided by the manufacturer, the product is accepted as complying with respect to that (those) characteristic(s).

- If the test result of B-sample for one or more of the same particular characteristics is outside the tolerance values given by the manufacturer, the product does not comply with respect to that (those) characteristic(s).

2.5 Certification decision

In the given certification scheme the certification decision is taken by the programme owner's Technical Committee. Where an inspection, whether announced or unannounced, reveals non-conformity of a product, the Technical Committee is notified by the certification body and meets (in person, or by other means) to recommend appropriate action to the certification body. The certification body decides what action needs to be taken e.g. whether Certification for that product, and any product family represented, should be suspended or cancelled with immediate effect. In this case, a notice is posted on the certification bodies website. The manufacturer is informed by the Technical Committee in writing within ten days of the steps which need to be taken to re-instate the Certification.

3 Experiences

During its certification activities in the given certification scheme, the certification body has experienced various cases over several years in which test results obtained from testing laboratories have been obviously wrong or at least questionable. Given the fact that often product families are tested any kind of inconsistency is certainly easier to spot than for individual product testing.

If not identified, such incorrect test results typically lead to a negative certification decision which in turn would lead to significant re-certification costs as well as losses in sales and time delays for the certificate holder.

The following two examples describe cases where obviously incorrect test results were identified and complaints were filed with the corresponding testing laboratories. Following up on these complaints the testing laboratories identified potential for improvement and thus were able to improve their performance.

3.1 Case 1 - Testing of characteristic opening size acc. to EN ISO 12956 [5]

For re-certification a product family of five nonwoven geotextiles covering the product specification profiles 1 to 5 as per Table 2 have been sampled by the certification body and tested in an accredited testing laboratory. The product Grades 1 to 5 differ in their mass per unit area and their corresponding mechanical and hydraulic parameters. Grade 1 is the lightest and 5 the heaviest. The internal quality control data of the manufacturer over multiple years is known to the certification body.

For the characteristic opening size, the certification scheme requires the manufacturer to declare a plus and minus tolerance on the declared value.

3.1.1 Test results of initial testing and re-testing vs. declared values and tolerances

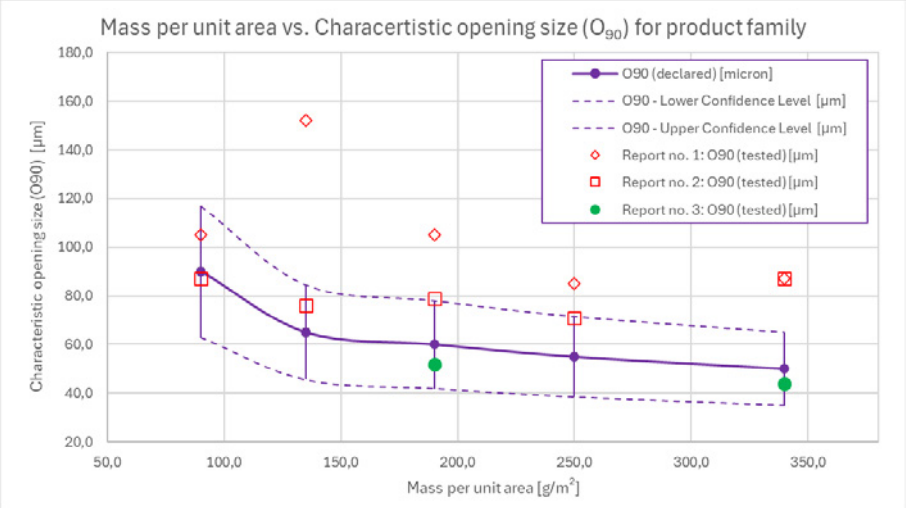


Fig. 1. Case 1 - Declared and tested characteristic opening size

3.1.2 Initial assessment - Report no. 1

Grade 1: test result is within 1.0 x declared tolerances: compliant
Grades 2-5: test results are outside of 1.5 x declared tolerances: failed

3.1.3 Complaint and discussion

When looking at the test results provided an extreme deviation from the declared values was noticed and an unusual distribution of individual values. This formed the basis for a complaint with the testing laboratory to check the test data and to re-test the characteristic opening size of the samples.

3.1.4 Re-testing - Report no. 2

The characteristic opening size for all five grades was re-tested.
Grade 1, 2, 4: test results are within 1.0 x declared tolerances: compliant
Grade 3: test result is outside of 1.0 x declared tolerance but within 1.5 x declared tolerances: B-Sample to be tested
Grade 5: test result is outside of 1.5 x declared tolerances: failed

3.1.5 Re-testing - Report no. 3

Since the test results of Report no. 2 were still inconsistent, Grades 3 and 5 were re-tested in a different accredited laboratory with the following results.
Grades 3, 5: test results are within 1.0 x declared tolerances: compliant

3.1.6 Final assessment

All five products were found to be compliant with the requirement of the certification scheme.

3.1.7 Findings

Based upon the discussion on these tests the laboratory has assessed the situation internally and found that a lack of training was the cause of these inconsistent test results.

3.2 Case 2 - Testing of water permeability acc. to EN ISO 11058 [6]

For re-certification, a product family of five nonwoven geotextiles covering the product specification profiles 1 to 5 as per Table 2 have been sampled by the certification body and tested in an accredited testing laboratory. The product Grades 1 to 5 differ in their mass per unit area and their corresponding mechanical and hydraulic parameters. Grade 1 is the lightest and 5 the heaviest. The internal quality control data of the manufacturer over multiple years is known to the certification body. For the water permeability the certification scheme requires the manufacturer to declare only a minus tolerance on the declared value.

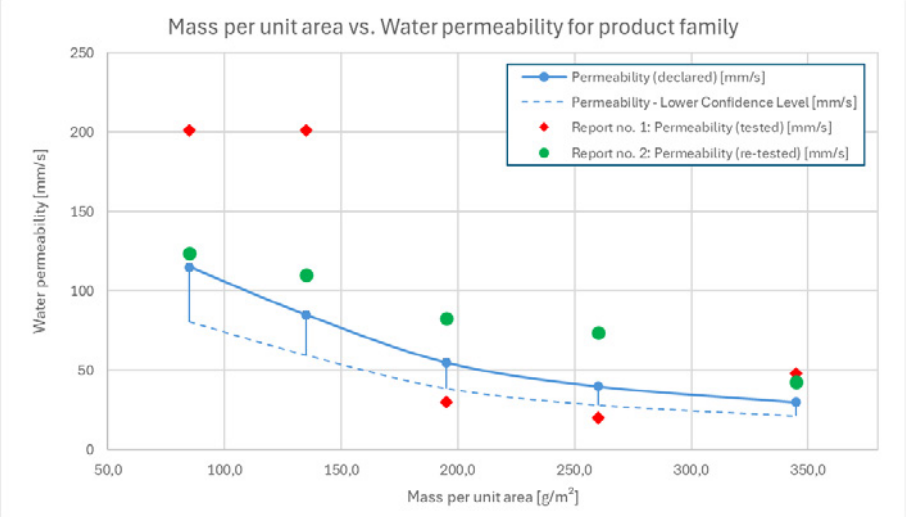


Fig. 2. Case 2 - Declared and tested water permeability

3.2.1 Initial assessment - Report no. 1

Grades 1, 2, 5: test results are within 1.0 x declared tolerances: compliant
Grades 3, 4: test results are outside of 1.5 x declared tolerances: failed

3.2.2 Complaint and discussion

When looking at the test results provided it was noted that Grades 1 and 2 had the same test results for each of the five specimens tested which was an indication for a data bias or technical issues of the testing equipment. Grades 3 and 4 were low as compared to recent quality control data of the manufacturer. This formed the basis for a complaint with the testing laboratory to check the test data and to re-test the water permeability of the samples. The result of the internal investigation by the testing laboratory revealed a defect in the test equipment.

3.2.3 Re-testing - Report no. 2

The water permeability for all five grades was re-tested.
Grades 1-5: test results are within 1.0 x declared tolerances: compliant

3.2.4 Final assessment

All five products were found to be compliant with the requirement of the certification scheme.

3.2.5 Findings

Based upon the discussion on these tests the laboratory has assessed the situation internally and found a defect piece of testing equipment that was replaced.

4 Lessons learned

4.1 Testing Laboratories

Despite the utmost diligence, errors occasionally occur. Handling complaints should be viewed positively, as they often reveal areas for improvement and uncover internal issues that might otherwise remain unnoticed. This is why ISO/IEC 17025, which sets the general requirements for the competence of testing and calibration laboratories, mandates accredited testing laboratories to maintain a documented process for receiving, evaluating, and resolving complaints.

ISO/IEC 17025 also outlines the requirements for managing nonconforming work. An example of this is when round robin test results show significant deviations from the robust average of other accredited laboratories, underscoring the importance of such testing to validate test results.

Additionally, it is advisable to conduct simple plausibility checks by experienced personnel, especially when testing product families, to ensure the validity of test results. It is acknowledged that there are limitations when testing individual products or when the technical characteristics of the products (expected values) are not known which is typically the case. In such cases, close communication with the certification body is crucial, as demonstrated in the presented examples.

4.2 Certification body

Just as testing laboratories must ensure the validity of their test results, certification bodies must ensure the validity of their certification decisions. The lessons learned by testing laboratories are largely applicable to certification bodies as well. According to ISO/IEC 17065, which sets requirements for bodies certifying products, processes, and services, certification bodies must maintain a documented process for receiving, evaluating, and making decisions on complaints and appeals.

However, while testing laboratories often only have limited information on the tested products, the certification body typically has a more comprehensive view within the given certification scheme. This broader perspective includes knowledge of the product performance from the manufacturer's internal quality control data, results of previous inspections and tests, and the declared performance of the products. This enables the certification body to perform more extensive plausibility checks on the test results.

This broader understanding is crucial, considering the significant consequences a negative certification decision, based on incorrect test results, can have for the certificate holder.

Recognizing all these aspects, the given certification scheme and its decision process, as outlined in chapter 2.4, have been amended to better address potentially incorrect test results:

- If the A-sample tested in Lab 1 is within 1.0 x the declared tolerances, the material is compliant.
- If the A-sample tested in Lab 1 is outside 1.0 x but still within 1.5 x the declared tolerances, the B-sample will be tested in a different laboratory (Lab 2).
- If the A-Sample tested in Lab 1 is outside 1.5 x the declared tolerances, the NorGeoSpec certification body (NCB) contacts the certificate holder to see whether he accepts the non-compliance or if he wants the A-sample to be re-tested in a different laboratory (Lab 2).
- If the certificate holder wants the A-sample to be re-tested in Lab 2 and the results are within 1.0 x declared tolerance the material is compliant. Note: In this case it can be assumed with a high level of certainty that the initial testing in Lab 1 was incorrect.
- If the A-sample tested in Lab 2 is outside 1.0 x declared tolerances the material is non-compliant

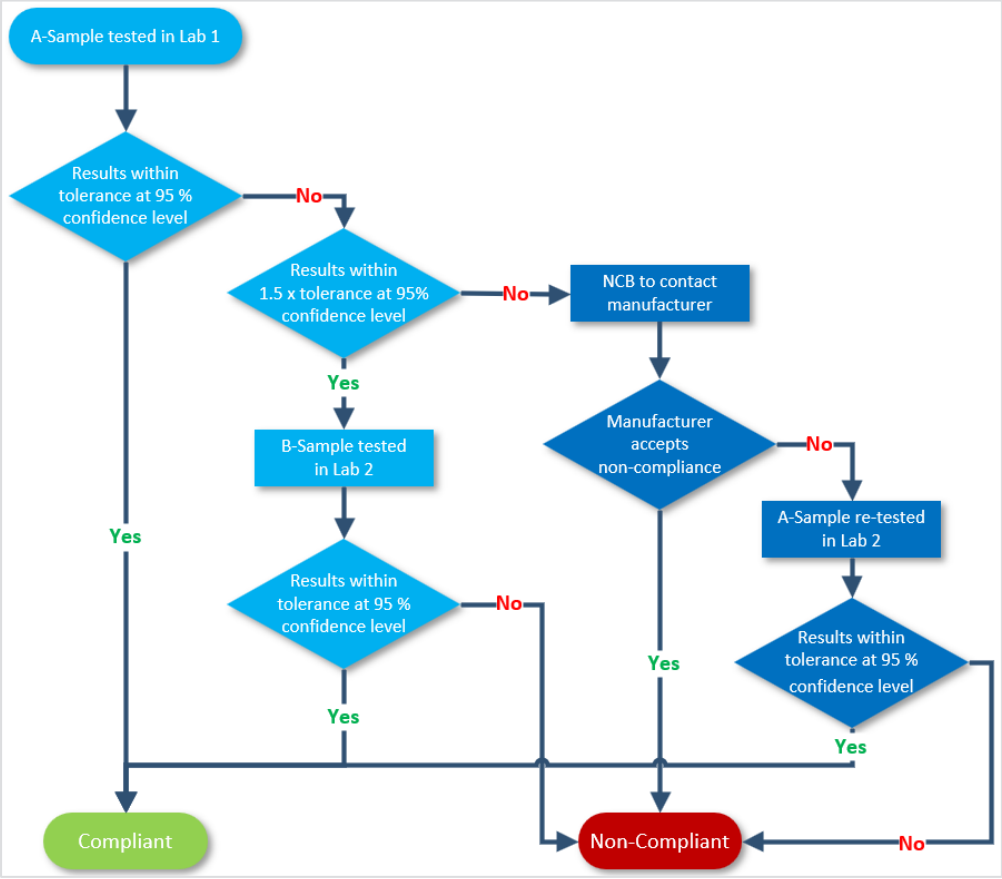


Fig. 3. Amended certification decision scheme with additions in dark blue

5 Conclusions

Plausibility checks on test results in testing laboratories as well as in certification bodies are an integral part of the corresponding normative requirements to ensure the validity of test results and of certification decisions. They significantly contribute to spotting inconsistent, questionable or incorrect test results.

It is worth noting that spotting incorrect test results can be difficult when only individual products are tested. However, in the examples presented product families of nonwoven geotextiles have been tested which only differ in the mass per unit area and therefore typically have a close correlation between the mass per unit area and the mechanical and hydraulic properties.

In the examples presented plausibility checks revealed inconsistent test results. Based on these findings, complaints by the certification body were received, evaluated and resolved by the testing laboratories leading to an improvement in performance of the testing laboratories with respect to training of personal as well as functional performance of testing equipment.

In both cases an open and transparent communication and prompt feedback in both directions has helped to quickly resolve these issues and to implement the necessary corrective actions to ensure the validity of test results and of the certification decision. For both, testing laboratories and certification bodies, such documented procedures are required to fulfil the normative requirements for accredited testing laboratories (ISO/IEC 17025) and certification bodies (ISO/IEC 17065).

The experiences with the two examples presented will be used for the upcoming revision of the decision rules of the programme owner as per Fig. 3. Using two different testing laboratories will significantly reduce the risk of products losing the certification due to incorrect testing.

The intention of this paper is not to shift the focus from product quality to the quality of testing and certification. In the examples presented, it was evident that the products initially failed due to incorrect test results rather than poor product quality. However, product quality issues still occur and are significantly more common than incorrect testing.

References

1. ISO/IEC 17065:2012 Conformity assessment - Requirements for bodies certifying products, processes and services
2. https://www.dakks.de/en/certification-bodies-for-products-processes-and-services.html, retrieved on 19.01.2025
3. ISO/IEC 17025:2017 General requirements for the competence of testing and calibration laboratories
4. NorGeoSpec 2012, Rev. 01, Issue: 14.12.2016, A Nordic system for the certification and specification of geosynthetics and geosynthetic-related products
5. EN ISO 12956:2020 Geotextiles and geotextile-related products - Determination of the characteristic opening size
6. EN ISO 11058:2019 Geotextiles and geotextile-related products - Determination of water permeability characteristics normal to the plane, without load

The influence of seating time on water flow of nonwoven geotextiles in permeability tests

Anna Markiewicz[1*], *Eugeniusz* Koda[1], *Ada* Skrońc[1] and *Przemysław* Soszyński[1]

[1]Warsaw University of Life Sciences - SGGW, Institute of Civil Engineering, 02-776 Nowoursynowska 159 St. Warsaw, Poland

Abstract. Determining the main hydraulic parameters of geotextiles is undoubtedly necessary for correctly selecting geotextiles in civil engineering constructions. Proper laboratory testing and subsequent determination of these parameters is important to ensure the effectiveness of the drainage system, or at least in avoiding the phenomenon of clogging. This paper presents the results of a study of the effect of seating time on the water flow of needle-punched nonwoven geotextiles. Seating time is a period during which the product is maintained under constant compressive stress before a measurement is made. The study results show that the water flow of geotextiles decreases with increasing seating time. It was confirmed that when a nonwoven geotextile sample is subjected to a given normal compressive stress, the water flow of the nonwoven geotextile does not immediately decrease to a final value. Moreover, the relationship between geotextiles' physical and hydraulic parameters and the seating time was shown.

Full paper to be published in:
https://www.e3s-conferences.org/articles/e3sconf/abs/2025/44/contents/contents.html

* Corresponding author: anna_markiewicz@sggw.edu.pl

Laboratory tests on stabilization of railway ballast with geogrid

Daniil Somov[1*], *Andrei* Petriaev[1]

[1]Emperor Alexander I St. Petersburg State Transport University, 9 Moskovsky pr, Saint Petersburg, 190031, Russia

Abstract. This article presents the results of an experimental research devoted to the study of the stability of the ballast prism of the railway track under the influence of dynamic loads. The aim of the work was to evaluate the effectiveness of two methods of stabilization: the technology of layer-by-layer compaction of ballast and reinforcement of ballast layer with geogrid. To conduct the research, a ballast prism model was created, on which dynamic tests were carried out to simulate the impact of a passing train. During the experiments, the ballast prism settlement was measured using each of the considered technologies, as well as in the control case without any additional measures. A detailed analysis of the data obtained is presented, including a comparative assessment of the magnitude and nature of settlement in the different test variants. The results demonstrate the effect of each technology on the deformation characteristics of the ballast prism and allow us to evaluate their effectiveness in reducing settlement and improving the overall stability of the railroad track. In particular, it is shown that the use of geogrid and layer-by-layer compaction leads to a significant reduction in vertical deformations compared to unreinforced ballast. The obtained conclusions are important for the optimization of structural solutions in the construction and reconstruction of railway tracks and can contribute to the improvement of their reliability and durability.

1 Literature review

Railway ballast, consisting of crushed stone, is an important element of a railway track. It provides stability, vertical and lateral support, distributes the load on the base and provides drainage. Increased stress on railway tracks due to increased freight and passenger traffic leads to wear and compaction of ballast, requiring frequent maintenance and increasing the need for new materials. The development of high-speed transportation also places increased demands on ballast, as it must provide stability and uniform load distribution to ensure safe and efficient traffic. According to [1], the dynamics of processes in the ballast layer is still insufficiently studied. This leads to significant and ever-increasing maintenance costs for railway tracks.

Lobo-Guerrero and Vallejo [2] found that ballast deformation occurs due to the complex interaction of several processes including settlement, particle redistribution, fracture and crushed stone wear. These processes, acting together, result in an overall deformation. Thakur

* Corresponding author: somovdaniil2000@gmail.com

[3] presented a description of a similar pre-maintenance ballast layer degradation at a site in New South Wales.

The mechanisms of ballast degradation as a function of load frequency are not well understood, nor is there a model that accounts for train speed and crushed stone particle degradation. This limits the ability to design track systems that can safely and economically support high-speed traffic. Addressing this problem requires studying ballast behavior at different frequencies and developing a more accurate cyclic compaction model that will allow engineers to more accurately predict ballast life cycle costs [3].

Raymond [4] investigated the effect of ballast reinforcement on its behavior under repeated loads by studying reinforced and unreinforced layers of granular material on different subgrade. It was found that mesh reinforcement reduced plastic settlement by 13-30%, especially on weak bases. Raymond also suggested that the use of geogrid on railroad track could increase the maintenance cycle from 3 months to 3 years. However, it should be kept in mind that the experiment was conducted on a reduced scale, using fine crushed stone and relatively large geogrid, which may have affected the results, although the overall conclusions are consistent with other studies.

Research conducted at the University of Illinois [5] has shown that geogrids can be effective for ballast reinforcement, but their effectiveness depends on the condition of the ballast. Triaxial tests using different types of geogrids showed that the bond between the geogrid and the ballast decreases when the crushed stone is degraded.

The deterioration of railway ballast due to cyclic loads results in the need for periodic replacement. Recycled ballast is a more economical alternative, but its significant settlement and deformation limit its use. This article [6] proposes a solution to this problem by stabilizing recycled ballast with geogrid. Laboratory tests with cyclic loading have shown that reinforcement improves the performance of recycled ballast, making it suitable for use in railway construction.

In this research [7], a full-scale section of railroad track was constructed to compare reinforced and unreinforced ballast. The geogrid placed at a depth of 7 inches under the sleepers showed significant improvements: settlement was reduced to 1 inch at some locations under the sleepers, and ballast contamination was reduced by 30% under the sleepers and 20% at the subgrade level. This demonstrates the high effectiveness of geogrid for ballast reinforcement. However, for optimum utilization of geogrid, it is necessary to determine its parameters: mesh size, geometry and number of layers. This article [8] studies the effect of the number of layers and mesh size of geogrid on ballast settlement using laboratory dynamic tests, which will help to determine the optimal characteristics for practical application.

The accuracy of laboratory ballast tests depends on adequate modeling of loads and lateral restraint. This research [9] developed and validated a methodology to ensure that laboratory and field conditions are appropriate. It was shown that reducing the lateral restraint increases permanent deformation and failure of the ballast. The results obtained allow more accurate prediction of the long-term behavior of ballast and planning of ballast maintenance activities.

In the study [10], a program of die tests of geomaterial-reinforced ballast was developed. Conducting these tests is necessary due to the lack of reliable data to evaluate the effect of geomaterials on the deformations of stabilized railway ballast. The main purpose of these tests was to study and evaluate the effect of different types of geomaterials on the deformability of crushed stone depending on the method of reinforcement and the magnitude of service loads.

Geogrid has been shown in [11] to be an effective solution for reducing lateral displacement of ballast subjected to cyclic loads. The tests proved that geogrid can effectively reduce lateral displacement, reduce settlement and minimize ballast particle failure.

Geogrid reinforcement of the sub-ballast layer provides higher shear strength compared to the use of geomembrane. Geogrid significantly increases the shear strength at the sub-ballast boundary compared to geomembrane. This is due to the mechanical interlocking of

the ballast particles in the cells of the geogrid, which improves load distribution and reduces lateral deformation. Geomembrane, being smooth and impermeable, does not provide this meshing and can even reduce friction between layers [12].

Fischer [13] conducted a long-term field study that investigated the effect of different types of geosynthetic reinforcement on the behavior of railway ballast. Five different types of geogrids were observed for more than eleven years on a busy main line in Hungary. The test results presented in the paper included a mathematical and statistical analysis to compare reinforced and unreinforced sections. Based on the analysis, differences in the behavior and deterioration of the railway track were identified when different types of geosynthetics were used. The work of [14] emphasizes the results of field studies that helped to quantify the performance of geosynthetic reinforcement of railway ballast. Experiments conducted using calibrated loading showed that geosynthetics improve track stability immediately after repair and this stability is maintained over time.

2 Experimental part

2.1 Materials

The composition of the model for full-scale tests of crushed stone ballast under cyclic loading is presented in Table 1. Basalt with nominal grain size from 22.4 to 63 mm with an average grain density of at least 2.4 g/cm^3, obtained by crushing dense rocks with subsequent sieving of crushing products, was used as ballast material.

Table 1. Composition of the model for testing.

Mesh size of square sieve, mm	Partial residue, % by mass
63	–
50	30
45	25
40	20
30	13
25	7
20	3
10	2
5	–



Fig. 1. Geogrid

Geosynthetic material is represented by geogrid (Figure 1), which consists of interconnected elements forming cells in the form of triangles and hexagons.

2.2 Laboratory equipment

Laboratory tests to optimize the ballast prism parameters are performed on an Amsler HB 250 testing machine (pulsator) (Figure 2). The load on the half ballast prism is applied through a reinforced concrete die representing a half sleeper. The dimensions of the metal box are 2,7x1x0,5 m.



Fig. 2. General view of the model on the test rig.

2.3 Test methodology

The schematic for the test is shown in Figure 3.

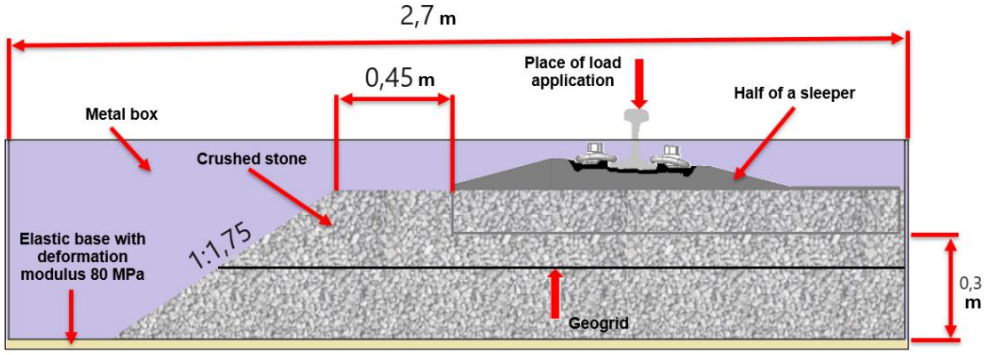


Fig. 3. Schematic of bench tests.

Before backfilling the crushed stone into the metal box, it was necessary to lay an elastic base 0,01 m thick with a deformation modulus of 80 MPa. To exclude local deformations, a 0,01 m thick sheet of plywood was laid on the elastic layer.

Crushed stone from the prepared grain composition had to be washed in order to remove dusty particles from the surface.

Next, the crushed stone of the prepared grain composition was laid.

A cyclic load must be applied to the model, which will give stresses under the die equal to the stresses under the sleeper from the train load. The area of the die is 0,405 m^2, hence the concentrated force should be 50 kN.

The technology of layer-by-layer compaction is that the crushed stone is compacted layer by layer every 0,1 m (Figure 4). Each layer is compacted by applying a dynamic load equal to 50 kN and a frequency of 8 Hz for 100 000 cycles. In case the thickness was less than 10 cm, more material should be poured on the compacted layer and then compacted again for 100 000 cycles with the load and frequency specified above. The backfilling is carried out in steps, which is necessary for further formation of the required slope gradient of the ballast slope. A reinforced concrete die is placed on the compacted crushed stone at a distance of 0,3 m below the sleeper in accordance with the scheme shown in Figure 3. The load is applied uniformly distributed over the surface of the stamp. The number of loading cycles is 2 000 000. During the tests, the value of vertical settlement is recorded.

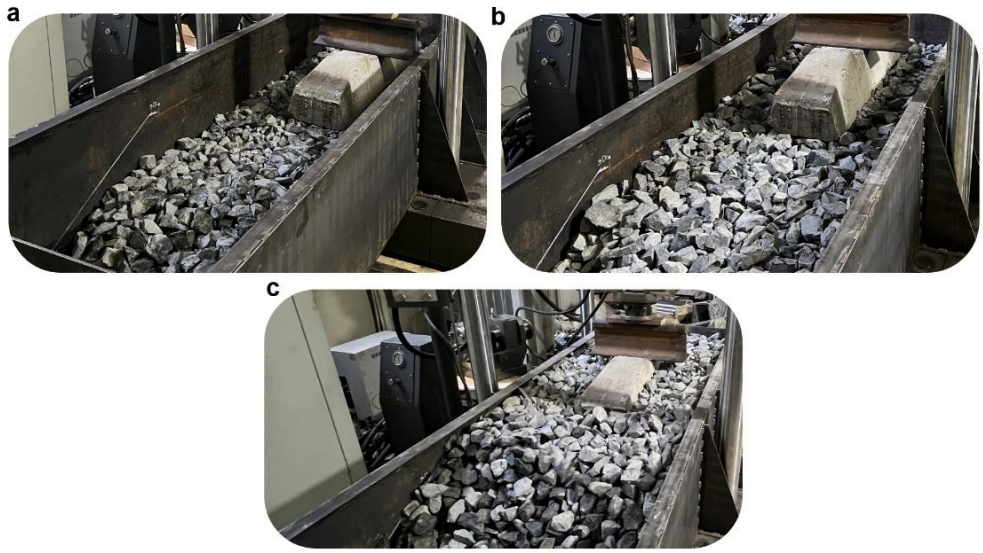


Fig. 4. a) First layer compaction; b) Second layer compaction; c) Final model.

The technology of layer-by-layer compaction with geogrid reinforcement of the ballast prism is similar to the previous technology. Two layers of crushed stone, each equal to 0,1 m, are compacted, followed by the placement of geogrid (Figure 5). The values of dynamic load, frequency and number of cycles remain unchanged.

To compare with the layer-by-layer compaction techniques, a test with a uniformly placed 0,3 m layer of ballast under the sleeper without prior layer-by-layer compaction was also performed.



Fig. 5. a) Compaction of the first layer; b) Compaction of the second layer; c) Geogrid placement; d) Final model.

3 Test results

The results of accumulation of residual strains of the die during cyclic loading during the model tests are shown in Figure 6.

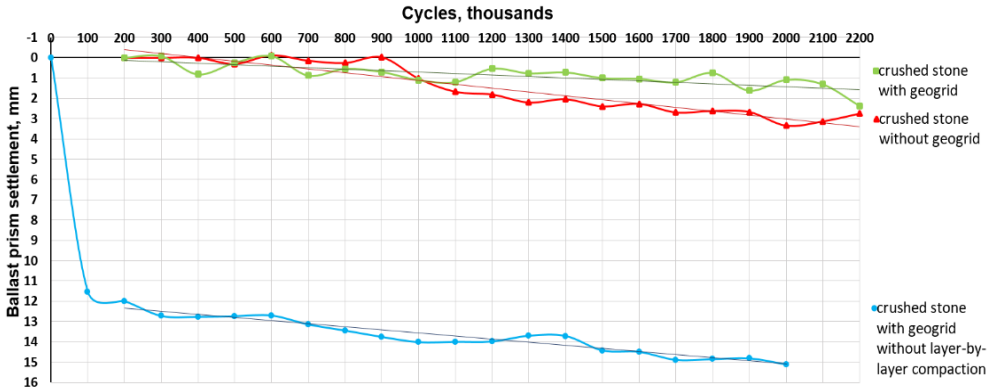


Fig. 6. Graph of ballast prism settlement intensity as a function of the number of load cycles with linear approximation of the data.

The graph illustrates the intensity of railway ballast settlement as a function of the number of load cycles for several technologies.

The ballast stabilization method with no layer-by-layer compaction showed the highest settlement over time. A sharp jump in settlement values in the first 200 000 cycles due to the lack of pre-compaction and further stabilization of settlement under cyclic loading due to the work of the reinforcing element can be seen. The settlement values are approximated by a straight line showing an approximately linear increase in settlement.

The technology of layer-by-layer compaction ballast without geogrid showed values of total settlement many times less than the previous method. However, the amplitude of the

values is more pronounced than for ballast with geogrid, thus increasing the intensity of settlement growth.

The technology of layer-by-layer compaction with the introduction of geogrid into the ballast prism proved to be the best. The intensity of settlement is significantly less than in the case without geogrid, as well as the amplitude of oscillations, which is significantly smaller. The linear approximation shows a smaller slope, indicating a lower intensity of precipitation.

For all three technologies, linear approximations are presented in Figure 6, which simplifies the visualization of the settlement intensity and also allows the calculation of the settlement intensity reduction coefficient (1).

The settlement intensity reduction coefficient:

$$K_g(s) = \frac{V(S)}{V_g(S)}, \qquad (1)$$

where $V(s)$ – is the intensity of settlement without geosynthetic material, mm/thousand cycles; $V_g(s)$ – is the intensity of settlement with geosynthetic material, mm/thousand cycles.

The calculated coefficient for each stabilization method is shown in Figure 7.

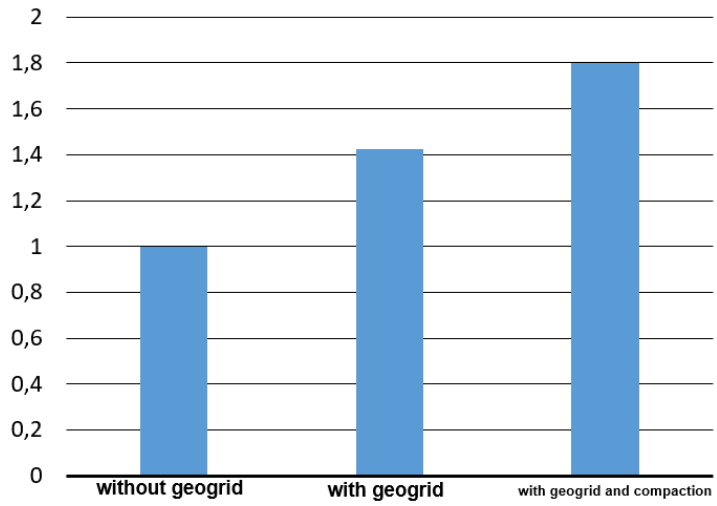


Fig. 7. Calculated the settlement intensity reduction coefficient

The results obtained prove the effectiveness of using geogrid to reduce the growth of ballast settlement intensity. Pre-compaction of the ballast with geogrid further increases the effectiveness of the reinforcement. Pre-compaction is integral to achieving low settlement values and more than doubles the effectiveness of geogrid. Linear approximations provide an estimate of the intensity of settlement for each method, confirming the advantage of using geogrid and pre-compaction - the intensity reduction factor increases with ballast prism stabilization methods. The amplitude of the curves indicates the non-uniformity of stress distribution in the ballast, which is more pronounced in the absence of geogrid.

Conclusions

Based on the presented text, the following conclusions can be formulated:

- The experimental study confirmed the effectiveness of both layer-by-layer ballast compaction and geogrid reinforcement to improve the stability of the railway track under dynamic loads.
- The combined application of these two methods provides the best results in reducing the intensity of ballast settlement accumulation.

- Geogrid significantly reduces both the intensity of settlement accumulation and its non-uniformity (amplitude of settlement fluctuations over time).
- Pre-compaction of the ballast further enhances the effectiveness of the geogrid and is a necessary part of achieving the lowest settlement values.
- The analysis of settlement intensity (settlement intensity reduction coefficient) confirms the advantages of using geogrid and pre-compaction. With the introduction of geogrid in the design of ballast prism the value of the coefficient is 1,4, with the use of layer-by-layer compaction and geogrid – 1,8.
- The obtained results allow to optimize design solutions during construction and reconstruction of railway tracks.
- The use of geogrid and layer-by-layer compaction is recommended to increase the reliability and durability of the track structure.

Future research

Further researches will be directed on specification of optimum parameters of layer-by-layer compaction and selection of geogrid type depending on specific conditions of railway track operation.

References

1. Popp, K., Knothe, K., & Popper, C. System dynamics and long-term behavior of railway vehicles, track and subgrade. In Report on the DFG Priority Program in Germany and Subsequent Research. Vehicle System Dynamics, 43(6-7), 485–538, 2005.
2. Lobo-Guerrero, S., Vallejo, L.E. Discrete Element Method Analysis of Railtrack Ballast Degradation during Cyclic Loading. Granular Matter 8, 195–204 (2006). https://doi.org/10.1007/s10035-006-0006-2
3. Thakur, P. K. Cyclic densification of ballast and associated deformation and degradation. Ph.D. Thesis. University of Wollongong, 2011.
4. Raymond, G. P. (2001). Reinforced ballast behavior subjected to repeated loading. Geotextiles and Geomembranes, 20(1), 39–61. https://doi.org/10.1016/S0266-1144(01)00024-3
5. Qian, Yu; Mishra, Debakanta; Tutumluer, Erol; and Kazmee, Hasan A.. (2015). "Characterize Behavior of Geogrid Reinforced Ballast at Different Levels of Degradation Through Triaxial Shear Strength Test and Discrete Element Modeling". Geotextiles and Geomembranes, 43(5), 393-402. https://doi.org/10.1016/j.geotexmem.2015.04.012
6. Indraratna, B., Salim, W., & Christie, D. Improvement of recycled ballast using geosynthetics. Rail international, 1177-1182, 2002.
7. Jowkar M. Performance of geogrid reinforced ballast under dynamic loading. Published Online First: 31 December 2011.
8. Abrashitov, A.; Sidrakov, A. Laboratory study of ballast material reinforced by flat geogrid under the dynamic load. MATEC Web Conf. 2019, 265, 01006, https://doi.org/10.1051/matecconf/201926501006.
9. Jideani, T C U, & Grabe, P J. (2019). The development of suitable cyclic loading and boundary conditions for ballast box tests. Journal of the South African Institution of Civil Engineering, 61(4), 59-72. https://doi.org/10.17159/2309-8775/2019/v61n4a6
10. Petriaev, A., Ganchits, V., Chetina, M., Kozlov, I., Petrenko, S. (2020). Stamp Test of Railway Ballast, Stabilized by Geogrids. In: Petriaev, A., Konon, A. (eds) Transportation Soil Engineering in Cold Regions, Volume 2. Lecture Notes in Civil Engineering, vol 50. Springer, Singapore. https://doi.org/10.1007/978-981-15-0454-9_6

11. Indraratna, B. & Hussaini, Syed & Vinod, J S. (2013). The lateral displacement response of geogrid-reinforced ballast under cyclic loading. Geotextiles and Geomembranes. 39. 20–29. https://doi.org/10.1016/j.geotexmem.2013.07.007
12. Biabani, M. & Indraratna, B. (2015). An evaluation of the interface behaviour of rail subballast stabilised with geogrids and geomembranes. Geotextiles and Geomembranes. 43. https://doi.org/10.1016/j.geotexmem.2015.04.002
13. Fischer, S. (2022). Geogrid reinforcement of ballasted railway superstructure for stabilization of the railway track geometry–A case study. Geotextiles and Geomembranes,50(5),1036–1051. https://doi.org/10.1016/j.geotexmem.2022.05.005.
14. Petriaev, Andrei. (2017). Stress Response Analyses of Ballasted Rail Tracks, Reinforced by Geosynthetics. Procedia Engineering. 189. 660-665. https://doi.org/10.1016/j.proeng.2017.05.105

Dry Abrasion Evaluation of Geotextiles with Different Test Standards

Gustavo Fierro[1*]

[1]R&D Corporate Manager at TDM Group, R&D Laboratory, Marqués de la Bula 339, Chorrillos - Lima, Perú

Abstract. Abrasion tests have been developed primarily for geotextiles and their main use has been with nonwoven geotextiles. However, very little or no information exists for woven geotextiles, even worse if they are made of polypropylene or polyester, polymers commonly used in their manufacture. In our R&D Laboratory facilities, this property has been investigated since its application is important to determine the durability of structures made with these Geosynthetics. Abrasion in geotextiles has been questioned due to its poor practical applicability and to which physical model the principle of the test refers. Although it was initially oriented to railways or pavements, currently the need is much greater. Nowadays woven geotextiles are used to confine soil as bags or as geotextile tubes, also in containment structures with the face exposed to wind and fine particles, in each case they generate loss of mass and finally reduction of resistance. This paper presents tests using ASTM D4886 and ISO 13427 standards and compares abrasion on nonwoven and woven geotextiles to understand the degree of resistance reduction. The results are compared over long laboratory periods to even be able to make some kind of approximation of this phenomenon for long site periods of time. The results are evaluated in search of an analytical expression that allows us to know the degree of resistance impairment and whether this can be associated with a real physical effect that can serve as a basis for a future methodology.

Full paper to be published in:
https://www.e3s-conferences.org/articles/e3sconf/abs/2025/44/contents/contents.html

* Corresponding author: gfierro@grupotdm.com

Considering the deformation of nonwovens to follow the behaviour on site

Henning Ehrenberg[1*] *and Jan* Retzlaff[2]

[1]Naue GmbH & Co. KG, 32339 Espelkamp, Germany
[2]GEOscope GmbH, 99427 Weimar, Germany

Abstract. An evaluation of the German GRC (Geotextile Robustness Class) system was done with large-scale test sections to model road constructions equipped with nonwovens showing different results in the performance according to their stress-strain behaviour. The GRC system itself was generally confirmed, but results after deconstruction show sometimes more and sometimes less damages under the same subgrade material and installation energy. Materials belonging to the same GRC have shown different performance on site depending on the stiffness of the original products. In following lab tests according to the established standards for testing the tensile strength (EN ISO 10319) and the puncture resistance (EN ISO 12236), SKZ (Süddeutsches Kunststoff Zentrum) recorded nearly the same deformation for all products. Because this did not explain the site observations, tests have been carried out with varying the technical testing conditions at several labs. By that, significant differences in the stiffness of the materials became visible during the test. Similar observations on sites have been made also on other test areas for hydraulic applications. Laboratory tests under the actual technical boundary conditions, do not show the typical variation in the stress-strain behaviour of geotextiles according to their behaviour shown in unbound layers of earth structures. These observations are done for tensile strength tests (EN ISO 10319) as well as for puncture strength tests (EN ISO 12236). The following article attempts to explain, the reasons for different performances between the actual laboratory tests and the materials behaviour on the construction site. It provides further details in modified test approaches in the laboratory and contains suggestions for amending the standards for tensile strength tests (EN ISO 10319) and for puncture resistance tests (EN ISO 12236) of nonwovens.

1 Introduction

In November 2020, test fields were set up in northern Germany near Wittenburg to check whether the rules for the GRC (GRK) of road construction nonwovens according to the M Geok E [1] regulations applicable in Germany are up to date [2, 3]. Different types of road construction nonwovens were tested for this purpose.

* Corresponding author: hehrenberg@naue.com

1. Needle punched and heavily thermally treated nonwovens,
2. needle punched and thermally treated nonwovens and
3. needle punched nonwovens

of the same classes (GRC 3, 4, 5 and as an additional test a potential GRC 6) were installed in the test fields, driven over in the installed state, excavated and then analysed and evaluated (Fig. 1 – 4).



Fig. 1 Overview of test section



Fig. 2. Overview of test section and load passes



Fig. 3 Deformation / damaging behaviour of a thermally untreated nonwoven after excavation



Fig. 4 Deformation / damaging behaviour of a thermally treated nonwoven after excavation.

The analyses generally confirmed the GRC (requests per class a minimum mass per unit area and a minimum puncture force). However, they did show different deformation behaviour under stress and, along with this deformation behaviour, different damage in the nonwovens. The thinner a nonwoven (heavily thermally treated, thermally treated, not thermally treated) with the same GRC (same mass per unit area, same strength) was, the more pronounced the tendency to damage / holes in the nonwovens was.

As these differences could not be explained with the 'standard' properties from tensile tests and puncture tests according to the standard (EN ISO 10319 and EN ISO 12236) [4, 5, 6], initial tests were already carried out by Zanzinger [2] to explain these differences. This was continued by the authors of this paper and is explained below.

2 Tensile strength and elongation following EN ISO 10319:2015 and EN ISO 10319:2024

The tests to describe the products used in the test fields in northern Germany were originally carried out in accordance with EN ISO 10319:2015. According to this standard, the elongation up to a preload of 1 % of the expected tensile strength is not included in the determination of the elongation at maximum tensile force. This means that for very

elongation-resistant products, a small proportion of the elongation is eliminated from the test result; for elongation-soft products, a significantly larger proportion of the elongation may be eliminated from the test result and will not be considered during the evaluation.

A revision of EN ISO 10319 was published in October 2024. According to this standard, elongation up to a preload of 1 % of the expected tensile strength is determined separately and, depending on the interpretation of the standard, may or may not be included in the determination of elongation at maximum tensile force. For nonwovens, it is also included that the tests should be carried out without a preload of 1 % of the expected maximum tensile force. Further clarification for the interpretation of the wording of this revision is needed.

2.1 Elongation measurement by EN ISO 10319 with and without 1 % preload

The following two chapters (2.1.1 and 2.1.2) show comparisons of new products, not exhumed, products with different production technologies, 2.1.1 needle punched and thermally treated and 2.1.2 needle punched.

In both cases (2.1.1 and 2.1.2) products, with roughly 170 g/m² and 300 g/m² and produced needle punched and thermally treated as well as needle punched only where tested.

2.1.1 The tests are done for all products with 1% preload as given in the standard EN ISO 10319:2015 and without preload. Elongation with needle punched and thermally treated products

Two examples of EN ISO 10319 of needle punched and thermally treated products with similar ultimate strength are shown below.

EN ISO 10319, roughly 170 g/m², 1.1 mm thickness, elongation difference with 1 % preload and without preload = 1.9 % (as average of 5 single tests each), Fig. 5.

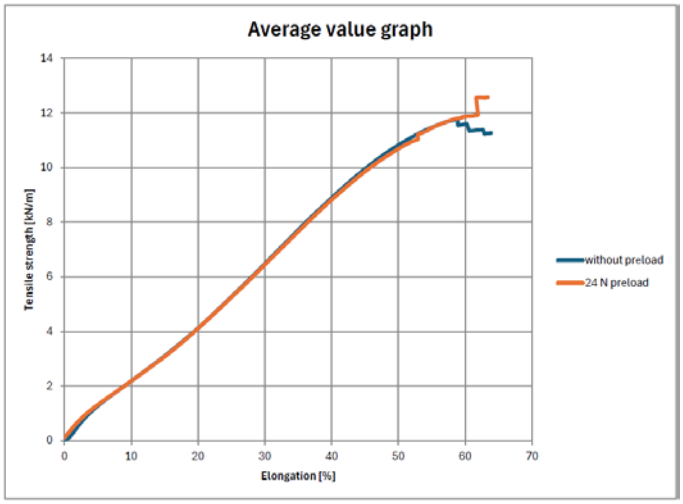


Fig. 5. Comparison of tensile strength / elongation curve of needle punched and thermally treated products with similar ultimate strength with roughly 170 g/m².

EN ISO 10319, roughly 300 g/m², 1.5 mm thickness, elongation difference with 1 % preload and without preload = 1.2 % (as average of 5 single tests each), Fig 6.

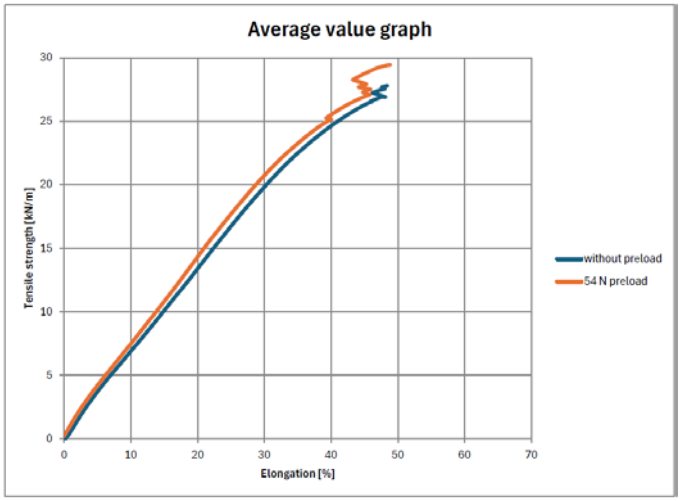


Fig. 6. Comparison of tensile strength / elongation curve of needle punched and thermally treated products with similar ultimate strength with roughly 300 g/m².

2.1.2 Elongation with needle punched products

Below are two examples of EN ISO 10319 of needle punched products with similar ultimate strength.

EN ISO 10319, roughly 170 g/m², 3.0 mm thickness, elongation difference with 1 % preload and without preload = 12.5 % (as average of 5 single tests each), Fig. 7.

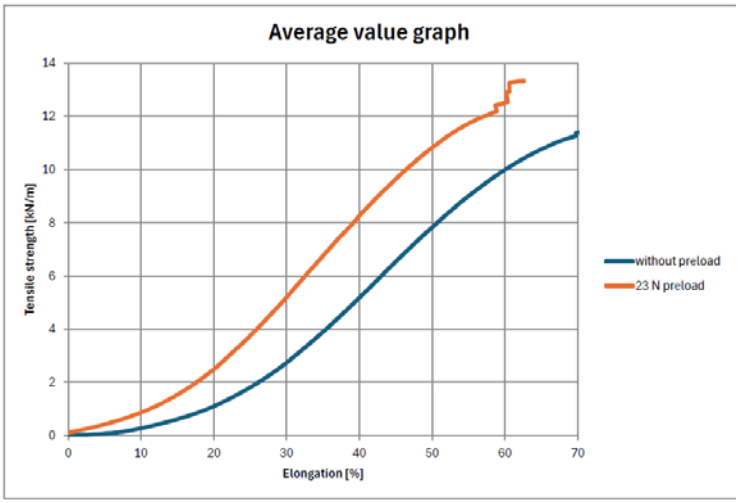


Fig. 7. Comparison of tensile strength / elongation curve of needle punched products with similar ultimate strength with roughly 170 g/m².

EN ISO 10319, roughly 300 g/m², 3.0 mm thickness, elongation difference with 1 % preload and without preload = 11.7 % (as average of 5 single tests each), Fig. 8.

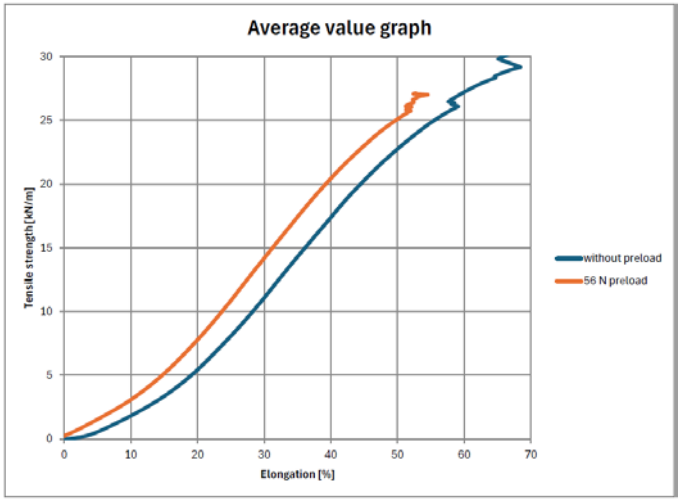


Fig. 8. Comparison of tensile strength / elongation curve of needle punched and thermally treated products with similar ultimate strength with roughly 300 g/m².

2.2 Comparison of results following 2.1.1 and 2.1.2

The results from 2.1.1 show that stiff (in terms of elongation) products, whether tested with or without 1% preload, show very comparable maximum elongations in the laboratory tests. In contrast, the results of 2.1.2 with weak (in terms of elongation) products show very different maximum elongations in the test with or without 1% preload.
The differences in weak products tend to decrease with higher mass.

Table 1. Elongation comparison with and without preload

Mass per unit area	Thickness	Elongation behavior	Elongation with preload	Elongation without preload	difference
170 g/m²	3.0 mm	weak	60.3 %	72.8 %	≈ 13 %
170 g/m²	1.1 mm	stiff	58.5 %	60.4 %	≈ 2 %
300 g/m²	3.0 mm	weak	54.4 %	66.1 %	≈ 12 %
300 g/m²	1.5 mm	stiff	47.5 %	48.7 %	≈ 1 %

2.3 Impact on energy index of results following 2.1 and 2.2

Sometimes a calculation of the energy index is required based on the measured tensile strength and elongation. According to the above information and the 2024 revision of EN ISO 10319, higher values of elongation will be determined in the future for the same products than before, as the measured tensile strength increases slightly (+1 %) and the measured elongation increases slightly (highly thermally treated, thermally treated) or more (not thermally treated) than before. This is positive, as it reflects the material behaviour on the side, as shown in [2, 3].

3 Puncture force and push-through displacement following EN ISO 12236:2006

The tests to describe the products used on the test fields in northern Germany were originally carried out in accordance with EN ISO 12236:2006. According to this standard, the push-through displacement up to a preload of 20 N is not included in the determination of the maximum push-through displacement. Here, too, this means that a small portion of the push-through displacement is eliminated from the result for very elongation-resistant products; for elongation-soft products, a significantly larger part of the push-through displacement can be eliminated from the result.

An upcoming revision of EN ISO 12236 in 2025 may take this into account and specify a preload of '0'N for tests on nonwovens.

3.1 Push-through displacement measurement by EN ISO 12236 with and without 20 N preload

The following two chapters (3.1.1 and 3.1.2) show comparisons of new products, not exhumed, with different production technologies, 3.1.1 needle punched and thermally treated and 3.1.2 needle punched.
In both cases (3.1.1 and 3.1.2) products with roughly 170 g/m² and 300 g/m² and produced needle punched and thermally treated as well as needle punched only where tested.
The tests are done for all products with 20 N preload as given in the standard EN ISO 12236:2006 and without preload.

3.1.1 Push-through displacement with needle punched and thermally treated products

The following shows 2 examples of EN ISO 12236 of needle punched and thermally treated products with similar ultimate strength.

EN ISO 12236, roughly 170 g/m², 1.1 mm Thickness, Push through displacement difference with 20 N preload and without preload = 6.6 mm (as average of 5 single tests each), Fig. 9

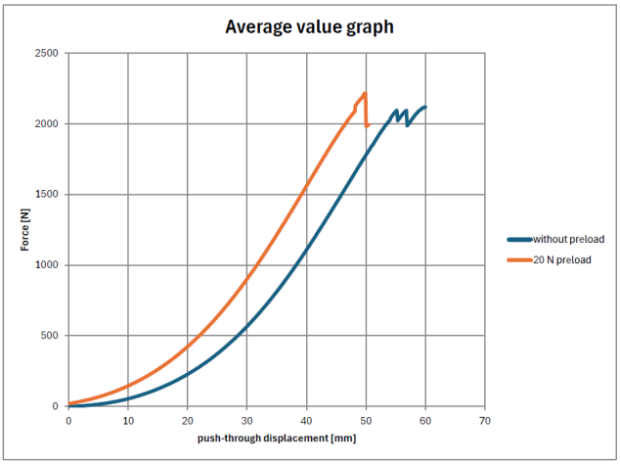


Fig. 9. Comparison of Force / push-through displacement curve of needle punched and thermally treated products with similar ultimate strength with roughly 170 g/m²

EN ISO 12236, roughly 300 g/m², 1.5 mm Thickness, Push through displacement difference with 20 N preload and without preload = 5.2 mm (as average of 5 single tests each), Fig. 10

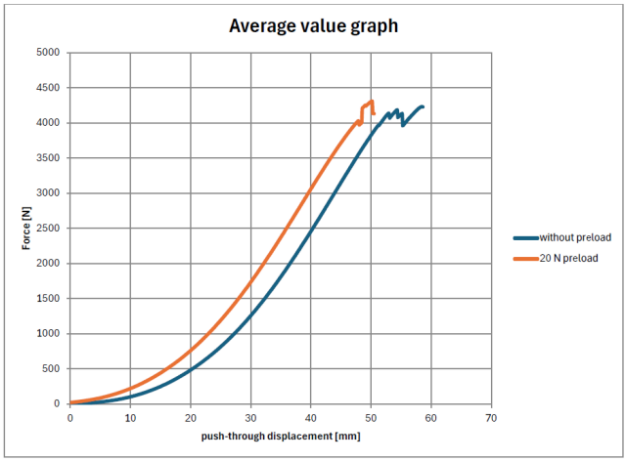


Fig. 10. Comparison of Force / push-through displacement curve of needle punched and thermally treated products with similar ultimate strength with roughly 300 g/m²

3.1.2 Push through displacement with needle punched products

Two examples of EN ISO 12236 of needle punched products with similar ultimate strength are shown below.

EN ISO 12236, roughly 170 g/m², 3.0 mm thickness, Push-through displacement difference with 20 N preload and without preload = 20.6 mm (as average of 5 single tests each), Fig. 11.

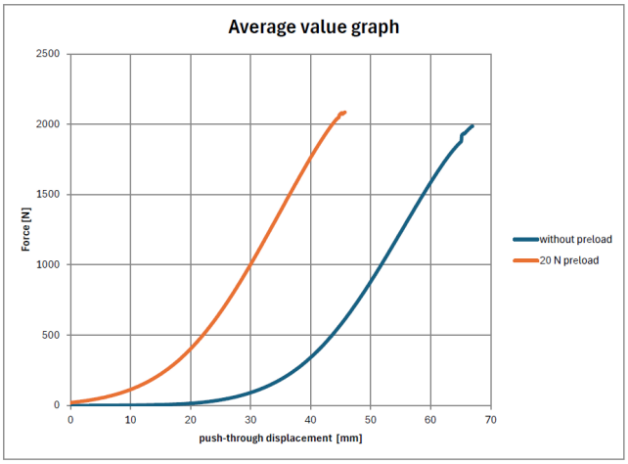


Fig. 11. Comparison of force / push-through displacement curve of needle punched products with similar ultimate strength with roughly 170 g/m².

EN ISO 12236, roughly 300 g/m², 3.0 mm thickness, Push-through displacement difference with 20 N preload and without preload = 11.3 mm (as average of 5 single tests each), Fig. 12.

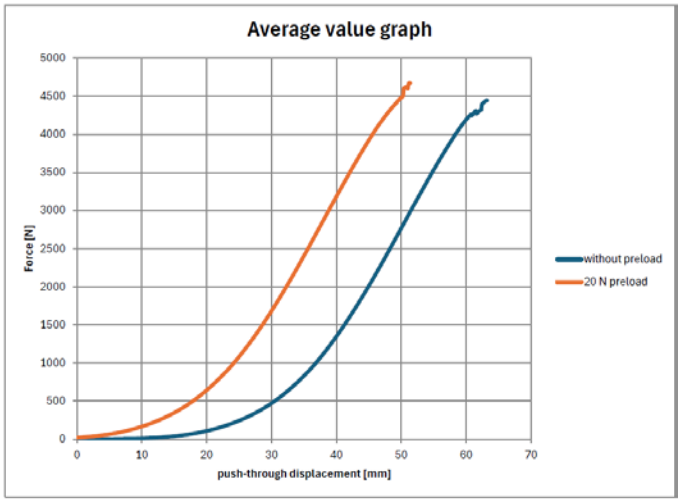


Fig. 12. Comparison of force / push-through displacement curve of needle punched products with similar ultimate strength with roughly 300 g/m².

3.2 Comparison of results following 3.1.1 and 3.1.2

The results from 3.1.1 show that stiff (in terms of elongation) products, whether tested with or without 20 N preload, show very comparable maximum elongations in the laboratory tests. In contrast, the results of 3.1.2 with weak (in terms of elongation) products show very different maximum elongations in the test with or without 20 N preload. The differences in weak products tend to decrease with higher mass.

Table 2. Push-through displacement comparison with and without preload

Mass per unit area	Thickness	Elongation behavior	Displace-ment with preload	Displace-ment without preload	difference
170 g/m²	3.0 mm	weak	45.8 mm	66.4 mm	≈ 21 mm
170 g/m²	1.1 mm	stiff	48.8 mm	55.4 mm	≈ 7 mm
300 g/m²	3.0 mm	weak	50.4 mm	61.7 mm	≈ 11 mm
300 g/m²	1.5 mm	stiff	49.2 mm	54.4 mm	≈ 5 mm

4 Summary

In order to be able to interpretate and evaluate field tests and their results, it is necessary to examine the products in laboratory tests in such a way that they correctly reflect the performance. The laboratory tests shown in this paper were carried out to explain the results of the field tests by SKZ with products of different manufacturing techniques, but of the same robustness classes (see Fig. 1-4).

The correct evaluation of the performance of nonwovens requires a test procedure that, in deviation from the previous standards (as of 2023/2024), determines the stretching behaviour without preload. Depending on the different manufacturing technique, the actual performance of nonwovens may be slightly or significantly higher than the results that exactly meet the current standards (2023/2024).

This paper does not intend to say that more field experiments need to be conducted, but it does say that when field experiments are conducted and product differences occur, laboratory experiments may need to be conducted to determine the causes of the differences and to draw the right conclusions.

These relationships are presented clearly (see Fig. 5-12) in this article and help to understand and to explain the differences in performance of products tested in the test fields in northern Germany.

References

1. M Geok E, Merkblatt über die Anwendung von Geokunststoffen im Erdbau des Straßenbaus, Forschungsgesellschaft für Straßen- und Verkehrswesen e. V., Cologne, 2016
2. H. Zanzinger, Überprüfung der Geotextilrobustheitsklassen hinsichtlich neuer Produktentwicklungen, FE 05.0199/2017/AGB, SKZ Würzburg, Germany, 2022
3. H. Zanzinger, J. Retzlaff, R. Kroh, Review of the German geotextile robustness classes (GRK) for separation layers with nonwoven geotextiles using large-scale field tests, in Proceedings of the 12th International Conference on Geosynthetics – 12 ICG Roma, September 17-21 (2023)
4. EN ISO 10319, Geosynthetics - Wide-width tensile test, Third Edition, 2015-05
5. EN ISO 10319, Geosynthetics - Wide-width tensile test, Fourth Edition, 2024-10
6. EN ISO 12236, Geosynthetics - Static puncture test (CBR test), Second Edition, 2006-09

Studies on the sound generated during the tensile test on nonwoven geotextiles

Francesco Niccolai[1*],

[1]ECOFIBRE s.r.l., Montale (PT), Italy

Abstract. The wide-width tensile test according to EN ISO 10319 standard is the main test to characterize the tensile strength of a nonwoven geotextile, which depends on the tenacity of the individual fibres it is made of, and also on the friction forces between the fibres bonded by needle punching treatment. The present study aims to analyze the possibility of determining the contribution to the wide-width tensile strength of individual fibres, recording and recognizing the noise that each individual fibre emits during breaking. By comparing the contribution to the strength of individual fibres and the tensile strength of the nonwoven geotextile, data on the friction forces between the fibres bonded by needle punching treatment can be obtained.

1 Introduction

Nonwovens geotextiles are made of mechanically needle-punched fibres and the tensile strength comes from the fibre entanglements. The mechanical breaking process of nonwovens is characterized by the procedures of the tensile test according to EN ISO 10319 (2024), [1], subsequently indicated only as wide-width tensile test, and this test measures only the values of strength and elongation and cannot provide information on the nature of the failure of the nonwoven itself. The comparison between the theoretical resistance of a film and a nonwoven made of the same material and the same mass per unit area, suggests that the breaking process, of film and nonwoven, is very different and greatly influenced by the intrinsic inhomogeneity of the nonwoven respect to a film. It is assumed that - during the breaking of the nonwoven - some fibres break while others slide between them generating force due to friction, but to date there is no method to characterize this phenomenon. The present study aims to find a method to identify the fibres that break during the tensile test, compared to those that slide, in order to integrate and expand the knowledge of the phenomenon of nonwovens breakage. In particular, taking inspiration from the standard ASTM D1577 (2018) Standard Test Methods for Linear Density of Textile Fibres [2], that give a method to determine the fibres yarn count measuring vibrations and from the techniques used to monitor and predict mechanical failures of machines analyzing their sounds, as example “Early detection and prediction of mechanical malfunction of machinery by sound analysis”, [3], it is supposed to be possible to identify and recognize the sound of fibre breaks during the wide-width tensile test.

* Corresponding author: niccolai.francesco@gmail.com

The study considers the wide-width tensile test on a typical range of nonwoven geotextiles made by high tenacity polypropylene fibres. In particular, nonwoven geotextiles considered are realized by high tenacity polypropylene fibres with a yarn count of 4.4 dtex (dtex is the weight in [g], of 10,000 m of yarn) and about 50 cN/dtex of tenacity as specified in table 1.

Table 1. Data of polypropylene fibre.

Parameter	Value	Unit	Description
Density (*d*)	910	kg/m³	Value from supplier datasheet
Yarn count (*Yc*)	4.4	dtex	Typical value from fibres suppliers datasheet,(dtex is the mass in g, of 10,000 m of yarn and it is related to the diameter of the fibre)
Fibre radius (*r*)	0.012405969	mm	Calculated starting from yarn count and density
Polypropylene Tenacity (*Tn*)	50	cN/dtex	Typical tenacity value from fibres suppliers datasheet
	455 455,000	N/mm² (kN/m² = kPa)	Conversion of tenacity (50 cN/dtex) to N/mm²
Fibre length (*L*)	70	mm	Typical value from fibres suppliers datasheet

In the wide-width tensile test, for nonwoven geotextiles, the specimen is 200 mm wide, the distance between the clamps is 100 mm and the speed test is 20 mm/min, as illustrated by Cazzuffi (1996) [4]. Experience made in Ecofibre's internal laboratory and declared values of others manufacturer of nonwoven geotextiles revealed that high tenacity polypropylene products generate a wide-width tensile strength of approximately 8 kN/m for every 100 g/m² of nonwoven geotextile product, following, this value is indicated as specific wide-width tensile strength (*Rsf*).

2 Comparison of film and nonwoven

The comparison between a homogeneous film and a nonwoven of the same mass per unit area can give us an idea of the influence of the nonwoven's inhomogeneity, also highlighting the margin of possible improvement on the nonwoven.

Considering a homogeneous film of 100 g/m², made of high tenacity polypropylene, it is calculated that the tensile strength resistance of this product will be 50 kN/m, equation (1) calc the thickness of 100 g/m² film considering density of polypropylene, and equation (2) calc tenacity of section of 1 m per thickness just calculated, multiplied per fibre tenacity as listed in Table 1:

$$T_f = W_f / d = 0.1 / 910 = 0.00010989\ m = 0.10989\ mm \quad (1)$$

R_f *film resistance[kN/m],* T_n *polypropylene tenacity [kN/m²],*

$$R_f = T_f \cdot 1000 \cdot T_n = 0.00010989 \cdot 455{,}000 = 50\ kN/m \quad (2)$$

where:
W_f = mass per unit area of film [kg/m²]
d = density of polypropylene[kg/m³]
Tf = thickness of film [m]

Taking in account that the specific resistance of the nonwoven geotextile is Rsf = 8 kN/m every 100 g/m², a resistance ratio $R_f / R_{sf} = 6.25$ is found, for the same mass per unit area and this index underline that the fibres of the nonwoven geotextiles are not homogeneously bound and participate in the breaking process differently respect the behaviour of a homogeneous

film. In order to investigate the behaviour of the nonwoven geotextile during the wide-width tensile test, we will have to monitor the breaking of the fibres in real time during the wide-width tensile test. Detecting the breaking point of fibres in real time, we will also be able to make considerations on the contribution that the individual fibres can give to the mechanical resistance of the specimen.

3 Acquisition and analysis of single fibre audio trace

In order to understand if exist possibility to recognize noise produced by fibre breaking, a series of audio acquisitions of the breaks of the individual fibres, during the tensile strength tests of fibres tests, performed according to the EN ISO 5079 (2020) standard [5], were performed. The audio acquisition device is an audio recorder capable of producing audio files in .wav format with a sampling rate of 48 kHz (time resolution 0.02 ms/sample), in which the audio signal is described with 16 bit depth and detectable frequencies from 0 to 8 kHz. The .wav files obtained were analyzed using the open-source software Audacity 2.1.2, [6], in Fig.1 sound spectrum of tensile strength tests of individual fibre test. Audio tracks of the single fibres were analyzed in order to verify the possibility of recognizing the breakage events, identifying the sound of the break by listening, and analyzing the waveform, and effectively a frequency perturbation during the break has noted, as highlighted in Fig.2a and 2b in two different scales.

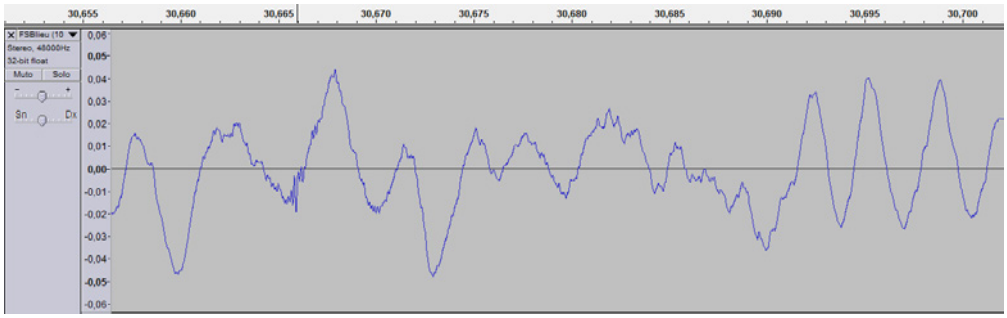


Fig. 1. Example of raw audio spectrum, in abscissa time in s and in ordinate amplitude (-1, 1)

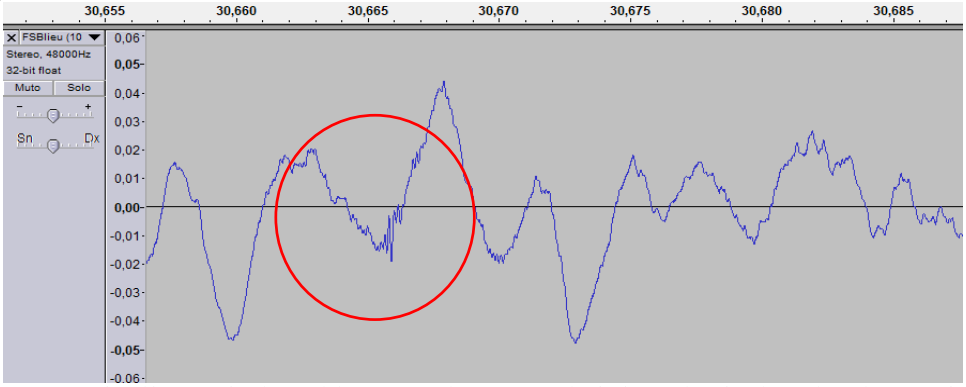


Fig. 2a. In detail perturbation of frequency in 5 ms period about, in abscissa time in s, and ordinate amplitude (-1, 1)

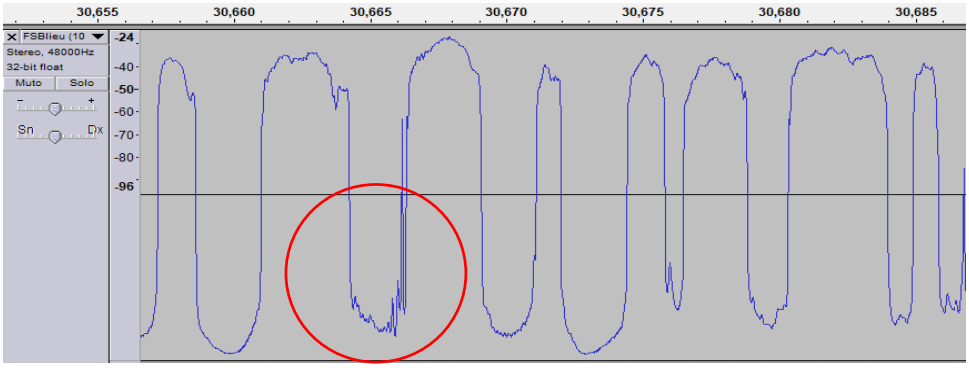


Fig. 2b. In detail perturbation of frequency in 5 ms period about, in abscissa time in s, and ordinate amplitude in dB.

This observation suggested the possibility of performing frequency analysis and, using the Audacity software, a frequency analysis of the waveform was performed using the STFT (Short Time Fourier Transform) algorithm. This type of analysis divides the audio signal into regular time intervals, and performs the FFT (Fast Fourier Transform) on the individual time intervals. A graph is then reassembled with time on the abscissa, frequencies on the ordinate, and a series of colors that identify the sound intensity measured in dB.

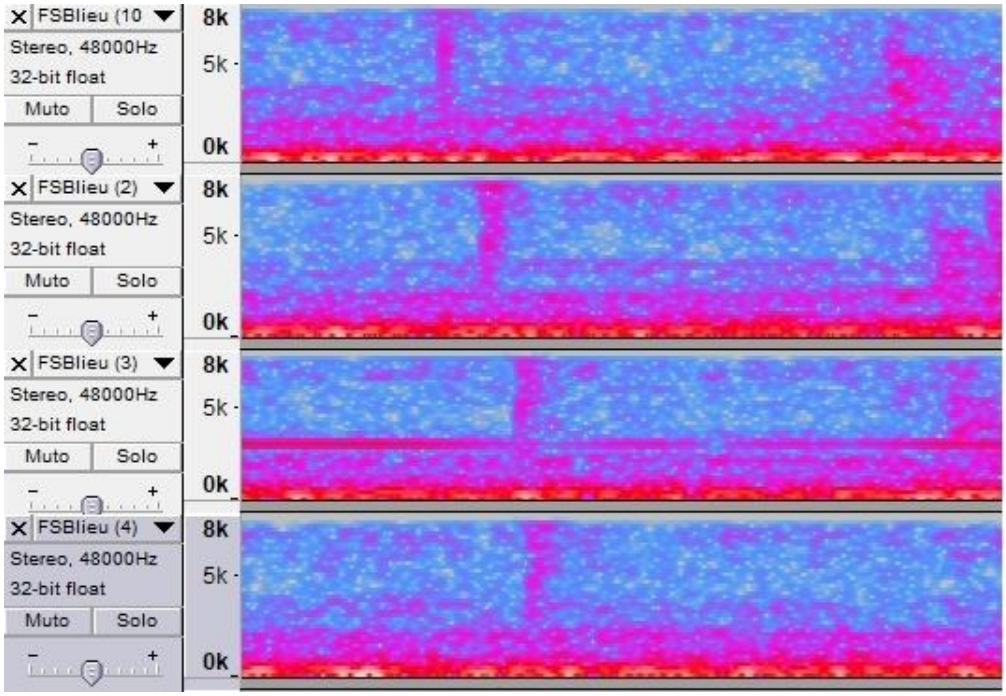


Fig. 3. Example images of frequency analysis

Audacity Spectrum Analysis Settings: Gain 20 dB, Range 80 dB, Algorithm "Frequencies", Window Size 256, window type Hann Window.

From the images shown in Figure 3 the breakage event is clearly identifiable and in this specific case has the following characteristics: event duration 4-5 ms, with characteristic frequencies between 3 and 8 kHz. These frequencies are well distinguished from the background noise, as listed in Table 2.

Table 2. Audio pattern characteristics according to the Audacity analysis

Time duration	4 – 5	ms
Frequency range	3 - 8	kHz
Acoustic intensity	60 - 80	dB

This observation and in reference of Standard Test Methods for Linear Density of Textile Fibres [2], allows us to hypothesize that each type of fibre has a characteristic sound pattern at breaking point and it can be well identified.

4 Acquisition and analysis of nonwoven audio track

Audio tracks of the noises were acquired during the wide-width tensile test, performed on the nonwoven geotextile and audio tracks were processed by frequency analysis STFT as already done for the single fibres. In order to make the results comparable, the frequency analysis parameters set on the Audacity software are the same used for the analysis of the single fibres. From the images shown in Figures 4a an 4b it is clear that the individual breaks can be identified by comparing the pattern defined for the single break. The trend in the number of breaks is clearly visible, increases with the increasing of elongation of the specimen and intensifies in proximity to the break. There are cases in which, in the same time interval, several fibre breaks can overlap; in this case , in order to count break events vs. time, we will have to consider the intensity of the sound to estimate the number of breaks in the unit of time.

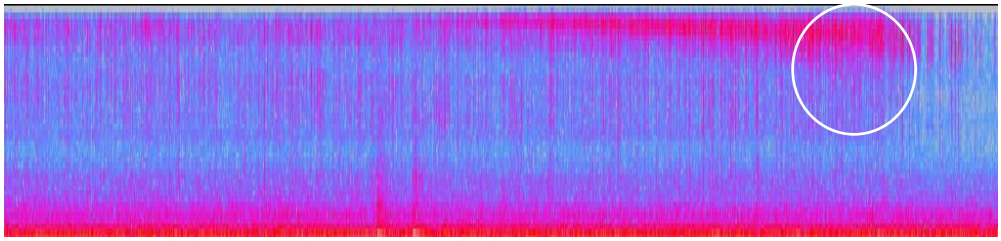


Fig. 4a. Example images of frequency analysis

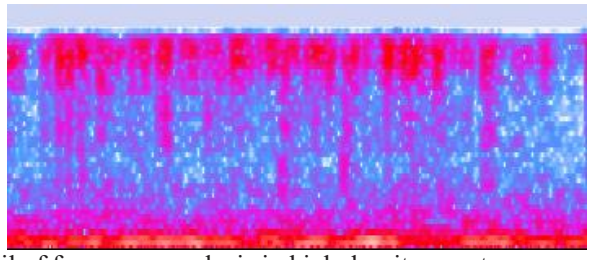


Fig. 4b. Image detail of frequency analysis in high density events zone

Overlapping of break events sound could be estimated considering the intensity of the sound, and in this case the conditions of sound acquisition have to be identical, it means that the instrument apparatus have to be developed in order to limit the background noise, and realize a standard noise condition.

5 Main comments on the preliminary results

The preliminary results presented in this study demonstrate the possibility of real-time monitoring of individual fibre breaks during the wide-width tensile test and the visual analysis of the spectra shows that the fibres start to break gradually, increasing the number of the elongation function.

If we reasonably assume that the force of nonwoven generated per unit time by the sample during the wide-width tensile strength test, is given by the sum of the fibre breaking force and from the force generated by the friction of the fibres between them, comparing the number of breaks in very small time intervals and the force provided by the sample in the same interval, we can understand how much the fibres tensile resistance contributes to the strength of the nonwoven geotextile, compared to the forces generated by the internal friction of the fibres equation [3].

$$F = n_f \cdot T_n \cdot Y_c + f_f \quad (3)$$

where:
F = nonwoven force during wide-width tensile strength test according to EN ISO 10319,
n_f = number of fibres at breaking point,
T_n = fibres tenacity,
Y_c = fibres yarn count,
f_f = others friction forces.

The ability to analyse the density of breaks in the time domain during the wide-width tensile test is an index of homogeneity of the needling process, that is the mechanical consolidation of the nonwoven. Logic suggests that the more homogeneous the needling process, the greater the resistance of the nonwoven fabric, so this type of method allows to characterize in depth the structure and performance of nonwovens.

6 Further developments

To perform a time domain analysis of fibre breaks during the wide-width tensile test, it is necessary to find or develop a specific software capable of acquiring and analysing the audio traces and automatically comparing the frequency pattern of the single break and the detectable patterns in the frequency spectrum of the wide-width tensile test. In particular, an algorithm must be found to estimate the number of break events overlapping, based on the noise intensity.

This type of investigation can be conducted with dedicated audio instruments, with detectable frequencies, sensitivity and sampling rates higher than those used for the present study, allowing a better characterization of the audio tracks.

It is possible to consider developing a tool to be installed on the dynamometers used for the wide-width tensile tests, with a setup designed to minimize background noise and create a standard noise condition and finally integrating the noise acquisition and subsequent analysis into the dynamometer control software.

The Author likes to thank Ecofibre for the support in carrying out this study, and for the availability and use of the internal Geosynthetics laboratory.

References

1. EN ISO 10319 (2024) Geosynthetics – Wide –width tensile test, CEN, Brussels, Belgium.
2. ASTM D1577 (2018) Standard Test Methods for Linear Density of Textile Fibres. ASTM, West Conshohocken, PA, United States.

3. Early detection and prediction of mechanical malfunction of machinery by sound analysis https://cordis.europa.eu/article/id/239883-sound-software-for-fault-detection-in-machinery/en.
4. D. Cazzuffi (1996) Evolution of European standardization on geotextiles, with special reference to mechanical tests, Proceedings "Index 96" Nonwoven Congress - Construction session, Geneva, Switzerland.
5. EN ISO 5079 (2020) Textile fibres - Determination of breaking force and elongation at break of individual fibres, CEN, Brussels, Belgium.
6. https://www.audacityteam.org/

SESSION 1 C
REINFORCEMENT APPLICATIONS (1)

Experimental Studies on Groups of Stone Columns with Various Shapes of Geotextile

Saeid Bazzazian Bonab[1*], *Seyed Hamid* Lajevardi[2]

[1]Department of Civil Engineering, National University of Skills (NUS), Tehran, Iran
[2]Department of Civil Engineering, Arak Branch, Islamic Azad University, Arak, Iran

Abstract. A wide range of treatments has been proposed to improve soft soils. However, increasing construction costs combined with today's environmental considerations will undoubtedly make the stone column technique a good alternative to the other techniques. In this paper, results obtained from stone columns installed in clay soil are presented and discussed. To do this and because in real conditions stone columns are used in groups, a series of experimental tests were performed on the groups of 3 and 12 stone columns and compared with the single stone columns. The stone columns were reinforced with a vertical encasement, horizontal layers, and a combination of both. It is found that, in a group of stone columns, the use of the combination of vertical encasement and horizontal layers outperformed other shapes. In addition, both group arrangements of stone columns result in more increase in bearing capacity in comparison with the single stone columns. However, the group of 3 stone columns had better efficiency despite its lower replacement area ratio.

Full paper to be published in:
https://www.e3s-conferences.org/articles/e3sconf/abs/2025/44/contents/contents.html

* Corresponding author: sbazazian@nus.ac.ir

Soil arching in geosynthetic and steel grid-reinforced pile-supported embankments

Suzanne van Eekelen[1*], *Marc* Schneider[2], *Marylin* Hell[3], *Paul* Pandrea[3], *Pascal* Schauber[4], *Michał* Topolnicki[5], *Karolina* Makowska[6], *Adam* Bezuijen[1,5], and *Hauke* Zachert[2]

[1]Deltares, Delft, Netherlands
[2]Technical University of Darmstadt, Department of Civil and Environmental Engineering, Institute of Geotechnics, Darmstadt, Germany
[3]Keller Holding GmbH, Germany
[4]Keller Fondations Spéciales, France
[5]Keller Polska, Poland
[6]SHM System, Poland
[5]Bezuijen Consult, Netherlands

Abstract. High-density deformation measurements were used to investigate the load distribution on, and the deformed shape of the basal reinforcement in pile-supported embankments. Two cases were analysed: a geosynthetic-reinforced (GR) embankment in Woerden, the Netherlands, and a steel-reinforced (SR) embankment in a large-scale model test (PEBSTER), conducted at the TU Darmstadt in Germany. The SR has an axial stiffness over 20 times higher than the GR, yet both embankments exhibited an inverse-triangular load distribution on the reinforcement. This consistent behaviour indicates that soil arching is independent of reinforcement stiffness. Predictions with the Concentric Arches model closely match the measured deflections in both cases. However, the model does not yet include the reinforcement above the piles, where the bending stiffness of the SR plays a role.

Full paper to be published in:
https://www.e3s-conferences.org/articles/e3sconf/abs/2025/44/contents/contents.html

* Corresponding author : suzanne.vaneekelen@deltares.nl

Experimental and numerical model in geosynthetic pile embankment

S. Hamid Lajevardi[1*], *Atefeh Tardast*[1], *Laurent Briançon*[2], and *S. Mohammad Mirhoseini*[1]

[1] Department of Civil Engineering, Arak Branch, Islamic Azad University, Arak, Iran
[2] Univ Lyon, INSA-Lyon, GEOMAS, F-69621, France

Abstract. Currently, geosynthetics are used to reinforce pile-supported embankments in soft soils. Geosynthetics are widely used to reinforce pile-supported embankments in soft soils. Numerous studies have examined various factors affecting load distribution, including pile group arrangement, the presence of pile caps, and the type and placement of the geosynthetic layer within the Load Transfer Platform (LTP). In such foundations, the primary concern is the distribution of load among the main structural components. Based on guidelines, the load is divided into three parts: the part which is directed to piles, the part which is transmitted to geosynthetic, and the part which is entered into soft soil. The soil arching and membrane effects are two effective phenomena in the load distribution process. In this study, the experimental results showed the increase in the load transferred on piles with geosynthetic and the geosynthetic focused the load on piles through the membrane effect, as confirmed by the numerical model.

Full paper to be published in:
https://www.e3s-conferences.org/articles/e3sconf/abs/2025/44/contents/contents.html

* Corresponding author : hamidlajevardi@yahoo.com

Piled embankments - Behaviour of geosynthetic basal reinforcement in condition of change of soft soil reaction

Andrzej Łopatka[1*],

[1]Przedsiębiorstwo Realizacyjne INORA Sp. z o. o. ul. Prymasa Stefana Wyszyńskiego 11, 44-100 Gliwice, Poland

Abstract. Foundation of embankments on piled subsoil is one of the most popular solution with soft soil conditions. In foundation system - piles are topped with one or more horizontal layers of geosynthetic reinforcement called – basal reinforcement. Due to geosynthetic reinforcement – a part of vertical load from area between piles is transferred to the bearing elements. Behaviour of basal reinforcement depends on many factors, like arrangement and dimensions of piles or caps, external loads, properties of mineral filling and geosynthetic reinforcement. One of the most important element is reaction of soft soil. Due to creeping behaviour of basal reinforcement and changes of loaded soil properties in time – taking into account a constant soil reaction is not appropriate solution at the design stage. The article presents the issue of changes in soil properties over time and their impact on the behaviour of the basal reinforcement. The predictions of reinforcement behaviour were made using the most currently popular and accepted design models.

Full paper to be published in:
https://www.e3s-conferences.org/articles/e3sconf/abs/2025/44/contents/contents.html

* Corresponding author: badania@inora.pl

On the construction rate of Geosynthetic-Reinforced and Pile-Supported Embankments

Viviana Mangraviti[1*]

[1]University of Padova, Department of Civil, Environmental and Architectural Engineering, Italy

Abstract. Geosynthetic-Reinforced and Pile-Supported Embankments are conventionally designed with simplified limit-equilibrium theories that prioritize ultimate limit state analysis. However, these methodologies exhibit a significant limitation in their inability to quantify the progressive settlement at the embankment crest during the construction phase, which is a critical phase in the occurrence of the soil arching mechanism. Recent advancements in the field have introduced a displacement-based mathematical model which can assess settlements, stresses, and geosynthetic forces during embankment construction with minimal computational effort. This paper compares full-scale test data with this mathematical model to examine the impact of embankment construction rate on the evolution of settlements during construction.

Full paper to be published in:
https://www.e3s-conferences.org/articles/e3sconf/abs/2025/44/contents/contents.html

* Corresponding author: viviana.mangraviti@unipd.it

Design of geosynthetics for rigid inclusion ground improvement: a simplified analytical method

Ana Maria Alzate[1*], *Bruno* Simon[1], and *Laurent* Briançon[2]

[1]Terrasol, CS 71230 75583 Paris Cedex 12, France
[2]GEOMAS, Université de Lyon, INSA-Lyon, 69621 Villeurbanne Cedex, France

Abstract. The French national project ASIRI+ (2019-2025) is the continuation of the ASIRI project (2005-2012). It aims to provide design recommendations for ground reinforced by rigid inclusions, which, in France, are typically based on the analysis of a unit cell accounting for the behavior of an infinite inclusion group. These so-called "biphasic models" provide all the necessary components for the structural design of rigid inclusions. New topics are introduced in ASIRI+ project, such as horizontal reinforcement of the granular platform using geosynthetics which permits the improvement of the performance of the load transfer platform. In this framework, this paper presents a simplified analytical method that incorporates geogrids into biphasic models. At the level of geosynthetics, which transfers the load to the tops of the inclusions, a relationship coupling the geosynthetic displacement with this load is introduced into the biphasic model equations. The results obtained using this methodology are compared to full-scale tests conducted by the laboratory GEOMAS and the CEREMA of Rouen.

Full paper to be published in:
https://www.e3s-conferences.org/articles/e3sconf/abs/2025/44/contents/contents.html

* Corresponding author: anamaria.alzate@setec.com

Lessons learned from the ASIRI+ project on the use of geosynthetics in load transfer platform

Alain Nancey[1*], and *Laurent* Briançon[2]

[1] Solmax France, 95873 Bezons, France
[2] GEOMAS -INSA Lyon, France

Abstract. Geosynthetics are used for the reinforcement of the granular layer acting as a load transfer platform in the case of embankments on piles or rigid inclusions. This article highlights the results obtained on the use of geosynthetics during the French national project ASIRI+ (2019 - 2025), an extension of the ASIRI project (2005-2012), aiming to provide recommendations for the design of a soil reinforced by rigid inclusions with practical suggestions for the installation. Full scale experiments, field monitoring, physical models at the centrifuge, as well as numerical models have been used to get a better understanding of the geosynthetic behaviour, confirming the interest of this reinforcement solution.

Full paper to be published in:
https://www.e3s-conferences.org/articles/e3sconf/abs/2025/44/contents/contents.html

SESSION 1 D
DESIGN AND MODELISATION (1)

Effects of grains characteristics and geogrid shape and rigidity on the behaviour of reinforced granular soil – 3D DEM study

Ahmad El Ayoubi[1*], *Fabrice* Emeriault[1], *Pascal* Villard[1], and *Luc* Sibille[1]

[1]Université Grenoble Alpes, CNRS, Grenoble INP, 3SR, Grenoble, France

Abstract. This study explores the impact of granular properties and geogrid characteristics on the behaviour of reinforced soil techniques, through DEM numerical simulations of triaxial compression tests. Three particle shapes (spheres, two different clumps) were examined, as well as two geogrid types (biaxial and triaxial). The results show that geogrids significantly increase peak strength and reduce lateral deformations, mainly due to better particle confinement. Clumps generally exhibit better shear strength, creating a more stable granular structure that interacts more effectively with geogrids. The study also reveals that particles interlocking in geogrid apertures predominates friction at the soil-geogrid interface. The stiffness of geogrids influences their effectiveness: above a certain threshold, geogrids offer near-saturated benefit performance. On the other hand, the shape and size of geogrid openings present a secondary impact when stiffness and effective area are maintained constant. This research highlights the importance of selecting geogrids according to soil granularity and can provide practical recommendations for the use of geogrids in geotechnical applications.

Full paper published in the September 2025 Special Issue of the French Geotechnical Journal **"Revue Française de Géotechnique"** _*https://www.geotechnique-journal.org*

* Corresponding author: ahmadaub04@gmail.com

Laboratory tests and numerical studies of a geosynthetic reinforced pile-supported embankment

Yining Hu[1]*, *Laurent* Briancon[1], and *Daniel* Dias[2]

[1] INSA LYON, GEOMAS, 69621 Villeurbanne, France
[2] Université Grenoble Alpes, CNRS, Grenoble INP, 3SR, 38000 Grenoble, France

Abstract. This paper presents laboratory tests examining geosynthetic-reinforced pile supported-embankments over soft soil. Many tests were carried out in a 4m x 4m x 0.9m pit including 16 piles, varying the load transfer platform thickness and geosynthetic reinforcement. A comprehensive monitoring program was implemented to track the load transfer inside the granular platform and the settlement. This research is a part of the cooperative national research project ASIRI+ (2019 - 2024) which gathers about forty organizations and aims to propose dimensioning rules in the field of soil reinforcement by rigid inclusions. These experimental results investigated the understanding of complex mechanisms developed inside the load transfer platform to evaluate the efficiency of the geosynthetic. In addition, a numerical model established by the software FLAC3D was employed to simulate the experimental tests. The ability of the numerical model to account for the settlement of the granular soil surface and the stress transmitted to the top of the subgrade layer was established by comparisons with the experimental data. From this calibrated numerical model, many simulations were performed to propose an optimal solution for the reinforcement by the geosynthetic.

Full paper to be published in:
https://www.e3s-conferences.org/articles/e3sconf/abs/2025/44/contents/contents.html

* Corresponding author: yining.hu@insa-lyon.fr

Strength prediction models for fiber-reinforced soils under effective stress triaxial compression testing

K. E. Bantralexis[1*], *A. G.* Vassou[1] *and I. N.* Markou[1]

[1]Democritus University of Thrace, Department of Civil Engineering, University Campus - Kimmeria, GR-67100 Xanthi, Greece

Abstract. The improvement of shear strength of soils is a common practice applied in numerous civil engineering projects. Geosynthetics like geogrids, geotextiles and fibers contribute significantly in soil strength improvement. Soil reinforcement with randomly oriented fibers has attracted extensive research attention. The shear strength of fiber-reinforced soils is often determined experimentally by performing triaxial compression tests under effective stress conditions. Presented in this paper are easy-to-use models for the strength prediction of fiber-reinforced soils under the aforementioned testing conditions. After an extensive literature review, a database of 436 measurements was created including data for all independent variables relative to the soil and fiber characteristics. This database was then processed and divided into two subsets: the first, consisting of 75% of the measurements, was used to develop the models by performing statistical analyses, whereas the second, with the remaining 25% of the measurements, served as a basis for their validation. The development of the models was achieved through multivariable linear regression analyses performed with suitable statistical software. After an extensive number of trials, three optimal models were derived that satisfy the statistical requirements, exhibiting R^2 determination coefficients greater than 0.95 and satisfactory estimation of the validation measurements at a rate reaching 81%.

Full paper to be published in:

https://www.e3s-conferences.org/articles/e3sconf/abs/2025/44/contents/contents.html

Geosynthetic overlap for reinforced piled embankment: centrifuge modelling

Luc Thorel[1*], *Mathieu* Guerois[1], *Thierry* Dubreucq[1], *Matthieu* Blanc[1]
[1] University Gustave Eiffel, Lab. Centrifuges for Geotechnics (GERS-CG), France

Abstract. The overlap of two geosynthetic strips, located at the base of the granular load transfer platform and above rigid inclusions, is being studied on small-scale instrumented models using the moving tray device in the geotechnical centrifuge at the University Gustave Eiffel. The width of the cover (in the range between zero and the pile spacing, for 3 area ratios of reinforced pile embankment) influences the efficiency of the load transfer and the differential settlement at the surface.

Full paper to be published in:
https://www.e3s-conferences.org/articles/e3sconf/abs/2025/44/contents/contents.html

Finite Element Modelling of geogrids in stabilisation function - Comparison study

Katarzyna Ria Zamara[1*], *Andrew* Lees[2], *Ben* Gorrill[1] and *Jacek* Kawalec[3]

[1]Tensar International Ltd, 2-4 Cunningham Court, Blackburn, BB1 2QX, United Kingdom
[2]Geofem Ltd, Dimostheni Severi 21, 1st Floor, Nicosia 1080, Cyprus
[3]Silesian University of Technology, Gliwice, Poland

Abstract. Finite element methods (FEM) are commonly used in geotechnical designs. These methods become particularly valuable when complex multistage scenarios with a variety of interactions need to be considered. Many advanced constitutive models describing soil behaviour exist. However, features in FEM software to model geogrids are often limited to elements that are represented as elastoplastic membranes that interact with the surrounding aggregate through an interface element. These methods, using limited parameters, are more suited to modelling the reinforcement function of geosynthetics. Since ISO 10318-1:2015+A1:2018 was published, a new function of geogrids was introduced: stabilisation. Stabilisation relies on the interlock between the geosynthetic and the granular material which confines the granular aggregate. This generates very small strains within the geosynthetic product. In addition, the confinement of the granular material, due to the stabilisation effect, influences beyond the thin layer of interface into the aggregate. The aim of this paper is to examine and assess the traditional feature that is available in popular FEM software Plaxis and compare it to the Tensar Soil Stabilised (TSS) constitutive model – a user defined soil model (USDM) available in software such Plaxis, Abaqus, Flac or Cesar. The TSS model aims to more accurately represent the geogrid and aggregate interaction by modelling the composite behaviour of the two materials.

Full paper to be published in:
https://www.e3s-conferences.org/articles/e3sconf/abs/2025/44/contents/contents.html

* Corresponding author: kasia.zamara@cmc.com

Numerical modelling of soil-reinforcement direct shear test with Mohr-Coulomb plasticity

Shuxiong Xiao[1*], *Ivan P.* Damians[1,2], *Wei Hu*[3]

[1]Department of Civil and Environmental Engineering, School of Civil Engineering, Universitat Politècnica de Catalunya-BarcelonaTech (UPC), Barcelona, Spain
[2]International Center for Numerical Methods in Engineering (CIMNE), Universitat Politècnica de Catalunya-BarcelonaTech (UPC), Barcelona, Spain
[3]Hunan Province Key Laboratory of Geotechnical Engineering Stability Control and Health Monitoring, Xiangtan, China

Abstract. The soil-reinforcement interaction issue is commonly encountered in the design of reinforced soil walls (RSWs). The prevalent laboratory approaches for soil-reinforcement interaction analyses are pull-out and direct shear tests, performing different loading-response mechanisms, both fundamental in the global performance and design of RSW systems. In comparison with the pull-out tests, direct shear has typically lower cost, higher simplicity, and can directly measure the interface shear strength parameters (i.e., friction angle and adhesion). This paper presents a 2D numerical modelling of soil-reinforcement direct shear test. The interface zone between soil and reinforcement is characterized by continuum elements, whose material behaviour is defined as linear elastic with Mohr-Coulomb (M-C) plasticity model for simplicity. The presented numerical method is examined by reported experimental data of sand-steel and sand-woven geotextile interface direct shear tests. Results indicate the M-C law generally performs well under different boundary conditions and loading pressures, except for shear strength overestimation when volumetric deformation is restricted. The present study may provide useful insight for element and material selection when modelling interface, relevant for soil-reinforcement interaction investigation and/or practical RSWs design.

1 Introduction

The common use of reinforcement material (basically steel- or polymeric-based elements), in the design of reinforced soil walls (RSWs) entails the analysis of soil-reinforcement interaction problem. As fundamental approaches, both pull-out test and direct shear test can reflect the global performance of RSWs system, showing different soil-reinforcement interaction response mechanisms. In comparison, direct shear test has a simpler set-up and typically lower cost than pull-out test, and can directly provide, at different confining pressures, the interface's strength and stiffness parameters required for the optimization of RSWs design.

So far, numerous studies of direct shear test data for soil-reinforcement interface have been reported. Direct shear failure mode can be elusive when different soil/reinforcement

* Corresponding author: shuxiong.xiao@upc.edu

types [1-3] and confining conditions [4-5] are involved, and the state variables [6-10] (e.g., porosity, suction, temperature, etc.) also exert considerable influences on the interface response. Numerical methods have been used to replicate the direct shear behaviour of soil-reinforcement interface, mainly by finite element methods [11-13]. In their studies the thin-layer element [14] has been used, combined with constitutive models [15-17] specially developed for interface modelling. However, up to a dozen -parameters are required for those models, and most of them are phenomenological with unclear physical meaning, which greatly increases the difficulty of calibration process. As one of the simplest and most practical plastic constitutive laws in geomechanics, Mohr-Coulomb failure criterion has shown certain accuracy in simulating reinforcement pull-out test and RSWs [18-20]. Considering that, whether the interface methodology of using linear elastic and Mohr-Coulomb plasticity with continuum element feasible for reinforcement direct shear test simulation is of common concern.

Therefore, in this paper, a numerical simulation of soil-reinforcement direct shear test is performed, focusing on the performance of Mohr-Coulomb plasticity model in simulating the interface. A 2D finite element numerical model was implemented to simulate direct shear responses. Then a simple and experiment-based parameter calibration method is proposed. Finally, the numerical model was validated through two sets of reported soil-reinforcement direct shear test data [4, 7].

2 Finite element numerical model

A 2D model was founded to simulate direct shear test on soil-reinforcement interface, using the finite element software CODE_BRIGHT [21]. The model replicates the typical direct shear test setup of soil-reinforcement interface, as shown in Fig. 1. In the model, the upper shear box is filled with soil, beneath the soil lays the reinforcement which glued by the steel block.

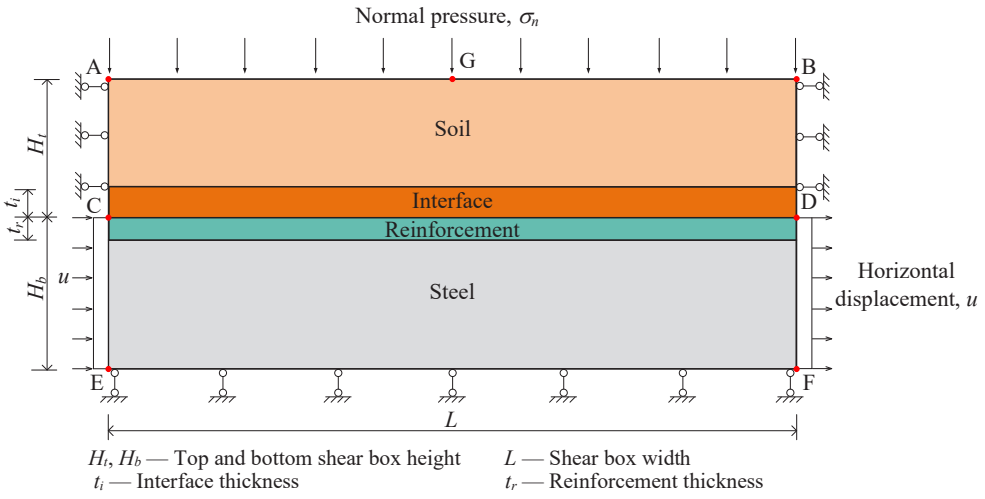


Fig. 1. Schematic diagram for the numerical model of soil-reinforcement direct shear test.

A defined interface zone replaces the soil adjacent to reinforcement, as this area behaves significantly distinguished from the surrounding soil due to the reinforcement constraint. The soil-reinforcement interface was implemented as continuum elements, which enables more control over strength, stiffness, element shape/size, and numerically agrees well with the results of zero-thickness element from other numerical software [18-20]. As to the material properties, for practicality and simplicity, the soil, reinforcement and steel were defined as linear elastic material [11, 13-14, 17], while the interface was modelled using a linear elastic

stiffness with a Mohr-Coulomb plastic constitutive law. This is because the interface plays a dominant role in the behaviour of the system.

The direct shear test procedure was reconstructed, depending on whether constant normal load (CNL) or constant volume (CV) path was loaded, by 2 or 3 stages: CNL scenario followed an order of pressurizing (σ_n applied on the top border, line AB) and shearing (horizontal displacement exerted on the lateral border of the lower box, line CE and DF), while for CV case an extra stage of fixing top border was inserted between the two stages to restrict the volume change. Note the lateral boundaries of the upper box (line AC and BD) were always fixed, as shown in Fig. 1.

Prior mesh optimization analyses (not included here due to page limitation) showed 3 transversal -vertical division of- mesh elements for interface satisfied the simulation requirement of good accuracy and few calculation expenses, which was thus used in all simulations of this study. The implemented 2D model, with fewer computational cost, can serve as an approximate alternative to 3D case because of the model continuity along the plane strain representation.

3 Calibration of soil-reinforcement interface

The soil-reinforcement interface was assumed as a Mohr-Coulomb plastic material with linear elasticity as aforementioned, 5 constitutive parameters: Young's modulus E, Poisson's ratio μ, cohesion c, friction angle φ and dilatancy angle ψ, were required for the simulation. In addition, the geometric thickness of the interface, t_i, should be prior determined before the 5 material parameters, a value between 5-10 times d_{50} (mean particle size of soil) could be a suitable choice according to the experimental evidence [1, 5, 11, 13, 15, 17].

The shear strength envelope of Mohr-Coulomb material follows the form of:

$$\tau_f = c + \sigma \tan\varphi \qquad (1)$$

where τ_f and σ denotes failure shear stress and normal stress in the shear plane respectively.

The shear plane in direct shear test is prior designated to the contacting surface between soil and reinforcement (line CD in Fig. 1), thus σ equals the loaded normal pressure σ_n, whereas the failure shear stress τ_f can be straightforwardly gained through measured shear stress-shear displacement (v-u) curve. Therefore, by Eq. (1), the friction angle φ can be calibrated through linear fitting of the τ_f - σ_n data, as shown in Fig. 2(a), where the sand-steel interface test [4] is selected as example to schematically explain how the parameters are calibrated.

The dilatancy rate for plastic material is defined as the ratio between plastic volumetric strain and deviatoric strain:

$$d = \tan\psi = \frac{d\varepsilon_v^p}{d\varepsilon_d^p} \qquad (2)$$

For the interface assumed thin enough (i.e., thickness $t \to 0$), strain states approximately obey [14]:

$$d\varepsilon_x = d\varepsilon_z = 0 \qquad (3)$$

$$d\varepsilon_y = \frac{dv}{t} \qquad (4)$$

$$d\gamma_{xy} = \frac{du}{t} \qquad (5)$$

where ε_x, ε_y, ε_z are 3 normal strain components, γ_{xy} is shear strain in x-y plane, and u, v respectively denotes shear and vertical displacement. Note that ε_y is very small when compared to the shear strain γ_{xy}, and the elastic strain proportion weakens as the plastic straining process proceeds, thus one may have:

$$\tan\psi = \frac{d\varepsilon_v - d\varepsilon_v^e}{d\varepsilon_d - d\varepsilon_d^e} \approx \frac{d\varepsilon_v}{d\varepsilon_d} \approx \frac{d\varepsilon_y}{d\gamma_{xy}} = \frac{dv}{du} \qquad (6)$$

By Eq. (6), the dilatancy angle can be obtained using the slope of measured *v*-*u* curve at large shear displacement, as depicted in Fig. 2(b).

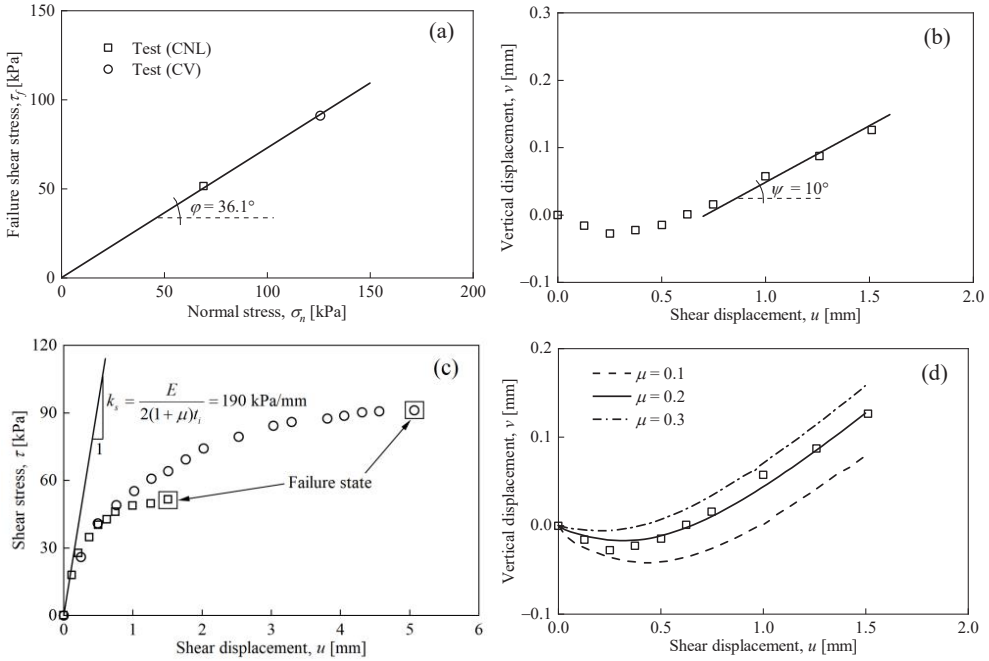


Fig. 2. Calibration of soil-reinforcement interface parameters: (a) friction angle φ, (b) dilatancy angle ψ, (c) Young's modulus E, and (d) Poisson's ratio μ. (data from [4])

The relationship between shear stiffness k_s and Young's modulus E can be deduced from elastic law [18] as:

$$k_s = \frac{E}{2(1+\mu)t_i} \qquad (7)$$

As the initial shearing phase is presumed elastic, in measured τ-u curve the slope of tangent line crossing origin is approximately the value of k_s. Using Eq. (7), with t known (2mm for this case) and a typical value of 0.3 set for μ, E can be secured. As displayed in Fig. 2(c), where k_s = 190 kPa/mm is obtained for this dataset, yielding to E = 1.0 MPa (rounded value), and the failure state is also marked in the figure as a complementary illustration to Fig. 2(a).

Once the strength parameters and stiffness of the interface calibrated, the Poisson's ratio may be tentatively determined to ensure the computed *v*-*u* curve conforming well to test data, as exhibited in Fig. 2(d), where μ = 0.2 seems to be a suitable choice. It is noteworthy all parameters can be derived from the CNL test data, as indicated by Fig. 2, where the calibration process isn't even affected if excluding the CV test data.

4 Results and discussion

To check the proposed numerical model, direct shear tests on sand-steel interface [4] and sand-woven geotextile interface [7] were simulated, corresponding to stiff and soft reinforcement scenarios respectively. The first case incorporated both CNL and CV loading paths, while the second case considered different loading pressures. With this simulation composition, the model performance under different boundary and loading conditions could be examined.

4.1 Simulation of sand-steel interface test

Zeghal and Edil [4] carried out direct shear tests between sand and steel, where both CNL and CV paths were loaded. The tested sand is a uniform (coefficient of uniformity C_u=1.8) silica sand, with a mean particle size d_{50} = 0.32 mm and relative density D_r = 70% prepared for the test. Small shear box size is used with H_t = H_b = 6.4 mm and L = 50 mm. The test applied an initial normal pressure of 69 kPa and ended approximately at a shear displacement of 1.5 mm and 5 mm respectively for CNL and CV conditions. Table 1 concluded the material properties used in the simulation, including sand and steel parameters, as well as interface parameters which has been calibrated in section 3. Interface thickness t_i = 2 mm is used for this case.

Table 1. Material properties for sand-steel interface test simulation [4].

Parameters	Materials		
	Sand	Interface	Steel
Unit weight, γ (kN/m^3)	20	20	75
Young's modulus, E (MPa)	86.3[a]	1.0	210 000
Poisson's ratio, μ (-)	0.3	0.2	0.3
Cohesion, c (MPa)	–	0.001	–
Friction angle, φ (°)	–	36.1	–
Dilatancy angle, ψ (°)	–	10	–

Notation: [a]Determined according to the empirical stiffness equation for dense sand [22].

Fig. 3 shows the comparison between the computed and measured results. Note that in all simulations of this study the computed shear stress and vertical displacement are extracted at the representative plane and point, i.e., shear plane (line CD) and top border midpoint (point G) respectively. As shown in Fig. 3(a-b), under CNL path the shear stress keeps increasing with shear displacement, while the volume change undergoes a so-called "phase transformation" process, namely, a transition from contraction to dilation [13,17]. It is also observed good consistency is reached between computed and measured results, showing the capacity of linear elastic with Mohr-Coulomb failure criterion model in capturing the typical behaviour of interface, including strain hardening, dilatancy and phase transformation.

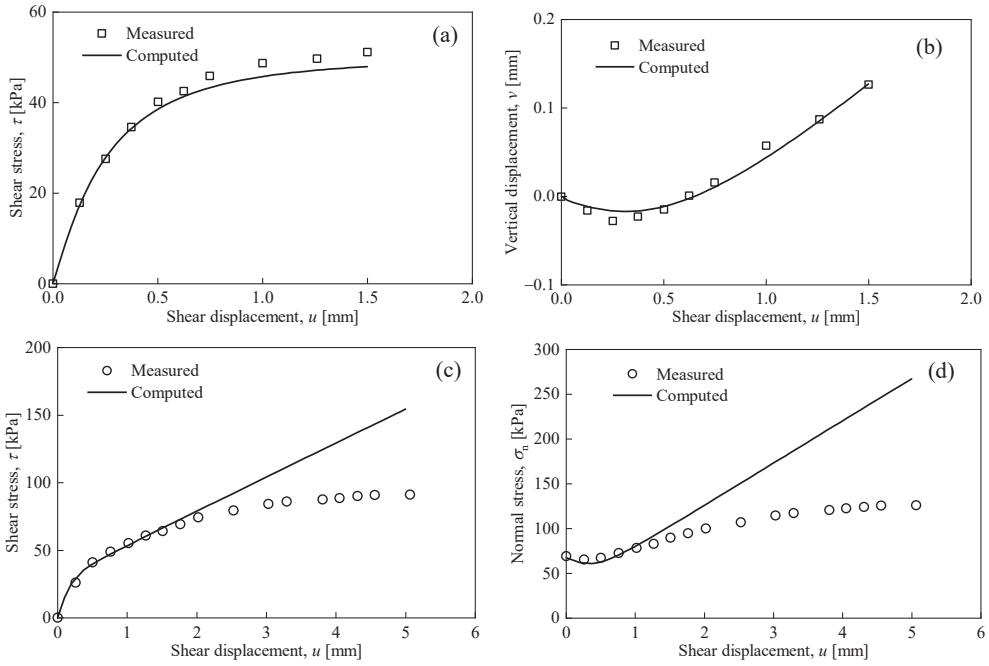


Fig. 3. Computed results against measured data of sand-steel interface direct shear test: (a-b) constant normal load (CNL) path; (c-d) constant volume (CV) path (data from [4])

The experimental CV responses of the direct shear system are also exhibited in Fig. 3(c-d), which manifests that, the shear stress increases at a decreasing rate, whereas the normal stress slightly drops down and levels off, both showing a stabilized tendency as shearing continues. One interesting thing is that, the model prediction matches the test data well at the initial shearing stage ($u < 2$ mm), but overestimations and deviations occur and become more significant when increasing the shear displacement further. This discrepancy may be attributed to the inherent deficiency of the Mohr-Coulomb plasticity, which assumes a constant dilatancy rate, resulting in continuous stress increase once volume change is not permitted. One effective way to eliminate the drawback is to formulate the dilatancy rate ψ as an attenuated parameter with shear strain, which may be a further area to investigate.

Table 2. Material properties for sand-woven geotextile interface test simulation [7].

Parameters	Materials			
	Sand	Interface	Woven Geotextile	Steel
Unit weight, γ (kN/m^3)	20	20	3.75[b]	75
Young's modulus, E (MPa)	87.9[a]	1.0	50[b]	210 000
Poisson's ratio, μ (-)	0.3	0.3	0.3	0.3
Cohesion, c (MPa)	–	0.001	–	–
Friction angle, φ (°)	–	42[b]	–	–
Dilatancy angle, ψ (°)	–	4[b]	–	–

Notation: [a]Determined according to the empirical stiffness equation for medium sand [22].
[b]Directly extracted from the test resource [7].

4.2 Simulation of sand-geotextile interface test

Afzali-Nejad et al. [7] conducted a series of direct shear tests (all under CNL path) on sand-woven geotextile interface, where particle shape, relative density, and pressure magnitude effects were investigated. The sand is classified as poorly graded sand with the following basic properties: specific gravity $G_s = 2.67$, $C_u = 1.53$, coefficient of curvature $C_c = 0.98$, $d_{50} = 0.65$ mm. The geotextile is woven and possesses properties as below: thickness $t_r = 0.5$ mm, mass per unit area 375 g/m^2, tensile strength 50 kN/m. The standard shear box is used in tests, with dimensions of $H_t = 22$ mm, $H_b = 11$ mm, and $L = 100$ mm. The medium sand case ($e_0 = 0.81$, $D_r = 43\%$) within the testing program is simulated here, where 3 different normal pressures (57, 107 and 207 kPa) are taken into account. Table 2 lists the modelling parameters for the materials composing the numerical model. In this case a thickness value $t_i = 3.5$ mm is adopted for the interface.

Fig. 4 presents the simulation results of sand-woven geotextile interface test under different normal pressures ($\sigma_n = 57$, 107 and 207 kPa). As shown in Fig. 4, higher pressure leads to a higher shear strength as expected, as well as lower dilatative deformation because increase of pressure suppresses the dilatancy magnitude. Overall, the computations keep a good agreement with the experimental observations, and the general phenomenon caused by normal pressure variation in direct shear test can be well reflected by the simulation, though more or less the discrepancy exists when coming to a specific loading case.

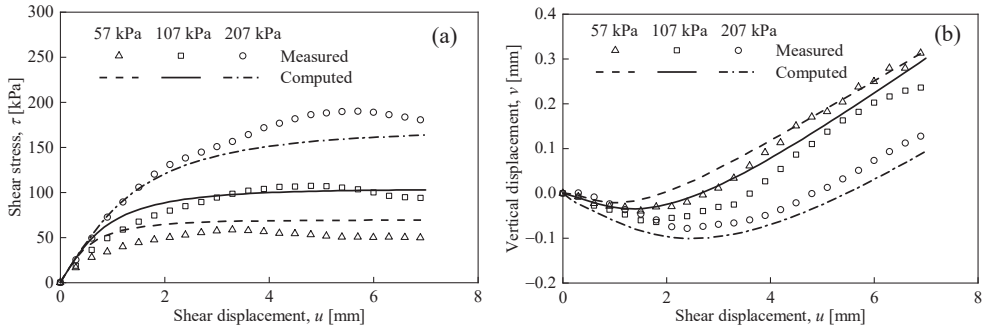


Fig. 4. Computed results against measured data of sand-woven geotextile interface direct shear test: (a) shear stress evolution and (b) vertical displacement evolution (data from [7])

5 Conclusion

The present study performs 2D finite element modelling of direct shear test on soil-reinforcement interface using the classic Mohr-Coulomb plastic constitutive law. A simple and experiment-based approach for calibrating the interface strength and stiffness parameters was proposed. The reported sand-steel and sand-woven geotextile direct shear tests were simulated to examine the numerical model. The following conclusion are addressed:

(1) The overall good agreement between computed results and measured data validated the effectiveness of continuum elements and linear elastic with Mohr-Coulomb failure criterion model in simulating soil-reinforcement interface.

(2) Simulation results revealed that the Mohr-Coulomb plasticity captured significantly well the typical behaviour of interface, including the strain hardening, dilatancy and phase transformation.

(3) The Mohr-Coulomb law generally showed a good performance when different boundary conditions and loading pressures were involved, yet it overestimated the shear strength and was incapable of modelling the asymptotic stress state when volumetric deformation was restricted.

The presented work may catch the attention of researchers who interested in selecting element type or constitutive law for interface modelling. The limitation of the present methodology is the inability in capturing the strain softening behaviour, the porosity effects, as well as the ultimate stress state under CV condition, future studies will be dedicated to the further investigation and improvement.

Acknowledgements

The authors wish to acknowledge the China Scholarship Council (No. 202306560015), the Department of Civil and Environmental Engineering (DECA) of Universitat Politècnica de Catalunya·BarcelonaTech (UPC), and the International Centre for Numerical Methods in Engineering (CIMNE).

Author contribution

S. Xiao: numerical model development, methodology, data curation, software, manuscript-writing. **I.P. Damians**: methodology, software, manuscript-review. All authors reviewed the manuscript.

References

1. A. Lashkari, V. Jamali, Global and local sand-geosynthetic interface behaviour. Géotechnique **71**(4), 346-367 (2021). https://doi.org/10.1680/jgeot.19.P.109
2. B. M. Bacas, J. Canizal, H. Konietzky, Frictional behaviour of three critical geosynthetic interfaces. Geosyn. Int. **22**(5), 355-365 (2015). https://doi.org/10.1680/jgein.15.00017
3. C. N. Liu, Y. H. Ho, J. W. Huang, Large scale direct shear tests of soil/PET-yarn geogrid interfaces. Geotext. Geomembr. **27**(1), 19-30 (2009). https://doi.org/10.1016/j.geotexmem.2008.03.002
4. M. Zeghal, T. B. Edil, Soil structure interaction analysis: modeling the interface. Can. Geotech. J. **39**(3), 620-628 (2002). https://doi.org/10.1139/t02-016
5. A. Afzali-Nejad, A. Lashkari, A. Martinez, Stress-displacement response of sand-geosynthetic interfaces under different volume change boundary conditions. J. Geotech. Geoenviron. Eng. **147**(8), 04021062 (2021). https://doi.org/10.1061/(ASCE)GT.1943-5606.0002544
6. J. T. DeJong, Z. J. Westgate, Role of initial state, material properties, and confinement condition on local and global soil-structure interface behavior. J. Geotech. Geoenviron. Eng. **135**(11), 1646-1660 (2009). https://doi.org/10.1061/(ASCE)1090-0241(2009)135:11(1646)
7. A. Afzali-Nejad, A. Lashkari, P. T. Shourijeh, Influence of particle shape on the shear strength and dilation of sand-woven geotextile interfaces. Geotext. Geomembr, **45**(1), 54-66 (2017). https://doi.org/10.1016/j.geotexmem.2016.07.005
8. T. B. Hamid, G. A. Miller, Shear strength of unsaturated soil interfaces. Can. Geotech. J. **46**(5), 595-606 (2009). https://doi.org/10.1139/T09-002

9. S. Maghsoodi, O. Cuisinier, F. Masrouri, Thermal effects on mechanical behaviour of soil-structure interface. Can. Geotech. J. **57**(1), 32-47 (2020). https://doi.org/10.1139/cgj-2018-0583
10. S. Q. Cui, C. Zhou, Q. Y. Mu, H. F. Pei, J. H. Yin, Coupled effects of temperature and suction on the shear behaviour of saturated and unsaturated clayey sand-structure interfaces. Géotechnique (2024). (**On line**) https://doi.org/10.1680/jgeot.22.00404
11. L. Hu, J. L. Pu, Application of damage model for soil-structure interface. Comput. Geotech. **30**(2), 165-183 (2003). https://doi.org/10.1016/S0266-352X(02)00059-9
12. G. Zhang, J. M. Zhang, Numerical modeling of soil-structure interface of a concrete-faced rockfill dam. Comput. Geotech. **36**(5), 762-772 (2009). https://doi.org/10.1016/j.compgeo.2009.01.002
13. M. Saberi, C. D. Annan, & J. M. Konrad, Implementation of a soil-structure interface constitutive model for application in geo-structures. Soil. Dyn. Earthq. Eng. **116**, 714-731 (2019). https://doi.org/10.1016/j.soildyn.2018.11.001
14. K. G. Sharma, C. S. Desai, Analysis and implementation of thin-layer element for interfaces and joints. J. Eng. Mech. **118**(12), 2442-2462 (1992). https://doi.org/10.1061/(ASCE)0733-9399(1992)118:12(2442)
15. L. Hu, J. Pu, Testing and modeling of soil-structure interface. J. Geotech. Geoenviron. Eng. **130**(8), 851-860 (2004). https://doi.org/10.1061/(ASCE)1090-0241(2004)130:8(851)
16. G. Zhang, J. M. Zhang, Unified modeling of monotonic and cyclic behavior of interface between structure and gravelly soil. Soil. Found. **48**(2):237-51 (2008). https://doi.org/10.3208/sandf.48.231
17. M. Saberi, C. D. Annan, J. M. Konrad, A. Lashkari, A critical state two-surface plasticity model for gravelly soil-structure interfaces under monotonic and cyclic loading. Comput. Geotech. **80**, 71-82 (2016). https://doi.org/10.1016/j.compgeo.2016.06.011
18. I. P. Damians, S. Olivella, R. J. Bathurst, A. Lloret, A. Josa, Modeling soil-facing interface interaction with continuum element methodology. Front. Built Environ. **8** 842495 (2022). https://doi.org/10.3389/fbuil.2022.842495
19. I. P. Damians, R. J. Bathurst, S. Olivella, A. Lloret, A. Josa, 3D modelling of strip reinforced MSE walls. Acta Geotech. **16**(3), 711-730 (2021). https://doi.org/10.1007/s11440-020-01057-w
20. I. P. Damians, A. Moncada, S. Olivella, A. Lloret, A. Josa, Physical and 3D numerical modelling of reinforcements pullout test. Sci. Report. **14**(1), 7355 (2024). https://doi.org/10.1038/s41598-024-57893-3
21. S. Olivella, A. Gens, J. Carrera, E. E. Alonso, Numerical formulation for a simulator (CODE_BRIGHT) for the coupled analysis of saline media. Eng. Comput. **13**(7), 87-112 (1996). https://doi.org/10.1108/02644409610151575
22. G. R. Lashkaripour, R. Ajalloeian, Determination of silica sand stiffness. Eng. Geol. **68**(3-4), 225-236 (2003). https://doi.org/10.1016/S0013-7952(02)00229-6

Prediction of rainfall induced geosynthetic-reinforced slope instability: machine learning algorithms perspective

Mehrez Jamei[1*], *Mbarka* Selmi[2], *Facker* Hamrouni[3]

[1]Northern Border University, College of Engineering, Civil Engineering Department, Arar, Saudi Arabia
[2]University of Gabes, National Engineering School of Gabes, Modeling in Civil and Environmental Engineering Laboratory, Tunisia.
[3]University Tunis Elmanar, National School of Engineering, Civil Engineering Laboratory, Tunis, Tunisia

Abstract. Rainfall-induced slope instability poses significant challenges in geotechnical engineering, particularly due to the increasing impacts of climate change. Heavy rainfall can trigger landslides, resulting in severe consequences like loss of life and infrastructure damage. Traditional predictive methods often rely on analytical approaches, while elastoplastic models and empirical methods have limitations in accuracy. Geosynthetics, such as geogrids, enhance soil properties, increasing resistance to sliding. Non-woven geosynthetics facilitate drainage to mitigate pore water pressure, thereby reducing failure risk. While previous studies have examined the roles of mechanical reinforcement and drainage separately, few have integrated both. This paper proposes a simplified model to explore the drainage capabilities of geosynthetics through finite element analysis. The study aims to predict slope instability under varying conditions, helping inform risk assessment and landslide mitigation strategies. A machine learning (ML) approach is also employed, utilizing algorithms like Random Forests and Support Vector Machines to analyze large datasets of historical rainfall, soil properties, and landslide occurrences. By training on 70% of the data and validating on 30%, the model can provide valuable insights into the likelihood of slope failures linked to rainfall. This information will be used to assess risk and inform decision-making for landslide mitigation strategies.

1 Introduction

* Corresponding author: mehrez.jamei@nbu.edu.sa

Rainfall-induced slope instability is a significant concern in geotechnical engineering and environmental management particularly in the last decades where the effects of climate changes seem more and more noticeable. Landslides triggered by heavy rainfall can lead to catastrophic consequences, including loss of life, infrastructure damage, and environmental degradation. Traditional methods of predicting slope instability often rely on analytical and numerical methods based on limit equilibrium and limit analysis. Elastoplastic constitutive models have been widely used based on inverse correction analysis as shear strength reduction method implemented in PLAXIS software. Some other empirical models and expert judgment, which can be limited in accuracy and adaptability. Geosynthetics or Geogrids help improve the mechanical properties of the soil, increase resistance to sliding [1], and reduce the risk of erosion [2]. Some geosynthetic products are designed to facilitate drainage [3], allowing excess water to escape from the slope. This is crucial in preventing the build-up of pore water pressure, which can lead to slope failure during heavy rainfall. In addition to slope reinforcement, geosynthetics can help control surface erosion during and after rainfall events, further protecting the slope from instability. Numerous previous studies have independently examined the roles of mechanical reinforcement and drainage [4]. Few of them have made attention by incorporating both drainage and mechanical interactions. In this paper, a simplified model is applied to investigate the drainage performance of geosynthetics, along with their role in mechanical reinforcement and enhancement. . Parametric study has been performed using a finite elements method to prepare sufficient data for machine learning analyses. Slope stability is influenced by various factors, including soil type, moisture content, topography, vegetation cover, and weather conditions [5]. Rainfall plays a critical role by saturating the soil, increasing pore water pressure, and reducing the effective stress within the slope material. As the soil becomes increasingly saturated, its shear strength decreases, making it susceptible to failure. The parametric study concerns the influence of hydraulic characteristics of soil and the non-woven geotextile: saturated permeability, air entry suction value, shape parameter of the water retention curve, initial saturation conditions (saturation water content and degree of saturation) and hydraulic boundary conditions such as the rainfall intensity. Machine learning (ML) algorithms enable the analysis of large datasets that include historical rainfall patterns, soil properties, topographical features, and past landslide occurrences. ML models can reveal complex patterns in the data, enabling reliable predictions of slope instability risk. The proposed paper aims to prepare the necessary data. After training, the model can predict the likelihood of slope instability under varying rainfall conditions. This information can be used to assess risk and inform decision-making for landslide mitigation strategies. Rainfall-induced changes in groundwater levels are a significant factor contributing to slope failures in various regions worldwide [6], where heavy precipitation has severely damaged roads. The installation of geotextile for drainage is proposed as an effective technique to alter flow paths and reduce soil pressure by lowering groundwater levels. This study evaluates the effectiveness of these non-woven geotextile drains in stabilizing residual slopes using a simple physical model, for which an elastoplastic model was also used to study the influence of the rainfall on the stability of soil without any drainage system. This study focuses separately on the water retention properties of various soil types and non-woven geotextiles, characterized by their water retention curves and unsaturated permeability. Utilizing the proposed model implemented in CODE-BRIGHT software, various aspects of drain efficiency are examined through changes in water pressure and displacement fields. Additionally, the paper addresses key parameters that influence soil water retention, such as saturation volumetric water content and air-entry suction. Based on the parametric study and published data on field slopes cases, including both failures non-failures, a ML method is used in the proposed paper. ML algorithms offer a promising alternative, enabling more accurate and dynamic predictions based on large datasets and complex patterns [7]. Simultaneously, based on the assumption of effective stress (see several discussions on its validity) a modified Mohr-Coulomb model has been proposed and implemented in CODE-BRIGHT. This model

includes a non-linear shear strength function that accounts for the impact of pore water pressure on effective cohesion under wet conditions. While significant findings have been made regarding the effectiveness of drains, a substantial gap remains in the literature regarding the relationship between the drainage efficiency and unsaturated soil properties. Therefore, this study aims to investigate the influence of unsaturated soil characteristics on stability of slopes enhanced by non-woven geotextile [8-9]. As noted by Hamrouni et al. (2021) [8], horizontal drains are typically situated in the upper regions of the slope, which is not always necessary. In many cases, the placement of these drains at the slope's surface level effectively reduces groundwater levels, thereby decreasing the risk of slope failure. Furthermore, Cai et al. (1998) [10] emphasized that minimizing the length of horizontal drains can enhance their effectiveness while also reducing the number of required drains. The studies conducted on the impact of horizontal drains (non-woven geotextiles) on groundwater levels indicate that, in general, slope stability improves with the intensity of rainfall, particularly when the water table is closely tied to the saturated hydraulic conductivity of the drains. However, there is limited research on the effects of unsaturated permeability and other properties over time. It is essential to recognize that investigating the efficiency of these drainage systems in the context of slope stability is valuable in geotechnical engineering and transportation planning.

2 Properties of the materials used in the study and Machine Learning interest

2.1 Properties of the materials

2.1.1 Hydraulic and Mechanical Soil properties

At a first step, silty sand and ash are considered as soils utilized to conduct the numerical simulations discussed in this paper. This choice was driven by the need to analyze the failure of the physical slope without any drainage system, caused by excess pore water pressure resulting from infiltration. The water content and displacement evolution were examined separately by [9]. The silty sand was sourced from a landslide site in Omigawa, Japan, while the ash was collected from a landslide location in Cervinara, Italy. As detailed in [8], the testing of two distinct physical models was found on the premise that these models provided well-defined background data. These physical models included not only specific instruments for controlling input data (such as water content, suction, and displacement) but also output data (including water content and soil displacement). Clearly, regarding hydraulic behavior, the two soil types exhibited distinct characteristics influenced by their unsaturated and water retention properties. Specifically, the shear strength parameters were as follows: φ' = 32° and c' = 0 kPa. Figure 1 presents the fitted water retention curves for both soils, highlighting the points representing the Van Genuchten model parameters. Table 1 summarizes the Van Genuchten data for the silty and ash soils. It is important to note the principal water retention curves for each soil type. Additionally, Equation 1 presents the Kozeny model used to estimate the intrinsic permeability of both soil types:

$$k_{sat} = k_0 \frac{n^3}{(1-n)^2} \frac{(1-n_0)^2}{{n_0}^3} \quad (1)$$

The saturated hydraulic conductivity for the silty sand and ash soil are respectively k_{sat} of 1.8 10^{-4} m/sec at a porosity n=0.471 and k_{sat} of 10^{-6} m/sec at a porosity n=0.69. The saturated hydraulic conductivity of the silty soil is also considered. The main mechanical properties of silty sand and ashes are respectively ϕ'=36°, c'=0kPa and ϕ'=38° , c'=0kPa.

Table 1. Van Genuchten equation parameters for both soil types.

Soil Type	Parameters of water retention curve			
	λ	P(MPa)	$S_{resid.}$	S_{max}
Silty sand	0.4	4.0 exp(-5)	0.22	1.0
Ash soil	0.6	9.0 exp(-4)	0.40	1.0

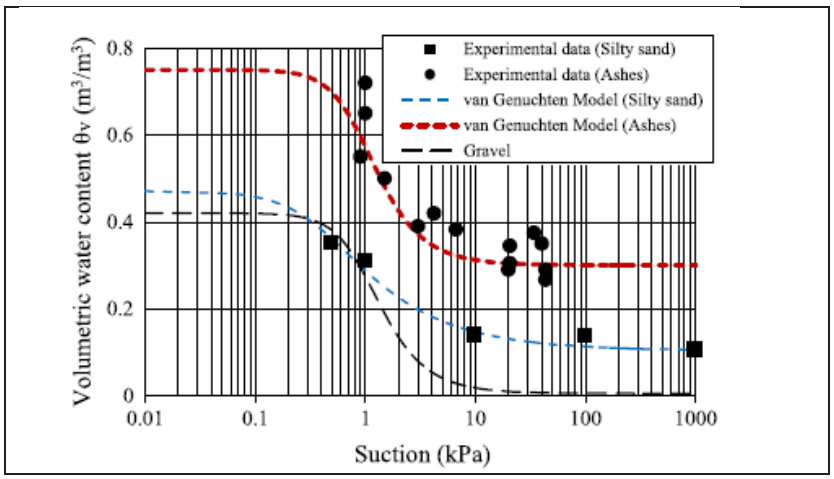


Fig. 1. Water retention curves of the considered soils

2.1.2 Hydraulic properties of the non-woven geotextile

Data provided by different sources ([11-13], giving the measured hydraulic properties of the non-woven geotextiles (saturated permeability, saturated permittivity and water content curve), is used. Nine types of geotextiles with their associated properties are summarized in Tables 2a and 2b.

Table 2a. Physical and saturated permeability of non woven geotextiles

	Geotextile characteristics				
Non-woven Geotextile type	Sample A	Sample B	Sample C	Sample D	Sample E
Type of fibers	Polyester short fibers	Polyester short fibers	Polyester long fibers	Polyester long fibers	Polyester long fibers
Production method	Needle punching and bending	Needle punching	Spun bonding	Spun bonding	Needle punching

Thickness (mm)	3	1.7	0.75	3	4
Surface mass (gr/m^2)	125	300	100	300	400
k_{sat} (m/sec), according to perpendicular direction of non-woven	$1.8\ 10^{-3}$	$3.4\ 10^{-3}$	$2.3\ 10^{-3}$	$1.7\ 10^{-3}$	$1.8\ 10^{-3}$

Table 2b. Physical and saturated permeability of non-woven geotextiles

	Geotextile characteristics			
Non-woven Geotextile type	Sample F	Sample G	Sample H	Sample I
Type of fibers	Polyester short fibers	Polyester short fibers	Polyester short fibers	Polypropylene short fibers
Production method	Needle-punching	Needle-punching	Needle-punching	Needle-punching and spun bonding
Thickness (mm)	2.3	1.8	2.3	3.7
k_{sat} (m/sec), according to perpendicular direction of non-woven	$5.0\ 10^{-2}$	$4.0\ 10^{-3}$	$4.0\ 10^{-3}$	$2.7\ 10^{-3}$
Reference	[11]	[11]	[12]	[13]

The water retention curves, presented in figure 2, were obtained by fitting the experimental data using van-Genuchten equation [14].

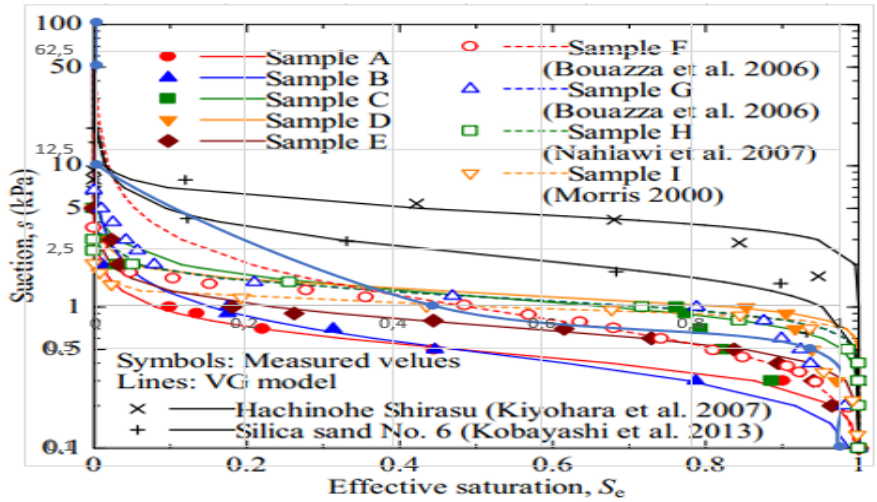


Fig. 2. Water retention curves of the two types of soil and non-woven geotextiles modeled by van-Genuchten model ([14]).

2.2 Brief information about the Machine Learning Algorithms

Random Forest (RF) is an ensemble machine learning technique that enhances predictive accuracy and robustness by combining multiple decision trees in parallel using bootstrap sampling. Each tree is trained on a random subset of the data through a process known as bagging and considers a random selection of influencing factors at each split, which introduces diversity among the trees. The final prediction is obtained by aggregating the outputs of all trees, typically using majority voting for classification tasks. This method helps reduce overfitting and enhances generalization, making RF particularly effective for complex datasets that include both numerical and categorical variables.

3 Physical numerical model and preliminary results

Figure 3 presents a schematic of the geometry used in the modeling. The geometry of the physical model corresponds to the laboratory model presented initially by [9].

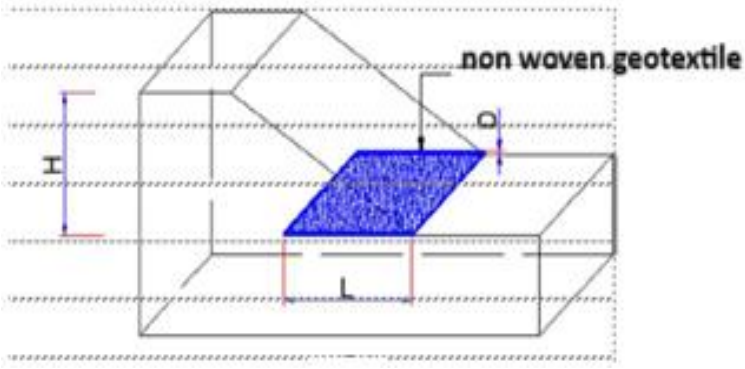


Fig. 3. Schematic of modeled geometry.

In Figure 3, H is the slope's high; L the length of non-woven geotextile and D is the thickness (tables 2a and 2b). Figure 4 gives the mesh implemented in Code BRIGHT and used in simulations, based on the hydromechanical model (see [8]) by varying the mechanical and hydraulic parameters of the soil and geotextiles.

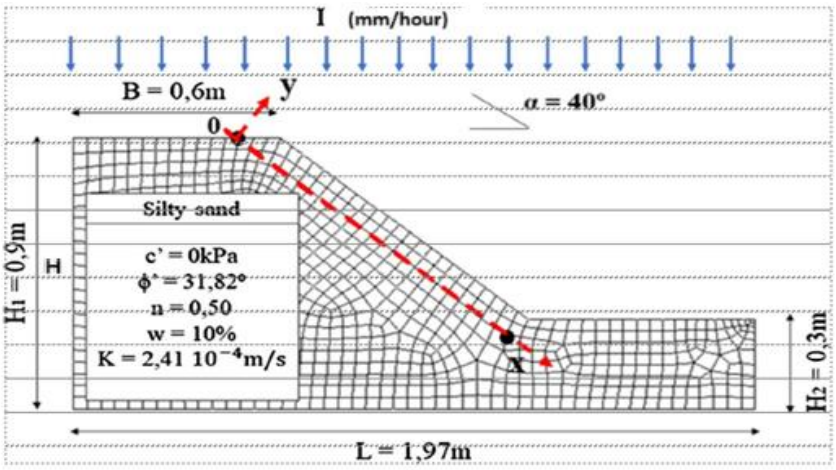


Fig. 4. Finite element meshing and geometric characteristics of the physical model (An example of soil parameters: φ' = 31.82° and c' = 0 kPa, porosity n = 0.5, initial water content ω = 10%, saturated permeability 2.41 10^{-4} m/sec)

3.1 Numerical Results

3.1.1 Role of permeability and permittivity

A series of simulations were conducted on the various types of geotextiles outlined in Tables 2a and 2b. By analyzing the data concerning drainage capacity measured by the discharge value q(l/sec), representative results highlighting the influence of geotextile type, are presented. The analysis focuses on the most effective non-woven geotextile, identified as type A, which demonstrated the best drainage performance.

Figures 5 and 6 depict the discharge during the infiltration period, with a rainfall intensity of 100 mm/min. To assess the variations in the saturated permeability of geotextile type A, Figure 5 reveals a lower performance linked to reduced permeability. Geotextile type A effectively facilitated drainage by 6000 seconds (100 minutes) in a progressive and continuous manner. However, when the permeability is decreased by a factor of ten, the onset of drainage is delayed, beginning at 9000 seconds (150 minutes). The drainage efficiency is also significantly impacted. When permeability is further reduced to 1.8 10^{-5} m/sec, drainage effectiveness is severely compromised.

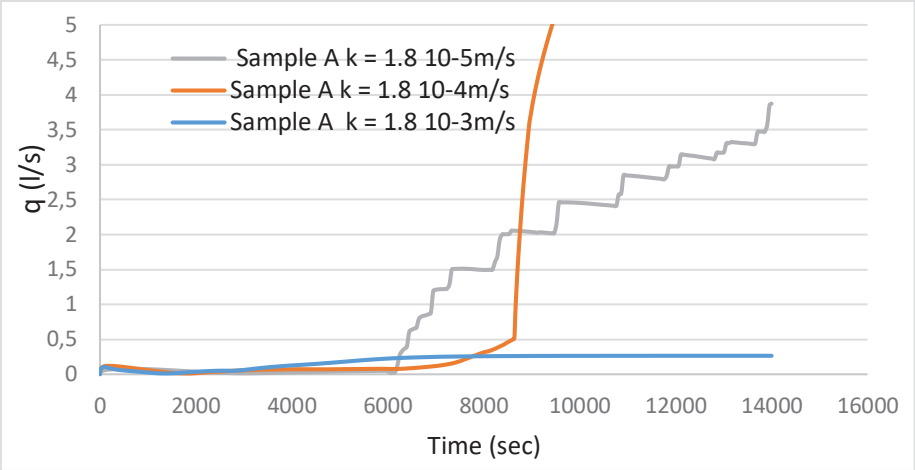


Fig. 5. Discharge of non-woven geotextile vs time: role of the permeability

3.1.2 Role of the permeability and the permittivity

Figure 6 illustrates the capacity of the non-woven geotextile and highlights the influence of permittivity (horizontal permeability). The efficiency of the non-woven geotextile is closely linked to the permittivity value, showing that efficiency significantly declines when permeability falls below approximately 1.8 10^{-4} m/sec.

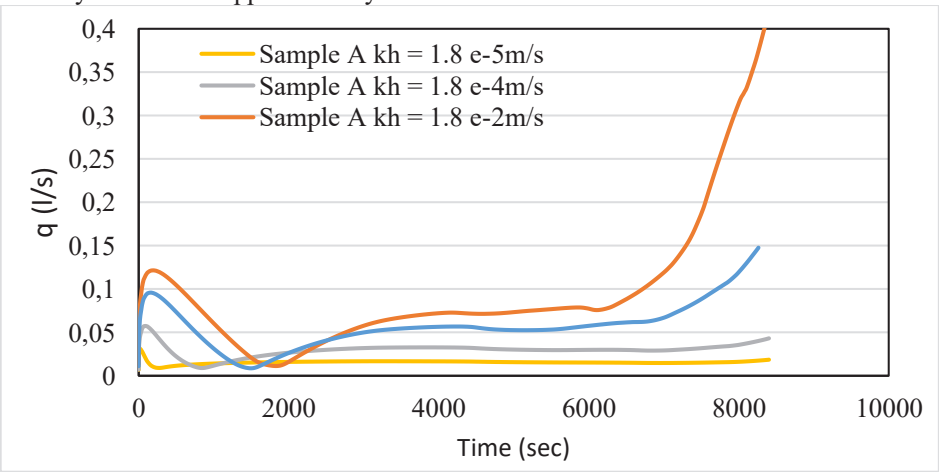


Fig. 6. Discharge of non-woven geotextile vs time: role of the permittivity

3.1.3 Role of the water retention curve

As initial results, the authors present the role of the main parameter of the water retention curve, specifically the shape parameter λ of the water content curve (with a focus on the geotextile A-water curve). Figure 7 clearly illustrates the effect of the shape factor λ on discharge and, consequently, on drainage efficiency.

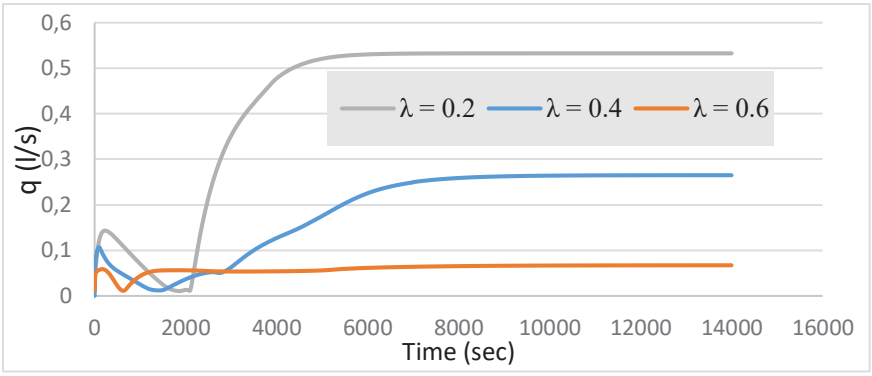


Fig. 7. Discharge of non-woven geotextile vs time: role of the shape factor λ

3.1.4 Role of the water pressure rate (variation of the ground-water level). Machine Learning (ML) prediction

As initial results, the authors present the role of the main parameter of the water retention curve. Several simulations demonstrated that this key parameter significantly influences drainage capacity and the discharge rate, helping to reduce water pressure by decreasing the average value of the water pressure rate r_u, defined as follows:

$$r_u = \frac{\bar{u}_w}{\sigma_v'}(z) \tag{2}$$

Where $\bar{u}_w$ is the average water pressure at a given depth and σ_v' is the effective vertical stress. When varying the following parameters: water pressure rate (r_u), friction angle (ϕ'), cohesion (c'), and geometric parameters of the slope, machine learning algorithms provided a measurement of the linear relationship, as shown in Figure 8. The drainage at the toe of the slope should reduce the effect of r_u and results are expected as follows:

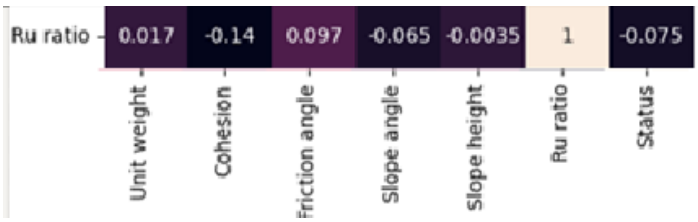


Fig. 8. Water pressure ratio linear correlation with other parameters: Regression coefficient

.

4 Conclusion

The study presents numerical results on the drainage performance of non-woven geotextiles in reducing pore water pressure caused by infiltration during rainfall. The modeling is developed within an unsaturated framework for both soil and geotextile. Unsaturated permeability and water retention curves are incorporated into the hydromechanical modeling proposed in [8] and implemented in the Code Bright software. Results indicate the influence of permeability and permittivity on drainage performance. Drainage effectiveness can be measured through the decrease in pore water pressure. Geotextile type A demonstrated the best performance, significantly reducing the water pressure rate.

References

1. Y. Guo, Y. Xue, Z. Han. Mechanical and deformation behavior of silt reinforced with wicking geotextile: An experimental study, Construction and Building Materials, (2025). https://doi.org/10.1016/j.conbuildmat.2025.141721
2. B. Finklenburg, E.-M. Klopries, H. Schüttrumpf . 2D failure mechanisms and failure modes of a new type of geotextile tubes used for river dikes. Geotextiles and Geomembranes, (2024). DOI: 10.1016/j.geotexmem.2024.03.009
3. J. Wang, R. Anda, Y. Cai Vacuum consolidation of dredged slurry improved by horizontal drainage-enhanced geotextile. Geosynthetics International. (2024). https://doi.org/10.1680/jgein.23.00087
4. Dong-dong Li, X. Cui, Ya-b. Han. An Experimental on Filtration and Clogging of Geotextile Filters around Drain Pipes in Fine Tailings. KSCE Journal of Civil Engineering. May (2024).
5. E. M. Palmeira,V. M. Souza, D. S.C. Santos, I. A.M.G. Góngora. Study on the hydraulic properties of internally unstable soil-nonwoven geotextile systems: Boundary values and preliminary estimates. Geotextiles and Geomembranes, (2025). https://doi.org/10.1016/j.geotexmem.2024.11.002
6. M. Jamei, H. Guiras & S. Olivella. Analysis of slope movement initiation induced by rainfall using the Elastoplastic Barcelona Basic Model, European Journal of Environmental and Civil Engineering. (2015). DOI: 10.1080/19648189.2014.996670
7. S.K Anuragi, D. Kishan, S.K Saritha. Comparative Analysis of Ensemble Learning Approaches for Slope Stability Prediction. SRRG Int. J. Civ. Eng. 11(5), 168-180. (2024).
8. F. Hamrouni, H. Trabelsi, M. Jamei. Numerical Analysis of the Drilled Horizontal Drains Efficiency in Physical Slope Model: The Role of the Soil Water Retention Property. Geotechnical and Geological Engineering 40(4). (2021). DOI: 10.1007/s10706-021-01894-w
9. R. Orenes, K. Farooq and I. Towhata. Deformation Behavior of Sandy Slopes during Rainwater Infiltration. SOILS AND FOUNDATIONS Vol. 44, No. 2, 15-30, Apr. 2004.
10. F. Cai, K. Ugai, A. Wakai, Q. Li . Efects of horizontal drains on slope stability under rainfall by three-dimensional finite element analysis. Computers and Geotechnics 23 (1998) 255-275. https://doi.org/10.1016/S0266-352X(98)00021-4.
11. Bouazza, A., Freund, M. & H. Nahlawi. Water retention of nonwoven polyester geotextiles. *Polymer Testing*, 25 (8), 1038–1043. (2006).
12. H. Nahlawi, A. Bouazza, J. Kodikara. Characterisation of geotextiles water retention using a modified capillary pressure cell. Geotextiles and Geomembranes 25(3):186-193. DOI: 10.1016/j.geotexmem.2006.12.001.
13. C. E. Morris. Unsaturated Flow In Nonwoven Geotextiles. ISRM International Symposium, Melbourne, Australia, November 2000. Paper Number: ISRM-IS-2000-099
14. M. Th. Van Genuchten. A Closed-form Equation for Predicting the Hydraulic Conductivity of Unsaturated Soils1. (1980). Soil Science Society of America Journal 44(5). DOI: 10.2136/sssaj1980.03615995004400050002x

Author Contribution Statement: The authors declare their equal contribution to data analysis, simulations, and the preparation of the manuscript.

SESSION 2 A
SUSTAINABILITY AND DURABILITY (2)

Geosynthetic multilayered composite: innovative development, applications and life cycle assessment

Marianna Ferrara[1]*, and *Giulia* Lugli[1]

[1]Officine Maccaferri Spa, Bologna, Italia

Abstract. Geosynthetics are polymeric products with a long history of use and development to address specific geotechnical needs. The products are typically differentiated into families, such as geotextiles, geogrids, geomembranes and others. These families are characterized by major functions, including separation, reinforcement, filtration, drainage, protection and barrier. Over time, products have been designed to address a wider range of functional issues while streamlining installation, cost-effectiveness and carbon footprint. This paper introduces a multicomposite geosynthetic that can integrate different functions within a single layer. The product's development is outlined, accompanied by an examination of its performance certification, case histories and life cycle assessment in comparison with traditional and standard geosynthetic solutions.

1 Introduction

Conventional civil engineering design has traditionally prioritized functionality, cost efficiency, and safety. However, sustainable engineering introduces a broader scope, emphasizing societal and environmental impacts. The concept of sustainable development, first defined in the 1987 Brundtland Report by the United Nations World Commission on Environment and Development [1], is described as "development that meets the needs of the present without compromising the ability of future generations to meet their own needs." As a result, modern engineering practices increasingly integrate sustainability principles, addressing environmental, social, and economic dimensions.

In the construction sector, there is growing recognition among public administrations, engineers, and stakeholders of the need to adopt sustainable methods that address environmental challenges. This awareness has been heightened by global acknowledgment of the adverse effects of human activity, driving the establishment of international frameworks such as United Nations directives and the Sustainable Development Goals (SDGs). Consequently, there is a shift toward innovative solutions that reduce environmental impacts while adhering to sustainability standards.

The use of geosynthetics in civil and environmental engineering has gained traction due to their durability, cost-efficiency, and sustainability attributes. Despite their advantages in diverse applications, quantitative comparisons between geosynthetics and conventional engineering methods remain limited in practice.

* Corresponding author: m.ferrara@maccaferri.com

2 Multilayered composite development

Geosynthetic composites that integrate multiple functions offer significant advantages over traditional mineral-based materials, particularly from environmental and economic perspectives. These advanced systems fulfill combined roles such as reinforcement, drainage, filtration, and moisture barrier functions, presenting a modern alternative to construction practices that rely on extensive extraction, transportation, and use of natural resources like gravel, sand, and clay. By reducing the depletion of finite mineral reserves, lowering greenhouse gas emissions associated with transportation, and minimizing ecological disruption from quarrying, geosynthetic composites greatly reduce the environmental footprint of construction projects. Additionally, their extended service life and durability decrease maintenance requirements, minimizing waste and conserving resources over time.

Economically, geosynthetic composites provide a cost-effective solution that lowers both initial and lifecycle expenses. Traditional approaches often require large volumes of material to achieve the desired functionality, resulting in higher transportation and installation costs. In contrast, geosynthetics are lightweight, easy to handle, and require less energy and labor during installation. Their multifunctionality within a single material also eliminates the need for separate components, simplifying construction processes and reducing costs further. The long-term reliability of these materials translates into decreased maintenance expenditures, offering significant financial benefits over time. Combining these environmental and economic advantages, geosynthetic composites align seamlessly with sustainable development principles, providing an advanced and practical alternative to traditional methods.

The multilayered geosynthetic system (Fig.1) examined in this study highlights a sophisticated engineering solution for landfill applications. This system integrates multiple critical functions, including separation, drainage, erosion control, and soil reinforcement, within a single composite.



Fig. 1. Multilayered geocomposite for landfill capping.

A needle-punched, thermo-calandered nonwoven geotextile component enhances filtration and separation by preventing material intermixing. A polypropylene (PP) extruded monofilament drainage core, designed with a “W-shaped” cross section and longitudinal parallel channels, delivers in-plane drainage, efficiently directing rainwater to the capping layer base and reducing infiltration into the underlying waste. Additionally, a three-dimensional (3D) monofilament geomat reinforced with a polyethylene terephthalate (PET) geogrid serves as an anti-erosion layer, stabilizing the soil veneer and mitigating stress on natural slopes from the overlying soil cover. This integrated approach underscores the

potential of advanced geosynthetic systems to address the complex challenges of landfill engineering effectively and sustainably.

3 Cases for LCA

A Life Cycle Assessment (LCA) was performed using the One Click LCA platform to evaluate and compare the environmental impacts of two technical solutions for capping systems in non-hazardous landfills. Importantly, the scope of the LCA encompasses the entire capping structure above the impermeabilization layer, meaning that the impermeabilization package itself is not included in the LCA boundary. This exclusion ensures consistency in the comparison, as the impermeabilization layers are common to all three solutions and do not influence the relative environmental performance of the drainage and reinforcement components. The two solutions are: Solution A, a traditional design featuring a 50 cm mineral drainage layer (typically sand or gravel), commonly used in standard landfill cover systems, and Solution B, which employs the geosynthetic multilayered composite mentioned before. The capping systems assessed are designed in compliance with the European Council Directive 1999/31/EC [2] on the landfill of waste, particularly concerning engineering requirements for final cover systems. Figures 2 and 3 illustrate the technical configurations of these systems.

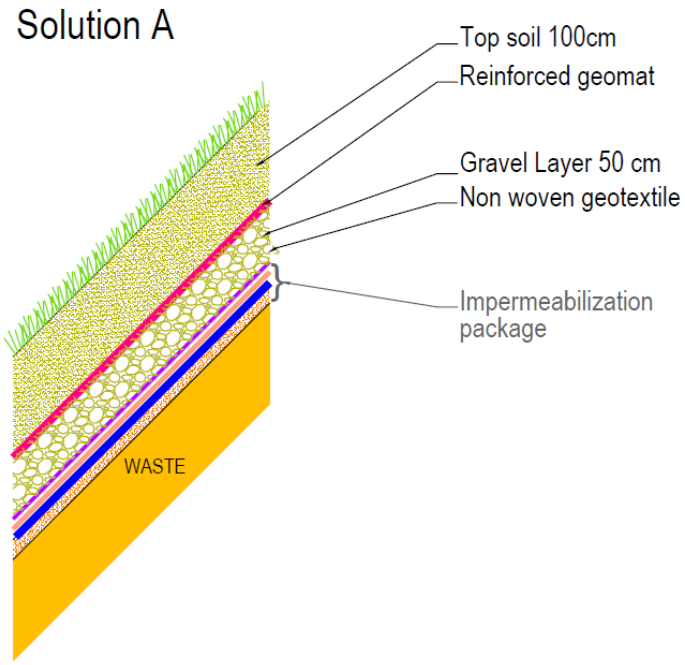


Fig. 2. Capping with 50cm mineral material as drainage layer.

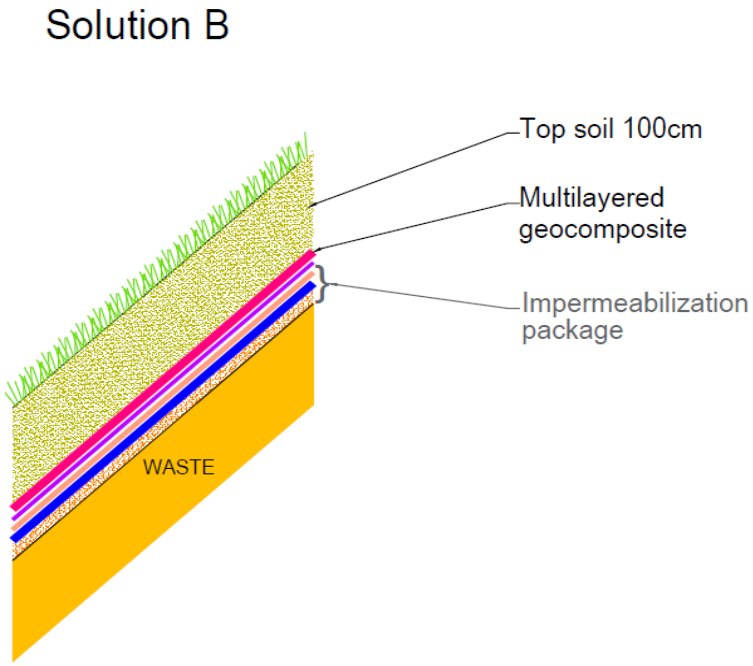


Fig. 3. Capping with a geosynthetic multicomposite as drainage layer and reinforced geomat.

The assessment was conducted in accordance with ISO 14040 and ISO 14044 standards [3, 4], covering the lifecycle of the materials and systems involved, from raw material extraction and manufacturing to transportation and installation phases. By leveraging extensive Environmental Product Declaration (EPD) databases and industry-specific modules [5, 6], One Click LCA facilitates the analysis of carbon footprints, energy consumption, resource efficiency, and other critical environmental indicators across the lifecycle stages of materials and systems.

The drainage performance equivalence between, 50 cm mineral drainage layer (minimum prescribed by EU Directive 1999/31/EC) in the traditional solution and the 8 mm thick drainage geocomposite part of the multicomposite, was verified based on the procedures outlined in ISO/TS 18228-4:2022 (Design using geosynthetics — Part 4: Drainage systems). This standard was used to evaluate the drainage capacity of geosynthetic solutions versus traditional mineral-based systems, ensuring consistent functional outcomes across all assessed alternatives.

To extend the scope of the study, a third alternative, Solution C, was introduced for comparative analysis. Solution C employs multiple separate layers of geosynthetics to fulfil the same functional requirements as the geosynthetic multilayered composite of Solution B. A significant advantage of the multilayered composite lies in its optimized performance, as its components are specifically engineered to operate synergistically. For instance, the drainage layer in Solution B not only facilitates effective water channelling but also supports the erosion control layer, ensuring efficient water management and slope stabilization. This integrated design mitigates the risks of system failure typically associated with poorly matched or interacting components.

Moreover, the multilayered composite structure offers additional benefits by requiring reduced material thickness compared to the layered assembly of separate products, thereby yielding material savings and reducing overall system weight. This reduction in weight translates to lower transportation costs and diminished stress on underlying layers or slopes. By consolidating multiple functionalities into a single, robust product, multilayered

composites present a cost-effective and environmentally sustainable solution that surpasses the performance of conventional multi-material systems in landfill capping applications.

4 Results and Discussion

The LCA results provide quantitative comparisons across key environmental categories, with Global Warming Potential (GWP) serving as a primary indicator. The figure below (Fig. 4) summarizes GWP contributions for each solution across major lifecycle phases. During the A1–A3 product stage, which accounts for raw material acquisition and manufacturing, Solution B demonstrated significantly lower GWP contributions than Solution A. This reduction is attributable to the lightweight and low-volume nature of polymer-based geosynthetics versus the high-density bulk materials required for mineral layers. In the A4 transport phase, Solution A showed a disproportionately high contribution to GWP, further reinforcing the environmental burden associated with hauling heavy mineral aggregates over long distances. The A5 construction phase also showed marked advantages for Solution B, primarily due to simplified logistics and mechanization during installation. Overall, this lifecycle breakdown highlights that environmental savings are not confined to a single phase but are distributed throughout the full system deployment.

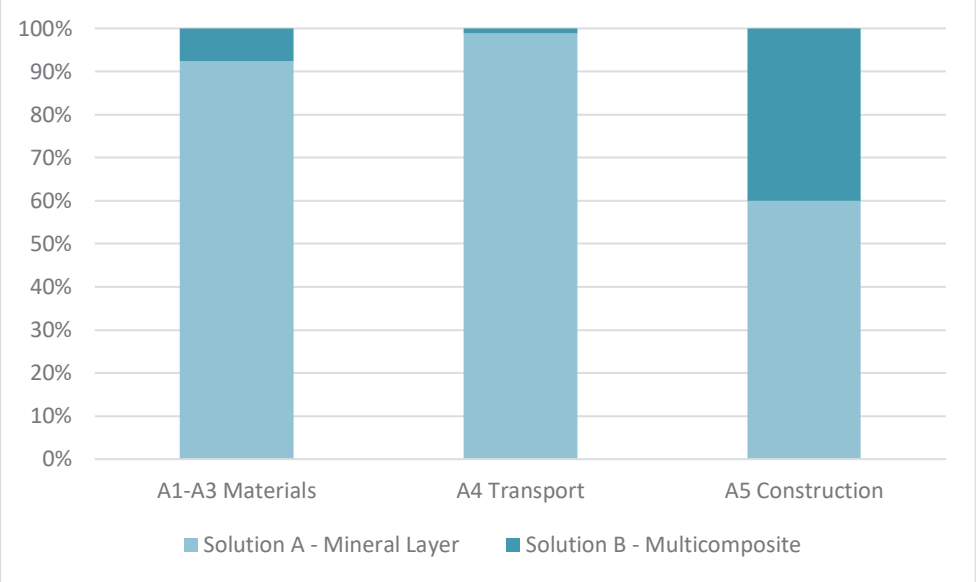


Fig. 4. Global Warming Potential percentage for each life-cycle stage analyzed.

Solution A, which utilizes a traditional 50 cm mineral drainage layer, exhibited the highest total GWP—estimated at approximately 118 kg CO_2-eq/m²—primarily due to the intensive extraction, processing, and transportation of gravel. Solution B, incorporating a geosynthetic multilayered composite, resulted in the lowest GWP (~7.501 kg CO_2-eq/m²) due to its integrated design, substantially lower material volume, and reduced transportation loads. A total landfill capping area of 10,000 m2 was considered to calculate these values.

In terms of installation-related emissions, Solution B once again proved superior. The prefabricated nature of the multilayered composite contributes to a 40–50% reduction in installation time, fewer heavy equipment operations, and lower fuel consumption compared to both mineral-based and separate-layer solutions. Fig. 5 quantifies the relative GWP impact during the construction stage (A5) for all three solutions. Solution A contributed 41% of total installation-related emissions (~0.18 kg CO_2-eq/m²), reflecting intensive use of heavy

machinery and prolonged site activity. In contrast, Solution B required significantly less construction effort, contributing only 27% (~0.12 kg CO_2-eq/m²), while Solution C, with its multiple components requiring sequential placement, fell in between at 32% (~0.14 kg CO_2-eq/m²) This analysis reinforces the operational efficiencies of integrated geosynthetic systems during field implementation.

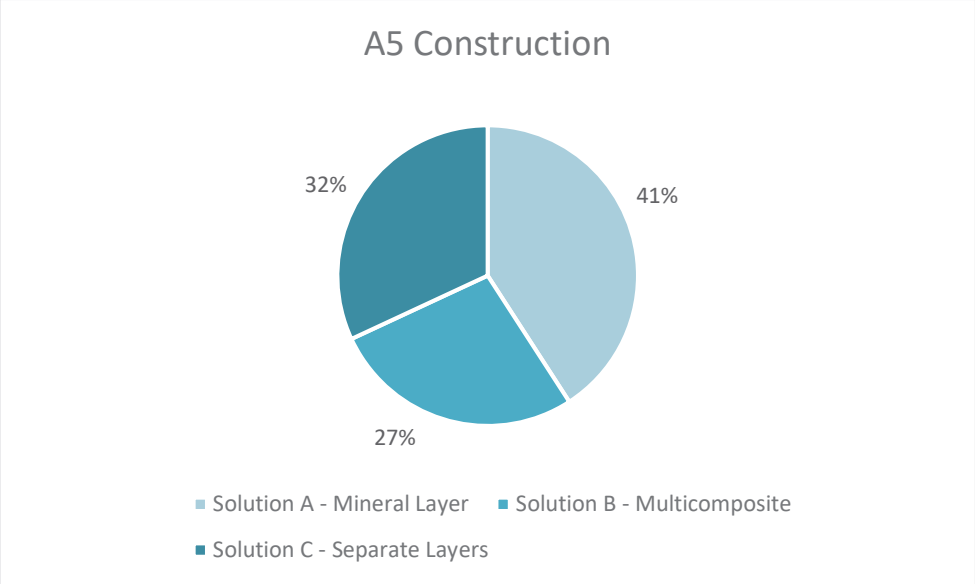


Fig. 5. Global Warming Potential percentage during installation for each solution.

Beyond global warming potential, Fig. 6 expands the assessment to encompass other environmental performance indicators, including ozone depletion (ODP), acidification (AP), eutrophication (EP), photochemical ozone creation (POCP), abiotic resource depletion (ADP), and water use. In nearly all categories, Solution B exhibited the lowest relative environmental burden, especially in categories linked to raw material production and resource extraction. For instance, in EP – Freshwater, EP-Marine and EP-Terrestrial, which reflect nutrient runoff and ecosystem eutrophication, the geosynthetic composite showed significantly reduced impacts compared to mineral-based and multi-layer synthetic alternatives. This comparison confirms that the environmental benefits of geosynthetic composites extend far beyond carbon emissions, providing broad-spectrum improvements in sustainability.

Moreover, Solution B reduced overall system weight by 60–70%, which translates to lower transportation emissions and reduced mechanical stress on landfill slopes—critical for long-term structural integrity and settlement control. Other LCA metrics such as cumulative energy demand, water usage, and raw material depletion further reinforced the sustainability of Solution B. For example, energy savings of up to 45% were observed compared to the conventional gravel-based system, driven by reduced processing and handling of heavy mineral materials.

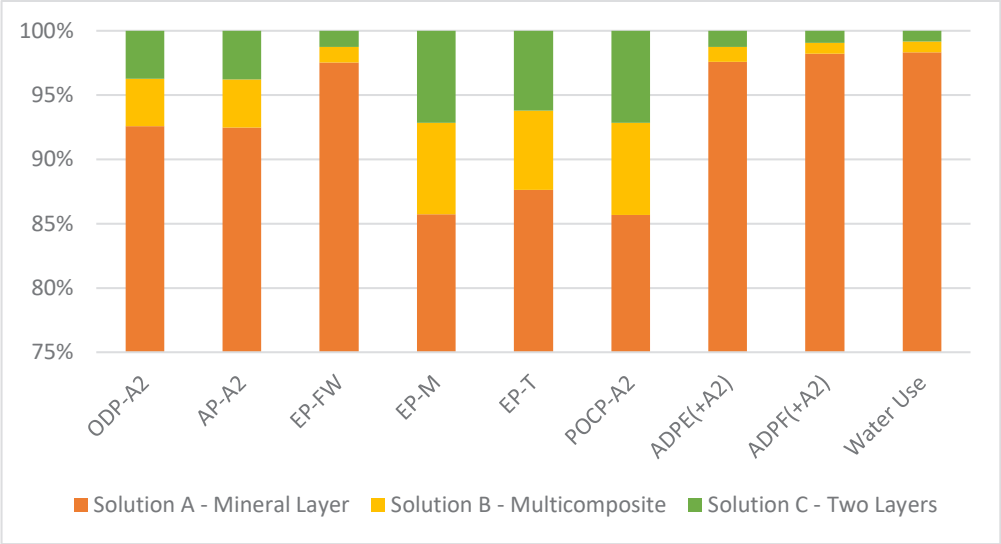


Fig. 6. Lifecycle impacts by solution as staked columns.

5 Conclusions

Using a multilayered composite in capping applications offers numerous advantages over employing separate products for each required function. One of the most significant benefits lies in the seamless integration of multiple functionalities—such as separation, drainage, erosion control, and reinforcement—into a single system.

This integration reduces material usage and simplifies installation, leading to considerable cost and energy savings. Furthermore, multilayered composites mitigate ecological degradation by reducing the need for materials such as sand, gravel, and clay, which are commonly extracted for conventional applications. Decreasing the extraction of these resources preserves natural ecosystems and minimizes disturbances caused by quarrying and mining activities.

The enhanced durability and extended service life of geosynthetic composites reduce the frequency of replacements and waste generation over time, further contributing to their sustainability credentials. Life cycle assessments have demonstrated the substantial environmental and economic benefits of these innovative materials, emphasizing their critical role in advancing sustainable engineering practices.

The findings of this study underscore the importance of adopting multilayered geosynthetic systems as a standard in landfill capping and beyond. Their broad applicability, environmental advantages, and cost-efficiency align with global sustainability goals, marking them as a cornerstone of modern civil and environmental engineering. Future research should explore the optimization of these systems across different geotechnical applications and regions, further reinforcing their role in sustainable infrastructure development.

References

1. United Nations World Commission on Environment and Development. (1987). Our Common Future (The Brundtland Report). Oxford: Oxford University Press.
2. European Council. (1999). Council Directive 1999/31/EC of 26 April 1999 on the landfill of waste. Official Journal of the European Communities, L 182, 1–19.

3. International Organization for Standardization. (2006). ISO 14040: Environmental Management – Life Cycle Assessment – Principles and Framework. Geneva: ISO.
4. International Organization for Standardization. (2006). ISO 14044: Environmental Management – Life Cycle Assessment – Requirements and Guidelines. Geneva: ISO.
5. Environmental Product Declaration of MacMat Geomat
6. Environmental Product Declaration of MacDrain W Drainage Geocomposite
7. International Organization for Standardization. (2022). ISO/TS 18228-4: Design using geosynthetics — Part 4: Drainage systems. Geneva: ISO.
8. Stolz, P., R., Frischknecht., Stucki, M., Busser, R., Itten, R., Frischknecht, R., & Wallbaum, H. (2019). Comparative life cycle assessment of geosynthetics versus conventional construction materials. European Association of Geosynthetic Product Manufacturers.

Potential release of microplastics from geosynthetic applications: a case study in Europe

Daniele Cazzuffi[1*], *Simon* De Meyer[2], and *Francesco* Fontana[3]

[1]CESI SpA, Italy
[2]Beaulieu International Group, Belgium
[3]A&B srl, Italy

Abstract. The theme of microplastics (MP) emissions is one of the focuses of possible environmental concerns when using geosynthetics in the civil engineering applications. For the construction of a new aircraft parking apron at the Ostend airport in Belgium, a relevant amount of gravel has been replaced with an appropriate woven geotextile for stabilizing the ground. The initial consideration for this decision was essentially due to the important economic and ecological advantages in terms of material savings, time needed for the installation and the overall construction costs. This paper reports the successive analyses showing a very relevant saving in CO_2 emissions (more than 77%), which would justify by itself the solution with geosynthetics, if compared with the use of granular material. The specificity and precision of the data available allowed the calculation of a dramatic saving (more than 97%) also in terms of MP emissions, due to the spare of trucks for the transport of materials, preventing also the MP formation connected to the truck's tires wearing.

1 Introduction

The Ostend-Bruges airport is located in Flanders, a region of Belgium, and acts both as a passengers and cargo operations. The cargo traffic in 2022 has been about 52 000 metric tons, while passengers traffic reached around 370 000 persons. The Ostend Airport continues to grow and fully commits to sustainability. In fact, during the autumn of 2023, over 60 000 solar panels are installed, providing the airport and the surrounding area with green energy. In this perspective, since April 2021 major works have been executed to renovate aircraft parking apron 2, to extend its service life by 40 years [1-2].

The project of aircraft parking renovation, consisting of 2 phases, was finalised in the summer of 2022. During the initial phase of the project, the eastern section of the air parking area was broken up and consequently only the western part remained in use for air traffic. After excavation, a woven geotextile was placed on the gravel base layer. On top, a sub-foundation layer composed of crushed concrete (0.20 m) and a foundation layer made of lean concrete (0.28 m) were constructed, see Figures 1 & 2. To finish, a concrete layer of 0.30 m thickness was poured on the foundations. In between the top and sub-layer, a thin bituminous interlayer was applied. This multi-layer approach is crucial to ensure the necessary load-bearing capacity for accommodating heavier aircrafts. The second phase, taking place from Jan 2022, focused on the renovation of the western part. Throughout this period, aircrafts were already able to utilize the renovated eastern part of the aircraft parking area [2].

* Corresponding author: daniele.cazzuffi@cesi.it

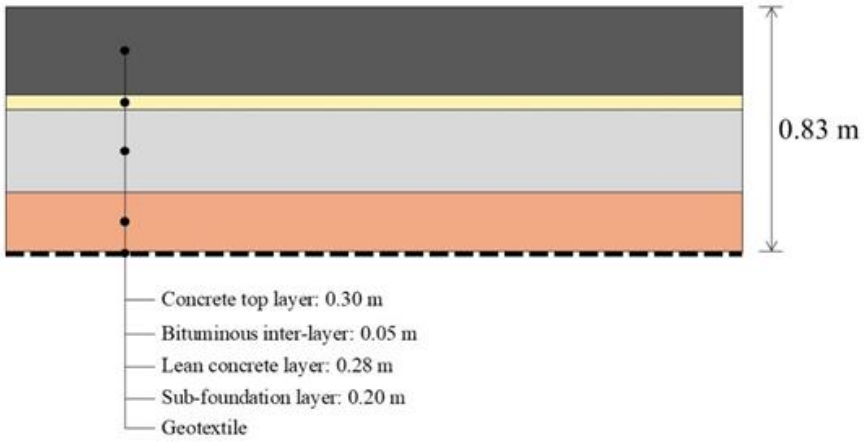


Fig 1. Cross section of the Ostend airport parking apron

1.1 Sustainability

The owners and the contractor paid a lot of attention to the sustainability themes and built a concrete plant able to produce up to 1000 m³ of concrete per day right close to the work site. In the context of circularity and sustainability, the broken-out concrete from the old pavement has been recycled by a COPRO-certified mobile crusher into 0/40 concrete aggregate reused in the foundation and sub-foundation layers of the aircraft parking apron. Thanks to this reuse, the broken-out concrete did not need to be transported to another site, and no new (sub) foundation materials needed to be supplied for the project. This on-site way of working reduces the number of trucks on the road needed to implement this project and significantly improves the environmental impact. The airport had to remain fully operational during the works, compelling the engineers to look for the quickest and still perfectly safe technical solutions [2].



(a) (b)

Fig. 2. An aerial (a) and ground (b) snapshot of the Ostend airport (Copyright: Ostend-Bruges Airport)

1.2 Geotextile benefits

The reinforcement of the sub-base layer aims to improve the load transfer on the track bed, and to limit differential settlements. The choice to use a geotextile to perform this function has been made because of many benefits, when compared to the alternative technical solution with a traditional layer of 0.10 m of gravel. The first benefit was the economic saving, then the time saving in installation, and, last but not least, the much lower environmental impact. The choice of the appropriate geotextile has been taken according to the recommendations of COPRO PTV 829, reported in table 1, identifying the type 2.6. As a result, the woven geotextile Terralys LF57/57 has been chosen [3].

Table 1. COPRO PTV 829 specifications in comparison with TDS of the selected woven geotextile

Characteristics	Method	Unit	Specifications PTV 829 – Table 2 Type 2.6	Measured properties of the selected geotextile
Tensile strength	ISO 10319	kN/m	≥50	57
Elongation	ISO 10319	%	≥10	14
Resistance to static puncture	ISO 12236	kN	≥3	5,6
Dynamic perforation resistance	ISO 13433	mm	≤14	9
Characteristics opening size (O_{90})	ISO 12956	µm	$O_{90}/d_{90} \leq 2$	$O_{90} = 190$ $d_{90} \geq 95$
Water permeability	ISO 11058	10^{-3} m/s	≥16	22

2 Environmental impact comparison

The benefits of using a geosynthetic compared to alternatives has already been proven in several papers, also on behalf of various associations, such as the International Geosynthetics Society (IGS) and European Association of Geosynthetics Manufacturers (EAGM) [4]. In line with previous cases, this Ostend project offered the chance to calculate with a very good approximation the environmental impacts of the alternative solutions without and with geotextiles, both in terms of CO_2 emissions and in terms of microplastics (MP) emissions.

2.1 CO_2 emissions savings

2.1.1 Solution with gravel

The area interested by the work is about 160 000 m². In terms of materials, the traditional solution with 0.10 m of gravel would have implied the use of:

$$160\,000\ m^2 \times 0.10\ m = 16\,000\ m^3 \text{ of gravel}$$

16 000 m³ of gravel at 1.5 ton per m³ gives a mass of 24 000 tons. The Global Warming Potential (GWP) of a ton of gravel is of 2.4 kg CO_{2eq} (average of 4 gravel EPDs available on the internet) [5].

The total emission of CO_{2eq} for the production of the necessary gravel amounts then to

24 000 x 2.4 kg = **57.6 tons**

Coming to the transport, the average truck load of 25 tons implies the use of

24 000 / 25 = 960 trucks

The traffic generated by the supplying of the gravel can be calculated knowing that the distance of the nearest quarry to source the gravel is 110 km from the work site of Ostend.

960 truck roundtrips of 110 x 2 km make a total of 211 200 km.

The consumption of diesel fuel per km of a heavy truck is 1 liter per 2.5 km, so the total need of fuel for the transport is:

211 200 km x 0.4 litres/km = 84 480 litres

For diesel fuel the emission of CO_2 is 2.5 kg per litre, leading to a figure of emission for the transport of the gravel to:

84 480 litres x 2.5 kg/litre = **211.2 tons**

A further emission of CO_2 is determined by the necessity to laying and compacting the gravel. With a productivity of 5.5 m^3 per hour, communicated by the contractor, a caterpillar has to work for 2 880 hours to lay and compact 16 000 m^3 of gravel with a consumption of 10 litres of diesel fuel per hour, it means 28 800 more litres of diesel fuel. The emission of CO_2 related to the installation is then:

28 800 litres x 2.5 kg/litre = **72 tons**

The total emission implied by the use of gravel amounts to

Production	tons 57.6
Transport	tons 211.2
Installation	tons 72
Total	**tons 340.8**

2.1.2 Solution with geotextile

The amount of geotextile needed is a little higher than the nominal surface, taking into account about 0.10 m of overlapping, so that the quantity considered has been 163 200 m^2. 163 200 m^2 of geotextile with a nominal area mass of 228 g/m^2 correspond to a mass of 37.21 tons. The global warming potential (GWP) of a ton of the selected geotextile is of 2 030 kg CO_{2eq} (see Figure 3) [5].

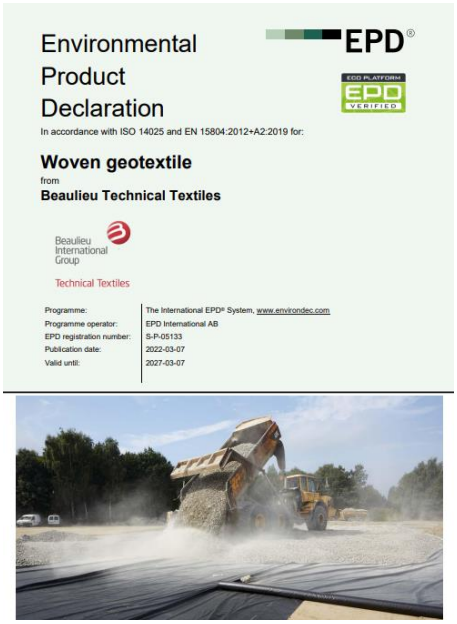


Fig. 3. Environmental Product Declaration (EPD) of the selected woven geotextile from Beaulieu Technical Textiles. [5]

The total emission of CO_{2eq} for the manufacturing process of the necessary geotextile amounts then to

37.210 x 2.030 = **75.54 tons**

Coming to the transport, the average truck load of 12 tons, implies the use of

37.210 / 12 = 3 trucks

The traffic generated by the supplying of the geotextile can be calculated knowing that the distance of the factory is 90 km from the work site in Ostend.

3 truck roundtrips of 90 x 2 km make a total of 540 km

Let's keep the consumption of diesel fuel per km of a heavy truck is 0.4 litres, even if the load per truck is one half if compared with gravel, so the total need of fuel for the transport is:

540 km x 0.4 litres/km = 216.8 litres

For diesel fuel the emission of CO_2 is 2.5 kg per litre, leading to a figure of emission for the transport of the geotextile to:

216.8 x 2.5 = **0.542 tons**

No further emission of CO_2 is determined by the installation phase, done by hand. The emission of CO_2 related to the installation is then:

163 200 m^2 x 0 = **0 tons**

The total emission implied by the use of geotextile amounts to

Production	tons 75.54
Transport	tons 0.542
Installation	tons 0
Total	**tons 76.08**

Resuming the comparison between the two solutions, the CO_2 emissions are:

With gravel:	340.8 tons
With geotextile:	76.08 tons

The choice of the solution with geotextiles has made possible a saving of 264.72 tons of CO_2, meaning a saving of **77.7%** of emissions.

2.2 Microplastics (MP) emissions savings

The big saving in terms of CO_2 emission could already be considered more than sufficient to justify the choice of a geotextile instead of gravel, but it has been considered important to make an assessment also in terms of microplastics (MP) emission, as this could be seen as a possible weak point for the application of geotextiles. Not so many specific and reliable studies on the release of microplastics from geotextiles are available in the literature yet, but it is possible to refer to existing assessments with opportune observations.

Of course, some MP emission is expected to occur by using a polymeric geotextile, but, as we have seen for the case of CO_2 emissions, the focus has to be driven on the comparison with the available alternative technological solutions that could be adopted to reach the desired development goal. Many studies have shown that the main source of MP in the oceans and in the environment at large is due to the consumption of the tires of the vehicles [6]. The rate of MP production due to tires consumption is deeply investigated and could be also detailed by the type of vehicle. With reference to the previous calculation of the traffic determined by the solutions with gravel or with geotextiles, it's easy to calculate in weight the amount of MP determined by the tire consumption. Following Baensch-Baltruschat et al. (2020) [7], we consider a rate of consumption of 1.092 g per km for a heavy truck with 10 wheels. This leads to calculate for the case of our project:

960 trucks x 220 km x 1.092 g = 230.63 kg with the use of gravel

3 trucks x 180 km x 1.092 g = 0.59 kg with the use of geotextile

Let's front now the much more challenging calculation of the emission of MP due to the use of the geotextile. It is possible here to refer to the recent study of Gustavsson et al. (2022) [8], a specific report requested by the Swedish government, after the inclusion of geotextiles in a list of possible MP sources by a study of the European Commission. This report leads to an estimation of two scenarios with an annual emission from a minimum of 0.013% of the product's weight, to a max emission of 0.2% in the worst possible case. Both scenarios do consider the exposure to degradation factors and relate the assessed emissions to the whole quantity estimated for the market.

The Swedish study also makes some assumptions about the cumulative release of MP vs. time, by analysing the case of application in the coastal protection, which is considered as the most aggressive case for geotextiles, in case of potential MP release, because both the exposure to UV and the possible mechanical abrasion could be assimilated to the one of tires. Let's examine the nature of these assumptions, and if and how they are applicable to our case, so to come to an estimation of the potential MP release in the specific case of Ostend project.

2.2.1 Service life and physical life

The service life of a geosynthetic is regulated in Europe according to the annex B of the specific Harmonized Standard, i.e. EN 13249 (2016), and it requires a minimum residual tensile strength of 50% after a determined time of accelerated oxidation process, in order to enable the manufacturers to declare 100 years of service life [9]. The Swedish report refers to this determined time applying a safety factor, that reduces the service life to one half (50%) in the worst scenario or to 80% in the "more likely" scenario. It should be noted that the figure in the harmonized standards is already quite prudential and conservative, as it has been set for engineering purposes, i.e. the survivability of a specific infrastructure for at least a century. According to Scholz et al. (2020), the half-life for the 50% reduction of the mechanical properties of a virgin polypropylene (PP) geotextile can be estimated in around 330 years [10].

It is worth to highlight that this indication, as well as the one of 100 years in the European harmonized standards, refers to the service life, and it has not to be confused with the physical life of the product: the loss of 50% of the mechanical performance cannot be proportioned to a corresponding physical fragmentation of the product.

2.2.2 Degradation factor

In the Swedish report, the main reason for the degradation of a geotextile is assumed as the action of UV oxidation, followed by possible abrasion for the case of hydraulic applications, mainly for coastal protections. A further factor for the durability reduction is considered by assuming a correct installation of the geotextile itself in the jobsite, even if they are reported in the obligatory accompanying document called Declaration of Performance.

In front of this remark, it has to be considered that the geotextiles allowing a service life expectation up to 100 years for sure do contain UV stabilizers, and the indication of max 30 days of exposure after the laying of the rolls on site indicates the start of a possible degradation due to the UV action, where, again, the potential degradation refers to the mechanical properties, not to the physical disintegration of the products.
This is valid in general terms, though in the case of the Ostend project we are examining, the UV matter has not been an issue at all, as the woven geotextile has been covered within the indicated terms, nor any remarkable abrasion can be considered, due the specific type of stress to which the geotextile is subjected, completely different from coastal applications.

It is worth to observe that MP are defined as fragments of bigger pieces of plastics, and they do not have to be confused with the substances possibly deriving by the decay of a polymer or its additives. This point is relevant when possible dangerous substances could be released by any product, but the topic here is other than MP release, and has to do with the ingredients constituting a product, not with the product's fragments as such. Many geotextiles are approved for the use in contact with drinkable water after severe control procedures of their chemical recipes, thus excluding absolutely the theoretical possibility of releasing dangerous substances, even in case of degradation.

2.2.3 Structure of the geotextile

When discussing about geotextiles, for the sake of simplicity, the Gustavsson et al. report does not distinguish among their constitutive polymers, nor among their internal structure, i.e. if wovens or nonwovens [8]. As a matter of fact, the structure of a geosynthetic plays an important role in its possibility to be prone to the mechanical and chemical injuries, and to photo-oxidation as well.

A nonwoven geotextile is made by a very high number of fibres, bonded by essentially three methods:

- heating

- needle-punching
- needle-punching and thermosetting

These structures are very different one to each other, and even much more different from a woven geotextile made with slit films, where no use of fibres is contemplated, Figure 4.



(a) (b)

Fig. 4. (a) woven geotextile, (b) nonwoven geotextile

Even the ratio between the mass per unit area and the surface exposed to oxygen varies very significantly depending on the structure of the product. Depending on the titre of fibres used (4.4 or 6.7 dtex), a PP nonwoven product with a mass per unit area of 228 g/m^2 presents from 8 to 10 times higher surface exposed to oxidation, compared to a slit film woven geotextile of the same mass per unit area.

2.2.4 Microplastics (MP) calculations

All of these observations lead to assess for our specific case an extremely low possibility of MP release, both in quantity and in time terms, because:

- There has not been any UV exposure longer than 30 days.
- The application excludes any movement causing abrasion.
- The temperature conditions are not extreme.
- The chemical environment is not aggressive.

As we have seen, the average figure of MP emission proposed by Gustavsson et al. (2022) as a “more likely” scenario of possible release, for any application and product, is already quite prudential in the direction of a high emission. By adopting it for assessing our case, the structure of the woven geotextile adopted in our project represents a further safety factor.

Still, by applying the indicated percentage of 0.013% to the quantity of 37 210 kg of PP woven geotextile, we obtain a theoretical possible MP release of 4.837 kg to be added to the quantity due to the tire consumption in connection with the geotextile transportation from the manufacturer factory to the jobsite.

This leads to a total potential emission due to the application of geotextile of:

Transport	kg	0.590
Product’s release	kg	4.837
Total	kg	5.427

This figure should be compared to the one due to the transport of the gravel (even without taking into account the extraction phase):

Gravel	kg	230.630

Geotextile	kg	5.427
Saving	kg	225.203

Therefore, the choice of the solution with geotextile has made possible a saving of 225.203 kg of microplastics, meaning a saving of at least **97.65%** of MP emissions, if compared with the solution with gravel.

3 Conclusions

For a project extending the aircraft parking apron of the Ostend airport in Belgium, two alternative technical solutions for stabilizing the foundation soil have been assessed in terms of environmental impacts due to total CO_{2eq} emissions and microplastics MP emissions: with a gravel layer, and with a geotextile layer. The adoption of the solution with a PP woven geotextile has led to very significative reductions of the impacts, particularly if compared to the traditional approach using a 0.10 m layer of granular material.

CO_2 emission has been reduced by 77.7%

Microplastics (MP) emission has been reduced at least by 97.65%

In conclusion, it is possible to assert that, in most of present applications, geosynthetics do represent a technology able to reduce the impact of the civil engineering projects both from the CO_2 and from the microplastics emissions point of view. Moreover, it's also important to note that - in the most probable future scenarios - geosynthetics will play a fundamental role also for allowing adequate constructions on derelict lands, where a lot of microplastics could be retrieved [15] and where geosynthetics will be also able to properly solve the environmental issues related to the confinement of the polluted soils.

References

1. Ostend-Bruges airport, Ostend-Bruges airport to become Belgium's second largest solar park, www.ostendebruges-aeroport.com/solarpark/, Accessed August 2023
2. COPRO, Ostend-Bruges Airport: A Lesson in Circularity, www.copro.eu/en/news/airport-ostend-bruges, Accessed August 2023
3. COPRO, PTV 829 (6.0) – Technical prescriptions for geotextile, https://www.copro.eu/nl/ptv-829, Accessed August 2023
4. P. Stolz, R. Frischknecht Comparative Life Cycle Assessment of Geosynthetics versus Conventional Construction Materials, www.eagm.eu. (2019)
5. EPD library, www.envirodec.com , www.epditaly.it.
6. NOC - National Oceanographic Centre Sources, amounts, & pathways of plastics entering the global ocean, NOC, Southampton, (2021)
7. B. Baensch-Baltruschat, B. Kocher, F. Stock, G. Reifferscheid. Tyre and road wear particles (TRWP) - A review of generation, properties, emissions, human health risk, ecotoxicity, and fate in the environment. Sci Total Environ. 2020 Sep 1;733:137823. doi: 10.1016/j.scitotenv.2020.137823. Epub 2020 Mar 10. PMID: 32422457, (2020)
8. N. Gustavsson, A. Bylund, L. Grabo, J. Groenholdt Palm, H. Nordzell, S. Snowbohm, Geosynthetics and microplastics in Sweden – an assessment. Ramboll Sweden AB, SE reg.no. 556133-0506, (2022)
9. CEN, European Committee for Standardization, Harmonized Standard EN 13249/2016 (annex B), Geotextiles and geotextile-related products – Characteristics required for use in the construction of roads and other trafficked areas, (2016)
10. P. Scholz, I. Putna-Nimane, I. Barda, I. Liepina-Leimane, E. Strode, A. Kileso, E. Esiukova, B. Chubarenko, I. Purina, F.G. Simon F.G., Environmental Impact of Geosynthetics in Coastal Protection. Materials (Basel). 2021 Jan 29;14(3):634. doi: 10.3390/ma14030634. PMID: 33573061; PMCID: PMC7866501, (2021)
11. D. Cazzuffi, K. Eufinger, CEN TC 189 reply to the BIOIS report and EC consultation on unintentional release of microplastics into the environment, (2022)
12. EC JrC - Symposium on Challenges of micro- plastic analysis - Bridging state of the art and policy needs, (online event 9 Sep 2021), (2021)
13. P.J. Kole, A. Löhr, F.I.G.A. Van Belleghem, A.M.J. Ragas, Wear and Tear of Tyres: A Stealthy Source of Microplastics in the Environment. Int J Environ Res Public Health. 2017 Oct 20;14(10):1265. doi: 10.3390/ijerph14101265. PMID: 29053641; PMCID: PMC5664766. (2017)
14. M.B. Tekman, B.A. Walther, C. Peter, L. Gutow, M. Bergmann, Impacts of plastic pollution in the oceans on marine species, biodiversity and ecosystems, 1-221 WWF Germany, Berlin. Doi: 10.5281/zenodo.5898684, (2022)
15. D. Haritval, G.V. Ramana, M. Datta, Microplastics in soil-like-material obtained during mining of a municipal solid waste dumpsite, Proc. 9th International Congress on Environmental Geotechnics, Chania, Greece, https://doi.org/10.53243/ICEG2023-129, (2023)

Potential microplastic release from gabion mattresses: a quantitative assessment

Gianluca Brocca[1*], *Francesco* Masola[2], *Maximilian P.* Born[3], and *Sebastian* Schiller[4]

[1] Officine Maccaferri S.p.A., DT Business Unit, Bologna, Italy
[2] Maccaferri Central Europe s.r.o., Senica, Slovakia
[3] Institute of Environmental Engineering – RWTH Aachen University, Aachen, Germany
[4] Beco Bermüller & Co Gmbh, Nuremberg, Germany

Abstract. Reno Mattresses offer a lasting and cost-effective alternative to traditional solutions for erosion control. Equipped with a state-of-the-art high-abrasion-resistance polymer coating, these gabion mattresses exhibit enhanced durability and corrosion protection, hence, longevity. However, the polymeric coating represents a potential microplastics (MP) source. Generally, the increasing prevalence of MP in the environment necessitates a critical evaluation of plastic-containing products for the construction industry, especially those used in and around aquatic environments.
Therefore, this study focuses on quantifying the potential MP release from this polymer coating throughout the product's life cycle, including installation and removal, under various erosion conditions, defined in a range from mild (E1) to extreme (E7). Combining laboratory tests, literature review, and field observations of 40-year-long installed gabion mattresses on the coast of the Baltic Sea, the investigations concluded that the risk of significant MP release is negligible across all impact classes, compared to the overall current MP influx. Even in extreme environments, polymer loss was around 1 % in 40 years, indicating limited MP formation. Additionally, the reduced construction volume compared to traditional loose stone solutions (riprap) results in decreased MP emissions from construction vehicles and the installation process. Therefore, regarding MP release, rock-filled gabion mattresses with high-abrasion-resistance polymer coating can be considered a suitable alternative to traditional construction methods for most intended applications.

1 Introduction

Rock-filled gabion mattresses are widely used to increase hydraulic erosion resistance in river training or coastal protection works. The units are manufactured with double-twist steel woven wire mesh, coated with technical polymer to prevent oxidation and to comply with EN 10223-3 [1] requirements. To holistically examine the influence of the polymer-coated gabion mattress on the aquatic environment, the potential abrasion of the polymer coating must be assessed, which would be equivalent to an undesirable entry of plastic into the water. An estimate of the potential microplastic (MP) input over the entire expected design life of

* Corresponding author: g.brocca@maccaferri.com

the gabion mattresses has been carried out based on several material investigations and load tests.

The increased use of plastics since the 1950s has inevitably led to the unintended release of plastics into the environment and waterways [2]. Environmental influences lead to the fragmentation of these plastics, which are called MP if they are smaller than five millimeters [3]. The impact of MP on the natural environment is widely recognized as negative, as the number of studies on adverse impacts increases.
This also includes plastics directly exposed to water, such as the polymeric coating of gabion mattresses.

Gabion mattresses are typically used to protect against erosion and provide high resistance to water flow and turbulent forces. Different types of gabion mattresses can have very different effectiveness as erosion control systems [4]. Recently developed rock-filled gabion mattresses have shown increased performance compared to older models [5].

These new mattresses are manufactured with double-twisted steel wire mesh coated with Zn-Al alloy and a high-abrasion-resistant polymer. The base, diaphragms, front, end, and sides are manufactured from a continuous mesh panel to increase structural strength. Units are equipped with special pre-formed bracing ties to provide tighter packing of the filling stones and to improve the mattress's hydraulic performance [4,5].

The required layer thickness of these new mattresses is drastically lower than with traditional stone finishes (e.g., Rip-Rap), leading to savings in material consumption (Figure 1).

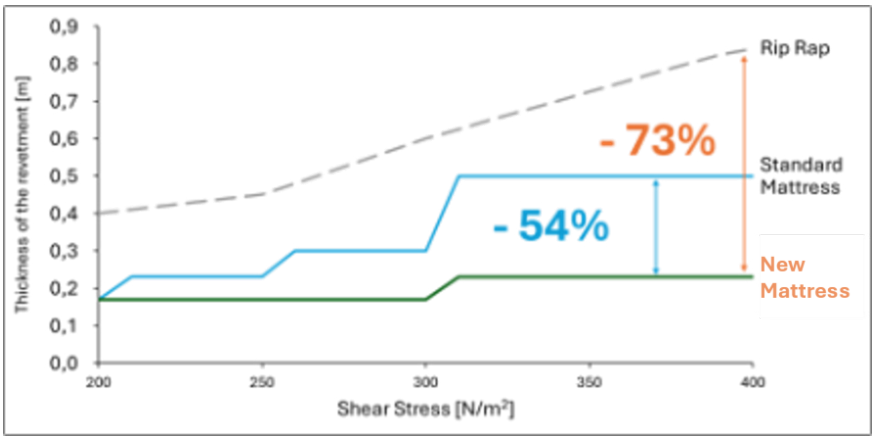


Fig. 1. Material saving potential using the newly developed gabion mattresses

According to a report by the European Commission (EC), geosynthetics account for 0.3% - 2.8% of the total MP input in the European Union (EU) [6].
The term *geosynthetics* covers several material categories, including geotextiles, geogrids, and geomats. Technical textiles used in the construction industry represent 20% of the total amount of this material category [7]. In a broader sense, gabion mattresses can be allocated to this material category. Therefore, a holistic investigation of this plastic coating installed directly in watercourses is necessary to evaluate its share in MP pollution.

To evaluate the potential MP input, both the available technical literature and the data from tests on mattresses, wire mesh, and polymer coating have been considered. Based on the abovementioned data, different “impact potential” classes were defined and assessed based on the exposure. Furthermore, a comparison between the mattress solution and the solution of loose stones (Rip-Rap) is briefly discussed, specifically regarding the potential MP emissions.

2 Literature Review

The literature review examined the risk of microplastic (MP) input and output from geosynthetics in the aquatic environment, which can occur during installation [8] and from improper handling [9]. Damage during installation and removal can sometimes be greater than the damage over the lifespan of geosynthetics. Factors such as subsoil grain size and weight per unit area of geosynthetics can influence tensile strength, causing fiber separation and expansion and, thus, MP release [9].

During their service life, geosynthetics are exposed to weathering, mechanical stress, UV radiation, biofouling, and further influences [8]. Stability decreases, especially if geosynthetics are not covered and remain exposed to sunlight, with UV radiation negatively affecting tensile strength and elongation-at-break. Elevated material temperatures also accelerate degradation, while oxygen pressure, salt water, changing water levels, moderate chemical loads, and biological degradation are of secondary importance for the plastics' fragmentation [17].

Stabilizers are added to geosynthetics to improve durability, thereby achieving a lifespan of over 100 years. However, these additives can leach into the environment. Yet, the exact impact on organisms, i.e., toxicity, especially regarding the prevalent concentration of additives in aquatic environments, is ongoing research [10, 18].

Field studies on the Baltic Sea near Kaliningrad showed that washed-up remains of plastic-coated wire mesh from gabions were found mostly in the form of "macro" plastics [8]. The study concludes that particular attention must be paid to the selection of materials as well as the professional installation and maintenance of geotextiles or plastics [8]. Therefore, it is crucial that gabions and mattresses have a good quality and high abrasion resistance polymer coating, to reduce the MP entry into the environment

3 Materials

The organic polymer coating under consideration (PoliMac) is a technical thermoplastic tailored for use in construction and characterized by very high material resistance to environmental influences. Compared to traditionally used PVC coating, the studied polymer has a lower density and particularly a higher abrasion resistance.

The tests conducted on the polymer coating under consideration examine various material aspects: corrosion, chemical weathering resistance, hardness, brittleness, abrasion, environmental harmlessness, elastic modulus, UV resistance, elongation at break, installation and removal damage, temperature influences and tensile strength. To assess the entry of MP into the environment, in addition to installation and removal, priority should be given to plastic-degrading factors and mechanical forces during the lifespan of the gabion mattress [3]. Furthermore, extreme temperatures can also promote fragmentation.

All these impacts, including installation and removal damage, have been analysed by TRI Environmental, Inc. [11] showing the improved performances of this special polymeric coating compared to traditional PVC. This results in an expected design life of polymeric coated gabion mattresses of 120 years in the exposure classes C2, C3, C4, and C5 as per EN 10223-3 [1].

4 Methods

To evaluate a potential MP entry into the environment from polymer-coated gabion mattresses, their use shall be considered in various environments. Since EN 10223-3 [1] only classifies two water-based environments (C4 and C5) and does not refine them further, seven water-based impact classes - E1 to E7 - are proposed and defined here (Table 1). The relevant impacts are briefly defined, and the investigations carried out are described.

Table 1. Impact classes and polymer coating assessment

Impact class	Medium	Description	Degrading effects	Resistance / test evidence
E1	Freshwater	Use in freshwater. Permanently below the water surface. Little to no water movement or other mechanical stress.	Frost, Hydrolysis, Biofouling (Installation time > 40 yrs)	Hydrolysis and biodegradation not considered (negligible processes) Frost resistance provided as proof
E2	Freshwater	Use in freshwater. Permanently below the water surface. With water movement and mechanical stress caused by sediments and small wind generated waves.	E1 + abrasive effects	E1 + Both hardness and abrasion resistance are significantly higher than standard PVC coatings
E3	Freshwater and air	Use in freshwater. Largely below the water surface with rare droughts. With water movement and mechanical stress from sediments. Example: free-flowing river.	E2 + UV radiation	E2 + UV radiation tested according to ISO 4892-3
E4	Air and freshwater	Use in freshwater. Mostly above the water surface with rare submersion. With strong water movement and greater mechanical stress from sediments. Example: flooding in a river.	E3 + increased temperatures, and mechanical stress	E3 + Vicat softening temperature >120°C as per ISO 306/A
E5	Saltwater	Use in saltwater. Permanently below the water surface. Intense water movement and mechanical stress. Example: coastal protection	Strong abrasive effects, salt water	E1 + Salt spray tests according to ISO 9227
E6	Saltwater and air	Application in salt water. Largely below the water surface. Intense water movement and other mechanical stresses. Example: coastal protection	E5 + UV radiation	E5 + UV radiation tested according to ISO 4892-3
E7	Air and saltwater	Application in salt water. Largely above the water surface. Extreme water movement and mechanical stress. Almost permanent exposure to UV radiation Example: Coastal protection for storm surges	E6 + Increased temperatures, extreme mechanical stress	E6 + Vicat softening temperature >120°C as per ISO 306/A + Study on polymeric coating exposed for more than 40 years

The resistance and test evidence reported in Table 1 refers to the results of [11], which shows that the organic polymer coating under consideration meets or exceeds the compliance and performance specifications outlined in ASTM A975 [19] for PVC. These results are further evaluated in [14].

5 Results

An exact calculation of the MP generation based on the reviewed literature sources and material studies is not possible. This is because MP research has not yet advanced to standardized material testing and does not enable robust assessments regarding technical plastics. Nevertheless, directions can be provided based on tests, the deployment locations, and the literature references.

The material tests on the examined polymeric coating indicate a high resistance to environmental influences; therefore, a lower MP input can be expected compared to conventional PVC coating. Of relevance are the resistance to UV degradation and the significantly increased abrasion resistance, which are particularly important in view of the findings of Simon and Scholz (2022) [8]. However, a distinction must be made according to exposure classes E1 - E7.

In Table 2 below, assessments for specific exposure classes (E1-E7) regarding the probability of significant microplastic generation from the polymer-coated gabion mattresses within their expected design life of 120 years are provided [16].

Table 2. Probabilities of a significant MP entry from polymer-coated gabion mattresses

Class	E1	E2	E3	E4	E5	E6	E7
Probability of a significant MP release	Negligibly low	Negligibly low	Very low	Very low	Moderately low	Low	Low

5.1 Evidence from structures in exposure class E7

In exposure class E7, the interaction of UV radiation, extreme mechanical stress, salt water, and increased temperatures stresses the material immensely. The testing on examined polymeric coating [11] shows high resistance against these stress factors, yet they were assessed individually, thus not considering parallel impacts. However, for a more detailed investigation of exposure class E7, old structures (> 40 years old) were recently examined to evaluate damage to the wire mesh coating and wire mesh samples tested [12]. This data represents a significant improvement in the estimation of MP entry.

The study on coating abrasion reveals a relatively low abrasion rate after 42 years. Therefore, it can be reasonably assumed that a comparably low mass loss for comparable installations and environmental conditions throughout its lifespan can be expected. The measurements on the wires and meshes were conducted on samples from a project site in Heiligenhafen (DE), located on the Baltic Sea. The gabion mattresses used as an erosion protection system for an embankment directly exposed to sea actions were installed in two phases: the first in 1981 (black polymeric coating) and the second in 1996 (grey polymeric coating).

The installed gabion mattresses were manufactured with lids made of 6x8 mesh type using a 2.2 mm zinc-coated steel wire with 0.5 mm of polymer coating, leading to an overall external diameter of 3.2 mm. The main ‘base’ units of the mattresses in contact with the soil used only zinc-coated steel wire and were not polymeric-coated, as can be seen in figure 2. The mattresses were exposed to highly aggressive environmental conditions (exposure class E7) including salt water, salt spray, wave attack and sediment action.

The tests were conducted on a minimum of three samples for each type of polymer-coated woven wire mesh in line with EN 10218-2, EN 10244-1 and EAD 200019-01-0102.

The measurements (Figure 3) [12] reveal that the polymeric coating's diameter is still within the prescribed tolerance (± 0.20 mm as per EN 10218-2 Table 2 [13]), resulting in a coating loss of approximately 1% in 42 years.



Fig. 2. Mattress protection system in Heiligenhafen. Left: black polymeric coating installed in 1981. Right: Grey polymeric coating, installed in 1996. (Pictures both from 1996)

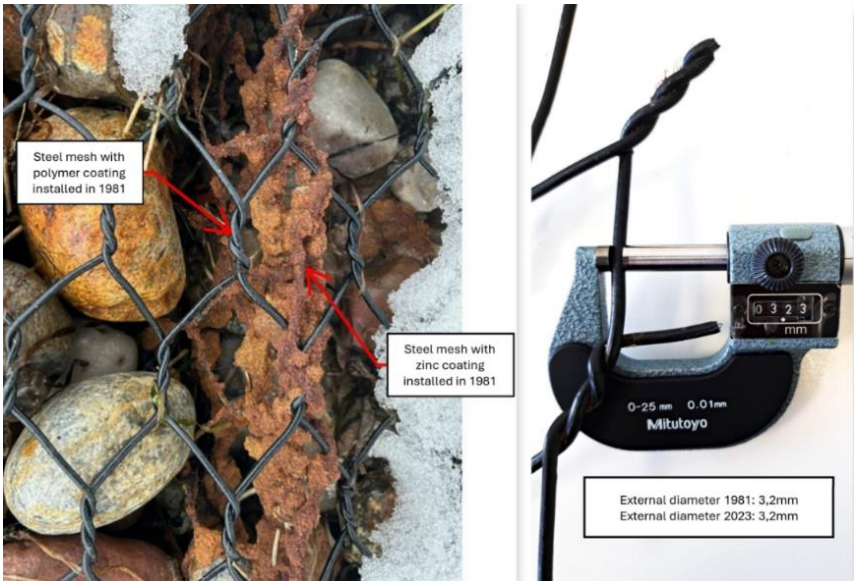


Fig. 3. Left: black polymeric coating installed in 1981 (picture of Dec. 2023) – Right: measurement of the coated wire external diameter. (Pictures of Jan. 2024)

6 Calculation example and comparison

Using new gabion mattresses as bank protection reduces the protection thickness by up to 73% compared to conventional "Rip Rap" stone finishes while offering the same hydraulic erosion protection [4,5]. Thereby, material consumption (stone / rock) and the number of truck transport rides to the construction site can be significantly reduced. This eventually means that MP discharged from truck tires during transport, a known source of MP, can be avoided. Other MP sources, such as the increased use of excavators on site to install the greater volume of Rip Rap compared to gabion mattress solution, could be added but are not analyzed here.

Considering the results of the measurements on the wire coating from the Heiligenhafen project site, in which the polymeric coating loss was approximately 1% after 42 years with

exposure class E7, the loss of polymeric coating for a design life of 50 years can be conservatively estimated to be between 5% and 10% of the total polymeric coating.

Therefore, concerning a real application, a comparison can be drawn in terms of microplastics generated between a project made with Rip Rap (loose stones) and with suited gabion mattresses. In the following example, a design life of 50 years was considered.

The river protection work analyzed here is a real case study on the Tenore River in the Province of Varese (Italy). It is part of a major project to construct the 'Pedemontana Lombarda' motorway.

The hydraulic erosion work consists of protecting a riverbank with an area of 5,400 m² with gabion mattresses. Each single unit is a 0.3 m thick mattress. Therefore, the total bulk volume of stones required is 1,620 m³. The mattress is made from mesh type 6x8 [1], with a wire diameter of 2.2/3.2 mm (int/ext), and is polymeric coated. The mattresses were filled with stones with an apparent unit weight of about 1,750 kg/m³, which led to a total of 2,835 tons.

The traditional solution that was considered is a revetment formed of large stones (Rip-Rap) with a thickness of 1 m, 70% greater thickness than the gabion mattress alternative. This equates to a stone total volume of 5,400 m³ which corresponds to a mass of 9,450 tons (at an apparent unit weight of 1,750 kg/m³) that must be transported from a quarry.

The analysis was carried out for both systems considering the transportation of the stones from a quarry 100 km away from the project site and, therefore, the round trip for each truck to be 200 km [14]. It should be noted that the distance between the construction site under consideration and the quarry is an assumed average that may vary and will depend on the region. Additionally, there are several MP-related emissions from quarrying operations that are not included here but are dependent on the moved mass of rock. The MP emissions per km truck journey is based on Kocher and Brose (2010) [15] and is 1,2 g/km. For the gabion mattress, the potential MP input due to both the transport of stones and polymeric coating is considered, while for rip rap solution only the transport of stones is considered.

Considering a load per truck of 20 tons [14], the MP emission due to transport can be calculated with the following formula:

$$m_{MP,t} = \frac{m_{s,RR}}{m_{Truck}} \cdot L_T \cdot m_{MP,gone} \quad (1)$$

Where:

$m_{MP,t}$	mass of MP emissions due to transport [kg]
m_s	mass of stones [kg]
m_{truck}	mass of the load per truck [kg]
L_t	distance of the transport route [km]
$m_{MP,gone}$	mass of MP emissions per km of truck journey [g/km]

Considering the above-mentioned data, the transport emission for Rip-Rap solution will be 113,4 kg, while the one for gabion mattresses is 34,0 kg

The potential MP input due to the polymeric coating, considering a potential loss of 10% along the design life and with a polymeric coating density of 947,5 kg/m³ results in 45,0 kg [16].

The total MP potential entry saved therefore results to be 34.4 kg. This saving would correspond to the MP generated by approx. 143 trucks travelling for the 200 km round trip. Yet, several further aspects are relevant for a holistic investigation of the MP generation. However, the calculations reveal a glimpse of its possible outcome.

7 Conclusions

Gabion mattresses represent a good alternative to traditional Rip-Rap stone protection in terms of erosion resistance as well as cost and construction volume savings. According to EN

10223-3 [1], the plastic coating is the only option to enable the solution to achieve a service life of 120 years.

The literature research and the material tests concluded that for most applications the probability of a significant entry of MP from the high abrasion resistance polymer coating of the new gabion mattresses analyzed is low to very low. Even for the impact class E7, results from a study reveal an average polymeric coating loss of 1% over 42 years and, thus, a low MP formation. However, an extrapolation on the gabions condition after 78 more years (thus, 120 years) can only be qualitatively drawn and is tried to be covered by the conservative approximation of 10% coating loss.

Furthermore, it should be considered that the reduction in construction volume due to the better efficiency of the new gabion mattresses compared to traditional rip rap stone protection also results in a reduction in the MP generated from truck tires and brakes, which can potentially exceed the theoretical input from the gabion mattresses. However, further aspects must be included for a holistic and concluding investigation, e.g., the location of generation.

The new gabion mattresses with a high abrasion resistance polymer coating have a low to very low probability of significant MP generation for the vast majority of applications for which they are intended. Therefore, in terms of MP generation they might be a more sustainable alternative to traditional construction methods in these application areas. However, an individual analysis for every application case is recommended, as conditions vary for every construction site. Furthermore, upcoming investigations on the impact of MP on the environment should be continuously included in these considerations.

Acknowledgment

The underlying work (literature work, calculations, conceptualization, etc.), except for the Heiligenhafen study, was part of a project commissioned by Maccaferri Central Europe S.R.O. to the Institute of Hydraulic Engineering and Water Resources Management of the RWTH Aachen University (IWW) which was finished in 2024. The intellectual property, except for the Heiligenhafen study, is held by Holger Schüttrumpf (IWW) and Maximilian P. Born (former employee of the IWW, now employed at the Institute of Environmental Engineering of the RWTH Aachen University).

Competing Interests

The underlying work (literature work, calculations, conceptualization, etc.), except for the Heiligenhafen study, was part of a project commissioned by Maccaferri Central Europe S.R.O. to the Institute for Hydraulic Engineering and Water Resources Management of the RWTH Aachen University which was finished in 2024. The co-author of this manuscript, Maximilian P. Born, was part of this project, and these competing interests are hereby indicated.

References

1. BS EN 10223-3:2013. Steel wire and wire products for fencing and netting. Hexagonal steel wire mesh products for civil engineering purposes. British Standards Institution (2013)
2. Janssens, Virginia: Plastics - The Facts 2022. With assistance of Plastics Europe AISBL, European Association of Plastics Recycling & Recovery Organisations. Edited by Plastics Europe AISBL. Plastics Europe AISBL. Brussels, Belgium. (2022)

3. M.P. Born, C. Brüll: From model to nature - A review on the transferability of marine (micro-) plastic fragmentation studies. In The Science of the total environment 811, p. 151389. DOI: 10.1016/j.scitotenv.2021.151389 (2022)
4. P. Di Pietro, N. Mazzon, F. Xu, B. Zhang: Hydraulic tests and interpretation of test data for erosion protection systems in open channel flow. Proceedings of International forum on land degradation, soil conservation and sustainable development, Dalian, China, pp. 99-105 (2021)
5. P. Di Pietro, G. Brocca, M. Vicari: Research study and new evaluation method for pre-filled mattresses as erosion protection systems of berthing structures against jet propeller action. 11th International Conference on Scour and Erosion (ICSE-11), Denmark, online library of ISSMGE. (2023)
6. European Commission: EU action against microplastics: Publications Office of the European Union. (2023)
7. F. Fontana, P. Rimoldi, M. Scotto, M. Vicari: Analysis of the generation of plastic debris and microplastics from geosynthetics. In Giovanni Biondi, Daniele Cazzuffi, Nicola Moraci, Claudio Soccodato (Eds.): Geosynthetics: Leading the Way to a Resilient Planet. London: CRC Press, pp. 365–374. (2023)
8. F. Simon, P. Scholz: Einfluss von Geokunststoffen auf die aquatische Umwelt; EI-GEO. Teilvorhaben: BAM. (2022)
9. D.M. Carlos, J.R. Carneiro, M. Pinho-Lopes, M. Lurdes Lopes: Effect of Soil Grain Size Distribution on the Mechanical Damage of Nonwoven Geotextiles Under Repeated Loading. In Int. J. of Geosynth. and Ground Eng. 1 (1). DOI: 10.1007/s40891-015-0011-9. (2015)
10. P. Scholz, et al.: Environmental Impact of Geosynthetics in Coastal Protection. In Materials (Basel, Switzerland) 14 (3). DOI: 10.3390/ma14030634. (2021)
11. Polimac Compliance Report, TRI Environmental, Inc, Austin, TX, USA(2021)
12. TSUS: Tests on Maccaferri Reno Mattress polymer coated wire mesh installed on the Baltic Sea in 1981 and 1996. Edited by BUILDING TESTING AND RESEARCH INSTITUTE, Slovak Republic (70240075). (2024)
13. CEN EN 10218-2:2012 - Steel wire and wire products - General - Part 2: Wire dimensions and tolerances. Brussels: European Committee for Standardization. (2012)
14. M. Stucki, S. Büsser, R. Itten, R. Frischknecht, H. Wallbaum: Comparative Life Cycle Assessment of Geosynthetics versus Conventional Construction Materials on behalf of the European Association for Geosynthetic Manufacturers (EAGM) Uster. 45th ed. Edited by Ground Engineering (10, 24-28). (2011)
15. B. Kocher, S. Brose: Stoffeinträge in den Strassenseitenraum - Reifenabrieb. Bremerhaven: Wirtschaftsverlag NW (Berichte der Bundesanstalt für Straßenwesen / V, 188). (2010)
16. Potential Microplastic Emissions from Reno Mattresses, RWTH Aachen University, Aachen, Germany (2024006) (2024)
17. A.L. Andrady: Microplastics in the marine environment, Marine Pollution Bulletin, Volume 62, Issue 8, 2011, pp. 1596-1605, ISSN 0025-326X. (2011)
18. R.M. Naga et al.: Additives of plastics: Entry into the environment and potential risks to human and ecological health, Journal of Environmental Management, Volume 348, 2023, 119364, ISSN 0301-4797. (2023)
19. ASTM A97: Standard Specification for Double-Twisted Hexagonal Mesh Gabions and Revet Mattresses (Metallic-Coated Steel Wire or Metallic-Coated Steel Wire With Polymer Coating) (2024)

High performance and recyclable geosynthetic for subgrade stabilisation and bearing capacity improvement

Alain Nancey[1*], and *Abdelkader* Abdelouhab[1]

[1]SOLMAX FRANCE, 95873 Bezons, France

Abstract. Environmental benefits and cost saving are parts of the requirements for all construction projects, additionally to the quality and the performance. It applies to the granular platforms which are the basis of many infrastructure's foundations, with the objectives of carrying the loads and controlling the deformation. Geosynthetics are known to reduce the needed quantity of granular fill material, but performance on real jobs is not sufficiently documented. As well, the interest of geosynthetics toward sustainability still needs to be highlighted, particularly because it covers many different aspects. Two jobs showing the multiple advantages of geosynthetics regarding economical end environmental benefits are presented in this paper. The first example shows that the bearing capacity requirement are more easily achieved using a high performance geosynthetic. In the second presented job which was a temporary road, additionally to the usual cost and environmental benefits linked to the reduction of the fill layer thickness, the same geosynthetic showed its ability for recycling.

1 Introduction

Since 1970, geosynthetics stabilise granular platforms in various type of infrastructure such as roads and railways. Their uses lead to a significant reduction of granular fill material. Bearing capacity improvement and trafficability by limiting surface deformation are the two main goals pursued in this stabilisation application. Separation, filtration, reinforcement and confinement or lateral restrain are the functions fulfilled by the geosynthetic. Stiffness and geosynthetic -soil interaction are the key characteristics to achieve the required performance of the reinforced platform, as demonstrated by Abou Chaz [1].

Comparison between the environmental performance of commonly applied construction materials (such as concrete, cement, lime or gravel) versus geosynthetic was carried out by ETH Zürich and ESU-services Ltd., commissioned by the European Association for Geosynthetic Products Manufacturers (EAGM) As seen in figure 1, the results given by Stolz [2] show that geosynthetic lowered about 30% the overall global warming impact of the construction effort during its 30 years lifetime compared to a road stabilised with cement/lime.

Based on the same cases, Retzlaff (3] made a cost comparison between the geosynthetic solution (case 2B from EAGM study) and the conventional solution (Case 2 A from EAGM study).

The cost calculation includes the site preparation, the removing of the topsoil with its temporary storage in the construction site area, the construction and compaction of the formation, the supply and the installation of the geosynthetic and the supply of the base course material 0/45mm. The carbon footprint with the use of geosynthetics is more than 30% lower than conventional solution without geosynthetics.

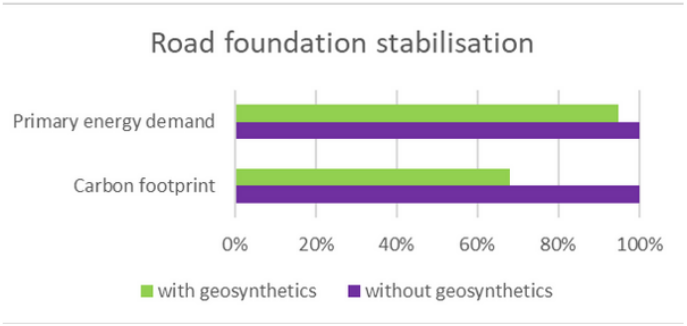


Fig. 1. Environmental impact of geosynthetic used in road stabilisation from Stolz [2]

The cost saving was significant as shown on figure 2. It demonstrates that the use of geosynthetics can reduce required quantities of fill material and save soil movements on the construction site.

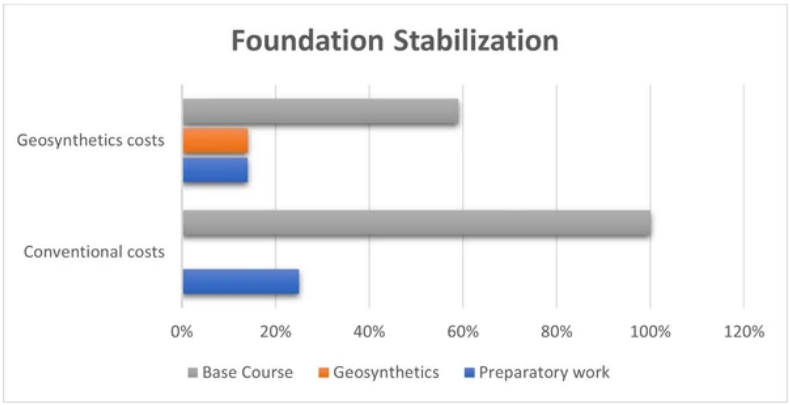


Fig. 2. . Economic impact of geosynthetic used in road stabilisation from Retzlaff [3]

To highlight supplementary advantages of the use of a high strength geotextile in road stabilisation, a first case study showing the benefits of the geosynthetic reinforcement on the bearing capacity and a second job more focused on the recycling of materials are presented hereafter.

2 Building a parking lot over soft soils at Teterow (Germany)

2.1 Overview

Teterow is a town on the eastern part of Germany, in the district of Rostock. The Lidl parking lot project aimed at reinforcing the base course to enhance the structural integrity of the commercial area.

On 12.09.2022, Erdbaulaboratorium Neubrandenburg GmbH (ELN) carried out an acceptance of the soil bearing capacity in the construction area of the planned parking expansion of the Lidl market in Teterow. After an initial soil excavation of 0.6 m, various materials were found, consisting primarily of humus-interspersed sands with deposits of bricks ([SU],[SE],[OH] according to the German soils classification [3].

Dynamic Deformation Modulus (according to TP BF-StB Part B 8.3), E_{vd} = 11 - 13 MPa ($E_{v2} \approx$ 10 MPa) have been measured and have shown insufficient load-bearing capacity, lower than the minimum E_{vd} = 25 MN/m² (or E_{v2} = 45 MPa) required at the base of the pavement structure by the project consultant.

Abou- Chaz [1] has shown that a stiff woven geotextile product having a high strength at low elongation (22 kN/m at 2%) in both directions significantly improved the behaviour of a granular layer installed on a very soft soil (CBR<1%), allowing a thickness reduction of 40%, compared to an unreinforced layer of 500 mm. The principle of this solution was chosen by the designer.

2.2 Solution

To solve this low bearing capacity issue, it was proposed to install 40 cm of [GW] crushed granular material (0/45) on a geosynthetic at the base which ensures the reinforcement and a permanent separation of the granular materials from the softer subgrade. The selected geosynthetic, MIRAFI® HMi-5 (figure 3), is a high-stiffness (tensile strength higher than 22 kN/m at 2% strain), flexible fabric for stabilising base courses in road construction. Its opening size (300 µm) prevents different soil layers from mixing and restricts the movement of soil particles while its permeability (20 mm/s) allows water to drain freely.

To validate fully the solution proposed, a minimum deformation modulus E_{v2} of 100 MPa or a corresponding minimum dynamic deformation modulus E_{vd} of 50 MPa must be proven by means of a test field.



Fig. 3. Geosynthetic installed on top of the subgrade.

2.3 Measurements

On 12.10.2022, new tests were carried at the surface of the granular layer (Figure 4):

- two tests documenting the existing areas without geosynthetic reinforcement (highlighted in yellow area n° 1 and area n° 2).
- two tests on areas with the 40 cm reinforced layer (area n° 3 and area n° 4).

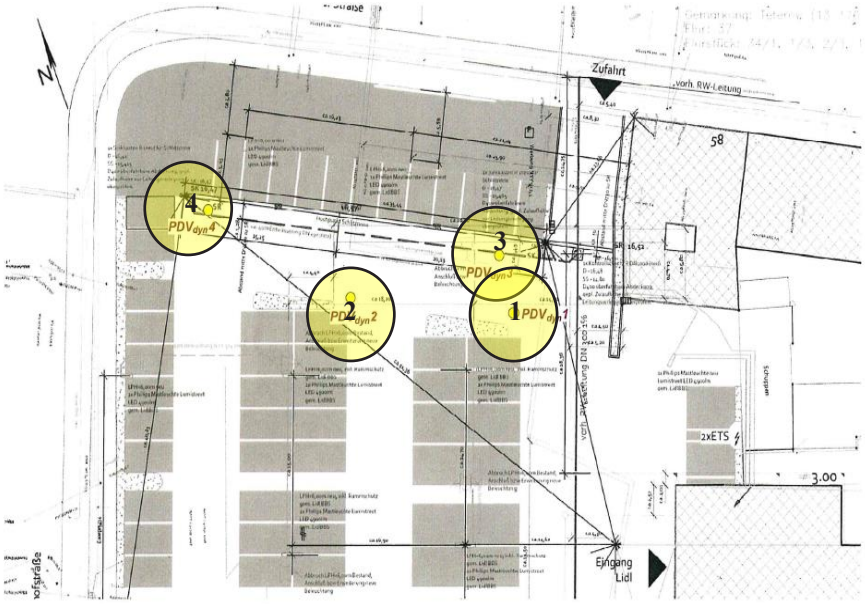


Fig. 4. Map of the parking area and dynamic E_{vd} tests position.

E_{vd} values presented on table 1 show clearly the positive effects of the high strength geotextile: separation between the soft soil and the granular layer, allowing a better compaction, and reinforcement that minimises the deformability of the granular layer. The unreinforced layer (test 1 and test 2) cannot deliver the minimum required E_{vd}.

Table 1. Dynamic plate test results.

	Dynamic deformation modulus E_{vd} (MPa)		Required E_{vd} MPa
Subgrade level	11.3 MPa	13.1 MPa	25
40 cm unreinforced layer	Test 1 : 24.9 MPa	Test 2: 16 MPa	50
40 cm reinforced layer	Test 3 : 59.5 MPa	Test 4: 57.7 MPa	50

These results provided the validation of this solution with the minimum 50 MPa required. The areas without reinforcement were later upgraded with the same geosynthetic.

3 Temporary road for an electric power plant (Netherland)

3.1 Overview

The supply of solar and wind energy is growing at a rapid pace and require new structure for the distribution. Tenne T as the Transmission System Operator (TSO) for the Netherlands, is expanding the high-voltage grid in the North of the Netherlands, to get all sustainably generated electricity to the right place and to guarantee supply to households and businesses.

As part of the construction of pylons for new high-voltage lines, a road was built on the agricultural land to transport construction machinery, with the constraint of returning the land to its original state after the end of the work. To minimize the impact on the environment, a temporary structure consisting of a geosynthetic, a layer of sand and concrete or steel plates (Figure 5) was put in place to ensure the stabilization of the platform. Without geosynthetics the sand thickness required should have been roughly 50% more than the amount finally used with reinforcement, as shown in [1,2,3] . This solution reduces consequently the truck traffic required to supply the site with granular material and its environmental impact.

The works were driven by Tenne T and SWITCH a contracting group as explained by Groen [4] who highlight the fruitful collaboration with the geosynthetic producer to reuse or recycle all the materials used on site.



Fig. 5. Temporary road structure

3.2 Lowering the environmental impact and recycling.

After the completion of the new high-voltage lines, the temporary road was fully dismantled, by removing first the concrete or steel plates, a large part of the sand in a second step and the geosynthetic in a third step. On the site having a total area of circa 500 000 m², 380 tonnes of polluted geosynthetic were removed (Figure 6), containing approximately 300 tonnes of sand and 80 tonnes of geosynthetic.

If the concrete or steel plates and the sand can be reused in other jobs or other applications, it is not possible for the geosynthetic that was polluted with the fine particles of soil and damaged by the installation and the de-installation. The remaining options are the disposal in landfill, incineration or recycling. Recycling textile material coming from the waste of the industry that are not contaminated by particles is already a common practice. At the contrary, the recycling of a geosynthetic used on site is a real challenge but that was the solution chosen for this job.



Fig. 6. Geotextile removal from the site

As stated by Groen [5]: " No existing process could efficiently recycle geotextile contaminated with a high soil particle content, necessitating an innovative approach to ensure the recycled material was devoid of soil particles." The cleaning process involved, consisted of extracting soil particles from the fabric. This was achieved by different steps of washing to ensure the resulting material was suitable for reuse in geosynthetic production. This required the production of high-quality pellets (figure 7), meeting stringent standards for reintroduction into the production chain, not impacting the performance of the product.



Fig. 7. Pellets prepared from recycled geotextile.

Indeed, the use of the recycled pellets for another geotextile production needs further investigations to check if their characteristics fit with the requirement of the considered process.

4 Conclusion

On two different projects, a geosynthetic used to reinforce a granular platform has proved that the requirement on bearing capacity can be achieved with less granular material, reducing the impacts on the environment. Furthermore, the second job highlights the first case where, after use, a geotextile was recycled into pellets to be reintroduced in a geosynthetic production cycle.

References

1. N. Abou Chaz, L. Briançon, P. Villard, C. Silvani, A. Nancey, A. Abdelouhab. (2023). Experimental and numerical studies of the geosynthetics reinforced platforms laid over soft subgrade soil. GeoAfrica (2023). https://doi.org/10.1051/e3sconf/202336802036
2. P. Stolz, R. Frischknecht, (Ed.) Comparative Life Cycle Assessment of Geosynthetics versus Conventional Construction Materials. Second edition. treeze Ltd. Uster (Swiss). Commissioned by the European Association of Geosynthetic product Manufacturers (EAGM) (2019)
3. J. Retzlaff, Cost comparison of geosynthetics versus conventional construction materials, a study on behalf of the EAGM, CASE 2: Foundation stabilisation EUROGEO 7, Warsaw, Poland (2022)
4. DIN 18196:2023-02, Erd- und Grundbau - Bodenklassifikation für bautechnische Zwecke
5. G. Groen, Recycling of geotextiles: a collaborative approach to enhance circularity in construction (to be published) EUROGEO 8, Lille, France

Geotextile Durability by Outdoor Weathering and Tensile Creep: Case Study

Mag Geisielly Alves Guimarães[1*], *Denise de Carvalho* Urashima[1], and *Beatriz Mydori Carvalho* Urashima[2]

[1]Federal Technological Education Centre of Minas Gerais, CEFET-MG, 1000 Imigrantes Avenue, Varginha, Minas Gerais, Brazil
[2]Osaka University, 565-0871 Suita, Osaka, Japan

Abstract. Designing with geosynthetics has been gaining market in recent years in different geotechnical and environmental applications. It is necessary to know its durability under degradation factors during the design life. This work evaluated the durability of geotextiles by simultaneous exposure to tensile creep and weathering for 90 days in the summer of 2020-2021. A polypropylene woven geotextile was used for research purposes for synergism durability analysis. Frames had a 22º slope to obtain higher global solar radiation. The creep load was set at 15% of the ultimate tensile strength. Laboratory tensile creep test was performed to evaluate synergistic degradation. Tensile creep tests with a 22° inclination proved effective in durability estimation by synergism between tensile creep and weathering. The study results have been promising in addressing the influence of the synergy of degradation factors and the achievement of partial reduction factors to apply in projects with geosynthetics.

1 Introduction

Geosynthetics' durability is a relevant criterion for its application in civil engineering in prolonged exposure to factors that can induce their degradation. This behaviour depends on the geosynthetic polymeric constitution, the physical structure, the storage and installation conditions, and the prolonged contact with degradation factors in various applications [1]. The acceptable durability for geosynthetics is related to their ability to perform satisfactorily and to maintain their functions under the conditions of use involved in the project. It is essential to obtain a greater knowledge of the factors that may result in geosynthetic material degradation [2,3].

The literature consensus is that geosynthetic exposure to weathering, especially ultraviolet radiation (UV) and temperature, is one of the main factors that lead to their degradation. Therefore, it is necessary to evaluate the degradation mechanisms, particularly for applications where the geosynthetic material will be exposed (i.e., above ground). For example, geotextiles can be applied to protect margins and breakwaters and build artificial islands as protective structures.

Moreover, waste containment systems (WCS) with geotextiles for dewatering and confinement of wastes in various industrial processes [4]. In these applications, the

* Corresponding author: mag@cefetmg.br

geotextiles are susceptible to weathering degradation, chemical degradation, and effects due to installation damage, cyclic loading, and tensile creep [5-7]. The adequate performance of engineering with geosynthetics is linked to understanding the complexity of the degradation mechanisms in an isolated way and the synergy effects of the factors [8,9].

This paper evaluated the durability of polypropylene woven geotextile by tensile creep and weathering synergism. The tests were conducted for 90 days in the summer of 2020-2021. Tensile creep laboratory tests were also performed to assess the synergism study. The durability parameters were performed by strip tests in specimens cut from the geotextile samples exposed to tensile creep and weathering tests.

2 Experimental study

2.1 Tested geotextiles

A polypropylene woven geotextile (GTXw) was used for research purposes for synergism durability analysis. Table 1 shows the properties obtained from sampling ten specimens. Sampling for tests was performed in the machine direction (MD), and obtained ten specimens after the tests. The number of ten specimens allows for obtaining tensile strength results with an expected error of up to 1%.

Table 1. Properties of the polypropylene woven geotextile.

Parameters	Value***
Mass per unit area [10]	252.8 g/m² (0.8%)
Thickness [11]	0.81 mm (2.1%)
Ultimate tensile strength [12]*	56.7 kN/m (0.8%)
Strain at ultimate tensile [12]*	14.8 % (3.3%)
Ultimate tensile strength [12]**	57.8 kN/m (2.0%)
Strain at ultimate tensile [12]**	14.0 % (4.3%)

*Mechanical property in the machine direction (MD), **Mechanical property in the cross-machine direction (CMD), ***Confidence interval (CI), with 95% of confidence level.

2.2 Tensile creep and weathering tests

The experiments were performed at the Federal Technological Education Centre of Minas Gerais (CEFET-MG), Varginha city, Minas Gerais State in south-eastern Brazil (-21.5490º south, -45.4194º west, at an altitude of 925.00 meters above sea level). Meteorological parameters were obtained in the meteorological station installed in Varginha city. These data are freely available at the National Institute of Meteorology. An estimation of the 4.2% UV radiation of global solar radiation (UV/G) was adopted in the durability tests [13-15]. Weathering durability tests were carried out in the summer of 2020-2021 (12/21/2020 to 03/20/2021), with a total exposure time of 90 days.

A frame was used for outdoor weathering tests by open exposure, which permits the air-free flow between the front and back of the samples [16,17]. This frame presents galvanized 30 mm × 30 mm wire mesh to prevent corrosion (Figure 1). The frame had a 22º slope, which is similar to the exposure location's latitude, and the face was inclined toward the Equator to obtain higher global solar radiation during the day [16,17]. The sample size of 420 mm x 900 mm was dimensioned to obtain ten specimens by strip tests.



Fig 1. Frame for weathering exposure.

Another frame with a 22º inclination was used for the synergism study by tensile creep and weathering. Figure 2 shows the frame for simultaneous exposure to tensile creep and weathering, which was employed in previous research [18]. The creep load was set at 15% of the ultimate tensile strength, and the loading was performed using static loads. The tensile creep load was applied simultaneously using a hydraulic jack to avoid the occurrence of strain along with the static loads' additions. This procedure was also established in previous research [18]. Samples sizes of 250 mm x 1350 mm in the MD were dimensioned to obtain ten specimens (strip tests) after the exposure period. The tensile creep tests were performed with replicates (2 samples) to get representative results for the durability analysis.

Creep strain (%) was analysed on the GTXw over time. Eight regions were established on the GTXw surface for strain measurements: six areas over the MD with nominal initial sizes of 100 mm and two of 50 mm in the CMD (Figure 2). Strain measurements were performed with the use of a digital pachymeter. A laboratory tensile creep test (Figure 3) also was performed with a standard atmosphere (20±2°C at 65±5% at relative humidity) over 90 days to evaluate synergistic degradation between tensile creep and weathering.

Strip tests obtained durability parameters [12]: 50 mm wide, 75 mm distance between the clamps, and 300 mm/min loading rate. Ten specimens were obtained from each sample submitted to durability tests. Ten specimens were obtained from each sample exposed on durability tests.

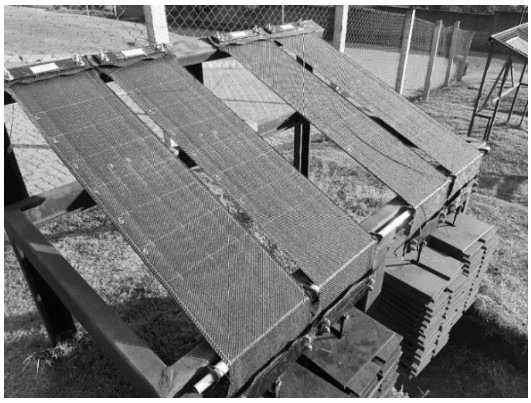


Fig 2. Frame for synergism study between tensile creep and weathering.

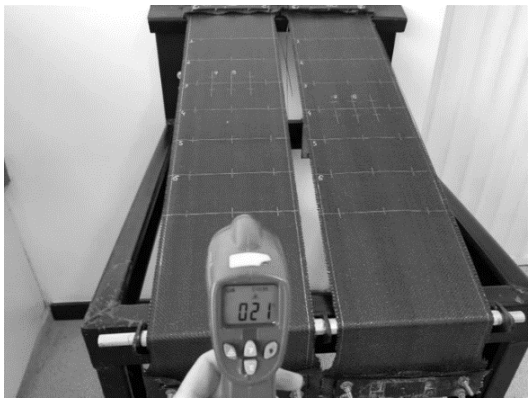


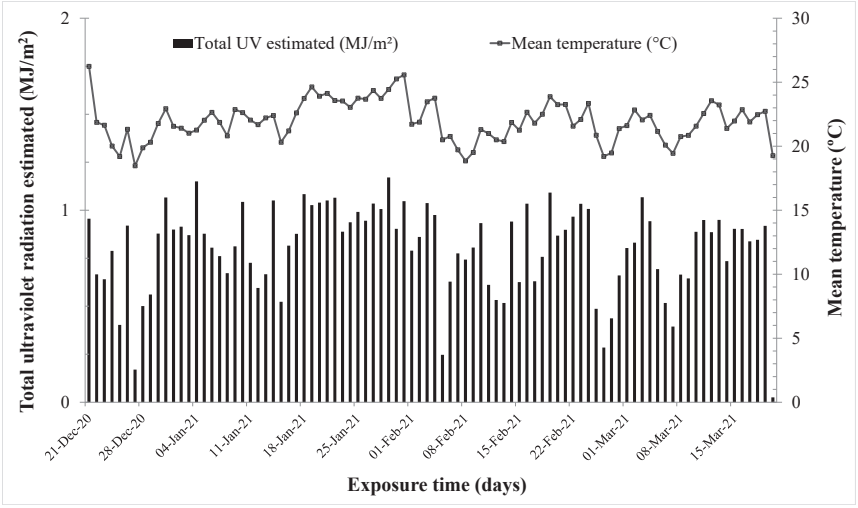
Fig 3. Laboratory tensile creep test.

3 Results and discussion

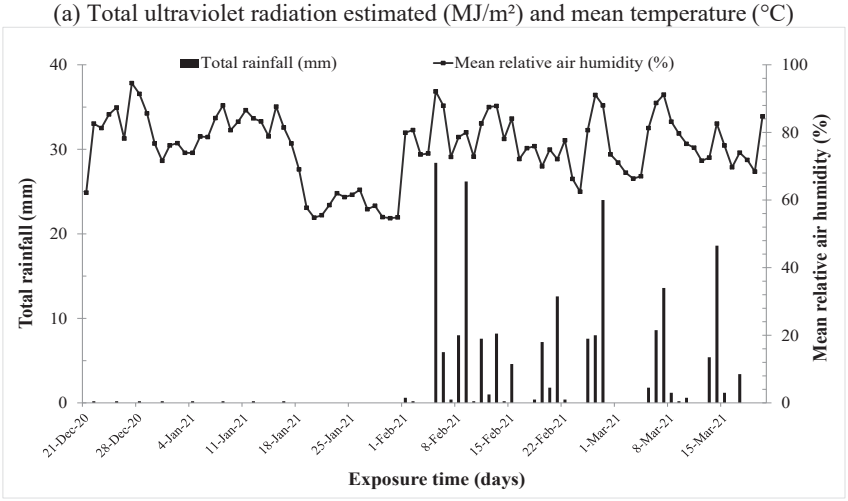
Figure 4 shows the climatic parameters obtained for the study site. The total ultraviolet radiation estimated was 74.3 MJ/m². The daily mean temperature of 22.2°C, and the mean relative air humidity was 73.8%. Total rainfall was 214.8 mm, with higher incidences in February/2021 (Figure 4b).

Table 2 summarizes the results obtained in the field and laboratory durability tests and the respective partial reduction factors. Weathering tests (open exposure) caused a tensile strength loss of 29.9%, and samples exposed to tensile creep and weathering simultaneously with a loss mean of 36.1%. Unlike the field creep tests (S1 and S2), no tensile strength losses were observed for laboratory tensile creep. Significant strain (%) reductions at ultimate tensile strength are obtained from samples exposed to tensile creep and weathering simultaneously. It is due to the climatic dynamics of the samples to weathering.

Although the research did not evaluate chemical changes in the geotextile subjected to weathering, research in the literature indicates that the incidence of weathering causes the breaking of chemical bonds by photodegradation, as well as the increase in temperature on the surface of exposed geosynthetics [19,20]. Both situations explain the changes in creep behavior in synergy with weathering.



(a) Total ultraviolet radiation estimated (MJ/m²) and mean temperature (°C)



(b) Total rainfall (mm) and mean relative air humidity (%)

Fig 4. Climatic parameters over the exposure time.

Table 2. Mechanical parameters retained after exposure periods.

Tests		Ultimate tensile strength, kN/m (Tmax)***	Strain at ultimate tensile, % (Ɛmax)***	Tensile strength loss
Field tests	Weathering*	39.7 ¨ (2.0%)	8.3 (2.9%)	29.9%
	S1*	36.4 (5.0%)	5.2 (5.6%)	35.8%
	S2*	36.0 (2.0%)	5.0 (4.1%)	36.4%
Laboratory	Tensile creep	56.9 (1.9%)	13.6 (3.4%)	0%

*Open exposure. **S1 (sample 1: creep tensile + weathering), and S2 (sample 2: creep tensile + weathering). ***The coefficients of variation (COV) are shown in parentheses.

Table 3 presents the average final creep strain obtained in the GTXw geotextile samples. Figure 5 shows the creep curves. Slight increases in longitudinal strains were observed over time for tensile creep under weathering (summer period). Longitudinal strains in samples 1 and 2 (S1 and S2) were 9.6% and 9.8%, respectively. S1 and S2 showed -4.8% and -5.0% in cross-section strains, respectively. Negative strains refer to contraction behaviour due to longitudinal strains.

Despite similarities in the creep curves over time (Figure 5), it is considered a higher average of final strains obtained by the tensile creep and weathering simultaneous compared to the laboratory creep, with differences in average final strains of 4.5% (Table 3).

Table 3. Average final creep strain over 90 days (summer 2020-2021).

Tests		Machine direction (MD)**	Cross-machine direction (MD)**
Field tests	S1*	9.6 (3.9%)	-4.8 (2.5%)
	S2*	9.8 (3.6%)	-5.0 (7.7%)
Laboratory	Tensile creep	5.2 (4.9%)	-1.6 (8.2%)

*S1 (sample 1: creep tensile + weathering), and S2 (sample 2: creep tensile + weathering). **The coefficients of variation (COV) are shown in parentheses.

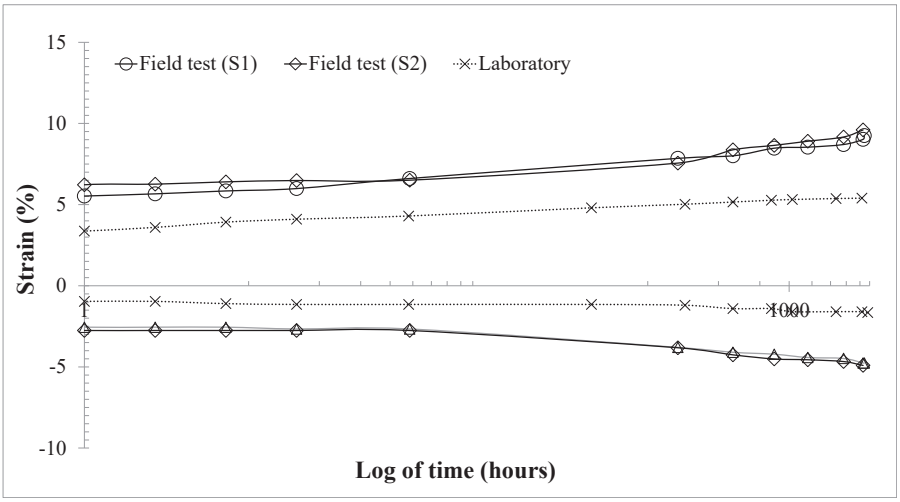


Fig 5. Tensile creep strains over 90 days.

4 Conclusion

Geosynthetic durability is a complex theme, and it's dependent on several factors which act synergistically and in a non-standard way. Polypropylene woven geotextile subjected to weathering and tensile creep degradation indicated the occurrence of synergism and mechanical properties changes over summer exposure. This geotextile was used for research purposes for synergism durability analysis and is not used in weathering exposure. Therefore, the results are for research purposes and are not used in dimensioning parameters.

Understanding climate dynamics is relevant to analyze their influence on geosynthetics' durability and the available properties dimensioning of above-ground. Although natural

degradation tests require longer durations than accelerated tests, these are of paramount importance because they represent the actual use conditions, especially in synergism studies of degradation factors. The influence of climatic dynamics is verified by the increase in tensile creep strains over time and tensile strength losses.

Tensile creep tests with a 22° inclination proved effective in durability estimation by synergism between tensile creep and weathering. This study can be used for other geotextiles and geotextile-related products.

The study results have been promising in addressing the influence of the synergy of degradation factors. In addition, greater knowledge of the geosynthetic degradation synergism in medium and long-term applications increases the reliability of design lifetime estimation and sustainable and economical engineering practices.

Acknowledgements
The authors thank the financial support of the Federal Technological Education Centre of Minas Gerais (CEFET-MG), and the National Council for Scientific and Technological Development (CNPq). Huesker is also acknowledged for providing the geotextile.

Fundings
This research received external funding: Federal Technological Education Centre of Minas Gerais, CEFET/MG (Propesq n° 088/12) and National Council for Scientific and Technological Development, CNPq (Demanda Universal n° 456236/2014-7).

Data availability statement
Publicly available datasets were analyzed in this study. This data can be found here: https://sig.cefetmg.br/sigaa/verArquivo?idArquivo=5008516&key=bca062432a0fbb4a8e62528974e07f4b (accessed on 10 December 2024).

Author contribution statement
Mag Geisielly Alves Guimarães (Conceptualization, Methodology, Formal analysis, Writing-Review and Editing), *Denise de Carvalho* Urashima (Conceptualization, Methodology, Formal analysis, Writing-Review and Editing), *Beatriz Mydori Carvalho* Urashima (Formal analysis, Writing-Review and Editing).

References

1. M.P. Lopes, and M.L. Lopes, A Durabilidade dos Geossintéticos (FEUP Edições, Porto, 2010)
2. ASTM D 5819. Standard Guide for Selectiong Test Methods for Experimental Evaluation of Geosynthetics Durability. ASTM International, West Conshohocken, PA, USA (2022)
3. ISO TS 13434. Geosynthetics - Guidelines for the Assessment of Durability. International Organization for Standardization, Brussels, Belgium (2020)
4. C.R. Lawson, Geotextile containment for hydraulic and environmental engineering. Geosynth. Int. **15**, 384-427 (2008). https://doi.org/10.1680/gein.2008.15.6.384
5. C. Hsieh, J.B. Wang, Y.F. Chiu, Weathering properties of geotextiles in ocean environments. Geosynth. Int. **13**, 210-217 (2006). https://doi.org/10.1680/gein.2006.13.5.210
6. R.W. Sarsby (Edited by). Geosynthetics in Civil Engineering (The Textile Institute, Woodhead Publishing Limited, Cambridge, 2007)
7. J.H. Greenwood, H.F Schroeder and W. Voskamp, Durability of Geosynthetics (The Netherlands, CUR committee C 187 - Building & Infrastructure, 2012)

8. J.R. Carneiro, P.J. Almeida, M.L. Lopes, Some synergism in the laboratory degradation of a polypropylene geotextile. Constr. Build. Mater. **25**, 586-591 (2014). http://dx.doi.org/10.1016/j.conbuildmat.2014.10.001
9. R.M. Koerner, Y.G. Hsuan, G.R. Koerner, Lifetime predictions of exposed geotextiles and geomembranes. Geosynth. Int. **24**, 198-212 (2017). https://doi.org/10.1680/jgein.16.00026
10. ISO 9864. Geosynthetics - Test method for the determination of mass per unit area of geotextiles and geotextiles-related products. International Organization for Standardization, Brussels, Belgium (2005)
11. ISO 9863-1. Geosynthetics - Determination of thickness at specified pressures - Part 1: Single layers. International Organization for Standardization, Brussels, Belgium (2016)
12. ASTM D5035. Standard Test Method for Breaking Force and Elongation of Textile Fabrics (Strip Method). ASTM International, West Conshohocken, PA, USA (2019)
13. J.F. Escobedo, E.N. Gomes, A.P. Oliveira, J. Soares, Modeling hourly and daily fractions of UV, PAR and NIR to global solar radiation under various sky conditions at Botucatu, Brazil. Appl. Energy **86**, 299-309 (2009). https://doi.org/10.1016/j.apenergy.2008.04.013
14. J.F. Escobedo, E.N. Gomes, A.P. Oliveira, J. Soares, Ratios of UV, PAR and NIR components to global solar radiation measured at Botucatu site in Brazil. Renew. Energy **36**, 169-178 (2011). https://doi.org/10.1016/j.renene.2010.06.018
15. J.F. Escobedo, A. Dal Pai, A.P. Oliveira, J. Soares, E. Dal Pai. Diurnal and anual Evolution of UV, PAR and NIR irradiations in Botucatu/Brazil. Energy Procedia **57**, 1130-1139 (2014). https://doi.org/10.1016/j.egypro.2014.10.099
16. ISO 877-1. Plastics - Methods of exposure to solar radiation - Part 1: General guidance. International Organization for Standardization, Brussels, Belgium (2009)
17. ISO 877-2. Plastics - Methods of exposure to solar radiation - Part 2: Direct weathering and exposure behind window glass. International Organization for Standardization, Brussels, Belgium (2009)
18. M.G.A. Guimarães, D. M. Vidal, D.C. Urashima, C.A.C. Castro. Degradation of polypropylene woven geotextile: tensile creep and weathering. Geosynth. Int. **24**, 213-223 (2017). https://doi.org/10.1680/jgein.16.00029
19. M.G.A. Guimarães, D.C. Urashima, D.M. Vidal, C.A.C. Castro, 2020. Influence of the open and backed exposures on the geosynthetics' durability by outdoor weathering. Braz. J. Dev. **6**, 37031-37049 (2020). https://doi.org/10.34117/bjdv6n6-295
20. F.P. La Mantia, M. Biondo, M. Ceraulo, M.C. Mistretta. In-line monitoring of the photooxidation behavior of a PP/clay nanocomposite through creep measurements. Polym. Degrad. Stab. **130**, 271-276 (2016). https://doi.org/10.1016/j.polymdegradstab.2016.06.022

Evaluation of the Degradation of Polypropylene Geotextiles under Real Coastal Conditions and UV Radiation Exposure

Ewerton Weynemi Cavalcante dos Santos*, *Lizandra* Maria Ferreira Gurgel[2], *Francisco* Felinto de Lima Neto [3] and *Fagner* Alexandre Nunes de França [3]
[1]Independent author, Brazil
[2]Universidade Federal Rural do Semi-Árido, Brazil
[3]Universidade Federal do Rio Grande do Norte, Brazil

Abstract. Geotextiles are permeable polymeric fabrics used in coastal protection to allow water flow while retaining fill material. These materials are usually minimally exposed to solar radiation (UV) and other atmospheric agents, often being covered by soil or liquids. However, exposure during installation can cause degradation. This study analyzed the impacts of weathering on a polypropylene geotextile exposed to different UV radiation conditions in Natal/RN, Brazil. The samples were exposed for 29, 58, and 90 days under four conditions: on a wooden table, on beach sand, immersed in seawater, and on beach sand submerged in seawater. After exposure, tensile strength tests were conducted. The results indicated that the transverse tensile strength of the exposed samples remained within the confidence intervals of the virgin geotextile ($50.92 \leq \mu \leq 56.46$ kN/m), suggesting no significant degradation during exposure. The samples immersed in seawater exhibited the lowest standard deviation in strength, with an average of 1.993 kN/m. On the other hand, the samples on beach sand submerged in seawater showed the lowest average strength, at 53.77 kN/m. In conclusion, exposure to coastal weathering during the studied periods did not significantly affect the geotextile's integrity.

1 Full paper to be published in:

2 https://www.e3s-conferences.org/articles/e3sconf/abs/2025/44/contents/contents.html

3

* Corresponding author: Wweynemi@gmail.com

Water Storages with PVC Liners and Floating Covers

Michael (Mike) A. Sadlier[1*]

[1] Geosynthetic Consultants Australia, Melbourne, Australia

Abstract. This paper discusses the advent of flexible PVC geomembranes with Ketone Ethylene Ester plasticiser packages and their growing use in geomembrane liner and floating cover systems for water reservoirs containing potable water. It will discuss the use of liner underdrain systems to capture any leakage and which also incorporate a conductive geotextile to enable effective Electronic Leak Location (ELL) surveys. This has resulted in reservoirs which have very low leakage rates.

1 PVC and Ketone Ethylene Ester Plasticisers

Flexible PVC (poly vinyl chloride) for geomembranes has been around for a very long time with the practice in the Americas tending towards relatively thin (less than 1 mm thick) unreinforced materials and the practice in Europe tending towards thicker materials usually with a woven scrim or other reinforcement. Plasticisers are used in the formulations to make the normally stiff PVC flexible. The traditional plasticisers were often unstable and stability for long term exposure required an additive package that included heat and light stabilisers. Stability for long term exposure was often variable but the Author experienced PVC roofing membranes in the 1970's that were capable of providing 30 years of exposed performance in the high UV Australian environment.

The Elvalloy plasticiser package for PVC is a proprietary ketone ethylene ester (KEE) package which is a solid polymeric plasticiser rather than liquid plasticiser. Once blended it is said to form an ethylene interpolymer alloy (also called EIA). These PVC formulations are capable of providing excellent performance in exposed applications and are also able to meet potable water requirements. They were initially available from the USA as fairly thin geomembrane materials and they are now available from Europe and the Middle East in thicker reinforced formats. The products retain their essential PVC characteristics of softness and flexibility. The reinforced products lay very flat with minimal wrinkles and this makes welding easy.

The Fabricated Geomembrane Institute [1] has published a guide to these PVC/EIAGeomembranes with a lot more information about the formulation, specifications and use of these materials.

Apart from the improved performance one of the benefits of the PVC/EIA technology is that we can use Nuclear Magnetic Resonance testing based on ASTM D8154+to determine the proportions of PVC and KEE in the formulation. An ashing test similar to ASTM D4128 that is used for HDPE is also required to determine the filler content. Being able to determine the KEE content by testing is a key benefit to specifiers and owners.

* Corresponding author: sadlierma@gmail.com

2 Potable Water Compatibility Testing

The National Sanitation Foundation in the USA has long used exposure testing to determine the suitability of geomembranes for use with potable water by chemical analysis of the exposed water. In Australia we have adopted under Australian Standard AS4020 a geomembrane exposure test using a tasting panel of people to determine whether excess taste and odour has been imparted to the water by the exposure to the geomembrane.

This standard was initially developed for domestic water pipes and fittings and is based on what is considered to be a standard exposure rate of 15 000 mm^2/L. This is rather severe for a geomembrane in a small reservoir and an exposure rate of 10 000 mm^2/L or less for a larger reservoir is considered more reasonable.

Some of the traditional plasticiser and stabiliser packages for PVC have some difficulty in meeting potable water requirements with strong UV stabilisers and we have seen products with different formulations for the two sides in order to accommodate the potable water on one side and the UV and general weathering exposure on the other side. The PVC/EIA materials are generally able to meet both the weathering requirements and the potable water requirements with the same formulation on both sides.

3 Floating Cover Issues including Maintenance

These floating covers are generally built in the empty basin with sand filled geomembrane tubes as ballast lines and matching floats. As the water level rises the ballast lines form trenches which enable the collection of rain water. A more detailed description of these covers was provided by Sadlier and Frobel [3] and Sadlier [4] [5].



Fig 1. A typical water reservoir cover with floats and ballast, access walkways to hatches and a sump as well as debris and ponded water. This one is CSPE (Chlorosulfonated Polyethylene).

In the past we would remove the surface water using a submersible pump installed in a

sump or basket in one of the cover trenches. These pumps suffered from difficulties with control using float switches that can be fouled as well as blockages from leaves and other debris. Access for maintenance was difficult and there is a trend now to use off-cover pumps where there is only a suction hose foot and level control switches in the sump. These pumps also have issues during long dry periods when the suction line can loose its prime.



Fig 2 An off-cover pump with a tank to prime the suction line

These floating covers normally have access hatches for diver access and water sampling along with associated walkways with foam flotation and non-skid surfaces. Health and safety issues and associated procedures have meant that these features are used infrequently.



Fig 3. A RPP (Reinforced Polypropylene) water reservoir floating cover with a toe line ballast arrangement Circa 2000 when new.

Combined with a general lack of maintenance mainly because the reservoir operators are reluctant to empty the reservoir, the wind blown soils tend to collect in the trenches and then

harbour growth of various kinds of vegetation.



Fig4. The same RPP reservoir cover as Fig 3 from a different view several years later with grass and trees growing in the trenches

4 Liner system configurations

Many of these reservoirs were originally built as post second World War employment projects and are cut to fill earthen basins with some sort of clayey liner of fairly low permeability. They have often been fitted previously with geomembrane liners and floating covers. Normally the floating cover material has exceeded its service capability and the projects are essentially renovations with new geomembrane liners and floating covers.

Depending on the conditions we have sometimes left the old liner in place and on other occasions it has been removed often to allow the installation of a new underdrain pipe network.

The new liner system will always have the new PVC liner installed over a conductive geotextile with a geonet or geocomposite as a planar underdrain. The geocomposite may or may not have a geotextile on the underside depending on whether the actual subgrade is the old liner, concrete or the low permeability original material. There is often an existing sump with a gravity outlet pipe which can be used for the underdrain but if there is no sump and gravity pipe a special down-the-slope underliner pump system will be installed. So all of the installations have an effective underliner drainage system that means that leakage can be captured and measured.

The conductive geotextile enables the liner to be Electronic Leak Location (ELL) tested by the ARC testing method. It was originally based on a robust and quite heavy grade of needle punched non-woven geotextile with graphene treatment. However some difficulties with the supply chain lead to some projects using a lighter weight heat bonded geotextile also with graphene treatment. This lighter weight heat bonded material suffered a lot of damage under foot traffic during installation that required repairs. The more robust needled non-woven is now preferred.

5 Leakage rate performance

Based on North American data Peggs and Giroud [1] discussed leakage rates in different across a variety of water reservoirs and the factors that influence leakage rates including the water heads and effectiveness of the leakage flow paths. They suggested action leakage rates for a variety of conditions which included an action leakage rate of around 2300 litres/hectare/day for a water depth of 4 m.

Several of these recent reservoir renovation projects have seen PVC liners installed over geocomposite drain systems with existing compacted clayey soils, concrete liner or old geomembrane retained as a de facto secondary liner. Sizes have ranged from 3000 sqm to 15,000 sqm with effective water depths of 4 to 8 m. Most have used conductive geotextile to facilitate leak location survey by the Arc Test method and others had water introduced to enable a dipole leak location survey.

The observed leakage rates were all less than 150 litres/hectare/day. Several of the more recent projects which benefited from the familiarity of the installation crews with the system have seen leakage rates less than 20 litres/hectare/day.

6 Summary

The paper has discussed the advent of flexible PVC geomembranes with ketone ethylene ester plasticiser packages and their growing use in geomembrane liner and floating cover systems for water reservoirs containing potable water.

It has discussed the use of liner underdrain systems to capture and monitor any leakage and the inclusion of a conductive geotextile to enable effective ELL surveys. This has resulted in reservoirs which have very low leakage rates.

References

1. Peggs I.D. and Giroud J.P.(2014) "Action Leakage Rate for Reservoir Liners" 10th ICG Berlin 2014
2. Fabricated Geomembrane Institute (2017) "Current Overview of EIA Geomembranes"
3. Sadlier, M.A., Frobel R.K (2018) "Current Developments and Trends for Water Reservoir Renovation with Geosynthetics" 11th ICG, Seoul, South Korea, October 2018
4. Sadlier M.A. (2022) "Liners and Covers for Reservoirs – Evaluation and Replacement" GeoANZ #1 2022.
5. Sadlier M. A. (2023) "Some current topics regarding liners and covers for water storages". 12th ICG Rome, Italy September 2023

SESSION 2 B

ESTING, QUALITY (2)

Design of unpaved forest roads - stress-strain response of a reinforced soil under triaxial conditions

David Carlos[1], *Olávio* Cafôfo[2], *Joaquim* Macedo[1], and *Margarida* Pinho-Lopes[1*]

[1]CERIS—University of Aveiro, Department of Civil Engineering, 3810-193 Aveiro, Portugal
[2]Megavia – Construções e Obras Públicas, SA, 2400-119 Leiria, Portugal

Abstract. Often, the design and construction of unpaved forest roads makes use of locally available soils. The road cross section consists of a base layer formed by locally available soil, good-quality aggregate or a mixture of these materials. To decrease the quantity of good-quality aggregates required for building such layer, using locally sourced soils is favoured. Including layers of geosynthetic reinforcements will contribute to reducing the quantities of granular material forming the base layer and/or increase its mechanical properties. This paper studied the influence of single pocket geocells on the mechanical response of a locally sourced soil (well-graded sand with gravel) close to an unpaved forest road (Aveiro, Portugal). The geocells were 3D printed, to define a reinforcement geometry adjusted to the soil characteristics, namely in terms of particle size distribution. The mechanical response of the composite material was characterised using triaxial tests. This allowed assessing its stress-strain response and any changes relatively to the unreinforced soil. The strength parameters of the composite material were estimated using equations from the literature. The study demonstrates that the inclusion of single pocket geocells enhanced the mechanical properties of the soil. These geocells increased the soil's peak friction angle and provided additional confining stresses.

Full paper to be published in:
https://www.e3s-conferences.org/articles/e3sconf/abs/2025/44/contents/contents.html

* Corresponding author: mlopes@ua.pt

Enhancing reinforced soil performance: polymeric coated steel woven wire mesh and geogrid interaction in composite systems

Gianluca Brocca[1*], *Marco* Vicari[1], and *Giulia* Lugli[2]

[1]Officine Maccaferri S.p.A., DT Business Unit, Bologna, Italy
[2] Officine Maccaferri S.p.A., GSY Business Unit, Bologna, Italy

Abstract. The pullout resistance at the interface of composite reinforcement systems is a fundamental element in the design of reinforced soil structures. A correct evaluation of this strength allows for the proper sizing of the reinforcement and ensures that the structure can withstand the expected stresses during its lifecycle. This research investigates the pullout behaviour of polymer-coated double twist wire mesh, conforming to EN 10223-3, used in reinforced fill (Terramesh) in various soil conditions and in combination with several polyester geogrids. This research, conducted following the EN 13738 standard methodology with modifications to accommodate the specific test setup, provide the experimental data necessary to calibrate the numerical models used in design and to verify the validity of the simplifying assumptions adopted.
The primary objective was to elucidate the interface friction factor between wire mesh facing elements and different structural fills, with a particular focus on the influence of steel wire mesh and geogrid interface. A comprehensive experimental program, encompassing several pullout tests, was conducted to evaluate the load-displacement response, ultimate pullout resistance, and failure modes of the reinforcement system. Normal load, and geogrid type were systematically varied to assess their impact on the pull-out capacity. The study aims to provide quantitative data on the performance enhancement achieved through the combined use of polymer-coated wire mesh and polyester geogrids. These findings are expected to contribute significantly to the design and optimization of reinforced soil structures, particularly those employing polymer-coated double twist wire mesh systems, by offering a deeper understanding of the underlying reinforcement mechanisms.

Full paper to be published in:
https://www.e3s-conferences.org/articles/e3sconf/abs/2025/44/contents/contents.html

* Corresponding author: g.brocca@maccaferri.com

Development of shear resistance at cohesive soil – geotextile interfaces

Ioannis Markou[1*], and *Evangelos* Evangelou[1]

[1]Democritus University of Thrace, Department of Civil Engineering, Soil Mechanics and Foundation Engineering Laboratory, University Campus – Kimmeria, GR-67100 Xanthi, Greece

Abstract. The shear resistance at cohesive soil – geotextile interfaces is important for the proper design of geotextile-lined structures. Although the interaction behaviour at cohesive soil – geotextile interfaces has been studied in the past, most of those research efforts have been focused primarily on the determination of the shear resistance at failure. Therefore, an attempt to quantify the development of shear resistance at the cohesive soil – geotextile interfaces with increasing shearing displacement is presented in this study. Toward this end, direct shear tests were conducted on soil – geotextile interfaces using a modified 100 mm shear box. A compacted cohesive soil of low plasticity (CL) was tested in contact with three woven and four non-woven geotextiles of five types. The direct shear tests yielded polynomial failure envelopes for the cohesive soil – geotextile interfaces, possibly indicating a transition from drained to undrained conditions at the interface with increasing normal stress. A special method for the determination of the interface shear strength parameters considering the non-linearity of the failure envelopes, is applied in the present study. The shear resistance parameters are functions of the shearing displacement at the cohesive soil – geotextile interfaces and their values at failure reveal a transition from "friction-like" behaviour to "adhesion-like" behaviour as normal stress increases.

Full paper to be published in:
https://www.e3s-conferences.org/articles/e3sconf/abs/2025/44/contents/contents.html

* Corresponding author: imarkou@civil.duth.gr

Evaluating the interaction between geogrid and recycled aggregate using pullout tests

Ahsan Rehman Khan[1*], *Gemmina* Di Emidio[1], *and Nicolas* Denies[2]

[1]Laboratory of Geotechnics, Dept. Civil Engineering, Ghent University, Belgium
[2]Buildwise, Unit Structural Work, Belgium

Abstract The understanding of the fill material-geogrids interface is critical in the design of the reinforced fill structure. Pullout tests are commonly used to characterize the interaction between fill material and geogrids. In recent years, recycled aggregate shows some promising results to be used as an alternative fill material. Nevertheless, the interaction between selected recycled aggregate and geogrids requires further investigation. This paper presents experimental results focusing on the interaction between one type of recycled aggregate and two different geogrids through a series of large-scale pullout tests. The pullout resistance of the geogrid is correlated with the confining stress. When the confining stress increases from 10 to 30 kPa, the peak value of the pullout resistance also increases due to the improved interlocking of recycled aggregate with the geogrid. Tighter interlocking provides greater resistance to the applied pullout force, leading to higher pullout resistance. Increased vertical confining stress enhances contact between the geogrid and recycled aggregate, creating a stronger bond resulting in dilatancy of the aggregates, which in turn results in higher frictional resistance against the pullout force. The results show that the tested recycled aggregate can be used as a fill material in a reinforced fill structure.

Full paper to be published in:
https://www.e3s-conferences.org/articles/e3sconf/abs/2025/44/contents/contents.html

* Corresponding author: ahsanrehman.khan@ugent.be

Influence of construction method on pullout resistance of polymeric strap reinforcement

Aníbal Moncada[1,2*], *Núria Girbau*[1], *Ivan P. Damians*[1,2,3], *Sebastià Olivella*[1,2], and *Richard J. Bathurst*[4]

[1] Department of Civil and Environmental Engineering (DECA), Universitat Politècnica de Catalunya·BarcelonaTech (UPC), Campus Nord UPC, 08034 Barcelona, Spain
[2] International Centre for Numerical Methods in Engineering (CIMNE), Campus Nord UPC, 08034 Barcelona, Spain.
[3] VSL International Ltd, Barcelona, Spain.
[4] Geoengineering Centre at Queen's-RMC, Civil Engineering Department, Royal Military College of Canada, Canada.

Abstract. The paper summarizes the results of several pullout box test series carried out on polymeric straps made of polyester (PET) yarns encased in polyethylene (PE) sheaths with a rough, continuous surface. The PET strap ultimate tensile strengths ranged from 30 to 100 kN/strap. Reinforcement specimens were subjected to pullout forces under different confining pressures using a large steel pullout box. Different reinforcement lengths and installation procedures were used. The test results were interpreted quantitatively with focus on damage to the sheath and yarn elements after pullout due to different installation/construction procedures. The consequences of damage during installation and pullout with respect to the long-term performance of strap reinforcement are explored. Implications to design and construction practice for PET strap reinforced soil walls are identified.

Full paper to be published in:
https://www.e3s-conferences.org/articles/e3sconf/abs/2025/44/contents/contents.html

* Corresponding author: anibal.moncada@upc.edu

Fibre reinforcement of a uniform sand: stress-penetration and stress-strain responses

Catarina Martins[1], *Daniela* Rodrigues[1], *David* Carlos[1], *Susana* Morais[2], *Joaquim* Macedo[1] and *Margarida* Pinho-Lopes[1*]

[1]CERIS—University of Aveiro, Department of Civil Engineering, 3810-193 Aveiro, Portugal
[2]Navigator Forest Portugal, SA, 4440-488 Porto, Portugal

Abstract. Fibres are one of many reinforcement types used to improve the mechanical response of soils, and can be natural, synthetic or waste. This paper studied the influence of polymeric fibres as randomly distributed reinforcement for sand. Fibres have proven useful for soil reinforcement, improving the strength and ductility of sands. Herein, the mechanical response of the sand-fibres composite material was characterised using CBR tests (stress-penetration response) and triaxial tests (stress-strain behaviour). The sand studied is a uniform material with an average particle size of 0.75 mm. Polypropylene fibres were used as reinforcement, with diameter and length of 0.031 mm and 12 mm, respectively. Two different fibre contents were studied (0.5% and 1.0%, in mass). The increase of fibre content led to an improvement of stress – penetration response for larger deformations. However, the CBR tests have some limitations, and the results may not be representative of the response under real conditions. The stress – strain behaviour, in general, was improved with the increase of fibre content, obtaining a better response with 1.0% of fibre content. The fibres need to be mobilised for the effect of reinforcement start to become effective. The soil-fibre interaction mechanism identified was the continuous thin filament fibre reinforcement.

Full paper to be published in:
https://www.e3s-conferences.org/articles/e3sconf/abs/2025/44/contents/contents.html

* Corresponding author: mlopes@ua.pt

SESSION 2 C
REINFORCEMENT APPLICATIONS (2)

Microgrid reinforcement of scaled railway ballast

Rafael Anjos[1*], *Victor* Neto[2], *Margarida* Pinho-Lopes[1], and *William* Powrie[3]

[1]CERIS, Department of Civil Engineering, University of Aveiro, Portugal
[2]TEMA, Department of Mechanical Engineering, University of Aveiro, Portugal
[3]Faculty of Engineering and Physical Sciences, University of Southampton, United Kingdom

Abstract. Ballasted tracks are predominant on railways worldwide. Previous research on random fibre reinforcement of scaled ballast has shown that flexible polymeric fibres can increase the shear resistance and ductility of the ballast. Owing to the difficulty of testing very coarse materials in standard laboratory apparatus, scaled-down materials have been introduced. A coarse aggregate with a particle size distribution curve parallel to that of full-scaled ballast can be used to investigate relevant shear stress-strain properties. Geogrids, usually as continuous sheets, interlock with aggregate particles, enhancing the overall shear resistance and stiffness. This paper investigates the reinforcement effectiveness of individual microgrids. obtained from a commercially available geogrid, mixed with a granular material corresponding to $^1/_3$-scaled railway ballast. Packing tests were used to inform the fibre mix design. The effect of microgrid shape and content on the mechanical behaviour of $^1/_3$-scaled ballast was investigated by means of a series of monotonic triaxial tests. Microgrids behave similarly to strip fibre random reinforcement, in reducing dilatancy while increasing the deviator stress. However, a benefit compared with strip fibre reinforcement is that the reduction in dilatation arising from the disruption to the packing caused by the microgrids does not result in a loss of stiffness.

Full paper to be published in:
https://www.e3s-conferences.org/articles/e3sconf/abs/2025/44/contents/contents.html

* Corresponding author: rafaelanjos@ua.pt

Geogrid-stabilized eco-friendly aggregates for pavement base – quantitative assessment using Bender Element sensor technology

Han Wang[1], *Hyojung* Ko[1], *Mingu* Kang[2], *Erol* Tutumluer[3*], and *Heather* Shoup[4]

[1]Graduate Research Assistant, University of Illinois Urbana-Champaign, IL 61801, USA
[2]Assistant Professor, University of St. Thomas, St. Paul, MN 55105, USA
[3]Abel Bliss Professor, University of Illinois Urbana Champaign, IL 61801, USA
[4]Central Office Geotechnical Engineer, Illinois Dept. of Transportation, Springfield IL 62704, USA

Abstract. Geogrids provide mechanical stabilization by effectively restraining aggregate movements in a granular layer which in turn improve pavement performance and extend its lifespan. This paper presents an experimental evaluation of a multi-axial extruded geogrid stabilizing two types of eco-friendly aggregates, i.e., virgin crushed limestone and recycled concrete aggregate, used in pavement unbound base/subbase applications. The study evaluated geogrid stabilized aggregate resilient modulus and permanent deformation characteristics and assessed the modulus enhancement provided by the geogrid. Repeated load triaxial tests were conducted on 152-mm (6-in.) diameter and 305-mm (12-in.) high cylindrical specimens, instrumented with embedded Bender Element (BE) shear wave transducers. Both control specimens and geogrid-stabilized specimens with geogrid placed at specimen midheight were constructed. During resilient modulus testing, shear wave velocity measurements were also taken by the transmitter-receiver BE sensor pairs embedded immediately above the specimen midheight to determine small-strain moduli. Specimen permanent deformations were then evaluated for up to 10,000 load repetitions. The geogrid-stabilized specimens had lower permanent deformations than the control specimens and provided considerable local stiffness enhancements for both the recycled and natural aggregates to demonstrate a sustainable geosynthetic application.

Full paper to be published in:
https://www.e3s-conferences.org/articles/e3sconf/abs/2025/44/contents/contents.html

* Corresponding author: tutumlue@illinois.edu

Experimental studies on the cyclic behaviour of reinforced unbound railway base courses

Claudia Bräunig[1*], *Ivo* Herle[1], and *Ulrike* Weisemann[2]

[1] Technische Universität Dresden, Institute for Geotechnical Engineering, 01069 Dresden, Germany
[2] Hochschule für Technik und Wirtschaft Dresden, Railway construction, 01069 Dresden, Germany

Abstract. In railway construction, base courses of unbound coarse-grained material are usually placed between the existing subgrade and the track. Geosynthetics, in particular geogrids, are used to improve the system behaviour. The reduction in the thickness of the base course due to the geogrid is based on empirical approaches. In this work triaxial tests were performed to investigate the influence of the geogrid. A specimen size of d · h = 100 · 200 mm was chosen. This small sample size saved material, reduced workload and allowed the use of a standard triaxial apparatus. However, the base course material and the geogrid had to be geometrically scaled. Cyclic triaxial tests were carried out on the unreinforced and reinforced specimens with the aim to reproduce the conditions caused by rail traffic loading. For this purpose, the low stress and high number of loading cycles N = 500,000 were chosen. It was shown that the inserted geogrid reduces the magnitude of deformation and the accumulated strains compared to the unreinforced material.

Full paper to be published in:
https://www.e3s-conferences.org/articles/e3sconf/abs/2025/44/contents/contents.html

* Corresponding author: claudia.braeunig@tu-dresden.de

Compaction of a geotextile-reinforced sand contaminated with tyre microplastics

Hakki O. Ozhan[1*], and *Murat* Yavuz[1]

[1]Civil Engineering Department, Yeditepe University, Inonu Mah., Kayisdagi Cad., 326A, 26 Agustos Yerlesimi, Atasehir-Istanbul 34755, Turkey

Abstract. In order to investigate the effect of placing geotextile and adding shredded tyre microplastics on the compaction performance of a sand that simulated a subbase soil contaminated with microplastics, up to two layers of a woven geotextile were placed in the sand and standard Proctor compaction tests were conducted. The effects of the number and location of the geotextile on γ_{dmax} of the sand were determined. The concentration of the shredded tyre microplastics in the sand was chosen as 0.1% by dry mass that represented an average tyre microplastics concentration in subbase soils due to the vehicle tyre abrasion on roads. Test results indicated that shredded tyre microplastics addition caused an increase in γ_{dmax} of the sand. Moreover, placing two layers of geotextiles resulted in the highest γ_{dmax} when compared with one geotextile layer placed either between the first and second or second and third compacted layers. γ_{dmax} of the sand without any reinforcement was measured as 15.99 kN/m^3 whereas two geotextile placement led to a γ_{dmax} of 16.58 kN/m^3. Microplastics addition caused γ_{dmax} to further increase to 16.69 kN/m^3. In conclusion, not only geotextile placement but also microplastic transfer contributed to the stability by enhancing compaction.

1 Introduction

The enhancement of the stability of a road or highway is provided by sufficient compaction of the subgrade layer. The main goal of compacting the subgrade layer of a road is to increase the maximum dry unit weight (γ_{dmax}) of the soil beneath the road pavement. There are several soil improvement methods for improving the stability of the road. Placing geotextile layers is one of these soil reinforcement techniques. Using geotextile in subgrade soil layer of a road or highway, generally enhances the mechanical properties of the soil [1-2]. However, the number and the exact location of the geotextile layers in the subgrade soil determine the level of the contribution to the stability of the road.

Kim et al. [3] performed Proctor compaction tests on a soil composed of silty sand. The effect of the placement of up to four geogrid layers in the soil was investigated. The results indicated that the soil with two geogrid layers had the optimum stability with a sufficient increase in the maximum dry unit weight (γ_{dmax}) and decrease in the optimum water content (w_{opt}). Moreover, Keskin et al. [2] conducted Proctor compaction tests on a sand deposit. The

* Corresponding author: hakki.ozhan@yeditepe.edu.tr

placement of geotextile layers enhanced γ_{dmax} value. The placement of one geotextile layer in the middle of the sand layer resulted in slightly higher (γ_{dmax}) than the placement of two geotextile layers at one third (1/3) and two thirds (2/3) of the total height. In another study, geotextile placement in a gravel-silt mixture, enhanced the bearing capacity [4].

The plastic particles with a particle size of 0.0001-5 mm are expressed as microplastics [5]. These particles both threaten the health and contaminate the environment [6]. The tyre microplastics transferred from the shredded vehicle wheels into the subbase layers can easily be digested by animals or plants and hence, health problems can take place. Furthermore, these microplastic particles might contaminate fruits and vegetables beneath the ground level. When we eat these products, the microplastics might also reach to our digestive or respiratory systems and as a result, serious health problems might occur [7-9]. Moreover, the tyre microplastics can hinder the agricultural productivity. They can even scatter into water sources or air by moving vertically or horizontally [6, 10, 11]. The microplastic particles can also be carried into the subsoil layers by various agents. The formation and transportation of microplastics due to the abrasion of the vehicle tyres on road surfaces can be considered as one of the main agents that contribute to the transfer of microplastics into the soil [12, 13]. According to several researches, the average microplastic concentration in soil was found to be not greater than 1% [14]. For instance, the amount of microplastics in a sandy soil deposit due to the abrasion of vehicle tyres on a road in Germany, was measured as 0.1% [15]. Furthermore, the concentration of the vehicle tyres' microplastics in the soil beneath a motorway in Germany was obtained between 0.016% and 1.59% [16].

The main objectives of this study were to assess the effect of placing geotextile layers in a sand layer on the compaction performance of the soil that simulated a subgrade beneath a road and investigate the effect of the shredded tyre microplastics on the compactibility of the sand that represented the subgrade soil contaminated with microplastics due to the abrasion of vehicle tyres on a road. Up to two layers of a woven geotextile were used in the standard Proctor compaction tests and the effects of the number and location of the geotextile on the maximum dry unit weight of the sand contaminated with microplastics were determined. The concentration of the shredded tyre microplastics in the sand was chosen as 0.1% by dry mass that represented the average tyre microplastics amount in subgrade soils due to the vehicle tyre abrasion on roads.

2 Materials

According to the granulometric curve (Figure 1) obtained from sieve analysis as outlined in [17], the sand used in this study was classified as a poorly graded sand (SP). Furthermore, the specific gravity (G_s) of the sand was measured as 2.67 [18].

The geotextile that was placed in the sand for reinforcement was a slit-film polypropylene woven geotextile having tensile strength (along machine direction), elongation (along machine direction) and apparent opening size of 65 kN/m, 12% [19] and 0.25 mm [20] respectively.

The shredded tyre microplastic particles that were mixed with the sand consisted of polystyrene polymer. As shown in Figure 2, approximately 93% of the tyre particles passed through the sieve with an opening size of 1 mm. Moreover, 60% of these microplastic particles were smaller than 0.5 mm [17]. Due to the fact that all of the shredded tyre particles were smaller than 5 mm, they were defined as microplastics. The specific gravity (G_s) of the tyre microplastics was measured as 1.14 [18] which was much lower than that of the sand.

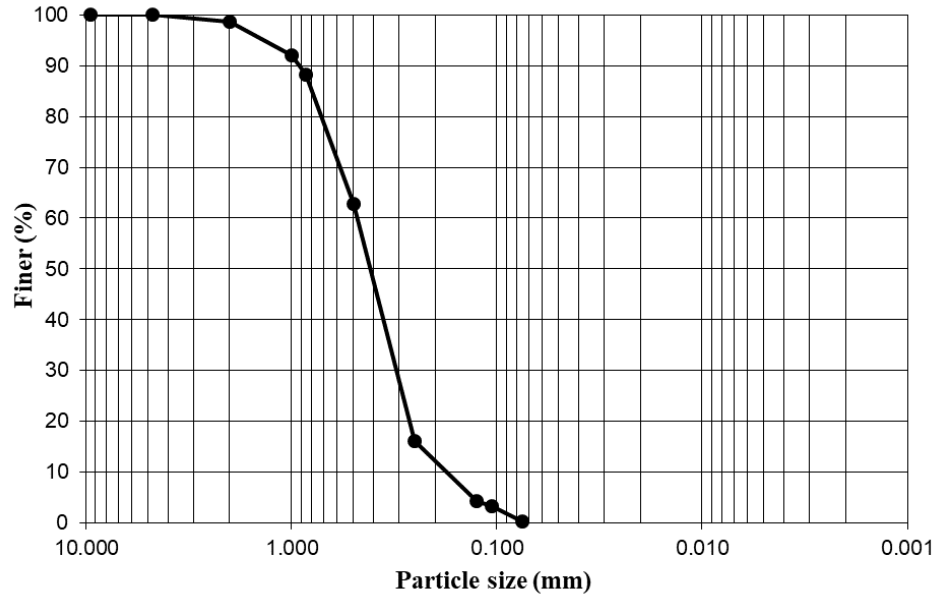


Fig. 1. Particle size distribution of the sand

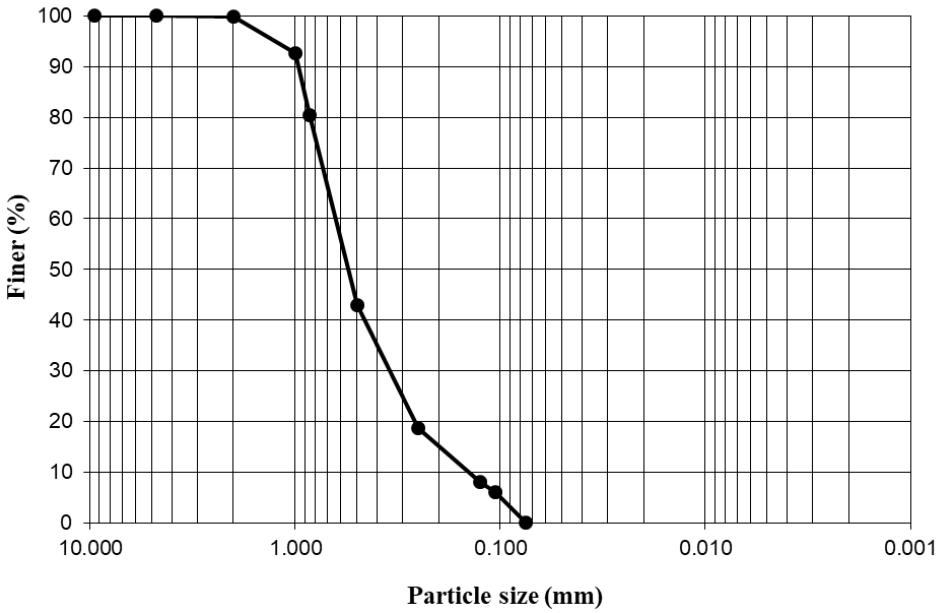


Fig. 2. Particle size distribution of the tyre microplastics

3 Methods

The woven geotextile layers were cut with a diameter (d) of 101.6 mm in order to fit in the Proctor compaction mold that had a height of 116.4 mm (h). First, almost one third of the mold (h/3) was filled with the sand and compacted as outlined in [21]. Then, one geotextile layer was placed on top of the compacted sand and afterwards, two thirds of the mold (2h/3) was filled with the sand and compacted again. Finally, one more layer of sand was filled in the mold and compacted up to the top (h) as shown in Figure 3a. Standard Proctor compaction test was repeated with one geotextile layer placed at two thirds (2h/3) of the mold after compacting the sand up to that height and before placing the last sand layer and compacting it up to the top (h) of the mold as shown in Figure 3b. The final standard Proctor compaction test (Figure 3c) was performed with two geotextile layers placed at one third (h/3) and two thirds (2h/3) of the mold respectively where the sand was compacted in three equal layers from bottom to top as outlined in [21].

Apart from placing geotextile layers in the sand, shredded tyre microplastics with a concentration of 0.1% by dry mass was also mixed with the sand and standard Proctor compaction tests were conducted on the tyre microplastics-added sand. First, the microplastic particles were added to the sand as shown in Figure 4. Then, the microplastics were mixed with the sand with the help of a shovel at a period of at least 10 minutes in order to obtain a homogeneous mixture [22]. 0.1% microplastics in the sand represented the average tyre microplastics amount that could be transferred into the subbase soil layers due to the abrasion of vehicle wheel tyres on roads [15, 16].

Standard Proctor compaction tests were also performed on 0.1% tyre microplastics-added sand with the same geotextile placements as followed before (one geotextile layer at h/3, one geotextile layer at 2h/3 and two geotextile layers at h/3 and 2h/3 of the compaction mold). As a result, the maximum dry unit weight (γ_{dmax}) and optimum water content (w_{opt}) of the sand were measured after the termination of the standard Proctor compaction tests.

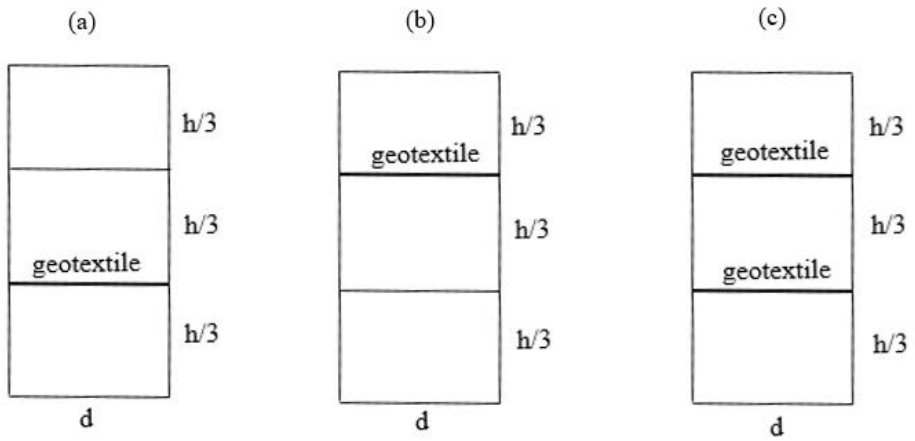


Fig. 3. Placement of (a): one geotextile layer at h/3; (b): one geotextile layer at 2h/3; (c): two geotextile layers at h/3 and 2h/3 of the compaction mold



Fig. 4. 0.1% tyre microplastics-added sand before the mixing process

4 Test results and discussion

Test results indicated that geotextile placement enhanced the compactibility of the sand by increasing γ_{dmax} as can be seen in Figure 5. The sand had γ_{dmax} of 15.99 kN/m^3 without any geotextile placement (NO GT). However, the woven geotextile placed at h/3 of the compaction mold (GT1) caused γ_{dmax} to increase to 16.19 kN/m^3. When the geotextile was placed at 2h/3 of the mold (GT2), γ_{dmax} further raised up to 16.38 kN/m^3. The highest γ_{dmax} was obtained when two layers of geotextiles were placed at h/3 and 2h/3 of the mold (GT1-GT2) with a value of 16.58 kN/m^3. When γ_{dmax} increased, w_{opt} of the sand decreased due to the placement of the woven geotextile as shown in Figure 6. w_{opt} of the sand for the tests with NO GT, GT1, GT2 and GT1-GT2 was measured as 16.7, 16.5, 16.2 and 15.9% respectively.

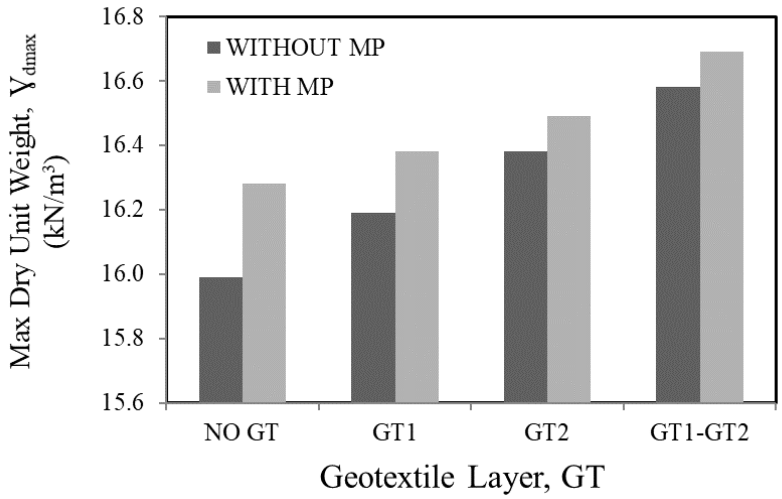


Fig. 5. γ_{dmax} change due to geotextile placement and microplastics addition to the sand

Tyre microplastics addition with a concentration of 0.1% to the sand also led to an increase in γ_{dmax} and a decrease in w_{opt}. As shown in Figure 5, γ_{dmax} of the sand with microplastics (MP) was measured higher than the sand without MP for all the tests (NO GT, GT1, GT2, GT1-GT2). For instance, microplastics addition caused γ_{dmax} of the sand without geotextile placement, to increase from 15.99 to 16.28 kN/m^3. When two layers of geotextiles were placed in the sand, γ_{dmax} also increased from 16.58 to 16.69 kN/m^3 due to the addition of 0.1% MP. w_{opt} of the sand decreased from 16.7 to 16.6% when 0.1% MP was added to the sand as can be seen in Figure 6. For the tests where the geotextile was placed in the sand, w_{opt} also slightly decreased as MP was added.

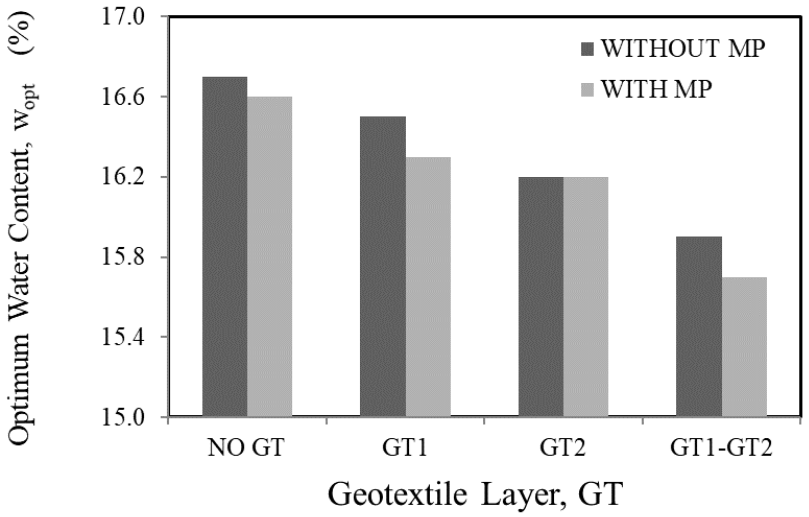


Fig. 6. w_{opt} change due to geotextile placement and microplastics addition to the sand

For all the standard Proctor compaction tests, dry unit weight (γ_d) increased up to a peak point and then decreased due to the addition of water as shown in Figure 7. As can be seen in Figure 7, γ_{dmax} increased and w_{opt} decreased when the number of the geotextile layers in the sand was increased for the test in which 0.1% MP was added to the sand.

The enhancement in the compactibility of the sand due to the placement of the geotextile could be attributed to the reduction in the lateral movement of the sand particles during the compaction process. The geotextile layer could minimize the displacement of the soil mass and hence, could result in an increase in the compaction energy. Furthermore, two geotextile layers could lead to additional reduction in the lateral displacement of the sand particles. On the other hand, when the geotextile layer was much closer to the top of the compaction mold, higher γ_{dmax} was measured. This result was obtained because the compaction energy exerted on the top sand layer could be slightly higher than the lower sand layers in the compaction mold.

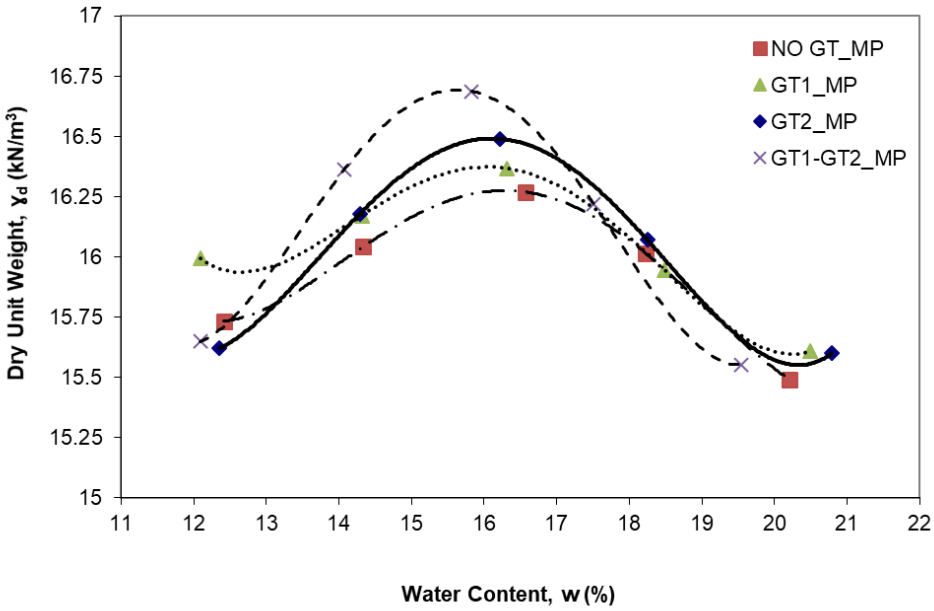


Fig. 7. Dry unit weight versus water content change of the microplastics-added sand during the standard Proctor compaction tests

The increase in the compaction degree of the sand due to the addition of 0.1% tyre microplastics could be attributed to the clogging of the voids between the sand grains. When tyre microplastics having a very low concentration (0.1%) was mixed with the sand, the microplastic particles that clogged the pores facilitated the compaction process and hence, resulted in an increase in the γ_{dmax} of the sand.

5 Conclusions

After the termination of the standard Proctor compaction tests conducted on a poorly graded sand (SP) reinforced with a woven geotextile and mixed with a concentration of 0.1% shredded tyre microplastics, the following conclusions were reached:

- Geotextile placement resulted in an increase in γ_{dmax} and a decrease in w_{opt}. As the number of the geotextile layers was increased to two, the highest γ_{dmax} was obtained. The sand without geotextile had γ_{dmax} value of 15.99 kN/m^3 whereas γ_{dmax} of the sand with one geotextile placed at h/3 and 2h/3 of the compaction mold was measured as 16.19 and 16.38 kN/m^3 respectively. The sand with two geotextiles placed at h/3 and 2h/3 of the compaction mold had γ_{dmax} of 16.58 kN/m^3.
- 0.1% tyre microplastics addition caused further increase in γ_{dmax} and decrease in w_{opt} of the sand. γ_{dmax} of 0.1% tyre microplastics-added sand without geotextile, with one geotextile placed at h/3, one geotextile placed at 2h/3 and two geotextiles placed at h/3 and 2h/3 of the compaction mold was measured as 16.28, 16.38, 16.49 and 16.69 kN/m^3 respectively.
- In conclusion, woven geotextile placement in a poorly graded sand (SP) enhanced the compaction degree by increasing the γ_{dmax} and reducing the w_{opt} of the sand. Moreover, placement of two geotextile layers resulted in a further increase in the compactibility.

- On the other hand, shredded tyre microplastics obtained from vehicle wheel tyres due to the abrasion of the tyres on roads, might easily penetrate into the subbase soil layers beneath the roads. Test results indicated that these microplastics increased the stability of the road by enhancing the compactibility.

Acknowledgements. The authors sincerely thank to Ymn Grup for providing the woven geotextile and to LASDER (Tire Industrialists Association of Turkey) for providing the shredded tyre microplastics that were used in the laboratory experiments of this study.

References

1. S.W. Perkins, Mechanical response of geosynthetic-reinforced flexible pavements. Geosynth. Int. **6**, 5, 347-382 (1999).
2. S.N. Keskin, O. Cimen, T.S. Göksan, S. Uzundurukan, M. Karpuzcu, Effect of geotextiles on the compaction properties of soils. İn Proceedings of the 2nd International Conference on New Developments in Soil Mechanics and Geotechnical Engineering, Near East University, Nicosia, North Cyprus, 28-30 May (2009), 420-424.
3. C. Kim, J.C. Im, J.W. Yoo, Effect of the geosynthetic installation on the compaction curve and compaction efficiency. KSCE Journal of Civil Eng. **22**, 12, 4841-4851 (2018).
4. K.S. Azar, R. Dabiri, The effects of geotextile layers on bearing capacity of gravel –silt mixtures. Trakya University Journal of Engineering Sciences, **16**, 2, 61-69 (2015).
5. R.C. Thompson, Y. Olsen, R.P. Mitchell, A. Davis, S.J. Rowland, A.W.G. John, D. Mcgonigle, A.E. Russell, Lost at sea: Where is all the plastic? Science, **304,** 838 (2004).
6. B.C. O'Kelly, A. El-Zein, X. Liu, A. Patel, X. Fei, S. Sharma, A. Mohammad, V.S.N.S. Goli, J. Wang, D. Li, Microplastics in soils: An environmental geotechnics perspective. Environ. Geotech. **8**, 8, 586-618 (2021).
7. M. Rezaei, M.J. Riksen, E. Sirjani, A. Sameni, V. Geissen, Wind erosion as a driver for transport of light density microplastics. Sci. Total Environ. **669**, 273–281 (2019).
8. J.C. Prata, J.P. da Costa, I. Lopes, A.C. Duarte, T. Rocha-Santos, Environmental exposure to microplastics: An overview on possible human health effects. Sci. Total Environ. **702**, 134455. (2020).
9. S.L.Wright, F.J. Kelly, Plastic and human health: A micro issue? Environ. Sci. Technol. **51**, 6634–6647. (2017).
10. L.Nizzetto, G. Bussi, M.N. Futter, D. Butterfield, P.G. Whitehead, A theoretical assessment of microplastic transport in river catchments and their retention by soils and river sediments. Environ. Sci. Process. Impacts, **18**, 1050–1059 (2016).
11. E. Zylstra, Accumulation of wind-dispersed trash in desert environments. J. Arid. Environ., **89**, 13–15 (2013).
12. P. He, L. Chen, L. Shao, H. Zhang, F. Lu, Municipal solid waste (MSW) landfill: A source of microplastics? - Evidence of microplastics in landfill leachate. Water Research, **159**, 38–45 (2019).
13. P.J. Kole, A.J. Löhr, F.G.A.J. Van Belleghem, A.M.J. Ragas, Wear and tear of tyres: A stealthy source of microplastics in the environment. Int. J. Environ. Res. Public Health, **14**, 10, 1-31 (2017).
14. M.M. Monkul, H.O. Ozhan, Microplastic contamination in soils: A review from geotechnical engineering view. Polymers, **13**, 23 (2021).
15. G. Dierkes, T. Lauschke, S. Becher, H. Schumacher, C. Földi, T. Ternes, Quantification of microplastics in environmental samples via pressurized liquid extraction and pyrolysis-gas chromatography, Anal. Bioanal. Chem. **411**, 6959–6968 (2019).

16. A. Müller, B. Kocher, K. Altmann, U. Braun, Determination of tire wear markers in soil samples and their distribution in a roadside soil. Chemosphere, **294**, 15, 133653 (2022). https://doi.org/10.1016/j.chemosphere.2022.133653
17. ASTM D6913, Standard test methods for particle-size distribution (gradation) of soils using sieve analysis. ASTM International, West Conshohocken, PA, USA (2017).
18. ASTM D854, Standard test methods for specific gravity of soil solids by water pycnometer. ASTM International, West Conshohocken, PA, USA (2014).
19. ASTM D4595, Standard test methods for tensile properties of geotextiles by the wide-width strip method. ASTM International, West Conshohocken, PA, USA (2017).
20. ASTM D4751, Standard test methods for determining apparent opening size of a geotextile. ASTM International, West Conshohocken, PA, USA (2021).
21. ASTM D698, Standard test methods for laboratory compaction characteristics of soil using standard effort. ASTM International, West Conshohocken, PA, USA (2012).
22. H.O. Ozhan, A.M.T. Elnemr, Compaction behaviour of a sandy road base contaminated with microplastics from vehicle tires. Soil Use Management, **40**, 3, e13090 (2024).

Ensuring the stability of high embankments on Ukrainian highways during reconstruction and repair using geosynthetic materials

Igor Gameliak[1], *Ganna* Zhurba[2], and *Tetiana* Diakovska[3]

[1]National Transport University, Department of System Design of Transport Infrastructure Object and Geodesy, 1 M. Omelianovycha-Pavlenka Str., Kyiv, Ukraine
[2]Euroizol Geosynthetics LLC, 7A Boryspilska St, Kyiv, Ukraine
[3]Hydrozahist LLC, 7A Boryspilska St, Kyiv, Ukraine

Abstract. Highway reconstruction in Ukraine often lacks detailed geological studies of slopes and foundations. Repairs usually involve excavation and reinforcement with cement-stabilized crushed stone and layered asphalt concrete, providing effective modulus of the pavement structure values of more than 350 – 400 MPa. However, damages frequently appear within 2–3 years due to weak foundations, soil heterogeneity, poor drainage, and increased traffic loads allowed since 2022. The primary causes of road collapses—weak bases, uncompacted layers, and inadequate drainage—have been known for decades. Increased loads have shifted the active zone from 1.5 to 2.5 m, causing even long-serving pavements to fail. This article examines reinforced embankments using geosynthetic materials in road repairs. These materials, selected for their mechanical strength and water filtering capacity, improve compatibility with subsidence soils and unstable layers. Comparisons of reinforcement strategies reveal significant improvements in embankment stability and durability with geosynthetics. Practical examples highlight their advantages in cost and installation time, reinforcing the importance of detailed engineering and geological studies for effective road repairs and reconstruction.

1 Introduction

The stability of high road embankments is a critical factor in highway reconstruction and repair, particularly in regions with complex soil and geological conditions. In Ukraine, such challenges are intensified by the frequent absence of detailed geological assessments, leading to recurring structural issues including cracking, settlement, slope instability, and landslides. These issues are often triggered by weak subgrades, insufficient compaction, poor drainage, and, more recently, the impact of increased traffic loads since 2022. Standard maintenance approaches, which typically involve excavation and reinforcement using cement-stabilized crushed stone and layered asphalt concrete to achieve effective modulus of the pavement structure values between 400 and 1200 MPa, have proven insufficient. Despite these efforts, structural damages frequently reappear within two to three years post-repair, highlighting the need for more resilient solutions.

Notable incidents across Ukraine emphasize the urgency of addressing these vulnerabilities:

1. Landslide on the Oriiv–Skhidnytsia Road (June 2020): Heavy rainfall triggered a landslide, rendering the road impassable and disrupting local connectivity.
2. Landslide on the H-09 Mukachevo–Lviv Highway (March 2024): In the Rakhiv district, intense precipitation caused severe damage to a key transport route.
3. Landslides in Zakarpattia (January 2024): Prolonged rainfalls led to widespread instability, affecting forest zones and nearby road infrastructure.
4. Landslide on the M-05 Kyiv–Odesa Highway near Troitske Village (July 2021): Prolonged rainfall caused partial embankment collapse and deformation of the road surface, significantly impacting one of Ukraine's most vital transportation corridors (Fig. 1).



Fig. 1. On the M-05 Kyiv-Odesa highway because of prolonged rains, a landslide and deformation of the road surface occurred

These events reflect a broader pattern of deterioration, often resulting from increased traffic that alters the active structural zone from 1.5 to 2.5 meters, leading to failure of formerly durable pavements. This shift underscores the limitations of traditional methods and the urgent need for innovative reinforcement solutions.

In response, the integration of geosynthetic materials has emerged as a promising strategy to enhance the durability and resilience of road embankments. Geosynthetics offer multiple benefits—reinforcing weak soils, evenly distributing loads, improving drainage, and reducing differential settlement—thereby addressing both mechanical and environmental challenges. This article investigates the application of geosynthetics in stabilizing high embankments, presenting case studies and methodologies aimed at achieving long-term infrastructure stability under increasingly demanding conditions.

2 Problem statement

The recurrent failure of highway embankments in Ukraine highlights the limitations of traditional reinforcement methods that do not account for site-specific geological conditions. The lack of comprehensive geological and engineering studies leads to the application of uniform solutions that fail to address the unique challenges posed by different soil

compositions and load requirements. This approach results in compromised structural integrity and reduced lifespan of repaired embankments.

2.1 Methodology overview

This study examines the application of geosynthetic materials to reinforce highway embankments during reconstruction and repair. Geosynthetics, including geotextiles, and geogrids, are selected based on their mechanical strength, compatibility with existing soil layers, and water filtration capacity. The selection process involves a thorough assessment of soil conditions to ensure optimal interaction between the geosynthetic materials and the native soil.

Practical examples are analysed to compare reinforcement strategies under varying conditions, focusing on the effectiveness of geosynthetics in enhancing embankment stability and durability. The study also considers factors such as cost implications and installation time to evaluate the feasibility of widespread implementation of geosynthetic reinforcement in highway maintenance practices.

3 Case Studies

3.1 Case Study 1: Major repair of Highway H-08 (Boryspil–Dnipro–Zaporizhzhia–Mariupol), section km 98+000–km 109+200, Cherkasy Region

The section between km 98+000 and km 109+200 underwent major repairs in 2020. The project involved reconstructing the embankment slopes by cutting terraces into the existing embankment body to improve stability. The road was opened to traffic on September 8, 2021. By July 2023, defects had manifested at km 98+800, characterized by longitudinal cracks up to 1 cm wide and settlement reaching 3 cm. The primary deformation occurred along the embankment slopes, suggesting insufficient load distribution and poor soil compaction during construction.

The cracking and settlement are likely due to a combination of factors:

- Inadequate embankment compaction, leading to differential settlement.
- Soil heterogeneity, with weak, dusty loess soils that are highly susceptible to moisture variations.
- Drainage deficiencies, resulting in water infiltration and reduced soil strength.

3.2 Case Study 2: Reconstruction of Highway H-08, section km 109+200–km 120+800, Cherkasy Region

This section underwent reconstruction in 2020, with the road opened to traffic on December 24, 2021. The embankment base was constructed using cement-stabilized crushed stone (PShS), and terraces were cut into the slope to improve structural integrity.

In November 2023, defects were observed at 119+200 km, including longitudinal cracks up to 1 cm wide and settlements up to 3 cm. Like the first case, the embankment showed signs of instability along the slope (Fig. 2)



Fig. 2. Cracks up to 1 cm wide and settlements of up to 3 cm at km 119+200

Analysis of Contributing Factors:

- Poor interface bonding between the new and existing embankment layers.
- Inadequate drainage, leading to water accumulation and soil softening.
- Construction technology issues, such as improper layering techniques and insufficient compaction near slope edges.

3.3 Case Study 3: Medium repairs of Highway H-16 (Zolotonosha–Cherkasy–Smila–Uman), section km 0+000–km 12+300, Cherkasy Region

The road section from km 0+000 to km 12+300 underwent medium-scale repairs in 2020. The work included milling the existing pavement, strengthening the base, and resurfacing with new asphalt layers. The road was reopened on July 30, 2021.

By November 2023, longitudinal cracks up to 5 cm wide and settlements of up to 6 cm were recorded at km 4+000. This section features an embankment with a height of 16.0 m from the base to the road surface, with a slope gradient of 1:1.75 (Fig. 3).



Fig. 3. Defects at km 4+000

Geotechnical Conditions:

- Embankment Soil: Light, dusty, flow-plastic loess-like silt (see Table 1 for soil properties).
- Subgrade Soil: Light, dusty loess-like sandy soil with moderate susceptibility to settlement.
- Slope Gradient: 1:1.2 in certain areas, increasing the risk of instability under dynamic loads.

Several factors contributed to the observed defects:

- Inadequate preparation of the subgrade, leading to localized settlement.
- Technological flaws during construction, such as poor joint treatment between asphalt layers, resulting in longitudinal cracks.
- Insufficient compaction at the pavement edges, which created weak zones prone to differential settlement.

Considering that all three studied cases stem from the same geographical context—bound by soft subgrades, poor drainage systems, and high traffic load—these cases share similar failure mechanisms and reinforcement strategies employed. These common features lead to similar design difficulties as well as solutions within the project's sites.

In order to avoid ambiguity and maintain cohesion, this publication focuses only on the most striking example, which in this case is the 16 m high embankment. This example was the choice because it demonstrates the most sophisticated design gilded with the success of the reinforcement measures taken using geosynthetics. The other case studies were deemed less interesting because they were too similar and lacked structural detail.

4 Characteristics of the soil

Table 1. Normative values of specific cohesion c_n, kPa (kgf/cm^2), angle of internal friction φ_n, deg. and modulus of deformation E, MPa (kgf/cm^2), of sandy soils of Quaternary deposits.

Sandy soils	Designation of soil characteristics	Characteristics of soils with a porosity coefficient e equal to			
		0.45	0.55	0.65	0.75
Gravelly and coarse	c_n	2	1	-	-
	φ_n	43	40	38	-
	E	50	40	30	-
Medium	c_n	3	2	1	-
	φ_n	40	38	35	-
	E	50	40	30	-
Fine	c_n	6	4	2	-
	φ_n	38	36	32	28
	E	48	38	28	18
Dusty	c_n	8	6	4	2
	φ_n	36	34	30	26
	E	39	28	18	11

Considering the presence of dusty sand within the quarry, characterized by a porosity coefficient of 0.85, the following geotechnical parameters were established after excavation and compaction to a reduced porosity coefficient $e = 0.75$. The derived design properties of the backfill material for subgrade applications beneath the road pavement are as follows: cohesion $c_n = 2$ kPa, internal friction angle $\phi_n = 26°$, and modulus of deformation E = 11 MPa. In the absence of experimental data for the precise determination of the backfill soil

properties, approximations were made based on the normative data from SNiP 2.02.01-83: Foundations of Buildings and Structures.

Based on the approximation analysis, two primary soil types were identified with a reliability level of 95%, which were subsequently adopted for further structural calculations:
Dusty sand:

- Unit weight: 19.8 kN/m³.
- Modulus of deformation: 17.2 MPa.
- Internal friction angle: 23.8°.
- Cohesion: 13.6 kPa.

Light dusty loam:

- Unit weight: 20.0 kN/m³.
- Modulus of deformation: 17.3 MPa.
- Internal friction angle: 21.2°.
- Cohesion: 25.8 kPa.

These parameters provide a basis for reliable geotechnical modelling and subgrade stability assessments in road construction projects.

5 Stability assessment and geosynthetic reinforcement

A stability analysis was conducted on a 16-meter-high embankment along Highway H-16 (Zolotonosha–Cherkasy–Smila–Uman) to evaluate its resistance to slope failure. The initial assessment, using Bishop's method, showed that the embankment did not meet the required stability factor of safety (FoS), with a coefficient of FoS = 0.79, which is lower than the minimum required threshold of 1.4. These results confirmed that without intervention, the embankment was at high risk of slope failure.

To improve embankment stability, three layers of geogrid reinforcement were installed within the embankment. The geogrid layers provided additional pullout resistance (C = 0.80) and increased the bearing capacity of the reinforcement elements to 30.76 kN/m. The application of geosynthetics effectively redistributed stress, improved embankment confinement, and enhanced resistance to lateral movement and deformation.

Following geogrid reinforcement, the embankment stability factor significantly improved (Tab. 2), achieving a final safety coefficient of FoS = 1.53, which exceeds the required minimum of 1.4. This demonstrates that the use of geosynthetics in embankment stabilization is a highly effective engineering solution, mitigating landslide risks and ensuring long-term structural integrity.

This comparison clearly demonstrates the effectiveness of geosynthetics in improving embankment stability. The safety factor nearly doubled, the landslide-inducing moment was significantly reduced, and passive resistance forces increased, ensuring greater structural integrity and reduced risk of failure.

The drawing shows a cross-sectional view of a 16-meter-high embankment slope. The upper 4 meters of the embankment consist of weak, active soil, which significantly influences the slope stability therefore it is focused on the reinforcement design. To highlight the critical active layer, this upper section has been drawn to a larger vertical scale and shows only active 4 m of depth (Fig. 4).

Table 2. Stability Parameters Before and After Reinforcement with Geosynthetic

Parameter	Before Reinforcement	After Reinforcement	Improvement
Safety Factor (FoS)	0.79	1.53	+93.7%
Soil weight over slip surface (kN/m)	4378	621	Reduced
Active forces (Fa, kN/m)	1801	282	Reduced
Passive Forces (Fp, kN/m)	1421	430	Increased
Landslide-inducing moment (Ma, kNm/m)	53366	2564	Reduced
Resisting moment (Mp, kNm/m)	42110	3912	Improved
Bearing capacity of reinforcement (kN/m)	–	31	Added
Pullout resistance (C)	–	0.80	Added

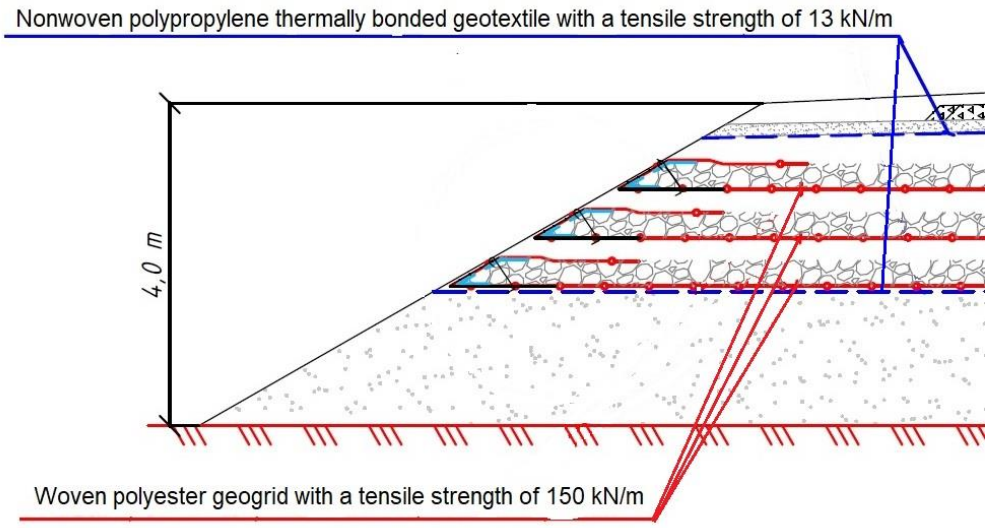


Fig. 4. Cross section of the reinforced embankment slope.

At the end of September 2024, the proposed stabilization solution was fully implemented. The entire pavement structure was dismantled over a 12–15 meter section, extending beyond the area where longitudinal cracking had appeared. The width of the replacement area was 1.5 meters wider than the subsidence zone, ensuring proper anchoring of the geosynthetic material within the embankment foundation.

Upon excavation, the soil beneath the lower base layer was found to be excessively saturated, with rut depths exceeding 29 cm when traversed by construction vehicles. To address this, the unstable soil was removed to a depth of 3.5–6.0 meters.

Subsequently, three reinforced layers were installed using high-strength woven polyester geotextile GT 400/50, employed as a wrap-around facing and reinforcement layer, featuring:

- Tensile strength of 440 kN/m longitudinally and 55 kN/m transversely.
- Elongation at break of up to 10%.
- Static puncture resistance of 14 kN.

After the reinforced base and asphalt concrete pavement were installed, traffic was restored. As of now, the road remains in good condition.

6 Conclusion and Recommendations

The analysis of high embankments on Ukrainian highways, particularly the 16-meter embankment on Highway H-16, has demonstrated that stability issues remain a critical concern in road infrastructure. Initial stability calculations revealed that without reinforcement, the embankment failed to meet the required safety factor, making it susceptible to landslides and deformation. The implementation of geosynthetic reinforcement, specifically a three-layer geogrid system, significantly improved structural integrity by enhancing load distribution, increasing passive resistance, and reducing landslide-inducing forces.

Despite the effectiveness of geosynthetics in improving stability, the recurrence of embankment failures across various road projects highlights the need for a more systematic approach to slope monitoring and stabilization in Ukraine. The current practice of assessing stability only at the design or repair stage does not provide sufficient long-term risk mitigation. Instead, a proactive, data-driven methodology is required to ensure embankment safety, particularly in areas prone to landslides and soil instability.

One of the primary challenges in embankment stability assessment is **insufficient geotechnical data at the planning and construction stages**. To improve this, it is essential to:

- Conduct detailed geotechnical investigations prior to construction, including soil composition, groundwater conditions, and slope stability modelling.
- Integrate in-situ testing methods, such as dynamic cone penetration (DCP) tests and geophysical surveys, to obtain a more accurate assessment of subsurface conditions.
- Require independent verification of soil parameters before approving embankment design specifications.

Given the increasing frequency of slope failures on Ukrainian highways**, it is necessary to create a comprehensive Landslide Inventory and Stability Passport System** for all embankments exceeding critical height thresholds. This system should include:

- A database of known landslide-prone areas, based on historical incidents, satellite imagery, and field inspections.
- A Stability Passport for each major embankment, documenting soil properties, construction details, stability assessments, and risk levels.
- Regular updates to embankment stability data, incorporating information from periodic surveys, rainfall impact studies, and deformation monitoring.

Current embankment assessments often rely on traditional stability calculations without incorporating **real-time environmental and operational conditions**. To enhance accuracy, it is recommended to:

- Use numerical modelling techniques, such as finite element analysis (FEA) and limit equilibrium methods (LEM), to simulate different loading conditions.
- Introduce continuous deformation monitoring systems, such as automated inclinometers, piezometers, and LiDAR scanning, to track changes in slope behaviour.
- Develop early warning mechanisms for critical sections, allowing timely intervention before failure occurs.

While geosynthetic reinforcement has proven effective in improving embankment stability, **the absence of national regulatory documents specific to geosynthetics in Ukraine limits their optimal use**. To address this, it is necessary to:

- Establish technical guidelines for geosynthetic material selection, installation, and performance verification.

- Require mandatory use of geosynthetics in embankments with high failure risk, especially in regions with loess, clay, or peat soils.
- Conduct long-term performance studies of geosynthetically reinforced embankments to refine design recommendations.

To reduce the frequency of embankment failures and costly emergency repairs, **a preventive maintenance approach should be adopted**, including:

- Regular slope inspections and drainage system evaluations to prevent water accumulation, which is a primary cause of instability.
- Immediate crack sealing and reinforcement at early signs of settlement to prevent progressive failure.
- Establishment of emergency response protocols for high-risk embankment sections, ensuring that stabilization measures can be deployed rapidly in case of slope movements.

The successful stabilization of high embankments depends not only on the application of advanced materials like geosynthetics but also on a comprehensive, long-term approach to slope monitoring and management. By implementing detailed geotechnical surveys, developing a national landslide inventory, adopting advanced stability modelling, and prioritizing preventive maintenance, Ukraine can significantly improve the resilience of its highway infrastructure. This proactive approach will reduce landslide-related disruptions, extend road lifespan, and ensure safer transportation networks for future generations.

References

1. G. Biondi, D. Cazzuffi, N. Moraci, C. Soccodato, Geosynthetics: Leading the way to a resilient planet, (Taylor & Francis, 2023). https://doi.org/10.1201/9781003386889
2. California Department of Transportation, Geosynthetic reinforced embankments. Caltrans Eng. Rep. (2023).
3. Naue GmbH & Co. KG, Erosion-stable road embankments – Design and selection of system solutions. Naue Publ. (2020).
4. Technobius, Evaluation of tensile strength characteristics of geosynthetic materials. Technobius Rep. (2023).
5. P. Ahlawat, M. Pardeep, V. Sharma, A review paper on geosynthetics in road construction. Int. J. Prog. Res. Eng. Manag. Sc. IJPREMS **3,** 4 (2023).
6. Texas A&M Transportation Institute, Geosynthetic reinforced steep slopes. TTI Res. Rep. (2017).
7. Geotexan, Embankment erosion control. Geotexan Tech. Artic. (n.d.). Web
8. I. P. Damians, Y. Miyata, P. Rimoldi, N. Touze, J. Kraus, Sustainability of geosynthetics-based landslide stabilization solutions. Springer Eng. Res. 3, 031-16898 (2023). https://doi.org/10.1007/978-3-031-16898-7_14
9. Ministry of Communities and Territories Development of Ukraine, ДБН В.2.3-4:2015 – Highways. Part I: Design, Part II: Construction (2015).
10. Ministry of Infrastructure of Ukraine, ГБН В.2.3-37641918-544:2014 – Highways. Application of geosynthetic materials in road structures. General requirements (2014).

SESSION 2 D
DESIGN AND MODELISATION (2)

Reinforced platforms with Geocells over tree root protection zones for the construction of an elevated woodland walkway

Muneeb Tahir[12*], *Pablo* Bernardini[123], and *Rozhan* Saeed[12]

[1] Geosynthetics Ltd., United Kingdom
[2] International Geosynthetics Society, IGS, United Kingdom
[3] Institution of Civil Engineers ICE, United Kingdom

Abstract. The Ellison Institute of Technology (EIT) Oxford Campus is a state-of-the-art research facility designed to tackle global challenges in healthcare, food security, clean energy, and government policy. The project, designed by Foster + Partners, includes an elevated Woodland Walkway traversing sensitive tree root zones and a historically significant burial ground. Construction required reinforced working platforms and access roads to support heavy machinery while preserving the site's environmental and historical integrity. The geotechnical design addressed challenges posed by soft soils with undrained shear strength below 50 kPa and California Bearing Ratio (CBR) values under 2%. With the use of Geocells for Tre Root Protection areas, and applying Reinforced Soil Raft method, the design ensured load distribution, minimized ground compaction, and allowed for water infiltration and oxygen exchange to protect tree roots. Extensive bearing capacity analysis and global stability assessments were conducted in compliance with Eurocode 7, resulting in reinforced platform thicknesses of minimum 400 mm. This paper details the innovative engineering solutions employed, demonstrating how sustainable geotechnical techniques can address environmental constraints while meeting structural demands, providing a model for integrating advanced engineering with ecological stewardship in sensitive construction projects.

1 Introduction

The Ellison Institute of Technology (EIT) Oxford Campus, designed by the world-renowned architectural firm Foster + Partners, is an ambitious interdisciplinary research facility poised to tackle some of humanity's most pressing global challenges. Spanning approximately 30,000 square meters, the campus will focus on four primary areas of innovation: healthcare, food security, clean energy, and government policy. EIT's mission is to create transformative solutions across these domains, facilitated by cutting-edge research laboratories, medical care facilities, and collaborative educational spaces. The campus is expected to be completed by 2026 and will serve as a hub for interdisciplinary research and development.

A notable feature of the Oxford campus design is the Woodland Walkway, see Figure 1, an elevated structure that will link the Collaboration Theatre with the Nest, crossing tree canopies and a historically significant burial ground. This structure epitomizes the integration of the built environment with natural landscapes, presenting unique engineering challenges—particularly in preserving the integrity of tree root zones and the burial ground beneath. As part of the construction process, 13 piling platforms and an access road, see Figure 2 were required to support heavy construction machinery and equipment, including piling rigs and construction traffic, while minimizing disruption to the underlying ground conditions.



Figure 1. Woodland Walkway

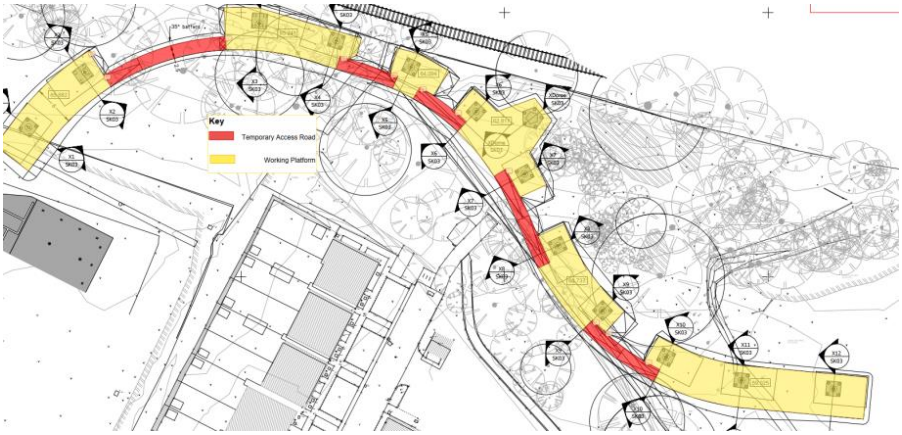


Figure 2. Working Platforms and Haul Road

1.1 Project Requirements

The design of the Cellular Confinement System (i.e. Cellweb Tree Root Protection) Working Platforms and Access Road was critical in addressing the environmental and historical challenges of this project. With soft soils (undrained shear strength < 50 kPa, CBR < 2%) and heavy construction loads (up to 30-ton piling rigs), there was significant risk to the subgrade's bearing capacity and tree root systems. To mitigate these, a geotechnical strategy was developed using the Reinforced Soil Raft method, for geogrids, adapted for the Geocells for Tree Root Protection, through an equivalent analysis of load distribution. The Geocell for Tree Root Protection system minimizes compaction while allowing water infiltration and oxygen exchange. The design process included reinforced platform thickness calculations and global stability analysis using GEO5 software in compliance with Eurocode 7. The final solution—200 mm Geocell Tree Root Protection layers, non-woven geotextiles, and clean angular stone—achieved reinforced thicknesses of minimum 400 mm, enabling construction

with minimal environmental impact. This project exemplifies the integration of advanced engineering techniques to balance infrastructure demands with environmental preservation.

2 Ground Conditions and Platforms

2.1 Ground Conditions

The soil profile at the site consists of Made Ground, featuring grass overlying dark brown, slightly gravelly, silty fine sand with rootlets, and gravel composed of concrete, limestone, sandstone, and charcoal, extending to 0.10 m. Beneath this is yellowish-brown, slightly gravelly, clayey fine-to-medium sand with similar gravel types. SPT N-values range from 4 to 37, with a mean internal friction angle of 32°. The design includes 13 working platforms and an access road, constructed at varying levels with heights from 0.70 m to 2.50 m, accommodating the site's geotechnical conditions. Key assumptions for platform heights are outlined below.

2.2 Platform Assumptions

2.2.1 Maximum Height Platform :

- Working Platform X9)

The geotechnical assessment of the site provided key parameters for the design of the reinforced platforms and access road. The **Table 1** below summarizes the existing and proposed levels, as well as the soil properties and design assumptions utilized in the analysis for Platforms X9 (maximum height), see **Fig. 3**. and X2 (minimum height), **see Fig. 4**.

Table 1. Geotechnical assessment of Working Platforms

Working Platform X9		**Working Platform X2**
Existing Level	58.20m AOD	64.57m AOD
Proposed Level	60.737m AOD	65.241m AOD
Level Difference	2.537m	0.67m
Foundation soil	Made Ground (Slightly gravelly silty fine SAND)	
CBR	1.72%	
Undrained Shear Strength: Cu	43kPa	
Unit weight: ɣ	18 kN/m3	
Assumed Undrained shear strength for design Cu	43kPa	

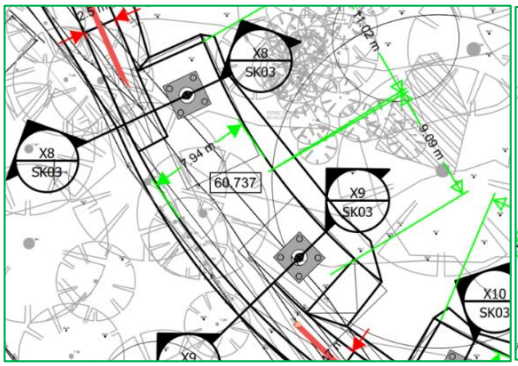


Fig. 3. Platform X9

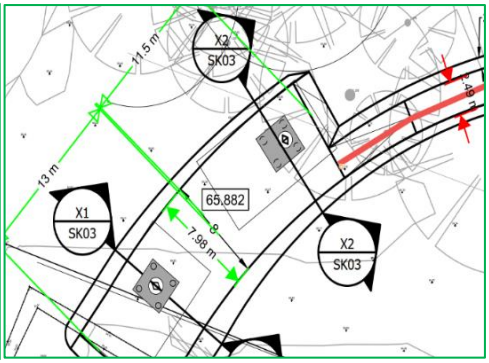


Fig. 4. Platform X2

3 Design methodology

3.1 Tree Root Protection Zones - Reinforced Soil Raft Method:

Verifications for the maximum axle and piling pressures and load cases using the Reinforced Soil Raft Concept. The methodology used is based on the design methods of reinforcement proposed by Giroud and Ah-Line-Bonaparte (1985), with an equivalent analysis for the Geocell Tree Root Protection. Where a load is applied directly to the soil, the bearing resistance can be estimated using established bearing capacity factors. We used Terzaghi's approach, to estimate the bearing capacity of the structure soil-foundation and verify if the factor of safety is adequate. A Safety Factor of 2.00 was used to obtain the allowable Bearing Capacity of the foundation soil.

3.2 Tree Root Protection Zones – Geocells Design Method:

The methodology used is based on the design methods of reinforcement of unpaved roads proposed by Webster (1981). The first step in the design of a Geocell reinforced pavement is to consider the ultimate bearing capacity of the pavement system under the greatest wheel load that it will have to support. This is undertaken following the guidance provided by Webster which uses conventional bearing capacity analysis to determine the applied and allowable pressure below the road pavement. The equations were derived for unpaved road design and make no allowance for the surfacing over the Geocell. They are therefore considered to be conservative when permanent surfacing is placed over the Geocell reinforced sub-base.

When additional sub-base is required beneath Geocell the depth of this material may be reduced by placement of surfacing material above. If the thickness of surfacing is equal to or greater than the required sub-base, then the sub-base may be omitted.

3.3 Tree Root Protection Zones – Global Slope Stability:

The calculations for the Geocell Reinforced Soil Slopes were run with the software GEO5 for global stability in accordance with Eurocode 7 DA1 Combination 1 & Combination 2. In this paper we are showing the results of the critical section (X6 &X7).

4 Design parameters and considerations

The thickness of the working platforms with Geocell Tree Root Protection was determined using the Reinforced Soil Raft and Geocell Design Methods, compared with Soil Stabilization, to achieve the minimum build-up for the required loadings. Following this, the cross-section with the maximum height was analysed for global stability using GEO5 software, in compliance with Eurocode 7 DA1 Combinations 1 & 2. The proposed solution included reinforcement with the minimum thickness and layers of Geocells, infilled with Clean Angular Stone (Type 4/20mm) as per BS7533-13 specifications, and separated by non-woven geotextile layers at the top and bottom.

4.1 Parameters for calculations

The parameters and assumptions used for the preliminary calculation are outlined in the following sections.

4.1.1 Soil Parameters

Table 2. Soil Parameters

Properties	**Infill Material of Geocells**	**Surface Material**	**Subgrade Parameters**
Stone Type	Clean Angular Stone (Type 4/20 mm)	MOT Subbase Type 1	Made Ground, described as slightly gravelly silty fine sand
Internal Friction Angle (ϕ'):	35 degrees	40 degrees	32 Degrees
Unit Weight (γ):	18 kN/m³	18 kN/m³	18 kN/m³
Maximum Particle Size	Ranging from 4 mm to 20 mm	Ranging from 4 mm down to dust	N/A
Cohesion (c):	0kPa	0kPa	N/A
California Bearing Ratio (CBR):	-	-	1.72%
Standard Penetration Test (SPT) Values (N)	-	-	4 to 37
Undrained Shear Strength (Cu):	-	-	43kPa

4.1.2 Loading parameters

Table 3. Loadings

HUTTE HBR207-4F Pilling Rig					
Load Case	1(Standing)	1(Handling)	1(Travelling)	2(Penetrating)	2(Extracting)
Track Length	1.09m	2.09m	2.94m	0.49m	0.40m
Track Width	0.6m	0.6m	0.6m	0.6m	0.6m
Pressure	350kPa	123.69 kPa	129.01 kPa	243.39 kPa	491 kPa
Note: The bearing pressures of the pile rig will need to be uprated by 33% due to the proximity of a Network rail asset. • 13t tracked excavator (max load 13 tonne)					

• XX Telehandler & 5t dumper (max load 5 tonne)
• HGV/std Construction Traffic (Max load 100kN/axle)

4.2 Geocells Tree Root Protection parameters

The specifications of the geosynthetic materials used in the design of the working platforms and access road are detailed below. These include the Geocell for Tree Root Protection System, see **Table 2**. and the non-woven Geotextile for separation, see **Table 3**. highlighting their key properties and performance characteristics.

Table 4. Geocell for reinforcement

Type	100% Virgin HDPE. Non-Thermally degraded. 0% Recycled HDPE
Name	Cellweb® - Tree Root Protection System
Expanded Cell Size – Width x Length	259mm x 224mm
Expanded Panel Size – Width x Length	2.56m x 8.10m
Effective Cell Diameter	190mm

Table 5. Geotextile for separation

Type	Polypropylene Non-woven Geotextile
Name	Geotextile Treetex
Resistance to Static Puncture	4kN
Dynamic Perforation Resistance (Cone Drop)	10mm
Opening Size O90	52mm
Water Flow rate	63 L/m2/s

The design process adhered to the partial factor requirements outlined in Eurocode 7 (BS EN 1997-1:2004), ensuring safety and reliability under varying load conditions. The **Table 4** below summarizes the partial factors applied to soil parameters and actions for Design Approaches DA1-C1 and DA1-C2.

4.3 Design Stages for Piling mat over Tree Root Protection

4.3.1 Reinforced Soil Raft Method

For the Access Road and working platforms, the subgrade at that level comprised Made Ground with very soft soils, described as Slightly gravelly silty fine SAND with a characteristic undrained shear strength Cu of 43 kPa and Internal friction angle, ϕ' 32˚. Due to the low strength of the subgrade as well as being a Tree Root Protection Zone and Heavy Loadings, the calculation was performed in following stages:

- Stage-1) Calculation of the access road to support heavy construction traffic of 30ton (travelling only) based on a bearing capacity analysis and improvement of the distribution of the loads. The result of Stage 1 was a minimum required reinforced buildup of 300mm.
    - **Heavy Construction Traffic:** 100 kN/axle
    - **Minimum Reinforced Platform Thickness:** 300 mm
    - **Allowable Bearing Capacity (q_{all}):** 150.31 kPa
    - **Design Pressure at the Base of Reinforced Platform (Reinforced):** 111.51 kPa
    - **Factor of Safety (FS):** 1.348

- Stage-2) Calculation of the working platform to support HUTTE HBR207-4F Pilling Rig based on a bearing capacity analysis and improvement of the distribution of the loads. The result of Stage 2 was a minimum required reinforced buildup of 400mm with 2 layers Geocell of 200mm.
    - **Piling Rigs: HUTTE HBR207-4F**
    - **Load Case: Worst-case, Load Case 1 (Standing)**
    - **Minimum Reinforced Platform Thickness: 400mm with 2 layers of Geocell of 200mm**
    - **Allowable Bearing Capacity (q_{all}): 145.26 kPa**
    - **Design Pressure at the Base of Reinforced Platform (Reinforced): 141.97 kPa**
    - **Factor of Safety (FS):** 1.023

(*) Note: A layer of 150mm MOT Subbase Type 3 as running surface has been recommended.

5 Solutions Working Platforms

To address the needs of the working platforms and access road, calculations were conducted to evaluate the rig, various loading cases, and construction traffic. Based on these analyses, a free-draining, coarse granular material—Clean Angular Stone Type 4/20mm—was chosen as the fill material. The thickness of the reinforced platforms was determined using the Reinforced Soil Raft method and the Tree Root Protection approach outlined previously. Below, the finalized solution for the platforms and access road is provided.

5.1 Final solutions reinforced platforms & access road

According to the design stages described above, the final solution for the Working Platform and Access Road was a minimum of 400m thick build-up (i.e. 2 Layers of Geocell of 200mm) infill Clean Angular Stone Type 4/20mm and two layers of non-woven geotextile for separation at the top and bottom, see **Fig. 5.** below.

The base of each platform had to follow the levels of the existing ground and reach the proposed top level in each location. The critical platform was X6-X7 with 10 layers of Geocell of 200mm and 150mm of Subbase Type 1 on the surface. The results of the Global Stability of Section X6-X7 are shown below with satisfactory results for overturning, slip and bearing capacity analyses, see **Fig. 6.** below.

(*) Note: A layer of 150mm MOT Subbase Type 3 as running surface has been recommended.

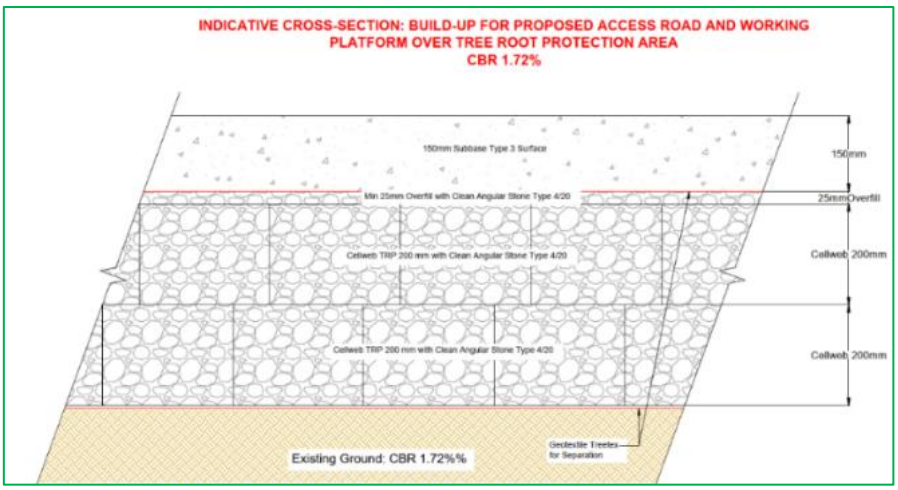


Fig. 5. Indicative Cross-section

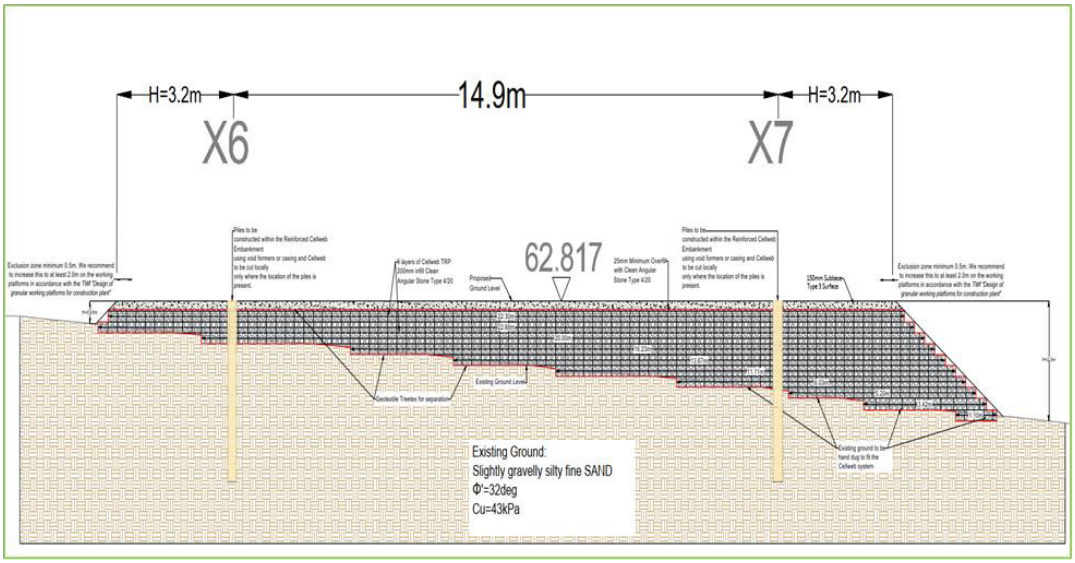


Fig. 6. Indicative Cross-section Platform X6-X7

5.2 Geo5 (Global Stability) Solution

The calculations for the Geocell Reinforced Soil Slopes were run with the software GEO5 for global stability in accordance with Eurocode 7 DA1 Combination 1 & Combination 2 for undrained and drained conditions in regards with Haul Road and Working Platforms. See below **Fig.7**. for indication cross section of worst-case working Platform (X6-X7) in GEO5.

Below are the results of the critical section (X6 &X7) working platform undrained as worst case with utilization of 76.7% in Combination 1 and 41.8% in Combination 2, see **Fig.8.**

For drained conditions, utilization of 36.9% in Combination 1 and 22.5% in Combination 2 were obtained, see **Fig.9.**

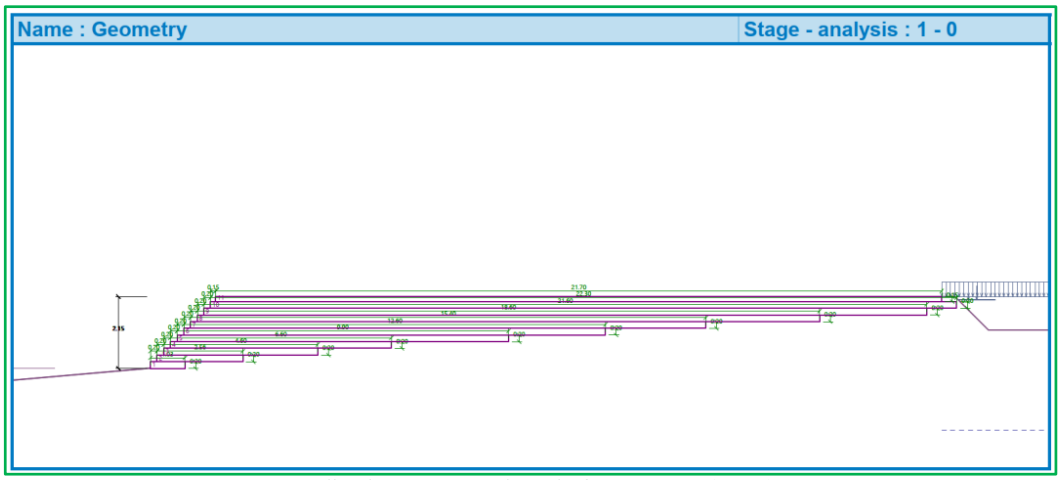


Fig. 7. Indicative Cross-section Platform X6-X7 (Geo5)

Slope stability verification (Bishop)
Combination 1
Sum of active forces : F_a = 4009.76 kN/m
Sum of passive forces : F_p = 5225.55 kN/m
Sliding moment : M_a = 159869.26 kNm/m
Resisting moment : M_p = 208342.81 kNm/m
Utilization : 76.7 %
Slope stability ACCEPTABLE
Combination 2
Sum of active forces : F_a = 525.33 kN/m
Sum of passive forces : F_p = 1257.77 kN/m
Sliding moment : M_a = 11068.70 kNm/m
Resisting moment : M_p = 26501.15 kNm/m
Utilization : 41.8 %
Slope stability ACCEPTABLE
Optimized slip surface for : Combination 1

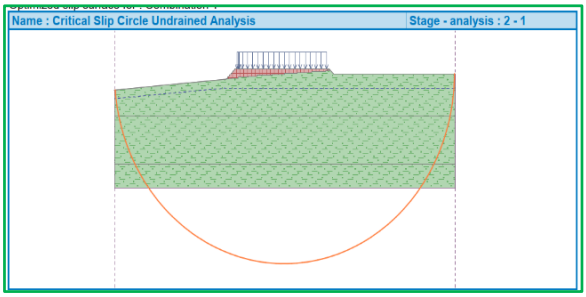


Fig. 8. Critical slip circle Undrained Analysis Platform X6-X7

Slope stability verification (Bishop)
Combination 1
Sum of active forces : F_a = 1513.89 kN/m
Sum of passive forces : F_p = 4100.63 kN/m
Sliding moment : M_a = 41858.96 kNm/m
Resisting moment : M_p = 113382.44 kNm/m
Utilization : 36.9 %
Slope stability ACCEPTABLE
Combination 2
Sum of active forces : F_a = 309.05 kN/m
Sum of passive forces : F_p = 1372.31 kN/m
Sliding moment : M_a = 9422.93 kNm/m
Resisting moment : M_p = 41841.59 kNm/m
Utilization : 22.5 %
Slope stability ACCEPTABLE
Optimized slip surface for : Combination 1

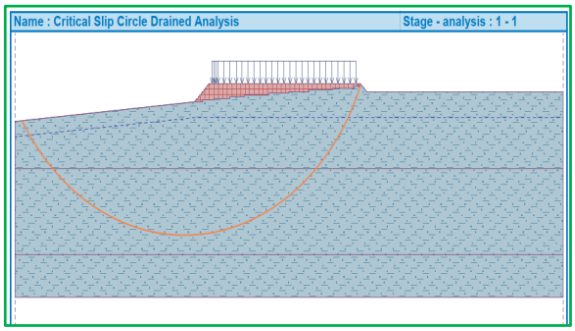


Fig. 9. Critical slip circle drained Analysis Platform X6-X7

6 Conclusions & Recommendations

The design and construction of the Ellison Institute of Technology (EIT) Oxford Campus presented unique challenges due to sensitive site conditions, including the proximity to tree root protection zones and the presence of soft, low-strength soils. To address these challenges, an innovative solution was developed involving the use of geosynthetic materials, specifically a system of cellular confinement and non-woven geotextiles. These measures ensured that construction activities could proceed safely without compromising the structural integrity of the underlying ground or the health of the tree roots.

The design process incorporated comprehensive bearing capacity analysis, global stability assessments, and the application of the Reinforced Soil Raft method, resulting in reinforced platform thicknesses capable of supporting heavy construction traffic and piling rigs. The final solution, which included of minimum 400 mm of reinforced material and clean angular stone as infill with a running surface with Subbase Type 3, effectively balanced load-bearing requirements with environmental sustainability.

The successful implementation of these solutions addressed the complex requirements of this high-profile project, protecting the tree root zones and preserving the historical ground while setting a benchmark for sustainable practices in sensitive environments. The integration of advanced geotechnical techniques and sustainable development methods highlights the importance of adopting innovative engineering approaches to meet the dual demands of environmental preservation and infrastructure development.

In conclusion, this project demonstrates how geosynthetic technologies can deliver sustainable and effective solutions, protecting natural environments while meeting modern construction needs. The methodologies and findings outlined in this paper provide a valuable reference for future projects prioritizing the preservation of sensitive ground conditions.

References

1. Giroud, J.P, Ah-Line, C., Bonaparte, R., Design of unpaved roads and trafficked areas with geogrids. Proceedings Symposium on Polymer grid reinforcement. Thomas Telford Ltd. London, UK (1984)
2. British Standard, BS 5837: 2012. Trees in relation to design, demolition and construction. Recommendations. British Standard Institution, London. UK. (2012)
3. British Standard, BS8004:2015 + A1: 2020 Code of practice for foundations. British Standard Institution, London. UK (2020)
4. Temporary Works Forum, TWf:2019 Design of granular working platforms for construction plants, A guide to good practice. Temporary Works Forum, London. UK (2019)
5. Tenax Spa. Reinforced Soil Raft Concept. Design guidance. Vigano, Italy (2011)
6. BRE. 2004. Working platforms for tracked plant: good practice guide to the design, installation, maintenance and repair of ground-supported working platforms. BRE. Watford. UK. (2004)
7. British Standard, PD 6694-1:2011+A1:2013. Recommendations for the design of structures subject to traffic loading to BS EN 1997-1:2004. British Standard Institution, London. UK. (2013)
8. Highway Works MCHW. Volume 1 Specification for Highway Works Series 5, Series 600 and Series 800. Highways Works, UK. (2016)

Comprehensive overview of soil erosion control: design of anti-erosive geomats for effective slope stabilization

Filippo Maria Santoli[1]*, *Giulia* Lugli[1], and *Fabrizia* Trovato[1]

[1] Officine Maccaferri SpA, Bologna, Italy

Abstract. Climate change is altering rainfall patterns, leading to more frequent events and intense downpours. These short intense rains, unlike the consistent precipitation of the past, increase soil erosion. The higher intensity and shorter duration make slopes more susceptible to instability, especially if they are already vulnerable, resulting in formation of gullies and other erosive features. The soil erosion can impact infrastructures, such as roads, railways, and buildings, and sensitive natural environments. Soil erosion control is essential for preventing slope instability and natural disasters, a clear method for designing and calculating soil loss is rarely used. The Revised Universal Soil Loss Equation (RUSLE) estimates annual soil erosion by considering factors: erosivity (R), erodibility (K), slope length and steepness (LS), coverage, management, and practices (CPM). An unprotected slope of bare soil has a C factor of one, whereas a protected slope with erosion control solution is characterized by a lower C factor. RUSLE method allows comparing soil loss with and without a protective solution. Extensive analysis and comparisons have shown that polymeric geomats represent among the most cost-effective and environmentally friendly solutions to reduce soil loss, providing significant protection to slopes, and benefiting both the environment and infrastructure. The calculation of soil loss for the first year of the project is not the only check to verify. To prevent the geomat breakage during installation and maintenance, securing it with anchorage is crucial. Proper analysis of slope stability during installation is necessary to prevent breakage and collapse that could lead to soil loss.

Full paper to be published in:
https://www.e3s-conferences.org/articles/e3sconf/abs/2025/44/contents/contents.html

* Corresponding author: f.santoli@maccaferri.com

Impact of structural intersections on reinforced soil structures: design and construction considerations

Francesco Masola[1*], *Fabrizia* Trovato[2], *Gianluca* Brocca[2] and *Marco* Vicari[2]

[1]Maccaferri Central Europe s.r.o., Technical Manager, 90501 Senica, Slovakia
[2]Officine Maccaferri S.p.A., Technical Department, 40132 Bologna, Italy

Abstract. During the construction of complex civil structures, it can happen that reinforced soil structures (RSS) are intersected by other structures that are part of the overall project. Although it is advisable that this does not happen, in many cases this is unavoidable, and it is therefore necessary to assess how these intersections affect the stability of the RSS and to implement measures to avoid problems during the construction phases. This paper investigates the management of intersections between drilled or beaten piles and steel profile into geogrids RSS, evaluating both possibility of geogrids installed prior or after the other structure. Various strategies for addressing these intersections are examined, including pre-cutting geogrids to create openings for the piles. A quantitative approach is presented to assess the reduced strength of the cut geogrids, incorporating a partial factor based on the influence area of the piles on the total area of the reinforced soil. The method is adjusted and proposed also for polymer-coated steel woven wire meshes (PWM) used as fill reinforcement. The paper further examines the practical implications of these strategies through a case study, where adjustments to the RSS were made to accommodate different interferences due to presence of drilled piles and intersection with guardrail foundations, introducing additional design considerations, such as structural interactions, load distribution, and long-term performance of the whole RSS. By providing both theoretical underpinnings and real-world examples, this paper offers valuable insights for engineers and practitioners involved in the design and construction of RSS incorporating these elements.

1 Introduction

The integration of reinforced soil structures (RSS) with other structural elements, such as drilled piles, presents unique challenges during design and construction. This paper explores the design and construction considerations for intersecting RSS with drilled piles, specifically when the geogrid reinforcement is installed prior to pile installation. Through a combination of theoretical analysis and practical case studies, this paper provides valuable insights for

* Corresponding author: f.masola@maccaferri.com

engineers and contractors involved in the design and construction of reinforced soil structures with intersecting elements.

1.1 Description of reinforcement types

1.1.1 Polymeric coated steel woven wire meshes (PWM)

Polymeric coated steel woven wire meshes (PWM) are CE-marked according to EAD 200026-00-0102 and comply with EN 10223-3, as well as BBA HAPAS certified. They feature an 8x10 mesh, Zn95%-Al5% metallic and polyolefin coatings, and wire diameters of 2.2-3.2 mm or 2.7-3.7 mm [1]. The mesh and wire diameters meet EN 10223-3 requirements for soil reinforcement, with a Class A Zn-Al coating (ISO 7989-2, EN 10244-2) and polyolefin polymer coating (EN 10245, EN 10223-3). Minimum short-term tensile strength is measured per EN 10223-3 and EAD 200026-00-0102. The main physical and mechanical properties are reported in Table 1.

Table 1. PWM reinforcements – physical and mechanical properties.

	Reference Norm	**PWM "reinforced"**	**PWM "light"**
Mesh type	EN 10223-3 EAD 200026-00-0102	8x10	8x10
Steel Wire diameter int./ext. (mm)	EN 10223-3 EAD 200026-00-0102	2.70 / 3.70	2.20 / 3.20
Zn-Al coating	ISO 7989-2 EN 10244-2 EAD 200026-00-0102	Class A	Class A
Organic Coating	EN 10245 EN 10223-3 EAD 200026-00-0102	Polyolefin	Polyolefin
Mesh tensile strength (kN/m)	EN 10223-3 EAD 200026-00-0102 ISO 10319	55 ± 5	40 ± 5

1.1.2 High Strength Geogrid Reinforcement

The geogrids employed in this case study are planar geosynthetic structures, characterized by a monoaxial array of composite strips. These geogrids are primarily utilized for soil reinforcement due to their structural capacity to enhance soil stability. They are CE certified for reinforcement applications, adhering to relevant harmonized standards, and additionally hold BBA HAPAS certification for compliance with BS 8006 design requirements and the specifications of Highways England and local highway authorities. The short-term tensile strength of these geogrids ranges from 30 kN/m to 1800 kN/m.

2 Cutting of soil reinforcements during the installation phase

To prevent damage to the geogrid during pile drilling, it is recommended to pre-cut the soil reinforcements before the pile installation. This involves creating square or circular openings in the PWM or in the geogrid, with sides larger than the diameter of the piles. By pre-cutting the PWM/geogrid, it is ensured that the piles can be drilled without pulling and ripping the reinforcement and compromising the structural integrity of the reinforced soil structure.

2.1 Cutting of PWM

The PWM reinforcements can be cut by using an angle grinder or a pincer, as shown in Fig. 1 and Fig. 2.



Fig. 1. PWM – marked area to indicate the pile position.



Fig. 2. PWM – cut reinforcement to ease the drilling operation.

2.2 Cutting of Geogrids

The geogrid reinforcements can be cut by using a cutter or a scissor, as shown in Fig. 3 and Fig. 4.



Fig. 3. Geogrid – marked area to indicate the pile position.



Fig. 4. Geogrid – cut reinforcement to ease the drilling operation.

3 Design strength reduction of the cut reinforcements

To evaluate the long-term design strength (LTDS) reduction of the cut geogrids, a specific partial factor shall be introduced in the calculations which will enhance the standard damage partial factor (f_{damage}) of the reinforcement. This factor is calculated considering the ratio between the number of strips that have been cut (n_{cut}) and the total number of strips in the machine direction (n_{st}) considering the whole design width of the facing. So that the percentage of damaged strips (D_{st}) is given by (1):

$$D_{st} = \frac{n_{cut}}{n_{st}} \quad (1)$$

Therefore, the partial factor (f_{cut}) can be calculated as follows (2):

$$f_{cut} = \frac{1}{(1-D_{st})} \quad (2)$$

This factor increases the standard damage partial factor f_{damage} of the reinforcement, so that the total damage partial factor shall be calculated as (3):

$$f_d = f_{damage} \cdot f_{cut} \quad (3)$$

Alternatively, the designer can decide to use a geogrid with a lower LTDS to take into account the reduction factor (i.e.: if in the project it is planned to use a geogrid with 200 kN/m nominal tensile strength, but due to the cut there is a partial factor f_{cut}=1,9, therefore it is possible to carry out the analysis in a conservative way by using a geogrid with 100 kN/m of nominal tensile strength).

By using the Limit Equilibrium Method (LME) for the stability, the presence of the piles which will carry horizontal loads and deformations are not taken into consideration.

Fig. 5 shows an example of a piling system intercepting the strips of a geogrid with a nominal tensile strength of 150 kN/m. The design width of the facing is 6 m and the drilled piling is made up of rows of 4 piles arranged at 1,5 m from each other and having a diameter of 0,5 m. The spacing between the rows is 2 m.
The square cuts regarding each pile intercept 9 strips of geogrid (Fig. 6), for a total of 36 strips cut in each row of piles.

Since on a 6 m width of geogrid of 150 kN/m nominal tensile strength there are 80 strips, the relevant damage affects the 45% of the geogrid ($D_{sw} = 0{,}45$) and the partial factor related to the damaged geogrids is $f_{cut} = 1{,}82$.
Therefore, to account for the damage due to cut strips, the damage partial factor of this geogrid (that is $f_{damage} = 1{,}02$ in gravel) interested by the piles has to be increased from the standard value to (4):

$$f_d = 1{,}02 \cdot 1{,}82 = 1{,}86 \quad (4)$$

Alternatively, the new partial factor can be directly multiplied by the total material safety factor ($f_m = 1{,}52$ for this 150 kN/m geogrid in gravel) increasing it to (5):

$$f_m = 1{,}52 \cdot 1{,}82 = 2{,}77 \quad (5)$$

so that this value can be directly modified in the stability calculation software.

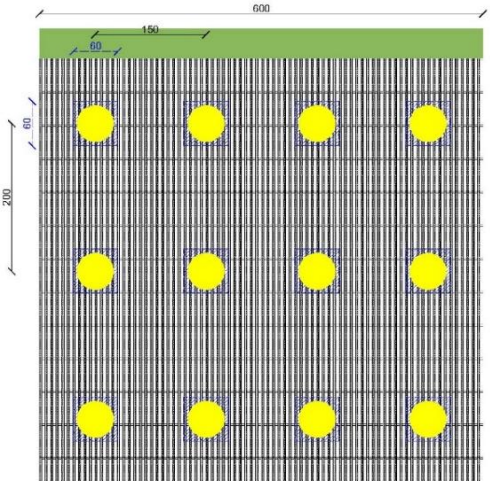


Fig. 5. Drilled piles interception detail.

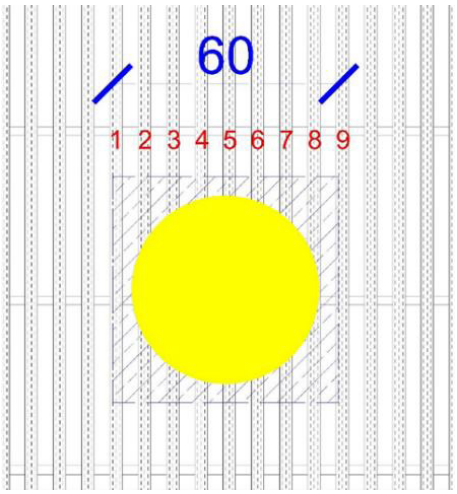


Fig. 6. Particular for the cut of each pile with the indication of the amount of cut strips.

The same methodology proposed for geogrids can be applied also to PWM, in this case to evaluate the partial factor (f_{cut}) the number of steel wires between two vertical elements (n_{sw}) and the number of steel wires cut (n_{cut}) shall be assessed to determine the percentage of damaged steel wires (D_{sw}):

$$D_{sw} = \frac{n_{cut}}{n_{sw}} \quad (6)$$

Therefore, for PWM the partial factor can be calculated as follows:

$$f_{cut} = \frac{1}{(1-D_{sw})} \quad (7)$$

Figure 7 shows a real application of an IPN 200 steel beams as foundation of noise barriers within a PWM structure. The steel beams were installed by pure driving. It can be seen that in the worst case the IPN 200 cuts 6 steel wires. Since on a 2 m width of wire mesh there are 24 steel wires, then the relevant damage affects 25% of the mesh ($D_{sw} = 0.25$) and the partial factor related to the damaged wires is $f_{cut} = 1{,}33$.

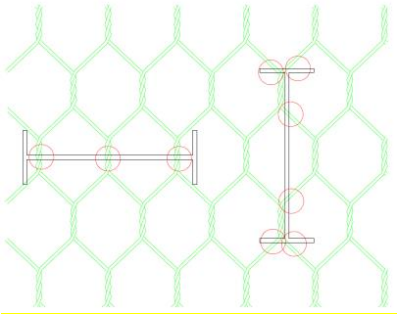


Fig. 7. Steel wires interested by the beam installation

Therefore, to account for the damage due to cutting wires, the damage partial factor of PWM units interested by the steel beams has to be increased from the standard value of 1,15

$$f_d = 1{,}15 \cdot 1{,}33 = 1{,}53 \quad (8)$$

4 Case Study: Project Linkeroever Oosterweel – Object G05

An example on how to manage the intersection between geogrids and drilled piles comes from a real application on a construction site in Antwerp, Belgium, in particular from the project "Linkeroever Oosterweel – Object G05" [2, 3]. During the execution phase it was necessary to evaluate the interference of the foundation piles of a bridge abutment with geogrids of a nominal tensile strength of 150 kN/m and the tails of PWM reinforcements of the facing.

There were two areas where the piles were close to the facing: the first area comprises 4 meters of facing with the piles intersecting the 3 m long PWM reinforcements (Fig. 8). In this case the closest pile is 2 m far from facing, so PWM reinforcements equal to 2 m, instead of 3 m, has been used.

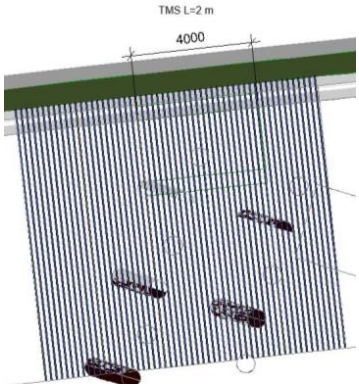


Fig. 8. View in 3D of the intersection of drilled piles with geogrids for the first area

Considering the piles diameter and their inter-axis, the strength of the geogrids for this section has been reduced as follows:

Up to geogrid length of 3 m → 67,5% of LTDS
Up to geogrid length of 4 m → 51,25% of LTDS
Up to geogrid length of 6 m → 35% of LTDS
Up to geogrid length of 7 m → 18,75% of LTDS

The second area comprises 10 meters of facing with the piles intersecting the 3 m long PWM reinforcements (Fig. 9).

In this case the PWM reinforcements have been removed and a wrap-around system behind the PWM units has been used (Fig. 10).

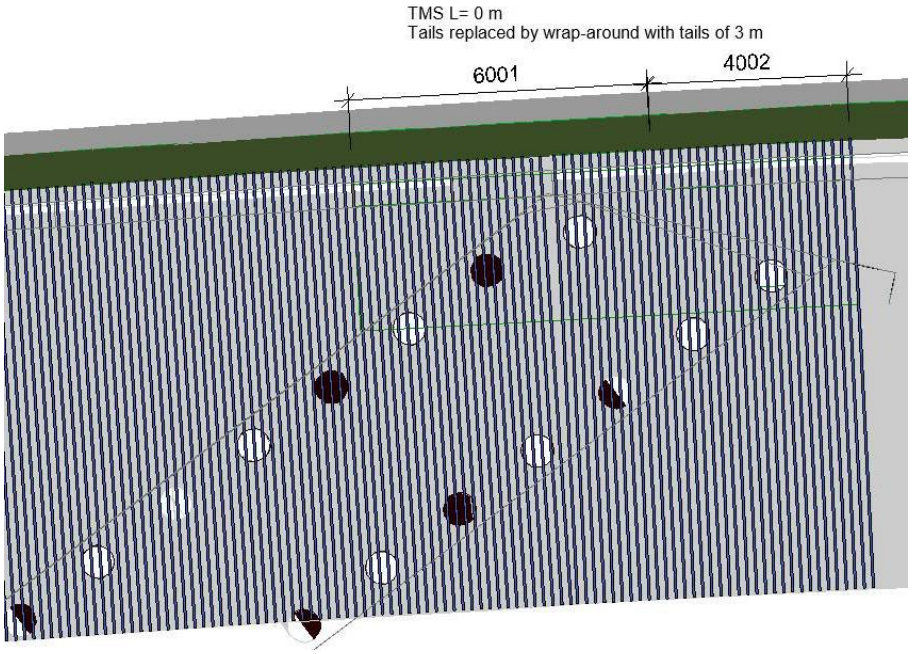


Fig. 9. View in 3D of the intersection of drilled piles with geogrids for the second area

Considering the piles diameter and their inter-axis, the strength of the geogrids for this section has been reduced as follows:

Up to geogrid length of 3 m → 67,5% of LTDS
Up to geogrid length of 5.6 m → 56,67% of LTDS
Up to geogrid length of 7.8 m → 35% of LTDS
Up to geogrid length of 9 m → 24,17% of LTDS

The final layout of geogrids is presented in the cross-section in Fig. 10.

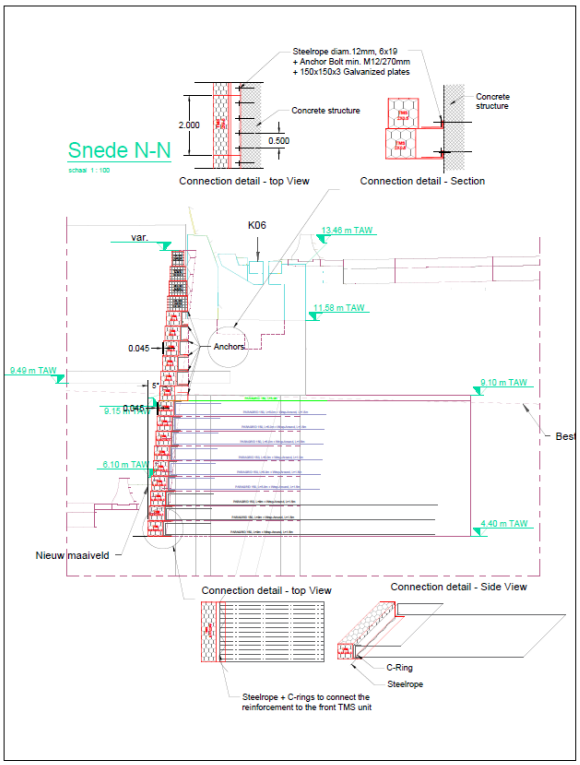


Fig. 10. Section with the particular of the direct anchorage of the PWM units in the facing and of the intersection between the drilled piles and the geogrid.

Finally, the drilling operations commenced after the complete construction of the reinforced soil structure, ensuring that the geogrid and PWM reinforcements remained undamaged (Fig. 11 and Fig. 12).



Fig. 11. Piling drilling operations for the Object G05 of the project "Linkeroever Oosterweel".

6 Conclusions & Recommendations

The design and construction of the Ellison Institute of Technology (EIT) Oxford Campus presented unique challenges due to sensitive site conditions, including the proximity to tree root protection zones and the presence of soft, low-strength soils. To address these challenges, an innovative solution was developed involving the use of geosynthetic materials, specifically a system of cellular confinement and non-woven geotextiles. These measures ensured that construction activities could proceed safely without compromising the structural integrity of the underlying ground or the health of the tree roots.

The design process incorporated comprehensive bearing capacity analysis, global stability assessments, and the application of the Reinforced Soil Raft method, resulting in reinforced platform thicknesses capable of supporting heavy construction traffic and piling rigs. The final solution, which included of minimum 400 mm of reinforced material and clean angular stone as infill with a running surface with Subbase Type 3, effectively balanced load-bearing requirements with environmental sustainability.

The successful implementation of these solutions addressed the complex requirements of this high-profile project, protecting the tree root zones and preserving the historical ground while setting a benchmark for sustainable practices in sensitive environments. The integration of advanced geotechnical techniques and sustainable development methods highlights the importance of adopting innovative engineering approaches to meet the dual demands of environmental preservation and infrastructure development.

In conclusion, this project demonstrates how geosynthetic technologies can deliver sustainable and effective solutions, protecting natural environments while meeting modern construction needs. The methodologies and findings outlined in this paper provide a valuable reference for future projects prioritizing the preservation of sensitive ground conditions.

References

1. Giroud, J.P, Ah-Line, C., Bonaparte, R., Design of unpaved roads and trafficked areas with geogrids. Proceedings Symposium on Polymer grid reinforcement. Thomas Telford Ltd. London, UK (1984)
2. British Standard, BS 5837: 2012. Trees in relation to design, demolition and construction. Recommendations. British Standard Institution, London. UK. (2012)
3. British Standard, BS8004:2015 + A1: 2020 Code of practice for foundations. British Standard Institution, London. UK (2020)
4. Temporary Works Forum, TWf:2019 Design of granular working platforms for construction plants, A guide to good practice. Temporary Works Forum, London. UK (2019)
5. Tenax Spa. Reinforced Soil Raft Concept. Design guidance. Vigano, Italy (2011)
6. BRE. 2004. Working platforms for tracked plant: good practice guide to the design, installation, maintenance and repair of ground-supported working platforms. BRE. Watford. UK. (2004)
7. British Standard, PD 6694-1:2011+A1:2013. Recommendations for the design of structures subject to traffic loading to BS EN 1997-1:2004. British Standard Institution, London. UK. (2013)
8. Highway Works MCHW. Volume 1 Specification for Highway Works Series 5, Series 600 and Series 800. Highways Works, UK. (2016)

Numerical modelling of MSE walls subjected to strong earthquake motions

Oltion Korini[1*]

[1]Terre Armée company, 280 avenue Napoléon Bonaparte, Rueil-Malmaison, France

Abstract. Practice has shown that reinforced soil walls are able to withstand quite well seismic events. Their modularity and soil – reinforcement interaction allow them to experience significant deformation without failing. Nevertheless, up to now it has been a challenge to estimate the residual deformation of a MSE wall after an earthquake. The most common seismic design approach is the equivalence with a pseudostatic force. This approach is generally conservative and as such it may overestimate the displacements of the structure. The seismic action is a variable motion that changes amplitude, direction, and frequency. Moreover, the amount of motion that a MSE wall will experience depends on its size and stiffness (natural frequency and internal design). This article presents a numerical (finite differences model) analysis of a typical MSE wall using a real earthquake recording. The goal is to evaluate the structure response during and after the seismic motion in terms of deformation and reinforcement tension. A case with longer reinforcement is included for studying the effect of longer strips in the dynamic response of the wall. A comparison is done with pseudostatic force approach to highlight the differences in the results.

Full paper to be published in:
https://www.e3s-conferences.org/articles/e3sconf/abs/2025/44/contents/contents.html

* Corresponding author: oltion.korini@terre-armee.com

Attenuation of environmental vibrations using geosynthetics

Alain Hérault[1*], *Philippe* Jean[2], and *Alexandre* Jolibois[3]

[1] Freudenberg Performance Materials, 68000 Colmar, France
[2] Centre Scientifique et Technique du Bâtiment, 77420 Champs-sur-Marne, France
[3] VINCI Construction - Direction de l'Habitat IDF, 92000 Nanterre, France

Abstract. Beyond the usual applications of drainage geocomposites, their environmental impact was considered through benefits, in terms of attenuation of vibration and structure-borne noise levels, of a vibration-damping geocomposite placed on or near a typical 4-floors building with an underground car park located 20 m from a railway line. The problem of train induced noise levels inside buildings is not new, but the means employed for its study have evolved with time mainly because of the increase of computing resources. Various numerical simulations and results obtained on the different floors of the typical building studied are detailed in this paper.

Full paper published in the September 2025 Special Issue of the French Geotechnical Journal **"Revue Française de Géotechnique"** *https://www.geotechnique-journal.org*

* Corresponding author: alain.herault@freudenberg-pm.com

A numerical assessment of the influence of compaction on the seismic performance of Geosynthetic-Reinforced Earth retaining walls

Domenico Gaudio[1*], *Ludovica* Cioffi[1], and *Luca* Masini[1]

[1]Department of Structural and Geotechnical Engineering, Sapienza Università di Roma, via Eudossiana 18, 00184, Rome, Italy

Abstract. Over the past three decades, field observations have demonstrated the resilience of Geosynthetic-Reinforced Earth (GRE) retaining walls to severe earthquakes. Seismic damage to GRE walls generally manifests as permanent deformations due to the transient activation of plastic mechanisms within the soil-reinforcement system, demonstrating their overall ductile behaviour. However, a limited understanding of the reinforcement-soil interactions under static and dynamic conditions and the lack of specific guidelines in many building codes for the seismic design of GRE walls have hindered their widespread adoption. In particular, the design parameters for both the backfill and the mechanical properties of the reinforcement are usually selected according to an overly conservative approach which neglects the effects of high compaction energy. As a result, a GRE wall in a well compacted granular soil is often designed with a soil shear strength that is much lower than the strength available. This paper discusses the effects of compaction on the initial stress and strain distribution in the reinforcement and their impact on the seismic performance of GRE walls. To this end, iterative pseudo-static and dynamic time-domain numerical analyses were carried out to assess how compaction affects both the plastic mechanisms and the seismic performance of reinforced soil walls.

Full paper to be published in:
https://www.e3s-conferences.org/articles/e3sconf/abs/2025/44/contents/contents.html

* Corresponding author: domenico.gaudio@uniroma.1.it

SESSION 3 A
SUSTAINABILITY AND DURABILITY (3)

Reuse and recycling of geosynthetics – Insights into an interdisciplinary research project for a circular economy

Niclas Depenbrock[1], *Frank* Heimbecher[1*], *Sabine* Flamme[1], *Simon* Ebbert[2], and *Martin* Tazl[3]

[1]Institute for Infrastructure, Water, Resources, Environment (IWARU), Münster University of Applied Sciences, Department of Civil Engineering, 48149 Münster, Germany
[2]HUESKER Synthetic GmbH, 48712 Gescher, Germany
[3]Naue GmbH & Co. KG, 32339 Espelkamp, Germany

Abstract. The article presents initial results and current challenges in closing the loop for geosynthetics. That includes the recycling of geosynthetics, the development of a new excavator attachment for reuse of geosynthetics, the integration of tracers for labelling and identification of geosynthetics and the establishment of efficient digital data management as the basis for a new business model to support the circular economy for geosynthetics. The project is structured around three large-scale tests. Each test aims to investigate the reuse and the recycling of different types of geosynthetics on a practical scale and to provide data for a comprehensive LCA. In the initial phase of the project, the focus was on products made from one type of raw material (e.g. polypropylene or polyester) and used for temporary structure*s (construction roads, crane platforms, etc.). A pre-treatment process is to be developed specifically for the recycling process, which will enable recovered geosynthetics to be incorporated into the existing recycling infrastructure.

1 Current situation and challenges

Geosynthetics (GSY) are established as reliable construction elements due to their economic and ecological advantages. Currently, almost exclusively primary raw materials are used in the production of geosynthetics. This ensures the required consistently high quality over the service life.

While the majority of geosynthetics are designed for long-term use of 25 to 100 years, estimated 10 to 15 % are used in temporary constructions with a service life of < 5 years. Examples of such constructions are reinforced sub-base layers and woven tubes for sludge dewatering. Temporary base-course reinforcement under access roads and crane-working platforms has become established as a standard construction method in the course of the expansion of renewable energies (windfarms, power lines, etc.) and is sometimes mandated by the authorities to protect the in-situ soil (e. g. on agricultural land) [1].

Regardless of the duration of the use phase, the geosynthetic product exhibits varying degrees of soil adhesion after deconstruction, depending on the product type and the removal conditions. The disposal of these geosynthetic-soil mixtures in Germany is currently carried out in waste incineration plants (WIP) due to a lack of alternatives (including take-back and processing concepts). Properties such as the high calorific value, the size of the respective compartments and soil adhesion make this disposal route increasingly difficult. In the context of hydraulic engineering, “disposal in the landfilled soil masses” has also been reported [2].

*Corresponding author: heimbecher@fh-muenster.de

Disposal as secondary fuel, e. g. in cement plants, or recycling, is currently not practised. Due to the rather unfavourable properties of the waste for incineration in a waste incineration plant (ash content up to 45 % by weight, calorific value of the plastics up to 42 MJ/kg), the capacities are very limited and the resulting disposal costs high. As there are no non-destructive deconstruction methods, the reuse of geosynthetic materials used for e.g. temporary structures is not practised at all. A description of the current common practice of the deconstruction process as well as material qualities for a wide range of different types of geosynthetics after deconstruction can be found in [3].

The usually high-quality plastics of largely homogeneous quality with a quantity of several megagrams per construction site are predestined for highergrade recycling. But in contrast to plastic packaging or other industrial products, appropriate return systems (deconstruction, logistics, processing, recycling) and successful approaches to closing the loop are not yet in place for products which have been in contact with the soil matrix.

Geosynthetic products must fulfil stringent requirements on durability. This is ensured by particularly high requirements for the raw materials. These are regulated in the harmonised application standards EN 13249 ff. and EN 13361 ff. [4,5]. This currently excludes the use of recycled materials for reinforcement products and for products with a service life of more than 5 years, so that virgin material is generally used in the manufacture of geosynthetics. Material to be recycled arising within production is an exception and can be used to 100 % without pelletisation in the treatment process. Its use is limited elsewhere to 10 % without additional proof. Only for individual, selected applications do products already exist which are made using high-purity recyclates derived from deposit bottle recycling [6]. However, this R-PET is subject to very high demand for use in other product areas (e. g. packaging), so that prices are currently significantly higher than those of virgin material.

To enable a closed-loop for geosynthetic-products following challenges need to be solved:

In order to be able to reuse a geosynthetic, non-destructive and regulated deconstruction methods are required. The reuse of dismantled GSY is particularly conceivable for products that were only used for a short time in their first (temporary) structure.

For recycling after (re-)use, there is a particular lack of return systems (appropriate deconstruction, logistics) and suitable processing technology for pre-processing the geosynthetics after deconstruction. These include suitable large-scale shredding technology and separation processes for the soil adhering to the geosynthetics.

For GSY, starting conditions for higher-value recovery are good, but there is a lack of appropriate recovery channels and business models. For recycling in recycling plants, the specifications of the respective plants must be observed. These specifications must be defined and guaranteed by upstream treatment processes, which have still to be developed, and by appropriate quality assurance systems.

2 Project scope & partners

To be able to meet the addressed challenges in the use of GSY at different levels (including administrative requirements, raw-material supply, social acceptance), the aim should be to close the loop completely. Figure 1 shows which new structures need to be created and which optimisations are required in all phases of the entire life cycle in order to achieve this goal. Based on this idealised life cycle, the following main tasks are covered:

- Optimizing the design for the reuse of geosynthetics in new structures
- If reuse is not possible, the design for the recycling of geosynthetics after (re)use in the existing plastics recycling infrastructure must be optimized.
- Production tests and analysis of geosynthetics from recycled materials
- Development and integration of tracers and sensors for traceability and determination of degradation of geosynthetics

- Continuous ecological and economic assessment of the entire life cycle to develop a business model (e.g. take-back system with subsequent pre-treatment for further recycling)
- Development of quality assurance measures & necessary regulatory framework conditions (e.g. liability for materials to be reused)
- Development of a digital data management system to maintain relevant life cycle information for closing the cycle

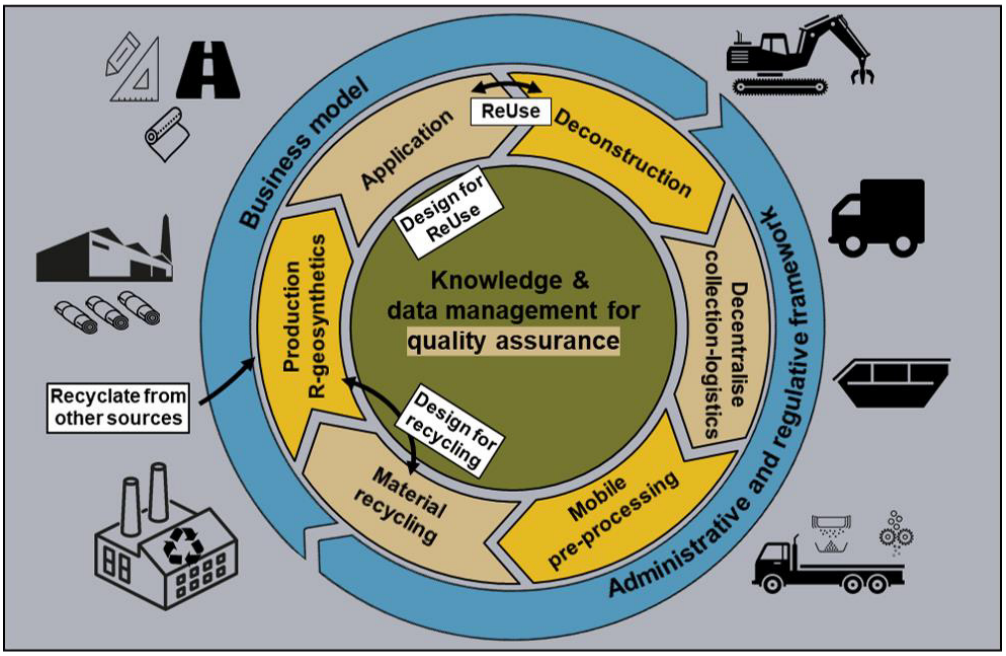


Fig. 1. Concept of closing the loop for geosynthetics.

The complexity of each life-cycle-stage as well as the flow of necessary information between the stages requires different stakeholders. For this purpose, relevant project partners for each life-cycle-stage were brought together for this interdisciplinary research project.

On scientific level working groups *infrastructure* and *resources* of IWARU (*Institute for Infrastructure, Water, Resources, Environment* at *Münster University of Applied Sciences*) working on the conception of the reuse and recycling process as well as the LCA of the newly developed processes. The *Chair of Computing in Engineering* at *Ruhr University Bochum* is working on developing digital structures that enable a consistent exchange of relevant data across the entire life cycle between the different stakeholders. Necessary partners from industry are involved in the project: The manufacturers *NAUE* and *HUESKER* supply materials for large-scale trials and test recycled materials in their production processes. The company *TIBATEK* developed a hydraulic-driven roll-up device as an attachment for excavators and wheel loaders for the non-destructive deconstruction of geosynthetics. Industry partner *TAILORLUX* develops a VIS/NIRS handheld spectrometer that can be used to identify materials chemometrically or using chemical markers (so-called TRACER). The engineering office *IBH-Herold & Partner* continuously compares the expectation horizon of the construction practice for closing the cycle with the knowledge generated within the project. The project consortium is complemented by advisory project partners, including manufacturers of mobile processing plants, recycling companies, authorities and representatives of the construction industry.

3 Current works and first results

The results of initial large-scale tests on the deconstruction, reuse and recycling of various geosynthetic products and accompanying half-scale laboratory tests carried out by IWARU are presented below.

3.1 Deconstruction process

In the current deconstruction process, geosynthetic layers are excavated and then removed from the structure using a sorting grab (Figure 2). The newly introduced deconstruction process uses a hydraulically driven roll-up device to recover the material after excavation without further destruction during the dismantling process (Figures 4.-5.).
Pulling-Forces are introduced into the geosynthetic material both during conventional deconstruction process as well as during the newly presented process. The question arises as to whether these forces can be relevant for the design of structures when considering the dismantling process.

To investigate this question two different geosynthetic products were covered with a compacted aggregate layer of 15 – 30 cm on an area between 1,0 – 2,0 m (width) x 3,0 – 5,0 m (length) in a half-scale laboratory test. The shorter side of the covered geosynthetic were connected to an indoor overhead crane. Geosynthetic and crane were connected with a load cell (Figure 3). The products were then pulled against the aggregate layer and the forces were measured over the pulling time to obtain the dimensions for the forces that occur during the deconstruction process when there is a remaining aggregate layer above the geosynthetic layer. A remaining aggregate layer is necessary to prevent the GSY from being damaged by the excavator shovel during excavation.



Fig. 2. Pulling-free of geosynthetic layer.

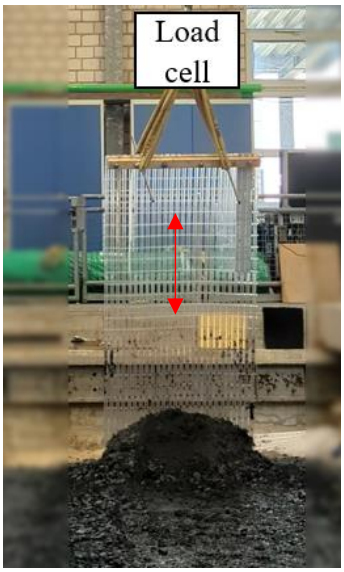


Fig. 3. Determination of pulling-force.

Considering the thickness of the aggregate layer and the width of the geosynthetic, the measured forces were in good agreement. The opening size of the product appears to play a negligible role (open geogrid vs. woven geotextile). It was found that the forces during pulling are once the remaining aggregates on top are at motion reach a constant maximum level between 2-4 kN/m depending on the thickness of the remaining aggregate layer on top (15-30 cm). This force-range is below the tensile strength of most available geosynthetic products. Depending on the skill of the excavator operator and the conditions on site, fewer residual aggregates than tested can be expected. However, practice shows that the removal of nonwoven products with low tensile strength in particular leads to significant tearing in the product during the removal process with a sorting grip [3]. Therefore, the way in which the tensile force is applied during the dismantling process is crucial.

This hypothesis was proven by large scale-test of the deconstruction of different geosynthetic products (approx. 3.500 m²). To simulate construction process und damaging induced during compaction geosynthetic layers where covered with 25 cm of 0/45 mm aggregate which were then compacted with a roller. This setup is in accordance to determine the reduction factor A_2 (EBGEO) for construction damage for the design-phase [7]. Figure 4 shows the winding process of a 300 g/m² nonwoven with a prototype of the new developed roll-up device. The damage was induced during the removal process of the aggregate layer. Despite the damage the nonwoven could be rolled up without tearing any further. If no damage occurred due to the removal of the aggregate layer, large quantities of undamaged products could be recovered (Figure 5).



Fig. 4. Rolling-up process of a 300 g/m² nonwoven.



Fig. 5: Undamaging recovery of a used geotextile.

3.2 Reuse

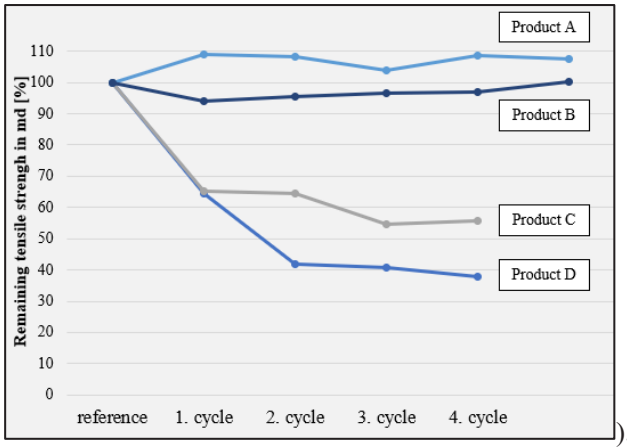
Specially geosynthetic products used in temporary constructions have a high potential to be reused for similar applications due to the reduced requirements concerning durability. To investigate these potential different products (1,0 x 5,0 m²) where covered several times with an aggregate 0/45 mm layer of approx. 15 cm and then compacted (Figure 6).



Fig. 6. Investigating reuse potential of different products.

After each compaction, the entire layer of aggregate was removed and a sample of the geosynthetic product was taken. A new layer of compacted aggregate was then applied to the same product. A sample from each simulated 'usage cycle' was then tested for its remaining tensile strength according to EN ISO 10319 [8]. Figure 7 shows remaining tensile strengths after up to 5 simulated cycles. It shows that there is a significant difference between products. While products A and B show no measurable loss of tensile strength after 5 cycles, products C and D go down up to less than 40% of remaining tensile strength. Even though the loss of tensile strength for product C and D comparable high after the first and second cycle, the loss in the additional cycles is less significant.

Analyses still to be carried out will show how representative the results from the half-scale tests presented are by comparing them with the results from the full-scale tests in the field (see 3.1). Also, the amount of damage induced to the products during the usage stage (e.g. rutting) has to be quantified and considered, when discussing a reuse of these products.



).

Fig. 7. Remaining tensile strength in md after simulated "usage-cycles".

3.3 Pre-treatment

If a reuse of a product is not possible (any more), they should be recycled. In order to be able to implement recovered geosynthetic products after dismantling into existing recycling processes (e.g. for plastic packaging or bottles), pre-treatment is necessary. This includes the production of piece sizes that can be processed by recycling plants. In addition, a large amount of soil adhering to the geosynthetic product must be removed. During first-large scale tests the shredding of different product-types was tested. Depending on the degree of contamination with remaining soil an additional sieving was necessary. Figure 8 shows an exemplary test-setup consisting of a shredder and a drum-sieve for the pre-treatment of a woven geotextile.

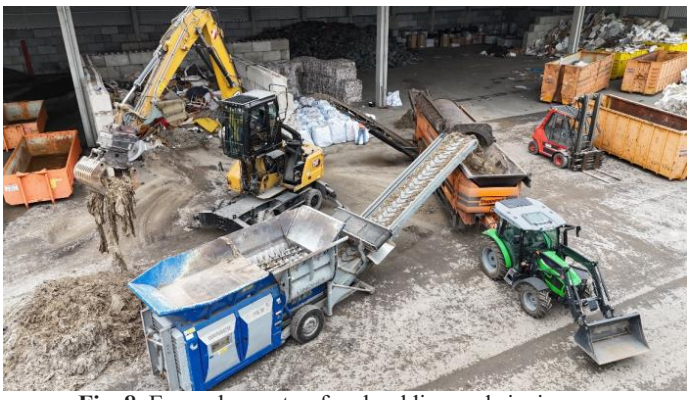


Fig. 8. Exemplary setup for shredding and sieving.

The large-scale tests showed that especially woven products with a high tensile strength demand high-power shredding technology to generated a satisfactory result.

3.4 Recycling

Pre-treated material (piece-size, reduction of adhering soil) was then tested for the ability of implementation in an existing recycling infrastructure. Fractions of different geosynthetic products where processed through a recycling plant in a large-scale. The process consisted

of further shredding, frictional washing, mechanical drying, agglomeration and granulation. Figure 9 shows two fractions after pre-treatment and during the process steps.

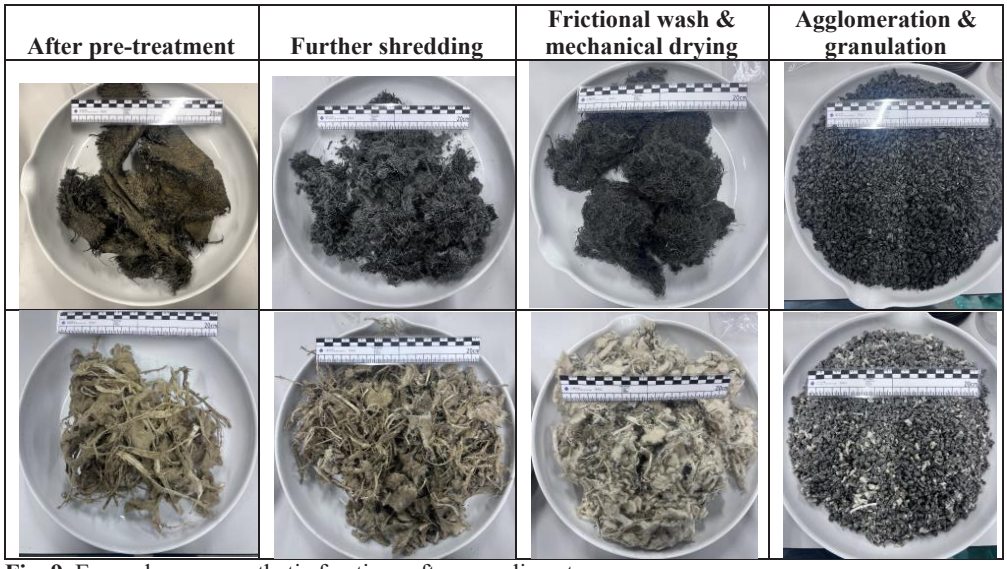


Fig. 9. Exemplary geosynthetic fractions after recycling steps.

It was possible to create an agglomerate from all the products tested (PET/PP wovens, PET geogrid, PP nonwoven + geogrid combination). An initial assessment by the operators of the recycling plant indicates that the agglomerate produced is suitable for further processing as a raw material for existing production processes for various products. However, the usability of the material produced for the manufacture of geosynthetics is still being investigated.

4 Conclusion and outlook

The large-scale trials show that it is possible to reuse and recycle geosynthetic products. However, the research activities are currently ongoing to fully close the loop for the products.

Further work within the presented part of the project will also address the data management needed to keep the information about the product/raw material in order to fulfil the high durability requirements of recycled geosynthetic materials. In addition, a newly developed VIS (visible infrared) and NIRS (near infrared) handheld spectroscope will be tested to detect possible degradation of the polymers as a basis for quality control of the recycling process as well as product identification on site.

All data obtained is analysed in a life cycle analysis (LCA) and life cycle costing (LCC). This information is used to develop ecologically and economically viable business models to close the loop for geosynthetics.

5 Acknowledgement

This project “Product stewardship through closed-loop geosynthetics - ProGeo-UP” is funded by the Federal Ministry of Education and Research of Germany (BMBF) as part of the funding measure "resource-efficient circular economy - plastic recycling technologies (KuRT)".

References

1. DIN 19639 (2019-09): Soil protection during planning and execution of construction projects. https://dx.doi.org/10.31030/3073049
2. L. Düster, C. Lechtenberg, Dietrich (2018) Entsorgung gebrauchter Geotextilien aus dem Wasserbau. https://www.researchgate.net/publication/324360718_Entsorgung_gebrauchter_Geotextilien_aus_dem_Wasserbau
3. N. Depenbrock, S. Flamme, F. Heimbecher, G. Walter (2022) Sustainability in Construction – Closing the Loop for Geosynthetics. In GeoResoures Journal **4**. https://www.georesources.net/download/GeoResources-Journal-4-2022.pdf#page=13.
4. EN 13249 (2016-12): Geotextiles and geotextile-related products – Characteristics required for use in the construction of roads and other trafficked areas (excluding railways and asphalt inclusion). https://dx.doi.org/10.31030/2580039
5. EN 13361 (2018-07): Geosynthetic barriers - Characteristics required for use in the construction of reservoirs and dams. https://dx.doi.org/10.31030/2682806
6. H. Hangen, M. Hempel, H. Hoyme, M.J. Plum (2021): Neue Herausforderungen an Geokunststoffe. Die zunehmende Diskussion über Kunststoffe in der Umwelt wird zum Treiber für die Weiterentwicklung. In: DER EISENBAHNINGENIEUR (**05**/2021). https://hdl.handle.net/20.500.11970/107052
7. Deutsche Gesellschaft für Geotechnik (Hg.) (2011): Recommendations for Design and Analysis of Earth Structures using Geosynthetic Reinforcements - EBGEO. Deutsche Gesellschaft für Geotechnik. ISBN: 978-3-433-02983-1
8. EN ISO 10319 (2015-09): Geosynthetics – Wide-width tensile test (ISO 10319:2015). https://dx.doi.org/10.31030/2273622

Towards a collaborative circular European geosynthetic economy

Francis Denoo[(1)], *Simon* De Meyer[(1)*] , and *Sara* Zamora[(1)]

[1]Beaulieu International Group, Belgium

Abstract. This whitepaper explores the path towards a collaborative and circular geosynthetic economy in Europe, emphasising sustainability in geosynthetics. These materials, essential in geotechnical and civil engineering, face growing concern over their environmental impact despite their durability and versatility. The paper examines challenges across the geosynthetics value chain, including chemical mapping, microplastic risks, and end-of-life solutions. It highlights the importance of stakeholder collaboration in addressing sustainability issues, such as incorporating recycled content, mitigating microplastic pollution, and creating effective recycling systems for temporary applications like geotextile-reinforced roads. The whitepaper promotes fostering partnerships and innovation, so that the geosynthetics industry can meet today's needs for a circular economy.

1 Sustainability in geosynthetics

Geosynthetics are widely used products in geotechnical and civil engineering, valued for their role in enhancing the stability and performance of soil and geological structures. Typically defined as materials containing at least one synthetic or natural polymer component, geosynthetics include products such as geotextiles, geogrids, and geocomposites. These products are prized for their durability, cost-effectiveness, and adaptability across diverse environments, making them indispensable in modern engineering applications. [1]

Despite their long lifespan and robust design, the sustainability of geosynthetics remains a topic of growing concern. As the infrastructure sector faces increasing pressures for environmental responsibility and resource efficiency, assessing geosynthetics' sustainability from multiple perspectives has become essential. Evaluating the environmental impact of these materials, from production to end-of-life, is crucial as the industry shifts towards greener practices, and increasingly focuses on environmental responsibility and resource efficiency. [2,3]

The geosynthetics industry is characterised by a complex, multi-stage value chain involving a variety of stakeholders, each playing a role in the product life cycle (see Figure 1). This complexity arises from the diverse components and materials – such as non-woven fabrics and films – that make up geosynthetic products. Manufacturers of these components contribute to the early stages of the value chain, while the finalised geosynthetics are typically distributed through intermediaries before reaching construction companies.

* Corresponding author: simon.de.meyer@bintg.com

Distributors play an essential role in this chain, often facilitating logistics between manufacturers and end users.

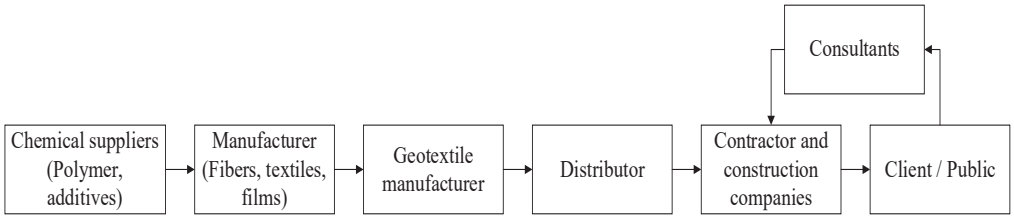


Fig. 1. General scheme of the geosynthetics value chain

1.2 Collaboration for sustainable practices

In this paper, we want to underscore the importance of collaboration across the geosynthetics value chain by presenting practical examples. We want to show that, by fostering partnerships among suppliers, manufacturers, distributors, and end users, the industry can more effectively implement sustainable practices, helping to address environmental challenges and promote a circular economy within the geosynthetics sector.

We will explore three key themes, each highlighting opportunities and potential strategies for advancing sustainability within the geosynthetics market. We will include practical examples and insights on how each can contribute in a collaborative, circular approach towards a sustainable European geosynthetic economy:

1. Chemical mapping 2. Microplastic risks 3. End-of-life solutions

2 Chemical mapping

In this paper, chemical mapping refers to the comprehensive process of identifying, cataloguing, and tracking every chemical substance used throughout the life cycle of geotextiles. This process includes gathering detailed information on each chemical's composition, function, source, and potential impacts on health, the environment, performance, regulations, and market demands.

Effective chemical mapping in geosynthetic products requires a structured system that links participants across the value chain, beginning with manufacturers and extending to the finished product's applications and relevant regulatory requirements. Figure 2 illustrates a graphical representation of such a system. The goal is to ensure traceability of raw material composition through to the final product, while also meeting current regulatory standards, performance requirements, and market demands.

However, due to the complexity and length of the geosynthetics value chain, obtaining accurate information at the right time can be challenging. Strong collaboration among stakeholders in the value chain is essential to facilitate the exchange of critical information – such as the product’s end-use applications, current and forthcoming regulations, and any chemicals or materials that may pose common issues over the product’s lifecycle.

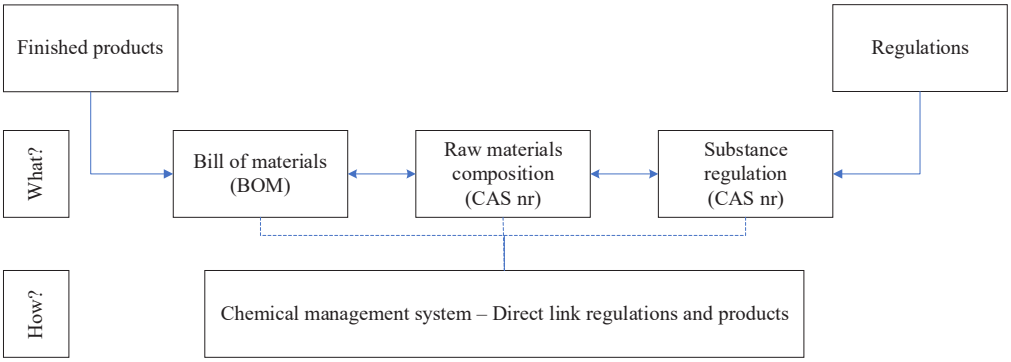


Fig. 2. Example of an integrated chemical tracking system within geosynthetic manufacture.

Implementing an optimal system for chemical mapping benefits geosynthetic products in multiple ways, particularly in promoting environmental and health safety, regulatory compliance, and adherence to standards necessary for market entry. Additionally, chemical mapping can support sustainability initiatives within the geosynthetics industry, such as incorporating recycled content, fostering innovation, and optimizing product lifespans.

2.1 Supporting the circular economy: incorporation of recycled content

Tracking chemical composition is essential for efficient recycling and reuse processes. By understanding the composition, origin, and characteristics of recycled raw materials, manufacturers can ensure that recycled geosynthetics meet safety standards and performance criteria when used in new products.

Several internal ongoing projects are evaluating the effects of incorporating recycled content in geosynthetic materials. For instance, one project investigated the integration of own reworked post-industrial polypropylene (PP) waste into woven geotextiles designed for road reinforcement. Mechanical testing was conducted on geotextile samples with and without recycled content to assess their tenacity and elongation properties. The results, obtained through tensile strength tests following ISO 10319, indicate that incorporating up to 10% post-industrial waste does not significantly alter the mechanical performance of the geotextile. These findings suggest that the addition of 10% of recycled content can be incorporated without compromising essential properties. (see Figure 3)

. Building on our internal efforts to incorporate recycled content into geosynthetics, another company-led project explores the integration of post-industrial waste into polypropylene fibres for nonwoven applications. While the previous study focused on woven geotextiles for road reinforcement, this project investigates how recycled content affects fibre properties to be used in nonwoven materials. In this study, fibres with recycled content ranging from 25% to 75% were produced and analysed to assess their thermal behaviour. Initial differential scanning calorimetry (DSC) results showed no strong correlation between the recycled content percentage and the material's thermal behaviour, although subtle variations in the melting peak's shape and position were observed (see Figure 4). Notably, the thermograms revealed that samples containing recycled content displayed a melting temperature comparable to that of the sample without recycled content. This behaviour may be attributed to the presence of residual thermal stabilisers in the recycled material. These findings are promising, as thermal stabilisers help protect polypropylene fibres from thermal degradation, potentially enhancing or maintaining minimum durability standards. To gain a more comprehensive understanding of the performance of polypropylene fibres with recycled content, additional testing is planned. This will include chemical analysis, durability

assessments using weathering meters and oven aging, and mechanical testing to evaluate long-term stability and mechanical integrity.

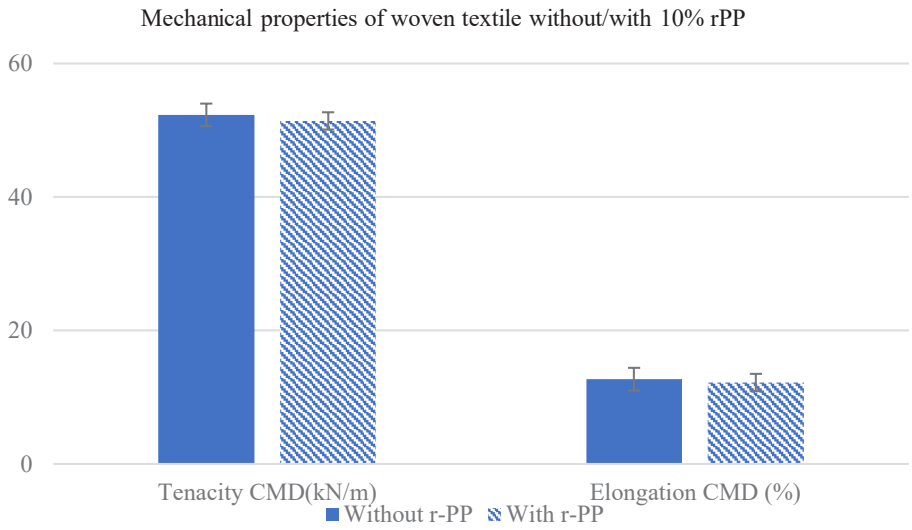


Fig. 3. Effect of incorporating 10% of recycled content into a woven geotextile material.

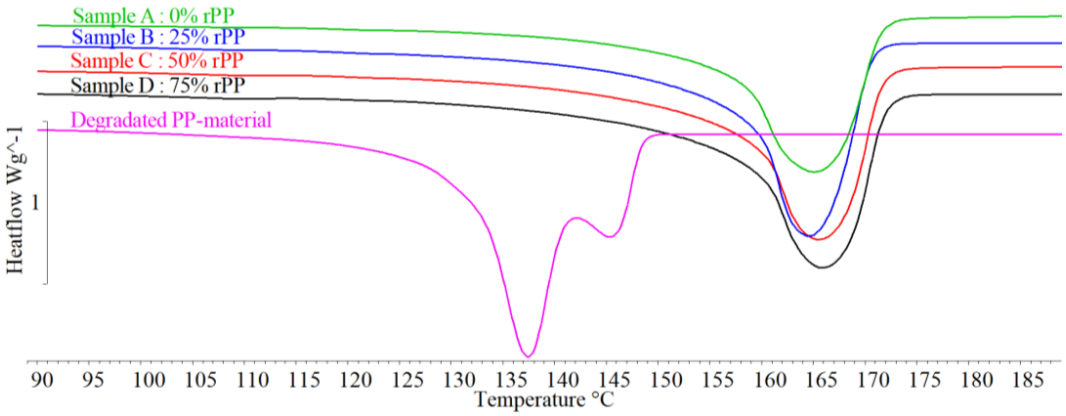


Fig. 4. DSC of PP fibre samples containing different % of recycled content (2nd heating).

These examples demonstrate the potential of using recycled content in geosynthetics. A chemical mapping system enables tracking and correlating results with future market demands for recycled content. Furthermore, both cases suggest that incorporating recycled content does not negatively affect the performance of the textiles or fibres.

It is worth noting that in these cases, only post-industrial waste from the manufacturers own processes was used as recycled content, simplifying raw material traceability. If external post-industrial or post-consumer waste were used, the complexity of maintaining traceability would increase. As authors, we believe that successful implementation of such a system in

these cases will rely on collaboration and communication among industry stakeholders such as suppliers and customers.

2.2 Innovation and optimization for extended product lifetime

Detailed chemical data drives innovation by allowing companies to optimise chemical inputs and identify safer, more sustainable alternatives. An additional ongoing project focused on enhancing the long-term performance of geotextiles exemplifies this potential.

Geotextiles are typically installed underground, where they are shielded from direct sunlight. However, UV exposure during the installation phase can pose a risk, as the material is subjected to both mechanical stress and sunlight degradation. Polypropylene, one of the most widely used materials in geotextiles, is particularly susceptible to UV-induced degradation, which can lead to a loss of mechanical integrity over time. Studies have shown that PP geotextiles without proper UV stabilizers can experience up to 90% strength loss within months of exposure, leading to premature failure [4]. To ensure geotextiles maintain their expected durability and performance throughout their service life, effective UV stabilization is essential. This is achieved by incorporating carefully selected UV additives into PP formulations. In particular, woven and nonwoven geotextiles rely on optimized UV stabilizers to withstand the critical installation period and ensure long-term functionality in their intended applications.

An internal project was conducted to evaluate the effectiveness of UV stabilizers in improving the durability of polypropylene fibres. This initiative involved a collaborative effort with multiple suppliers to screen and select the most promising additives for PP to be used in geosynthetics applications. Selected additives were incorporated at varying concentrations into a standard PP fibre formulation to assess their impact on UV resistance. The modified fibre formulations were then subjected to controlled UV exposure in a xenon light chamber, following a modified version of the ISO 105-B04 protocol. At predefined intervals, fibre samples were retrieved and mechanically tested to evaluate their retained tenacity. The extent of UV degradation was quantified by determining the time required for the fibres to reach 60% of their initial tenacity. Figure 5 visually demonstrates the close relationship between additive selection and performance, highlighting how tailored additive choices can meet the specific demands of each application.

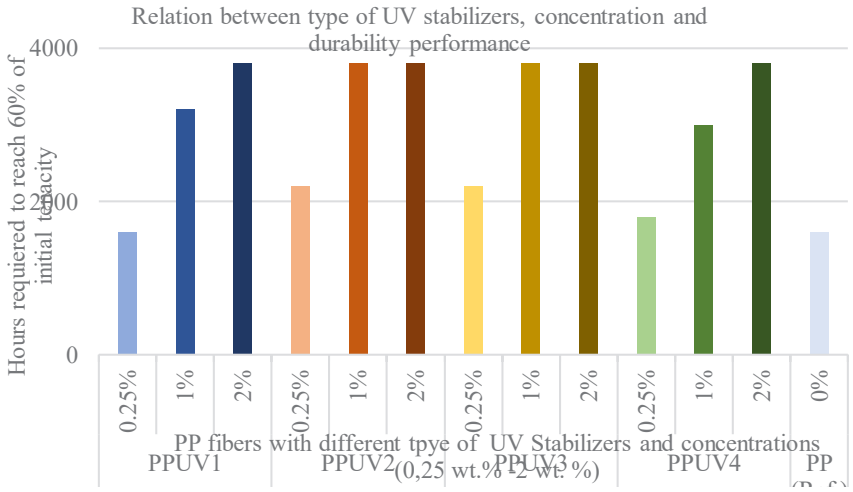


Fig. 5. Relation between type of UV additive and concentration vs end product durability performance

3 Microplastics risks

According to the European Chemicals Agency (ECHA), microplastics are solid particles made up of polymer mixtures. They can be classified into two main categories: [5]

- Unintentionally formed: resulting from the wear and tear of larger plastic items
- Deliberately manufactured: produced intentionally for specific applications.

The release of microplastics is a significant issue, as their continuous discharge leads to persistent pollution of ecosystems and food chains. [6] Although awareness of microplastics has grown over the past decade, many factors remain unclear, making it challenging to quantify their effects on the environment and human health.

In 2024, the European Environment Agency (EEA) published a report offering a preliminary evaluation of microplastics unintentionally released into the environment within the EU. The estimated data derived from this EEA report highlights paints, tyres, and pellets as the primary sources of unintentional microplastic pollution, with geotextiles ranking fifth. Nevertheless, it is important to note that the estimated microplastic release from geotextiles accounts for less than 2% of the total estimated emissions from the six sources evaluated. The report also notes that due to insufficient data and reliable estimates for many sources (including geotextiles), scenario-based estimates with varying emission levels were necessary. [6]

Although geotextiles do not top the list of major sources of unintentional microplastics, as shown in Figure 5, the authors of this paper believe it is crucial for stakeholders within the geosynthetics industry to continue researching and assessing the impact of geosynthetics on microplastic release, while identifying opportunities to contribute positively to this issue. One example of evaluating and quantifying the role of geosynthetics in microplastic release is outlined by Fontana et al. in the study titled “Use of geosynthetics and reduction of environmental impacts in the construction of a new parking apron at Ostend airport in Belgium”. In this paper, a comparative analysis was carried out to examine the environmental impact of a woven geotextile compared with a traditional material, such as a gravel layer. The findings revealed that using a polypropylene woven geotextile significantly lowered environmental impacts compared to the conventional approach involving granular materials: [7]

- CO_2 emissions were reduced by 77.7%.
- Microplastic emissions were decreased by at least 97.65%.

The main factor driving these reductions was the avoidance of transporting large quantities of material to the construction site, thereby significantly minimising microplastic loss associated with tyre wear during transportation

Regarding the quantification of microplastic release directly from geosynthetics, some analyses can be found in the literature. A comprehensive overview is provided in the assessment conducted by the Swedish Environmental Protection Agency in 2022. This report emphasises the importance of clearly defining boundaries and assumptions, such as g/m², material type, installation methods, and product life conditions, as these factors significantly influence the total estimation of microplastic release under varying degradation conditions. [8]

It is well established that geosynthetic degradation is influenced by factors such as abrasion, mechanical stress, UV exposure, chemical exposure, and hydrolysis. However, the relationship between the degradation of geosynthetics under these conditions and the volume of unintentional microplastic release remains unknown. [8]

The authors of this paper extend an open invitation to all stakeholders in the geotextile industry - manufacturers, researchers, policymakers, and end users - to join forces and drive collaborative initiatives aimed at comprehensively addressing the microplastics challenge. By pooling resources, expertise, and innovation, the geotextile community can develop standardised methodologies, conduct comprehensive evaluations, and generate important insights to better understand and mitigate microplastic release from geotextiles. Moreover,

aligning these efforts with evolving EU policy goals and staying informed about regulatory updates will be crucial for ensuring compliance and fostering proactive solutions. Collaboration across the value chain is essential to ensuring that geotextiles not only meet sustainability standards but also contribute to the environment and the circular economy.

4 End-of-life solutions for geotextiles in temporary roads

The global transition to sustainable energy demands vast infrastructure projects, including wind farms and upgraded power grids. These initiatives often require temporary roads, used to transport heavy equipment across challenging terrains such as farmland or natural habitats.

Geotextiles, vital for separating and reinforcing these temporary roads, pose a significant sustainability challenge: their longevity - designed to last at least a century - is in stark contrast to their short-term use. Developing end-of-life (EOL) solutions for geotextiles is therefore crucial to ensuring sustainability within this growing market.

4.1 The challenge: balancing durability and sustainability

Temporary roads are, by definition, transient, but geotextiles are engineered for durability, resisting wear and tear for decades. This mismatch creates a critical question: can materials designed to last 100 years find a sustainable application in temporary contexts?

Addressing this challenge will require a shift from linear usage models to circular business practices, where geotextiles are reused, recycled, or repurposed rather than disposed of after a single use.

The environmental stakes are high. Geotextiles prevent fertile subsoil from mixing with construction materials like gravel or sand, protecting the land they traverse. But as infrastructure projects increase, so does the volume of discarded geotextiles. Without effective end-of-life solutions, this could result in significant environmental and logistical challenges. Important questions to consider are:

- What is the most sustainable end-of-life solution?
- Is it necessary to use material that is designed to last hundred years, when only used temporarily?
- How do we obtain the highest value from the used material?

4.2 Route to circularity

To achieve a circular economy for geotextiles, stakeholders across the value chain must collaborate to align environmental goals with economic feasibility. This requires innovations in material design, end-of-life processing, and market incentives. In this route to circularity, some of the key points to focus on are:

4.2.1. Material design for purpose

The choice of material is critical. Polypropylene geotextiles currently offer an attractive solution in terms of durability, cost, and carbon footprint when compared to other traditional geosynthetic materials such as PET [9]. However, designing geotextiles with durability that is adapted to temporary applications could reduce waste and resource usage.

4.2.2. Recycling and downcycling

Post-use geotextiles must undergo rigorous cleaning and processing to remove soil and contaminants, enabling recycling into secondary applications. For instance, shredded and re-granulated PP can be reintroduced into the production cycle, either for new geotextiles or other products like drainage crates. However, recycling of geotextiles often leads to downcycling, where material quality is reduced. Chemical recycling, which can restore polymers to near-virgin quality, may offer a more sustainable long-term solution, though scalability remains difficult.

4.2.3. Biodegradable materials

Misconceptions around biodegradable alternatives, such as polylactide (PLA), must be addressed. Although they seem appealing, these materials have limitations in terms of mechanical properties and additionally require more controlled sorting and recycling technologies when compared to traditional materials as PP or PET. [10] . Therefore, the focus on enhancing the recyclability and circular potential of existing polymers is still relevant and of great value.

4.2.4. Overcoming legislative hurdles

Regulatory hurdles, such as restrictions on cross-border waste transportation and a lack of EOL certification, complicate recycling efforts. Policymakers should support the industry by defining clear end-of-waste criteria, enabling used geotextiles to re-enter production cycles as secondary raw materials. In addition, virgin PP often remains cheaper than recycled material, which makes the use of recycled content less interesting. Financial incentives will therefore be equally important.

4.2.5. Cross-sector collaboration

Creating a circular geotextile economy demands an ecosystem of cooperation. Manufacturers, distributors, contractors, and recyclers must establish clear processes for harvesting used geotextiles, cleaning and sorting them onsite, and transporting them to recycling facilities.

5 Conclusion: towards a shared vision

This paper highlights the importance of collaboration, innovation, and circularity in the geosynthetics industry to enhance sustainability and environmental performance. Through the analysis of chemical mapping, microplastic risks, and end-of-life solutions, key insights emerge regarding how geosynthetics can transition toward a more circular economy:

- Chemical mapping plays a crucial role in ensuring regulatory compliance, product safety, and sustainability. By tracking and documenting the chemicals used throughout the geotextile value chain, manufacturers can optimize formulations, enhance product performance, and enable the successful incorporation of recycled content.
- Microplastics risks associated with geosynthetics remain an area of ongoing research. Although geotextiles are not among the primary sources of unintentional microplastic release, the industry must proactively assess and mitigate potential impacts. The study underscores the necessity of collaboration across the value chain, engaging researchers, manufacturers, and policymakers to develop a science-based approach to addressing this challenge.
- End-of-life and circularity strategies for geosynthetics are essential to closing the material loop. While geosynthetics are designed for long-term durability, their disposal remains a challenge. Achieving circularity for geotextiles in temporary roads requires a

shift in mindset. Stakeholders must prioritize long-term sustainability over short-term cost considerations. Industry leaders have set ambitious targets, such as Beaulieu's commitment to using over 50% renewable and recycled raw materials by 2030. But to realize these ambitions, cooperation across the value chain is paramount.

References

1. J. Dąbrowska, A. Kiersnowska, Z. Zięba, Y, Trach. Sustainability of Geosynthetics-Based Solutions, Environments. **10**(4):64. (2023)

https://doi.org/10.3390/environments10040064

2. L. Barlow, S. Metaxas, Carbon Cost in Infrastructure. SWECO. (2020)

https://www.swecogroup.com/urban-insight/climate-action/report-carbon-cost-in-infrastructure-the-key-to-the-climate-crisis/

3. European Commission, Buildings and construction. (2025)

https://single-market-economy.ec.europa.eu/industry/sustainability/buildings-and-construction_en

4. C. V. S. Benjamim, B. S. Bueno, P. C. Lodi, and J. G. Zornberg, Installation and Ultraviolet Exposure Damage of Geotextiles. (2008)

https://sites.utexas.edu/zornberg/files/2022/03/Benjamim_Bueno_Lodi_Zornberg_2008.pdf

5. European Chemicals Agency, Microplastics. (2025)

https://echa.europa.eu/hot-topics/microplastics

6. European Commission, COMMISSION STAFF WORKING DOCUMENT IMPACT ASSESSMENT REPORT: Combatting microplastic pollution in the European Union. (2023)

https://eur-lex.europa.eu/legal content/EN/TXT/HTML/?uri=CELEX:52023SC0332

7. F. Fontana, D. Cazzuffi, S. De Meyer, Use of geosynthetics and reduction of environmental impacts in the construction of a new parking apron at Ostend airport in Belgium. (2024)

8. N. Gustavsson, A. Bylund, L. Grabo, J. Grönholdt Palm, Geotextiles and microplastics in Sweden. (2022)

9. The Association of Plastic Recyclers, Virgin vs. Recycled Plastic Life Cycle Assessment Energy Profile and Life Cycle Assessment Environmental Burdens. (2020)

10. K. Trivedi, M. K. Gupta, H. Singh, PLA based biocomposites for sustainable products: A review, Advanced Industrial and Engineering Polymer Research. **6**, 382–395 (2023)

https://doi.org/10.1016/j.aiepr.2023.02.002

Recycling of geotextiles: a collaborative approach to enhance circularity in construction

Gijs Groen[1*], and Juergen *Gruber*[2]

[1]SOLMAX NETHERLANDS B.V. 7559 SC, Hengelo, the Netherlands
[1]SOLMAX AUSTRIA GMBH, Schachermayerstraße 18, 4021 Linz, Austria

Abstract. The construction sector is a major contributor to waste in Europe, producing over 850 million tonnes annually, with polymer-based materials like geosynthetics significantly underrepresented in circular economy (CE) strategies. This study analyses a groundbreaking initiative in the Netherlands that successfully recycled 500,000 m² of geotextiles from temporary construction roads. Employing innovative recycling technologies, including an innovative recycling process, and fostering multi-stakeholder collaboration among project owners, contractors, manufacturers, and recyclers, the project demonstrated the technical feasibility of geotextile recovery and reuse. Inspired by Mariana Mazzucato's mission-oriented innovation framework, the initiative prioritized directionality, additionality, and spillovers to address systemic challenges. Key outcomes included reduced CO_2eq emissions, resource conservation, and reintegration of recycled granulates into production cycles. While economic and technical barriers, such as the high content of soil and cost disparities, remain, this initiative exemplifies the transformative potential of CE principles when coupled with innovation and stakeholder cooperation. This case study provides a replicable model for tackling waste challenges in polymer-based materials, advancing CE practices in large-scale infrastructure projects, and contributing to broader sustainability objectives within the construction industry and beyond.

Full paper to be published in:
https://www.e3s-conferences.org/articles/e3sconf/abs/2025/44/contents/contents.html

* Corresponding author: ggroen@solmax.com

Simple constitutive methods to represent the tensile response of a laboratory-aged nonwoven geotextile

António Miguel Paula[1*], *José Ricardo* Carneiro[2], and *Margarida* Pinho-Lopes[3,4]

[1]GiCos, Sustainable Construction Research Group com sede no IPB, Instituto Politécnico de Bragança, Campus de Santa Apolónia, 5300-253 Bragança, Portugal
[2]CONSTRUCT, Faculty of Engineering, University of Porto, Rua Dr. Roberto Frias, 4200-465 Porto, Portugal
[3]RISCO, Department of Civil Engineering, University of Aveiro, Campus Universitário de Santiago, 3810-193 Aveiro, Portugal
[4]CERIS, Department of Civil Engineering, University of Aveiro, Campus Universitário de Santiago, 3810-193 Aveiro, Portugal

Abstract. Simple constitutive models (polynomial and hyperbolic-based) were used to represent the tensile response of a nonwoven polypropylene geotextile. The model parameters were defined for a virgin sample and for samples submitted to two degradation mechanisms: thermo-oxidation and artificial weathering. Thermo-oxidation tests were carried out by the oven-ageing method (exposure in air, 110 ºC, in the dark during 56 and 112 days). The artificial weathering tests were performed in a laboratory weatherometer with exposure to ultraviolet radiation and water spraying. The virgin and laboratory-aged samples were characterised by tensile tests. The laboratory-aged samples exhibited some changes in their tensile properties. The best constitutive model to approximate the response of the geotextile (virgin and laboratory-aged samples) was the polynomial (order 6). However, the model parameters have no physical meaning. The hyperbolic-based model fitted well the experimental data. Model parameters *a* and *b* have physical meaning as they were related to tensile properties. The fit improved by using correction factors. Hyperbolic-based model parameters for the laboratory-aged samples were adequately estimated from tensile properties of the virgin sample and reduction factors for the laboratory ageing induced. This latter approach for estimating model of aged samples is promising and should be explored further.

Full paper to be published in:
https://www.e3s-conferences.org/articles/e3sconf/abs/2025/44/contents/contents.html

* Corresponding author: mpaula@ipb.pt mailto:author@email.org

Investigation of durability of geotextiles tubes in marine conditions

Soon Hoe Chew[1], *Jun Ming* Soh[1], *Yun Mei* Lim[1], *Jinyu* Deng[1], *Yeow Chong* Tan[2], *Audrey* Yim[2], *Abel* Quek[2], *Dao Jing* Lim[2], *Stacy* Low[2], and *Dylan* Chang[2]

[1]National University of Singapore, Civil and Environmental Engineering Department, 21 Lower Kent Ridge Road, Singapore 119077
[2]Housing & Development Board, Building & Infrastructure Group, 480 Lor 6 Toa Payoh, Singapore 310480

Abstract. Geotextile tubes are widely used in coastal protection structures like revetments, breakwaters, and containment bunds. Geotextile sheets that make up the tube are exposed to harsh environmental conditions, such as UV radiation and wave action. Thus, it is crucial to assess the long-term durability of geotextile materials used to form geotextile tubes, especially since these structures are designed to last 50 years or more. A study was conducted on samples from a 6-year-old geotextile tube that was part of a containment bund on Singapore's northeast coast. Samples were taken from multiple sections along the bund. At each section, samples were retrieved from three orientations: top facing, diagonal facing and side-corner facing of the tube. Physical and mechanical properties of these samples were tested and evaluated. Results showed an increase in mass per unit area, a decrease in thickness, and a retained tensile strength of 18-80% compared to virgin samples of the same grade. A study comparing this durability result with the durability results of a stronger grade of geotextile was conducted. In addition, extensive vegetation growth was observed on the geotextile tube bund. A survey of the plant species was conducted, and the results and observations of the survey were discussed.

Full paper to be published in:
https://www.e3s-conferences.org/articles/e3sconf/abs/2025/44/contents/contents.html

SESSION 3 B
TESTING, QUALITY (3)

Laboratory investigation of geopolymer stabilized subgrade soil reinforced with Alkaline binder-coated Natural Jute Sheet

Aaqib Ali[1*], *Mazhar* Syed[2], *Mubashir* Aziz[1,2], and *Umair* Ali[1,2]

[1]Department of Civil and Environmental Engineering, King Fahd University of Petroleum & Minerals, Dhahran 31261, Saudi Arabia
[2]Interdisciplinary Research Center for Construction and Building Materials, King Fahd University of Petroleum & Minerals, Dhahran 31261, Saudi Arabia

Abstract. Soft subgrade soils often pose significant challenges in pavement design due to their low bearing capacity and high compressibility, and poor durability under repeated loading. As sustainable alternatives to conventional stabilizers gain attention, alkali-activated materials and natural fiber reinforcements offer promising solutions. This study explores the enhancement of subgrade soil strength through reinforcement with a natural jute sheet coated in a geopolymer-based alkaline binder (AB). The investigation examined the performance of stabilized subgrade soils under varying water-to-binder ratios and curing durations. Subgrade performance was assessed through California Bearing Ratio (CBR) and flexural strength tests, along with resilient modulus evaluation. The CBR value of the treated soil increased from 4.1% in untreated samples to 19.4% in AB-treated jute reinforced specimens. The resilient modulus also improved significantly, rising from 17.3 MPa (untreated) to 81.9 MPa (reinforced). Flexural strength increased by 216% compared to the untreated sample, confirming improved load-bearing capacity. Furthermore, 2D finite element simulations demonstrated a 71% reduction in vertical deformation under wheel load in the reinforced soil. The pressure bulb analysis confirmed more uniform stress distribution and reduced settlement, validating the effectiveness of this sustainable reinforcement method in improving subgrade performance.

Full paper to be published in:

https://www.e3s-conferences.org/articles/e3sconf/abs/2025/44/contents/contents.html

* Corresponding author: g202210600@kfupm.edu.sa

Laboratory tests of the impact of stones on geotextiles and calculation model

Adam Bezuijen[1*]

[1]Bezuijen Consult, Berkel en Rodenrijs, Netherlands

Abstract. Laboratory tests have been performed to test the influence of stone impact on a geotextile. According to the Dutch guideline for this type of structures, the vulnerability for stone impact should be limited for non-woven geotextile with a high elongation at break. However, laboratory experiments and field tests showed that also these non-wovens are damaged regularly. A calculation model is used to investigate what are the important parameters for damage of the geotextile during impact. Shape of the block and friction between layers appear of importance. The amount of penetration of the stone into the soil below the geotextile is of less importance. Results are compared with laboratory tests.

Full paper to be published in:
https://www.e3s-conferences.org/articles/e3sconf/abs/2025/44/contents/contents.html

* Corresponding author: adambezuijen@bezuijenconsult.nl

Study of installation of prefabricated vertical drain through a geotextile tube bund

Jun Ming Soh[1*], *Soon Hoe* Chew[1], *Yun Mei* Lim[1], *Jinyu* Deng[1], *Yeow Chong* Tan[2], *Audrey* Yim[2], *Abel* Quek[2], *Dao Jing* Lim[2], *Stacy* Low[2], and *Dylan* Chang[2]

[1]National University of Singapore, Civil and Environmental Engineering Department, 21 Lower Kent Ridge Road, Singapore 119077
[2]Housing & Development Board, Building & Infrastructure Group, 480 Lor 6 Toa Payoh, Singapore 310480

Abstract. Traditional coastal protection and containment structures, such as sand dykes and concrete seawalls and barriers, are increasingly being replaced by geotextile tube bund as a sustainable alternative. In this application, it is common to encounter a layer of seabed soft clay beneath the bund. Ground improvement treatment of this soft clay layer using a cost-effective method, such as Prefabricated Vertical Drains (PVD), will be necessary. However, there are concerns regarding the difficulty of PVD's mandrel penetrating the high-strength geotextile material of the tube. To address this, a laboratory testing apparatus was developed at the National University of Singapore (NUS) to simulate PVD penetration through geotextile sheets anchored in a round frame. A full-scale anchor plate and a full cross-section size of mandrel were used in this test. The study tested two different anchor plate designs on one or two layers of geotextile. Results indicated that while anchor plate design affects the penetrating force and zone of disturbance to the geotextile, the force required to penetrate through geotextile using any of the tested anchor plate designs remains small compared to typical PVD installation forces through sand layers above soft soil. Field data of the PVD installation process was also collected to validate these lab test findings. Field data show minimal differences in the force-depth relationship when PVDs were installed through areas with and without geotextile tubes. Contractors also reported no change in the production rate of PVD installation due to the presence of geotextile tubes, demonstrating that geotextile tubes can be effectively integrated into containment bund structures without impacting PVD installation performance.

Full paper to be published in:
https://www.e3s-conferences.org/articles/e3sconf/abs/2025/44/contents/contents.html

* Corresponding author: ceesjm@nus.edu.sg

Interaction properties between cohesive soils and woven geotextiles – experimental and numerical analysis

Matei-Stelian Serbulea[1*]

[1]Technical University of Civil Engineering Bucharest, Romania

Abstract. Though retaining walls made of reinforced soil already became a classical type of structure, common engineering practice state the use of cohesionless materials reinforced with geogrids. Unfortunately, it is often found the case when only local cohesive materials are available as an economically feasible solution, when the interaction from the soil mass and the reinforcement is governed by adhesion forces. The paper shows how the interaction properties may be described out of test data obtained from an interface shearing test and the adequate numerical simulation using Coulomb model accounting for contact pressure and slip rate.

1 Introduction

This paper aimed at obtaining a proof of concept for a test necessary to define the interaction properties between cohesive soils and geotextiles. This is necessary in order to be a starting point of a research program investigating the behavior of soil reinforced in-mass with synthetic fibers similar to steel fiber reinforced concrete.

For finding the shear strength parameters of soil-geosynthetic interface it is generally used the test procedure given by ASTM D5321/5321M-21 [1], since the adoption of the ISO 12957-2 [2] by CEN is still ongoing. The Standard is focused on the interface between coarse-grained materials and geogrids, where the mechanisms of interlocking outweigh the mere in-plane friction, meaning that for the object of the research theme, a non-standard test method needed to be devised in order to obtain the sought interaction parameters between geotextile and fine-grained (cohesive) soils. Testing coarse materials has the advantage of material being quasi-incompressible, unlike cohesive materials which rise the problem of the geosynthetic displacement from the shearing plane before and during the test due to the soil deformability. In order to partially mitigate this phenomenon, it was chosen to keep just one half of the shearing box filled with soil while the other was fitted with the geotextile fixed on a wooden pseudo half-sample, quasi-incompressible. The reason for using the wooden support was the difficulty to glue the geotextile fibers to a stiffer one, made of steel, so it was decided to choose a mechanical installation system using staples keeping the geosynthetic in place while being anchored in wood.

The necessity of performing direct shearing tests to assess the contact mechanical parameters between cohesive soils and geotextiles yielded since the value of adhesion was about five times less in pull-out tests with respect to direct shearing [6], greatly depending

* Corresponding author: matei.serbulea@gmail.com

on the type of geotextile (better for nonwoven). The tests have been carried-out as in the case of the present paper, on samples with rectangular cross-section of 63mm side, but the geotextile was placed perpendicular to the shearing surface. The range of normal stresses was up to 600kPa.

The EN ISO 17892-10:2018 [3] standard for direct shearing testing requires at paragraph 6.1.2 that the maximum allowable soil grain size should be less than 1/6 of the sample height and if grains are larger than 1/10, this should be reported. Similarly, the American standard ASTM D3080/D3080-23 [4], states at 6.2.2 that the largest grain size should be smaller than 1/6 of the sample thickness. This means that the usual parallelepipedal shear box size of 60mmx60mmx20mm fulfills these requirements for fine grained soils such as the one used for this paper, having the grain size distribution in the Fig. 1. The maximum grain size is far less than the one required by standards, so the test results are valid from this point of view.

The dimensions for classical geotechnical tests were genereally used in several research works such as Pegfei et. al. [6], who studied the soil-geotextile interface behaviour subjected to frost cycles (using small size shear box) or Noorzad and S. H. Mirmoradi [5] performed a set of 144 unconfined compression tests and 72 UU triaxial tests on samples of 38mm in diameter and 76mm height in natural state along with one to three layers of geotextile layers placed in horizontal equally spaced layers noticing the alteration of soil stiffness due to the presence of the reinforcement, while the increase of shearing strength depended on the initial values of the un-reinforced soil.

The soil used for testing was an undisturbed silty clay (PI = 37%) with the grain size distribution described in **Fig. 1**, with a unit weight of 18.47kN/m^3, moisture content 34% (saturated) and CI = 0.82. The tests have been performed at the natural moisture content, without additional saturation.

The oedometer test performed on this type of soil showed an oedometer modulus of 6231kPa (over the loading steps 200 to 300kPa, according to the Romanian classification principle). The swelling pressure was 58.79kPa.

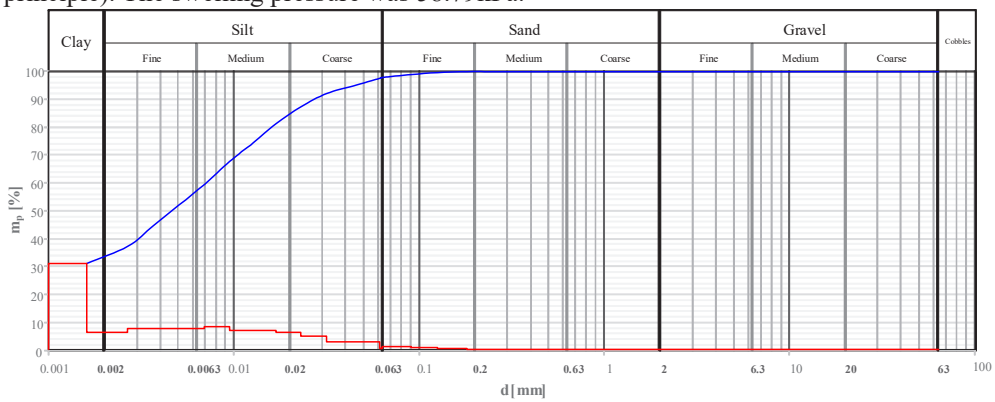


Fig. 1. The grain size distribution of the soil sample used for testing (blue – grading curve, red – bar chart distribution)

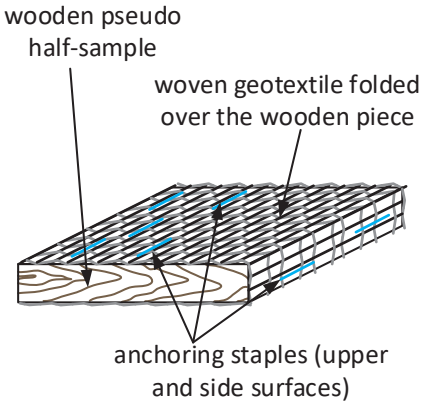
2 Test setup

The purpose of the test was to assess the difference between the intrinsic shearing strength properties of a soil sample and the interaction between the geotextile and the soil. Even if the final point is to study the contact with lean fibers, for this preliminary test was used a woven geotextile for improved anchorage. The fabric margins were glued (over a brim of about 1mm wide) to avoid unravelling.

The geotextile sample was anchored by stapling on the face not in contact with the soil as well as on the side (Fig. 2 a.), while on the contact face the staples were used along the side opposed to the relative motion in order to keep the fabric stretched during installation

(Fig. 2 b.). The choice of stapling instead of glueing [7], was to allow the proper mobilization of the fabric and to avoid partial detachment due to the binding between acrylate and fabric.

The thickness of the wooden support was chosen to match half of a normal sample thickness (10mm) so that the usual direct shear setup to be used.



a. Sketch of the wooden half-sample (view from the top and side anchoring surfaces)



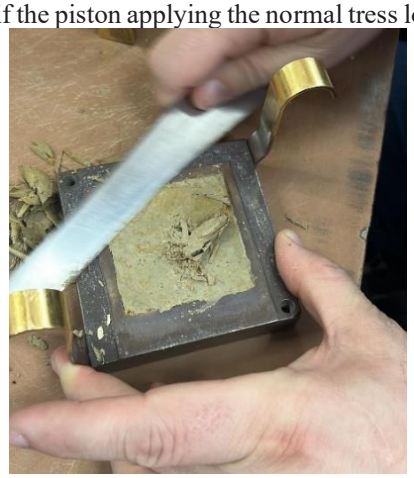
b. Wooden pseudo half-sample (view from the soil side)

Fig. 2. The set-up for the woven geotextile attachment to the wooden piece installed in the upper part of the shearing box

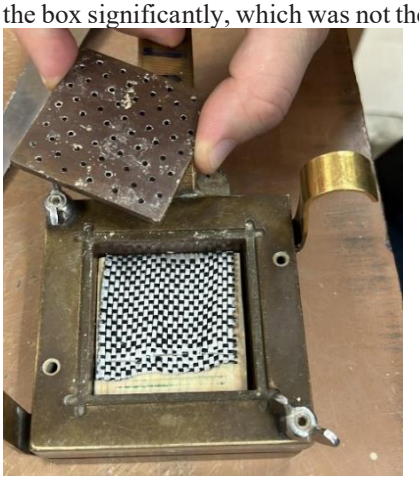
One of the most important parts of the test procedure was to ensure the correct position of the fabric, perfectly at the interface between the two halves of the shearing box. In order to attain this, the soil sample was trim at its normal size, loaded in the shearing box and left to consolidate under the normal stress to be applied for each sample.

After a new consolidation stage with the final set-up, the shearing stage was performed as in the case of a normal CD test, using a shearing rate of 0.025mm/min.

The installation principle was to bring the lower half of the soil sample as close as possible to the compaction degree corresponding to almost zero settlement under the applied normal stress. After the consolidation process was over, each shear box was swiftly removed and trimmed to the interface between the two boxes (Fig. 3 a). Of course, some swelling was to be expected, leading to the geotextile to sink in the soil, but this penetration was assessed to match the thickness of the fabric itself. The main concern was not to have the wooden support overpass the shearing surface and block the test. Another reason for having the wooden + fabric sample thickness equal to the upper half of soil sample thickness was to visually check if the piston applying the normal tress lowers in the box significantly, which was not the case.



a. Trimming the excess soil after consolidation



b. Installation of the upper part of the shearing box containing the wooden piece with attached geotextile

Fig. 3. Shearing box set-up

3 Test results

The number of samples tested was chosen to make sure that the number of results obtained by linear regression are enough to confirm a certain pattern. The soil sample was chosen from a shallow position (2m deep) in order to avoid the effects of over-consolidation, issue that was initially confirmed by oedometer test.

After the test end it was noticed the the position of the interface was maintained (Fig. 4 a.) and it was noticed a good connection of the woven fabric with the soil, judging from the imprinted pattern into the latter (Fig. 4 b.).

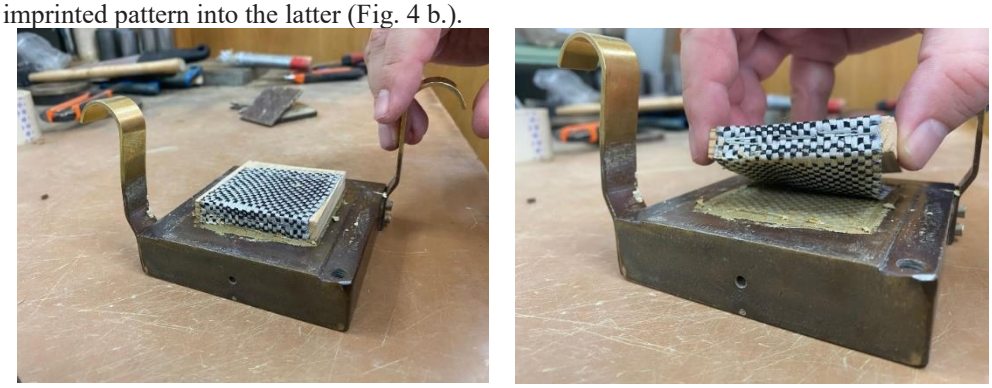


Fig. 4. Pictures showing that the wooden piece kept the geotextile in the right position at the box interface without soil swelling or upper part penetration downwards

In some case the staples used on the interface surface left skid marks (Fig. 5), yet not material bulging was noticed to justify considering this issue to have influenced the results.



Fig. 5. Three of the samples showing the geotextile imprint in the soil and the dragging marks during shearing

Studying the soil-geotextile mobilization curves it may be noticed (Fig. 6) that in the case of the samples loaded with 250kPa (green), 300kPa (yellow) and 350kPa (orange) the wooden half-sample was tripped in the shearing box, but this effect did not alter the results, occurring to displacement far from the peak value of the interaction stress.

The shape of the mobilization curves proves furthermore that the soil samples behave as normally consolidated for the applied normal stress.

The tripping of the upper wooden half-sample did not tear or even disturb the geotextile fabric and the fact that the apertures did not clog with soil prove the fact that the interface failure occurred indeed at the interface and not within the soil sample. The parameters of the intrinsic lines for the soil in natural state and for the interaction between soil and geotextile are given in Fig. 7 and Tab. 1.

Comparing the two sets of values it may be noticed that, at least for this type of material couple, the geotextile seems to have lower friction with the soil than the intrinsic value, yet displays adhesion almost double than the cohesion. These effects impact less the response of the interaction in terms of reactive tangential stress for the low range of stresses, yet it is important for the range of applied normal stresses larger than 250kPa.

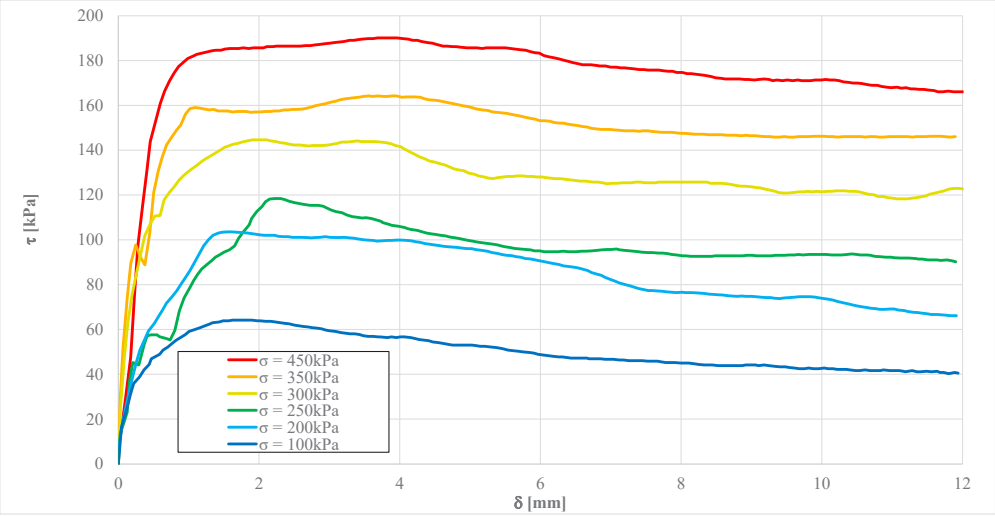


Fig. 6. Mobilization diagram for the six samples of soil interaction with the woven geotextile

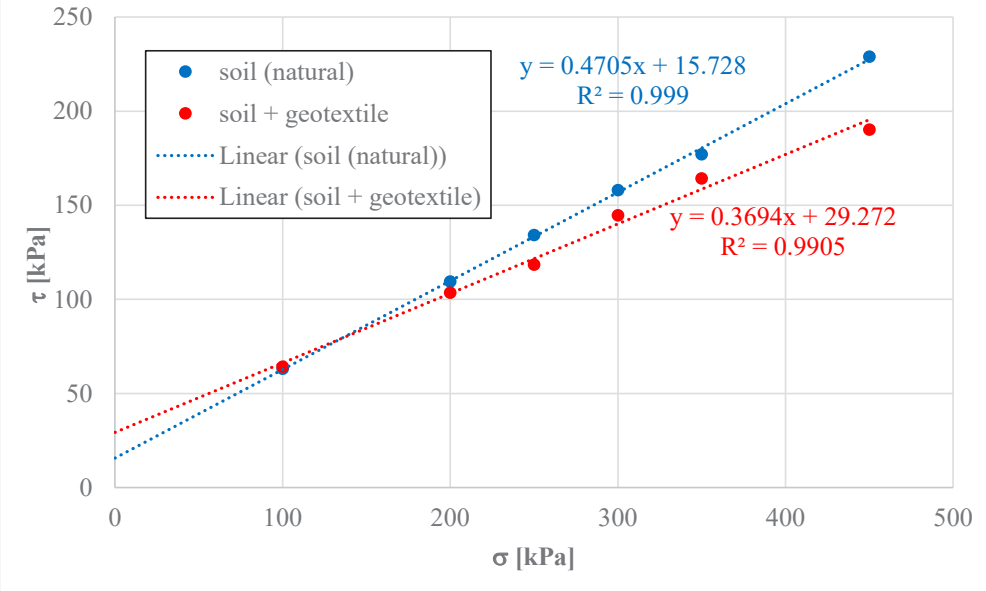


Fig. 7. Results of shearing the natural soil (blue) and interaction of soil with the woven geotextile

Tab. 1. The shearing strength and interaction parameters for the soil and soil + geotextile

Material	R2	ϕ [°]	c (a) [kPa]
Natural soil	0.9990	25.20	15.73
Soil + geotextile	0.9905	20.27	29.27

4 Data processing

One of the most important information to characterize the geotextile-soil interaction is the mobilization of the response (shear stress, friction, adhesion and so on) with the slip or slip rate. Starting from the curves plotted in **Fig. 6**, the tangential stress interaction property may be used directly as long as the normal stress does not vary along the interface and/or time history. This is usually a rare case, since most of the time it is important to study the evolution of the reinforced structure under loads leading to failure.

As a consequence a far better approach is to use friction and adhesion curves in terms of slip rate. The experimental data is very seldomly obtained as a smooth variation with fixed sampling intervals, so a hyperbolic regression curve typical for this type of evolution was used [9].

The accuracy of regression was evaluated in the first step of processing, after the coordinate system transformation, with respect to the assumed linearity (**Fig. 8**). It may be noticed that the coefficient of determination (R^2) has acceptable values even when limiting the analysis to slip value of 3mm (5% slip rate). Beyond this limit, the failure is attained and the post-elastic behavior horizontally plateaus. The regression curves resulted form interpolation are displayed in **Fig. 9**.

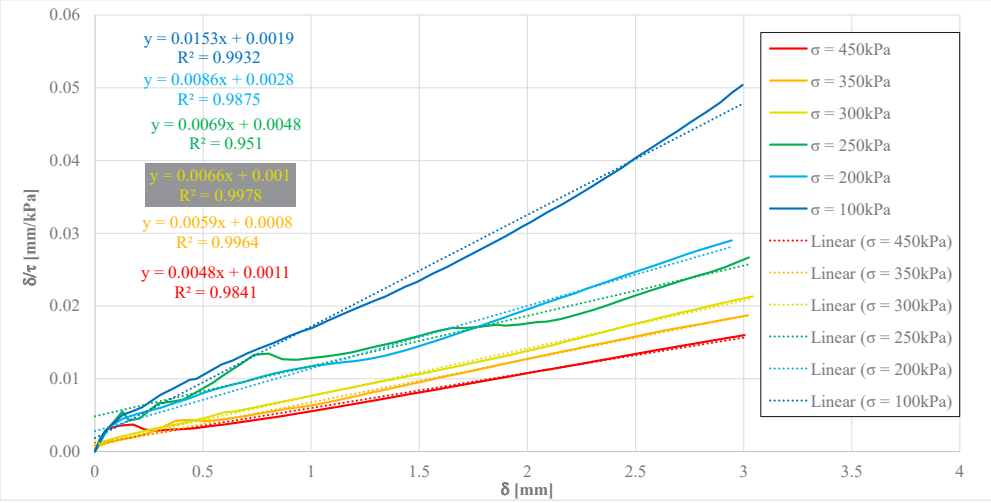


Fig. 8. Coordinate system transformation and check for linearity

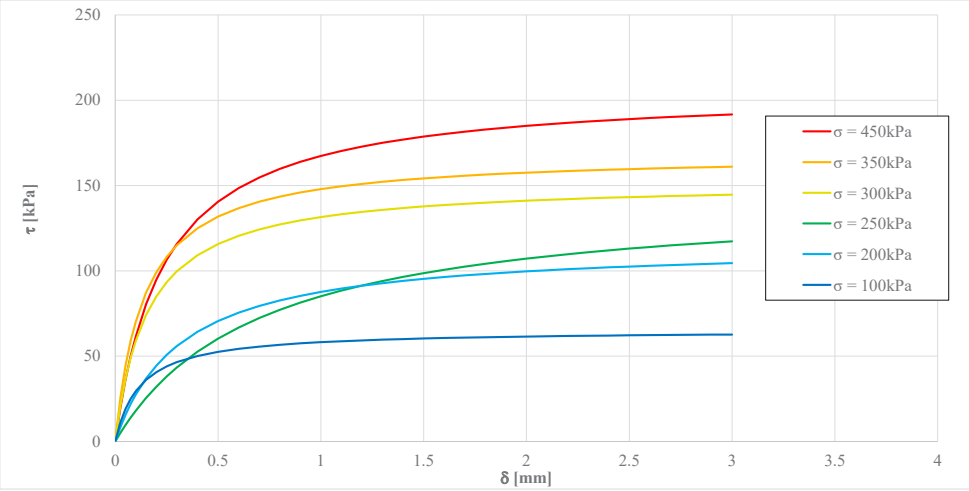


Fig. 9. Resulting hyperbolae regressed from the test data

Computing the tangential stresses for predefined slip rates or slip, resulted the separated mobilization curves for the friction and adhesion (**Fig. 10**, **Fig. 11** and **Tab. 2**). Usually, the friction is expressed in terms of slip rate, while adhesion in terms of slip.

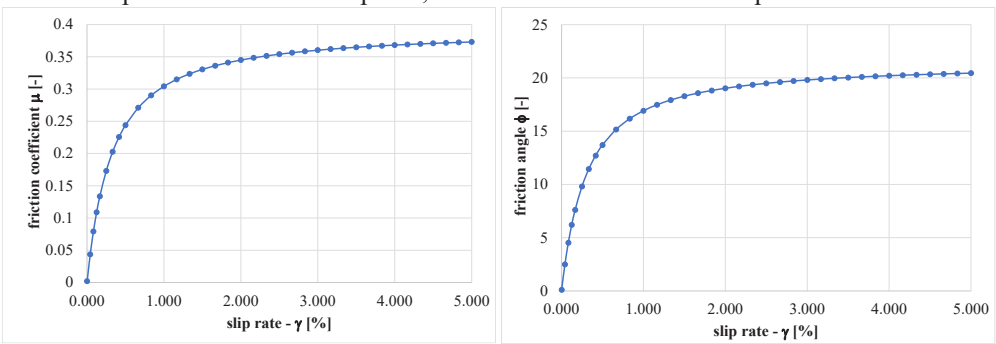


Fig. 10. Variation of friction properties with the slip rate

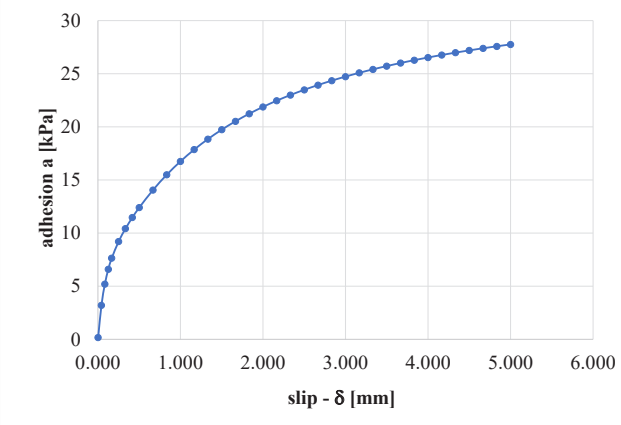


Fig. 11. Variation of adhesion with the slip

Tab. 2. Tabulated values for the friction variation with slip rate and adhesion with slip

ε (%)	μ (-)	ϕ (°)
0.002	0.002	0.11
0.125	0.109	6.21
0.250	0.173	9.81
0.500	0.244	13.70
1.000	0.304	16.92
1.500	0.330	18.28
2.000	0.345	19.03
2.500	0.354	19.49
3.000	0.360	19.81
3.500	0.365	20.04
4.000	0.368	20.21
4.500	0.371	20.34
5.000	0.373	20.45

δ (mm)	a (kPa)
0.001	0.16
0.075	6.59
0.150	9.20
0.300	12.40
0.600	16.75
0.900	19.73
1.200	21.87
1.500	23.48
1.800	24.72
2.100	25.71
2.400	26.52
2.700	27.19
3.000	27.75

5 Discussion based on a simplified numerical model

In order to check the behaviour of the interface considering the mobilization of friction and adhesion versus the application of the full value, a simple model was used similar to the physical one in the shear box. A difference, in order to capture the detachment of the parts was to allow this phenomenon to occur, instead of confining the parts in a frictionless restraining outer box.

The analysis has been carried-out in explicit dynamic conditions to allow the run after separation. The total applied displacement at a constant rate reached a maximum of 12mm. The normal stress applied on the stiff part (equivalent of the top wooden part) was 100kPa, value that lead at the end of a distribution of the contact pressure as described in **Fig. 12**. As expected, comparing the results of analysis where the progressive mobilization of friction was applied versus full friction coefficient all along the loading, it may be noted a difference of orders of magnitude in shear stress (**Fig. 14**), larger reactive stress in the latter case and about 12% larger slip in the former hypothesis.

Base on these remarks we consider that for full scale structures of cohesive soil reinforced with geotextiles, the use of full value of the interaction parameters between reinforced layers leads to unconservative results, limiting the horizontal displacements and over-evaluating the stresses bared by the reinforcement. This may be distinctively noticed analysing the development of the plastic equivalent strains in the soil part (**Fig. 16**).

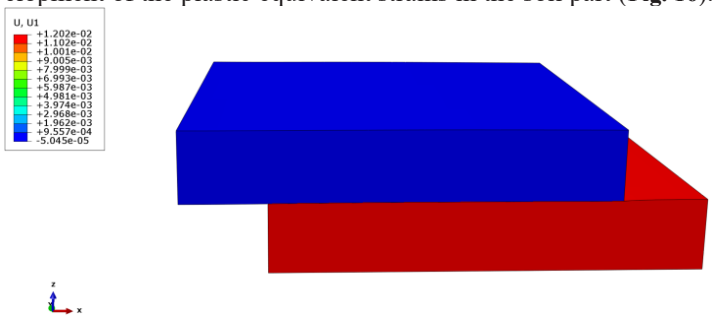


Fig. 12. Position of the parts in the end of the analysis

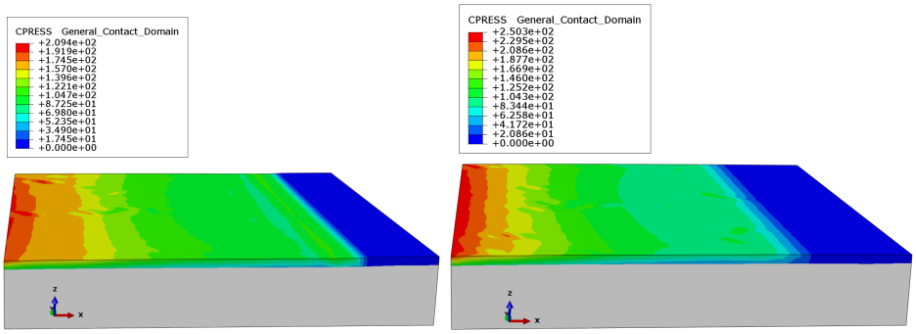


Fig. 13. Contact pressure as seen on the top of the soil part (left – mobilized contact, right – full contact)

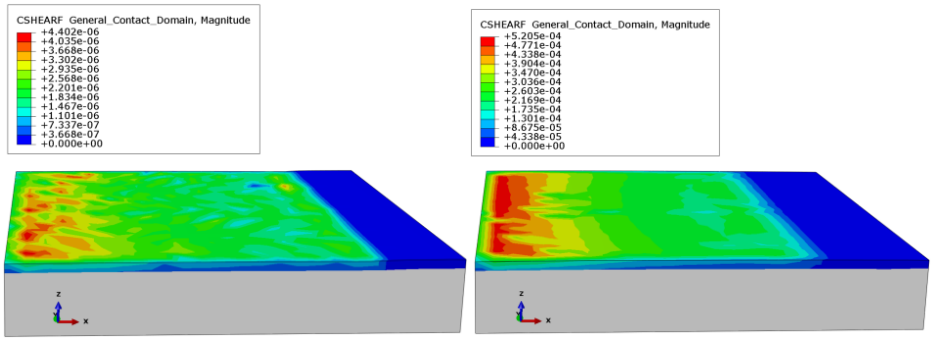


Fig. 14. Contact shear stress as seen on the top of the soil part (left – mobilized contact, right – full contact)

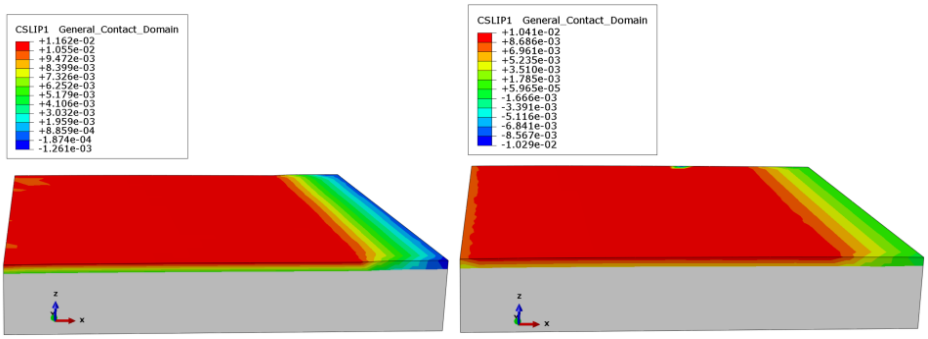


Fig. 15. Contact slip as seen on the top of the soil part (left – mobilized contact, right – full contact)

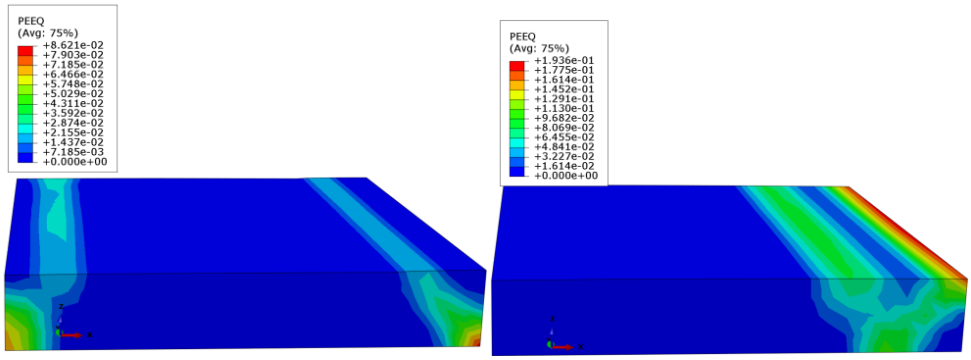


Fig. 16. Plastic equivalent strains of the soil part (left – mobilized contact, right – full contact)

All the numerical simulations have been done using Abaqus/Explicit and the author wishes to express his gratitude for the support of Caelynx Europe and especially Dr. Ștefan Castravete.

References

1. American Society for Testing Materials, ASTM D5321/D5321M Standard Test Method for Determining the Shear Strength of Soil-Geosynthetic and Geosynthetic-Geosynthetic Interfaces by Direct Shear, ASTM (2021).
2. International Standard Organization, ISO 12957-2 Geosynthetics — Determination of riction characteristics — Part 2: Inclined plane test, ISO (2024).
3. G. Athanasopoulos, Results of direct shear tests on geotextile reinforced cohesive soils. Geotextiles and Geomembranes **14**, 11, pp. 619-644 (1996).
4. European Committee for Standardization, EN ISO 17892 Geotechnical investigation and testing - Laboratory testing of soil - Part 10: Direct shear tests, CEN-CENELEC (2018).
5. American Society for Testing Materials, ASTM D3080/D3080M Standard Test Method for Direct Shear Test of Soils Under Consolidated Drained Conditions, ASTM (2023).
6. P. He, H. Cao, J. Dong, G. Hou, Y. Mu and J. Zhang, Effects of wet-dry-freeze-thaw cycles on the response of the frozen soil-composite geotextile interface in direct shear tests. Case Studies in Thermal Engineering **63** (2024).
7. R. Noorzad and S. H. Mirmoradi, Laboratory evaluation of the behavior of a geotextile reinforced clay. Geotextiles and Geomembranes **28**, 4, pp. 386–392 (2010).
8. S. Muthy, A. Sridharan and Bindumadhava, Evaluation of Interfacial Frictional Resistance. Geotextiles and Geomembranes, **12**, 3, pp. 235-253 (1993).
9. J. Duncan and C.-Y. Chang, "Nonlinear Analysis of Stress and Strain in Soils. Journal of the Soil Mechanics and Foundations Division **96**, 5 (1970).

Simulation and applicability evaluation of nonwoven geotextile composite for adsorption of cesium Ions in radiation-contaminated soil

Han-Yong Jeon[1*], *Gyunghwa* Nam[2], and *Ju Hee* Cha[3]

[1]Department of Chemical Engineering, Inha University, Incheon 22212, South Korea
[2]GSI-Korea, Incheon 22212, South Korea
[2]Composite Materials Team, DYETEC Institute, Daegu 41706, South Korea

Abstract. In this study, zeolite and Prussian blue were selected as adsorbents for the removal of cesium components from radioactive contaminated water, and their particle sizes and cesium adsorption performances were evaluated. Additionally, nonwoven geotextiles designed for cesium adsorption were manufactured, and their adsorption performance was analyzed based on the concentration of cesium ion-contaminated water as well as their effectiveness in acidic and alkaline environments. Among the tested adsorbents, Prussian blue demonstrated a higher adsorption performance compared to zeolite. The results of the adsorption tests indicated that the particle size of the adsorbent is a critical factor influencing the adsorption performance of cesium ion adsorption geotextiles. Furthermore, the adsorption efficiency of the adsorbents was found to vary depending on the pH of the contaminated water.

Full paper to be published in:
https://www.e3s-conferences.org/articles/e3sconf/abs/2025/44/contents/contents.html

* Corresponding author: hyjeon@inha.ac.kr

SESSION 3 C
REINFORCEMENT APPLICATIONS (3)

Enhanced evaluation methodology for asphalt reinforcement: methodological updates and laboratory testing protocols

Mohammad Sadeghian[1*], *Eelke* Vromans[1], and *Germain* Auray[2]

[1]Kiwa KOAC B.V., Wilmersdorf 50, 7327 AC Apeldoorn, The Netherlands
[2]Bekaert France SAS, 3 boulevard de Belfort, 59000 Lille, France

Abstract. This paper presents advancements in asphalt reinforcement testing methodologies, focusing on improved accuracy and reliability in three-point bending (3PB) and four-point bending (4PB) tests. Key updates include the transition from displacement-controlled to stress-controlled mode in 4PB tests, enabling complete specimen rupture and eliminating extrapolation, thus providing precise stress (σ6, i.e. stress level at which the mixture would fail after 1 million cycles) values for enhanced evaluation of reinforcement performance. Sample preparation has also been refined, with a shift to single-layer reinforcement placement and adjustments to density grouping, minimizing variability and improving consistency. Additionally, modifications to 3PB tests include the use of fracture energy metrics, capturing the reinforcement's ability to absorb energy and resist cracking, yielding a more comprehensive assessment. These methodological changes align laboratory testing with real-world conditions, ensuring more robust and statistically reliable results. By reducing the impact of sample variability and incorporating new evaluation criteria, the updated protocols provide manufacturers and stakeholders with dependable tools for assessing and developing asphalt reinforcement products. This study contributes to the advancement of testing standards and methodologies, fostering collaboration within the industry to support the design and development of longer-lasting and more durable asphalt pavements.

1 Introduction

Geogrids are a type of geosynthetic material widely used in the pavement industry, particularly for reinforcing asphalt layers. Since their initial study in the 1980s, geogrids have garnered attention for their ability to enhance pavement performance by reducing the thickness of the pavement structure and extending its fatigue life, offering both economic and durability benefits [1, 2]. These materials improve the structural integrity of asphalt layers by mitigating stress and absorbing strain, which effectively reduces reflective cracking and prolongs the pavement's overall lifespan [3].

While both laboratory and field methods are employed to assess the effectiveness of geogrids in asphalt layers, this paper focuses on laboratory-based testing, which provides a controlled environment for evaluating geogrid performance. Among the various laboratory

* Corresponding author: mohammad.sadeghian@kiwa.com

methods, three-point bending (3PB) and four-point bending (4PB) tests are most commonly used due to their ability to assess different performance aspects of geogrids. The 4PB test is often utilized to evaluate complex modulus and fatigue properties, while the 3PB test is employed to assess fracture characteristics and strength under static loading conditions. Virgili et al. (2009) [4] used the 4PB test to evaluate the impact of fiberglass and polyester geogrids on reflective cracking, concluding that these materials significantly improve asphalt layer resistance to cracking. Arsenie et al. (2012) [5] also employed the 4PB test to investigate the effectiveness of fiberglass geogrids, noting a 40% increase in fatigue life under dynamic loading conditions. Meanwhile, the 3PB test, well-regarded for its reliability in static testing, has shown promise in evaluating fracture energy. Romeo et al. (2014) [6] utilized the 3PB test to highlight the superior performance of fiberglass geogrids coated with elastomeric polymers, which exhibited improved resistance to cracking. These studies demonstrate the relevance and effectiveness of both 3PB and 4PB tests for evaluating geogrid performance.

Since 2008, Kiwa KOAC laboratory (previously called KOAC NPC) has been actively involved in testing and evaluating a wide range of geogrid materials, continuously refining our methodologies in line with new research findings and technological advancements. We have contributed significantly to promoting the application of 3PB and 4PB tests for geogrid evaluation and have consistently updated our protocols to enhance their accuracy and reliability. This paper presents recent advancements to our 3PB and 4PB testing methods, which provide a more precise and comprehensive evaluation of geogrid performance. These improvements represent a step forward in standardizing testing methods for geogrids and contribute to the overall enhancement of asphalt reinforcement practices.

2 Methodology

Before explaining the updates and improvements in our testing protocol and methodology, the 4PB and 3PB tests should be explained.

2.1 Four-point bending test (4PB)

The four-point bending test is used for decades in road engineering in the Netherlands. A theoretical explanation of this test is given in the report: “The theory of the four-point dynamic bending test” [7]. A summarization of the theory is given in the European norm: ”EN 12697-24” [8] and “EN 12697-26” [9].

An overview of the test set-up is given in **Fig** 1.

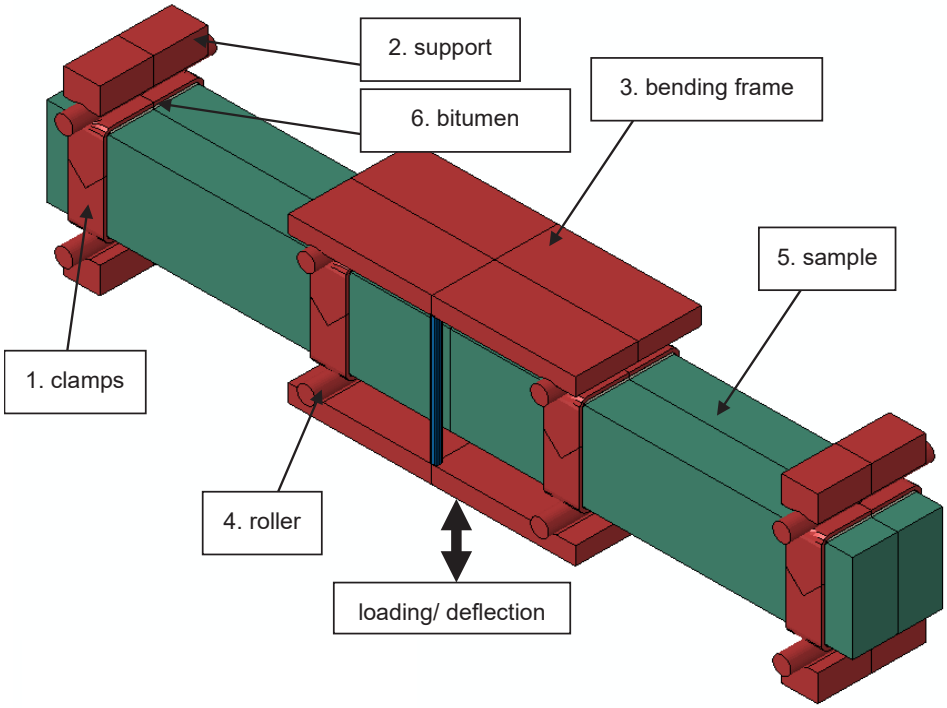


Fig 1. Schematic overview of the four-point bending test.

In this test, the bending frame is oscillated vertically using a sinusoidal waveform. With the supports fixed, the beam undergoes bending, resulting in pure bending at the midpoint, where shear forces are absent. The deflection of the beam is measured at the center of the specimen using a displacement transducer. This deflection leads to the elongation of the beam's surface on both sides, which is termed strain (ε). By conducting tests at various strain levels, a fatigue curve is generated. A key parameter derived from this curve is the strain corresponding to 1 million load cycles, denoted as ε6.

The 4PB test is widely used in the Netherlands to assess the stiffness and fatigue characteristics of asphalt mixtures. Stiffness is determined through a frequency sweep test conducted at 20°C, followed by a fatigue test on the same samples to obtain the ε6 value. The fatigue termination criterion for the 4PB fatigue test is the conventional method of reducing the stiffness of the beam samples to 50% of its initial value. This criterion remains in use in the Netherlands today for evaluating the fatigue resistance of asphalt mixtures. Additionally, the test is performed exclusively in strain-controlled mode, meaning that the strain level is maintained consistently across all cycles, while the reduction in stiffness over time is measured.

The first four-point bending (4PB) test for evaluating asphalt reinforcement was conducted in our laboratory in 2008. Initially, the test was designed to replicate the standard conditions used in fatigue testing of asphalt mixtures. This approach employed strain-controlled mode and a termination criterion based on a 50% reduction in initial stiffness, in line with conventional fatigue testing protocols. However, the results obtained did not show a clear distinction between beams with and without asphalt reinforcement. In many cases, the termination criterion was met due to factors unrelated to the reinforcement itself, such as poor aggregate-bitumen interlock or low beam density, rather than the effectiveness of the asphalt reinforcement.

Recognizing the need for more robust results, we revised our methodology. The first significant adjustment was the introduction of notches in the middle of the beam samples, a technique sourced from the literature [10] to better activate the reinforcement and promote clearer differentiation between reinforced and non-reinforced beams. While notching provided some improvement, it did not fully address the challenge of activating the reinforcement's performance.

A key realization was that the asphalt reinforcement's primary function is to delay the propagation of reflective cracking through the asphalt layer. To better evaluate this effect, we revised the testing protocol further, transitioning from strain-controlled mode to stress-controlled mode. This adjustment allowed for more severe damage to the samples, making the impact of the asphalt reinforcement more evident. Moreover, the conventional termination criterion based on stiffness reduction was no longer suitable under these new conditions. Therefore, we opted to terminate the test once the beam reached complete rupture (zero stiffness), which provided a more accurate representation of the reinforcement's effect (see Fig 2).

These methodological changes led to more consistent and reliable results, with clear differentiation between beams with and without reinforcement. To ensure the robustness of the results, we repeated the test on six different types of asphalt reinforcement produced in Europe. The refined testing approach not only improved the clarity of the results but also enhanced the reliability of the evaluation, making it more suitable for the assessment of asphalt reinforcement in real-world applications.

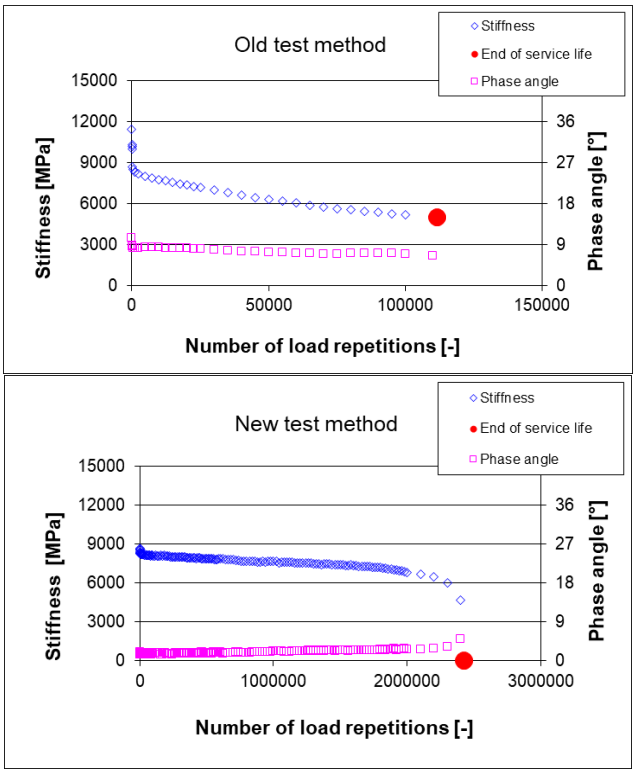


Fig 2. Representation of old (strain-controlled mode) and new (stress-controlled mode) test results.

By adopting the stress-controlled mode, we established a new criterion to evaluate the effectiveness of asphalt reinforcement. Instead of using ε_6—the strain level associated with 1 million load cycles—we introduced s_6, defined as the stress level corresponding to 1 million load cycles. Comparing the s_6 values for beams with and without asphalt reinforcement

provides a more distinct assessment of the reinforcement's effectiveness. It is important to note that ongoing research is investigating whether s_6 is the most appropriate parameter for this evaluation. For the purpose of assessing asphalt reinforcement, we utilized s_6 as an alternative to ε_6, recognizing that further studies are needed to validate its suitability.

Over the past 16 years, further insights have been gained regarding the influence of asphalt reinforcement on specimen stiffness. We observed that adding asphalt reinforcement often does not significantly impact the stiffness of the specimen, due to the relatively small surface area of the reinforcement within the cross-sectional area of the asphalt mixture. This can be confirmed through straightforward analytical calculations. When stiffness variations are observed, they are typically attributable to variations in the asphalt mixture composition or differences in specimen preparation, rather than to the presence of the reinforcement itself.

In the four-point bending test, it is essential to focus on the phase of micro-crack growth within the specimen to accurately demonstrate the reinforcement's effect. As micro-cracks form and the asphalt mixture weakens, the reinforcement engages, supporting the load and delaying complete failure. This phase of crack growth, defined here as the second stage of fatigue, is where the asphalt reinforcement most significantly contributes to the fatigue life of the specimen. Our findings confirm that the presence of asphalt reinforcement plays a critical role in extending the fatigue life during this second stage, underscoring its importance in enhancing the durability of asphalt pavements.

2.2 Three-point bending test (3PB)

Another laboratory test utilized in this study is the three-point bending (3PB) test. This monotonic test is designed to assess the fracture strength of asphalt samples. In the Netherlands, the 3PB test is commonly used to evaluate the strength, fatigue, and stiffness of asphalt in dike construction, following the guidelines outlined in STOWA 2010-W06 [11]. While 3PB is widely employed in monotonic loading for strength measurements, it can also be adapted for dynamic loading to characterize the stiffness and fatigue properties of asphalt.

An overview of the test set-up is given in Fig 3.



Fig 3. Overview of the three-point bending test.

In the context of asphalt reinforcement, 3PB is primarily applied in monotonic loading to assess its effect, as discussed in the literature referenced in the introduction. However, using the 3PB test for measuring the strength of asphalt in dike construction requires specific modifications to make it suitable for evaluating the influence of asphalt reinforcement. These

adaptations are essential to ensure that the test captures the reinforcement's contribution to the overall performance of the asphalt sample.

To adapt the three-point bending (3PB) test for evaluating the effects of asphalt reinforcement, several modifications were necessary. The standard beam sample size used for asphalt in dike applications is 50 mm ×50 mm ×225 mm. However, this small sample size is unsuitable for assessing asphalt reinforcement due to the typical mesh size of the reinforcement materials. As a result, the first refinement involved revising the beam sample dimensions to ensure compatibility with the reinforcement's characteristics.

The standard 3PB test for dike construction traditionally focuses on measuring strength, which is calculated from the peak load in the load-displacement curve. While strength improvement is a valuable parameter, it alone does not provide a comprehensive assessment of the effects of asphalt reinforcement. To address this limitation, the test was modified to include additional metrics derived from the load-displacement curve. These metrics include the peak load and the energy required for crack propagation, commonly referred to as fracture energy [12]. Fracture energy quantifies the material's ability to resist cracking, offering a more detailed evaluation of the reinforcement's effectiveness.

These refinements were inspired by the BEFIM project (Projet national français pour le développement industriel du béton fibré métallique) [13], where the 3PB test was utilized to evaluate steel fiber-reinforced concrete. The project emphasized two critical parameters: maximum loading and post-peak energy, also referred to as the softening region. Maximum loading corresponds to the peak load the specimen can withstand before failure, while post-peak energy reflects the material's toughness and ductility. The latter is calculated by integrating the area under the load-deformation curve beyond the peak load for deformations of 5 mm and 10 mm. While these values represent fine deformation thresholds, they are not fixed. Through extensive testing of asphalt reinforcements, we observed that samples with reinforcement often exhibit greater deformation, continuing well beyond 10 mm in some cases. Using these thresholds allows for a consistent comparison of fracture energy, but the extended deformation seen in reinforced samples further highlights the reinforcement's ability to absorb energy and sustain loads, providing additional insights into its effectiveness.

Adopting these parameters for asphalt reinforcement testing allows for a more detailed analysis of the softening region, capturing the material's ability to absorb energy and sustain loads after cracking. By incorporating these metrics, the refined 3PB test provides valuable insights into the reinforced asphalt's performance in terms of strength, durability, and resistance to cracking.

Furthermore, based on extensive experience with conducting 3PB tests, significant limitations were identified due to the variability in asphalt reinforcement mesh sizes and the bonding between the reinforcement and the surrounding asphalt layers. To address these challenges, we propose shifting from testing beam samples to testing asphalt slabs. Testing a slab measuring 350 mm ×350 mm ×480 mm, instead of a beam measuring 75 mm ×75 mm× 480 mm, eliminates issues related to large mesh sizes, which can make beam testing impractical for some types of asphalt reinforcement. Additionally, slab testing better replicates field conditions by encompassing larger areas of reinforcement and asphalt interaction.

For instance, in the case of steel cord reinforcement, a typical beam may only accommodate two or three cords due to mesh size constraints, which diminishes the reinforcement's impact in the analysis. By contrast, testing larger slabs accommodates the full-scale geometry of the mesh, ensuring more accurate results and better alignment with real-world applications. Recognizing these advantages, we have modified our testing equipment to accommodate both beam and slab samples for the 3PB monotonic test. This enhancement provides a more robust and reliable evaluation of asphalt reinforcement under laboratory conditions, yielding results that closely correspond to field performance.

2.3 Sample fabrication

The enhancements made to our testing methodology are not limited to the refinement of the 3PB and 4PB test protocols. Over the past 16 years of testing, significant changes have also been introduced to the sample fabrication process.

The first major change was shifting from applying two layers of asphalt reinforcement to a single layer within one slab. Initially, it was assumed that using two layers would better highlight the effects of asphalt reinforcement, as the difference between results with and without reinforcement was often minimal. However, this approach introduced discrepancies between small-scale testing and field conditions. It became evident that the observed limitations were primarily related to the test control mode, as explained in previous sections, rather than the number of reinforcement layers. Transitioning to a single reinforcement layer aligned the test conditions more closely with real-world scenarios while maintaining consistency in results.

Another critical aspect of the sample fabrication process is the placement of the asphalt reinforcement at one-third of the slab height. For example, in a slab with a total height of 75 mm, an initial layer of 25 mm (small slab) is compacted, followed by the installation of the asphalt reinforcement. A second layer of 50 mm (big slab) is then compacted on top of the reinforcement. This layering technique ensures proper integration of the asphalt reinforcement within the sample structure.

A key consideration during this fabrication process is the thickness of the small slab, as it determines the type of asphalt mixture that can be used. For instance, when using a 25 mm thick base layer, it is recommended to select an asphalt mix with a maximum aggregate size of 8 mm or smaller. This ensures adequate compaction and uniform distribution of the asphalt mixture, ultimately improving the reliability of the test results.

Lastly, the number of samples fabricated for testing plays a crucial role in ensuring consistent results. As two asphalt slabs need to be fabricated and the reinforcement layer installed between them, variations in the density of the samples can lead to scattered results. To address this, it is highly recommended to fabricate additional slabs initially and measure their densities. Based on these measurements, samples with similar densities can be grouped together, resulting in greater consistency and reliability in the test outcomes.

An overview of the sample fabrication is given in Fig 4.





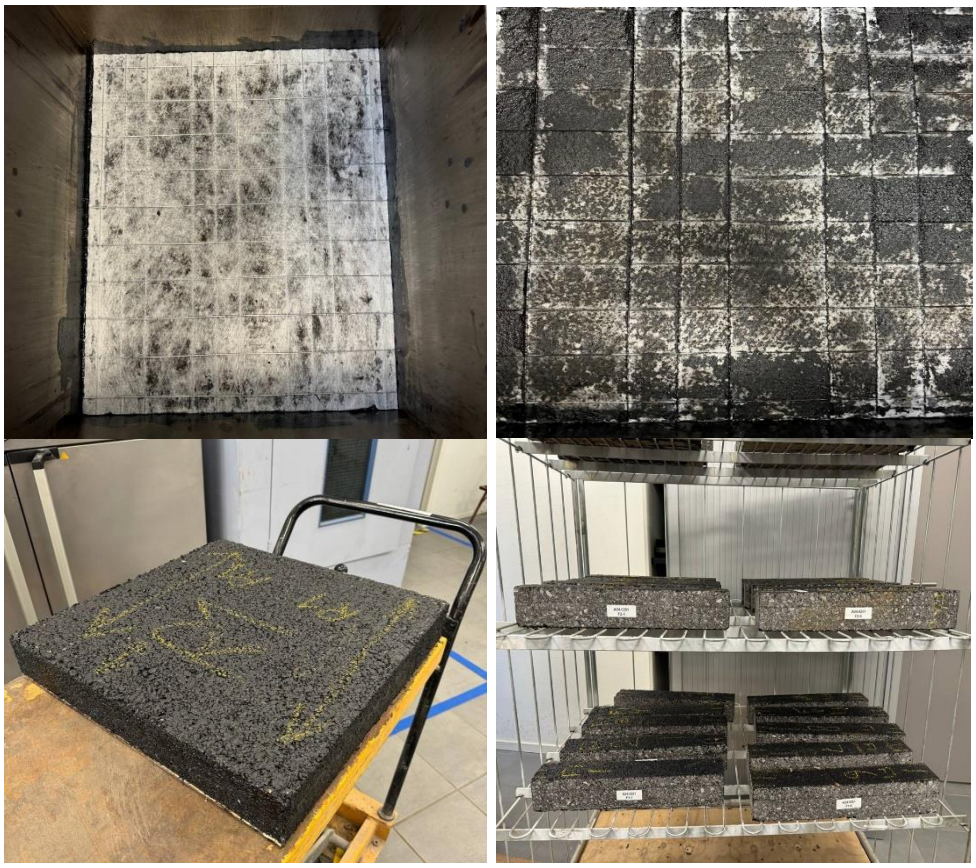


Fig 4. Overview of the sample fabrication.

3 Standardization and adaptation for broader use

The refinements described in this study, although developed within a specific industrial context, provide a foundation that can be standardized and adapted for broader use by other laboratories. Transitioning from strain-controlled to stress-controlled testing in 4PB offers a methodological improvement that enhances the differentiation of asphalt reinforcement performance. This adjustment, alongside the introduction of s6 as an evaluation parameter, ensures that fatigue behavior is assessed comprehensively, even without direct access to proprietary test results.

The shift from beam to slab testing in 3PB addresses key limitations such as mesh size compatibility and alignment with field conditions. By standardizing slab dimensions, reinforcement placement, and sample preparation protocols (e.g., density grouping), other laboratories can replicate these advancements to achieve more consistent and reliable outcomes.

While proprietary data cannot be shared, the refinements themselves are based on fundamental principles of material testing, which can be generalized and incorporated into broader testing frameworks. Publishing the methodology and collaborating with industry stakeholders could facilitate the creation of standardized guidelines. These would allow other laboratories to adopt these innovations while tailoring them to their specific testing needs and client requirements.

4 Conclusion

This study has highlighted the significant advancements made over the past 16 years in evaluating asphalt reinforcement through laboratory testing, including the refinement of 4PB and 3PB test methodologies and improvements in sample fabrication processes. These refinements have enhanced the accuracy, reliability, and applicability of test results, providing better insights into the performance of asphalt reinforcement under various conditions.

In the 4PB test, transitioning from strain-controlled to stress-controlled mode and revising the termination criteria to focus on complete rupture have addressed limitations in differentiating between reinforced and non-reinforced samples. These changes have enabled a more robust evaluation of the reinforcement's ability to delay reflective cracking, particularly during the second stage of fatigue. The introduction of the s6 parameter further enhanced the assessment, offering a clearer distinction of reinforcement effectiveness.

For the 3PB test, modifications to the sample dimensions, test metrics, and evaluation methods have improved the assessment of asphalt reinforcement. Incorporating fracture energy and post-peak energy metrics allows for a detailed analysis of the reinforcement's contribution to crack resistance and energy absorption. Additionally, the shift from beam to slab testing ensures compatibility with larger mesh sizes and better replicates field conditions, yielding more reliable results.

Enhancements in sample fabrication have also played a critical role in improving test consistency. The transition from two-layer to single-layer reinforcement and the strategic placement of reinforcement within the slab have aligned testing more closely with real-world applications. Moreover, addressing density variations by grouping samples with similar densities has further reduced result scatter, enhancing overall reliability.

These advancements collectively provide a more accurate and comprehensive evaluation framework for asphalt reinforcement, bridging the gap between laboratory testing and field performance. By refining both testing methodologies and sample preparation processes, this study contributes to the development of more effective testing standards for asphalt reinforcement, ultimately supporting the design of longer-lasting and more durable asphalt pavements. Future research should focus on further validating the s6 parameter and exploring the potential of alternative evaluation methods to continue improving the assessment of asphalt reinforcement.

References

1. S.F. Brown, J.M. Brunton, D.A.B. Hughes, B.V. Brodrick, Polymer grid reinforcement of asphalt. Asphalt Paving Technology, 54, 133-148 (1985).
2. I.L. Al-Qadi, W.G. Buttlar, J. Baek, M. Kim, Cost-effectiveness and performance of overlay systems in Illinois, Volume 1: Effectiveness assessment of HMA overlay interlayer systems used to retard reflective cracking. FHWA-ICT-09-044, Illinois Center for Transportation (2009).
3. A. de Bondt, Effect of reinforcement properties. In: Proceedings of the 4th International RILEM Conference on Reflective Cracking in Pavements—Research in Practice, Vol. 5, pp. 13-22 (2000).
4. A. Virgili, F. Canestrari, A. Grilli, F.A. Santagata, Repeated load test on bituminous systems reinforced by geosynthetics. Geotextiles and Geomembranes, 27(3), 201-210 (2009).

5. I.M. Arsenie, C. Chazallon, A. Themeli, J.L. Duchez, D. Doligez, Measurement and prediction model of the fatigue behavior of glass fiber reinforced bituminous mixture. In: 7th RILEM International Conference on Cracking in Pavements: Mechanisms, Modeling, Testing, Detection and Prevention Case Histories, pp. 415-423, Springer Netherlands (2012).
6. E. Romeo, F. Freddi, A. Montepara, Mechanical behaviour of surface layer fiberglass-reinforced flexible pavements. International Journal of Pavement Engineering, 15(1), 95-109 (2014).
7. A.C. Pronk, The theory of the four point dynamic bending test, *Report P-DVWV-96-008*, Public Works and Water Management, (1996).
8. Royal Netherlands Standardization Institute, NEN-EN 12697-24 (en), Bituminous mixtures – Test methods for hot mix asphalt – Part 24: Resistance to fatigue, June (2012).
9. Royal Netherlands Standardization Institute, NEN-EN 12697-26 (en), Bituminous mixtures – Test methods for hot mix asphalt – Part 26: Stiffness, March (2012).
10. S.A. Safavizadeh, A. Wargo, M. Guddati, Y.R. Kim, Investigating reflective cracking mechanisms in grid-reinforced asphalt specimens: Use of four-point bending notched beam fatigue tests and digital image correlation. *Transportation Research Record*, 2507(1), 29-38 (2015).
11. Foundation for Applied Water Research (STOWA), State of the art asphalt dike coverings. Amersfoort, (2010).
12. H.R. Radeef, N. Abdul Hassan, A. R. Zainal Abidin, M. Z. H. Mahmud, M. K. I. Mohd Satar, M. N. Mohd Warid, Z. H. Al Saffar, Determining fracture energy in asphalt mixtures: A review. IOP Conference Series: Earth and Environmental Science, 682(1), (2021).
13. R. Lacroix, P. Rossi, BEFIM: The French National Project for the industrial development of metal fibre reinforced concrete. *RILEM Proceedings PRO*, 15, (2000).

Geogrids in road applications for mitigating reflective cracking: A case study from Portugal

José Neves[1*], *Fernanda* Caetano[2], and *Carla* Beja[3]

[1]CERIS, Department of Civil Engineering, Architecture and Environment, Instituto Superior Técnico, Universidade de Lisboa, 1049-001 Lisboa, Portugal
[2]BRISA, Department of Pavements, 2785-599 São Domingos de Rana, Portugal
[3]S&P Clever Reinforcement Ibérica, 2845-408 Amora, Portugal

Abstract. Road pavements are a major field of application for geosynthetics to perform various functions, including reinforcement and stabilisation. Knowledge of the mechanisms of interaction between geosynthetics and paving materials has also been well developed for a long time. This paper focuses on applying geogrids in road flexible pavements to mitigate reflective cracking in asphalt overlays. Based on a case study, the paper aims to analyse the benefit of the use of fiberglass geogrid to reduce crack propagation. The fiberglass geogrid was placed underneath the wearing course of the rehabilitated pavement of a highway in Portugal. Three-point bending tests were performed in the laboratory to analyse the benefit of the presence of the geogrid regarding the potential of crack propagation reduction. The increase of the energy quantified after failure has demonstrated the greater capacity to absorb the energy applied over time due to the presence of the geogrid. This behaviour indicates the benefit of including the fibreglass geogrid to reduce the reflective cracking potential.

1 Introduction

Road pavement maintenance and rehabilitation should be guided by sustainability principles, helping to achieve the Sustainable Development Goals (SDG) set by the United Nations. Consequently, road administrations must promote adequate infrastructure quality through technical, cost-effective, environmental, and social actions.

One current approach to extending the life of the pavement is the asphalt overlay. The asphalt overlay consists of a new layer constructed directly on top of an existing pavement or after removing the existing cracked wearing course. This procedure allows the functional and structural properties of the existing pavement to be recovered. However, when some level of cracking remains on the final surface before the asphalt overlayer construction, crack reflection is a phenomenon that leads to the propagation of cracks from the lower layer to the asphalt overlayer. This phenomenon leads to early cracking at the pavement surface, reducing the useful life of the rehabilitation action. The most traditional solution to overcome this problem is to increase the depth of asphalt removal. However, this solution generates more reclaimed asphalt pavement (RAP), which is no longer sustainable.

* Corresponding author: jose.manuel.neves@tecnico.ulisboa.pt

Geogrids are geosynthetic materials used in road construction, typically made from polyester, fibreglass, polypropylene, or carbon. Their effectiveness depends on the geogrid's tensile strength, stiffness, aperture size, and material. Proper installation and bonding between the geogrid and adjacent layers are also crucial for effective performance. Geogrids can perform various purposes in the payment structure, such as mitigating the reflective cracking phenomenon [1-4].

Geogrids mitigate reflective cracking in asphalt overlays through some mechanisms, such as the reduction of the tensile stresses and crack growth rate. Geogrids develop tensile forces near a crack tip, reducing the stress and strain experienced by the asphalt material. This is achieved through the geogrid's ability to structurally strengthen the pavement by changing its response to loading. In addition, geogrids have been shown to significantly reduce the rate of crack propagation in reinforced asphalt overlays compared to unreinforced samples [5, 6]. Many studies have been conducted to evaluate the impact of geogrids on pavement performance through laboratory tests that the many frequents are three point bending tests (3PB) and four point bending tests (4PB) [7, 8].

In the case of previous wearing course removal, the geogrid is likely to be located at the interface with the asphalt overlayer. However, it is well known that when geogrid is placed at the bottom of an asphalt overlay, the cracks initiate directly to propagate upwards through the overlay, eventually reaching the pavement surface. While the geogrid may offer some resistance, this placement does not entirely prevent the upward propagation of cracks [9-11].

Based on a case study, this paper aims to demonstrate that the location of the geogrid directly on the bottom of the asphalt overlayer can be suitable for mitigating crack reflection during the pavement rehabilitation design period. Although not the most efficient location, it has the advantage of being easily implemented and reducing milling depth with a consequent reduction in reclaimed asphalt pavement (RAP). The paper presents a case study in Portugal, describing the geogrid application, and the three point bending tests performed in laboratory to confirm the efficiency of cracking propagation.

2 Methodology

2.1 Case study description

The case study was the Highway A6 (Marateca/Caia) on the Évora Poente/Évora Nascente section in Portugal (Figure 1a). The pavement rehabilitation was carried out in 2014 to eliminate existing ruts and areas of more pronounced degradation (cracks and ravelling) (Figure 1b). The rehabilitation sub-section had a length of around 16,320 m, between km 59+100 and km 75+420, and a typical cross-section profile of 2×2 lanes.



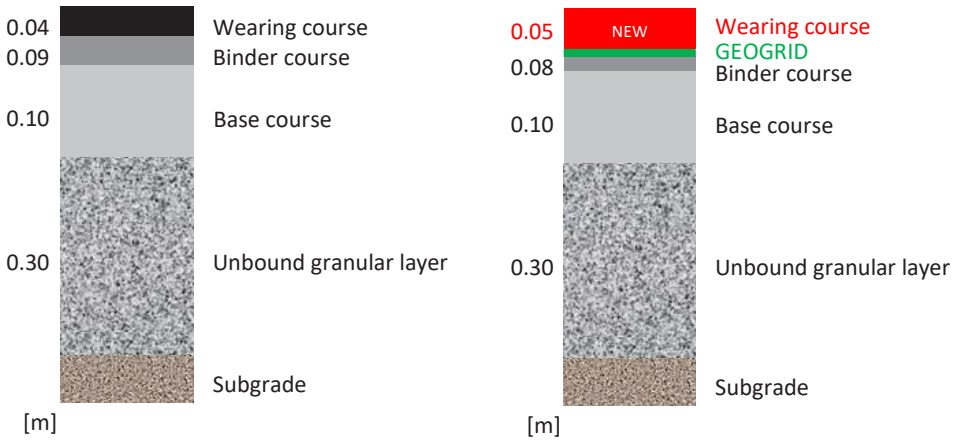
a) b)

Fig. 1. Portuguese Highway A6.

The existing pavement structure is shown in Figure 2a. It is a flexible pavement composed by unbound granular material (0.30 m) and hot bituminous mixtures (0.23 m): wearing course of modified open graded asphalt concrete, AC 14 surf PMB 45/80-65 (0.04 m); binder

course of dense graded asphalt concrete, AC 20 bin 35/50 (0.09 m); and base course of dense graded asphalt concrete, AC 20 base 35/50 (0.10 m). Figure 1b shows the main distresses of the wearing course: cracking and ravelling.

The pavement rehabilitation essentially consisted of milling the existing wearing course within 5 cm and replacing it with a new bituminous mixture: AC 14 surf PMB 45/80-65. In cases where cracking remained after the milling operation, the cracks were sealed (slurry-seal), and a fibreglass geogrid, pre-coated with bitumen, was installed with the main objective of reducing reflective cracking (Figure 2b).



a) Existing pavement b) Rehabilitated pavement

Fig. 2. Pavement structures.

2.2 Geogrid application

A fibreglass geogrid was used in the pavement rehabilitation. This type of geogrid is a synthetic fibre of glass filaments (in the longitudinal and transverse directions). The fibres are produced by agglomerating glass filaments with polyester resin and applying a catalyst to facilitate the polymerisation of the materials. The geogrid is pre-coated and impregnated with bitumen to promote greater adhesion between the geogrid and the pavement layers, a fundamental condition for good performance after its application.

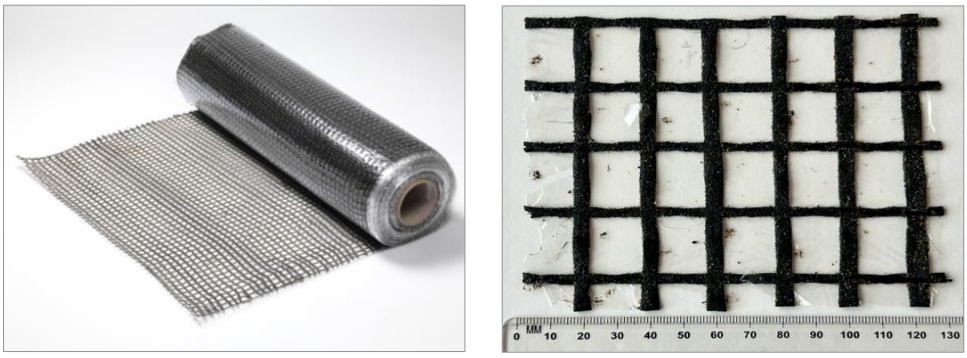


Fig. 3. Fiberglass geogrid.

The fibreglass geogrid was placed after the existing wearing course milling. Previously, the pavement surface was cleaned, dried and free of loose material, dust, oil or other foreign material. All significant depressions or elevations and cracks greater than 2 mm were repaired

to make the surface even and homogeneous. The geogrid was applied over the bituminous emulsion, after the rupture, to promote adequate adhesion between the geogrid and the bituminous base mixture. The tack coat was a thermoadherent cationic bitumen emulsion C60BP4 TA applied at 0.45 kg/m^2 rate. Figure 4 shows some details of the mechanical application of the geogrid.

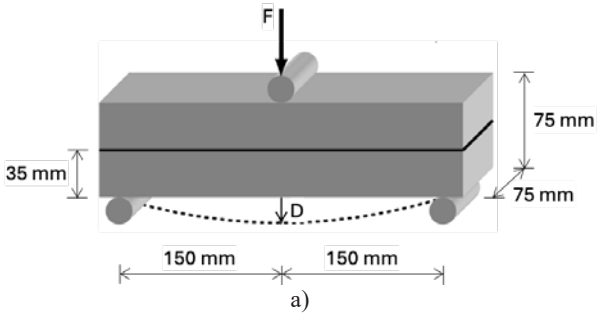


Fig. 4. Geogrid application.

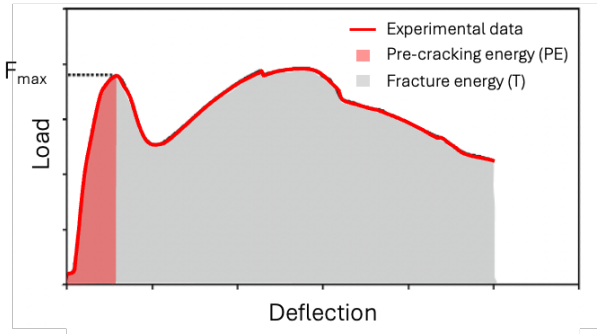
The use of mechanical equipment favours the correct application of the fibreglass geogrid. This type of application promotes its perfect extension, without folds or creases, and bonding to the pavement's surface. After constructing of the upper wearing course, this procedure helps ensure that the geogrid is perfectly integrated into the interface of the bituminous mixture's layers.

2.3 Cracking propagation assessment

To assess the behaviour of the fibreglass grid in terms of crack propagation, 3PB tests were carried out in laboratory on a double-layered specimen [12]. This type of test applies an increasing monotonic load until failure on prismatic specimens compacted in the laboratory as shown in Figure 5. The methodology used in the tests is described in detail by Canestrari et al. [13].



a)



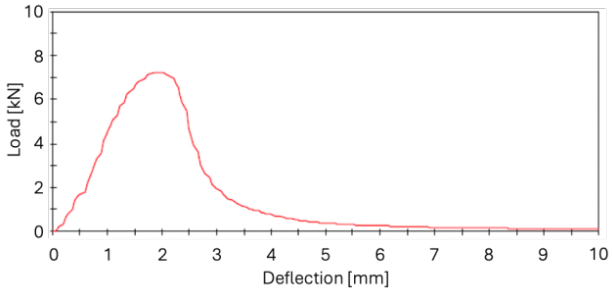
b)

Fig. 5. Scheme of 3PB test and results analysis (adapted from [13])

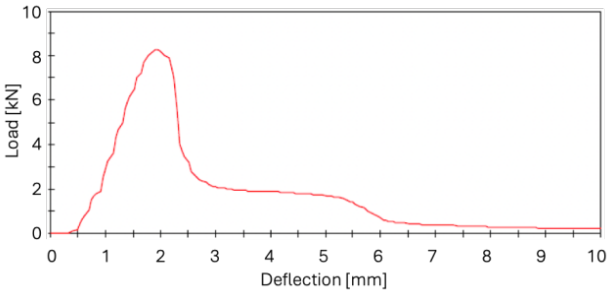
Two sets of prismatic specimens were compacted in the laboratory: one without any reinforcement (unreinforced) and the other reinforced with the fibreglass geogrid (reinforced). The specimens were prepared by roller compactor according to EN 12697-33 [14]. Two bituminous mixtures were used: asphalt concrete AC 14 surf 35/50 in the upper layer, and asphalt concrete AC 20 bin 35/50 (with 20% RAP) in the bottom layer. A thermoadherent cationic bitumen emulsion C60BP4 TA, modified with elastomeric polymers, was applied in the interface of the two layers at a rate of 0.35 kg/m^2. Prismatic specimens were then cut with a cross-section of 75×75 mm^2 and a length of 300 mm. The interface was placed 35 mm from the base of the specimen. Figure 5a shows the schematic representation of test load application and specimen geometries. The load application rate during tests was 50.8 mm/min and tests were performed at 20°C.

3 Results and discussion

Figure 6 shows the curves obtained for the two types of specimens – unreinforced and reinforced – during the 3PB tests. The behaviour of the specimens was assessed through the methodology proposed by Canestrari [11] and illustrated in Figure 5b: the maximum load (F_{max}) and the correspondent maximum deflection (D_{max}); the energy released during the pre-cracking period (PE); and the energy corresponding to the cracking presented by the specimen during the test (T). The energy released during the pre-cracking period considers the start of cracking of the specimen when the load is applied, while the energy after rupture assesses the behaviour of the reinforcement in terms of crack propagation (see Figure 5b).



a) Unreinforced specimen



b) Reinforced specimen

Fig. 6. Example of the flexural behaviour during 3PB tests (adapted from [12]).

During tests, the specimens started cracking at the base due to tensile stress, and the crack propagated to the top. The crack always occurred in the direction of the load application and propagated vertically without the two layers being separated by the existing interface. Figure 7 shows the maximum values of load and deflection recorded in the tests (F_{max} and D_{max}), as well as the values of the energy during the pre-cracking period (PE) and the energy corresponding to the global behaviour of the specimen during the test (T). These results show that the maximum load and deflection values, and pre-cracking energy value are similar for the two specimens (unreinforced and reinforced). However, the energy quantified after cracking was higher for the reinforced specimen, reflecting a greater capacity to absorb the energy applied over time due to the presence of the geogrid [12]. This type of behaviour is confirmed in the literature and indicative of the benefit of the inclusion of the fibreglass geogrid related to the reduction of reflective cracking potential [13, 15, 16].

In addition to the 3PB tests, other laboratory tests were carried out to confirm the benefits of the geogrid on the pavement: Leutner shear test, resistance to permanent deformation test, fatigue resistance and stiffness tests in a four-point bending configuration (4PB). The tests confirmed that geogrid reinforcement did not significantly influence stiffness and strength, while the speed of crack propagation was positively reduced [12].

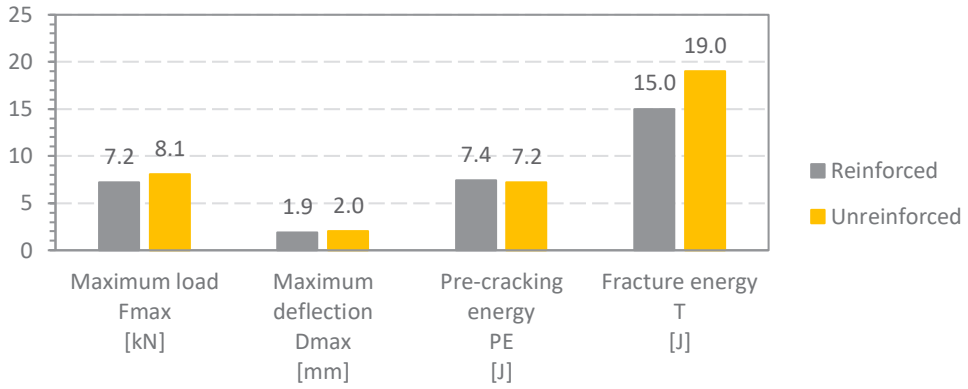


Fig. 7. Results of 3PB tests.

4 Conclusion

This paper described a case study in Portugal on the effectiveness of fibreglass geogrid in preventing reflective cracking in the asphalt pavement. Laboratory three-point bending tests compared reinforced and unreinforced specimens, demonstrating that the geogrid increased

the energy absorption capacity after cracking. This procedure is the simplest and easiest to implement, especially when thin asphalt overlayers are involved. In fact, the use of three-point bending and four-point bending tests can validate the benefits of geogrids in asphalt overlays. Laboratory tests can offer critical data that inform both design practices and material innovation, leading to longer lasting and more cost effective pavements. Further developments on laboratory tests should continue to be developed and implemented.

The results presented in the paper are intended to promote the implementation of geogrids to mitigate crack reflection in asphalt overlayers. This technique can contribute economically to reducing the depth of milling, with the consequent environmental advantage associated with reduced waste production.

Acknowledgement

The first author would like to acknowledge the support of the Foundation for Science and Technology (FCT) through funding FCT-IDB/04625/2020 from the research unit CERIS (Civil Engineering Research and Innovation for Sustainability), hosted by the Department of Civil Engineering, Architecture and Environment (DECivil) of Instituto Superior Técnico (IST), University of Lisbon (ULisboa).

References

1. A. Khodaii, S. Fallah, F.M. Nejad, Effects of geosynthetics on reduction of reflection cracking in asphalt overlays. Geotextiles and Geomembranes **27**, 1-8 (2009). https://doi.org/doi:10.1016/j.geotexmem.2008.05.007
2. P. Hornych, M.N Nguyen, M. Gharbi, Utilisation des géogrilles dans le renforcement des chaussées. IFSTTAR (2015). http://confjeri.ch/wpcontent/uploads/4.-Presentation_Hornych.pdf
3. J.G. Zornberg, Functions and applications of geosynthetics in roadways. Procedia Engineering **189**, 298-306 (2017). https://doi.org/10.1016/j.proeng.2017.05.048
4. J.P. Giroud, J. Han, E. Tutumluer, M.J.D. Dobie, The use of geosynthetics in roads. Geosynthetics International **30**, No. 1 (2023). https://doi.org/10.1680/jgein.21.00046
5. V.V. Kumar, G.H. Roodi, S. Subramanian, J.G. Zornberg, Installation of geosynthetic interlayers during overlay construction: Case study of Texas State Highway 21. Transportation Geotechnics **43**, 101127 (2023). https://doi.org/10.1016/j.trgeo.2023.101127
6. E.J. Rueda, J.G. Bastidas-Martinez, J.C. Ruge, Y. Alayón, J. Olivos, Laboratory Analysis of an Asphalt Mixture Overlay Reinforced with a Biaxial Geogrid. Coatings **13**, 99 (2023). https://doi.org/10.3390/coatings13010099
7. M. Orešković, Š. Bohuš, A. Virgili, F. Canestrari, Simplified methodology for fatigue analysis of reinforced asphalt systems. Materials and Structures **57**, 34 (2024). https://doi.org/10.1617/s11527-024-02305-1
8. D. Ragni, F. Canestrari, F. Allou, C. Petit, A. Millien, Shear-torque fatigue performance of geogrid-reinforced asphalt interlayers. Sustainability **12** (11), 4381 (2020). https://doi.org/10.3390/su12114381
9. I. Arsenie, Étude et modélisation des renforcements de chaussées à l'aide de grilles en fibre de verre sous sollicitations de fatigue, Ph.D. thesis, Université de Strasbourg (2013)
10. M.L. Nguyen, J. Blanc, J.P. Kerzreho, P. Hornych, Review of glass fibre grid use for pavement reinforcement and APT experiments at IFSTTAR. Road Materials and Pavement Design **14** (Sup 1), 287-308 (2013). https://doi.org/10.1080/14680629.2013.774763

11. N.S. Correia, E.R. Esquivel, J.G. Zornberg, Finite-element evaluations of geogrid-reinforced asphalt overlays over flexible pavements. Journal of Transportation Engineering, Part B: Pavements **144** (2018). https://doi.org/10.1061/JPEODX.0000043
12. LNEC, Study for the emission of an application document (DA) for S&P Glasphalt ® G, Phase 2 - Evaluation of the geogrid's performance after application, LNEC 58/2018-DT/NIT, National Laboratory for Civil Engineering, Portugal (in Portuguese) (2018).
13. F. Canestrari, L. Belogi, G. Ferrotti, A. Graziani, Shear and flexural characterization of grid-reinforced asphalt pavements and relation with field distress evolution. Materials and Structures (2013). https://doi.org/10.1617/s11527-013-0207-1
14. CEN, EN 12697-33:2019+A1:2022, Bituminous mixtures – Test method – Part 33: Specimen prepared by roller compactor, European Committee for Standardization (2022)
15. A. Graziani, C. Sangiorgi, F. Canestrari, Fracture characterization of grid-reinforced asphalt pavements. In: Chabot, A., Buttlar, W., Dave, E., Petit, C., Tebaldi, G. (eds) 8th RILEM International Conference on Mechanisms of Cracking and Debonding in Pavements. RILEM Bookseries, vol 13. Springer, Dordrecht (2016). https://doi.org/10.1007/978-94-024-0867-6_9
16. A. Zofka, M. Maliszewski, D. Maliszewska, Glass and carbon geogrid reinforcement of asphalt mixtures. Road Materials and Pavement Design **18** (Sup 1), 471-490 (2017). https://doi.org/10.1080/14680629.2016.1266775

Comparative analysis of thermal and mechanical degradation in glass fiber and PVA geocomposites in asphalt pavement

Pedro Júlio Castro dos Santos[1], *Micheline* dos Anjos e Mello[1], *Fagner* Alexandre Nunes de França[1], *Francisco* Claudio Marques da Silva Júnior[2], and *Ênio* Fernandes Amorim[1]

[1]Federal University of Rio Grande do Norte (UFRN), Natal-RN, Brazil
[2]Independent researcher, Sousa-PB, Brazil

Abstract. Resurfacing is a common solution for addressing crack propagation in pavements, but it results in negative environmental impacts due to the large amount of bituminous material used. As a more sustainable alternative, geosynthetics prevent propagation of crack, reducing maintenance costs and the amount of bituminous material. However, this solution requires certain precautions to preserve their properties against thermal and mechanical degradation. This paper analyzes the effects of high asphalt temperature (167°C) and compaction on two types of geocomposites, glass fiber and PVA, both with a nominal strength of 50 kN/m. The geocomposites were implanted on an asphalted surface before the application of asphalt concrete and subsequent compaction. The exhumation of the geocomposites made it possible to characterize the tensile strength in two stages: one with heating only and the other with heating and compaction. In the first stage, the tensile strength was 42 kN/m and 47 kN/m, with grip displacement of 11.1 mm and 28.9 mm, for glass fiber and PVA, respectively. In the second stage, with the increase of mechanical stress, the values were 9 kN/m and 20 kN/m for tensile strength, and 9.7 mm and 19.7 mm for grip displacement, respectively. Although the PVA showed higher peaks in tensile strength, the glass fiber showed lower average grip displacements, indicating better retention of mechanical properties and greater effectiveness as an anti-reflective crack barrier.

1 Introduction

Pavements are constructed with the objective of providing comfortable and safe driving conditions, as well as withstanding the effects of traffic and weather over a specified lifespan. However, throughout their service life, pavements deteriorate, leading to negative impacts, such as the emergence of distresses that reduce the functional and structural quality of the pavement [1].

There are various types of defects that pavement can exhibit, with cracks being particularly noteworthy. Cracks appear due to the combined effects of traffic and the environment. As a consequence of their presence, several problems arise, such as traffic discomfort, reduced safety conditions for users, water infiltration into the lower layers with a consequent reduction in structural capacity, and the pumping of fines [2].

Typically, simple resurfacing is adopted to solve the problem of cracked pavements. However, in a short time, the cracks reflect or propagate from the old layer to the new one. Crack reflection or propagation is one of the main issues affecting pavements. To prevent crack reflection, which reduces the service life of the restored pavement, an anti-reflective crack system should be employed. This system consists of using special intermediate layers positioned between the new layer and the cracked pavement [3].

Among the existing systems, geosynthetics stand out due to their ease of installation, lower cost, availability, and adaptability to different climatic conditions [4]. These materials are placed on cracked pavements before the overlay is applied, aiming to function as reinforcement or stress-absorbing layers, thereby delaying crack propagation. Additionally, they can be made from various materials, including glass fiber and polyvinyl alcohol (PVA) [5].

Although both glass fiber and PVA geocomposites offer significant advantages in preventing crack reflection, they have distinct characteristics that can influence their selection depending on the specific conditions of the project. Glass fiber geocomposites are more suitable for environments with high temperatures and heavy traffic due to their thermal and mechanical resistance [6]. On the other hand, PVA geocomposites are more flexible, cost-effective, and provide better adhesion to asphalt, making them ideal for areas where stress absorption is crucial for pavement integrity [7].

However, the choice between glass fiber and PVA can be influenced by damage resulting from transportation, handling, storage, and on-site installation processes; internal actions (polymer evolution); and external factors, which can be mechanical—such as creep and relaxation—physical, chemical, or bacteriological, potentially affecting the properties of these materials [1].

To ensure the proper functioning of the geosynthetic, it is necessary to guarantee its durability by identifying the main degradation elements present at the application site of the geosynthetics. This aims to ensure the conservation of its properties within the minimum required values, as well as to evaluate the resistance of the materials to these agents [8].

In the case of geosynthetics used in crack reflection systems, they can be damaged in two ways: by mechanical effect, due to the compaction of the asphalt concrete, and by thermal effect, due to the high temperatures of the asphalt mixture [9].

With this in mind, the objective of this work is to evaluate and compare the effects of temperature and the compaction of asphalt concrete on the tensile strength properties of fiberglass and PVA geocomposites used in asphalt resurfacing.

2 Material and methods

A field simulation of the installation of geosynthetics, composed of fiberglass and PVA, used as a crack reflection system, was developed to verify the impact caused by the thermal and mechanical damage to which these materials are subjected during this procedure. In this simulation, the bonding coat was not used to facilitate the exhumation of the samples, thus avoiding exposing the geosynthetics to possible additional damage.

2.1 Material

The polymer materials used in the research were commercial geocomposites, provided by Huesker Ltda., which are applied in asphalt reinforcement and consist of geotextiles adhered to geogrids, fully impregnated with bitumen. They differ in their raw material and/or tensile strength (Figure 1).

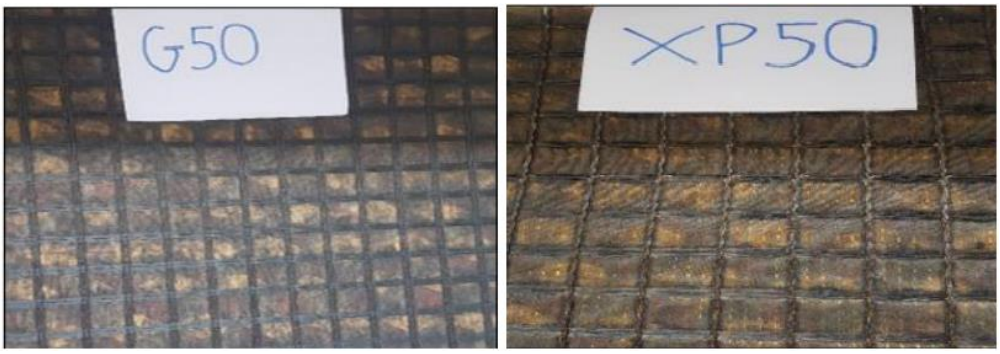


Fig. 1. Geosynthetic materials.

Therefore, in this study, the fiberglass geocomposite with a tensile strength of 50 kN/m (GCO–G50) and the PVA (GCO – XP50), both with a tensile strength of 50 kN/m, were used. Their properties can be seen in Table 1.

As for the asphalt material, C-grade asphalt concrete was used, produced at 167ºC, composed of 26% gravel, 24% sand, 24% stone dust, 21% crushed stone, 6% petroleum asphalt cement, and 1% filler. The asphalt concrete was manufactured and supplied by TCPAV - Tecnologia em Construção e Pavimentação Eireli.

Table 1. Properties of geosynthetic materials.

Properties	Type of geosynthetic	
	GCO-G50	GCO-XP50
Polymer	Fiberglass	PVA
Deformation at nominal tensile strength	≤ 3%	≤ 6%
Tensile strength (MD + CMD)*	50 kN/m	50 kN/m
Bitumen content of the coating	> 60%	> 60%
Tensile strength after installation damage test (DIN EN ISO 10722)	> 90%	> 90%
Mesh opening	3 cm	4 cm
* MD: in the direction of the equipment CMD: transversal to the equipment		

2.2 Methodology

The materials were divided into two sections. Each section served as a sample for each of the two damage situations: thermal damage (TD) and thermal and compaction damage (TCD). In the end, the samples from each situation were approximately 1.0 meter × 2.5 meters.

2.2.1 Application and installation location

The simulation procedure was carried out at the facilities of TCPAV - Tecnologia em Construção e Pavimentação Eireli, located in Macaíba, in the state of Rio Grande do Norte, with geographic coordinates 5º 51' 04.03" S and 35º 17' 46.77" W. On 12/09/2021, at 1:00 PM, the geosynthetics were installed on an asphalt surface, which was previously cleaned with brooms to remove impurities and granular materials that could compromise the performance of the materials. The cleaning was crucial to ensure that the geocomposites were applied under suitable conditions, avoiding interferences that could affect the test results.

After cleaning, the geocomposites were arranged in two distinct rows. The first row contained samples exposed exclusively to the high temperature of the asphalt concrete, while the second row consisted of samples that would also be subjected to additional mechanical stresses. To secure the materials, asphalt concrete was applied to the edges of the geosynthetics, followed by the placement of asphalt concrete over the entire area of the geocomposites. The application of the asphalt concrete was carried out with the aid of shovels for transportation and plows for the uniform distribution of the mixture, as illustrated in Figure 2 (a). For the samples in the row subject to thermal and mechanical damage, the asphalt concrete was compacted using a BOMAG BW 90 AD tandem double drum roller, as shown in Figure 2 (b).



Fig. 2. (a) Deposition of asphalt concrete; (b) Compaction of asphalt concrete.

2.2.2 Exhumation and sample preparation

The exhumation procedure was carried out on 12/10/2021 around 4:00 PM, with extreme care to avoid possible mechanical damage. The removal of the asphalt layer was done with the aid of shovels, but predominantly manually.

After the exhumation of the samples, the specimens were prepared to be tested according [10] for determining tensile properties of geogrids by the single or multi-rib tensile method. The method used in the test was the single element method (Method A).

2.2.3 Uniaxial tensile test

The tensile tests were conducted at the Geotechnical Laboratory of the Federal University of São Carlos – LabGEO/UFSCar, according [10]. The grips used in the tests were of the roller type, which means that part of the specimen was wrapped around each grip. In this situation, to measure the deformations in the specimens, video extensometry is required. This tool could not be used due to the time available for the research, as tests using it require more execution time.

Because of this, the graphs presented in this study are of tensile strength (kN/m) vs. grip displacement (mm). The initial distance between the grips is 200 mm for all specimens, and with the application of tensile stress, this distance increases, either due to the deformation of the specimen in its part wrapped around the roller-type grip or in the free section between grips.

Thus, it was not possible to obtain the secant modulus of the tested materials. Therefore, in this study, a beta (β) parameter will be used as an indicator of the stiffness of the geosynthetics and as a comparison element between the proposed situations. This parameter can be defined as the slope of the tensile strength (kN/m) vs. grip displacement (mm) curve.

3 Results

For a better comparison of the behavior of the geocomposites in the various scenarios, representative curves of the proposed situations are displayed. The representative curve is the one that presents typical values and shapes among the set of curves obtained from the tensile tests of the specimens.

3.1 GCO – G50

The representative curves of GCO – G50 (fiberglass geocomposite with a tensile strength of 50 kN/m) are presented in Figure 3. The average tensile strength for the virgin sample was 52 kN/m, with a CV of 9%, and the corresponding displacement was 11.7 mm, with a CV of 11%. In this case, the average tensile strength obtained from the specimen tests (52 kN/m) was 4% higher than the reference value provided by the manufacturer (50 kN/m). Regarding the slope, its average value was 3.84, with a CV of 24%.

For the situation where the sample was exposed to thermal damage, the GCO-G50 showed an average tensile strength of 42 kN/m, with a CV of 17%. The average grip displacement was 11.1 mm, with a CV of 10%. The average slope was 3.43, with a corresponding CV of 19%.

In the situation where the GCO-G50 sample was directly subjected to thermal and mechanical damage, the average tensile strength was 9 kN/m, the average grip displacement was 9.7 mm, and the average β parameter was 0.95. The CVs were 52%, 43%, and 46% for tensile strength, displacement, and slope, respectively.

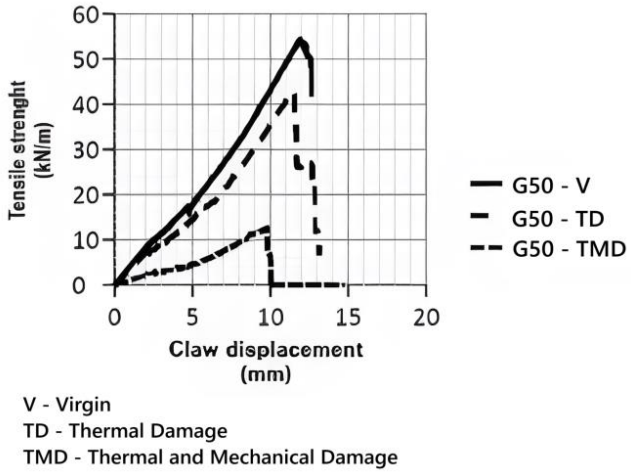


Fig. 3. Representative curves for GCO – G50

3.2 GCO – XP50

The representative curves of GCO – XP50 (PVA geocomposite) can be observed in Figure 4. The average tensile strength for the reference situation of GCO – XP50 was 53 kN/m, the corresponding displacement was 32.3 mm, and the average slope was 1.57. Regarding the CVs, for tensile strength it was 6%, for grip displacement it was 8%, and for the β parameter it was 42%. In this case, the average tensile strength obtained from the specimen tests (53 kN/m) was 6% higher than the reference value provided by the manufacturer (50 kN/m).

For GCO – XP50 exposed to thermal damage, the average tensile strength was 47 kN/m, with a CV of 14%. The average grip displacement was 29.9 mm, with a CV of 12%, and the average slope was 1.39, with a CV of 15%.

In the case of GCO-XP50 subjected to thermal and mechanical damage, the average tensile strength was 20 kN/m, with a CV of 22%. The average grip displacement was 19.7 mm, with a CV of 18%, and the average β parameter was 1.20, with a CV of 38%.

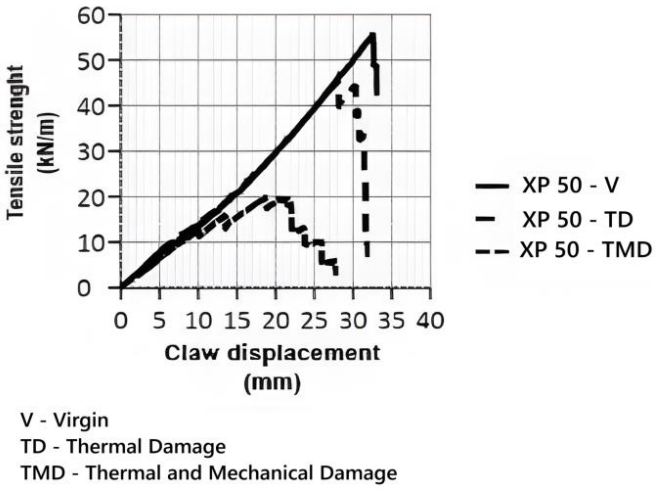


Fig. 4. Representative curves for GCO – XP50

4 Discussion

4.1 Comparison between situations

4.1.1 GCO – G50

According to Table 2, it is possible to conclude that mechanical damage had a strong influence on the loss of strength, as the sample subjected only to thermal damage showed a reduction of 19%. In turn, the sample that also suffered mechanical action showed a reduction of 82%.

Regarding the average grip displacement, in the case of thermal and mechanical damage, there was a reduction of 17% for both cases. For the samples with thermal damage, there was a reduction of 5%.

Concerning the slope, a trend of reduction can be observed, more pronounced for the situation of thermal and mechanical damage, with a decrease of 75%, while the reduction was 10% for the sample subjected to thermal damage.

Table 2. Variation GCO – G50

Type	Tensile strength (kN/m)	Claw displacement (mm)	β
TD	-19%	-5%	-10%
TMD	-82%	-17%	-75%

4.1.2 GCO – XP50

According to Table 3, it is possible to observe the influence of mechanical damage on the loss of tensile strength for GCO – XP50. For the sample exposed only to high working temperatures, there was a reduction of 12%. In turn, when the geocomposite was also subjected to compaction, there was a reduction of 63%.

The grip displacement results also follow this trend, as the sample that suffered thermal and mechanical action showed a reduction of 39%. Conversely, in the case of exposure only to thermal damage, the displacement reduction was 7%.

The average slope also showed a trend of reduction due to the applied damage. The greatest reduction was for the sample that suffered thermal and mechanical damage, with 23%. Conversely, the smallest reduction occurred for the sample exposed only to thermal damage, with 11%.

Table 3. Variation GCO – XP50

Type	Tensile strength (kN/m)	Claw displacement (mm)	β
TD	-12%	-7%	-11%
TMD	-63%	-39%	-23%

4.2 General comments

Regarding the virgin samples, both GCO-G50 and GCO-XP50 showed higher tensile strength than that presented by the manufacturer (50 kN/m), with increases of 4% and 6%, respectively. The most homogeneous material in terms of strength was GCO - XP50, due to its lower CV value.

In general, with the application of damage, there was a reduction in the tensile strength property and in the slope, used as an indicator of stiffness, which is in accordance with [11]. The cases with thermal and mechanical damage showed the highest reductions in tensile strength for both types of geosynthetics and the highest coefficient of variation values, as presented in [12].

When analyzing thermal damage, all parameters showed a reduction, with GCO-G50 being the material that presented the greatest reduction in tensile strength, which was 19%. However, the GCO-XP50 geosynthetic suffered the greatest reductions in grip displacement and slope, which were 7% and 11%, respectively.

In [12], for the analysis of the temperature effect alone, among the types of geocomposites used, the fiberglass one also showed the greatest reduction in tensile strength.

When analyzing the cases of thermal and mechanical damage, it is possible to observe the influence of compaction on installation damage, as the trend was a reduction in parameters and an increase in CVs when compared only to the thermal damage situation. In this situation, GCO-G50 showed the greatest changes in strength and slope, with reductions of 82% and 75%, respectively. For this geocomposite, high CV values can also be seen, the highest for all cases regarding tensile strength, 53%, and grip displacement, 43%. GCO - XP50 was the least susceptible to damage when analyzing tensile strength and slope, as it had the smallest reductions in these parameters, with tensile strength decreasing by 63% and slope by 24%.

The highest CV values are expected for the condition involving both thermal and mechanical degradation, as the compaction procedure may have been unevenly performed across parts of the sample. In the study by [11], the material that showed the greatest reduction in mechanical properties after being subjected to installation damage was reinforced with fiberglass. According to the author, this occurred due to the breakage of these fibers after the damage was applied.

Regarding the stiffness of the evaluated materials, it can be seen in Figure 5 that, regardless of the situation, GCO-G50 is the stiffest material and GCO-XP50 is the most extensible, as the latter showed greater variation in the grip displacement tests. It can also be observed, in all cases, a reduction in tensile strength and the corresponding grip displacement value when compaction damage is considered. Furthermore, both the fiberglass geosynthetic (GCO-G50) and the PVA geosynthetic (GCO-XP50) showed significant differences when comparing the situation with only thermal damage to that with both thermal and mechanical damage.

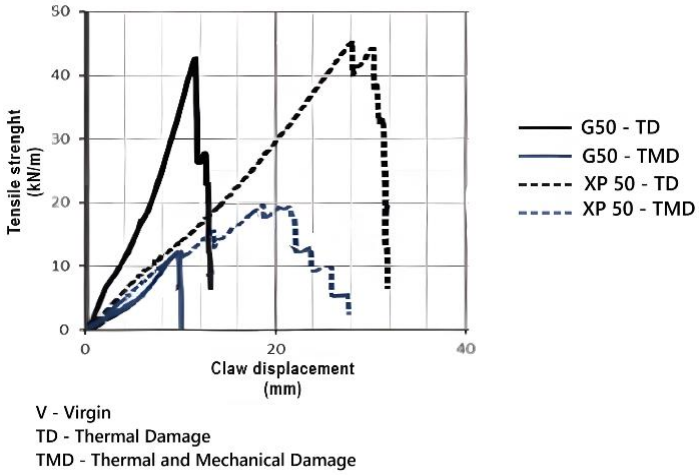


Fig. 5. TD and TMD curves for 50 kN/m geocomposites.

5 Conclusion

Geosynthetics used in pavement restoration are subjected to the high temperatures of asphalt concrete, averaging 150ºC, as well as the mechanical action of asphalt mixture compaction. To evaluate these damages, two distinct types of geocomposites were separated into two groups: the first group consisted of samples exposed to thermal damage, and the second group consisted of samples subjected to both thermal and mechanical damage. The damages were evaluated using parameters obtained from uniaxial tensile tests conducted according [10] for all samples. Based on the results, it was possible to conclude that:

• Both geosynthetics showed changes in their parameters and loss of strength for all damage situations;

• GCO-G50 exhibited the greatest changes in strength and slope, with reductions of 82% and 75%, respectively, for the thermal and mechanical damage situation;

• Compared to GCO-50, GCO-XP50 was less susceptible to degradation in both damage situations, but its grip displacement was approximately 160% greater in the first situation and about 103% greater in the second situation.

In conclusion, it is observed that both materials suffer a reduction in tensile strength values when subjected to thermal and mechanical conditions, causing significant deformations in the materials. Although the PVA geocomposite showed higher tensile strength values throughout the test, the fiberglass geocomposite exhibited lower average grip

displacements. It is important to note that greater displacement indicates greater deformation under load, which can compromise pavement stability. Therefore, this indicates that the fiberglass geocomposite has better retention of mechanical properties, making it more effective as a crack reflection barrier.

In summary, both geocomposites degrade under thermal and mechanical conditions, highlighting the need for careful implementation. Thus, the choice of the appropriate material to act as a crack reflection system should consider both tensile strength and grip displacement to ensure the longevity and efficiency of the pavement.

References

1. S. P. C. N. M. Moreira, *Efeitos da danificação mecânica de geossintéticos no comportamento como filtro em sistemas de cobertura de estruturas de confinamento de resíduos*, Master Thesis, University of Porto, Graduate Program in Environmental Engineering, 2009
2. R. Bandaru, Cost effective prevention of reflective cracking in composite pavements, Master Thesis, Federal University of Luisiana States, 2010
3. J. C. Vertematti, *Manual Brasileiro de Geossintéticos*, *(*Blucher, São Paulo, 2015)
4. N. Sudarsanan, S. R. Mohapatra, R. Karpurapu, V. Amirthalingam, Use of natural geotextiles to retard reflection cracking in highway pavements. J. Mat. Civ. Eng., **30**, 4, 2018. https://doi.org/10.1061/(ASCE)MT.1943-5533.0002195
5. J. W. Button, R. L. Lytton, Guidelines for Using Geosynthetics with Hot-Mix Asphalt Overlays to Reduce Reflective Cracking. J. Transp. Res. Rec.: J. Transp. Res. B., **2004**, 1, 2007. https://doi.org/10.3141/2004-12
6. M. Farzana, M. M. Haque,S. M. Sonali, M. Z. I. Mollah, M. A. Amin, Mohammad, S. A. Khan, F. Islam, R. A. Khan, Thermo-mechanical properties and applications of glass fiber reinforced polymer composites. J. MCMS, **5**, 3, 2023. DOI:10.33552/MCMS.2023.05.000614
7. A. C. Mesquita, *Estudo da polimerização do acetato de vinila utilizando a radiação ionizante*. OCLC 55921128, Master Thesis, Federal University of São Paulo, 2002
8. J. H Greenwood, H. F. Schroeder, W. Voskamp, Durability of Geosynthetic, (CRC Press, 2016)
9. J. Norambuena-Contreras, I. Gonzalez-Torre, D. Fernandez-Arnau, C. Lopez-Riveros, Mechanical damage evaluation of Geosynthetics fibers used as anti-reflective cracking systems in asphalt pavements. J. Constr. and Build. Mat., **109**, 7, 2016. https://doi.org/10.1016/j.conbuildmat.2016.01.057
10. ASTM D6637, Standard Test Method for Determining Tensile Properties of Geogrids by the Single or Multi-Rib Tensile Method, American Society for Testing and Materials, West Conshohocken, 6 p., 2015. DOI: 10.1520/D6637-11
11. I Gonzalez-Torre, M. A Calzada-Perez, A. Vega-zamanillo, D. Castro-Fresno, Damage evaluation during installation of geosynthetics used in asphalt pavements. J. Geosyn. Inter., **21**, 6 (2014). https://doi.org/10.1680/gein.14.00025
12. L. M. M Azevedo, *Instalação de geossintéticos em pavimentos flexíveis com CBUQ: danos de instalação*, Master Thesis, Federal University of Rio Grande do Norte, Graduate Program in Geotechnical Engineering, 2019

Evaluation of geotextile's stiffening function using accelerated pavement testing

Gino Sicha[1*]

[1]The University of Texas at Austin, Department of Civil Architectural and Environmental Engineering, 2515 Speedway, USA

Abstract. This study focuses on quantifying the potential benefits of using geotextiles to stiffen the base of flexible pavements and the mechanisms developed when placing them at the interface between a soft subgrade with high water content and a granular base. The analysis is based on experimental results of four identical pavements conducted using a one-third scale Model Mobile Load Simulator (MMLS3) device. The subgrade material used in this study consisted of a soil mixture containing 50% kaolin and 50% Monterey sand #30 and a base material corresponding to a uniform angular aggregate. A control pavement model was built and tested as an initial reference. The second pavement model involved using a non-woven geotextile to differentiate the benefit provided only by the geotextile's separation function. The third and fourth pavement models involved using woven geotextiles with different mechanical properties to quantify the benefit provided by the geotextile's stiffening function. The traffic benefit ratio (TBR) obtained showed an important increase in performance with the increase of geotextile's unconfined stiffness. The lateral restraint mechanism provided by the geotextile unconfined stiffness was correlated to the increase in TBR.

1 Introduction

This study aims to quantify the benefits of geotextiles' stiffening function when used for base stabilization applications in pavements constructed on soft subgrades. Additionally, this study intends to experimentally demonstrate the underlying mechanisms responsible for the observed pavement performance improvement theoretically discussed in [1]. Prior research has shown experimentally that geotextiles can serve various applications at the subgrade-base interface, including intermixing mitigation, base stabilization, and subgrade stabilization [2,3,4,5,6]. While field evaluations can assess overall pavement performance [7], they often struggle to isolate the individual benefits of these applications and the specific mechanisms at play. Conversely, smaller laboratory testing studies may not fully capture the complex effects of traffic loading conditions. To address these limitations, an accelerated pavement testing (APT) program was conducted using reduced-scale pavement models under controlled environmental conditions. The key performance indicators, such as surface rutting, as well as directly measuring parameters like horizontal base particle displacements, and vertical stress distributions were measured.

* Corresponding author: gino.sicha@utexas.edu

The APT data presented compares four pavement models including a control non-stabilized model, a model using a low stiffness geotextile for separation, and two geotextile-stabilized models with different geotextile's tensile properties. By employing advanced instrumentation and measurement techniques, this study intends to comprehensively capture the relevant performance improvements and base stabilization mechanisms provided by the geotextiles, going beyond the limitations of typical field or standalone smaller scale laboratory evaluations.

2 Materials and methods

2.1 Pavement models

Four pavement models were tested, each incorporating a 140mm water table in the subgrade. The models were constructed with three distinct layers: a 152.4mm clay subgrade, 127mm gravel base, and 25.4mm hot mix asphalt layer. Each pavement model's dimensions were 1829mm in length, 1219mm in width, and 305mm in height. While one section served as a control without any geotextile, the other three sections featured geotextiles of varying stiffness placed between the base and subgrade layers.

A custom hydraulic system was engineered to establish and maintain the water table in the subgrade. This setup included an external reservoir linked to the pavement frame, a valve for water level control and a flow meter for water volume measurement. The frame featured a waterproof liner and incorporated a drainage layer consisting of a geonet sandwiched between two geotextiles to maintain consistent water flow during the flooding process.

Testing utilized a scaled-down mobile load simulator (MMLS3), which operated with four small wheels at one-third the size of standard truck tires. These wheels moved in a single direction with 620 kPa of pressure at a rate of two cycles per second.

2.2 Material characterization

The subgrade consisted of a mix of kaolin and Monterey sand #30 (50% in weight of each). The maximum dry unit weight of the subgrade mixture corresponded to 1.8 g/cm3 at 16% optimum moisture content. The kaolin had a liquid limit of 50, plastic limit of 30, and plasticity index of 20. An angular uniform aggregate was used as the base material. The asphalt layer consisted of a thin overlay mixture class A. The binder was classified as PG 76-22. The asphalt mix had a maximum specific gravity of 2.394 and was compacted to achieve 6.8% air voids. As for the geotextiles used, model 2 incorporated a thin non-woven polypropylene geotextile and models 3 and 4 used woven polypropylene geotextiles with different stiffness. Unconfined tensile testing of the geotextiles showed stiffness values at 5% elongation of 45 kN/m, 579 kN/m, and 809 kN/m for the geotextiles used in models 2, 3, and 4 respectively.

2.3 Instrumentation

Surface rutting measurements were taken using a profilometer to evaluate the impact of MMLS3 dynamic loading. Additionally, various monitoring devices were embedded during construction to track the pavement models' performance. These included moisture sensors, earth pressure cells and base artificial particles. The stress distribution from traffic loading was monitored using six earth pressure cells positioned at depths of 63.5mm and 152.4mm below the surface, placed at varying distances from the wheel path. Base layer particle movement was tracked using linear potentiometers connected to "tell-tales" attached to custom-made markers consisting of nuts and bolts installed at different heights within the

base layer. A more extended description of the material characterization and instrumentation is presented in [8].

3 Results and Discussion

3.1 Quantification of pavement performance

The pavement improvement was quantified using the traffic benefit ratio (TBR), which compares the number of load cycles needed to reach a specific rutting levels between an improved pavement using geotextiles and a control pavement [9]. Fig. **1** presents the TBR results for three test sections compared to the control section: pavement model 2 (with a low-stiffness geotextile) and pavement models 3 and 4 (with stabilizing geotextiles). The data demonstrates that geotextile benefits increased with greater surface rutting. At 12.7mm of rutting, the TBR values showed significant variations among the models. Pavement model 2 required twice as many loading cycles compared to the control, while model 3 needed 11 times more cycles, and model 4 demonstrated the highest performance with 27 times more cycles than the control section. While Model 2's geotextile was intended to only prevent layer mixing, Models 3 and 4's geotextiles provided additional base and subgrade stabilization. When isolating these stabilization benefits at 12.7mm rutting depth, the performance improvements were substantial. Model 3 showed 5.5 times better performance than separation alone, while Model 4 demonstrated even greater improvement at 13.5 times better than separation alone.

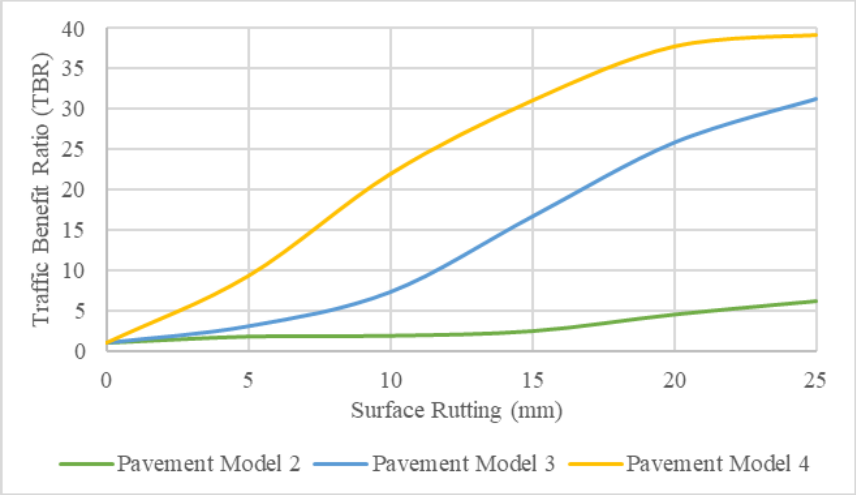


Fig. 1. Traffic benefit ratio for different levels of rutting.

3.2 Lateral restraint mechanism

This analysis focused on understanding how high-stiffness geotextiles stabilize the base layer by examining changes in lateral particle movement during traffic loading. This analysis utilized data from artificial particles positioned at various depths and distances from the wheel path within the base layer. Fig. **2** illustrates the base lateral displacement patterns across the four pavement models evaluated after approximately 1000 loading cycles. The figure presents the transverse distance from wheel path to pavement edge on the x-axis and the depth on the y-axis. In pavement models without stabilization (PM1 and PM2), significant

horizontal displacement occurred, decreasing as depth and distance from the wheel path increased. Notable displacement near the subgrade-base interface indicated unrestricted lateral movement of base particles in these models. In contrast, the geotextile-stabilized models (PM3 and PM4) demonstrated markedly reduced horizontal displacement. The lower half of the base layer showed minimal lateral displacement, suggesting a redistribution of lateral particle flow. This reduction in particle movement near the geotextile can be attributed to two factors: the interaction between angular base particles and the geotextile, and the geotextile's inherent stiffness. The data suggests that the resulting geotextile-base composite structure exhibited higher stiffness near the geotextile, effectively limiting lateral particle movement. However, the geotextile-stabilized models showed higher displacements in the upper half of the base layer. This suggests that the effect of geotextiles in mitigating lateral displacement of unbound aggregates reduces with distance. The combination of concentrated stresses in the upper base region and the diminished geotextile effect likely caused increased lateral particle flow in this area. Furthermore, comparison between the stabilized models revealed that pavement model 4, which used a stiffer geotextile than model 3, exhibited lower horizontal displacements. This observation suggests that increased geotextile stiffness enhances the lateral restraint mechanism for unbound base particles reducing the base modulus degradation with the increase of loading cycles.

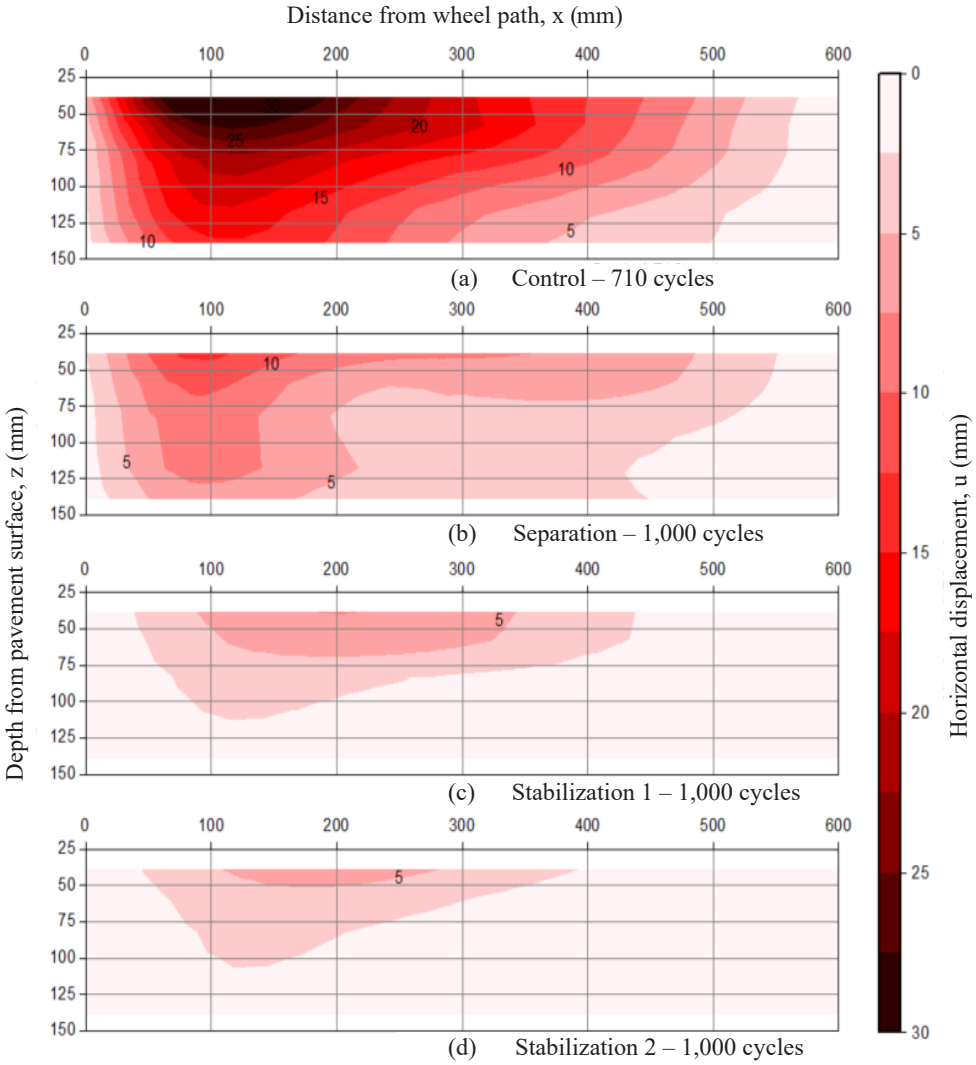


Fig. 2. Horizontal displacements contours after 1000 cycles or end of testing: (a) Pavement model 1;(b) Pavement model 2; (c) Pavement model 3; (d) Pavement model 4 [10].

3.3 Geotextile-aggregate composite stiffness

The aggregate-geotextile composite stiffness is considered a key property to characterize the lateral restraint mechanism for base stabilization. When using geotextile, two main parameters have been identified as important contributors to the composite stiffness including the geotextile's confined stiffness and the geosynthetic-aggregate interface shear [11]. In this analysis the geosynthetic-aggregate interface shear was assumed almost identical when using GT3 and GT4 as they correspond to the same family of products and the base aggregate was not modified between pavements. On the other hand, the unconfined stiffness was used for this evaluation since it can be correlated to the confined stiffness of the geotextile, and it is a property of the geotextile much simpler to quantify. Thus, the TBR and the geotextile unconfined stiffness was evaluated in Fig.3. The x-axis corresponds to the unconfined stiffness of the geotextile at 5% of strain and the y-axis corresponds to the TBR up to 15 mm of surface rutting. The data shows little contribution of the low stiffness geotextile (GT1) to

stiffening of the base layer of pavement model 2. However, GT2 and GT3 show an important contribution in the TBR improvement with increase of surface rutting. Additionally, the increase of geotextile's unconfined stiffness showed higher impact in the TBR suggesting a strong correlation between these two parameters.

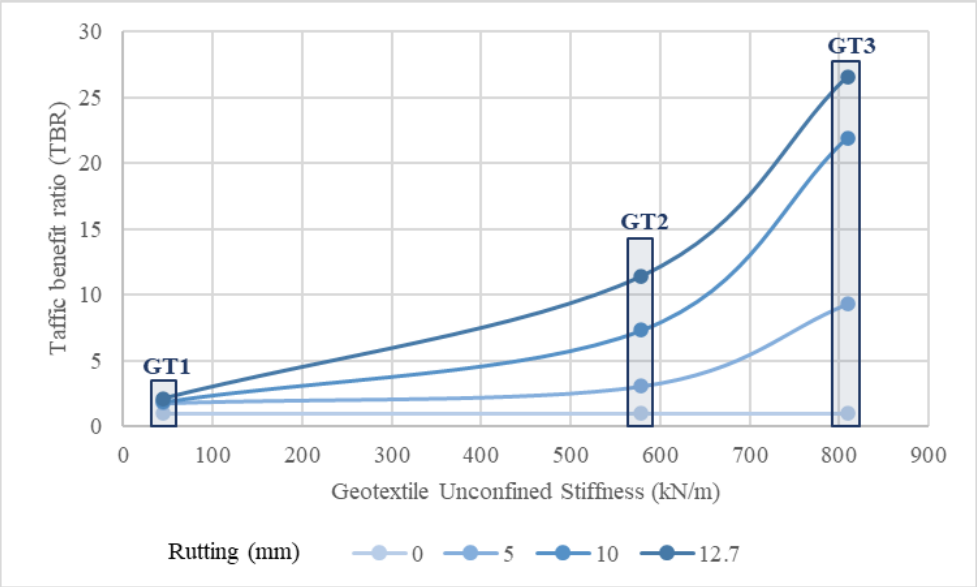


Fig. 3. Correlation between TBR and Geotextiles Unconfined Stiffness.

3.4 Vertical stress variation

Vertical stresses were measured using earth pressure cells (EPCs) installed at two depths: 63.5mm within the base layer, and 152.4mm at the subgrade-base interface, all located directly under the wheel path. Fig.4 shows the data collected from the sensors. The x-axis and y-axis correspond to the number of cycles and vertical stresses respectively. The data shows that at the start of testing (N=1 cycles), the initial stresses induced were similar across all pavement models, regardless of the geotextile used suggesting that geotextiles had minimal impact on the initial stress distribution. However, the rate of stress increase under the wheel path differed between non-stabilized and geotextile-stabilized models as loading continued. The geotextile-stabilized models (PM3 and PM4) experienced a slower rate of stress increase compared to the non-stabilized ones (PM1 and PM2). The reduced stress concentration in the geotextile-stabilized models can be attributed to the lateral restraint mechanism provided by the geotextiles (GT2 and GT3) helping to mitigate the degradation of the base layer's modulus over loading cycles. It is important to point out that some strain was required to mobilize the geotextiles as discussed in Giroud & Han (2004) to develop the mechanisms providing base stabilization of the pavements.

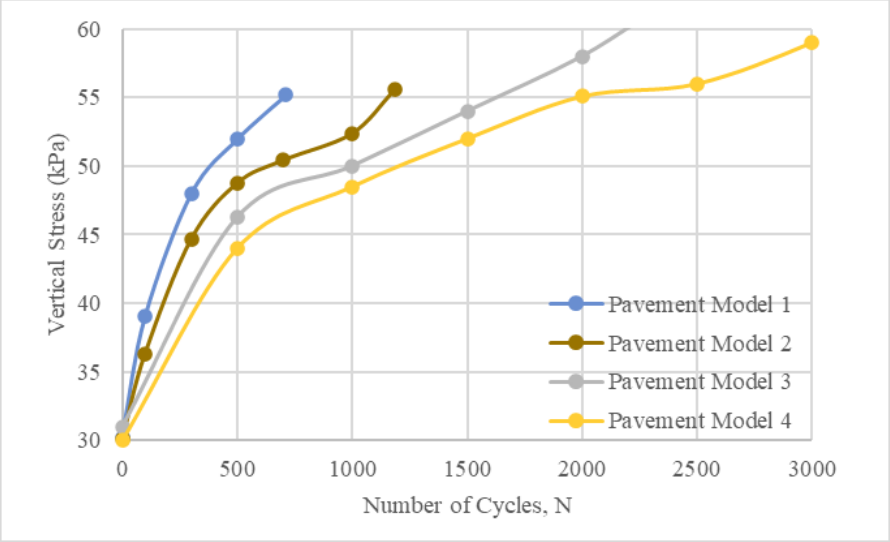


Fig.4. Vertical stresses under the wheel path at 63.5mm from the surface for different loading cycles of the four pavement models evaluated.

4 Conclusion

This study used accelerated pavement tests (APTs) to evaluate the mechanisms involved in stabilizing unbound aggregate base layers in flexible pavements by placing higher-stiffness geotextiles at the subgrade-base interface. Two non-stabilized pavement models were tested including a control model and one with a lower-stiffness separation geotextile. Two additional models incorporated geotextiles for base stabilization. The performance and mechanisms of the models were monitored by measuring surface rutting, horizontal base particle displacements, vertical stresses. The key findings of this study were:

- The geotextile-stabilized models (PM3 and PM4) showed significantly lower surface rutting compared to the non-stabilized models, quantified by Traffic Benefit Ratios (TBRs) of 11 and 27 respectively at 12.7mm rutting, versus only 2 for PM2 using a geotextile for separation only.
- The geotextile-stabilized models exhibited lateral restraint mechanism of base particles near the geotextile interface. The development of this mechanism was linked to reduction of the rate of stress concentration under the wheel path reducing the base modulus degradation over cycles.
- The geotextiles did not show initially an impact stress distribution; however, their base stabilization benefits developed over time as loading progressed. Higher geotextile stiffness seemed to improve the geotextile-aggregate composite stiffness, enhancing lateral restraint and pavement service life.

Acknowledgments

The author gratefully acknowledged the financial support provided by Solmax to this study.

References

1. J. Zornberg, Functions and Applications of Geosynthetics In Roadways. Procedia Engineering, 189, 298–306 (2017).
   https://doi.org/10.1016/j.proeng.2017.05.048
2. E. Cuelho, S. Perkins, Morris, Relative Operational Performance of Geosynthetics used as Subgrade Stabilization. Western Transportation Institute (2014).
3. M. Abu-Farsakh, S. Hanandeh, L. Mohammad, Q. Chen, Performance of geosynthetic reinforced/stabilized paved roads built over soft soil under cyclic plate loads. Geotextiles and Geomembranes, 44, 6, 845–853, (2016).
   https://doi.org/10.1016/j.geotexmem.2016.06.009
4. B. Kermani, S. Stoffels, M. Xiao, Evaluation of effectiveness of geotextile in reducing subgrade migration in rigid pavement. Geosynthetics International, 27, 1, 97–109 (2020).
   https://doi.org/10.1680/jgein.19.00052
5. X. Sun, J. Han, J. Fei, J. Guo, W. Zhang. Geosynthetic-stabilized flexible pavements: Solution derivation and mechanistic-empirical analysis. Geotextiles and Geomembranes, 48, 4, 468–478 (2020).
   https://doi.org/10.1016/j.geotexmem.2020.02.005
6. M. Singh, A.Trivedi, S. Shukla, Evaluation of geosynthetic reinforcement in unpaved road using moving wheel load test. Geotextiles and Geomembranes, 50,4, 581–589 (2022).
   https://doi.org/10.1016/j.geotexmem.2022.02.005
7. E. Hoppe, M. Hossain, A. Moruza, C. Weaver, Use of geosynthetics for separation and stabilization in low-volume roadways (FHWA/VTRC 20-R8). Virginia Center for Transportation Innovation and Research. (2019).
   https://www.virginiadot.org/vtrc/main/online_reports/pdf/20-r8
8. G. Sicha, Evaluation of separation function with geotextiles using accelerated pavement testing conditions, Master Thesis, The University of Texas at Austin, Department of Civil Architectural and Environmental Engineering (2021).
9. AASHTO. R 50-09 Standard Practice for Geosynthetic Reinforcement of the Aggregate Base Course of Flexible Pavement Structures (2009).
10. G. Sicha, Evaluation of pavement performance improvement with geotextiles using accelerated pavement testing, PhD Thesis, The University of Texas at Austin, Department of Civil Architectural and Environmental Engineering (2024).
11. J. Zornberg, G. Roodi, R. Gupta, Stiffness of Soil–Geosynthetic Composite under Small Displacements: I. Model Development. Journal of Geotechnical and Geoenvironmental Engineering, 143,10 (2017).
    https://doi.org/10.1061/(ASCE)GT.1943-5606.0001768

Instrumentation of geogrids using novel non-invasive electrical sensing

Trigg Sharp[1][1], *Christos* Mias[1], *Kasia* Zamara[2] and *Gary* Fowmes[1]
[1]School of Engineering, University of Warwick, Library Road, Coventry, CV4 7AL, UK
[2]Tensar International, Sett End Rd W, Blackburn BB1 2PU, UK

Abstract. Accurate strain measurement of geogrids has been challenged by several factors, many of which are due to the unfavourable environmental conditions which geosynthetics are subject to. Existing contributions have seen deployment of standard strain measurement techniques including piezoresistive and fibre-optic sensors. These have faced limitations with poor survivability, low accuracy, and changes to the physical geogrid structure which subsequently alter geogrid behaviour. This report presents a novel, non-invasive, electrical sensor designed for use on geosynthetics specifically. A direct shear apparatus (DSA) was used to apply confining pressure up to 300kPa and strain up to 9.0% to the sensor-enabled geogrids in both dry and wet soil conditions to assess the performance of the novel sensor. Signal phase angle was measured at a range of frequencies at 1mm DSA intervals. Geogrid strain was derived from DSA displacement and a linear response between phase angle and strain has been observed. The findings of this study indicate that the sensor is sensitive to strain and resistant to adverse environmental conditions without modification to the geogrid structure. This is significant as it means that the sensor can be used for instrumentation in field-based applications, particularly where the geogrid is used for soil stabilisation.

Full paper to be published in:
https://www.e3s-conferences.org/articles/e3sconf/abs/2025/44/contents/contents.html

1 Corresponding author: Trigg.Sharp@warwick.ac.uk

SESSION 4 B
TESTING, QUALITY (4)

Geosynthetic Clay Liners, why hydraulic conductivity (k-value) is the wrong value for a tender

Henning Ehrenberg[1*] and *Christian* Niehues[1]

[1]Naue GmbH & Co. KG, 32339 Espelkamp, Germany

Abstract. Today, geosynthetic clay liners (GCL or GBR-C) are used in many applications as an alternative to compacted clay liners (CCL), as they offer considerable ecological advantages and protect the natural clay resource. Tenders/specifications for geosynthetic clay liners mainly contain requirements for hydraulic conductivity (k-value). This value alone leads the customer / user in the wrong direction when selecting the product to be used. This value alone does not provide any information about the flow rate through the sealing layer, as this can only be correctly determined together with the thickness (indirectly the mass) of the sealing layer. However, determining the thickness is also subject to errors. Alternatively, the permittivity or the index flux can be evaluated and shall be used in specifications. The paper shows the influence of the mass/thickness on the results and the real flow rate, also in comparison to other sealing elements such as clay.

1 Introduction

Geosynthetic clay liners (GCL), also known as clay geosynthetic barriers (GBR-C) are used in many applications as an alternative to compacted clay liners (CCL), as they offer considerable ecological advantages and protect the natural clay resource. Specifications for geosynthetic clay liners mainly contain requirements for hydraulic conductivity (k-value). This value alone leads the customer / user in the wrong direction when selecting the product to be used. This value alone does not provide any information about the flow rate through the sealing layer, as this can only be correctly determined together with the thickness (indirectly the mass) of the sealing layer. Alternatively, the permittivity or the index flux can be evaluated and shall be used in specifications.

Fig. 1. shows the basic principle curve of hydraulic conductivity (k-value), permittivity and index flux as a function of mass per unit area.

This paper shows the influence of the mass per unit area of the bentonite on the results also in comparison to other sealing elements such as clay.

* Corresponding author: hehrenberg@naue.com

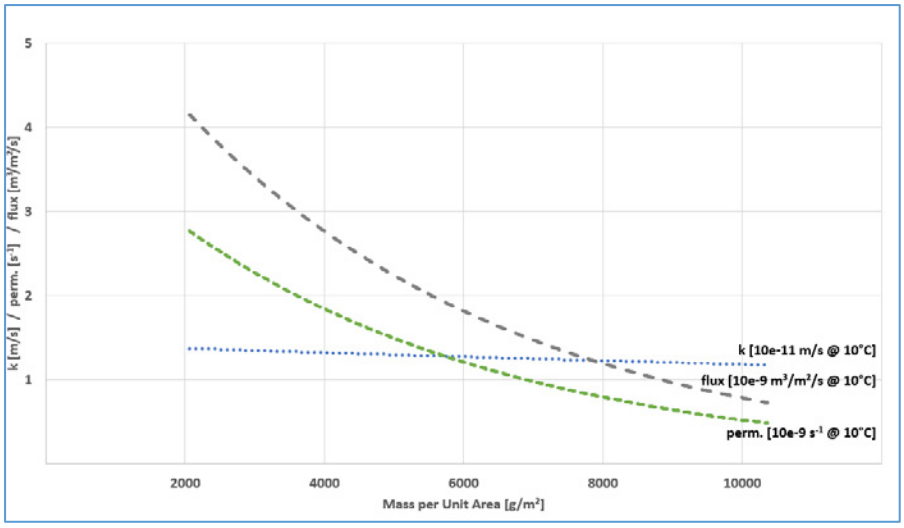


Fig. 1: Principle curve of k-value, permittivity and flux as a function of bentonite

2 Index flux measurement following ASTM D5887 and EN 16416

In ASTM D5887 (Standard Test Method for Measurement of Index Flux Through Saturated Geosynthetic Clay Liner Specimens Using a Flexible Wall Permeameter) [1] and in EN 16416 (Geosynthetic clay barriers – Determination of water flux index – Flexible wall permeameter method at constant head) [2] equations are given to calculate from the measured flow-through volumes in the test (the test method itself is nearly identical following ASTM D5887 and EN 16416) hydraulic properties.

It should be noted that the flux in ASTM D5887 and EN 16416 ensures that products can be directly compared under the same test conditions.

2.1 Index flux measurement following ASTM D5887

Chapter 10 of ASTM D5887 shows the calculation of the flux, q_i as follows:

$$q_i = (Q) / (At) \qquad (1)$$

where:
q_i = flux, (m³/m²)/s,
Q = quantity of flow, taken as the average of inflow and outflow, m³,
A = cross-sectional area of nominal 100 mm diameter porous end piece, 0.00785 m², and
t = interval of time, s, over which the flow occurs.

Annex X2 of ASTM D5887 gives the calculation of the hydraulic conductivity based on Flux test data and for constant head:

$$k_T = (QT) / (Ath) \qquad (2)$$

where:
k_T = hydraulic conductivity (at measured temperature), m/s,
Q = quantity of flow, taken as the average of inflow and outflow, m³,
T = thickness of specimen (clay part), m,
A = cross-sectional area of clay component, m²,
t = interval of time, s, over which the flow Q occurs, s,
h = difference in hydraulic head across the specimen, m, of water.
The temperature range during the test shall be 21°C +/- 2°C)

The measurement of the thickness of "the clay" of a GCL specimen shall be measured and measurements must be completed within 10 min after dismounting the test specimen. The dismounted test specimen is cut across its diameter. First, utilizing a sharp razor knife, the upper geotextile backing is cut. Next, the clay portion of the GCL is cut with the razor knife. Finally, the cut area is carefully folded back and the lower geotextile backing is cut with a pair of scissors. The cut geotextile backing can be gently peeled away from the clay portion using the blade of the razor knife until the clay portion is clearly defined. The thickness of the exposed clay portion is directly measured (per test methods D374/D374M) at three different locations along the cut diameter (d) using calibrated calipers or similar devices capable of measuring to the nearest 0.3 mm [0.01 in.] or better. Fig. 2 give recommended locations for measuring clay thickness.

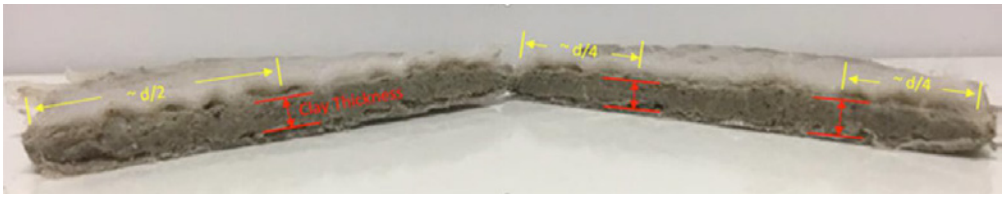


Fig. 2: example from ASTM D5887 where/how to measure the clay thickness, with d as the sample diameter

2.2 Water flux index measurement following EN 16416

Chapter 8 of EN 16416 shows the calculation of the flux, q_i as follows:

$$q_i = (V) / (At) \qquad (3)$$

where:
q_i = flux, (m³/(m² s)) at test temperature,
V = quantity of flow, taken as the average of inflow and outflow, in m³,
A = cross-sectional area of nominal 100 mm diameter porous end piece, in m²,
t = interval of time over which the flow occurs, in s,

The flux value q_{10} shall be reported in m³/(m² s) after being corrected to the flux at 10 °C by using RT_{10} (RT_{10} is the ratio of viscosity of water at test temperature to the viscosity of water at 10 °C).

Annex A of EN 16416 gives the calculation hydraulic conductivity at the test temperature, k_T as follows:

$$k_T = q_i / i \qquad (4)$$

where:
k_T = hydraulic conductivity at the test temperature in m/s
q_i = flux, (m³/(m² s)) at test temperature,
i = hydraulic gradient in the test

The hydraulic gradient i can be calculated according to:

$$i = \Delta H / d \qquad (5)$$

where:
ΔH = head loss across the specimen, in m
d = thickness of the specimen, in m

The thickness (d) should be measured immediately at the end of the test using the apparatus and following the procedure of EN ISO 9863-1 at 35 kPa using a loading plate of an area of 25 cm².

The hydraulic conductivity k_{10} should be reported in m/s after being corrected to the hydraulic conductivity at 10 °C by using RT_{10} (RT_{10} is the ratio of viscosity of water at test temperature to the viscosity of water at 10 °C).

Annex A of EN 16416 also gives calculation of the permittivity at the test temperature (Ψ_T) in 1/s and Ψ_T can be calculated:

$$\psi_T = q_i / \Delta H \qquad (6)$$

where:
ψ_T = permittivity at the test temperature in 1/s or s^{-1}
q_i = flux, in m³/(m² s) at test temperature,
ΔH = head loss across the specimen, in m

The permittivity Ψ_{10} should be reported in m/s after being corrected to the permittivity at 10 °C by using RT_{10} (RT_{10} is the ratio of viscosity of water at test temperature to the viscosity of water at 10 °C).

2.3 Summary of ASTM D5887 and EN 16416

Both methods (ASTM D5887 and EN 16416) give as the main value to evaluate the flux in m³/m² s under a water head of 1.5m. The results of both methods can be compared with each other, however, the temperature differences in each test method (ASTM D5887 (21° +/-2°C) vs. EN 16416 (reported at 10°C) must be taken into account. At the same temperature, the same flux values should be obtained.

Both standards give further procedures how to calculate hydraulic conductivity based on the flux values in the appendix, resp. annex. However, the evaluation of the GCL thickness is described differently.

In ASTM D5887 a way is described to measure the thickness of the clay portion on its own. However, the accuracy and reproducibility of the method is questionable. The sample preparation of the cut edges and the definition of the measuring points are prone to errors.

In EN 16416 a way is described to measure the thickness of the entire GCL. As a result, a higher thickness gives a higher hydraulic conductivity (more permeable). The thickness measurement here includes the geotextile part of the GCL, which can be a non-woven fabric on one side and a woven fabric on the other, but sometimes also non-woven fabrics on both sides or a non-woven fabric on one side and a non-woven fabric/woven fabric combination on the other.

Assuming that a GCL always has the same amount and type of bentonite, but has different total thicknesses due to the textile structure around it, a higher hydraulic conductivity (more permeable) is calculated as the thickness increases, although the permittivity and flux remain the same. This clearly shows the negative influence of increasing thickness on the result, as the thickness comes from structures that do not influence the permeability of the GCL.

EN 16416 also provides the option of determining the permittivity. The permittivity results from the flux in relation to the water head (here in both cases, ASTM and EN) 1.50 m water head. The determination of the thickness plays no role in the permittivity. Permittivity is the base value for calculating flux with different (other than 1.5 m) water heads.

3 Bentonite mass per unit area, k-value, permittivity and flux

Although ASTM D5887 and EN 16416 already specify the meaningful properties in the main part of the standard, flux, the wide-ranging k-value is still required in specifications. Often the k-value is specified, however as described earlier the much more important and clearer value is flux and should be specified.

As already shown in Fig. 1 based on the evaluation of more than 1000 single tests, the mass per unit area of the bentonite has a significant influence on the flux or permittivity, while the k-value remains more or less the same even with increasing bentonite mass per unit area.

In [3] first results and background about the impact of mass per unit area of bentonite onto the lab results as well as on the behaviour on site are presented. This paper shows the tendency of the decreased flux or permittivity with increased mass, also on long-term values. The following Fig. 3 gives a bit more details of such this evaluation, but now with a much higher number of tests. The increase in mass per unit area from 3,000 g/m² bentonite to 6,000 g/m² results in roughly a 50% reduction of the flux value from roughly 3.3 x 10^{-9} m³/m² s to roughly 1.7 x 10^{-9} m³/m² s. The k-value, on the other hand, remains the same over the same range of evaluated mass per unit areas.

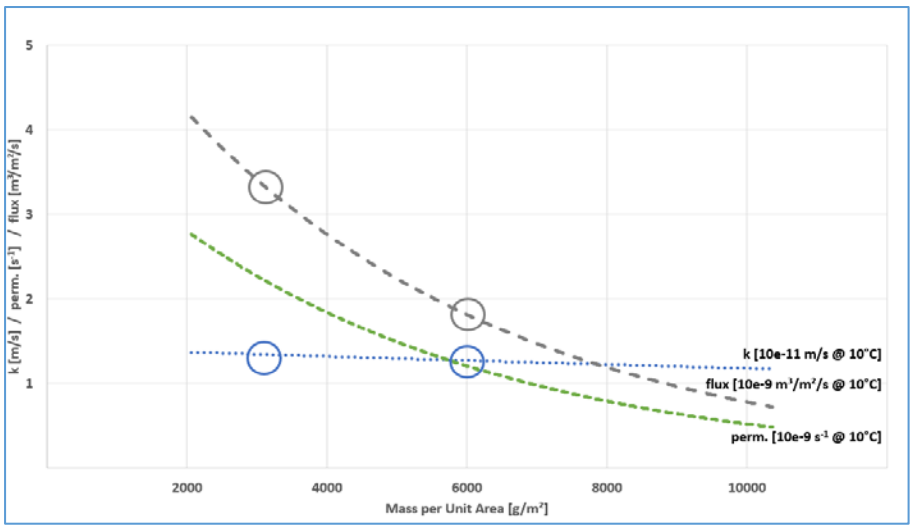


Fig. 3: Principle curve of k-value, permittivity and flux as a function of bentonite mass, highlighted for roughly 3,000 g/m² and roughly 6,000 g/m² bentonite

This example illustrates why the k-value should not be part of a specification, or rather should not be a criterion without the corresponding permittivity or index flux. K-value alone leads the user of GCL in a completely wrong direction and promotes that the mass does not actually play a role, as the k-value is always the same.

The permittivity can be used as an alternative; this is also independent of the thickness and can also be determined from the flux. The flux gives a true volume under the water head of 1.5 m. The permittivity can be used to determine a volume in relation to other water heads.

Flux (or permittivity), one of these, are the main values to use in a specification. They show the values that shall be really of interest for the designer and they also qualify indirectly the amount of bentonite to be used. These results show that a higher bentonite mass per unit area has a significant positive influence on the hydraulic properties.

It should also be noted that the above-mentioned values are short-term permeability values.

The below presented Fig. 4, summarized from a paper presented at the 10th IGS in Berlin [4] shows the decrease of long-term permittivity from roughly 1.5 x 10^{-8} 1/s to roughly 1.0 x 10^{-8} 1/s to roughly 0.6 x 10^{-8} 1/s with the increasing of bentonite amount from roughly 4000 g/m² bentonite to 7000 g/m² bentonite. The dashed blue line in the 2 graphs of Fig. 4 is intended to illustrate the jump in long-term permittivity with increasing bentonite mass. These evaluations were done for the certification process for GCLs in German landfill caps for a durability of > 100 years.

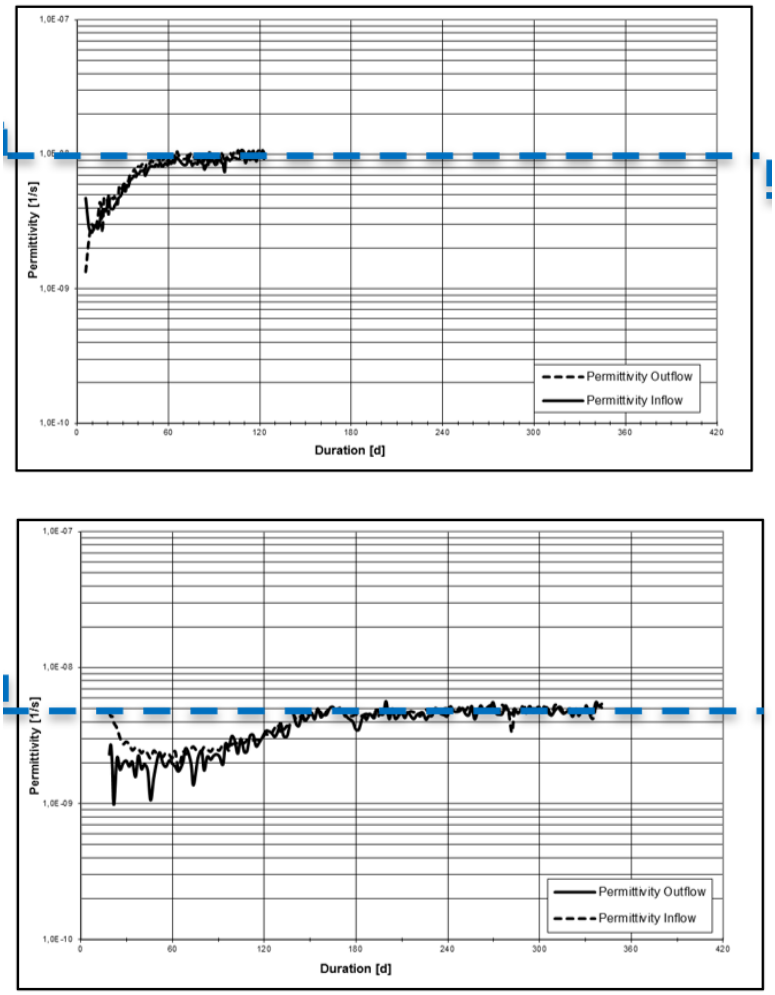


Fig. 4: Principle curve permittivity as a function of bentonite mass per unit area, highlighted for approx. 4,000 g/m² (upper part) to 7,000 g/m² (lower part) bentonite

These results show that a higher bentonite mass has a positive influence (depending on mass difference) on the short-term hydraulic properties (see Fig. 3), but also on the long-term hydraulic properties (see Fig. 4).

4 Bentonite mass per unit area, k-value, permittivity and flux in practice

In the following a practical example is being used for the demonstration of a basic performance calculation. The example is a water pond with a constant water head over the GCL of 1.5 m and compares the water loss per day for a sealed area of one hectare (10,000 m²) on the basis of the results from Fig. 3.

The calculation can be done based on flux:

$$Q = q_{10} \, x \, A \, x \, t \qquad (7)$$

Q = quantity of flow in volume/area/time,
q_{10} = flux, (m³/(m² s)) at 10°C und a given water head of 1.5 m,
A = area, in m²,
t = interval of time over which the flow occurs, in s,

Bentonite mass roughly 3000 g/m²:
Q = 3,3 x 10^{-9} m³/m² s x 10.000m² x 86400 s = 2.26 m³/ha/day

Bentonite mass roughly 6000 g/m²:
Q = 1,7 x 10^{-9} m³/m² s x 10.000m² x 86400 s = 1.16 m³/ha/day

The calculation can also be done based on permittivity:

$$Q = \Psi_{10} \, x \, \Delta H \, x \, A \, x \, t \qquad (8)$$

Q = quantity of flow in volume/are/time,
Ψ_{10} = flux, (m³/(m² s)) at 10°C und a given water head of 1.5 m,
ΔH = water head above the sealing, in m
A = area, in m²,
t = interval of time over which the flow occurs, in s,

Bentonite mass roughly 3000 g/m²:
Q = 2,2 x 10^{-9} s^{-1} x 1.5 m x 10.000m² x 86400 s = 2.26 m³/ha/day

Bentonite mass roughly 6000 g/m²:
Q = 1,13 x 10^{-9} s^{-1} x 1.5 m x 10.000m² x 86400 s = 1.16 m³/ha/day

Permittivity and equation 8 can be used also to calculate for e.g. the water flow through a sealing element in a capping of a landfill, assume again 10,000m² = 1 ha, but with a drainage gravel in 30 cm thickness and depending to that drainage element a water head of 30 cm above the sealing element:

Bentonite mass roughly 3000 g/m²:
Q = 2,2 x 10^{-9} s^{-1} x 0.3 m x 10.000m² x 86400 s = 0.45 m³/ha/day

Bentonite mass roughly 6000 g/m²:
Q = 1,13 x 10^{-9} s^{-1} x 0.3 m x 10.000m² x 86400 s = 0.23 m³/ha/day

Finally the permittivity and equation 8 can be used also to calculate for e.g. the water flow through a sealing element in a capping of a landfill, assume again 10,000m² = 1 ha, but with a geosynthetic drain (GCO) with 1 cm thickness and depending to that drainage element a water head of 1 cm above the sealing element:

Bentonite mass roughly 3000 g/m²:
Q = 2,2 x 10^{-9} s^{-1} x 0.01 m x 10.000m² x 86400 s = 0.015 m³/ha/day

Bentonite mass roughly 6000 g/m²:
Q = 1,13 x 10^{-9} s^{-1} x 0.01 m x 10.000m² x 86400 s = 0.007 m³/ha/day

These examples show the influence of the mass of the bentonite on the real flow through a seal when considering practical surfaces. The influence does not become clear in the singular consideration of the k-value, it becomes clear in the consideration of permittivity and/or flux and even more so in the calculation of the water losses / seepage of sealed surfaces.

These examples also show the influence of the water head and in case of the two examples for a landfill cap it shows clearly the influence of the system that was build – a GCL with drainage gravel or a GCL with a geosynthetic drainage composite – which show also clearly the influence of the whole system build.

Further examples of these calculations are given in [3], here using k-value as a basis for comparing GCL and CCL. It should be noted that if GCL is calculated based on k-value, the same thickness must be used in the calculation of Q (with whatever error this was determined, see section 2.3) as was used in the determination of the k-value.

5 Summary

The examples shown above clearly demonstrate the influence of increasing mass on the performance as a sealing element of GCLs. Furthermore, it is shown that hydraulic conductivity (k-value) as the sole value of hydraulic performance in a specification is in no way sufficient. At least the flux or the permittivity must be required.

The performance of the sealing element can be significantly increased by the choice of the surrounding layers, which was demonstrated with the GCL/GCO system.

References

1. D5887/D5887M – 23, Standard Test Method for Measurement of Index Flux Through Saturated Geosynthetic Clay Liner Specimens Using a Flexible Wall Permeameter, ASTM (2023)
2. EN 16416:2023, Geosynthetic clay barriers – Determination of water flux index – Flexible wall permeameter method at constant head, CEN (2023)
3. K. von Maubeuge, Bentonite Mass Per Unit Area Requirements for Geosynthetic Clay Liners (GCLs) and Related Topics for Multi-Component GCLs, Geosynthetics Conference, Portland (2015)
4. H. Ehrenberg, K. von Maubeuge, T. Egloffstein, Investigations on the Influence of Different Calcium Concentrations on the Permittivity of GCLs, 10th ICG Berlin. (2014)

Parameters affecting the vertical deformations of GCLs during hydraulic conductivity tests

Nilhan Demirci[1], *Tuğçe* Özdamar Kul[2], and *Ali Hakan* Ören[3*]

[1]Graduate School of Natural and Applied Science, Dokuz Eylul University, Izmir, Turkiye
[2]Department of Civil Engineering, Dokuz Eylul University, Izmir, Turkiye
[3]Department of Civil Engineering, Dokuz Eylul University, Izmir, Turkiye

Abstract. The hydraulic conductivity and swelling behaviours of geosynthetic clay liners (GCLs) are closely related to each other. An alternative system was developed to measure the swelling or compression (vertical deformation) behaviour of GCLs during permeability tests by simply modifying flexible wall permeameters. In this system, the cell part of the flexible wall permeameter was removed, thereby allowing the application of vertical stress on the specimen to be provided by a simple frame system. The vertical deformations were determined using dial gauges, which were placed on the frame. In this study, vertical deformation and hydraulic conductivity were examined depending on the concentration of test liquid, mass per unit area (MPUA) of GCL, and vertical stress. GCLs within 3.0-5.5 kg/m^2 MPUA were subjected to hydraulic conductivity tests under two different vertical stresses and with various $CaCl_2$ solutions. The results showed that the hydraulic conductivity increased, and the pattern of vertical deformations remarkably changed when the concentration of permeant increased. Furthermore, reducing the vertical stress applied on GCLs resulted in an increase in vertical swelling; however, there was no definite relationship between hydraulic conductivity and effective stress. Similarly, reducing the MPUA of GCLs decreased the vertical swelling, but increased the hydraulic conductivity from 2.8×10^{-11} m/s to 3.4×10^{-7} m/s.

Full paper to be published in:
https://www.e3s-conferences.org/articles/e3sconf/abs/2025/44/contents/contents.html

* Corresponding author: ali.oren@deu.edu.tr

Hydraulic conductivity of geosynthetic clay liner containing polymerized bentonite with low mass per unit area

A. Hakan Ören* and *Taylan Cem* Aytekin [2]

[1] Department of Civil Engineering, Dokuz Eylul University, Izmir, Turkiye
[2] Graduate School of Natural and Applied Science, Dokuz Eylul University, Izmir, Turkiye

Abstract. The hydraulic performance of geosynthetic clay liners (GCLs) has been of interest since the 1990s. Conventional GCLs are made up of sodium bentonite. During the last decade, polymerized bentonite has been started to be used in GCLs to improve the barrier performance of GCLs against aggressive leachates. In this study, a GCL roll which had been used in a landfill liner was supplied from the construction site. The bentonite of the GCL was polymerized (P-GCL). The mass per unit area (MPUA) of the GCL was within the range of 3.2-4.0 kg/m^2, which was low compared to GCLs reported in the literature. The aim of this study is to investigate the hydraulic performance of P-GCL to deionized water (DIW) and trona ash leachate (TAL) as a function of mass per unit area. The hydraulic conductivity of P-GCL to deionized water was high at the beginning of the tests (10^{-7} m/s). However, the hydraulic conductivity gradually decreased to 2.0×10^{-11} m/s. Then, hydraulic conductivity tests were conducted on non-prehydrated and prehydrated P-GCLs using trona ash leachate. Even though GCLs were prehydrated with deionized water, the hydraulic conductivity was above the allowable limit suggested for the barriers (1.0×10^{-9} m/s), indicating the role of mass per unit area on the hydraulic conductivity.

Full paper to be published in:
https://www.e3s-conferences.org/articles/e3sconf/abs/2025/44/contents/contents.html

* Corresponding author : ali.oren@deu.edu.tr

Semi-permeable membrane behaviour of conventional and enhanced Geosynthetic Clay Liners

Davide Bernardo[1*], *Jonathan* Domizi[2], *Evelina* Fratalocchi[2], *Francesco* Mazzieri[2]

[1] STS Mobile, Via Giovanni Conti, 60131 Ancona, Italy
[2] Università Politecnica delle Marche, Department of Science and Engineering of Materials, Environment and Urban Planning, 60131 Ancona, Italy

Abstract. The semipermeable membrane behavior of conventional and enhanced Geosynthetic Clay Liners (GCLs) is viewed with great interest in pollutant containment applications, as the consequent reduction of diffusive flow and the onset of chemical osmosis improves the containment properties. In this context, an experimental apparatus was developed to characterize the semipermeable membrane behavior of GCLs. Preliminary results were obtained on conventional GCLs and a Dense PreHydrated and polymer-enhanced (DPH) GCL. The measured values of the chemico-osmotic efficiency coefficient ω are comparable with literature data. In addition, owing to the possibility of monitoring the total vertical stress, the equipment allows determining the at the same time the swelling coefficient $\bar{\omega}$. In this way, a complete picture of the behavior of the charged porous medium in response to chemical exposure is obtained and it is possible to determine on the same specimen the relevant parameters for the application of advanced theoretical models of chemical-osmotic phenomena in clays and GCLs.

Full paper to be published in:
https://www.e3s-conferences.org/articles/e3sconf/abs/2025/44/contents/contents.html

* Corresponding author: davidebernardo@hotmail.it

Laboratory procedures for the modification of soluble and exchangeable cations of geosynthetic clay liners

Nicolò Guarena[1*], *Francesco* Mazzieri[2], *Andrea* Dominijanni[1], *Evelina* Fratalocchi[2], and *Mario* Manassero[1]

[1]Polytechnic University of Turin, Department of Structural, Geotechnical and Building Engineering, 10129 Turin, Italy
[2]Polytechnic University of Marche, Department of Science and Engineering of Materials, Environment and Urban Planning, 60131 Ancona, Italy

Abstract. A novel dialysis procedure to modify the exchange complex composition of the bentonite component of geosynthetic clay liners, as well as to remove the excess soluble salts from the bentonite pores, has been developed in order to overcome the limitations associated with the currently used dialysis methods. Indeed, when the bentonite to be purified is characterized by an aggregated fabric, the presence of less accessible pores does not allow the interlayer exchangeable cations to be replaced by the cationic species contained in the dialysing solution, thus undermining the effectiveness of dialysis in homo-ionising the bentonite specimen. For such a reason, the novel dialysis procedure that is proposed in this study comprises a preliminary treatment phase, which comes before the homo-ionisation phase and is aimed to promote the break-up of the bentonite tactoids through dialysis cycles with deionised water. A natural powdered bentonite has been tested in the laboratory to evaluate the enhancement in the bentonite sodium homo-ionisation that is due to the adoption of the newly developed dialysis procedure, in substitution to the currently used one, showing that such substitution results in an increase in the exchangeable sodium percentage from 35% to 78% at the expense of a decrease in the exchangeable calcium percentage.

Full paper to be published in:
https://www.e3s-conferences.org/articles/e3sconf/abs/2025/44/contents/contents.html

* Corresponding author: nicolo.guarena@polito.it

SESSION 4 C
REINFORCEMENT APPLICATIONS (4)

Use of asphalt interlayer multiaxial geocomposite to enhance an asphalt overlay fatigue performance and bottom-up cracking prevention in motorway rehabilitation project

Michal Golos[1*], *Kamila* Kornacka[1], and *Jacek* Kawalec[1]

[1]Tensar, Division of CMC, Units 2-4 Cunningham Court, Shadsworth Business Park, Blackburn, UK

Abstract. The use of asphalt interlayer multiaxial geocomposite to enhance asphalt overlays results in a substantial life increase of the road pavement. It can provide the higher traffic capacity that would result in an increase of fatigue life of the asphalt pavement eventually. It can be obtained by two main benefits: (1) no need to increase asphalt overlay thickness to achieve an increased pavement life, or (2) to reduce the thickness of an asphalt overlay without any compromise on the value of pavement life. Both economic and environmental advantages of this approach seem to be obvious and can be quantified. This paper presents an example of the multiaxial geocomposite application on the heavily trafficked motorway rehabilitation project in one of the European countries. The calculation of the rehabilitated asphalt pavement with the enhancement of the asphalt overlay reinforced by geocomposite based on the modified concept of the Mechanistic-Empirical pavement design method will be also outlined. In addition, the entire installation process related to the multiaxial geocomposite will be presented and photos from installation will be shown.

1 Introduction

Maintenance of pavement is becoming a global challenge as road administration due to expanding road networks, even with same budget could dedicate less and less funds per km of road for engineering works. As a consequence of such rapid expansion, it is observed that there is continuous pressure to optimize solutions and search for methods and/or products which could increase the life of pavements. Geosynthetics becomes one of the main directions of interest in this context. Modern geogrids and geocomposites could provide significant extension of pavement life if properly implemented into pavement design and if properly installed [1, 2, 3, 4, 5, 6].

The main objective of the paper is to present the benefits of the new geocomposite asphalt interlayer for improving the pavement life. The paper presents a successful case of motorway pavement rehabilitation with the use of multiaxial geocomposite asphalt interlayer introduced into design for heavy trafficked motorway pavement life extension.

[1*]corresponding author: michal.golos@cmc.com

2 The starting position. Condition of the existing pavement

The pavement rehabilitation project was related to the heavily trafficked motorway section of a length of slightly more than 5km. Analysed motorway section is located in one of the European countries and it was constructed in 2005-2006. After approx. 15 years of continuous operation the pavement surface was in relatively poor condition. Investigations executed by the expert company commissioned by the Contractor revealed not only surface deteriorations but also structural issues on a major part of the length of the analysed section. There was an extensive network of longitudinal, transverse and 'alligator' cracking. Figures 1 and 2 reflect the examples of single longitudinal cracking in the wheel paths that might trigger and develop into alligator cracking, eventually. Moreover, at some locations, a number of breaks and chips in some deteriorated patches were found.



Fig. 1. Wheel path longitudinal cracking that may develop to the alligator pattern of fatigue cracking (to the courtesy of Contractor).



Fig. 2. Wheel path longitudinal cracking (to the courtesy of Contractor).

After milling process of a surface and binder course, one could have seen an exceptionally large number of longitudinal and transverse cracks on the asphalt base course layer (Figure 3). In addition, a disaggregated asphalt mix layer as well as improper inter-layer bonding connection between existing asphaltic base and binder courses were detected (Figure 4).



Fig. 3. Condition of existing pavement after milling, depicting both longitudinal and transverse cracking.



Fig. 4. Finely milled surface of the existing asphaltic base course.

The client, the National Road and Motorway Authority, needed a long-term validated solution to withstand the heavy traffic by the rehabilitated pavement section with the new - relatively thin and economically verified - asphalt overlay. Although the initially assumed traffic capacity was determined as up to slightly more than 50 mln 100kN Equivalent

Standard Axle Load (ESAL), after thoroughly verified traffic study, this value was substantially increased, reaching finally an enormous value of almost 63 mln 100kN ESALs.

All above mentioned and recorded distresses together with an incredibly high level of anticipated traffic level led to the decision of reconstruction of existing pavement, by milling 2 upper existing asphalt layers (wearing and binder courses) and replacing them with 2 new asphalt layers – stone mastic asphalt as a wearing (SMA 11) and asphalt concrete (AC 16) as a binder courses, both with polymer modified bitumen PMB and additionally enhanced by the geocomposite incorporating multiaxial geogrid, hereafter referred to as the Multiaxial Geocomposite Asphalt Interlayer (MGAI).

3 Benefits of asphalt overlay enhanced by Multiaxial Geocomposite Asphalt Interlayer

It is vital for providing the adequate performance of an asphalt interlayer implemented between old existing pavement and a new asphalt overlay to mitigate and eventually delay fatigue crack propagation. Multiaxial Geocomposite Asphalt Interlayer (MGAI) was developed for achieving above purposes and for solving the bottom-up cracking distress. In this approach the asphalt overlay is enhanced by a geocomposite of monolithic multiaxial geogrid and heavy-weight non-woven fabric, and the asphalt interlayer either increases the fatigue life of such overlay (compared to the same overlay thickness without MGAI) or allows to reduce the overlays thickness eventually, while achieving the same pavement life as slightly thicker overlay which does not incorporate any asphalt interlayer.

This approach is illustrated on the Figure 5 [3, 4], where: Section A is a typical section with a new asphalt overlay (H) designed for a respective fatigue life of a pavement (N_0), which is not enhanced by any asphalt interlayer. Section B is a section with a new asphalt overlay of the same thickness H, as presented in Section A, however enhanced by MGAI and thus providing a significant benefit of an increased fatigue life of a pavement ($N >> N_0$). Whilst finally section C is a section with a new asphalt overlay (h) enhanced by MGAI and designed for at least the same fatigue life as the Section A ($N \geq N_0$) but providing here a benefit of a slightly thinner overlay thickness ($h < H$).

Moreover, for the most efficient usage, it is heavily recommended to locate MGAI at the bottom of the lowest asphalt course, which usually - and also in the analysed case - is a bottom of the new asphalt overlay.

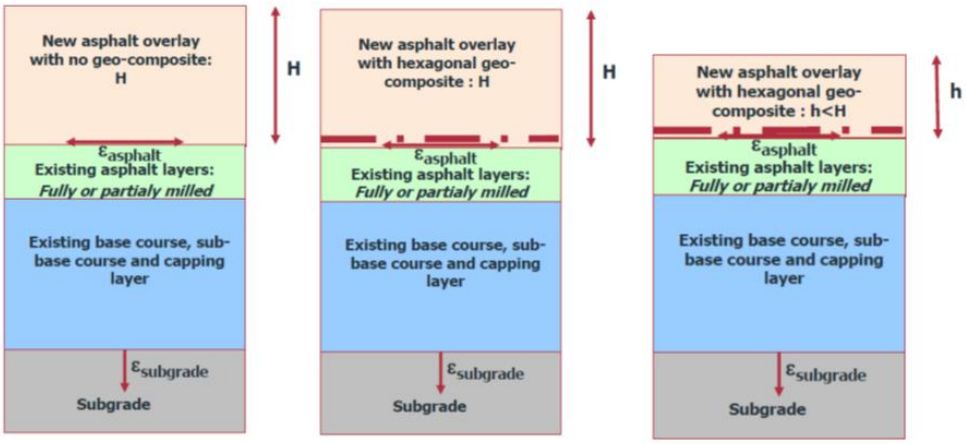


Fig. 5. Fatigue life enhancement by incorporating MGAI presented on three sections (A - control with designed thickness, B - enhanced and with same thickness as control section and C - enhanced and with reduced thickness than the control one) [3, 4].

From the geosynthetic point of view, a multiaxial geocomposite is a structural composite consisting of (1) polypropylene monolithic multi-axial paving geogrid with integral junctions

bonded to (2) a polypropylene non-woven paving fabric (Figure 7). The multi-axial grid controls strains in the overlay by an optimal interlock with the asphalt mix and provides maximum reinforcement and effective crack control in all directions, hence creating not only structural reinforcement (R) function, but even somehow stabilisation (S) function of the asphalt interlayer. The paving fabric initially functions as an installation aid, however after saturation with bitumen, it provides a SAMI (Stress Absorbing Membrane Interlayer) effect by enabling lateral strain distribution between cracked underlay (existing asphalt layers in our case) and the new asphalt overlay (two asphalt layers – binder and wearing courses, in our case), what means a stress relief (STR) function. Once saturated and additionally impregnated with bitumen the fabric delivers a waterproof interlayer barrier (B) function.

All above benefits of asphalt overlay enhanced by MGAI have been proven by the laboratory testing of the fatigue life of double-layered asphalt specimens that was performed in the scheme of four-point bending tests (4PB) of large asphaltic concrete beams in the controlled strain mode - both for geocomposite enhanced and control specimens. Based on the fatigue performance results obtained from the extensive tests program, that was carried out at Gdansk University of Technology, Poland, one can conclude that the rated product has a clear and positive effect on asphalt overlay performance and thus has an evident potential to extend the asphalt pavement fatigue life [4]. A couple of specific conclusions which were crucial for further product implementation in the design approaches have been outlined:

- Enhancing the asphalt pavement with MGAI significantly increases its fatigue life.
- The effect of asphalt enhancement is more beneficial in the case of new pavements (thicker asphalt layers and lower tensile strain at the bottom of these layers) which were simulated by the plain (un-notched) samples during the test research. A relative increase in fatigue life (RI) by a shift factor of 6-18 (in the range of or pre-set strain level of 200 to 80 microstrains, respectively) is achievable, compared to the control system (as depicted in Figure 6 [5]).
- Nevertheless, in terms of rehabilitated pavements overlaid by new asphalt courses, which were simulated by the notched beams during the test research (in contrary to the new pavements - thinner asphalt layers and higher tensile strain at the bottom of these layers), a relatively high shift factor can be achieved as well. A relative increase in fatigue life (RI) by a shift factor of 4-10 (in the range of or pre-set strain level of 200 to 80 microstrains, respectively) is achievable, compared to the control system (as depicted in Figure 6 [5]).

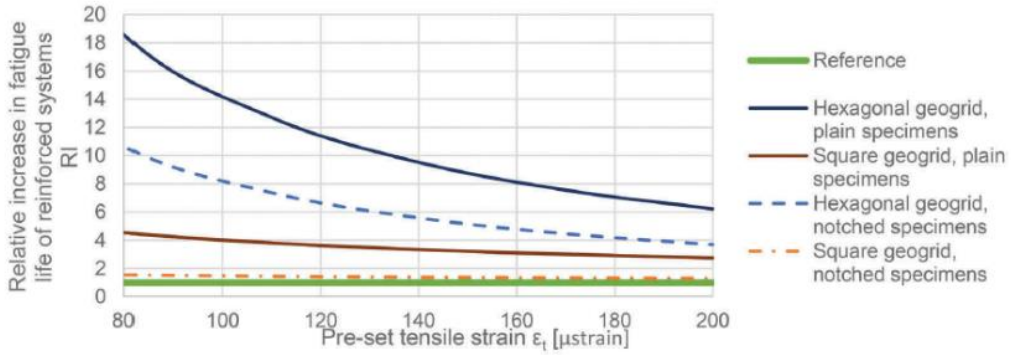


Fig. 6. Relative increase in fatigue life (RI) of double-layered beams enhanced by MGAI product (upper solid and dashed lines) based on the research at Gdansk University, Poland [5] (also the bi-axial geocomposite was tested – middle solid and dashed lines).

- Introducing MGAI enhancement at the bottom of asphalt overlay mitigate and delay the occurrence of fatigue (bottom-up) cracking in the upper asphalt layers, as depicted in Figure 8 [1, 4] and extend the asphalt overlay and pavement durability [6].



Fig. 7. View of the Multiaxial Geocomposite Asphalt Interlayer, PP geogrid bonded to PP non-woven fabric.

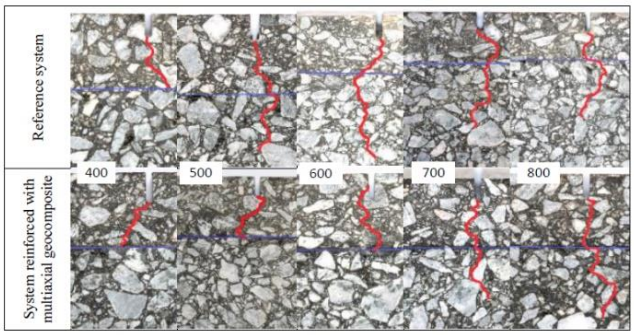


Fig. 8. Photographs of notched samples after fatigue testing with highlighted cracks based on the research at Gdansk University, Poland [1, 4].

• By introducing MGAI enhancement at the bottom of asphalt overlay it would be expected that overall stiffness can be slightly reduced, as a consequence of slight differential movements between the two asphalt layers [4, 5, 7]. It can also affect the shearing strength of interlayer bonding, but this should not have a destructive effect on overall pavement performance. Moreover, a control de-bonding mechanism is supposed to have a positive effect that provides a SAMI-like effect and STR function, initiated by the bitumen-saturated heavy-weight fabric component. As a consequence, it delays crack propagation in the new asphalt overlay [5, 6].

There is a strict relation between mitigation of the bottom-up fatigue cracking occurrence and the increase of the fatigue life of an asphalt overlay and entire pavement eventually. The fatigue life of asphalt layers is defined as a number of standard axles load which can be applied before a given percentage of a pavement surface area will be covered with cracks. In the Mechanistic-Empirical Pavement Design Method (M-EPDM) approach it is calculated with the help of an appropriate Transfer Function. Fatigue cracking development depends on the magnitude of horizontal tensile strain at the bottom of lowest asphalt layer. Therefore, the modified M-EPDM including the enhancement of MGAI, has been utilised for calculation of an analysed motorway pavement section. It has been predominantly based on the well-received results achieved at Gdansk University testing facility and described at the point 4.

4 Design process

The analysed section of the motorway was divided into two sections: section 1 of total 1050 meters and section 2 of total 4200 meters. This division was caused by significant differences in the thickness and parameters of the existing pavement layers along the investment. The list of thicknesses and stiffness/elasticity modules of the existing structure layers after milling the cracked wearing and binder course is presented in Table 1. For the asphalt layers, the air voids content and the volumetric content of asphalt were also determined, which amounted to 6.0% and 8.6%, respectively, for both sections for the lowest asphalt layer.

For both sections, an overlay in the scheme of a new 40 mm thick wearing course and a new 80- or 90-mm thick binder course was designed. In order to increase fatigue life and slow down the propagation of cracks from the old asphalt package, MGAI was used, placed directly on the existing asphalt base after milling. The parameters for the new asphalt layers were adopted in accordance with the applicable guidelines for the domestic requirements of flexible pavements design and presented in Table 2.

Table 1. Parameters of the existing road construction

Layer	Layer thickness [mm]		Layer stiffness/elasticity modulus [MPa]		Poisson's ratio [-]	Air voids content [%]	Asphalt volume content [%]
	Section 1	Section 2	Section 1	Section 2			
the asphalt base upper layer remained after milling	100	100	6856	6854	0.3	-	-
the asphalt base bottom layer remained after milling	81	85	6856	6854	0.3	6.0	8.6
existing unbound subbase layer	210	90	352	391	0.3	-	-
Subgrade	-	-	111	286	0.35	-	-

Table 2. Parameters of the new asphalt layers for an overlay

Layer	Layer thickness [mm]		Layer stiffness/elasticity modulus [MPa]		Poisson's ratio [-]	Air voids content [%]	Asphalt volume content [%]
	Section 1	Section 2	Section 1	Section 2			
Wearing course SMA 11 PMB 45/80-55	40	40	7300	7300	0.3	-	-
Binder course AC16 W 35/50	80 or 90	80	10300	10300	0.3	7.3	9.9
MGAI	-	-	-	-	-	-	-

Due to reduced values or total lack of adhesion at the interface of existing asphalt base layers (what was determined during pre-construction research) and the possibility of a slight decrease in adhesion at the geocomposite installation level, an additional ALK (*reduced shear spring compliance*) coefficient was used [8]. There were a number of calculation attempts including different ALK coefficients, however the final values assumed for the adhesion reduction scheme by 50% and 30%, respectively have been determined. These coefficients are equal to 1.0 m for the existing asphalt base – asphalt base interface and 0.3 m for the new binder course – existing asphalt base course interface, i.e. at the geocomposite installation level.

The required fatigue life was determined based on the General Traffic Measurement and amounted to 62.8 million standard 100 kN axles over 20 years of road operation, which is the highest traffic category in the classification applicable in the domestic requirements. The designed new pavement structure using asphalt interlayer geocomposite was verified computationally using the modified Mechanistic-Empirical Pavement Design Method. Stresses and strains in the pavement structure were calculated according to the multilayer elastic half-space theory. The Asphalt Institute transfer functions for fatigue cracking of asphalt layers and for permanent deformation of the subgrade were used.

The following assumptions were made for the calculation of the pavement structure: surface is loaded with a design axle of 100 kN (load on the wheel of 50 kN), contact pressure between the wheel and the pavement is 850 kPa, equivalent diameter of the wheel trace is 0.32 m and the time of loading the pavement with the wheel is 0.02 s.

To determine the fatigue life of asphalt layers, the following equations were used:

$$N_c = 18.4*10^{M}*6.167*10^{-5}*\varepsilon_h^{-3.291}*E^{-0.854} \quad (1)$$

$$M = 4.84\ \{\frac{Vb}{Va + Vb} - 0.69\} \quad (2)$$

The durability due to permanent deformation of the subgrade was determined using the following equation:

$$N_{DEF} = \{\frac{k}{\varepsilon_v}\}^{1/m} \quad (3)$$

The calculated fatigue life is the lower value of two criteria:

$$N = \min \{N_c; N_{DEF}\} \quad (4)$$

where:

N_c – number of loads applied until fatigue cracking occurs on 20% of the lane area,
ε_h – tensile deformation at the bottom of the asphalt layers,
E – stiffness modulus of the lowest asphalt layer,
V_b – asphalt content [% by volume],
V_a – air voids content [% by volume],
N_{DEF} – the number of loads to create a structural rut with a critical depth of 12.5mm,
ε_v – vertical compressive strain at the top of the subgrade,
k,m – empirical coefficients: k = 0.0105, m = 0.223.
N – number of design axles in the assumed operating period – fatigue life of the pavement.

To calculate the durability of the pavement with MGAI, the shift factor, named Fatigue Resistance Improvement Factor (FRIF) was used. The FRIF value of 2.5 was assumed based on analyses verifying the impact of using the MGAI to increase the durability of the pavement structure (reference to point 3). When determining the value of the factor, its value was reduced due to the fact that the interlayer was placed directly on the milled and prepared pavement, without a leveling layer. The results of the calculations are shown in Table 3.

Table 3. Results of the calculations

	Section 1 overlay			Section 2 overlay	
	Without MGAI	With MGAI		Without MGAI	With MGAI
	40 + 80 mm	40 + 80 mm	40 + 90 mm	40 + 80 mm	40 + 80 mm
Tensile strains at the bottom of new asphalt layers [μm/m]	80.4	45.6	45.3	70.1	45.7
Compressive strains at the top of the subgrade [μm/m]	195.3	205.9	193.4	146.4	170.8
Fatigue life from fatigue cracking of asphalt layers criterion	5.8	57.5	58.6	9.2	56.8
Fatigue life from permanent deformation of the subgrade criterion	57.5	45.4	60.1	209.8	105
Designed life of the pavement [mln]	5.8	45.4	58.6	9.2	56.8
Required fatigue life [mln]	62.8				
Percent of achieved required fatigue life [%]	9	72	93	15	90

Ultimately, the overlay of 40 + 90 mm for the first section and 40 + 80 mm for second section was adopted. Thanks to the use of MGAI it was possible to significantly increase the fatigue life compared to the unreinforced construction and approach the required fatigue life - at least 90% of the required fatigue life was achieved. The final results have been accepted by the Client eventually.

5 Installation process of MGAI

The reconstruction works were split into two phases; the 1st phase took place in October/early November 2021, whilst the 2nd phase was carried out on the very next year, between July and September. The entire work comprises three main sub-processes, i.e. (1) milling of the existing asphalt layers, (2) multiaxial geocomposite asphalt interlayer installation over the mechanically sprayed tack coat and (3) paving & compaction of the new asphalt overlay.

Following the geocomposite manufacturer's installation guideline [9], finely milled substrates with a maximum rill depth ≤ 10mm are acceptable for the installation of the product. However, in the executed project the rills could be found substantially higher/deeper than 10mm, sometimes reaching even 20+mm (see Figure 4).

A proper installation process of MGAI product seems to be extremely important to achieve the final effect of good performance. The properly carried out installation process consists of the five following key sub-processes:

5.1 Bond coat application

A bitumen bond coat is a mechanically spray-applied cationic bitumen emulsion directly to the substrate. The bitumen spray rate of 1.2 - 1.5 kg/m^2 of residual bitumen was recommended by producer's installation guideline. As the Contractor used a bitumen emulsion with a bitumen solid content of ≥69%, the amount of freshly sprayed bitumen emulsion varied between the values of 1.75 - 2.0 kg/m^2, as depicted in the Figure 9.

5.2 Installation of the asphalt interlayer

Geocomposite is simply unrolled immediately onto the freshly sprayed bond coat. While manual unrolling is perfectly possible, the use of a purpose-built interlayer installation machine enables a faster installation, to a higher quality. In the analysed case rolls of both 3.8m and 1.9m width were mostly installed by machine, while some of them were installed also manually, e.g. 0.95m width. However, the most commonly used method was a so-called semi-mechanical installation method, as it is depicted in the Figure 10.



Fig. 9. Tack (bond) coat spraying process by using bitumen emulsion tankers.



Fig. 10. Semi-mechanical and partially manual installation process accompanied by the brushing operation.

5.3 The brushing or brooming process to accompany unrolling the interlayer

Brushing also helps a lot to achieve a firm and wrinkle free contact between the product and the existing surface. Thus, immediately after product installation (while bitumen emulsion's breaking process occurs) pressure with brooms or brushes was applied to geocomposite to get rid of any wrinkles and folds and to assist the fabric to be initially saturated by the bitumen, that is precipitated from bitumen emulsion (Figure 10).

5.4 Pneumatic Tyre Roller (PTR) passing over the interlayer

Few passes of PTR over the fully installed product (while bitumen emulsion's curing process occurs) are highly recommended to achieve the better bonding of the fabric to the surface (Figure 11). An effectiveness of the well-conducted PTR pressing operation can be easily tested just after the operation on site. It's heavily recommended to do at randomly selected locations a kind of on-site easy testing, that means a number of attempts of separation/delamination the grid from the fabric by holding the grid's node and trying to lift it up. The more the grid tends to delaminate from the fabric, the better performance and higher value of bonding between existing substrate and product's fabric is then achieved (Figure 12). If the fabric seems to be no sticky, then the section gets ready for the paving operation.



Fig. 11. PTR compaction process conducted after product installation and brushing processes.



Fig. 12. On-site testing of the bonding strength by lifting the grid up.

5.5 Asphalt paving and compaction processes

Once the bitumen emulsion is fully broken and cured, asphalt binder course paving (placed directly over an interlayer) and compaction processes using traditional paving and compaction machines should occur (see Figure 13 and 14). Then finally, the paving process of SMA 11 PMB wearing course was carried out.



Fig. 13. Paving operation of an asphalt binder course of 80 (90) mm just over the MGAI product.



Fig. 14. Compaction operation of an asphalt binder course of 80 (90) mm.

Apart from the well-adjusted product selection and design calculation (outlined in the points 3 and 4), an excellent installation process of multiaxial geocomposite asphalt interlayer is an important milestone to achieve the highest quality of a final accomplishment [9].

6 Summary and conclusions

Although not much time have passed since the Multiaxial Geocomposite Asphalt Interlayer was installed (3 years form the 1st phase of installation), however based on 3 key elements, i.e. an appropriately selected technology, well-designed solution and properly installed

interlayer, one can expect a long-lasting solution without evident signs of fatigue of a new asphalt overlay. Hence, it can be concluded, that the MGAI could provide significant extension of pavement life without increasing asphalt overlay thickness, if appropriately implemented into pavement design and properly installed.

The lessons taken from the installation is that installation procedure must be strictly followed and even minor departures may result in problems visible at compaction of asphalt binder course.

The solution will be subject of further regular monitoring over years to observe long time performance of MGAI and to compare it with predicted by design behaviour of the motorway pavement structure.

References

1. P. Jaskula, D. Rys, M. Stienss et al., The effect of multiaxial geocomposite reinforcement on fatigue performance and crack propagation delay in double-layered asphalt beams, Road Mater. Pavement Des., **24**, 352-368 (2023). https://doi.org/10.1080/14680629.2023.2180998
2. P. Jaskula, D. Rys, M. Stienss et al., Fatigue Performance of Double-Layered Asphalt Concrete Beams Reinforced with New Type of Geocomposites, Materials, **14:2190** (2021). https://doi.org/10.3390/ma14092190
3. M. Golos, P. Mazurowski, Pavement Optimisation with Aggregate Base or Asphalt Layers Stabilised with Hexagonal Geogrids, IOP Conf. Ser. Mater. Sci. Eng., **1202, no. 1**, p. 012024 (2021). https://doi.org/10.1088/1757-899x/1202/1/012024
4. M. Golos, P. Jaskula, Asphalt Overlay Enhancement with Fatigue High-Performing Multiaxial Geocomposite, in Proceedings of the 10th International Conference on Maintenance and Rehabilitation of Pavements, MAIREPAV10, **2**, 375-385, Guimares, Portugal, July (2024).
5. P. Jaskula, D. Rys, M. Stienss, C. Szydlowski, M. Golos, J. Kawalec, Laboratory fatigue assessment of large geocomposite-reinforced double-layered asphalt concrete beams, Eleventh International Conference on the Bearing Capacity of Roads, Railways and Airfields, **3**, 65–74 (2022). https://doi.org/10.1201/9781003222910-7
6. P. Jaskula, D. Rys, M. Stienns et al, Delay of crack propagation in 4PB test of double-layered geocomposite reinforced asphalt concrete beams, 12th Int Conf Geosynth, Roma (2023).
7. CEN EN 15381: Geotextiles and geotextile-related products - Characteristics required for use in pavements and asphalt overlays (2008).
8. P. Jaskula, Adhesiveness of asphalt layers in multi-layer road surface systems, habilitation thesis, Gdansk University of Technology, Poland, 2018.
9. Tensar International Limited, *Installation Guide for Tensar AX5-GN Asphalt Interlayer*, Tensar Installation Guideline, IG/AX5-GN (23.11.2020).

Influence of different paving geosynthetics on crack growth phases and strain behavior in asphalt overlays

Natalia S. Correia[1], *Ana Laura C. S.* Bernardinelli[1], *Karolina Maria* Santos[1] and *Amir* Shahkolahi[2]

[1]Department of Civil Engineering, Federal University of Sao Carlos, Brazil
[2]Global Synthetics, Queensland, Australia

Abstract. This study aimed to assess the impact of different paving geosynthetics on crack propagation and the mitigation of reflective cracking in asphalt mixtures based on four-point bending tests combined with Digital Image Correlation (DIC). The study evaluated pre-notched beam configurations of double-layered asphalt slabs, both with and without paving geosynthetics. DIC analysis was used to measure strain patterns in the central area of the specimens during crack propagation. Results clearly showed that paving geosynthetics significantly delayed crack propagation, as reinforced beams endured more cycles than the control beam. Geosynthetic-reinforced asphalt samples achieved tensile strains reduction factors ranging from 0.07 to 0.36, indicating their superior effectiveness in mitigating strain concentrations and maintaining the neutral axis position for longer periods. Findings highlight the critical role of interface shear bond and reinforcement characteristics in prolonging pavement service life.

Full paper to be published in:
https://www.e3s-conferences.org/articles/e3sconf/abs/2025/44/contents/contents.html

[1] Corresponding author: ncorreia@ufscar.br

Steel grids performance and environmental impact in asphalt

Germain Auray [1*], and *Abdelghani* Mekkaoui[1]

[1]Bekaert France SAS, Building Products, 3 Boulevard de Belfort, 59000 Lille, France

Abstract. Since the creation of Steel grids in the 1970s, the advancement of wire rope and cable technology in recent years has allowed to create efficient, robust and recyclable grids, while respecting the environment and the most severe conditions of trafficability. The expansion of road networks and the number of vehicles in the world are constantly increasing. Road maintenance is becoming very expensive. The new maintenance technologies with steel grids have allowed 100% recyclable low-cost maintenance with unique reinforcement performance in asphalt. In this article we will first present the performance of steel grids in asphalt reinforcement. The ductility of the steel and coated grid composite has proven effective for crack mitigation in laboratory tests. In the second part, we will present the maintenance cost savings and carbon footprint reduction by using metal grids with a comparison to traditional solutions in a large-scale project.

1 Introduction

In the 1930s, a first use of steel wire mesh in asphalt reinforcement was made in Michigan, USA [1], with the same state of mind than reinforced concrete.

In the 1990s, several scientific publications showed the performance of steel grids in asphalt reinforcement as interlayers, to delay reflective cracking, increase bearing capacity, increase service life and reduce the thickness of the asphalt. Thus, asphalt reinforcement with steel grids has been implemented in design methods for roads [2].

The expansion of road networks and the number of vehicles in the world are constantly increasing. The road network in France increased by 11.5% between 2005 and 2020, with a total of around 1.1 million kilometres following the French Ministry of Ecological Transition.

Road maintenance is becoming very expensive. Several techniques and processes have emerged to fight against cracking in roadway structures.

Steel grids have allowed 100% recyclable low-cost maintenance with unique reinforcement performance in asphalt. In order, to quantify the performance of these products, laboratory tests have been developed by Bekaert in collaboration with external laboratories, governmental and academic partners.

* Corresponding author: abdelghani.mekkaoui@bekaert.com

2 Characteristics of steel grids for road

Two steel products were tested. A square steel wire mesh (FF-1C and FF-2C) and a hexagonal twisted steel mesh (MT) pictured in Figure 1.

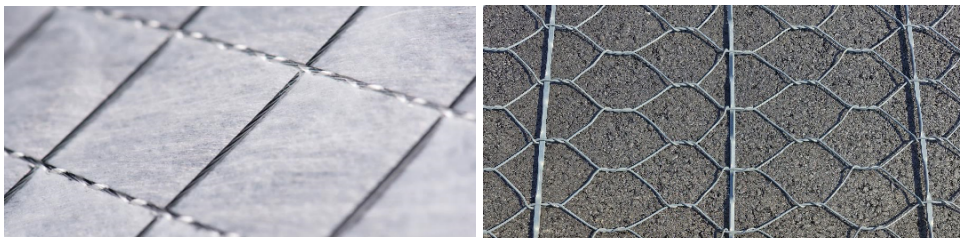


Fig. 1. Square steel wire mesh grid (left) and hexagonal twisted steel mesh grid (right).

Fortifix® FF-1C and FF-2C are advanced steel cord structures delivered on a synthetic carrier with highest steel density. The mesh grid is built from steel cords longitudinal and cross direction, the steel cords are stitched to the carrier. The technical specifications of the products are detailed in Table 1.

Table 1. Technical specifications of the products FF-1C and FF-2C.

Square steel wire mesh grid		
Products	FF-1C	FF-2C
Grid opening CMD × MD (mm)	40 × 30	(50) × 50
Mesh tensile strength CMD × MD* (kN/m)	54 × 42	32 × 31
Elongation (%)	1.7	1.7
Young's modulus (GPa)	190	190
Tensile stiffness (kN/m)	2900 × 3900	2300 × 2300
Durability	Zn coated-class D	Zn coated-class D
Weight (g/m²)	353	253
Carrier	PET non-woven	PET non-woven
Bitumen retention (g/m²)	500	500

Mesh Track® MT is a woven hexagonal wire netting, manufactured of heavy Bezinal® coated class B steel wire, reinforced in transversal direction, at regular intervals, by flat twisted reinforcing wires interwoven in the mesh. The technical specification of the product is detailed in Table 2.

Table 2. Technical specifications of the product MT.

Hexagonal twisted steel mesh grid	
Product	MT
Mesh dimensions (mm)	80 × 118
Pitch on transversal wire (mm)	245
Mesh tensile strength kN/m	40 x 50
Young's modulus (GPa)	200
Tensile stiffness (kN/m)	23000 x 29000
Durability	Zn(95) AI(5)
Weight (g/m²)	1730

As a main characteristic of all steel grids, it's very important to mention that steel grids are not affected by installation damage and that the performance delivered in laboratory conditions is very likely to be equivalent on jobsites as long as the other parameters of installation are correctly managed (for more information refer to installation guidelines of each product). Also, it's possible to extract steel material and 100% recycle it which makes an interesting advantage in terms of environmental impact.

3 Crack delaying in cyclic bending

We have recently tested FF-1C and FF-2C in the reference laboratory for asphalt KIWA/KOAC/NPC in the Netherlands. All test conditions and full results are available in report on demand. The test conditions are also reported in [3]. As an extract we refer to the cyclic testing according to set-up depicted on Figure 2.

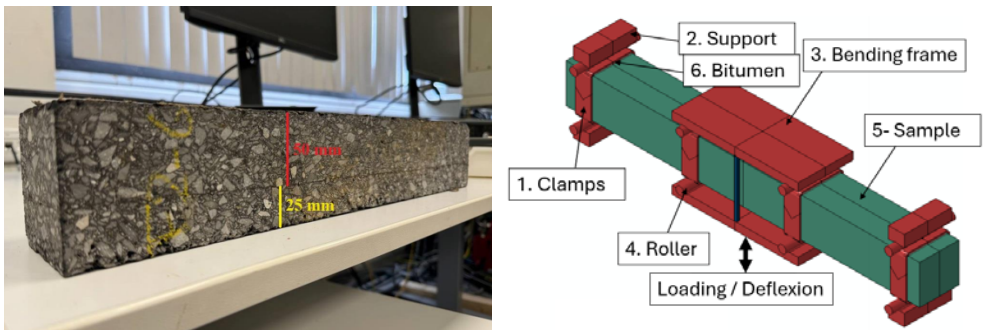


Fig. 2. Picture and drawing of test set-up.

With notched beams in 4 point bending test at -5°C and 30 Hz, we are assessing the capacity of the reinforced samples (FF-1C and FF-2C) to delay the crack propagation to the top compared with unreinforced samples (Ref). This solicitation models the fatigue repetitive flexural movement of traffic in asphalt layers. We obtained following results in Table 3.

Table 3. results of 4PB cyclic tests on notched beams.

	σ6 notched (MPa)	ε6 notched (µm/m)	Cycles. Nb σ6 = 1.97 MPa	Cycles nb ε6 = 255 µdef	Gain on cycles Nb for σ6	Gain on nb cycles for ε 6	Gain on σ6	Gain on ε6
Ref.	1.97	255	1,000,000	1,000,000				
FF-1C	2.32	324	3,692,122	5,439,585	x3.7	x5.4	17%	27%
FF-2C	2.30	292	3,739,887	3,343,849	x3.7	x3.3	17%	15%

σ6 is the stress estimated for 1 million cycles of loading, ε6 is the deformation estimated for 1 million cycles of loading. These are reference values for estimating fatigue behaviour in asphalt layers. And we computed in the table the gains obtained using the 2 steel grids in numbers of load cycles or on these reference values σ6 and ε6.

The figures are demonstrating a clear capacity of steel grids to delay crack propagation and increase number of loading cycles. In some specific configurations the ratio has been even evaluated up to 13 times better.

4 Crack delaying in composite solicitation (cyclic bending + tension)

A specific test has been developed in CEREMA laboratory France [4] to model reflective cracking travelling through the structure. The test set up is as described in Figure 3.

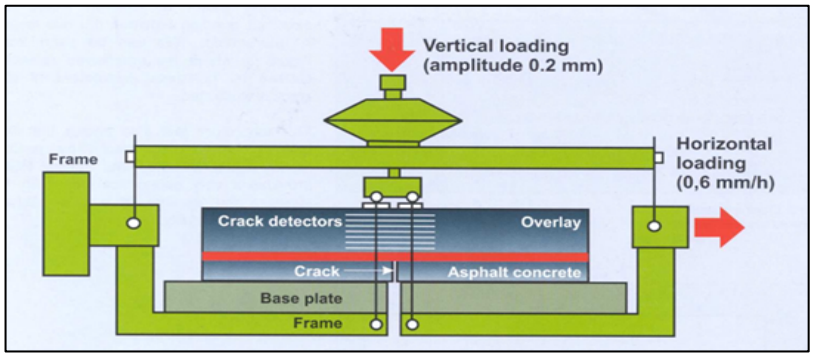


Fig. 3. CEREMA test principles.

It consists in measuring the time for a crack from the foundation course to rise to the top of the overlay, under the effect of simultaneous stresses, simulating thermal shrinkage (horizontal movement) and traffic (flexural behaviour). Under the same temperature conditions (the test is carried out at 5°C), the time for the crack to rise to the surface is compared to the time for the crack to rise through control layers (a reference asphalt only without interlayer and a bituminous sand interlayer) with perfectly determined characteristics.

When we tested FF-1C, FF-2C and MT, delamination or anchorage failure was not reported, thus we can compare the results of the graph below Figure 4.

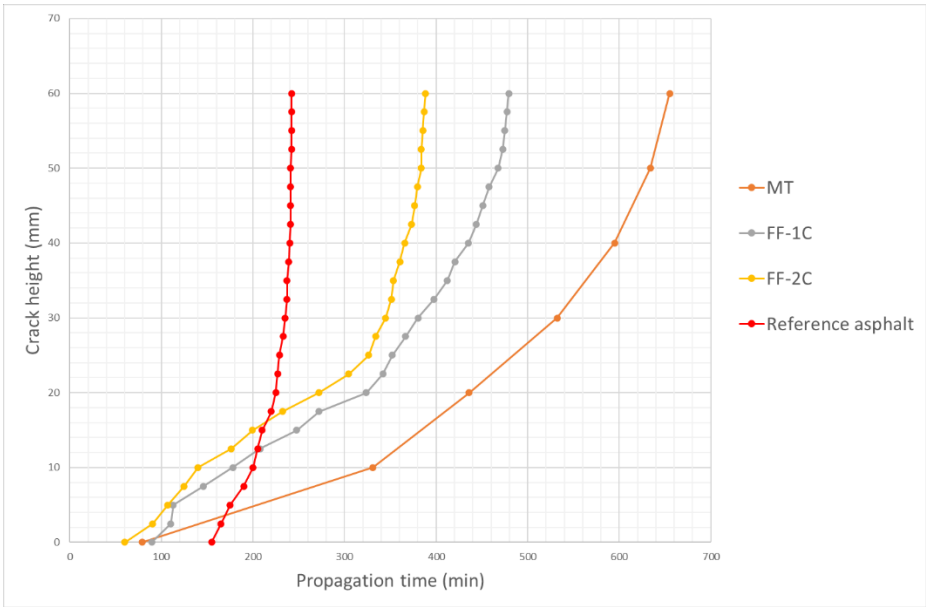


Fig. 4. Propagation crack height during time.

According to these results, if we look at the total time it takes for a crack to propagate up to the top, we see that compared to a reference asphalt we are significantly improving crack control as presented in Table 4.

Table 4. Performance ratio of the products vs asphalt reference.

Products	Asphalt Ref.	FF-1C	FF-2C	MT
Time of the test [min]	242	481	392	568
Total performance increase vs reference	-	1.98x	1.62x	2.35x

Now for each product or system tested, installation of products, tensile strength, raw material of the product and the bitumen emulsion are different and not controlled by the laboratory. It is difficult to compare between different solutions in this set-up especially the time for the first crack to appear in the overlay. In this analysis we are interested to see the performance of the product in crack propagation control, so we have looked at the time between the appearance of the first crack until the end of the test reported in Table 5.

Table 5. Performance ratio of the products vs asphalt reference.

Products	Asphalt Ref.	FF-1C	FF-2C	MT
Time to full cracking from crack initiation @60mm [min]	87	392	264	576
ratio vs reference	-	4.5×	3.0×	6.6×

Once the crack appears, interlayers should normally delay the crack spreading in the asphalt. We observe that steel grids are very efficient in terms of delaying crack propagation. Compared to the same test that we have seen for some other types of systems in glass fibres or polypropylene fibres for instance, MT is delivering solid performances

on that analysis while FF-1C and FF-2C are also performing good with a limited thickness and amount of bitumen emulsion involved in the installation.

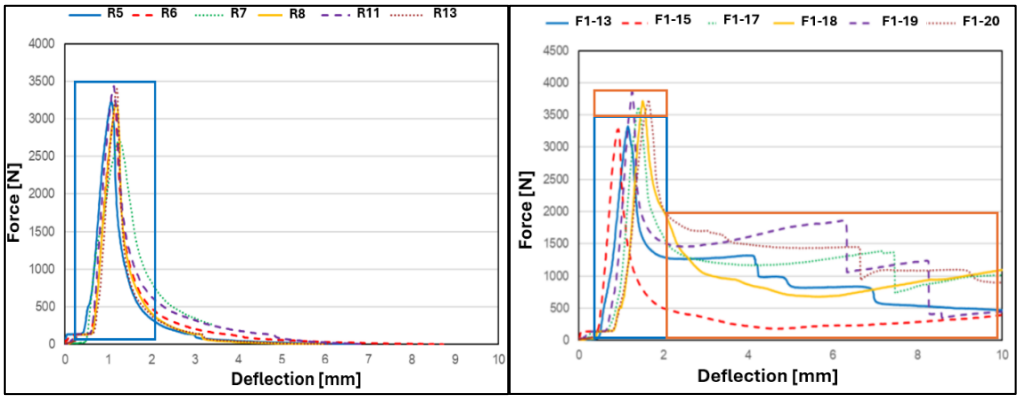
Steel grid interlayers are 3 to 7 times more efficient than the reference asphalt and we can say that the ductility of the interface reinforced by steel grids is the most efficient due to the capacity of steel to sustain the crack opening. It demonstrates similar effects as the thermal plate test campaign on steel grids reinforced asphalt, also modeling effect of thermal cracks, published in [5].

MT has already been evaluated long ago and is validated in a specific design methodology for optimizing thicknesses of asphalt structures. It will not be presented in the next chapters of this paper, but it was interesting to place it on this test as comparative benchmark not really evaluated before.

5 Crack propagation control

What if the crack is already at the top? It is fine to delay crack propagation to it is maximum with interlayers but it is also obvious that cracks will appear after a certain period. We wanted to model how steel grids could bridge and redistribute cracks, resulting in lower crack width, and so continuously act as a reinforcement in post crack situation. We have developed a 3 point bending notched test program based on energy distribution post crack. This has been done in collaboration with Dutch external laboratory (same report as previously mentioned). This is also extending the publication [5] which was using the same philosophy of testing in 4 point bending set-up.

To base our assessment on existing energy redistribution methodology and materials we have used the BEFIM French national project methodology [6]. It's interesting to note that it exists similarities within the crack control behaviour of asphalt interlayers and steel fibres reinforced concrete helping to visualize and analyse post crack behaviour. The main learnings are explained in Figure 5 on force vs deflection graphs.



Asphalt reference notched beam

Steel reinforced notched beam

- Phase 1 □ : Asphalt behavior
- Phase 2 □ : Impact of steel on asphalt behavior

Fig. 5. Effect of steel grids on peak load and post crack control.

We clearly identify an important post crack behavior of the reinforced asphalt against un-reinforced which is demonstrating the capacity of Steel grids to bridge the cracks, distribute cracks and lower the opening size of the cracks. As already mentioned post crack performance is based on energy absorption (area under the curve). When looking at these criteria, we obtained following results:

Table 6. Performance ratio in percentage (increase due to grids) of the steel grid reinforced layers vs asphalt reference or reinforcement type 1 vs type 2.

	Fmax (kN)	E5mm (J)	E10mm (J)
FF-1C vs Ref	+13%	+210%	+470%
FF-2C vs Ref	+4%	+192%	+425%
FF-1C vs FF-2C	+8%	+6%	+9%

Steel grids are slightly improving the maximal load at first crack (Fmax = peak load), but the most important is to see how sustainable the action of these products is, until very long deformations. It emphasizes the ductility effect mentioned in previous chapter since we dissipate 3 to 9 times more energy for redistributing the crack compared to unreinforced asphalt at 5 mm and 10 mm displacements.

6 Uncracked fatigue performances

Within the same set-up of paragraph 3 we have tested un-notched beams. In 4 point bending test at -5°C and 30 Hz, we are assessing the capacity of the reinforced samples with steel grids to basically reinforce asphalt before failure. The identified parameters are the same as for table 3 are shown in Table 7.

Table 7. Performance ratio of the products vs asphalt reference.

	σ6 (MPa)	ε6 (μdef)	Cycles. Nb σ6 = 2.09 MPa	Cycles nb ε6 = 279 μdef	Gain on nb cycles for σ6	Gain on nb cycles for ε6	Gain on σ6	Gain on ε6
Reference	2.09	279	1,000,000	1,000,000				
FF-1C	2.83	369	3,251,187	2,639,897	×3.3	×2.6	35%	33%
FF-2C	2.45	322	3,522,688	2,417,601	×3.5	×2.4	17%	16%

The figures are demonstrating a clear capacity of steel grids to reinforce asphalt before failure. In some specific configurations the ratio has been even increased to 30 times better. We know this is a parameter used for design, and we are currently assessing how to compute all these results in road design software's to provide some guidelines for future design.

7 Example of reduction of the carbon footprint of a reinforced road structure

7.1 How to measure the reduction of a carbon footprint of a reinforced road structure

Life cycle assessment is a science-based calculation method to quantify the environmental impact of materials throughout the lifetime. GHG (Green House Gas) emission values are obtained either by using the EPD documents from the supplier or generic values from a recognized LCA provider.

Road reinforcement strategies could reduce the carbon footprint in several ways:

- Reduced Materials: Grids may reduce asphalt thickness. Less material means less production and transportation, which reduces the carbon footprint.
- Increased Durability: Grids increase the durability of asphalt, delaying cracking and extending pavement service life. Fewer frequent repairs and replacements reduce emissions associated with maintenance work.
- Improved Structural Performance: By reinforcing the structure of the asphalt, grids help maintain a smoother road surface. A smoother road reduces the rolling resistance of vehicles, which reduces fuel consumption and CO2 emissions from vehicles.
- Construction Efficiency: Grids should be easier and faster to install than other reinforcement methods, reducing construction time and emissions associated with construction equipment

From all these elements above, we can compare the products and their effectiveness in reducing carbon footprint.

7.2 Example of projects reinforced with steel cable grids

7.2.1 Project Inputs

As a typical structural road renovation project, a road with 4cm wearing course and 8cm binder course is selected. For structural renovation a hexagonal twisted steel mesh (MT) solution is prescribed with 3cm reduced binder course thickness.

As example of anti-reflective road renovation, same thickness of road considered for a square steel wire mesh (FF) and traditional renovation method. These parameters are summarized in Table 8.

Table 8. Traditional structure solution VS MT and FF structures solution.

	Structural Overlay Renovation		**Anti-reflective Crack Renovation**	
1000m2 road	Traditional Overlay no interlayer	MT	Traditional Overlay no interlayer	FF

Wearing Course AC11 *thickness in cm*	4	4	4	4
Tack Coat *kg/m2*	0.3	0.3	0.3	1.8
Binder Course AC22 thickness *in cm*	8	5	8	8

The LCA calculations following in next paragraph have been carried on a 1000 m² surface of road for a service lifetime of 15 years, in a full lifecycle assessment cradle to cradle according to EN 15804 standard.

For MT renovation we have considered only the benefit for optimizing the thickness of asphalt. For FF renovation we have considered the maintenance process according to our experience in Table 9.

Table 9. Evaluated Maintenance of traditional roads vs reinforced roads.

	5 first years of exploitation	**5 years middle period**	**5 last years of exploitation**
Traditional road	No maintenance	2% wearing course surface	5% wearing course surface
Reinforced road	No maintenance	No maintenance	2% wearing course surface

The equivalent CO2 impact values used in the calculations are publicly available in EPD's or generic information from an experienced LCA provider (in our case OneClick LCA) and declared in Table 10.

Table 10. Selected Materials equivalent CO2 impact.

Type of material	**Eq CO2 impact**
Wearing course AC11	0.04 kgCO2eq /kg
Tack Coat	0.35 kgCO2eq/kg
Binder Course	0.038 kgCO2eq/kg
FF reinforcement	0.44 kgCO2eq/m²
MT reinforcement	1.38 kgCO2eq/m²

From our mean projects data in Europe, we estimated the distance for transporting the mesh from production site to jobsite is 370 km and the distance for transporting asphalt is 90 km.

Of course, all inputs are subjected to discussions and could be adjusted for specific cases, but we wanted to set a starting point in evaluating the performances.

7.2.2 LCA Results

Main results are presented in Figure 6.

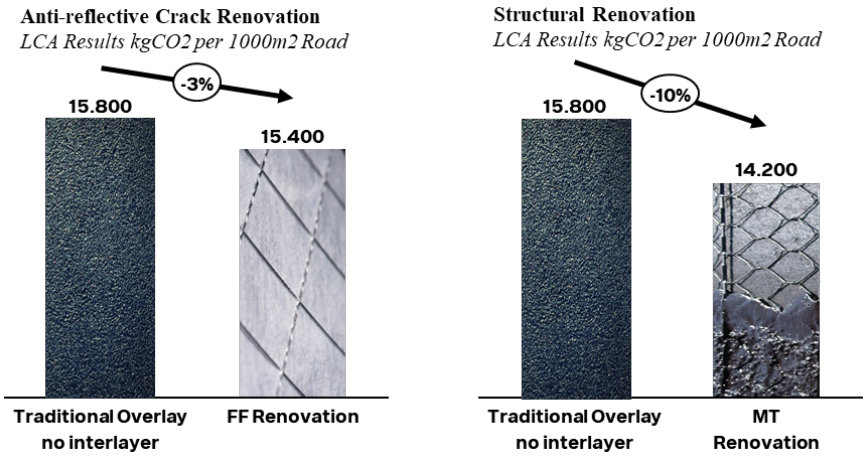


Fig. 6. LCA Results in kgCO2e for 1000 m² Road.

For structural overlay renovation, thanks to thickness reduction it resulted in ~10% lower carbon emission in the case of MT. For Anti-reflective cracking renovation, despite the higher initial material input, the FF solution optimized maintenance of wearing course contributes to reduced long-term environmental impacts by -3%.

These findings suggest that incorporating hexagonal twisted steel mesh for structural overlay renovation and a square steel wire mesh for anti-reflective renovation into road renovation projects can contribute to lower carbon emissions and improved sustainability. By reducing the maintenance demands, extending the service life of asphalt pavements and in MT case reducing the asphalt thickness, this solution addresses the environmental challenges in road construction.

8 Conclusion

With this wide study covering different aspects of asphalt reinforcement and crack control we are demonstrating the performance of steel grids in various contexts. Steel grids in asphalt are, depending on the context we are using them, enhancing bearing capacity, fatigue properties, crack propagation and crack control with the main supplementary properties of not being affected by installation damage or fragile to solicitations. On contrary we have observed a very interesting ductility behaviour on several tests which is demonstrating outstanding sustainability in crack control when crack is already there. This is going one step further in interlayers evaluation than only delaying the crack to appear on top. For the first time we are looking also into crack mitigation by trying to reduce crack width and continue crack control as far as possible in time before maintenance. That makes steel grids a unique solution for renovating roads and an interesting enabler for more environmentally friendly products with long lasting effects especially when thinking that steel could be extracted at end of life and is infinitely recyclable.

References

1. E.G. Williams, Application of wire mesh reinforcement to asphaltic concrete pavement overlays. Highway Materials Res. Lab. Report. Lexington, KY, USA (1954)
2. D. Léonard, A. Vanelstraete, S. Parewyck, Structural design of flexible pavements using steel netting as base reinforcement. International Journal of Geomechanics **2**, 3 (2002)
   https://doi.org/10.1061/(ASCE)1532-3641(2002)2:3(291)
3. M. Sadeghian, E. Vromans, G. Auray, Enhanced evaluation methodology for asphalt reinforcement. In Proceedings of Eurogeo8 conference, Lille, France, 15-18 September (2025) (to be published)
4. P. Dumas, J. Vecoven, Processes reducing reflective cracking: synthesis of laboratory tests. 2th International RILEM Conference on Reflective Cracking in Pavements, State of the Art and Design Recommendations, pages 246–253 (1993)
5. F. Vervaecke, H. Cornelius, P. Straubinger, Performance testing of a steel cord based crack-preventing interlayer. Proceedings of the 7th International Conference Bituminous mixtures and pavements, Thessaloniki, Greece, 12-14 June (2019)
   https://www.taylorfrancis.com/chapters/edit/10.1201/9781351063265-80/performance-testing-steel-cord-based-crack-preventing-interlayer-vervaecke-cornelus-straubinger
6. BEFIM, Projet National IREX, Recommandations techniques pour la conception et la réalisation des dallages en béton de fibres métalliques, CSTB, February (2002)

Application of geosynthetics in linear concrete pavements improved by adding carbon nanotubes CNTs

Mouloud Abdessemed[1*], *Noureddine* Ouadah [1]

[1]Laboratory of Geo-Materials and Civil Engineering, University of Blida1, Algeria

Abstract. Geosynthetic products such as geogrids, despite their various uses, cannot alone improve the stiffness, or ductility, of pavements when used for reinforcement. this paper studies the behaviour of cement concrete slabs enhanced with carbon nanotubes (CNTs) in addition to geogrids application. Experimental work was carried out in the laboratory, on small-scale slab models simulating real rigid road or airfield pavements. All these slabs were mechanically tested to failure under monotonic loading using a "four-point" bending test. In order to calibrate the experimental results obtained, a numerical analysis was conducted using the finite element method using appropriate commercial software. The results showed that CNTs significantly improve the mechanical properties of modified concrete, with a strength gain of 40%. Hybrid combinations (CNT-enhanced concrete + geogrid), showed improvements in breaking strength, stress, strain, and Young's modulus, by 40% to 70%, which shows the applicability of the hybrid combination used, offering considerable gains in stiffness and ductility and can be beneficial in ensuring the longevity of rigid pavements, with savings in their long-term maintenance.

1 Introduction

Linear infrastructures, such as roads, freeways and airstrips, are an important driver of economic development, given the services they provide for passenger, vehicle, urban and public transport traffic [1]. This is why these infrastructures must meet the needs of the population [2]. To achieve this, it is essential to keep these infrastructures in optimum condition, through ongoing maintenance and, where necessary, rehabilitation, so that they remain efficient, durable and usable for traffic services [3, 4]. The most common types of linear infrastructure are rigid or flexible road and/or airport pavements, characterized by a pavement body composed of sub-layers capable of withstanding traffic loads and various internal and external stresses [5]. Road and/or airport pavements are subjected to excessive traffic loads, due to passing vehicles, exceptional road loads and aircraft weights (during take-off and landing). This leads to deformations and potential stresses in the pavement, resulting in harmful growths of deterioration, such as cracking in heavily stressed areas.
This is why it is increasingly necessary to protect these pavements by applying reliable, effective rehabilitation techniques. Among these reinforcement techniques, those known as

* Corresponding author: abdesmoul@yahoo.fr

"geosynthetic products", and more specifically geogrids, have proved to be an appropriate solution for repairing damage to rigid pavements and thus increasing their ductility [6, 7]. Other types of reinforcement have also been used successfully, such as the insertion of fibers with plastic residues, bars and metal meshes [8, 9]. Numerous experimental studies, both in situ and in the laboratory, have demonstrated the ability of geogrids to improve the structural performance of pavements thanks to their higher modulus of elasticity, as well as their ability to retard the propagation of reflection cracks. Other researchers have shown that the addition of carbon nanotubes (CNTs) at a volume fraction of 0.005 to 0.02% to concrete improves the latter's strength by at least 20%, thus reducing the energy dissipated [10].

This paper presents a study on the effect of the behavior of rigid cement concrete slabs modified by the insertion of carbon nanotubes (CNTs) and reinforced with layers of geogrids. This is experimental laboratory work involving the production of small-scale slabs (simulating rigid pavements), 400 x 400 x 50 (mm) in size. The aim of this work is to analyze the effect of nanotubes, at different percentages, on the behavior of manufactured slabs (reinforced or unreinforced), by determining stresses and strains at the most stressed points, which will give a good idea of the expected improvements.

2 Experimental program

In this study, four-point mechanical bending tests are envisaged on cement concrete slab samples, with enhanced mechanical properties via the addition of CNTs (0.005 wt.%) (Figure 1), and the incorporation of geogrid layers positioned at one-third and two-thirds depths from the underside of the slab tested. The CNT dosage was selected based on prior research [11]. A total of 20 slab specimens were fabricated, divided into two batches: Batch 1 comprised ordinary cement concrete slabs (without CNTs), while Batch 2 included cement concrete modified with 0.005 wt.% CNTs. Each batch featured slabs reinforced with one or two geogrid layers (Table 1).

2.1 Materials used

The materials used were cement concrete, CNT nanotubes and two types of geogrid. All these materials were selected on the basis of test conditions, availability of equipment and instrumentation, and compliance with standards [12]. For the concrete composition, CEM IIA 42.5 cement was used, with aggregates crushed to a maximum size of 15 mm, as well as fine limestone aggregates to form the samples [13]. The water/cement ratio (w/c) was 0.52. Additives (plasticizer and trainer) were added to achieve a high slump and ensure adequate contact and interaction with the added nanotubes and geogrid. The composition (per $1m^3$ of concrete) of the mix used is detailed in Table 2. The compressive strength of the concrete, measured on day 28, is 35 MPa.

The composition of the concrete was modified to improve it, by inserting CNT nanotubes, with a percentage of 0.005%. The nanotubes used were of the "Multi-walled carbon nanotubes MWCNT's" type [14]. Two types of geogrid were used, G1 and G2 (Figure 2), as shown in Figures 2a and 2b. Type "G1" is a woven glass fiber grid, while type "G2" is a non-woven glass fiber grid [15].

While prior studies recommend geogrids "manufactured via extrusion, punching, and flooding processes", glass fiber geogrids (GFGs)—whether woven or non-woven— are widely adopted materials for attenuating reflection cracks in semi-rigid or rigid asphalt pavements, with a few optimizations for adequate pavement treatment (pavement wearing

courses)][16]. In this study, we further optimized the system by integrating CNTs, leveraging their synergistic benefits with geogrids to enhance the stiffness of the hybrid "Geogrid-CNT" reinforcement, consistent with findings in our earlier research (Khengaoui et al. in 2024 [9] and Guirous et al. in 2024 [10].

Table 1. Nomination and identification of tests.

Number	Type of concrete	Type of reinforcement	Appointment	Location
01	Ordinary	Without	BB	-
02	Modified	Without	BM	-
03	Ordinary	One layer grid G1	BG1	1/3 of the base
04	Modified	One layer grid G1	MG1	1/3 of the base
05	Ordinary	One layer grid G2	BG2	1/3 of the base
06	Modified	One layer grid G2	MG2	1/3 of the base
07	Ordinary	Two layers grids G1	BG1G1	1/3 and 2/3 of the base
08	Modified	Two layers grids G1	MG1G1	1/3 and 2/3 of the base
09	Ordinary	Two layers grids G2	BG2G2	1/3 and 2/3 of the base
10	Modified	Two layers grids G2	MG2G2	1/3 and 2/3 of the base
11	Ordinary	Two layers grids G1G2	BG1G2	1/3 and 2/3 of the base
12	Modified	Two layers grids G1G2	MG1G2	1/3 and 2/3 of the base

Table 2. Test concrete components.

Constituent	Kg/ m^3)
Cement	350
Sand 0/1	254
Sand 0/3	610
Gravel 3/8	418
Gravel 8/15	659
Water (litre)	182
Plasticizer	37.8
Air entertainer	0.12



Fig. 1. Concrete materials before and after mixing with CNTs.



Fig. 2. Two types of geogrid used, G1 and G2.

2.2 Test procedure and instrumentation

The experimental laboratory study consisted in manufacturing the 24 specimens (slabs) listed, measuring 400 mm, with a span of 360 mm. The distance between the loading points was 120 mm, and the total load (P) was applied via two steel rollers (each applying P/2) at two symmetrically positioned points along the span (Figure 3).

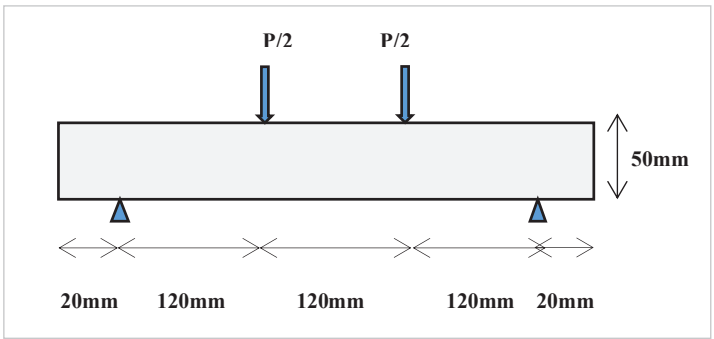


Fig. 3. 4-point bending diagram.

The test was carried out on a servo-hydraulic loop testing machine, using displacement control at a constant rate of 0.04 MP/second, and the loads acting on the slabs were measured using a 600 kN transducer, where each slab is loaded to failure (Figure 4).



Fig. 4. Bending test machine.

The static diagram, before and after slab reinforcement, was chosen to induce flexural failure while respecting the a/h ratio, where a: represents the distance between the support and the point of load application and h: the height of the slab [17]. The physical and mechanical properties of ordinary concrete, CNT nanotubes, modified concrete and the two geogrids used are presented in Table 3.

Table 3. Mechanical properties of materials used in tests.

Property	Unit	Concrete		Geogrid		Nanotubes
		Ordinary	modified	type1	type2	CNTs
Density		2.5	2.5	/	/	1.6
Geometry	mm	400×400	400×400	30×30	30×30	10^{-6}
Elastic modulus	GPa	21	27	750	850	950
Tensile strength	MPa	35	43.5	4200	4800	5000
Elongation at failure	%	-	-	1.8	2.1	-

3 Results and discussion

3.1 Bending results

The first results obtained from the experimental laboratory investigation are presented in Table 4. These are mid-span measurements for all tested slabs under ultimate limit states (force and displacement) during the four-point bending test. In all cases, specimens exhibited ductile failure without tearing or delamination of the embedded geogrid layers, confirming the flexibility of the slab tested and the monolithic behavior of all the constituent materials.

Table 4. Nomination and identification of tests.

Identification slab	Limit force value (kN)	Displacement value (mm)
BB	16.65	0.308
BM	19.95	0.284
BG1	19.82	0.301
MG1	21.25	0.278
BG2	20.04	0.302
MG2	21.32	0.259
BG1G1	20.39	0.264

MG1G1	21.56	0.241
BG2G2	20.55	0.274
MG2G2	21.74	0.247
BG1G2	21.08	0.261
MG1G2	22.12	0.237

Limiting forces for the reference slab in ordinary concrete (BB) were measured at 16.65 kN, compared with 19.95 kN for that in modified concrete (BM), i.e. again, caused by the addition of CNTs, of the order of: 19.85%. Insertion of the G1 geogrid gave values of 19.82 kN and 21.25 kN, respectively, for ordinary and modified concrete, i.e. gains of : 19% for BG1 and 27.63% for MG1.

For reinforcement with G2 geogrid, the values are of the order of 20.04 kN for BG2 and 21.32 kN for MG2, giving percentage gains of 20.36% for ordinary concrete and 28.05% for modified concrete. The application of two layers of geogrids appears to provide greater benefits in terms of the stiffness of the slab tested. In fact, two layers of G1 geogrids, giving values of 20.39kN and 21.56 kN, respectively, for the ordinary concrete slab and the CNTs-modified concrete slab, yielded gains of the order of 22.46% and 29.49%. For the second G2 geogrid, with two layers inserted, the ultimate force values are of the order of : 20.55 kN (ordinary concrete) and 21.74 kN (modified concrete), i.e. gains of 23.42% and 30.57%, respectively. For the last combination (2 different geogrid layers), we found: 21.08 kN (BG1G2) and 22.12 kN (MG1G2), i.e. gains of 26.60% and 32.85%, respectively.

Comparing the reinforcement with grids G1 (BG1) and G2 (BG2), the values are 19.82kN and 20.04kN respectively, representing appreciable percentage gains of : 19.04% and 20.36%. The G2 geogrid appears to perform better than the G1 geogrid, and the proposed reinforcement with just one layer of geogrid gives a significant gain of around 20%. For modified concrete, the reinforcement provided by these geogrids is of the order of : 21.25 kN for MG1 and 21.32 kN for MG2, i.e. percentages of : 27.63% and 28.05%. We can see that it is very useful to use concretes improved by the addition of CNTs in addition to geogrid reinforcement. When reinforced with these two geogrids, displacements are not overly influenced.

For displacements, the maximum value was found to be 0.308 mm, for the reference beam (unimproved concrete), while that of the CNTs-improved concrete was of the order of 0.284 mm, i.e. a reduction of 7.80%. For slabs reinforced with a geogrid layer, we found values of: 0.301 mm (for BG1), 0.278 mm (for MG1), i.e. reductions of 2.28%, for the former and 9.74% for MG1 (inserting G1 geogrid and CNTs nanotubes). Also, for the G2 geogrid, with gains in displacement reduction of the order of : 1.95% (BG2) and 15.91% (MG2). For reinforcement with two layers of geogrids, the values found for “G1G1” were: 0.264 mm (ordinary concrete) and 0.241 mm (improved concrete), i.e. a reduction of 14.28% and 27.80%, respectively. Similarly, for double reinforcement with G2 geogrid, or values of: 0.274mm (for BG2G2), i.e. a gain of 11.04% and 0.247mm (for MG2G2), i.e. a gain of 19.81%. Finally, for the combination (G1-G2), the values are of the order of: 0.261mm (for BG1G2), i.e. a gain of 15.26% and 0.237mm (for MG1G2), i.e. a gain of 23.05%.

3.2 Dissipation energy evaluation

Table 5 below shows the dissipation energy values for all slab types, with the various combinations applied. These values confirm the advantage of slabs with improved (modified) concrete over slabs with ordinary concrete, as well as the advantage of slabs reinforced with two layers of geogrid, over unreinforced slabs or slabs reinforced with only one layer of geogrid.

In fact, the dissipation energy for the reference slabs is of the order of 2.56 kN-mm (ordinary concrete slab) and 3.83 kN-mm (modified concrete slab), giving a 49.61% greater stiffness. The geogrid, with a layer (G1 or G2), appears to have no influence on the slab for concrete modified with CNTs, with average stiffness gains of 14%, compared with influences (for ordinary concrete) of an average value of 20.51%. CNTs inserted in the concrete give certain flexibility to the slab tested [18].

Table 5. Nomination and identification of tests.

Number/ slab	Identification slab	Dessipated energy (kN-mm)
01	BB	2.56
02	BM	2.83
03	BG1	2.98
04	MG1	2.95
05	BG2	3.19
06	MG2	2.76
07	BG1G1	2.69
08	MG1G1	2.60
09	BG2G2	2.82
10	MG2G2	2.68
11	BG1G2	2.75
12	MG1G2	2.62

In the case of double reinforcement (two layers), the insertion of nanotubes does not provide any additional stiffness for the slab tested, where the values are of the order of : 2.60 kN-mm (gain of 1.56%) for MG1G1, 2.68 kN-mm (gain of 4.69%) for MG2G2 and 2.62 kN-mm (gain of 2.35%) for MG1G2. Double-reinforced geogrids, on the other hand, gave greater stiffness, with ordinary concrete, for the slab tested, with an average energy dissipation of 2.75 kN-mm, a gain of 7.5%.

3.3 Elastic modulus measurement

Young's modulus values at the elastic phase of each load-displacement evolution (Figure 5) [19], show that this modulus varies according to the type and number of geogrids and the composition of the concrete used. For ordinary concrete (BB), the slabs gave an E value equal to 54.06 kN/mm², compared with 70.25 kN/mm² for the modified concrete (BM) slab, an increase of 29.95%. Similarly, for slabs reinforced with a G1 geogrid layer, we found values of 65.85 kN/mm² (BG1) and 76.44 kN/mm² (MG1), i.e. a gain of 16.10%, compared with an increase of 30.62% (for reinforcement with G2 geogrid). Double reinforcement gave increases, between ordinary and modified concrete, of : 15.82% (reinforcement with two layers of G1), 17.36% (reinforcement with two layers of G2) and 15.56% (combined reinforcement with layers of G1 and G2.

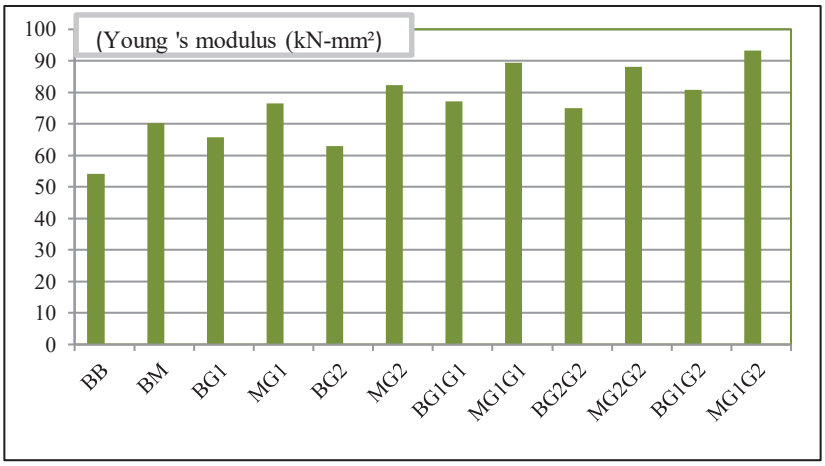


Fig.5. Elastic modulus values for slabs tested.

4 Conclusion

The study conducted on the application behavior of geosynthetics (geogrids) in rigid slabs (simulated to concrete pavements), improved by the addition of carbon nanotubes CNTs, led to the following conclusions:

- The experimental study carried out on a series of 24 concrete slabs, reinforced with different types of geogrids and 0.005% CNTs, was able to simulate the behavior of rigid pavements, statically loaded to failure;
- The application of innovative products such as geogrids, combined with carbon fiber-based nano-composites, shows that promising results can be obtained, with gains of up to 40% in terms of ultimate strength and/or maximum displacement;
- The “hyride” combination of geogrid sheets + CNT nanotubes is a highly effective alternative solution, and can replace traditional methods that are costly and require large-scale layouts;
- Calculations of the dissipation energies of the various slabs tested showed a slight increase in flexural rigidity, especially for slabs made of modified concrete (addition of CNTs) and/or reinforced with geogrid sheets;
- Ultimate forces (see rupture), stresses, strains and Young's modulus were increased by 40% to 70%, compared with the reference values, showing that the insertion of geogrids, combined with concrete modified with CNTs, is highly beneficial for the rehabilitated pavement;
- The results of this laboratory study can be put to practical use, given the considerable gains in rigidity (see ductility) and can be beneficial in ensuring the longevity of rigid infrastructures (roads, airfields), thus guaranteeing savings in their long-term maintenance.

The authors would like to thank all those who helped them and made the task of carrying out the investigations in the experimental part easier, as well as those who provided the geosynthetic products. Master2 students: Bouzar Yahia, for his contribution to the experiment, and Abdessemed Anfel. N. Houda, for his contribution to the formatting and verification of the article's content.

References

1. S. Polyzos, D. Tsiotas, The contribution of transport infrastructures to the economic and regional development. Theor.and Emp.Resear.in Urb. Manag.**15(1),** 5-23 (2020).
2. N. Kaiser, C.K. Barstow, Rural transportation infrastructure in low-and middle-income countries: a review of impacts, implications, and interventions. Sustain.**14(4)**, 2149 (2022).
3. J. Santos, C. Torres-Machi, S. Morillas, V. Cerezo, A fuzzy logic expert system for selecting optimal and sustainable life cycle maintenance and rehabilitation strategies for road pavements. Intern. J.of Pav. Eng. **23(2)**, 425-437 (2022).
4. M. Mohamed, A. Mouloud, Experimental study of the behavior of light embankments made of a new polystyrene reinforced by a polyglass geo-membrane. Rev. Rom. de Mater. **53(1**), 73-81 (2023).
5. L. Žiliūtė, A. Laurinavičius, Traffic Load Impact on the Initiation and Development of Plastic Deformations in Road Asphalt Pavements. The Bal; J. of Road & Brid. Eng. **8(3)**,220-226 (2013).
6. M. Abdessemed, S. Kenai, S. Khengaoui, Diagnostic d'une Infrastructure Linéaire Rigide-Analyse Expérimentale après Renforcement par Geogrilles. Acad. J.of Civ. Eng. **38(2**), 144-148 (2021).
7. A.S. Al-Hedad, M.N. Hadi, Effect of geogrid reinforcement on the flexural behaviour of concrete pavements. Road Mat. and Pav. Des. **20(5**), 1005-1025 (2019).
8. S.A. Altoubat, J.R. Roesler, D.A Lange, K.A. Rieder, Simplified method for concrete pavement design with discrete structural fibers. Cons. and Buil. Mat. **22(3**), 384-393. (2008). https://doi.org/10.1016/j.conbuildmat.2006.08.008.
9. S. Khengaoui, M. Abdessemed, S. Kenai, N. Ouadah, Using a combination of geogrids and steel mesh to improve the performance of concrete pavements: Experimental study and numerical analysis. Rev. Rom. de Mat. **54 (1**), 65-76 (2024).
10. L. Guirous, M. Abdessemed, N. Ouadah, Fracture strength of geogrid-reinforced concrete pavements with carbon-fiber composites insertion. Mat. (Rio de Janeiro), **29(3**), e20240175 (2024). https://doi.org/10.1590/1517-7076-RMAT-2024-0175.
11. M.A. Qissab, S.T. Abbas, Effect of Multi-Walled Carbon Nanotubes on Mechanical Properties of Concrete. Al-Nah. J. for Eng. Sc. **19(2)**, 194-201 (2016).
12. F. Schladitz, M. Frenzel, D. Ehlig, M. Curbach, Bending load capacity of reinforced concrete slabs strengthened with textile reinforced concrete. Eng. Str. **40**, 317-326 (2012). https://doi.org/10.1016/j.engstruct.2012.02.029.
13. J. Zelić, Properties of concrete pavements prepared with ferrochromium slag as concrete aggregate. Cem. and Conc. Res. **35(12**), 2340-2349 (2005). https://doi.org/10.1016/j.cemconres.2004.11.019.
14. A.M. Anwar, M.S. Khalafalla, E.K. Mohamed, Effect of nano-composites on the dynamic properties of repaired flexural elements. Wat. Sc. **32**, 276–286 (2018). http://doi.org/10.1016/j.wsj.2018.07.003.
15. R. Bazine, M. Abdessemed, S. Kenai, N. Ouadah, Experimentation and numerical analysis of the influence of geogrids with emulsion insertion on the behavior of bituminous pavements- Case of Ouargla aerodrome, Mat. de Const. **74**(353), e339-e339 (2024). https://doi.org/10.3989/mc.2024.355723.
16. G. Zhang, H. Zhang, W. Sun, Effect of coating optimization on performances of glass fiber geogrid for semi-rigid base asphalt pavement. Geot. and Geom. **50(2**), 337-346 (2022).

17. M. Abdessemed, Experimental study and modelling of the behaviour of reinforced concrete beams strengthened by composite materials under bending - Case of bridges, Ph.D. thesis, National Polytechnic School of Algiers (2011).
18. O. Noureddine, A. Mouloud, K. Fouad, Static and dynamic behavior of concrete structures reinforced with nanotubes modified composites. Rev. Rom. de Mat. **52(1)**, 26-37 (2022).
19. A. Laichaoui, M. Abdessemed, A. Bali, S. Kenai, The use of carbon fibre composite for strengthening reinforced concrete beams. Stud. in Eng. and Exact Sc. **5(2)**), e11975-e11975 (2024).

SESSION 5 A
SUSTAINABILITY AND DURABILITY (4)

Long-Term Durability of HDPE Geomembranes in Mining: A Non-Parametric Statistical Approach

Beatriz Urashima[1*], *Toru* Inui[1], *Lucas* Deleon[2], *Anderson* Duarte[2], *Denise* Urashima[3] and *Renato* Santos[2]

[1]The University of Osaka, Graduate School of Engineering, Suita Campus, Osaka, Japan
[2]Federal University of Ouro Preto, Graduate Program in Geotechnical Engineering, Ouro Preto, Brazil
[3]Federal Center for Technological Education of Minas Gerais, Graduate Program in Civil Engineering, Varginha Campus, Varginha, Brazil

Abstract. The long-term reliability of geomembranes is essential for maintaining environmental safety and protecting human health, particularly when applied in demanding environments such as mining. This study evaluates the long-term performance of a 2 mm high-density polyethylene (HDPE) geomembrane after 12 years at a gold mining tailings pond in Brazil. As built performance data were unavailable, so analyses were based on GRI GM13 standard. Three samples from various dam locations were analysed using the Kernel Density Estimator (KDE) for non-parametric statistical analysis. The geomembrane's failure probability in terms of tensile strength was 19%, indicating an 81% success rate as a hydraulic barrier. The lowest stress crack resistance (SCR) among samples exceeded the 50% SCR of the GRI GM13 standard. Significant antioxidant depletion was noted in the Standard Oxidative Induction Time (Std-OIT) tests, down to 14% of the minimum GRI GM13 value, while the High-Pressure Oxidative Induction Time (HP-OIT) showed only slight depletion, down to 80% of the minimum GRI GM13 value. Environmental analysis revealed no significant contamination, confirming the geomembrane's effectiveness.

Full paper to be published in:
https://www.e3s-conferences.org/articles/e3sconf/abs/2025/44/contents/contents.html

* Corresponding author: urashimabeatriz@gmail.com

Durability Assessment of HDPE Geomembrane in a Concrete Water Supply Canal: A 10-Year Case Study

Beatriz Urashima[1*], *Toru* Inui[1], *Lucas* Deleon[2], *Denise* Urashima[3] and *Daniel* Meucci[4]

[1]The University of Osaka, Graduate School of Engineering, Suita Campus, Osaka, Japan
[2]Federal University of Ouro Preto, Graduate Program in Geotechnical Engineering, Ouro Preto, Brazil
[3]Federal Center for Technological Education of Minas Gerais, Graduate Program in Civil Engineering, Varginha Campus, Varginha, Brazil
[4]AzulPack TechGround, Barueri, São Paulo, Brazil

Abstract. In 2008, a 1.5 mm smooth high-density polyethylene (HDPE) geomembrane was applied as a lining over 800 m of a concrete water supply canal in southeaster Brazil. This study aims to enhance the understanding of geomembrane durability through a case study of a HDPE geomembrane after 10 years, comparing samples submerged in water with those exposed to weather. Mechanical parameters such as tensile strength, tear resistance, and puncture resistance were tested and compared to GRI GM13 standard. Submerged samples primarily faced mechanical damage risk from debris, while weather exposed samples suffered mainly from mechanical, thermal and UV degradation. Results indicated that all parameters for submerged samples exceeded GRI GM13 requirements. Conversely, weather exposed samples showed some variations from the values established by the GRI GM13 Standard. Of the 11 parameters tested, 7 met the GRI GM13 standards, including tensile strength and tear resistance in both machine (MD) and transverse (TD) directions, and puncture resistance. Only transverse elongation at break showed a 40% reduction in the minimum value of GRI GM13. Most of the parameters for the weather-exposed samples were within 80% of the results for the submerged samples, with the exceptions of the tensile strength and elongation at break-both in transverse direction-, which were within 50%.

Full paper to be published in:
https://www.e3s-conferences.org/articles/e3sconf/abs/2025/44/contents/contents.html

* Corresponding author: urashimabeatriz@gmail.com

Comparative Performance Evaluation of Smooth and Textured White Geomembranes Under UV Exposure

Maria Alejandra Aparicio-Ardila[1*], and *Jefferson* Lins da Silva[1]

[1] São Carlos School of Engineering (EESC), University of São Paulo (USP), São Carlos, Brazil

Abstract. High-density polyethylene (HDPE) geomembranes are widely utilized in environmental protection projects, where they are produced in various colours to meet specific technical requirements. The addition of colour to these geomembranes involves the use of additives other than carbon black, which is traditionally employed for its cost-effectiveness and superior Ultraviolet (UV) protection properties, giving HDPE geomembranes their characteristic black colour. This study examines the degradation of smooth and textured HDPE geomembranes with a white surface. These geomembranes, with a nominal thickness of 1.00 mm, were manufactured using both flat die and round die processes and subjected to accelerated UV aging for 500 and 1000 hours, with the white surface exposed. Physical and mechanical tests were conducted to assess the performance of the geomembranes post-exposure. Initial High Load Melt Index (HLMI) and Low Load Melt Index (LLMI) values indicate differences in manufacturing processes and composition despite both geomembranes achieving similar HLMI values after 500 hours of UV exposure. The textured geomembrane exhibited a significant reduction in strain at break, likely linked to its high standard deviation, a typical characteristic of textured geomembranes. Despite these differences, both geomembranes subjected to accelerated ageing exceeded the minimum tensile property requirements specified by the GRI-GM13.

Full paper to be published in:
https://www.e3s-conferences.org/articles/e3sconf/abs/2025/44/contents/contents.html

* Corresponding author: maparicio@usp.br

Service life of a bituminous geosynthetic barrier: accelerated ageing tests

Wilma Hahn[1*], *Robin* Kroh[1], *Helmut* Zanzinger[1], *Anja* Armani[1], *Bertrand* Breul[2], and *Edgar* Doledec[2]

[1]SKZ – Testing GmbH, 97076 Würzburg, Germany
[2]IKO-Axter, 75009 Paris, France

Abstract. For decades bituminous geosynthetic barriers (GBR-B) are widely used in geotechnical applications such as barriers against different liquids. Detailed knowledge about the longevity and therefore the service life of GBR-Bs is not available to the same extent as it is for other geosynthetic products, such as polymeric geosynthetic barriers (GBR-P). In this study, a SBS stabilized GBR-B and its components are subjected to accelerated ageing with various ageing conditions: oven ageing and leaching tests in water at different elevated temperatures. Quality-determining mechanical, physical and chemical properties are monitored during the entire ageing process, i.e. tensile tests, flexibility at low temperatures, flow resistance at elevated temperatures, ring and ball tests and water permeability tests. Also, dynamic mechanical analysis (DMA) was performed to gain an additional evaluation of the progress of ageing of the bitumen component in a GBR-B. The geotextile component was subjected to hydrolysis and tested by tensile tests. The test program performed in this research covered the test procedure for GBR-Bs according to EN 13361:2018, regarding leaching and resistance to oxidation for a service life of 50 years. All requirements were fulfilled, as the PET fibres of the nonwoven geotextile (GTX-NW) were well surrounded with bitumen and therefore well protected against hydrolysis attack. Even at higher temperatures and after longer durations of ageing, the evaluated GBR-B still fit the requirements stated in the standard, which opens a discussion about an even longer service life of GBR-Bs beyond 50 years.

1 Introduction

Bitumen has been used for waterproofing purposes since the real beginning of developed human civilization. At the real beginning it was used in the natural form [1]. The first idea to produce the composite reinforced prefabricated product came in the last century. Within the needs of better properties for this composite structure usage the need of an improvement appeared. Because of industrial production there was a need to start to use distilled bitumen [2]. Then the first step of modification of the distilled bitumen for the usage in prefabricated panels was the oxidation of the bituminous blend. In the middle of the 20th century, the first idea of modification of bituminous blend by additives came. This resumed, in the seventies, on the modification by elastomeric additives [3]. That established the base for the massive

* Corresponding author: w.hahn@skz.de

usage of composite prefabricated bituminous membranes in the construction and waterproofing activities [4]. On this base, the principle of modern bituminous composite geomembranes has been formulated. Nowadays the bituminous geomembranes (GBR-B) are being successfully used at numerous jobsites. GBR-B can be prescribed in a wide range of applications, where the conditions are more and more critical due to climate change, project remote locations, project specifications, et cetera [5]. As the amount of GBR-B used in the world increases, new questions are being brought to the civil engineers' and contractor's attention, mostly on its service life and technical properties limits. This study is positioned as a deepening of the GBR-B ageing and technical properties behaviour under oxidation and hydrolysis.

At the moment, the durability of a BGM is measured in terms of how its key components, namely the polyester geotextile and the bitumen, maintain their mechanical properties and low permeability over time under operating conditions [6]. Also, actual CE marking, through geomembranes application standard, requires oxidation (EN 14575) [7] and UV exposure (EN 12224) [8] testing to evaluate the durability of the product.

The application of a geomembrane as bottom lining in a Heap Leach Pad or in a deep reservoir request different kind of performances that GBR-B are complying to. GBR-Bs will not face the same chemical environment and/or strain from one site to the other. Even applied on a canal, the submerged part of the GBR-B will age differently than the exposed part located on the crest or the berm [9]. It is common for manufacturer to extend GBR-B warranty from 10 years if exposed and up to 20 years if covered, to reflect the stability and performances of the product. But the structures waterproofed with GBR-B are likely to be in full function much longer. This is the reason why we need to understand the GBR-B ageing mechanism in the different conditions.

A better knowledge of this factor could help the industry by considering the GBR-B's real limit of use and aim new research on the improvement of this measured durability. And harsher testing environments should be already given a thought as the conditions on sites will continue decrease. But many ancient achievements, including the Tigre at Assur (Mesopotamia) dikes, still bear witness to the exceptional longevity of bitumen, like other noble materials such as stone, iron or wood. So hopefully, continuous developments on GBR-B will allow the technology to surpass those new threats and keep the wind in the bow.

2 Experimental part

2.1 Material investigated

The principle of a Bituminous Geomembranes (GBR-B) is like roofing membranes and are, in some ways, still related to them. The product's main structure is based on a reinforcement which can be, either a combination of a non-woven polyester geotextile (GTX-NW) associated with a glass fleece (to maintain the width of the geomembrane during its impregnation at a high temperature), or a single composite reinforcement made with glass and non-woven polyester fibres (see Fig. 1). Reinforcements are completely impregnated with a bituminous compound (bitumen, elastomer and filler). The top of the structure is sanded to provide grip for installation workers. On the bottom is a terephthalic film to limit perforation of any vegetation roots through the geomembrane. For this study, a single reinforcement product has been used [10].

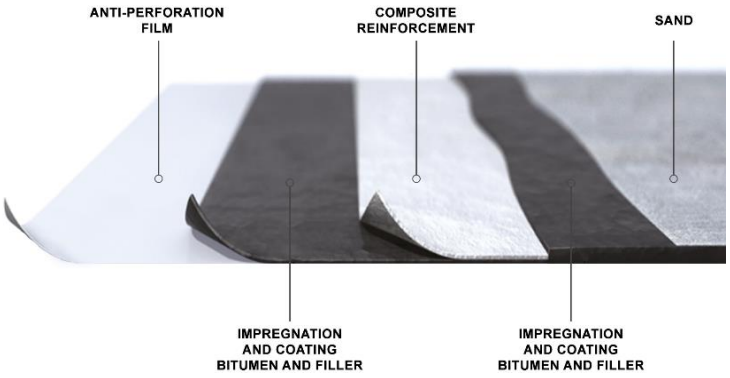


Fig. 1. Single reinforcement Bituminous Geomembrane typical cross-section

The mechanical resistance of GBR-B is provided by its polyester fibres (polyester is resistant to temperatures up to 230 °C compared to polypropylene geotextile generally resistant to temperatures below 120 °C). The watertightness and durability are guaranteed by impregnating and coating the reinforcement with the bituminous blend. These layers ensure the protection of the reinforcement against potential negative impact of the environment where the bituminous geomembrane was installed. These coating layers ensure also the possibility of seaming the geomembrane panels to each other to obtain a continuous waterproofing surface. The composite structure of the bituminous membrane, together with the proper combination of mechanical resistance of the reinforcements and viscoelastic behaviour of the SBS-modified bituminous blend gives the excellent fatigue behaviour which became the base for the worldwide successful exploitation, especially when harsh conditions could be expected.

2.2 Accelerated ageing tests

Determination of resistance to oxidation of the GBR-B was carried out according to EN 14575 [7] in an WTB Binder oven. The ageing was performed at 60 °C, 70 °C and at 80 °C. Ready-to-test specimens were stored. The properties of the aged samples were compared to properties in as-delivered state (ADS).
The determination of resistance to leaching of the GBR-B was carried out according to EN 14415, method A [11]. The tests were carried out in osmosis water at test temperatures of 50 °C, 60 °C and 70 °C. The medium was stirred continuously and replaced after every 14 days. Ready-to-test specimens were stored. To avoid additional thermal impact, no redrying in oven was performed.
The determination of resistance to hydrolysis in water of the GTX-NW was carried out according to EN 12447 [12], in osmosis water at 70 °C. The medium was stirred continuously and not replaced. Ready-to-test specimens were stored for a total of 28 days.

2.3 Index tests in ADS and after ageing

Tensile tests on the GBR-B were carried out according to EN 12311-1 [13] using a universal testing machine by Zwick. The tests were performed in machine direction (MD) with five specimens for each ageing condition. The strain was measured by an optical extensometer. Test speed was 50 mm/min.

Tensile tests on the GTX-NW were carried out according to EN 29073-3 [14] using a universal testing machine by Zwick. The tests were performed in cross machine direction (CMD) with each six specimens in ADS and after ageing. Test speed was 100 mm/min.

Determination of flexibility at low temperature of the GBR-B was carried out according to EN 1109 [15]. Five specimens were tested in MD at each ageing condition. In ADS, the failure temperature was determined. After aging, the test was performed only at the determined temperature.

Determination of flow resistance at elevated temperature of the GBR-B was carried out according to EN 1110 [16] in a WTB Binder oven. Specimen size was 100 mm x 50 mm. In ADS, the failure temperature was determined. After ageing, the test was performed at the expected failure temperature and if necessary, at up to two further temperatures.

The determination of water flow rate of the GBR-B was carried out according to EN 14150 [17] with a volume measurement device type B.

Determination of softening temperature (ring and ball temperature) of the bituminous binder was carried out according to EN 1427 [18]. For this test, semi-finished products were made by moulding hot bituminous binder in a plate-shaped form.

Dynamic mechanical analysis of the GBR-B was performed according to EN ISO 6721-1 [19], using the DMA/SDTA 861 instrument from METTLER TOLEDO. For the load type, the corresponding specimen holder provided by the manufacturer was used. Prior to the measurement, the respective specimen to be examined was placed in the fixture, fixed and cooled down to the starting temperature in the closed specimen chamber. A sinusoidal load with a specified force amplitude of max. 20 N was then applied to the specimen with a frequency of 1 Hertz. The resulting, also sinusoidal, variation of specimen strain and its phase shift δ with respect to the applied force were recorded and used to calculate the dynamic storage modulus E'. Over the course of the measurement, the sample chamber was heated from -20 °C at a heating rate of 2 K/min to +100 °C. To reduce the values determined, only the mean value of E' between 25 °C and 40 °C was calculated for this investigation (see Fig. 2.).

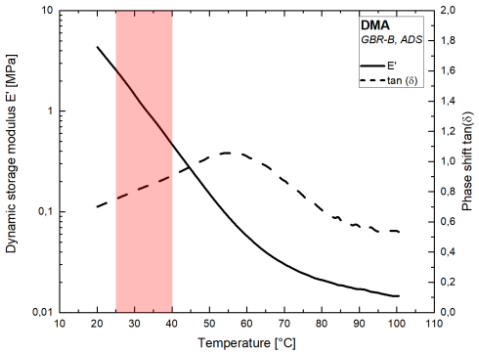


Fig. 2. Example for the evaluation of dynamic storage modulus E' of the GBR-B in ADS in a temperature range between 25 °C and 40 °C.

3 Test results

3.1 Evaluation of test results with the requirements of EN 13361:2018

In Tab. 1 the requirements of EN 13361:2018, annex A, table A.7 and A.8 [20] regarding a service life of 50 years are compared to the test results obtained in this investigation.

Table 1. Ageing tests according to EN 13361:2018 for a service life of 50 years.

Property	Test conditions	Requirement according to EN 13361:2018, table A.7 + A.8	Assessment for a service life of 50 years

Resistance to leaching	56 days in water at 50 °C	Ring and ball > 100 °C (on elastomeric bituminous binder)	fulfilled 115 °C
		Change in tensile strength and change in elongation at break in MD < 25%	fulfilled strength: -3 % elongation: +3 %
	28 days in water at 80 °C	Residual tensile strength in MD ≥ 50% (only GTX-NW)	not fulfilled * strength: -98 %
Resistance to oxidation	180 days in air at 70 °C	Ring and ball ≥ 90 °C (on elastomeric bituminous binder)	fulfilled 107 °C
		Change in tensile strength and change in elongation at break in MD < 25%	fulfilled strength: +6 % elongation: -12 %
		Flexibility at low temperatures ≤ -5 °C	fulfilled ≤ -40 °C
		Flow resistance at elevated temperatures ≥ 90 °C	fulfilled 100 °C
		Water flow rate ≤ 10^{-5} m³/(m²·d)	fulfilled ≤ 10^{-6} m³/(m²·d)

* The test was performed for 28 days in water at 70 °C in CMD.

As indicated in Tab. 1, the requirements regarding a service life of 50 years, in the means of resistance to leaching and oxidation, were fulfilled for the GBR-B and its elastomeric bituminous binder, except for the GTX-NW.

Microbiological resistance and weathering resistance are not part of this investigation.

3.2 Evaluation of test results at more severe test conditions

In Tab. 2, the obtained test results were evaluated with requirements of EN 13361:2018, annex A, table A.7 and A.8, but more severe test conditions were applied, i.e. increased test temperatures, and longer test durations.

Table 2. Assessment of the requirements of EN 13361:2018 with more severe test conditions.

Property	Test conditions	Requirement according to EN 13361:2018, table A.7 and A.8	Assessment for a service life of 50 years
Resistance to leaching	56 days in water at **60 °C**	See Tab. 1	fulfilled **
	56 days in water at **70 °C**		
	112 days in water at 50 °C		
Resistance to oxidation	180 days in air at **80 °C**		
	392 days in air at 70 °C		

** Water flow rate after 392 d oxidation at 70 °C was not tested.

As indicated in Tab. 2, the requirements of EN 13361:2018, annex A, table A.7 and A.8 with more severe test conditions, in the means of increased test temperatures or test durations, were fulfilled for the GBR-B and its elastomeric bituminous binder. Only water flow rate of the GBR-B after 392 days oxidation at 70 °C has not been tested.

The resistance to hydrolysis of the GTX-NW at severe test conditions was not included in this test program, as the actual requirement regarding a service life of 50 years (see Tab. 1) was already not fulfilled.

4 Discussion

4.1 Discussion of test results compared to the requirements of EN 13361:2018

The investigated GBR-B and its elastomeric bituminous binder fulfils the requirements of EN 13361:2018 for a service life of 50 years related to leaching and oxidation as the main degradation mechanisms. No significant change in mechanical and hydraulic properties of the GBR-B and its elastomeric bituminous binder were detected at the test conditions stated in Tab. 1.

Instead, a significant drop in tensile properties after a short test duration (see Tab. 1) was detected for the hydrolysis test of the GTX-NW, failing the requirement of ≥ 50% residual tensile strength in MD after 28 days at 80 °C significantly.

In Fig. 3 the residual tensile strength of the GTX-NW for the hydrolysis test at 70°C is compared with the residual tensile properties of the GBR-B after leaching at 70 °C. Both tests were performed in water with the same quality regarding the water grade and in the same type of water basin.

Obviously, the GTX-NW alone is little to not stabilized against hydrolytic degradation, resulting in an almost complete loss of tensile properties after a short test time. In contrast, the GBR-B shows no significant drop in tensile properties at the same test temperature over the same test duration. Even at longer test durations the tensile properties of the GBR-B remain within the requirements of EN 13361:2018.

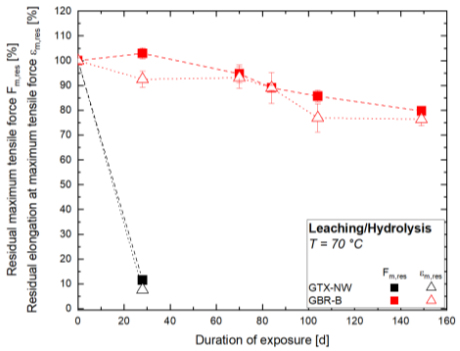


Fig. 3. Residual tensile properties after hydrolysis of the GTX-NW and leaching of the GBR-B at a test temperature of 70 °C vs. duration of exposure.

As the GTX-NW within the GBR-B is largely responsible for the mechanical properties of the composite, especially the tensile properties, it can be assumed that the GTX-NW is well protected against hydrolytic degradation by the surrounding elastomeric bituminous binder. The preparation of specimens for tensile testing by stamping leads to fresh cut edges on narrow test specimens, which allow additional water to enter and thus a hydrolytic attack on the PET fibres embedded in bitumen. In the application, GBR-B have a very low proportion of open cut edges due to the large roll widths and water ingress to the PET fibres is therefore generally very limited. Taken this into account, the protection of the GTX-NW by the surrounding elastomeric bituminous binder can be considered even better, leading to the discussion as to whether testing the GTX-NW itself is necessary for the assessment of service life of GBR-Bs.

4.2 Discussion of test results at more severe test conditions

The investigated GBR-B not only fulfilled the requirements of EN 13361:2018 for a service life of 50 years, but also showed good performance regarding leaching and oxidation at even more severe test conditions.

Regarding leaching in water, additional testing was performed at 60 °C and 70 °C for 56 days, which represents an increase of test temperature by 10 K and 20 K respectively, compared to the requirements of EN 13361:2018. Also, the test duration was increased by doubling the required test duration of 56 days to a total of 112 days. In all cases of leaching in water at more severe test conditions, the requirements regarding change in tensile properties (< 25%) of the GBR-B and softening temperature (> 100 °C) of the elastomeric bituminous binder were fulfilled. Even by increasing the test temperature by 20 K up to 70 °C with simultaneous increasing the test duration up to 150 days, the tensile properties only decreased within the requirements of EN 13361:2018 (see Fig. 3).

In addition to leaching tests, the resistance to oxidation of the GBR-B and its elastomeric bituminous binder was investigated with more aggressive test conditions compared to those indicated in EN 13361:2018. Similar to the leaching tests in water, the test conditions for the oxidation tests were adapted by increasing the test temperature (from 70 °C to 80 °C) and the test duration (from 180 days to 360 days). In both cases the quality-determining properties of the GRB-B, i.e. tensile properties, flexibility at low temperature, flow resistance at elevated temperature and water flow rate, showed no change or only increased or decreased within the requirements of EN 13361:2018. Also, the softening temperature (ring and ball) of the elastomeric bituminous binder after oxidation was above the required 90 °C. The water flow rate after testing at 70 °C for 392 days has not been tested.

In summary, it can be shown that the mechanical and hydraulic functionality of the GBR-B can be maintained after leaching and oxidation tests with significantly more severe test conditions than indicated in EN 13361:2018. This opens the discussion, whether the requirements of EN 13361:2018 are still applicable, or whether a service life of more than 50 years, regarding leaching and oxidation, should be considered for comparable GBR-B. If one assumes that the requirements of EN 13361:2018 guarantee a service life of 50 years, then a service life of 100 years may be possible with testing at double the test duration or with a temperature increase of 10 K or even 20 K, as it's done within the standardization of geotextiles and geotextile-related products, e.g. EN 13252:2016 [21].

Obviously, there is an upper temperature limit for bituminous geosynthetics. Also test durations should be economical. However, the test results obtained show that the investigated GBR-B far exceeds the requirements regarding service life, thus the improved performance should be considered in the standardization.

4.3 Service life estimation by Arrhenius extrapolation

In order to substantiate the results from the oxidation and leaching tests of the GBR-B for a service life of 50 years and beyond, additional evaluation based on the Arrhenius approach was performed. As some tests are still ongoing, the following observations are based on interim results from the oxidation tests in air. Furthermore, only elongation is considered, as the tensile force of the GBR-B showed no significant change during oxidation so far.

In Fig. 4, left the residual elongation at maximum tensile force of the GBR-B during oxidation in air at different test temperatures and its linear regression lines is presented graphically. Also, the failure criterion of 75% residual elongation at maximum tensile force is indicated, which equals a change of < 25% in tensile properties according to the requirements of EN 13361:2018.

In Fig. 4, right times-till-failure, which are the intersection points of the linear regression lines with the failure criterion (see Fig 4, left), are plotted logarithmically (Arrhenius-typical) against inverse temperature. Also, linear regression of times-till-failure and the resulting

Arrhenius-extrapolation to lower temperatures is shown. At a temperature of 20 °C, which represents a standard application temperature for geosynthetic barriers, the extrapolated service life is approximately 150 years (for now), which fortifies the assumption in section 4.2 regarding a service life of beyond 50 years and even 100 years, at least for the oxidative degradation of the GBR-B in air.

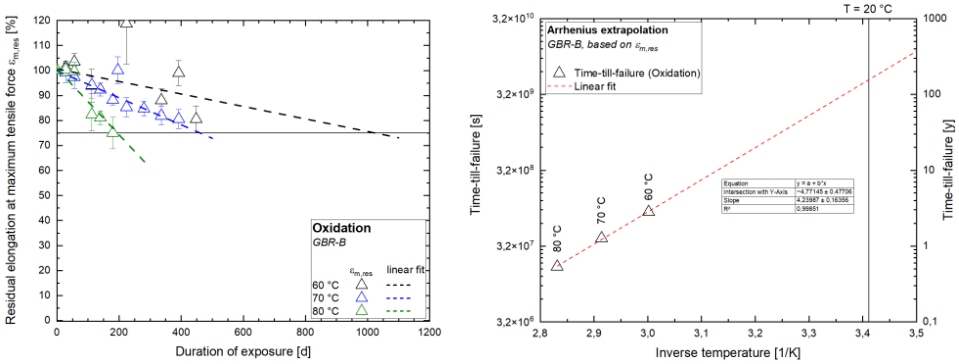


Fig. 4. $\varepsilon_{m,res}$ of the GBR-B after oxidation at 60 °C, 70 °C and 80 °C with indication of the failure criterion of 75% $\varepsilon_{m,res}$ (left) and (Interim-)Arrhenius extrapolation of times-till-failure based on $\varepsilon_{m,res}$ of the GBR-B after oxidation in air (right)

4.4 Dynamic mechanical analysis (DMA) of the GBR-B

In addition to the determination of quality-determining properties of the GBR-B and its elastomeric bituminous binder according to EN 13361:2018, DMA was performed on the GBR-B in ADS and after ageing to obtain an alternative parameter for the degradation of the GBR-B, especially for the embrittlement of the bituminous component of the GBR-B. The dynamic storage modulus in a temperature range of 25 °C to 40 °C was evaluated.

In Fig. 5 the residual tensile properties and the dynamic storage modulus during oxidation in air at 70 °C and leaching in water at 50 °C are presented graphically. As the residual tensile properties of the GBR-B, especially the residual elongation at maximum tensile force only decreases slowly during oxidation in air, the dynamic storage modulus shows a significant increase during duration of exposure, indicating an embrittlement of the bituminous component of the GBR-B even after short test times. For example, after 140 days of oxidation at 70 °C, the tensile properties hardly changed, resulting in a residual maximum tensile force of >100% and a residual elongation of 93% (see Fig. 5, left). In contrast, the dynamic storage modulus increased approximately by a factor of 2.5 from 1.3 MPa in ADS to 3.4 MPa after oxidation, indicating a decrease in flexibility of the elastomeric bituminous binder.

An increase of the dynamic storage modulus of the bituminous component also occurs during leaching in water (see Fig. 5, right), while tensile properties remain unaltered, indicating a change in flexibility of the elastomeric bituminous binder like the observations during oxidation.

As already indicated, after oxidation and leaching according to the requirements of EN 13361:2018 and with even more severe test conditions, the quality-determining properties of the GBR-B and its elastomeric bituminous binder still fulfils the requirements regarding longevity and service life. Nevertheless, DMA, especially the dynamic storage modulus, can give an additional parameter for the embrittlement of the bituminous component of the GBR-B, as quality-determining properties like tensile properties are mostly influenced by the reinforcement, e.g. GTX-NW, within the GBR-B. Also, embrittlement of the bituminous component can be tested on the GBR-B itself, avoiding additional testing on the elastomeric bituminous binder only.

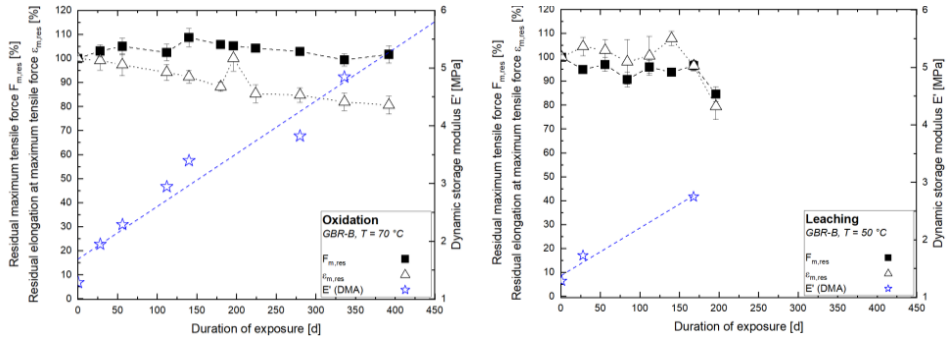


Fig. 5. Residual tensile properties and dynamic storage modulus during oxidation in air at a test temperature of 70 °C (left) and leaching in water at a test temperature of 50 °C (right).

5 Summary & Outlook

The investigated GBR-B easily fulfils the requirements of EN 13361:2018 regarding a service life of 50 years based on oxidation in air and leaching in water. Even with more severe test conditions, i.e. increasing the test temperature by 10 K and even 20 K or extending the test duration, the quality-determining properties of the GBR-B still complied with the requirements of EN 13361:2018. This opens the discussion as to what extent this increased performance of comparable GBR-B should be considered in future standardization. The obtained results indicate that, based on the requirements of EN 13361:2018, a service life of beyond 50 years is possible. Even a declaration of 100 years is conceivable, which is indicated by Arrhenius extrapolation of test results obtained from the oxidation test in air. Nevertheless, additional investigation regarding the service life, e.g. Arrhenius based evaluation of data from the leaching tests in water, is needed to affirm a service life of beyond 50 years or even 100 years.

The GTX-NW of the composite showed hardly any stabilization against hydrolytic attack, resulting in a complete loss of tensile properties after a short test time. However, the GBR-B itself showed no change in tensile properties at identical test conditions. As mechanical properties of the GBR-B, especially tensile properties, are mostly determined by the reinforcement component, an excellent protection of the GTX-NW fibres by the surrounding elastomeric bituminous binder can be assumed. This opens the discussion as to what extent the GTX-NW component must be tested individually.

As an additional parameter for the embrittlement of the GBR-B, especially the bituminous component, DMA was performed on exposed GBR-Bs after ageing. A steady increase of dynamic storage modulus during oxidation and leaching was obtained, indicating a change in flexibility of the bituminous component with the advantage that testing can be performed directly on the GBR-B and thus not on an extra sample of the elastomeric bituminous binder. To establish DMA as an additional quality-determining parameter for GBR-Bs, further investigation is needed, especially regarding the correlation of DMA with other quality-determining properties of the GBR-B, which are directly influenced by an embrittlement of the bituminous component and are crucial for the mechanical and hydraulic functionality.

References

1. H. Abraham, Asphalts and allied substances, their occurrence, modes of production, uses in the arts and methods of testing, 4th ed., (D. Van Nostrand Company, Inc., New York, 1938)

2. D. Whiteoak,. The Shell Bitumen Handbook, 4th ed., (Shell Bitumen UK., Chertsey, 1990)
3. J. Zhu, B. Birgisson, N. Kringos, Polymer modification of bitumen: Advances and challenges, Eur. Pol. J. **54**, 18 (2014). https://doi.org/10.1016/j.eurpolymj.2014.02.005
4. A. Scuero, G. Vaschetti, Geomembrane sealing systems for dams: ICOLD Bulletin 135, Innov. Infrastruct. Solut.. **2**, 29 (2017). https://doi.org/10.1007/s41062-017-0089-0
5. Design and Application Handbook, (IKO-AXTER SAS, 2025)
6. E. Escobar, N. Daly, B. Breul, An approach to longevity and durability of bituminous geomembranes (BGM), in Proceedings of the GeoAmericas 4 conference, International Geosynthetics Society Conferences, Rio de Janeiro, Brazil, April 26-29 (2020)
7. EN 14575:2005-04 Geosynthetic barriers - Screening test method for determining the resistance to oxidation.
8. EN 12224:2000-09 Geotextiles and geotextile-related products - Determination of the resistance to weathering.
9. N. Touze-Foltz, F. Farcas, Long-term performance and binder chemical structure evolution of elastomeric bituminous geomembranes, Geotex. and Geomem. 45, 121 (2017). https://doi.org/10.1016/j.geotexmem.2017.01.003
10. J. Scheirs, A guide to Polymeric Geomembranes: A Practical Approach (John Wiley and Sons, 2009). https://doi.org/10.1002/9780470748213
11. EN 14415:2004-05 Geosynthetics - Screening test method for determining chemical resistance for landfill applications
12. EN 12447:2021-09 Geotextiles and geotextile-related products - Screening test method for determining the resistance to hydrolysis in water
13. EN 12311-1:1999-09 Flexible sheets for waterproofing - Part 1: Bitumen sheets for roof waterproofing; Determination of tensile properties
14. EN 29073-3:1992 Textiles - Test methods for nonwovens - Part 3: Determination of tensile strength and elongation
15. EN 1109:2013-04 Flexible sheets for waterproofing - Bitumen sheets for roof waterproofing - Determination of flexibility at low temperature
16. EN 1110:2010-12 Flexible sheets for waterproofing - Bitumen sheets for roof waterproofing - Determination of flow resistance at elevated temperature
17. EN 14150:2019-06 Geosynthetic barriers - Determination of permeability to liquids
18. EN 1427:2015-07 Bitumen and bituminous binders - Determination of the softening point - Ring and Ball method
19. EN ISO 6721-1:2019-05 Plastics - Determination of dynamic mechanical properties - Part 1: General principles
20. EN 13361:2018-03 Geosynthetic barriers - Characteristics required for use in the construction of reservoirs and dams
21. EN 13252:2016-10 Geotextiles and geotextile-related products - Characteristics required for use in drainage systems

Durability of three PVC-P geomembranes during two years of accelerated ageing laboratory tests

Guillaume Stoltz[1*], *Julien* Aubriet[1], *Gisèle* Bambara[1], *Laurent* Sauger[2], *David* Chamoley[3],and *Sébastien* Bouteille[3]

[1]INRAE, Aix Marseille Univ, RECOVER, Aix-en-Provence, France
[2]CEREMA, Lyon, France
[3]CETU, Lyon, France

Abstract. PVC-P geomembranes have demonstrated their performance in sealing shallow and medium-depth tunnels. In the case of very deep tunnels, there are additional issues, such as the higher temperature than at the surface. In the case of the future Lyon-Turin tunnel, depths can exceed 2000 meters, which can lead, due to the geothermal gradient, to temperatures exceeding 60°C. In these extreme conditions, the durability of PVC-P geomembranes remains to be demonstrated. Test specimens of three 3 mm thick PVC-P geomembranes, produced by 3 different producers, were placed for 2 years in 5 baths: 3 baths containing water at temperatures of 23°C, 45°C, and 70°C and 1 bath containing a sulfuric acid solution at 45°C and finally a last bath containing a calcium hydroxide solution at 45°C. At different immersion times in these baths (8, 12 and 24 months), test specimens were removed and mechanical tests (traction and static puncturing test) were carried out. Measurements of plasticizer contents were also carried out. The results show that the mechanical properties of the three tested geomembranes remained stable over time, as did the plasticizer dosage measurements.

Full paper to be published in:
https://www.e3s-conferences.org/articles/e3sconf/abs/2025/44/contents/contents.html

* Corresponding author: guillaume.stoltz@inrae.fr

Aging of PVC geomembranes for dams: monitoring of aging and end of service life

Olivier Bory[1*], *Julien* Cintract[1], and *Leslie* Martin[1]

[1]EDF CIH, Savoie Technolac, 4 allée du lac de Tignes La Motte Servolex France

Abstract. The use of PVC-P geomembranes is a classical solution to ensure the watertightness function of a new dam, or to renovate the watertightness of an old dam. This technique is relatively recent in the field of dams. Some dam owners are now confronted with the issues of ageing and end of life of PVC geomembrane. EDF has developed a methodology and a non-destructive tool to monitor the ageing and estimate the remaining service-life of PVC geomembranes. This article presents this methodology, provides feedbacks, and proposes some elements for the analysis of PVC geomembranes' end-of-life for dams. Case studies will be presented.

1 Introduction

Geomembrane is a widespread solution for sealing a dam, for rehabilitations or new constructions.
The use of geosynthetics as water barriers is one of the numerous uses of geosynthetics in hydraulic applications.
According to the bulletin 135 of ICOLD [1], the database (up to 2009) counts more than 250 uses of geomembrane for dams (even more today), with a very large use of PVC-P geomembrane (63 %) compared to other type (LLDPE, HDPE, EPDM, CSPE, PP, CPE, Bituminous,…).
EDF operates more than 50 dams that uses a geomembrane for their watertightness function (both new constructions and rehabilitations). PVC-P geomembranes are also the most common product used. The oldest PVC-P geomembrane, for this owner, is 50 years old, used in 1973 for a dam sealing.

Geomembranes, and more broadly geosynthetics, are products that appeared around the 1960-70s for civil engineering applications. References were few at the beginning, the time for the profession to appropriate, master and develop these products. From the 1990s, they were more widely used, particularly for dams waterproofing rehabilitation. This success can be explained by their good technical and economic performance.
Nevertheless, long-term aging of geosynthetics in real-life conditions has been the subject (until now) of some communication on only a few dams. Far from being exhaustive, we can cite in particular recent publications : [2 - 6].

* Corresponding author: olivier.bory@edf.fr

The evolution of long-term performance on hydraulic structures in real conditions, maintenance needs, end-of-life, were not well known on varied sites and conditions, mainly due to the lack of old references.
For a dam operator, it is useful to monitor and control aging of PVC-P geomembranes installed on dams, in order to accurately assess the future maintenance needs and anticipate the end of life.

Up to date, several dam operators have reached the end of service life of the PVC-P geomembrane and have removed or replaced them.
This paper presents the methodology used by one dam's operator, provides some feedback, and proposes some elements for the analysis of PVC geomembranes' end-of-life for dams.

2 Methodology for PVC Geomembrane aging monitoring

2.1 Relevant properties

The theoretical principles and mechanisms of the aging of PVC materials have been rather well described by numerous authors and papers in literature ([2 - 6] to mention just a few).

For dam application, the most interesting properties to analyze are:
- permeability;
- low temperature behavior;
- tensile and shear strength and elongation;
- static and dynamic puncture;
- joint strength shear and peeling;
- repairability (ability to carry out repairs with resistant welds).

Most of them are quite well correlated with plasticisers'content, which makes it one of the best indicators of PVC-P geomembrane aging. Two correlations content are illustrated on Fig 1.

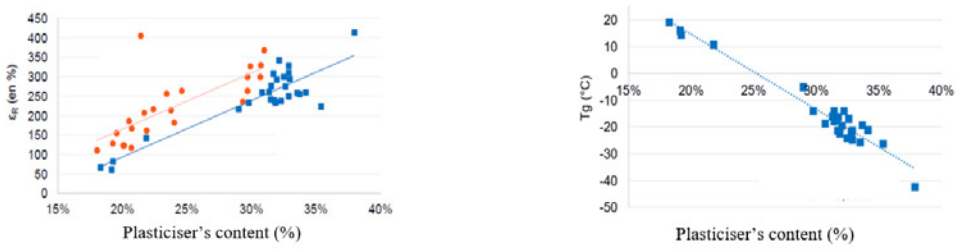


Fig. 1. Relationship between elongation at break ε_R (left) or glass transition temperature T_g (right) and plasticiser's content for different PVC-P geomembranes (data from case studies on EDF dams).

Based on one dam operator's experience, for these different properties, thresholds have been defined below which the density of defects (cracks, tears, …) increased substantially, requiring more maintenance, and decreasing the welding capacity. With the experience accumulated over many years, several categories could be defined (see section 3.4)

2.2 Spatial variation of properties

The durability of geomembrane depends on their weathering properties, and on their resistance to specific loads during service, such as extreme temperatures, frost, freeze/thaw, ice, impacts by floating debris and boats, wind and waves, vandalism etc.

Not all geomembranes have the same behavior due to their different chemistry, basic ingredients, and manufacturing process. That is why, it is important when considering waterproofing dam projects to select a geomembrane that can provide the best performance and the best durability according to the environment in which it will be used.

The properties of a geomembrane (cf. §2.1) can be very heterogeneous between several dams, but also within a single dam. The initial composition and the quality of the geomembrane are obviously crucial points that influence behaviour over time. But also the local atmospheric conditions, water level variation, specificity of the project (support, exposure, …) are various factors that impact local properties.

The case of La Girotte dam (Fig. 2.) illustrates this variability. A PVC-P geomembrane has been installed on this multiple arch dam (on arch V11-12) in 1994. Properties of the geomembrane were measured on different locations (Fig. 3.) in 2018 and shows heterogeneous properties. The geomembrane has reached his end of service life in 2018 and has been removed.

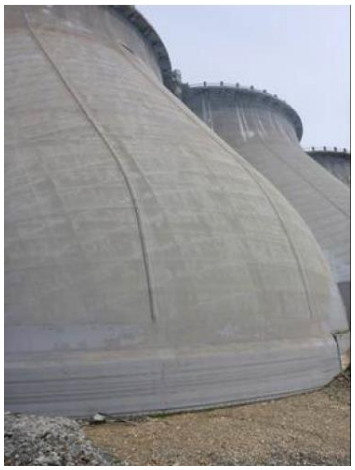


Fig. 2. La Girotte dam, arch 11-12 sealed with PVC-P geomembrane

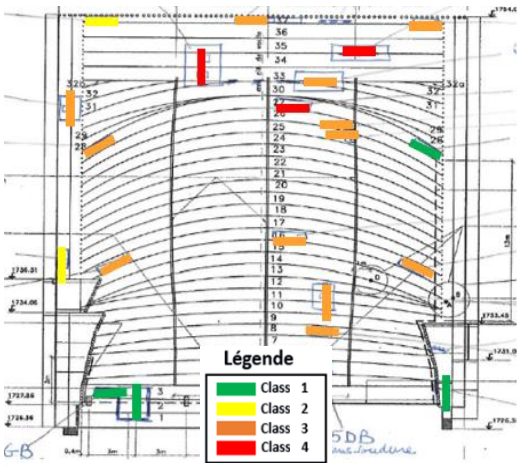


Fig. 3. La Girotte dam, arch 11-12: spatial variability of the properties of the PVC-P geomembrane. Classification of properties from Class 1 (good condition) to Class 4 (poor condition)

To provide the best appreciation of the conditions and properties of the PVC-P geomembrane over time, a regular monitoring of the geomembrane on site, combined with regular laboratory tests are essential.

2.3 Plasticiser's content evaluation

2.3.1 Laboratory test

Tests are carried out on samples exhumed form the dam to determine to which extent their properties (listed in §2.1) have changed during service. The tests performed show if the geomembrane properties at the time of the test within acceptable limits.
Although standards are available to measure plasticisers' content (ISO 6427 or DIN 53738), significant variations in results may be observed between several laboratories (Fig. 4). Deviations of up to 78% from the reference value have been observed.

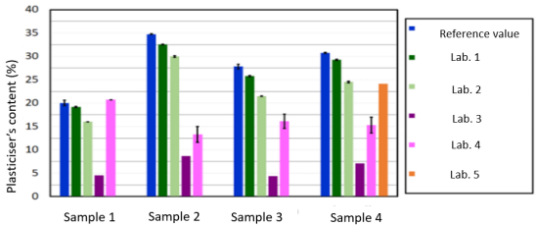


Fig. 4 Results of a benchmark on plasticiser's content evaluation from 5 laboratories

Following this, it is advisable to select and qualify only some laboratories and protocols to carry out this type measurements.

2.3.2 Non-invasive methods

The measurement of the plasticisers' content on samples taken in the field is very accurate (with qualified laboratories and protocol), but nevertheless suffers from two difficulties:
- Samples are small and local, whereas the geomembrane surface could be large, and aging effects are not always homogeneous (in particular because the exposure is variable on the same dam). Several samples should also be taken (Fig. 5.) to cover different exposures.
- But unless aging indicators have been installed (Fig. 6.) on the dam, taking a sample always represents a risk, since the geomembrane must then be closed with a patch, the welding of which being increasingly difficult over time (Fig. 7.).

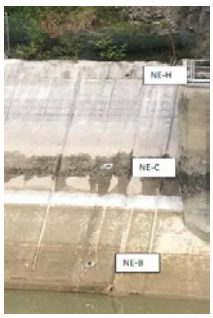


Fig.5. Sampling with different exposures

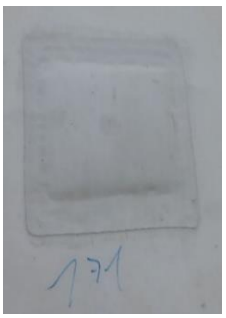


Fig.6. Aging indicator





Fig. 7. Example of sampling and repair

These difficulties could be overcome by a non-invasive tool (not requiring sampling) that can measure the plasticisers'content. An example is illustrated on Fig. 8. and Fig. 9. The scanner, usable on site measures an electromagnetic property (raw data : dielectric permittivity) that is directly correlated to the plasticisers'content. A significant number of measurements are taken with the scanner, and then, thanks to correlations, they are converted into value of plasticisers'content.

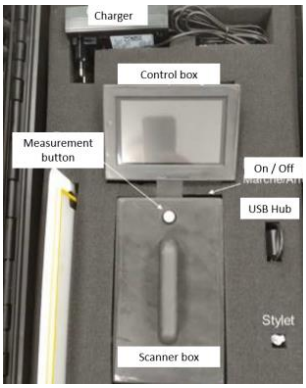


Fig. 8. Scanner able to measure plasticiser's content



Fig. 9. On-site scanner measurement

To achieve a sufficient accuracy of the correlation between raw data and plasticisers'content, an on-site calibration is often necessary. Compared with sample and standard test, accuracy is a little less precise. So sampling and laboratory tests are still necessary, but their number can be reduced very significantly. Indeed, scanner measurements allowing many measures on many positions, provide information on the spatial heterogeneity of the conditions of the geomembrane, without the risk of multiplying sample collection. See § 4.4.2 for an example of application and analysis.

3 Analysis of end of service life

Defining a single end of service life criterion does not seem relevant, because each structure has site constraints and specific issues. This thought must therefore be carried out and discussed on a case-by-case basis. Some elements that can be used in the analysis are proposed below.

3.1 Low temperature behaviour

The glass transition temperature is the temperature below which the material exhibits non-ductile behaviour, i.e. it can fail in a brittle manner due to an impact. For uncovered geomembranes, this parameter is quite indicative of the fragility of the geomembrane in winter. A glass transition temperature higher than the temperatures commonly encountered in winter increases the risk of the geomembrane cracking, especially if it can be subjected to impacts: floating bodies, falling ice or blocks, etc.
For covered geomembranes, this parameter is less interesting, because (i) they are less exposed to extreme cold, and (ii) they are often protected from shocks.

3.2 Tensile, shear, punching strength, elongation at break

French and International Standards proposed limit values for theses parameter. It could also be compared to the design values. These values are less critical for covered geomembranes, with damped differential settlements.
Limit values of these parameter should be set with feedback and adapted with the site's conditions and issues.

3.3 Repairability

This property decreases over time, and could become critical, when it is no longer possible to repair defects easily, which could also multiply at the same time.
An unrepaired defect could lead to a considerable leakage, causing a drop the performance of the sealing function.
The experience and knowledge of the welder is crucial. In the most difficult cases, several welding techniques must be mastered.

3.4 Definition of an aging index

In order to facilitate the analysis of the condition of a PVC-P geomembrane, an aging index has been defined, based on the plasticiser's content. According to this aging index, the value 100 % corresponds to the best possible condition when leaving the factory. The value 0% corresponds to the worst condition observed on a geomembrane on a dam.
Thanks to numerous feedbacks, four aging classes (Table 1) could be defined.

Table 1. Aging classes defined, thanks to cumulative feedback on several dams with PVC-P geomembranes.

Aging index	Conditions	Maintenance needs
80 à 100 %	New	None whose origin would be due to aging
40 à 80 %	Good	Defects caused by aging are scarce and very occasional and require low maintenance (frequency of around 10 years) and easy (welds easy to perform).
20 à 40 %	medium	Defects caused by aging are frequent and require heavy maintenance (frequency between 1 and 4 years) and difficult maintenance (welds are difficult to perform). Depending on the case, the end of life is approaching, and a replacement should be studied.
0 à 20 %	bad	Defects are frequent and widespread and cannot all be repaired, even with the best welders. Depending on the case, the geomembrane reaches the end of its life and a replacement should be studied.
< 0 %	Very bad	Defects are frequent and widespread. Repairs are practically no longer possible. The geomembrane has generally exceeded its end of life

The proposed monitoring principle of a PVC-P geomembrane for dam consists of regularly checking this index, in different position. Thus, the aging kinetics can be assessed, which anticipate the transition to a higher state of degradation or the approach of the PVC-P geomembrane' end of life.

Fig. 10. shows Aging Index of several dams, at different locations and for different operating time.

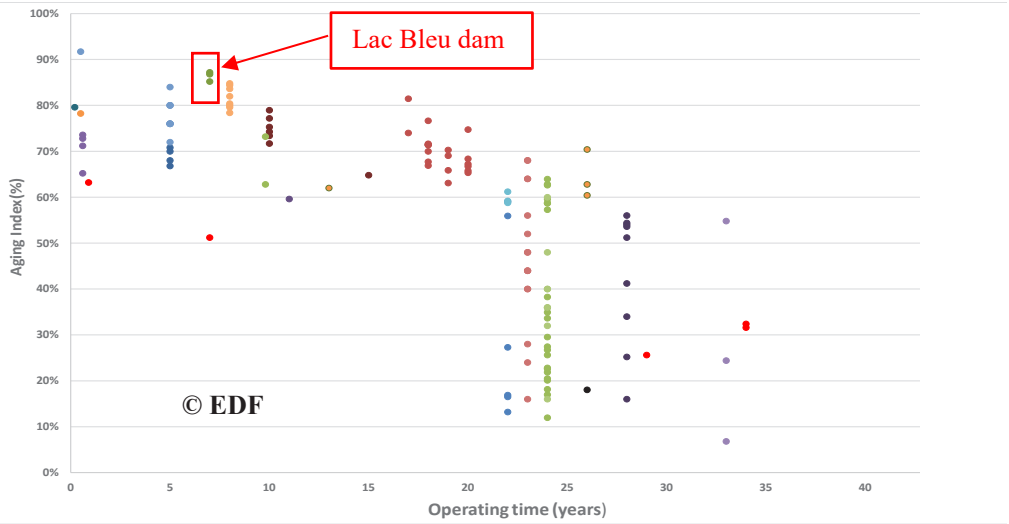


Fig. 10. Aging Index vs operating time (years). Each color corresponds to one dam. Each point corresponds to one measure on a dam.

Several lessons could be learned from Fig. 10.:

1) Aging of PVC-P geomembranes is very heterogeneous between each dam, and sometimes on the same dam.
2) Aging kinetics are generally slow at first (consumption of protective additives), but can then accelerate (when additives are consumed).
3) Aging analysis should be carried out on each dam, with end of service life criteria to be studied according to the associated issues (safety, economic, etc.) and site constraints.
4) For the same structure, it is possible that only a fraction of the surface crosses a threshold. This may be the case for an area that would not have the same exposure, for instance the part above the water level which is often more exposed to U.V.s. The maintenance strategy can take this into account.
5) For a PVC-P geomembrane on a dam, it is possible on a given date to measure the Aging Index on different positions, place them on the Fig. 10 and evaluate state of aging compared to other geomembranes of other dams, and so estimate residual service life and to anticipate maintenance works.

For instance, the case study of Lac bleu shows (Fig. 10) that the geomembrane is still in a good state (Aging Index > 80%), homogeneous, the kinetic of aging is rather slow (compared to other dams) and age-related defects (and therefore maintenance works requirements) are not to be expected for at least the next 10 years.

4 Case study: Lac bleu dam

The most pioneering applications of PVC-P geomembranes, employed to rehabilitate concrete and masonry dams, were in the alpine regions in Europe, at more than 1500 m elevation. In particular, this paragraph focuses on a concrete and upstream masonry facing dam, in the French Alps, that were rehabilitated with this technology in 2017.

4.1 Location and main features

The Lac Bleu dam is located in Bagnères-de-Luchon, in Pyrénées'montains, near the franco-spanish border. The Lac bleu dam is a slightly arched gravity cyclopean concrete dam built in two campaigns between 1944 and 1945 and impounding in 1945. The existing face of this dam is a masonry upstream face. The dam is 12,5 high (at maximum).

4.2 Story of the failures of the waterproofing system

Since 1992, a relatively high level of calcification has been observed in the barbicans, a sign of the slow dissolution of the concrete cement making up the dam.
In 2014, geotechnical and geophysical surveys were undertaken to acquire data on the condition of the dam body and the nature and quality of the foundation.
On this occasion, the monitoring system, which included only a leakage measurement device, was supplemented by the installation of two piezometers at the concrete-rock contact at the spillway. These tests identified: an heterogenous concrete quality; a significant cracking, particularly at the head of the structure.(the concrete joints appear to be in good condition, however, and the contact appears sound and bonded on most of the test holes) ; a significant leaks through the structure and its foundation

These disorders had long-term consequences on the stability of the structure.
In 2017, to ensure its stability, the structure was reinforced by :

- Sealing the upstream face with a flexible composite geomembrane, also known as geocomposite, formed by a geomembrane layer, placed externally and having an hydraulic barrier function, by a geotextile layer, placed internally witch increase the mechanical protection and by a geodrain, having a drainage function.
- Installing vertical passive tie rods

4.3 The new impervious facing

The geocomposite waterproofing device was installed on the entire upstream facing (covering a surface area of 450 m^2), to prevent water infiltration and avoid water circulating in the body of the dam (avoid pressurizing cracks).



Fig. 11. Photo of the upstream face of the Lac Bleu dam

This PVC-P geomembrane was left exposed to the environment, which at such elevation is quite demanding. The mechanical characteristics of this geomembrane had to be compatible

with the following operating and environmental constraints specific to the structure, in particular:

- The high altitude of the structure (elevation 2265 m) and the extremely low temperature induce: UV rays exposure, freeze/thaw cycles and the risk of degradation in the presence of ice and snow in the reservoir ;
- The presence of a spillway at the middle of the dam, which implies stress on the membrane and its attachments;
- The near-vertical upstream face, made of masonry blocs;
- Submergence of the waterproofing system's upper attachment;
- The presence of water with a low mineral content (very pure high-altitude water) ;
- The rapid and frequent fluctuation of water level.

The waterproofing solution consist in a flexible geosynthetics system composed by :

- a 2,5 mm thick, flexible and UV-stabilized PVC-P geomembrane thermally-bonded during fabrication with a 500 g/m^2 non-woven geotextile ;
- a anti-puncturing non-woven geotextile of 1 000 g/m^2 ;
- a new drainage system below the geomembrane liner constituted by geodrain (made of polyethylene) of 50 cm high at the bottom ;
- a stainless steel anti-intrusion plate at drains and aerators ;
- 2,5 mm thick PVC cover strips (without geotextile) to cover the tensioning anchoring profiles and to patch the scaffolding anchors.

The seaming of the geomembrane sheets is made during construction at site by means of seaming machines, which can be either automatic double track or manual single track.
Several protruding blocks on the masonry upstream face have been received.
A drainage system for any potential geomembrane's leaks was created. 2 independent drainage compartments were created, separated by a tensioning profile, to make it easier to identify the origin of any leaks. The drainage system consists of:

- 2 ventilation boreholes with 50/60 tubing at the top of each compartment to maintain atmospheric pressure between the geomembrane and the facing ;
- 2 drains with 50/60 tubing at the lower central part of the dam, on either side of the compartmentalizing section.

18 control spot zones (3 lines of 6 patches distributed in the lower, middle and upper parts of the dam) were welded onto the complex, in order to monitor ageing at regular intervals.
A control sample is also stored at the powerhouse, for comparison.

4.4 Geomembrane expertise

4.4.1 Visual inspection

In the lower part of the structure, there is a slight deposit of fine sediment on the surface of the geomembrane. Visually, the geomembrane is in very good condition: no chalking (oxidation) ; no macro or micro-cracking ; no yellowing ; smooth, shiny surface ; flexible behavior, no brittle behavior when cut (sample areas) ; no loss of thickness (sampling areas). Locally, however, some vertical anchoring profiles were deformed, probably due to ice pressure. As a result, some of the fastening screws are protruding and puncturing the geomembrane.

4.4.2 Scanner data

In order to estimate variations in geomembrane condition at more points than just the sampling zones, the scanner (non-destructive tool that an operator applies to the geomembrane, measuring a physical quantity correlated with the PVC-P geomembrane ageing indicator, see § 2.3.2) was used. The tool needs to be calibrated on site to obtain a direct reading of the ageing indicator. In the absence of calibration, relative measurements can be used to observe variations in the ageing indicator.

30 measurements were carried out in total on the geomembrane of the Lac Bleu dam. The scanner measurements show a generally homogeneous state of the geomembrane over the entire height, with a standard deviation of the aging indicator measurements of around +/- 7%.

This homogeneity is explained by a relatively uniform exposure of the geomembrane to solar radiation (UV and temperature) and to water.



Fig. 12. Scanner measurement on the upstream face of the Blue Lake dam

4.4.3 Laboratory testing data

Samples were taken both above and below the normal water level and in different parts of the upstream face, with the aim of studying the different behaviour of the same geomembrane under different conditions of exposure. The samples were analyzed in a qualified laboratory with specific protocol (see § 2.3.1). Each sample is tested twice. The level of plasticizers and the aging index is then calculated. All samples still have a good aging index and high level of plasticizers. Considering the date of installation of the membrane, the kinetics of aging is relatively slow. Indeed, exposure to solar radiation is rather moderate, despite the altitude. UV protection additives are still present and effective.

The graph on **Fig. 10** illustrates the aging index of PVC geomembranes observed on several structures and at different exposure times. The measurements taken on the geomembrane of the Lac Bleu dam after 7 years of exposure are reported. We observe that the aging index are overall very good (equivalent to a new state), thus allowing us to conclude that the aging of the Lac Bleu membrane follows relatively slow kinetics.

5 Conclusion

Monitoring the aging of PVC-P geomembranes used for watertightness is useful for dam operators, in order to anticipate and optimize maintenance and/or substitutions works, post-pone the end of life as far as possible with a controlled risk of breakdown, and optimized the planning of the necessary lowering of water level and shutdown for works. A method and an aging index is proposed for this purpose.

References

[1] Geomembrane Sealing Systems for Dams : *Design Principles and review of experience*, ICOLD Bulletin 135, 2010.
[2] M. Blanco et al, 2022, *Long-term performance of PVC-P geomembrane installed in "Los Llanos de Mesa" reservoir*, EUROGEO 7 Conference Proceedings
[3] J.P. Giroud, 2021, "*Discussion of 'Lifetime assessment of exposed PVC-P geomembranes installed on Italian dams'* by D. Cazzuffi & D. Gioffrè", Geotextiles and Geomembranes, Vol. 49, No. 5, October 2021, pp. 1447-1448.
[4] D. Cazzuffi et al, 2020, *Lifetime assessment of exposed PVC-P geomembranes installed on Italian dams*, Geotextiles and Geomembranes 48 (2020) 130-136
[5] R. M.Koerner et al, 2017, *Lifetime predictions of exposed geotextiles and geomembranes*. Geosynth. Int. 24 (2) 198–21.
[6] J.P.Benneton et al, 2008, *Durabilité des géomembranes - Vieillissement physico-chimique et endommagement mécanique,* LCPC, Paris

SESSION 5 B

HYDRAULIC APPLICATIONS (1)

Issues of steep sideslope liners that remain exposed and are later covered

Richard Thiel*

Thiel Engineering, Oregon House, CA, USA

Abstract. The steepness of sideslope bottom liner systems for landfills, heap leach pads, and tailings dams often precludes the safe placement of overliner cover soil at the end of construction. As a result, a composite liner system might remain exposed for months or even years before it is eventually covered. In this case the following liner design and operational issues present themselves: degradation of a GCL while the liner system is exposed, toe wrinkle formation, wind uplift, eventual overliner soil cover placement, future downdrag, and selection of design shear strength parameters for short- and long-term conditions. Suggestions to address these issues are proposed.

Full paper to be published in:
https://www.e3s-conferences.org/articles/e3sconf/abs/2025/44/contents/contents.html

* Corresponding author: richard@rthiel.com

Performance of geosynthetics in methane oxidation systems

Vanessa Di Battista[11], *Sophie* Filion[2], and *Alexandre R.* Cabral[1]

[1]Université de Sherbrooke, Département de génie civil et du bâtiment. Sherbrooke, Canada
[2]Carelton University, Department of Civil & Environmental Engineering, Ontario, Canada

Abstract. Landfills are a major source of methane emissions contributing to climate change. These emissions can be fugitive emissions from capped landfills, where hotspots form due to vulnerabilities (e.g., holes, fissures) in the cover. A research project investigating the use of "biowindows" for the biological oxidation of methane has been initiated by the Université de Sherbrooke. This study will examine the performance of geosynthetic drainage composite as a gas distribution layer (GDL) and a wicking geotextile as a separation layer between the methane oxidation layer and GDL. This study is a pilot scale installation with ten 2 m x 2 m biowindows fed directly by landfill gas. As occlusion due to moisture retention is a major impediment to gas transport and system efficiency, this study examines the inclusion of geosynthetics and their effects on gas transport and system efficiency.

Full paper to be published in:
https://www.e3s-conferences.org/articles/e3sconf/abs/2025/44/contents/contents.html

[i] Corresponding author: vanessa.di.battista@usherbrooke.ca

Gas capture and extraction using multi-linear drainage geocomposite

Hajer Bannour[1*], *David* Beaumier[1], and *Stephan* Fourmont[2]

[1]Groupe CTT, 3000 Ave Boulle, Saint-Hyacinthe QC J2S 1H9, Canada
[2] Afitex-Texel, 1300, 2e Rue, Parc industriel. Sainte-Marie QC G6E 1G8, Canada

Abstract. The design of gas drainage systems is essential for mitigating environmental impacts, especially in contaminated soils (e.g., hydrocarbons, radon) and landfill covers (e.g., methane and carbon dioxide management). This study experimentally investigates the gas drainage capacity and transport through mini pipes within multi-linear drainage geocomposites, as these mini pipes primarily determine the system's overall drainage capacity. Initially, the assessment of the discharge capacities was performed on air, and CO_2 through various mini-pipe diameters and lengths to characterize the flow rate as a function of the gradient. Finally, the drainage capacity through mini-tube connections and their integration into the principal collection system was examined. These two steps enable the estimation of both linear and singular head losses, considering the extended lengths of the mini-pipes and their connections. The final objective is to extend these findings to gases such as methane and radon by establishing discharge equivalencies among various fluids. This experimentation is supported by well-known fluid transport concepts, allowing for the modeling and reproduction of the drained flow rate as a function of the fluid gradient. This paper presents the methodology and results of the proposed study, along with various analyses of equivalency considerations to enhance gas drainage system design.

Full paper published in the September 2025 Special Issue of the French Geotechnical Journal **"Revue Française de Géotechnique"** *https://www.geotechnique-journal.org*

* Corresponding author: hbannour@gcttg.com

Feedback on long-term integrity of Multi-linear drainage geocomposites installed on landfill final covers after 10 and 12 years of operation

Mathilde Riot[1], *Cris* Ciuperca[2], *Pascal* Saunier[3], and *Stephan* Fourmont[3]

[1]Afitexinov, 13-15, rue Louis Blériot 28300 Champhol, France
[2]Sperling Hansen Associates, 1225 E Keith Rd #8, North Vancouver, BC V7J 1J3, Canada
[3]Afitex-Texel Geosynthetics, 1300, 2e Rue, Parc industriel Sainte-Marie QC G6E 1G8, Canada

Abstract. The use of drainage geocomposites in landfill final covers facilitates surface water drainage, contributing to long-term stability. However, validating their durability beyond accelerated laboratory aging tests remains a challenge. The most direct method involves exhuming geocomposites after prolonged field exposure and analyzing their mechanical and hydraulic properties. This study presents two case studies involving multi-linear drainage geocomposites installed in landfill final covers, one exhumed after 10 years in France and the other after 12 years in Canada. The samples underwent laboratory analysis to compare residual properties with original specifications, providing insights into long-term performance.

Full paper to be published in:
https://www.e3s-conferences.org/articles/e3sconf/abs/2025/44/contents/contents.html

Installation of geosynthetics at the Cerro do Lobo Tailings Storage Facility

Madalena Barroso[1*], *João* Manso[1], *Andrea* Brito[1], *João* Marcelino[1], *Rui* Galrão[2] and *Mafalda* Oliveira[2]

[1]Laboratório Nacional de Engenharia Civil, Lisboa, Portugal
[2]Lundin Mining Corporation, Neves-Corvo Mine, Portugal

Abstract. The Cerro do Lobo Tailings Storage Facility is part of the Neves-Corvo Mine, located in Portugal. The mine is operated by Somincor, a Portuguese company and a subsidiary of Lundin Mining Corporation. The mine has been in operation since 1988 and processes copper and zinc with an annual capacity of 2.8 million tonnes and 2.5 million tonnes, respectively. The facility consists of a zoned rockfill tailings dam. The tailings storage area was recently expanded by approximately 10%. This expansion involved the construction of a new embankment in the southern area of the tailings facility. Technical assistance for the design and construction of the new southern embankment was provided by an independent and impartial research and development institute. The embankment incorporates a liner system with geosynthetic barriers. The use of geosynthetic barriers presented several challenges during both the design and construction phases. This paper discusses the main challenges faced during the construction of the liner system, mainly related to the installation of the geosynthetics.

1 Introduction

The Neves-Corvo Mine, which includes the Cerro do Lobo Tailings Storage Facility, is operated by the Portuguese company Somincor, a subsidiary of Lundin Mining Corporation. In operation since 1988, the mine comprises two plants: the copper plant and the zinc plant. The copper plant processes copper ore and has a capacity of approximately 2.8 million tonnes per annum, while the zinc plant, capable of processing both zinc and copper ores, recently underwent a significant expansion to a capacity of 2.5 million tonnes per annum [1].

The Tailings Storage Facility (TSF) consists of a zoned rockfill tailings dam. It was originally designed for sub-aqueous tailings disposal, covering 191.5 ha (1.9 km²) with a capacity of 17 Mm³. In 2010, it was redesigned as a thickened tailings facility, incorporating a thickened tailings plant to increase storage capacity without further raising the main and perimeter dams. The new design adopted a co-disposal system, combining thickened tailings with potentially acid-generating waste rock. The waste rock was used to create peripheral berms that defined tailings areas and levels. This redesign increased the storage capacity to 33.3 Mm³ by expanding vertically to five levels [1].

* Corresponding author: mbarroso@lnec.pt

In 2022, Somincor secured approval to expand the Cerro do Lobo facility's footprint to the south, ensuring sufficient storage capacity until 2033. The expansion involved the construction of a new embankment in the southern area of the tailing facility.

The construction of the southern embankment began in 2022. The expansion increased the footprint by 18.5 ha (out of a total of 210 ha or 2.1 km²) and increased the storage capacity to 50 Mm³. This was achieved by both horizontal and vertical expansion from Level 5, at 266.5 m, to Level 13, at 283.5 m. The facility continues to use the co-disposal system for thickened tailings and waste rock [1].

Mining Company received technical advice on the design and construction of the new southern dam from the *Laboratório Nacional de Engenharia Civil*, an independent and impartial research and development institute.

The new southern embankment incorporates a geosynthetic liner system with geosynthetic barriers. The use of geosynthetic barriers presented several challenges during both the design and construction phases. This paper focuses on the primary challenges faced during the construction of the liner system, particularly those associated with the installation of the geosynthetics.

2 Cerro do Lobo TSF southern embankment

2.1 Main features

The Cerro do Lobo TSF is part of the Neves-Corvo Mine (Figure 1), located in the Alentejo district of southern Portugal, approximately 200 km from Lisbon.

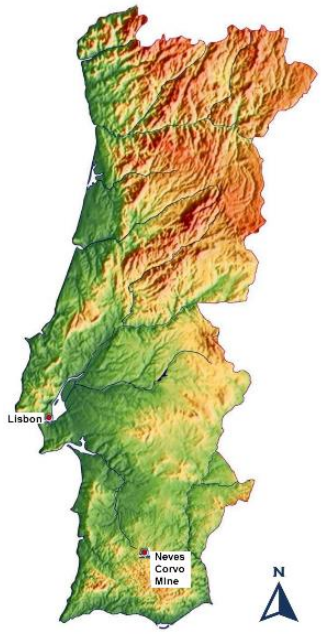


Fig. 1. Location of the Neves-Corvo Mine.

The southern embankment, whose location is shown in Figure 2 and Figure 3, is intended to contain the tailings up to Level 8, at 272 m. It has a maximum height of 17 m, with upstream and downstream slopes of 1(V):2.5(H) and 1(V):2(H), respectively.

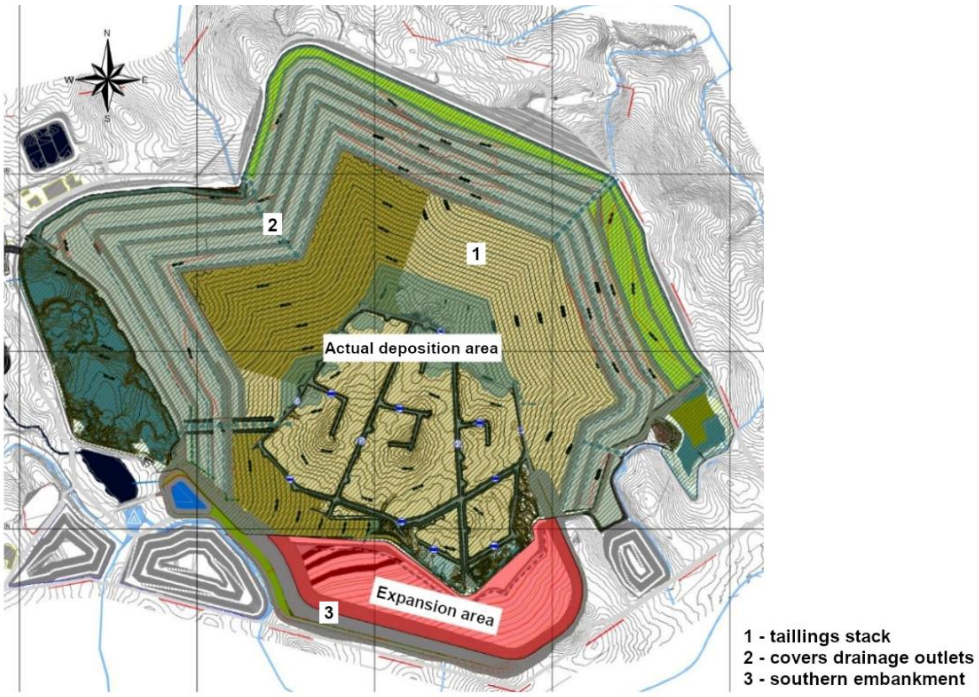


Fig. 2. Location of the southern embankment of the Cerro do Lobo TSF (adapted from [2]).



Fig. 3. Aerial view of the southern embankment of the Cerro do Lobo TSF (Courtesy of TPF Company).

The southern embankment (Figure 4) consists of rockfill material and soil-rockfill mixtures from *in situ* excavation. On the upstream slope, it includes a liner system.

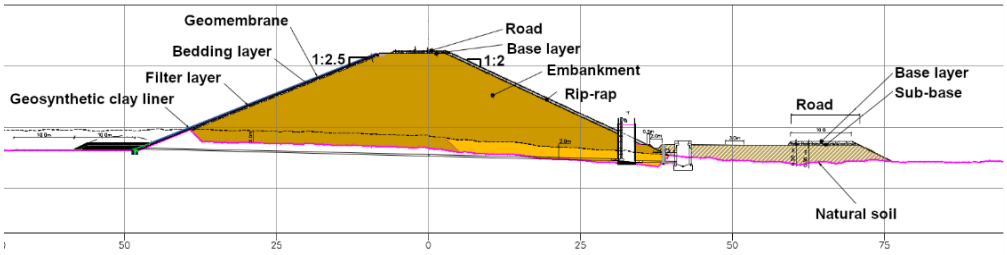


Fig. 4. Cross section of the southern embankment (adapted from [2]).

2.2 Liner system

The liner system of the southern embankment comprises of the following elements, from bottom to top [3] :

- bedding layer (soil with $D_{30} < 20$ mm $< D_{70}$), with a thickness of 0.30 m;
- filter layer (soil with D_{85}>0.30 mm, 0.10 mm< D_{15} <0.2 mm);
- geosynthetic clay liner (GCL) consisting of a sodium bentonite layer (4.5 kg/m²) sandwiched between two polypropylene geotextiles, one woven (100 g/m²) and one nonwoven (200 g/m²);
- high-density polyethylene (HDPE) geomembrane, 2.5 mm thick, with smooth surfaces on both sides.

The GCL with sodium bentonite was selected for its low permeability and self-healing properties, ensuring the integrity of the containment barrier and minimising contaminant migration.

The 2.5 mm thick HDPE geomembrane was selected to provide increased mechanical strength, durability, and protection against punctures, reducing the risk of failure and extending the service life of the system.

3 Geosynthetics

3.1 Overview

As part of the technical advice provided to Somicor during the design and construction of the southern embankment, various activities were undertaken to ensure that the installer/contractor complied with the project plans and specifications. Among the activities conducted are the following:

- supervision of the procedures for the transport, handling, and storage of geosynthetics;
- supervision of the procedures for the installation of the geosynthetics and any necessary repairs after installation;
- carry out observations/inspections to assess the quality of the geosynthetic installation;
- monitoring the results of quality control tests on the seams, including:
  - non-destructive tests to check the continuity;
  - destructive tests to evaluate the mechanical strength (peel and shear tests).

The following sections describe some of the main activities carried out during the installation of the geosynthetics.

3.2 Anchorage system

Anchors play a vital role in the design and installation of geosynthetic liners on exposed slopes, ensuring stability, durability and long-term performance. They prevent slippage due to gravity and secure the geosynthetics at critical points to resist wind uplift, hydrostatic pressure and sliding forces.

The anchorage system designed for the southern embankment consisted of anchorage trenches located at the top of the embankment and at the toe of the slope. The trenches were backfilled with soil.

Figure 5 illustrates the configuration of the anchor trench at the top of the embankment. As shown in the figure, the square trench (1.0 m × 1.0 m) is positioned at the end of the geomembrane runout section, which has a design length (L_{RO}) equal to 0.5 m.

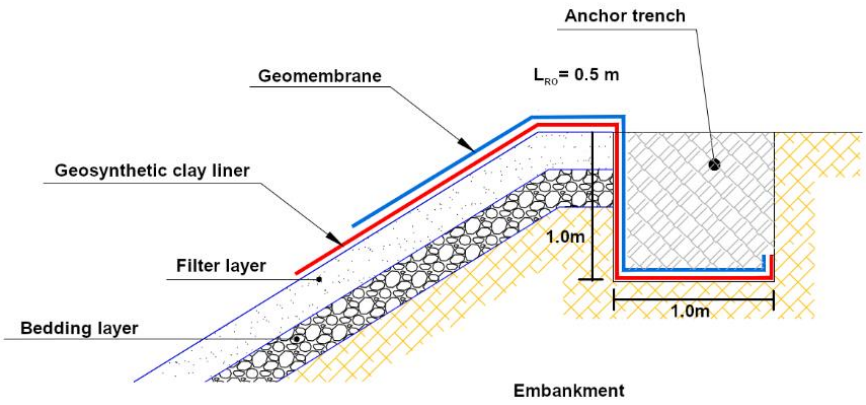


Fig. 5. Cross section of anchor trench and geomembrane runout design (adapted from [2]).

The construction of the anchor trench at the top of the embankment encountered some difficulties during the initial phase of the geosynthetic installation. The main issue was the geomembrane runout length, which was shorter than specified in the design (Figure 6a). During a construction quality assurance inspection, the importance of complying with the specified geomembrane runout length was emphasized to prevent long-term geomembrane rupture. Subsequently, this issue was corrected, as shown in Figure 6b.

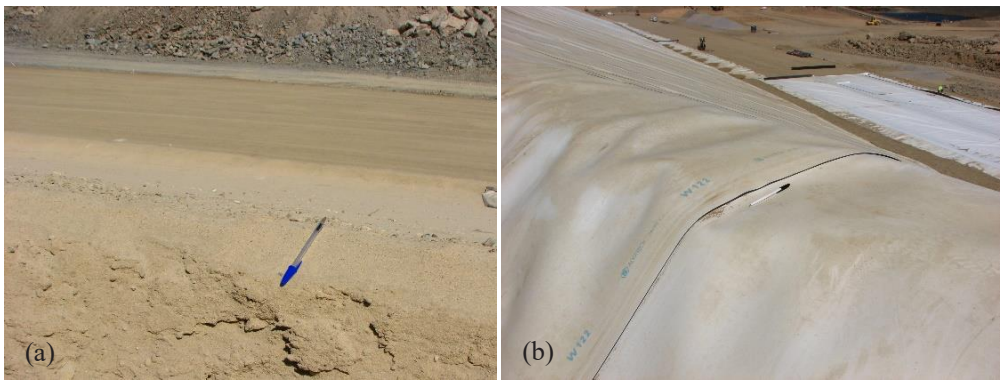


Fig. 6. View of the anchor trench and length of geomembrane runout: (a) before the correction; (b) after correction.

3.3 Geosynthetic support surface

The characteristics of the support surface for geosynthetics are essential to ensure the performance and durability of the system. The surface influences the interaction between the geosynthetics and the soil, affecting the deformation, durability, and stability of the geosynthetics. The support surface should be uniform, without significant irregularities or depressions that could damage the geosynthetics. It must also be adequately compacted to ensure even load distribution. The surface should be free of sharp objects that could damage the material during installation or over time.

It was observed that the installation of the geomembrane was delayed compared to the geosynthetic clay liner on the embankment slope (Figure 7a), leaving a large part of the support surface exposed to rain and wind. This exposure led to the development of irregularities in the support surface, as shown in Figure 7b.

To avoid excessive exposure of the bentonite panels to UV radiation, it was recommended that the geosynthetic clay liner be installed at the same time as the geomembrane. It was also recommended that the characteristics of the support surface be checked prior to installation to ensure proper contact with the geosynthetics, as this is critical to the long-term performance of the HDPE geomembrane.

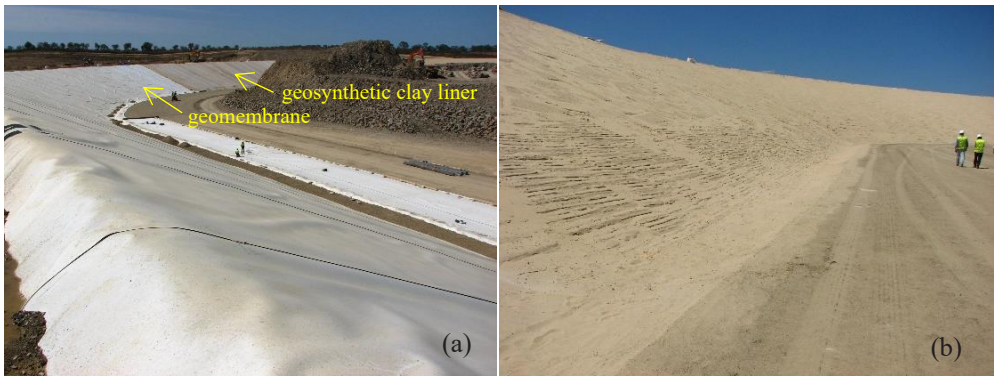


Fig. 7. View of the geosynthetics support surface: (a) delay in installation of the geomembrane compared to the geosynthetic clay liner (b) irregularities caused by wind.

3.4 Quality control of geomembrane seams

3.4.1 Criteria for the quality control

Seams are often the weakest point in a geomembrane liner. Quality control ensures that seams meet or exceed the required strength and performance criteria, reducing the risk of failure under load.

Quality control of geomembrane seams includes specific criteria and test methods to ensure that they meet performance requirements and provide a reliable barrier. These criteria generally fall into two categories: integrity/continuity and mechanical strength.

For integrity/continuity, the acceptance criteria are based on the results of non-destructive tests: the air channel pressure test for hot wedge (dual track) seams and the spark test for extrusion fillet seams. For mechanical strength, the acceptance criteria are based on the results of destructive tests: shear and peel tests for both hot wedge seams and extrusion fillet seams.

The air channel pressure test was carried out in accordance with ASTM D5820 [4]. The seam was accepted when the air pressure in the seam channel remained stable for the required time (2.5 bar for 5 minutes) without a pressure drop. Figure 8 shows a test being carried out.



Fig. 8. Air channel pressure test ongoing

The spark test was carried out in accordance with ASTM D6365 [5]. A copper wire was inserted into the overlap area of the top and bottom geomembrane panels during welding. The seam was acceptable if a high-voltage detector detected no discontinuities in the seam.

Shear and peel tests (Figure 9) were performed in accordance with ASTM D6392 [6]. The peel test measures the resistance to peeling forces, while the shear test measures the resistance to shear stress.

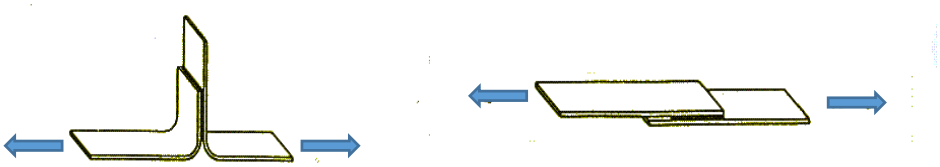


Fig. 9. Scheme of peel and shear tests.

Seams were considered acceptable if the strength met or exceeded the following values shown in Table 1.

Table 1. Seam strength for HDPE geomembrane at southern embankment based on tests conducted according to ASTM D 6392.

	Hot wedge seam	**Extrusion fillet seam**
Shear strength (kN/m)	≥ 35.5	≥ 35.5
Peel strength (kN/m)	≥ 28.4	≥ 22.8

3.4.2 Test results

Non-destructive tests were performed on all seams along their entire length during installation. Destructive tests were conducted at regular intervals, specifically every 200 m of seam length.

The results of the non-destructive and destructive tests met the specified acceptance criteria, except in a few cases. Wherever the test results did not comply with the acceptance criteria, the seams were replaced.

4 Conclusions

This paper presents some of the main challenges encountered during the construction of the liner system on the new southern embankment of the Cerro do Lobo Tailings Storage Facility, with particular emphasis on those related to the installation of the geosynthetics.

The issues identified through the construction quality assurance procedures were properly addressed, ensuring a high level of quality in the installation of the geosynthetics at this site.

References

1. Lunding Mining Corporation, GISTM Public Disclosure Report. Neves-Corvo Mine Cerro do Lobo Tailings Storage Facility. 6 p. https://lundinmining.com/site/assets/files/8904/neves-corvo_tsf_gistm_public_disclosure_report_2024.pdf (2024).
2. Golden, Projeto de licenciamento da expansão da IRCL para o PEZ (DGEG- LNEC). (Volume I - Tomo 1.2. Análise de Consolidação dos rejeitados e de estabilidade. Relatório 1899306-132-RI.2-v2-00, 2021) (in Portuguese).
3. J. Manso, M. Barroso, A. Brito; J. Marcelino, J., Instalação de Resíduos Mineiros de Cerro do Lobo. (Segundo relatório de acompanhamento da obra da Expansão Sul. LNEC - Proc. 0502/1201/23439. Relatório 148/2024 – DG/NGOH, 2024) (in Portuguese).
4. ASTM D5820-95 (2018), Standard practice for pressurized air channel evaluation of dual seamed geomembranes. American Society for Testing and Materials (2018).
5. ASTM D6365 − 99 (2018), Standard Practice for the Nondestructive Testing of Geomembrane Seams using the Spark Test. American Society for Testing and Materials (2018).
6. ASTM D6392 – 23, Standard Test Method for Determining the Integrity of Nonreinforced Geomembrane Seams Produced Using Thermo-Fusion Methods. American Society for Testing and Materials (2023).

Raising waste storage facilities - design in line with the latest French recommendations

Mame Coumba Faye[1*], *Abdelkader* Abdelouhab[2]

[1]SOLMAX, Ingénieure d'affaires, 95873 Bezons, France
[2] SOLMAX, Docteur en géotechnique, 95873 Bezons, France

Abstract. Geosynthetics play an important role in the design of landfill sites. They contribute to environmental protection, structural stability and cost reduction. Raising the height of landfill cells places additional stresses on existing structures. This leads to additional deformation, promoting differential settlement and damage to waterproofing systems. The use of geosynthetic reinforcements can absorb these deformations and ensure the durability of the structure. In this article, we present two examples of ISD landfill riser projects using polyethylene terephthalate (PET) reinforcement geosynthetics. The first project concerns the raising of a landfill cell on its side in the Paris region, using a reinforcement geosynthetic. The height of the new waste is 23 m, with potential subsidence zones 1 m in diameter. The second project concerns the raising of a landfill in the north-west of France, with a new waste height of around ten meters and potential subsidence zones of 1 to 1.5 m in diameter.

1 Introduction

The need for waste storage is growing all the time, while available space is shrinking because of the economic and environmental impact. In fact, many old landfill sites are either leaky or have unsuitable sealing systems. It is therefore necessary to adapt the design of waste storage facilities. Existing landfill sites may be extended by creating new landfill extensions, by storing all or part of the new waste in existing bins. These extensions generate overloads on the existing waste block, creating additional deformations. Reinforcing geosynthetics are used in the design of fusegates to take up deformations, guarantee the longevity of the sealing system and the stability of the structure.

2 ISD extension: principles

The main types of ISD raising are shown below:

- **Pure vertical extension** : resting on the top of an existing landfill. The main issues in this configuration are differential settlement of the old waste, and gas and leachate drainage.

* Corresponding author: mfaye@solmax.com

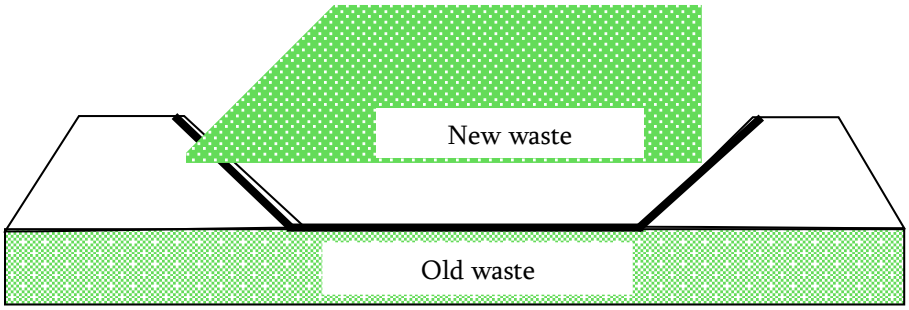


Fig. 1. Vertical extension

- **Extension on lateral support**: resting on bedrock and the flank of the existing landfill, with problems linked to deformation of the old waste mass at the junction between the latter and the bedrock.

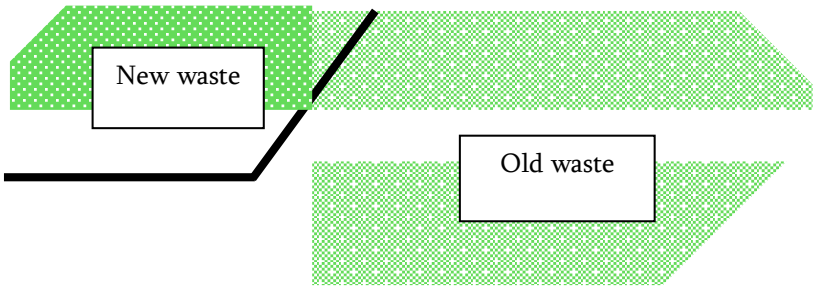


Fig. 2. Extension on lateral support

- **Mixed support extension**: a combination of the two previous extensions with the issues outlined above.

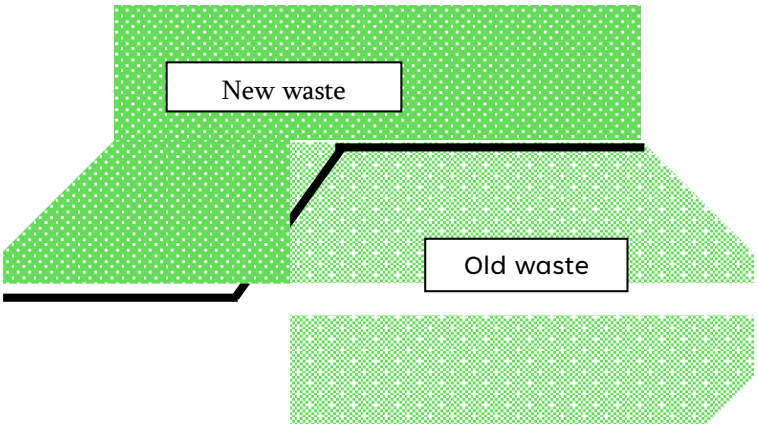


Fig. 3. Extension on mixed support

3 Selection and sizing of reinforcement geosynthetics

3.1 Choice of reinforcement geosynthetic

In France, the design of ISDND extensions may be done in accordance with BRGM's "Guide de recommandations pour la conception des extensions d'ISDND en appui sur des casiers anciens" [1] and CFG's "Fascicule Installations de stockage de déchets" [2]. These guides recommend the use of a geosynthetic reinforcement in the transition zone between old and new waste cells. The hydrolysis phenomena that occur in long-term in waste deposits, geosynthetics must have good resistance in this environment. Alkaline hydrolysis can cause some polymers to lose their potential stiffness. The BRGM guide therefore recommends the use of Polyvinyl Alcohol (PVA) reinforcement geosynthetics [1].
When hydrolysis at a neutral acid pH, PET shows no significant loss of stiffness. PET offers good chemical resistance to most acids and many solvents.

Resistant against	Polymer, under short and long loading duration									
	PA (6 and 6.6)		PET		PP		PE		Plasticized PVC	
	Short[1]	Long[1]	Short	Long	Short	Long	Short	Long	Short	Long
Dilute acids	+	o	++	+	++	++	++	++	+	o
Concentrated acids	o	–	o	–	++	+	++	+	o	–
Dilute alkali	++	+	++	o	++	++	++	++	++	+
Concentrated alkali	o	–	o	–	++	++	++	++	+	o
Salt (prine)	++	++	++	++	++	++	++	++	++	++
Oil (mineral)	++	++	++	++	+	o	+	o	+	o
Glycol	+	o	++	o	++	++	++	++	++	++
Micro organisms	++	+	++	++	++	++	++	++	+	o
UV Light	+	o	+	o	o	–	o	–	+	–
UV Light (stabilized)	++	+	++	+	++	+	++	+	++	+
Heat, dry (up to 100°C)	++	+	++	++	++	+	++	o	+	o
Steam (up to 100°C)	++	+	o	–	o	–	o	–	o	–
Moisture absorption	++	++	++	++	++	++	++	++	+	+
Detergents	++	++	++	++	++	++	++	++	++	++
Tendency to creep	++	+	++	++	+	o	+	o	+	o

Degree of resistance: – = not resistant; o = moderate; + = passable; ++ = good.
This assessment of resistance is valid under normal conditions and temperatures:
1. During construction stage, 2. During usage, 3 Depending on type of plasticizer.

Fig. 4. Extract of" Geosynthetics in civil engineering – GPTM Van Santvoort" **[3]**

To determine the long-term resistance of geosynthetics, a chemical reduction factor is taken into account. This factor depends on pH level, temperature and service life.

Strength losses for high-tenacity PET fibers have been evaluated by Elias and Van Schoors, and are summarized in the table below:

Table 1. PET resistance loss [3]

pH	7	9	10	11	12
Loss per year (%)	0,08	0,25	0,35	0,5 à 1,1	4,1

At pH levels below 9 (the case for most decomposing waste), the risk of chemical degradation is very low.

In addition, the reduction factor to be taken into account, for different temperatures and as a function of time, can be calculated from Arrhenius curves (see Fig.4).

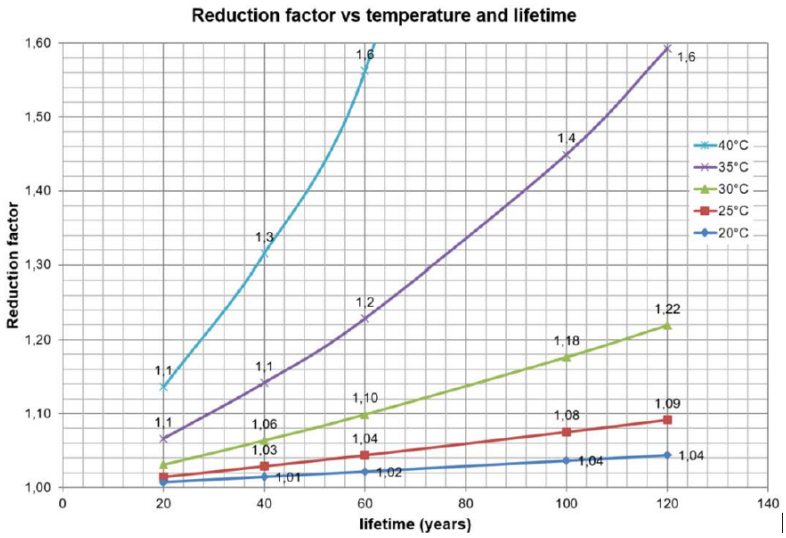


Fig. 5. Arrhenius curves

3.2 Design principle

The geosynthetic reinforcement must be dimensioned to reduce differential settlements in order to avoid failure or loss of functionality of the sealing system. The geosynthetic is designed according to the RAFAEL calculation method for securing structures in areas at risk of collapse. To simulate localized subsidence, a nominal subsidence diameter (D) of 1 to 2 m is taken into account. When localized subsidence occurs in old waste, the reinforcing geosynthetic placed in the subgrade deforms into a membrane and comes under tension above the subsidence zone. This transfers the load to the anchoring zones, preventing the structure from collapsing.

The data required to design reinforcement structures are [1] and [2]:

- The nominal diameter of the localized settlement (1 m < D < 2 m) ;
- The maximum permissible deformation for the service life of the structure (less than or equal to 3%);
- Surcharge due to new waste limited to n x D

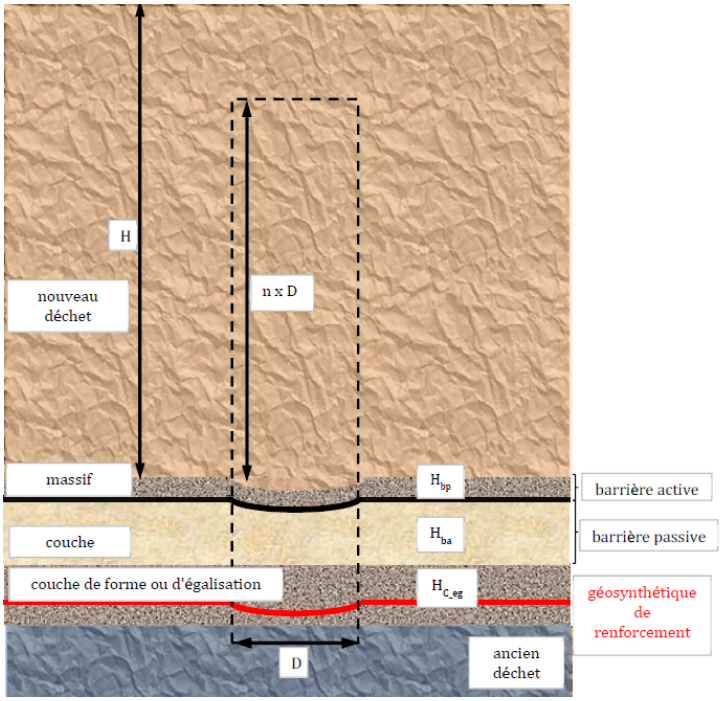


Fig. 6. Schematic cross-section of ISDND extension

The justification of the geosynthetic and the stability of the cavity is based on the Eurocodes and standard XP G38-065. For these structures, a uniform vertical stress distribution is assumed. This is determined using the following formula:

- **ELS :**

$$\sigma=(\gamma waste*n*D+\gamma ba*Hba+\gamma bp*Hbp+\gamma Ceg*HCeg+P)+Q \quad (1)$$

- **ELU :**

$$\sigma=\gamma Gsup*(\gamma waste*n*D+\gamma ba*Hba+\gamma bp*Hbp+\gamma Ceg*HCeg+\gamma GSup*P)+\gamma QSup*Q \quad (2)$$

Next, the required tractions at ELS and ELU are determined using formulas (3) and (4) below:

$$T_{d,ELS} = \frac{\sigma_{v,k}.D}{2}.\sqrt{1+\frac{1}{6.\varepsilon_{max}}} \quad (3)$$

$$T_{d,ELU} = \frac{\sigma_{v,d}.D}{2}.\sqrt{1+\frac{1}{6.\varepsilon_{ult}}} \quad (4)$$

The progressive mobilization and the geosynthetic elongation in the anchorage areas (Briançon and Villard 2006) is taken into account in the design.

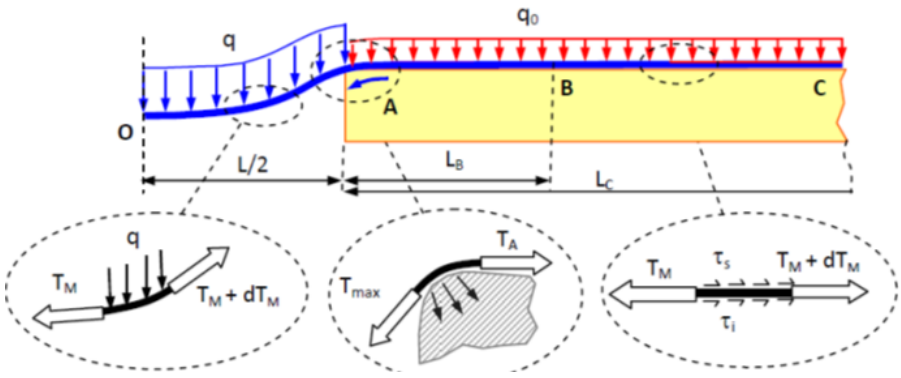


Fig.7 . Geosynthetic elongation in anchorage (Briançon and Villard)

4 Case studies

In this chapter, we present two examples of landfill raising projects where geosynthetic reinforcement made of Polyethylene Teraphthalate (PET) was used.

4.1 Extension of a household waste bin

The first example concerns a project to raise the height of a landfill receiving household waste in the Paris region. The project involves raising the side of a landfill cell using a PET reinforcement geosynthetic (see Fig. 7). A geosynthetic clay liner and a geomembrane will be used to seal the storage site.

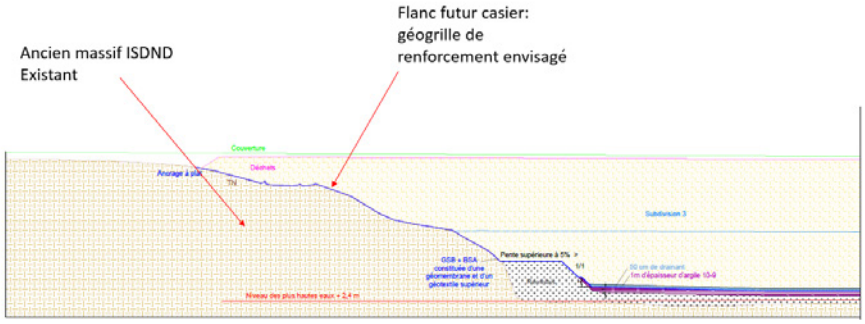


Fig. 8. Extension of an ISDND for household waste

The parameters taken into account for the design of the reinforcement geosynthetic are summarized in Table 2 below.

Tableau 2. Calculation parameters

Width or diameter of localized settlement zone (D)	Height of overlying waste (H)	Active barrier height (Hba)	Passive barrier thickness (Hbp)	Thickness of levelling layer above reinforcement (HC_eg)
1 m,	23 m	0,5 m	0,5 m	0,8 m

To limit deformation and damage to the waterproofing system, we recommended the use of a reinforcing geosynthetic made of polyethylene teraphthalate (PET) with a short-term tensile strength of 800 kN/m.

4.2 Extension of a final waste landfill

The landfill studied for this project is located in north-western France. It is a landfill for storing millions of m3 of hazardous waste.
As part of the project, it is planned to raise the height of the new waste by 10 to 12 m over a surface area of 16,200 m². The waterproofing of the old landfill is provided by a geosynthetic clay liner (GCL) combined with a geomembrane. Raising the landfill could lead to differential settlement of the old waste.
In order to limit settlement and consequent damage to the sealing system, geosynthetic reinforcement was used.

The parameters taken into account for the design of the reinforcement geosynthetic are summarized in Table 3 below.

Table 3. Calculation parameters

Width or diameter of localized settlement zone (D)	Height of overlying waste (H)	Active barrier height (Hba)	Passive barrier thickness (Hbp)	Thickness of levelling layer above reinforcement (HC_eg)
1 - 1,5 m	> 11 m	0,5 m	1,0 m	0,5 m

Based on these data, we prescribed the following reinforcement geosynthetics:

- For a zone of localized subsidence 1.5 m in diameter, a PET reinforcement geosynthetic with a short-term tensile strength of 1400 kN/m ;
- For a 1 m diameter subsidence zone, a PET geosynthetic reinforcement with 600 kN/m short-term tensile strength.

5 Conclusion

Geosynthetic reinforcement of landfills as part of ISDND upgrades makes it possible to:

- prevent differential settlement during and after waste deposition;
- prevent damage to the lining system;
- resolve economic and environmental constraints.

PET geosynthetics can be used and offer good resistance.

The current calculation method is used to estimate the tensile strength of geosynthetics.

This calculation method leads to conservative results when the diameter of the subsidence is well estimated.

Further studies and experiments are needed to improve or define a realistic design method.

References

1. B. Chevrier, P. Michel, F. Garrido, Guide de recommandations pour la conception des extensions d'ISDND en appui sur des casiers anciens, BRGM/RP-69455-FR (2020)
2. CFG, Fascicule Installations de stockage de déchets – guide d'utilisation des normes de dimensionnement dans la conception des ouvrages avec géosynthétiques : géotextiles et produits apparentés (2021)
3. G.P.T.M Van Santvoort, Geotextiles and Geomembranes in Civil Engineering (1994)

SESSION 5 C
REINFORCEMENT APPLICATIONS (5)

Stabilisation and bearing capacity improvement of granular platform

Alain Nancey[1*], *Nisrine* Abou Chaz[2], *Laurent* Briancon[3], *Pascal* Villard[2], and *Claire* Silvani[3]

[1] Solmax, Bezons, France
[2] 3SR, Université Grenoble Alpes, Grenoble INP, CNRS, Grenoble, France
[3] GEOMAS INSA, Lyon, France

Abstract. Building roads or platforms on weak soil is a remaining challenge. The reduction of granular material required for the subbase is more and more crucial, for cost reasons but also for a much lower impact of the earthworks on the environment. Geosynthetics have proved that they offer an effective and efficient solution. Design methods using geosynthetics have been developed for subbase stabilisation but may strongly differ depending on the model and the calibration behind. An experimental study, completed by numerical modelling has been carried out to understand better the behaviour of geosynthetic at the base of a granular layer on a weak soil.

Full paper to be published in:
https://www.e3s-conferences.org/articles/e3sconf/abs/2025/44/contents/contents.html

* Corresponding author: anancey@solmax.com

The role of mechanically stabilized base on the performance of top asphalt layer

Leoš Horníček[1*], *Zikmund* Rakowski[2], *Jacek* Kawalec[2], *and Jiří* Pospíšil[1]

[1]Czech Technical University in Prague, Faculty of Civil Engineering, Prague, Czech Republic
[2]Tensar International s.r.o., Český Těšín, Czech Republic

Abstract. The paper describes a laboratory study aimed at the influence of a granular layer mechanically stabilized by a multiaxial geogrid as the base on the performance of the top asphalt layer. Full-scale models with standard and composite bases were assembled in the laboratory facility of the Czech Technical University in Prague. Comparative models were dynamically loaded with the same amount of 100,000 loading cycles and equipped with few types of gauges. The settlement of a concrete circular loading plate placed on the top surface of the asphalt layer was a key parameter. Furthermore, observations included a precise deformation of geogrid, deformation of the contact between the asphalt layer and aggregate base, and horizontal pressures on the experimental box side wall as well. Comparison of the performance of the models showed a very positive influence of the mechanically stabilized layer leading even to the possibility of some reduction of asphalt and base thickness. It has economic sense, of course, but it also could solve a lack of proper natural aggregate which is already observed in some regions.

Full paper to be published in:
https://www.e3s-conferences.org/articles/e3sconf/abs/2025/44/contents/contents.html

* Corresponding author: leos.hornicek@fsv.cvut.cz

Research on geogrid stabilization of paved and unpaved roads

Giulia Lugli[1], *Pietro* Rimoldi[2*], *Gianluca* Spadaro[1], *Fabrizia* Trovato[3]

[1]Officine Maccaferri spa, GSY Business Development Department, 40132 Bologna, Italy
[2]Civil Engineering Consultant, 20157 Milano, Italy
[3]Officine Maccaferri spa, GSY Technical Department, 40132 Bologna, Italy

Abstract. Biaxial geogrids can be used for stabilising the base and subbase of paved and unpaved roads built on soft subgrade. Traffic Benefit Ratio (TBR) and Layer Coefficient Ratio (LCR) are used as the performance parameters in available design methods for road stabilisation. TBR and LCR values are peculiar to each combination of a specific biaxial geogrid, of the thickness and properties of the granular layers for base and subbase, and of the type of soft subgrade. The paper presents extensive research for evaluating the performance of extruded biaxial geogrids. In this study, large-scale experiments, including cyclic plate load tests, were conducted on various geogrid stabilised sections within a 2 m × 2 m × 1.1 m test box. The tests were carried out for both unstabilised and geogrid stabilised sections, both paved and unpaved, by applying a repeated load with a maximum force of 40 kN, equivalent to an applied pressure of 560 kPa, in the form of a load pulse with a loading period of 0.7 seconds and a rest period of 0.3 seconds. Over 10,000 loading cycles were applied on unpaved sections, while over 100,000 cycles were applied on paved sections. The research afforded the values of TBR and LCR referred to subgrades with different CBR values in the range from 1 to 10. The results of this study highlight the significant role that geogrid stabilisation can play in enhancing the performance of both paved and unpaved road sections.

1 Introduction

Permanent roads are generally constructed with an asphalt or concrete course on a granular base and a subbase layer which supports and distributes the traffic load to the subgrade layer. The subgrade often consists of fine cohesive soils that are unable to support it adequately.

Traditional solutions to place a road on weak subgrade are to excavate all or part of it and replace it with good quality soil. Alternatively, the subgrade can be improved by adding cement, lime or excess aggregate to increase its mechanical properties. In any case traditional solutions are often costly and always time-consuming.

Geosynthetics are a versatile and a cost-effective alternative, offering many advantages over traditional solutions including overall cost reduction, reduced construction time, improved environmental sustainability and more effective control of material quality.

* Corresponding author: pietro.rimoldi@gmail.com

Geosynthetics can stabilise unbound granular layers, that form the road foundation, essentially by two mechanisms: confinement and tensioned membrane mechanisms.

In confinement mechanism, geosynthetics provide stabilisation by limiting the movements of the particles constituting the aggregate layer. By providing lateral restraint, the confinement mechanism improves the mechanical properties of the aggregate layer by controlling the lateral deformations. In the confinement mechanism geosynthetics typically operate at low strain levels.

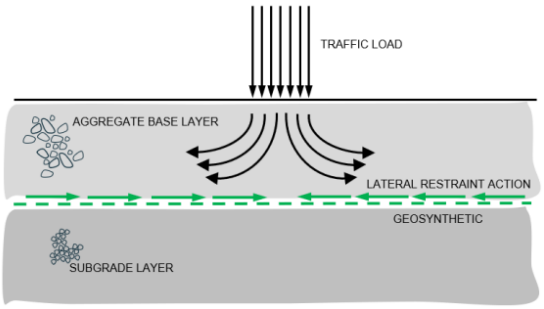


Fig. 1. Confinement mechanism.

In the tensioned membrane mechanism, geosynthetics anchored on either side of the loaded area, act as a tensioned membrane, supporting the aggregate layer and helping to reduce deformations. The tensioned membrane mechanism requires consistent out of plane deformation to be activated. In the tensioned membrane mechanism, geosynthetics operate at relatively high strain levels.

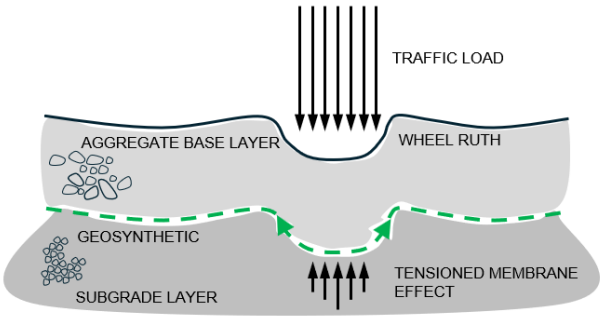


Fig. 2. Tensioned membrane mechanism.

The design of flexible road pavements incorporating geosynthetics to stabilise the base and subbase layers is usually carried out according to the AASHTO Guide for design of pavement structures [1]. The AASHTO design method is based on the empirical equation below:

$$logW_{18} = Z_R\, S_0 + 9.36\log(SN+1) - 0.20 + \frac{\log\left(\frac{\Delta PSI}{4.2-1.5}\right)}{0.40+\frac{1094}{(SN+1)^{5.19}}} + 2.32\log(Mr) - 8.07 \quad (1)$$

characterised by the structural number *SN*, consisting in an equivalent thickness which expresses the required structural strength of the pavement. The structural number is expressed by the following equation:

$$SN = a_1 d_1 + a_2 d_2 m_2 + a_3 d_3 m_3 \quad (2)$$

where *a* is the layer coefficient expressing the strength of the layer, *d* is thickness of the layer and *m* is the drainage coefficient of the layer; subscripts 1, 2, 3 refer to asphalt layer, base

and subbase. Hence SN represents the thickness of an ideal single layer having the layer coefficient equal to 1.0.

According to GMA's White Paper II (Berg et al., 2000) [2], the following empirical factors can be incorporated into the design to account for the contribution of a geosynthetic:

- Traffic Bearing Ratio (TBR) as the ratio of the number of load applications of the stabilised section to the number of load applications of the unstabilised section.
- Base Course Reduction Factor (BCR) as the ratio of the reduction in thickness of the stabilised layer to the thickness of the unstabilised layer.
- Layer Coefficient Ratio (LCR) as ratio of the layer coefficient of the stabilised layer to the layer coefficient of the unstabilised layer.

All of them can only be estimated from full-scale tests, which may be supplemented by large-scale laboratory tests performed under cyclic loading conditions, which must be validated and certified by a third party testing institute.

In the LCR design approach, the influence of a specific geosynthetic on the layer coefficient of the layer in which the geosynthetic is placed is implemented in the design according to the following equation:

$$SN_R = a_1 d_1 + LCR_2\, a_2 d_2 m_2 + LCR_3\, a_3 d_3 m_3 \quad (3)$$

LCR factor depends on the support provided by the underlying layers and it is usually plotted as function of their CBR. Therefore, even for the same geosynthetic, different LCR values need to be assumed when resting on different supporting layers.

2 Aim of the study

The paper presents the results of an extensive test campaign carried out at the Department of Civil Engineering of the Indian Institute of Science in Bangalore (India), to evaluate the performance of extruded biaxial polypropylene geogrids in stabilising unbound granular layers which constitute the typical foundation of flexible paved roads. Extensive analyses and elaborations of the raw test results allowed to obtain coherent values of the design parameters TBR and LCR for stabilised paved and unpaved roads. The following sections describe in detail the test procedure, the adopted setup and the materials involved in the series of tests.

3 Test apparatus

Testing setup was designed in accordance with the specifications reported in ASTM D8462-22 [3], which provides recommendations for the execution of Cycling Plate Load (CPL) tests, intended as performance tests to quantify the benefits provided by the stabilising geosynthetic incorporated within the unbound granular layers included in road pavement structure, and the provisions as per IRC SP:59 [4].

CPL is a laboratory test used to accelerate rutting in a road pavement structure using a cyclic plate load. Although the load application differs from real roads, the results of similarly constructed CPL tests are useful for evaluating and comparing the performance of various products or cross sections.

The test setup, shown in Figure 3, consisted of a large rigid vessel measuring 2 m × 2 m × 1.1 m, to accommodate the road pavement cross sections to be tested, minimizing boundary effects, and subjected to a cyclic load to simulate traffic load by means of a load assembly equipped with a 5 kN capacity load cell.

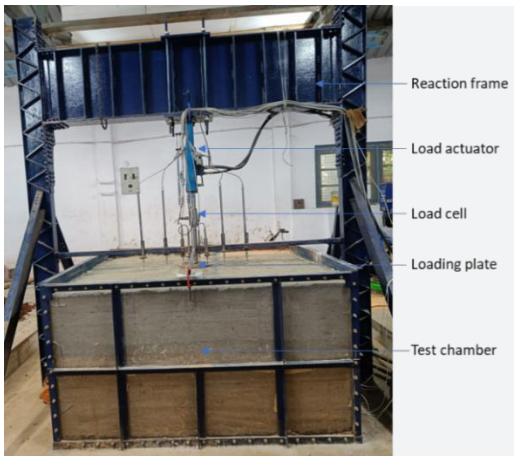


Fig. 3. CPL test setup used in the research.

To obtain an accurate measurement of the progressive cumulative displacements induced by the applied load, the unit has been equipped with linear variable differential transformers (LVDTs).

A 300 mm diameter bearing plate was used for the test phase, simulating the traffic load, whereas a 400 mm diameter bearing plate was used for the conditioning phase. A ball bearing system was used between the load shaft and the bearing plate to prevent any eccentric loading. An additional nitrile rubber pad was fitted immediately below the bearing plate to reduce the concentrated stresses due to minor surface irregularities.

The test sections were subjected to a repeated loading, in order to evaluate, for a given displacement, the influence of the stabilising geogrids to be tested, with a maximum load of 40 kN, corresponding to an equivalent applied pressure of 560 kPa, applied in the form of load pulses, with a loading period of 0.7 seconds and a rest period of 0.3 seconds.

Over 10,000 loading cycles were applied to the unpaved sections, while over 100,000 cycles were applied to the paved sections.

Prior to the application of the above described load, the test sections were subjected to a conditioning phase consisting of a repeated load with a maximum of 20 kN applied for 1,000 cycles to simulate traffic during the construction phase.

4 Tested materials

4.1 Subgrade material

The subgrade is the natural soil layer that rests immediately below the aggregate layers that form the road pavement structure. Its characteristics directly influence the performance of the above road pavement structure. Natural red soil (including 2 % gravel, 95 % sand, and 3 % silt and clay) was used as subgrade layer in this series of tests. The influence of the subgrade was simulated by varying the moisture content and bulk density to achieve the target subgrade CBR values of 1 %, 2.5 %, 5 % and 10 %.

4.2 Base and Subbase materials

A mix of crushed aggregate from a nearby quarry was used to construct the base and the subbase layers. The aggregates were screened to comply with the grading recommended by the Indian Ministry of Road Transport and Highways (MORTH) [5], with particles size in the range from 0.1 mm to 50 mm, as shown in Figure 4 right.

4.3 Geogrids

This paper examines the stabilising contribution ensured by biaxial extruded polypropylene geogrids Maccaferri MacGrid EG S to the aggregate layer in which they are incorporated. The characteristics of the tested geogrids are shown in Table 1.

Table 1. Extruded biaxial polypropylene geogrids characteristic

	Standard	Unit measure	Geogrid #1	Geogrid #2	Geogrid #3
Tensile strength	ASTM D 4759 EN ISO 10319	kN/m	20	30	40
Tensile strength at 2% strain		kN/m	7.0	11.0	14.0
Tensile strength at 5% strain		kN/m	14.0	21.0	28.0
Junction strength efficiency	GRI GG2 / GG1	%	> 90		

4.4 Asphalt layer

Bituminous wearing course was constructed using dense bituminous macadam in accordance with MORTH [5] and IRC SP:59 [4] specifications with binder content of 4.5 % by weight and minimum Resilient Modulus of 3,000 MPa.

5 Test procedure

The subgrade was first conditioned to achieve the required moisture content to obtain the desired subgrade CBR values. The conditioned subgrade soil was then compacted in the test box in 50 mm lifts using a manual hand compactor. To ensure adequate bonding between the layers, the surface of each lift was lightly scratched before the next layer was placed, as shown in Fig. 4 left.



Fig. 4. Subgrade layer laying process (left); photo of the aggregates used for base and subbase (right).

Once the designed subgrade thickness of 600 mm had been achieved, the subbase layer was constructed in 50 mm thick lifts using a vibratory plate compactor to achieve the planned 200 mm thickness as shown in Figure 5.



Fig. 5. Subbase layer compaction.

The execution of the tests on the stabilised road pavement sections required the installation of a panel of 1.9 m × 1.9 m geogrid placed on top of the compacted subbase layer, as shown in Figure 6. J-bolts and weights were positioned at the edges to prevent any wrinkle.



Fig. 6. Placement of the stabilizing geogrid in the testing box.

Then the base layer was constructed in 50 mm thick lifts using a vibratory plate compactor to achieve the planned 200 mm thickness.

The surface of the base, representing the surface layer for the unpaved tests, was then prepared for the placement of the bearing plate and the installation of LVDTs to measure surface deformations.

For the paved tests, a primer had to be applied on the surface of the base layer to provide the necessary adhesion between base and asphalt layer. A 1 m × 1 m × 0.09 m asphalt slab was confectioned at the asphalt plant using specially fabricated molds and then laid on top of the base layer adding the same thickness of granular soil used for the construction of the base layer all around the slab, to ensure a proper confinement to the bitumen slab (Fig. 7).

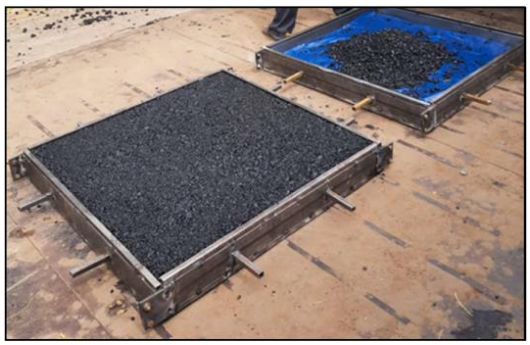


Fig. 7. Preparation of asphalt slabs for paved tests.

The schemes in Figures 8, 9, 10, 11 illustrate the test sections by specifying the layer thicknesses for each.

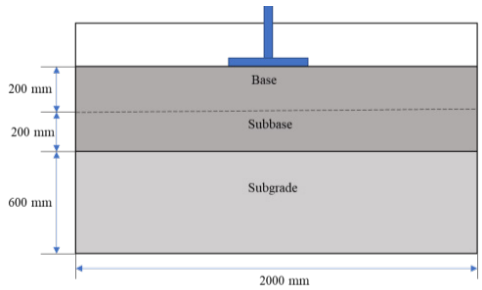


Fig. 8. Unstabilised unpaved test section.

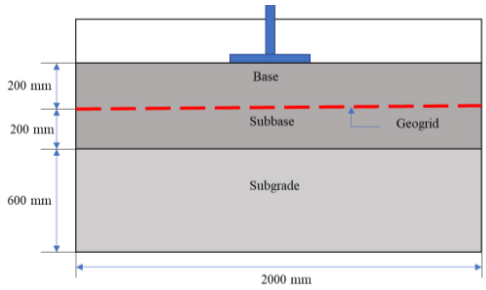


Fig. 9. Stabilised unpaved test section

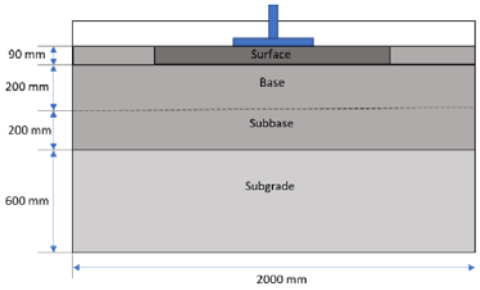


Fig. 10. Unstabilised paved test section.

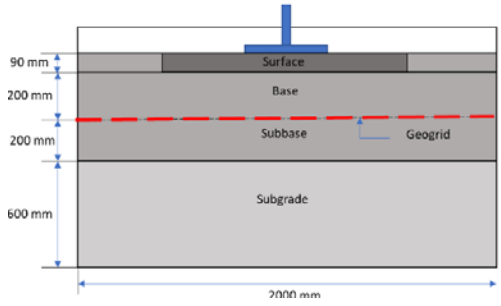


Fig. 11. Stabilised paved test section.

6 Test results

Tests were performed for the planned subgrade CBR values (1 %, 2.5 %, 5 %, 10 %), on both stabilised and unstabilised test sections, and both unpaved and paved test sections, for all the three grades of extruded biaxial geogrids involved in the research. The 20 mm rut depth required to evaluate the TBR values was only achieved for subgrade CBR of 1 %, while for the remaining subgrade CBR values of 2.5 %, 5 % and 10 % the rut depth remained below this target value. For these CBR values, the 20 mm rut depth was then extrapolated as a function of the number of applied loading cycles. The extrapolation functions that fit the measured deformations within the acceptable range were found to be exponential functions given by following equations:

$$N = c_1 \cdot d^{c_2} \quad (4)$$

$$N = k_1 \cdot d^{k_2} + k_3 \quad (5)$$

where N is the number of loading cycles corresponding to rut depth d and c_1, c_2, k_1, k_2, and k_3 are fitting parameters. The goodness of fit R^2 for both equations is greater than 0.99 for all the measured data. However, the number of loading cycles corresponding to a rut depth of 20 mm is greater with equation (4) than with equation (5). Therefore, in order to obtain a conservative estimation of the corresponding TBR and LCR, the number of loading cycles for the unstabilised cases was estimated using equation (4), while for the stabilised cases using equation (5); this approach provides a higher number of cycles for the unstabilised case and a lower number of cycles for the stabilised case, thus affording the minimum values of the calculated TBR and LCR. Extensive analyses and elaborations of the raw test results, applying the above described extrapolation methods with progressive refinements of the fitting parameters, allowed to get the curves in Figures 12 and 13.
For clarity and synthesis, only CPL test results related to subgrade CBR values of 2.50 % for Geogrids #1, #2, #3 and CBR value of 5 % for the Geogrid #2 are reported below in Figures 12 and 13.

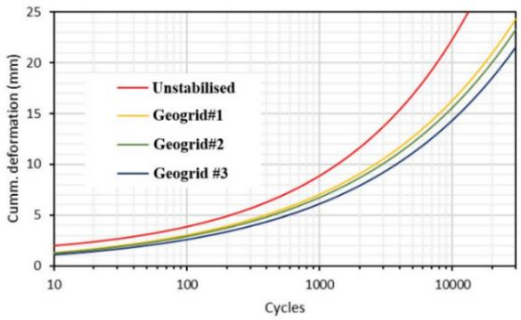


Fig. 12. Test results for unstabilised and stabilised unpaved sections with subgrade CBR = 2.5 %.

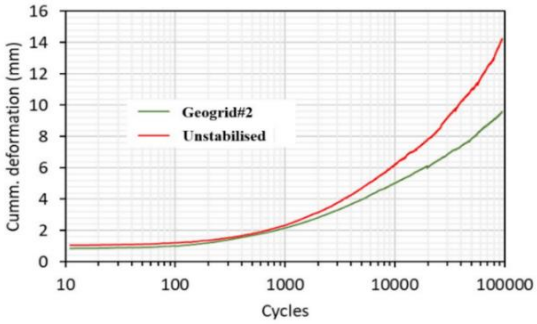


Fig. 13. Test results for unstabilised and stabilised paved sections with subgrade CBR = 5 %.

7 Testing results analysis

TBR is conventionally evaluated at a standard rut depth of 20 mm, which is consistent with the rutting failure criterion for flexible road pavements according to the relevant norms.

Extensive analyses and elaborations of the test results, summarised in the curves in Figures 12 and 13, finally afforded to obtain the TBR values estimated based on 20 mm ruth depth, as reported in Table 2.

The corresponding LCR values were then obtained, through other extensive analyses and elaborations, using AASHTO equation (1) to calculate the traffic on the unstabilised sections W_{18U}, from which, based on TBR values, the traffic on the stabilized sections W_{18R} was estimated. Using again AASHTO equation (1), the structural number of the stabilized sections SN_R was then calculated, from which finally the LCR was derived from equation (3). LCR values, estimated according to this procedure, are summarized in Table 3.

It is noted that the CBR values in Tables 2 and 3 take into account the test setup, where below the geogrid there are two layers, the subbase and the subgrade; therefore Tables 2 and 3 show the effective CBR values, which has been evaluated by calculating firstly the equivalent modulus $M_{r,eff}$ of the subgrade made up by the two combined layers, through an elastic layered analysis, at equal value of surface deflection, and then converting the $M_{r,eff}$ values to effective CBR values.

Table 2. TBR values summary

	TBR			
	CBR 1.5 %	**CBR 3.7 %**	**CBR 9.5 %**	**CBR 18.5 %**
Geogrid#1	3.28	2.62	2.53	2.48
Geogrid#2	3.53	2.90	2.75	2.60
Geogrid#3	3.91	3.20	3.03	2.80

Table 3. LCR values summary

	LCR			
	CBR 1.5 %	**CBR 3.7 %**	**CBR 9.5 %**	**CBR 18.5 %**
Geogrid#1	1.69	1.64	1.55	1.48
Geogrid#2	1.84	1.75	1.60	1.50
Geogrid#3	2.05	1.93	1.70	1.53

The comparison of the results obtained from paved tests and unpaved tests, as shown in Figure 14, indicates that similar LCR values can be obtained with unpaved tests with a lesser number of loading cycles compared to the number of loading cycles required for paved tests.

This finding indicates that unpaved tests may serve as a reliable approximation for assessing the performance of paved sections, potentially reducing the time and resources required for testing. The research therefore suggests then the LCR values obtained from unpaved tests can be directly used for the design of paved sections without the need for any correction factor, thus simplifying the design process and the implementation of stabilising geogrids in various road pavement structures.

Overall, the study demonstrates, as evidenced by the increased TBR and LCR values, that the incorporation of stabilising geogrids in pavement design is an effective strategy for improving road life, reducing maintenance costs and optimising the amount of aggregate to be sourced, making this approach particularly effective for both new constructions and rehabilitation projects. In addition to the already mentioned benefits, the use of stabilising geogrids has the further advantage of making more sustainable road projects.

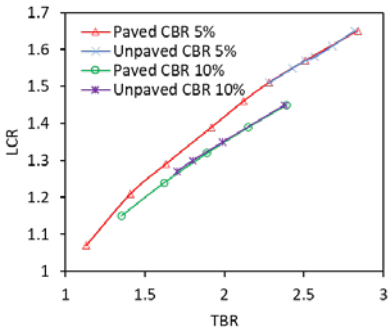


Fig. 14. Comparison of LCR for paved and unpaved tests for subgrade CBR of 5 % and 10 %.

Conclusions

A summary of the major findings and results of the research, qualitatively valid for any pavement system and quantitatively valid for the specific system that was tested, are presented below:

- The test setup and the testing method were in accordance with the specifications of ASTM D8462-22 [3] and IRC SP:59 [4].
- 10,000 load cycles were applied for unpaved tests, while 100,000 cycles were applied for paved tests.
- The stabilising contribution of the tested geogrids was quantified in terms of TBR (Traffic Benefit Ratio) and LCR (Layer Coefficient Ratio), which resulted mainly influenced by CBR of the subgrade and the stiffness of the stabilising geogrid.
- The LCR values were observed to increase with the increase of the tensile strength of the stabilising geogrid and to be higher for subgrade with lower CBR values than for subgrade with higher CBR values.
- The TBR was observed to increase with the increase in cumulative permanent deformation. This was reflected in LCR as a function of cumulative permanent deformation; the higher the considered cumulative permanent deformation, the higher the LCR for a given condition of subgrade CBR and stabilising geogrid. This is due to the activation of the stabilising geogrids as the number of load cycles increases.
- The research indicates that the LCR obtained from the unpaved test can be used for the design of paved sections with no correction factor.

References

1. AASHTO, Guide for design of pavement structures. American Association of State Highway and Transportation Officials, Washington DC, USA (1993)
2. R.R. Berg, B.R. Christopher, S. Perkins, Geosynthetic reinforcement of the aggregate base/subbase courses of pavement structures. Geosynthetic Materials Association White paper II, Roseville, USA (2000)
3. ASTM International, ASTM D8462-22: Standard test method for cyclic plate load tests to evaluate the structural performance of roadway test sections with geosynthetics. West Conshohocken, PA, USA (2022)
4. Indian Road Congress, IRC SP:59 Guidelines for use of geosynthetics in road pavements and associated works (First Revision), New Delhi, India (2019)
5. MORTH, Specifications for road and bridge works (Fifth edition). Indian Road Congress, New Delhi, India (2013)

Case studies of use of multiaxial stabilisation geogrids in heavy duty pavements

Piotr Mazurowski[1] and *Kasia* Zamara[2]

[1]Tensar Polska Sp. Z o.o., Azymutalna 9, 80-298 Gdańsk, Poland
[2]Tensar International Ltd, Cunningham Court, Shadsworth, Blackburn BB1 2QX, United Kingdom

Abstract: Use of multiaxial stabilisation geogrids in paved and unpaved roads is a most common type of application of this family of geosynthetics. In those kind of structures geogrids are subject to multiple, cyclic, but relatively low loads. It is less known that stabilisation geogrids can be equally successfully used in industrial pavements subject to very high loads, such as ports and container storage areas. This paper presents two case studies of pavements constructed in installation terminals at off-shore windmills construction facilities. Unpaved structures, consisting only of aggregate stabilised with geogrid, were designed and constructed for these two projects. Both pavements were designed to carry very high loads from cranes and assembled wind tower parts stored in the area – uniformly distributed load of up to 500 kPa or loads from elements weighting up to 1000T. In both cases challenging ground conditions, with low bearing capacity and compressible organic soils, had to be addressed, which required detailed settlement analysis.

1 Introduction

Geosynthetics can perform a variety of different functions in civil engineering applications. Most common functions utilised in pavement construction are separation, filtration, reinforcement, stabilisation (described in [1] as 'stiffening') and drainage [1]. Two of those – reinforcement and stabilisation – can provide substantial benefits to pavement life, which can be quantified and used in pavement design. [2] provides guidelines for development of design approach for geosynthetics in flexible pavements based on performance tests, including full scale trafficking tests.

Use of geogrids for stabilisation of aggregate was recognized by standardisation organisations as a separate function of geosynthetic relatively recently. International Organization for Standardisation (ISO) defines the stabilisation function by means of aggregate interlock and confinement, as opposed to reinforcing function being corelated to geogrid tensile strength, as: "improvement of the mechanical behaviour of an unbound granular material by including one or more geosynthetic layers such that deformation under applied loads is reduced by minimizing movements of the unbound granular material" [3]. ASTM defines it as: "the ability of one or more geosynthetics layers to reduce deformation under applied loads to limit the movements of unbound granular material or improve sub-grade support" [4].

1 Corresponding author: piotr.mazurowski@cmc.com

Stabilisation geosynthetics, especially geogrids, do not rely on tensile strength to increase performance of aggregate layer. They provide a mechanism where the aggregate particles within the granular layer interlock with the geogrid and the subsequent particle confinement prevents deformation. When unbound well graded aggregate is placed and compacted on a layer of stabilisation geogrid, aggregate particles penetrate through and interlock within the geogrid apertures and are confined by its stiff ribs (Fig 1). A geogrid/aggregate composite is created, in which lateral restraint provided by the geogrid reduces strains and thereby increases the stiffness of the layer compared to the same layer without geogrid. Such layer of aggregate stabilised with geogrid is often referred to as Mechanically Stabilized Layer (MSL).



Fig. 1. Aggregate particles interlocked within stabilisation geogrid

Increase in aggregate properties due to stabilisation with geogrids can be quantified. Lees and Clausen [5] developed a method for derivation of strength parameters of granular soils stabilised with multiaxial stabilisation geogrids with the use of large triaxial tests. This approach has been then utilised by one stabilisation geogrids manufacturer to develop new design methods for working platforms and unpaved roads.

Years of practical experience with the use of geosynthetics in real life projects, as well as numerous research [6-7] proved that there is no direct correlation between tensile strength of geosynthetic and their performance in pavement applications. However, according to Authors observations, it seems that still a lot of engineers recognize tensile strength as a primary characteristic of geosynthetic used in pavements, and tend to use as strong material as possible in designs, especially in structures subject to high loads.

This paper describes two case studies of projects in which multiaxial stabilisation geogrids were used in heavy duty pavements subject to very high loads from different kinds of structures for off-shore windfarms construction. Geogrids used were of relatively low tensile strength, however due to stabilisation effect described above they worked perfectly well in aggregate-only pavements, and provided safe, economical and environmental friendly solutions.

2 Serial production plant for large-scale steel structures in Szczecin, Poland

Serial Production Plant For Large-Scale Steel Structures is located in Szczecin, a port city in North-West Poland. It is located in industrial area along the Odra river, on the small island called Ostrów Brdowski. This part of the city is known for very complicated ground conditions, with deep deposits of organic soils, which is understandable, given its proximity to the river and to the Szczecin Lagoon. This is, however, a perfect location for a facility producing structures used for off-shore windfarms construction, as Odra river and Szczecin Lagoon enable easy connection to Baltic Sea.

Production plant on the Ostrów Brdowski island was constructed in 2015 (Fig. 2). Its main purpose is production, assembly and storage of large-scale structures for off-shore windfarms. As a part of the plant, one of the largest production halls in Poland was constructed, with height of 42 m and volume of 1,100,000 m^3.



Fig. 2. Aerial view of Production Plant in Szczecin *(source: https://atlasward.pl/niezwykla-realizacja-hali-na-wyspie/)*

Apart from production and paint halls construction, significant part of the project was construction of pavements for transportation and storage of ready-made structures. A big variety of different structures, like monopiles and jackets, can be produced in this facility, including jackets of maximum weight up to 1000 T (Fig. 3). Such jackets have to be safely transported after assembly, stored, and then transported again to the wharf, where they are loaded on barges and shipped to destination location by the sea.

Ground conditions at the project location are challenging. Subgrade consist of thin (up to 1.5 m) layer of made ground, below which there is a 6-8 m thick deposit of organic soils – peats and organic clays. Example of geological profile from the project location is shown in Fig. 4.

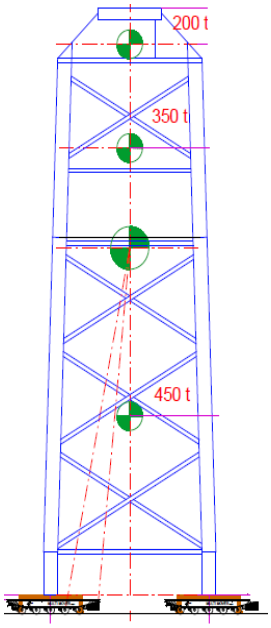


Fig. 3. Outline of loads applied by jacket during transport by SPMTs *(source: "Construction of Serial Production Plant for Large-scale Steel Structures on Brdowski Ostrów in Szczecin", design by Biuro Projektów Budownictwa Morskiego Projmors, Gdańsk, 2012)*

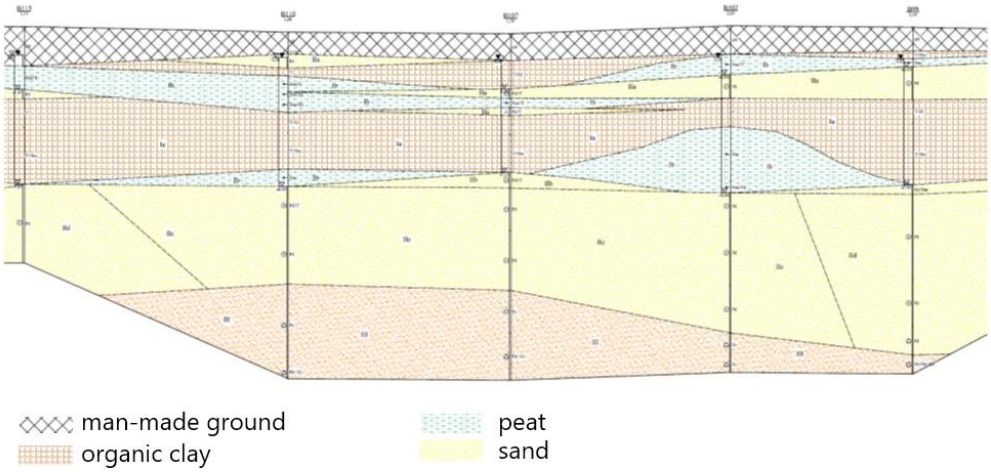


Fig. 4. Example of geological profile of subgrade at Ostrów Brdowski island *(source: "Construction of Serial Production Plant for Large-scale Steel Structures on Brdowski Ostrów in Szczecin", design by Biuro Projektów Budownictwa Morskiego Projmors, Gdańsk, 2012)*

Two main issues had to be addressed at the design stage: potential settlements of subgrade and its low bearing capacity.

The issue of settlements was solved by the use of vertical wick drains and overload embankment. As there was not enough embankment material available at the site, overloading was performed in stages: part of the area was overloaded for 3 months, and then material was moved to next part of the area, and so on. 90% consolidation of weak soils was achieved this way.

The second problem to solve was construction of pavement on a low bearing capacity subgrade, capable of withstanding extreme loads applied by 1000 T jacket during

transportation and storage. Subgrade below the pavement was assumed to have undrained shear strength of Cu = 32.5 kPa. Jackets are transported in vertical position, by SPMTs (Self-Propelled Modular Transporters), and stored also in vertical position.

Unpaved aggregate-only pavement structure was chosen for this project, as it is significantly cheaper than any paved (concrete, asphalt of paving blocks) structure. This type of pavement has one important disadvantage, which is surface rutting caused by moving vehicles and machinery, but this can be relatively easily solved by regular maintenance. However, this approach can only work if any rutting is happening at the surface of the structure only, and subgrade is protected from deformations.

Solution adopted for this project was the design of the unpaved structure consisting of high-quality crushed aggregate stabilised with multiaxial stabilisation geogrids. Design analysis included calculation of maximum rut on top of the pavement resulting from SPMTs passes, as well as checking of bearing capacity of the structure loaded with 1000 T jacket. Total designed pavement thickness is 80 cm, with three layers of geogrids (see Fig. 5). In total, more than 150,000 m^2 of stabilisation multiaxial geogrids were installed in this project (Fig. 6)

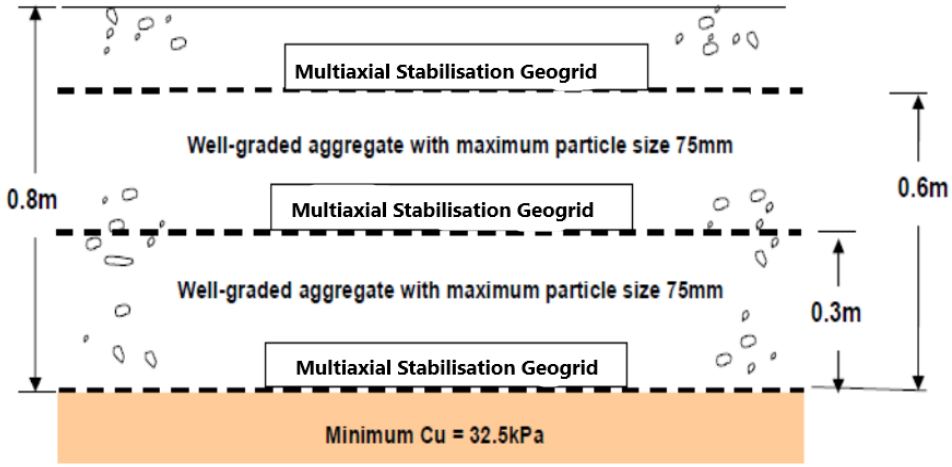


Fig. 5. Unpaved pavement structure designed for Production Plant in Szczecin *(source: geogrid manufacturer archive)*



Fig. 6. Installation of multiaxial geogrids *(source: geogrid manufacturer archive)*

3 Installation terminal for off-shore windfarms in Świnoujście, Poland

Installation Terminal for Off-Shore Windfarms is a big terminal located in Świnoujście port, north-west Poland, at Baltic Sea shore, about 70 km north of Szczecin. Its construction started in 2023, and it is scheduled to be finished early 2025. This terminal is planned as a storage and reloading facility for all kinds of elements needed for off-shore windfarms construction, like jackets, blades, turbines, towers etc. Total area of the terminal is about 20 hectares (Fig. 7).

Subgrade at the facility area consists of 1.5 – 2.5 m layer of man-made ground, below which there is a 9-10 m thick layer of fine sand with pockets of organic clay. Below this there is 1 – 3 m thick layer of organic clay, and below that there is fine and medium sand. Example of geological profile from the project location is shown in Fig. 8.



Fig. 7. Aerial view of Installation Terminal in Świnoujście under construction *(source: https://24kurier.pl, photo: Dariusz Gorajski)*

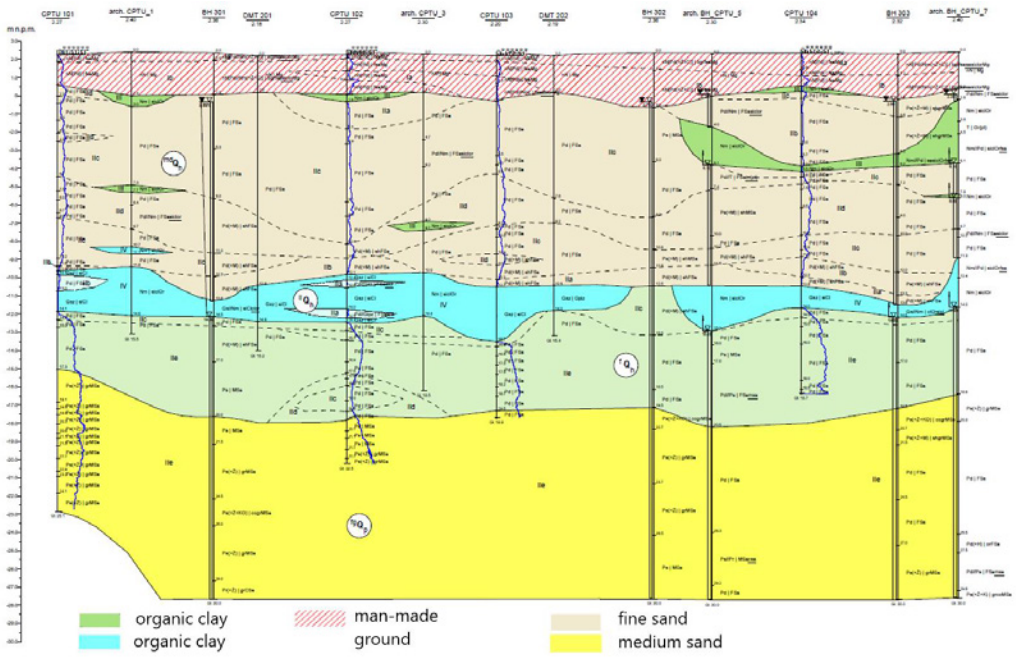


Fig. 8. Example of geological profile of subgrade at Installation Terminal in Świnoujście *(source: Ground Investigation Survey by Geoprojekt Szczecin, 2023)*

From pavement types perspective, the terminal area is divided into four parts:

- Concrete pavement along the wharf
- Unbound aggregate pavement at crane operating area
- Unbound aggregate pavement at storage area
- Paver blocks pavement at parkings and internal roads area

Apart from parkings and internal roads area, all other pavements were to be designed for very heavy loads, either 250 kPa in the storage area or 500 kPa in the wharf and crane operating areas.

Concrete wharf pavement was designed as reinforced concrete plate founded on set of concrete piles. Other pavements (apart from parkings and internal roads area) were designed as unbound aggregate pavements, stabilised with multi-shape stabilisation geogrids. Unbound aggregate pavements consists of either high quality recycled concrete or crushed aggregate, depending on material availability.

Extensive calculations of pavement structures were performed, both for bearing capacity and for settlements (Fig. 9), for a wide range of different loads in different locations with different ground conditions. Loads from all different structures, which can be stored in the facility, were checked (monopiles, transition pieces, nacelles, sections of towers, rotor blades, offshore substations, cable baskets, GSBs) as well as loads from two types of cranes: LR13000 and CC8800. All structures were verified both for storage conditions and transport with SPMTs. Analysis showed that potential settlements are within range acceptable by customer, so there was no need for any expensive deep soil improvement techniques, like piles, columns or wick drains (apart from concrete wharf, as mentioned above). Long term settlements were not a concern, as there is an assumption that any surface deformations will be repaired as part of routine maintenance. Bigger concern were immediate and short term settlements (up to several days after the load is applied), especially differential settlements, as they can be dangerous and difficult to react to. However, the analysis showed that these settlements are within acceptable range and ensure safe operations at the facility.

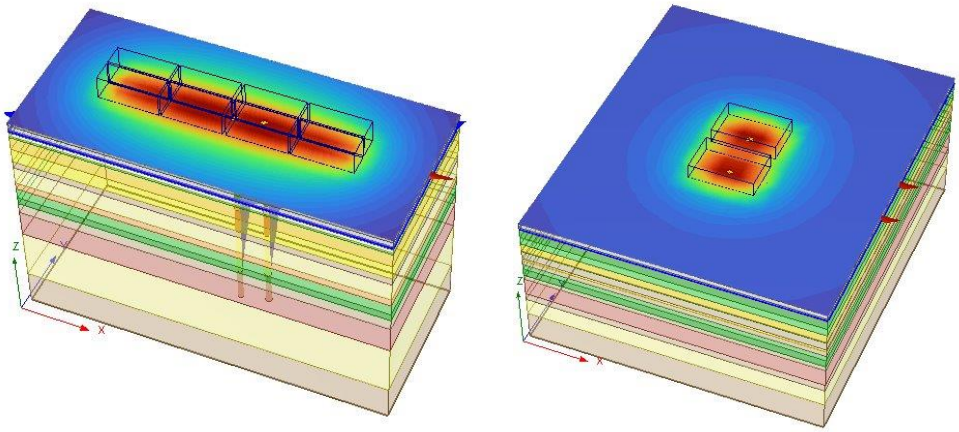


Fig. 9. Examples of visualizations of settlements analysis results: rotor blade (left), CC8800 crane (right) *(source: geogrid manufacturer archive)*

Bearing capacity and settlements analysis took into account enhanced parameters of aggregate stabilized with multi-shape stabilisation geogrids. Three types of unbound aggregate pavements were designed as a result of all the analysis:

- 109 cm thick pavement with three layers of multi-shape geogrid for crane operating areas
- 80 cm thick pavement with two layers of multi-shape geogrid for storage areas in eastern part of the facility (worse ground conditions)
- 70 cm thick pavement with two layers of multi-shape geogrid for storage areas in western part of the facility (better ground conditions)

Fourth type of pavement was designed for parkings and internal roads, but as it was a typical pavement for cars and trucks traffic, such extensive analysis was not required. It was designed as 50 cm thick pavement with two layers of geogrids.

More than 370,000 m^2 of multi-shape stabilisation geogrids were installed on this project (Fig. 10).



Fig. 10. Installation of geogrids and aggregate *(source: geogrid manufacturer archive)*

4 Conclusions

Case studies described above are just two examples of many projects constructed around the world proving high efficiency of stabilisation geogrids in heavy duty pavements applications. Use of Mechanically Stabilised Layers provides designers, contractors and clients with opportunities to construct reliable, economical, easy to construct and environmentally friendly pavements for all kinds of loads, from typical vehicles traffic to very heavy loads from transport of industrial structures. These case studies also confirm the reasoning which led to establishing a new geosynthetic function – stabilisation – as a function, which is separate and different from reinforcement function. Stabilisation geosynthetics do not require a high tensile strength to perform properly in pavements, even pavements subject to extreme loads.

References

1. J.G. Zornberg, Functions and applications of geosynthetics in roadways, Transportation Geotechnics and Geoecology, TGG 17-19 May 2017, St. Petersburg, Russia, 298-306 (2017) https://doi.org/10.1016/j.proeng.2017.05.048
2. American Association of State Highway and Transportation Officials, Standard Practice for Geosynthetic Reinforcement of the Aggregate Base Course of Flexible Pavement Structures, AASHTO R 50-09, Washington, USA (2009)
3. ISO, Geosynthetics – Part 1: Terms and definitions, 10318-1:2015 Amendment 1-2018. ISO/TC 221 Geosynthetics. Geosynthetics (2015)
4. ASTM, Standard terminology for geosynthetics, ASTM D4439 (2023)
5. A. Lees and J. Clausen, Strength envelope of granular soil stabilized by multi-axial geogrid in large triaxial tests, Canadian Geotechnical Journal 57, 3 (2020) https://doi.org/10.1139/cgj-2019-003
6. C.G. Jenner, G.R. Watts and D.I. Blackman, Trafficking of reinforced unpaved subbases over a controlled subgrade, in Proceedings of the 7th Int. Conf. on Geosynthetics, Nice, France (2002)
7. J. Cook, M. Dobie and D. Blackman, The development of APT methodology in the application and derivation of geosynthetic benefits in roadway design. In: Aguiar-Moya, J., Vargas-Nordcbeck, A., Leiva-Villacorta, F., Loría-Salazar, L. (eds) The Roles of Accelerated Pavement Testing in Pavement Sustainability. Springer, Cham. (2016) https://doi.org/10.1007/978-3-319-42797-3_17

Advanced multi-composite products for road stabilization: a comparative design and LCA analysis

Fabrizia Trovato[1*], *Jayakrishnan* P.V.[2], *Giulia* Lugli[1] and *Pietro* Rimoldi[3]

[1]Officine Maccaferri S.p.A, Geosynthetic Business Unit, 40132 Bologna, Italy
[2]Maccaferri Middle East, Technical Department, Dubai, UAE
[3]Civil Engineering Consultant, 20157 Milano, Italy

Abstract. In the construction sector, there is a growing emphasis on sustainable solutions driven by global recognition of the negative impacts of human activities on the environment. Among these solutions in civil engineering applications, geosynthetics have proven to be a versatile and high-performing alternative to traditional materials, offering significant advantages in terms of reducing resource consumption and minimizing CO_2 emissions. When two or more geosynthetics are coupled together to create a single product, the result is a high-performance product called a multi-composite geosynthetic. These are engineered to enhance project efficiency and sustainability, ensuring faster and more efficient installation in terms of time, costs, and CO_2 emissions from production and installation operations. A notable example of this innovation is the use of multi-composite geosynthetics for road applications, which incorporate a biaxial geogrid with a drainage geocomposite. These components work together to stabilize subgrades, facilitate water drainage, and reduce aggregate layer thickness due to the reinforcement element. In this paper, the results of a comparative design calculation based on the AASHTO 1993 method will be presented to better illustrate how the inclusion of a multi-composite geosynthetic within the road structure can impact the reduction of various layers in comparison to an unreinforced road section. These results will be used to perform a comparative Life Cycle Assessment analysis, confirming the effectiveness of the multi-composite solution compared to traditional design methods.

1 Introduction

In recent years, the construction sector has placed increasing emphasis on sustainability, as public administrations and engineers have become more aware of the environmental challenges posed by traditional practices. Global recognition of the negative environmental impacts of human activities has led to the adoption of international directives like the United Nations Sustainable Development Goals (SDGs). In response, the European Union, with the introduction of the new Construction Products Regulation (CPR) [1], encourages the industry to consider sustainable solutions that reduce resource exploitation, promote circularity and

* Corresponding author: f.trovato@maccaferri.com

minimize environmental footprints. This results in a growing trend toward adopting customized, eco-friendly solutions that align with modern sustainability standards.

Among the various solutions available in the civil and geotechnical engineering sectors, geosynthetic products have already proven to be a widely adopted technology among contractors and stakeholders, thanks to their versatility and ability to meet diverse project requirements, while providing an efficient and sustainable alternative to conventional materials. When multiple geosynthetics are combined into a single product, the result is a high-performance multi-composite geosynthetics which further improve project efficiency and sustainability compared to individual components. An example of this innovation is multi-composite geosynthetics for road applications, which combine a biaxial geogrid with a drainage geocomposite, to reduce the thickness of aggregate in the base and subbase layers.

They enable a cost-effective design not only by reducing the thickness of granular layers but also by lowering CO_2 emissions given by a faster installation and minimizing resource extraction.

The scope of this paper is to present the results of a comparative design calculation based on the AASHTO 1993 (American Association of Highway and Transportation Officials) method [2], illustrating how the inclusion of a multi-composite geosynthetic in the road structure can reduce the thickness of various layers compared to an unreinforced road section. These results will then be used for a comparative Life Cycle Assessment (LCA) [3] to evaluate the sustainability benefits of geosynthetics and confirm the effectiveness of the multi-composite solution over traditional design methods.

2 Multi-composite geosynthetics

2.1 Application overview

Geosynthetics are polymer-based engineered materials designed for various functions in civil engineering, geotechnical, and environmental applications. As defined by ISO 10318 [4], geosynthetics include various functionalities, offering advanced solutions for infrastructure development. Key functions such as filtration, separation, drainage, reinforcement, barrier, and protection make geosynthetics a sustainable and efficient alternative to traditional construction methods, which instead rely on extraction, consumption and transportation of natural resources such as gravels or other mineral-based materials.

Paved roads that handle high traffic volumes typically consist of asphalt layers placed above base and subbase layers made of gravel aggregate. These layers work together to support and distribute traffic loads to the subgrade. However, challenges arise when the subgrade consists of soft clay, silt, or organic soil, which is highly water-sensitive and lacks the necessary strength to adequately support traffic loads.

Traditional solutions like excavating and replacing weak subgrade layers or using stabilization techniques can be costly and time-consuming. The inclusion of geosynthetics for stabilization optimizes road design by reducing the thickness and the depletion of natural aggregates, thereby lowering the overall project costs. These projects often span kilometres and involve complex installation, so saving material on layer thickness offers significant economic and environmental benefits.

The use of multi-composite geosynthetic can further enhance these advantages, by integrating multiple functions within a single system, significantly reducing the installation procedures that would otherwise be required when laying individual geosynthetic components. It consists of a drainage core made of channelized monofilaments, thermally bonded with two nonwoven geotextiles for separation and filtration purposes, and a high modulus polypropylene biaxial extruded polypropylene geogrid. The result is an engineered product specifically designed for road applications, produces through an advanced

manufacturing process that enables the lamination of two or more components directly at the factory (Fig.1).

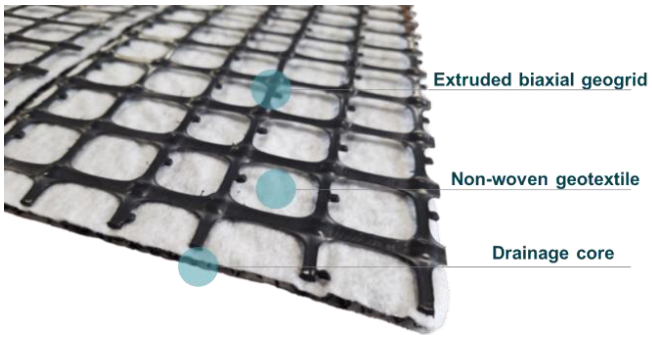


Fig. 1. Multi-composite geosynthetic for road stabilization.

2.2 Multi-composite components

The three main components of the multi-composite for road stabilization are:

- High-modulus polypropylene geogrids, produced through an extrusion process with tensile strengths ranging from 20 to 40 kN/m in both directions, stabilize the unbound granular layers beneath the road pavement. They enhance the rigidity of the layers through an interlocking mechanism between the unbound materials and the mesh of the extruded PP geogrid;
- The drainage core, composed of a geomat with a W-shaped profile and an average thickness of 9mm, provides high resistance to compressive loads, minimizes compressive creep, and maintains a high flow rate. This configuration allows water to drain from both the top and bottom as well allowing the drainage of capillary rise water from the subgrade;
- Two layers of nonwoven geotextiles: each with an average mass of 130 g/m², act as external filters to prevent soil mixing and maintain the integrity of the base and subbase layers with the subgrade.

The multi-composite product, with an average thickness of 11 mm, is tested to determine the key parameters required for designing a paved road following the AASHTO 1993 method. The characteristics of the products are shown in Table 1.

Table 1. Multi-composite for road stabilization - performance

	Standard	Unit	Value
Tensile strength MD & CMD	EN ISO 10319	kN/m	33 & 26
Tensile strength at 2% strain MD & CMD		kN/m	14
In plane flow capacity MD			
S/S i=1; 20kPa – Short term	EN ISO 12958	l/(m s)	3.20
R/S i=0.03; 20kPa – Short & Long term(100y)			0.45 & 0.41
R/S i=0.03; 100kPa – Short & Long term(100y)			0.36 & 0.32

3 Improved design of paved roads

The AASHTO 1993 method, the most widely used approach for flexible pavement design, applies empirical equations based on multilayer elastic theory. It determines a target thickness, known as the Structural Number (*SN*), which depends on expected traffic for the design life and subgrade properties. The *SN* is calculated by summing the structural contributions of the asphalt layer, base course, and subbase course, considering their thickness (d_i), layer coefficients (a_i), and drainage coefficients (m_i), as applicable (Eq. (1)):

$$SN = a_1 d_1 + a_2 d_2 m_2 + a_3 d_3 m_3 \quad (1)$$

The incorporation of extruded geogrids as reinforcement in the base or subbase layers enhances the structural performance (SN_R) of flexible pavement systems. This is achieved by increasing the layer coefficient (a_i) of the aggregate base and granular subbase courses. Accordingly, the AASHTO Eq. (1) gets modified as Eq. (2):

$$SN_R = a_1 d_1 + LCR_2\, a_2 d_2 m_2 + LCR_3\, a_3 d_3 m_3 \quad (2)$$

LCR is the layer coefficient ratio, which has a value always higher than unity. *LCR* value is determined based on the results from laboratory testing (ASTM D8462) on flexible pavement systems with and without geogrid.

Reinforcement alone is not always sufficient to stabilize a road section. Water is one of the primary causes of pavement distress, and effective drainage significantly extends roadway lifespan. Modern roads with proper drainage can last two to three times longer than undrained sections [5]. Incorporating a drainage layer into the road structure enables rapid water removal.

The AASHTO 1993 design method accounts for drainage using the time-to-drain principle, which estimates the time needed for the pavement system to drain after a significant moisture event. Table 2 defines poor to excellent drainage based on the time required for 50% of free water to drain from a saturated pavement section.

Table 2. AASHTO definitions for pavement drainage recommended for use in both flexible and rigid pavement design

Quality of Drainage	Water Removed Within
Excellent	2 hours
Good	1 day
Fair	1 week
Poor	1 month
Very Poor	Does not Drain

The formula for the calculation of the time to drain t depends on geometric factors and intrinsic characteristics of the drainage layer. Key geometric factors include the width of the roadway W, longitudinal and transverse slope S_R, and the thickness of the layers H the water must travel through to reach the drainage system. Regarding the intrinsic properties, the most important parameters, especially when considering conventional design are porosity (N_0) and the coefficient of permeability (k), both of which are related to the transmissivity of the drainage layer and play a critical role in ensuring effective drainage.

For a conventional design (unreinforced section), the drainage consists of an open-graded, free-draining base layer, which requires asphaltic or cement stabilization binders to facilitate construction, increasing the density of the base. Additionally, a dense-graded subbase layer is usually placed beneath the base for structural purposes and to prevent the migration of subgrade particles. Due to the low permeability of these layers, the drainage path to the edge of the road is extremely slow

Placing a drainage geocomposite within the subgrade-base or subgrade-subbase significantly reduces the drainage time by shortening the drainage path to the thickness of the base, rather than the entire width of the roadway.

Multi-composite geosynthetic, which not only include a drainage layer but also an extruded geogrid, provides an optimal solution to enhance both drainage and pavement stabilization. The combined effect of this innovative material allows for the simultaneous improvement of the parameters *ai* and *mi* of the AASHTO 93 formulation, thereby leading to an improvement of the SN. In the following chapter, four case studies are presented to show the calculations performed to demonstrate how the influence of an advanced product, such as multi-composite geosynthetics, can lead to a reduction in thickness and optimization of the road base. These case studies will also serve for conducting a LCA study to evaluate the environmental performance following the requirements of ISO 14040 and 14044 standards.

4 Comparison between case studies

The four case studies (A, B, C, and D) were modelled based on a 2.0 km long highway section with a 7.0 m wide two-lane configuration, a 2% slope, a total design ESAL (W18) of 18,000,000, a reliability level of 95%, and a subgrade CBR of 1%.

The initial unreinforced pavement section (**Case A**) consists of 10 cm of asphalt surface course, 60 cm of well-graded base granular material with k =2.50 m/day and N_0=0.30 and 100 cm of mixed granular subbase material with k = 0.70 m/day and N_0=0.20. In this case, the time to drain is strongly influenced not only by k, N_0 coefficients and the thickness of the base and subbase layers but primarily by the horizontal drainage time required for water to travel across the entire width of the roadway, which is the critical factor to be considered. The calculations performed according to AASHTO 93 (Table 3) show that the quality of drainage for the layers is considered fair/poor, meaning m_2= and m_3=0.8, assuming the road is exposed to moisture levels approaching saturation for 2–25% of the time.

In **Case B** the introduction of a drainage geocomposite (gcd) is considered between the subbase and the subgrade. In this case, the time to drain depends on the drainage rate of the base and subbase layers into the drainage geocomposite, plus the time to drain for the geocomposite drainage layer (horizontal drainage time).

The drainage composite has a flow rate of Q = 0.44 l/(m·s) = 4.4×10^{-4} m²/s under a gradient of 0.03 and a normal load of 50 kPa. Considering a drainage thickness of 0.009 m, it is possible to calculate the velocity of water traveling through the geocomposite and a horizontal drainage time of 0.04 hours, which is considered negligible. By adding this time to the time for drainage, calculated following the same procedure as in Case A and shown in Table 3, we can find that the drainage geocomposite increase the quality of drainage from fair/poor to fair/excellent, leading to an increase in the m_3 parameter.

The same considerations apply to **Case C**, where the inclusion of an advanced multi-composite between the subbase and the subgrade not only enhances drainage efficiency but also strengthens the pavement structure through the integration of an extruded geogrid. The improved drainage reduces the need for a thick subbase, while the geogrid increases tensile stiffness across all layers above it, optimizing stress distribution. This combined effect resulted in a substantial reduction in the thickness of both the base and subbase layers, with base thickness reduced by up to 50% and subbase by 45% compared to an unreinforced section. This optimization was achieved even with the installation of just a single layer, strategically positioned at the interface between the subbase and subgrade.

Comparable thickness reductions achieved with the use of the multi-composite in Case C could be obtained in **Case D** by incorporating extruded polypropylene geogrids at the subgrade-subbase and subbase-base interfaces. To achieve comparable results in thickness reductions, higher grade extruded geogrids with a characteristic tensile strength of 40 kN/m were utilized. This resulted in Layer Coefficient Ratio (LCR) values of 1.40 and 1.85, depending on the CBR of the underlying layers. With these geogrids, the base thickness was reduced by approximately 33% and the subbase thickness by about 40% compared to Case A. This option, despite offering a significant advantage in terms of reducing the thickness of

natural coarse gravel layers, with a major impact on construction and sustainability costs, does not provide improvements in the overall drainage quality. Therefore, if the subgrade consists of fine-grained, water-retentive materials, this could potentially impact the long-term durability of the pavement due to reduced moisture removal efficiency leading then to a more frequent maintenance.

Table 3 summarizes the comparison of the four case study designs. These results will be used to perform a Life Cycle Assessment comparing traditional design with sustainable alternatives.

Table 3. Results comparison of road sections design

	Case A Unstabilized		**Case B** Gcd		**Case C** Multi-composite		**Case D** Extruded PP GG	
	Base Course	**Subbase Course**	**Base Course**	**Subbase Course**	**Base Course**	**Subbase Course**	**Base Course**	**Subbase Course**
Time Factor (T_{50})	0.40	0.51	0.40	0.23	0.40	0.23	0.40	0.51
"m" Factor	12.25	17.50	12.25	0.29	12.25	0.29	12.25	17.50
Time to Drain [days]	4.96	8.89	4.96	0.07	4.96	0.07	4.96	8.89
Quality of drainage	fair	poor	fair	excellent	fair	excellent	fair	poor
m coefficient for %time 2-25%	**1**	**0.8**	**1**	**1.3**	**1**	**1.3**	**1**	**0.8**
LCR	-	-	-	-	-	**1.65**	**1.40**	**1.85**
Thickness of layers	**0.60 m**	**1.00 m**	**0.60 m**	**0.70 m**	**0.30 m**	**0.55 m**	**0.40 m**	**0.60 m**
%reduction	-	-	-	**-30%**	**-50%**	**-45%**	**-33%**	**-40%**

5 LCA analysis

As per ISO 14040, the LCA is conducted in four distinct phases such as (1) goal and scope, (2) life cycle inventory (LCI), (3) life cycle impact assessment (LCIA) and (4) results and interpretation. These phases are often interdependent, as the results of one phase can shape the approach and implementation of the others.

5.1 Goal and scope

The objective of this LCA study is to evaluate the environmental performance of the four road sections by comparing the impact of a traditional design with a geosynthetics-based solution. The aim is to assess the sustainability benefits of geosynthetics and validate the enhanced effectiveness of the multi-composite solution over conventional approaches.

The analysis was conducted for the four case studies schematized in Fig. 2 using One Click LCA [6], a cloud-based software designed for assessing sustainability in engineering designs. The software uses curated databases (e.g., Ecoinvent) as well as industry-provided environmental product declaration (EPD) in accordance with EN 15978 [7]. The data points comply with EN 15804 [8] and/or ISO 14025 [9].

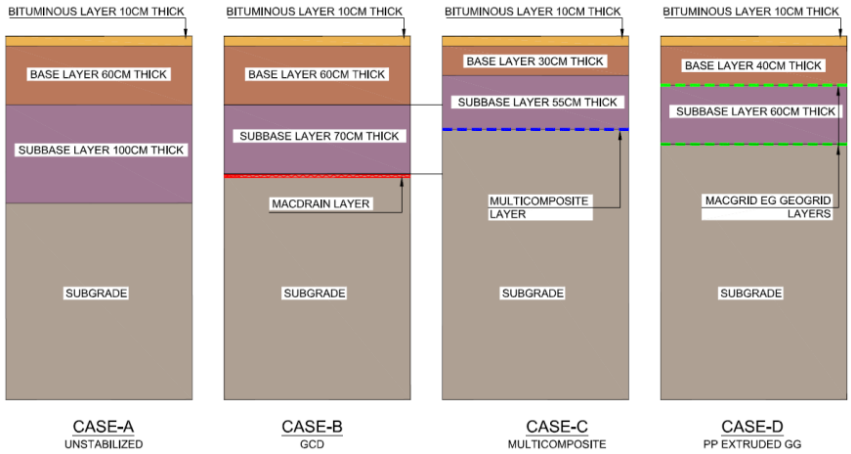


Fig. 2. Details of four cases of road pavement solutions

The functional unit (FU) for this comparative LCA study is a 2 km running length road section with a carriageway of 7 m. The design lifespan is 30-year.

EN 15804 defines a standardized life cycle model for building and construction works, enabling modular stage comparisons across projects. Depending on the LCA objectives, certain stages may be excluded when detailed data is unavailable or to minimize uncertainties. This LCA analysis includes the product stage (A1-3) and the construction process stage (A4-5). Stages B1-3, C1-4, and D are excluded due to scope limitations and insufficient data regarding the use and end-of-life phases specific to the project.

5.2 Life cycle inventory

The life cycle inventory of the present case studies primarily relies on environmental product declarations (EPDs) for the main products such as drainage geocomposite, multi-composite, extruded PP geogrids, non-woven geotextile, developed according to EN 15804, and data from One Click LCA.

- **Product stage (A1 to A3)**: In accordance with EN 15804, the A1-3 stage includes materials, products, energy consumption, and waste processing up to disposal or reaching the end-of-waste state. The material inventory in Table 4 provides a comprehensive breakdown of the resources utilized for the four case studies.

Table 4. Inventory of materials for the product stage.

Item	Material	Unit	Case A	Case B	Case C	Case D
1	Base course (granular material)	m^3	12,600	12,600	6,300	8,400
2	Subbase (mixed or stabilized granular materials)	m^3	21,000	12,600	11,550	12,600
3	Drainage geocomposite	m^2	-	22,412	-	-
4	Extruded PP geogrids	m^2	-	-	-	46,293
5	Non-woven geotextile	m^2	21,600			21,600
6	Multi-composite	m^2	-	-	2,130	-

- **Transportation stage:** The A4 stage covers the transportation of materials from the factory or quarry to the construction site, assuming that trucks operate at full

capacity on outbound trips and return empty. With Bologna as the assumed site location, the transportation distances are estimated as follows:

- 50 km for items 1 and 2, representing the distance from the quarry where granular materials are extracted;
- 850 km for geocomposite materials and PP extruded geogrids and multi-composite;
- 150 km for the supply of non-woven geotextile material.

- **Installation stage:** The A5 stage primarily assesses the environmental impacts associated with the installation process, including the assembly of materials and products. All construction equipment used for road section construction - such as soil spreading and compaction - has been modelled with diesel engines or diesel-powered generators [10]. The fuel consumption for installing geosynthetic layers, mainly carried out by excavators and wheel loaders, is estimated at 1.0 MJ/m^2. The total fuel and energy consumption during the installation stage has been calculated based on the total tons of soil to be spread and compacted, as well as the total m^2 of geosynthetics to be installed. Results are: Case A = 86,246 MJ; Case B= 69,586 MJ; Case C= 55,837 MJ and Case D=108,078 MJ. Compared to other geosynthetic solutions, Case D had the highest consumption due to the double layer of geogrids between the base/subbase and subbase/subgrade that requires doubled transportation and installation.

5.3 Life cycle impact assessment and results interpretation

The life cycle impact assessment (LCIA) results for the study, are summarized in Table 5 and Fig. 3, and correspond to the stages A1-3 and construction process stage A4-5. The study evaluates several midpoint indicators such as total global warming potential (GWP-t), potential for depletion of the ozone layer (ODP), acidification potential (AP), Eutrophication Potential-Particulate Matter Formation (EP-P), water use and the abiotic depletion of minerals (ADPE) and fossil fuels (ADPF). This is essential to comprehensively address the environmental impacts of the solution different options.

Table 5. Comparison of midpoint indicators for the four types of road stabilization solutions.

Impact category	Unit	Case A	Case B	Case C	Case D
GWP-t	Kg CO2 eq	5.11E+07	4.54E+07	3.21E+07	3.63E+07
ODP	kg CFC11 eq	7.00E+00	5.53E+00	3.84E+00	5.00E+00
AP	Mol H+ eq	2.42E+05	2.18E+05	1.37E+05	1.76E+05
EP-P	kg P eq	2.50E+01	1.80E+01	1.36E+01	2.08E+01
ADPE	kg Sb eq	1.53E+05	1.14E+05	8.17E+04	9.55E+04
ADPF	MJ	1.04E+09	9.63E+08	7.36E+08	7.62E+08
Water use	m^3	1.15E+07	1.02E+07	6.11E+06	9.52E+06

The main environmental impact indicators for Case A are higher compared to the other cases, followed by Case B, Case D, and finally Case C with multi-composite geosynthetics. For example, the Global Warming Potential (GWP-t) is linked to the extraction and transportation of large quantities of mineral materials, leading to increased CO2 emissions. Additionally, the Abiotic Depletion Potential of Elements (ADPE) is elevated due to the significant extraction of mineral resources, especially when compared to geosynthetic-based solutions.

Case C, which incorporates multi-composite geosynthetics, consistently shows the lowest impact values across all parameters. One particularly interesting indicator in this analysis is EP-P (Eutrophication Potential–Particulate Matter Formation), which is mainly

influenced by the materials and processes that contribute to eutrophication and particulate matter emissions. Unlike the other indicators, where Case A is always the highest, in the case of EP-P, Case D (with geogrids) ranks second, surpassing Case B. In Case D, the use of extruded PP geogrids resulted in a relatively high EP-P value compared to the other cases, except for Case A. This is because, although the geogrids reduce the need for large quantities of mineral materials, they do not significantly improve drainage quality. Over time, this could lead to increased particulate matter formation due to the presence of water in the subbase.

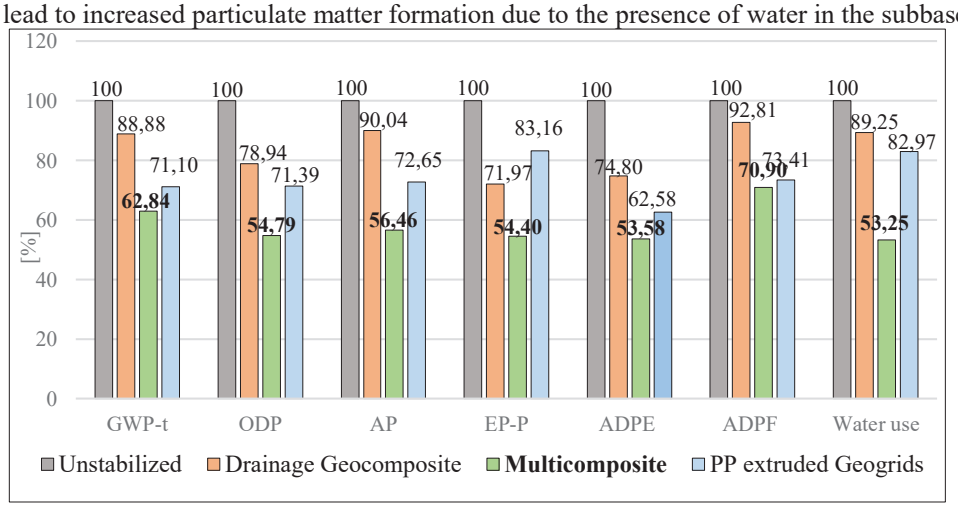


Fig. 3. Comparison of midpoint indicators for the four road stabilization solutions, with each indicator scaled to 100% for the case with the highest environmental impact.

The environmental benefits of using multi-composite in Case C is proved from its ability to integrate multiple functions within a single solution. Unlike traditional solutions that require separate components - such as gravel and geotextiles for drainage and separation or geogrids and geotextiles for reinforcement and separation, multi-composites drastically simplify the installation process (A5 stage), reducing both labour demands and logistical complexities.

Table 6. GWP-total [kg CO2e] during installation for each case

	Case A	Case B	Case C	Case D
A5-Construction	**7907**	**6379**	**5119**	**9908**

Finally, despite geosynthetics such as drainage geocomposite, multi-composite, and geogrids being transported from greater distances compared to the components in Case A, their overall environmental impacts are relatively low. This is due to their significantly lower impacts during the production stage (A1-3) compared to other primary materials in Case A, indicating the general effectiveness of geosynthetic materials.

6 Conclusions and discussion

This paper highlights the effectiveness of geosynthetic-based solutions for road stabilization from both design and environmental perspectives. The comparative analysis confirms that integrating geosynthetics into road structures enhances performance, reduces the thickness of gravel layers, and lowers environmental impact compared to unreinforced sections.
Among the four case studies analysed, the multi-composite geosynthetic emerged as the most efficient and sustainable alternative by integrating reinforcement and drainage functions into a single product. Although the inclusion of extruded geogrids between layers (Case D) achieves comparable thickness reductions, the use of a multi-composite geosynthetic (Case C) enables a road design with "excellent" drainage quality rather than "poor" (ASTM, 1993).

This improvement not only enhances the Structural Number by accelerating horizontal drainage but also prevents water stagnation between the subbase and weak subgrade. As a result, overall durability is improved, and the road's design life is extended.

The effectiveness of geosynthetics in road applications has also been demonstrated through Life Cycle Assessment. The accuracy of the selected data was crucial to ensure that the LCA results are reliable. Therefore, it is essential to use verified and up-to-date data sources, such as Environmental Product Declarations (EPD) and recognized databases like Ecoinvent. While all geosynthetic solutions analysed provided benefits in terms of material savings and reduced environmental impact, the multi-composite geosynthetic stands out as the most advanced and well-balanced option.

By combining multiple functions into a single product, it optimizes road design and simplifies installation, leading to significant cost and energy savings. This makes multi-composite geosynthetics the most efficient solution among the four case studies presented, aligning with industry goals for greener and more sustainable infrastructure development.

References

1. Regulation (EU) 2024/3110 of the European Parliament and of the Council of 27 November 2024 laying down harmonised rules for the marketing of construction products and repealing Regulation (EU) No 305/2011.
2. AASHTO, Guide for Design of Pavement Structures, American Association of State Highway and Transportation Officials, Washington, D.C. (1993).
3. ISO 14040. Environmental Management – Life Cycle Assessment – Principles & framework. International Organization for Standardization, 14040 (2006)
4. ISO 10318-1:2015, Geosynthetics - Part 1: Terms and definitions, (2020)
5. H.R. Cedergren, Drainage of highway and airfield pavements, Robert E. Krieger Publishing Co. Inc., Malabar, FL. (1987)
6. One Click LCA Ltd, Life Cycle Carbon – Global Available on https://oneclicklcaapp.com). Helsinki, Finland (2024)
7. EN 15978, Sustainability of construction works - Assessment of environmental performance of buildings - Calculation method (2012)
8. EN 15804, Sustainability of construction works - Environmental product declarations - Core rules for the product category of construction products (2012)
9. ISO 14025. Environmental labels and declarations — Type III environmental declarations - Principles and procedures. International Organization for Standardization, Geneva, Switzerland. (2006)
10. A. Elsing, I. Fraser, M. Stucki, S. Büsser, R. Itten, R. Frischknecht, H. Wallbaum, Comparative LCA of geosynthetics versus conventional construction materials, case 2, foundation stabilization, in Proceedings of the 5th European Geosynthetics Congress. Valencia, Spain, September 16-19 (2012)

Refinement of the design method for geogrid stabilisation of railway ballast and subballast

Pietro Rimoldi[1*], *Fabrizia* Trovato[2]

[1]Civil Engineering Consultant, 20157 Milano, Italy
[2]Officine Maccaferri SpA, 40132 Bologna, Italy

Abstract. A new design method for geogrid stabilisation of railway bases was presented by the same Authors, which allows to evaluate the thickness of ballast and subballast layers stabilized with geogrids, taking into account the wheel loads, the number of passages, the railway geometry, the subgrade characteristics and the geogrid properties. In the present paper the design method has been refined with an improved analytical model, allowing an easier calculation of the subballast thickness.

1 Introduction

A new design method for geogrid stabilisation of railway bases was presented by Rimoldi and Trovato [1], which allows to evaluate the thickness of ballast and subballast layers stabilized with geogrids, taking into account the wheel loads, the number of passages, the railway geometry, the subgrade characteristics and the geogrid properties. In the present paper the design method by Rimoldi and Trovato [1] has been refined with an improved analytical model: in particular, the Odemark theory [2], which transforms a multilayer system into an equivalent single layer system, has been implemented according to El-Badawi and Kamel [3], allowing an easier calculation of the subballast thickness. The proposed method is based on established engineering principles, and it incorporates the latest research findings on railway ballast behaviour and properties, ensuring a comprehensive design approach.

2 Development of a new design method

Geogrids offer a practical solution for stabilising ballast and/or subballast, in order to mitigate settlements and increase the life cycle. A systematic design approach for geogrid stabilized railway ballast/subballast has been developed, considering wheel loads, frequency of passages, railway geometry, subgrade characteristics, and geogrid properties. The proposed design method is based on the same principles established by the Leng and Gabr method [4] for designing geogrid stabilization of road bases. Adapting this method to railways involves placing geogrids at the base of the ballast, as shown in Fig. 1.

Odemark theory [2] transforms a multilayer system into an equivalent system, where layer thicknesses are adjusted to ensure that all layers have the same elastic modulus. This equivalent system behaves like an elastic half-space, allowing the application of Boussinesq theory to determine the stress distribution due to the applied stress on the surface.

* Corresponding author: pietro.rimoldi@gmail.com

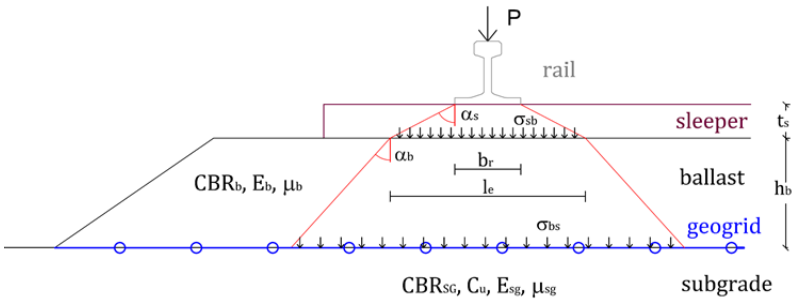


Fig. 1. Schematic of the model for the stabilisation of ballast

For a two-layer system consisting of ballast and subgrade (Fig. 2), the equivalent thickness of the ballast (h_e), ensuring it matches the elastic modulus of the subgrade (E_{sg}), is given by:

$$h_e = h_b \cdot \chi_1 \quad (1)$$

$$\chi_1 = \left[\frac{E_b \cdot (1-\mu_{sg}^2)}{E_{sg} \cdot (1-\mu_b^2)}\right]^{1/3} \quad (2)$$

where: h_b = thickness of ballast (m), E_b = elastic modulus of ballast (kPa), E_{sg} = elastic modulus of subgrade (kPa), μ_b = Poisson's ratio of the ballast (default value = 0.35), μ_{sg} = Poisson's ratio of the subgrade (default value = 0.42); χ_1 = Odemark coefficient ballast – subgrade.

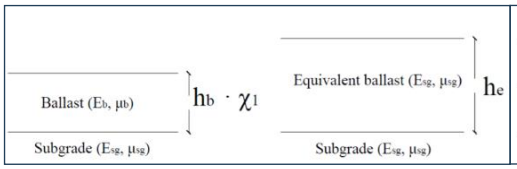


Fig. 2. Odemark transformation of the ballast thickness h_b in an equivalent thickness h_e

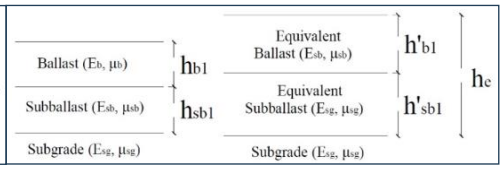


Fig. 3. Odemark transformation for the case of ballast and subballast

With reference to Fig. 3, when the railway structure includes the ballast thickness h_{b1} and subballast thickness h_{sb1}, the thickness h_e, calculated for a single granular layer (Fig. 3), has to be divided into the equivalent thickness h'_{b1} of the ballast and the equivalent thickness h'_{sb1} of the subballast. According to El-Badawi and Kamel [3], the equivalent thicknesses are calculated as:

$$h'_{b1} = h_{b1} \cdot \chi_1 \quad (3)$$

$$h'_{sb1} = h_{sb1} \cdot \chi_2 \quad (4)$$

$$\chi_2 = \left[\frac{E_{sb} \cdot (1-\mu_{sg}^2)}{E_{sg} \cdot (1-\mu_{sb}^2)}\right]^{1/3} \quad (5)$$

$$h_e = h'_{b1} + h'_{sb1} \quad (6)$$

where: E_{sb} = elastic modulus of subballast, μ_{sb} = Poisson's ratio of the subballast (default value = 0.30); χ_1 = Odemark coefficient ballast – subgrade; χ_2 = Odemark coefficient subballast – subgrade

In the presently proposed design method the following formulas, commonly used in road engineering, are applied:

- Modulus of the subgrade E_{sg} (MPa) (Shell formula, from Heukelom and Foster [5]), valid for fine soils with CBR ≤ 10: $E_{sg} = 10 \cdot CBR_{sg}$ (7)

- Modulus of the ballast E_b (MPa) and subballast E_{sb} (MPa) (from Giroud and Han [6]):

$$E_b = 36 \cdot CBR_b^{0.3} \qquad E_{sb} = 36 \cdot CBR_{sb}^{0.3} \tag{8}$$

with: CBR_{sg} = CBR index of subgrade, CBR_b = CBR index of ballast, CBR_{sb} = CBR index of subballast.

It must be noted that experimental evidence indicates that the modulus of limestone ballast is usually lower than the modulus of basalt and granite ballast; hence it is suggested to assume $CBR_b = 90$ for limestone ballast, and $CBR_b = 100$ for basalt and granite ballast. Typical values for suballast are: $CBR_{sb} = 20 \div 30$.

With the Odemark transformation expressed by equation (1), the half space below the sleeper become uniform, elastic and isotropic, that is, in the conditions for the validity of the well known Boussinesq theory.

The present method assumes that the vertical stresses are distributed through the equivalent granular layer according to the well known Boussinesq theory for rectangular loaded area. If the load from sleeper to ballast is assimilated to a uniform load on a rectangular area, the Boussinesq theory allows to obtain the value of the vertical stress σ_c at any point along the vertical line passing by one corner of the rectangle. With reference to Boussinesq theory and applying the following equations (9) and (10)

$$R_1 = (L^2 + z^2)^{0.5} \quad R_2 = (B^2 + z^2)^{0.5} \quad R_3 = (L^2 + B^2 + z^2)^{0.5} \tag{9}$$

$$\sigma_z = \frac{q}{2\pi} \cdot \left[\arctan\left(\frac{L \cdot B}{z \cdot R_3}\right) + \frac{L \cdot B \cdot z}{R_3} \cdot \left(\frac{1}{R_1^2} + \frac{1}{R_2^2}\right)\right] \tag{10}$$

it is possible to calculate the ratio of the vertical stress at top and bottom of ballast as:

$$\frac{\sigma_{sb}}{\sigma_{bs}} = \frac{2\pi}{\left[\arctan\left(\frac{L \cdot B}{z \cdot R_3}\right) + \frac{L \cdot B \cdot z}{R_3} \cdot \left(\frac{1}{R_1^2} + \frac{1}{R_2^2}\right)\right]} \tag{11}$$

where: σ_z = induced vertical stress at depth z below one corner of the rectangle (kPa), q = uniform pressure on the rectangular area (kPa); z = depth below surface (m); L, B = length and width of the rectangle (m).

2.1 Load transfer and design rail seat load

In a ballasted railway track, the rails transfer the wheel loads to the supporting sleepers, which are spaced evenly along the rail length. Similarly, sleepers transfer the load from the rail to the wider ballast area. The ballast and subballast layers spread the high imposed stress from the sleeper/ballast interface to the subgrade layer at a reduced intensity.

For design purposes, the sleeper - ballast contact pressure is generally considered to be uniform on the effective sleeper area l_e, shown in Fig. 1. In the presently proposed method, the load from the rail spreads inside the sleeper according to the load spreading angle α_s, that is symmetrically to the rail centre (Fig. 1). For standard concrete sleepers the value $\alpha_s = 55°$ provides a value l_e practically equivalent to the value provided by the AREMA manual [7], while the value $\alpha_s = 60°$ provides a value l_e practically equivalent to the value provided by the Japanese National Railways (JNR) method (Atalar et al. [8]).

Hence the load spreading angle should be assumed as: $\alpha_s = 55° \div 60°$. Then:

$$l_e = b_r + 2 \cdot t_s \cdot \tan \alpha_s \tag{12}$$

where: l_e = effective length of sleeper (m); b_r = rail width (m); t_s = sleeper thickness (m).

The sleeper - ballast contact area A_{sb} (m^2) and contact pressure σ_{sb} (kPa) are therefore:

$$A_{sb} = l_e \cdot b_s \tag{13}$$

$$\sigma_{sb} = P / (l_e \cdot b_s) \tag{14}$$

where: P = design rail seat load (kN); b_s = sleeper width (m).

In equation (14), for calculating the average sleeper - ballast contact stress, note that the rail seat load P differs from the wheel load P_d. In facts, track deflection shows that only three sleepers bear the load; additionally, research indicates that 40 % to 60 % of the wheel load is supported by the sleeper directly beneath the wheel. In the more conservative scenario, where the load is shared by 3 sleepers, 50 % of the load directly stresses the sleeper beneath the axle of the train, while each of the two adjacent sleepers bears 25 % of the load from the axle; consequently, if W is the axle load, the rail seat load P generated by a wheel on the most heavily loaded sleeper can be approximated as:

$$P = 50\ \% \cdot W / 2 = W / 4 \tag{15}$$

With regard to the loads generated by the wheels of trains: for cargo trains the load model is usually composed of 4 x 250 kN axles arranged with spacing of 1.60 m. In case of high-speed trains, the heaviest axle load (in driving cars) is typically equal to 170 kN/m. Hence, for cargo train load: P = 250 / 4 = 62.5 kN. For a high speed train the highest rail seat load can be assumed as: P = 170 / 4 = 42.5 kN.

To consider the dynamic component of wheel load, the static wheel load shall be multiplied by an influence coefficient generally known as the Dynamic Amplification Factor (DAF). In the presently proposed method, the DAF according to AREMA manual [7] will be used:

$$P_{dyn} = \varphi \cdot P \tag{16}$$

where: P_{dyn} and P are the dynamic and static wheel load (kN), respectively; and φ is the dimensionless DAF, which is given by:

$$\varphi = 1 + \frac{0.0052\ C}{D_w} \tag{17}$$

where: C is the train speed (km/h), and D_w is the wheel diameter (m).

For cargo train: C = 100 km/h, D_w= 0.90 m; the typical value of DAF is: φ = 1.58.

For high speed trains: C = 300 km/h, D_w = 0.92 m; the typical value of DAF is: φ = 2.70.

Hence the design rail seat load should be assumed equal to: $P_{dyn} = \varphi \cdot W / 4$ (18)

2.2 Applied stress on subgrade

The load spreading model here assumed is the trapezoidal distribution, as proposed by Indraratna et al. [9], shown in Fig. 4, which is a simple approach for estimating the variation in vertical stress with depth. According to this method, it is assumed that the vertical stress decreases with depth in the form of a trapezoid according to the load spreading angle, α_b, as shown in Fig. 4. Subsequently, the stress at the equivalent depth h_e below the sleeper is:

$$\sigma_{bs} = \sigma_{sb} \cdot \frac{A_{sb}}{A_{bs}} \tag{19}$$

$$A_{sb} = l_e \cdot b_s \tag{20}$$

$$A_{bs} = (l_e + 2 \cdot h_e \cdot \tan\alpha_b) \cdot (b_s + 2 \cdot h_e \cdot \tan\alpha_b) \tag{21}$$

where: σ_{sb} is the average value of vertical stress below the sleeper (i.e. above the ballast), from Equation (14); A_{sb} is the sleeper/ballast contact area; A_{bs} is the ballast / subgrade contact area; and h_e is the equivalent thickness of ballast, from equation (1).

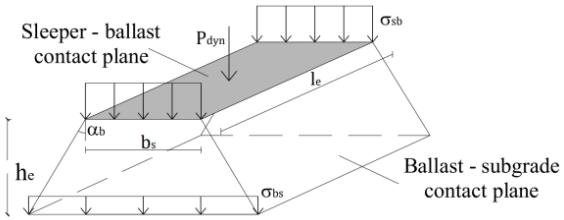


Fig. 4. Stress distribution on the subgrade from sleeper - ballast contact stress by trapezoidal distribution

2.3 Allowable settlement and plastic deformations

The allowable settlement of the rail tracks is very limited, of the order of 1 to 5 mm; above these values trains are bound to reduced speed. At the base of the ballast or subballast allowable settlements are larger, since only part of the settlements at subgrade interface is transmitted to the sleepers and rails. The thresholds for permanent allowable settlements of rails are of the order of a few millimetres in the presence of a light seismic event, while it shall be of the order of several centimetres for heavy seismic events. Therefore, it can be assumed that the settlement limit at the interface with the subgrade is equal to 50 mm, while at the top of ballast it can be assumed equal to 5 mm.

For unstabilised ballast, Sayeed [10] has proposed an empirical model for better prediction of the accumulated plastic deformation of ballast. In the present method, a modification of the Sayeed model [10] is used for the evaluation of the accumulated plastic deformation of unstabilised ballast; the modified model is expressed by the following formula:

$$\varepsilon_{bu} = x \cdot \alpha^{y} \cdot [1 + \ln (N)]^{\nu} \quad (22)$$

where: ε_{bu} is the cumulative plastic strain of unstabilised ballast (%); N is the number of load applications on the ballast; and α, x, y and ν are regression parameters depending on the ballast type, as summarized in Table 1 (modified from [**Erreur ! Source du renvoi introuvable.**]).

At present there are no published method for evaluating the accumulated plastic deformation of stabilised ballast. Yet, the model of Vecchiotti and di Prisco [11] set the following formula for the estimation of the settlement r:

$$r = \beta \, \text{Log} \, N \quad (23)$$

with: N = number of load cycles; β = coefficient depending on the applied load.

The formulas for calculating the coefficient β are:

- for unstabilised ballast: $\beta_u = (0.0655 \, P_{dyn} - 0.8256)$ (24)
- for stabilised ballast: $\beta_s = (0.05163 \, P_{dyn} - 0.4245)$ (25)

with: P_{dyn} = design rail seat load (kN), from Equation (16).

Hence, in absence of any other data, in the present method the accumulated plastic deformation of stabilised ballast ε_{bs} is evaluated as:

$$\varepsilon_{bs} = \varepsilon_{bu} \cdot (\beta_s / \beta_u) \quad (26)$$

Table 1. Material parameters for various types of ballast (modified from [6])

Ballast type	x	y	ν	α
Basalt	4.82	1.42	0.49	0.30
Granite	1.27	2.41	0.48	0.67
Dolomite	4.23	1.15	0.32	0.40

The most advanced model that is currently used to predict the cumulative plastic strain and cumulative plastic deformation of track fine-grained subgrade soils were presented by Li and Selig [12]; this model is modified in the present method as following:

$$\varepsilon_{sp} = \frac{\xi}{100} \cdot N^{\vartheta} \cdot \left(\frac{\sigma_{bs}}{q_c}\right)^{\omega} \quad (27)$$

$$r_u = \varepsilon_{sp} \cdot H_s \quad (28)$$

$$r_u = \sum_{i=1}^{n} \varepsilon_{spi} \cdot H_{si} \quad (29)$$

where: ε_{sp} is the cumulative plastic strain of track subgrade soil; σ_{bs} is the vertical stress applied at the ballast – subgrade interface; q_c is the bearing capacity of the subgrade soil; N is the number of load repetitions in the subgrade; ξ, ω and ϑ are material parameters given in Table 2; r_u is the rut depth at the ballast – subgrade interface in case of unstabilised ballast / subballast; H_s is the thickness of the soft subgrade layer; ε_{spi} and H_{si} are the cumulative plastic strain and layer thickness for the i-th subsoil layer, in case of stratified subsoil. For practical design purposes, the considered thickness of the soft subgrade may be limited to 5.0 m.

At present there are no published method for evaluating the rut depth at the ballast - subgrade interface in case of stabilised ballast / subballast. Due to lack of any other data, as done above, in the present method the rut depth at the ballast – subgrade interface in case of stabilized ballast/subballast is evaluated as:

$$r_s = r_u \cdot (\beta_s / \beta_u) \quad (30)$$

Table 2. Material parameters for various types of soil (modified from Li and Selig [12])

Subgrade soil type	ξ	ω	ϑ
Fat clay (CH)	1.20	2.4	0.18
Lean Clay (CL)	1.10	1.8	0.16
Elastic silt (MH)	0.84	2.0	0.13
Silt (ML)	0.64	1.7	0.10

2.4 Load spreading angle in ballast

We have previously assumed the trapezoidal distribution of the load inside the ballast; now, for simplifying calculations, let's reduce the rectangular loaded area below the sleeper to a square load area of size a_t, having the same area of the rectangular one; hence:

$$a_t = (l_e \cdot b_s)^{0.5} \quad (31)$$

With reference to Fig. 4, still considering the trapezoidal distribution according to the load spreading angle α_b, the square loaded area at the ballast – subgrade interface will have size: $a_b = a_t \cdot \tan \alpha_b$.

The load from sleeper to ballast shall be the same load that is transferred to the subgrade; hence, considering the equivalent thickness h_e (see Equation (1) and Fig. 1), it shall be:

$$\sigma_{sb} \cdot a_t^2 = \sigma_{bs} \cdot a_b^2 = \sigma_{bs} \cdot (a_t + 2 \cdot h_e \cdot \tan\alpha_b)^2 \quad (32)$$

Therefore, we can calculate the load spreading angle α_{b1}, to be intended as the value at the first application of the train wheel load, as:

$$\tan\alpha_{b1} = \frac{a_t}{2\,h_e} \cdot \left(\sqrt{\frac{\sigma_{sb}}{\sigma_{bs}} - 1}\right) \quad (33)$$

where $(\sigma_{sb} / \sigma_{bs})$ has to be calculated with equation (11).

Based on cyclic plate load tests, Leng and Gabr [13] have shown that the spreading angle α_b of the load decreases with the number of load cycles. This corresponds to the intuitive concept that a large number of wheel passages results in a degradation of the ballast, due to the displacement of the grains of soil and the horizontal tensile stresses that are generated

because of Poisson's ratio of the ballast, which in turn causes a decrease in the elastic modulus E_b of the ballast: since a less rigid layer spreads the loads worse than a more rigid layer, it is intuitive that as the number of passages increases the load spreading angle decreases.

Therefore Leng and Gabr [13] introduced the coefficient λ_2 of degradation of the angle α, defined as:

$$\lambda_2 = \frac{\tan\alpha_{bN}}{\tan\alpha_{b1}} = \frac{1}{1+k_2 \cdot \log N} \quad (34)$$

where: tan α_{bN} = tangent of the angle of load distribution at the N-th loading cycle, tan α_{b1} = tangent of the initial angle of load distribution (for N = 1) from Equation (33); N = number of load cycles, k_2 = parameter that defines the degradation of tanα_b.

2.5 Effect of geogrids for stabilisation of ballast

Based on cyclic plate load tests (Leng and Gabr [13]) and in situ tests (Fannin and Sigurdsson [14]), it was shown that the introduction of geogrid stabilisation in the ballast delays and minimizes the degradation of the load spreading angle with the number of passages. In fact, the open structure of geogrids allows the interlocking of the grains of soil, so that the grains are confined by the geogrid, which provides tensile forces at low strain; interlocking and geogrid tensile forces (which produce horizontal compressive stresses on soil granules) prevent lateral movement and expansion of soil under load, produced by the Poisson's ratio of the soil. Thus, the elastic modulus of the ballast is maintained for much longer as the number of passages increases and consequently the degradation of the angle of load diffusion decreases. Based on the above experimental evidence and empirical criteria, the influence of the geogrid is introduced by Leng and Gabr [4] by means of the tensile strength of geogrids $T_{2\%}$ at 2% strain. The coefficient k_2, which defines the degradation of α_b, is related to $T_{2\%}$ by the following empirical equation:

$$k_2 = (a_t / h)^{0.81} \cdot \text{Max}\,[(0.58 - 0.000046\, T_{2\%}^{4.5}), 0.15] \quad (35)$$

The minimum value of k_2 is for N = 1 and is equal to 0.15. Equation (35) contains the intuitive fact that as the thickness h of the ballast increases the degradation of α_b (and then the coefficient k_2) is decreased.

2.6 Bearing capacity mobilization factor

The load bearing capacity of the subgrade, according to the scheme in Fig. 4, is defined with the classic formula:

$$q_c = N_c \cdot c_u \quad (36)$$

where: N_c = bearing capacity factor; c_u = undrained shear strength of subgrade (kPa).

Leng and Gabr [4] assumed the following values for the bearing capacity factor N_c:

- N_c = 3.80 for unstabilised unpaved roads (N_c value in the case of saturated cohesive soil conditions at the elastic limit in axially symmetric conditions);
- N_c = 6.04 for unpaved roads stabilised with geogrids (N_c value in the case of saturated cohesive soil with maximum shear stress at the interface).

The same N_c values will be assumed here for unstabilised and stabilised railway ballast and subballast.

The well known empirical relation between CBR_{sg} value and the undrained shear strength of subgrade c_u (kPa) can be used (Giroud and Han [6]):

$$c_u = 30 \cdot CBR_{sg} \quad (37)$$

Leng and Gabr [4] introduced the bearing capacity mobilization factor, m, which allows the expression of mobilized resistance as a function of the bearing capacity and the vertical stress applied on subgrade:

$$m = N_{cm} / N_c = \sigma_{bs} / (N_c \cdot c_u) \quad (38)$$

where: N_c = bearing capacity factor of the subgrade; N_{cm} = mobilized bearing capacity factor of the subgrade.

Leng and Gabr [4], based on experimental evidence, found the following empirical relationship:

$$m = \left(1 - e^{-0.78 \cdot \left(a_t / h\right)}\right) \cdot \frac{N_{cm}}{N_c} \quad (39)$$

The mobilization of bearing capacity of the subgrade occurs at the cost of a settlement on the upper surface of the subgrade itself, i.e. in proportion to the depth of the rut that is created at the ballast – subgrade interface. Leng and Gabr [4] assumed that at the critical value r_{cr} of the rut depth the entire load bearing capacity of the subgrade is mobilised; the critical rut depth r_{cr} (m) is related to the number of passes through the following empirical relationship (Leng and Gabr [4]):

$$r_{cr} = 0.025 \cdot (0.125 \cdot \log N + 1.5) \quad (40)$$

By assuming that the mobilization of bearing capacity increases linearly with the rut depth r at the ballast – subgrade interface, Equation (39) becomes:

$$m = \left[1 - e^{-0.78 \cdot \left(a_t / h\right)}\right] \cdot \frac{r}{r_{cr}} \quad (41)$$

where the rut depth r has to be calculated with Equation (28) or (29) for unstabilised ballast, and with Equation (30) for stabilised ballast.

The mobilized bearing capacity q_{cm} becomes: $q_{cm} = m \cdot N_c \cdot c_u$ (42)

2.7 Minimum thickness of ballast and subballast

The vertical stress at ballast – subgrade interface σ_{bs} shall be less than the load bearing capacity mobilized in the subgrade, so as not to cause failure of the subgrade due to an excess of localized settlements, that is of rut depth. Still considering the load from sleeper to ballast applied on a square area of size a_t, and the trapezoidal distribution of load in ballast (Fig. 4), the following condition shall be verified:

$$\sigma_{bs} = \frac{P_{dyn}}{(a_t + 2 \cdot h \cdot \tan\alpha_{bN})^2} \leq m \cdot N_c \cdot c_u \quad (43)$$

From equation (43) we obtain the minimum equivalent thickness h_e of ballast:

$$h_e = \frac{1}{2 \cdot \tan\alpha_{bN}} \cdot \left(\sqrt{\frac{P_{dyn}}{m \cdot N_c \cdot c_u}} - a_t\right) \quad (44)$$

The model described above is based on the results of cyclic loading tests performed in the laboratory (Leng and Gabr [13]). To make the method more closely related to actual conditions, a model factor, equal to 0.85, is introduced in Equation (44); then, assuming that the degradation of the load spreading angle in ballast with the number of passes is given by Equation (34), Equation (44) becomes:

$$h_e = \frac{0.85 \cdot (1 + k_2 \cdot \log N)}{2 \cdot \tan\alpha_{b1}} \cdot \left(\sqrt{\frac{P_{dyn}}{m \cdot N_c \cdot c_u}} - a_t\right) \quad (45)$$

Since (P_{dyn} / a_t^2) shall be equal to the vertical stress transmitted from sleeper to ballast, σ_{sb}, Equation (45) can be rewritten as:

$$h_e = \frac{0.85 \cdot a_t \cdot (1 + k_2 \cdot \log N)}{2 \cdot \tan\alpha_{b1}} \cdot \left(\sqrt{\frac{\sigma_{sb}}{m \cdot N_c \cdot c_u}} - 1\right) \quad (46)$$

Considering that the thickness h_e of the base appears in both members of Equation (45) or Equation (46), they should be solved by an iterative process.

By solving Equation (45) with respect to the known load P_{dyn}, we obtain the following equation:

$$P_{dyn} = m \cdot N_c \cdot c_u \cdot \left(\frac{2 \cdot h_e \cdot \tan\alpha_{b1}}{0.85 \cdot (1+k_2 \cdot \log N)} + a_t\right)^2 \quad (47)$$

By solving Equation (46) with respect to the known vertical stress σ_{sb} we obtain the following equation:

$$\sigma_{sb} = m \cdot N_c \cdot c_u \cdot \left(\frac{2 \cdot h_e \cdot \tan\alpha_{b1}}{0.85 \cdot a_t \cdot (1+k_2 \cdot \log N)} + 1\right)^2 \quad (48)$$

Given that the P_{dyn} or σ_{sb} value is known, Equation (47) or Equation (48) can be used to calculate h_e, as example with the solver function of a spreadsheet.

The actual thickness of ballast is:

$$h_b = h_e / \chi_1 \quad (49)$$

Equations from (45) to (49) afford to calculate the minimum thickness both for unstabilised ballast, h_{bu}, and for stabilised ballast, h_{bs}: for unstabilised ballast, the parameter k_2 has to be calculated from Equation (35) with $T_{2\%} = 0$, and the parameter m has to be calculated using the rut depth r_u from Equation (28) or (29); for stabilised ballast the coefficient k_2 has to be calculated from Equation (35) with the $T_{2\%}$ value for the selected geogrid, and the parameter m has to be calculated using the rut depth r_s from Equation (30); the value of h used at each iteration influences the parameters k_2, tan α_{b1}, and m.

When the equivalent total thickness h_e is composed of the ballast thickness h'_{b1} and subballast thickness h'_{sb1} (Fig. 3), from Eqs. (3) ÷ (6) we get:

$$h_e = h_{b1} \cdot \chi_1 + h_{sb1} \cdot \chi_2 \quad (50)$$

If we set the value of the ballast thickness h_{b1}, as a predefined value (like $h_{b1} = 0.35$ m), or $h_{b1} = ((100 - P_r) \cdot h_b / 100)$, where P_r is the required percent reduction of the ballast thickness, obtained from Eq. (49), the subballast thickness is given by:

$$h_{sb1} = \frac{h_e - h_{b1} \cdot \chi_1}{\chi_2} \quad (51)$$

The above formulas can be used to calculate the thickness of ballast and subballast both in the unstabilised and stabilised cases.

Note that, for the stabilised design with ballast and subballast, the above formulas are valid only if both ballast and subballast are stabilised with geogrids having the same tensile strength at 2 % strain, $T_{2\%}$; anyway, the opening size of the geogrid for ballast stabilisation and for subballast stabilisation need to be different and suited to the granular size distribution of the two materials.

Compared to the case of design with ballast only, the design with ballast and subballast requires a higher total granular thickness, yet the thickness of ballast can be reduced.

3 Conclusions

The paper presents a design method for geogrid stabilised railway ballast and subballast, which considers the wheel loads, the number of wheel passes, the geometry of the railroad, the characteristics of the subgrade and the properties of geogrids.

This design method is a refinement of the method presented by Rimoldi and Trovato [1].

For the development of the design method the latest research on the behaviour of unstabilised ballast, subballast, and subgrade under railway loading has been considered.

The authors believe that the proposed design method for geogrid stabilised ballast and subballast is an important advancement, which will allow important savings in the use of selected granular materials in railway projects.

References

1. P. Rimoldi, F. Trovato, Design of geogrid stabilisation for railway ballast and subballast, in Proceedings of the Sixth International Conference on railway technology: Research, Development and Maintenance, 18.7; Prague, Czech Republic (2024)
2. N. Odemark, Investigations as to the elastic properties of soils and design of pavements according to the theory of elasticity. Statens Vag Institute Meddeland 77, Stockholm, Sweden (1949)
3. S.M. El-Badawy, M.A. Kamel, Assessment and improvement of the accuracy of the Odemark Transformation Method. International Journal of Advanced Engineering Sciences and Technologies **6**, 1, 105 – 110 (2011)
4. J. Leng, M.A. Gabr, Deformation-resistance model for geogrid-stabilised unpaved road. Journal of Transportation Research Board **1975**, National Research Council, Washington, DC, USA, 146-54 (2006)
5. W. Heukelom, C.R. Foster, Dynamic testing of pavements. Journal of Soil Mechanics and Foundations Division. American Society of Civil Engineers **86** No. SM1 (1960)
6. J.P. Giroud, J. Han, Design method for geogrid-stabilised unpaved roads – Part I: theoretical development. ASCE Journal of Geotechnical and Geoenvironmental Engineering **130** (2004)
7. AREMA, Manual for railway engineering. American Railway Engineering and Maintenance of Way Association. Lanham, Maryland, USA (2019)
8. C. Atalar, B.M. Das, E.C. Shin, D.H. Kim, Settlement of geogrid reinforced railroad bed due to cyclic load, In Proceedings of the International Conference on Soil Mechanics and Geotechnical Engineering. Istanbul, Turkey (2001)
9. B. Indraratna, M.W. Salim, C. Rujikiatkamjorn, Advanced rail geotechnology - Ballasted track (Taylor & Francis Group), London, UK (2011)
10. A. Sayeed, Design of ballasted railway track foundations using numerical modelling with special reference to high speed trains. Ph.D. thesis, Curtin University, Perth, Australia (2016)
11. M. Vecchiotti, C. di Prisco, Comportamento meccanico di rilevati ferroviari rinforzati sottoposti a carichi ciclici, in Proc. XVIII Convegno Nazionale Geosintetici. L'Ingegnere e l'Architetto, n.1. In Italian (2006)
12. D. Li, E.T. Selig, Cumulative plastic deformation for fine-grained subgrade soils. Journal of Geotechnical Engineering **122**, 1006-13 (1996)
13. J. Leng, M.A. Gabr, Characteristics of geogrid-stabilised aggregate under cyclic load. Journal of Transportation Research Board **1786**, National Research Council, Washington, DC, USA, pp 29-35 (2002)
14. R.J. Fannin, O. Sigurdsson, Field observations on stabilization of unpaved roads with geosynthetics. ASCE Journal of Geotechnical Engineering **122** (1996)

SESSION 6 A
REINFORCEMENT APPLICATIONS (5)

Determination of the Reduction Factors applied to polymeric coated woven steel wire mesh reinforcement according to German recommendation

Francesco Masola[1*], *Paolo* Gualandi[1], *Pietro* Rimoldi[2], *Sebastian* Schiller[3], and *Marco* Vicari[4]

[1] Maccaferri Central Europe s.r.o., Senica, Slovakia
[2] Civil Engineering Consultant, Milano, Italy
[3] BECO Bermüller & Co GmbH, Nürnberg, Germany
[4] Officine Maccaferri SpA, Bologna, Italy

Abstract. In Germany the design of reinforced soil structures must comply with the technical regulations set in DIN 1054 norm, which refers to the German guidelines EBGEO (2011). A specific Section of EBGEO requires the determination of five Reduction Factors to be applied to the characteristic tensile strength of geosynthetic and geosynthetic-related products reinforcements, for taking into account all factors which may decrease the available tensile strength over the full design life of the project. In practical terms this means that installation damage, as well as chemical and physical degradation tests, are required for defining the Reduction Factors which need to be accounted for to reduce the tensile strength from the characteristic value to the design value. The present paper is aimed at presenting the durability criteria for polymeric coated woven steel wire mesh reinforcement and the way to derive the Reduction Factors required by EBGEO guidelines for this peculiar class of geosynthetics.

1 Introduction

1.1 Products presently used for soil reinforcement

The products presently used for soil reinforcement can be classified in three homogeneous classes:

- Geosynthetics (GSY, purely polymeric products): the tensile resistant elements are polymeric;
- Polymeric coated woven steel wire meshes (PWM): the tensile resistant elements are metallic, made of steel wires, which shall be metallic coated (typically with zinc aluminium alloys) and polymeric coated (i.e. with PVC, PE, PA6 or other polymers);

* Corresponding author: f.masola@maccaferri.com

- Purely metallic products: the tensile resistant elements are metallic, usually made of steel, which may be metallic coated (zinc, zinc – aluminium, etc.).

The durability of PWM should be addressed with specific criteria, which consider the mode of development of corrosion in the metallic core when the product is placed in soil; the set criteria shall be subject to laboratory testing for the definition of the durability and of the Reduction Factors for design of reinforced fill structures.

1.2 Durability of geosynthetics and of polymeric coated steel meshes

Polymeric coated steel meshes show a totally different behaviour than fully polymeric geosynthetics; as example, the installation damage will produce the following effects:

- on geogrid made up of polyester yarns with polymeric coating: the polyester yarns (tensile resistant elements) will be immediately damaged to a lesser or larger extent;
- on steel wire mesh with metallic and polymeric coating: the steel wires (tensile resistant elements) will suffer negligible immediate damage, while the polymeric coating may get damaged at multiple points; in points where only light scratches or bruises occurred on the polymeric coating, the metallic coated steel wire will not be exposed to outside environment (the compacted soil), hence the steel wire will not suffer damages even in the long term; only in points where the polymeric coating suffered nicks exposing the metallic coated steel wire to the surrounding compacted soil the tensile resistant elements may suffer long term damage, due to oxidation produced by contact with the chemicals contained in the soil.

By analysing existing norms, like EN 10223-3 [1], EN 14475 [2], and ISO/TS 20432 [3], it appears that different approaches should be used for the two classes of products; the approach to the durability of PWM for soil reinforcement is now presented in accordance with the new Eurocode 7 - BS EN 1997-3:2025 [4].

2 Reinforced soil systems based on polymeric coated steel woven wire meshes

Two main reinforced soil systems based on PWM are available on the market:

- with gabion facing (Fig. 1);
- with wrapped-around facing (Fig. 2).

These reinforced soil systems are usually produced and CE-marked in compliance with EAD 200026-00-0102 [5], and EN 10223-3 [1].

The systems are usually based on a polymeric coated steel wire mesh, mesh type 8x10 and wire diameter of 2.7-3.7 mm or 2.2-3.2 mm (internal/external wire diameter).

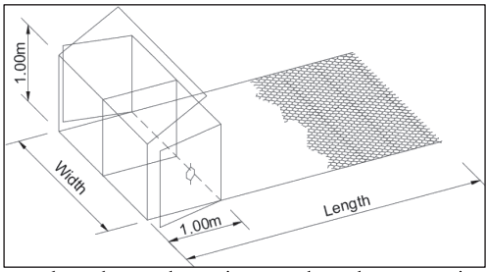


Fig. 1. Reinforced soil system based on polymeric coated steel woven wire meshes with gabion facing

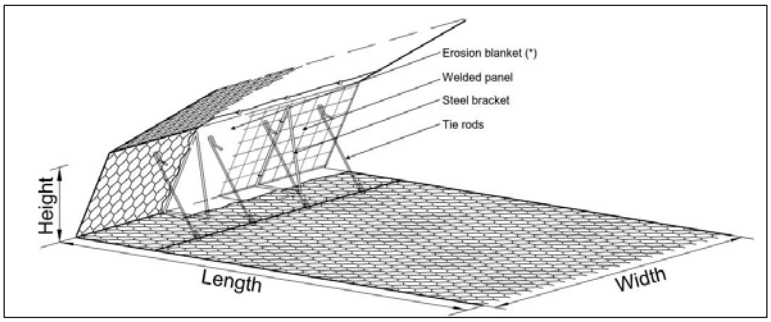


Fig. 2. Reinforced soil system based on polymeric coated steel woven wire meshes with wrapped-around facing

The double twisted steel wire mesh usually has a Zn-Al coating of Class A, in accordance with ISO 7989-2 [6] and EN 10244-2 Table 2 [7]; plus a polyolefin coating, in accordance with EN 10245-1 [8] and EN 10223-3 [1].

2.1 Intended use of the product

Reinforced soil systems with PWM reinforcement are intended to be used for:

- Earth retaining structures (vertical, battered or inclined walls, bridge abutments, bulk storage facilities) with a facing to retain the fill placed between the reinforcing layers;
- Reinforced steep slopes with built –in deformable facing units;
- Self-standing embankments (example: for rockfall protection, or noise bunds).

3 Design of reinforced soil structure in Germany according to the national guideline EBGEO

In Germany the design of reinforced soil structures must comply with the technical regulations set in DIN 1054 norm [9], which makes reference to EBGEO – "Empfehlungen für den Entwurf und die Berechnung von Erdkörpern mit Bewehrungen aus Geokunststoffen" (Recommendations for Design and Analysis of Earth Structures using Geosynthetic Reinforcements) [10] for the design of flexible reinforcement elements, hence evidence must be provided that design is in accordance with the rules set in EBGEO [10].

The design of reinforced soil structures based on polymeric coated woven steel meshes shall always be carried out with the analyses that investigate the Ultimate Limit States (ULS) and Serviceability Limit States (SLS) set in Section 3 and Table 3.1 of EBGEO [10].

Moreover, all requirements set in the new EuroCode 7 - BS EN 1997-3:2025 [4] must be fulfilled, also considering that no statement in EBGEO can contradict the EuroCode 7 and any contradictory statement in EBGEO, if any, has to be considered as invalid.

4 Reduction factors according to EBGEO

Section 2.2.4 of EBGEO [10] requires the determination of Reduction Factors to be applied to the characteristic tensile strength of geosynthetic reinforcements, for taking into account all factors which may decrease the available tensile strength over the full design life of the project. EBGEO [10] requires that product properties (hence also the Reduction Factors) shall be demonstrated by testing. Obviously testing shall be performed according to norms that are applicable to the specific product.

EBGEO [10] requires the determination of 5 Reduction Factors:

- Reduction Factor A1 for the long term effects of tensile creep;

- Reduction Factor A2 for damage during transportation, installation and compaction;
- Reduction Factor A3 for junctions, joints, seams, and connection to other structural elements;
- Reduction Factor A4 for environmental chemical impacts, including also:
  - microbiological resistance
  - biological resistance and vandalism
  - weathering resistance (UV resistance)
- Reduction Factor A5 for predominantly dynamic actions.

The 5 Reduction Factors shall be applied to the short term tensile strength (it is noted that the short term tensile strength is usually named Ultimate Tensile Strength T_{ULT}).

The Wide Width Tensile Test EN ISO 10319 [11] applies to polymeric coated steel wire meshes as well.

The following minimum values are usually reported in the CE Marking of the PWM products:

T_{ULT} = 50.0 kN/m for mesh type 8x10 with 2.7/3.7 mm diameter wire

T_{ULT} = 35.0 kN/m for mesh type 8x10 with 2.2/3.2 mm diameter wire

The determination of the 5 Reduction Factors for PWM products is now analysed.

4.1 Reduction Factor A1 from creep testing

For steel, that is the tensile resistant element of polymeric coated steel wire mesh products, the effects of creep begin to become noticeable at around 35 % of its absolute melting temperature (T_m). For low carbon steel, T_m = 1600 K therefore the temperature at which creep phenomena starts is approx. equal to 560 K (287 °C), well above the typical service temperatures (20 - 40 °C) of the PWM in reinforced soil structures.

It has to be noted that even the mesh structure doesn't show any creep: in facts, when subject to a tensile force the mesh elongates but, if the force becomes constant in time, the deformation becomes constant as well, without any further elongation; that is, even the mesh structure does not show the time-dependent creep elongation commonly observed in polymeric geogrids.

For these reasons, it is appropriate to set:

A1 = 1.0

4.2 Reduction Factor A2 for damage during transportation, installation and compaction

The A2 Reduction Factor in EBGEO [10] is perfectly equivalent to the reduction factor η_{dmg} defined in Clause 9.3.5 of BS EN 1997-3:2025 [4] as a reduction factor accounting for the adverse effects of mechanical damage to the steel during transportation, installation, and execution.

Hence, as required by Clause 9.3.5 of BS EN 1997-3:2025 [4], the value of the A2 Reduction Factor can be assessed by testing in accordance with EN 17738 [12], as the ratio of the tensile strength of damaged specimens divided by the tensile strength of the undamaged specimens.

It has to be noted that:

- damage to the coating does not decrease the tensile strength in the short term, hence it is accounted for in the determination of A2, as it may induce corrosion of the exposed wire.
- The determination of A2 shall account for the long term effect of corrosion of the steel wires due to the local loss of protection caused by mechanical and chemical damage to the polymeric coatings, exposing the steel wires to the surrounding environment.
- The polymeric and the zinc-aluminium alloy coatings have no structural function, since their only purpose is to protect the steel wires.

- As required by Clause 9.3.5 of BS EN 1997-3:2025 [4], the value of A2 shall be based on the residual strength of the product ignoring the wires that are exposed and assumed to be ineffective due to loss of polymeric coating. This assumes that the undamaged polymeric coating does not degrade chemically up to a level such that its protective function is lost over the design service life, as later demonstrated.

Mechanical damage, which affects the tensile strength of polymeric coated steel wire meshes, can develop basically during installation, due to friction of the coarse aggregates during compaction of the soil layers; it is related to possible scratches, cuts, bruises, consequent to the mechanical friction of the sharp edges of stones during compaction of coarse soil.

To provide the longest corrosion protection to the steel wire mesh, the steel wire is galvanized with a Zn/Al alloy (metallic coating), and additionally coated with a polymer of required characteristics.

It is obvious and it can be easily demonstrated that the steel wires, that is the tensile resistant elements of PWM products, are not damaged in EN 17738 test [12]; therefore there is no decrease of the short term tensile strength.

Hence, the evaluation of the durability of PWM reinforcement will require the evaluation of the number of wires which can be considered as instantly corroded at the points where the polymeric coating is damaged and the steel wire is exposed.

In facts, for practical purposes, the steel wire can be considered as totally corroded in very short time at the point of coating damage; that is, the steel wire can be considered as instantly corroded or, which is the same, it can be considered as totally cut and not contributing anymore to the tensile strength of the steel mesh: this conservative assumption allows to include the long term effect of mechanical damages into the A2 reduction factor.

Hence the long term effect of installation damage can be evaluated by the following procedure, which is consistent with ISO/TS 13434 [13] (Fig. 3):

- perform the installation damage procedure according to EN 17738 [12];
- retrieve the damaged specimens;
- carry out a visual and microscopic inspection for setting the points where the steel wire became exposed;
- cut the steel wires at the points where they were exposed (taking into account that multiple damages on the same steel wire will be counted as just one wire exposed);
- perform tensile tests according to ISO 10319 [11] on the reference specimens and the damaged specimens with cut wires;
- the ratio between the tensile strength of specimens with the cut wires to that of undamaged specimens with no cuts provides the minimum percent retained strength, which is equal to the value of the Reduction Factor A2.

Tests according to the above procedure performed on typical steel mesh reinforcement (polymeric coated mesh type 8x10 and 2.7 mm diameter wire), provided the values of A2 listed in Table 2 [14].

Table 2. Reduction Factor A2 for typical steel mesh reinforcement (polymeric coated mesh type 8x10 and 2.7 mm diameter wire)

Fill material	Maximum particle size (mm)	A2
Crushed stones	< 200	1.22
Coarse gravel	< 38	1.15
Sandy gravel	< 9.5	1.05
Sands	< 2	1.00
Silts and clays	< 0.06	1.00

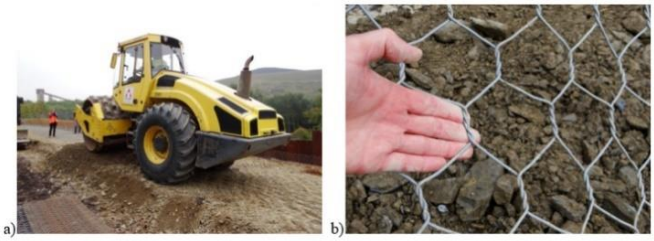


Fig. 3. Procedure for installation damage of PWM [14]: a) coarse fill compaction on the sample; b) retrieving sample and identifying local damages; c) microscopic examination to assess exposure of the metallic core; d) indicating points where the metallic core is exposed and the wire will be cut

4.3 Reduction Factor A3 for junctions, joints, seams, and connection to other structural elements

Polymeric coated steel wire mesh products are always installed with no junction, joint or seam along the direction of tensile resistance. The only structural element to which polymeric coated steel wire mesh products might be connected is the facing; but in the systems shown in Fig. 1 and Fig. 2 the steel wire meshes constitute even the facing element, without discontinuity with the reinforcing element.

Therefore for these polymeric coated steel wire mesh products it is appropriate to set:
A3 = 1.0

4.4 Reduction Factor A4 for environmental chemical impacts

The chemical resistance of polymeric coated steel wires depends on the environment where they work during their service life. It has to be noted that the polymeric coating has no structural function, since it has only to provide protection to the steel wire. Hence the durability of the polymeric coating shall be evaluated, considering its function, as the maximum time when it is still able to provide protection to the steel wire.

In the case of polymeric coatings protecting the steel wire, the most representative property is the elongation at break: in fact at 50 % of the initial value the residual elongation drops rather quickly. Low elongation results in an embrittlement of the coating and in lack of flexibility to protect the metal wires.

The service life of the polyolefin polymeric coating T_{pc} shall be assessed as follows: the service life T_{pc} is assumed to be equal to the embrittlement time, defined by testing specimens of the polymeric sleeves (the coating separated from the inside steel wire), using the thermal oxidation test EN 60216-8 [15] followed by tensile tests according to EN ISO 527 [16] modified (specimens are tubular rather than butterfly shaped): the embrittlement time is assumed to be the time required to reduce the elongation at break of specimens to 50 % of the original elongation at break of virgin specimens. The test procedure consists in performing an initial characterization of the mechanical properties (tensile strength and elongation) of the polymeric sleeves, and then exposing them in oven at different temperatures for a scheduled number of hours. After such exposure, specimens are tested for tensile elongation, recording the percentage values of the retained elongation. For each exposure temperature and for the group removed from the oven after each heat-ageing period, the mean value of the per cent residual tensile strain relative to the initial strain value is plotted as a function of the logarithm of the time of ageing (see Fig. 4 left); the point at which each curve intersects the horizontal line representing the endpoint criterion (tensile

elongation at break = 50 % of the initial elongation at break) is taken as the time to end-point of the temperature group. Using the Arrhenius regression method, the logarithms of the mean times to end point are plotted versus the reciprocal values of the exposure temperatures (see Fig. 4 right). The intersection of this curve with the inverse of the selected reference temperature (20 °C) provides the service life T_{pc}. It is noted that for the typical polymeric coating of PWM products the service life T_{pc} is higher than 100 years at 20 °C (Fig. 4 right).

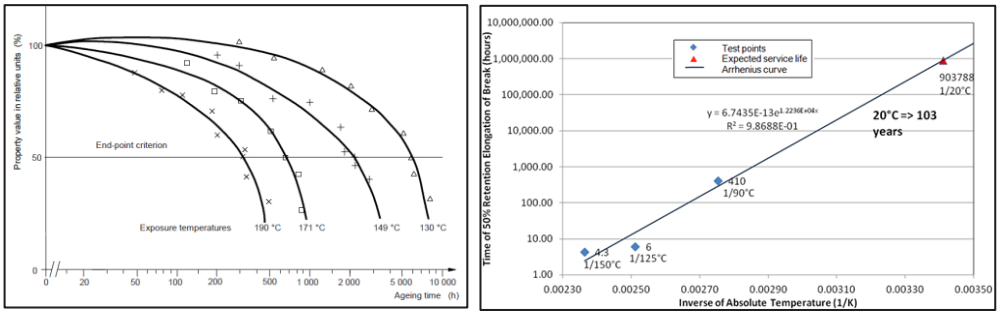


Fig 4. Left: plot of accelerated testing results for determining the time to reach the end-point at each temperature; right: Arrhenius plot for typical PWM products to set the expected service life at 20°C

Moreover, compression molded plaques of polyolefin polymeric coating were exposed to two years of oven-aging at three separate temperatures. The tensile strength, and the High-Pressure Differential Scanning Calorimetry (HPOIT) were tested at 3, 6, 12, 18, and 24 months. The tensile strength results showed no significant change. The HPOIT results showed small decreases in the values across two years time. When a service lifetime estimate was performed on the HPOIT results, it was found that the data suggested a service lifetime greater than 500 years at 25°C. Knowing that the coating is protected from oxidation as long as additives are present, these data show that the service life of the polyolefin polymeric coating is greater than 125 years at 25°C with a reduction factor of four [17].

The durability of the steel wires placed in soil relies primarily on the durability of the polymeric coating:

- the expected service life of the steel wire can be assumed to be at least equal to the expected service life of the polymeric coating if the coating remains intact or just slightly damaged, that is when in no point the steel wire is exposed to the external environment;
- only at points where physical and/or chemical and/or thermal degradation of the polymeric coating exposes the steel wire the metallic coating of the wires will start to rust and corrode.

Hence the lower limit of durability of the steel wires can be identified in the situation when local damages to the polymeric coating occur: where the metallic wire is exposed to the external environment then rust and corrosion start to develop.

When the polymeric coating is damaged and the metallic coated wire gets exposed to the outside environment (usually the compacted soil), corrosion of the steel wire may be produced by the chemical composition of such environment, and corrosion may propagate along the wire.

In this situation two phenomena need to be considered:

1) diffusion of corrosion along the wire starting from the point where the polymeric coating is damaged;
2) accelerated corrosion due to differences of electric potential between adjacent points of damage along the same wire or between points of damage along different wires.

The constant exposure to outside environment always occurs (even without damage) at the ends of the steel wire mesh panels, where the full cross-section of the steel wire is in contact with the surrounding environment. Hence this is surely the worst case, since corrosion will affect the whole cross section of the wire since the beginning.

The evaluation of corrosion propagation can be made by using end cut wires as reference specimens and referring to the corrosion spread test defined in ASTM A975 [18]. The procedure consists of immersing 250 mm long wire samples in a 5 % solution of HCl by weight. Samples are removed from the solution and analysed after 100, 500, 1000, 1500, 2500 hours of immersion. After immersion the polymeric coating shall be removed, and the length of the corroded wire measured. The part of the wire with reduced diameter is considered as corroded. The average corrosion lengths measured versus time plot shall show the maximum length after which there is no more increase in length with time: this measured maximum length shall be always less than a mesh repetition.

The corrosion spread test allows to verify that the corrosion, when exposed to such an aggressive acid environment (theoretical pH = 0.137), does not progress further with time and that it remains confined within the size of a single mesh only, equal to 40 mm for 8x10 mesh type. Tests using ASTM A975 [18] procedure on PWM have shown that the maximum corrosion length (mm) is always less than a mesh repetition and has the tendency to reach a plateau after approx. 1500 h, as shown in Fig. 5. As the length of corrosion penetration is less than half the twisted length (Fig. 5), then corrosion occurring in one wire will not affect any other wire of the hexagonal mesh; therefore the effect of corrosion will be limited to the single wire where damage occurred.

The corrosion spread test is focused on the evidence that very low pH (acid environment with pH lower than 0.2) produces the highest corrosion rates in steel, while very high pH (alkaline environment) has negligible effects on corrosion; this is consistent with the common experience that concrete, that is a highly alkaline material, does not produce corrosion of steel bars, rather it protects the steel from corrosion.

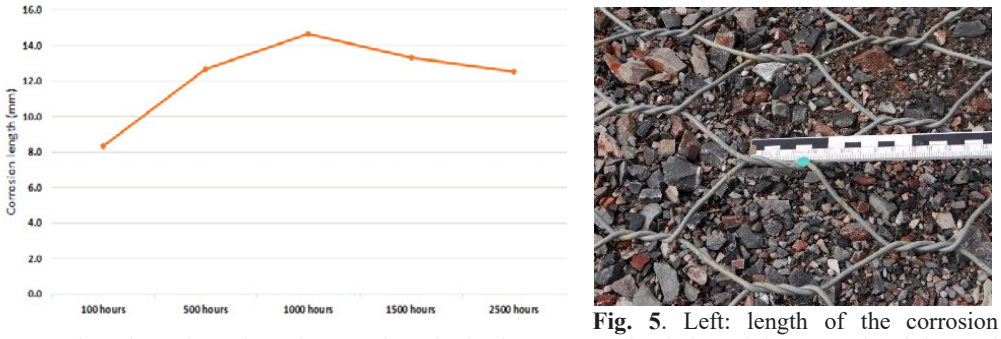


Fig. 5. Left: length of the corrosion penetration along the polymeric coated steel wire in a 5 % HCl solution; right: example of the steel wire mesh with damage in the twisted segment

Regarding the possible corrosion due to differences of electric potential between two points (i.e., stray currents near railway tracks), being the polymeric coating of steel wires dielectric, it provides electrical insulation to the steel wire itself and avoids electrical connections between adjacent wires; hence, as per TNO Delft [19], corrosion cannot occur if the polymeric coating is not deeply damaged,

Regarding the microbiological resistance, neither the polymeric coating nor the steel wires suffer any damage from microbiological attack when tested according to EN 12225 [20]; hence for this component of the A4 Reduction Factor it is appropriate to set:

$\mathbf{A4_{microbiological\ resistance} = 1.0}$

Practical evidence and experience show that PWM are not damaged by rodents and it is very difficult to be purposely damaged by vandals; in any case damages by vandalism can only be addressed on a case-by-case basis; hence for this component of the A4 Reduction Factor it is appropriate to set:

$\mathbf{A4_{biological\ resistance\ and\ vandalism} = 1.0}$

Regarding weathering resistance (UV resistance), both EBGEO [10] and Annex B of EN 13249 [21] and EN 13251 [22] requires accelerated weathering tests according to EN 12224 [23]; anyway the result of such test determine only the maximum time of exposure to sunlight before the product is covered with soil. In the case of PWM the tensile resistant element is the steel wire, which is not affected by UV radiation; hence testing according to EN 12224 [23] always results in retained strength of 100 %. Therefore for PWM the maximum time of exposure to sunlight before the product is covered with soil is 1 month.
Furthermore, in compliance with EN 10223-3 [1], for PWM reinforcements the mechanical characteristics of the polymer base compound after a UV-rays exposition of 4000 h to Xenon Arc or 2500 hours QUV-A cannot change more than 25 % from the initial test results.
According to the results of the above mentioned tests, for the $A4_{weathering}$ factor for PWM products it is appropriate to set:
$A4_{weathering}$ = 1.0

Overall, considering the various components of environmental degradation and their potential interactions, in favour of safety for the A4 Reduction Factor it is appropriate to set:
A4 = 1.05

4.5 Reduction Factor A5 for predominantly dynamic actions

According to EBGEO [10], for reinforced soil structures subject to predominantly static actions, like those built with the systems in Fig. 1 and Fig. 2, it is:
A5 = 1.0.

5 Conclusion

The durability criteria for polymeric coated woven steel wire mesh reinforcement and the way to derive the Reduction Factors required by the German guidelines for this peculiar class of geosynthetics have been presented, also considering the new EuroCode 7 - BS EN 1997-3:2025 [4]. The importance of the polymeric coating in protecting the steel wires against corrosion has been emphasized; moreover, how installation damage to this coating and environmental factors influence the long-term performance has been shown.

It has been shown that, by applying the appropriate reduction factors, engineers can ensure the structural integrity and long-term performance of reinforced soil structures utilizing polymeric coated woven steel wire meshes, in compliance with German regulations.

References

1. EN 10223-3:2014. Steel wire and wire products for fencing and netting - Part 3: Hexagonal steel wire mesh products for civil engineering purposes
2. EN 14475:2006. Execution of special geotechnical works - Reinforced fill
3. ISO/TS 20432:2022. Guidelines for the determination of the long-term strength of geosynthetics for soil reinforcement
4. BS EN 1997-3:2025. Eurocode 7 Geotechnical Design – Part 3: Geotechnical structures
5. EAD 200026-00-0102. Steel mesh systems for reinforced fill. EOTA
6. ISO 7989-2:2007. Steel wire and wire products - Nonferrous metallic coatings on steel wire - Part 2: Zinc or zinc-alloy coating
7. EN 10244-2:2023. Steel wire and wire products - Non-ferrous metallic coatings on steel wire - Part 2: Zinc or zinc alloy coatings

8. EN 10245-1:2011. Steel wire and wire products. Organic coatings on steel wire - General rules
9. DIN 1054:2005. Subsoil - Verification of the safety of earthworks and foundations - Supplementary rules to DIN EN 1997-1 (Baugrund - Sicherheitsnachweise im Erd- und Grundbau - Ergänzende Regelungen zu DIN EN 1997-1)
10. EBGEO (2011). Recommendations for Design and Analysis of Earth Structures using Geosynthetic Reinforcements (Empfehlungen für den Entwurf und die Berechnung von Erdkörpern mit Bewehrungen aus Geokunststoffen). German Geotechnical Society (Deutsche Gesellschaft für Geotechnik, DGGT). Published by Ernst & Sohn Verlag für Architektur und technische Wissenschaften GmbH & Co. KG, Berlin, Germany
11. EN ISO 10319:2024. Geosynthetics - Wide-width tensile test
12. EN 17738:2023. Geotextiles and geotextile-related products - Damage during installation procedure - Full scale test
13. ISO/TS 13434:2007. Geosynthetics – Guidelines for the assessment of durability
14. J. Müller-Rochholz, Expertise MRG 2-24. Reduction Factors for Maccaferri Terramesh System, Maccaferri Terramesh Green/Mineral and Terramesh Green/Mineral Light (Polimac). Creep rupture, Damage during Installation and environmental influences, 2024
15. EN 60216-8:2013. Electrical insulating materials. Thermal endurance properties - Instructions for calculating thermal endurance characteristics using simplified procedures
16. EN ISO 527 - Plastics. Determination of tensile properties
17. TRI Environmental. Accelerated Aging of the PoliMac Coating Used with Maccaferri Double Twist Steel Wire Products, 2024
18. ASTM A975-2024. Double-Twisted Hexagonal Mesh Gabions and Revet Mattresses (Metallic-Coated Steel Wire or Metallic-Coated Steel Wire with Polymer Coating
19. TNO Delft. Report R11812 - Evaluation of possible stray current effects on Maccaferri products in rail environment, 2013
20. EN 12225:2020. Geosynthetics - Method for determining the microbiological resistance by a soil burial test
21. EN 13249:2016. Geotextiles and geotextile-related products - Characteristics required for use in the construction of roads and other trafficked areas (excluding railways and asphalt inclusion)
22. EN 13251:2016. Geotextiles and geotextile-related products - Characteristics required for use in earthworks, foundations and retaining structures
23. EN 12224:2000. Geotextiles and geotextile-related products - Determination of the resistance to weathering

Durability Analysis of High-Density Polyethylene Geomembrane Immersed in Brine and Tailings Solutions

Siamak Paulson[1*]

[1]Sigma Geo Environment, Technical Director, 53 Metroplex Av Murarrie QLD, Australia 4172

Abstract. The high-density polyethylene geomembrane has been widely used within the lining system of various containment facilities in mining and coal seam gas sectors. These have proven to be very effective in most cases, however some notable failures have occurred which could be attributed to either the aggressive nature of the contained solution, or the makeup of the geomembrane. These failures have consequently highlighted the fact that the use of minimum specification provided in GRI GM13 should be reassessed for application in conjunction with unusual liquors. This paper investigates the performance of several geomembrane products immersed in CSG Brine and Tailings solutions. Some of the geomembranes analysed are considered a GRI GM13 compliant geomembrane, while the others are considered high-performance products. The retention of antioxidants for each specimen over a period of up to 150 days was assessed at 21, 40, 60 & 75 degrees Celsius using Arrhenius analysis of Standard Oxidative Induction Time (ST-OIT) and High-Pressure Oxidative Induction Time (HP-OIT) test methods. The analysis presented in this paper depicts a clear performance difference between the GRI GM13 compliant geomembrane and the high-performance geomembrane. It is also shown that the nature of the liquor in contact with the geomembrane can present a noticeable influence on the results.

1 Introduction

Standard durability tests in GRI-GM13 are commonly considered adequate for Manufacturing Quality Control (MQC) of geomembrane products; however, may not be sufficient for site-specific mining applications. Thus, a comprehensive assessment of geomembrane compatibility in these environments is crucial to ensure satisfactory performance and avoid catastrophic failures. This paper presents durability studies with a high-performance geomembrane at various temperatures and durations using brine and tailing solutions from actual mine sites.

* siamak.paulson@sigma-geo.com.au

1.1 Material tested

1.1.1 GRI-GM13 compliant geomembrane

High Density Polyethylene (HDPE) geomembrane typically comprises 96-97% Polyethylene resin, 2-3% carbon black, and small amounts of antioxidants and stabilizers. Carbon black protects against UV radiation, while antioxidants and stabilizers prevent oxidation. The GRI Standard Specification GM13 for smooth/textured HDPE geomembranes is widely used in the industry.

1.1.2 High-performance HDPE geomembrane

The high-performance geomembrane product is manufactured to exceed the GRI-GM13 and undergoes stringent testing regimes. It has been widely adopted in waste containments and mining applications where long-term performance under harsh chemical exposures is critical. To ensure suitability for such demanding environments, extensive durability tests were conducted to demonstrate the geomembrane's performance in mining solutions.

1.2 Experimental Descriptions

1.2.1 Immersion testing with mining solutions

The mechanisms of HDPE geomembrane degradation are UV degradation, thermal degradation, oxidative degradation and the synergic effects of these mechanisms occurring simultaneously. Long-term performance of HDPE geomembranes depends on several aspects, which include field temperature, exposure conditions, covered or protected conditions, geomembrane type and its formulations, etc.
To understand the geomembrane degradation mechanisms in mining applications, immersion tests simulating the actual mining condition, brine solution (pH 9 from a Coal Seam Gas brine pond) and copper tailing solutions from a mine site with different temperatures. The immersion durations were set at 60, 90, and 150 days, with testing temperatures of 21 C, 40 C, 60 C, and 75 C. The samples underwent testing in both pre- and post-immersion as shown in Figure 1.



Fig. 1: The immersion apparatus: samples immersed in 40 C brine solution

1.2.2 Oxidation Induction Time (OIT)

Oxidation induction time is a crucial parameter for HDPE geomembranes, indicating their resistance to oxidative degradation over time. It measures the duration until the material starts to undergo oxidative changes when exposed to environmental factors such as heat, UV radiation, and chemicals as shown in the degradation model of most geomembranes (GRI White Paper 6: Geomembrane Lifetime Prediction) as shown in Figure 2.

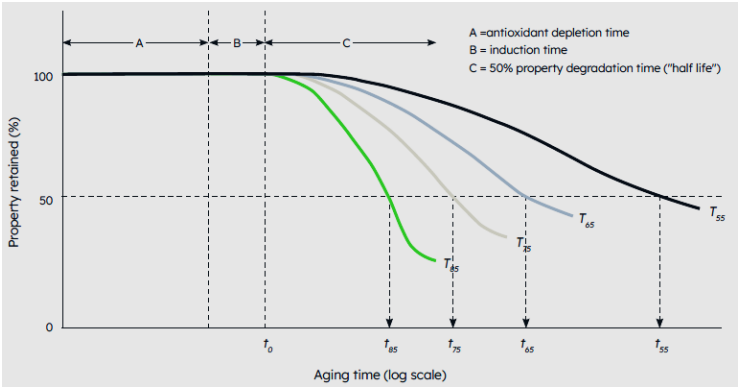


Fig. 2: Three Individual Stages in the Aging of Most Geomembranes (Robert M. Koerner & et. al., 2005)

1.2.3 Standard Oxidation Induction Time (ST-OIT)

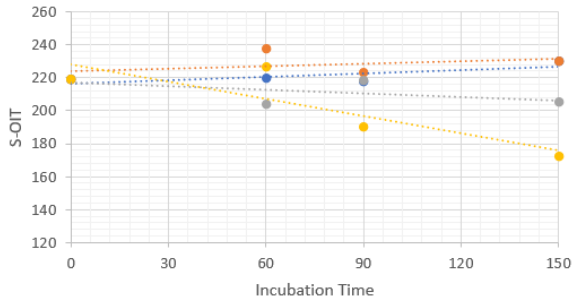
Standard Oxidation Induction time (ST-OIT 200 C, 35kPa; ASTM D3895) was used to detect hindered phenol and phosphite antioxidants. Samples immersed in brine demonstrated no significant reduction of ST-OIT at lower temperatures, with slight reductions at 60 C and 75 C after 60 and 90 days whilst samples exposed to tailing solutions exhibited significant reductions over time as shown in Figure 3. However, test results after brine shows reduction less than 15% and after tailing shows reduction less than 25%. Both of the test result remains a value of above 100 minutes, which is the minimum requirement of a standard GRI GM 13 HDPE geomembrane.

1.2.4 High Pressure Oxidation Induction Time (HP-OIT)

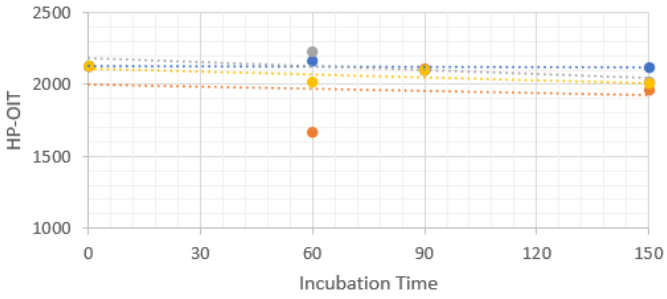
High Pressure Oxidation Induction Time (HP-OIT, 150 C, 3450 kPa: ASTM D5885) tests was conducted to monitor the synergists and hindered amine light stabilizers (HALS). The stabilizers can slow down the aging reaction and indicate the service life of geomembrane even after exposure. The reduction in HP-OIT was less than 15% with individual HP-OIT values consistently meeting or exceeding the specification limits.

2 Results and Discussions

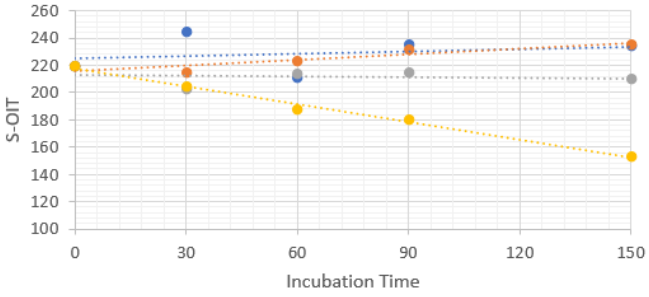
The results from ST-OIT and HP-OIT on geomembrane samples after immersion in Brine and Tailings are presented in Figure 3. Graphs provided for each showing the ST-OIT and HP-OIT after 30, 60, 90, 120 and 150 days of immersion.
From these graphs it can be seen that the ST-OIT and HP-OIT after immersion in brine and tailings have generally decreased with the increase in temperature.



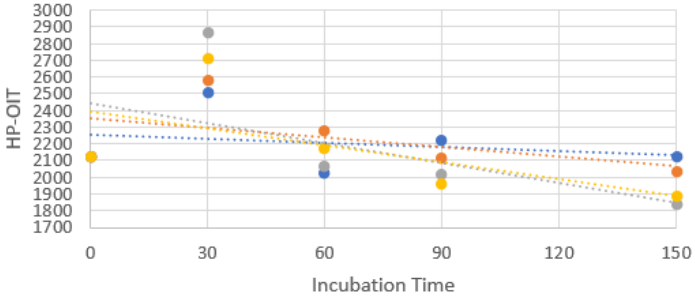
ST-OIT after tailings



HP-OIT after tailings



ST-OIT After Brine



HP-OIT after Brine

Fig. 3: ST-OIT & HP-OIT after Brine and Tailing Immersion

Arrhenius modelling (Koerner et. al. 1992) was used to calculate the rate of antioxidant depletion at different temperatures using the depletion rates obtained experimentally for ST-

OIT and HP-OIT. The results are shown in Figures 4 -9. It can be seen in these graphs that the ST-OIT and HP-OIT reductions in the high-performance geomembrane has been significantly less than GRI-GM13 geomembrane after immersion in brine and tailings solutions. Similarly, a significant improvement can be seen in the antioxidant depletion rate for the high-performance geomembrane than the GRI GM13 geomembrane.
It should be noted that several tests were conducted as replicates in this study due to various errors during the testing process where unreliable data were obtained. Also, the ST-OIT results on high-performance geomembrane samples after immersion in Tailings and Brine did not produce adequate number of data points for use in the Arrhenius analysis, hence, these graphs are not presented in this paper.

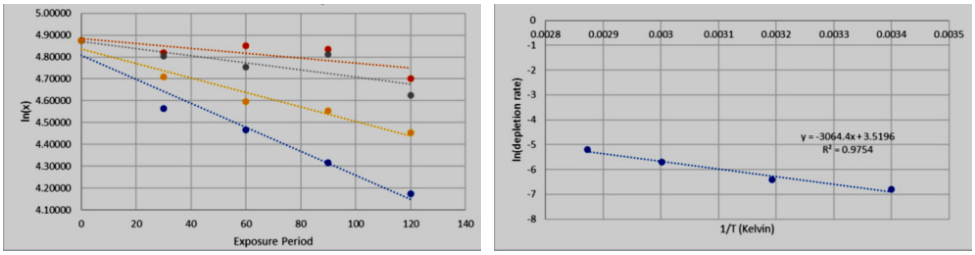


Fig. 4: GRI GM13 Geomembrane Immersion in Tailing Liquor, Arrhenius ST-OIT Prediction Depletion Time 7 years

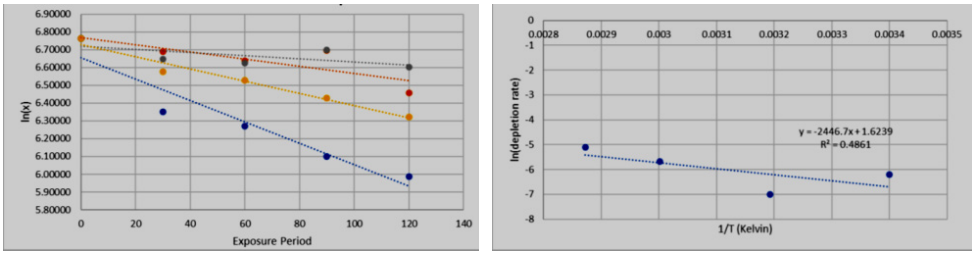


Fig. 5: GRI GM13 Geomembrane Immersion in Tailing Liquor, Arrhenius HP-OIT Prediction Depletion Time 9 years

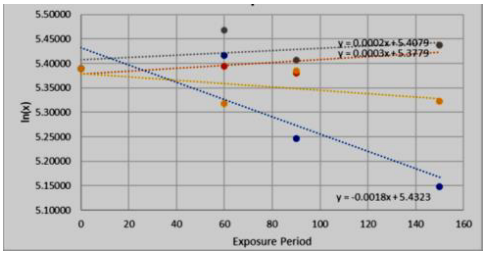


Fig. 6: High-performance Geomembrane Immersion in Tailing Liquor, ST-OIT

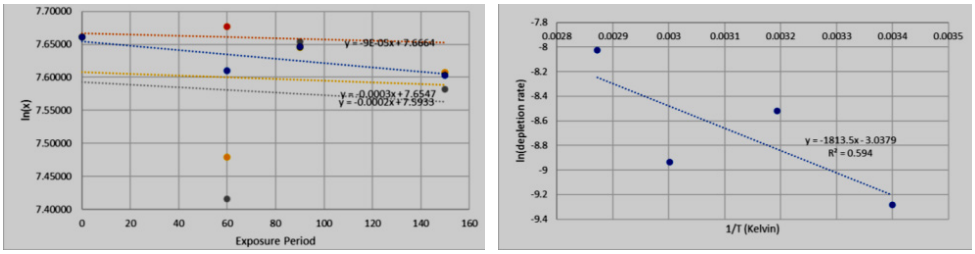


Fig. 7: High-performance Geomembrane Immersion in Tailing Liquor, Arrhenius HP-OIT Prediction Depletion Time 144 years

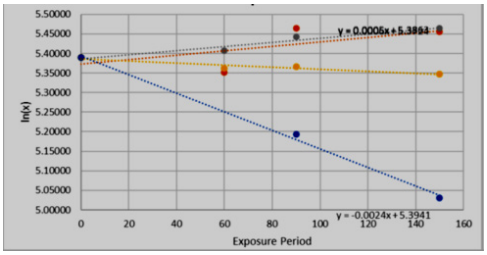


Fig. 8: High-performance Geomembrane Immersion in Brine Liquor, ST-OIT

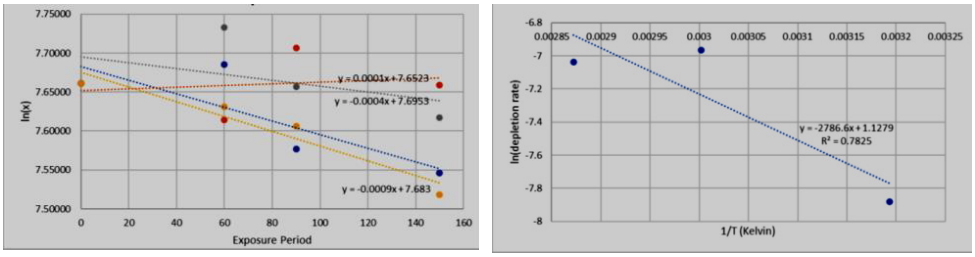


Fig. 9: High-performance Geomembrane Immersion in Brine Liquor, Arrhenius HP-OIT Prediction Depletion Time 50 years

3 Conclusions

The durability assessment of HDPE geomembrane in aggressive chemical such as one in mining industry shall be subjected to a higher standard of assessment as any failure may cause catastrophic contamination. The immersion tests provide a direct assessment on the durability and chemical stability/ compatibility of a particular geomembrane.

From the above laboratory testing, it can be concluded that temperature has a detrimental effect on the durability of HDPE geomembrane & different chemical solutions will affect the durability of HDPE geomembrane differently. The high-performance geomembrane has been proven in this study to perform satisfactorily in aggressive brine and tailing solutions even at an elevated temperature of up to 75 C after 90 days of immersion.

Antioxidant depletion rate predicted at 60 C for high-performance geomembrane based on preset test conditions also indicated satisfactory performance with respect to the industry requirement. The findings provide critical insights into the geomembrane's long-term performance, ensuring its reliability in environments with mining exposure. This study enhances confidence in the use of high-performance geomembrane, supporting their application in vigorous mining conditions.

4 References

1. R. M. Koerner, Y. G. Hsuan, G. R. Koerner, Geosynthetic Institute GRI White Paper 6: Geomembrane Lifetime Prediction Unexposed and Exposed Conditions, Original June 7, 2005 – Updated February 8, 2011.
2. R. M. Koerner, A. E. Lord Jr, Y. H. Hsuan, Arrhenius Modelling To Predict Geosynthetic Degradation, Geotextiles And Geomembranes, Vol 11, Issue 2, 1992.
3. R. M. Koerner, Y G. Hsuan, Lifetime Prediction of Polymeric Geomembranes Used in New Dam Construction and Dam Rehabilitation, Geosynthetic Research Institute and Drexel University, Proceeding of State Dam Safety Conference, Pennsylvania, June 4-6, 2003
4. ASTM D3895-19, Standard Test Method for Oxidative-Induction Time of Polyolefins by Differential Scanning Calorimetry, Last Updated: Aug 21, 2023.
5. ASTM D5885/ D5885M-20, Standard Test Method for Oxidative Induction Time of Polyolefin Geosynthetics by High-Pressure Differential Scanning Calorimetry, Last Updated: Sep 14, 2020.

25 Years of Experience with a Lysimeter System with Geosynthetic Clay Liners

Antje Müller-Kirchenbauer[1] and *Henning* Ehrenberg[2*]

[1]University of Applied Sciences and Arts (HSBI), 32427 Minden, Germany
[2]Naue GmbH & Co. KG, 32339 Espelkamp, Germany

Abstract. Since 1999, a lysimeter facility with 6 test areas has been installed in a hillshaped soilbody in northern Germany, in which long-term tests with geosynthetic clay liners are carried out. Inside of the hill is a measuring room which contains the devices for measuring the precipitation, the amount of drainage water above the GCLs and the amount of permeation water passing through the GCLs every 10 minutes since 25 years. Based on this data, the Long-Term behaviour was investigated under various boundary conditions and the efficiency of the Geosynthetic Clay Liners under different boundary conditions was analysed. Different types of geosynthetic clay liners were investigated and it was considered under different overload-situations. The paper provides an overview of the general test set up and the most important findings on long-term permeability, influences from dry-wet and freeze-thaw cycles, and other findings from 25 years of testing the lysimeter system.

Full paper to be published in:
https://www.e3s-conferences.org/articles/e3sconf/abs/2025/44/contents/contents.html

* Corresponding author: hehrenberg@naue.com

EVOLUTION OF RECYCLED CONSTRUCTION AGGREGATES (RCA) pH AND ITS COMPATIBILITY WITH GEOSYNTHETICS

Abdelkader Abdelouhab[1*], *Alain* Nancey[1] and *Dick* Janse[2]

[1]Solmax, 9, rue Marcel Paul - B.P. 40080, F-95873 Bezons Cedex, France
[2]Solmax, Europalaan 206 7559 SC Hengelo The Netherlands

Abstract. Recycled Construction Aggregate (RCA) is now commonly used as a fill material in reinforced soil structures, often in combination with geosynthetic reinforcement. However, the alkalinity of recycled materials in contact with geosynthetics made from Polyethylene Terephthalate (PET) can lead to varying degrees of reduction in the mechanical resistance of the geosynthetic. When RCA is first produced, the concrete elements within it typically have a high initial alkalinity (pH > 9). However, the actual pH of mixed RCA varies depending on site conditions and time. A literature review has shown that while RCA initially has a high pH, the recycling process and its transformation into granulates lead to a gradual decrease in pH due to several influencing factors. Over time, the pH can drop to values below 9. Through a literature review and simplified laboratory tests, this paper examines the evolution of RCA's pH and the key parameters influencing its changes. This study serves as an initial contribution to a better understanding of the conditions that determine the compatibility of RCA with PET geosynthetic reinforcement.

Full paper published in the September 2025 Special Issue of the French Geotechnical Journal **"Revue Française de Géotechnique"** _*https://www.geotechnique-journal.org*

* Corresponding author: aabdelouhab@solmax.com

Long-term performance of PET geogrids with LLDPE coating in alkaline conditions

Giulia Lugli[1], *Quintilio* Napoleoni[2], and *Moreno* Scotto[1]

[1]Officine Maccaferri Spa, Bologna, Italy
[2]DICEA – University of Rome "Sapienza", Rome, Italy

Abstract. The increasing demand for sustainable construction practices and cost minimization has driven interest in utilizing locally available soil for reinforced fill structures. However, cohesive soils often require chemical stabilization to meet engineering standards, creating highly alkaline conditions that can affect the durability of polymeric reinforcements. Conventional PET geogrids are generally considered unsuitable in environments where pH exceeds 9 due to their susceptibility to hydrolysis. While this concern is valid, it may not fully consider the various types of coatings and industrial production processes available, which can significantly impact reinforcement performance. This study investigates the long-term performance of high-strength PET geogrids with LLDPE coatings in highly alkaline environments through laboratory experiments and real-world exhumation campaigns. The research examines the role of PE sheathing in mitigating the penetration of alkaline solutions, preserving the mechanical properties of geosynthetic reinforcements. Findings from field tests at multiple sites in the UK and Italy, where geogrids were exposed for up to 20 years, confirm that the protective LLDPE coating effectively prevents degradation, with residual tensile strengths exceeding 96% of the characteristic values. The results highlight the need to reconsider existing durability standards, which primarily assess uncoated PET, to account for the protective role of advanced coatings.

Full paper published in the September 2025 Special Issue of the French Geotechnical Journal **"Revue Française de Géotechnique"** *https://www.geotechnique-journal.org*

SESSION 6 B
HYDRAULIC APPLICATIONS (2)

First innovative and sustainable GCL-application in Dutch flood defence at Beesel

Rijk Gerritsen[1], *Jan-Willem* Bardoel[2], *Kees* Dorst[3], *Jan* Meerkerk[4]

[1] Naue Nederland,'s-Heerenberg, Holland
[2] Water Authority Limburg / DoWaCo, Roermond, Holland
[3] ABT engineering firm, Velp, Holland
[4] Contractor combination Heel & Beesel (Mourik and FL), Haghorst, Holland

Abstract. As an innovation within the Flood Protection Programme (HWBP) in the Netherlands, the flood defence at Beesel has been reinforced using a Geosynthetic Clay Liner (GCL, bentonite mats) over two levee sections. The implementation of GCL's on a levee is a first-time project in the Netherlands. The GCL were applied over a total length of 530 metres on the outer slope, the crest and part of the inner slope of the levee. An extensive guideline for the application of bentonite mats in Dutch levees has been written. This article describes the considerations for bentonite mats within the assessment framework 'Sustainable levees'. Furthermore, the article extensively discusses the design aspects of the project in Beesel, implementation, management and maintenance.

1 Introduction

In order to comply with the legal flood protection standard, the levees along the Meuse River, near Beesel in Limburg region, have been raised and strengthened. As an innovation within the Flood Protection Programme (HWBP), the dike core has been covered with a bentonite mat as equivalent to a traditional clay layer.

The implementation of GCL's in a levee is a first-time project in the Netherlands. A major advantage of this method is that it allows optimal use of locally available soil. Knowledge and experience was brought in from hydraulic engineering projects in Germany, where the technique of GCL's on flood defences has been used for over 20 years [1].

With a very thorough development phase from 2015 onwards, the technique has also been introduced to flood defences in the Netherlands. In 2019, GCL's were used for the first time in the Netherlands as an anti-piping measure in the foreland between the levee and the river, at a levee reinforcement in Neer [2]. In 2022, GCL's were applied to the outer slope, the crown and part of the inner slope of the levee in Beesel (Fig. 1). The project was carried out by the contractor Heel & Beesel Levee Reinforcement Combination (Mourik and FL).



Fig. 1. Installation GCL's at the levee reinforcement project at Beesel on the outer slope, the crest and part of the inner slope and covering with a top layer of soil.

2 POV Levee Reinforcement with locally available soil

Strengthening flood defences faster, cheaper, and more sustainable with locally available soil: that is the objective of the POV-DGG program (Cross-project exploration of dike reinforcement with locally available soil). This exploration is an initiative of the HWBP and aims for an optimal composition and shape of a flood defence, with maximum use of locally available soil. This is also known as 'soil-driven design'. One of the innovations from the POV DGG is the application of GCL's on levees [3].

Levee reinforcements normally require a large amount of high-quality clay to seal the levee and make it erosion resistant. However, good quality levee clay is becoming increasingly scarce in the Netherlands. This type of clay is often not available within a reasonable distance from the project site. For some projects, levee clay has been transported in large quantities from Belgium over a distance of more than 200 km. Transporting large quantities of soil over long distances results to high CO_2 emissions and high construction costs. In many projects, the bentonite mat together with a layer of local soil can replace the entire clay covering, eliminating the need for the supply of this specific clay. This makes a significant difference in transport intensity: one truck can transport about 4000 m^2 of bentonite mats, which corresponds to 250 trucks of clay. This also has a positive effect on road safety and noise disturbance. The use of bentonite mats is a reinforcement measure that increases the possibilities for the use of locally available soil.

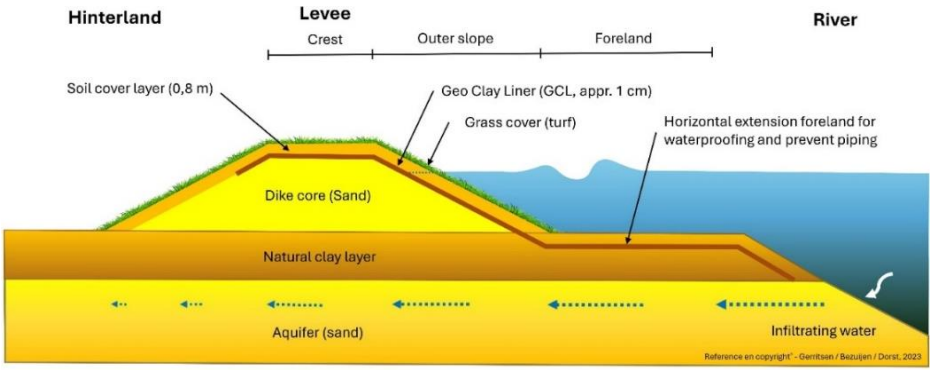


Fig. 2. Schematic cross-section: GCL as sealing of the outer slope, crest and a part of the inner slope of the levee, or to extend the seepage length in the foreland to prevent piping, as a replacement for a traditional clay lining.

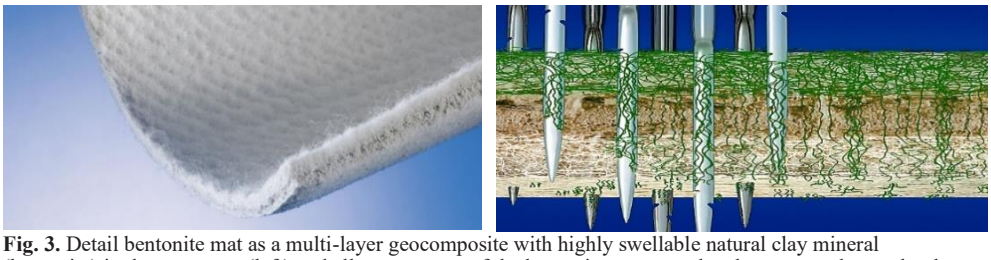


Fig. 3. Detail bentonite mat as a multi-layer geocomposite with highly swellable natural clay mineral (bentonite) in the core zone (left) and all components of the bentonite mat are robustly connected to each other by needle punch technique (right).

3 What are Geosynthetic Clay Liners (GCL)

Geosynthetic Clay Liners (GCL's) or so called bentonite mats are a multi-layer geocomposite with highly swellable natural clay mineral (bentonite) in the core zone, see Fig. 3. The geotextile bottom and top layer determine the technical strength properties and robustness of the bentonite mat. The core with ≥ 4500 gram/m^2 of high-quality sodium bentonite determines the long-term sealing properties [4]. All components of the bentonite mat are robustly connected to each other by use of the needle-punch technique (Fig. 3). Bentonite naturally has a low internal friction angle of about 8 degrees, but the needle-punch technique firmly connects the layers to each other and increases the internal friction angle. This makes the bentonite mats suitable for installation on a slope. The connection of the top and bottom layer is tested in a laboratory using so-called peeling tests (Fig. 4). The mats should have a strength of ≥100 N/10 cm in accordance with the guidelines [5]. For the shear strength of bentonite mats, it is important not only to look at the internal shear resistance, but also at the shear strengths on the bottom or top side in combination with the soil conditions. These shear strengths are determined using so-called 'direct shear' tests.

Bentonite mats are produced and delivered to a project site in 'dry' form (approx. 10% water content in the bentonite). The sealing effect of the bentonite mat is created by water absorption after installation. When hydrating the bentonite, a molecular bond is formed with the so-called bentonite plates, in which the mat swells homogeneously. The swelling capacity of the bentonite is tested with the so-called 'swell index test', in which two grams of dry bentonite should swell to a minimum of 24 ml within one day (Fig. 4). For swelling of the mat during installation, it is important that the mat has sufficient homogeneous load with ground pressure to prevent excessive swelling. When using bentonite mats, the absolute minimum cover is 0.3 m, but for levees a soil cover of 0.80 to 1.20 m is recommended (see Management and maintenance aspects).

Bentonite mats were developed in the 1980s, providing more than 40 years of experience in design, properties, and applications. In hydraulic engineering and levees, there is already more than 20 years of experience [1]. A significant part of all experience has been gained in Germany with hundreds of civil and environmental projects. This also includes applications on levees, such as along the Lippe, Kinzig and Elbe. The application of high-quality bentonite mats on levees is a mature and fully accepted construction technique in Germany. The guidelines for German applications are found in [5]. For use in levees, Naue developed the high quality GCL Bentofix® B4000. This GCL mat was also used for the levee reinforcement in Beesel. The bentonite mat distinguishes itself in the use of certified raw materials for the geotextiles, high-quality properties of the geotextiles both the top and bottom layer (robustness), high shear strengths and the quality of the bentonite.

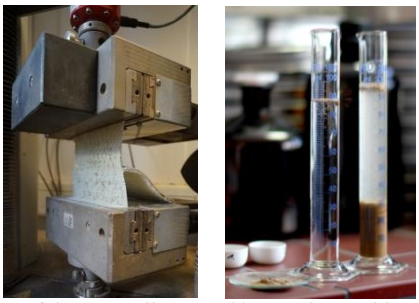


Fig. 4. Laboratory test connection of the geotextile top and bottom layer with so-called peeling tests in tensile equipment (4a - left) and laboratory test of bentonite swelling capacity with the 'swell index test', in which 2 grams of dry bentonite should swell to at least 24 ml within 1 day (4b - right).

4 Assessment framework bentonite mats in sustainable levees

The Flood Protection Programme (HWBP) faces the task of realising safe levees within the agreed frameworks of financial budget and construction time. In addition, all HWBP alliance partners have committed themselves to ambitions in terms of energy, climate and circularity. These ambitions are based on various Dutch government agreements, such as the Climate Agreement, the National Raw Materials Agreement, and the Green Deal Sustainable Civil Engineering 2.0. With the consequence that levee reinforcements should be circular and climate neutral as much as possible by 2030. Application of geosynthetics to levees can contribute to multiple sustainability and climate change topics, [6], [7] and [8].

To make sustainability more specific and concrete, the HWBP has developed the sustainability rose (Fig. 5). The base of the approach and the centre of the rose is the focus on constructing levees in a sober and efficient manner. Around this, three main sectors have been defined with Energy & Climate, Circularity and Spatial Quality [9]. Innovations for levee reinforcements play a vital role within the HWBP programme. The use of bentonite perfectly meets the sustainability goals and has the following advantages comparing a traditional clay lining:

1. Climate proof: good resistance to dehydration. This becomes more and more important given the increasingly dry and hotter periods due to climate change.
2. Incentive for the use of locally available soil. Substantial reduction in soil transport and reduction in use of primary construction materials (sand, clay).
3. Reduction of CO_2 emissions during the construction. The production and supply of bentonite mats can be compared to the (large-scale) extraction and transport of traditional clay. The reduction of CO_2 emissions is of increasing importance for the realisation of climate-neutral levee reinforcement projects.
4. When applied in the foreland as an anti-piping measure: fast construction and less deep excavation.
5. A special type of bentonite mat with sand inlay (tri-composite) can be placed under water In that case, no dewatering is required.
6. Delivery of ready-to-use product. Homogeneous product properties with continuously guaranteed quality based on intensive production quality checks.
7. Technically high-quality geo-building material with a long, demonstrable technical and functional life time of up to 100 years.
8. Important for management and maintenance: low-maintenance or maintenance-free application. If damage occurs due to unforeseen circumstances, it can be repaired.
9. High installation speed with 1500 m^2/day, resulting to shorter realisation time in levee reinforcement projects. Faster to apply than a traditional clay cover with need for multiple layered compaction in 30 cm thickness each.
10. Cost-effective: substantially lower construction costs.

If the above properties are translated to the sustainability rose, the application of bentonite mats contributes to 6 of the 12 quadrants. This is visualized with the orange dots in Fig. 5.

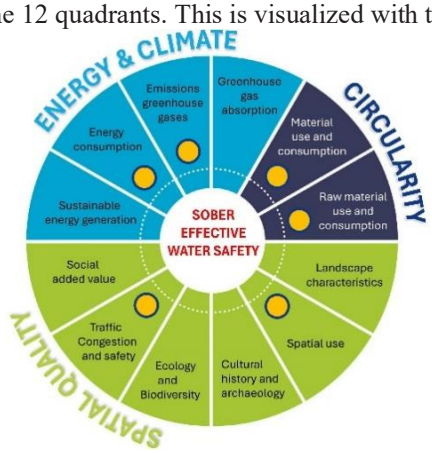


Fig. 5. Sustainability quadrant overview by Flood Protection Program (HWBP) with the contribution of bentonite mats (orange dots) in 6 of the 12 quadrants – edited Gerritsen 2025.

5 Guideline Geosynthetic Clay Liners to levees

To enable the application of levees with Geosynthetic Clay Liners in the Netherlands, a technical working group of experts prepared a comprehensive guideline at the initiative of Water Authority Limburg in collaboration with Arcadis [10]. This guideline covers the design, implementation, assessment, management and maintenance of bentonite mats in the foreland and slopes of primary and regional flood defences. Application, specification, and testing criteria have also been established, in line with fundamentals on flood protection [11] and [12]. The NL-guideline is based on knowledge and experience gained from the design and application of bentonite mats in German levee construction and has been extended to Dutch design and assessment practice.

6 Design levee reinforcement

For the levee reinforcement in Beesel, the application of bentonite mats is designed at the outer slope, the crest and part of the inner slope in the following levee sections:

- Beesel levee section 4 and levee section 5-1, length 280 m[1] (Fig. 6 left).
- Beesel levee section 9 and 10, length 250 m[1] (Fig. 6 right).

A detailed construction design was made by engineering firm ABT, including stability and flow calculations. The finite element program PLAXIS was used for the calculations (see Fig. 7). Initially, the intention was to apply the bentonite mats also on the entire inner slope, as a applicable measure against infiltration to the core of the dike during wave overtopping. However, groundwater flow calculations with PLAXIS showed that the pressure in the core near the inner toe under normative conditions could increase due to seepage water from underneath the dike. The high phreatic water level in the core has a negative influence on the stability of the lining on the inner slope and could (theoretically) lead to excessive tensile forces in the bentonite mats. On the basis of additional stability calculations carried out with PLAXIS, it was established that the tensile strength in the bentonite mats was well within the margin, even with the occurrence of limited deformations of the inner slope. In the end, it was decided not to use the bentonite mats on the lower half of the inner slope. This creates a

natural relief zone on the inner slope for water overpressure to escape. The analyses have shown that the application of the bentonite mats on the outer slope and the crest results to the same geohydrological situation as for the levee sections where a clay revetment with erosion resistance class 1 has been.

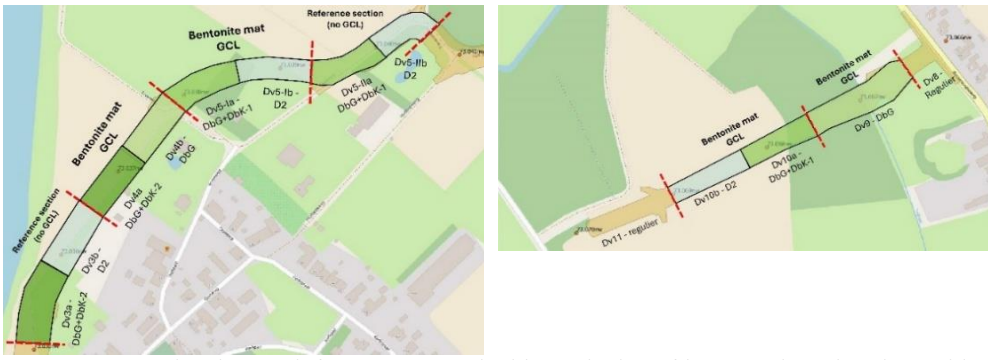


Fig. 6. Top view levee reinforcement Beesel with numbering of levee sections, locations with bentonite mat and overview of grass mixtures for monitoring the development of grass cover.

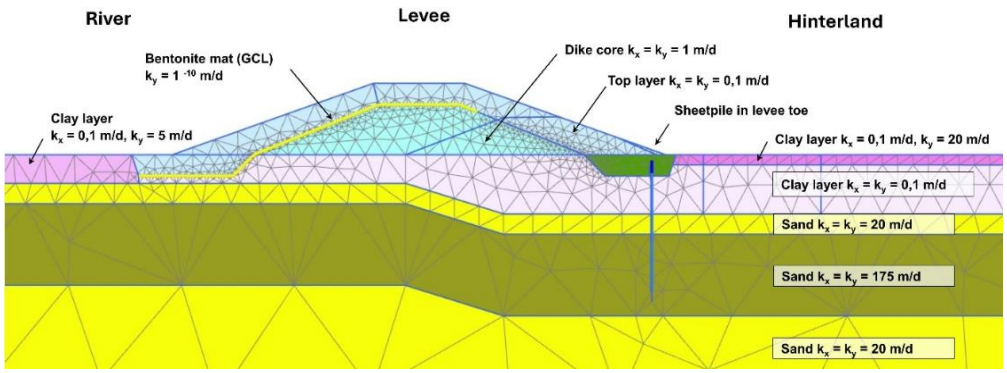


Fig. 7. Overview schematization levee in PLAXIS-software with bentonite mats in the flow calculations performed to determine the geohydrological situation under normative conditions, including the permeability factors used (k-value in m/day).

Another important design aspect was the thickness of the cover layer at the top of the crest. From German design practice, several aspects were known that needed to be considered in the design of this thickness, such as minimum thickness regarding the swelling of the mat, weather influences (frost-thaw), traffic loads, current and wave attack and uplift and shear due to water pressure. These aspects sometimes have contradictory requirements. In the construction design, the various aspects have been made transparent and the influence of each aspect on the design has been determined with the help of sensitivity calculations. In Beesel, the minimum construction height of the bentonite mat (above the normative river water level at extreme conditions, including settlements during its entire lifespan) and the maximum construction height of the crest of the levee were determining factors. As a result, there was only a limited thickness on the crest for the cover layer and the maintenance road. The application of soil stabilization with GeoCrete offered a solution here. This technique also leads to optimal use of locally available soil by mixing the existing soil with a stabilizer. This creates a stable, hard, and erosion-resistant layer on top of the crown. The strengthened maintenance path thus ensures sufficient weight and sealing of the bentonite mats in the crest of the levee, despite the limited thickness in which the stabilisation is applied (25-35 cm).

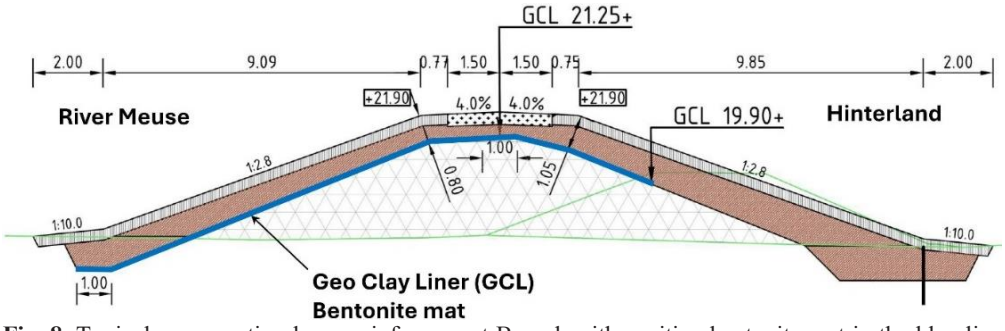


Fig. 8. Typical cross-section levee reinforcement Beesel, with position bentonite mat in the blue line on the outer slope, crest and part of the inner slope of the levee.

Specific point of attention was the connection of the bentonite mats to other objects to which the bentonite mats are connected. At the structures the bentonite mats are set up vertically against the concrete and then secured with stainless steel strips (see Fig. 9a - left). A layer of bentonite paste has been applied between the concrete and the bentonite mats as a watertight connection.



Fig. 9. Detail of the bentonite matt clamp construction with metal strips, carried out for connection to the concrete inlet works (Fig. 9a - left) and installing bentonite mats to the levee and rolling them out using a spreader bar (Fig. 9b – right).

7 Execution

The bentonite mats were applied on the outer slope with an inclination of 1:2.5, the 4.5 m wide crest of the levee, and a part of the inner slope (see Fig. 8). The height of the levees varies from 2 to 4 meters, depending on the location. A total of 13,500 m² of bentonite mats were supplied and installed. The bentonite mats were delivered on rolls and installed with a spreader bar (Fig. 9b – right). The mat overlaps are sealed with prefabricated bentonite-impregnated and marked overlap zones. This has the advantage that bentonite powder or paste does not have to be applied separately. As a realistic installation speed, a production of approx. 1500 m^2/day, including covering with soil has been achieved. With 15 m^1 of bentonite mat in the cross section, this corresponds to 100 metres of levee per day. The equipment consisted of a crane for the profiling of the levee and a crane with a spreader bar for the installation of the bentonite mats (Fig. 10). A shovel and bulldozer were used to cover the bentonite mat with the soil cover layer. It is important, especially in more rainy conditions with a wet surface, that installed bentonite mats are covered with a soil cover as soon and much as possible. This is necessary for the counter-pressure when the bentonite mats hydrate and swell. Therefore, it is not desirable to apply bentonite mats in wet conditions with continuous and heavy rainfall.

From the preliminary design phase, it was planned to install the bentonite mats with one lane on the inner slope, one lane on the outer slope and an overlap of at least 1.0 meters on

the crest. Important here was to overlap from the river side to the inner levee side, so that high water cannot run underneath the connection on the crest. Evaluation of the construction method before installation revealed that it was possible to install the bentonite mats over the entire levee profile in one movement by using a crane with a long reach. This method eliminated the overlap on the crest. This also saved surface area of bentonite mat in the levee profile and made installation easier and faster.

8 Anti animal-digging measure

The area around a natural creek in Beesel is the habitat of the beaver and the badger. Stone deposits have been placed on the stream banks to discourage digging. Additionally, the flood defence is preventively protected against animal digging by applying a protective steel grid (so-called anti-beaver netting) to the slopes at specific locations. Before applying the steel mesh, a cover layer of soil with a thickness of 0.4 metres was first applied on top of the bentonite mat (Fig. 10b right). After the installation of the mesh, the slope was finished with a soil cover layer with a total thickness of 0.8 to 1.2 meters.



Fig. 10. Installing bentonite mats to the levee and rolling them out using a spreader bar (Fig. 10a - left) and covering bentonite mats with a soil layer and applying beaver netting as a measure against animal burial levee section Beesel (Fig. 10b – right).

9 Vegetation monitoring

The bentonite mat forms an almost water-impermeable layer. In wet periods (rain, high water), the cover layer on the GCL may retain a lot of water. In dry periods, the mat may form a blockage for the capillary ascent, causing the cover layer to dry out. Both situations can therefore have an effect on vegetation development, depending on the properties of the cover.

With the aim to optimise the turf and vegetation compound on GCL's in future projects, a four-year monitoring programme was launched from the spring of 2024. Various reference and test sections have been constructed with two different cover layers (more clayey and sandy) and with three different grass and herb mixtures. The sections have an average length of 70 m.

The following grass/herb mixtures were applied throughout the reference and test sections:

- D2 (standard grass mixture for levees)
- Levee base Grass (DbG)
- DbG + basic herbs 1 (DbK-1: DbG: 90% and DbK: 10%)
- DbG + basic herbs 2 (DbK-2: DbG: 70% and DbK: 30%)

Moisture sensors have been installed in the cover layer in the reference and test sections. The monitoring of the vegetation (development and root growth) is mapped every two years, establishing relationships with occurred conditions and moisture measurements. After four years, grass sod pulling tests are also planned to measure the strength of the vegetation.

10 Management and maintenance aspects

After installation, in normal circumstances, bentonite mats are maintenance-free. Installed bentonite mats which meet the product requirements hydrate within a few days, forming a homogeneous and durable sealing system. This is important in levee construction, as some levee improvements are completed just before the high-water season. Bentonite mats are high-quality construction materials whose technical lifetime of 100 years can be proven by certified laboratory tests in advance. They do not decompose or degenerate into micro-plastics. At the end of its lifetime, a construction with bentonite mats can be removed, adjusted, or expanded if necessary.

For levees, a soil cover of 0.80 to 1.20 metres on the bentonite mat is recommended. Reason is the final situation were the levee is maintained by mowing equipment (heavy tractors). It is also recommended to install bentonite mats below the frost line (0.6-0.8 m) to prevent freezing and thawing effects, which could affect the lifetime.

In Germany the BAW (Bundesanstalt für Wasserbau) took several samples from 4 to 12-year-old mats from the Lippe, Kinzig and Elbe dikes (see Fig. 11). The Tests showed that no significant mechanical-physical changes or aging occurred. The water permeability of the samples was found to be unchanged, between 2.5 and 8.0 x 10^{-11} m/s. The results of the various test series have shown that bentonite mats do not experience any significant loss of quality after several years. Baseline is that the mat has been carefully installed and the levee has been properly maintained, meaning that trees and deep growing roots should be prevented.



Fig. 11. Test trench and inspection of bentonite mats at the Elbe levee Wittenberge from BAW Germany (Fig. 11a left) and detail sampling of hydrated bentonite mat at the Elbe levee Wittenberge by BAW Germany (Fig. 11b right).

11 Conclusion

The levee reinforcement in Beesel is a unique project in the Netherlands, in which GCL's have been successfully applied for the first time on the outer slope, crest and part of the inner slope of a dike. The application of bentonite mats in levee projects encourages the use of locally available soil, substantially reduces the number of transport movements, lowers CO_2 emissions and is cost-efficient compared to application of a traditional clay layer.

The innovative application of bentonite mats encourages other levee reinforcement projects to construct cheaper and faster and contribute positively to several sustainability

topics. Application of innovative building techniques become increasingly important due to climate change effects with increasing intense rainfall, higher river discharges and dryer periods over longer time.

References

1. Werth, K.; Heerten, G.; Pries, J.-K.; Klompmaker, J. 20 years' experience with GCLs in dams and dykes. Proceedings GBR-C 2k10, 3rd International Symposium on Geosynthetic Clay Liners, Würzburg, Germany, 15–16 September 2010.
2. Maubeuge, von, K., Gerritsen, R.H., Ehrenberg, H., Geosynthetics: responsible and sustainable solutions to reduce environmental impact, pag. 49-56, Geokunst, 2022.
3. Bardoel, J.W., Dijkversterking Beesel Waterschap Limburg, Pilot bentonietmatten: innovatief en duurzaam, pag. 4-6, Civiele Techniek, special Waterbouw, 2022.
4. Von Maubeuge, K.P.; Ehrenberg, H. Investigation of Bentonite Mass per Unit Area Requirements for Geosynthetic Clay Liners. Proceedings 10th International Conference on Geosynthetics, Berlin, Germany, 21–25 September 2014.
5. BRAD 16, Brandenburgische Richtlinie für die Anwendung Geosynthetischer Tondichtungsbahnen im Deichbau, Landesamt für Umwelt, 2016.
6. Gerritsen, R.H., Bezuijen, A., Dorst C., Klimaatverandering en weersextremen: toepassing van geokunststoffen bij waterkeringen en kustverdediging, deel 1 (pag 46 – 51), deel 2 (pag 48 - 53), Geokunst, 2019.
7. Gerritsen, R.H., Bezuijen, A., Dorst, C., Climate change and extreme weather conditions: Applications of geosynthetics securing flood defenses and coastal protection, pag. 291-303, Geosynthetics: Leading the Way to a Resilient Planet, Proceedings 12 ICG – Biondi et al (eds), 2023, ISBN 978-1-003-38688-9, 2023.
8. Rimoldi, P., Shamrock, J., Kawalec, J, Touze, N., Sustainable Use of Geosynthetics in Dykes, https://doi.org/10.3390/su13084445, Sustainability, MDPI, 2021.
9. HWBP (Hoogwaterbeschermingsprogramma), Waterschap Rivierenland, Handreiking Bouwstenen Duurzame Dijken, 2022.
10. Koopmans, R., Dorst, C., Zuijlen, van J., Dijken met GCL (bentonietmat), Handreiking voor toepassing van GCL in voorlanden en op taluds van primaire en regionale waterkeringen (groene versie), POV-DGG Dijkversterking met gebiedseigen grond, 2023.
11. Expertise Network for Flood Protection (ENW). Fundamentals of Flood Protection, English ed.; Ministry of Infrastructure and the Environment and the Expertise Network for Flood Protection: Hague, The Netherlands, 2017.
12. International Levee Handbook; CIRIA: London, UK, 2013.

Benefits in cost and environment for channel revetment with geocells

Wladimir Caressato Junior[1*], *Gustavo* Fierro[2]

[1]Tecnologia de Materiais Brasil Ltda., Technical Coordinator, 7415322, Jaguariúna, Brazil.
[2]Tecnología de Materiales S.A., R&D Corporate Manager, 6215354 Lima, Peru

Abstract. Drainage systems are vital for urban infrastructure, ensuring efficient water flow and reducing flood risks. Traditional reinforced concrete solutions, while durable, are costly and environmentally impactful. Concrete-filled geocells offer a promising alternative with lower costs and improved sustainability. This study compares both approaches in terms of costs, resource use, and environmental impact. Two drainage systems were designed with varying flow rates, using a trapezoidal section. HDPE geocells were evaluated against cast-in-situ reinforced concrete, focusing on installation efficiency and cost-effectiveness. The analysis considered direct execution costs, time estimates, required resources, fuel consumption, machine operation hours, and human labor hours. The results showed that geocells can reduce direct costs by up to 66% due to the smaller volume of material and easier installation. Machine hours and fuel consumption decreased by up to 35% and 21%, respectively, emphasizing the environmental and social benefits. The use of geocells provides significant economic and environmental advantages, aligning with global sustainability goals. Future research will assess long-term performance and maintenance.

1 Introduction

Drainage systems are essential for urban infrastructure, ensuring effective water flow management and minimizing flood risks. While traditional solutions like reinforced concrete offer durability, they are often costly and environmentally impactful. Recent advancements in geotechnical materials, such as concrete-filled geocells, provide a sustainable alternative. This study compares these two approaches in terms of costs, resource use, and environmental impact. Two drainage systems were designed for varying flow rates, using a trapezoidal section with defined dimensions and slopes. HDPE geocells were compared to cast-in-situ reinforced concrete, emphasizing installation efficiency and cost-effectiveness. The cost analysis included direct expenses like materials, labor, and equipment, using market data to identify cost differences.

The resources required for both systems, including materials, machines, labor, as well as fuel consumption, were calculated based on machine operating hours and task efficiency, and environmental impacts were assessed by quantifying carbon emissions from material production to transportation and equipment use, with additional assessment of material recyclability and reuse.

* Corresponding author: wcaressat@tdmbrasil.com.br

2 An example of project to be evaluated

In this study, we will analyze a channel lining project for hydraulic structures as a reference (Fig. 1). Two alternatives will be considered: Reinforced Concrete Lining and Geocell Concrete-Filled Lining. The estimated quantities will be used exclusively to assess the direct costs associated with each lining solution. Indirect costs will not be considered, as they are assumed to be approximately equivalent (a conservative assumption). The objective is to center the comparison on the criteria used for selecting the lining solution.

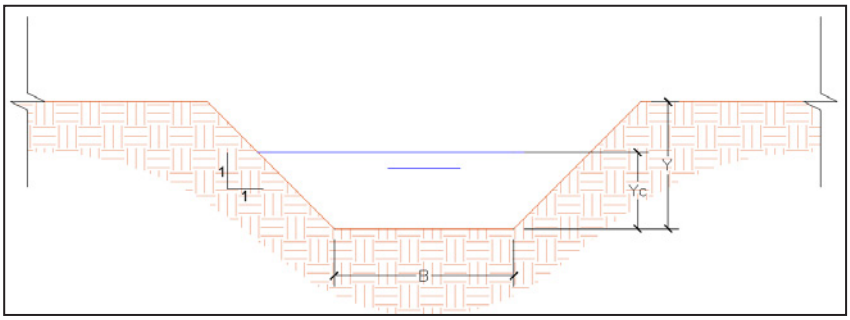


Fig. 1. Typical trapezoidal cross-section of a canal lining project.

The study consists of evaluating variations in flow rates between 1 and 80 m³/s and the consequent variation in geometry (base and height), in a section of a trapezoidal channel with a slope inclination of 1H:1V, lined with concrete of f'c = 210 kg/cm², surface roughness of 0.018, longitudinal length of 5,000 m and 0.5% bottom slope.

It is assumed that the sections meet the geotechnical and hydraulic stability requirements. For the lining design [1], we considered the information presented in Table 1.

Table 1. Estimated geometry for revetment design in the example project.

Description	Flow Rate Q = 1m³/s	Flow Rate Q = 7m³/s	Flow Rate Q = 20 m³/s	Flow Rate Q = 80m³/s
Base (m)	0.70	1.50	3.00	4.50
Height (m)	0.55	1.10	1.50	2.60
Water depth (m)	*0.45*	0.92	1.22	2.15
Speed (m/s)	*1.62*	2.63	3.38	4.81

2.1 Alternative details for a geocell and concrete revetment structure

After evaluating the following methodologies found in references [2, 3, 4, 5], for different hydraulic requests presented, the use of the geometric characteristics of the geocells was defined, as Table 2. The geocells used in this study are materials manufactured in HDPE in accordance with current ISO [6] and ASTM [7] standards and recommendations of the Geosynthetics Institute [8].

Table 2. Estimated geocell geometry for lining design

Description	Flow Rate Q = 1m³/s	Flow Rate Q = 7m³/s	Flow Rate Q = 20 m³/s	Flow Rate Q = 80m³/s

Revetment Thickness	50mm	100mm	100mm	150mm
Geocell Opening Size	416x374mm	416x374mm	416x374mm	416x374mm

Fig. 2 shows a typical detail of the application of HDPE geocells filled with concrete and the accessories required for lining drainage channels.



Fig. 2. Alternative revetment with concrete filled geocells.

2.2 Basic details for a reinforced concrete revetment structure

For the design of the reinforced concrete lining, the methodologies [9, 10, 11] were reviewed, and considering the flow rates presented in item 1, the concrete thicknesses and number of reinforcement layers were defined. In all cases, metal reinforced bars are used, following ASTM A615 standard [12], considered as concrete reinforcement.

Table 3. Estimated reinforced concrete geometry for lining design.

Description	Flow Rate Q = 1m³/s	Flow Rate Q = 7m³/s	Flow Rate Q = 20 m³/s	Flow Rate Q = 80m³/s
Revetment Thickness	75mm	150mm	175mm	225mm
Number of Armor layers	1	2	2	2

Fig. 3 shows a typical detail of the application of reinforced concrete for lining drainage channels.

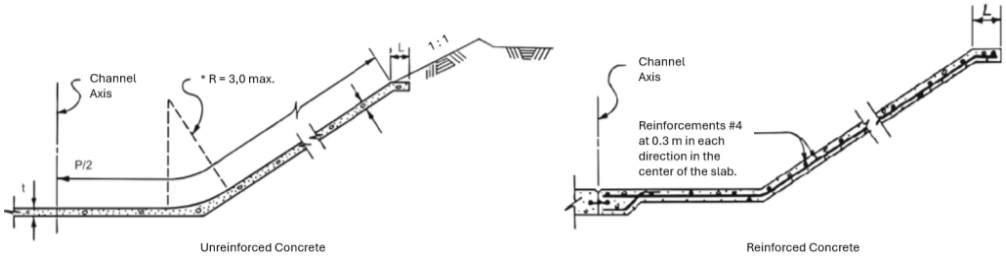


Fig. 3. Typical reinforced concrete structure to revetment channel.

2.3 Resume of quantification of principal revetment activities

For this comparison, we considered only the Direct Cost of the activities, understanding that other complementary tasks will be almost the same for both alternatives. Table 4 and Table 5 summarize the quantities.

Table 4. Geocell + Concrete total quantifications for 5km channel length.

			Flow Rate Q = 1m³/s	Flow Rate Q = 7m³/s	Flow Rate Q = 20 m³/s	Flow Rate Q = 80m³/s
Item	**Activity**	**Unit**	**Quantity**	**Quantity**	**Quantity**	**Quantity**
01	Earth Movement					
01.01	Channel excavation material	m³	2,130	13,242	32,480	134,922
01.02	Removal of excess material	m³	2,769	17,214	42,224	175,398
02	Geocell + Concrete					
02.01	Formwork	m²	500	1,000	1,000	1,500
02.02	Sup & Inst HDPE Geocell	m²	18,467	32,437	47,095	74,399
02.03	Concrete f'c=210 kg/cm2	m³	923	3,244	4,709	11,160

Table 5. Reinforced Concrete total quantifications for 5km channel length.

			Flow Rate Q = 1m³/s	Flow Rate Q = 7m³/s	Flow Rate Q = 20 m³/s	Flow Rate Q = 80m³/s
Item	**Activity**	**Unit**	**Quantity**	**Quantity**	**Quantity**	**Quantity**
01	Earth Movement					
01.01	Channel excavation material	m³	2,314	14,562	36,060	144,508
01.02	Removal of excess material	m³	3,009	18,931	46,877	187,860
02	Reinforced concrete					
02.01	Formwork	m²	19,200	33,550	48,600	76,600
02.02	Corrugated steel	kg	99,190	340,050	486,075	767,720
02.03	Concrete f'c=210 kg/cm2	m³	1,381	4,860	8,232	16,734
03	Complementary activities					
03.01	Waterproof channel joints	ml	18,425	34,900	50,650	80,000

3 Cost estimation

For a more comprehensive comparative effect, cost analyses were performed for the eight (8) scenarios studied. The unit price references were considered based on the values currently practiced in Brazil (February/25).

In addition to the installation and material supply costs, for the present study, considering both alternatives, Geocell + Concrete and Reinforced Concrete, the location of the concrete consumables (aggregate, water, backfill, cement) was at an average distance of 5.0 km, thus including the material transportation costs in our analyses.

Fig. 4 expresses the compared value as 100% of the cost due to the reinforced concrete revetment, showing how the use of geocells demonstrates a significant cost reduction.

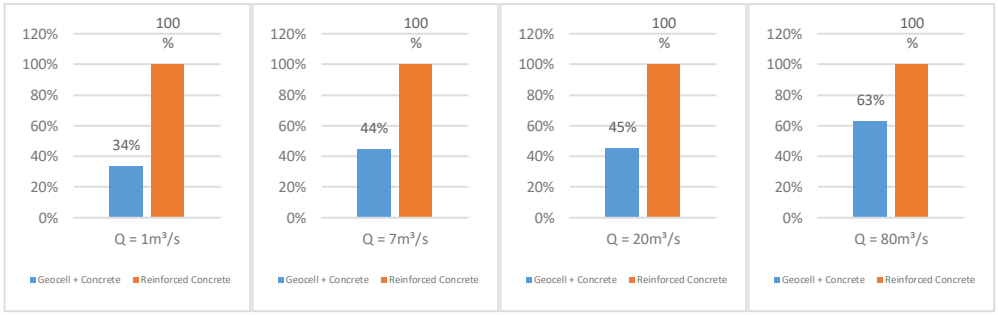


Fig. 4. Cost reduction of 66%, 56%, 55% and 37% respectively.

4 Time estimation

Fig. 5 and Fig. 6 show time schedules considering the scenario for a channel flow of 80 m³/s. The problem with reinforced concrete is the large volume of forms and metal meshes to be installed, which due to low productivity requires a high number of people working at the same time.

In project planning [13, 14], it is possible to design different scenarios and installation schedules, where the advantage of using Geocells, which in the case presented would be 37% in time, compared to reinforced concrete, could be achieved, but with the complication of managing many people at the same time on site.

Item	Acitivity	Unit	Quantity	Crew	Time (Month)
01	EARTH MOVEMENT				
01.01	CHANNEL EXCAVATION IN LOOSE AND REFINED MATERIAL	m³	144.508	2	5
01.02	REMOVAL OF EXCESS MATERIAL	m³	187.860	6	6
02	REINFORCED CONCRETE				
02.01	FORMWORK	m²	76.600	5	20
02.02	CORRUGATED STEEL FY= 4200 kg/cm2 GRADE 60	kg	767.720	5	20
02.03	CONCRETE f'c=210 kg/cm2	m³	16.734	5	7
03	COMPLEMENTARY ACTIVITIES				
03.01	WATERPROOF CHANNEL JOINTS	ml	80.000	10	8

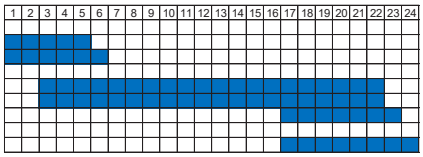


Fig. 5. Reinforced concrete schedule requires about continuous 24 months. For a 5km channel length.

Item	Acitivity	Unit	Quantity	Crew	Time (Month)
01	EARTH MOVEMENT				
01.01	CHANNEL EXCAVATION IN LOOSE AND REFINED MATERIAL	m³	134.922	2	4
01.02	REMOVAL OF EXCESS MATERIAL	m³	175.398	6	6
02	GEOCELL + CONCRETE				
02.01	FORMWORK	m²	1.500	1	2
02.02	SUP & INST. GS-15 HDPE GEOCELL TW352 h=50mm	m²	74.399	1	2
02.03	CONCRETE f'c=210 kg/cm2	m³	11.160	5	5

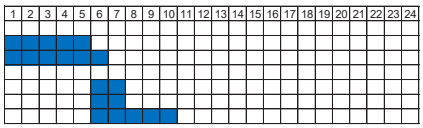


Fig. 6. Geocell+Concrete schedule requires about continuous 10 months. For a 5km channel length.

5 Environmental impact estimation

To obtain an overview of the environmental impacts generated by canal lining projects, we will consider some main variables, such as diesel consumption, machine hours and man hours worked. The criteria used to carry out this comparison will be presented below.

Fig. 7 shows the diesel consumption of the equipment involved in the activities shown in tables 4 and 5. For this estimate, an average distance of 5.0 km from the locations of withdrawal, borrowing or disposal of resources (quarry, water, sand, landfill, etc.) was considered.

Fig. 7 expresses the compared value as 100% due to diesel consumption for a reinforced concrete lining, showing how the application of geocells generates significant reduction. In different scenarios, diesel reductions of up to 21% can be found.

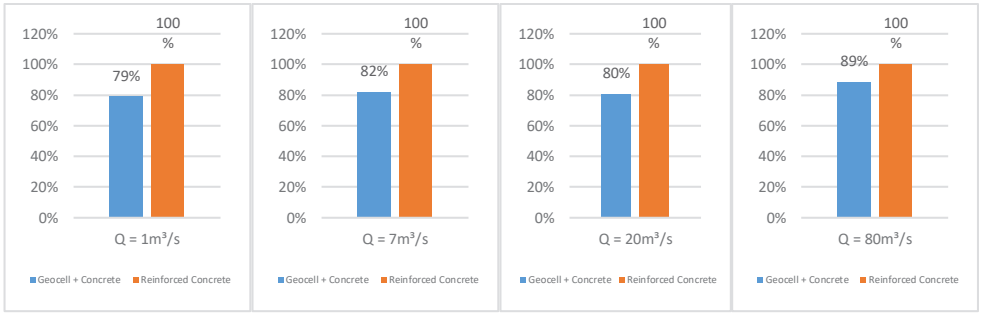


Fig. 7. Reduction in diesel consumption of 21%, 18%, 20% and 11% when the material is at an average distance of 5.0km from the construction site.

Also Fig. 8 shows the Machine Hours for both alternatives. In some cases, there are up to 35% fewer machine hours worked in the option using Geocells. This means that there will be 35% less dust generation and traffic volume in the project's surroundings and consequently noise produced in the environment, in addition to less deterioration of the region's roads and highways. These issues are of great interest to be considered when evaluating alternatives from the point of view of environmental and economic impact, especially in relation to the maintenance of access roads to the construction site.

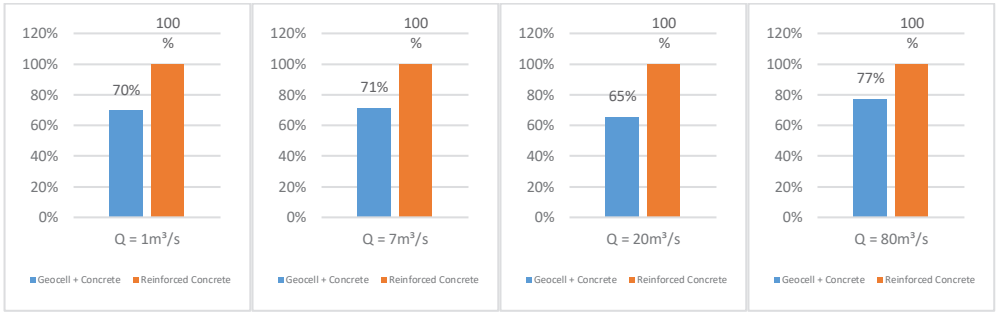


Fig. 8. Reduction in Machine Hours of 20%, 19%, 35% and 23% when the material is at an average distance of 5.0km from the construction site.

The man-hours worked to complete both alternatives were also analyzed. In the case of smaller linings, we can observe reductions of around 80%, while in larger channels, the reductions are around 53%. Such reductions allow large projects to be carried out in remote areas, using local labor from small towns, without the need for excessive mobilization of workers from large urban centers.

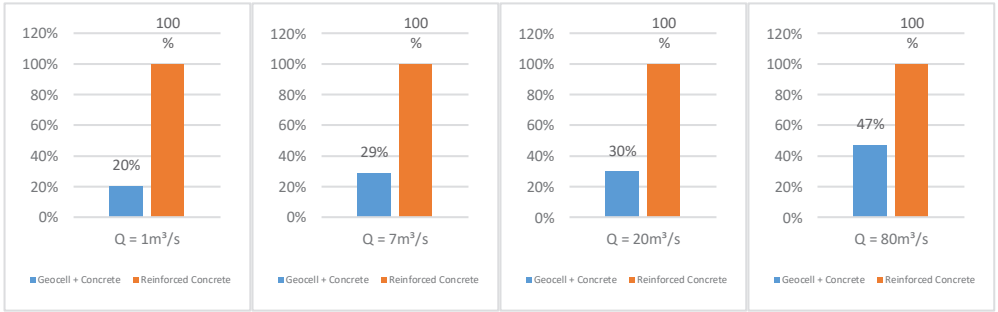


Fig. 9. Reduction in Man-Hour Worked of 80%, 71%, 70% and 53% when the material is at an average distance of 5.0km from the construction site.

6 Conclusions

The following conclusions can be drawn from this study:

In addition to the reduction in thickness provided by the use of geocells, compared to reinforced concrete, with the use of geosynthetic material, due to its constant height, it is possible to better control the volume of concrete required to make the entire canal lining.

In the different scenarios analyzed, a reduction in direct costs of 37% to 66% can be observed using standard HDPE geocells [6, 7, 8].

Evaluating the total execution time of the project, even considering a greater number of teams working at the same time, compared to the process of installing geocells with concrete, we had reductions of up to 58% in the execution schedule.

Regarding the environmental impact, diesel consumption was reduced by 11% to 21% in the alternative with geosynthetics. Consequently, CO2 emissions and machine hours are also reduced when using surface lining systems with HDPE geocells.

In addition to reducing CO2 emissions and diesel consumption, if we reduce machine hours, there is also less dust generation, noise emissions and road maintenance work in the local environment, thus generating an economic and social benefit for the regions close to the project.

Greater productivity and shorter execution times result in reductions in man-hours worked. With reduction levels that can reach up to 80%, we allow us, in remote regions, to use local labor, promoting local development without the need to import labor, in addition to the probability of accidents due to the reduced work schedule.

With the benefits presented here, aligned with the wide range of methodologies, calculation procedures and studies, on a small and large scale, related to the use of geocells for hydraulic works, the notable benefits of the application of geosynthetics in engineering works are increasingly demonstrated, whether in terms of direct and indirect project costs, as well as in issues related to sustainability and the well-being of society.

References

1. V. Chow, Hidraúlica de canales abiertos (Mc Graw-Hill, Bogotá, 1988).
2. W. Caressato Junior, G. Fierro, Criterios de dimensionamiento para proyecto de revestimiento de canales con geoceldas, in Proceedings of the XXXI Congreso latino americano de hidráulica, Colombia, Bogotá, 1-4 October (2024).
3. W. Caressato Junior, Use of HDPE geocells to replace rip rap and reinforced concrete in superficial drainage structures in photovoltaic power stations, in Proceedings of the 4th Pan american conference on geosynthetics, Geoamericas, Brazil, Rio de Janeiro, 26-29 April (2020).
4. R. Koerner, Designing with geosynthetics fifth edition (Pearson Prentice Hall, New Jersey, 2005).
5. J.C. Vertematti, Manual brasileiro de geossintéticos – 2 Edição (Editora Blucher, São Paulo, 2015).
6. ISO 13426-1, Geotextiles and geotextile-related products — Strength of internal structural junctions — Part 1: Geocells, International Organization for Standardization, pp. 1-10, Geneva, Switzerland (2019).
7. ASTM D8269, Standard guide for the use of geocells in geotechnical and roadway projects, ASTM International, pp. 1-11, Pennsylvania, USA (2021).
8. GRI Standard GS-15, Test methods, test properties and frequency for geocells made from high density polyethylene (HDPE) strips, Geosynthetics Institute, pp. 1-9, Pennsylvania, USA (2016).

9. Bureau of Reclamation, Construção de projetos de irrigação – Manual de irrigação, Secretaria de recursos hídricos, Brasil, Brasília (2002a).
10. Bureau of Reclamation, Elaboração de projetos de irrigação – Manual de irrigação, Secretaria de recursos hídricos, Brasil, Brasília (2002b).
11. Bureau of Reclamation, Operação e manutenção de projetos de irrigação – Manual de irrigação, Secretaria de recursos hídricos, Brasil, Brasília (2002c).
12. ASTM A615/A615M, Standard specification for deformed and plain carbon-steel bars for concrete reinforcement, ASTM International, pp. 1-5, Pennsylvania, USA (2022).
13. W. J. Del Pico, Project control: integrating cost and schedule in construction, John Wiley & Sons, 53-102, USA, New Jersey (2013).
14. T. Omotayo, U. Kulatunga, B. Awuzie, Continuous cost improvement in construction - Theory and practice, Routledge,153-188, USA, New York (2022).

Central quay, Cardiff - regenerated concrete river bank

Pablo Bernardini[1*], *Patricia* Guerra-Escobar[1], *Rozhan* Saeed[1], and *Muneeb* Tahir[1]

[1] Geosynthetics Ltd., United Kingdom

Abstract. Central Quay is a scheme to redevelop the iconic former Brains Brewery site in central Cardiff on the banks of the River Taff. The project requires a green and visually pleasing solution to protect and regenerate a 300 m length of river frontage. The initial option involved breaking out the existing concrete flood wall and decreasing the angle of the riverbank to create a natural vegetated slope. However, the brief was revised due to land loss and the high carbon footprint of this solution. A new approach was required to create a vegetated face over the existing 45° - 60° concrete slope. The proposed solution was a 150 mm deep geocellular confinement system to retain the growing medium and enable sustainable vegetation. Key challenges included securing the geocells to concrete and preventing topsoil washout during flooding. Resin anchor pins and polymeric reinforcing tendons were used to support the geocells. High-performance turf matting was applied for additional soil protection. The solution was effective, offering permanent protection and a natural green riverbank.

1 Introduction

The Central Quay project in Cardiff focuses on transforming and regenerating the iconic former Brains Brewery site into a vibrant mixed-use development spanning 2.5 million square feet. The redevelopment includes apartments, hotels, offices and leisure facilities, as well as the rejuvenation of the River Taff's neglected waterfront. Situated near Cardiff Central railway station and the Principality Stadium, this ambitious scheme aims to revitalise the area and enhance its connectivity and appeal.

As part of this initiative, a parcel of land known as the Brewhouse (formerly Plot 8) is being redeveloped for commercial use. A critical component of the project involves stabilising and vegetating the unsightly concrete slopes along the riverbank to create a greener, visually appealing, and environmentally sustainable river frontage.

Therefore, the design was developed to provide a vegetated engineered solution for the challenging riverbank conditions. The proposed intervention focuses on improving both the aesthetic and environmental performance of the site.

2 Project Geometry

The original riverbank consisted of a steep concrete slope over an existing sheet pile wall running parallel to the River Taff. The design focused on a 200 m stretch of the riverbank, which was later extended to 300 m, see yellow area in



Fig *1*.
Fig 1 Proposed Plan View (yellow area).

The sheet pile wall is located at 1.50 m above average river level, the levels varied between 5.00 m to 5.62 m above ordnance datum (AOD). The concrete slope height varies approximately between 2.20 m to 3.50 m. The existing slope angles varied between 45° - 62°; the maximum slope angle was 62°.

Above the existing concrete slope there is a brick masonry wall acting as flood defence to a maximum level of 8.90 m above ordnance datum (AOD). The upper masonry flood wall is to be replaced and 5no. ecological refuge areas are proposed to be constructed along the length of the flood wall, creating wildlife wetland habitats as well as overtopping spill areas for flood waters (see light blue areas in Figure 1).

As part of the initial design, the concrete slope forming part of the flood defences was to be reprofiled to a consistent angle of 1V:1.5H with the concrete facing removed. However, this option was discarded due to land lost and spatial constraints for a riverside walkway.

Therefore, an engineering solution was required to ensure vegetation establishment without reducing the top spacing.

3 Ground Conditions & Groundwater

3.1 Ground Conditions

The ground conditions at the Central Quay site are varied, comprising made ground, superficial deposits, and weathered bedrock. A summary of each strata encountered is provided below.

It is important to note that instability was observed in most trial pit sides, ranging from minor spalling to complete collapse. Similar instability was also encountered in the boreholes, requiring casing within the made ground, superficial deposits and in some areas the Mercia Mudstone. These findings highlight the significant stability challenges that may arise if the existing concrete flood wall is removed, particularly in managing both soil and groundwater variability.

The site is underlain by made ground, encountered at depths ranging from 1.5 m to 3.2 m, with thicker deposits (up to 6.0 m) found in the western part of site, likely due to the historical location of the River Taff channel. The made ground consists of crushed demolition materials, including brick, concrete, and ash, transitioning to sandy gravel, silty clay, and gravelly clay. Boulders and cobbles were frequently encountered. Strength tests showed SPT N values between 1 and 16, with higher values (up to >50) at depths with cobbles or obstructions.

Tidal Flat Deposits are described as soft to very soft, grey to brown, silty clay with sandy and gravelly layers. The deposits were found to a maximum depth of 5.9 m and SPT N values typically ranged from 1 to 9.

River Terrace Deposits described as medium to dense sandy gravel with cobbles, encountered at depths of 4.0 m to 6.0 m and SPT N values ranged from 6 to 49, with softer layers of clay found in places.

Beneath the superficial deposits lies the Mercia Mudstone Formation, found at depths between 10.0 m and 10.8 m. The mudstone is weathered, firm to stiff, with fractured sections.

The formation contains weak mudstone or siltstone, which is classified as partially weathered (Grade III to II), often fractured and filled with clay or gravel. SPT N values in the bedrock were typically above 100, indicating strong materials.

The summary results of the geotechnical parameters used for design are summarised in Table 1:

Table 1 Summary of Geotechnical Parameters.

Strata	**Moisture Content (%)**	**Liquid Limit (%)**	**Plastic Limit (%)**	**Plasticity Index (%)**	**% Passing 425 µm**	**Unit Weight (kN/m^3)**	**Drained Angle of shearing Resistance (°)**
Made Ground (cohesive)	12.4 – 17	29 – 39	15 – 16	13 – 23	43 – 63	18	25 - 28
Tidal Flat Deposits	21.7 – 62.1	57 – 78	27 – 31	30 – 47	76 – 100	18	21 - 24

3.2 Groundwater

Groundwater was encountered at varying depths, with shallow seepage observed between 1.4 m and 2.5 m in the made ground. Groundwater levels in the superficial deposits were typically deeper, ranging from 3.8 m to 5.4 m depth. Water monitoring data provided revealed groundwater levels ranging from 5.46 m to 6.86 m above ordnance datum (AOD).

The water table fluctuates seasonally, with some boreholes showing a quick inflow, and may be affected by other factors and the presence of the adjacent River Taff with potential flood risk, therefore groundwater levels have been assumed near to ground level, corresponding an extreme flood event.

Rapid drawdown conditions were analysed, which is considered critical when flood waters recede, causing a saturated condition in the soil banks. Rapid drawdown affects granular soils primarily, which saturate quickly upon sudden raised water levels.

3.3 Surcharges

A surcharge load of 10 kN/m² applied as a strip load above the slope crest has been considered, in accordance with BS6031:2009, which allows for unforeseen slope loading.

4 Design Methodology

4.1 Design Method

The basis of the solution was to use 150 mm deep geocell to provide a honeycomb matrix that could contain the topsoil that would provide the growing medium to enable the slope to sustainably vegetate.

The net sliding force was calculated to design the number/spacing and type of tendons/anchors including the required safety factors ([1]). The design accounted for the slope geometry, including the length and the slope angle. As well, the weight, type and geotechnical parameters of infill, the presence of the existing concrete slope, played an important role in the design. Additionally, space constraints made it impossible to implement a traditional anchor trench at the crest, increasing the challenges ([2-9]).

4.2 Implemented solution

After ruling out the option of regrading the existing concrete flood defence wall to a consistent angle of 1V:1.5H due to land loss and spatial limitations for a riverside walkway. An engineering solution was required to ensure vegetation establishment without reducing the top spacing; 2 areas were identified for the solution:

- Slopes $\alpha \leq 45°$: geocell panels of 2.56m width with four tendons per panel.
- Slopes $45° < \alpha \leq 62°$: geocell panels of 2.56m width including six tendons per panel

The solution involved drilling a fixing pin into the concrete at the slopes toe and crest. The required number and spacing polymeric reinforcing tendons were designed to provide the tensile strength to support the filled geocell at the required slope angle. The tendons were threaded through the perforations in the geocell side walls and secured to the pins at the slope toe and crest. Additional support to the system and to minimise sagging of the geocell, was provided by threading a tensioned steel curtilage wire through the top edge of the geocell.

To ensure that the topsoil would not be washed out of the cells when the River Taff was in flood condition, a layer of turf reinforcement matting was placed over the top of the filled geocell to encapsulate the topsoil and for effective erosion control. (See Fig *2*)

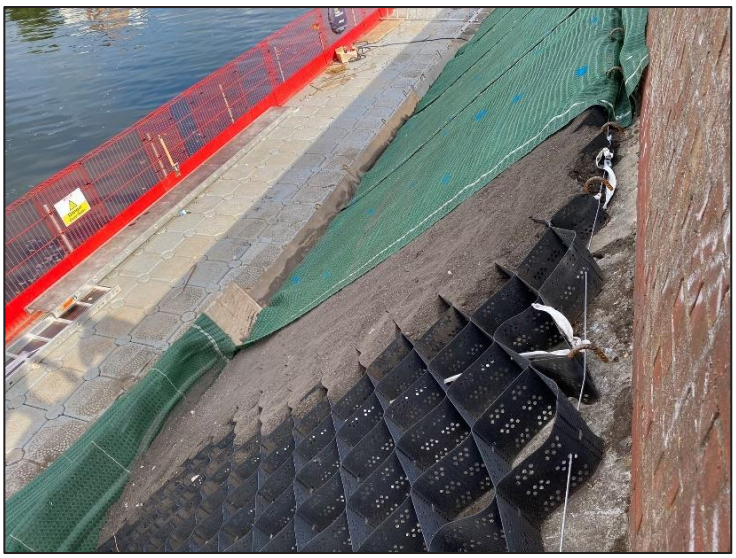


Fig 2 Geocell with tendons, reinforcement matting tendons & tensioned steel curtilage wire through the top edge of the geocell.

However, due to the presence of the sheet piled wall at the toe of the slope it was not possible to have the usual toe anchor trench to secure the lower edge of the turf reinforcement matting. Therefore, to prevent scour, it was wrapped around the lower edge of the geocell and then extended 1.0 m back up the concrete slope beneath the filled geocell.

The reinforcement matting was secured to the surface by using plastic ZIP anchors installed through the topsoil and secured into the existing concrete slope.

4.3 Construction sequence

Even with a viable solution developed and agreed, access to the slope remained difficult meaning that installation could only be undertaken from a floating pontoon on the river.

1. Remove existing vegetation.
2. Conduct visual inspection: assess the existing concrete revetment, identify any required remedial works and propose solutions for approval by the designer/client.
3. Perform concrete remedial works.
4. Anchor the turf reinforcement matting at the toe of the concrete slope using resin pins. Allow the resin to set, ensuring a minimum 750 mm underlap for the geocell.
5. Position and secure the 150 mm geocell with tendons, using two pins at the crest and toe to hold the tendons in place.
6. Drill resin-anchored pins for turf reinforcement matting at a density of three pins per square meter.
7. Fill the geocell with seeded topsoil. (See
8.
9.

10. **Fig *3***)



Fig 3 Geocell with Tendons infill with Topsoil Overlay by Turf Reinforcement Matting.

11. Place the turf reinforcement matting over the installed geocell.
12. Secure the turf reinforcement matting pins with load plates, spring washers and nuts.
13. Apply hydroseeding to the slope face to promote vegetation growth.

5 Environmental Performance

The solution was designed to meet the client's requirements for a visually pleasing and vegetated riverbank. It prevented soil erosion while allowing native vegetation to thrive reducing the earthworks and excavation.

Below there is a summary of the environmental performance of this solution:

- **Sustainable vegetation establishment:**
  The geocellular confinement system enabled the transformation of a steep,

unsightly concrete slope into a vegetated sustainable green frontage. This approach provided a growing medium for vegetation and enhanced biodiversity along the riverbank.

- **Erosion control:**
  The combined use of geocells and turf reinforcement matting ensured long term soil stability. Preventing soil erosion during river flooding, preserving the integrity of the slope.
- **Land preservation:**
  By maintaining the original steep slope angle, the project avoided encroaching on valuable riverside space, preserving land for a new cycle/walkway while delivering a green, visually appealing environment.
- **Aesthetic and ecological improvement:**
  The vegetated slope replaced a neglected, overgrown concrete surface, significantly improving the visual and ecological quality of the waterfront.
- **Adaptable engineering for environmental challenges:**
  Innovative anchoring techniques and materials minimised the environmental impact of the installation, using fewer fixings and reducing construction disturbance on the riverbank.
- **Carbon footprint improvement:**
  This innovative engineering solution minimised the construction disturbance on the riverbank, preserving natural habitats and reducing emissions associated with extensive groundworks.

This innovative engineering solution required fewer resources, lowering the carbon footprint associated with material production, transportation and installation. (See Fig 4 & Fig 5).



Fig 4 Implemented vegetated reinforced slope.



Fig 5 Implemented vegetated reinforced slope from the other side of the River Taff.

6 Conclusion

As shown above, the use of geocellular confinement system and turf reinforcement matting effectively stabilised the steep concrete slope, providing a cost efficient vegetated sustainable green solution that maintained the structural integrity of the site. The extended length of the project highlights its environmental and aesthetic success.

The methodology ensured rapid installation maintaining the original steep slope angle, reduced material usage and improved the riverfront's ecological and visual value.

References

1. StrataWeb Design and Construction Manual for containment systems, slope protection, erosion control, and base reinforcement. Strata Global Geosolutions Manual (Cumming, GA 30040 USA, 2016)
2. British Standard, BS8002:2015. Code of practice for Earth Retaining Structures. British Standard Institution, London. UK. (2015)
3. BS 6031:2009 Code of Practice for Earthworks. British Standard Institution, London. UK. (2019)
4. British Standard EN 1997-1:2004+A1:2013 Eurocode 7: Geotechnical Design, Part 1: General Rules. British Standard Institution, London. UK. (2013)
5. British Standard EN 1997-2:2007 Eurocode 7: Geotechnical Design, Part 2: Ground Investigation and Testing. British Standard Institution, London. UK. (2007)
6. NA+A1:2014 to BS EN 1997-1:2004+A1:2013 UK National Annex to Eurocode 7: Geotechnical Design, Part 1: General. British Standard Institution, London. UK.(2013)
7. British Standard, BS8006-1:2010. Code of practice for the Strengthened/ Reinforced Soils and other fills. British Standard Institution, London. UK. (2010)
8. Highway Works MCHW. Volume 1 Specification for Highway Works Series 600 and Series 800. Highways Works, UK. (2016)
9. R.M. Koerner, Designing with Geosynthetics, (Pearson, 2005).

Innovation in Reservoir Design with Bituminous Geomembranes (BGM)

Natalie Daly[1*], *Edgar* Doledec[2], *Ted* Aguirre[1]and *Emilio* Escobar[3]

[1]Axter Coletanche Inc, Canada
[2]IKO Axter SAS, France
[3]IKO Axter Chile, Chile

Abstract. This paper will investigate the use of bituminous geomembranes (BGMs) as a sustainable geosynthetic lining solution for reservoirs, focusing on their efficacy in water storage infrastructure. The selection of an appropriate geosynthetic material is critical, necessitating characteristics such as efficient installation across varying weather conditions, cost-effectiveness, longevity when left exposed, and ease of maintenance. BGMs stand out due to their low thermal expansion coefficient, density greater than 1 g/cm³, and demonstrated long-term durability in exposed conditions. Their flexibility and bituminous properties allow for seamless connections to different surfaces. This paper will overview the benefits of BGM and examine its application in two innovative reservoir projects. In the United States, BGM was selected by the Roza Irrigation District to line a comprehensive irrigation scheme reservoir and its associated canals in the Columbia River Basin. Years later, samples of the exposed material were examined and tested, which will be reviewed in this paper. In Chile, BGM was employed to line raw water storage reservoirs supporting the Santiago potable water system's treatment plant. The Chilean methodology included an asphalt layer, and a concrete slab placed directly on top of the BGM, facilitating periodic cleanup and sediment removal from the reservoirs. These reservoir project examples will underscore the innovative application of BGMs in enhancing the sustainability and efficiency of reservoir design.

1 Introduction

Reservoirs are crucial elements of global water management infrastructure, storing enormous quantities of water annually. These structures, built from various materials including soil and concrete, face significant challenges, particularly water loss through bottom and side leakage. This issue poses substantial economic concerns for owners and operators. As climate change leads to higher temperatures and increased aridity, exacerbating water scarcity, addressing these challenges becomes increasingly urgent.

* Corresponding author: ndaly@axtercoletanche.com

Historically, reservoir protection relied on concrete or clay. However, projects using these materials often show a marked decrease in satisfactory performance within five years of completion, largely due to suboptimal design. In response to the need for a more sustainable approach, geomembrane liners have emerged as a promising alternative. This article examines the effectiveness of the BGM as an innovative solution to these issues.

A major obstacle in reservoir lining is the dewatering process during construction. The BGM's high density, exceeding 1 g/cm³, allows for underwater repairs and installations, offering a practical advantage in tackling construction phase challenges. Through detailed case studies, this paper demonstrates how BGMs not only address these challenges but also show long-lasting durability under various weather conditions. Beyond its durability, BGM offers easy maintenance and repair, establishing itself as both a technically and economically viable selection for reservoir lining.

For now, the long-term performance of a bituminous geomembrane (BGM) is evaluated by the ability of its primary constituents—polyester geotextile and bitumen—to preserve their mechanical integrity and impermeability under sustained operational conditions [1]. Compliance with CE marking, as stipulated in geomembrane application standards, necessitates durability assessment through standardized oxidation resistance testing (EN 14575) [2] and ultraviolet (UV) aging tests (EN 12224) [3].

2 The composite structure of the Bituminous Geomembrane

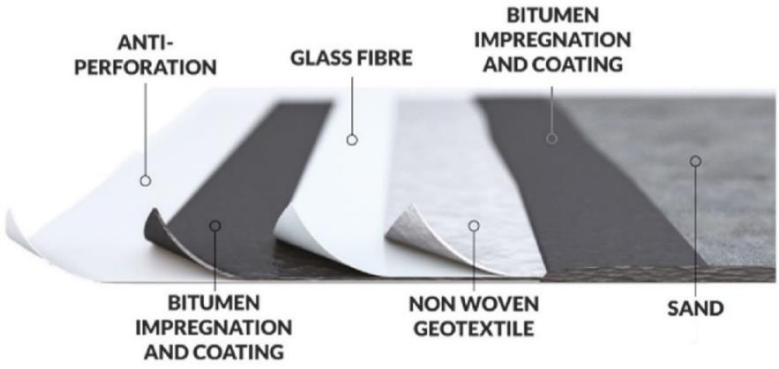


Fig. 1. Bituminous Geomembrane (BGM) roll and cross-section

The BGM's main composition (Fig. 1) consists of a non-woven polyester geotextile that is fully saturated with elastomeric bitumen, enhanced by an internal glass fleece to strengthen the structure during manufacturing at a temperature of 160°C (320°F). The top layer is coated with sand, which provides traction for installation workers. At the bottom, an anti-perforation film is included to prevent vegetation roots from penetrating the liner. Produced in France under strict quality control and assurance standards, the BGM is carefully inspected in an ISO 9001 and ISO 14001 certified facility [4, 5].

A key feature of the BGM, combined with elastomeric bitumen, is its ability to be installed in cold climates, capable of withstanding temperatures as low as -35˚C (-31˚F). This makes it ideal for use in colder regions like Canada, the northern United States, and parts of northern and eastern Europe, as well as in high-altitude areas. The product is offered in a variety of thicknesses, from 2.2 to 5.6 mm (87 to 220 mils), allowing for flexibility to meet different project needs.

2.1 Reasons for selecting a BGM waterproofing solution

BGM offers several technical advantages for lining reservoirs:

- With a density greater than water (1.276 g/m³,), BGM presents a cost-effective solution, enabling installation in flowing water. Underwater seams are easily achieved with a bituminous mastic to join the panels.
- It is certified by the NSF/ANSI 61 international standard for potable water storage in reservoirs holding over 283.9 m³ (75,000 gallons) [6].
- BGM has exceptionally low and consistent permeability (6 x 10^{-14} m/s according to ASTM E96), ensuring effective water containment [7].
- Thanks to its low thermal coefficient (ASTM D696), BGM maintains a wrinkle-free surface, improving both its appearance and functionality. It also allows for continuous installation across a wider temperature range compared to polymeric geomembranes [8].
- As bituminous compounds generally have a high friction angle, the sanded surface of BGM further enhances this property. This non-slip surface minimizes the risk of slipping for both people and animals near canals or reservoirs.
- The integrated geotextile gives BGM excellent puncture resistance of 450 to 650 N (100 to 146 lbf) for index puncture (ASTM D4833), and superior resistance to hydrostatic and puncture by aggregates [9]. This allows for coarse materials to be placed directly above the membrane without requiring extra protection, as well makes it suitable for heavy equipment movement during installation and maintenance (Fig. 2).



Fig. 2. Direct trafficability on BGM

- It is compatible with asphalt and concrete layers placed directly above the membrane, aiding in maintenance and providing additional load-bearing capacity.
- BGM can be easily bonded to various surfaces, including concrete (Fig. 3), steel, or high-density polyethylene (HDPE), making it adaptable to a variety of project needs.



Fig. 3. Bonding to concrete

3 Exposed reservoir in Washington, USA

The Wasteway 5 Re-Regulation Reservoir project, located 7 miles northeast of Sunnyside, Washington, in Washout Canyon off Highway 241, is a joint initiative between the US Bureau of Reclamation, the Washington State Department of Ecology, and the Roza Irrigation District. HDR Engineering (Pasco, WA) and Shannon and Wilson (Seattle, WA) led the engineering services, while Rotschy Inc. (Vancouver, WA) managed the installation.

The project involved the use of a BGM, with a thickness of 4 mm (157.5 mils) and a unit mass of 4.85 kg/m² (143 oz/yd²), covering an area of 188,000 m² (2,100,000 ft²). The Dam Safety Commission of Washington State approved the project on November 30th, 2015. With an estimated budget of US$31 million, the re-regulation reservoir was designed with a geomembrane liner to hold a capacity of approximately 200,000 hectares, enabling water to be pumped from the Roza canal into the reservoir via turbine pumps and gravity feed.

BGM was selected as the optimal solution due to its cost-effectiveness and efficient installation process, ensuring significant savings while maintaining high standards of quality and durability. The decision to use an exposed liner was driven by the limited availability of easily accessible fill for a covered liner alternative.

To streamline the process, specialty-length rolls of 100 m (328 ft) were manufactured to eliminate the need for seams on the slopes (Fig. 4). These rolls met specific shipping requirements, resulting in substantial cost savings. Comprehensive quality assurance and quality control (QA/QC) measures were applied, including geo-electrical leak detection (water puddle method), air lance, and ultrasound seam testing, all pre-approved by the Dam Safety Commission and the Department of Ecology.

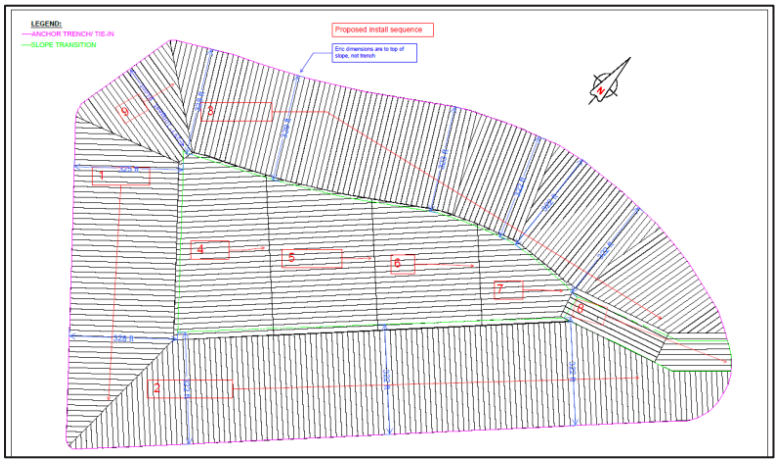


Fig. 4. Pannel Layout of BGM to minimize material loss.

The reservoir, situated on a 17-hectare site about 9.5 km (6 miles) north of Sunnyside, WA, has an average depth of 32 m (105 ft). It serves two main canals, providing irrigation for apple orchards, vineyards, hops, alfalfa, and other crops. The project is expected to conserve around 10 million m³ of water each season, a vital measure for water efficiency, especially after the severe drought of 2016.

Installation began in March 2017 (Fig. 5). and was completed by the end of summer, ensuring a reliable water source for local farmers (Fig. 6). Following the installation of BGM, HDR engineering monitored the reservoir for three weeks and reported no leakage during this crucial period.



Fig. 5. Installation of BGM Pannels

Yearly maintenance checks are conducted during the lowest reservoir levels, with ongoing regular monitoring and visual inspections. Every five years a thorough inspection is done, which requires emptying the reservoir. Special attention is given to structural battening, which must be cleaned before visual inspections. Additionally, electrical leak detection testing should be performed every 10 years. In case of significant unexpected incidents, a detailed review of the liner's stability in the affected areas is advised.



Fig. 6. The Wasteway 5 Re-Regulation Reservoir works complete

3.1 Testing of exposed BGM after years of service

An ageing and durability study was conducted for the BGM at the Wasteway 5 Re-Regulation Reservoir, USA after 8 years of service. The study was influenced by a recent rare flood event, triggered by an atmospheric river that impacted the area. A private property adjacent to the reservoir experienced significant flooding, with over 3 m (10 feet) of water filling a small valley. This caused extensive seepage under the cement-capped dike structure, directing water towards the aquifer beneath the Roza Reservoir. As the floodwaters infiltrated, they reached the reservoir and seeped upward, forming pockets of water beneath

the liner. After the flood subsided, the water drained, leaving behind voids and eroded slopes beneath the BGM liner. Importantly, the BGM liner remained fully intact, with no failure or seam separation despite the important differential settlements, therefore still acted as a sufficient waterproofing system.

The BGM was however deformed due to the displacement of the underlying subgrade, so samples of the liner were sent to a laboratory for testing. The samples taken to be tested were from 3 zones (Fig. 7) of the reservoir:

- The 100% submerged zone
- The tidal zone (water fluctuation)
- The 100% exposed zone.



Fig. 7. Varying zones of the reservoir

Recent meteorological data for Sunnyside, Washington, indicates that the rainiest month at the reservoir location is December, with an average rainfall of approximately 39mm. See Tab.1 for a detailed overview of meteorological conditions during the summer and winter months.

Tab. 1. Average historical meteorological conditions in Sunnyside, WA [10].

	Summer	**Winter**
Average high temp (T°C)	33	3
Average low temp (T°C)	17	-3
Average Daylight (h)	346	147
Rainfall (mm)	2	39
UV index	7	2

3.2 Test results of exposed BGM after years of service

Tests were conducted on samples of these 3 zones acc. to ASTM testing methods. The tidal zone and submerged zone are compared to the control specimen, the exposed zone, which is compliant with the 2016 technical data sheet of the original product. Tab. 2 shows the % variation of tensile strength acc. to ASTM D7275 for both the machine direction (MD) and cross machine direction (CMD) [11]. The tests resulted in no more than a 5% variation in tensile strength and no more than a 10% variation in elongation for the specimens.

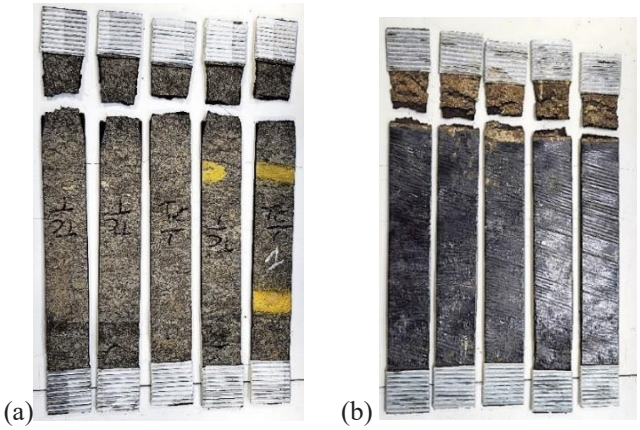
Tab. 2. Tensile strength acc. to standard ASTM D7275

		Variation of strength	Variation of elongation
Exposed zone	Control specimens – MD	-	-
	Control specimens – CMD	-	-
Tidal zone	Test specimens – MD	-4.07	-4.39
	Test specimens – CMD	+2.66	+8.70
Submerged zone	Test specimens – MD	-0.72	-3.24
	Test specimens – CMD	+4.34	+0.68

Tab. 3 shows values in kN/m for the seam shear strength acc. to ASTM D7056 [12]. The values obtained are > 80% of the tensile strength specification in CMD, which is presented value of 15 kN/m in the technical data sheet for the product. There were no suitable samples retrieved from the jobsite to perform testing for the submerged zone. Fig. 8 shows the seam shear strength specimens all failed outside the joint, which means the seam is adequate.

Tab. 3. Seam shear strength acc. to standard ASTM D7056

		Tensile strength at break (kN/m)
Exposed zone	Seam – CMD	12.90
Tidal zone	Seam – CMD	15.80
Submerged zone	Seam – CMD	NA



(a) (b)

Fig. 8. Surface (a) and under face (b) samples tested under shear for ASTM D7056.

In summary, the tested values for BGM are compliant with the existing specification after 8 years of service life. The BGM samples has negligible differences between the zones but showed less discrepancy in the submerged zone compared to the tidal zone.

4 Water storage facility in Chile

The Maipo River, a key water source for the Santiago de Chile metropolitan area, frequently faces high turbidity events that have led to temporary closures of the Vizcachas water treatment plant, causing interruptions in the city's water supply. To address this issue, Santiago's water utility, Aguas Andinas, launched the Estanques Pirque project. This initiative involves the storage of 1.5 million m³ of raw water from the Maipo River in six strategically placed reservoirs. These reservoirs provide a backup water supply for the Vizcachas plant during times of high turbidity, ensuring the city's water needs are met. With the capacity to supply the entire metropolitan area for up to 34 h, the Estanques Pirque project is vital for maintaining water resilience in Santiago [13].

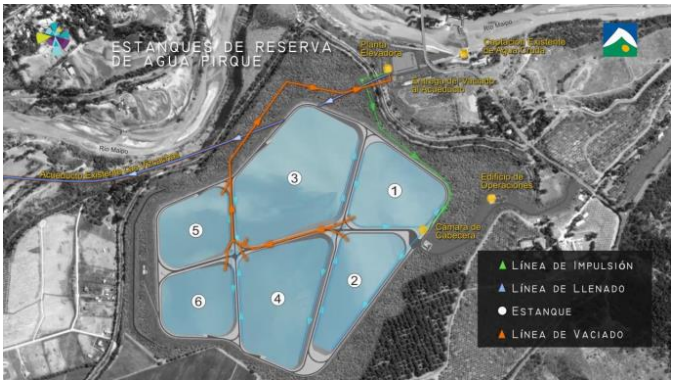


Fig. 9. Plan view of Estanques Pirque reservoirs in Chile [14].

The reservoirs (Fig. 9) are designed to a maximum depth of 6 m (20 ft), with a 1 m (3 ft) clearance between the top of the walls and the highest water level to prevent overflow. The walls have a slope ratio of 2.5H:1V. Given the expected sediment accumulation from the raw water, periodic mechanical cleaning of the reservoir floor is required. This, along with the

need to store water for individual use, led the consulting engineering firm to select a BGM (ASTM D5199) that is 4 mm (157.5 mils) thick, with a unit weight of 4.85 kg/m² (143 oz/yd²) for ASTM D3776 [15-16]. The total amount of BGM supplied for the project was around 480,000 m² (517,000 ft²).

The lining system (Fig.10) for the reservoir floor is carefully engineered, consisting of multiple layers arranged in the following order from bottom to top:

- 5 cm (2 in) levelling asphalt layer
- 5 cm (2 in) drainage asphalt layer
- 4 mm (157.5 mils) thick BGM
- 5 cm (2 in) asphalt pavement directly on top of BGM
- 15 cm (6 in) concrete slab

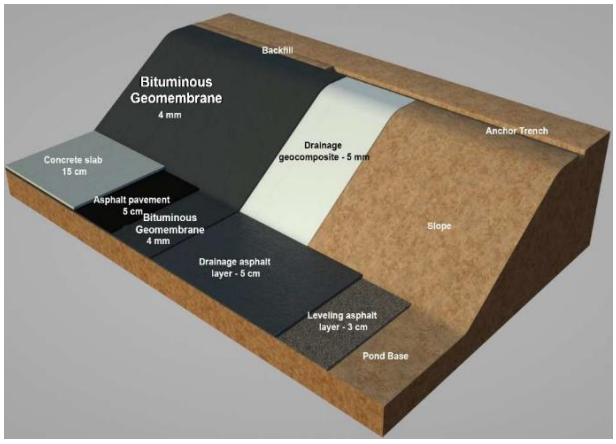


Fig. 10. Cross section of lining structure

The decision to use BGM for the project was based on several key benefits, including its NSF/ANSI 61 certification, which confirms its suitability for storing water intended for drinking water systems. This certification highlights its adherence to international water quality and safety standards. Additionally, BGM is the only geomembrane that can directly withstand the application of asphalt concrete at temperatures up to 140°C (284°F). This unique property enables efficient sediment removal through mechanical methods, offering a practical solution for maintenance and cleaning.

These exceptional qualities make BGM an ideal choice for the project, meeting the rigorous requirements for structural compatibility, water quality, and maintenance efficiency.



Fig. 11. Works completed for six reservoirs in use

5 Conclusion

The BGM showcases its versatility and durability across a wide range of applications, demonstrated in projects such as the Wasteway 5 Re-Regulation reservoir and the Aguas Andinas Estanques Pirque water storage facility. Certified for potable water storage, BGM is compatible with various surfaces and maintains its durability under different conditions, making it a dependable choice for ensuring water quality and security. Its adaptability to challenging landscapes and project needs is reflected in its support for exposed liner options and innovative installation techniques. As a result, BGM provides a long-lasting solution, contributing significantly to the enhancement of water storage infrastructure and meeting the growing demands of water resource management with efficiency and sustainability.

Offering both cost-effectiveness and durability, BGM meets rigorous standards and is approved by regulatory authorities. The success of the two reservoir projects highlights its adaptability, proving its effectiveness in protecting water resources, improving structural integrity, and ensuring long-term sustainability. As a resilient and efficient geomembrane, BGM is an ideal choice for addressing the various challenges of water storage, containment, and conservation.

References

1. E. Escobar, N. Daly, B. Breul, An approach to longevity and durability of bituminous geomembranes (BGM). *GeoAmericas 4 Proc.*, Int. Geosynthetics Soc. (2020)
2. European Committee for Standardization, EN 14575:2005 - Geosynthetic barriers - Screening test method for determining the resistance to oxidation (2005)
3. European Committee for Standardization, EN 12224:2000 - Geotextiles and geotextile-related products - Determination of the resistance to weathering (2001)
4. International Organization for Standardization, *Quality management systems*, ISO 9001:2015 (2015)
5. International Organization for Standardization, *Environmental management systems*, ISO 14001:2015 (2015)
6. NSF International, *NSF/ANSI 61-2023: Drinking water system components* (2004)
7. ASTM International, *Standard test methods for water vapor*, ASTM E96 (2024)
8. ASTM International, *Standard test method for coefficient of linear thermal expansion of plastics between −30°C and +30°C*, ASTM D696 (2024)
9. ASTM International, *Standard test method for index puncture resistance of geomembranes and related products*, ASTM D4833 (2024)
10. Sunnyside, Washington Monthly Climate Averages. https://www.weatherworld.com/climate-averages/wa/sunnyside.html
11. ASTM International, *Standard test method for tensile properties of bituminous geomembranes (BGMs)*, ASTM D7275 (2024)
12. ASTM International, *Standard test method for determining the tensile shear strength of prefabricated bituminous geomembrane seams*, ASTM D7056 (2024)
13. Aguas Andinas, Megaestanques de Pirque – inauguramos la obra que permitirá abastecer de agua a Santiago durante 34 horas. https://www.aguasandinas.cl/web/aguasandinas/-/megaestanques-de-pirque-inauguramos-la-obra-que-permitira-abastecer-de-agua-a-santiago-durante-34-horas
14. Estanques Pirque, Aguas Andinas. YouTube: https://www.youtube.com/watch?v=C-CM_PWrm-c

15. ASTM International, *Standard test methods for mass per unit area (weight)*, ASTM D3776 (2024)
16. ASTM International, *Standard test method for measuring the nominal thickness of geosynthetics*, ASTM D5199 (2024)

Climate resistance of GCL-reinforced sealing systems based on lysimeter testing

Christian Niehues[1] and *Lars* Vollmert[1]

[1] Naue GmbH & Co. KG, 32339 Espelkamp, Germany

Abstract. Mineral sealing systems are widely used in geotechnical engineering. Applications are well known in dykes, landfill cover systems, retention ponds, tailings, reservoirs, environmental and groundwater protection. In all applications, these systems are covered and protected with topsoil. While the topsoil has to be protected against erosion by making use of vegetation, the thickness and quality of the cover soil and type of vegetation are of direct influence for the entire function of the system. One central aspect is that the performance of any mineral sealing system varies depending on certain parameters such as water content and strain state of the mineral layer. One potential threat for the sealing capability of a mineral layer is desiccation, which causes shrinkage and ultimately results in the formation of cracks, which – at least in the case of compacted clay liners – are considered irreversible. To prevent such impacts on the performance on mineral liners, the water balance of such systems is to be simulated under extrapolation of data for precipitation, taking climate change into account. Both thickness and permeability of the protective layer need to be designed and implemented in accordance with simulation scenarios that show no risk of desiccation. This process may lead to considerable efforts not only in simulating but also implementing such designs. The presented paper evaluates the results of lysimeter trials with a particular focus on the performance of GCL after dry periods. The results show that the tested GCL have favourable performance in terms sealing performance even after dry periods, indicating good resilience against impacts associated with climate change. In this paper, we will also discuss further developments on GCL as the multicomponent GCL which aim to even increase the resilience against desiccation.

1 Introduction

Sealing systems play a crucial role in climate change mitigation, whether in landfills to prevent generation and emission of greenhouse gases or in structural water management to reduce the effects of extreme weather events.

One group of sealing components are the mineral sealing layers, where the impermeability is achieved by a mineral material of such nature that granulometry and mineralogy only allows for small pore diameters and thus low permeability. However, changes in water content and thus the cohesion of the fine particles in such layers as well as deformations of the layer (e.g. as consequence of settlements) pose a threat to the performance of such mineral layers as these factors may trigger crack formation [1].

GCL are also attributed to the group of mineral sealing components, as the sealing performance is based on the sealing capacity of bentonite, specifically the swelling properties of the main mineral montmorillonite. The desiccation behaviour however differs from such of conventional clay.

To assess the long-term performance of GCL under varying soil cover conditions and bentonite fillings (powder and granular bentonite), a lysimeter test field was constructed in 1998 and started data collection in January 1999. Depending on the setup, the GCL were covered with 0.5-1.0m recultivation soil. The details on the test setups are given in [4].

The latest results of these lysimeter trials have been presented in [2]. The results general show that with 1.0m cover soil, the measured permeations are generally low. This is judged both by percentage of precipitation that actually permeated through the GCL (system efficiency) and by comparing common yearly allowed permeation into municipal solid waste landfills (20 mm/a according to [5]) to actual permeation. The permeation rates increased noticeably with only 0.5m cover soil, especially when granular bentonite is used [2].

The following research aims to examine whether effects of extended drought periods become visible in the permeation rates in the lysimeter trials. The focus is to allow conclusions on the sensitivity of GCL on extreme weather conditions and the in-situ behavior and sealing performance after extended dry periods.

2 Evaluations

In order to assess the resilience of GCL under conditions that correlate with the effects of climate change, such as extended dry periods, the long-term precipitation data of the lysimeter test fields were evaluated. The data from [2] provide insights on specifically dry periods followed by noticeable precipitations. In specifically dry periods, the system components – both cover soil and GCL – suffer from desiccation. Subsequent rainfall events will give an indication whether the sealing performance was compromised. Such behavior is indicated by a noticeable increase in measured permeation of the sealing component in the lysimeter trials.

2.1 Precipitation

From the location of the lysimeters in central Germany, the water balance can be expected to be humid in the long term. This is supported by the long-term annual precipitation average, which is 702.1 mm as per recorded data. However, recent summers (especially 2018, 2020) were recorded with total accumulated rainfall sums which range well below the long-term average. During these years, significant impacts associated with heat and water shortage on human health, agriculture and waterway transport have been reported as well (e.g., [6]), proving that these years were significantly dry.

Table 1. Recorded rainfall on lysimeter site

Year	Rainfall [mm]
2018	417.7
2019	734.0
2020	288.3
2021	525.8

It can be concluded that the recorded time span includes abnormally dry periods.

2.2 Typical coherence of measured data

Considering that the cover soil of the lysimeters is not fully saturated, the typical sequence

of measured data is as follows: Following rainfall events, a part of this precipitation is subsequently recorded as drainage runoff in a later time interval. The delay and attenuation effect of measured volume between precipitation and drainage runoff is due to water retention and evapotranspiration within the cover soil. The following figures are illustrative examples which were elaborated in the course of this work.

In the case that the sealing performance of the GCL is not affected by desiccation effects, the recorded permeation remains marginal compared to the drainage runoff (see Fig. 1).

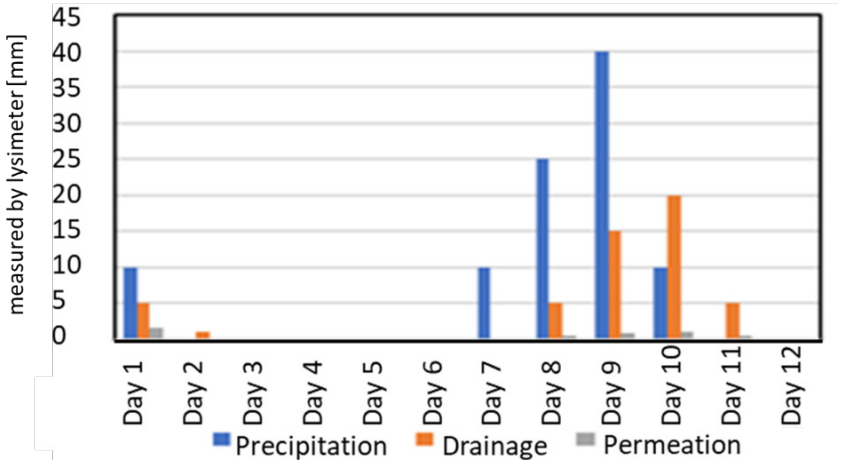


Fig. 1: Typical response curve of rainfall and drainage runoff with marginal permeation indicating good sealing performance of GCL

In the case that the performance of the GCL is negatively affected after a dry period – such as from crack formation and/or dilatation of pores – the overall permeation would be a noticeable percentage of the drainage runoff, as seen in Fig. 2.

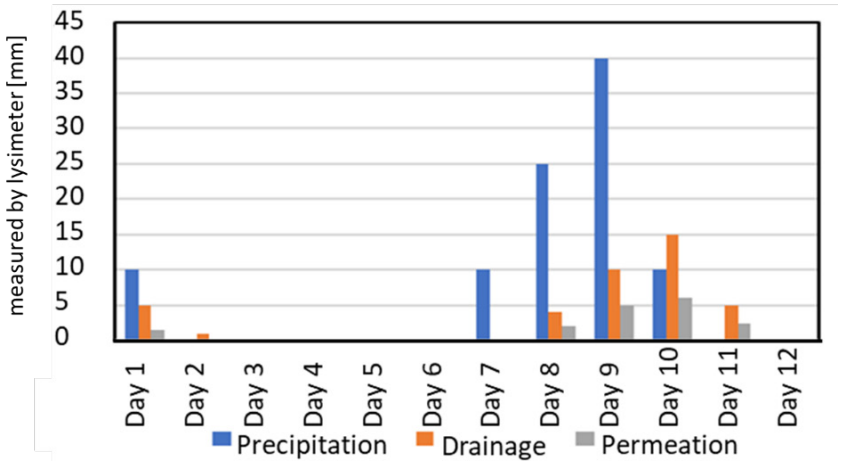


Fig. 2: Typical response curve of rainfall and drainage runoff with noticeable permeation indicating increased GCL permeability

2.3 Evaluation of example period

The recordings of [2] contain data that validate the theoretical expectations formulated under 2.2. Fig. 3 shows data from a GCL with powder sodium bentonite. The drainage runoff is delayed after rainfall events. The permeation is negligible, showing that the powder sodium bentonite GCL had not been compromised with desiccation.

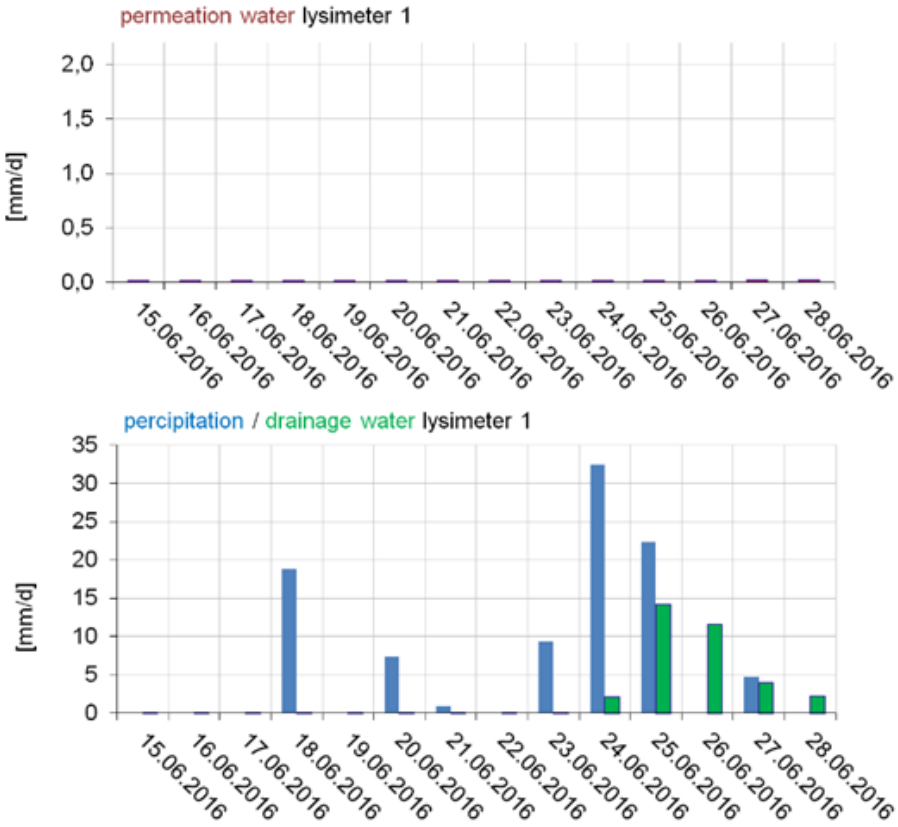


Fig. 3: Lysimeter data from [2] – Lysimeter 1 with powder sodium bentonite GCL

Further data from lysimeter 3 with a granular sodium bentonite GCL indicate the same delay between rainfall and runoff maxima. In the case of lysimeter 3, an increased permeation was noted after one significant rainfall event. After two days, the permeation rate through the GCL, however, decreased disproportionately to the decrease in rainfall/drainage runoff, indicating that the GCL with granular sodium bentonite was only temporarily affected by desiccation and reverted to homogeneous initial sealing performance after rehydration, in spite that a notable water head in the drainage was recorded on 27.06.2016 (Fig. 4).

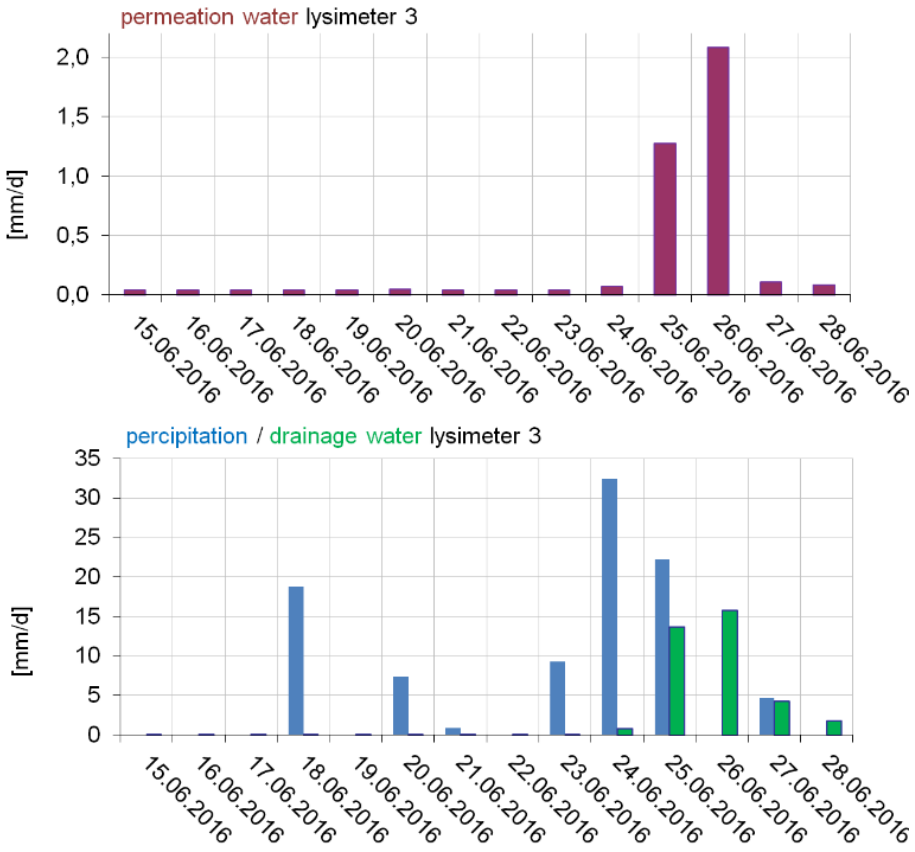


Fig. 4: Lysimeter data from [2] – Lysimeter 3 with granular sodium bentonite GCL

2.4 Evaluation of long-term data

The indicative model in 2.2 was validated with data from a restricted period of 14 days in 2.3. It has also been found in [2] that the general impact of desiccation is reversible in the tested GCL setups.

The central aspect to judge resilience to climate change is the specific evaluation of sealing performance after long-term dry periods. In 2.1, specific years with precipitation below long-term average have been identified. It will be evaluated whether the measured permeations after long drought periods show noticeable peaks, indicating that desiccation may have compromised the sealing performance of the GCL as a result of extended dry periods. If such peaks are recorded, the consecutive question is whether the effects of desiccation on the GCL are permanent or reversible.

In Fig. 5, the long-term data from the lysimeter trials for lysimeter 1 (powder sodium bentonite GCL, 1.0m soil cover) are shown. Periods with marginal precipitation can be identified (red markup), especially in the years with accumulated rainfall sums below long-term average. The corresponding permeation data show no peaks following these dry periods (red arrows) resp. no permeation water. Further setups and results have been discussed in [2]. It was found that in lysimeter setups using only 0.5m soil cover on the GCL, the effect of increased permeation after long drought periods is more significant. Still this increase was found to be temporary, with the permeation rate through the GCLs being near zero again after rehydration of the bentonite. These increased permeations after dry periods with soil covers of only 0.5m were recorded for both powder sodium bentonite GCL and granular sodium bentonite GCL. The absolute values of permeation were higher in the lysimeter setup with

granular sodium bentonite GCL.

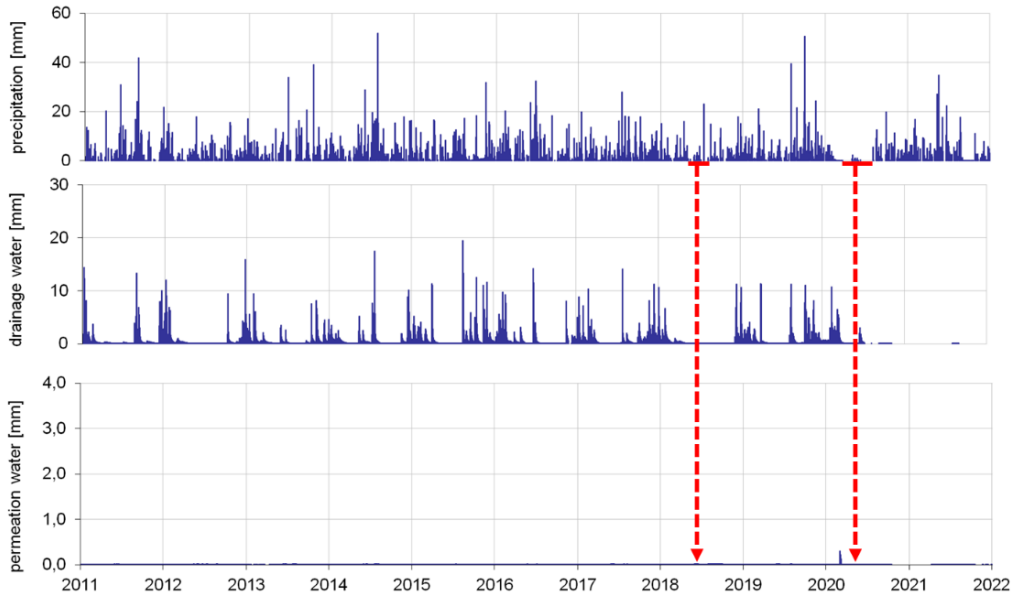


Fig. 5: Lysimeter data – Modified long-term data for lysimeter 1, adapted from [2]

3 Increasing desiccation resistance

The data indicate that the setups with GCL are in general resilient to dry periods within systems that allow for adequate confining pressure and internal water retention. This was the case for all systems with 1.0m soil cover. At lower soil covers (e.g. 0,5m), and thus lower confining pressures and less water retention, temporary permeations after dry periods were recorded.

For projects of such nature that even more severe desiccation is to be anticipated, or the cover soil is limited due to geometrical conditions, modifications of GCL products have been made to compensate the effect of intense desiccation or low soil covers. One such modification is the multicomponent GCL [6].

Multicomponent GCL are equipped an attached geofilm or thin membrane or coating (Fig. 6), which – when installed towards the cover soil – acts as a diffusive barrier and prevents desiccation of the bentonite core of a GCL. The effect has been investigated in desiccation trials ([7]).

Under this aspect, the resistance to climate change induced desiccation and thus the long-term sealing performance of GCL is elevated even more compared to conventional compacted clay liners, as clay is vulnerable to crack formation caused by loss of optimum water content.



Fig. 6: Principle of a coated multicomponent GCL

4 Summary and conclusions

In this paper, long-term lysimeter trials with sealing systems built with different GCL and soil covers have been evaluated. Specific for these trials is that the recorded data include extraordinarily dry periods. While the findings [2] interpreted the results in general, the given conclusions focus on the behaviour of GCL under specifically dry conditions.

Even under challenging climatic conditions, sodium bentonite GCL with 1.0m soil cover maintained the sealing properties after dry periods. Noticeable permeations of powder sodium bentonite GCL did not correlate with dry periods in setups of 1.0m cover soil

Setups with granular bentonite GCL however showed overall more permeation after dry periods, but also reverted to low permeations after rehydration.

All setups with 0.5m cover soil showed noticeable permeation after dry periods

In all cases, permeations correlating with precipitation after dry periods were measured only temporarily and permeations returned to zero after a while

For applications that are very sensitive to water ingress, or project conditions allow only low soil covers, or strong impact of desiccation is to be expected, multicomponent GCL with increased desiccation resistance offer a potential solution

Overall, GCL can be judged as resilient towards extended drought periods which are one central aspect of climate change. Conventional compacted clay liners are prone to be irreversibly altered in permeability once the water content has significantly changed. This is of special relevance for infrastructure like dams / dykes or even stormwater retention ponds that rely on sealing capability of mineral liners (compacted clay liners or GCL) to mitigate other effects of climate change, such as heavy precipitation events.

This provides the designer and user with a tool that summarises the findings and knowledge from more than 30 years of using GCLs and also gives recommendations on which type of barrier should be used.

References

1. G. Heerten, R.M. Koerner, Cover systems for landfills and brownfields. Land Contamination & Reclamation **16(4)**, 343-355 (2008)
2. A. Müller-Kirchenbauer, H. Ehrenberg, 25 Years of Experience with a Lysimeter System with Geosynthetic Clay Liners, in Proceedings of EuroGeo 8 – 8th European Regional Conference on Geosynthetics, Lille, France, September 15-18 (2025)
3. A. Müller-Kirchenbauer, W. Blümel, K.P. von Maubeuge, Long-term efficiency of GCLs with regard to natural drying and wetting cycles, in Proceedings of EuroGeo 4 - 4th European Geosynthetis Conference, Edinburgh, Scotland, September 7-10 (2008)
4. BMUV: Verordnung über Deponien und Langzeitlager (Deponieverordnung – DepV), Bonn/Berlin, Germany (2009)
5. O. Rakovec, L. Samaniego, V. Hari, Y. Markonis, V. Moravec, S. Thober, M. Hanel, R. Kumar, The 2018–2020 Multi-Year Drought Sets a New Benchmark in Europe. Earth´s Future, **10(3)** (2022)
6. K.P. von Maubeuge, A. Shahkolahi, Design requirements and long-term performance of multi-component coated GCLs, in Proceedings of the 12th International Conference on Geosynthetics, Rome, Italy, September 17-21 (2023)
7. C. Boley, R. Höppner, The desiccation process of Geosynthetic Clay Liners above different subsoils and climatic changes, in Proceedings of the 10th International Conference on Geosynthetics, Berlin, Germany, September 21-25 (2014)

SESSION 6 C
REINFORCEMENT APPLICATIONS (6)

Design of GRS bridge abutment using river debris as backfill material

Stanislav Lenart*[1] *and Siva Ram* Karumanchi[1]

[1] Slovenian National Building and Civil Engineering Institute (ZAG), Dimičeva 12, SI-1000 Ljubljana, Slovenia

Abstract. The Horizon Project CIRCUIT (2024) seeks to construct a new bridge on a local road in the municipality of Črna na Koroškem, Slovenia, replacing the existing structure over a torrential creek. The project incorporates geosynthetic-reinforced soil (GRS) with cast-in-place concrete full-height rigid facing (FHR) for the bridge abutments, providing robust scour protection. In August 2023, severe flooding caused by heavy rainfall deposited large quantities of river debris—comprising silty sand and gravel—classified as non-hazardous inert waste in the area designated for the bridge construction. To enhance sustainability, this debris has been repurposed as backfill material for the new GRS bridge abutments. This paper details the material testing and design considerations for constructing the bridge abutments under these revised conditions.

Full paper to be published in:

https://www.e3s-conferences.org/articles/e3sconf/abs/2025/44/contents/contents.html

*Corresponding author: stanislav.lenart@zag.si

Design and construction of non-load bearing reinforced soil bridge abutments for high speed two to span over large diameter sleeve columns

Mitul Dalwadi[1*], *Skevi* Perdikou[2], *Chaido* Doulala-Rigby[1], and *Jacek* Kawalec[3]

[1]Tensar International Ltd, 2-4 Cunningham Court, Blackburn, BB1 2QX, United Kingdom
[2]Geofem Ltd, Dimostheni Severi 21, 1st Floor, Nicosia 1080, Cyprus
[3]Tensar International, s.r.o, Hrabinska 498/19, 737 01 Cesky Tesin, Czech Republic

Abstract. Addison Road, a public highway located in Buckinghamshire, United Kingdom, was proposed to be realigned, and as part of this realignment, a new single span steel-concrete composite bridge was proposed, spanning semi-integrally between piled support columns sleeved through reinforced soil abutment walls. The columns are 1.2 m in diameter and are sleeved in 1.7 m diameter precast concrete rings so that the columns are isolated from the reinforced soil block. The challenge was to design and construct 6.5 m high non-load bearing reinforced soil bridge abutments and wing walls, the concrete facing panels of which had to span across the 1.7 m diameter sleeved concrete columns that are supporting the bridge superstructure, thereby significantly reducing the amount of geogrid reinforcement available (coverage) near concrete facing panels. The bespoke, first time designed and supplied 4m wide concrete panels facing reinforced soil retaining system using HDPE geogrid as soil reinforcement layers was adopted as the preferred solution. This paper discusses the successful design and construction of the geogrid-reinforced soil retaining structures using both conventional and 3-D finite element analysis. The project was successfully constructed in 2023 and opened to traffic in 2024.

1 Project Background

The High Speed two (HS2) is Great Britain's new high-speed railway line and comprises 140 miles of track. Once operational, HS2's British-built bullet trains will provide zero-carbon journeys between the UK's two largest cities, Birmingham and London, while freeing up space on the existing mainline for more freight and local services. HS2 Ltd awarded the Area Central contract C2 (1MC06), which covers the route from the North Portal of the Chiltern Tunnels to Long Itchington Wood, to the Eiffage, Kier, Ferrovial Construction and BAM Nuttall (EKFB) joint venture. The proposed design for HS2 in the Calvert area interfaces with NR infrastructure, sharing the same corridor with the existing Aylesbury to Claydon Junction line (MCJ) between Quainton and Calvert for approximately 8 km and passing beneath the existing Oxford to Bletchley line (OXD) near Calvert. Both MCJ and OXD lines are planned to be upgraded, requiring new bridge structures. Addison Road, a public highway located close to Calvert, Buckinghamshire, needed to be realigned approximately 60 m east

* Corresponding author: mitul.dalwadi@cmc.com

of the existing Network Rail (NR) overbridge, which crosses over the Network Rail OXD line. The realigned Addison Road is supported on a new single 40 m span overbridge that spans over the revised track alignments, comprising the Up & Down Bletchley (OXD) lines, Claydon Loop line and IMD transfer line [1]. The design of non-load bearing bridge abutments and wing walls at Addison Road for an overbridge was subcontracted to Tensar by Arcadis Setec COWI (ASC) Design Joint Venture (DJV) working for (EKFB), a joint venture delivering the design and construction of Britain's High Speed Two (HS2) Rail Main Works Civils Contract C23 in April 2020.

1.1 Addison Road Overbridge- Structure configuration

The realigned Addison Road, a rural 6 m wide single carriageway public highway is supported on a new 40 m, single span, semi-integral overbridge which is skewed at 23°. The bridge comprises a reinforced concrete deck on steel beams simply supported on a capping beam at either end. Each capping beam bears on a single row of four 1.2 m in diameter reinforced concrete columns. The columns pass through non-load bearing reinforced soil abutment walls. The reinforced concrete columns are encased within 1.7 m diameter sleeves formed of reinforced concrete manhole rings to avoid transferring loads between the reinforced soil and support columns. The bridge structure includes two types of wing walls, as shown in Figure 1:

- The upper reinforced concrete wing walls which retain the highway and support very high containment class parapets and are supported by the reinforced soil abutment and lower wing walls.
- The lower reinforced soil wing walls that extend away from the abutments and parallel to the NR track. The reinforced soil walls support load from the upper wing walls.



Fig. 1. Constructed structure: Addison Road bridge

1.2 Addison Road Overbridge- Ground condition

Table 1 summarises foundation soil types and thicknesses adopted for the proposed non-load bearing reinforced soil bridge abutments and wingwalls at both sides founded at approximately 83.5 m level. A detailed formation soil assessment and interpretation can be found in the design submission ref 1MC06-CEK-BR-REP-CS06_CL09-000098, Rev C01, dated 11/04/2022 [2].

Table 1. Ground conditions (Adopted for assessment)

Geological unit	**Top of Stratum range** (mAOD)	**Thickness** (m)
Alluvium	85.1	2.7
Oxford & Kellaways Clay Formation (soft to firm Clay)	82.4	1.1
Oxford & Kellaways Clay Formation (stiff to very stiff Clay)	81.3	21.8
Predominately Mudstone, but with weathered Mudstone and bands of Limestone (Cornbrash formation)	59.5	Not proven

2 Development of the preferred solution – choice of large precast panels

The clear distance between the four 1.7 m diameter concrete sleeve columns varies between 2.2 m and 4.7 m (refer to figure 2), and the minimum distance between sleeve columns and the outer edge of the non-load bearing reinforced soil abutment is approximately 0.7 m. A solution was required that could span across the four 1.7 m sleeved concrete columns in a way that could deal with the variable force distribution due to their non-symmetrical location and could mitigate uncertainties of imbalanced forces in the facing units due to tight and uneven column spacing.



Fig. 2. Sleeved Columns arrangement

The chosen solution was to design and construct bespoke, extraordinary large reinforced concrete (RC) precast facing units, measuring 4 m wide by 1.5 m high by 0.2 m thick for the non-load bearing bridge abutment reinforced soil walls, as shown in Figure 3 (Left), that could span across the sleeved concrete columns instead of the standard 1.5 m x 1.5 m RC precast facing panels, which were adopted for the wing walls where there were no sleeved concrete columns to span. The whole remaining area of lower wing walls away from the large sleeved columns was designed and constructed with typical 1.5 m x 1.5 m precast panels (ARES panel system). To ensure efficient connectivity between the concrete panel facing units and high-strength geogrids and to achieve the required connection capacity, HDPE geogrid tails were cast in the precast concrete facing panels. The panels were manufactured off-site under strict quality control and later connected to the required geogrid design lengths on-site during construction. The geogrids act as the primary soil-reinforcing layers. RE500 series High-Density Polyethylene (HDPE) geogrids are stiff monolithic geogrids with integral junctions and are inert to all chemicals naturally found in soils. They are not susceptible to hydrolysis and are resistant to aqueous solutions of salts, acids, and alkalis (pH 4.0 to 12.5), making them a perfect geogrid that can be inserted during concrete panel casting

without any compromise on long-term durability considering the alkaline environment associated with concrete. Figure 3 (Right) shows short starter tails of HDPE geogrid securely cast into the back of the panels at predetermined spacings. This enables a high-strength connection to be subsequently formed with the primary reinforcement length using an HDPE circular bodkin and without the concern of corrosion. The RE500 geogrids carry the European CE registration and the independent HAPAS (ex-British Board of Agrément (BBA)) certification. Partial material factors were obtained from the BBA certificates to design the reinforced soil walls.



Fig.3. Left: 4m Wide Panel, Right: HDPE geogrid connection

3 Design Development

The next phase was to finalise the dimensions of the facing units and the design of the reinforced soil system to meet ultimate limit state (ULS) and serviceability limit state (SLS) criteria for the required 120 years design life of the structure. This was done in stages, as explained below. It is also important to note that all these stages are interlinked, and appropriate design iterations were carried out before the final design stage was reached and prior to the construction of reinforced soil walls.

3.1 Structural Design of Precast facing Panel

Three main variants of the large-width facing panels were identified from the initial assessment of the reinforced soil wall geometry, i.e., a half-height panel, a full-height panel of 1.5 m high and an upper panel up to 2 m in height. The structural design of reinforced concrete panels (Grade C40/C50) was carried out in accordance with BS EN 1992-1 and the UK NA for BS EN 1992-1. In order to design the 4 m wide RC panels, a uniformly distributed load was applied until the shear in the RC panel was equivalent to the combined design strength of the total number of geogrid reinforcement layers attached to the RC panel. An additional steel reinforcement layer on the outer face of the facing panels was designed, as these panels are required to span across the sleeved columns where the geogrid presence will be minimum. The development of these extraordinary large facing panels went through a rigorous process, both from a technical and construction perspective, before the panel design was finalised for production. The process included design checks and modifications to cater for practical and efficient lifting and demoulding stages of panel assembly.

3.2 Design assessment of Reinforced Soil System

The design assessment of the 6.5 m high non-load bearing reinforced soil walls and lower wing walls was carried out incorporating polymeric HDPE geogrids, classified as ‘extensible’ reinforcement, utilising a tie-back wedge design method in accordance with BS

8006-1:2010+A1:2016 [3] and for a design life of 120 years. Precast reinforced concrete panels, i.e., 4 m x up to 2 m high for non-load bearing bridge abutments and 1.5 m x 1.5 m for lower wing walls, were modelled as facing panels. The shear strength properties for the various soil types used for design and their extent are as shown in Table 2 and in Figure 4 respectively. The upper RC wing wall was modelled as a 100 kN/m^2 permanent surcharge, and transient/traffic loading was modelled as an additional 20 kN/m^2. The lateral offset provided between the reinforced soil facing panels and the rail running edge is greater than 4.5 m to mitigate the risk of train impact on the substructure due to train derailment, in accordance with Network Rail Standard NR/L3/CIV/020. Therefore, the reinforced earth wingwalls were not assessed against train impact loading. The geogrid layout was assessed for internal sliding, rupture, pull-out, and wedge failure. For ULS, the assessment is related to tensile creep rupture in the reinforcement, whereas, for SLS, the serviceability limits are checked in terms of the axial tensile strain (<1%) in the reinforcement, which is not to be exceeded between the completion of the construction (typically 1 month) and the end of the selected design life of the structure, which is 120 years. For SLS criteria, the geogrid layers are not assessed against the rupture but against the average post-construction strain over the geogrid length. External stability was carried out by Geofem and is detailed in section 3.3.

Table 2. Design parameters for reinforced soil wall

Soil Type	ϕ'	c' (kN/m^2)	γ' (kN/m^3)
Reinforced fill	42°	0	20
Retained fill	38°	0	20
Foundation Soils (Excavated and replaced with engineered fill)	38°	0	20

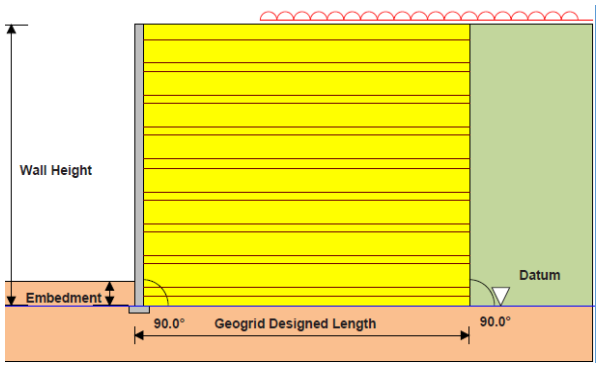


Fig. 4. Soil Zone-Reinforced/Retained and foundation

3.3 Foundation Design and External Stability Assessment

The foundational designs of the non-load bearing reinforced soil abutment and lower wing walls were performed using three-dimensional (3D) finite element analysis (FEA) using Plaxis. A 3D analysis approach was used to take account of the gaps in the geogrid for the pile sleeves and the bearing piles themselves in contributing to differential settlement. The sleeves above each pile location were modelled by leaving voids in the geogrid layer and by reducing the density of the fill within the sleeves to zero while retaining the same mechanical properties. A two-dimensional (2D) plane strain FEA was performed for the lower wingwalls as the cross section of these walls remained constant except for the varying height of the wall. Table 1 summarises foundation soil types and thicknesses for the proposed reinforced soil

non-load bearing bridge abutments and wingwall founded at approximately 83.5 m AOD level. The Oxford and Kellaways Clays had similar properties, so they were combined with one layer but with a division at 71.3 m AOD between an upper clay where stiffness and undrained shear strength were increasing with depth and a lower clay where these values were constant. The top of the Cornbrash formation (limestone with mudstone) was taken as the level of the fixed base (59.5 m AOD) to the FEA mesh since the strains at this depth and in the stiff limestone and mudstone were expected to be insignificant. A horizontal ground surface, i.e., 83.5 mAOD, at reinforced soil wall formation level was adopted for the ULS analysis, while the initial ground level of 85.44 mAOD was adopted in the SLS analysis to include excavation on formation level. Groundwater level was modelled at the formation level as a conservative assessment. The total permanent and variable surcharge on the retained side was set to 126 kN/m^2 to include the Eurocode 7 Design Approach 1 Combination 2 (DA1(2)) partial factor of 1.3 on variable loads. The modelling work aligns with the protocols set out in the published guide [4], ensuring the adopted methods adhere to recognised industry standards. The linear elastic perfectly plastic (LEPP) Mohr-Coulomb constitutive model was used for the soil layers. The analyses were run for both undrained and drained input parameters for the alluvium and clay layers to check both short-term and long-term conditions, respectively. Preliminary analysis predicted sliding failure in the undrained case and bearing failure in the drained case with no ground improvement of the foundation soil. For an optimal safety margin, the following measures were implemented:

- Alluvium and upper clay replacement with Class 1A ϕ' =38° and γ =20kN/m^3 material, 3.0 m in depth below the foundation level of reinforced soil wall (the improved foundation FEA model)
- Geogrid reinforcement length of 8 m for non-load bearing wing walls and 6.5 m for the wing walls

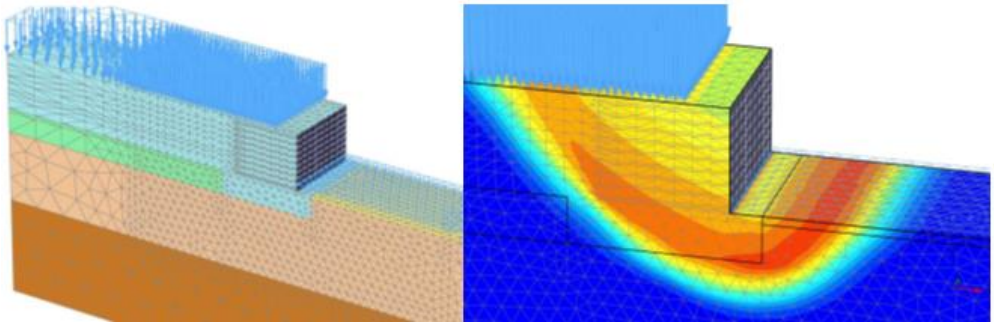


Fig. 5. Left: 3D FEA model of abutment wall, Right: Critical failure mechanism (Drained condition)

Figure 5 (Left) shows a 3D Plaxis model with a 3m foundation replacement. Assessments for reinforced soil structures yielded a safety factor (via shear strength reduction) exceeding 1.25. Figure- 5 (Right) shows bearing failure as the critical mechanism in the verification of ULS for external stability of the abutment wall in the drained case. In the SLS analyses, an approximate prediction of post-construction displacements was obtained by subtracting the undrained analysis displacements from the drained. These showed 33 mm settlement at the wall facing, increasing to a near-uniform 78 mm beyond the reinforced soil mass and ground improvement (refer to figure 6). The predicted differential post-construction settlement between the piles (without the bridge loads applied) and the top of the fill above the piles was 24 mm. The maximum differential settlement along the line of the facing of the abutment wall was predicted to be 1 in 685 (Refer to figure 7), which is within acceptable criteria for concrete panel facing [5].

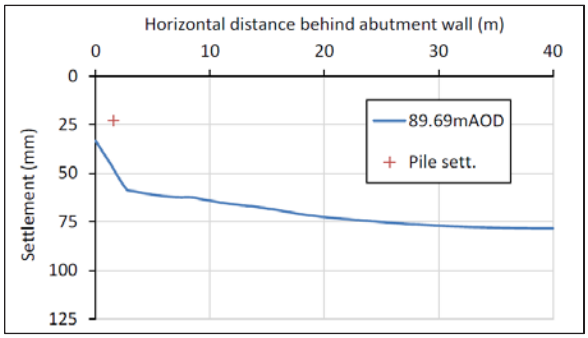


Fig. 6. Predicted post-construction phase settlement

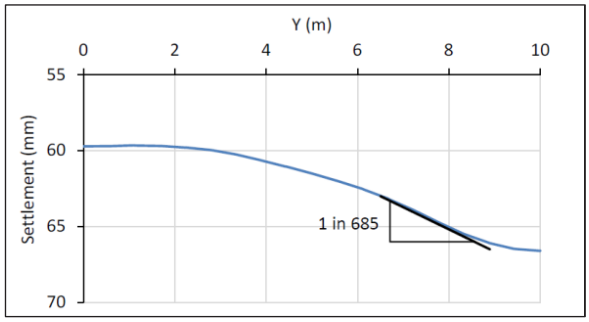


Fig. 7. Predicted settlement of abutment wall facing base

4 Final Design

Additional analysis of the reinforced soil wall was performed in FEA to assess the effect of the settlement on the geogrid layers considering a rigid foundation. Settlement-induced tensile forces in the geogrid layers were then derived by subtracting forces in the geogrid from the improved foundation FEA model and an FEA model considering a rigid foundation. The conventional tie-back wedge analysis does not consider the effect of foundation settlement. So, the difference in tensile forces in geogrid layers was then added to the tensile forces (T_{req}) from conventional tie-back wedge analysis. The increased tensile force in geogrid layers was then checked against the long-term design strength of each geogrid layer to ensure that they still achieved the target factor of safety in ULS conditions as defined in BS8006. Final design and drawings (Refer to figure 8) were prepared [2], and the summary is below:

- Non-load bearing reinforced soil bridge abutment designed using 8 m long HDPE geogrid mechanically connected to large facing units of 1.5 m high and up to 2 m high for reinforced fill and retained fill as per table 2.
- Lower wing walls were designed using 6.5 m long HDPE geogrid mechanically connected to facing units of 1.5 m wide and up to 1.5 m high for reinforced fill and retained fill as per table 2.
- Foundation soil replacement with Class 1A material, 3.0 m in depth for all reinforced soil sections

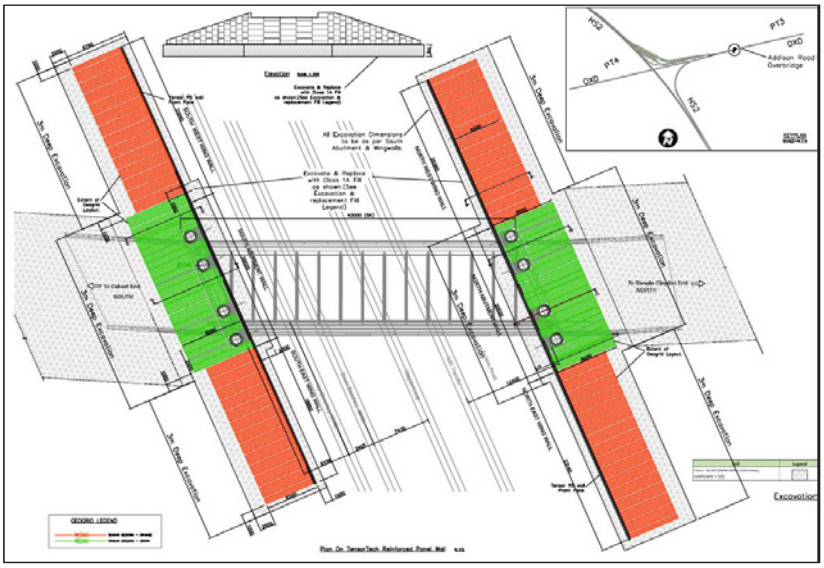


Fig. 8. Showing one of the detailed drawings produced for construction

5 Construction

The project was approved for construction in September 2022. The concrete panels were precast with the HDPE geogrid tail cast within the facing unit off-site and were subsequently carefully transported to the site for assembly, thereby ensuring the highest level of quality assurance in production. During assembly, the short geogrid tails of the facing panels were connected to the full design geogrid length on site using polymeric bodkins, providing superior connection strength and enabling high-efficiency transfer of the load to the soil reinforcement layers (Refer to figure 9). The primary geogrid layers were lightly tensioned using a tensioning beam, so any slack in the layer from the face units to the entire length was removed. Reinforced fill material was then placed before the release of the tension beam, followed by appropriate compaction as specified in Series 600 of the Specification for Highway Works. The construction of a geogrid-reinforced retaining wall using HDPE geogrid is a straightforward procedure with no issues on buildability. Construction drawings



Fig. 9: Construction images (Panel installation, Bodkin Connection, Panel arrangement-elevation)

included site-specific detailing for geogrid placement around columns and to ensure the careful cutting of these layers was carried out to avoid any additional reduction in the percentage coverage area of geogrid. Figure 9 shows construction images of the wall.

6 Conclusion

The design of these reinforced soil walls commenced in April 2020. The project team faced unprecedented challenges due to Covid-19, but with sheer dedication and excellent teamwork, the scheme design was delivered at the requested time. However, construction work only started in late 2022, and the full Addison Road Overbridge scheme was successfully completed and opened to traffic in 2023. The newly constructed Addison Road overbridge (refer to figure 10) serves as a public highway located close to Calvert, Buckinghamshire, and is an important asset for HS2 and Network Rail infrastructure. The project demonstrated how the collaboration from project consultant to specialist designer and from project contractor to specialist contractor resulted in a successful project using large facing panels with HDPE geogrids for a design life of 120 years.



Fig. 10. Constructed Addison Road Overbridge

7 Acknowledgement

The authors are grateful to High Speed 2 Ltd. and EKFB for allowing us to publish this case study. We would also like to thank Arcadis Setec COWI (ASC) DJV, Buckingham Group Contracting Limited and PC Construction for their support and for the successful construction of the project.

8 References

1. Project document: Reinforced Soil Specialist Consultant Scope of Works prepared by Arcadis, March 2020.
2. Project document: High Speed 2 - 1MC06 - Stage One C2 - MWCC –North Portal of Chiltern Tunnels to Brackley Addison Road Overbridge Reinforced Earth Design and Calculation Report - 1MC06-CEK-BR-REP-S06_CL09-000098, Rev C01, dated 11/04/2022.
3. BS8006-1:2010+A1:2016, Code of practice for strengthen/reinforced soils and other fills.
4. A. Lees, Geotechnical finite element analysis: a practical guide (ICE publishing 2016).
5. BS EN 14475:2006 Execution of special geotechnical works —Reinforced fill.

History and performance of the first MSE walls reinforced with polymeric strips in Türkiye

Hakan Özçelik[1*]

[1]Consultant, Senior Geotechnical Engineer, 06830 Ankara, Türkiye

Abstract. MSE wall technology was first introduced to the Turkish market and to the General Directorate of Highways in 1986 with a system that uses precast panels and polymeric strips. The first wall was built near Ankara. In 1987, for the Second Bosphorus Crossing Project – Istanbul, all the wing walls of the overpasses at the Trans European Motorway (TEM) and connecting roads on the European side were also constructed with the same system. Another wall for a hotel construction in Kusadasi near Izmir was built in 1988, supporting a road in front of the hotel. The walls during their 38 years of service life were subjected to severe earthquakes. Strips exhumed from Ankara and Istanbul walls after 20 and 22 years of construction respectively were tested. This paper discusses the history, performance of the walls after earthquakes, the results of the exhumed polymeric strip tests and their present state.

Full paper published in the September 2025 Special Issue of the French Geotechnical Journal **"Revue Française de Géotechnique"** *https://www.geotechnique-journal.org*

* Corresponding author: hakan@hakanozcelik.com

Influence of different construction methods on full-height precast facing reinforced soil walls

Khashayar Malekmohammadi [1,2 *] and *Ivan P.* Damians [1,2,3]

[1] Department of Civil and Environmental Engineering, Universitat Politècnica de Catalunya·BarcelonaTech (UPC), Spain
[2] VSL Construction Systems, Barcelona, Spain
[3] International Centre for Numerical Methods in Engineering (CIMNE), Barcelona, Spain

Abstract. Reinforced soil walls (RSW) have been extensively employed worldwide for many decades, showcasing their efficacy and versatility in diverse geotechnical contexts. The field of RSW is constantly advancing, propelled by ongoing research and significant advancements in design and construction methods. The inherent complexity of soil-structure interaction behaviour poses significant challenges for researchers investigating RSW systems. Among these, the wall-facing system is pivotal to performance outcomes. This study focuses on full-height precast concrete wall facings by applying numerical simulations to investigate the impact of construction techniques on the performance of the facing toe as well as facing/foundation relationship. The numerical evaluation is performed by altering construction and design features from actual site conditions and common practice and assess their influence on the deformation of the RSW system, particularly, on the full-height facing panels component. The findings demonstrate that the configuration of the facing toe has a substantial impact on the overall performance of the facing. Differences in connection design result in distinct deformation patterns, underscoring the significance of thorough design of connection approaches. These findings can provide useful insights for improving the design and construction of RSW structures, especially those that use full-height precast concrete facing panels.

Full paper to be published in:
https://www.e3s-conferences.org/articles/e3sconf/abs/2025/44/contents/contents.html

* Corresponding author: khashayar.malekmohammadi@upc.edu

The stabilisation of a cut slope utilising percussion driven earth anchors

Elliot Harris

Abstract. This report examines the stabilisation of a major cut slope in Edginswell, Torquay, UK, undertaken to facilitate the construction of a retail development. The project involved the excavation of a 137.00 m long slope with a maximum height of 5.25 m. Percussion Driven Earth Anchors (Mechanical Anchors) were integral to the stabilisation strategy. The slope was divided into two distinct sections: the lower half was excavated at an 80 ° angle and stabilised with a welded gabion panel system incorporating non-woven filter fabric to mitigate material loss, while the upper half was cut at a 60 ° angle and supported by a flexible facing designed to promote vegetation growth. The report details the selection and design of geosynthetic materials for use between Mechanical Anchor positions, highlighting compliance with BS EN 1997-1 [1] and BS 8006-2 [2] standards. It addresses the unique challenges of applying these standards to Mechanical Anchors, as opposed to alternative traditional grouted anchoring systems. This case study underscores the role of innovative engineering practices in delivering sustainable and effective slope stabilisation solutions.

1 Project overview

1.1 Background

The proposed construction of a retail premises off Orchard Way in the Edginswell area of Torquay, Devon, England entailed the establishment of a large portal-frame warehouse/store structure and accompanying infrastructure. The proposed development involved substantial cutting as part of enabling works to create commercial plots.

1.2 Form of development

To prepare the commercial plots, extensive excavation was necessary. The excavation involved a 5.25 m high cutting extending over a length of 137.00 m. Due to site constraints, the proposed scheme was an 80 ° cut on the lower 3.00 m of the slope, transitioning to a 60 ° cut on the upper 2.25 m, as seen in Figure 1. Cut heights remained relatively constant throughout the excavation.



Figure 1. Completed works prior to hydro mulching application.

1.3 Technical overview

It was determined that Percussion Driven Earth Anchors (Mechanical Anchors) offered a viable solution for stabilising the proposed cutting. Mechanical Anchors speed of deployment and immediately quantifiable loads allowed for a top-down construction approach in individual berms, ensuring temporary stability in the short term and adherence to the work schedule.

1.4 Ground conditions

The ground conditions encountered within the area of the cut slope comprised the Watcombe Breccia Formation, consisting of interbedded reddish brown, sand, silt and clay. The materials of each type often contain gravel as secondary constituent, and the silts and clays typically contain sand as an additional secondary constituent. Overall, sand beds predominated, typically comprising slightly gravelly silty/clayey sand.

2 Ultimate limit state design

Stability of the cut slope was verified in Ultimate Limit State (ULS) (GEO and STR) utilising Design Approach 1 (DA1), employing a partial factor approach to address the risk of the structure reaching a limit state. This approach considers uncertainties and variations in material properties and loading conditions.

Design Approach 1 applies partial factors either to actions (A) or the effects of actions, as well as to material (M) parameters and resistances (R). Design values for actions were derived by multiplying the representative value by the partial factor, while design values for material properties and resistances were derived by dividing the characteristic value by the partial factor.

The following combinations of sets of partial factors were verified in accordance with Design Approach 1:

Combination 1 (DA1-1) (STR): *A1* "+" *M1* "+" *R1* (1)
Combination 2 (DA1-2) (GEO): *A2* "+" *M2* "+" *R1* (2)

(where "+" implies: "to be combined with").

In addition, BS 8006-2 [2] provides two further Sets of partial factors (Set 1 and Set 2) to ensure ULS would not occur in the reinforced anchored structure. The partial factors were adjusted from those specified in BS EN 1997-1 [1], with increases to some material properties and anchor resistance factors.

Both BS EN 1997-1 [1] and BS8006-2 [2] assume the design of the structure is for the worst credible geometry, therefore no partial factor relating to this aspect were applied. Partial factors were not differentiated based on whether the works were temporary or permanent. Instead, this distinction was reflected in the selection of material properties and anchoring resistance.

2.1 Serviceability limit state design

Since the analytical and numerical methods available do not provide reliable predictions of the deformations of a natural slope, the occurrence of Serviceability Limit State (SLS) was avoided by limiting the mobilised shear strength. BS EN 1997-1 [1], outlines important considerations for handling limit states, particularly when no reliable calculation model is

available for a specific limit state. If such a scenario arises, an analysis of another limit state should be conducted using factors to ensure that the likelihood of exceeding the specific limit state is sufficiently improbable. A limit equilibrium analysis was undertaken for the slope for day-to-day normal circumstances. SLS design was undertaken with partial factors set to 1.0, as specified in BS EN 1997-1 [1].

3 Remediation strategy

3.1 Design standard

The Mechanical Anchor design was predominantly undertaken in accordance with BS EN 1997-1 [1] and BS 8006-2 [2]. Mechanical Anchors differ to Grouted Anchors, BS 8006-2 [2] is considered applicable for the purposes of determining forces within reinforced slopes and for analysing flexible facings.

3.2 Computational and analytical techniques

To analyse the stability of the cut slope, Rocscience Slide2, a 2D limit equilibrium analysis software, was employed for assessing both internal and external stability of the reinforced slope.

The 'Optimisation' option was selected during analysis to model a comprehensive search for potential shear surfaces passing through the slope and identify those with the lowest over design factor (ODF) (least stable) at all stages of construction.

3.3 Ultimate limit state stability analysis

Failure surfaces can vary in shape, ranging from planar to circular or more complex shapes. In normal circumstances BS EN 1997-1 [1] suggests where ground materials are relatively homogeneous and isotropic, circular failure surfaces can be assumed. However, as the Site comprises interbedded layered soils with variations in shear strength, a non-circular failure surface was also considered.

Due to the proposed steep cut angles, external stability checks for bearing capacity, forward sliding, and overturning were necessary. Analysis of sliding stability considers the ability of steep slopes to resist sliding along the base of the reinforced block in response to lateral earth pressure. Bearing capacity can become a concern due to the unbalanced loads from the excavation which could have led to heave at the base. Traditionally, sliding and bearing capacity checks were performed as if the reinforced slope were a gravity retaining wall or reinforced earth structure. However, the anchor zone does not behave as a rigid block, and discrete soil boundaries typically do not exist behind or below it. Anchored slopes align more closely with slope stability principles. BS 8006-1 [3], specifies potential bearing capacity issues be assessed through an external circler analysis, while possible forward sliding identified using an external non-circular wedge analysis as this assesses forward sliding across a planar surface.

ULS analysis of internal failure surfaces were undertaken in accordance with BS 8006-2 [2] utilising Set 1 and 2 partial factors, which take precedence over BS EN 1997-1 [1].

ULS analysis for external failure surfaces occurring outside the anchorage zone were consequently undertaken in accordance with partial factors of Combination 1 (DA1-1) and 2 (DA1-2) of BS EN 1997-1 [1].

The verification through partial factors on actions and material properties ensured geotechnical (GEO) limit states were met. The structural (STR) limit state was also assessed by partial factors on actions, hence structural verifications were also verified through DA1-1 and Set 1.

3.4 Ultimate limit state design anchoring strategy

The design aim was to arrive at a Mechanical Anchor layout and facing design for which the factored resisting forces exceeded the factored driving forces for any calculated failure mechanism, both in the short term and the long term and for each stage of construction.

Within the 2D, limit equilibrium design software, Mechanical Anchors were modelled through the influence on the slices where they intersect the slip. Mechanical Anchors are assumed within the analysis to increase the normal force acting on the base of the slice, thereby increasing the frictional shear resistance of that slice.

The free anchor length was determined to ensure adequate performance in maintaining the overall stability of the supported structure, while also being positioned beyond any potential ground rupture. This was proven analytically using the Boussinesq [4] method to determine the pressure distribution generated by the anchor head. A 20% stress zone was employed to verify that the anchor was positioned sufficiently beyond the calculated slip surfaces.

Where Mechanical Anchors are proposed in poor soils or near to surface, the free anchor length was also increased to locate the anchor bearing head (fixed length) in more competent ground.

Mechanical Anchors were designed to prevent both local overstressing and the risk of progressive failure. Mechanical Anchor spacings were restricted to ensure each anchor could locally withstand the loads placed upon it. For cuts slopes between 60 ° and 90 °, BS8006-2 [2] suggests anchor spacings be between 0.75 m to 1.50 m vertically and 0.50 m to 2.00 m horizontally. Vertical spacings between anchor rows are traditionally kept constant with depth to avoid construction error. ULS analysis also ensured that vertical spacings between anchor rows were not excessive. This is because this method includes mechanisms which daylight on the slope face.

Mechanical Anchoring positions were proposed to be installed across 5no. rows at 1.00 m vertical (elevation) spacings for ease of installation and at a lateral spacing of 1.20 m, which was determined to give the most economical solution. To enhance slope coverage, a diamond (horizontal offset) grid pattern was implemented between rows of anchors. An additional anchor row was required for areas where slope topographies varied, resulting in excessive space between the upper anchor and the top of the cutting. This was determined through ULS analysis, as failures occurred above the upper row of anchors.

Practical considerations dictate installing anchors perpendicular to the slope face. However, to avoid collision issues, rows 1 and 2 deviated by a 10 ° incline above perpendicular, while row 3 was set at a 20 ° angle above perpendicular. To accommodate the angle variance, a hemispherical washer was employed in these rows.

The stability analysis confirmed that the Over Design Factor (ODF) $\geq$ 1.000 in both the circular and non-circular slip analysis for external stability assessment. This indicated there was no concern regarding sliding or bearing capacity with the proposed anchoring strategy.

3.5 Temporary works

To ensure a safe working environment during anchor installation and prevent collapse of the cut face, a staged excavation approach was implemented following guidance from BS8006-2 [2]. This involved an incremental construction process where excavation increments were followed by the placement of Mechanical Anchors and a surface facing. Each horizontal anchoring level had to be completed and secured before further excavation could proceed. This sequential process continued until the full depth of the excavation was achieved.

Phased excavation assessments were undertaken to enable a top-down construction, as well as ensuring overstressing of Mechanical Anchor positions did not occur during the construction. Each berm was assessed for temporary stability while the corresponding anchoring row were installed and secured. Overall slope stability for temporary cuttings were

determined in accordance with the principles of BS EN 1997-1 [1], including the selection of appropriate soil parameters for designing temporary slopes. An overdig allowance of 0.50 m was accounted for between rows of anchor installations.

Face stability assessment tests, detailed in BS EN 14490 [5], were also conducted to assess temporary stability and excavation bench heights. The test involved excavating a trial pit to a batter and depth equal to the slope angle and bench height proposed. The width of excavation was not less than twice the bench height, with the observation period representative of the anticipated time between anchor installations. On-site observations revealed that sufficient temporary stability was ensured by the presence of fine material, providing a small amount of cohesion between the grains.

Good earthworks practices were followed during anchoring works, and all excavated slopes were required to be supported at the end of each shift. Faces were not exposed during adverse weather conditions and the period between trimming the slope face and anchor installation was minimised to mitigate the risk of face collapse.

3.6 Anchor limit state design

In accordance with BS EN 1997-1 [1], the ULS design force to be resisted by the anchors ($E_{ULS;d}$) must not exceed the design resistance of an anchor that meets ultimate limit state criteria ($R_{ULS;d}$). The ULS design force ($E_{ULS;d}$) is determined as the greater of:

- The design force required to prevent any ultimate limit state in the supported structure ($F_{ULS;d}$), or
- The maximum anchor design force, including the effect of lock-off load, necessary to prevent a serviceability limit state in the supported structure ($F_{Serv;d}$), multiplied by a partial factor (γ_{Serv}).

$$E_{ULS;d} \leq R_{ULS;d} \quad (3)$$

$$\text{where } E_{ULS;d} = \max(F_{ULS;d}\,;\, F_{Serv;d}) \quad (4)$$

$$\text{and } F_{Serv;d} = \gamma_{Serv} \times F_{Serv;k} \quad (5)$$

The values of $F_{Serv;k}$ and $F_{ULS;d}$ were derived from the slope stability analysis for Serviceability and Ultimate Limit States, respectively.

3.7 Anchor geotechnical ultimate limit state resistance

In the early phase of project design, an analytical approach was employed to assess ultimate anchor pull-out resistance. This assessment was subsequently confirmed by pre and post construction testing.

It is possible to derive anchor performance prior to conducting the slope stability assessment, it is however considered more practical to establish anchor dimensions once a known/initial required ULS design force is calculated ($E_{ULS;d}$). The anchoring design process continued to evolve with several iterations to adjust anchor spacings and quantities based on anchor performance calculations. This refinement of the slope stability assessment continued until a suitable specification was achieved.

BS EN 1997-1 [1] does not specify a method for calculating anchor performance through analytical calculations. It also does not provide guidelines for attaining adequate ultimate load capacities while meeting the Proof Loads (P_p) requirements to satisfy Creep Rate or Load Loss.

BS 8006-2 [2] outlines the ULS approach for deriving anchor design bond stress (τ_{bd}) and characteristic bond stress (τ_{bk}), Table 1. These values correspond to lumped factors ranging from 1.5 to 3.0 applied to ultimate resistances in anchor design (τ_{bu}). The variation in the range of the partial factors (γ_k, $\gamma_{\tau b}$) accounts for whether the anchors are utilised in a

temporary or permanent application.

Table 1. Ultimate Limit State Approach to Deriving Design Values BS8006-2 [2]

Method of Determining Ultimate Bond Stress τ_{bu}	Factors for Determining Characteristic Bond Stress from Ultimate Values. $\tau_{bk} = \tau_{bu} / \gamma_k$	Factors for Determining Design Bond Stress from Characteristics Values for Set 1, $\tau_{bd} = \tau_{bk} / \gamma_{\tau b}$	Factors for Determining Design Bond Stress from Characteristics Values for Set 2, $\tau_{bd} = \tau_{bk} / \gamma_{\tau b}$
Effective	γ_k = 1.00 to 1.35	$\gamma_{\tau b}$ = 1.11	$\gamma_{\tau b}$ = 1.5
Total	γ_k = 1.35 to 2.00	$\gamma_{\tau b}$ = 1.11	$\gamma_{\tau b}$ = 1.5

By employing the aforementioned criteria, it was possible to establish theoretical ultimate load requirements for anchor performance. This approach ensured that the anchoring design met the stipulated Proof Load (P_p) requirements in accordance with BS EN 1997 [1], before initiating anchor investigation or suitability testing.

The geotechnical ULS resistance of anchors was confirmed suitable through on-site testing. Testing was conducted following the manufacturer's recommendations. Testing protocols for Mechanical Anchors deviates slightly from BS EN 22477-5 [6]. Unlike grouted anchors, where an unloading sequence is commonly employed to ascertain the apparent free length, this step is omitted as this value is already known due to it being a grout free system.

Investigation tests were guided by analytical calculations performed in advance to determine anchoring loads. The objective was to align the chosen anchoring specification as closely as possible with the potential final anchor scheme.

The investigation tests determined the anchor specification derived analytically to be suitable. The client initially requested a full hard armour finish over the slope face. However, through negotiation and by demonstrating the cost savings and ecological benefits of a vegetated finish, a hybrid approach was agreed upon. This solution consisted of a 60° upper vegetated cut slope and an 80° lower cut slope with a hard armour gabion façade.

3.8 Surface finish

The client initially requested a full hard armour finish over the slope face. However, through negotiation and by demonstrating the cost savings and ecological benefits of a vegetated finish, a hybrid approach was agreed upon. While a 70 ° cut was originally requested, vegetation concerns led to a solution consisting of a 60 ° upper vegetated cut slope and an 80 ° lower cut slope with a hard armour gabion façade, all within the 70 ° cut allowance

This approach satisfied the client's requirement for a hard armour finish, providing the desired aesthetic appearance and minimal maintenance while reducing the need for a gabion façade at height. This minimized the risks associated with working at height and reduced installation labour.

The 60 ° upper slope angle was determined in consultation with a hydro mulching specialist. As the cut face predominantly faced north, the specialist advised that nitrate-fixing vegetation would be necessary and that 60 ° was the maximum angle at which they could confidently guarantee successful vegetation uptake.

3.8.1 Slope Stabilization & Mesh Facing

The anchored scheme included a flexible steel mesh facing over the entire slope to resist lateral forces between anchor positions. The mesh acted as a tensioned catenary system, preventing instability or excessive deformation.

Careful consideration was given to the mesh's ability to function as a flexible structural restraint. This involved evaluating:

- Loads imparted by anchor head plates to ensure no puncturing failure under working conditions, as per BS 8006-2 [2].
- The facing's ability to restrain surface soil between anchor positions, modelled in two dimensions (ignoring side friction) using shallow two-part wedge mechanisms to achieve force equilibrium.

Several steel mesh options were evaluated, with the final selection chosen for its higher tensile strength and resistance to elongation under load, making it better suited as a tensioned catenary between anchors. This ensured facing deflection remained below 35mm between anchoring positions.

The mesh was primarily installed without overlap, though small overlaps were introduced where necessary to accommodate site-specific geometry.

3.8.2 Upper 60 ° Vegetated Slope

To protect against degradation and softening, a woven coir mat was placed beneath the mesh to enhance contact with the hydro mulch application. The coir matting was deliberately selected with large apertures to:

- Allow direct contact between the hydro mulch and the ground.
- Facilitate connection with the slope face.
- Gradually degrade over time, providing nutrients and a substrate for vegetation establishment.

The slope face was left slightly friable to encourage vegetation growth. A smoother, smeared finish was avoided, as it could create a desiccated surface that roots would struggle to penetrate, leading to vegetation failure.

3.8.3 Lower 80 ° gabion façade

A gabion façade was proposed for the steeper 80 ° cutting. To prevent the potential washout of fines and voiding behind the gabions, a non-woven filter fabric was placed beneath the mesh as a drainage layer.

Both the non-woven filter fabric and the coir matting were installed with a minimum 500mm lap between adjacent sheets.

3.8.4 Durability considerations

Exposed facings are vulnerable to environmental damage. The site's atmosphere was classified as Category C4 under BS EN 9223 [7], indicating a corrosive environment. All proposed facing materials were confirmed to have BBA certification for a 120-year design life under these conditions.

3.9 Gabion design

The 80 ° anchored cutting was adorned with a 300 mm gabion façade. The gabions adhered to MCHW Series 600, Clause 626, using PVC-coated galvanized welded mesh, compliant with BS EN 10244-2 [8] (Class A) and BS EN 10245-1 [9] and BS EN 10245-2 [10]. A welded gabion was chosen for its ability to maintain shape better than woven alternatives, and to prevent bulging when filled. The mesh panels were constructed from 75 mm x 75 mm square mesh, utilising 3.8/4.3 mm diameter wire throughout. Factory-assembled joints were secured with clips or C-rings at every aperture.

A "High Corrosivity" C4 environmental condition, as defined by MCHW 1 Clause 626, was selected. The gabion materials were BBA/HAPAS certified, ensuring a 120-year design life under this environmental condition.

Assembly of the gabion units was undertaken using continuous tie lacing wire, helicals, C-rings, or a combination thereof. All joining accessories matched the corrosion protection specification of the parent mesh material.

To prevent weak joints, larger stones were prohibited. Careful filling of gabion baskets was essential to avoid damaging the corrosion protection and to prevent material escape or movement. Stones were hand-placed to achieve a 'dry stone' finish, ensuring both structural performance and aesthetic appeal.

To prevent distortion and stone migration, gabion boxes were fitted with transverse vertical diaphragm panels at 1.00 m intervals and internal bracing wires installed at 1/3 and 2/3 of the gabion's height. Internal ties, configured as figure-eight, single ties, or corner ties, were securely fastened, ensuring they wrapped around a minimum of three vertical wires on both the front and rear faces of the gabion.

Gabions were constructed vertically and leaned back against the 80 ° cutting to enhance resistance to overturning. They were built without overlapping panels to facilitate future maintenance and decommissioning.

Gabion baskets were secured to the slope face using C-clips, which were fastened between the gabions and the mesh. Additionally, the baskets were tied back at each anchor position by large washer plates and a further nut to the threaded anchor bar, to ensure there is no risk of collapse of the baskets, Figure 2.



Figure 2. Gabion basket fastening.

The gabions were filled with Class 6G stone material. Strict control of fill placement was maintained to ensure maximum load spread and structural integrity, with fill material sizes limited to avoid voids and weakness planes. The maximum size of fill material was selected to not exceed two thirds of the minimum dimension of the gabion compartment (200 mm) with the minimum size of the fill material not less than the size of the mesh opening (100 mm).

Whilst the gabion façade will not be assumed to provide any additional buttressing to the slope, an additional assessment was undertaken to determine its contribution to stability. Gabions were not relied upon for overall slope stability due to time delays for installation and the need to allow for any future maintenance requiring un-filling of the gabions.

The Javankhoshdel et al. [11] methodology for modelling gabions was utilised to assess overall slope stability. The Javankhoshdel et al. [11] method calculates Mohr-Coulomb parameters for the gabion wall materials.

Internal stability analysis caused by external loading, such as overturning, sliding, and shear stress acting on the gabions, was deemed unnecessary due to the gabions primarily functioning as a façade and were not loaded by external forces. However, Compressive stress acting on the gabion of the corresponding row was evaluated for each gabion block to ensure instability did not occur due to the weight of subsequent gabion rows above.

A strip foundation was proposed at the base of the gabion baskets. Sliding resistance of the footing was checked to ensure adequate shear resistance along the foundation base.

Additionally, overturning stability was evaluated to ensure compliance with the ULS EQU in accordance with BS EN 1997-1 [1]. Due to the difficulty of obtaining undisturbed samples of granular materials and thus the Poisson's ratio, foundation settlement was estimated using correlations based on the results of the in-situ SPT N testing.

Foundations were proposed to be a minimum thickness of 300mm with a width of 600mm founded 450mm below formation level. Any soft spots were removed and filled with additional concrete.

4 Conclusion

4.1 Problem resolution

The design primarily followed the guidance of BS EN 1997-1 [1] and BS 8006-2 [2]. Although a Mechanical Anchor is grout free, as it mobilises resistance from a fixed point, BS 8006-2 [2] is considered still applicable as it outlines methods for determining forces within reinforced slopes and for analysing flexible facings.

Unlike a grouted system that primarily relies on skin friction, where even slight movements can lead to rupture and shearing of the grout-to-soil interface, Mechanical Anchors utilise end bearing, where the degree of movement is less critical. This distinction underscores the importance of considering the specific characteristics and behaviour of Mechanical Anchors in their design process and how they differ from grouted alternatives.

4.2 Mechanical anchor considerations

Mechanical Anchors offer significant cost advantages over grouted systems due to reduced labour and time requirements and the elimination of specialist installation equipment. Their cost-effectiveness is further enhanced by the absence of grout curing times and the lack of predrilling requirements, which streamline the installation process and lead to faster project completion.

Mechanical Anchors can also be installed with conventional handheld equipment, making them well-suited for sites with spatial constraints.

Moreover, Mechanical Anchors provide immediate feedback on performance, allowing for rapid adjustments to anchor designs in response to unforeseen ground conditions.

4.3 Surface facing considerations

While the gabion façade achieved the desired aesthetic finish, its design presented challenges. The construction involved a top-down approach to stabilize the cut slope with Mechanical anchors, followed by a bottom-up method for the gabion wall. This sequence made it impractical to install the anchor top details on the outer face of gabions, which would have facilitated future testing and maintenance.

Installing anchor top plates on the outer face of the gabion façade might have been feasible using a method of controlled, sequenced unloading and reloading of the Mechanical Anchors. This would involve placing and filling the gabions before reloading the anchors, and incorporating sleaves on the protruding rod sections to allow movement and prevent damage during the filling process. While this approach could have created a seamless system for future maintenance, it would have extended work schedules and potentially created unsafe conditions, with contractors working close to temporarily unsupported slopes.

4.4 Closing statement

Mechanical Anchors are widely regarded as an effective solution for various applications, often aligning well with the technical standards established for grouted alternatives.

However, it is crucial for designers to be aware of the limitations and potential challenges associated with Mechanical Anchors to ensure their optimal use.

The authors would like to express their gratitude to Platipus Anchors Ltd for their support in conducting this study. Special thanks to Geoffrey Stevenson and Sami Hoq for their assistance with data collection, technical discussions, and logistical support. The data supporting the findings of this study are available upon reasonable request from the corresponding author. Due to confidentiality agreements, certain data may be restricted.

References

1. British Standards Institution (BSI), 2013. BS EN 1997-1:2004+A1:2013 - Eurocode 7: Geotechnical design - Part 1: General rules. London: BSI.
2. British Standards Institution (BSI), 2017. BS 8006-2:2011+A1:2017 - Code of practice for strengthened/reinforced soils and other fills - Part 2: Reinforced soils and fills. London: BSI.
3. British Standards Institution (BSI), 2016. BS 8006-1:2010+A1:2016 - Code of practice for strengthened/reinforced soils and other fills - Part 1: General principles. London: BSI.
4. Warrington, D., 2020. Analytical Boussinesq solutions for strip, square, and rectangular loads [online]. Available at: https://vulcanhammer.net/2020/01/29/analytical-boussinesq-solutions-for-strip-square-and-rectangular-loads/ [Accessed 18/03/2025].
5. British Standards Institution (BSI), 2010. BS EN 14490:2010 - Execution of special geotechnical works. Soil nailing. London: BSI.
6. British Standards Institution (BSI), 2018. BS EN ISO 22477-5:2018 - Geotechnical investigation and testing - Testing of geotechnical works - Part 5: Testing of grouted anchors. London: BSI.
7. International Organization for Standardization (ISO), 2012. ISO 9223:2012 - Corrosion of metals and alloys — Corrosivity of atmospheres — Classification, determination and estimation. Geneva: ISO.
8. British Standards Institution (BSI), 2023. BS EN 10244-2:2023 - Steel wire and wire products. Non-ferrous metallic coatings on steel wire. Zinc or zinc-alloy coatings. London: BSI.
9. British Standards Institution (BSI), 2011. BS EN 10245-1:2011 - Steel wire and wire products. Organic coatings on steel wire. General rules. London: BSI.
10. British Standards Institution (BSI), 2001. BS EN 10245-2:2001 - Steel wire and wire products. Organic coatings on steel wire. PVC coated wire. London: BSI.
11. S.Javankhoshdel, , L.J. Sy, T. Ma, B. Cami, T. Yacoub, Limit equilibrium analysis of gabion walls. In: GeoCalgary 2022 - 75th Canadian Geotechnical Conference, Calgary, Canada, 2-5 October (2022)

SESSION 7 B
TESTING AND QUALITY(5)

Comparing continuous filament and staple fibre geotextiles for geomembrane puncture protection

Monique Albertyn[1*]

[1]Kaytech Engineered Fabrics, Technical Marketing and Design Department, 9 Kariga Street, Kaymor Industria, Western Cape, South Africa, 7350

Abstract. Geotextiles are widely used as cushioning barriers in geosynthetic lining systems, such as landfills and dam liners, to protect geomembranes from damage caused by angular and rigid drainage materials. Such materials can cause both physical damage and strain-related stress cracking, potentially compromising the liner's integrity. Protection geotextiles help distribute localized stresses, preserving the structural integrity of the liner. Specifications like those in GRI-GT12 often emphasize mass as the primary performance measure, overlooking critical mechanical properties like puncture resistance. This study compares the performance of continuous filament and staple fibre nonwoven geotextiles—both conforming to GRI-GT12—through independent laboratory testing under varying pressures. These findings underscore the need to move beyond mass-based specifications and adopt performance-driven criteria to ensure more effective and reliable geomembrane protection. The study concludes that continuous filament geotextiles provide superior performance and cost-efficiency, making them a more effective solution for geomembrane protection in high-stress environments.

1 Introduction

Geotextiles serve a vital function in geosynthetic lining systems, particularly as cushioning layers in landfill cells. The geomembrane component must be shielded from damage caused by adjacent crushed stone drainage layers. Over time, these stresses can result in physical or strain-induced damage, leading to serious environmental hazards.

The Geosynthetic Research Institute (GRI-GT12, 2010) [1] guidelines currently emphasize geotextile mass as the basis for protection specifications. However, Koerner [2] and Bouazza & Rahman [3] argue that mechanical performance properties—such as puncture resistance, tensile strength, and strain capacity—are more indicative of actual field performance than mass alone. While mass has long been regarded as a convenient measure, it is becoming increasingly clear that performance-based properties offer a more accurate evaluation of effectiveness. To this end, independent laboratory tests were performed on various continuous filament (CFN) and staple fibre (SFN) geotextiles conforming to GRI-GT12 [1] specifications.

2 Why use a protection geotextile?

*Corresponding author: moniquea@kaytech.co.za

Experimental investigation of a PVC geomembrane response to different tensile loading modes

Nesrin Akel[1*], *Laurent* Josseaume[1], *Guillaume* Stoltz[1], *Antoine* Wautier[1], *Nathalie* Touze[2] and *François* Nicot[3]

[1] INRAE, Aix Marseille Univ, RECOVER, Aix-en-Provence, France
[2] Université Paris-Saclay, INRAE, SDAR, Jouy-en-Josas, France
[3] Université Savoie Mont-Blanc, ISTerre, Le Bourget-du-Lac, France

Abstract. Geomembrane are not meant to support mechanical actions, however, one of the main causes of the malfunctioning of their waterproofing properties is attributed to the unexpected tensile forces that may be generated during its service life, and that may potentially lead to failure. Driven by this meticulous problem, this study focuses on characterizing the tensile behaviour of Polyvinyl Chloride geomembranes by evaluating their failure criteria in terms of resistance and elongation. A wide range of tensile loading rates was applied to investigate the rate-dependent effects on the material's ultimate properties. Additionally, complementary long-term (creep) tests were conducted to examine the impact of the loading weight on the failure thresholds. Based on these results, this study proves that creep behaviour can be predicted through tensile tests, provided the environmental conditions remain constant. The results highlight the important role of the loading rates on the GM performance, providing a solid base for engineering design.

Full paper to be published in:
https://www.e3s-conferences.org/articles/e3sconf/abs/2025/44/contents/contents.html

* Corresponding author: nesrin.akel@inrae.fr

Internal temperature change of various types of geomembranes subjected to tensile test

Hamza Tahir[1*], *Guillaume* Stoltz[1], *Nesrin* Akel[1], *Guillaume* Veylon[1], and *Laurent* Peyras[1]

[1]INRAE, Aix Marseille Université, RECOVER, Aix-en-Provence, France

Abstract. Geomembranes are nowadays commonly used for waterproofing of dams around the world. One characteristic taken into consideration while designing a geomembrane for a site is their tensile strength. Up to now, it is well established that the tensile strength of geomembranes is temperature dependent. For the typical polymers of geomembranes (Bitumen, EPDM, HDPE, PVC, PP), the greater the temperature during the test, the lower the tensile strength and vice versa.

To obtain comparable results between different geomembranes and between different laboratories that perform tensile tests on geomembranes, the typical test standards require a constant temperature during the test. However, when a geomembrane specimen is subjected to a tensile force, the phenomenon of heat dissipation due to the deformation of the specimen can locally modify the constant temperature conditions and therefore the behaviour of the specimen subjected to the test.

This paper focuses on quantifying the internal temperature change for various types of geomembranes during tensile tests in an attempt to better characterize the tensile strength of geomembranes. For this research, a thermal infrared camera was used to quantify the temperature change during tensile tests. Through numerous laboratory tests, it was found that the internal temperature change during tensile tests is not the same for the various types of geomembranes and is not uniform during the test. The temperature rise is significant for certain geomembranes such as, PVC and HDPE, while it is insignificant for others such as, bitumen. These results suggest that the composition of the geomembranes is the major reason that explains the various observed behaviours.

Full paper to be published in:
https://www.e3s-conferences.org/articles/e3sconf/abs/2025/44/contents/contents.html

* Corresponding author: hamza.tahir@inrae.fr

Effect of tensile load and temperature on bituminous geomembrane seams

Eric Blond[1*], *Jean-Pierre* Giroud[2], and *John* Scheirs[3]

[1]Eric Blond Consultant Inc, Montréal, Québec, Canada
[2]JP Giroud Consultant, Paris, France
[3]ExcelPlas Pty Ltd, Moorabbin, Victoria, Australia

Abstract. Geomembranes, and their seams, are exposed in the field to tensile loads and elevated temperatures. The tensile-shear strength of bituminous geomembrane seams was assessed through laboratory testing under temperatures ranging between 23 and 80°C. Constant-load (creep) tests were conducted under temperatures ranging between 23 and 60°C to measure the seam separation rate and failure time as a function of temperature. The results show that both the short-term tensile-shear strength of bituminous geomembrane seams and the seam separation rate under constant loading are a function of temperature. A theoretical analysis of the creep tests shows that the behavior of the seams is consistent with published data on the viscosity of bitumen. A practical consequence of the tests is that, unless the tensile loads exerted on a bituminous geomembrane seam dissipate (which may happen in the field under certain conditions), the relative displacement of the two seamed geomembrane sheets is likely to continue at a rate depending on tensile load and temperature, until full separation of the seam. The data provided in the paper are expected to have an impact on the way bituminous geomembrane seams are evaluated and the way bituminous geomembranes can be safely used in containment facilities.

Full paper to be published in:
https://www.e3s-conferences.org/articles/e3sconf/abs/2025/44/contents/contents.html

* Corresponding author: eric@ericblond.com

Performance testing of strained BGM welds

Preston Kendall[1], *Pau* Llinas[2], and *Mukula* Hettihewage[2]

[1]IKO Coletanche USA, Suite 400, 531 Roselane St, Marietta, GA 30060, USA
[2]Axter Australia 1302 / 50 Cavill Ave, Surfers Paradise, Queensland 4217, Australia

Abstract. Geomembranes are essential for liquid containment, with bituminous geomembranes (BGMs) benefiting from a unique composition of polymer-modified bitumen and polyester geotextile. This study examines the strain response of BGM liner systems, focusing on weld seams, which are typically the weakest points. Through uni-axial creep and multi-axial burst (MAB) testing, the viscoelastic behavior of BGM welds was investigated. Creep tests showed no rupture at 30% strain and showed substantial stress relaxation. MAB tests demonstrated that both BGM material and welds could handle strains nearing 30% before ultimate rupture suggesting BGMs have good strain tolerance compared to other geomembranes. This research provides insights into BGM performance under stress, guiding design and installation in containment applications. Further research is recommended to refine stress calculations for composite materials like BGMs and to broaden the comparative analysis with other geomembrane types.

Full paper to be published in:

https://www.e3s-conferences.org/articles/e3sconf/abs/2025/44/contents/contents.html

SESSION 7 C
REINFORCEMENT APPLICATIONS (7)

Oosterweel connection - optical fiber monitoring of a 17-meter high reinforced fill structure

Nicolas Denies[1*], *Maximilien* Van Breusegem[1], *Jan* Couck[2], *Jos* van der Ploeg[3], *Nathan* Lauwers[4], *Steven* De Maesschalck[5], *Francesco* Masola[6] and *Jan* Ruigrok[7]

[1]Buildwise, 1342 Limelette, Belgium
[2]Vlaamse Overheid, Afdeling Geotechniek, 9052 Zwijnaarde, Belgium
[3]Lantis, 2000 Antwerpen, Belgium
[4]Stadsbader, 8530 Harelbeke, Belgium
[5]Texion Geokunststoffen, 2000 Antwerpen, Belgium
[6]Maccaferri, 40132 Bologna, Italy
[7]Arcadis Nederland, 3812 GV Amersfoort, The Netherlands

Abstract. As part of the infrastructure works on the Antwerp Ring, a large number of reinforced fill structures have been constructed in recent years. These structures include reinforced fills with gentler slopes as well as those featuring vertical or near-vertical facings. Within the framework of this extensive road infrastructure project, the client Lantis has selected a reinforced fill structure approximately 17 meters high and 160 meters long, with a near-vertical facing for monitoring deformations in the geogrids ensuring its stability. This paper presents the instrumentation of the geogrids using optical fiber technology and the results of measurements conducted over the past three years at the site. The results are analyzed in accordance with design requirements and their projections.

Full paper to be published in:
https://www.e3s-conferences.org/articles/e3sconf/abs/2025/44/contents/contents.html

* Corresponding author: nicolas.denies@buildwise.be

Geometric changes of reinforced soil walls: monitoring and impact on facing conditions during construction and using stage

Maciej Machowski[1*],

[1]Przedsiębiorstwo Realizacyjne INORA sp. z o.o., P. S. Wyszyńskiego 11, 44-100 Gliwice, Poland

Abstract. The article explores reinforced soil walls, focusing on the use of different reinforcement types and facings, and introduces a novel method for inspecting geometric changes using 3D laser scanning. This method, rarely applied to reinforced soil retaining walls, allows for precise monitoring of wall deformations, which is crucial for ensuring structural safety. The author discusses potential risks associated with exceeding deformation limits and highlights how laser scanning can support safety analysis. Real-life examples show how this technology captures geometry and geometric changes during both construction and operation, offering detailed measurements and facilitating ongoing maintenance. The article emphasizes the growing need for advanced technologies in the construction industry, particularly for large surface area structures like reinforced soil walls. It also addresses challenges in displacement estimation during the design phase and monitoring during construction and operational stages. The insights provided are valuable for all stakeholders in the investment process, including designers, contractors, supervisors, and infrastructure managers.

Full paper to be published in:
https://www.e3s-conferences.org/articles/e3sconf/abs/2025/44/contents/contents.html

* Corresponding author: tech@inora.pl

Numerical study on the performance of reinforced fill structure using marginal fill

Ahsan Rehman Khan[1*], *Gemmina* Di Emidio[1]

[1]Laboratory of Geotechnics, Dept. Civil Engineering, Ghent University, Belgium,

Abstract. Reinforced fill structures (RFS) play a vital role in geotechnical engineering applications which includes retaining walls, embankments, retaining landfill structures, & slope stabilization. The use of geosynthetics enhances the stability of soil, helps to distribute the loads evenly and reduces settlement. They also provide a better alternative in terms of cost, aesthetics, simplified construction and adaptability to different site conditions. The choice of a backfill material is a critical parameter in the design and construction of a RFS. Usually, granular material is considered to be a conventional backfill material because of various benefits i.e. having high strength & good drainage capability. But due to shortage of granular soil, it is necessary to study other alternatives. The use of marginal fill as an alternative has been pointed out as a sustainable and effective means of attenuating the environmental impacts and reducing natural resource depletion. This paper presents a numerical study within the finite element method framework. The findings demonstrate that marginal fill can provide a reliable, environmentally sustainable option for RFS.

Keywords: Reinforced fill structure, marginal fill, sustainable, finite element method

Full paper to be published in:
https://www.e3s-conferences.org/articles/e3sconf/abs/2025/44/contents/contents.html

* Corresponding author: ahsanrehman.khan@ugent.be

Green vegetated reinforced soil wall with geogrid and site won materials for Raleigh park, Barnstaple

Rozhan Saeed*, *Patricia* Guerra-Escobar, *Pablo* Bernardini, *and Muneeb* Tahir

Geosynthetics Ltd., United Kingdom

Abstract. For a new residential development called Railegh Park, it was required to design and construct a reinforced soil wall using site won materials. The project is located in Barnstaple, Devon in the South West of the UK. This paper explores the design and construction of the reinforced soil wall utilizing geogrid reinforcement, built with site-won granular head deposit material classified as Class 1A/1B. The wall is 200m approx. and reaches a maximum height of 6.2 meters with a 70-degree slope face. The design considers a live load landscape surcharge of 10 kPa on top of the wall and aims for a design life of 120 years. The analysis encompasses three different combinations (A, B, and C) to ensure comprehensive assessment and optimization of structural integrity. The resulting optimal design includes 17 layers of geogrid reinforcement. Each layer is wrapped around using Erosion Control mat Landlok at intervals of 600mm, providing enhanced stability and erosion resistance. Additionally, a steel mesh system was employed to support the steep face slope, achieving an angle of 70 degrees. This paper demonstrates that with proper design and material selection, it is feasible to construct durable and stable reinforced soil walls using site-won materials, capable of meeting long-term performance requirements under specified loading and environmental conditions.

1 Introduction

1.1 Project Description

The Raleigh Park project is a site located at Raleigh Park, North Road, Barnstaple, United Kingdom . The site is located approximately 1km north of Barnstaple town centre as shown on Figure 1 below. The construction of a reinforced soil wall using geogrid reinforcement was required. One of the key challenges was to utilize site-won materials—materials sourced directly from the construction site—for the wall's construction. The use of site-won materials offers numerous benefits, including cost savings, environmental sustainability, and practical advantages in terms of material availability. This report explores the benefits, challenges, and considerations of using site-won granular materials in the design and construction of a reinforced soil wall, incorporating geogrid reinforcement to enhance structural integrity and stability.

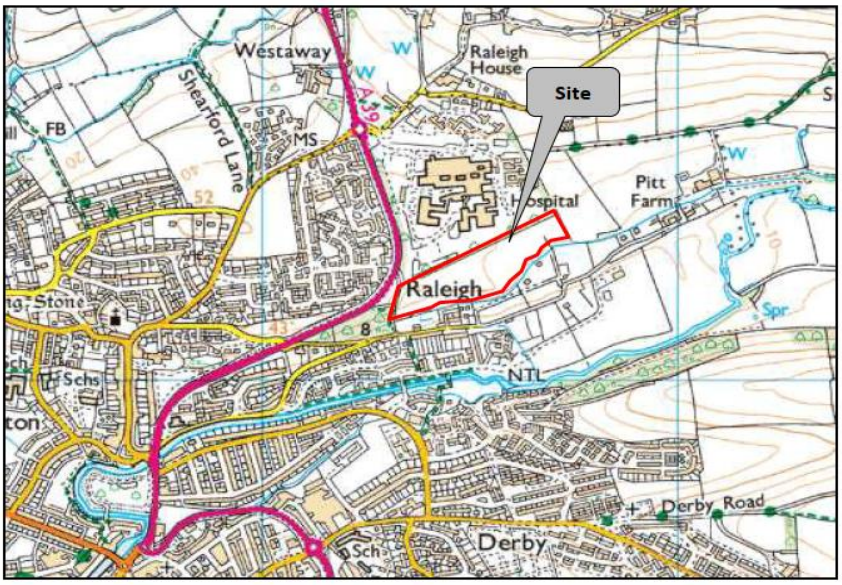


Fig. 1. Site Location

1.2 Project Background

The project involves the construction of a reinforced soil wall as part of a residential development located in Barnstaple, Devon. The site encompasses approximately 4.17 hectares of grassed agricultural land, with varied topography that includes gently sloping areas and a more pronounced slope in the southern part of the site. Given the site's geographical location, a reinforced soil wall was needed to support a steep slope with a maximum height of 6.2 meters.

The goal of using site-won materials was to reduce transportation costs, minimize environmental impact, and ensure that the materials used were suitable for the local conditions.

1.3 What is Site-Won Materials?

Site-won materials refer to soils that are available on the construction site itself, including soil, gravel, rock, and other aggregates. These materials are typically excavated, processed, and used directly in the construction process, as opposed to purchasing imported materials. Site-won materials can be used for various construction elements, including embankments, foundations, and in this case, reinforced soil walls.
In the context of this project, the site-won materials used for the construction of the reinforced soil wall were granular deposits found within the site boundaries, classified as Class 1A/1B. These materials were deemed suitable for use with geogrid reinforcement to provide the necessary strength and stability for the wall.

1.4 Benefits of Using Site-Won Materials

Using site-won materials in the construction of reinforced soil walls provides several key benefits:

- **Cost Reduction:**
  One of the primary advantages of using site-won materials is the cost savings associated with avoiding the need to purchase and transport materials from external suppliers. Transportation costs, which can be significant, are minimized, reducing the overall construction costs for the project.

- **Environmental Sustainability:**
  By using materials that are already available on-site, the need for quarrying or transporting materials from other locations is reduced, which helps to minimize the environmental impact of the construction process. This can lead to lower carbon emissions and reduced fuel consumption, contributing to a more sustainable construction project.

- **Availability and Practicality:**
  Site-won materials are immediately available, which can help speed up the construction process. Since these materials are sourced locally, there is no reliance on external suppliers, which can help mitigate supply chain delays or material shortages.

- **Material Compatibility:**
  The use of site-won materials ensures that the materials are well-suited to the local environmental conditions. In the case of the reinforced soil wall, the site's granular deposits were classified as suitable for use in the wall design, ensuring compatibility with the geogrid reinforcement system.

- **Reduced Waste:**
  When site-won materials are used efficiently, there is often less waste generated during construction, as any surplus material can be re-used on-site for other purposes (e.g., landscaping, drainage works).

2 Design Considerations

2.1 Design and Construction of the Reinforced Soil Wall with Geogrid

The reinforced soil wall was designed to provide the necessary structural support for the steep slope, with a maximum height of 6.2 meters and a 70-degree slope face. To ensure the stability of the wall and prevent failure, geogrid reinforcement was incorporated. The Geogrid helps to reinforce the soil by providing tensile strength and improving the shear strength of the soil structure.

- **Geogrid Selection:**
  The geogrid used in the design was selected based on its ability to withstand the loads and environmental conditions expected over the wall's 120-year design life. The geogrid was installed in layers, with each layer extending horizontally to increase the wall's resistance to sliding and deformation. The geogrid layers were spaced at 600mm intervals to optimize the wall's performance.

- **Layering System:**
  The wall design consisted of 17 layers of geogrid reinforcement, as shown on Figure 2 below, each carefully wrapped in an erosion control mat to prevent soil erosion in the face. The layers were strategically placed to support the lateral pressure and the loading on the top of the wall.

- **Steel Mesh Support:**
  In addition to geogrid reinforcement, a steel mesh system was employed to support the steep slope face, helping to achieve the 70-degree angle required. The steel mesh provided additional strength and stability, ensuring the integrity of the wall during the construction process.

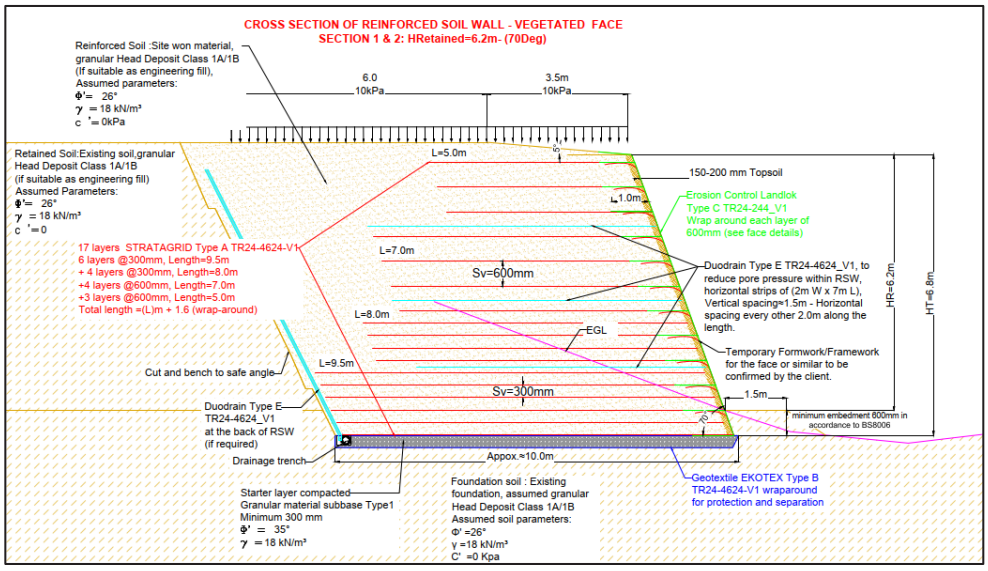


Fig. 2. Geometry cross section of Reinforced Soil Wall.

2.2 Challenges and Considerations

While the use of site-won materials offers significant benefits, there are some challenges and considerations that need to be addressed:

- **Material Quality Control:**
  It is essential to ensure that the site-won materials meet the necessary engineering specifications for the project. In this case, the granular material was classified as Class 1A/1B, suitable for use in reinforced soil walls, but this classification required careful testing and analysis to ensure compliance with standards.

- **Material Processing:**
  Site-won materials may require processing, such as grading, compaction, or stabilization, before they are suitable for use in the construction of a reinforced soil wall. This can add additional time and cost to the project, although the overall benefits still outweigh the costs.

- **Design Adaptation:**
  The wall design must be flexible to accommodate variations in the quality of site-won materials. For instance, if the material's properties are not uniform across the site, adjustments to the geogrid reinforcement or wall geometry may be necessary to ensure the wall's stability.

2.3 Soil Parameters and Surcharges

The following geotechnical properties have been assumed for the calculations of the reinforced soil wall.

Table 2. Soil properties used in calculations.

Soil Type	Soil Description	Soil Class	Effective Angle of Shearing Resistance ϕ'(°)	Unit Weight γ (kN/m³)	Effective Cohesion C' (kpa)
Reinforced Fill	Site won material, granular Head Deposit	Class 1A/1B	26	18	0
Backfill	granular Head Deposit	Class 1A/1B	26	18	0
Starter Layer	Compacted Granular material Subbase	Type 1	35	18	0
Foundation Soil	Existing foundation assumed granular Head Deposit Class	Class 1A/1B	26	18	0

- **Groundwater:** No presence of groundwater table in this case.

3 Sustainable Reinforced Soil Wall solution

3.1 Design Method and Standards

The design for the internal and external stability of the reinforced soil wall and the global stability for the design approaches 1 and 2 [1, 2 ,3 ,4 ,5]. The final design proposal consisted of uniaxial woven geogrids with ultimate tensile strength of 60kN/m as reinforcement with the use of compacted site won granular material classified as Class 1A/1B. The total running length of the reinforced soil wall is approximately 200m with a maximum height of 6.8m and a slope angle of 70 degrees. Figure 3 shows the construction stage of reinforced soil wall.

3.2 Sustainable Reinforced Soil Wall Design

The reinforced soil wall and its construction stages are outlined as follows, with additional details illustrated in Figures 3, 4, and 5. The wall has a maximum height of 6.8 meters and a slope angle of 70 degrees, extending approximately 200 meters in length. It is designed to withstand a surcharge of 10 kPa, with geogrid reinforcement applied at 300/600 mm spacing across 17 layers.

The geogrid reinforcement includes the following configurations:

- 6 layers of geogrid (60 kN/m) spaced at 300 mm, with lengths of 9.5 meters plus a 1.6-meter wrap-around.
- 4 Layers of geogrid (60 kN/m) spaced at 300 mm, with lengths of 8.0 meters.
- 4 Layers of geogrid (60 kN/m) spaced at 600 mm, with lengths of 7.0 meters plus a 1.63-meter wrap-around.
- 3 layers of geogrid (60 kN/m) spaced at 600 mm, with lengths of 5.0 meters plus a 1.63-meter wrap-around.

The foundation begins with a 300 mm starter layer of compacted granular material (Type 1), separated by a geotextile wrap. The reinforced fill material consists of site-won granular Head Deposit Class 1A/1B, while the retained fill and foundation soil are also granular Head Deposit Class 1A/1B.To protect against erosion and wash-out, each 600 mm compacted fill layer is covered with an Erosion Control TRM wrap on the face. External formwork is constructed using a steel mesh framework to maintain the 70-degree slope angle.

A reinforced soil wall with geogrid is a sustainable solution due to its efficient use of materials and its ability to reduce environmental impact. Geogrids, typically made from polymers, provide tensile strength to the soil, allowing for the construction of steep and stable walls with minimal excavation and backfill requirements. This reduces the need for extensive concrete or steel reinforcements, which have a higher carbon footprint. Additionally, the flexibility of geogrid-reinforced walls makes them resilient to seismic activity and differential settlement, ensuring long-term durability and reducing the need for frequent repairs. By integrating locally available soil and reducing construction waste, these systems align with principles of sustainable engineering, making them an eco-friendly choice for modern infrastructure projects.



Fig. 3. The construction stage: Shows placing layers of Geogrid filling with site-won material.



Fig. 4. The construction stage: showing face framework and Erosion control for protection.



Fig. 5. The construction stage: showing the final face of the Reinforced Soil Slope.

4 Conclusion

The use of site-won materials in the construction of the reinforced soil wall for the Raleigh Park project with geogrid reinforcement provides several advantages, including significant cost savings, environmental sustainability, and the practicality of using locally available materials. When combined with geogrid reinforcement, site-won materials can offer a durable, stable, and cost-effective solution for constructing reinforced soil walls, capable of meeting long-term performance requirements.

This approach demonstrates that with proper testing, design, and material selection, reinforced soil walls built with site-won materials can provide an effective and sustainable solution for managing steep slopes and other challenging site conditions. As such, the project serves as a model for future construction efforts that prioritize cost efficiency, sustainability, and the responsible use of local resources.

References

1. British Standard, BS8002:2015. Code of practice for Earth Retaining Structures. British Standard Institution, London. UK. (2015)
2. British Standard, BS8006-1:2010. Code of practice for the Strengthened/ Reinforced Soils and other fills. British Standard Institution, London. UK. (2010)
3. British Standard EN 1997-1:2004+A1:2013 Eurocode 7: Geotechnical Design, Part 1: General Rules. British Standard Institution, London. UK. (2013)
4. British Standard EN 2011-PD 6694-1: Recommendations for the design of structures subject to traffic loading, London. UK. (2011)
5. S.Strata. Use of Geogrids for Soil Reinforcement. Manual for Reinforced Walls and Slopes, Embankment on Soft Soils and Foundation Reinforcement, UK. (2015)

Slope protection using geosynthetic materials - a case study on the graveyard complex of mataram royal king

Dhinta Ayundya Nurjannah[1*], *Nadya Ayu* Anindita[1], *Dandung Sri* Harninto[2], *Ardyan* Badriza[3], and *Jaja* Subagja[4]

[1]PT. Geoforce Indonesia, Engineering Department, 10210 Central Jakarta, Indonesia
[2]PT. Geoforce Indonesia, President Director, 10210 Central Jakarta, Indonesia
[3]PT. Geoforce Indonesia, Construction Department, 10210 Central Jakarta, Indonesia
[4]PT. Geoforce Indonesia, Sales Department, 10210 Central Jakarta, Indonesia

Abstract. This paper presents the study case of landslide occurred at the Imogiri Cemetery, Mataram Royal Kings Graveyard Complex. On March 17, 2019, a landslide occurred, it was expected to have been triggered by heavy rainfall of 148 mm/day intensity. The study was carried out by slope stability modelling using PLAXIS software. Based on the results of field observations and numerical analysis, the type of slope failure that has occurred is a translational landslide. The failure line is between hard soil layer that tends to be horizontal and weak surface soil. In anticipating the occurrence of subsequent landslides, a reinforcement solution is needed with a combination of Geosynthetic and bored pile at the bottom of the slope which functions as a counterweight. The output of this analysis safety factor value is around 1.55 for the static load. This design also considered the earthquake pseudo-static load, where the result of the safety factor was 1.15 and fulfilled the criteria stated in Indonesian National Standard for Geotechnic Design Requirement (the slope safety factor must be above 1.10). The combination of Geosynthetic and Bored Pile application work effectively as a retaining wall because it is a more economical solution, faster and more environmentally friendly.

Full paper to be published in:
https://www.e3s-conferences.org/articles/e3sconf/abs/2025/44/contents/contents.html

* Corresponding author: dhintaayundya1608@gmail.com

SESSION 7 D
DESIGN AND MODELISATION (3)

Seismic performance of reinforced soil walls on Big Almaty Ring Road in Kazakhstan

Anna Kuznetsova[1*], *Evgeniy* Orlov[2], and *Svetlana* Park[2]

[1]Soterra Engineering, 105066, 13/1 Niznaya Krasnoselskaya, Moscow, Russia
[2]AsiaGeoCentre, 050012, 68-bDosmukhamedova, Almaty, Kazakhstan

Abstract. Almaty region was subjected to a severe 6.1 MSK earthquake on the 4th of March 2024. Dozens of reinforced soil walls (RSW) were hit by the impact. This made it possible to conduct the first study of the seismic resistance of RSW in Kazakhstan. During the site visits, a visual inspection was carried out, confirming the absence of structural defects in the structures. This article describes the condition of two notable non-load bearing bridge abutments and one longitudinal wall. The first one – 15 m high Aksenger – the tallest RSW abutment in Kazakhstan with no sighs of seismic impact. The second one - Sewer collector – in comparison with failed traditional abutment on the other side of a bridge. The last one – longitudinal retaining wall with built-in corrugated steel culvert.

1 Reinforced soil walls seismic behaviour

In the last decades of 20the century a new technology of reinforced soil wall (RSW) construction had been developed widely in US, Europe and Asia. In CIS countries it had arrived in early 2000s starting from Russia and Kazakhstan.

The most complex and extensive investigation of RSW seismic behaviour was described by Tatsuoka et al [1] after the Hyogo-ken Nanbu (Kobe) earthquake (M = 7.2). This topic was further developed in the form of experimental study of an earthquake performance of modular-block reinforced soil retaining walls which were backfilled with sand using large scale benchmark shaking table tests by Ling et al [2].

The first experiment on this topic on the post-soviet area was held in Russia in 2009 by prof. Belayev [3]. It was related to ongoing Sochi Winter Olympic Games 2014 preparation and provided a gateway for RSW as a cost-effective, sustainable and resilient technique.

Each seismic region has unique combination of earthquake parameters. And even though in Kazakhstan hundreds of RSW have been constructed during the last 20 years, no research or monitoring program was conducted on this topic.

The article describes the first stage of Kazakhstan RSW seismic behavior monitoring that consisted of objects selections, visual inspection and maintenance data collection. The overall aim of the study is to confirm the effectiveness of using RSW in the seismic conditions of eastern Kazakhstan.

* Corresponding author: anna.kuznetsova@soterra.ru

2 Almaty earthquake

Almaty and its environs belong to the Almaty seismically active region of MSK 9-10 zone in south-eastern Kazakhstan. In the beginning of 2024 two earthquakes hit the city. On the 23rd of January – relatively soft with an epicenter at a distance of 264 km and 6.7 magnitude. City residents felt a swaying, like in a moving train carriage. On the 4th of March a 6.1 magnitude severe high frequency earthquake occurred with an epicenter located 43 km from Almaty. Due to its proximity, it had a stronger impact. It caused local utilities damages, cracks in the walls of houses and broken window glasses. Metro was evacuated, classes have been cancelled in schools and universities. The danger of the last earthquake is that it occurred on the Kemin fault, that was an epicenter of the strongest 1911-year event that almost destroyed the predecessor of Almaty town Verniy. And therefore, this leads seismologists to think that this fault may come back to life again.

A few RSW with high density polyethylene (HDPE) uniaxial Tensar geogrids and TW1 modular block facing on Big Almaty Ring Road (BAKAD) and adjacent territories had been affected by the event. This had provided a perfect opportunity to verity a high seismic resistance of this type of structures specifically for Kazakhstan.

2.1 Aksenger

In 2022 a RSW non-bearing bridge abutment was constructed as a part of a flyover on CH 210+10 of BAKAD. Setting an absolute hight record of that time for Kazakhstan with almost 16m tall modular block facing.

Due to the weak soils in the foundation (Cu=35kPa), structure was based on piles as shown on the Figure 1. Geogrid spacing 450-300mm, design strength - 65,27kN/m.

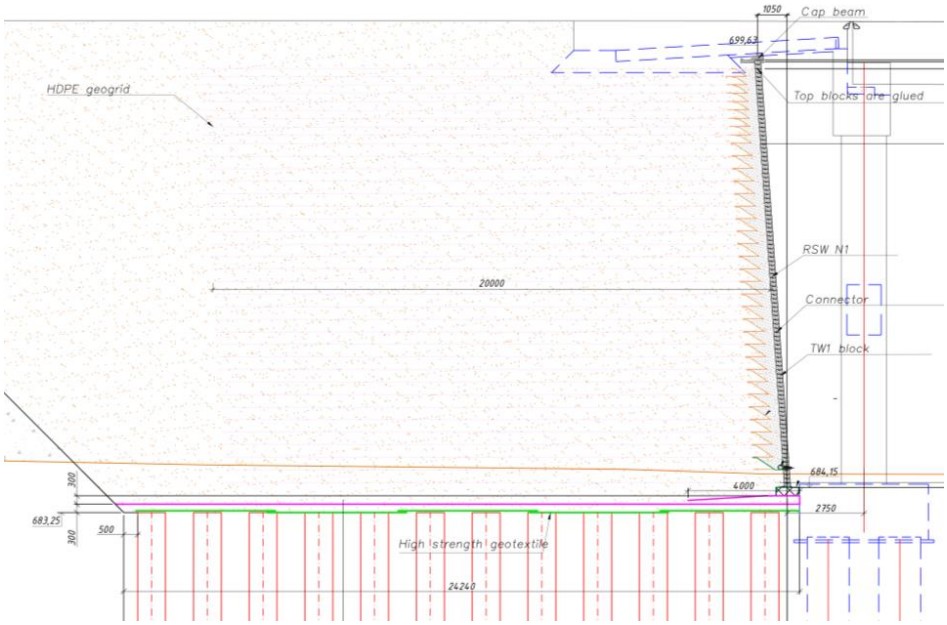


Fig. 1. Aksenger RSW design.

Visual inspection results and construction phase photos confirmed the excellent condition of the object as shown on the Figures 2-3.

a)



b)

Fig. 2. Aksenger side view: a) during construction and b) after earthquakes.

a)



b)



Fig. 3. Aksenger view along the flyover axile: a) during construction and b) after earthquakes.

No defects, or block displacements had been observed.

2.2 Sewer collector

In 2022 a non-load bearing RSW abutment was constructed on CH 356+22 across the sewer collector. Foundation soil was presented by soft silty clay (c=16,6kPa, φ=16.5°) and this caused an extensive reinforcement length as shown on the Figure 4. Geogrid spacing 450mm, design strength - 40,15kN/m. The second abutment was built in a traditional technique.

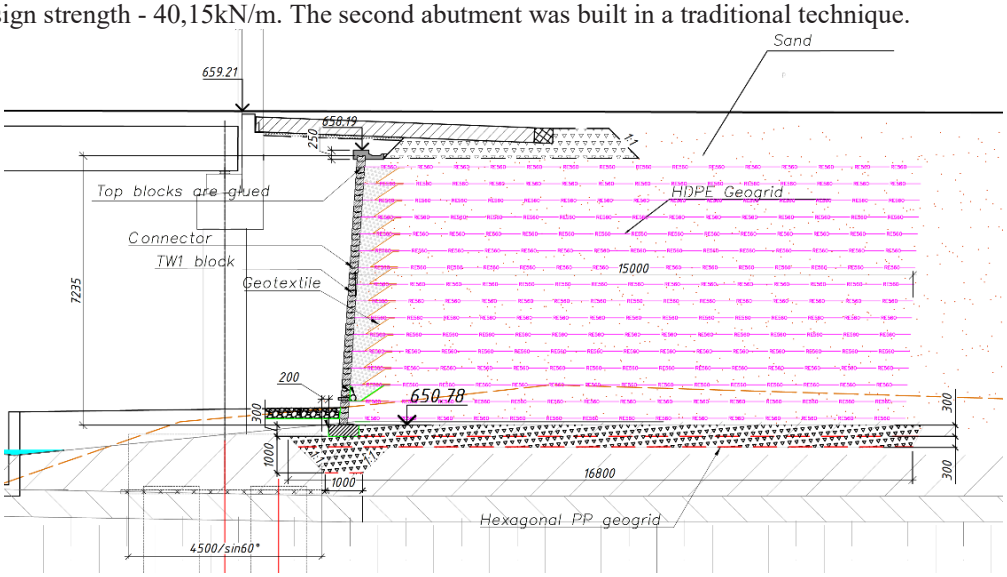


Fig. 4. Sewer collector RSW design.

Visual inspection results and construction phase photos confirmed the excellent condition of the object as shown on the Figures 5-6.

a)



b)



Fig. 5. Sewer collector wall side view: a) during construction and b) after earthquakes.

a)



b)



Fig. 6. Sewer collector wall facing : a) during construction and b) after earthquakes.

The RSW abutment withstood the earthquake without deformation or destruction unlike the traditional construction in front of it.

Two abutments are shown on the Figure 7. Comparing to the perfectly stable RSW, the other abutment was hit by seismic event and soft soil issues.



Fig. 7. Bridge overview.

On spring, significant deformations occurred along the traditional approach. It was decided to provide an additional load banquet at the toe, preventing slip surface formation. Newly constructed reinforced concrete retaining wall at the toe is shown on the Figure 8, 9.



Fig. 8. Repair measures.

Later it was also covered by boulders more evenly.



Fig. 9. Repair measures final state.

Cracked and sealed concrete slabs on the road shoulder, shown on the Figure 10 testify to what had happened. Also, a top layer of asphalt was milled and a new overlay installed.



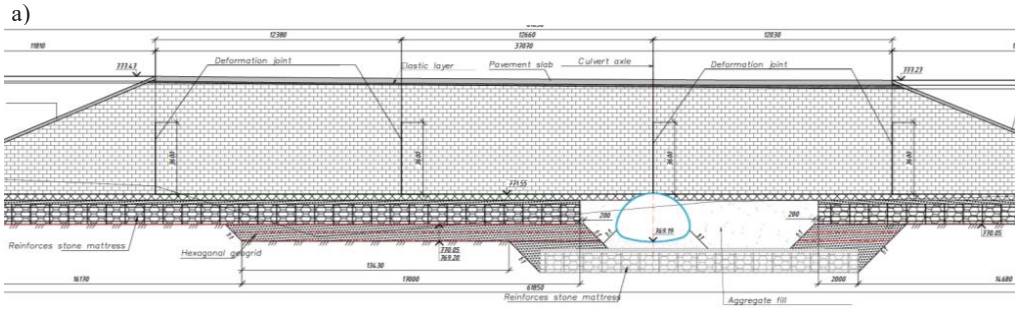
Fig. 10. Repaired shoulder.

Further condition monitoring is important to determine the effectiveness of the measures taken.

2.3 Olympic village

In 2020 an access to the Republican Olympic training base in Almaty region was constructed. Geogrid spacing 450mm, design strength – 21,44kN/m. The road passes through a ravine with 20m deep soft (Cu=40kPa) soil foundation. A stiff geogrid reinforced stone platform was proposed to provide a global stability and reduced settlement. In the lowest ravine point a corrugated steel pipe was installed as shown on the Figure 11.

a)



b)

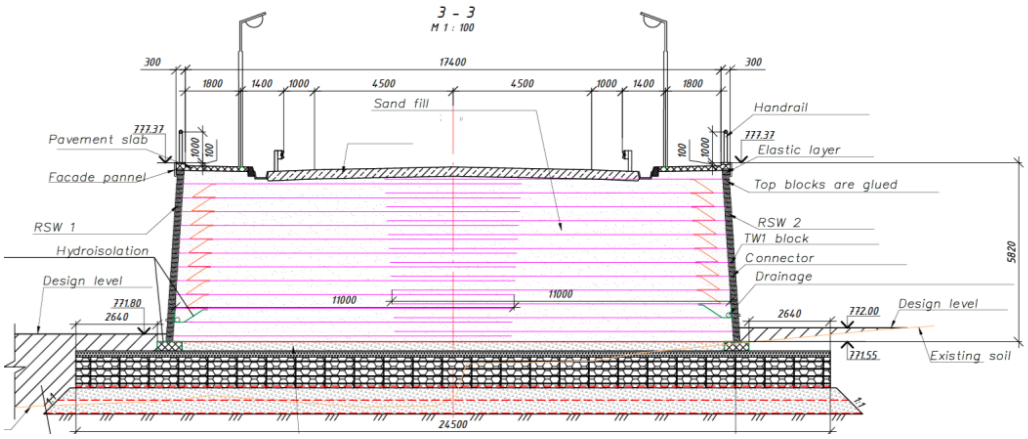


Fig. 11. RSW facade and section: a) Facade view and b) Cross-section.

Due to the low strength of foundation, the entire structure was built with a 10cm additional rise to compensate a long-term settlement. However, after 3 years of operation, there was no significant settlement and the site remains elevated relative to the design level.

After seismic events no signs of deformations have been observed as show on the Figure 12.



Fig. 12. Olympic village RSW.

Pavement, handrail and barrier along the site are perfectly even as shown on the Figure 13. This is a clear proof of the soft soil settlement issues absence and no deformations caused by earthquakes. Handrail hight is taller right above the culvert and this creates an optical curvature illusion.



Fig. 13. Olympic village pavement and barrier.

3 Conclusion

Almaty region of Kazakhstan is located in a hight seismicity area. Events with magnitude 4 are usual and are observed several times a year. Stronger earthquakes up to 6 occur 1-2 times a year. Two events in the beginning of 2024 had shown a significant impact on buildings and infrastructure. That danger of further lithological processes activation forces local scientists to search more actively for earthquake-resistant technologies.

Three structures, described in the paper are based on soft soil foundations with three different options for solving this problem:

- concrete piles on Aksenger;
- longer grids on Sewer collector;
- geogrid reinforced stone platform on Olympic village.

All structures demonstrated excellent performance under seismic conditions. Reinforces soil walls had proved their high resilience and resistance specifically to Eastern Kazakhstan type of earthquake.

Authors would like to acknowledge Daulet Murzagulov for providing photos from construction and operation phases.

References

1. F. Tatsuoka, J. Koseki and M. Tateyama, Performance of reinforced soil structures during the 1995 Hyogo-ken Nanbu Earthquake, in Proceedings International Symposium on Earth Reinforcement, IS Kyushu 96, Balkema, Vol 2, 105-140 (1996).
2. H.I. Ling, Y. Mohri, D. Leshchinsky, C. Burke, K. Matsushima, & H. Liu, Large scale shaking table tests on modular-block reinforced soil retaining wall. J. Geotech. Geoenviron. Eng. **131(4)**, 465–476, (2005)
3. V.S. Belayev,Testing of reinforced soil structures. Railway Track and Facilities Journal **3**, 33-35, (2011)

Selection of intensity measures for displacement prediction of geosynthetic reinforced soil walls under seismic loading

Cihan Cengiz[1*], *Ismail Emrah* Kilic[2], and *Erol* Guler[3]

[1]Deltares, Boussinesqweg 1, 2629 HV Delft, the Netherlands
[2]Royal HaskoningDHV, 3818 EX Amersfoort, the Netherlands
[3]George Mason University, 4400 University Dr, Fairfax, VA 22030, USA

1. **Abstract.** The accurate prediction of damage in Geosynthetic Reinforced Soil (GRS) walls is critical for the safe and cost-effective design of infrastructure systems, particularly in seismic or extreme loading environments. This paper investigates the selection of appropriate Intensity Measures (IMs) for predicting damage to GRS walls under various loading scenarios. A comprehensive analysis is conducted, comparing different IMs based on their correlation with wall performance indicators, including displacement, reinforcement strain, and facing deformations. The study explores the suitability of IMs such as peak ground acceleration (PGA), spectral acceleration, and Arias intensity, focusing on their ability to provide reliable predictions of wall damage under dynamic conditions. Numerical simulations are employed to model the behavior of GRS walls under seismic loads, and empirical data from previous tests is used to validate the results. The findings suggest that certain IMs, particularly those capturing energy dissipation and frequency content, offer enhanced predictive capability compared to traditional measures. This research provides valuable insights into the selection of IMs for improving the design and resilience of GRS walls, with implications for both the seismic and geotechnical engineering communities.

Full paper to be published in:
https://www.e3s-conferences.org/articles/e3sconf/abs/2025/44/contents/contents.html

* Corresponding author: cihan.cengiz@deltares.nl

Design method for combined geocell and geogrid stabilisation of paved roads

Pietro Rimoldi[1*]

[1]Civil Engineering Consultant, 20157 Milano, Italy

Abstract. Paved roads are often built on soft soils. The effect of repeated and cyclic loads on soft soils generates absolute and differential settlements, which may quickly degrade the quality of roads. Geocells and geogrids improve the modulus and strength of the stabilised composite layers and the durability of the road structure, while drastically reducing the required quantity of aggregate materials. The paper aims to present the design methods for combined geocell and geogrid stabilisation of paved roads. The proposed design method takes into account the wheel loads, the number of passages, the geometry, the subgrade characteristics, the geocell and geogrid properties. A final design example is included.

1 Concepts and fundamental principles

According to ISO 10318-1 [1], geogrids are bi-dimensional geosynthetics which can be defined as "planar, polymeric structure consisting of a regular open network of integrally connected, tensile elements, which can be linked by extrusion, bonding, or interlooping or interlacing, and the openings of which are larger than the constituents"; geocell are defined as "manufactured, three-dimensional, expandable, polymeric structure consisting of contiguous discrete cells which are subsequently filled". The typical structure of geogrids and geocells is shown in Fig. 1. The primary mechanisms by which geosynthetics can limit the deformations of a granular layer is the confinement mechanism, which requires that confining stresses on the soil particles are developed. For 2D geosynthetics the confinement can occur via interlock and/or surface friction; for interlock to be effective the geosynthetic is required to have apertures (see the structure of geogrids in Fig. 1) into which granular particles can penetrate; in case of geocells, confinement is afforded by the walls of the cells (Fig. 1). Geogrids and geocells provide the lateral restrain mechanism for horizontal stresses generated by the self weight of soil and by wheel loading. The magnitude by which the horizontal and vertical strain in the aggregate layer can be reduced depends on the stiffness of the composite layer, which a function of the geosynthetic tensile stiffness required for the stress equilibrium as well as of the efficiency of the aggregate/geosynthetic interaction. During the application of loads to the base and subbase, the interaction with geosynthetics distributes stresses throughout the stabilized granular layers, thus reducing any stress transmitted to the underlying subgrade.

* Corresponding author: pietro.rimoldi@gmail.com

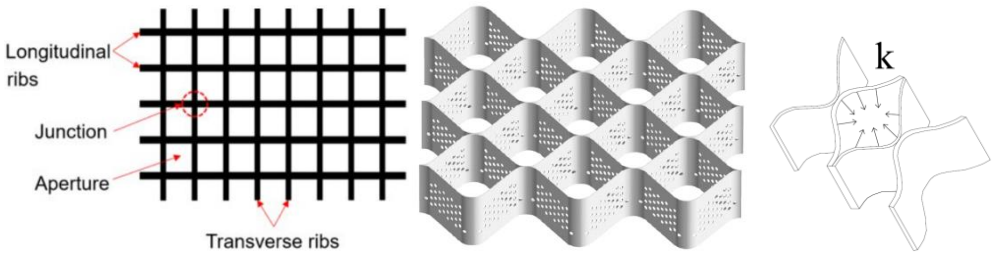


Fig. 1. Typical structure of geogrids (left) and geocells (centre), and primary mechanism of confinement by the 3D structure of geocells (right). (k = 3D confining stresses)

The creation of a confined zone with limited particle movement naturally limits the deformation of the granular layer as a whole. The resultant reduced stress transmission to the subgrade limits its deformation. It is typically the underlying subgrade that is the weakest material in the construction section and one of the principles aimed in developing a confined and stabilized granular layer is to limit any stress and strain transmission to this weaker layer.

Reducing the horizontal strains means to decrease the Poisson ratio of the soil – geosynthetic composite material compared to the Poisson ratio of the unstabilised soil; reducing the Poisson ratio means to increase the horizontal stiffness; like for a beam, the increased horizontal stiffness means that the geosynthetic stabilized soil layer is able to distribute the vertical stresses σ_{v0} applied at the top surface on a wider area (Fig. 2); the improved vertical load distribution on the subgrade affords a higher bearing capacity of the stabilized system compared to that of the unstabilised system.

While vertically loaded, additional shear stresses are transmitted from the aggregate to the geosynthetic which results in horizontal strains. The shear resistance caused by friction or mechanical interlock generates a physical restraint of the aggregate particles. The stiffness provided by the geosynthetic reduces the development of lateral tensile strains and stresses in the base aggregate over a defined height above the geosynthetic, called the 'confined zone', by preventing the development of explicit displacements of the aggregate (Fig. 3). In the case of geocells, the fully confined zone includes two parts: 1) the cell height, and 2) a limited thickness above and possibly beneath the geocell. Above the confined zones, a transition zone is developed, which extends until there is no influence on the granular layer from the geogrid or geocell (unconfined zone). From Fig. 3 it is evident that, when a relatively high aggregate thickness is required, designing with multiple layers of geosynthetics would allow to reduce or eliminate the unconfined zone, thus affording a more effective stabilization.

2 Design method for paved roads

The proposed design method for combined geocell and geogrid stabilisation of paved roads is modified from the AASHTO (1993) Guide [2], largely based on empirical equations.

The scheme of the unstabilised and geogrid + geocell stabilised paved road is shown in Fig. 4. The AASHTO equation for designing flexible road pavements has the following form:

$$\log_{10}(W_{18}) = Z_R \times S_o + 9.36 \times \log_{10}(SN+1) - 0.20 + \frac{\log_{10}\left(\frac{\Delta PSI}{4.2-1.5}\right)}{0.40 + \frac{1094}{(SN+1)^{5.19}}} + 2.32 \times \log_{10}(M_R) - 8.07 \quad (1)$$

where:

W_{18} = predicted number of 80 kN (18 kips) ESALs

Z_R = standard normal deviate (example : Z_R = -1.645 for 95 % reliability)

S_o = combined standard error of the traffic prediction and performance prediction

SN = Structural Number (inches)

ΔPSI = difference between the initial design serviceability index, p_o, and the design terminal serviceability index, p_t

M_R = subgrade resilient modulus (psi)

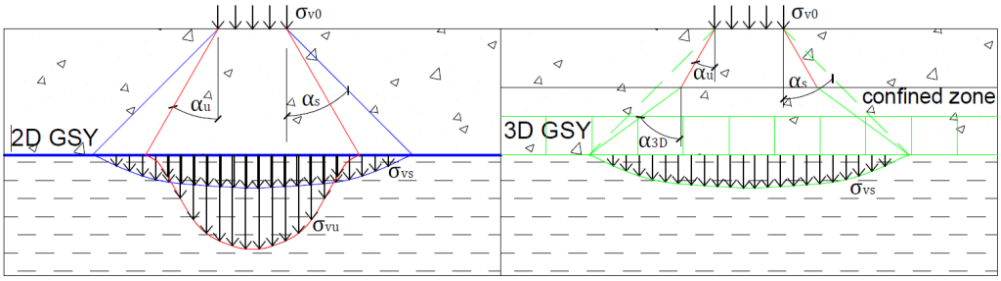


Fig. 2. Increase of the load distribution angle with geogrid (left) and geocell (right) confinement of granular layers (σ_{v0} = vertical stress applied at the top surface; σ_{vs} = vertical stress on the subgrade with stabilized granular layer; α_u = load spreading angle with unstabilized granular layer; α_s = load spreading angle with stabilized granular layer; α_{3D} = load spreading angle within 3D structure)

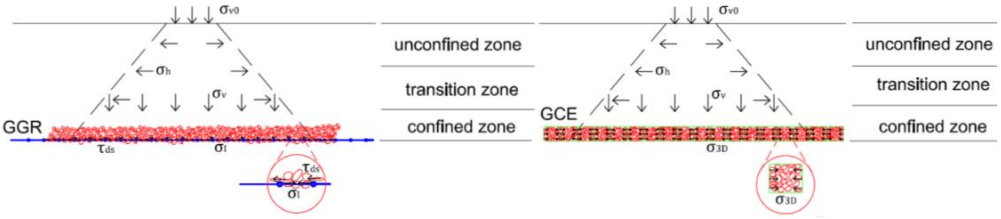


Fig. 3. Transition zones with geogrids (left) and geocells (right). (σ_{v0} = vertical stress applied at the top surface; σ_h = horizontal stress; σ_v = vertical stress at the subgrade interface; σ_{3D} = geocell confining stress; GGR = geogrids; GCE = geocells)

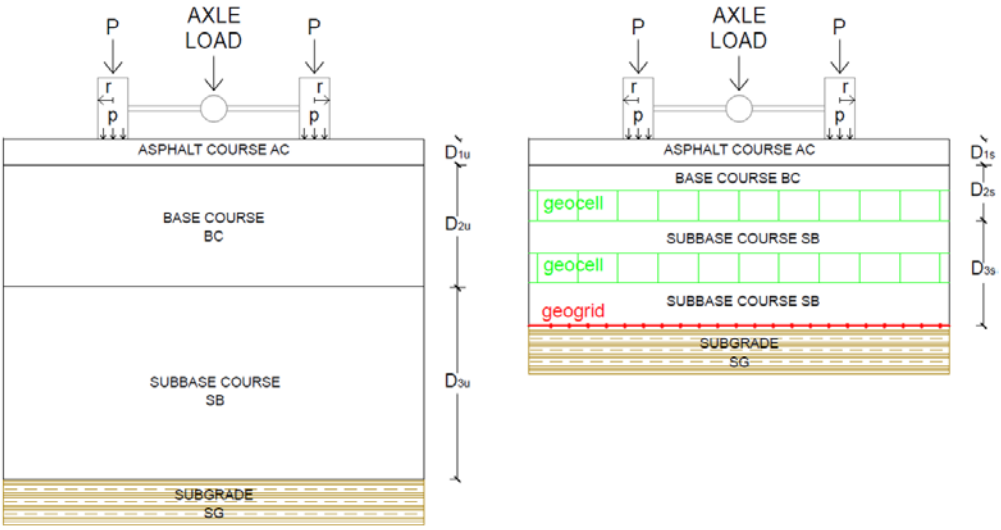


Fig. 4. Schemes of the unstabilised (left) and the geogrid + geocell stabilised paved road (right)
References for the input parameters related to loads, pavement structure and subgrade support can be found directly in the AASHTO (1993) Guide [2].

2.1 Layers contribution

The AASHTO method utilizes the term Structural Number (SN) to quantify the structural strength of a pavement required for a given combination of soil support, total traffic, reliability, and serviceability level. The required SN is converted to actual thickness of

asphalt, base and subbase courses by means of appropriate layer coefficients representing the relative strength of the construction materials.

The design equation for the unstabilised paved road is as follows:

$$SN = a_{1u} \cdot D_1 + a_{2u} \cdot D_{2u} \cdot m_2 + a_{3u} \cdot D_{3u} \cdot m_3 \quad (2)$$

where:
a_{iu} = i-th layer (unstabilised) coefficient
D_i = i-th layer (unstabilised) thickness (inches or mm)
m_i = i-th layer drainage coefficient

The subscripts 1, 2 and 3 refer to the asphalt course AC, aggregate base course BC, and subbase course SB (if applicable), respectively.

Typical values of SN can be between 1 and 10 inches (25.4 – 254 mm).

2.2 Layer coefficients

Layer coefficients are empirical relationships between the Structural Number (SN) and layer thicknesses which express the relative ability of a material to function as a structural component of the pavement. The magnitude of the layer coefficient is a function of the modulus of the material of each layer.

Typical layer coefficients are:

- Asphalt course = 0.44
- Crushed aggregate for base course = 0.12 – 0.14
- Engineered fill for subbase course = 0.10 – 0.11

The asphalt pavement contribution to the Structural Number is given by the term $a_1 \cdot D_1$; in this term the wearing course contribution is neglected and only the binder contribution is taken into account; hence a_1 and D_1 refer to the binder course only.

Reference values for layer coefficients can be found in the AASHTO Guide [2].

2.3 Drainage coefficients

The drainage characteristic of the pavement is accounted for through the use of specific coefficients m_i. When no data is available for evaluating the drainage coefficients, it is assumed that: $m_i = 1.0$

3 Design of the unstabilised paved road

The procedure for designing the layout of the unstabilised paved road is the following:

1) set analysis period Y, standard normal deviate of reliability Z_R, combined standard error S_o, ΔPSI, as indicated in AASHTO (1993) Guide [2];
2) calculate the traffic load in the design lane W_{18}, as indicated in AASHTO Guide [2];
3) set the CBR value of the subgrade, CBR_{sg};
4) calculate the resilient modulus, M_r, of subgrade with the following equations:

$$M_r = 17.6 \, (CBR_{sg})^{0.64} \quad \text{(MPa)} \quad (3)$$

$$M_r = 2.552 \, (CBR_{sg})^{0.64} \quad \text{(psi)} \quad (4)$$

5) solve Eq. (1) using the M_r value in psi and get SN (inches); calculate SN in mm:

$$SN_{mm} = SN_{inches} \cdot 25.4 \quad (5)$$

6) set the asphalt type, asphalt thickness D_1 and layer coefficient a_1 based on empirical or numerical calculations or national regulations, considering the minimum asphalt and base / subbase course thickness as indicated by AASHTO (1993) [2]

7) set base course type and layer coefficient a_{2u}; set the drainage coefficient m_2 as indicated by AASHTO (1993) [2]
8) calculate the base course modulus E_{bcu} with the following formula:

$$E_{bcu} = (10^{((a_2 + 0{,}977) / 0{,}249)}) / 145 \quad \text{(MPa)} \quad (6)$$

9) set subbase type and layer coefficient a_{3u}; set the drainage coefficient m_3
10) calculate subbase course modulus E_{sbu} with the following equation:

$$E_{sbu} = (10^{((a_{3u} + 0{,}839) / 0{,}227)}) / 145 \quad \text{(MPa)} \quad (7)$$

11) calculate the thickness of subbase course: Eq. (2) can be solved for one variable only, usually for the base thickness D_2, once the asphalt thickness D_1 has already been set based on other criteria. When the subgrade is very soft (example: $CBR_{subgrade} < 2.0$) it is usually required to design for base + subbase. In these case usually the subbase is used also to provide a working platform for construction. Since Eq. (2) can be solved only for either base or subbase thickness, it is suggested that the subbase thickness D_{3u} is designed to resist the construction activities before building the base and asphalt layers. During construction activities the subbase works like an unpaved road, loaded by the passages of trucks and dumpers. Hence the subbase can be designed as an unstabilised aggregate layer, using as example the Giroud - Han method [3], with the following input parameters:
- number of passages: $N = 100 – 10{,}000$ (depending on total construction activity prior of building base and asphalt layers);
- allowable rut depth: $S_3 \leq 25$ mm (if larger rut depth is allowed, then ruts shall be filled and graded before the construction of the base layer);

12) calculate the thickness of base course: now the only unknown is the base course thickness D_{2u}, which can be easily calculated with Equation (2).
13) Alternatively, the thickness of the unstabilised base and subbase courses can be calculated using Equation (2) by a trial-and-error procedure.

4 Modified AASHTO method for stabilised paved roads

The structural contribution of geocells and geogrids to a flexible pavement system can be quantified by the increase in the layer coefficients of the aggregate base and subbase courses.

Equation (2) now becomes:

$$SN = a_1 \cdot D_{1s} + a_{2s} \cdot D_{2s} \cdot m_2 + a_{3s} \cdot D_{3s} \cdot m_3 \quad (8)$$

where a_{2s} and a_{3s} are the layer coefficients, obtained from the values of the increased modulus of base and subbase due to geocells and geogrids stabilisation.
The Modulus Improvement Factor (MIF), proposed by Pokharel [4], is expressed as:

$$MIF = E_{cs} / E_{cu} \quad (9)$$

where E_{cs} and Ecu are the moduli of the stabilized and unstabilised layers.

MIF values are determined based on the results from laboratory testing on flexible pavement systems with and without geocells and geogrids.

Suggested values of MIF for combined geocell and geogrid stabilisation are presented in the charts in Fig. 5, providing MIF as a function of the modulus of the unstabilised layer and of the modulus of the below layer for: 1 layer of geocells, 2 layers of geocells, and 1 layer of geogrids + 1 layer of geocells.

These charts have been obtained by the Author, adapted from Vega et al (2018) [5], and are valid only for extruded biaxial geogrids with 30x30 kN/m tensile strength and for tough geocells with $AR \leq 2$, made up of perforated strips having tensile strength (from ISO 10319 [6] tests) higher than 16 kN/m, with less than 3 % accumulated permanent deformation (tensile creep).

MIF charts for other types of geocells and geogrids shall be obtained through performance testing including validation of geosynthetics properties for design life, specific type of fill material, and modulus of subgrade (Rajagopal, et al, 2012 [7]).

4.1 Geocell geometry and aspect ratio

The stabilization effect of geocells highly depends on the geometry of the product, since at equal properties the confining effect increases with the Aspect Ratio AR:

$$AR = \text{(cell diameter B / cell height h)} \quad (10)$$

In fact, the geometry of the geocell, particularly the cell size and cell height, affects the magnitude of stabilisation. The diameter of the cells affects the density of confinement: a small-diameter cell size with a higher cell height provides a larger MIF than a large-diameter cell size with a lower cell height. It means that, if cell diameter is too large compared to cell height, the lateral confinement provided by geocells cannot limit the lateral displacements of the volume of fill in each cell. Hence the intensity of the confining stresses depends on the Aspect Ratio of the geocell and on the tensile properties of the geocell.

As above mentioned, the confined zone includes two parts (Fig. 3): cell height and limited thickness above the geocell.

With reference to Fig. 6, the aspect ratio AR can be calculated as follows:

- Cell height (see Table 1): h_{cell} = 50, 75, 100, 120, 150, 200 mm
- Distance between weld seams (see Table 1): d_{ws} = 330, 356, 445, 660, 712 mm
- Number of cells / m^2 (see Table 1): N_{cells} = 40, 35, 22, 10, 8
- Cell area (m^2): $A_c = 1 / N_{cells}$ (11)
- Cell diameter (m): $D_c = ((4/\pi) \cdot A_c)^{0.5}$ (12)
- Aspect Ratio: $AR = D_c / h_{cell}$ (13)

From Author's analyses, an empirical approximation of the thickness of the fully confined zone is given by two times the cell height divided by the Aspect Ratio; hence the confined zone can be assumed to have a thickness equal to:

$$h_{cz} = (2 / AR) \cdot h_{cell} \quad (14)$$

From above statements, with reference to Fig. 6, two criteria have to be met for optimal confinement of geocells:

- Aspect Ratio: $AR \leq 2$ (15)
- stabilized layer thickness: $h_{cz} \geq H$ (16)

where H is the thickness of the layer under consideration.

The values of AR can be estimated from Table 2.

This means that the geocell diameter cannot be selected independently from the cell height, but the geocell diameter (or, which is the same, the distance between weld seams) shall be selected according to condition (15). This also means that the calculated stabilized layer thickness H (as example: the thickness h_{bcs} of the geocell stabilised base course) shall

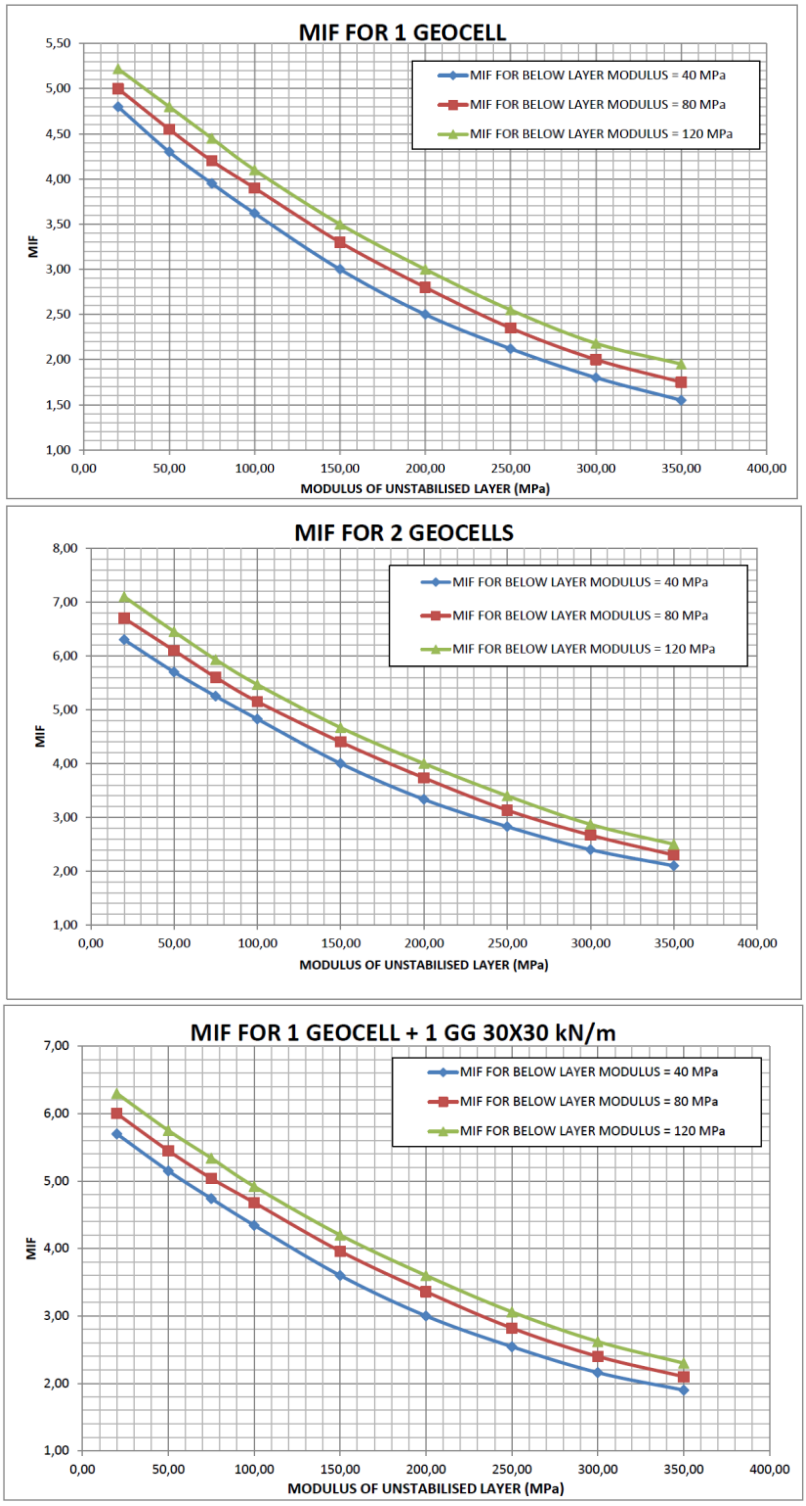


Fig. 5. Charts for 1 layer of geocells, 2 layers of geocells, and 1 layer of geogrids + 1 layer of geocells (geocells with AR ≤ 2), providing MIF as a function of the modulus of the unstabilised layer and of the modulus of the below layer (adapted from Vega et al, 2018 [5])

be compared with the selected geocell height h_{cell}: if the condition (16) is not satisfied, the design with just 1 geocell layer is not optimal; hence a design layout with 2 geocell layers or 1 geocell + 1 geogrid should be applied.

When using a design layout with 2 geocell layers, the confined zone can be assumed to have a thickness equal to twice the confined thickness for 1 geocell, hence the condition on stabilized layer thickness becomes:

$$h_{cz\text{-}2\ GCE} = 2 \cdot (2 / AR) \cdot h_{cell} \geq H \quad (17)$$

When using a design layout with 1 geocell + 1 geogrid, the confined zone can be assumed to have a thickness equal to:

$$h_{cz\text{-}GCE+GG} = [(2 / AR) \cdot h_{cell} + h_{GG}] \geq H \quad (18)$$

where h_{GG} is the thickness of the zone stabilised by the geogrid (see Fig. 3), which can be assumed to be equal to the thickness of the soil layer between the geogrid and the geocell, with the maximum value:

$$h_{GG} \leq 0.25 \text{ m} \quad (19)$$

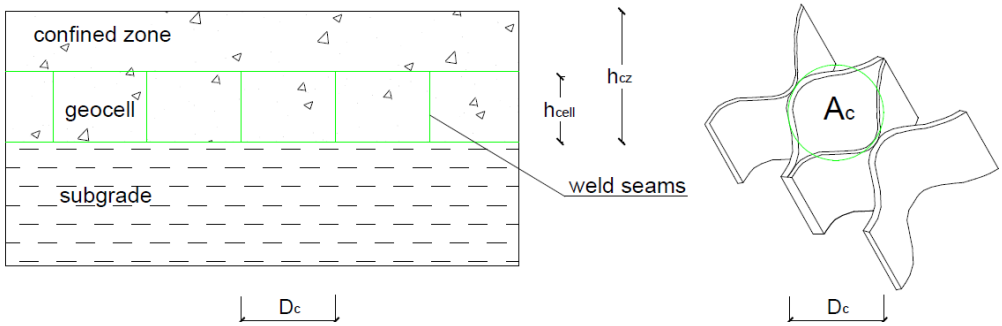


Fig. 6. Scheme for geocell geometry and Aspect Ratio

Table 1 – Aspect Ratio AR vs cell diameter and geocell height

GEOCELL GEOMETRY						
distance between weld seams	**mm**	**330**	**356**	**445**	**660**	**712**
cells density	$1/m^2$	40	35	22	10	8
cell area	m^2	0,0250	0,0286	0,0455	0,1000	0,1250
cell diameter	**m**	**0,178**	**0,191**	**0,241**	**0,357**	**0,399**
Geocell height	**mm**	**Geocell Aspect Ratio AR**				
	50	3,568	3,814	4,811	7,136	7,978
	75	2,379	2,543	3,207	4,757	5,319
	100	1,784	1,907	2,405	3,568	3,989
	120	1,487	1,589	2,005	2,973	3,324
	150	1,189	1,271	1,604	2,379	2,659
	200	0,892	0,954	1,203	1,784	1,995

4.2 Design procedure for geocell stabilised paved road

The procedure for designing the layout of the geocell and geogrid stabilised paved road is the following:

1) get SN from the previous calculation for unstabilised road
2) select the geocell layout (1 geocell, or 2 geocells, or 1 geocell + 1 geogrid) for base and subbase stabilisation
3) set MIF_{bc} from Fig. 5, based on the previously calculated modulus E_{bcu} of the unstabilised base (Eq. 11) in abscissa of the charts and the previously calculated modulus E_{sbu} of the unstabilised subbase (Eq. 12) to select the curve in charts

4) set MIF_{sb} from Fig. 5, based on the previously calculated modulus E_{sbu} of the unstabilised subbase (Eq. 7) in abscissa of the charts and the modulus E_{sg} of the subgrade (Eq. 3) to select the curve in charts
5) calculate the stabilised modulus and the stabilised layer coefficient of the base course:

$$E_{bcs} = MIF_{bc} \cdot E_{bcu} \quad \text{(MPa)} \qquad (20)$$

$$a_{2s} = 0.249 \log_{10} (145\ E_{bcs}) - 0.977 \qquad (21)$$

6) calculate the stabilised modulus and the stabilised subbase layer coefficient of the subbase course:

$$E_{sbs} = MIF_{sb} \cdot E_{sbu} \quad \text{(MPa)} \qquad (22)$$

$$a_{3s} = 0.227 \log_{10} (145\ E_{sbs}) - 0.839 \qquad (23)$$

7) calculate the thickness of the stabilised subbase course: Equation (8) can be solved for one variable only, usually for the base thickness D_{2s}, once the asphalt thickness D_{1s} has already been set based on other criteria. Like for the unstabilised subbase thickness, it is suggested that the stabilised subbase thickness D_{3s} is designed to resist the construction activities before building the base and asphalt layers, using the Pokharel method [4] with the MIF values obtained from Fig. 5, for the same above suggested input parameters
8) Check the condition on the stabilised subbase course thickness with Equations (10) ÷ (19)
9) Calculate the thickness of the stabilised base course: now the only unknown is the base course thickness D_{2s}, which can be easily calculated with Eq. (8).
10) Check the condition on the stabilised base course thickness with Equations (10) ÷ (19)
11) Alternatively, the thickness of the stabilised base and subbase courses can be calculated using Eq. (8) by a trial-and-error procedure; in any case the condition on the stabilised base and subbase course thickness shall be checked with Equations (10) ÷ (19).

5 DESIGN EXAMPLE

Let's design a paved road for the following input data:
Subgrade CBR_{sg} = 1; Initial service index: p_0 = 4.2; Terminal service index: p_t = 3.0; Reliability level: R = 99.0 (Standard normal deviate Z_R = -2.346); Combined standard error: S_0 = 0.45; Traffic in the design lane W_{18} = 16 Million ESALs.

Solving Equation (1) we get the required Structural Number: SN = 9.33 in = 0.237 m

Let's design the road structure using the following materials:

- Asphalt, with a_{1u} = 0.44
- Highly compacted granular base course, with a_{2u} = 0.14
- Granular subbase course, with a_{3u} = 0.11

For the drainage coefficients let's assume: $m_2 = m_3 = 1.00$

Let's design the unstabilised subbase thickness using the Pokharel method [4] for unpaved roads, for number of passages N = 1,000 and allowable rut depth S_3 = 25 mm.

Using the Pokharel method [4] and Eq. (2) we get the design of the unstabilised road:

- asphalt thickness = 100 mm
- base course thickness = 0.50 m
- subbase course thickness = 1.12 m

Let's now design the stabilised paved road with the following layout:

- base course stabilisation: 1 layer of geocells with h_{cell} = 150 mm, d_{ws} = 330 mm;
- subbase course stabilisation: 1 layer of geocells with h_{cell} = 200 mm, d_{ws} = 356 mm + 1 layer of extruded biaxial geogrids with 30 x 30 kN/m tensile strength.

From Eqs. (3), (6) and (7) we get: M_r = 17.62 MPa; E_{bcu} = 211 MPa; E_{sbu} = 104 MPa
From Fig. 5, with the above Moduli, we get: MIF_{bc} = 3.0; MIF_{sb} = 4.0
From Eqs. (20) and (21) we get: E_{bcs} = 633 MPa; a_{2s} = 0.259

From Eqs. (22) and (23) we get: $E_{sbs} = 418$ MPa; $a_{3s} = 0.247$

Let's design the stabilised subbase thickness using the Pokharel method [4] for unpaved roads, for number of passages N = 1,000, allowable rut depth $S_3 = 25$ mm, and $MIF_{sb} = 4.0$.

Using the Pokharel method [4] and Eq. (8) we get the design of the stabilised subbase:

- Geogrid stabilised thickness: $h_{cz\text{-}GG} = 0.25$ m
- Geocell stabilised thickness: $h_{cz\text{-}GCE} = 0.28$ m

Now let's check the condition on the stabilised layer thickness for subbase course:

- Geocell Aspect Ratio: AR = 0,954 (from Table 2)
- $h_{cz\text{-}GCE+GG} = (2 / 0.954) \cdot 0.2 + 0.25 = 0.67$ m ≥ 0.53 m → OK

Then from formula (8) we get: $D_{2s} = 0.24$ m

Let's check the condition on stabilised layer thickness for base course:

- Geocell Aspect Ratio: AR = 1,189 (from Table 2)
- $h_{cz\text{-}GCE+GG} = (2 / 1.189) \cdot 0.15 = 0.252$ m ≥ 0.24 m → OK

Therefore the design of the stabilised road is:

- asphalt thickness = 100 mm
- base course thickness = 0.24 m, stabilised with 1 layer of geocells with $h_{cell} = 150$ mm and $d_{ws} = 330$ mm
- subbase course thickness = 0.53 m, comprised with 1 layer with thickness of 0.25 m stabilised with extruded biaxial geogrids with 30 x 30 kN/m tensile strength and 1 layer with thickness of 0.28 m stabilised with geocells with $h_{cell} = 200$ mm and $d_{ws} = 356$ mm.

Hence the design with geocells and geogrids stabilisation afforded the total saving on (base + subbase) thickness = 1.72 m – 0.77 m = 0.85 m = 52.5 % saving

6 SUMMARY

The paper has presented the design method for combined geocell and geogrid stabilisation of paved roads, which takes into account the wheel loads, the number of passages, the geometry, the subgrade characteristics, the geocell and geogrid properties. Suggested values of the Modulus Improvement Factor (MIF) are presented. The design with geocells and geogrids stabilisation affords to considerably reduce the (base + subbase) thickness of paved roads.

References

1. ISO 10318-1. Geosynthetics - Part 1: Vocabulary
2. AASHTO (1993) "Guide for Design of Pavement Structures," American Association of State Highway Transportation Officials, Washington D.C
3. Giroud, J.P. and Han, J. (2004) Design method for geogrid-reinforced unpaved roads; I. development of design method, and II. calibration and applications. ASCE Journal of Geotechnical and Geoenvironmental Engineering. Vol. 130, No. 8, 775-797.
4. Pokharel, S.K. (2010). Experimental study on geocell-reinforced bases under static and dynamic loading, PhD dissertation, Civil Environmental an Architectural Eng and Graduate Faculty of The University of Kansas, USA.
5. Vega, E., van Gurp, C., Kwast, E. (2018). Geokunststoffenals Funderingswapening in Ongebonden Funderingslagen (Geosynthetics for Stabilization of Unbound Base and Subbase Pavement Layers), SBRCURnet (CROW), Netherlands.
6. ISO 10319:2015. Geosynthetics - Wide-width Tensile Test. ISO, Geneve, Switzerland
7. Rajagopal, K, Veeragavan, A., and Chandramouli, S. (2012). Studies on geocell reinforced road pavement structures, 5th Asian Regional Conference on Geosynthetics

Effects of density of geofoam cushion on seismic performance of the retaining wall: experimental study

Ayşe Edinçliler[1*], and *Bilge Sultan* Demirtaş[1,2]

[1]Boğaziçi University, İstanbul, Türkiye.
[2]İstanbul Gelişim University, İstanbul, Türkiye.

Abstract. In recent years, three important factors have been taken into account in designing safe and useful retaining walls in seismically active regions: cost, environment and earthquake performance. One of the improvement methods defined in the literature is the inclusion of the lightweight, compressible cushion layer behind the retaining wall. The lightweight materials as tire waste-sand mixtures and EPS Geofoam have various advantages such as low unit weight, low bulk density, and high vibration absorption capacity. EPS Geofoam has recently been proposed as a seismic cushion, which is an energy absorption layer due to the higher damping properties of lightweight materials depending on their density compared to the sand. This study covers the evaluation of the shaking table experiments performed on a 1/25 scaled wall model in the rigid-sided plexiglass soil box. This study aims to determine the effects of geofoam density on the seismic performance of the retaining wall with the cushion under real earthquake motion. Shaking table test results of the retaining wall with cushion are compared with the uncushioned case. Test results revealed that the cushion density has an important effect on improving the seismic performance of the wall.

Full paper to be published in:
https://www.e3s-conferences.org/articles/e3sconf/abs/2025/44/contents/contents.html

* Corresponding author: aedinc@bogazici.edu.tr

SESSION FRANCOPHONE

Réhausse des installations de stockage des déchets (ISD) – conception selon les dernières recommandations des guides du CFG et du BRGM

Mame Coumba Faye[1*], *Abdelkader* Abdelouhab[2]

[1]SOLMAX, Ingénieure d'affaires, 95873 Bezons, France
[2] SOLMAX, Docteur en géotechnique, 95873 Bezons, France

Résumé. Les géosynthétiques jouent un rôle important dans la conception des installations de stockages des déchets (ISD). Ils participent à la protection de l'environnement, la stabilité des ouvrages et la réduction des coûts. Les réhausses des casiers entrainent des contraintes supplémentaires sur les structures existantes. Ainsi des déformations supplémentaires apparaissent en favorisant un tassement différentiel et l'endommagement des systèmes d'étanchéité. L'emploi de géosynthétiques de renforcement permet d'absorber ces déformations et d'assurer la pérennité de la structure. Nous présenterons dans cet article deux exemples de projets de réhausses de casiers d'ISD pour lesquels des géosynthétiques de renforcement en polyéthylène téréphtalate (PET) ont été utilisés. Le premier projet concerne une réhausse d'un casier sur le flanc en région parisienne avec l'utilisation d'un géosynthétique de renforcement. La hauteur des nouveaux déchets est de 23 m avec des zones d'affaissement potentiels de 1 m de diamètre. Le deuxième projet concerne une réhausse au sein d'une ISD dans le Nord-Ouest avec une hauteur de nouveaux déchets d'une dizaine de mètres et des zones d'affaissements potentiels de 1 à 1,5 m de diamètre.

1 Introduction

Les besoins en stockage de déchets sont de plus en plus croissants alors que les espaces disponibles se réduisent du fait des impacts économiques et environnementaux. En effet, de nombreuses anciennes décharges sont ne sont pas étanches ou présentent un système d'étanchéité non adapté. Ainsi, il est nécessaire d'adapter la conception des installations de stockage des déchets. Les extensions des ISD existants se font par la création de réhausses en stockant entièrement ou partiellement les nouveaux déchets sur les casiers existants. Ces extensions génèrent des surcharges sur les massifs de déchets existants créant ainsi des déformations supplémentaires. Des géosynthétiques de renforcement sont utilisés dans la conception des réhausses afin de reprendre les déformations, de garantir la pérennité du système d'étanchéité et la stabilité de l'ouvrage.

* Corresponding author: mfaye@solmax.com

2 Réhausse d'ISD : principes

Les principaux types de réhausse d'ISD sont présentés ci-aprés :

- **Extension verticale pure** : en appui sur le sommet d'un casier existant. Les principales problématiques dans cette configuration sont les tassements différentiels des anciens déchets ainsi que le drainage des gaz et des lixiviats.

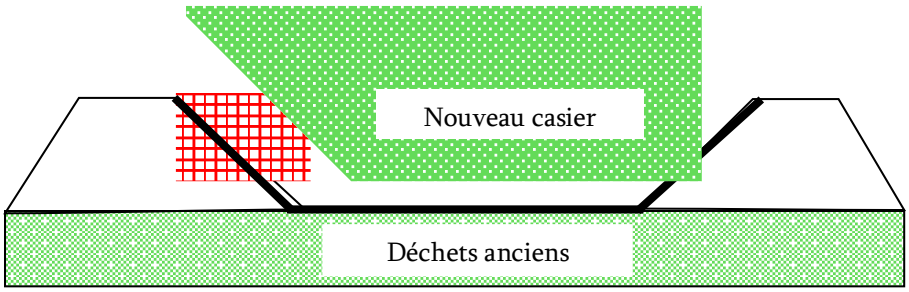


Fig. 1. Extension verticale pure

- **Extension en appui latéral** : en appui sur le substratum et le flanc du casier existant avec des problématiques liées aux déformations du massif de déchets anciens à la jonction entre ce dernier et le substratum.

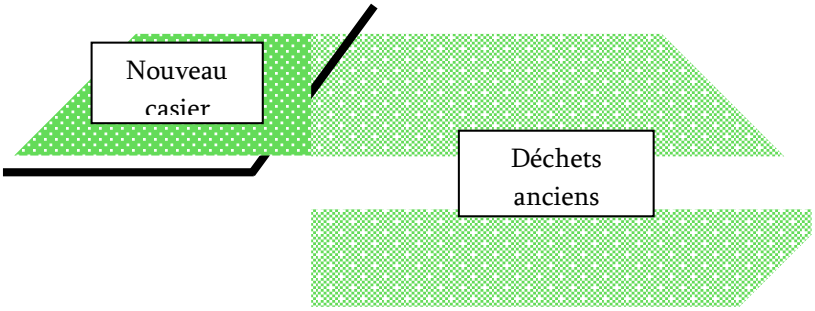


Fig. 2. Extension en appui latéral

- **Extension en appui mixte**.: une combinaison des deux précédentes extensions avec les problématiques énoncées précédemment.

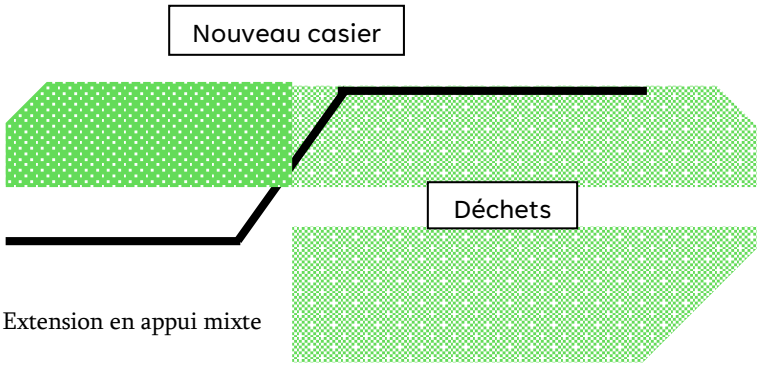


Fig. 3. Extension en appui mixte

3 Choix et principe de dimensionnement du géosynthétique de renforcement

3.1 Choix du géosynthétique de renforcement

En France, la conception des extensions d'ISDND repose sur "*Le guide de recommandations pour la conception des extensions d'ISDND en appui sur des casiers anciens* » du BRGM [1] et le « *Fascicule Installations de stockage de déchets* » du CFG [2]. Ces guides préconisent la mise en œuvre d'un géosynthétique de renforcement dans la zone de transition entre les anciens casiers et les nouveaux déchets. Compte tenu des phénomènes d'hydrolyse, survenant dans les massifs de déchets à long terme, le géosynthétique doit présenter une bonne résistance dans cet environnement. Les phénomènes d'hydrolyse d'origine alcaline peuvent entrainer une perte de raideur de certains polymères. Le guide du BRGM recommande alors l'utilisation des géosynthétiques de renforcement en Polyvinyle Alcool non hydrosoluble (PVA) [1].

A contrario, en cas d'hydrolyse à un pH neutre acide, le PET ne présente pas de perte de raideur significative. Ainsi, le PET offre une bonne résistance chimique à la plupart des acides et à de nombreux solvants.

Resistant against	Polymer, under short and long loading duration									
	PA (6 and 6.6)		PET		PP		PE		Plasticized PVC	
	Short[1]	Long[1]	Short	Long	Short	Long	Short	Long	Short	Long
Dilute acids	+	o	++	+	++	++	++	++	+	o
Concentrated acids	o	–	o	–	++	+	++	+	o	–
Dilute alkali	++	+	++	o	++	++	++	++	++	+
Concentrated alkali	o	–	o	–	++	++	++	++	+	o
Salt (prine)	++	++	++	++	++	++	++	++	++	++
Oil (mineral)	++	++	++	++	+	o	+	o	+	o
Glycol	+	o	++	o	++	++	++	++	++	++
Micro organisms	++	+	++	++	++	++	++	++	+	o
UV Light	+	o	+	o	o	–	o	–	+	–
UV Light (stabilized)	++	+	++	+	++	+	++	+	++	+
Heat, dry (up to 100°C)	++	+	++	++	++	+	++	o	+	o
Steam (up to 100°C)	++	+	o	–	o	–	o	–	o	–
Moisture absorption	++	++	++	++	++	++	++	++	+	+
Detergents	++	++	++	++	++	++	++	++	++	++
Tendency to creep	++	+	++	++	+	o	+	o	+	o

Degree of resistance: – = not resistant; o = moderate; + = passable; ++ = good.
This assessment of resistance is valid under normal conditions and temperatures:
1. During construction stage, 2. During usage, 3 Depending on type of plasticizer.

Fig. 4. Extrait de" Geosynthetics in civil engineering – GPTM Van Santvoort" **[3]**

Les pertes de résistance, pour des fibres PET à haute ténacité, ont été évaluées par Elias et Van Schoors, et sont synthétisés dans le tableau ci-dessous:

Table 1. Perte de resistance du PET en fonction du PH[3]

pH	7	9	10	11	12
Perte par an (%)	0,08	0,25	0,35	0,5 à 1,1	4,1

Ainsi pour des pH inférieurs à 9 (cas de la plupart des déchets en décomposition), le risque de dégradation chimique est très faible.

Par ailleurs, le facteur de réduction à prendre en compte, pour différentes températures et en fonction du temps, peut être calculé à partir des courbes d'Arrhenius (cf Fig.5).

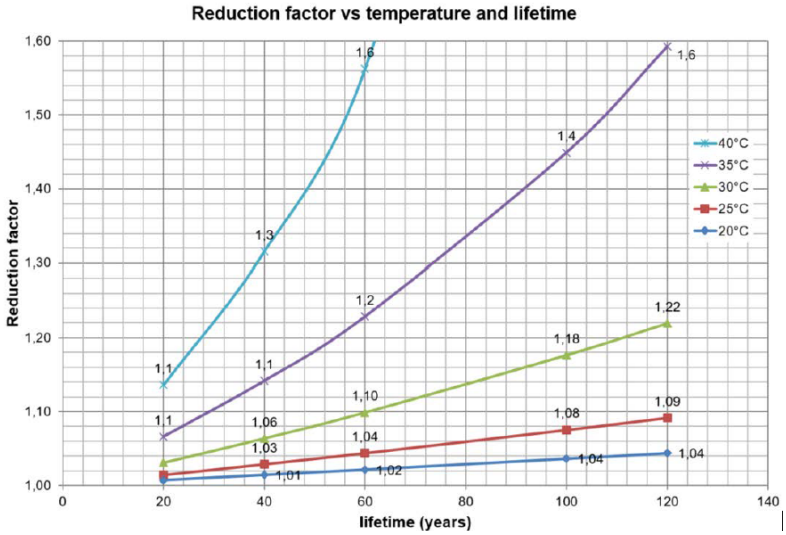


Fig. 5. Courbes d'Arrhenius

Pour déterminer la résistance à long terme du géosynthétique, des facteurs de réduction liés au pH, à la température et à la durée de vie sont pris en compte. Ainsi, les produits en PET peuvent être utilisés jusqu'à un pH de 9. Enfin, signalons que les matériaux présentent rarement un pH supérieur 9 et il n'y a généralement pas de contact direct avec le produit.

3.2 Principe de dimensionnement

Le géosynthétique de renforcement doit être dimensionné de sorte à réduire les tassements différentiels afin d'éviter la rupture ou la perte de fonctionnalité du dispositif d'étanchéité. Le dimensionnement du géosynthétique est réalisée selon la méthode de calcul RAFAEL pour la sécurisation des ouvrages en zone à risque d'effondrement. Pour simuler les affaissements localisés, un diamètre nominal d'affaissement (D) de 1 à 2 m est pris en compte. Lorsqu'un affaissement localisé survient dans les déchets anciens, le géosynthétique de renforcement mis en place dans la couche de forme, se déforme en membrane et se met en tension au-dessus de la zone d'affaissement. Un transfert de charge se fait alors vers les zones d'ancrage empêchant ainsi l'effondrement de la structure.
Les données nécessaires au dimensionnement des ouvrages de renforcement sont [1] et [2]:

- Le diamètre nominal de l'affaissement localisé ($\mathbf{1\ m < D < 2\ m}$) ;
- La déformation maximale admissible pour la durée de service de l'ouvrage

(Inférieure ou égale à 3%). Elle correspond à la déformation admissible pour une géomembrane en PEHD de 2 mm de la barrière active;

- La surcharge due aux nouveaux déchets limitée à n x D

La figure 6 présente une coupe schématique d'une réhausse d'ISDND avec les composants et paramètres pris en compte.

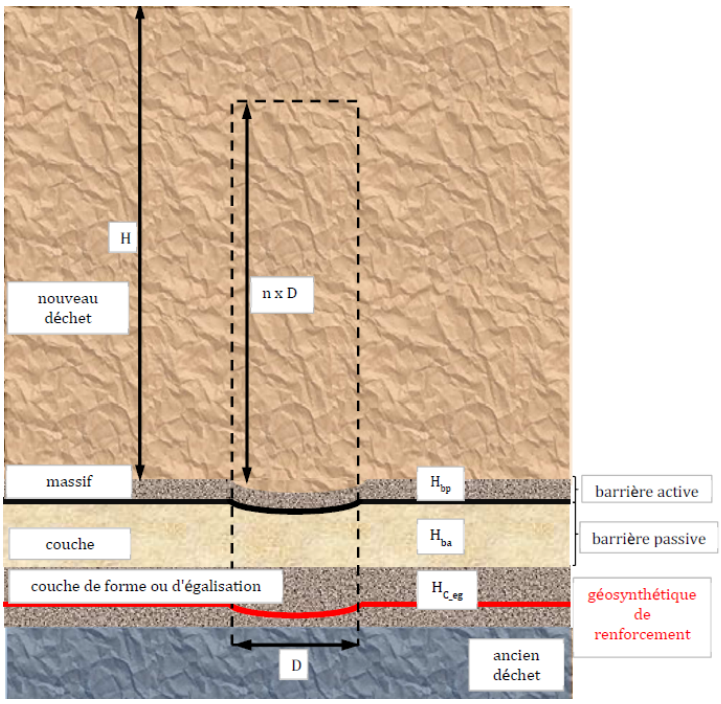


Fig. 6. Coupe schématique d'une réhausse

La justification du géosynthétique et de la stabilité de la cavité repose sur les Eurocodes et la norme XP G38-065. Le principe consiste à fixer la déformation maximale admissible pour la durée de vie de l'ouvrage.

Pour ces ouvrages, il est considéré une distribution verticale et uniforme de la contrainte. Celle-ci est déterminée ? à l'ELS et à l'ELU, par les formules suivantes :

- **A l'ELS :**

$$\sigma=(\gamma déchet*n*D+\gamma ba*Hba+\gamma bp*Hbp+\gamma Ceg*HCeg+P)+Q \quad (1)$$

- **A l'ELU :**

$$\sigma=\gamma Gsup*(\gamma déchet*n*D+\gamma ba*Hba+\gamma bp*Hbp+\gamma Ceg*HCeg+\gamma GSup*P)+\gamma QSup*Q \quad (2)$$

Avec :

γdéchet = Poids volumique des déchtes ;

n = facteur d'effet de voute (n=3 pour les OM) ;

D = Diamètre de l'affaissement ;
γba = Poids volumique de la barrière active ;
Hba = Epaisseur de la barrière active ;
γbp = Poids volumique de la barrière passive ;
Hbp = Epaisseur de la barrière passive ;
γCeg = Poids volumique de la couche d'égalisation ;
HCeg = Hauteur de la couche d'égalisation ;
P = Surcharges permanentes ;
Q = Surcharges temporaires ;
γGSup = 1,35
γQSup = 1,50

Ensuite, les tractions nécessaires à l'ELS et L'ELU sont déterminées grâce aux formules (3) et (4) ci-dessous :

$$T_{d,ELS} = \frac{\sigma_{v,k} \cdot D}{2} \cdot \sqrt{1 + \frac{1}{6 \cdot \varepsilon_{max}}} \quad (3)$$

$$T_{d,ELU} = \frac{\sigma_{v,d} \cdot D}{2} \cdot \sqrt{1 + \frac{1}{6 \cdot \varepsilon_{ult}}} \quad (4)$$

Avec :
εmax : déformation maximale admissible
εult : déformation maximale ultime.

En cas d'affaissement localisé, des glissements surviennent au niveau des ancrages. Ainsi, la mobilisation progressive et l'élongation des géosynthétiques dans les zones d'ancrage (Briançon et Villard 2006) doivent être prises en compte dans la conception.

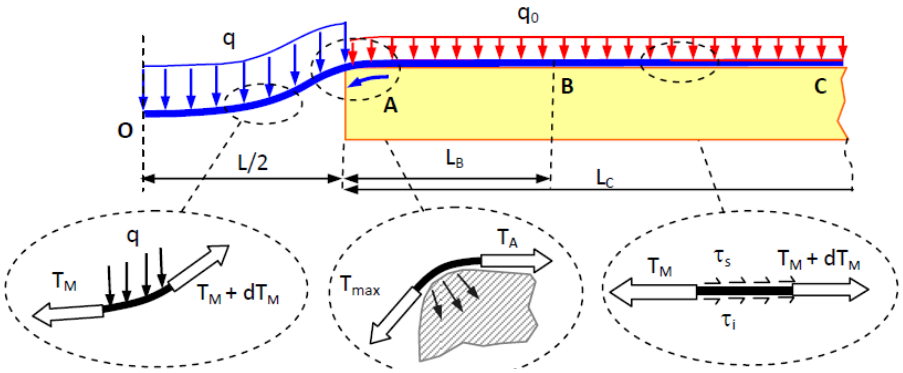


Fig. 7. Prise en compte des glissements au niveau des ancrages (Briançon et Villard, 2008)

4 Etudes de cas

Nous présenterons dans ce chapitre deux exemples de projet de réhausse d'ISDND pour lesquelles des géosynthétiques de renforcement en PET ont été utilisés.

4.1 Réhausse de casier de déchets ménagers

Le premier exemple concerne un projet de réhausse d'une ISDND recevant des déchets ménagers en région parisienne. Dans le cadre du projet, il est prévu la réhausse sur le flanc d'un casier avec l'utilisation d'un géosynthétique de renforcement en PET (cf Fig 7). L'étanchéité du stockage est assurée par un géosynthétique bentonitique et une géomembrane.

La figure ci-dessous présente le projet de réhausse de l'ISDND.

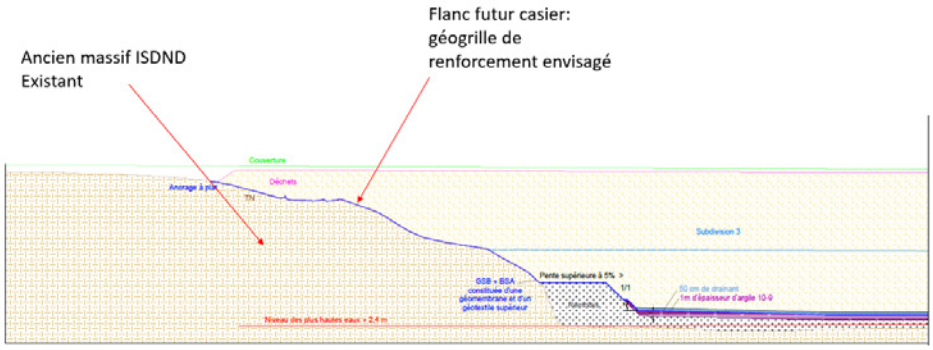


Fig. 8. Réhausse d'une ISDND de déchets ménagers

Les paramètres pris en compte pour le dimensionnement du géosynthétique de renforcement sont synthétisés dans le tableau 2 ci-dessous.

Tableau 2. Paramètres de calcul.

Largeur ou diamètre de la zone de tassement localisée (D)	Hauteur des déchets sus-jacents (H)	Hauteur de la barrière active (Hba)	Epaisseur de la barrière passive (Hbp)	Epaisseur de la couche d'égalisation au-dessus du renforcement (HC_eg)
1 m,	23 m	0,5 m	0,5 m	0,8 m

Afin de limiter les déformations et l'endommagement du sytème d'étanchéité, nous avons préconisé l'utilisation d'un géosynthétique de renforcement en PET de 800 kN/m de résistance à la traction à court terme.

4.2 Réhausse de casier de déchets ultimes

La décharge étudiée dans le cadre de ce projet se situe dans le Nord-Ouest de la France. Il s'agit d'un centre de stockage de déchets ultimes permettant le stockage de millions de m3 de déchets dangereux.

Dans le cadre du projet, il est prévu une réhausse avec une hauteur de nouveaux déchets de 10 à 12 m sur une surface de 16 200 m². Le système d'étanchéité de l'ancienne décharge est assurée par un revêtement d'argile géosynthétique (GCL) associée à une géomembrane. La réhausse pourrait engendrer des tassements différentiels des anciens déchets.
Afin de limiter les tassements et par conséquent l'endommagement du système d'étanchéité, un renfort en géosynthétique a été utilisé.

Les paramètres pris en compte pour le dimensionnement du géosynthétique de renforcement sont synthétisés dans le tableau 3 ci-dessous.

Table 3. Paramètres de calcul.

Largeur ou diametre de la zone de tassement localisée (D)	Hauteur des déchets sus-jacents (H)	Hauteur de la barrière active (Hba)	Epaisseur de la barrière passive (Hbp)	Epaisseur de la couche d'égalisation au dessus du renforcement (HC_eg)
1 à 1,5 m	> 11 m	0,5 m	1,0 m	0,5 m

Sur la base de ces données, nous avons prescrit les géosynthétiques de renforcement suivant :

- Pour une zone d'affaissement localisée de 1,5 m de diamètre, un géosynthétique de renforcement en PET présentant une résistance à la traction de 1400 kN/m à court terme ;
- Pour une zone d'affaissement de 1 m de diamètre, un géosynthétique de renforcement en PET de 600 kN/m de résistance à la traction à court terme.

5 Conclusion

Dans le cadre des réhausses d'ISDND, le renforcement géosynthétique des décharges permet :

- d'éviter les tassements différentiels pendant et après le dépôt des déchets ;
- d'éviter l'endommagement du système d'étanchéité ;
- de résoudre les contraintes économiques et environnementales.

Les géosynthétiques en PET peuvent être utilisés.

La méthode de calcul actuelle permet d'estimer la résistance à la traction du géosynthétique

Cette méthode de calcul conduit à des résultats conservateurs lorsque le diamètre de l'affaissement est bien estimé.

De nouvelles études et expériences doivent être menées pour améliorer ou définir une méthode de conception réaliste.

References

1. B. Chevrier, P. Michel, F. Garrido, Guide de recommandations pour la conception des extensions d'ISDND en appui sur des casiers anciens, BRGM/RP-69455-FR (2020)
2. CFG, Fascicule Installations de stockage de déchets – guide d'utilisation des normes de dimensionnement dans la conception des ouvrages avec géosynthétiques : géotextiles et produits apparentés (2021)
3. G.P.T.M Van Santvoort, Geotextiles and Geomembranes in Civil Engineering (1994)

Utilisation des géosynthétiques dans le cadre des travaux de « digues » du site pilote écrêteur de crue Seine-Bassée

Alexandre Valenziano[1], *et Pascal* Laugier[2]

[1]Antea Group, Pôle Infrastructures, 45166 Olivet Cedex, France
[2]EPTB Seine Grands Lacs, Direction de la Bassée et de l'Hydrologie, 75012 Paris, France

Résumé. Le site pilote Seine-Bassée est le premier ouvrage écrêteur de crue d'un ensemble de neuf espaces endigués localisés dans le lit majeur de la Seine. Cette opération consiste en la création d'un espace d'environ 4 km², ceinturé par un remblai périphérique (dit « digue »), dont la fonction est de stocker temporairement les eaux de la Seine lors des crues majeures. Cela permettrait une diminution de la ligne d'eau en aval et réduirait les dommages socio-économiques dus aux inondations en Île-de-France. Les travaux prévoient notamment la réalisation de 7,6 km de remblais (« digues ») offrant une capacité de stockage de 10 millions de m3; d'une station de pompage en Seine d'une capacité de 42 m3/s et de deux stations de relevage permettant de limiter les impacts piézométriques locaux. Le site pilote est considéré comme un aménagement hydraulique et un barrage de classe C. Les travaux se sont réalisés sur 4 ans (de 2021 à 2025). Cet article porte sur l'intégration des géosynthétiques au niveau des différents organes de sécurité de la « digue ».

1 Introduction

Le site pilote Seine-Bassée se situe en Seine-et-Marne (77), à cheval sur 4 communes (Châtenay-sur-Seine, Gravon, Egligny et Balloy). D'une superficie d'environ 4 km², et d'une capacité de stockage de 10 millions de m3, il permet de stocker temporairement les eaux de la Seine en période de crue afin d'abaisser la ligne d'eau en aval, et ainsi limiter les impacts socio-économiques dus aux inondations en Île-de-France. Il est le premier d'un programme de 9 casiers d'une capacité de stockage totale de 55 millions de m3 afin de réduire le niveau d'eau en Île-de-France de 40 cm lors d'un pic de crue de la Seine. Le site pilote permettrait à lui seul une atténuation des crues de la Seine jusqu'à 15 cm.

Cet ouvrage, classé Aménagement hydraulique et Barrage de Classe C, est composé des éléments suivants (localisés sur la Fig. 1) :

- 7,6 km de remblais périphériques (« digues ») ;
- une station de pompage en Seine équipée de 8 pompes d'une capacité totale de 42 m3/s ;
- un déversoir de sécurité d'une capacité de 42 m3/s ;
- deux stations de relevage connectées à des drains actifs positionnés en pied de remblais périphériques afin de limiter les impacts piézométriques locaux. Ces drains actifs, d'une

longueur de 700 m et 500 m, sont respectivement implantés dans l'angle nord-ouest et sud-est du site pilote ;

• deux ouvrages de continuité hydro-écologique.

Le contexte géologique de la zone est le suivant : alluvions modernes sur alluvions anciennes, reposant sur la Craie du Campanien. Les étangs présents à l'intérieur du site sont d'anciennes gravières (exploitation d'alluvions anciennes).

Au moment d'une crue, le casier sera rempli par actionnement des pompes de la station pour une durée de près de 3 jours. Les eaux seront ensuite stockées jusqu'à la décrue de la Seine, puis rejetées gravitairement dans la Seine par ouverture des vannes de la station de pompage. Le bassin étant situé en contexte alluvionnaire, l'impact sur la piézométrie locale n'est pas négligeable lorsque celui-ci est rempli. Ainsi, les stations de relevage raccordées aux deux drains actifs permettront de maintenir la nappe à un niveau bas en pied d'ouvrage. Le déversoir de sécurité, situé au niveau de la digue sud, permettra quant à lui un rejet du « trop-plein » en Seine en cas d'élévation incontrôlée de la cote d'eau.

La digue sud se distingue par le fait que les deux talus sont sollicités. Le talus intérieur l'est par le remplissage du bassin et le talus extérieur par les crues de la Seine.

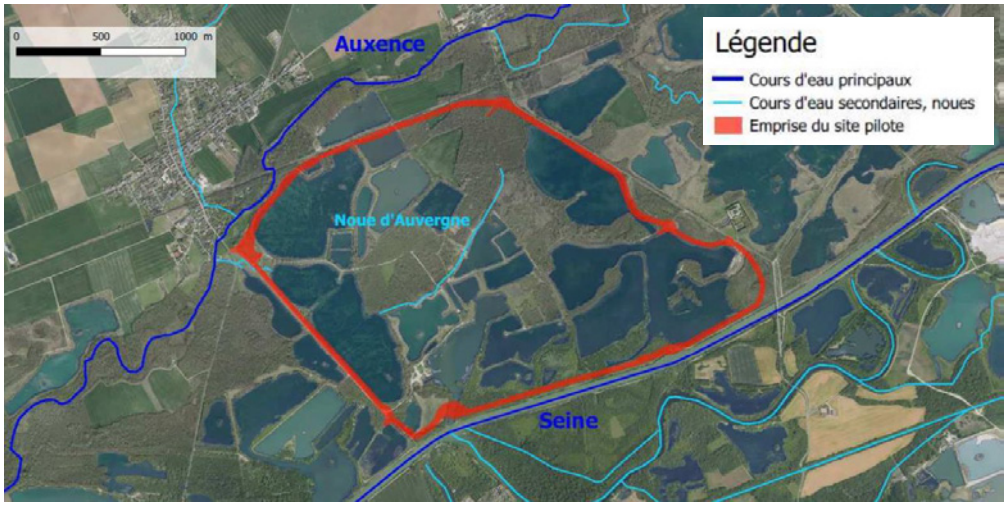


Fig. 1. Localisation de l'ouvrage projeté (Source : EPTB Seine Grand Lac & Hydratec, 2020)

2 L'érosion, mécanisme prépondérant à l'origine de la rupture des digues et barrages

Le mécanisme d'érosion est divisé en 2 groupes distincts : l'érosion interne et l'érosion externe.

L'érosion interne se décompose en 4 différents processus (Cf. Fig. 2) :

• L'érosion régressive se caractérise par la formation d'un passage appelé « renard hydraulique » de l'aval vers l'amont, par départ des particules à l'aval. Ce passage provoque la réduction du chemin d'écoulement, et donc du gradient hydraulique de l'ouvrage, ce qui implique des vitesses d'écoulement plus élevées au sein de ce dernier. Il y a rupture lorsque le passage formé atteint la moitié de la largeur de la digue.

• L'érosion de contact se développe à l'interface de 2 couches de perméabilité très différente. Les vitesses d'écoulement élevées au sein de la couche en matériau grossier entraînent le détachement de particules de la couche de matériau fin.

• L'érosion de conduit se caractérise par le détachement des particules de sol au niveau d'un chemin d'écoulement préférentiel, le long d'un conduit ou d'un trou préexistant. Le développement de ce type d'érosion n'est possible que si la nature des matériaux de « l'encaissant » est un minimum cohésive. Dans le cas contraire, le conduit s'effondrera sur lui même, ce qui stoppera la poursuite du phénomène.

• La suffusion est une instabilité interne d'un sol à granulométrie discontinue. Lors de ce phénomène, les particules fines libres sont entraînées à travers les particules grossières. Elle n'apparaît que dans les sols où les fines ne comblent pas les vides des particules granulaires.

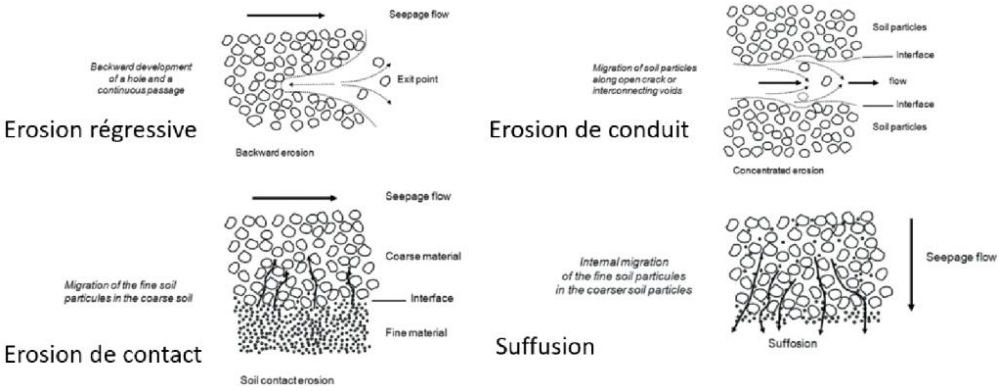


Fig. 2. Différents processus d'érosion interne (Source : The International Levee Handbook, 2013 [1])

L'érosion externe peut se traduire de différentes manières (Cf. Fig. 3) :

• Coté zone protégée, par des interactions avec l'environnement (pluie, gel, ruissellement, animaux) et les activités anthropiques (cheminements « sauvages », passage d'engins) ;

• Coté eau, par l'action des vagues et des courants ;

• Par surverse.

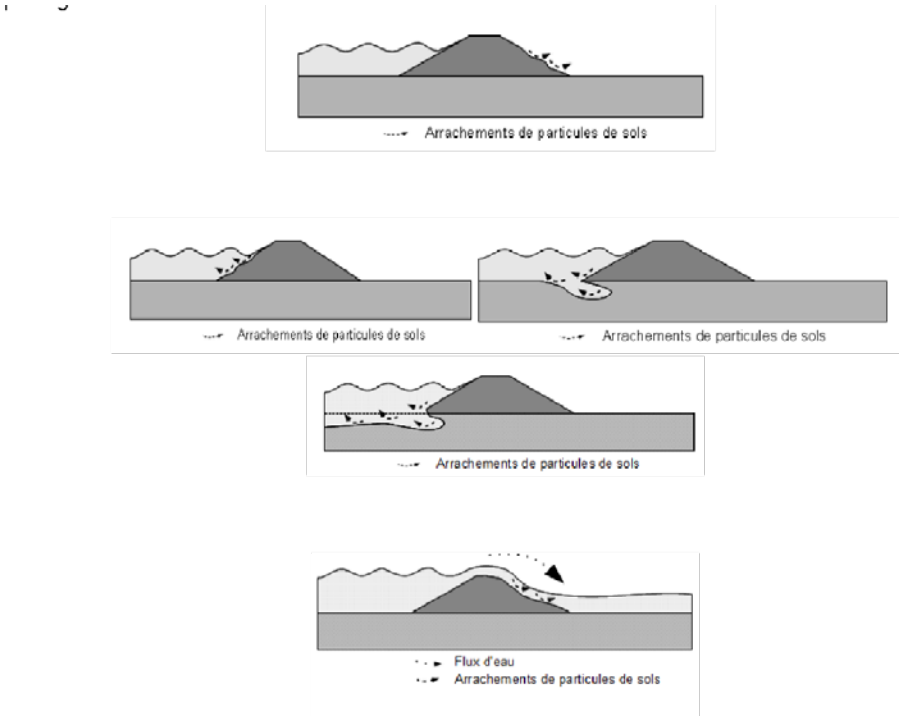


Fig. 3. Différents processus d'érosion externe (Source : Référentiel technique digues maritimes et fluviales, 2015 [5])

D'après l'étude statistique menée par Foster (2000) [6], les mécanismes d'érosion interne et externe seraient respectivement à l'origine de 50 et 45 % des ruptures de barrage en remblai.

Il est donc nécessaire d'intégrer des dispositions constructives suffisamment robustes et pérennes afin de sécuriser les ouvrages en terre contre ces phénomènes.

C'est pour répondre à cet objectif que les géosynthétiques et produits assimilés ont fait partie intégrante de la conception des « digues » de la Bassée.

3 Présentation des « digues » du site pilote La Bassée

D'une hauteur limitée (3 m en moyenne), les remblais périphériques présentent la particularité d'être implantés partiellement sur des plans d'eau. Une vidange de ceux-ci et un batardage n'étant pas envisageable au regard du linéaire des travaux, les remblais en eau ont été conçus avec des matériaux insensibles à l'eau (au sens du Guide de Terrassement Routier, 2000, [2] et [3]). Cela permet de s'affranchir des modalités de compactage. Ces matériaux étant perméables, il a fallu coupler cette disposition constructive à un écran étanche ancré jusqu'aux alluvions anciennes. Il permet de limiter le débit de contournement de l'ouvrage (par les terrains d'assise).

Des risques de claquage hydraulique de la couche d'alluvions modernes ayant localement été mis en évidence par les calculs, des puits de décompression jusqu'au alluvions anciennes ont été réalisés sur certains secteurs.

Sur les portions terrestres, un décapage de la terre végétale sur 30 cm, et un terrassement/re-compactage des matériaux en place sur 1 m de profondeur ont été réalisés sur l'ensemble du linéaire. En plan d'eau, la vase résiduelle a été curée avant mise en œuvre des remblais insensibles à l'eau. Aucune section de digue ne repose entièrement sur les matériaux insensibles.

Un matelas drainant a été réalisé en pied d'ouvrage, parement extérieur, afin de limiter le risque d'érosion interne. Une fibre optique passive est posée en son sein pour la détection d'éventuelles fuites anormales dans l'ouvrage. Le matelas est raccordé à un fossé de pied de « digue ». Malgré la sollicitation de l'ouvrage par les crues de la Seine, ces dispositions n'ont pas été réalisées coté intérieur afin de ne pas accentuer la saturation du corps de digue lorsque l'ouvrage sera rempli, d'autant plus que l'ouvrage sera en cours de remplissage au moment d'une crue dans son fonctionnement normal (afin de limiter fortement les gradients hydrauliques dans l'ouvrage). Une coupe type de l'ouvrage issue du CCTP est présentée en Fig.4.

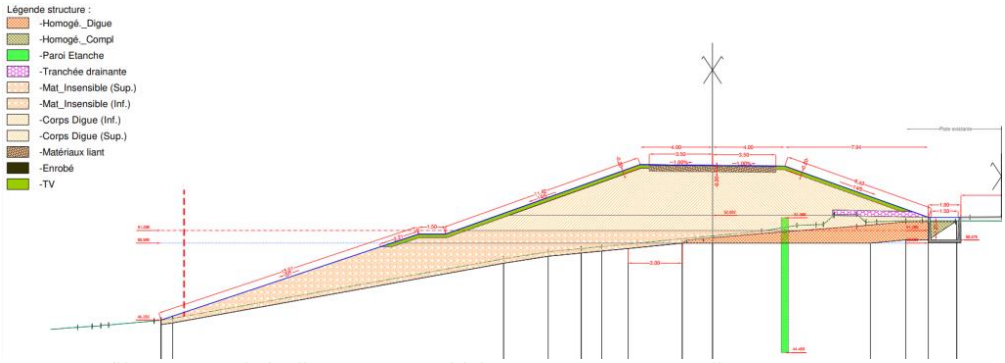


Fig. 4. Profil en travers de la digue – Cas remblais en eau (Source : Terélian, 2022)

Sur deux tronçons, un drain actif a été réalisé afin de limiter l'impact piézométrique local engendré par le remplissage du site. Le drain actif conçu correspond à une conduite circulaire en béton de DN 1000 à 2000 mm, avec des trous de diamètre 20 mm implantés selon un maillage de 20 cm par 20 cm (hors cunette), positionnée dans une tranchée drainante. La coupe type est présentée en Fig. 5.

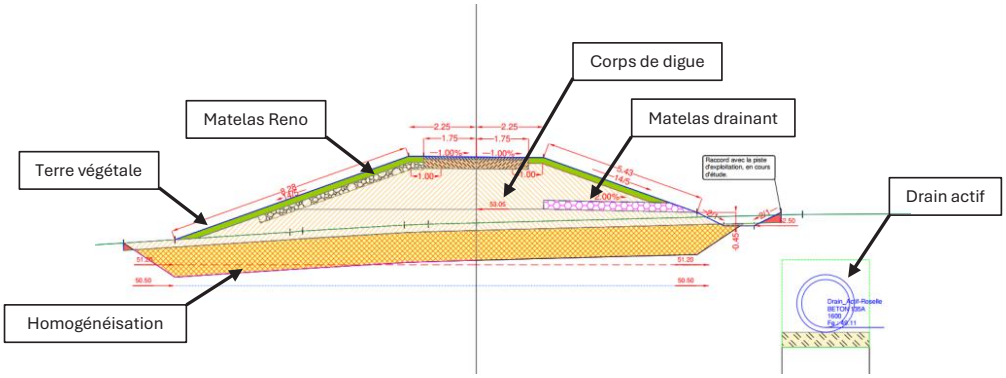


Fig. 5. Profil en travers de la digue – Cas drain actif (Source : Terélian, 2022)

4 Les géosynthétiques dans les dispositifs de protection contre l'érosion interne

Comme présenté précédemment, l'érosion interne est un problème de migration des particules de sol au sein de l'ouvrage, engendré par les écoulements internes. La maîtrise de ce risque passe donc par un contrôle des écoulements et la mise en place de filtres au niveau de points stratégiques.

Deux types de filtres sont utilisés sur les ouvrages hydrauliques :
- Les filtres granulaires ;
- Les géotextiles de filtration.

Pour le site pilote Seine-Bassée, le choix s'est porté sur les géotextiles de filtration de par leur rapidité de mise en œuvre, et leur plan de contrôle en usine. Ils ont été utilisés à 3 niveaux (Cf. Fig. 6 et 7) :

- A l'interface entre le corps de digue et les matériaux insensibles à l'eau pour se prémunir contre le développement d'érosion de contact ;
- Autour du matelas drainant, vis-à-vis du risque d'érosion régressive dans le corps de digue ;
- Au niveau du drain actif autour de la tranchée pour limiter le risque d'érosion régressive et de suffusion dans les terrains d'assise ;
- Au niveau du drain actif autour de la buse béton afin d'empêcher le matériau granulaire de rentrer dans les perforations de la buse béton (les perforations étant de 80 mm et le drainant mis en œuvre d'une granulométrie 20/50 mm).

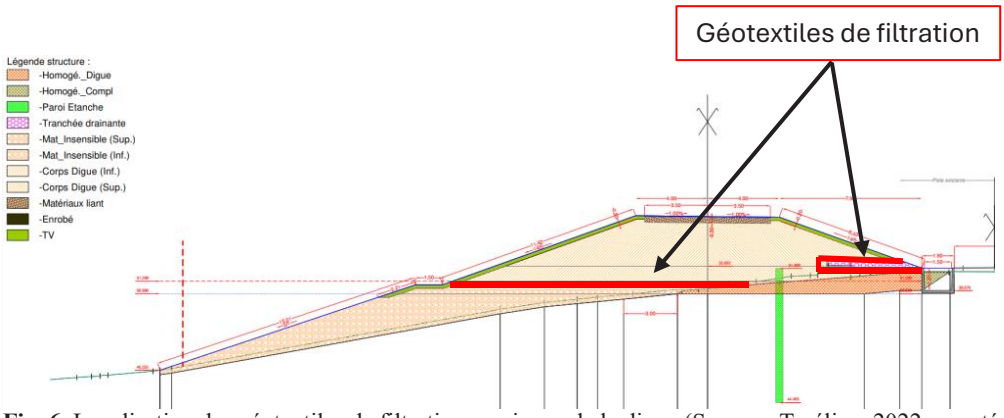


Fig. 6. Localisation des géotextiles de filtration au niveau de la digue (Source : Terélian, 2022, annoté par Antea Group, 2025)

NB : Le géotextile de filtration positionné entre le matériau insensible et le corps de digue n'a pas fait l'objet de préconisations particulières concernant son épaisseur. En effet, le matériau insensible étant par nature drainant, la digue a été conçue de façon à avoir une charge hydraulique assez « profonde ». C'est pour cela que des écrans étanches ont été réalisés sur ces tronçons spécifiques.

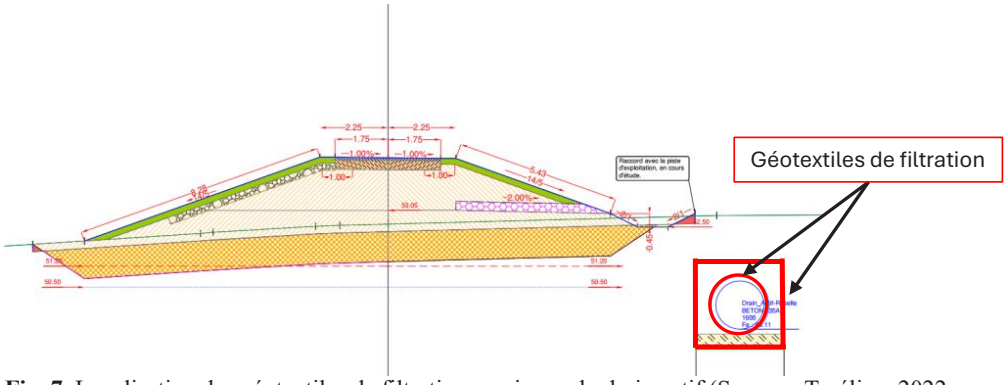


Fig. 7. Localisation des géotextiles de filtration au niveau du drain actif (Source : Terélian, 2022, annoté par Antea Group, 2025)

Les géotextiles utilisés ont été dimensionnés selon les recommandations du Comité Français des Géosynthétiques [4], de la NF G38-061 et sont certifiés ASQUAL.

Les caractéristiques du produit utilisé sont présentées dans le Tableau 1.

Tableau 1. Caractéristiques du géotextile de filtration utilisé

Caractéristiques	Valeur	Tolérance
Perméabilité normale au plan (vh50)	60 l/m²s	- 18 l/m²s
Capacité de débit sous 20 kPa	$4x10^{-6}$ m²/s	- $1,2*10^{-6}$ m²/s
Ouverture de filtration (O90)	80 µm	+/- 20 µm
Durabilité présumée dans les sols naturels de 4 < pH < 9 pour des températures de sol < 25°C	100 ans	-

5 Les géosynthétiques dans les dispositifs de protection contre l'érosion externe

Pour pallier au risque d'érosion externe, les parements intérieurs ont été renforcés par la pose d'une géogrille tri-dimensionnelle et d'une géogrille anti-fouisseur. La géogrille tridimensionnelle a pour objectif de permettre la fixation du système racinaire de l'enherbement et ainsi améliorer la résistance du talus au clapot et aux vagues. La géogrille anti-fouisseur vise à limiter la création de terrier dans la digue. Les animaux visés sont généralement les lapins, lièvres, blaireaux, ragondins et taupes.

Les parements extérieurs étant moins sollicités, seule la géogrille anti-fouisseur a été mise en œuvre.

Ces dispositions constructives sont représentées sur la Fig. 8.

Les géosynthétiques ont été ancré en crête de digue dans une tranchée de 30x30 cm (du fait de la faible sollicitation mécanique). Des épingles de fixation ont été mises en œuvre au niveau des recouvrement de lés.

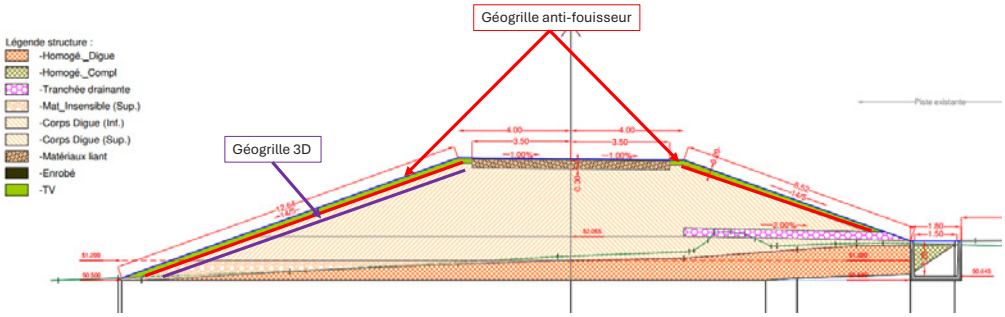


Fig. 8. Localisation des dispositions constructives en parement de digue – Section courante (Source : Terélian, 2022, annoté par Antea Group, 2025)

Le CCTP du marché prévoyait initialement un grillage anti-fouisseur correspondant à un grillage en acier galvanisé double torsion, d'une maille 6x8 cm, et d'un diamètre de fil 2,2 mm. Les produits disponibles sur le marché, répondant à ces critères présentent des résistances à la traction de 30 à 50 kN/m. Le choix s'est donc orienté vers une géogrille en polypropylène présentant une résistance à la traction similaire (40 kN/m).

La géogrille anti-fouisseur a été préférée à un grillage métallique classique du fait de la possibilité de la souder à la géogrille tridimentionnelle et des caractéristiques du polypropylène (bonne résistance à la traction, durabilité élevée et bonne résistance chimique). Cette solution a permis d'augmenter les cadences de pose tout en augmentant les caractéristiques mécaniques de la géogrille tridimentionnelle (les deux géogrilles étant soudées, le complexe géosynthétique hérite des propriétés mécaniques des deux matériaux). Les modalités de soudure entre les deux géosynthétiques n'ont cependant pas été précisées par le fabriquant.

Ce type de géogrille anti-fouisseur a déjà été utilisé au niveau des digues de Fauquembergues (62), ouvrages bordant des champs d'inondation contrôlés de l'Aa, travaux finalisés en 2020.

Les caractéristiques des géogrilles sont présentées dans les Tableaux 2 et 3.

Tableau 2. Caractéristiques de la géogrille anti-fouisseur

Caractéristiques	Valeur	Tolérance
Maille	30*30 mm	-
Matériau	Polypropylène	-
Résistance à la traction, SP/ ST	40 / 40 kN/m	- 0
Allongement à la traction maximale, SP / ST	7,0 / 7,0 %%	+3,0 / – 2,0-
Durabilité présumée dans les sols naturels de 4 < pH < 9 pour des températures de sol < 25°C	100 ans	-

Tableau 3. Caractéristiques de la géogrille tridimensionnelle

Caractéristiques	Valeur	Tolérance
Matériau	Polypropylène	-
Diamètre du filament	1,1 mm	-
Masse surfacique	600 g/m²	-

Ces aménagements ont été complétés par la pose de matelas gabions de part et d'autre de la digue au droit des zones de Run-Up et de franchissement (l'ouvrage ayant fait l'objet d'une dérogation sur la hauteur de la revanche) ; comme représenté sur la Fig. 9.

L'ensemble de ces renforcements a été recouvert de 15 cm de terre végétale, ensemencée par hydroseeding.

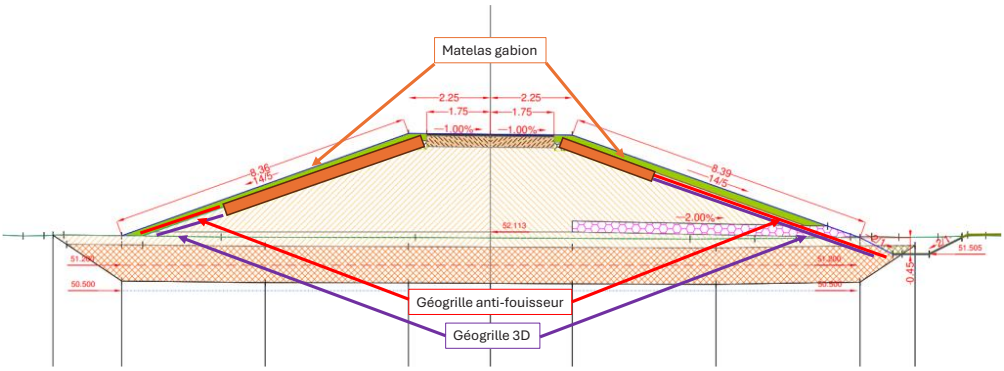


Fig. 9. Localisation des dispositions constructives en parement de digue – Section « renforcée » (Source : EPTB Seine Grand Lac & Hydratec, 2021, annoté par Antea Group, 2025)

Les caractéristiques majeures du matelas gabion sont présentées dans le Tableau 4 :

Tableau 4. Caractéristiques du matelas gabion

Caractéristiques	Valeur	Tolérance
Epaisseur	23 cm	-
Maille	60 x 80 mm	- 0 / + 8
Diamètre du fil nu	2,2 mm	-
Résistance à la traction	37 kN/m)	-
Résistance au poinçonnement	42 kN	-
Matériau de remplissage	Grave calcaire 90/120	-

6 Conclusion

L'utilisation des géosynthétiques et produits assimilés (matelas gabions) lors de la construction des « digues » du site pilote Seine-Bassée ont permis de mieux maitriser le risque d'apparition d'érosion interne ou externe au niveau de l'ouvrage. Ils ont été mis en œuvre sur les différentes parties de la « digue » : les géotextiles de filtration au niveau de l'interface corps de digue/matériau insensible à l'eau, du matelas drainant et du drain actif, les géogrilles tridimensionnelles et anti-fouisseur, ainsi que les matelas gabion, au niveau des parements de digue intérieur et extérieur. Ces solutions présentent l'avantage de disposer d'un plan de contrôle en usine (offrant plus de garanties qu'un plan de contrôle en chantier) et de permettre une mise en œuvre rapide, bienvenue sur des chantiers de grande ampleur aux contraintes de planning importantes.

Références

Ouvrages

1. CIRIA, Ministère de l'Ecologie, du Développement durable et de l'Energie, USACE, The International Levee Handbook. (2013)
2. SETRA / LCPC, Réalisation des remblais et des couches de forme - Fascicule I - Principes généraux (2000)
3. SETRA / LCPC. Réalisation des remblais et des couches de forme - Fascicule II - Annexes techniques (2000)
4. Comité Français des Géosynthétiques, Recommandations pour l'emploi des Géosynthétiques dans les systèmes de Drainage et de Filtration (2014)

Article de revue

5. P. Chassé, Y. Deniaud, D. Goutaland, J.M. Kahan, P. Lebreton, et al.. Référentiel technique digues maritimes et fluviales. MEDD - DGPR, pp.191 (2015)
6. M. Foster, R. Fell and M. Spannagle, The statistics of embankment dam failures and accidents, Can. Geotech. J. 37: 1000–1024 (2000)

AMELIORATION DES SOLS PAR INCLUSIONS RIGIDES ET APPORT DES GEOSYNTHETIQUES

SOIL IMPROVEMENT *BY RIGID INCLUSIONS AND ADDITION OF GEOSYNTHETICS*

Thouna Hamidechi Boulmaali [1], Said Tabti [1]

[1] Afitex Algérie Alger- Algérie

RESUME. Dans le cadre de la réalisation du projet d'Autoroute Est Ouest, lot Est sur un linéaire de 84 km (El Taref vers frontières tunisiennes), le terrain du PK 397 +500 au PK 398+065 se caractérise par un sol compressible. Plusieurs solutions ont été proposées mais l'amélioration de sol par Inclusions Rigides associée à un géotextile de renforcement bidirectionnel s'est avérée la solution la mieux adaptée. Le nombre et /ou l'entraxe des pieux est le sujet de cette présentation ainsi que le type du géotextile de renforcement utilisé pour assurer le transfert des charges.

ABSTRACT. As part of the implementation of the East West Highway project, East lot over 84 km section (El Taref towards Tunisian borders), the land from PK 397 +500 to PK 398+065 is characterized by a compressible soil. Several solutions proposed but the improvement of the soil by Rigid Inclusions associated with a bidirectional reinforcement geotextile appeared to be the best suited for this case. The number and/or spacing of the piles is the subject of this presentation as well as the type of reinforcement geotextile ensuring the transfer of loads.

1 Introduction

Le terrain de PK397+500 à PK398+065 est un sol compressible, il s'agit d'une couche épaisse d'argile marneuse (Profondeur maximale de 27 mètres), intercalée par des lentilles et des poches sableuses.

La dernière mesure du tassement de la plateforme a été effectuée le 16/04/2022 au niveau du PK397+500 sous le remblai d'essai de 11,23 m de hauteur. Le tassement final a atteint 73,3 cm, dont 39 cm produit durant la constitution du remblai, sachant qu'il avait été estimé à 90 cm.

1.1 Topographie et géomorphologie

La zone d'étude où se trouve le pont est une zone de plaine, de relief plat et ouvert, avec une altitude comprise entre 23,05 et 24,51 m (**Fig. 1**).



Fig. 1. Photographie de la plateforme à côté de OA 397.1

1.2 Lithologie de la strate

D'après le rapport de reconnaissance géologique établi par COJAAL [3], la stratigraphie de la zone est constituée, de haut en bas, d'argile, de sable argileux, lâche-intense, et d'argile marneuse. Le profil établi résulte des sondages géologiques en colonne effectués à proximité de la semelle de l'OA397 (**Fig. 2**).

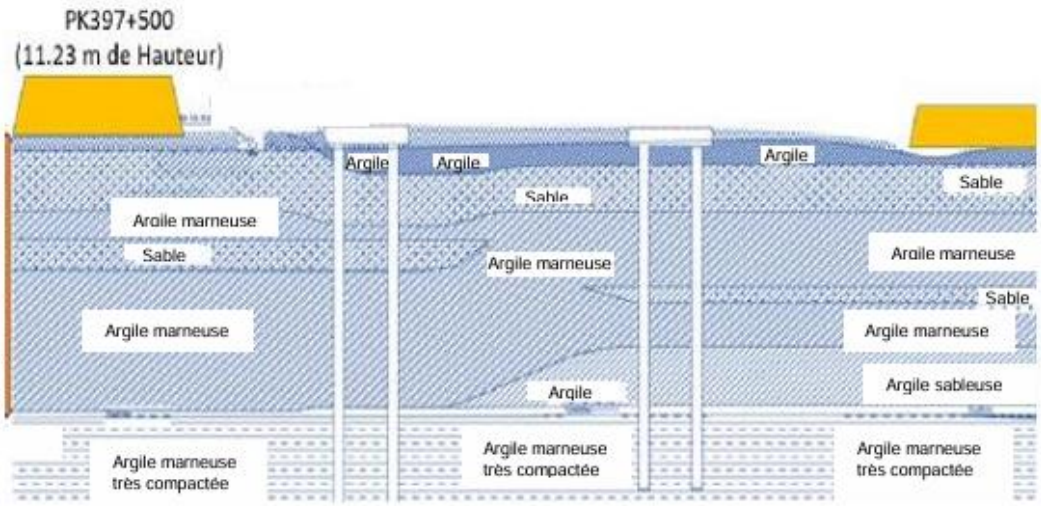


Fig. 2. Schéma lithologique simplifié de la section PK397+700-398+065

2 Les variantes de confortement de la plateforme et la solution adéquate

Deux variantes ont été présentées lors de la réunion du 14-7-2022 avec l'ensemble des intervenants (BCE, BCS, maitre d'ouvrages et l'entreprise CITIC), la première solution sans renforcement destinée à évaluer le tassement et le temps de consolidation et la deuxième solution avec des Inclusions Rigides. Vu que le délai de réalisation de la première solution par consolidation tend vers des durées très importantes (plus de 18 mois dans le cas le plus favorable), le maitre d'ouvrage a opté pour la solution des Inclusions Rigides qui consiste à transférer directement la charge due au remblai vers le substratum rigide de Marne compacte [2, 6].

2.1 Présentation des solutions

Dans ce schéma de fondation par Inclusions Rigides, plusieurs variantes ont été envisagées à des fins de comparaison en faisant varier l'espacement des pieux (l'espacement des pieux de la variante 1 est de 6,0 m * 6,0 m, l'espacement des pieux de la variante 2 est de 7,0 m * 7,0 m (**Fig.3**).

Une solution de renforcement mixte associant un réseau de pieux et un renfort géosynthétique placé à la base du remblai a été retenue. Les charges verticales dues au remblai sont transmises aux pieux directement par le sol de remblai par effet voûte, et indirectement par l'intermédiaire du renfort géosynthétique par effet membrane (**Fig. 4**).

La longueur des pieux est fixée à 31 m en respectant la règle classique des 3 diamètres d'ancrage du pieu dans la couche résistante (DTU 13-2 / P 11-212). [4]

Le choix de Géotextile de renforcement dépend de la distance (s-b) entre les têtes des pieux de dimensions 3 m x 3 m x 0,65 m.

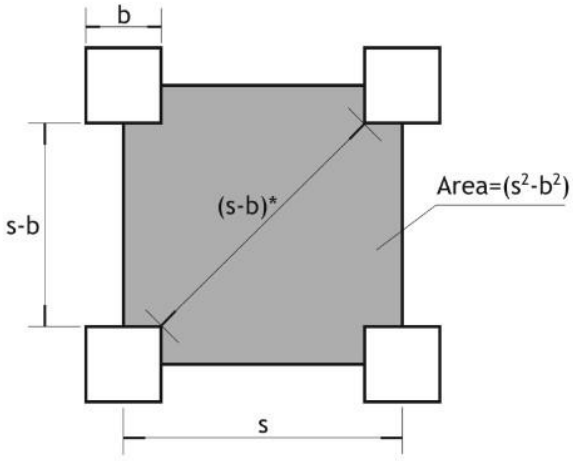


Fig. 3. Schéma de fondation par Inclusions Rigides

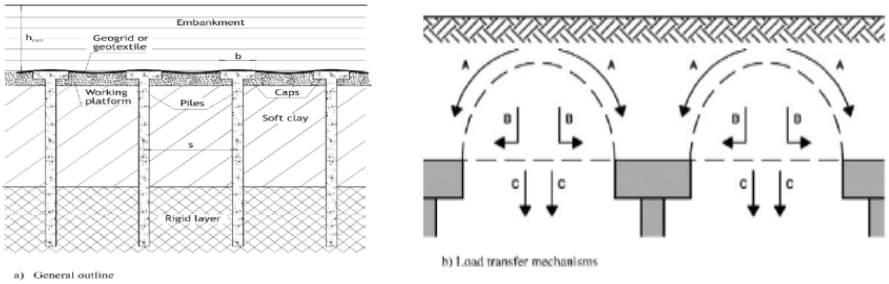


Fig. 4. Remblai sur pieux renforcé par géosynthétique

3 Analyse du schéma de fondation sur pieux

3 .1 Procédure de réalisation des pieux

3.1.1 Ordre d'exécution

Ordre général d'exécution : Levé et traçage → Excavation de la tranchée de boue → Enterrement du tube protecteur → Fixation du trépan de la foreuse au centre du pieu → Création d'un forage atteignant le fond du pieu de référence → Conformité du dégagement du forage → Descente du tube → Coulage du béton → Levée du tube → Déplacement de la foreuse → Entretien. L'intervalle d'exécution entre deux forages ne doit pas être inférieur à 12 heures en cas d'exécution en alternance.

3.1.2 Exécution du forage

Lors de l'exécution du forage du pieu, la ligne de contrôle de la cote de la tête du pieu doit être marquée sur la paroi du tube protecteur selon le point de référence de la cote. Les relevés des forages doivent être effectués au cours de l'exécution.

3.1.3 Tube guide et entonnoir

Il faut choisir le tube guide avec un diamètre de 30cm, et l'entonnoir avec une capacité de 1,5m³.

Les joints du tube guide doivent être étanches lors de son assemblage (Bague d'étanchéité et lubrifiant requis).

Le test d'étanchéité et le test de pression doivent s'effectuer sur le tube guide avant sa première utilisation. Il est qualifié quand aucune fuite n'est détectée sous pression de l'eau de 0,6 MPa pendant 20 minutes.

L'extrémité inférieure du tube guide se situe à 30 cm-50 cm au-dessus du fond de forage. L'entonnoir sera mis à l'extrémité supérieure du tube guide.

3.1.4 Coulage du béton sous l'eau

La résistance du béton requise pour l'étude du pieu est de RN27. La dimension maximale pour l'agrégat grossier (gravier) ne doit pas être supérieure à 25 mm. Pour l'essai d'affaissement au cône d'Abrams, l'affaissement de 180～220mm doit être respecté. On utilise du ciment de silicate ordinaire, qui peut être additionné, le cas échéant, d'un adjuvant réducteur d'eau à haut rendement, dont la quantité est déterminée sur la base des essais. Le béton préparé doit présenter de bonnes propriétés. Le béton ne doit pas présenter des

phénomènes de ségrégation au cours du transport et de la coulée. Le premier coulage de béton doit être effectué jusqu'à plus de 2 m en dessus de l'extrémité inférieure du tube guide, de façon à ce que le tube enfoncé dans le béton au cours du premier coulage soit d'environ 3 m. La profondeur du tube enfoncé dans le béton est entre 2 m et 6 m lors du coulage ; une personne doit être désigné pour effectuer des mesures en temps voulu pour maîtriser la hauteur de levage du tube. Lors de chaque démontage de tube, il faut mesurer et calculer sa profondeur enfoncée, puis déterminer la longueur à démonter de façon à ce que le béton reste en découlement, et enregistrer les relevés de coulage. Le coulage du béton doit être continu et sans interruption. Après démontage, le tube doit être placé dans une étagère et nettoyé à temps. Lorsque le béton est injecté jusqu'à moins de 5 m de la partie supérieure du forage, le tube ne peut plus être levé. Quand le béton atteint la cote de référence, le tube peut être complètement retiré. L'injection dépassant la cote de référence de la tête du pieu ne doit pas être inférieure à 1 m pour assurer la résistance du béton au niveau de la tête du pieu après suppression de la laitance.

3.1.5 Rebouchage du forage et mise en place de la semelle du pieu

Une fois le pieu terminé, le béton au niveau de la tête du pieu doit être recépé rapidement de façon manuelle ou à l'aide du perforateur à air comprimé. La dalle positionnée sur la tête du pieu est installé à la cote de référence avec une précision de ± 2 cm.

3.2. Procédure de renforcement par Géotextile

Cette procédure a pour but de justifier le rôle d'un géotextile de renforcement comme solution complémentaire à la solution « pieux » et de décrire sa mise en œuvre.

3.2.1. Géotextile de renforcement

Le géotextile retenu est un géotextile composite de renforcement et de séparation, tissé tricoté tramé, à mise en tension immédiate. La structure du géotextile est illustrée Fig. 5 et Fig. 6. L'assemblage par tissage-tricotage-tramage du géotextile tissé en polypropylène (fonction séparation) et les câbles polymères haute résistance (fonction renforcement) vont permettre une mise en tension immédiate, ce qui permet de reprendre les efforts instantanément et de limiter la déformation initiale lors de la mise en tension. [1].

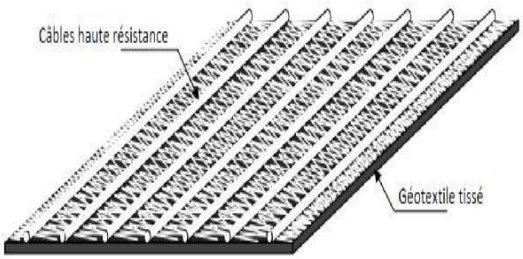


Fig. 5. Structure du Géotextile de Renforcement



Fig. 6. Photographie de Géotextile de renforcement

3.2.2. Caractéristiques et principe de fonctionnement

Le Géotextile de renforcement, par son procédé de fabrication, permet de dissocier les fonctions séparation et renforcement (**Fig.7**). En effet, la résistance en traction du géotextile est obtenue par l'action des câbles polymères haute résistance. La fonction séparation est, quant à elle, assurée par le géotextile tissé dont l'ouverture de filtration est constante et ce quelle que soit la résistance à la traction du géotextile. Ce produit ou d'autre similaire, doit être conforme à la norme ISO 10319 [5].
Le géotextile présente en plus des performances de résistance :

- des résistances élevées au poinçonnement et à la perforation,
- une résistance élevée lors de la mise en œuvre même dans des conditions agressives,
- une perméabilité parfaitement contrôlée pour l'utilisation en fondation.

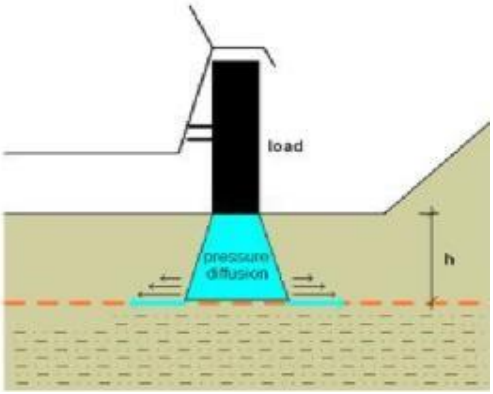


Fig. 7. Fonction de Renforcement

Dans le cas des remblais sur Inclusions Rigides renforcés par géosynthétique, une partie des contraintes verticales du remblai supérieur est transmise aux pieux par effet voûte au sein du remblai et par effet membrane par géosynthétique (**Fig.8**). La présence du géosynthétique permet également de limiter la déflexion de surface.

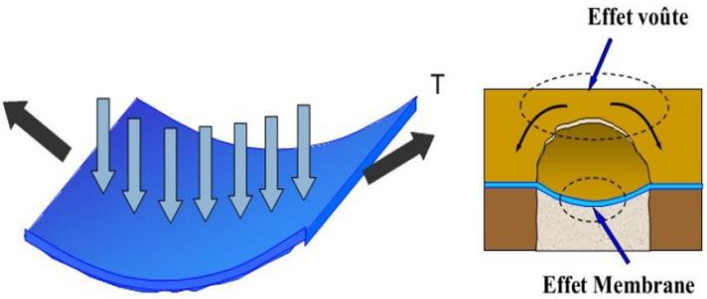


Fig. 8. Effet membrane et effet voûte – Source : J.P. GOURC

3.2.3. Mise œuvre du Géotextile de Renforcement

* Stockage

Le géotextile, afin de conserver toutes ces propriétés, ne doit pas être exposé à l'eau, au gel, aux rayons du soleil, aux déchirures et perforations, etc.

* Installation

Elle s'effectue sur plateformes compactées et nivelées, sans éléments saillants susceptibles d'endommager les nappes de géotextile. L'étalement est réalisé par déroulement manuel ou avec un engin de chantier, avec découpage éventuel des nappes à des longueurs appropriées.

La concordance du sens de pose du géotextile sera impérativement vérifiée avant tout remblaiement. En effet, la résistance des géotextiles est fréquemment plus importante dans le sens production (sens de la longueur du rouleau).

*Recouvrements

Le recouvrement dans le sens perpendiculaire au sens de travail (côte à côte) peut se faire par tuilage sur au moins 50 cm (**Fig.9**). Dans le cas des zones à risques de cavités, le recouvrement dans le sens perpendiculaire au sens de travail sera fonction du diamètre maximal de la cavité.

* Mise en place du sol

Pour le réglage et le compactage du sol, il conviendra de respecter les règles édictées par le CCTP et les fascicules de Recommandations pour les Terrassements routiers.

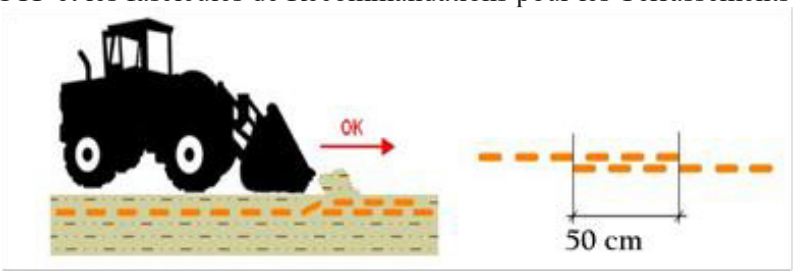


Fig. 9. Recouvrement des nappes de Géotextile de Renforcement

3.2.4. Protection du Géotextile de Renforcement et finitions

Le géotextile de renforcement travaille en tant qu'armature, sa dégradation éventuelle serait très préjudiciable pour la pérennité de l'ouvrage.

Il convient donc d'assurer une protection minimale de toutes les nappes visibles des ouvrages renforcés par Géosynthétiques.

Les exigences concernent essentiellement :

- Le rayonnement solaire,
- La protection mécanique (vandalisme, poinçonnement par chute de pierres…).

3.2.5. Hypothèses géotechniques et dimensionnelles

La justification du géotextile se fait selon la procédure suivante :
1- On calcule la contrainte verticale σ_v agissant sur la base du remblai par la formule de Terzaghi :

$$\sigma_v = \frac{(s-b)\left(\gamma_{emb} - \frac{c_{emb}}{(s-b)}\right)}{Ktg\,\phi_{emb}}\left(1 - e^{-Ktg\,\phi_{emb}\frac{h_{emb}}{(s-b)}}\right) + q.e^{-Ktg\,\phi_{emb}\frac{h_{emb}}{(s-b)}} \quad (1)$$

s-b : la distance entre deux semelles, avec s = 6 m ou 7 m et b=3 m

ϕ : Angle de frottement du remblai de 35°
h_{emb} : Hauteur de remblai de 11,2m
q : La charge du trafic de 20 kPa
C: La cohésion de remblai de 10 kN/m^2
γ_{emb} : Le poids volumique du sol de remblai de 17,68 kn/m^3
K : Coefficient de poussée des terres de 1,46

2- On calcule l'effort de traction agissant sur le géotextile pour une déformation maximale ε_{ult} de 10%, et q désigne la contrainte verticale (en prenant en compte les coefficients partiels sur les matériaux et les surcharges).

$$T_{max;ELU} = \frac{q.(s-b)}{2}\sqrt{1 + \frac{1}{6.\varepsilon_{ult}}} \quad (2)$$

La résistance à la traction du géotextile doit être :

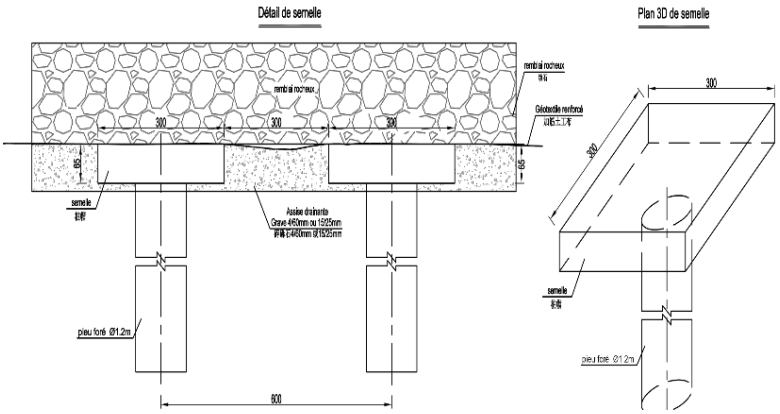
$$R_t \geq T_{max;ELU} \times \Gamma_{Geo} \quad (3)$$

Avec Γ_{Geo}, le Coefficient partiel défini par :

$$\Gamma_{Geo} = \gamma_{MT} \times \Gamma_{flu} \times \Gamma_{veil} \times \Gamma_{inst} = (1{,}25 \times 1{,}7 \times 1{,}1 \times 1{,}2) \quad (4)$$

4 Analyse comparative des solutions pieux

Plusieurs variantes vont être étudiées et ce pour déterminer celle qui techniquement et financièrement est la plus adaptée au cas d'étude présenté sur les Fig.10 et Fig.11.



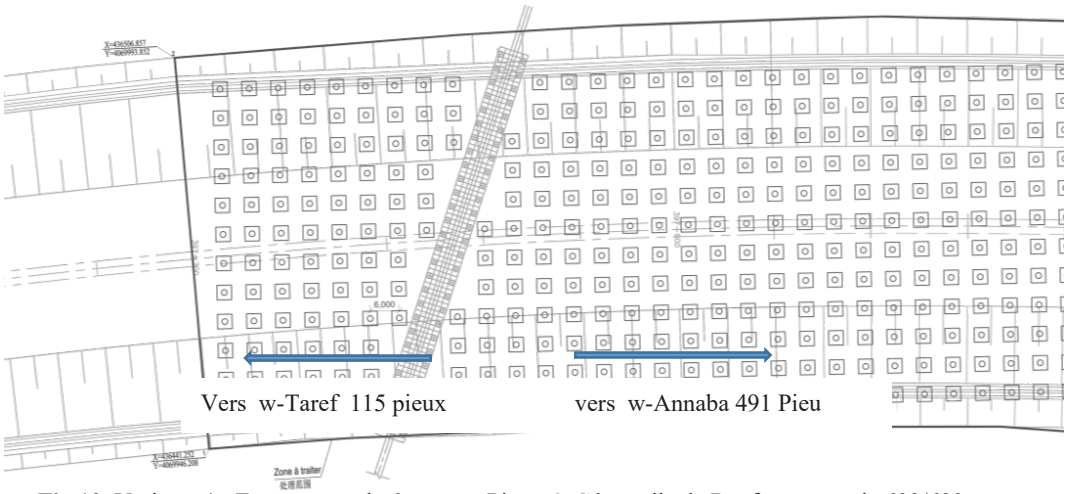


Fig.10. Variante 1 : Espacement de 6 m entre Pieux & Géotextile de Renforcement de 600/600

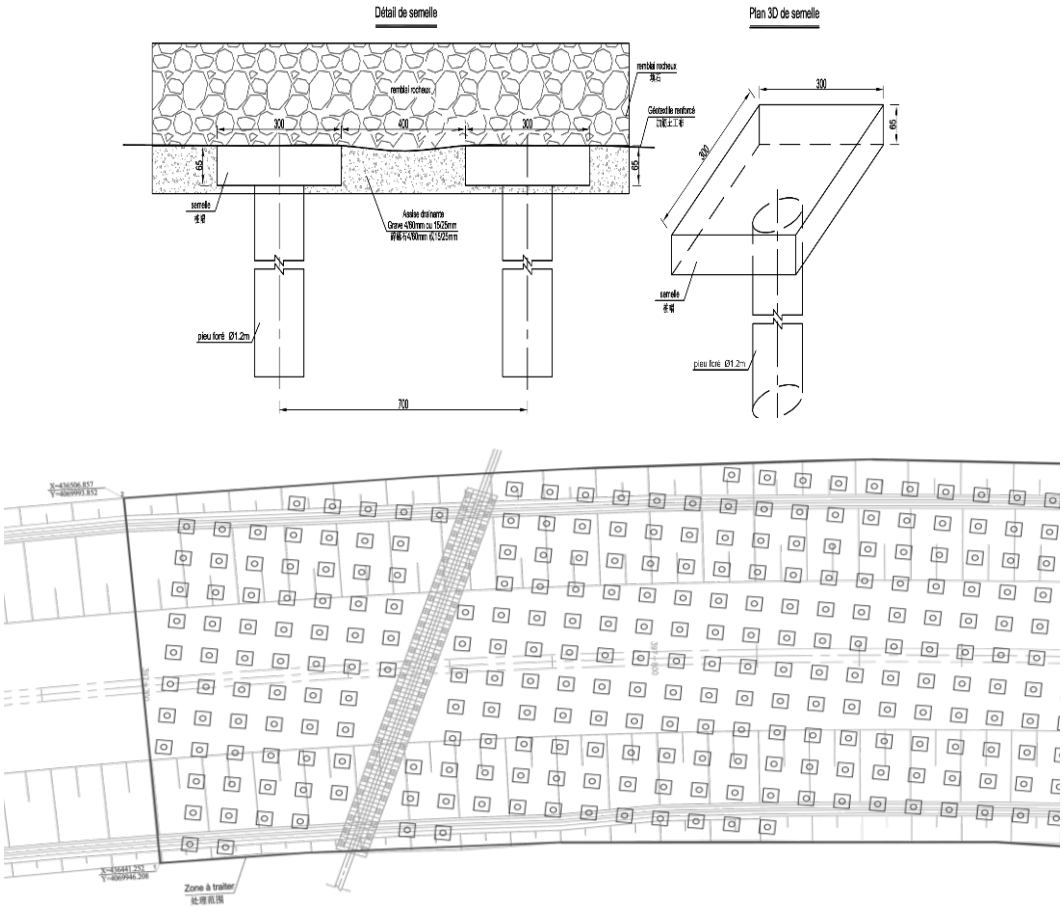


Fig.11. Variante 2 : Espacement de 7 m entre Pieux & Géotextile de Renforcement de 800/800

Les résultats de calcul pour les deux variantes et des entraxes de 6 m et 7 m sont présentés et récapitulés dans le tableau 1 & le tableau 2 ci-dessous.

Tableau 1. Dimensionnement des géosynthétiques suivant les deux variantes

s-b (m)	σ_v (kN/m²)	$T_{max;ELU}$ (kN/m)	Γ_{Geo}	R_t	Géotextile recommandé
3	59,52	157	2,8	441	600/600
4	77,26	268	2,8	750	800/800

Tableau 2. Estimation des coûts suivant les deux variantes

Variante	Entraxe (m)	Nombre de pieux	Nombre de semelles	Diamètre (m)	Longueur du pieu (m)	Classe de géotextile de renforcement	Quantité de géotextile de renforcement	Durée des Travaux	Coût de construction (DA)
Variante 1	6	606	606	1.2	31	Type 600/600	28 120 m2	3 mois pour l'exécution des pieux, et 2 mois pour l'exécution de la plate-forme 5 mois au total	644.086.511,26
Variante 2	7	451	451	1.2	31	Type 800/800	28 120 m2	2,5 mois pour l'exécution des pieux, et 2 mois pour l'exécution de la plate-forme 4,5 mois au total	497.680.995,64

Selon les résultats du tableau 2, un renforcement de 800/800 est à adopter. Par ailleurs, la difficulté de fabrication d'un géotextile de renforcement bidirectionnel de forte résistance, comme le 800/800, à conduit l'entreprise a choisir un géotextile de renforcement monodirectionnel 800/50 posé en deux nappes croisées avec une couche de remblai (TUFF) intermédiaire de 15-20 cm (**Fig.12**) et ce selon les recommandations du Fabricant des géosynthétiques.

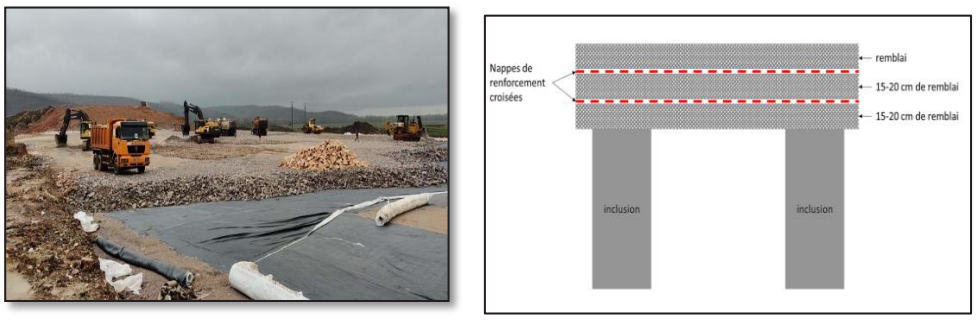


Fig. 12. Détail de la pose des nappes de géotextiles de renforcement croisées

5 Conclusion

Sur la base de l'analyse préliminaire ci-dessus, l'entreprise chinoise CITIC-CRCC a estimé que l'entraxe des inclusions rigides (pieux forés) ajusté à 7 m, est préférable à celui de 6 m et ce en associant un géotextile de renforcement de 800/800 kn/m au lieu de 600/600 kn/m. Cela conduira à un délai plus court de quinze jours avec 151 pieux, soit 40 000 m^3 de béton armé en moins, avec un gain sur le coût de la construction de la plateforme routière de l'ordre de 146 millions Dinars Algérien.

En conclusion, faire contribuer la résistance à la traction du géotextile de renforcement aide fortement à désigner le meilleur entraxe des pieux. La solution technique « Renforcement sur Inclusions Rigides» est recommandée pour pouvoir avoir le meilleur délai des travaux et un gain sur le coût de la construction. Sans oublier aussi les avantages à ne pas négliger pour l'environnement en particulier avoir épargné l'émission de 47 tonnes de CO2 dans l'atmosphère ainsi que réduire le potentiel du réchauffement climatique dû au CH4 qui est 20 fois supérieur à celui du CO2.

Références

1. Fascicule préliminaire Guide d'utilisation des normes de dimensionnement dans la conception des ouvrages avec géosynthétiques : géotextiles et produits apparentés

2. Combarieu O. - Amélioration des sols par inclusions rigides verticales. Application à l'édification de remblais sur sols médiocres. Revue française de géotechnique. n° 44. 1988, p. 57-79.
3. Rapport de reconnaissance géologique établi par COJAAL (2014).

4. Règle classique des 3 diamètres d'ancrage du pieu dans la couche résistante (DTU 13-2 / P 11-212).

5. Norme ISO 10 319 –geosynhtnetiques essais de traction des bandes larges

6. Article de recherche Rev. Fr. Geotech. 2020 « Amélioration des sols par inclusions rigides : le rôle des géosynthétiques dans la plateforme de transfert de charge » Bruno Simon, Laurent Briançon et Luc Thorel.

Techniques de renforcement par géosynthétiques d'un glissement de terrain

Mossedek KHELIFI[1], *Messaoud* ZERMANI[2]

[1] Afitex Algérie, Alger, Algérie
[2] Afitex Algérie, Alger, Algérie

Résumé . Les fortes pluies caractérisant la région du Nord Est de l'Algérie dans la localité de Jijel, ont causé d'importants glissements de terrain sur la Route Nationale RN 77 et le chemin CW 137 A . Le projet consiste à la réalisation des travaux de confortement du chemin N° 137 A, et le traitement des glissements de terrain. La solution retenue consiste à dimensionner et réaliser un massif renforcé par géosynthétiques avec parement en treillis Métallique. Les produits géosynthétiques utilisés sont : Un géocomposite de drainage, un géotextile de séparation et filtration et un géotextile de renforcement. Mots-clés : geocomposite-glissement-géotextile-drainage-renforcement.

Abstract. The heavy rains characterizing the north-eastern region of Algeria in the locality of Jijel, caused significant landslides on the National Route RN 77 and the CW 137A road connecting Texenna to Selma. The project consists of carrying out work to reinforce road N ° 137 A, and treat landslides. The chosen solution consists of dimensioning and producing a solid structure reinforced by geosynthetics with a metallic lattice facing. The Geosynthetic Products used are: drainage geocomposite,geotextile of separation and filtration 200 g / m².150 g / m² and reinforcing geotextile in successive layers. Keywords: geocomposite-slip-geotextile-drainage-reinforcement.

1 Introduction

Les glissements de terrain sont des mouvements de masses compactes et de terrains meubles glissants vers l'aval. Ils résultent d'une rupture par cisaillement et se produisent en général sur des talus ou des versants de pentes modérées à raide. L'ampleur d'un glissement de terrain peut varier d'un simple bloc qui se détache d'une falaise à une vaste zone englobant des dizaines de kilomètres carrés et des millions de mètres cubes de débris.

Le but principal de ce travail étant le confortement de l'un des glissements de terrain dans la localité de jijel (Est algérien), par l'apport d'un géosynthétiques de renforcement [1, 2, 3].

Les zones instables recensées à travers le réseau routier de cette localité montrent l'apparition d'autres glissements potentiels en d'autres endroits, d'où la généralisation future de ses solutions de confortement par géosynthétiques

2 Présentation du procédé (massif renforcé par géotextile de renforcement).

Un massif renforcé par géotextile de renforcement est constitué de plusieurs nappes successives intercalées dans un remblai technique sélectionné. L'intervalle entre les nappes de renforcement est déterminé par calcul. Plusieurs types de parement peuvent être associés au remblai renforcé :

- Parement en Blocs cellulaires en béton Atalus
- Parement en Treillis Métallique
- Parement à retournement en Géotextile de renforcement associé avec Géofilet (végétaliser)

2.1 Dimensionnement

Dans son principe de fonctionnement, le remblai transmet par frottement aux nappes géo synthétiques, les efforts qui se développent dans la masse ; ces nappes se mettent en tension et le remblai possédera alors dans le même sens que les renforcements, une résistance à la traction dont la valeur est directement proportionnelle aux efforts repris par les nappes ; celles-ci reportent les efforts de la zone active, à l'aval, vers la zone résistante à l'arrière du massif.

Pour le dimensionnement de ces ouvrages on utilise des logiciels combinés à des calculs manuels.

Le logiciel nous donne les cercles de ruptures les plus défavorables par la méthode de Bishop (Méthode des tranches), on considèrera les données suivantes :

- Les caractéristiques du sol en place
- Les caractéristiques du remblai technique
- La résistance à la traction du géotextile de renforcement à utiliser
- Les caractéristiques géométriques de l'ouvrage à réaliser.

2.2 Conception et principe de dimensionnement

Les calculs à effectuer pour les soutènements en massif renforcé d'après les normes NF P 94-270, XP G 38-064 sont les suivants :

- La stabilité générale : (stabilité au glissement le long de la surface de rupture du massif renforcé)
- La stabilité mixte : (stabilité au glissement le long des surfaces de rupture qui longent au moins une nappe de géosynthétiques
- La stabilité interne : (Résistance à la traction des géosynthétiques et résistance en ancrage)
- La stabilité externe : (stabilité du massif renforcé vis-à-vis du glissement et du poinçonnement)

2.2.1 Stabilité interne, mixte et générale : permettent de déterminer l'effort de traction Tmax;d au sein de chaque nappe pour assurer la stabilité de l'ouvrage

Les cercles de ruptures sont décrits dans la figure 1.

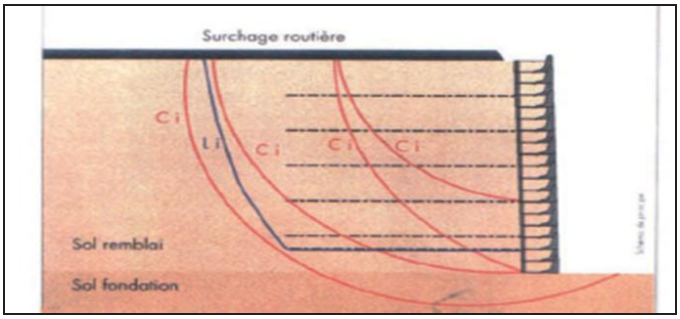


Fig. 1. Schéma des cercles de ruptures

2.2.2 Stabilité externe, glissement et poinçonnement, calcul manuel.

Poinçonnement : Vérifier si la portance du sol support est suffisante pour supporter le poids du Massif renforcé

Glissement : Vérifier que le frottement mobilisé à la base est suffisant et que le Massif ne peut glisser sous l'effet des poussées des terres

La figure 2 montre le calcul manuel des efforts.

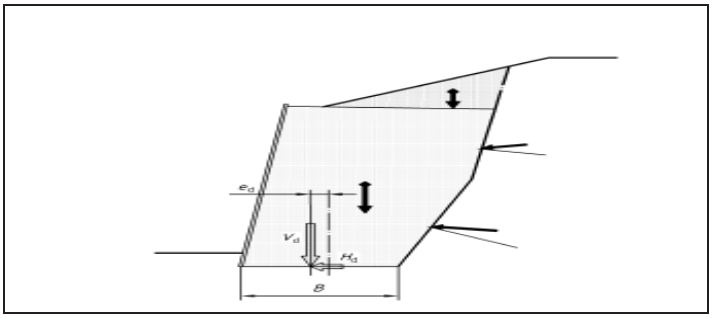


Fig. 2. Calcul manuel des efforts

2.2.3 *Coefficients de pondération :* Plusieurs facteurs de sécurité pour les états limites ultimes sont considérés dans les calculs de stabilité à savoir :

Coefficient de résistance en traction $\gamma_{M;\tau}$:

Le coefficient $\gamma_{M;\tau}$ est également pris en compte pour la vérification de la résistance structurelle des éléments de renforcement géosynthétiques d'un ouvrage en sol renforcé vis-à-vis d'une rupture par traction.

Ainsi la résistance à la traction caractéristique du géotextile de renforcement lors d'une combinaison fondamentale sera pondérée d'un coefficient selon la formule suivante :

$$R_{t;d} \leq \frac{R_{t;k}}{[\gamma_{M;t}.\Gamma_{flue}.\Gamma_{viel}.\Gamma_{end}]}$$

Ces valeurs sont celles recommandées par la norme NF EN 1997-1 et la norme NF G38-064, et rappelées dans la norme NF94-270, pour la vérification des états limites ultimes.

2.2.4 Condition de vérification

$$R_{t;d} \leq \frac{R_{t;k}}{[\gamma_{M;t}.\Gamma_{flue}.\Gamma_{viel}.\Gamma_{end}]}$$

$R_{t;d}$: c'est la résistance ultime en traction de la géogrille
***$R_{t;k}$*:** désigne la résistance a la traction de la géogrille garantie par le fabricant (caractérisée et mesurée selon la norme ISO 10319)

3 Cas du glissement de Jijel

Lors de la période hivernale de l'année 2018, du fait des fortes pluies caractérisant la région de la localité de Jijel, plusieurs glissements de terrain ont eu lieu, nécessitant des interventions pour redonner à la route son aspect normale (Figure 3).



Fig. 3. Plan de situation de la Zone de glissement

3.1 Contexte géomorphologique et hydrologique des Sites

La localité de Jijel est principalement constituée de massif métamorphique et se situe dans la zone géologique des montagnes plissées du littoral méditerranéen.

Le cas traité du projet présente un relief très accidenté, dans un versant montagneux caractérisé par des pentes et fort déclivité qui permet la circulation d'eau souterraine.

3.2 Choix de la geogrille

Dans le cadre de ce projet, le dimensionnement s'est fait selon la formule :

$$R_{t;d} \leq \frac{R_{t;k}}{[\gamma_{M;t}.\Gamma_{flue}.\Gamma_{viel}.\Gamma_{end}]}$$

Le calcul par logiciel , en tenant compte des données géotechniques, et des valeurs des coefficients de réduction définis dans le tableau ci-dessous, nous donnes une valeur $R_{t;d}$ de 40 kN/m au minimum.

Tableau 1. Coefficients réducteurs / sécurité

Coefficients réducteurs / sécurité	Valeur
Endommagement Γ_{end}	1.20
Vieillissement Γ_{viel}	1.20
Fluage Γ_{flu}	1.52
Sécurité partielle $\gamma_{M,t}$	1.25

D'où le choix de la géogrille en PET caractérisée par un effort de traction de 110 kN/ml

3.3 Massif renforcé par géotextile avec parement en treillis métallique.

Un massif renforcé par géogrille de renforcement avec parement en treillis métallique est constitué par l'ensemble masque drainant en géocomposite, tranchée drainante, géogrille de renforcement avec un parement en treillis métallique, confinement de la terre végétale par un géotextile , et remblai technique

3.4 Profil géométrique du massif renforcé « Glissement PK 00+100 ».

La figure 4 montre le Profil massif renforcé

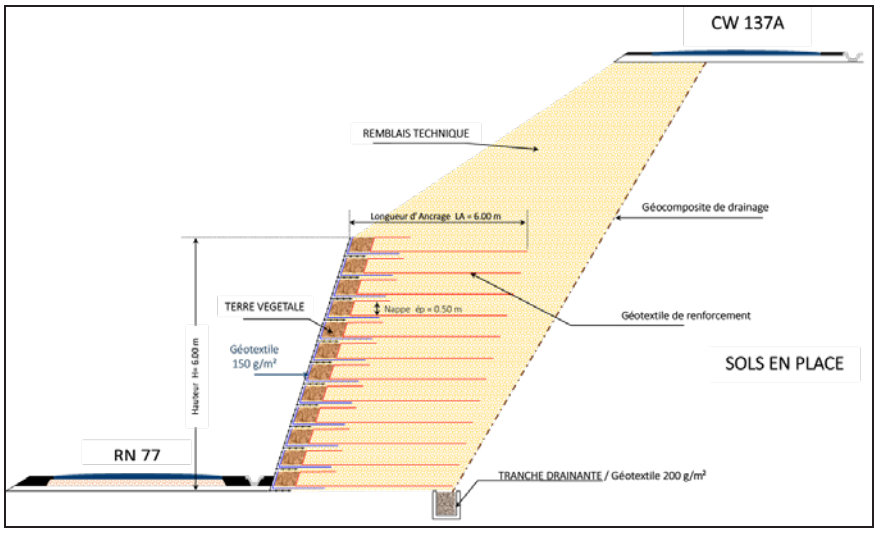


Fig. 4. Profil massif renforcé PK00 + 100

Les photos des figures 5 et 6 montrent l'aspect du glissement de terrain et le traitement par géosynthétique.



Fig. 5. Avant traitement



Fig. 6. Après traitement

Conclusion

Ce cas étudié montre que la technique de traitement de certains glissements de terrain et confortement de talus, réalisés grâce à des massifs renforcés par géotextile à parement en treillis métallique ou autres, constitue une réelle alternative innovante et économique par rapport aux solutions classiques de soutènement.

Les principaux avantages de cette technique résident dans :

- La grande souplesse des massifs renforcés par géosynthétiques
- L'utilisation des matériaux locaux
- L'intégration des ouvrages dans leurs environnements.
- L'esthétique développée
- La rapidité d'exécution.

Références

1. Alexiew D. (2012). High geogrid-reinforced walls with a flexible stone-filled facing in a mountainous seismic region. Proc. Second Pan American Geosynthetics Conference & Exhibition GeoAmericas 2012, Lima, Peru, no pp. on the CD
2. Alexiew D. (2005). Design and construction of geosynthetic-reinforced « slopes" and "walls": commentary and selected project examples. Proc. 12th Darmstadt Geotechnical Conference. Darmstadt Geotechnics No. 13, TU Darmstadt, Institute and Laboratory of Geotechnics, Darmstadt, March 2005, pp. 167-186
3. Arab R. (2007) Traitement d'un glissement de terrain et reconstruction de la chaussée avec un remblai renforcé par géosynthétiques dans la willaya de Bejaia – Algérie. Colloque « sols et matériaux à problème ». 9-11 février 2007, Tunisie ; PP. 157-162.

Amélioration de la portance d'une plateforme par inclusion de nappes géosynthétiques

Farid CHERIFI[1], Said TABTI[2]

[1]Afitex Algérie, Alger, Algérie
[2]Afitex Algérie, Alger, Algérie

Résumé. L'étude présentée expose une amélioration de la portance du sol d'une plateforme de stockage de conteneurs d'un port à Alger. Cette plateforme, située à proximité d'une ancienne installation de stockage de déchets réhabilitée, est constituée principalement de remblais et de déchets de faible portance. Pour dimensionner correctement cette plateforme et son système de fondation, il était indispensable d'évaluer la portance du sol support. Les essais de plaque ont montré l'augmentation de la capacité portante avec l'utilisation des géosynthétiques.

Abstract. The study presented demonstrates an improvement in the load-bearing capacity of the soil of a container storage platform at a port in Algiers. This platform, located near a former rehabilitated waste storage facility, consists mainly of embankments and waste with low load-bearing capacity. To correctly design this platform and its foundation system, it was essential to assess the load-bearing capacity of the supporting soil. Plate tests showed the increase in load-bearing capacity with the use of geosynthetics.

1 Introduction

Les géosynthétiques sont utilisés pour assurer, entre autres, la fonction de renforcement des plateformes. Des géogrilles ont été utilisées pour la première fois pour ce type d'ouvrage en 1980 [1].

Le géosynthétique de renforcement facilite le compactage [2], améliore la portance du sol, apporte un confinement de la couche d'agrégats et permet la diffusion de la charge sur une surface plus grande ; diminuant donc la contrainte locale appliquée.

L'essai effectué est un essai à la plaque, avec deux méthodes d'application : une charge de 566 kPa, à savoir un essai à charge monotone et un essai à charge cyclique avec une fréquence de 1Hz.

Dans ce contexte, l'utilisation de nappes géosynthétiques (pour améliorer la stabilité de ces remblais) est une technique de renforcement de sol efficace [3].

2 Rappel sur la classification des sols

Pour les besoins de ce projet, nous nous intéressons particulièrement à deux types de sols :

2.1 Sols sensibles à l'eau

Ce sont des sols dont l'état varie en fonction de leur teneur en eau (comportement solide, plastique, liquide). Une teneur en eau excessive se traduit par :
- Une portance médiocre.
- De faibles caractéristiques mécaniques : grande compressibilité et faible cohésion.
- Une sensibilité importante au gel.

2.2 Sols évolutifs ou fragmentables

Ce sont des sols « rocheux » compacts à l'état naturel, susceptibles de se fragmenter ou de se dégrader sous l'effet de sollicitations :
- A court terme : lors de la mise en œuvre (extraction, transport, compactage).
- A long terme : sous l'action de contraintes mécaniques (effet de la circulation ou de stockage lourds) ou encore en présence de l'eau ou du gel.

Le tableau 1 renseigne sur les correspondances des valeurs de déformation statique (EV_2) et les caractéristiques des sols référencés dans [4].

Tableau 1. Classe d'arase

Classe d'arase	**AR0**	**AR1**	**AR2**	**AR3**	**AR4**
Compacité (si D ≤20 mm)		≥ 95% de l'Optimum Proctor Normal			
Portance minimum requise «EV_2» (MPa)	< 20	≥ 20	≥ 50	≥ 120	≥ 200
Commentaires	caractéristiques insuffisantes : matériaux impropres nécessitant une substitution ou une amélioration avec, si nécessaire, un drainage	Matériau sensible à l'eau	Matériau insensible à l'eau soit naturellement (VBS < 0,1) soit par traitement avec un réactif adapté (CBR > IPI) Matériau sensible à l'eau mais convenablement drainé	Matériau insensible à l'eau graveleux ou rocheux mais posant des problèmes de réglage ou de traficabilité	

3 Le projet

Le sol en place présente une problématique liée à une très faible portance et pose de réelles difficultés de stabilité des plateformes pour le stockage des conteneurs (figures 1 et 2),



Fig. 1. Vue de la section à traiter.



Fig. 2. Gros plan de la section à traiter.

Compte tenu des problèmes d'affaissements rencontrés sur ces terrains, une évaluation approfondie a eu lieu. L'entreprise, choisie à cet effet, a proposé des solutions spécifiques par un renforcement du substrat avec un traitement à la chaux. Ce traitement sur ce terrain mou et instable n'a pas donné les résultats attendus c'est-à-dire que sur une partie d'une plateforme où il a été appliqué, le terrain reste instable.

La solution alternative proposée par le bureau d'études pour résoudre les problèmes d'instabilité a suggéré l'utilisation des géosynthétiques en base de remblai afin de limiter les épaisseurs de couche de forme et éviter une substitution des matériaux. Les étapes suivantes ont ainsi été réalisées :

1. Evaluation du terrain : la première étape a consisté à évaluer attentivement le terrain destiné au stockage des conteneurs. Ceci revient à identifier les zones molles qui pourraient nécessiter un traitement particulier et vérifier s'il y a des zones avec de fortes saturations en eau ou si le sol est instable. Le tableau 2 résume respectivement les valeurs moyennes de quelques caractéristiques physiques et mécaniques des sols les plus défavorables rencontrées sur site.

Tableau 2. Caractéristiques du sol

Caractéristiques du sol	Valeurs
Teneur en eau ω (%)	135
Indice des vides e	2.0
Porosité η (%)	66.67
Masse volumique sèche Ps (t/ m ^{3})	0.3
Cohésion non drainée Cu (kPa)	25

La nature de ce sol est à dominante argileuse, mais caractérisée par un taux de déchets pouvant atteindre 20 %, d'une teneur en matières organiques très importante.

- Une teneur en eau de 135 %,
- Une masse volumique P_s qui est de 0.3 t/m ^{3}.
- Une cohésion non drainée étant de 25 kPa.

2. Elimination de la couche organique constituée en majorité de déchets, les herbes et les racines.

3. Excavation : creuser jusqu'à atteindre des couches de substrats plus stables sur toute les surfaces, en enlevant les terres molles et instables.

4. Renforcement réalisé par des géosynthétiques spécifiquement choisis en vue de consolider le sol et prévenir les affaissements en adoptant trois variantes de dispositions constructives :

- Géotextile 300 g/m²
- Géogrille de résistance à la traction de 35 kN/m.
- Géotextile 300 g/m²et géogrille de 35 kN/m simultanément.

5. Choix d'un matériau stabilisant constitué d'un gravier et d'un liant.

6. Compactage à l'aide d'une plaque vibrante après mise en œuvre du gravier stabilisant.

3 Caractéristiques des géosynthétiques utilisées

3.1 Géotextile de séparation et filtration de masse surfacique 300 g/m²

Le géotextile non tissé aiguilleté en polypropylène de fibres courtes mis en œuvre a été choisi pour ses caractéristiques hydrauliques (perméabilité, ouverture de filtration).

Les caractéristiques mécaniques et hydrauliques du géotextile en question sont indiquées dans le tableau 3.

Tableau 3. Caractéristiques du géotextile 300g/m²

Propriétés	Unités	Norme	Valeur
Masse surfacique	g/m²	EN ISO 9864	300
Epaisseur sous 2 kPa	mm	EN ISO 9863-1	1.60
Résistance à la traction SP	kN/m	EN ISO 10319	20
Résistance à la traction ST	kN/m		25
Résistance au poinçonnement CBR	kN	EN ISO 12236	3.40
Perméabilité normal au plan	m/sec	EN ISO 11058	0.040
Ouverture de filtration	mm	EN ISO 12956	65

3.2 Géogrille de renforcement

Concernant la géogrille, Hufemusa et al. [5] ont montré que la résistance à la traction à 2 % de déformation devait être supérieure ou égale à 8 kN/m si la hauteur de l'excavation était inférieure à 5 mètres. Imanishi et al. [6] ont présenté le cas d'un remblai dont la teneur en eau de 100 %.

La géogrille utilisée est constituée de câbles de renforcement en polyester haute ténacité.

Le tableau 4 résume les caractéristiques de la géogrille utilisée.

Tableau 4. Caractéristiques de la géogrille

Propriétés	Unités	Norme	Valeur
Masse surfacique	g/m²	EN ISO 9864	135
Résistance à la traction SP	kN/m	EN ISO 10319	35
Résistance à la traction ST	kN/m		35
Résistance à la traction à 2 % de déformation	kN/m	EN ISO 10319	8
Arrête	mm		25/25

4 Essai de plaque

L'essai de plaque vise à mesurer la façon dont le sol des plateformes se déforme sous l'application d'une charge lourde.

Les plates-formes concernées par cet essai sont destinées au stockage des conteneurs.

Le module de déformation statique est donné par la relation (1).

$$EV_2 = \frac{\pi}{4}(1-u^2)\frac{pd}{Z_2} \qquad (1)$$

Où

- EV_2 : module de déformation de la plateforme au point d'auscultation, en MPa.
- u : coefficient de Poisson du matériau
- p : pression moyenne exercée, en MPa.
- d : diamètre de la plaque, en mm.
- Z_2 : enfoncement de la plaque lors du 2eme cycle de chargement, en mm.

5 Résultats obtenus

Les résultats de l'essai de plaque sur trois plateformes sont présentés dans les tableaux 5, 6, 7, 8 et les figures 3 et 4.

Ces résultats résument à chaque fois une moyenne de trois essais pour chaque zone.

L'épaisseur de la couche de forme reconstituée de gravier est de 0.50 mètres.

Le même protocole de compactage a été adapté pour toutes les variantes.

Tableau 5. Module de déformation statique (EV_2) des trois plateformes sans traitement par géosynthétiques.

Localisation	EV_2 (MPa)
Plateforme 1	48
Plateforme 2	53
Plateforme 3	49

Tableau 6. Module de déformation statique (EV2) des trois plateformes en utilisant un géotextile de 300 g/m²

Localisation	EV_2 (MPa)
Plateforme 1	47
Plateforme 2	54
Plateforme 3	45

Tableau 7. Module de déformation statique (EV2) des trois plateformes en utilisant une géogrille de 35 kNm

Localisation	EV_2 (MPa)
Plateforme 1	70
Plateforme 2	73
Plateforme 3	69

Tableau 8. Module de déformation statique (EV_2) des trois plateformes en utilisant un géotextile 300 g/m² surmonté d'une géogrille 35 kN/m

Localisation	EV_2 (MPa)
Plateforme 1	94
Plateforme 2	95
Plateforme 3	93

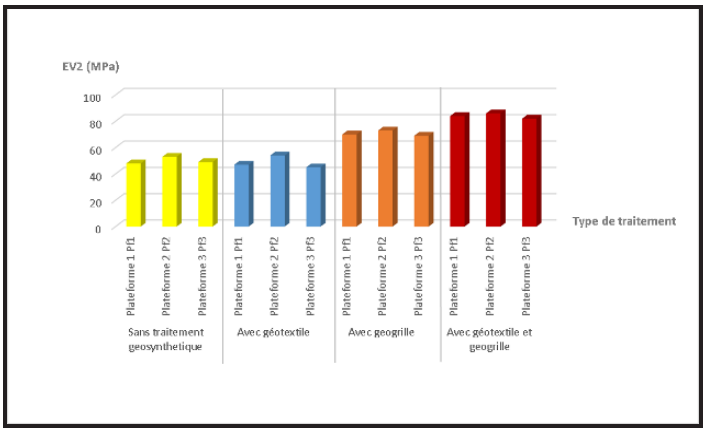


Fig. 3. Evolution du module EV_2 par type de traitement géosynthétiques des plateformes.

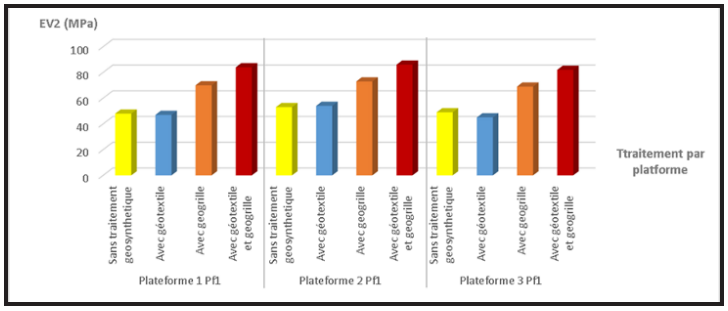


Fig. 4. Evolution du module EV_2 des trois plateformes en fonction du traitement géosynthétiques.

6 Mise en œuvre

Les Figures 5 et 6 illustrent la mise en œuvre de la géogrille et du géotextile au droit des emplacements des conteneurs où il y a un risque d'affaissement.



Fig. 5. Mise en place du géotextile et de la géogrille



Fig. 6. Mise en place de la couche de forme.

7 Conclusion

Afin d'augmenter la portance des trois plateformes, différentes variantes de renforcement par géosynthétiques ont été testées et comparées par des essais à la plaque.
- Variante 1 : Géotextile 300 g/m² seul
- Variante 2 : Géogrille de résistance en traction de 35 kN/m
- Variante 3 : Géotextile 300 g/m² et Géogrille 35 kN/m

Les valeurs du module EV_2 sont assez différentes, le renforcement étant mis en place à la base de la sous-couche de 30 cm d'épaisseur. Les conclusions sont les suivantes :
- Le compactage du sol ne résulte guère en une amélioration de la portance de ce dernier.
(EV_2 : respectivement 48 MPa, 53 MPa, 49 MPa au droit des trois plateformes)
- Le géotextile de séparation seul n'a pas amélioré la portance du sol.
(EV_2 : respectivement 47 MPa, 54 MPa et 45 MPa au droit des trois plateformes)
- Une amélioration de la portance par utilisation de la géogrille.
(EV_2 : respectivement 70 MPa, 73 MPa et 69 MPa au droit des trois plateformes)
- La portance des trois plateformes supports des conteneurs a été sensiblement améliorée par l'utilisation combinée du géotextile surmonté d'une géogrille.
(EV_2 : respectivement 94 MPa, 95 MPa et 93 MPa au droit des trois plateformes)

Ce travail a permis un développement d'un protocole efficace pour tester la portance de toutes les plateformes de stockage existantes car souvent implantées sur des sols peu porteurs. La mesure des tassements permet également de compléter les mesures à la plaque.

Références

1. Giroud, J.P. "An assessment of the use of geogrids in unpaved roads and unpaved areas", Proceedings of the Jubilee Symposium on Polymer Geogrid Reinforcement, Institution of Civil Engineers, London, UK, (2009). pp. 23-36.

2. Bloise, N., & Ucciardo. On site test of reinforced freeway with high-strength geosynthetics. In eurogeo (2000)

3. Cancelli, A., & Montanelli, F. In-ground test for geosynthetic reinforced flexible paved roads. In twelfth european conference on soil mechanics and geotechnical engineering (Volume 2). (1999)

4. Guide technique de conception et de dimensionnement des structures de chaussées métropolitaines, grand Lyon la métropole, Version Mars 2017 (2017).

5. Hufemusa R. et al. Experience: full-scale field tests on geosynthetic reinforced unpaved roads on soft soils (2005)

6. Imanishi H., Hirat T., Takaba Y., Adachi M. Embankment technology with geogrid on very soft clay, 7th International Conference on Geotextiles, Nice, France, (2002) Vol. 1, pp. 177-180.


EUROGEOSS
LILLE 2025 15-18 September

EUROGEO8

LILLE 2025 15-18 September

WWW.EUROGEO8.ORG

Edited by vertcom

ORGANIZED BY CFG COMITÉ FRANÇAIS DES GÉOSYNTHÉTIQUES

UNDER THE AUSPICES OF IGS INTERNATIONAL GEOSYNTHETICS SOCIETY